Faculty of Engineering

Czech University of Life Sciences Prague

Conference Proceeding

5th International Conference TAE 2013

TRENDS IN AGRICULTURAL ENGINEERING 2013

3 - 6 September, 2013

Prague, Czech Republic

CZECH UNIVERSITY OF LIFE SCIENCES PRAGUE

2013

Faculty of Engineering

Czech University of Life Sciences Prague

Conference Proceeding

5th International Conference TAE 2013

TRENDS IN AGRICULTURAL ENGINEERING 2013

3 - 6 September, 2013

Prague, Czech Republic

CZECH UNIVERSITY OF LIFE SCIENCES PRAGUE

2013

Title: Trends in Agricultural Engineering 2013

Editor: © 2013 Czech University of Life Sciences Prague; Faculty of Engineering (www.tf.czu.cz)

The conference is organised in cooperation with CIGR (www.cigr.org)

Type publication: Conference Proceedings

Approved: Deanship of Faculty of Engineering; Czech University of Life Sciences Prague

Edition: First

Circulation: 180

Imprint date: 2013

The articles in the publication are reviewed

The Conference Proceedings designed by Jan Malaťák and Martin Libra

ISBN: 978-80-213-2388-9

Note: Objective correctness and language guaranteed by authors

DEAR COLLEAGUES AND FRIENDS

It is my privilege and great pleasure to invite you to participate in the 5th International Conference "Trends in Agricultural Engineering 2013" to be held September 3 - 6, 2013 in Prague, Czech Republic.

I would like to remember the successful past conferences held in 1994, 1999, 2007 and 2010 where we have experienced a growing number of participants - from 107 back in 1994 to 157 in a year 2010. The organizers of the oncoming event hope that the fifth conference will be the valuable successor of the previous conferences. Its participants will have an excellent opportunity to exchange new experience, ideas and scientific results in the wide range of scientific disciplines.

The history of nineteen years of the conferences dedicated to this topic also represents the changes in this discipline during the years. At the beginning of this period the main domain of the discipline consisted mainly in agricultural machinery improvement, development of automation and robotics. Now, the main role consists of detection of the product quality and in developing agricultural technologies more precisely and friendly towards the environment.

I am looking forward to meeting you all at the conference. We will work hardly not only to offer an interesting scientific programme but also to bring you an attractive social and cultural activities during you stay in Prague. I share this feeling with all my colleagues in Local Organisation Committee that are ready to prepare the best conditions for you.

Martin Libra
Chairman of the Scientific Board

SCIENTIFIC BOARD

- Prof. Martin Libra (chairman, Czech Republic)
- Prof. Vladimír Jurča (Dean, Czech Republic)
- Prof. Jiří Blahovec (Czech Republic)
- Prof. Richard J. Godwin (Great Britain)
- Prof. Jozef Horabik (Poland)
- Prof. Wouter Saeys (Belgium)
- Prof. Dmitry Strebkov (Russia)
- Prof. Zdenko Tkáč (Slovakia)
- Prof. Stavros Yanniotis (Greece)

LIST OF REVIEWERS

- Prof. Radomír Adamovský
- Assoc. Prof. Miroslav Andrt
- Prof. Jiří Blahovec
- Prof. Zdeněk Bohuslávek
- Prof. Milan Brožek
- František Dvořák, PhD.
- Assoc. Prof. Eloy Fernández Cusimamani
- Assoc. Prof. David Herák
- Assoc. Prof. Petr Heřmánek
- Prof. Josef Hůla
- Assoc. Prof. Rostislav Chotěborský
- Assoc. Prof. Boleslav Kadleček
- Prof. Miroslav Kavka
- Prof. Pavel Kic
- Milan Kroulík, PhD.
- Prof. František Kumhála
- Zdeněk Kvíz, PhD.
- Prof. Martin Libra
- Assoc. Prof. Jan Malaťák
- Jiří Mašek, PhD.
- Miroslav Mimra, PhD.
- Assoc. Prof. Miroslav Müller
- Prof. Petr Němec
- Assoc. Prof. Pavel Neuberger
- Assoc. Prof. Martin Pexa
- Martin Polák, PhD.
- Prof. Josef Pošta
- Prof. Józef Horabik
- Assoc. Prof. Miroslav Přikryl
- Assoc. Prof. Miroslav Růžička
- Assoc. Prof. Adolf Rybka
- Assoc. Prof. Petr Šařec
- Prof. Jaromír Volf
- Josef Zeman, PhD.
- Retta Zewdie, PhD.

LOCAL ORGANIZING COMMITTEE

- Prof. Martin Libra (chairman)
- Assoc. Prof. Jan Malaťák (secretary)
- David Hoffmann
- Lukáš Dlabal
- Zdeňka Váchová
- Jarmila Jiříčková
- Jiří Zeman
- Helena Loneková, PhD.

CONTENTS

Invited Lectures

Papers

Letters

IMPROVED SOIL AND WATER MANAGEMENT

Richard J. Godwin

Harper Adams University, Great Britain

Abstract

This paper is written as a result of a series of lectures given over the early few months of 2013 to help farmers and land managers handle the very serious problems of water logging in fields arising from the prolonged period of rainfall in the summer, autumn and winter of 2012 in England. The paper covers some of the fundamental aspects of soil and water management, the description of the current problems, the short/medium/long term action that should be taken and stresses the benefits of controlled traffic, reduced vehicle contact pressure and soil loosening.

Keywords: soil, water management

Introduction

Fundamental aspects

Fig. 1 shows the basic constituents making a healthy mineral based agricultural soil where approximately half of the soil volume (soil solid) is either mineral or organic matter, with the remaining volume (soil void) either water or air. The water/air ratio is dynamic - fluctuating with rainfall/irrigation, drainage status and crop use. Further details of the soil water balance are shown in Figure 2, this illustrates the different effect of soil texture on the moisture status. The "saturation" line depicts the condition when the soil void is full of water; this is not an ideal state as it does not allow the plant roots and other soil flora and fauna to have access to oxygen for respiration. The "field capacity" line represents an ideal condition where water is freely available with sufficient air void for respiration. Finally the permanent wilting point shows the condition when there is insufficient water to sustain crop growth; and although there can be up to 20% of water by volume in a clay soil the crop cannot extract the water from the soil.

Also shown in Fig. 2 are the conditions in "freely draining sand" and a silty clay and clay soil in the Uck and Bourne catchment where the soil is saturated at the surface, but at is at field capacity at 150 mm depth. This illustrates the common condition of a "perched water table" where the soil is saturated at the surface but the water does not infiltrate deeply into the soil. This is different from the "commonly held model" where saturation occurs from a rising water table that might occur in flatter landscapes in river valleys such as the fens and Somerset levels in the UK, the polders in Holland and prairie land in the US mid west.

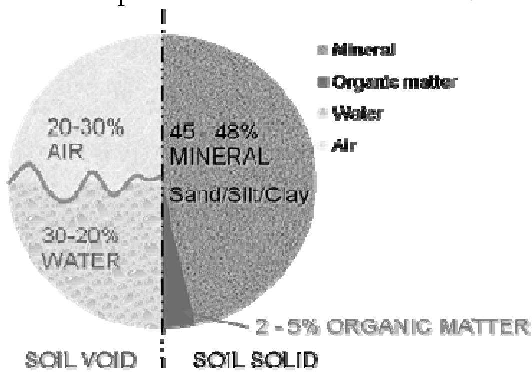

Fig. 1 Soil Constituents

The zone between field capacity, if the land is well drained, and saturation is an ideal area to temporarily store water in cases of excess rainfall which can then prevent surface runoff and flooding (Godwin, Dresser, 2003).

The series of photographs in Fig. 3 show the flow of water, over an 8 minute period, into the soil in two tanks of sand; on the left coarse sand overlying fine sand and on the right fine sand overlying coarse sand. It can be readily seen that the water moves readily from the coarse sand into the fine but not in the reverse case until a crack appears after 8 minutes of infiltration.

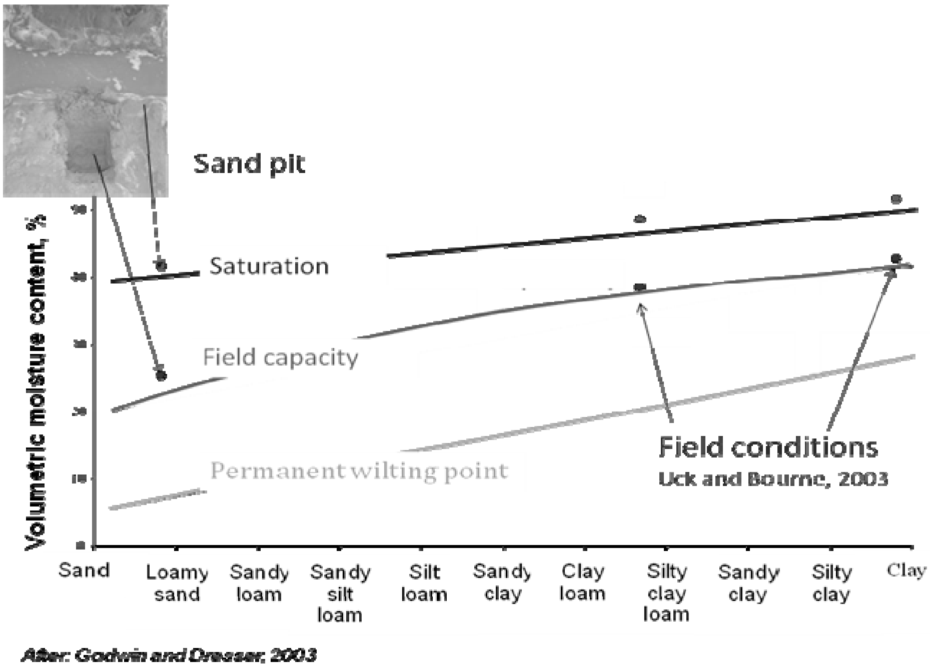

Fig. 2 Perched water tables and storage capacity (Godwin, Dresser, 2003)

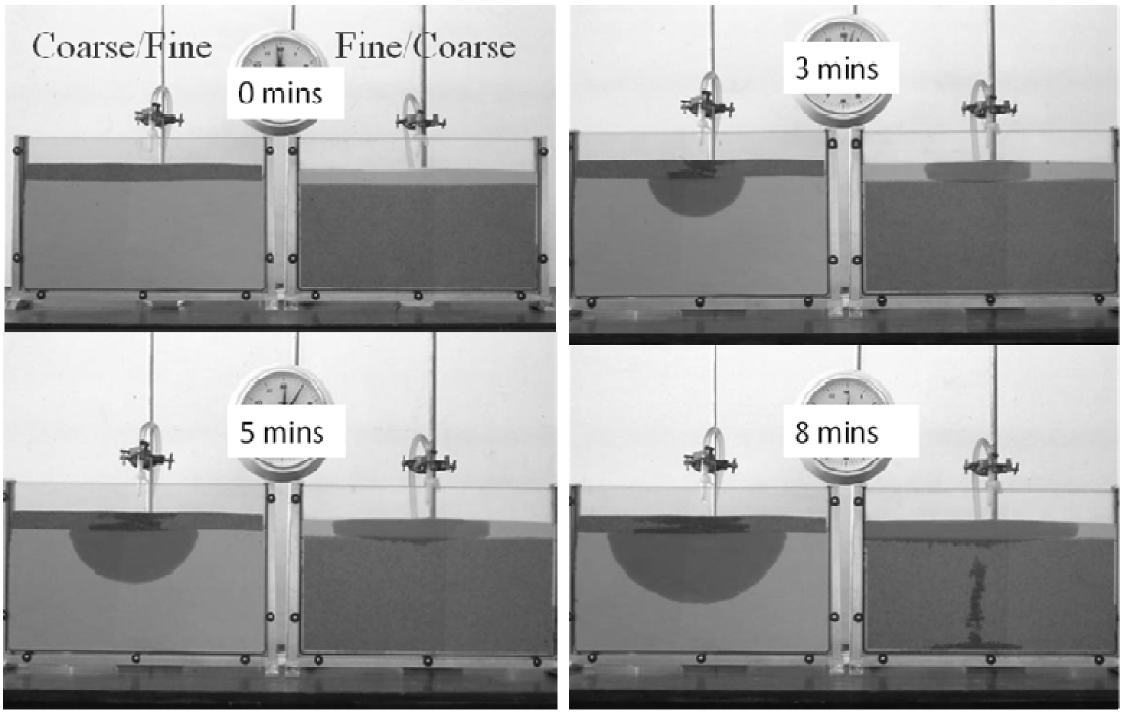

Fig. 3 Infiltration of water over time into 2 tanks of sand: coarse/fine left, and fine/coarse right

Infiltration rate is influence by both soil texture (where sand>loam>clay) and surface cover as shown in Fig. 4. The rate reduces with time as surface damage occurs and soil pores become saturated, runoff starts to occur when the rainfall rate exceeds the infiltration rate. Fig. 4 demonstrates clearly that soils with a permanent pasture or heavy mulch have infiltration rates very much greater than clean tilled and bare soils. Fig. 5 shows how the number of wheel passes effects the infiltration rate, where any number above a single pass reduces the infiltration rate to <1mm/hr.

Not only does the numbers of passes reduce infiltration rate but it also increases soil bulk density from 1.42 g/cc to 1.62 g/cc which can have a dramatic effect on crop yields, as shown in Fig. 6. This shows that an increase in soil density can cause a significant reduction on maize silage yield.

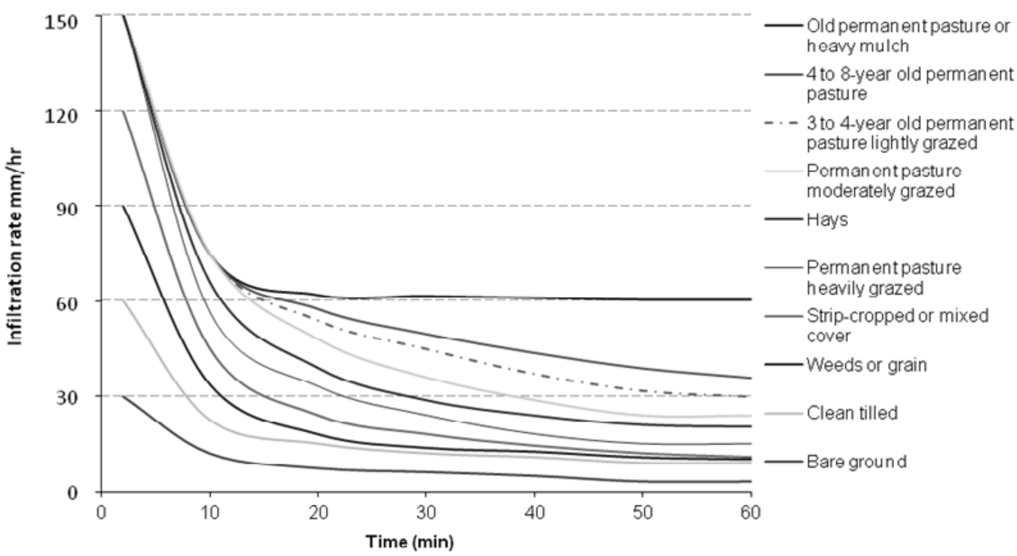

Fig. 4 Effect of time and surface condition on infiltration rate. (Differentiated from data in Holtan and Kirkpatrick, 1950)

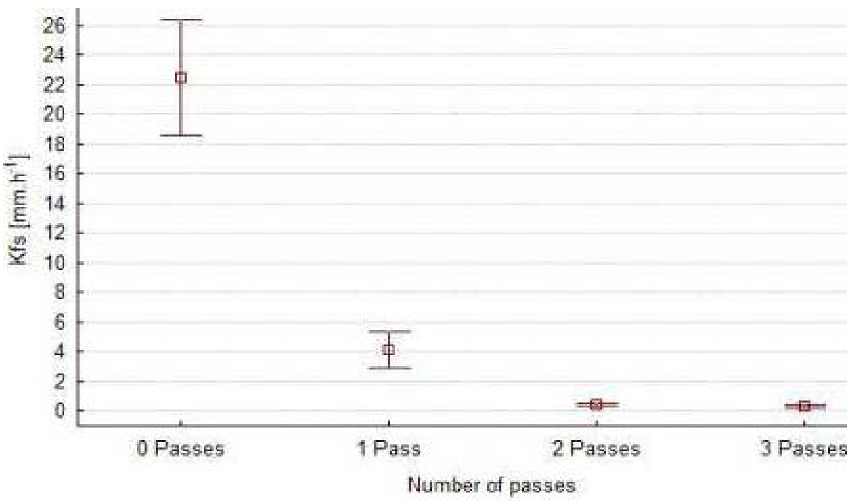

Fig. 5 Effect of number of wheel passes on infiltration rate (Chyba, 2012)

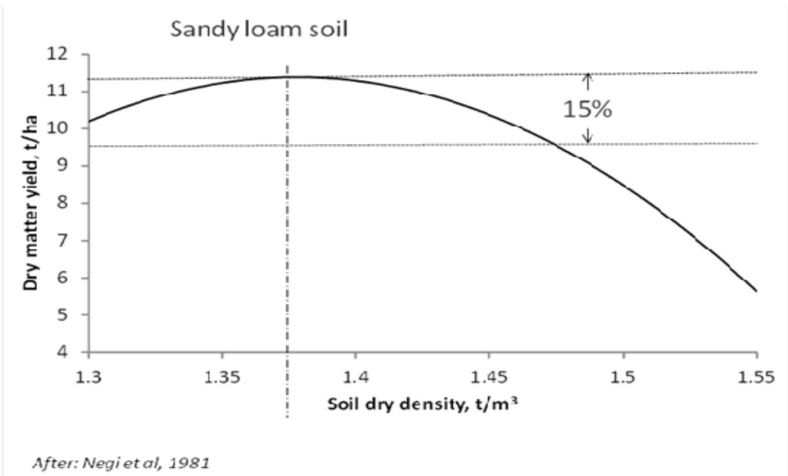

Fig. 6 Relationship between soil bulk density and maize silage yield (Negi et al., 1981)

Current problems

The adverse weather conditions in 2012 have lead to either localised water logging or over complete fields preventing crop establishment or restricted development. A summary of the effects of water logging (where the soil profile is saturated) on the yield of winter wheat is given in Tab. 1 from data given in Belford et al. (1981). The effect of this, whilst very serious, does not result in total crop failure proving that a crop has been established. The problem in many parts of the UK was that soil conditions did not allow crop establishment and farmers and land managers have been asking what can they do to "repair the damage" for the following seasons. Many fields had water "ponded" on the soil surface, often at the headlands and close to old established drainage ditches that have not been maintained for 30 – 40 years.

Tab. 1 Effect of water logging on winter wheat yield (Belford et. al., 1981).

1. For all treatments, grain losses were much less than expected from the extent of tiller loss in winter.
2. Losses after single water logging events ranged from 2 % (after 47 days) to 16 % (after 80 days with the water-table at the soil surface).
3. Yield losses after three water loggings at the seedling, tillering and stem elongation stages of growth were additive, and totalled 19 %.
4. In many treatments, grain loss was associated with lighter individual grain weights, suggesting that the size of the root system or efficiency of water and nutrient uptake by roots at the later stages of growth may have been less after earlier water logging.
5. The importance of nitrogen fertilizer in maintaining a satisfactory plant nitrogen status was shown as vital.

Generally good drainage will improve crop yield even in less sever climatic conditions as was shown by data from FDEU (1975) at Drayton where the yield of winter wheat improved from 4.5 t/ha by 1.0 t/ha from drainage with mole drains and 0.6 t/ha with drains and subsoil loosening. Positive yield responses were also recorded at Brooksby by 0.5 t/ha from the addition of mole drains. Good drainage is also critical for trafficability as can be seen from Fig. 7, as the depth of the water table has a very significant effect on soil strength. The effect was illustrated in the summer of 2007 when 40 % of the pea harvest in certain areas in the UK was lost due to the 25 t pea harvesting equipment becoming stuck in the fields.

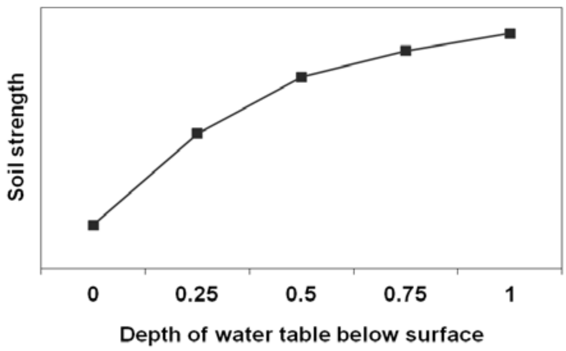

Fig. 7 Effect of depth of water table on soil strength

Advice on repairing the damage

The best advice that can be given to farmers for the short, medium and long term repair of the problems is given in Tab. 2. Much of this is not "new" information, just good soil and water management practices that may have been forgotten, never learnt, skipped a generation and not now supported by an "extension service", as described in Godwin et al., (2008).

Tab. 2 Action points for repairing the damage in the short/medium/long term

<u>Short Term</u>

1. Study "old" drainage plans
2. Walk ditch drains
3. Check that tile drains, plastic pipes mole drains are working
4. Clean blocked ditch and open drains
5. Flush pipe drains
6. Ensure that outfall lateral drains are working
7. Install "short life" mole drains if appropriate to remove excess water
8. Broadcast seed to establish a crop to remove surplus water by evapo-transpiration
9. Map damaged areas for repair when conditions permit

<u>Medium Term</u>

1. Mole drain clay soils with perched water tables to connect with gravel backfill on top of field drains
2. Loosen compacted top and sub-soils after the next harvest

<u>Long Term</u>

1. Install pipe/ditch drains
2. Mole drain clay soils with perched water tables to connect with gravel backfill on top of field drains
3. Consider "grass waterways" for open field ditch drains and erosion prevention
4. Grade/fill low spots

5. Improve arterial drains
6. Reduce surface compaction by reducing traffic intensity (consider Controlled Traffic and or Lower Pressure Farming practices)
7. Improve soil organic matter content.

Fig. 8, shows that the "natural" system drainage system, picking up on the serious "wet spots" in the field may have economic advantages over "regular" and "herringbone" systems, also remember to consider intercepting any runoff from other parts of the catchment that may cause flooding on key fields.

Reducing the intensity of wheel traffic by either controlled traffic or lower pressure footprints from lower pressure tyres and or rubber belted tracks could make a significant improvement. The data from Kroulik et al., (2011) in Fig. 9 shows that up to 85 % of a field growing winter wheat can be covered in wheel marks with conventional plough based system, this reduces to 65 % and 45 % for minimum tillage and direct drilling respectively. Table 6 summarises the potential benefits from controlled traffic where the wheel tracks of all vehicles follow common (or near common) predetermined pathways. Whilst this is a simple concept and is greatly assisted by GPS assisted steering and guidance there are a number of technical issues to be resolved concerning machine and track widths (usually with the combine harvester) but also the issues with matching narrower tractor track widths with that of the combine.

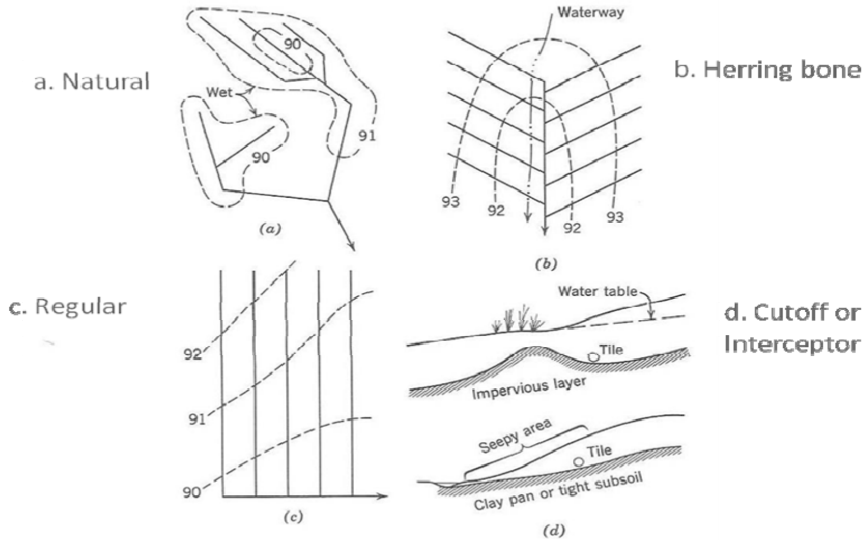

Fig. 8 Alternative drainage designs (Schwab et al., 1993)

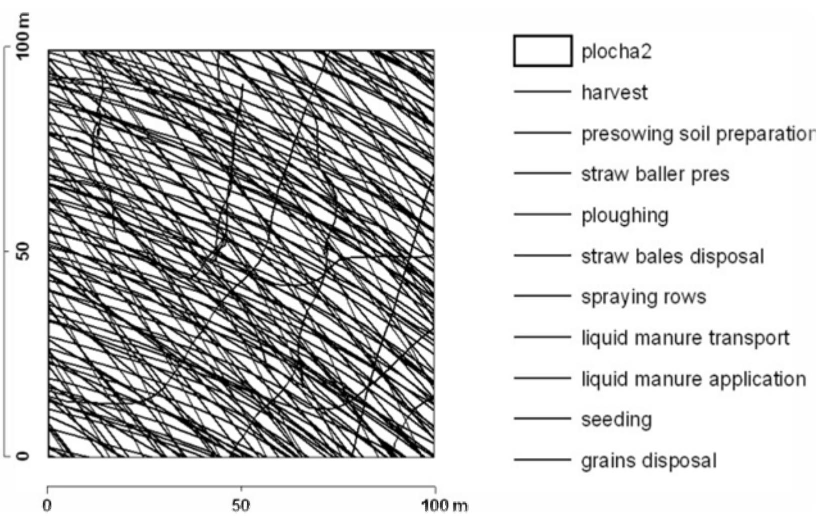

Fig. 9 Random traffic patterns in Czech Republic during wheat production (Kroulik et al., 2011)

An alternative approach is to replace the high inflation pressure tyres with those with lower pressure (Ultraflex or Axiobib tyres) or rubber belted tracks. This is a simpler solution and is relatively cheap (some of the cost of which is recovered by improved fuel economy (Michelin, 2012), trafficability and manoeuvrability. The negative aspect however is that some pressure is still applied to the soil – albeit much reduced from the more conventional tyre (MachXbib) as shown by Smith et al (2013) in Fig. 10. The estimated costs for the Ultraflex (Axiobib) tyres are Euro 1.20/ha for 280 hp tractor and Euro 0.60/ha for a combine (Mozziconacci, (Michelin), 2012) and Euro 4 to 5/ha for the rubber tacks for a combine (Tyrell (Claas), 2012 and Blessley (CaseIH), 2013). The paper by Ansorge and Godwin (2007) demonstrates the benefit of rubber belted tracks over conventional tyres in detailed laboratory studies for large combine harvesters together with the 63 % reduction in tillage energy needed to repair any compaction.

A study at Harper Adams University (Smith et al., 2013) is currently investigating the effects of both controlled traffic and lower ground pressure farming systems compared to regular field traffic and their interaction with tillage system (deep (250 mm), shallow (100 mm) and direct drilling) on soil properties and crop growth.

If subsoil compaction has been caused then attention should be paid to mechanically alleviating the damage, the recommendations given by Spoor and Godwin (1978) give a guide to the farmer on the most appropriate design of equipment using either:- “winged tines”, with their reduced specific resistance (draught force/area of soil disturbed) as shown in Fig. 11, or “winged tines with shallow leading tines” which give a further 45% reduction in specific resistance but are less readily available commercially. The concept of the ideal tine spacing is shown in Fig. 11 for simple tines and the optimum for friable/hard soil conditions is given in Tab. 7 for the three alternative tine configurations. Remember not to compact the freshly loosened soil.

Tab. 6 Perceived benefits of controlled traffic farming systems
(Chamen, 2011 & Proceedings of the 1st International Conference on Controlled Traffic Farming, 2013, Toowoomba, Queensland)

Reduces compaction – may reduce area trafficked to as little as 10 %
Improved yields – in the range 9 -16 %
Possibly double cropping
Improved rainfall utilisation
Reduced runoff and flooding – infiltration rate increased by 400 %
Reduced erosion
CTF and minimum tillage/direct drilling are natural bed fellows
Reduced machine costs, fuel use and tillage costs – by 22 %

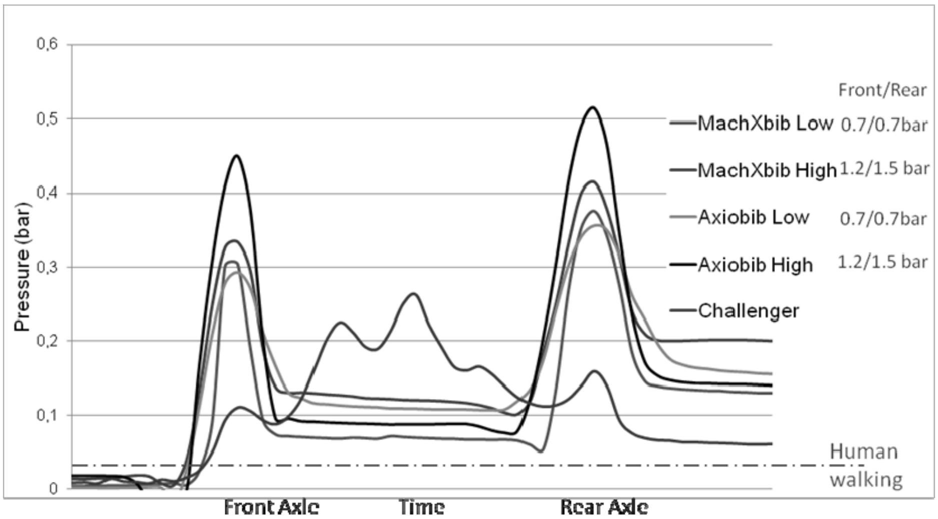

Fig. 10 Soil pressures at 30cm below the soil surface of high and low tyre inflation pressure tyres (MachXbib and Axiobib) fitted to a 12t 4WD tractor compared to a 16t rubber tracked Challenger tractor. The pressure of a human walking is also shown. (Smith et al., 2013)

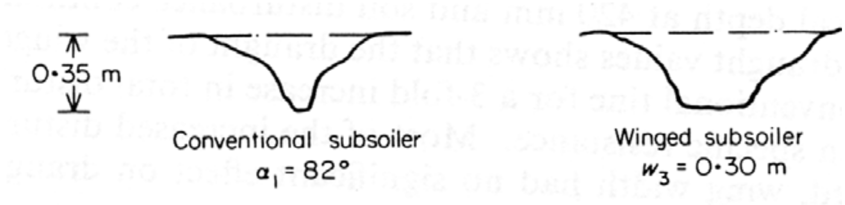

Draught force	20.43 kN	26.58 kN
Disturbed area	0.098 m^2	0.0184 m^2
Specific Resistance	208 kN/m^2	144 kN/m^2

Fig. 11 The effect of wings on soil disturbance, draught force and specific resistance. (Spoor, Godwin, 1978)

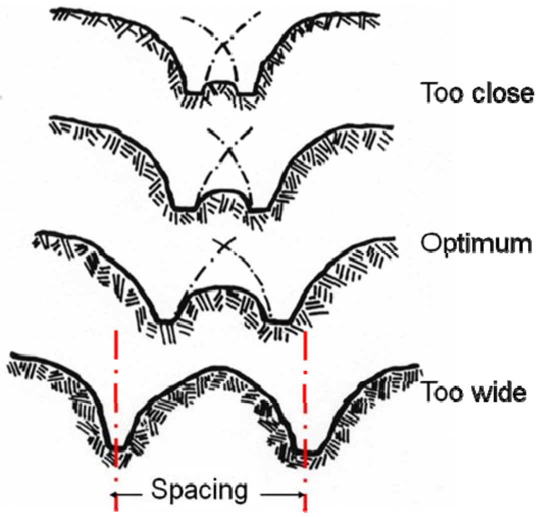

After: Godwin, Spoor and Soomro, 1984

Fig. 11 The effects of simple tine spacing on soil disturbance. (Godwin et al., 1984)

Tab. 7 Tine spacing (Spoor, Godwin, 1978)

Simple tine	-	1.5 x depth of work
Winged tine	-	2.0 x depth of work
Winged tines + shallow leading tines	-	2.5 x depth of work of deep tine

Concluding remarks

1. Improved soil and water management is achieved by:

a. Reducing traffic intensity & contact pressure

b. Checking, maintaining and improving drainage infrastructure

c. Considering the short, medium and longer term actions listed above

d. Minimise compaction and repair the damage if required.

2. Remember prevention is better than cure.
3. Water does not flow from small to large pores.
4. Regular inspections of drainage systems are needed.
5. Restoration of an existing system is generally cheaper and quicker than the installation of a new system.
6. Remember "Man has only a thin layer of soil between him and starvation" (*Anonymous*)

References

Ansorge D., Godwin R.J., 2007. The effect of tyres and a rubber track at high axle loads on soil compaction, Part 1: Single axle-studies. Biosystems Engineering, 98(1).

Belford R.K., 1981. Response of winter wheat to prolonged water logging under outdoor conditions, Journal of Agricultural Science, 97: 557-568.

Blessley C., 2013. Farmers Weekly Seminar, Cereals Event.

Chamen W.C.T. The effects of low and controlled traffic systems on soil physical properties, yields and the profitability of cereal crops on a range of soil types. PhD Thesis, Cranfield University, Bedfordshire, UK

Chyba J., 2012. The influence of traffic intensity and soil texture on soil water infiltration rate. MSc Thesis Harper Adams University College, Shropshire, UK.

Godwin R.J., Spoor G., Soomro M.S., 1984. The effect of tine arrangement on soil forces and disturbance. Journal of Agricultural Engineering Research, 29: 47-56.

Godwin R.J., Dresser M.L., 2003. Review of soil management techniques for water retention and minimising diffuse water pollution in the River Parrett Catchment. R & D Technical Report P2-261/10/TR. Environment Agency. ISBN 1844321460

Godwin R.J., Spoor G., Finney J.B., Hann M.J., Davies B.D., 2008. The current status of soil and water management in England. RASE, Stoneleigh, Warwickshire.

Kroulik M., Kviz Z., Masek J., Misiewicz P., 2011. Benefits of GPS agricultural guidance for sustainable agriculture. 19th International Soil Tillage Research Organisation Conference, Uruguay.

Mozziconacci L., 2012. Personal Communication, Michelin.

Negi S.C., McKyes E., Raghavan G.S.V., Taylor F., 1981. Relationships of field traffic and tillage to corn yields and soil properties. Journal of Terramechanics, 18(2): 81-90.

Holtan N.H., Kirkpatrick M.H., 1950. Rainfall, infiltration and hydraulics of flow in runoff computation. Transactions of the American Geophysical Union, 31: 771-779.

Schwab G.O., Fangmeier D.D., Elliot W.J., Frevert R.K., 1992. Soil and Water Conservation Engineering, 4th Edition, J. Wiley & Sons, New York.

Spoor G., Godwin R.J., 1978. Experimental Investigation into the Deep Loosening of Soil by Rigid Tines. Journal of Agricultural Engineering Research, 23(3): 243-258.

Smith E., Misiewicz P.A., White D.J., Chaney K., Godwin R.J., 2013. Effect of traffic and tillage on soil properties and crop yield. Paper No 1597846, ASABE International Meeting, Kansas City.

Tyrell T., 2012. Personal Communication, Claas UK.

EXPERIMENTAL STUDIES AND MODELING OF GRAIN SILO LOADS

Józef Horabik[1*], Marek Molenda[1], Montross[2] M.D., Ross[2] I.J., Rafał Kobyłka[1]

[1]Institute of Agrophysics Polish Academy of Sciences, 20-290 Lublin, Poland
Phone: +48 81 74 450 61, Fax: +48 81 74 450 67, E-mail: j.horabik@ipan.lublin.pl
[2]Dept. of Biosystems and Agric. Engng, University of Kentucky, Lexington, KY 40546-0276

Abstract

Experimental studies and DEM simulations of load in a grain silo were presented and discussed in the paper. Experiments were performed on model silos of 0.6, 1.2 and 2.4 m in diameter. The vertical wall and bottom loads and moments of force exerted on the wall and the floor were analysed during centric and off-center filling and discharge. It was shown that off-center filling of the silo produced a preferred orientation of in nonspherical grain that resulted in asymmetry of silo wall loads as well as in anisotropic airflow resistance within the bulk grain.

Keywords: DEM simulations, grain silo, grain, storage

Introduction

Storage, handling and processing of granular materials are employed in numerous industries and are of interest to various branches of science and technology such as physics, chemistry, mechanics, agriculture and engineering. Agriculture and the food industry are, next to chemical, power, and pharmaceutical industries the largest producers and users of granular materials. Two basic conditions have to be fulfilled for equipment used for storage and processing of granular materials: predictable and safe operations and obtaining high quality finished products.

Since the pioneering work of Janssen (1895), numerous experimental and numerical research studies have been conducted to determine static and dynamic pressures and flow regimes in silos (Holst et al., 1999; Jenike, 1964; Roberts, Wensrich, 2002). Initiation of discharge of granular solids from silos lead to dramatic stress redistributions which result in silo wall pressure ramps, and the majority of silo failures take place at the onset of discharge. One symptom of unstable behaviour is the localized shear zones in the interior of the granular material (Wójcik, Tejchman, 2009). Eccentric discharge has been shown to create very strong load asymmetry and these studies have led to recommendations for silo design codes (Borcz, Abd, 1991; Eurocode 1, 2003; Guaita et al., 2003; Łapko, 2010).

At the same time granular material models were intensively developed providing constitutive laws of material (Drucker, Prager, 1952; Mühlhaus, Vardoulakis, 1987). However, the effects of the microstructure within the material was not considered in most of continuum mechanics models. Distinct Element Method (DEM) has provided new possibilities for deeper insight into the micro-scale behaviour of bulk solids, which are not available with traditional continuum mechanics (Cundal, Strack, 1979). DEM simulations can provide good agreement with experimental data if the proper material parameters are determined (Anand et al., 2009; Kuwabara, Kono, 1987; Thornton, Ning, 1998).

Granular materials of biological origin constitute a class of materials distinguished by large deformability of particles and strong dependence of their mechanical properties on moisture content. Contrary to materials of mineral origin, moisture penetrates inside grain, leading in some cases to qualitative changes in physical properties. These differences bring about certain peculiar behaviours and the necessity of adjustments to material models, experimental techniques and technological solutions. The most important is that stored grain is a respiring biological material subjected to microbiological activity. For high-quality preservation during storage, a multidisciplinary approach applying knowledge from several fields: biology, chemistry, toxicology, engineering and mathematical modeling to the study of the complex interactions among physical, chemical and biological variables in stored-grain ecosystem is necessary (Jian, Jayas, 2012).

This paper presents a review of experimental studies of loads in model silos of different scales selected from several research projects performed by the authors. Special attention was paid to the effects typically found in cereal grain. These include, deposition of cutin on frictional forces, impact of anisotropy, elasticity and swelling of grain on silo loads. Some of these effects were modeled with DEM and compared with corresponding experimental tests.

Experimental setup

Experiments on model silos have been conducted in the Granular Mechanics Laboratory of the Department of Biosystems and Agricultural Engineering at the University of Kentucky, USA on silos of diameters 0.6, 1.2 and 2.4 m and in the Institute of Agrophysics PAS on a silo with a diameter of 0.4 m. The majority of tests were performed on smooth and corrugated-walled model silos 2.4 m in diameter and 7.3 m high. The wall and floor of the silo were each supported independently on three load cells to isolate the wall and floor loads (Fig. 1b). Such an experimental configuration allowed for determination of vertical wall and floor loads (F_z), and of the resultant moment (M) exerted by grain on the wall and floor of the silo (Horabik et al., 1992):

$$F_z = F_1 + F_2 + F_3$$

$$M = \left| \sqrt{M_x^2 + M_y^2} \right|$$

$$M_x = R(F_1 \sin\alpha_1 + F_2 \sin\alpha_2 + F_3 \sin\alpha_3)$$

$$M_y = R(F_1 \cos\alpha_1 + F_2 \cos\alpha_2 + F_3 \cos\alpha_3)$$

Moment of force served as a global measure of the asymmetry of pressure distribution (Fig. 1c). The silos were filled to a height to diameter ratio (H/D) of about 2.75. The wall loads were compared for centric or eccentric filling and centric or eccentric unloading of smooth and corrugated-walled bins (Fig. 1a). Tests were performed using soft red winter wheat.

Silo loads

Investigations on a smooth-walled model silo filled with wheat showed wear-in effect that resulted in a 70 % decrease in the wall coefficient of friction. The comparison presented in Fig. 3 shows that experimental values of loads are in good agreement of experimental results from four bins of diameter in a range from 0.4 to 4.1 m with theoretical estimation by Janssen‘s equation applying measured values of pressure ratio and coefficient of wall friction (Molenda et al., 1995, 1996).

During prolonged sliding, like movement along a silo wall during discharge, cutin a wax-like substance from the grain seed coat accumulates on the smooth contact surface. Cutin acts as a lubricant, that smoothes the contact surface and changes its frictional properties. Although determination of the exact value of the angle of wall friction in the initial period of frictional contact is difficult to accurately determine, although a three-fold reduction in the angle of friction (Fig. 2) was observed (Molenda et al., 1996).

Relatively low modulus of elasticity has been observed in grain (about 20 MPa)(Horabik, Molenda, 2005), that can influence the pressure distribution in a bin. It was observed that during the final stage of discharge, as the ratio of the grain height to the bin diameter decreased below approximately 1, the total friction force of grain on the bin wall changed its direction from a downward direction to an upward direction (Horabik et al., 1992). The elastic recovery of grain in the dead zone of the bin caused by decrease in the grain column height from the discharging grain resulted in the upward movement of grain in the dead zone and in the upward friction force on the wall.

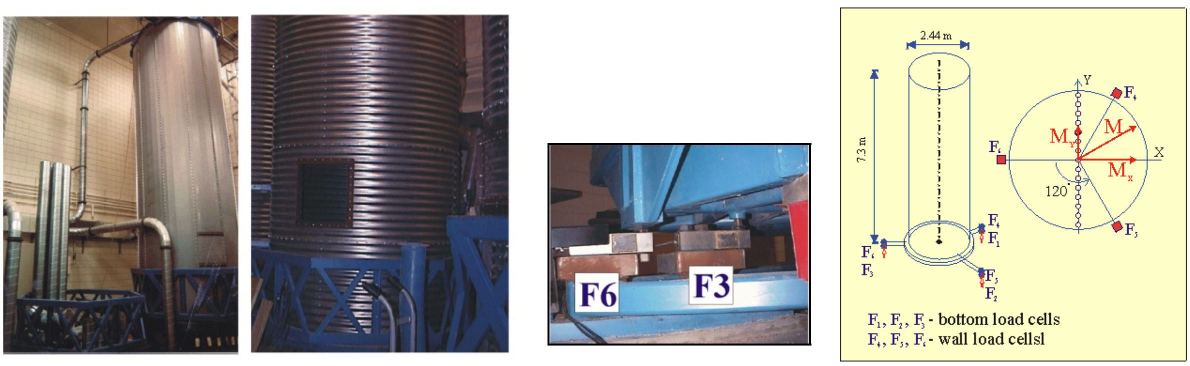

Fig. 1 Experimental silos, detail of load cells locations and schematic diagram

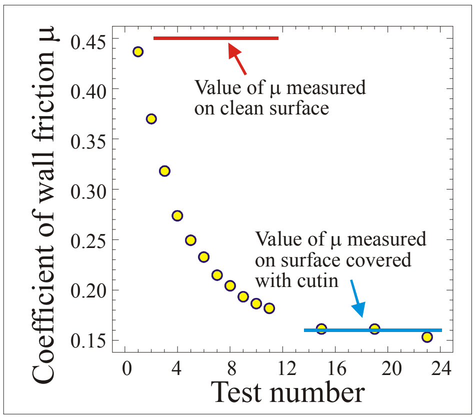

Fig. 2 Wall friction coefficient as influenced by silo discharge number (Molenda et al., 1996)

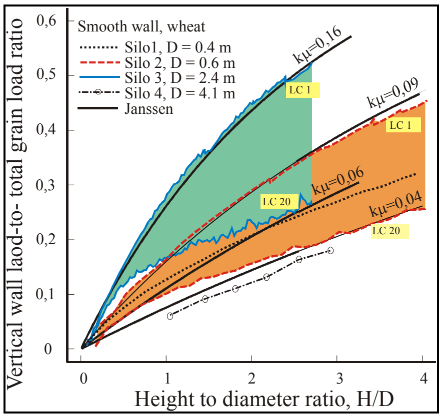

Fig. 3 Range of variability of the vertical wall loads in different model silos (Molenda et al., 1995)

DEM simulations generally produce a huge scatter of inter-particle forces which after averaging provide useful information. An example of the horizontal forces acting on a vertical wall in quasi-static assemblies (6000 particles in two dimensions) is presented in Fig. 4a. Analysis of the distribution of horizontal forces averaged for 10 particle–wall contacts (Fig. 4b) indicated a moderately smooth increase in the force with increase in particle bedding depth (Sykut et al., 2008). The DEM values are considerably larger as compared to Janssen (1895) solution. Similarly Balevičius et al. (2011) obtained good agreement of lateral pressure distribution vs. material depth with experimental data which were significantly larger then Janssen (1895) solution and Eurocode 1 (2003) recommendations. González-Montellano et al. (2012) obtained the pressure distribution of pressure in particles similar to maize grains along the vertical direction of the wall reaching its maximum at the silo-hopper transition using DEM. Masson and Martinez (2000) reported on the impact of anisotropy of contact orientations on the pressure distribution.

Asymmetry of loads

Eccentric discharge of the silo generates strong load asymmetry (Eurocode 1; Fig. 5). As suggested by silo users, such load asymmetry may lead to ovalization of the wall or create particularly high loads that may lead to silo failure. The moment of force exerted on the wall was determined for smooth and corrugated wall model bin with a diameter 2.4 m (Fig. 6). The moment was found to be the highest for the discharge orifice located at half the radius of the silo floor. Smoother silo wall resulted in larger asymmetry of load distribution (Molenda et al., 2001).

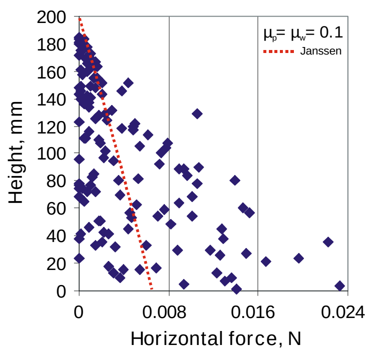

Fig. 4a Scater of wall horizontal force

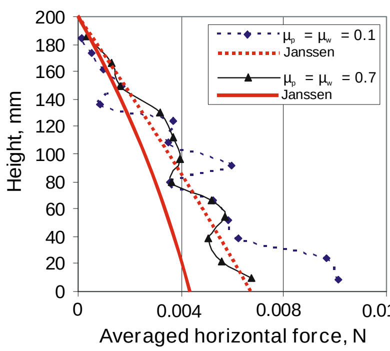

Fig. 4b Wall horizontal force averaged for 10 particle–wall contacts compared to Janssen solution

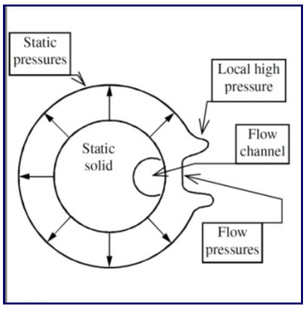

Fig. 5 Pressure distribution during off-center discharge according to Eurocode 1 (2003)

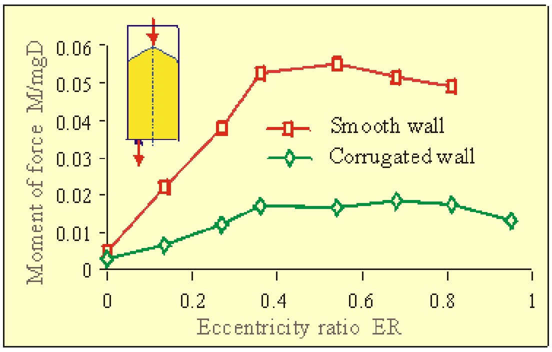

Fig. 6 Nondimensional moment of force exerted on the smoot and corrugated silo wall as a function of the orfice eccentricity ratio (Molenda et al., 2001)

Non-axial filling of the silo was also found to produce asymmetric load distribution. This asymmetry is a result of anisotropy of the bedding of granular material produced by grains rolling along the surface of the cone of natural repose. The potential for eccentric filling to decrease load asymmetry during eccentric discharge was investigated by Molenda et al. (2002). Line A on Fig. 7 represented the resultant moment of force exerted by grain on the silo wall during discharge when filling and discharge gates were located on the same side of the silo. Load asymmetry increased momentarily after opening the discharge gate. Line B represented the wall moment versus time relationship for the test when the filling chute and the discharge gate was located on the opposite sides. For this condition, load asymmetry decreased at the onset of discharge (Molenda et al., 2007).

To explain a role of off-center filling in reduction or increase of resultant moment of force the anisotropy of bulk of grain should be considered. When the long axes of nonspherical grains are oriented along certain directions, the bedding showed anisotropic properties. In the case of wheat, the length of grain is approximately twice its width. Slow rolling of wheat grains along the cone of natural repose is an easy way to observe an example of formation of anisotropic bedding. Determination of the angle of internal friction with a triaxial shear test and a direct shear test have shown (Fig. 8) that the angle of internal friction increased with an increase in the angle between direction of preferred orientation of grains and the direction of sliding (Horabik, Molenda, 2005). Horabik et al. (1988) indicated that anisotropy of bedding resulting from preferred spatial orientation of grains created during off-center filling results in significant silo loads asymmetry during discharge.

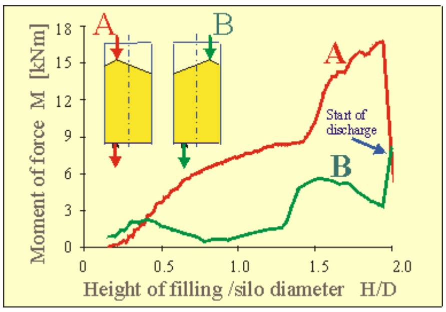

Fig. 7 Moment of force exerted on silo wall for off-center filling and discharge: filling and discharge on the same side (A) and on the opposite sides (B) (Molenda et al., 2002)

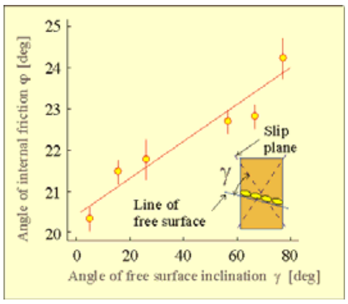

Fig. 8 Angle of internal friction as a function of the inclination angle of slip plane in the triaxial compression test to the preferred orientaion of grains (Horabik, Molenda, 2005)

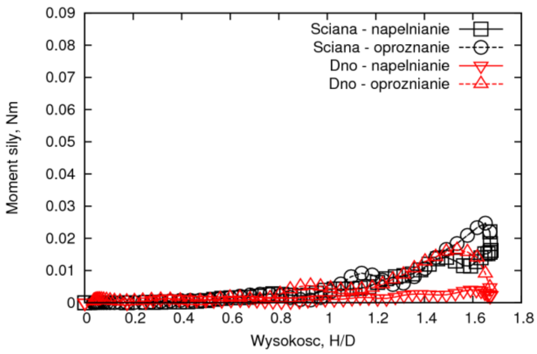

Fig. 9a Moment of force exerted on wall and bottom of the model silo during centric filling and discharge (Kobyłka, Molenda, 2013)

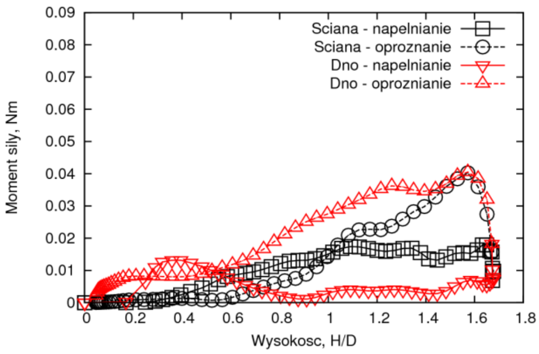

Fig. 9b Moment of force exerted on wall and bottom of the model silo during off-center filling and centric discharge (Kobyłka, Molenda, 2013)

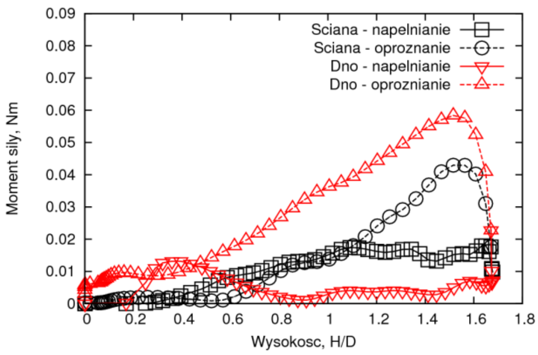

Fig. 9c Moment of force exerted on wall and bottom of the model silo during off-center discharge (Kobyłka, Molenda, 2013)

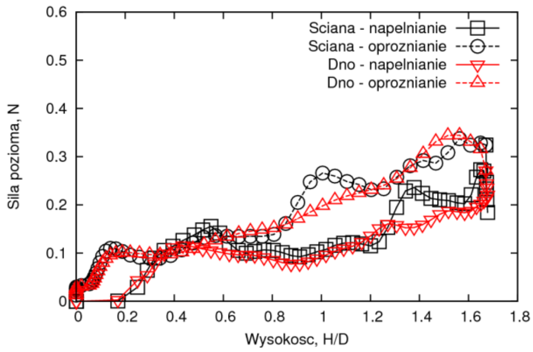

Fig. 9d Resultant lateral force exerted on wall and bottom of the model silo during off-center discharge (Kobyłka, Molenda, 2013)

The DEM modeling of off-center filling and discharge of a model silo 24 times smaller than experimental one provided similar results to experimental findings. Simulations performed for 30 000 particles in a model silo of 10 cm in diameter indicated some minor asymmetry of loads during centric filling and discharge (Fig. 9a), which increased for off-center filling (Fig. 9b) and off-center discharge (Fig. 9c). Resultant lateral force (Fig. 9d) exerted on the wall and the bottom corresponded to a resultant moment of force (Kobyłka, Molenda, 2013).

To model properly dynamics of discharge, like a rapid, thin ouflow of particles, the contact model for DEM simulations must be selected very carefuly as cereal grains reveal different behaviour depending on moisture content (Wiącek, Molenda, 2011). The mechanical properties of grains are strongly influenced by the moisture content which plays a role similar to that of temperature for thermoplastics and metals. Wojtkowski et al. (2010) found that an elastoplastic model (Thornton, Ning, 1998) was efficient for simulation of the behavior of dry rapeseed while a viscoelastic model of Kuwabara and Kono (1987) gave closer estimates of experimental data for wet seeds. Parafiniuk et al. (2013) used both models to simulate discharge of dry and wet rapeseeds from a model silo obtaining good agreement with experimental results. In case of wet cohesive grains the adhesion forces should be considered, like for example a liquid bridge force (Anand et al., 2009).

Swelling pressure

The uncontrolled increase of moisture content may take place in stored grain due to grain respiration or as a result of wetting with ambient air during aeration. Increased grain moisture content leads to an increase in volume. Walls of the silo confine deformation of the grain in the horizontal direction that may lead to an increased lateral pressure (Blight, 1986; Britton et al., 1993; Dale, Robinson, 1954). A theoretical model was developed to estimate the relationship between increased moisture content and increased lateral pressure (Zhang, Britton, 1995). The model was based on the assumption that an increase in grain volume was equal to the volume of absorbed water (Fig. 10). In the next step of the approximation, a decrease in grain elasticity due to moisture content increase was taken into account (Horabik, Molenda, 2000). When kernels swell the contact forces increased. At the same time the modulus of elasticity decreased. As a consequence, the pressure reached its maximum value and then decreased.

Resultant volumetric strain, ε_v, is a sum of two independent components: strain generated by external pressure, ε_c, and strain resulting from grain swelling, ε_u. The model adequately predicted the upper limit of pressure increase reached under a condition of high initial compaction of material when the moisture content increase was below 2 %.

Experimental data for the examination of pressure increase caused by water absorption consisted of a model silo (0.61 m in diameter and 0.75 m high) with instrumentation to determine the radial distribution of vertical pressure on the floor and top cover of the silo, and the mean lateral pressure (Fig. 11). The set up was equipped to generate, dose and apply moist air to the grain contained in the model silo (Horabik, Molenda, 2000).

Radial distributions of normal pressure σ_v on the floor of the model silo are shown in the Fig. 12 for several values of increased water content. Pressure increase was found to be highest at the center of the floor and decreased towards the wall due to a decrease in rate of water adsorption along the path of air movement. The rate of mean lateral pressure σ_n increase was found to be 125 kPa/kg/kg (Fig. 13).

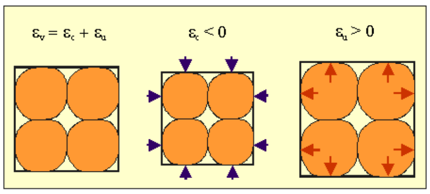

Fig. 10 Volumetric strain ε_v resulting from compaction by confining pressure ε_c and swelling of kernels ε_u

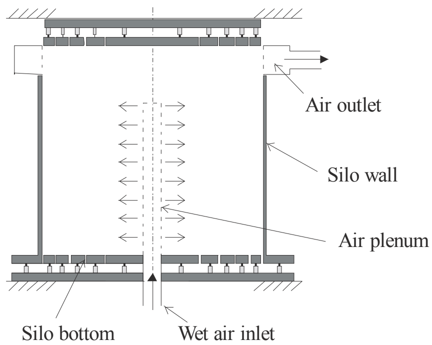

Fig. 11 Model silo with wetting equipment

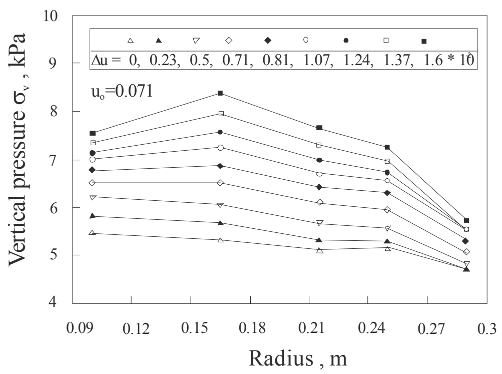

Fig. 12 Radial distribution of vertical pressure σ_V on the silo bottom as influenced by the moisture content increase

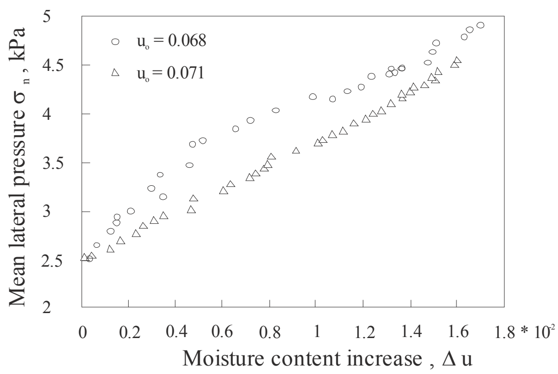

Fig. 13 Mean lateral pressure σ_n on the silo wall as influenced by the moisture content increase

It was found that effective bulk modulus of grain expressed as a power function of confining pressure according to Walton (1987) reflected real compression conditions between kernels. The model properly described the swelling pressure when the moisture content increased up to 2 %.

Airflow resistance in bulk of grain

Knowledge of airflow patterns within a grain bin is crucial factor for the efficient and safe use of a number of technologies such as air movement through a bin for aeration, chilling, fogging, fumigation, modified atmospheres or drying. Usually for design purposes, homogeneity and isotropy of the grain bulk have been assumed to simplify the design process. Experimental studies have indicated that airflow resistance depends on the airflow direction related to grain orientation (Molenda et al., 2005). Kumar and Muir (1986) found that for an airflow velocity of 0.077 $m.s^{-1}$ the pressure drop in the vertical direction was up to 60 % higher than in the horizontal direction for wheat and barley. Standard ASAE D272.3 (ASAE, 2007) recommends using a pressure drop in the horizontal direction of 60–70 % of that in the vertical direction. Łukaszuk et al. (2008) has shown that not only global porosity, but also the orientation of the pores were factors that caused variability in the pressure drop. They estimated the variation in the pressure drop in both the horizontal and vertical directions in a grain bulk due to the filling method (Łukaszuk et al., 2009). A study was conducted to estimate variability of airflow resistance of wheat caused by filling method and airflow direction. A grain chamber in the form of a cubic box with 0.35 m sides was used (Fig. 14 and Fig. 15). Airflow resistance along three perpendicular directions: two horizontal X and Y, and vertical direction Z was determined. In each wall of the cube circular openings 0.16 m in diameter were machined and covered with perforated steel. Each wall of the chamber was equipped with cylindrical air collectors (supply or outlet) 0.16 m in diameter and with four connectors for installation of pressure transducer. Pressure drop was measured at a distance of 0.25 m for airflow velocities in a range from 0.03 to 0.35 $m.s^{-1}$.

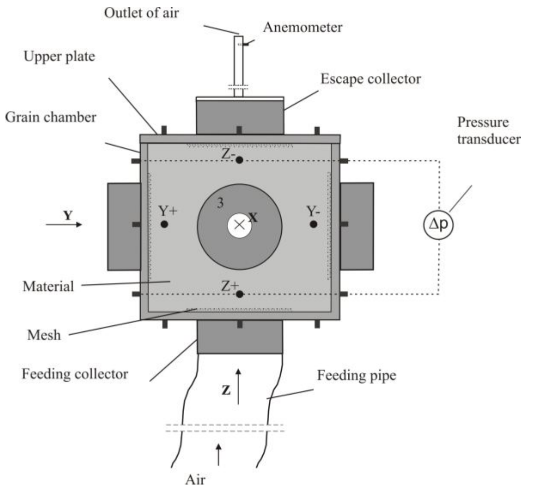

Fig. 14 Schematic of the apparatus for measuring airflow resistance in cubic sample of grain

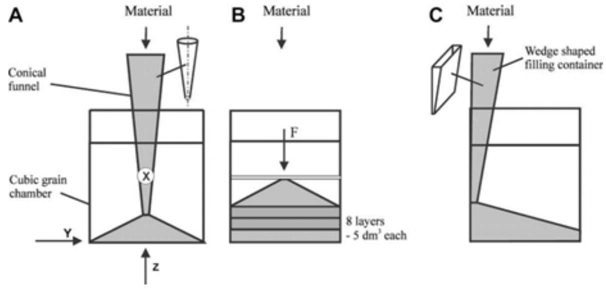

Fig. 15 Methods of filling the test chamber

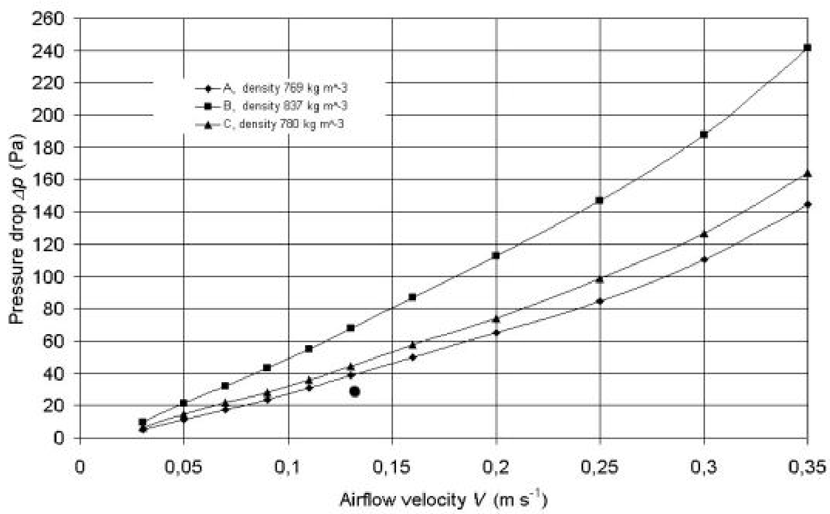

Fig. 16 Pressure drop Δp in bulk of wheat versus air velocity V in vertical direction Z for three filling methods (Łukaszuk et al., 2009)

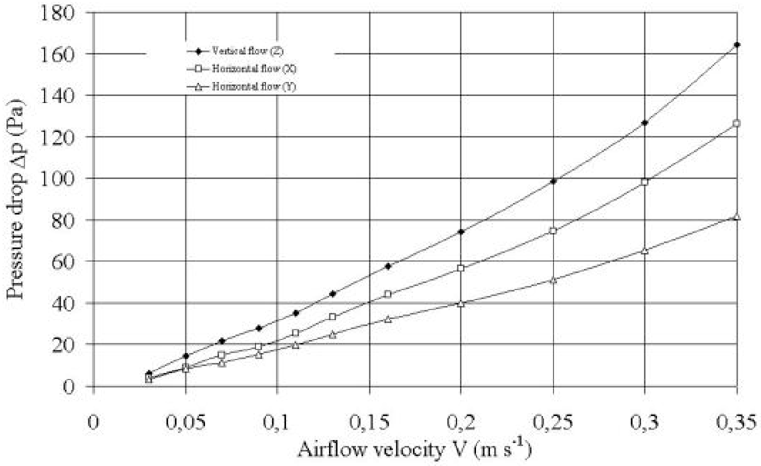

Fig. 17 Pressure drop Δp in bulk of wheat versus air velocity V for three airflow directions Z, X and Y for filling method C (Łukaszuk et al., 2009)

Fig. 16 illustrates relationships of pressure drop at a distance of 0.25 m versus airflow velocity in vertical direction Z of samples formed with three filling methods. Pressure drop increased with an increase in bulk density and airflow velocity. At an airflow velocity of 0.3 m.s^{-1} a pressure drop of 118.2 Pa was found for filling method A, while in the case of method B it was 1.65 times higher. In the case of filling method C, the lowest airflow resistance was in the Y direction and the highest in the Z direction (Fig. 17). Tests utilizing filling methods A and B in resulted in substantially different directional airflow resistances than filling method C. The pressure drop in the X direction was higher than the Y direction over the whole range of velocity. At an airflow velocity of 0.3 m.s^{-1} the pressure drop in the Y direction was 61.2 Pa, while in X direction it was 90.1 Pa, that is approximately 1.5 times higher. Method C, that used wedge shaped filling container, produced a grain sample that was not axially symmetric. Subsequent layers of grain were moving down the angle of repose of the conical surface.

Asymmetric filling (method C) resulted in substantial differences in the pressure drop between the X and Y directions. Along the X direction, parallel to the orientation of the kernels, as the kernels moved in the Y direction along the angle of repose, the pressure drop was higher than in the Y direction, but still lower than airflow in the vertical direction. At an airflow velocity of 0.3 ms^{-1}, the pressure drop in the X direction was 1.5 greater than the Y direction for wheat grain. Variations in pressure drop could be a significant factor in the design and operation of equipment in technologies utilizing flow of gases through the granular materials such as drying, aeration, cooling or fumigation.

Conclusions

Experimental research and DEM simulations of loads in grain silo confirmed a strong influence of material properties and filling and discharge method on the load distribution. Total vertical wall load decreased during the initial period of operation due to cut in deposition smoothed the contact surface. Swelling of grain due to moisture addition resulted in increased pressure that is another example of phenomena typical for biological materials that are not seen with other materials. Off-center discharge produced a strong asymmetry in wall loads. This asymmetry may be reduced or increased with off-center filling. Similar findings were obtained from DEM simulations, which proved to be a promising method for design of storage structures for granular materials. Airflow resistance of bulk of grain was found to be influenced by the preferred orientation of nonspherical grains.

References

Anand A., Curtis J.S., Wassgren C.S., Hancock B.C., Ketterhagen W.R., 2009. Predicting discharge dynamics of wet cohesive particles from a rectangular hopper using the discrete element method (DEM). Chemical Engineering Science, 64: 5268–5275.

ASAE, 2007. ASAE D272.3 MAR1996 (R2007). Resistance to airflow of grains, seeds, other agricultural products and perforated metal sheets. ASABE Standards 4: 627–633.

Balevičius R., Sielamowicz I., Mróz Z., Kačianauskas R., 2011. Investigation of wall

stress and outflow in a flat-bottomed bin: A comparison of the DEM model results with the experimental measurements. Powder Technology, 214: 322-336.
Blight G.E., 1986. Swelling pressure of wetted grain. Bulk Solids Handling, 6(6): 1135-1140.
Borcz A., Abd R.H., 1991. Wall pressure measurements in eccentrically discharged cement silos. Bulk Solids Handling, 11(2): 469-476.
Britton M.G., Zhang Q., McCullagh K., 1993. Moisture induced vertical loads in model grain bin. ASAE Paper No. 93-4503, St. Joseph, MI.
Cundall P.A., Strack O.D., 1979. A discrete element model for granular assemblies. Géotechnique, 29(1): 47-65.
Dale A.C., Robinson R.N., 1954. Pressure in deep grain storage structures. Agricultural Engineering, 35(8): 570-573.
Drucker D.C., Prager W., 1952. Soil mechanics and plastic analysis or limit design. Quarterly of Applied Mathematics, 10(2): 157-165.
Eurocode 1, 2003. Actions on structures. Part 4. Actions in silos and tanks. Ref. No EN 1991-4.
González-Montellano C., Gallego E., Ramírez-Gómez Á., Ayuga F., 2012. Three dimensional discrete element models for simulating the filling and emptying of silos: Analysis of numerical results. Computers and Chemical Engineering, 40: 22-32.
Guaita M., Couto A., Ayuga F., 2003. Numerical simulation of wall pressure during discharge of granular material from cylindrical silos with eccentric hoppers. Biosystems Engineering, 85(1): 101-109.
Holst J.M.F.G., Ooi J.Y., Rotter J.M., Rong G.H., 1999. Numerical modeling of silo filling II. Discrete element analyses. Journal of Engineering Mechanics-ASCE, 125: 104–110.
Horabik J.A., Ross I.J., Schwab C.V., 1988. Effects of spatial orientation on grain load distribution. Transactions of the ASAE, 31(6): 1787-1793.
Horabik J., Schwab C.V., Ross I.J., 1992. Non-symmetrical loads in a model grain bin during eccentric discharge. Transactions of the ASAE, 35(3): 987-992.
Horabik J., Molenda M., Ross I.J., 1992. Friction force reversal in a model grain bin during emptying. International Agrophysics, 6: 167-171.
Horabik J., Molenda M., Schwab C.V., Ross I.J., 1995. Wall and bottom loads in grain bins of different diameters. Bulk Solids Handling, 15(2): 215-218.
Horabik J., Molenda M., 2000. Grain pressure in a model silo as affected by moisture content increase. International Agrophysics, 14(4): 385-392.
Horabik J., Laskowski J., 2005. Mechanical Properties of Granular Agro-Materials and Food Powders for Industrial Practice. Part I: Molenda, M., Horabik, J.: Characterization of mechanical properties of particulate solids for storage and handling. Institute of Agrophysics, Lubin, 1-145.
Janssen H.A., 1895. Versuche über Getreidedruck in Silozellen. Verein Deutscher Ingenieure, Zetschrift (Düsseldorf), 39: 1045-1049.
Jenike R., 1964. Storage and flow of solids. University of Utah: Utah Engineering Experimental Station Bulletin.
Jian F., Jayas D.S., 2012. The Ecosystem Approach to Grain Storage. Agric. Res., 1(2): 148-156.
Kobyłka R., Molenda M., 2013. DEM modelling of silo load asymmetry due to eccentric filling and discharge. Powder Technology, 233: 65-71.
Kumar A., Muir W.E., 1986. Airflow resistance of wheat and barley affected by airflow direction, filling method and dockage. Transactions of the ASAE 29: 1423–1426.
Kuwabara G., Kono K., 1987. Restitution coefficient in a collision between 2 spheres. Japanese Journal of Applied Physics 26: 1230–1233.
Łapko A., 2010. Pressure of agricultural bulk solids under eccentric discharging of cylindrical concrete silo bin. International Agrophysics, 24: 51-56.
Łukaszuk J., Molenda M., Horabik J., Szot B., Montross M.D., 2008. Airflow resistance of wheat bedding as influenced by the filling method. Res. Agr. Eng., Vol. 54(2): 50-57.
Łukaszuk J., Molenda M., Horabik J., Montross M.D., 2009. Variability of pressure drop in grain generated by kernel shape and bedding method. J. Stored Products Research, 45(2): 112-118.
Masson S., Martinez J., 2000. Effect of particle mechanical properties on silo flow and stress from distinct element simulations. Powder Technology, 109: 164-178.
Molenda M., Horabik J., Ross I.J., 1995. Reduction of wall friction in initial period of grain silo operation. 10th International Conference on Reinforced and Posttensioned Concrete Silos and Tanks, Kraków 24 - 26.11., 165-172.
Molenda M., Horabik J., Ross I.J., 1996. Wear-in effects on loads and flow in a smooth-wall bin. Trans. of the ASAE, 39(1): 225-231.
Molenda M., Horabik J., Ross I.J., 2001. Comparison of loads on smooth- and corrugated-wall model grain bins. International Agrophysics, 15(2): 95-100.
Molenda M., Horabik J., Thompson S.A., Ross I.J., 2002. Bin loads induced by eccentric filling and

discharge of grain, Transactions of ASAE 45 (3): 781–785.
Molenda M., Montross M.D., McNeill S.G., Horabik J., 2005. Airflow resistance of seeds at different bulk densities using Ergun's equation. Trans. ASAE, 48 (3): 1137-1145.
Molenda M., Montross M.D., Horabik J., 2007. Non-Axial Stress State in a Model Silo Generated by Eccentric Filling and Internal Inserts. Particle & Particle System Characterization, 24: 291-295.
Mühlhaus H.B., Vardoulakis I., 1987. The thickness of shear bands in granular materials. Géotechnique, 37(3): 271-283.
Parafiniuk P., Molenda M., Horabik J., 2013: Discharge of rapeseeds from a model silo: physical testing and Distinct Element Method simulation. Computers and Electronics in Agriculture (in press).
Roberts A.W., Wensrich Ch.M., 2002. Flow dynamics or 'quaking' in gravity discharge from silos. Chemical Engineering Science, 57(2): 295-305.
Sykut J., Molenda M., Horabik J., 2008. Influence of filling method on packing structure in model silo and DEM simulations. Granular Matter, Vol. 10: 273-278.
Thornton C., Ning Z., 1998. A theoretical model for the stick/bounce behaviour of adhesive, elastic–plastic spheres. Powder Technology 99: 154–162.
Walton K., 1987. The effective elastic moduli of a random packing of spheres. J. Mech. Phys. Solids (35)2: 213-226.
Wiącek J., Molenda M., 2011. Moisture-dependent physical properties of rapeseed – experimental and DEM modeling. International Agrophysics, 25: 59-65.
Wojtkowski M., Pecen J., Horabik J., Molenda M., 2010. Impact of rapeseed against flat surface: Physical testing and DEM simulation with two contact models. Powder Technology, 198: 61-68.
Wójcik M., Tejchman J., 2009. Modeling of shear localization during confined granular flow in silos within non-local hypoplasticity. Powder Technology, 192: 298–310.
Zhang Q., Britton M.G., 1995. Predicting hygroscopic loads in grain storage bins. Transactions of the ASAE 38(4): 1221-1226.

PRECISION AGRICULTURE TECHNOLOGY FOR SUSTAINABLE GOOD AGRICULTURAL PRACTICE

Wouter Saeys*, Josse De Baerdemaeker

KU Leuven, Department of Biosystems-MEBIOS, Kasteelpark Arenberg 30 , B3001 Leuven, Belgium,
E-mail: Wouter.saeys@biw.kuleuven.be

Abstract

In the last decades the reduction of protectionist regulations through international trade agreements has led to a globalization of the food market. Although this has promoted the availability for the consumer of a wider variety of food products at lower prices, governments, retailers and consumers around the globe are becoming more and more concerned about the safety and quality of their food products. As food is produced on a global scale, national governments and consumers have lost control over the production methods. Therefore, traceability and verification of good agricultural practices (GAP) is becoming very important. Apart from food safety and quality, this also involves considerations in the environmental impact and sustainability of the production and transport of the available food products. Precision agriculture and the technologies developed for it, including automation and robots, have high potential for reducing the environmental impact of production and for providing the necessary information for verifying the origin and compliance with GAP criteria. Apart from providing governments, retailers and consumers with the information needed to assure food quality and safety, precision agriculture technologies can also help producers to meet the GAP criteria and relief them from the administrative load related to proving compliance. In this paper, some novel developments in agricultural automation and their potential for food safety assurance are discussed.

Keywords: precision agriculture, food safety, good agriculture practice

Introduction

Since the WTO's Agriculture agreement negotiated in the 1986-1994 Uruguay round protectionist systems of quota, import taxes and export subsidies on agricultural products have been significantly reduced. As the competition on the food market became more fair, our food basket became significantly more international. While most consumers enjoy the availability of a wide variety of food products at very competitive prices, some recent food scandals have led to an increasing concern about the safety and sustainability of our food products. To reassure consumer's confidence in his food, both governments and private organizations (e.g. retailers) have taken initiatives to guarantee food safety and sustainability. Good Agricultural Practices (GAP) and traceability of all products back to their origin have been defined by all players in the food chain as the keys to satisfy this consumer demand. This has led to the definition of international standards for agricultural production, such as Global G.A.P. (SCP, 2010), which are administered and maintained through international partnerships between producers, traders and retailers.

Precision agriculture aims to improve on the current agricultural practices in terms of efficiency and sustainability by taking the spatial variability into account to adapt treatments to the local situation. As such, one could argument that successful precision agriculture would be 'Better Agricultural Practice'. While the full potential of precision agriculture still has to be realized, the sensing and automation tools developed in the context of precision agriculture could already be used as tools for complying with the regulations and for documenting this compliance in an automated way.

Shared aims of Good Agricultural Practices and precision agriculture

Good Agricultural Practice schemes, like the ones defined by Global G.A.P. (SCP, 2010), cover the entire agricultural production process from seed to non-processed end product considering the following basic concepts:

- Food safety criteria derived from HACCP principles.
- Reduction of the level of residues on the food crops by limiting the use of chemicals.
- Minimization of the negative impacts of Agricultural Production on the Environment.
- Occupational health and safety criteria including social responsibility.
- Animal welfare criteria.

The basic principles of precision agriculture can be seen as an extension of good agricultural practices by matching the supplied inputs (seed, nutrients, plant protection agents, tillage,...) with higher precision than would be obtained in traditional uniform farming. For example, in the case of reduction of the level of residues on the food crops good agricultural practice under traditional uniform farming would involve spraying certified herbicides or pesticides at the right time and in the right dose. Precision agriculture aims at improving on this current good practice by only applying these chemicals at the locations where these are needed based on the detection of weeds or diseases. Similarly, in precision lifestock farming one would go beyond the current good agricultural practice of treating all animals equally well by optimizing the treatment (feed, medication, housing,..) for every individual animal.

Apart from going beyond the current definition of good agricultural practices, the use of information and communication technology in precision agriculture systems would make it much easier to document the production process and its compliance with the standards. As such, the implementation of precision agriculture technologies could adhere to the “Lead Principle” that states: “*Environmental information communicated along the food chain, including to consumers, shall be scientifically reliable and consistent, understandable and not misleading, so as to support informed choice*” (Globalg, 2012). In the following sections, the potential for convergence between the GAP and precision agriculture initiatives will be discussed for the different GAP principles.

Traceability

As precision agriculture aims at locally optimized treatments based on information gathered at different moments during the growing season and over different seasons, Global Positioning Systems (GPS) play a key role in many precision agriculture applications. Thanks to the realizations in the context of precision agriculture, an increasing fraction of the self-propelled agricultural machinery is equipped with a GPS system providing information on the location and time of different treatments. While this is essential for navigation purposes and localized treatments during subsequent runs, it also provides large potential for product traceability. By adding the GPS coordinates to the shipping documents one could not only trace the product back to the farm where it came from, but even to the field and the location within that field.

An example of such a traceability system which is already commercially available is an RFID tagging system which can be mounted on a large square baler. This system adds an RFID tag to every bale on which the GPS coordinates are stored together with other information collected during harvest such as the time of harvest, the moisture content of the crop at harvest and the weight of the bale (Roberts, 2009). This allows livestock producers to check whether good agricultural practices were applied when harvesting the crop before deciding to feed this to their animals.

This is just the start, as also in crops for human consumption the GPS coordinates of the field and the location in the field where the crop has been harvested could be linked to the products during harvest. In the case of self-propelled harvesting machines such as combine harvesters, forage harvesters or grape harvesters vehicle-to-vehicle communication is already investigated to allow automatic planning of the logistics and control of the unloading process. This vehicle to vehicle communication could, however, also be used to transfer information on the location and quality properties of the harvest crop from the harvesting machine to the transportation vehicle on or at the side of the field. This information could then be further transferred in a similar way to the road transportation vehicle or at the grain station.

A similar approach would also be possible in crops which still involve a large amount of manual labor during harvest, such as fruit and vegetables by attaching RFID tags to the harvesting crates and linking the GPS coordinates and other quality parameters to these crates. For this purpose, the recently introduced harvest crate transporting robots (Ringer, Humpal, 2004) which use GPS for their navigation through the orchard provide new opportunities.

Attaching the GPS coordinates of the field or location in a field where the food and feed products were harvested to the product would be very useful to trace the product back to its roots. While this would allow to trace problems with the final product back upstream through the food production chain, it would not allow to see what has happened at that location during crop growth and to check that Good Agricultural Practices have been applied here. To reach this goal all treatments applied to that (location in the) field should be registered in a database. For example, in the case of the detection of dangerous pathogens like the EHEC bacteria on vegetables, it would be very useful to trace these vegetables back to the location in the field where these were grown and to the manure which has been applied here for fertilization. This is not so futuristic as it may seem, as in regions with concentrated livestock production, like the Netherlands and Belgium, GPS-logging of manure transport and application is already mandatory. In the case of herbicides and pesticides section control based on GPS to minimize over application due to overlap and unintended spraying of neighbor crops is already commercially available and might become mandatory in the near future (Ringer, Humpal, 2004). Good agricultural practices require that farmers register any chemical treatment by specifying the time and dose of application. As most sprayers are already equipped with computer controllers, it would be possible to add extra functionalities such an automatic read out of the product specifications from the package. By linking this information to the database of the crop the dose could be automatically set and spraying accidents could be avoided by giving an alarm when an unauthorized product is loaded. It is actually not unthinkable that such systems with automatic product identification and logging of the time, location and doses of application would eventually become mandatory.

Reduction of residues

Although section control based on GPS can already result in a serious reduction of the herbicide and pesticide use without loss of efficacy, it still assumes that the field is homogeneously infested with the targeted weeds or pests. This is, however, seldom the case as weeds and pest typically emerge locally and spread from the point(s) of emergence. Therefore, the largest reduction in the use of herbicides and pesticides would be obtained when these would only be applied where the targeted weeds or pests are present.

Slaughter et al. reviewed the state of the art on automatic weed control systems and concluded that the major challenge remains the automatic detection and identification of weeds in the field under variable weather conditions (Slaughter et al., 2008). Most researchers have focussed on the use of spectroscopy or image processing to discriminate between weeds and crop based on the differences in their spectral properties (Vrindts et al., 2002), respectively their shape properties or a combination of both.

When the weed has been detected it can either be sprayed with herbicide or treated thermally or mechanically. While most researchers have proposed systems attached to a regular tractor, a few fully autonomous weed control robots have been demonstrated in the field. Blackmore suggested that small autonomous robots could perform the weeding tasks more efficiently than one or a few large machines (Blackmore, 2009). Recently, researchers are investigating the potential of small unmanned aerial vehicles or drones as tools for scouting fields for weed patches, which would then provide the coordinates of the detected weed patches to small weeding robots (Fernandez-Quintanilla et al., 2011). When such an automatic system for weed detection and treatment would be in place, the occurrence of weed populations and the administered treatments could be easily registered and made available in the GAP database.

Residues of pesticides form an even bigger threat to human and animal health than herbicides. The best way to reduce the use of pesticides is by preventing the incidence of pests and minimizing their intensity when they occur. This can be obtained by regularly monitoring the crop to detect the pests and diseases at an early stage. As a contactless and non-destructive detection method is desired, several researchers have investigated the potential of optical measurement techniques such as NIR spectroscopy and fluorescence imaging for early disease detection. For example, Moshou et al. successfully discriminated winter wheat plants infected with yellow rust from healthy and nutrient stressed plants using an in-field combination of a hyperspectral and multispectral imaging system (Moshou et al., 2011). This and other researchers indicate that automatic disease detection by remote sensing with unmanned aerial vehicles or small driving robots may become possible in the near future. Further research is, however, required to fully explore this potential.

Similar to disease control the use of pesticides can be reduced by early detection of potential pests. This requires tight monitoring of the insect population to allow rapid action when pests start to develop. However, the use of insecticides to avoid pests caused by harmful insects is becoming more and more controversial as it often also kills the good insects such as bees which are essential for the pollination. Therefore, several insecticides such as neonicotinoids are being banned and farmers are turning more and more towards pest control through the use of natural predators. This concept is known as integrated crop protection. Good pest management requires regular monitoring of the insect population, which is typically done with insect traps. This is a labor intensive process as the trapped insects have to be identified and counted manually. Moreover, as pests typically develop locally this has to be done at multiple places in the field, orchard or greenhouse. To obtain an efficient pest management it would thus be very useful to have an automatic system for insect identification and counting. A first attempt in this direction was reported by Brydegaard et al., who demonstrated the feasibility of Light Detection and Ranging (LiDaR) sensors for insect monitoring (Brydegaard et al., 2009).

Minimization of the environmental impact

Together with toxic residues of herbicides and pesticides, eutrophication due to over application of nitrogen and phosphorous fertilizers is one of the major negative environmental impacts of agriculture. As under application of fertilizer leads to yield loss, while over application leads to nutrient leaching to soil and surface waters, good agricultural practice implies that the correct dose of fertilizer is applied at the correct moment in the correct way. To determine the correct dose one should subtract the amount of nutrient available in the soil from the nutrient demand of the crop.

The traditional way to determine the nutrient availability in the soil, also known as the soil fertility, is by taking a sample and analyzing this wet chemically in the laboratory. While this is an approved and reliable method, it is a labor intensive and cumbersome procedure. Therefore, typically only one (mixed) sample is taken per field, while there can be large variability in the soil fertility within a field. To promote more precise fertilization several researchers have investigated the potential of sensor technologies for rapid on-site and even on-line measurement of the nutrient content of the soil. The two most studied methods are Visible and Near Infrared (Vis/NIR) Spectroscopy and electrochemical sensors. As the latter involves a serious time lag between sample collection and sensor read out, it cannot be used for on-the-go soil fertility measurement (Adamchuk et al., 2006). On the other hand Vis/NIR spectroscopy on soil is typically performed in reflectance mode where the soil is illuminated and the diffusely reflected spectrum is acquired with a spectrophotometer. As such, this measurement does not require sample preparation and can be performed in a rapid and contactless way. Mouazen et al. successfully implemented a fiber-optics probe in a subsoiler to measure the diffuse reflectance spectrum of the freshly cut soil in the plough zone and predict some selected soil fertility parameters on-the-go (Mouazen et al., 2007). By combining the predicted nutrient content for all scanned lines in a field and interpolating between the lines with spatial interpolation procedures, soil fertility maps can be produced. So far, useful prediction results have been obtained for the moisture and organic matter contents, but the prediction performance for N, P and K is not yet good for precise fertilization purposes. Therefore, further research is required to increase the accuracy for these major nutrients and to obtain better robustness of the predictions against variations in the spectral signals related to the on-the-go acquisition.

Apart from the distribution of the major soil fertility parameters throughout a field precise fertilization also requires a system which allows to apply for every nutrient the difference between the amount required by the plant and the amount available in the soil. In the case of mineral fertilizer this could be obtained by locally adapting the applied dose of single nutrient or mixed fertilizers. For example, banded application of nutrients near the plant rows could already increase the nutrient efficiency and reduce the leaching losses. This type of machinery also opens opportunities to apply different doses to the different rows or different places within the row by measuring the actual position with GPS and actuating flow control valves based on the application maps. While this type of systems may become possible in the near future, it will not be sufficient to optimize nutrient application as in many regions a large part of the nutrients are applied in the form of manure. As the nutrient composition of manure can vary considerably, good agricultural practice requires that the nutrient content of the applied manure is measured in order to optimize the dose and register the amount of applied nutrients. Several researchers have shown the potential of for on-line manure composition measurement. For example, Saeys et al. obtained very good prediction accuracy for dry matter content and good accuracy for organic matter content and total nitrogen, while only approximate prediction could be made for ammonium nitrogen, phosphorus and magnesium (Saeys et al., 2005). For potassium and calcium they were only able to discriminate between high and low values. Such an on-line manure composition sensor could then be combined with a precise manure flow control system to optimize the applied dose (Saeys et al., 2008). As the nutrient content of manure cannot be optimized on the go, such a system with on-line measurement of the manure composition and flow control based on this, would not allow to match the plant needs for all nutrients. Therefore, manure application should be combined with mineral fertilizer application to fill the gaps for the nutrients which could not be matched with manure. This could either be done by actively adding mineral fertilizer to the manure during application or by mapping the applied doses for all nutrients to create mineral fertilizer application maps to be used in a subsequent fertilization run.

Even when the amount of applied nutrients could be perfectly matched to the available nutrients in the soil, this would most likely not lead to an optimal match between the provided nutrients and the plant needs. Apart from the nutrient availability many other factors like genetics, local environmental conditions and the occurrence of diseases and pests determine the local growth. So, the average estimate for the nutrient demand of a crop may be too high at some locations and too low at others. Therefore, the crop status should be monitored during the growing season and the fertilization should be adapted to the crop status. With respect to crop status monitoring most researchers have focused on estimation of the nitrogen status of the crop based on its chlorophyll content. Especially optical sensors measuring in reflectance mode in the wavelength range around the chlorophyll absorption wavelength at 680 nm have been reported to allow accurate estimation of the chlorophyll content. While many systems use an external light source, some systems are passive and use the sun as the light source (Reyniers et al., 2006). In this case, it is important to include some reference measurement to compensate for variations in the light intensity due to season, time of the day and the presence of clouds.

Conclusions

In this paper it has been shown that the main aims of the international standards for good agricultural practices are very similar to the aims of precision agriculture. On one hand precision agriculture shares the aim to reduce the use of chemicals and the negative impact of agriculture on the environment, while on the other hand it provides the information and communication technology to easily document the production process and its compliance with standards. As precision agriculture aims at providing the technology to farm more precise, its ambition goes beyond what is today recognized as good agricultural practice. By moving away from uniform treatments which neglect the variability in soil fertility and the occurrence of weeds, pests and diseases, to optimized treatments based on measurements with sufficient spatial resolution, precision agriculture has high potential for reducing the negative impact of agriculture on the environment especially in terms of nutrient leaching and chemical residues. The use of Global Positioning Systems (GPS) on agricultural machinery makes it possible to automatically register all treatments for a given location in the field and couple all this information to the final product during harvest. In this way, precision agriculture technology could allow automatic collection of the information to be registered with respect to the control points and compliance criteria of Global G.A.P. or another international scheme for Good Agricultural Practices. As such precision agriculture technology could provide farmers confronted with the globalized food market with the tools to restore the confidence of retailers and consumers in their products.

References

Adamchuk V.I., Hummel J.W., Morgan M.T., Upadhyaya S.K., 2006. On-the-go soil sensors for precision agriculture. Comput.Electron.Agr., 44: 71–91.

Blackmore B.S., 2009. New concepts in agricultural automation. Precision in arable farming - current practice and future potential. Stoneleigh Park, Kenilworth, Warwickshire, UK, Home Grown Cereal Authority, 28-29 October.

Brydegaard M., Guan Z., Wellenreuther M., Svanberg S., 2009. Insect monitoring with fluorescence lidar techniques: feasibility study, Appl. Opt., 48: 5668-5677.

Fernandez-Quintanilla C., Dorado J., San Martin C., Conesa-Munoz J., Ribeiro A., 2011. A Five-Step Approach for Planning a Robotic Site-Specific Weed Management Program for Winter Wheat. RHEA-2011, 3-12.

Globalg A.P., 2012. Integrated Farm Assurance, 1-12. Available at: http://www.globalgap.org/uk_en/what-we-do/

Moshou D., Bravo C., Oberti R., West J.S., Ramon H., Vougioukas S., Bochtis D., 2011. Intelligent multi-sensor system for the detection and treatment of fungal diseases in arable crops, Biosyst.Eng., 108(4): 311-321.

Mouazen A., Maleki M., De Baerdemaeker J., Ramon H., 2007. On-line measurement of some selected soil properties using a VIS-NIR sensor. Soil & tillage research, 93(1): 13-27.

Reyniers M., Vrindts E., De Baerdemaeker J., 2006. Comparison of an aerial-based system and an on the ground continuous measuring device to predict yield of winter wheat. Eur.J.Agron., 24: 87-94.

Ringer J.D., Humpal R.A., 2004. Sprayer section control valve switching. US Patent nr US 6776355 B2.

Roberts J.S., 2009. System and method for identifying bales of hay. US Patent nr US7621111 B2.

Saeys W., Mouazen A.M., Ramon H., 2005. Potential for Onsite and Online Analysis of Pig Manure using Visible and Near Infrared

Reflectance Spectroscopy. Biosyst.Eng., 91(4): 393–402.
Saeys W., Deblander J., Ramon H., Anthonis J., 2008. High-performance flow control for site-specific application of liquid manure, Biosyst.Eng., 99: 22 – 34.
SCP, 2010. European Food Sustainable Consumption and Production (SCP) Round Table, 1-12. Available at: www.food-scp.eu/files/Guiding_Principles.pdf
Slaughter D.C., Giles D.K., Downey D., 2008. Autonomous robotic weed control systems: A review. Comput.Electron.Agr., 61: 63–78.
Vrindts E., De Baerdemaeker J. Ramon H., 2002. Weed detection using canopy reflection. Precis. Agric., 3(1): 63-80.

ELECTRIC POWER SYSTEMS ON THE BASIS OF N. TESLA TECHNOLOGIES

Strebkov D.S.

State Scientific Institution “All-Russian Scientific-Research Institute
for Electrification of Agriculture”
(GNU VIESH at the Russian Academy of Agricultural Sciences (RAAS,)
109456, 1st Veshnyakovsky pr., 2, Moscow, Russian Federation
www.viesh.ru

Abstract

Resonant electric power systems with the use of single-line waveguide lines at highfrequency are considered. The results of comparison of classical electrical engineering with resonant electrical enineering proposed by N. Tesla 100 years ago, are given. In such characteristics as current density and line losses, energy trasmission distance, transmission capacity, the possibility of cable and wireless power transmission the Tesla electrical systems exceed the classical energy supply systems. The results of the GNU VIESH research for the development of electric power supply systems proposed by N. Tesla, are considered. The future world energy model based on solar energy and N. Tesla technologies for electric power transmission is suggested. The ten trends of the future development and application of resonant systems for electric power transmission are described. In future electrified mobile robots with external wireless electric power supply will allow to organize agricultural production on the principle “Industrial factories on the fields” with full automation of technological processes.

Keywords: electric power system, N. Tesla

Introduction

At UPGrid-2012 forum Mikhail Kurbatov, RF Deputy Minister of Energy said that there exist in Russia over 2 million kilometers of overhead transmission lines more than half of which have already used their rated resource. They have to be replaced in the coming 15 years. Oleg Budarin, the head of the Federal Grid Company of the Unified Energy System of Russia (UES FGC) stated: “We are expecting new materials and technologies of power transmission over long distances. However, speaking of breakthrough solutions for electric grids, none have been demonstrated in recent years” (Power Engineering and Industry of Russia, 2012). In fact, breakthrough technologies for electric grids and systems already exist.

History of science demonstrates that very occasionaly global inventions come to life that considerably change our perception of the outside world and the prospects of humanity development. As an example we can mention the discovery of electricity, the emergence of nuclear and solar energy, of aircraft and rocket engineering, computers and telecommunication technologies.

However, nowadays we witness and participate in the development of advanced technologies that change the world making it better, cleaner and safer. First and foremost we should mention technologies proposed by N. Tesla a hundred years ago. N. Tesla developed electric engineering solutions with the use of alternate current but he was not able to implement his major project of “The global system for electric power supply” for reasons described in his work (Tesla, 2008): … “My project was retarded by laws of nature. The world was not prepared for it. It was too far ahead of time. But the same laws will prevail in the end and make it a triumphal success”.

"Perhaps it is better in this present world of ours that a revolutionary idea or invention instead of being helped and patted be hampered and ill-treated in its adolescence - by want of means, by selfish interest, pedantry, stupidity and ignorance; that it be attacked and stifled; that it pass through bitter trials and tribulations, through the heartless strife of commercial existence. ... So all that was great in the past was ridiculed, condemned, combatted, suppressed - only to emerge all the more powerfully, all the more triumphantly from the struggle." It is so similar to the attitude to scientists in Russia since 1991.

N. Tesla left behind thousands of pages of his books desribing the experiments results, articles and patents (Tesla, 2008; Tesla, 1886).

The comparison of classical electric engineering with N. Tesla electric engineering solutions

Fig. 1 demonstrates one of electric circuits of the resonant single-wire electric power supply system proposed by N. Tesla and updated at GNU VIESH (Tesla, 1886; Strebkov, Necrasov, 2008).

At the beginning of the 19th century there were no diodes and transistors and for pumping resonant circuit and a transformer N. Tesla used the method of impact incitation with a spark arrester with 96 % transmision efficiency (Tesla, 2008). At the end of the 20th century we used a thyristor frequency converter with 25 kW capacity, water cooling with 86 % efficiency and 400 kg weight. Currently frequency converters on silicon transistors with 97 % efficiency and 30 kg weight are applied. The ReFuSol company developed and brought to market 20 kW inverters on silicon carbide transistors with 98 % efficiency.

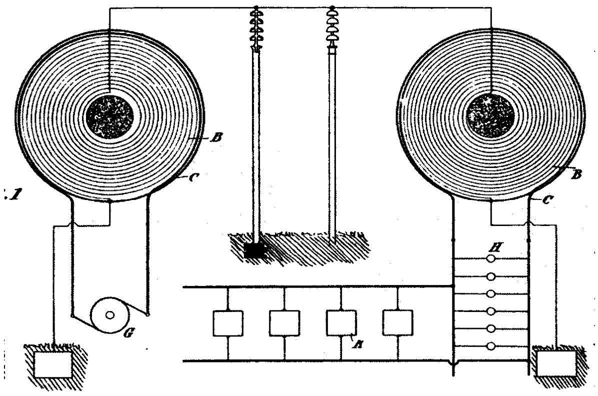

Fig. 1a Resonant single-wire electric power supply system developed by N. Tesla (1897)

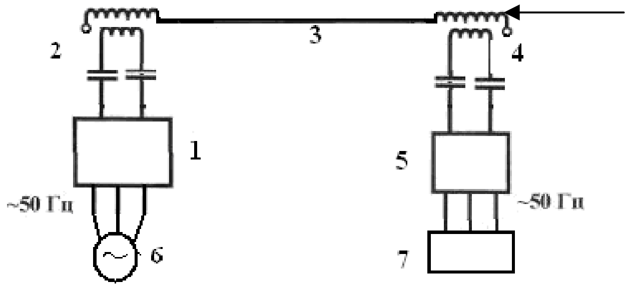

Fig. 1b State-of-the art resonant system for electric power supply:
1 – frequency converter; 2, 4 – two resonant high-frequency Tesla transformers; 3 – single-wire high voltage line; 5 – inverter; 6 – generator; 7 – load

In contrast to DC power transmission lines with converting substations at a high-voltage side of transformers, we use frequency converters and inverters at low-voltage side of transformers, which reduces their price to 100-200 USD per 1 kW.

The Table presents the comparison of classical electric engineering studied by future electric engineers for three terms, with N. Tesla electric engineering techique.

Table The comparison of classical electric engineering with N. Tesla technique in the field of electric power transmission

№№	Classical electric engineering based on the use of alternative current in a closed circuit	N. Tesla electric engineering based on the use of reacive current in an open-circuit line
1	**2**	**3**
1	AC frequency – 50 Hz (Europe), 60 Hz (USA), 400 Hz (aviation)	AC frequency - 500 Hz- 500 kHz
2	The modes of quenching of resonant characteristics of the line, transformers with a closed core, three- and one-phased overhead transmission lines are used	The resonant modes of the line operation, resonant circuits, resonant transformers with an open core or without a core, waveguide single-conductor cable lines, as well as the globe as a single-conductor line are used
3	Potentials at outlets of high-voltage winding of a single-phase trasformer are equal in value and opposite in sign	Potential of one of the outlets of high-voltage winding of the Tesla transformer is equal to zero and the potential of the second outlet has maximum in modulus positive or negative value
4	A single-layes electric coil is classical inductance	A single-layer electric coil in various applications is an earth loop, a time-delay curcuit, a spiral waveguide, a spiral antenna or an electric resonator
5	The tranformer has low-voltage and high-	The high-voltage Tesla transformer has additional single-

№ №	Classical electric engineering based on the use of alternative current in a closed circuit	N. Tesla electric engineering based on the use of reacive current in an open-circuit line
	voltage winding made in the form of multilayered coils with lamped parameters and there is classical theory of calculation of transformers winding	layer high-voltage winding which is an electric resonator with lamped parameters and it is impossible to calculate the parameters of the electric resonator using classical theory of electric circuits (Strebkov, Necrasov, 2008; Strebkov, 2007)
6	Loss of phase in power transmission lines is emergency for consumers	The open circuit mode of the generator is an operating mode of electric power transmission
7	Electric power from the generator is transmitted to the customer in a continuous mode	A pulse mode of energy pumping into the Tesla trasformer from a transmitting resonant circuit is used.
8	The circuit must be closed to provide current flow	in closed current flows in a open-circuit line
9	Closed current of the generator must pass through the load and return to the generator	Unclosed current flows from the generator to the load not returning to the generator
10	Current must be equal for all sections of closed circuit. It holds for direct currents and quasi-steady alternating currents with 50 Hz frequency and circuit length of up to 100 km	Current at various line sections can flow in opposite directions and assume any values from zero to maximum
11	Electric power is transmitted with the use of active current in a closed circuit	Electric power is transmitted with the use of reactive capacitance current in an open-circuit line
12	During electric power transmission in a closed line travelling current and voltage waves emerge	During electric power transmission in an open-circuit line standing (stationary) current and voltage waves emerge
13	Current and voltage waves in a line match in phase: $\varphi=0$, $\cos\varphi=1$	Current and voltage waves in a line are phase shifted by 90^o: $\varphi=90^o$, $\cos\varphi=0$
14	Crests and nodes of current and voltage waves are cuncurrent and match along the line length	Crests and nodes of current and voltage waves are non-cuncurrent and are located at various sections of the line. At the moment when voltage in the whole line is equal to zero, current in the line has maximum value and vise versa
15	Crests and nodes of current and voltage move along the line	Crests and nodes of current and voltage are rigidly settled along the line
16	Maximum effective current density in the line is 1,5-3,5 A/mm^2 (Smirnov, Antipov, 1984)	Maximum effective current density in the line made of copper conductor at ambient temperature is 600 A/mm^2. The parameters of the GNU VIESH operating plant are as follows: conductor diameter - 80, мкм, transmission capacity – over 20 kW, voltage – 6,8 kW
17	Losses in electric power transmission in the line are 8,5 % (normative), 10-20 % (actual)	Losses in electric power transmission in the line are 1-3 % (N. Tesla experimental data)
18	In the mode of active power transmission voltage along the line is constant and there is an angle between voltage vectors at the sending-end and receiving end on the line	An angle between voltage vectors at the sending-end and receiving end of the line is equal to zero, and voltage value is measured over wide range and is determined by the line quality factor
19	Active transmission capacity is regulated by changing angle between voltage vectors at the sending-end and receiving end of the line, as well as voltage value	Active transmission capacity is regulated by changing voltage and frequency value
20	When frequency is changed by 2 %, transmission capacity undergoes slight change	When frequency is changed by 2 %, transmission capacity is reduced down to zero
21	The Umov-Poynting vector is directed along the line from the generator to the load	The Umov-Poynting vector changes its direction each quarter wave
22	Power transmission distance is 2000-3000 km (Smirnov, Antipov, 1984)	Power transmission distance is limitless within the Earth bounds

№ №	Classical electric engineering based on the use of alternative current in a closed circuit	N. Tesla electric engineering based on the use of reacive current in an open-circuit line
23	Maximum transmission capacity of a three-phase power transmission line is limited by electromagnetic stability of the line at the level of 6 GW (Smirnov, Antipov, 1984)	Maximum transmission capacity of a three-phase power transmission line is limited by electric strength of insulation and exceeds 100 GW
24	Wireless power transmission is impossible at the 50-60 Hz frequency and is economically unsound at high frequencies	Wireless power transmission is highly efficient and will be widely used in railroad and automobile transport and in rocket and space technologies
25	In DC power transmission lines 500-750 kW converting substations are used	Converting substations are used at the transformer low-voltage side with 0,4-10 kW voltage

In such parameters as current density and line losses, power transmission distance, transmission capacity, the possibility of cable and wireless power transmission N. Tesla electric systems exceed classical electric power supply systems.

In radio engineering threre are examples of single-conductor power transmission systems at frequency 100 times exceeding the frequency used by N. Tesla: a beam antenna, a single-conductor wave-guide, electromagnetic and galvanic coupling between resonant circuits. The theory of coupled resonant circuits can be used in the theory of power transmission through single-conductor lines. In the theory of coupled resonant circuits power transmission effciency tends to 100 % while power transmitted between resonant circuits tends to zero. Maximum capacity is transmitted with 50 % efficiency because of energy losses in circuits (Kalashnikov, Stepun, 1965). To raise transmission efficiency up to 96 % N. Tesla used pulse mode of pumping the Tesla transformer, wherein in power transmission through a single-conductor line, transmitting circuit opened and provided infinite resistance for reflected waves, corresponding to the mode of open-circuit line of the generator (Tesla, 2008; Strebkov, 2007). This provided the mode of standing waves and prevented losses in series transmitting circuit where the Tesla transformer pumping currents amount to tens of thousands of amperes at 70 kW supply voltage and idling losses power of 3 hp.

Classical electrical engineering should be supplemented by a section describing N. Tesla resonant electric engineering solutions.

Trends of future development of electric engineering and energy industry

N. Tesla has left behind the following technologies for further development:

1. Single-wire resonant technologies for power supply to stationary consumers.
2. Technologies for wireless power supply to surface and sea transport.
3. Technologies of directional electric power transmission through conducting channels in atmosphere and space.

In 21st century these technologies make it possible to develop:

1. fuel-free rockets with electric rocket motors, which increase layload mass taken into orbit, from current 5% up to 90% of the rocket total weight;
2. extremely long-range electric power transmission lines with lower losses than in superconducting cable lines;
3. a unified energy system of Russia from Chukotka to Kaliningrad;
4. a global solar energy system with terawatt transcontinental power exchange and twenty-four-hour electric power generation for million years in the amount of 20 000-50 000 TW·h, corresponding to the Earth current and future energy consumption;
5. plasma chlorine-free technologies of solar-quality silicon production in the amount of 1 mln tons per year for yearly construction of photovoltaic solar power palnts with total capacity of 150 GW;
6. hydrogen energetics due to 10 times reduction of costs on water electrolysis;
7. electric cars without accumulators with limitless distance of run;
8. contactless electric power supply systems for railroad transport, trolley-cars, air and sea transport;
9. mobile electric robots providing automated soil tillage, cultivation and harvesting agricultural crops without herbicides and pesticides;
10. underground shielded cable lines that can replace all overhead power transmission lines.

All the ten directions of the development of energy technologies for future world has been developed in GNU VIESH for 20 years and are protected by fifty Russian patents. The basic content of these patents and the research results have been publshed in the study (Tesla, 1886) that will be issued in the fourth edition in 2013. Over 80 experimental low-power electric devices using Tesla technologies, are described in the book (Juferev et al., 2010).

Let us consider each of these trends in more detail.

N. Tesla resonant technologies for electric power transmission are based on the use of reactive currents in single-conductor open lines. In 1927 N. Tesla (2007) wrote: “In 1893 I demonstrated that there is no need to use two conductors for electric power transmission… Irreversible power transmission through a single conductor was practically substantiated”.

D. Maxwell confirmed the existence of unclosed currents: “Outstanding complexity of agreeing laws of electromagnetcs with the existence of unclosed currents is one of the reasons why we should admit the existence of currents generated by displacement change”.

N. Tesla suggested power transmission through a conducting channel in atmosphere with the use of X radiation. In 1927 Tesla wrote. (Tesla, 2008): “More than twenty-five years ago my efforts to transmit large amounts of power through the atmosphere resulted in the development of an invention of great promise, which has since been called the "Death Ray". The underlying idea was to render the air conducting by suitable ionizing radiations and to convey high tension currents along the path of the rays. Experiments, conducted on a large scale, showed that with pressures of many millions of volts virtually unlimited quantities of energy can be projected…” .

We have obtained five patents for electric power transmission through laser, electron and microwave beams between objects in the Earth atmosphere, in space and between the Earth and space objects. Technogies of directional wireless electric power transmission develop N. Tesla technologies for using conducting channels as a guide system (single-conductor wave-guide) for transmission of electromagnetic high-potential energy at 10-500 kHz and voltage level from hundreds of kilovolts to tens of millions of volts. In this process energy transmitted through a conducting channel exceeds energy spent on formation and maintaining a conductive channel 10^2-10^6 times.

On July 15, 2012 the manned spaceship “Soyuz” was launched to perform works at the international space station. For 529 seconds of rocket engines operation 300 t of liquid fuel were consumed. This means that launch mass of the spaceship exceeded 300 t while payload mass was less than 5%. The use of electric rocket motors with wireless electric power transmission to the spaceship from a terrestrial energy system will make it possible to reduce the rocket mass and energy consumption, as well as space flights costs tens of times.

Another N. Tesla approach was to use the Earth as a single-conductor line for electric power supply to ground, sea and air electric tranport vehicles. In his speech on the occasion of receiving the Thomas Edison Award at the session of the American Institute of Electrical Engineers on May 18, 1917 N. Tesla stated: “Years ago I was in the position to transmit wireless power to any distance without limit other than that imposed by the physical dimensions of the globe. In my system it makes no difference what the distance is. The efficiency of the transmission can be as high as 96 or 97 per cent, and there are practically no losses except such as are inevitable in the running of the machinery. When there is no receiver there is no energy consumption anywhere.

When there are no receivers, the plant consumes only a few horsepower necessary to maintain the vibration; it runs idle, as the Edison plant when the lamps and motors are shut off.".

The project envisaged the setting-up of a network of electric power plants equipped with the systems for power transmission to any part of the globe on the surface of ground, oceans or in atmosphere using the Earth as a single-conductor line. At the same time N Tesla suggested lighting of oceans and cities at night time due to atmosphere ionozation. Still, testing of experimental systems in Colorado Springs and near New York revealed ecological problems in the process of the system operation: sparks from water taps and horses’ hooves, glowing of human hands and hair, a failure at the electric power supply station, etc.

In order to set up the global energy system developing N. Tesla ideas, we proposed electric energy transmission through high-voltage single-conductor cable gas-insulated lines and the use of three solar energy plants in deserts of Australia, Africa and Latin America as energy sources (Fig. 2, Fig. 3) (Strebkov, Necrasov, 2008).

Each solar energy plant size is 200×200 km, efficiency - 25 %. They produce electric energy in the amount of 20 000 TW*h per year on a 24-hour basis, which corresponds to the world energy consumption in 2010.

Thus Russia proposed the model of the future world development based on direct conversion of solar energy at solar power plants and transcontinental terawatt power streams with the use of resonant wave-guide technologies suggested by N. Tesla.

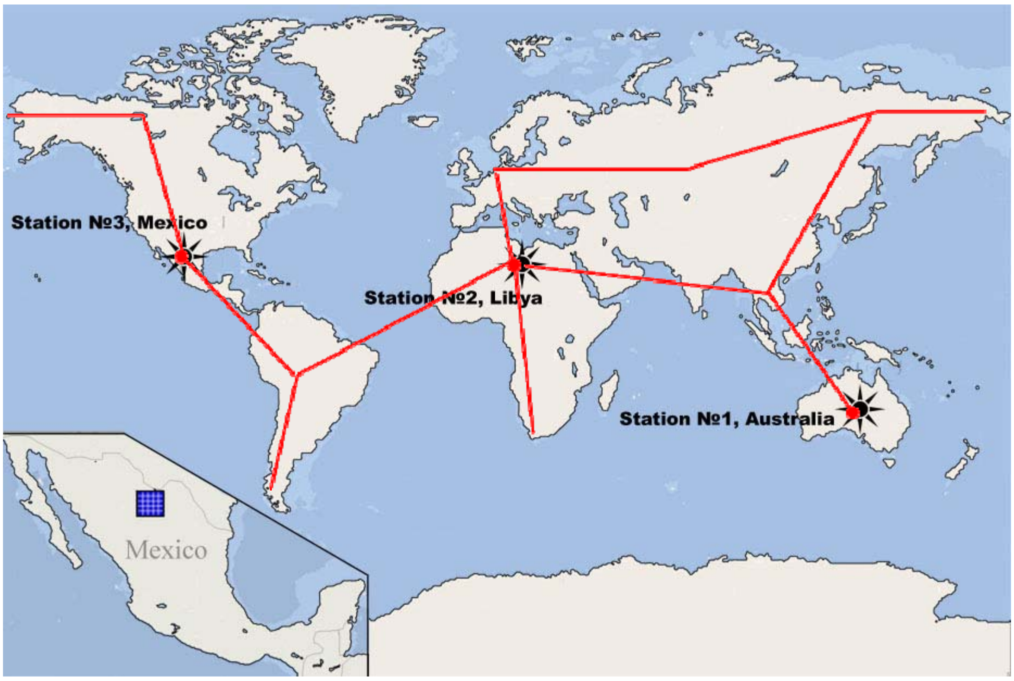

Fig. 2 The global solar energy system comprising three solar power plants

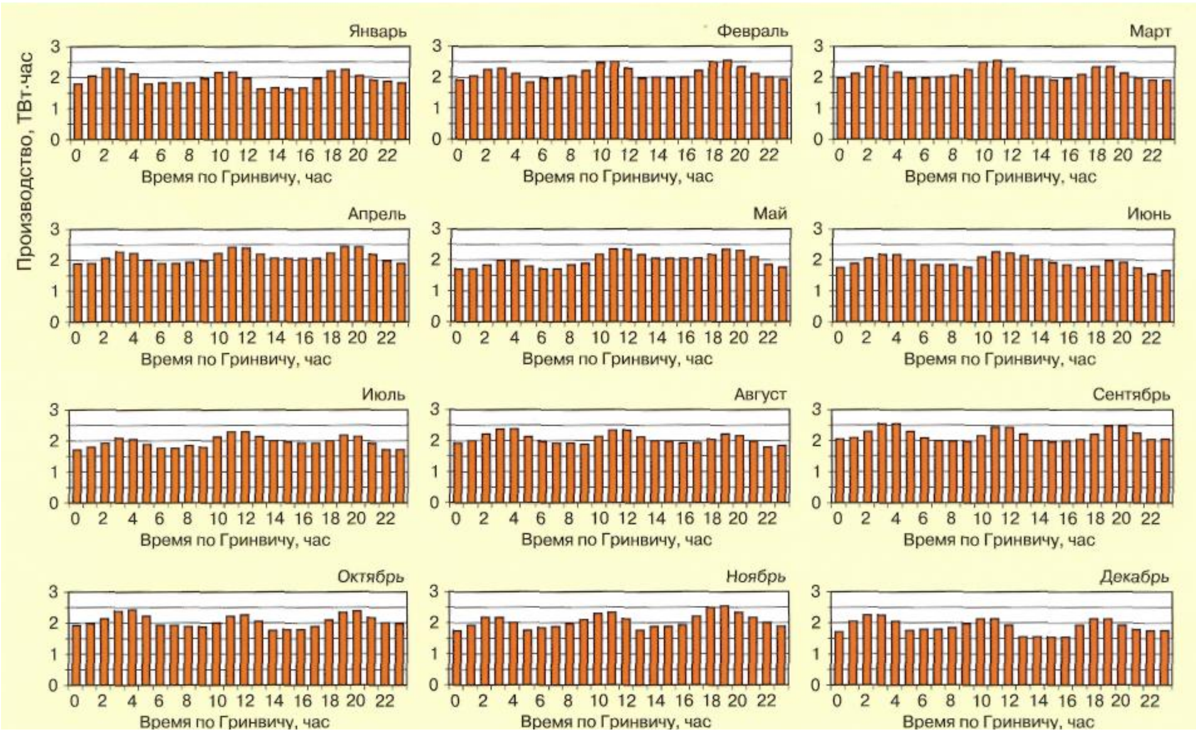

Fig. 3 Full-time production of electric energy by the global solar power system in the amount of 20 000 TW per year for millions of years

The use of insulated single-conductor cable lines instead of the Earth will make it possible to eliminate ecological problems related to the implementation of the N. Tesla project for the setting-up of the global power suply system. N. Tesla published two patents on cable single-wire lines (Tesla, 1886), that can be used for the project of the unified energy system of Russia from Chukotka to Kaliningrad. The first patent suggests using cables with special shields reducing radiation losses practically down to zero. The cable conductor diameter is 1-5 mm that provides low electric capacity of the cable. In the second patent N. Tesla offered to lay wave-guide single-conductor cable lines in the permafrost zone to increase insulation strength, and to create permafrost zone around a cable with the use of electrically insulated metal pipe through which gas or liquid low-temperature refrigerant is pumped.

Single-conductor cable lines covered by N. Tesla patents will replace overhead electric power transmission lines, which will considerably increase reliability of electric power supply, reduce rate of injuries caused by electricity and free considerable areas of fields, cities and forests in Russia.

Mono-electrode high-frequency plasmatrons developed in GNU VIESH make it possible to set up solar-grade chlorine-free silicon production in the amount of 1 mln tons per year to provide the construction of solar energy plants with capacity of 150 GW, while current solar energy production is 30 GW per year. N. Tesla technologies allow to develop special mono-electrode electrolysis units and reduce energy consumption in the process of water electrolysis for hydrogen production tenfold.

N. Tesla developed the conactless method of electric power supply to railway transport from a single-conductor cable laid in the gound (Tesla, 1886). The GNU VIESH specialists developed and patented experimental models of cars of the future without accumulators, that are fed from an energy system through air interspace from a single-conductor cable laid near the pavement surface. Electric energy costs of a light electric car will be 1 USD per 100 kilometer of road, electromobiles price will be reduced twice due to the absence of accumulators and it will be less expensive than cars with internal combustion engines. In addition ecological problems of large cities and highways will be solved. Troleyless systems of electric power supply will raise reliability of tramway cars and high-speed trains and will make it possible to use electric heavy-payload trucks on interurban roads. We proposed systems for electric power transmission to underwater vehicles with submergence depth of up to 10 km and to aircraft in atmosphere.

In his letters of July 14 and 17 N. Tesla (2007) wrote:

“With the use of a standing waves generator and receiving equipment installed and adjusted in any distant location it is possible to transmit distincts signals, control or activate devices...

With the use of a transmitter electricity moves in all directions equally through ground and air but energy is spent only at the location where it is accumulated and used to perform operations. Though electric oscillations can be detected on the whole Earth both on the surface and high in the air, energy would actually be not consumed.

Electromagnetic energy of a transmitter is transmitted to a location of the Earth or its atmosphere where there is a receiver with resonant frequency adjusted to the transmitter frequency”.

Electric tractors and robotized mobile equipment in agriculture will get energy from a cable laid in the ground but it will be necessary to provide for a special permanent path (track) for a left of right train of wheels of an electrified mobile vehicle. In the future electrified mobile robots with external power wireless power supply will make it possible to organize agricultural production on the principles of “Industrial Factories on Fields” with full automation of techniological processes.

Humanity will be able to unify energy systems of all the countries into a global solar energy system of the Earth to provide decent living conditions for everyone and to implement large-scale scientific and technological projects both on the Earth and in space.

Conclusions

1. The results of comparison of parameters of a classical electric power supply system with an electric power supply system using single-wire wave-guide lines with high frequency, proposed by N. Tesla 100 years ago, are presented. In such characteristics as current density and line losses, energy trasmission distance, transmission capacity, the possibility of cable and wireless power transmission the Tesla electrical systems exceed the classical energy supply systems
2. The future world energy model based on direct solar energy conversion and transcontinental terawatt power transmission with the use of resonant wave-guide technology developed by N. Tesla, is proposed.
3. The trends of the future development of electric engineering and energy technologies for agriculture, space exploration, solar energy, hydrogen energy and electric transport based on resonant wave-guide methods of electric power transmission and application are suggested.
4. In future electrified mobile robots with external power wireless power supply will make it possible to organize agricultural production on the principles of “Industrial Factories on Fields” with full automation of technological processes.

References

Juferev L.J., Strebkov D.S., Roschin O.A., 2010. Esperimental modeles of resonant electric power transmission systems. M. GNU VIESH, 180.

Kalashnikov A.M., Stepun A.V., 1965. Fundametals of Radio Engineering. M., 148: 34-35.

Power Engineering and Industry of Russia, 2012. November 2012, n.22 (210): 12-13.

Strebkov D.S., Necrasov A.I., 2008. Resonant methods of electric power transmission and application. Moscow, GNU VIESH, the 3rd, 350.

Strebkov D.S., 2007. Design of high voltage resonant generator. Electro, 3: 39-41.

Smirnov A.D., Antipov K.M., 1984. Reference book for power engineer. M. Energoatom publishing house, 418: 370.

Tesla N., 1886. Patents. N.Tesla Museum.

Tesla N., 2008. Colorado-Springs notes. 1899-1990. Agni Publ. house. Samara 2008: 457. (in Russian).

Tesla N., 2007. Agni Publ.house. Samara 2007: 579. (in Russian).

AFLATOXIN IN FOOD AND FEED: FOOD SAFETY ISSUES AND CONTROL

Stavros Yanniotis*, Maria Georgiadou

Agricultural University of Athens, Iera Odos 75, 11855 Athens, Greece.
E.mail:yanniotis@aua.gr

Abstract

Mycotoxin contamination of agricultural commodities is considered a serious food safety issue worldwide. Among the most dangerous mycotoxins are aflatoxins produced by Aspergillus flavus and A. parasiticus. The presence of aflatoxins represent a serious problem in cereals, nuts, dried fruits and other food products. They can be produced either in the field or during processing or storage. Their elimination from food and feed is of great concern due to the fact that they are highly toxic, mutagenic, teratogenic and carcinogenic compounds. A great number of publications concerning aflatoxin contamination of various products have been generated over the last several years of research and investigations. A review of the problem of aflatoxins in food and feed is presented with emphasis on control measures.

Keywords: aflotoxin, food, feed

Introduction

Aflatoxins are the most prominent group of mycotoxins. They are undoubtedly the most documented of all mycotoxins since they have been detected in many agricultural commodities, with significant presence in corn, wheat, cottonseed, groundnuts and tree-nuts (Smith E.J., 1997). Aflatoxins B_1, B_2, G_1 and G_2 are the four major aflatoxins, based on their blue or green fluorescence under ultraviolet light. Additionally, about a dozen other have been described, among them aflatoxin M_1, which is secreted in milk when cows metabolize aflatoxin B_1 from feed into a hydroxylated derivative. By chemical definition, aflatoxins are difuranocoumarin derivatives and they have been implicated as causative agents in human hepatic and extrahepatic carcinogenesis (Massey et al., 1995; Liu, Wu, 2010). Due to their toxic and carcinogenic effect in humans and animals, maximum tolerated levels have been established worldwide to safeguard the health of the consumers. More than a hundred countries have similar aflatoxin regulatory laws, but allowable threshold levels vary (Van Egmond, Jonker, 2005). Research on aflatoxins have gained great attention since they are the hazardous category with the highest number of notifications within EU during last decade (Annual Reports of European Rapid Alert System for Food & Feed – RASFF) representing an additional cost in the production and loss of income for producers, distributors and other stakeholders.

Causative Pathogens and Aflatoxin Formation

Aflatoxin production is confined to certain strains of Aspergillus sc Flavi as secondary metabolites. These fungi are plant pathogens that have a broad host range. They are isolated from a wide range of climate zones (Cotty, Jaime-Garcia, 2007). Contamination of food and feed by aflatoxin can occur in the field or during subsequent processing and storage. At pre-harvest stages aflatoxin contamination is associated not only with favorable environmental conditions, but also with insect and bird damage, which provide entry sites for the fungus (Doster, Michailides, 1999; Georgiadou et al., 2012). Infection with Aspergillus fungi and the presence of aflatoxin before harvest will presumably lead to further build up after harvest (Georgiadou et al., 2012; Olsen, 1999). It is also likely that infected crops will provide a source of inoculum for spread of the fungus to healthy food during inadequate processing or under poor storage conditions (Olsen, 1999). Post-harvest aflatoxin contamination can also be a problem in the case of improper storage conditions, primarily high relative humidity and insect activity.

Many biotic and abiotic factors are known to affect aflatoxin production by toxigenic strains of Aspergilli. Nutritional and environmental factors including temperature, pH and water activity have been shown to affect aflatoxin production (Yu et al., 2008). Among all factors, water activity plays a key role in the development of the fungi and aflatoxin production (Hill et al., 1985). Additionally, drought, close planting, competition from weeds, reduced fertilization and other factors that cause stress to host-plants enhance the growth of these fungi (Yu et al., 2008).

The genetics of aflatoxin synthesis has been greatly improved with the advent of the genome sequence of A.flavus and the application of molecular tools, which allow rapid genetic analysis of individual genes within the genome (Payne, Yu, 2010). This field of research has lead to a deeper understanding of the biology of this fungus and the role of fungal secondary metabolism.

Control Strategies at Pre-Harvest Stages

Both mould growth and aflatoxin production are undesirable and should be prevented. This can be achieved by preventing infection in the first place or by modifying the environment to inhibit mould growth and mycotoxin production.

Preharvest prevention

The incorporation of good agricultural practices at farm level including improved irrigation techniques, fertilizer applications, pest control will help prevent Aspergillus infection (Olsen, 1999; Codex Alimentarius, 2005). Appropriate use of fungicides during production process have been shown to effectively control Aspergillus species, but results in very limited reduction of the fungus or the toxin (Abbas et al., 2009). It is also recommended to avoid practices that disperse dust to aerial parts of the crops and manipulate the irrigation, which could limit colonisation by the fungi (Doster, Michailides, 1994).

Resistant crop lines

Efforts have been made to develop resistant commercial crop varieties that counteract A.flavus invasion and inhibit aflatoxin formation, identifying pathogen-related, insect- and drought-resistant proteins or other biochemical or genetic resistance markers (Yu et al., 2008; Abbas et al., 2009). These sources of resistance have been incorporated into breeding programmes and prototypes of genetically engineered crops were developed in corn (Naidoo et al., 2002) and peanuts (Liang et al., 2005) but have not shown adequate levels of resistance to aflatoxin producing fungi (Munkvold, 2003). Transgenic Bt peanut (Weissinger et al., 2002) and Bt corn have been also assessed for resistance to fungal colonization and aflatoxin contamination but similar studies did not chart consistent results (Odvody et al., 2000; Dowd, 2001; Abbas et al., 2008). The development of resistant hybrids appears to be a very promising technology, but commercial hybrids are still not available (Abbas et al., 2009).

Biocontrol agents

Among approaches that were investigated to manage aflatoxin contamination, biological control methods have shown great promise. Numerous organisms, including bacteria (Palumbo et al., 2006; Dalie et al., 2010), yeasts (Hua et al., 1999; Antonopoulos et al., 2012) and nontoxigenic fungal strains of A. flavus and A. parasiticus, (Cotty, Bayman, 1993; Abbas et al., 2006; Pitt, Hocking, 2006; Atehnkengab et al., 2008; Georgiadou et al., 2012) have been tested for their ability in controlling aflatoxin contamination. Positive results in reducing aflatoxin contamination have been achieved by applying nontoxigenic strains of A. flavus and A. parasiticus in fields of cotton, peanut, maize and pistachio. The idea driving this approach is that the nontoxigenic strains applied to soil occupy the same niches as the natural occurring toxigenic strains and therefore, they are capable of competing and displacing toxigenic strains. Currently, two biocontrol agents are commercially available in U.S.A: Afla-Guard registered for use on peanuts and corn and AF36 primarily registered for use on cotton and recently on pistachios. Current efforts are aimed at identifying additional atoxigenic atrains for use in other regions of the world, including Africa (Donner et al., 2010) and Europe (Georgiadou et al., 2012).

Control Strategies at Post - Harvest Stages

Preventive measures

The most important preventive measure after harvest should be to prevent further growth of the fungi and accumulation of toxin. This can be achieved by application of proper curing, drying, sorting and storage procedures. The maintenance of safety during storage and transportation depends on the moisture content, the relative humidity, the temperature and hygienic conditions (cleanliness, insect control). Although prevention is considered as the basic strategy to deal with aflatoxin contamination problem, the contamination is often unavoidable and still remains a serious problem associated with many important agricultural commodities.

Sorting

The aim of the sorting process is to eliminate products with off-standard characteristics that are related qualitative and quantitative with the presence of aflatoxigenic fungi and aflatoxin contamination. On the other hand, if aflatoxin production occurs during storage, a different distribution would arise and the removal of such contamination would be difficult. In any case, the knowledge of the physical and chemical characteristics of the agricultural product is essential for the design and operation of sorting systems. Several studies on corn (Huff, 1980; Huff, Hagler, 1982; Huff, Hagler, 1985; Pearson, Wicklow, 2006; Pearson et al., 2001), on pistachios (Pearson, 1996; Pearson, Schatzki, 1998; Pearson et al., 2001), on almonds (Pearson, 1999; Pearson, Young, 2002), on peanuts (Dickens, Whitaker, 1975) and on wheat (Pearson et al., 2008) have shown that foodstuffs most likely to be infected by moulds and contaminated with aflatoxin, have several characteristics which distinguish them from normal. The volatile profile of susceptible agricultural products has been also investigated as an early indicator of quality deterioration and possible aflatoxin contamination (Borjessön et al., 1989; Kaminski, Wasowicz, 1991; Jelen, Wasowicz, 1998; Schnürer et al., 1999; Magan, Evans, 2000). Georgiadou et al. (2013) studied the volatile profile of healthy and aflatoxin contaminated pistachios.

Additionally, efforts have been made to reduce aflatoxin contamination using sorting based on fluorescence in tree-nuts (Tyson, Clark, 1974; McClure, Farsaie, 1980; Pelletier, Reizner, 1992; Hadavi, 2005) and in corn (Shotwell et al., 1975). However, fluorescence sorting was not effective in all cases (Steiner et al., 1992). In recent years, research has been conducted to evaluate near infrared (NIR) spectroscopy as a method for aflatoxin detection in nuts (Pearson, 1999; Pearson, Young, 2002; Hirano et al., 1998; Haff, Pearson, 2006; De Mello, Scussel, 2009) and corn (Baye et al., 2006).

The X-ray imaging technique has been used to evaluate the quality in grains and nuts. Continuous line scan X-ray systems are currently available for the food industry for inspection applications involving the removal of rocks, glass, metal and bone from food commodities (Keagy et al., 1996; Williams et al., 1984; Haff, Pearson, 2007) and the detection of various fungal infections (Pearson, Wicklow, 2006; Narvankar et al., 2009) and insect damages (Keagy et al., 1996; Keagy, Schatzki, 1993; Karunakaran et al., 2004a; Karunakaran et al., 2004b). Yanniotis et al. (2011) have shown that X-ray imaging of pistachio nuts has a potential for the detection of nuts with internal necrotic spots which are correlated with aflatoxin contamination. The necrotic spot detection by X-rays is possible due to high differences in the absorption coefficient between healthy and injured tissue (Proshlyakov et al., 2013).

Decontamination and detoxification

Five main approaches are directed to the reduction or detoxification of aflatoxins in agricultural commodities: 1) food and feed processing, thermal inactivation, irradiation 2) biocontrol and microbial inactivation 3) dietary modification and chemoprevention 4) solvent extraction, chemical degradation and 5) reduction in toxin bioavailability by selective chemisorption with clays. Detoxification processes involve degradation, destruction and/or inactivation of aflatoxin (Smith E.J., 1997). In any case, the degradation products must be safe and the nutritional or palatability properties of the decontaminated commodities must not be reduced.

Even though aflatoxins exhibit high decomposition temperatures ranging from 237oC to 306 oC, the use of heat to inactivate aflatoxin in contaminated food has been attempted. However, results were not consistent and the extent of the destruction was very dependent on the initial level of contamination, heating temperature, time, moisture content, pH and ionic strength of the food (Rustom, 1997; Yazdanpanah et al., 2005). Alternatively, the use of UV and gamma radiation to inactivate aflatoxins was investigated leading to the formation of less toxic photodegradation products (Rustom, 1997). Solar energy also destroyed aflatoxins in some foods like peanuts but results from naturally contaminated samples were not encouraging indicating that when aflatoxin was present as a natural contaminant is strongly bound to the protein and appear to be less susceptible to photodegradation than the free toxin (Rustom, 1997).

Degradation or binding of aflatoxin by microbial systems is also under research (Smith E.J., 1997; Dalie et al., 2010). A decontamination method using low pressure cold plasma (LPCP) for the elimination of Aspergillus parasiticus from nut surface has been proposed by Basaran et al. (2008) but further research need to be undertaken.

The toxicity of aflatoxins may be strongly influenced by dietary chemicals that alter the normal responses of mammalian systems to these chemicals. A number of chemical factors, including nutritional components, food and feed additives, as well as other chemical compounds like oltipraz and chlorophylin, triterpenoids, sulforaphane or dietary intervention like broccoli sprouts and polyphenols in green tea, increase animals’ detoxification processes (Kensler et al., 2004) or prevent chromosomal damage (Hayes et al., 1998). Extraction with solvents such as 95 % ethanol, 90 % aqueous acetone, 80 % isopropanol, hexane-methanol, methanol-water, acetonitrile-water, hexaneethanol-water and acetone-hexane-water has been used to remove aflatoxins from the oilseeds peanut and cottonseed but materials treated in this way may only be suitable for animal feeding (Rustom, 1997). Although, no fully approved methods exist for aflatoxin detoxification in human food, ammonia either in gaseous form or as an ammonium hydroxide solution, ozonation and reaction with sodium bisulfite have been tested to degrade aflatoxins in various feedstuffs but the toxicity of the reaction products must be elucidated (Smith E.J., 1997).

Noticeable reduction in the bioavailability of the aflatoxins has been shown by the addition of phyllosilicate clays - HSCAS (Hydrated Sodium Calcium Alumino Silicate) or other organic materials (e.g. yeast cell walls) to the feed intake, which selectively chemisorb aflatoxins in the gastrointestinal tract of animals (Smith E.J., 1997). Selected calcium montmorillonite clays (e.g. NovaSil Plus, NSP) have proven to be the most highly selective and effective enterosorbents, which tightly bind and inactivate aflatoxins in the gastrointestinal tract of multiple animal species (Wang et al., 2005).

Conclusions

Aflatoxins pose a serious threat to animal and human health and efforts continue to be devoted, worldwide, to preventing or eliminating them. Research during recent years has revealed critical points on the way, the conditions and the time that aflatoxins are produced. These findings have formed the basis for coping with the problem in the pre-harvest stages and also the potential for post-harvest elimination. Pre-harvest strategy is focused in genetic improvement to develop resistance to either fungal invasion or aflatoxin formation, the use of biocompetitors in the field and improvement of cultural practices. More work needs to be done on the control of aflatoxins in the postharvest phases. Future approaches may include the development of a rapid, low-cost detection tool for monitoring the aflatoxin presence in food and feed at farm or processing level.

References

Abbas H.K., Zablotowicz R.M., Bruns H.A., Abel C.A., 2006. Biocontrol of aflatoxin in corn by inoculation with non-aflatoxigenic Aspergillus flavus isolates. Biocontrol Sci. Technol., 16(5): 437-449.

Abbas H.K., Accinelli C., Zablotowicz R.m., Abel C.A., Bruns H.A, Dong Y., Shier W.T., 2008. Dynamics of mycotoxin and Aspergillus flavus levels in aging Bt and non-Bt corn residues unser mississippi no-till conditions. J.Agric. Food Chem., 56: 7558-7585.

Abbas H.K., Wilkinson J.R., Zablotowica R.M., Accinelli C., Abel C.A, Bruns H.A., Weaver M.A., 2009. Ecology of Aspergillus flavus, regulation of aflatoxin production, and management strategies to reduce aflatoxin contamination of corn. Toxin Rev., 28: 142-53.

Antonopoulos D.F., Georgiadou M., Agoritsis S.P., Gianniotis S., Tsitsiyiannis D.I., 2012. Biological control of the toxigenic fungus Aspergillus flavus and aflatoxins that are produced to the shelled pistachio nuts “Aiginis”. 2nd Conference of Agricultural Biotechnology, Athens, 10: 4-5.

Atehnkengab J., Ojiamboac P.S., Ikotunb T., Sikorad R.A., Cotty P.J., Bandyopadhyay R., 2008. Evaluation of atoxigenic isolates of Aspergillus flavus as potential biocontrol agents for aflatoxin in maize. Food Additives and Contaminants, 25(10): 1264–1271.

Basaran P., Basaran-Akgul N., Oksuz L., 2008. Elimination of Aspergillus parasiticus from nut surface with low pressure cold plasma (LPCP) treatment. Food Microbiology, 25: 626-632.

Baye T.M., Pearson T.C., Settles A.M., 2006. Development of a calibration to predict maize seed composition using single kernel near infrared spectroscopy. J. Cereal Sci., 43(2): 236-243.

Borjessön T., Stöllman U., Adamek P., Kaspersson A., 1989. Analysis of volatile compounds for detection of moulds in stored cereals. Cereal Chemistry, 66: 300-304.

Codex Alimentarius, 2005. “Code of Practice for the prevention and reduction of aflatoxin contamination in tree nuts” CAC/RCP, 59.

Cotty P.J., Bayman P., 1993. Competitive exclusion of a toxigenic strain of Aspergillus flavus by an atoxigenic strain. Phytopathology, 83: 1283-1287.

Cotty P.J., Jaime-Garcia R., 2007. Influences of climate on aflatoxin producing fungi and aflatoxin contamination. International Journal of Food Microbiology, 119: 109-115.

Dalie D.K.D., Deschamps A.M., Richard-Forget F., 2010. Lactic acid bacteria – Potential for control ofmould growth and mycotoxins: A review. Food Control, 21: 370-380.

De Mello F.R., Scussel V.M., 2009. Development of physical and optical methods for in-shell brazil nuts sorting and aflatoxin reduction. Journal of Agricultural Science, 1(2): 3-14.

Dickens J.W., Whitaker T.B., 1975. Efficacy of electronic color sorting and hand picking to remove aflatoxin contaminated kernels from commercial lots of shelled peanuts. Peanut Sci., 2(2): 45-50.

Donner M., Atehnkengab J., Sikorad R.A., Bandyopadhyay R., Cotty P.J., 2010. Molecular characterization of atoxigenic strains for biological control of aflatoxins in Nigeria. Food Addit.Contam., 27: 576-590.

Doster M.A., Michailides T.J., 1994. Development of Aspergillus moulds in litter from the pistachio trees. Plant disease, 78(4): 393-397.

Doster M.A., Michailides T.J., 1999. Relationship between Shell Discoloration of Pistachio Nuts and Incidence of Fungal Decay and Insect Infestation. Plant Disease, 83(3): 259-264.

Dowd P.F., 2001. Biotic and abiotic factors limiting efficacy of Bt corn in indirectly reducing mycotoxin levels in commercial fields, J.Econ.Entomol.,94: 1067-1074.

Georgiadou M., Agoritsis S.P., Vichou K., Vardouniotis G., Yanniotis S., Paplomatas E.I., Cotty P.J., Tsitsiyiannis D.I., 2012. Genetic and molecular characterization and evaluation of the Greek non-toxigenic isolations of the fungi Aspergillus as potential biocontrol agents against aflatoxins. 16th Hellenic Congress in Phytopathology, Salonica, 10: 16-18.

Georgiadou M., Dimou A., Yanniotis S., 2012. Aflatoxin contamination in pistachio nuts: A farm to storage study. Food Control, 26, 2012, p. 580-586.

Georgiadou M., Gardeli Chr., Komaitis M., Tsitsigiannis D.I., Paplomatas E.J., Yanniotis S., 2013. Volatile compounds of healthy and aflatoxin contaminated pistachios, paper in preparation.

Hadavi E., 2005. Several physical properties of aflatoxin-contaminated pistachio nuts: Applicattion of BGY fluorescence for separation of aflatoxin – contaminated nuts, Food Additives & Contaminants, 22(11): 1144-1153.

Haff R.B., Pearson T.C., 2006. Spectral band selection for optical sorting of pistachio nuts defects. Trans. ASABE, 49(4): 1105-1113.

Haff R.B., Pearson T.C., 2007. An automatic algorithm for detection of infestation in X-ray images of agricultural products. Sensing Instr. Food Qual. Safety, 1(3): 143-150.

Hayes J.D., Pulford D.J., Ellis E.M., McLeod R., James R.F.L., Seidegard J., Mosialou E., Jernstrom B., Neal G.E., 1998. Regulation of rat glutathione-S-transferase A5 by cancer chemopreventive agents: mechanisms of inducible resistance to aflatoxin B1. Chemico-Biological Interactions 111/112: 51–67.

Hirano S., Okawara N., Narazaki S., 1998. Near infrared detection of internally mouldy nuts. Biosci. Biotechnol. Biochem., 62(1): 102-107.

Hill A.R., Wilson D.M., McMillian W.W., Widstrom N.W., Cole R.J., Sanders T.H., Blankenship P.D., 1985. «Ecology of the Aspergillus flavus group and aflatoxin formation in maize and groundnut», Proceedings of the International mycotoxin symposium Sydney – Australia, Trichothecenes and Other Mycotoxins Ed. J.Lacey, 8: 79-95.

Hua S.S.T., Baker J.L., Flores-Espiritu M., 1999. Interactions of saprophytic yeasts with a nor mutant of Aspergillus flavus. Appl. Environ. Microbiol., 65(6): 2738-2740.

Huff W.E., 1980. A physical method for the segregation of aflatoxin-contaminated corn. Cereal Chem.,57: 236-238.

Huff W.E., Hagler W.M., 1982. Evaluation of density segregation as a means to estimate the degree of aflatoxin contamination of corn. Cereal Chem., 59(2): 152-154.

Huff W.E., Hagler W.M., 1985. Density segregation of corn and wheat naturally contaminated with aflatoxin, deoxynivalenol and zearalenone. J.Food Prot., 48(5): 416-420.

Jelen H., Wasowicz E., 1998. Volatile fungal metabolites and their relation to the spoilage of agricultural commodities. Food Reviews International, 14: 391-426.

Kaminski E., Wasowicz E., 1991. The usage of volatile compounds produced by moulds as indicators of grain deterioration. In: Cereal grain: mycotoxins, fungi and quality in drying and storage,edited by J.Chelkowski Amsterdam, Netherlands: Elsevier, 229-280.

Karunakaran C, Jayas D.S., White N.D.G., 2004a. Detection of internal wheat seed infection by Rhyzopertha dominica using X-ray imaging. Journal of Stored Products Research, 40: 507-516.

Karunakaran C, Jayas D.S., White N.D.G., 2004b. Identification of wheat kernels damaged by the red flour beetle using X-ray images. Biosystems Engineering, 87(3): 267-274.

Keagy P.M., Schatzki T.F., 1993. Machine recognition of weevil damage in wheat radiographs. Cereal Chemistry, 70: 696-700.

Keagy P.M., Parvin B., Schatzki T.F., 1996. Machine recognition of Navel Orange Worm Damage in X-ray images of pistachio nuts. Lebensm.-Wiss. u. Technol., 29: 140-145.

Kensler T.W., Egner P.A., Wang J.B., Zhu Y.R., Zhang B.C., Lu P.X., Chen J.G., Qian G.S., Kuang S.Y., Jackson P.E., Gange S.J., Jacobson

L.P., Munoz A., Groopman J.D., 2004. Chemoprevention of hepatocellular carcinoma in aflatoxin endemic areas. Gastroenterology, 127: 310–318.
Liang X., Holbrook C.C., Lynch R.E., Guo B.Z., 2005. Beta-1,3-glucanase activity in peanut seed (Arachis hypogaea) is induced by inoculation with Aspergillus flavus and copurifies with a conglutin-like protein. Phytopathology, 95: 506-511.
Liu Y., Wu F., 2010. Global burden of aflatoxin-induced hepatocellular carcinoma: a risk assessment. Environ. Health Perspect, 118: 818-824.
Magan N., Evans P., 2000. Volatiles as an indicator of fungal activity and differentiation between species and the potential use of electronic nose technology for early detection of grain spoilage. Journal of Stored Products Research, 36: 319-340.
Massey T.E., Stewart R.K., Daniels L.M., Ling L., 1995. Biochemical and molecular aspects of mammalian susceptibility to aflatoxin B1 carcinogenicity. Proceed. Soc. Exp. Biol. Med., 208: 213-227.
McClure W.F., Farsaie A., 1980. Dual-wavelength fiber optic photometer measures fluorescence of aflatoxin contaminated pistachio nuts. Trans. ASAE, 23(1): 204-207.
Munkvold G.P., 2003. Cultural and genetic approaches to managing mycotoxins in maize. Annual Review of Phytopathology, 41: 99-116.
Naidoo G., Forbes A.M., Paul C., White D.G., Rocheford T.R., 2002. Resistance to Aspergillus ear rot and aflatoxin accumulation in maize F1 hybrids. Crop Sci., 42: 360-364.
Narvankar D.S., Singh C.B., Jayas D.S., White N.D.G., 2009. Assessment of soft X-ray imaging for detection of fungal infection in wheat. Biosystems Engineering, 103: 49-56.
Odvody G.N., Chilcutt C.F., Parker R.D., Benedict J.H., 2000. Aflatoxin and insect response of near-isogenic Bt and non-Bt commercial corn hybrids in South Texas. In Proc. Aflatoxin/Fumonisin Workshop, ed. Robens JF. Beltsville MD: USDA-ARS.
Olsen M., 1999. Mycotoxin Prevention and Decontamination. Case study: Prevention of aflatoxins in pistachio. MYC-CONF/99/6d
Palumbo J.D., Baker J.L., Mahoney N.E., 2006. Isolation of bacterial antagonists of Aspergillus flavus from almonds. Microb. Ecol., 52(1): 45-52.
Pearson T.C., Wicklow D.T., 2006. Detection of corn kernels infected by fungi. Trans. ASABE, 49(4): 1235-1245.
Pearson T.C., Wicklow D.T., Maghirang E.B., Xie F., Dowell F.E., 2001. Detecting aflatoxin in single corn kernels by transmittance and reflectance spectroscopy. Trans. ASAE, 44(5): 1247-1254.
Pearson T.C., 1996. Machine vision system for automated detection of stained pistachio nuts. Lebensm.Wiss.-Technol., 28(6): 203-209.
Pearson T.C., Schatzki T.F., 1998. Machine Vision System for Automated Detection of Aflatoxin-Contaminated Pistachios, J.Agric.Food.Chem., 46: 2248-2252.
Pearson T.C., Doster M.A., Michailides T.J., 2001. Automated Detection of pistachio defects by machine vision" Applied Engineering in Agriculture, 17: 81-84.
Pearson T.C., 1999. Use of near infrared transmittance to automatically detect almonds with concealed damage. Lebensmittel-Wissenschaft und Technologie, 32(2): 73-78.
Pearson T.C., Young R., 2002. Automated sorting of almonds with embedded shell by laser transmittance imaging. Applied Eng. Agric., 18(5): 637-641.
Pearson T.C., Brabec D., Haley S., 2008. Color image based sorter for separating red and white wheat. 2(4): 280-288.
Payne G.A., Yu J., 2010. Ecology, development and gene regulation in Aspergillus flavus. In Aspergillus:Molecular Biology and Genomics, ed. M.Machida, K.Gomi., Norwich, UK:Caister Acad. Press., 157-171.
Pelletier M.J., Reizner J.R., 1992. Comparison of fluorescence sorting and color sorting for the removal of aflatoxin from large groups of peanuts. Peanut Sci., 19(1): 15-20.
Pitt J.I., Hocking A.D., 2006. Mycotoxins in Australia: biocontrol of aflatoxin in peanuts. Mycopathologia, 162(3): 233-243.
Proshlyakov A., Yanniotis S., Blahovec J., 2013. Pistachio deterioration detected by X-ray Absorption. Czech Journal Food Science, 31(2): 126-131.
Rustom I.Y.S., 1997. Aflatoxin in food and feed: occurrence, legislation and inactivation by physical methods. Food Chemistry, 59(1): 57-67.
Schnürer J., Olsson J., Börjesson T., 1999. Fungal volatiles as indicators of food and feeds spoilage. Fungal Genetics and Biology, 27: 209-217.
Shotwell O.L., Goulden M.L., Jepson A.M., Wolck W.F., Hesseltine C.W., 1975. Aflatoxin occurrence in some white corn under loan. Association with bright greenish-yellow fluorescence in corn. Cereal Chem., 52: 670-677.
Smith E.J., 1997. Aflatoxins in "Handbook of Plant and Fungal Toxicants" Ed. by J.P.Felix O'Mello, CRC Press New York , 19: 269-285.

Steiner W.E., Brunschweiler K., Leimbacher E., Schneider R., 1992. Aflatoxins and fluorescence in brazil nuts and pistachio nuts. J.Agric.Food Chem., 40(12): 2453-2457.

Tyson T.W., Clark R.L., 1974. An investigation of the fluorescent properties of aflatoxin infected pecans. Trans.ASAE, 17(5): 942-945.

Van Egmond H.P., Jonker M.A., 2005. Worldwide regulations on aflatoxins p.77-93 ed.Abbas H.K. Aflatoxin and Food Safety, Boca Raton, FL:CRC Press.

Wang J.S., Luo H., Billam M., Wang Z., Guan H., Tang L., Goldston T., Afriyie-Gyawu E., Lovett C., Griswold J., Brattin B., Taylor R.J., Huebner H.J., Phillips T.D., 2005. Short-term safety evaluation of processed calcium montmorillonite clay (NovaSil) in humans. Food Additives and Contaminants, 22: 270–279.

Weissinger A., Wu M., Liu Y.S., Ingram K., Rajasekaran K., Cleveland T.E., 2002. Development of transgenic peanut with enhanced resistance against preharvest aflatoxin contamination, Mycopathologia, 155: 97.

Williams D., Sawyer C., Conklin W.C., Robe K., 1984. X-ray scanner removes stones from almonds on conveyor belt. Food Processing, 44(11): 56-57.

Yanniotis S., Proshlyakov A., Revithi A., Georgiadou M., Blahovec J., 2011. X-ray imaging for fungal necrotic spot detection in pistachio nuts. Procedia Food Science, 1: 379-384.

Yazdanpanah H., Mohammadi T., Abouhossain G., Cheraghali A.M., 2005. Effect of roasting on degradation of aflatoxins in contaminated pistachio nuts. Food and Chemical Toxicology, 43: 1135-1139.

Yu J., Payne G.A., Campbell B.C., Guo B., Cleveland T.E., Robens J.F., Keller N.P., Bennett J.W., Nierman W.C., 2008. Mycotoxin Production and Prevention of Aflatoxin Contamination in Food and Feed. Gustavo H.Goldman & Stephen A.Osmani «The Aspergilli», Mycology, 26, CRC Press, 27: 457-472.

THE INFLUENCE OF LOW RATE WATER VAPOR CONDENSATION TO PERFORMANCE OF SENSIBLE HEAT RECOVERY

Daniel Adamovsky*

University Centre for Energy Efficient Buildings, Czech Technical University in Prague, Nam. Sitna 3105, Kladno, Czech Republic, Phone: +420 224 354 316; E-mail: daniel.adamovsky@fsv.cvut.cz

Abstract

The article describes influence of low rate of water vapor condensation to the performance of flat-plate compact air-to-air heat recovery heat exchanger in a ventilation unit. For evaluation besides sensible, latent and overall efficiency exergy analysis is also used. Exergy based approach to tested heat exchanger balance determines whether additional heat flux due to condensation is used efficiently.

Keywords: low rate water, heat recovery

Introduction

In buildings with high ventilation requirements are applied strict rules of energy policy. For appropriate annual performance of entire ventilation system highly efficient heat recovery must be applied transferring as much as possible of heat from exhaust to outside air (El Fouih et al., 2012.. Water vapor condensation affect actual performance and however it is usually in overall analysis of heat recovery neglected, it needs to be examined. This is important mainly for indoor environments with high moisture production such as stables, or swimming pool halls.

Heat exchanging surface in compact heat exchangers is created from multiple parallel plates providing air flow channels. Each plate is exposed on one side to outside air and on the other side to exhaust air. If cooled by outside air so the surface temperature drops below the dew point temperature of exhaust air, condensation of water vapor occurs. Condensation causes droplets or very thin water layer in compare to thickness of heat exchanging plate or width of flow channel. If more intense condensation occurs, drained condensate flowing on the surface may in extreme glut air flow channels. Large compact heat exchangers may also experience cooling of the surface due to flow of liquid condensate together with back evaporation into air stream. The article presents analysis of air-to-air sensible heat type heat exchanger with low rate water vapour condensation and discussion whether it is preferable to avoid condensation at all or utilize a positive influence.

Two air flows pass through a heat recovery heat exchanger; outside air of mass flow rate m_e and exhaust air of mass flow rate m_i. Temperature of outside air is lower than the dew point temperature of exhaust air so at a part of heat exchanging surface water vapor condensation from exhaust air occurs and the heat transfer rate includes also latent heat (Fig. 1).

Heat exchangers efficiency η defines ratio of actual heat transfer rate Q from exhaust indoor air i to outside air e to the maximum possible heat transfer rate Q_{max} as in (1) (Shah, Sekulic, 2003).

$$\eta = \frac{Q}{Q_{max}} \tag{1}$$

The heat transfer rate is obtained from the energy balance of both outside and exhaust air flows neglecting any heat losses. In the case of water vapor condensation from exhaust air, heat balance (2) contains on the right side heat transfer rate associated with the condensate drained from the heat exchanger. It is assumed that condensed water as it leaves heat exchanger has the same temperature as air flow i at the outlet.

$$Q = m_e(h_{e2} - h_{e1}) = m_i[(h_{i1} - h_{i2}) - (x_{i1} - x_{i2}) \cdot h_w] \tag{2}$$

The heat transfer rate Q is in (3) to (5) expressed in sensible and latent heat parts. This division to both parts of transfer rate is simplified, as both occur simultaneously and influence each other if condensation occurs. The influence of sensible Q_S and latent Q_L heat flux transferred from exhaust air in transfer rate Q to the change of specific enthalpy of outside air (h_{e2}-h_{e1}) with respect to (2) is as follows.

Theoretical Analysis

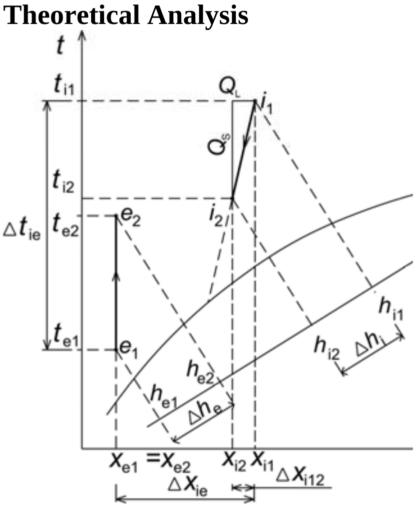

A	Area of heat exchanging surface [m²]		*Subscripts*
C	Air flow stream heat capacity, [W/K]	e	exterior(outside) air
c_p	Specific heat capacity, [J/(kg.K)]	ex	exergy
E	Exergy of a heat flux, [W]	i	indoor exhaust air
ΔE	Dissipation rate, [W]	L	latent heat
h	Specific enthalpy, [J/(kg.K)]	min	minimum value
l_{23}	Latent heat of evaporation, [J/kg]	max	maximum value
$LMTD$	Log mean temperature difference [K]	S	sensible heat
m	Mass flow rate of dry air, [kg_{da}/s]	da	dry air
Q	Heat transfer rate, [W]	w	water
T	Thermodynamic temperature, [K]	wv	water vapor
t	Temperature, [°C]	0	dead state for exergy analysis
U	Overall heat transfer coefficient [W/(m².K)]	1	inlet
x	Specific humidity, [kg_{wv}/kg_{da}]	2	outlet
η	Efficiency, [-]		

Fig. 1 Nomenclature and scheme of moist air processes in outside air *e* and exhaust air *i*

$$Q = Q_S + Q_L = m_e \Delta h_{e,S} + m_e \Delta h_{e,L};\ Q_S = U \cdot A \cdot LMTD \tag{3}$$

$$\Delta h_{e,S} = \frac{Q_S}{m_e} = \frac{m_i \left[c_{p,da}\left(t_{i1} - t_{i2}\right) + c_{p,wv}\left(x_{i1}t_{i1} - x_{i2}t_{i2}\right) - c_{p,w}t_{i2}\left(x_{i1} - x_{i2}\right)\right]}{m_e} \tag{4}$$

$$\Delta h_{e,L} = \frac{Q_L}{m_e} = \frac{m_i\left[\left(x_{i1} - x_{i2}\right)l_{23}\right]}{m_e} \tag{5}$$

Sensible heat flux Q_S could be also expressed on the basis of overall heat transfer coefficient U through entire heat exchanging surface and log mean temperature difference (3).

Maximum possible heat transfer rate in ideal counter-current heat exchanger with infinite surface area and zero heat losses is defined in literature on the basis of difference between inlet air temperatures t_{i1} and t_{e1} (6) (Shah, Sekulic, 2003; Kays, London, 1998). This applies of sensible heat only (6). Latent heat maximum heat transfer rate has similar description based on difference between inlet air specific humidity x_{i1} and x_{e1} (7). On behalf of both sensible and latent, maximum heat transfer rate is expressed by difference between inlet air specific enthalpy h_{i1} and h_{e1} (8).

$$Q_{max,S} = C_{min}\left(t_{i1} - t_{e1}\right) \tag{6}$$

$$Q_{max,L} = m_{min}\left(x_{i1} - x_{e1}\right)l_{23} \tag{7}$$

$$Q_{max} = m_{min}\left(h_{i1} - h_{e1}\right) \tag{8}$$

Applying separately each partial heat flux against its maximum into (1) will result in three efficiencies – sensible heat efficiency η_S, latent heat efficiency η_L, and overall efficiency η.

$$\eta_S = \frac{Q_S}{Q_{max,S}} = \frac{m_i\left[c_{p,sv}\left(t_{i1} - t_{i2}\right) + c_{p,vp}\left(x_{i1}t_{i1} - x_{i2}t_{i2}\right) - c_{p,w}t_{i2}\left(x_{i1} - x_{i2}\right)\right]}{C_{min}\left(t_{i1} - t_{e1}\right)} \approx \frac{C_i\left(t_{i1} - t_{i2}\right)}{C_{min}\left(t_{i1} - t_{e1}\right)} = \frac{C_e\left(t_{e2} - t_{e1}\right)}{C_{min}\left(t_{i1} - t_{e1}\right)} \tag{9}$$

$$\eta_L = \frac{Q_L}{Q_{max,L}} = \frac{m_i\left(x_{i1} - x_{i2}\right)l_{23}}{m_{min}\left(x_{i1} - x_{e1}\right)l_{23}} = \frac{m_i\left(x_{i1} - x_{i2}\right)}{m_{min}\left(x_{i1} - x_{e1}\right)} \tag{10}$$

$$\eta = \frac{Q}{Q_{max}} = \frac{m_i\left[c_{p,sv}\left(t_{i1} - t_{i2}\right) + c_{p,vp}\left(x_{i1}t_{i1} - x_{i2}t_{i2}\right)\right] + m_i\left[\left(x_{i1} - x_{i2}\right)l_{23}\right]}{m_{min}\left(h_{i1} - h_{e1}\right)} \tag{11}$$

Exergy analysis will help in detection how increased heat transfer rate due to water vapor condensation is usefully utilized. Exergy represents not only heat transfer rate, but also quality in terms of usability. Basically a heat transfer rate between higher temperatures has higher usability than between lower temperatures, although the temperature difference is identical. Thus exergy states potential of energy availability. Exergy of air flow heat flux represents (12), which is agreement with (Bejan, 1997) if pressure drop of heat exchanger is neglected.

$$E = Q\left(1 - \frac{T_0}{T}\right) = m(h - h_0)\left(1 - \frac{T_0}{T}\right) \qquad (12)$$

Heat recovery heat exchanger balance of exergies at inlets and outlets follows (13), where ΔE is dissipation rate, which means unutilized exergy. That is the key value for following analysis as it is desired to decrease ΔE utmost.

$$E_{e1} + E_{i1} = E_{i2} + E_{e2} + \Delta E \qquad (13)$$

Exergy analysis has important requirement in setting of dead state condition as a benchmark for all considered exergies. Usually temperature T_0 is established, but in case of moist air processes with changes of water vapor content it is necessary to define the dead state as any other moist air state with 3 properties. Atmospheric pressure together with temperature T_0 = 273.15 K, specific humidity x_0 = 0 g_{wv}/kg_{da} was defined. Dead state significantly influence quantity of exergy, discussion in case of sensible heat transfer in a heat exchanger has (Boelman, Sakulpipatsin, 2004).

Measurements

Experiment was performed in the Demonstrational Laboratory of Building Services at Faculty of Civil Engineering Czech Technical University in Prague. Measured data were obtained on air-handling unit Duplex TC CHW 1500 with horizontally located plastic counter-current heat recovery heat exchanger with total area A = 99,87 m^2.

Measured values represent velocity of air flows, air temperature and relative humidity at heat exchanger inlets and outlets. Velocities were measured in straight circular ducts 250 mm diameter at the inlets of outside and exhaust air. Sensors were rotating vanes FV A915 S220 with accuracy ±3 % of measured value. Air temperatures were measured at all inlets and outlets, three temperature sensors were located near air inlet/outlet distanced 330 mm from each other. Totally 12 NiCr-Ni (type K) temperature sensors were applied. Maximum deviation defined by sensor producer is ±1.5 °C. Air flow relative humidity was measured using single capacitive humidity sensor FHA 646 E1 located at each inlet and outlet. Humidity and temperature measuring accuracy of these sensors is 2% and 0.3 K respectively.

Measured states were limited to one operational state with balanced air flows. Final air mass flow rates were m_i = 0.160 kg_{da}/s and m_e = 0.156 kg_{da}/s. Measurement was carried in late winter conditions when outside air temperature was between 9 to 13.2 °C and exhaust air inlet temperature was between 25.5 to 26.7 °C. Humidity of exhaust air was controlled by a steam humidifier between 50 to 61.8 %. In most cases exhaust air at outlet was saturated. Observed condensation on heat exchanging plates had form of small local droplets. Weight of condensed water could not be accurately determined. Finally 46 air states were obtained.

Results

The main parameter hereafter discussed is condensation rate described in terms of difference between specific humidity of exhaust air inlet and outlet. Results of experiments depict Fig. 2.

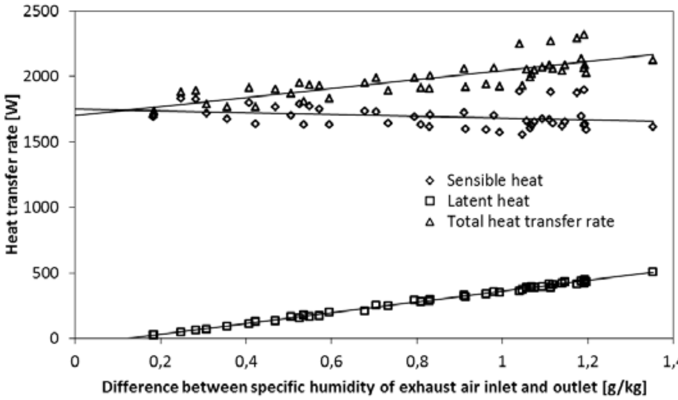

Fig. 2 Heat transfer rate against difference of exhaust air inlet and outlet specific humidity
(Trend lines: Total: y = 343.61x + 1701.5, R^2 = 0.66; Sensible: y = -67.202x + 1751.1, R^2 = 0.064; Latent: y = 410.82x – 49.651, R^2 = 0.99)

Three lines show trends in latent, sensible and total heat transfer rate against condensed water vapor from exhaust air. Basically with rising difference between specific humidity x_{i1} and x_{i2} due to water vapour condensation total heat grows on account of linearly increasing latent heat flux. The maximum achieved difference was 1.35 g_{wv}/kg_{da} and resulting condensing rate was 0.227 g_{wv}/s, so the latent heat of water vapor condensation enhanced the heat transfer rate for 509 W (24 % of 2125 W). Experimental data were validated comparing calculated heat transfer rate Q_e and Q_i. Data considered for following evaluation are within acceptable error band of -5 to +10 % (Seara et al., 2011).

Discussion

Increase of heat transfer Q rate due to water vapor condensation in exhaust air causes rise of specific enthalpy of heated exterior air h_{e2} (5) as well as temperature t_{e2}. Increase of both properties linearly depends on latent heat flux. Every gram of condensed water vapor increases heat transfer rate for 360 W and outlet heated air temperature for 2.5 K.

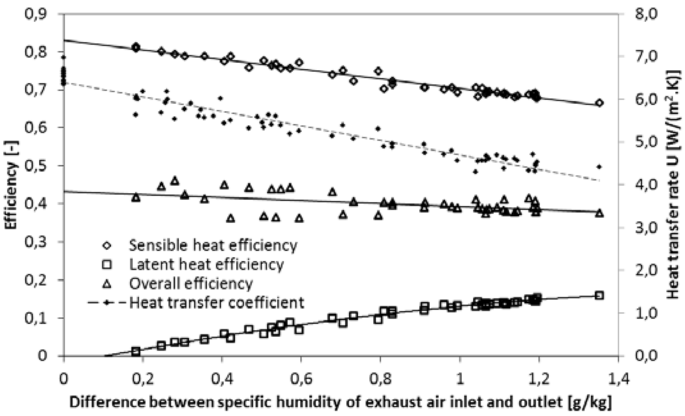

Fig. 3 Resulting efficiency and overall heat transfer coefficient
(Trend lines: Overall: y = -0.04x + 0.4331, R^2 = 0,27; Sensible: y = -0.1271x + 0.8306, R^2 = 0.96; Latent: y = $-0.0063x^3 - 0.0404x^2 + 0.1984x + 0.0207$, R^2 = 0,98; U: y = -1,7x + 6,4, R^2 = 0.94)

Sensible, latent and overall efficiency of the tested heat exchanger according to (9), (10), (11) presents Fig. 3. With rising intensity of water vapor condensation obviously increases the latent heat efficiency η_L. In (10) numerator increase with rising difference between specific humidity of exhaust air at the inlet and outlet of the heat exchanger thus the latent heat transfer rate Q_L also increase. Despite of this, η_L reaches maximum value only 16 % utilizing less than 1/6 of maximum transfer rate $Q_{max,L}$. Flat-plate compact heat exchangers due to separation of air flows have strong limitation in utilization of latent heat potential. This is in accordance with results published in (Seara et al., 2011).

It is noticeable from Fig. 3 that sensible heat efficiency η_S decreases. Values reach range from 66 to 81 % - this corresponds to temperature efficiency provided by heat exchanger producer. Sensible heat transfer rate Q_S following (9) is not directly dependent on condensation rate, but grows with higher difference between temperatures of air flows inlets (t_{i1}-t_{e1}), the same is observed for maximum sensible heat transfer rate $Q_{max,S}$ (Fig. 4). But transferred sensible heat Q_S rises slower than potential $Q_{max,S}$ may suggest, so η_S decreases. Due to water vapour condensation drops overall U (Fig. 3) of heat transfer in the heat exchanger (3). When droplets occur on the heat exchanging plate, simultaneously direct convective heat transfer from exhaust air into solid plate is influenced. It is supposed that partially convective heat transfer is locally hindered where water droplets occur and backward evaporation into exhaust air may arise as well. This may be proved by saturated exhaust air at heat exchanger outlet. It is complicated phenomena, so the explanation for this case is simplified.

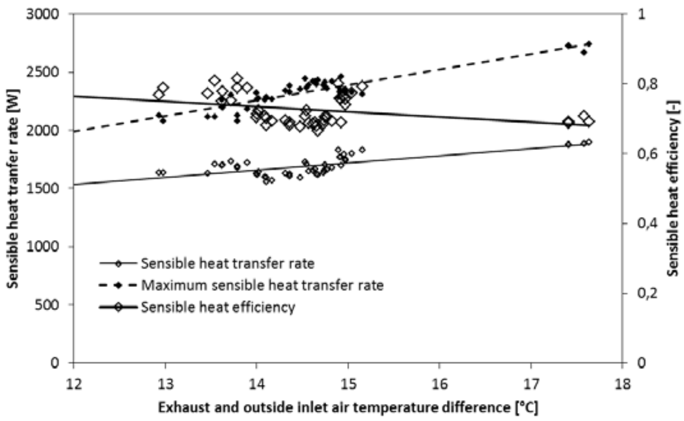

Fig. 4 The progress of sensible heat transfer rate and sensible efficiency across measured data (Trend lines: Sensible: y = 61,70x + 794,25, R^2 = 0,54; Max. sensible: y = 133,30x + 393,16
R^2 = 0,84; Sensible heat eff.: y = -0,0147x + 0,9416, R^2 = 0,13)

Overall efficiency η comprises both sensible and latent heat in heat transfer rate. As the latent heat efficiency is quite small, so does the overall efficiency. Obtained results are from 36 % to 46 %. The reason lies in low utilization of latent heat potential and as discussed above a part of sensible heat transfer rate is unutilized. In overall view less than half of entire potential provided by difference of specific enthalpy (h_{i1}-h_{e1}) is utilized. Among plate heat exchangers only total heat exchangers can provide significantly higher transfer of latent heat due to direct transfer of water vapor through a dividing membrane (Kwak, Bai, 2009).

Despite of limited use of latent heat potential in regular compact heat exchanger still the question of efficient use is important. In ventilation of moisture loaded indoor environments condensation of water vapor in heat recovery devices often occurs, so it is desirable to recognize its profitability. The answer gives exergy analysis in progress of dissipation rate ΔE from heat exchanger exergy balance (13) (Fig. 5).

The difference (E_{i1}-E_{i2}) between exhaust air exergy of heat flux between the inlet and outlet increase with rising amount of condensed water vapor, so energy potential available for outside air increase. The aim of efficient utilization lay in maximization of (E_{i1}-E_{i2}) and increase of (E_{e2}-E_{e1}). Maximizing (E_{i1}-E_{i2}) means to recover from exhaust air maximum possible energy thus decrease E_{i2}, which states leaving potential in exhaust air after heat exchanger. Measurement results show small grows of (E_{i1}-E_{i2}), so exhaust air still contains usable energy in forms of sensible and latent heat as well. Solution for further utilization may be in two-pass heat exchangers serially connected.

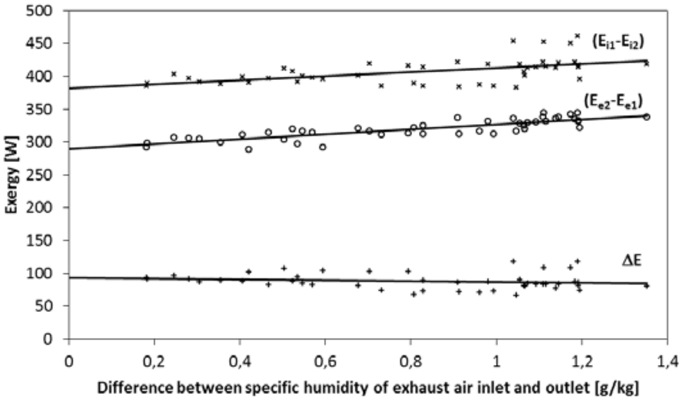

Fig. 5 Exergy balance
(Trend lines: (E_{i1}-E_{i2}): y = 31,066x + 381,92, R^2 = 0,28; (E_{e2}-E_{e1}): y = 37,26x + 289,11, R^2 = 0.70; ΔE: y = -6,1939x + 92,812, R^2 = 0,03)

Trend line of (E_{e2}- E_{e1}) increases and proves utilization of latent heat in the outside air flow. The growth of (E_{e2}-E_{e1}) in the state of maximum measured condensation is nearly the same as growth of (E_{i1}-E_{i2}) in the same state, both lines are almost parallel. This demonstrates full utilization of latent heat from exhaust air water vapor condensation. Support for this conclusion is visible in the line of dissipation rate ΔE, which is constant irrespective to the amount of condensed water vapor (ΔE trend line 3.4% drop is neglected due to measurement accuracy). In tested heat exchanger maximum value of ΔE was 118 W, which is 14 % of exergy of exhaust air at the inlet E_{i1}. Dissipation rate quantify irreversible transformation of energy thus any optimization approach need to decrease this rate with benefit to E_{e2}.

Conclusion

Condensation of water vapor in sensible heat recovery devices causes additional heat flux transferred from exhaust air into heat exchanging plate and then to outside air. Concurrently convective heat transfer is also influenced. Despite of negative influence and limited utilized potential of latent heat, the total heat transfer rate increases while low rate of water vapor condensation occurs. The utilized portion in a heat exchanger designed for sensible heat transfer is smaller than 1/6 of maximum latent heat transfer rate, but constant dissipation rate with rising condensation rate proves that it is efficiently used in the outside air flow. Thus the latent heat is not dissipated as anergy. Its significance is not large as it would be in a regenerative type of air-to-air heat recovery exchanger, but should not be neglected mainly in moisture loaded indoor environments and need not to be avoided.

Acknowledgement

This work has been supported by the European Union, OP RDI project No. CZ.1.05/2.1.00/03.0091 – University Centre for Energy Efficient Buildings.

References

Bejan A., 1997. Advanced Engineering Thermodynamics. New York: John Wiley and Sons, Inc., 850, 2nd edition.
Boelman E.C., Sakulpipatsin P., 2004. Critical analysis of exergy efficiency definitions applicable to buildings and building services. In: Proceedings of Plea2004 - The 21th Conference on Passive and Low Energy Architecture, Eindhoven, 6.
El Fouih Y., Stabat P., Rivière P., Hoang P., Archambault V., 2012. Adequacy of air-to-air heat recovery ventilation system applied in low energy buildings. Energy and Buildings, 54: 29–39.
Kays W.M., London A.L., 1998. Compact heat exchangers. Krieger Publishing Co, Florida, 335, 3dr eddition, reprint.
Kwak K., Bai C., 2009. A study on performance improvement of corrugated type total heat exchanger considering the structure of flow passage on surface. Journal of Mechanical Science and Technology, 23: 1528-1535.
Seara J.F., Diz R., Uhiá F.J., Dopazo A., Ferro J.M., 2011. Experimental analysis of an air-to-air heat recovery unit for balanced ventilation systems in residential buildings. Energy Conversion and Management, 52: 635–640.
Shah R.K., Sekulic D.P., 2003. Fundamentals of heat exchanger design. J. Wiley and Sons, New Jersey, 941.

HORIZONTAL GROUND HEAT EXCHANGERS – SOURCE OF ENERGY FOR HEAT PUMPS

Radomír Adamovský, Pavel Neuberger, Michaela Šeďová

Czech University of Life Sciences Prague, 16521 Prague 6 – Suchdol, Czech Republic, Phone: +420 22438 4176 Fax: +42023438 1828, E-mail: adamovsky@tf.czu.cz

Abstract

The objective of our study was to measure temperatures and analyse temperature changes in the ground massif with a horizontal linear heat exchanger and a slinky coil heat exchanger, both of which are used as sources of energy for heat pumps. Assess the regeneration ability of the energy potential of the ground massif during the heat exchangers' operating stagnation period. Furthermore, to determine specific thermal outputs extracted from the ground massif and assess the possibilities of increasing the heat exchangers' outputs.

Keywords: energy, horizontal linear heat exchanger, slinky coil heat exchanger, heat pumps

Introduction

A global review of the utilisation of geothermal energy for direct consumption (Lund et al., 2011), based on an investigation conducted in 78 countries, showed that in 2009 the total installed output of geothermal sources amounted to 48,493 MW. Acquired from these sources was 423,830 TJ of thermal energy per year. Approximately 47.2 % of this energy was acquired by using heat pumps of the ground–water type. Heat from the soil or ground massif is utilised through horizontal and vertical heat exchangers constructed from polyethylene tubes resistant against point loads and development of cracks. Installation of horizontal ground heat exchanger is compared to vertical ground heat exchangers which are less demanding on investment, but an adequate area is required to install them. Horizontal ground heat exchangers are available in three basic configurations – linear, helix and slinky coil. All three configurations were tested in year-round trials conducted at the Research Centre for Energy and Environment in Lecce, Italy (Congedo et al., 2012). Monitored were the flows of heat extracted by ground heat exchangers, as well as temperatures of the surrounding ground massif. The monitoring showed that the most important parameters from the heat flow from the ground massif point of view are the coefficient of thermal conductivity of the ground massif, and the velocity of the heat-carrying fluid flowing inside the exchanger's tubes. Installation depth of the heat exchanger in the ground massif did not play an important role. From the point of view of configuration geometry, as best was judged the horizontal helix heat exchanger. Song et al. (2006) analysed the most important parameters which have an effect on the value of the coefficient of thermal conductivity of the ground massif. Experiments conducted showed that the coefficient of thermal conductivity of the ground massif of temperature 10 – 40 °C reaches, at normal humidity, an average value of 2.3 W/m.K, in a dry state 0.55 – 0.6 W/m·K, and in moist soil 2.7 W/m.K. With the growing moisture content in the soil, the coefficient of thermal conductivity increases, however this increasing trend is gradually reduced. When the moisture content exceeds a certain concrete value, thermal conductivity then remains almost constant. However, frozen ground massif has quite different properties. Experimental measurements showed that for instance the coefficient of thermal conductivity of clay with above-zero temperatures was 1.616 W/m·K, and when frozen 2.454 W/m.K. The coefficient of thermal conductivity of the ground massif when frozen is thus higher. The reason for this is a difference in the values of the coefficient of thermal conductivity of water in a liquid state (0.58 W/m.K) and that of ice (2.25 W/m.K). Tarnawski et al. (2009) observed that heat transfer in laminar flow depends on the time the fluid remains inside the absorption tubes and on the tubes' diameter, and on the density, thermal conductivity and specific thermal capacity of the absorption fluid. Heat transfer between the absorption tube wall and the fluid thus increases with the decreasing operating temperature, concentration of the antifreeze mix and the tubing length, and with the increasing tube diameter and the velocity of the heat-carrying fluid flow. The effect of various covers of the ground massif with a horizontal ground heat exchanger on temperature distribution and heat flows extracted from the ground massif was monitored at the University at Buffalo (Rezaei et al., 2012). When the rock massive was covered by an insulation layer of recycled tyres, the flow of the heat extracted from the ground massif during winter months increased by 17%.

The objective of our studies was to determine temperatures and analyse changes in temperatures in the ground massif with horizontal ground heat exchanger of the linear and of the slinky coil type, used as a source of energy to heat pumps, and to assess the regeneration ability of the ground massif's energy potential during the period of the exchanger's operating stagnation. Furthermore, we wanted to determine specific thermal outputs extracted from the ground massif and assess the possibilities of increasing the heat exchangers' outputs.

Material and methods

The monitored ground exchangers serve as sources of energy to IVT PremiumLine EQ E17 heat pumps (Industriell Värme Teknik, Tnanas, Sweden) of nominal thermal output 17 kW (0/35°C). These heat pumps are together with other three units used to heat an administrative building and production halls of VESKOM s.r.o. in Dolní Měcholupy.

The linear horizontal ground heat exchanger was made from polyethylene tubes PE 100RC 40 x 3.7 mm (LUNA PLAST a.s., Hořín, Czech Republic), resistant against point loads and development of cracks. It is not installed on a sand bed. The exchanger tubing of overall length 330 m is installed at depth 1.8 m in three loops at 1 m spacing. The length of each loop is 54.62 m. The ground massif to the depth of about 2 m is formed by dark sandy-earthy soil, course gravel, crushed stones and fragments of bricks. The heat-carrying fluid flowing through the heat exchanger is a mix of 33 % ethyl alcohol and 67 % water. Temperature sensors used to measure the ground massif temperature were installed in a plane perpendicular to the exchanger tubing, at 5 m distance from its beginning. A schematic diagram of the temperature sensors locations is presented in Fig. 1.

A schematic diagram of the horizontal ground heat exchanger of the slinky coil type is presented in Fig. 2. The exchanger is made from polyethylene tubing PE 100RC 32 x 2.9 mm, resistant against point loads and development of cracks. It is not installed on a sand bed. The exchanger tubing of an overall length 200 m is installed at depth 1.5 m in 53 coils. The ground massif and the heat-carrying fluid are of the same composition as those of the linear exchanger.

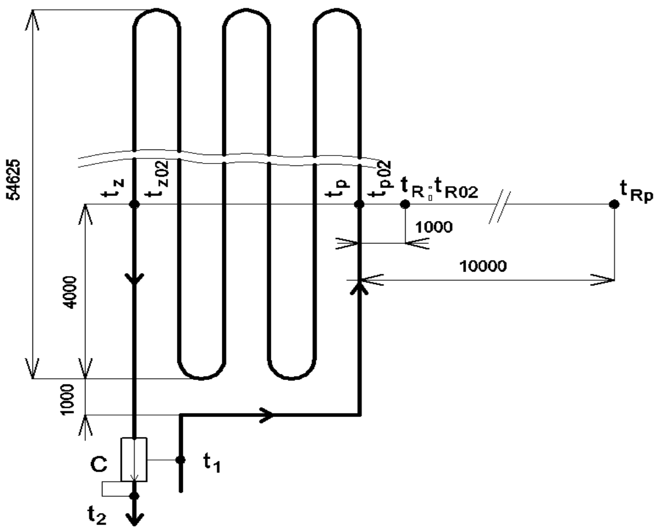

Fig. 1 Schematic diagram of the linear horizontal ground heat exchanger and locations of temperature sensors

Legend to Fig. 1: t_z – a temperature sensor installed in depth 1.8 m next to the tubing running towards the heat exchanger evaporator; t_p – a temperature sensor installed in depth 1.8 m next to the tubing running away from the heat exchanger evaporator; t_{z02}; $t_{p0,2}$ – a temperature sensor installed in depth 0.2 m above the tubing; t_1 – a temperature sensor of the heat-carrying fluid at the point of entry to the exchanger; t_2 – a temperature sensor of the heat-carrying fluid at the point of exit from the exchanger; C – an electronic heat consumption meter.

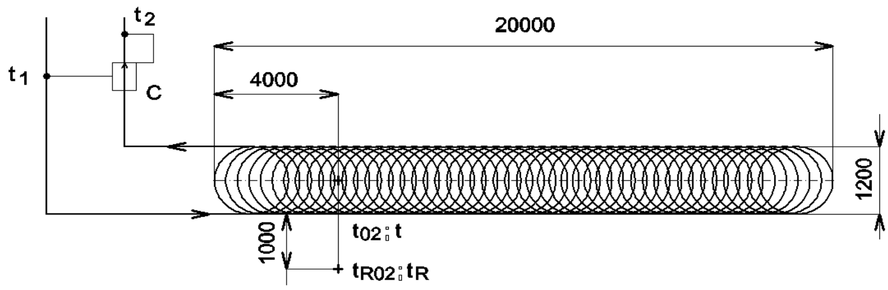

Fig. 2 Schematic diagram of the slinky coil ground heat exchanger and locations of temperature sensors
Legend to Fig 2: t - a temperature sensor installed in depth 1.5 m near the exchanger; t_R – a reference temperature sensor installed at a distance of 1.0 m from the exchanger, at depth 1.5 m; t_{02} – a reference temperature sensor installed at depth 0.2 m, above the heat exchanger; t_{R02} – a reference temperature sensor installed at a distance of 1.0 m from the exchanger, at depth 0.2 m

Temperatures of the ground massif were measured with PT 1000A resistance temperature sensors (manufacturer GREISINGER Electronic GmbH, Regenstauf, Germany) and recorded at 15-minute intervals. Temperatures of the surrounding environment t_e were measured at height 2 m above ground level and a distance of 20 m from the horizontal ground heat exchangers. Total thermal flow extracted by the horizontal ground heat exchangers was measured by MTW 3 electronic heat consumption meters (manufacturer Itron Inc. Liberty Lake, USA).

Results and discussion

1. *Temperatures of the ground massif*

The measurements took place during the period from 1st March 2011 to 28th February 2012. Average daily temperatures of the ground massif are presented in Fig. 3 to Fig. 5. Equations of the ground massif temperature curve around the linear exchanger t_L, the slinky coil exchanger t_S and the temperature of the surrounding environment t_e as a function of the number of days from the measurement commencement have the following form:

$$t_L = 6.408 \cdot \sin\left(\tau \cdot \frac{2 \cdot \pi}{365} + 4.822\right) + 10.841 \qquad (R^2 = 0.981) \qquad (1)$$

$$t_S = 9.89 \cdot \sin\left(\tau \cdot \frac{2 \cdot \pi}{365} + 5.343\right) + 11.111 \qquad (R^2 = 0.960) \qquad (2)$$

$$t_e = -10.506 \cdot \sin\left(\tau \cdot \frac{2 \cdot \pi}{365} + 2.372\right) + 11.713 \qquad (R^2 = 0.777) \qquad (3)$$

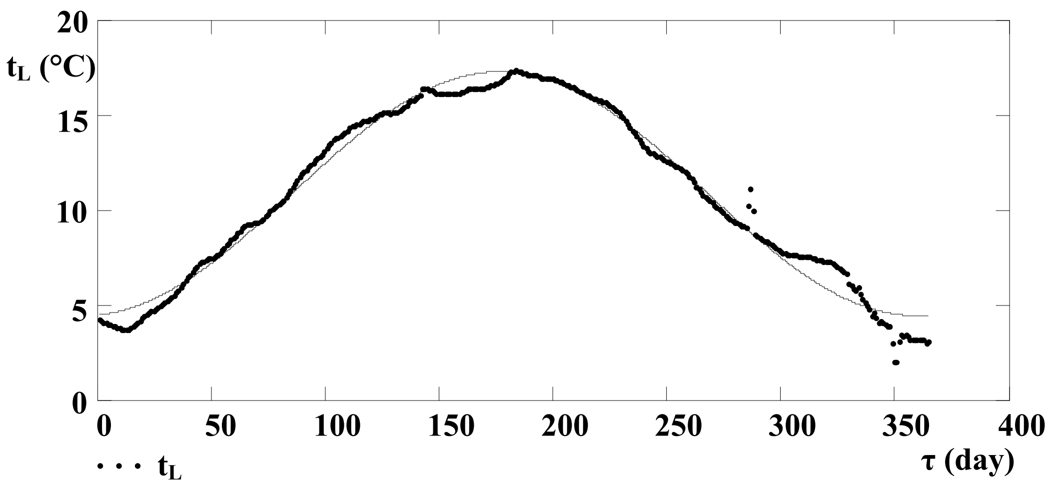

Fig. 3 Temperatures of the ground massif around the linear exchanger t_L

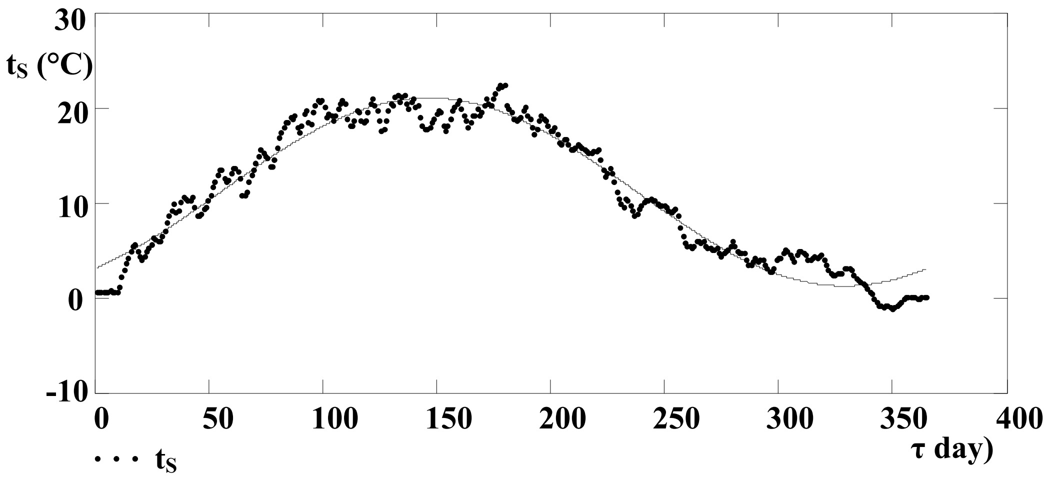

Fig. 4 Temperatures of the ground massif around the slinky coil exchanger t_S

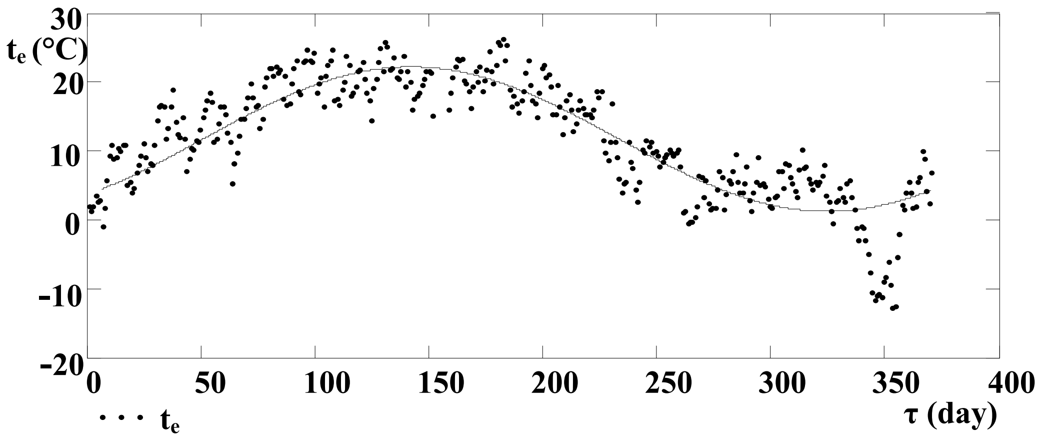

Fig. 5 Temperatures of the surrounding environment t_e

The curve of average daily temperatures of the ground massif around the exchangers can be divided into three phases:

Phase A – the end of the 2010/2011 heating season. The phase covers the period from 1st March to 5th June 2011, lasting 97 days.

Phase B – a stagnation period, exchangers are not in operation. The phase covers the period from 6th June to 6th September 2011, lasting 93 days.

Phase C – start and duration of the 2011/2012 heating season. The phase covers the period from 7th September 2011 to 28th February 2012, lasting 175 days.

Fig. 3 shows that the temperature of the ground massif t_L around the linear exchanger was throughout the entire monitored period in positive values. During the heating season 7th September 2011 to 28th February 2012, the average temperature t_L = 10.19 °C, maximum $t_{Lmax.}$ = 17.12 °C, and minimum $t_{Lmin.}$ = 2.03 °C. Temperatures of the ground massif t_S (Fig. 4) around the slinky coil exchanger towards the end of the heating season were, starting from 5th February 2012 in negative values. During the heating season from 7th September 2011 to 28th February 2012, the average temperature was t_S = 6.99 °C, maximum $t_{Smax.}$ = 19.24 °C and minimum $t_{Smin.}$ = -1.15 °C. Fig. 5 shows the average temperature curve of the surrounding environment.

The results of the study show that an average temperature of the ground massif near the slinky coil heat exchanger was lower and even dropped into negative values. The lower temperatures of the ground massif induce a lower evaporation temperature in the evaporator, which may have a negative impact on the heat pump's heating factor.

From the point of view of the source's energy potential and its life, important is to compare the initial and the final temperatures of the ground massif around the exchanger in several heating seasons. The difference in temperatures at the beginning of the 2010/2011 heating season (30th August 2010) and the 2011/2012 heating season (8th September 2011) was in case of the linear exchanger 0.18 K. The difference in temperatures of the ground massif at the end of the 2009/2010 heating season (21st June 2010) and the 2010/2011 heating season (16th June 2011) was 0.47 K. For the slinky coil exchanger, the differences in temperature at the beginning of the 2010/2011 heating season (30th August 2010) and the 2011/2012 heating season (7th September 2011) was only -0.04 K. The temperature difference of the ground massif at the end of the 2010/2011 heating season (22nd March 2011) and the 2011/2012 heating season (22nd March 2012) was -1.58 K. These temperature differences, which are within the measurements accuracy, show that horizontal ground heat exchangers can be regarded as very stable sources of energy to heat pumps. Thus the results of the more than two-year monitoring study did not confirm the opinions expressed by some designers and investors concerning the energy potential of the ground massif.

2. Specific thermal outputs of heat exchangers

An example of a curve of specific thermal flows q of both types of horizontal ground heat exchangers on a typical day during the heating season, 24th January 2012, is presented in Fig. 6.

The diagram in Fig. 6 indicates that the specific thermal outputs of the slinky coil heat exchanger q_S are higher than the specific thermal outputs of the linear heat exchanger q_L. On average, q_S was on the specified day greater by 1.59 W/m, with maximum difference in the highest thermal outputs q_S - q_L between 5:00 am and 10:00 am amounting to 5.93 W/m. To the greater specific thermal outputs of the slinky coil exchanger correspond lower temperatures of the ground massif around the heat exchanger.

The process of heat transfer in the ground massif with the horizontal ground heat exchanger can be in simplified terms ascribed to (Šeďová et al., 2013) the greater thermal resistance of the ground massif R_z (m.K/W), respecting the exchanger's three main parameters, the installation depth, the spacing and the tubing diameter, but also to the coefficient of thermal conductivity of the ground massif, λ_z (W/(m.K)). The coefficient of thermal conductivity of the ground massif ranged between λ_z = 1.5 and 1.9 W/(m.K). Thermal resistance of the ground massif at the given configuration of the linear exchanger then acquired the value R_z = 1.14 – 1.44 m.K/W. Increasing the tubing installation depth would result in an increased thermal resistance of the ground massif, and increasing the tubing spacing or diameter would reduce the thermal resistance.

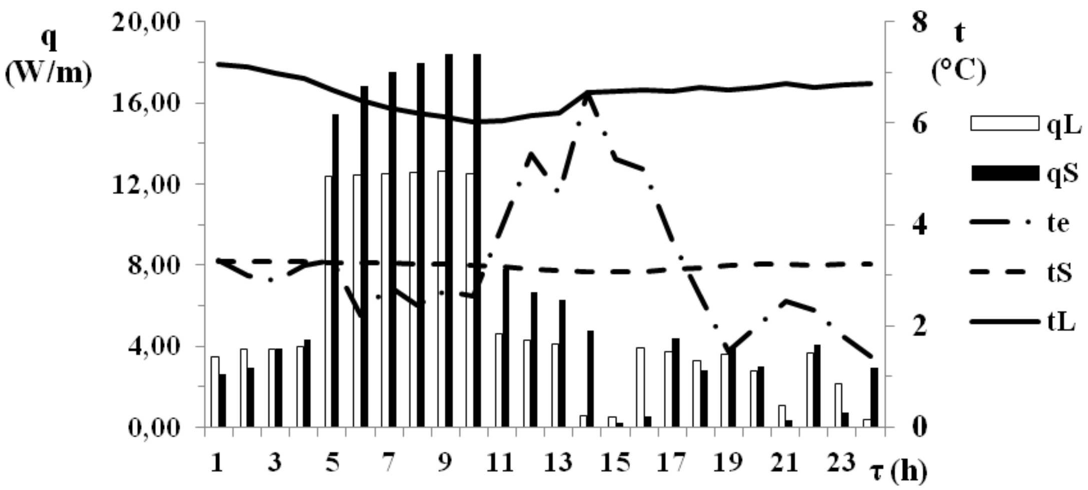

Fig. 6 Specific thermal output of the horizontal linear ground heat exchanger q_L and the slinky coil heat exchanger q_S on 24/1/2012

During the study of the horizontal ground heat exchangers we achieved a heat transfer coefficient between the heat exchanger wall and the heat-carrying fluid α = 43 – 55 W/m^2.K. Both exchangers worked within the limits of laminar flow, with Reynolds's criterion Re = 550 – 1300. With turbulent flow we would achieve a heat transfer coefficient greater by an order of magnitude. However, the effect of turbulent flow should not be overestimated. Turbulent flow for the antifreeze heat-carrying fluid induces a significant increase in the output of circulation pumps, and hence a reduction in the energy effect of the entire system. Only a comprehensive energy and economy analysis will be able to determine the effectiveness of achieving a turbulent flow inside the ground heat exchanger's tubing.

Conclusion

The outcomes of our study are findings concerning a temperature profile in the ground massif with a linear horizontal heat exchanger and with a slinky coil exchanger. Equations (1) and (2) together with Figs. 3 and 4 specify temperature curves of ground massif around the heat exchangers during a heating season and during the ground exchanger stagnation period. An adequate energy potential of the ground massif with horizontal ground heat exchangers was demonstrated by a minute difference in the ground massif temperatures at the beginning of a heating season over the period of several years. This observation has been also substantiated by the results of comparisons of ground massif temperatures around the exchangers and temperatures of the ground massif on reference planes. Specific thermal outputs of the ground heat exchangers have been determined (Fig. 6). The study showed higher specific thermal outputs of the slinky coil type of a heat exchanger. However, at the end of a heating season the temperatures of the ground massif around the exchanger reached negative values.

Acknowledgements

This work was supported by the Technology Agency of the Czech Republic, Project No. TA02020991 Optimization of the energetic parameters of the horizontal ground heat exchangers with respect to soil and hydrological conditions at the specific location.

References

Congedo P.M., Colangelo G., Starace G., 2012. CFD simulations of horizontal ground heat exchangers: A comparison among different configurations. Applied Thermal Engineering 33–34, 24–32.

Lund J.W., Freeston D.H., Boyd T.L., 2011. Direct utilization of geothermal energy 2010 worldwide review. Geothermics 40/3, 159–180.

Rezaei B.A., Kolahdouz E.M., Dargush G.F., Weber A.S., 2012. Ground source heat pump pipe performance with Tire Derived Aggregate. International Journal of Heat and Mass Transfer 55/11-12, 2844-2853.

Song Y., Yao Y., Na W., 2006. Impacts of soil pipe thermal conductivity on performance of horizontal pipe in a ground-source heat pump. Proceeding of the Sixth International Conference for Enhanced Building Operations, Shenzhen, China, November 6 – 9, http://esl.tamu.edu.

Šeďová M., Adamovský R., Neuberger P., 2013. Analysis of ground massif temperatures with horizontal heat exchanger. Research in Agricultural Engineering 59/3, In press.

Tarnawski V. R., Leong W. H., Momose T., Hamada Y., 2009. Analysis of ground source heat pumps with horizontal ground heat exchangers for northern Japan. Renewable Energy 34, 127–134.

RES-BASED MICROGRIDS FOR ENVIRONMENTALLY FRIENDLY ENERGY SUPPLY IN AGRICULTURE

Vytautas Adomavicius[1], Valeriy Kharchenko[2*], Jonas Valickas[3], Valentin Gusarov[2]

[1]Kaunas University of Technology, Kaunas, Lithuania
[2*]All-Russian Scientific Research Institute for Electrification of Agriculture, Moscow, Russia
VIESH, 1st Veshnyakovsky pr., 2, Moscow 109456, Russia
Phone: +7 (499) 171-27-43; Fax: +7 (499) 170-51-01, E-mail: viesh@dol.ru
[3]Panevezys Institute at Kaunas University of Technology, Panevezys, Lithuania

Abstract

Possibilities of RES-based microgrids development in rural areas are analysed in this paper. One of feasible schemes of the microgrid for a small rural settlement is proposed and described. Status, benefits and advantages of the power and heat energy supply by means of the microgrids are reviewed, usage of adjustable energy generators and energy storage systems, functions of the control system and outlook for the microgrids development are discussed on purpose to substantiate good chances for the anticipated breakthrough of this promising technology of energy generation and supply.

Keywords: energy, res-based microgrid

Introduction

Microgrid can be installed almost in every locality. However, rural areas in many cases have some advantages versus urban ones in sphere of the RES-based energy production, which should make up a substantial share of the energy produced in the microgrid. Superiority of rural areas for installation of microgrids can be easily explained: roughness of ground surface in general there is lower and accordingly wind speeds are higher than in urban and periurban areas, there are more possibilities to install small-scale hydro electric power plants. Besides, bio oil, which is one of the fuels used in the CHP plant based on the Diesel engine, can be produced in a local farm and possibly can be purchased for a lower price, other biomass fuels of various types also mostly can be found in the close surrounding areas. Fossil fuels can be used in the microgrids as well, but renewable energy sources have a priority due to the good environmental characteristics, universal availability and socio-economic benefits.

Normally power plants running on local, free, non-fuel and non-polluting primary energy sources are included in a microgrid first of all. It can be PV systems, wind turbines and small-scale hydro power plants. Their cumulative capacity usually makes up a major part of the total power integrated in microgrid. Large extent integration of RES-based power plants in the microgrid allows considering it as environmental friendly. The environmental aspect of energy production is becoming more and more substantial. Climate extremities, which are evident through the frequent huge floods, long drafts, strong hurricanes, large scale forests fires, heat and frost waves and rising of the average air temperature in the Earth during the last years are giving us tips that this thin and vulnerable atmosphere of our planet may be is not the place for unlimited emissions of various pollutants and greenhouse gases from industry, transport, households and agriculture. Further ignoring of environment protection will lead to the huge losses made by the pollution induced natural disasters what became very evident during the last decade.

Apart from the good environmental characteristics, microgrids have more advantages. Unstable power produced by PV power plants and wind turbines is balanced and used locally by the loads of the microgrid and only a surplus of electricity, which is not consumed inside, can be supplied into electric grid. It allows avoiding of power losses in the grid of the power system and makes fewer problems for the power grid operator due to the decreased total capacity of unstable power flows inside the power system.

Energy produced in a rural microgrid can be used in buildings, farms and local enterprises. Microgrid can be designed only for power production, only for heat production or it can be combined – for heat and power production. Combined heat and power (CHP) production in the microgrid allows achieving of the best fuel consumption factor. Electrical vehicles also can be connected in the microgrid as loads of the local power grid. It could be very convenient and beneficial for the cars owners. About 90 % of the presently operating microgrids have power capacity below 1 MW and cover areas less than 1 km^2.

Structure of microgrid

Optimal architecture of microgrid, its siting and sizing of the included power generation systems can be designed on basis of various criteria: power supply reliability, minimal price of generated power, minimal environment pollution or on the integral criterion. Number of the used renewable energy sources in a microgrid may be various. Even one energy source having substantial resources may be gainful (Adomavicius, Ramonas, 2011). One of the feasible versions of microgrid scheme for small rural settlement is shown in Fig. 1. It has the energy generation facilities and the loads connected over the microgrid's bus. The microgrid's bus MGB has the link with the electric grid EG of the main power system. Power trade between the microgrid and the electric grid of power system can be performed if it is beneficial for both sides.

Energy generation facilities of the microgrid comprises of the PV power plant with the PV array, the battery for power storage B, the small wind turbine SWT with the rectifier R, the battery chargers Ch-1 and Ch-2, the power conversion system based on the grid-tied inverter GTI, the DC choppers DC/DC-1–DC/DC-3 (inductor L, diode VD and transistor VT), the power storage condenser C_K, the middle scale wind turbine WT, the hydro electric power plant HEPP, the fuels cells PEM FC with the grid-tied inverter DC/AC, the CHP plant, the microgrid's control system MCS and a number of switches S, S1–S5 and S_1–S_3.

Every building in the microgrid area has a power inlet PINi. Some buildings also have heat energy inlet H. Perfectly insulated buildings (passive buildings) need not to be heated because the heat released from the domestic electrical appliances (refrigerator, TV, PC, lighting system, etc.), the food processing equipment and from the inhabitants bodies being in the building is sufficient to keep standard temperature in the living spaces. Buildings having energy efficiency class "A" require very small quantities of heat energy (15 kWh /m^2 per heating season or in average about 5 W/m^2) even in a cold month of heating season and usage of electricity for space heating is quite affordable and convenient in this case.

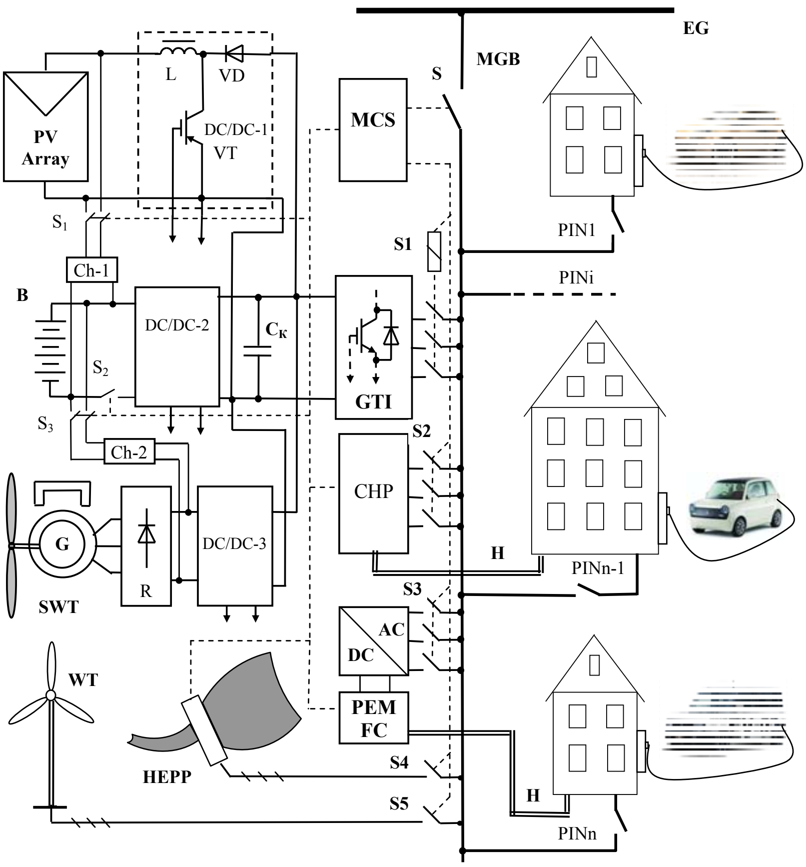

Fig.1 Feasible version of microgrid scheme for rural settlement

There is no need to have three energy inlets (power, heat and natural gas) in the passive buildings or buildings of energy efficiency class “A”. In summer domestic hot water (DHW) in the buildings with only one energy inlet (electricity) can be produced by solar collectors, in autumn, winter and spring – by the hybrid system comprised of solar collectors and electrical heaters.

Balancing power sources

The power being produced in a microgrid has to be balanced as well as in the large-scale nation-wide power system: the total power generation capacity must be equal to the total power demand at any moment. Balancing of power in microgrid is necessary not only because the demand of power can be different at any moment, but also because such RES-based power generation systems as wind turbines and PV power plants have unstable output of power what depends on natural conditions. This is why adjustable power sources have to be included during the designing of microgrid. Some power generation technologies are suitable for the produced power variations accordingly to the demanded power; however some of them are hardly adjustable (or not adjustable) and have not acceptable efficiency in the considerable part of the necessary power control range. Uncontrolled power sources can be used for covering the base loads in microgrids. Adjustable and fast coming into operation power sources are suitable for power balancing. Presently small-scale cogeneration technologies (or micro-CHP), which can be used for power balancing and/or covering base loads in microgrids, are produced industrially (Slowe, 2006). They are presented in Tab. 1.

Internal combustion engine (ICE) – generator sets and fuel cells are suitable for both purposes (balancing and covering base loads). There are more than dozen of fuel cells types but PEMFC and SOFC have the best characteristics and parameters for satisfying requirements of power balancing in the microgrid. Data of SOFC and PEMFC as power balancing plants are presented in Tab. 2. SOFC and PEMFC can be fueled by hydrogen, natural gas, methane, and methanol. Gas reformer or electrolyser with hydrogen storage equipment has to be used depending on the chosen fuel. The main disadvantage of the SOFC – it has a longer start-up time when cold (up to 4–6 hours).

Tab. 1 Efficiency and purpose of cogeneration technologies (Source: UNEP)

Technology	Fuel	Capacity, MW	Electrical efficiency	Total efficiency	Purpose	
					Balancing	Base
Gas turbine	Gas and liquid fuel	0,25–50+	25–42 %	65–87 %	–	+
Combined cycle power plant	Gas and liquid fuel	3–400+	35–55 %	73–90 %	–	+
ICE–generator set	Gas and liquid fuel	0,003–20+	25–45 %	65–92 %	+	+
Stirling engine–generator set	Gas and liquid fuel	0,003–1,5+	~40 %	65–85 %	–	+
Micro turbine	Gas and liquid fuel	0,025–0,3+	15–30 %	60–85 %	–	+
Fuel cells	Gas and liquid fuel	0,003–3+	~37–50 %	~85–90 %	+	+

Tab. 2 Data of SOFC and PEMFC as power balancing plants (Source: DK Styrelsen)

FC as balancing plants, running on natural gas							
Technical and financial data	Measures	2015		2020		2030	
		SOFC	PEMFC	SOFC	PEMFC	SOFC	PEMFC
Capacity of one unit	MW	0,1	0,1	0,5	0,5	0,5	0,5
Total efficiency	%	90	85	92	92	92	92
Electricity efficiency at full load	%	>52,5	>50	>55	>55	>55	>55
Electricity efficiency at 25 % load	%	45	45	50	50	52	52
Start-up time, when warm	s	90	60	90	60	90	60
Working temperature	ºC	750	70	650	80	650	80
Construction time	years	1	1	1	1	1	1
Technical lifetime	years	3	3	5	5	5	5
Investment	€/W	2,0	2,0	0,4	0,4	0,4	0,4
Operation and maintenance costs	€/MWh	25	25	10	10	10	10

Power storage systems also are used in microgrids not only for power reserving but also for power balancing. In this case their power output has to be controlled. Available power storage technologies, their application areas and the main parameters are presented below.

Energy storage

Various heat energy and power storage systems experienced significant qualitative and quantitative development during the last two decades. This trend will remain in future years due to the further development of smart grid, microgrids and stand-alone power systems. A number of various power storage technologies presently are used in the power systems. Many of the existing power storage technologies can be used in the microgrids but to a lesser capacity. Types of necessary power storage systems and their storage capacity depend on the specific parameters of the microgrid generators and characteristics of loads. Typical parameters of the power storage technologies used for various purposes in the power systems are presented in Tab. 3 (Tinkler, 2009).

PHES or CAES, or flow batteries or hydrogen storage system (in future) or their combination can be used also in the microgrids for power balancing and reservation. Small-scale CAES systems (up to 1 MWh) can be installed on the ground on basis of high pressure pipes, which normally are used for the natural gas pipelines.

Flywheels, supercapacitors, SMES, batteries may be used for improving the quality parameters and stability of electric power supply in the power system or microgrids.

However in many cases typical microgrids, which have not dramatically changing loads inside and have well designed compatibility of unstable and adjustable power generating systems, do not require many types of power storage systems. Properly chosen efficient power storage system(s) allow better exploiting of the installed generation capacities, reducing of fuel burning and thus pollution of environment as well.

Tab. 3 Typical parameters of power storage technologies used in power systems

Storage technology	**Typical power**	**Typical energy**	**Typical discharge time**	**Round trip efficiency**	**Life cycle**	**Maturity**
PHES	100 MW – 4000 MW	500 MWh – 15 GWh	4–12 h	80 %	40 years	Mature
CAES	25 MW – 3000 MW	200 MWh – 10 GWh	1–20 h	75 %	30 years	Mature
Flow batteries	100 kW – 10 MW	1 MWh – 100 MWh	10 h	60–80 %	10^3–10^4 cycles	Demo objects
Hydrogen storage	10 MW	Unlimited	> 5 h	20–36 %	3-5 years	Demo objects
Batteries: NiCd, Lead-acid, NiMH, Li-ion	1 kW – 500 kW	1 MWh – 100 MWh	1 h–8 h	60–90 %	10^3–10^4 cycles	Mature
NaS batteries	1 MW	1 MWh	1 h	75–80 %	10^3–10^4 cycles	Demo objects
SMES	10 kW – 10 MW	10 kWh – 1 MWh	1–30 min.	95 %	10^6 cycles	Demo objects
Flywheels	500 kW – 1 MW	100 kWh – 100 MWh	< 5 min.	85–90 %	10^6 cycles	Mature
Supercapacitors	< 250 kW	10 kWh	< 1 min.	90 %	10^6 cycles	Mature

Explication of abbreviations: PHES – Pumped Hydro Energy Storage, CAES – Compressed Air Energy Storage, SMES – Superconducting Magnetic Energy Storage.

Principles of the microgrid control

Microgrid's control system MCS (Fig. 1) in general is responsible for optimal power and heat generation and supply. First of all it means power balancing in the microgrid and keeping standard and stable parameters of generated power. It can be considered that MCS operates efficiently when every energy generator in the microgrid is kept operating efficiently, the price of produced energy and pollution of environment are possibly minimal and the reliability of power and heat supply is secure enough. Forecast of solar, wind and hydro energy resources, power interchange between the microgrid and grid of the power system, possibilities to control the loads also should be taken into consideration. Efficiency of microgrid operation depends on many factors and all possible measures have to be taken on every step of microgrid designing and installation for achieving this goal (Adomavicius et al., 2013). For example, one multi-inlet universal power converter can be used for a number of small-scale power sources (Chen at al., 2007), (Ramonas, Adomavicius, 2011), which is shown in Fig. 1 (DC/DC-1–DC/DC-3, C_K and GTI).

Algorithm of power and heat energy flow control in the microgrid has to be elaborated on basis of economic calculations of the most efficient modes of operation of the microgrid generators and loads. There are many approaches for solving this problem. Some algorithms are based on minimization of losses in the microgrid. Energy management in microgrids and buildings is analysed in paper (Stluka et al., 2011) and in some other. In general, efficient power and heat management in a microgrid and control of various configurations of the microgrids is a large-scale optimization problem and it will remain an important topic for researches in future years.

Microgrids have good possibilities for development in future. It can be expected because of the necessity to solve problems of environment pollution and climate crisis, unemployment, energy independence and reliability of energy supply. From other hand, gradual decrease of the RES-based power prices (especially from the PV power systems), innovations and improvements in power storage, FC and other technologies also paves the way for the breakthrough of microgrids.

Conclusions

Microgrids is rapidly rising technology of energy production and distribution and it have better possibilities for development in rural areas versus urban and periurban areas due to the better resources and availability of renewable energy.

Falling prices of PV modules create favourable conditions for considerable breakthrough of PV power plants and microgrids globally. Environmental and climate crises act as catalyst.

Fast development of microgrids based on substantial integration of the non-polluting and free energy resources leads to the possibility of shaking off (or at least considerable mitigating of the impact) from periodical increases of fossil fuel prices in the market.

References

Adomavicius V., Ramonas C., 2011. Small scale wind energy systems for farmsteads. Research papers of Aleksandras Stulginskis University, 43(4): 5-16.

Adomavicius V.B., Kharchenko V.V., Gusarov V.A., 2013. Possibilities of Enhancing Economic Efficiency of Microgrids. The 10th International Conference Renewable and Small Energy Systems, Proceedings, Moscow, 108–123. (in Russian language)

Chen Y.M., Liu Y.C., Hung S.C., Cheng C.S., 2007. Multi-Input Inverter for Grid-Connected Hybrid PV/Wind Power System. IEEE Transactions on Power Electronics, 22(3): 1070-1077.

Ramonas Č., Adomavičius V., 2011. Grid-tied Converter with Intermediate Storage Chain for Multipurpose Applications. Electronics and Electrical Engineering, 7(113): 15-20.

Slowe J., 2006. Micro-CHP: Global Industry Status and Commercial Prospects. 23rd World Gas Conference, Amsterdam, 9.

Stluka P., Godbole D., Samad T., 2011. Energy Management for Buildings and Microgrids. 50th IEEE Conference on Decision and Control and European Control Conference, Orlando, Fl., USA, December 12–15, 5150–5157.

Tinkler M.J., 2009. Electricity Storage: A Key Component of Our Emerging Energy Future. Third Industrial Revolution. Canadian Executive Round Table Meeting, Toronto, Ontario, May 28, 31.

EFFECTIVENESS INDICATORS OF FOOD PROCESSING LINES

Zdenek Ales, Vladimir Jurca, Vaclav Legat

Czech University of Life Sciences Prague, 16521 Prague 6 – Suchdol, Czech Republic,
Phone: +420 22438 3254, E-mail: ales@tf.czu.cz, jurca@tf.czu.cz, legat@tf.czu.cz

Abstract

The development of science and technology is linked to a number of requirements for food processing lines. One of the main characteristics observed during the operation of food processing lines is their effectiveness. When monitoring the effectiveness of food processing lines, the attention is mostly paid to the production quality, performance and availability. Availability is closely related to maintenance, which helps to maintain quality of production by ensuring reliable and serviceable condition of production equipment. It is crucial to focus on the elimination of corrective maintenance its localization in order to find out cause of failure, because only a properly executed maintenance contributes to increased availability of food processing line. The current concept of measuring the effectiveness of the food processing lines must be focused on finding weak points, i.e. to focus on the food processing line as on the interaction between a set of machines in one unit. Main objective of this paper is to acquaint the reader with newly proposed tool for evaluation of failures of food processing lines.

Key words: effectiveness indicators, maintenance, Breakdown Downtime Matrix, failure

Introduction

Food processing line is generally system composed of number of production equipment. In order to achieve proper competitiveness of production it is necessary to monitor and evaluate several operational parameters. One of these parameters is effectiveness. Measuring the effectiveness of production machines (including food processing lines) is one of the important factors of economy of operation (Legat et al., 1996).

Generally, there are several indicators for numerical representation of effectiveness in the manufacturing organization (Drozyner, Mikolajczak, 2007).

These indicators are one of the key performance indicators KPIs. Key performance indicators are a set of standards focused on aspects that critically affect the present or the future success of the organization (Nakajima, 1988; Reyes, 2010).

Key performance indicators must be defined to meet the following general characteristics:

- Non scale – indicator is not evaluated in monetary terms,
- Repeated measurements (e.g. daily, weekly, monthly, quarterly...),
- Value of indicator can be used as a basis for decision-making of top management,
- Understanding the indicator and possible follow-up measures are required for all employees,
- Indicator includes responsibility for the individual or team,
- Indicator has a significant impact - affects most critical success factors of the organization,
- Indicator has a positive impact - positively affects other performance measures.

When monitoring the effectiveness of food processing lines, the attention is mostly paid to the production quality, performance and availability (Jurca, Ales, 2007). The importance of these factors supports the fact that the food processing lines work with a material that is in most cases perishable.

Material and method

Before the actual determination of effectiveness indicators, it will be necessary to define the time of losses that may potentially occur during total available time. Generally, there are these times losses:

- **Non-scheduled time t_{non}** – All time the food processing line is not being used.
  Organizational downtime t_{org} - food processing line downtime due to organizational causes (time for personal relaxation, lack of staff…).
- **Logistic downtime t_{log}** - machine downtime due to logistical reasons (lack of material,

material damage, incorrect order, lead time, warehouse, insufficient stock, etc.).

- **Preventive maintenance downtime t_{pre}** - food processing line downtime due to preventive maintenance, which cannot be done during operation (Hartmann, 1992).
- **Setup and adjustment downtime t_{set}** - food processing line downtime due to necessary setup and adjustment (e.g. replacement of worn tools) [6].
- **Corrective (functional and minor) maintenance downtime t_{cor}** - food processing line downtime due to failures and caused other dependent losses (greater extent of damage, safety hazards, adverse environmental impacts) including minor failures (e.g. product blocked in the machine). The issue of corrective maintenance is greater than it is shown in Fig. 1. Fig. 2 describes possible causes of failure in general which may occur during operation. Font size in Fig. 2 represents possible probability of failure cause in operation.
- **Loss time due to reduced performance efficiency t_{per}** - time loss due to lower performance due to worsen technical state (loss adjustment, wear, corrosion, deformation, cracks, etc.).
- **Loss time due to production of non-conforming products t_{pro}** – there are generally two categories of non-conforming product origin:

  a) as a result of defective manufacturing process, which is caused by a poor monitoring, improperly performed maintenance (repair), and adjusting the parameters influencing the capability of food processing line.

  b) due to start of production process to a stable state.

Losses of production effectiveness can be similarly interpreted by cause and effect diagram as shown in Fig. 1.

For a calculation of effectiveness indicators it is necessary to begin with definition of available time. Available time can be defined as the calendar time, which can be potentially used for production, for example, 8,760 h per year, 24 hours per day, etc. Available time may in the limiting case be equal to the net operating time, in the event that there are no time losses and food processing line is required continuously. This situation is almost impossible in real operation because work shift usually consists (besides net operating time) of a number of time losses and downtimes.

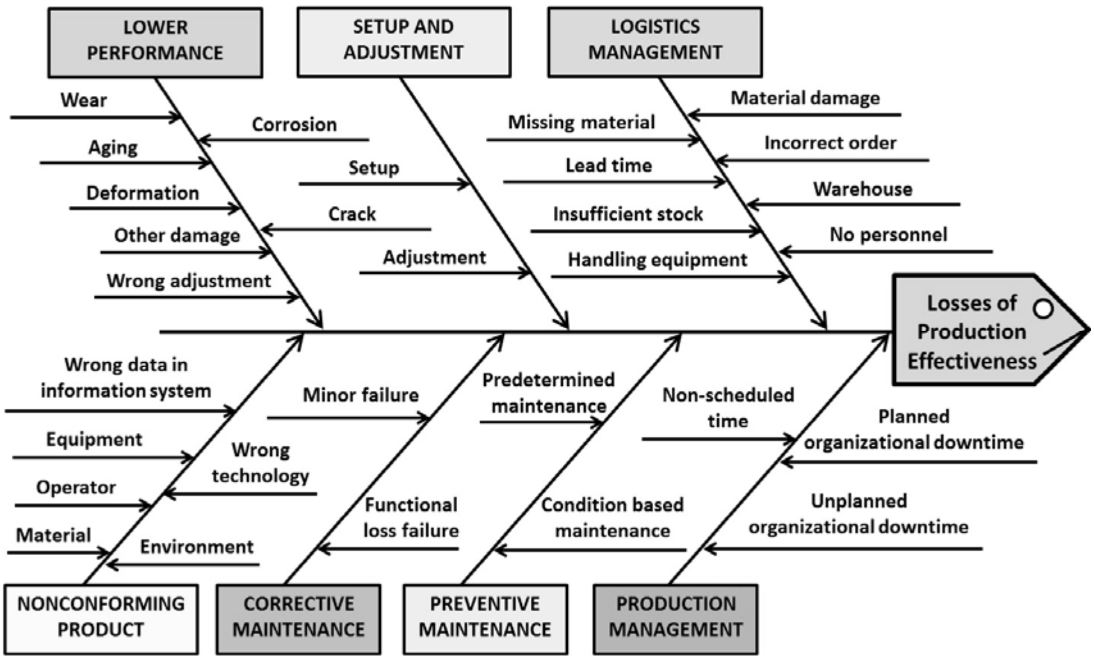

Fig. 1 Cause and effect diagram of losses of production effectiveness

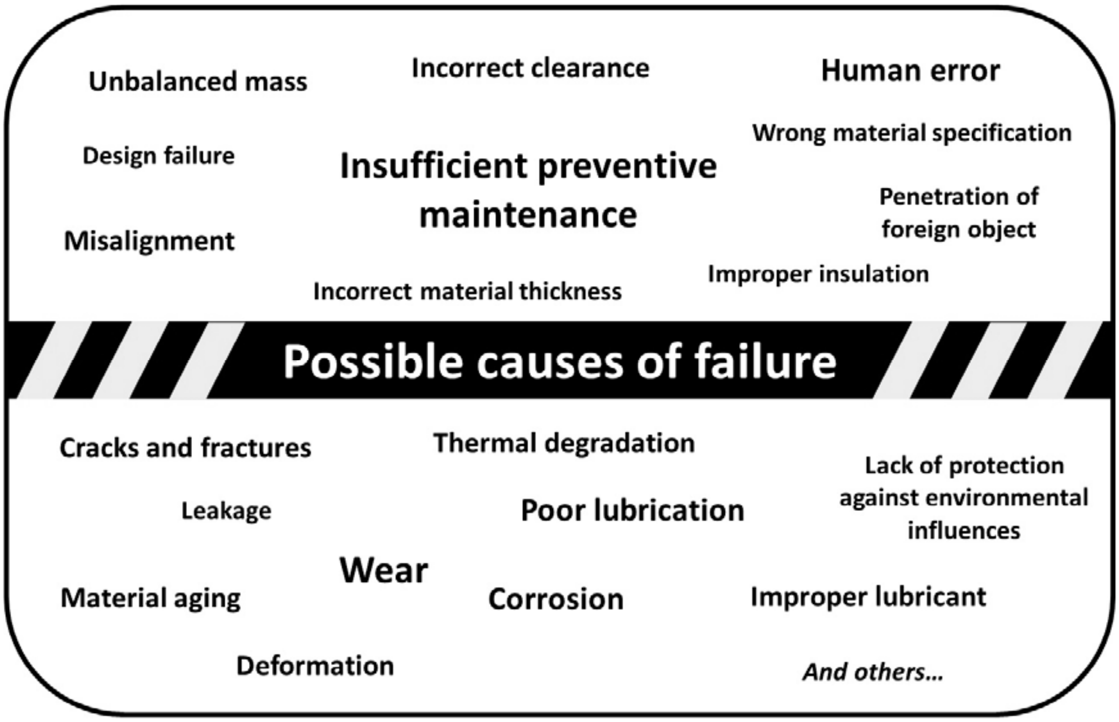

Fig. 2 Possible cause of failure of food processing line

Various operational or production times are calculated by subtracting the time of loss from total available (calendar) time as it is shown in Table 1. Calculated operational and production times are used to construct the coefficients, which are used for calculation of effectiveness indicators.

Fig. 3 Describes the breakdown of the total available (calendar) time the individual operating and production times and each time losses that can occur during operation

Tab. 1 Calculations of operational and production times

Type of time	Calculation (verbally)	Calculation
Running time t_{run}	Total available time t_{ava} – Non-scheduled time t_{non}	$t_{run} = t_{ava} - t_{non}$
Running time without organizational and logistic downtimes t_{orl}	Running time t_{run} – Organizational downtimes t_{org} – Logistic downtimes t_{log}	$t_{orl} = t_{run} - t_{org} - t_{\log}$
Operating time t_{ope}	Running time without organizational and logistic downtimes t_{orl} - Preventive maintenance downtimes t_{pre} – Setup and adjustment downtimes t_{set}	$t_{ope} = t_{orl} - t_{pre} - t_{set}$
Net operating time t_{net}	Operating time t_{ope} – Corrective maintenance downtimes t_{cor}	$t_{net} = t_{ope} - t_{cor}$
Usable operating time t_{usa}	Net operating time t_{net} - Loss time due to reduced performance efficiency t_{per}	$t_{usa} = t_{net} - t_{per}$
Net productive time t_{npr}	Usable operating time t_{usa} - Loss time due to production of non-conforming products t_{pro}	$t_{npr} = t_{usa} - t_{pro}$

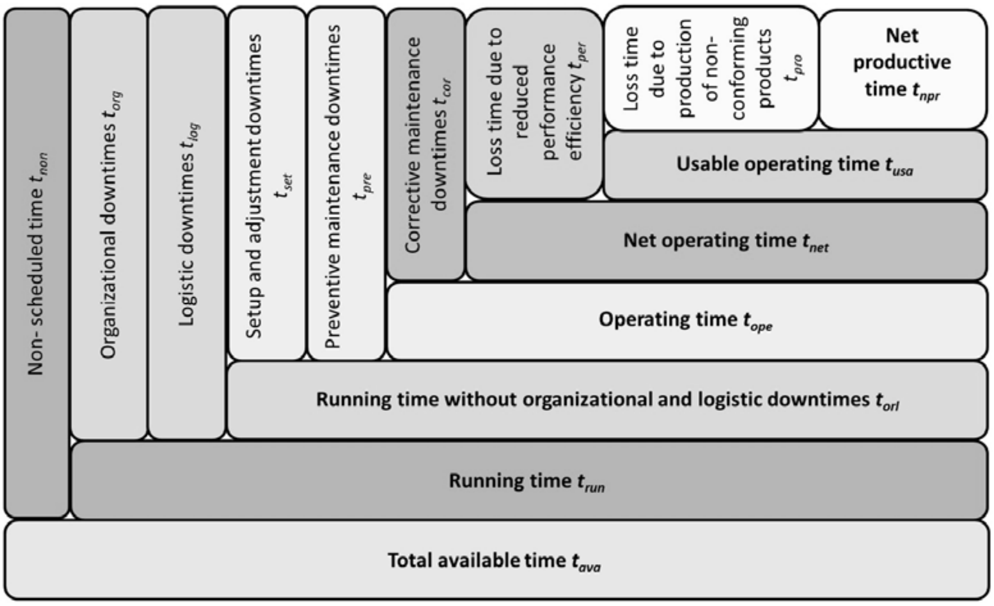

Fig. 3 Total available time breakdown

Coefficients for calculation of effectiveness indicators of food processing line are calculated by operating and production times in different ratios. It is possible to define these coefficients:

- ***Coefficient of Non-scheduled time, organizational and logistic downtimes N*** - this coefficient is calculated as total available time without non-scheduled time, organizational and logistical downtimes divided by total available time. (1)

$$N = \frac{t_{orl}}{t_{ava}} = \frac{t_{ava} - t_{non} - t_{org} - t_{\log}}{t_{ava}} \quad (1)$$

- ***Coefficient of Organizational and logistic downtimes O*** - this coefficient is calculated as running time without organizational and logistical downtimes divided by running time. (2)

$$O = \frac{t_{orl}}{t_{run}} = \frac{t_{ava} - t_{non} - t_{org} - t_{\log}}{t_{ava} - t_{non}} \quad (2)$$

- ***Coefficient of preventive Maintenance downtimes, setup and adjustment downtimes M*** - this coefficient is calculated as operating time divided by running time without organizational and logistical downtimes. (3)

$$M = \frac{t_{ope}}{t_{orl}} = \frac{t_{ava} - t_{non} - t_{org} - t_{\log} - t_{pre} - t_{set}}{t_{ava} - t_{non} - t_{org} - t_{\log}} \quad (3)$$

- ***Coefficient of Failures F (breakdowns)*** - this coefficient is calculated as net operating time divided by operating time. (4)

$$F = \frac{t_{net}}{t_{ope}} = \frac{t_{ava} - t_{non} - t_{org} - t_{\log} - t_{pre} - t_{set} - t_{cor}}{t_{ava} - t_{non} - t_{org} - t_{\log} - t_{pre} - t_{set}} \quad (4)$$

- ***Coefficient of Availability A*** - this coefficient is calculated as coefficient of preventive maintenance downtimes, setup and adjustment downtimes *M* multiplied by coefficient of failures *F*. (5)

$$A = M \times F = \frac{t_{net}}{t_{orl}} \quad (5)$$

- ***Coefficient of Performance P*** - this coefficient is calculated as usable time divided by net operating time. (6)

$$P = \frac{t_{usa}}{t_{net}} = \frac{t_{ava} - t_{non} - t_{org} - t_{\log} - t_{pre} - t_{set} - t_{cor} - t_{per}}{t_{ava} - t_{non} - t_{org} - t_{\log} - t_{pre} - t_{set} - t_{cor}} \quad (6)$$

- ***Coefficient of Quality Q*** - this coefficient is calculated as net productive time divided by usable time. (7)

$$Q = \frac{t_{npr}}{t_{usa}} = \frac{t_{ava} - t_{non} - t_{org} - t_{\log} - t_{pre} - t_{set} - t_{cor} - t_{per} - t_{pro}}{t_{ava} - t_{non} - t_{org} - t_{\log} - t_{pre} - t_{set} - t_{cor} - t_{per}} \quad (7)$$

Tab. 2 Calculation of effectiveness indicators of food processing line

TEEP	*Total Effective Equipment Productivity*	$\frac{t_{npr}}{t_{ava}} = N \times A \times P \times Q$
OEOE	*Overall Equipment and Organizational Effectiveness*	$\frac{t_{npr}}{t_{run}} = O \times A \times P \times Q$
OEE	*Overall Equipment Effectiveness*	$\frac{t_{npr}}{t_{orl}} = A \times P \times Q$
NEE	*Net Equipment Effectiveness*	$\frac{t_{npr}}{t_{net}} = F \times P \times Q$

Results

Effectiveness indicators of food processing line can be calculated by combining various products of different coefficients. The best-known effectiveness indicators, including their calculations are shown in Table 2.

Tab. 2 shows that effectiveness indicator TEEP includes all defined loss times and downtimes. Conversely, effectiveness indicator NEE includes only coefficient of failures *F*, coefficient of performance *P* and coefficient of quality *Q*. The most widely used indicator in practice is Overall Equipment Effectiveness OEE. OEE includes coefficient of availability *A* (coefficient of preventive maintenance, adjustment and adjustment *M*, coefficient of failure *F*), coefficient of performance *P* and coefficient of quality *Q*.

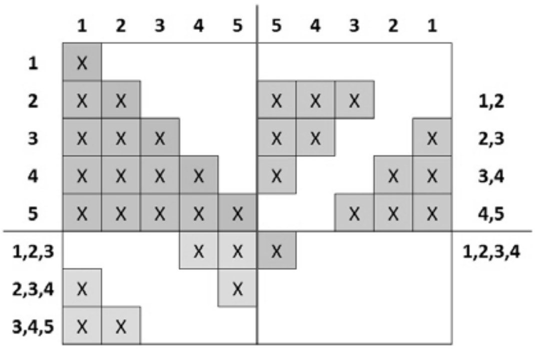

Fig. 4 Example of B-D Matrix for five machines

In terms of dependability it is clearly obvious that coefficients of failures have impact on final value of all effectiveness indicators. For keeping records and consequent evaluation of failure downtimes authors proposed visual tool called Breakdown Downtime Matrix (B-D Matrix). General structure of B-D Matrix is based on all possible combination of equipment breakdown downtimes which may occur during operation. In fact, B-D Matrix is a table that is divided into two halves and all values of equipment downtimes caused by failure are entered into proper intersection according to number of broken machines. In general, different scenarios may occur when downtime of one (or more) machine can happen at a certain time. Limit situation (unlikely) may occur when there are all machines in food processing line in downtime. If all values of downtimes are summarized in B-D Matrix, then resulting value represents corrective maintenance downtime t_{cor} of whole food processing line during monitored period. Fig. 4 shows structure of B-D Matrix for 5 production machines joined in food processing line. The values of particular downtimes obtained from B-D Matrix can be processed using Pareto diagram and then evaluate the weaknesses of failure occurrence of individual machines in food processing line.

Conclusion

Paper describes methodology on how to calculate various effectiveness indicators of food processing lines. Selection of particular indicators depend each user and also depend on the specific conditions of operation and type of processing equipment. The authors designed a tool called B-D Matrix for better visualization of the values of downtimes caused by failures.

It is relevant to point out the disadvantages of effectiveness indicators, consisting in the fact that they do not take into account other relevant factors (e.g. operating costs, value of inventories of spare parts, the productivity of the manufacturing process, age of production equipment, etc.) and that there is a problem with finding all the necessary input data. Constant increase of effectiveness indicators may lead to excessively high costs of operation and maintenance. Currently, the effectiveness indicators are implemented into Overall Equipment Efficiency - Downtime Management (OEE-DTM systems), which allows real-time information collected from the production process and subsequently automatically evaluates its effectiveness. OEE-DTM system partly eliminates subjective influence personnel to data entry and identifies weaknesses in the manufacturing process, which can be eliminated by corrective measures.

Acknowledgement

Grant project of the Ministry of Industry and Trade of the Czech Republic No. FR-TI2/202 "Information system of effectiveness and performance monitoring of production equipment – OEE-DTM".

Reference

Drozyner P.; Mikolajczak P., 2007. Assessment of the effectiveness of machine and device operation. Exploatacja i niezawodnosc, Polish Maintenance Society, 3(35): 72-75. ISSN 1507-2711

Hartmann E., 1992. Successfully installing TPM in a non-Japanese plant: total productive maintenance. Pittsburgh, Pa.: TPM Press, 221. ISBN 18-822-5800-2

Jurca V., Ales Z., 2007. Maintenance Management Efficiency Evaluation. Exploatacja i niezawodnosc, Polish Maintenance Society, 33: 13-19. ISSN 1507-2711

Legat V., Žaludová A., Červenka V., Jurča V., 1996. Contribution to optimization of preventive replacement. Elsevier Science Limited. Reliability Engineering and System Safety, 51: 259–266. ISSN 0951-8320

Nakajima S., 1988. Introduction to TPM: total productive maintenance. Cambridge, Mass.: Productivity Press, XX: 129. ISBN 09-152-9923-2

Garza-Reyes J.A., Eldridge S., Barber K.D., Soriano-Meier H., 2010. Overall equipment effectiveness (OEE) and process capability (PC) measures: A relationship analysis, International Journal of Quality & Reliability Management, 27(1): 48–62.

ENERGY AND EXERGY ANALYSIS OF FROZEN CHERRY PRODUCTION PROCESS

Z. Deniz Alta*, Can Ertekin

Akdeniz University, 07059, Antalya, Turkey
Phone: 90 242 3106545, Fax: 90 242 2274564, E-mail: denizalta@akdeniz.edu.tr

Abstract

In this paper, energy and exergy analyses are presented for processing of frozen cherry for a factory in Turkey. Data were collected from each of the defined basic unit operations: weighing and loading, pre washing, removing the stalks, separating the seeds, inspection and sorting, IQF freezing and packaging. The average energy intensity for processing a batch of 146 tonnes cherry to 99.28 tonnes of frozen cherry was estimated as 0.4 MJ/kg. The types of energy used in the manufacturing of frozen cherry were electrical and manual with the respective proportion of 99.78 % and 3.22 % of the total energy. The most energy consumed unit was IQF Freezing, followed by inspection & sorting which accounted for about 87.59 % and 5.67 % of the total energy input, respectively. Weighing and loading unit consumed the least energy, which is about 0.03 % of the total energy input. The exergy analysis revealed that the IQF freezing operation was responsible for most of the inefficiency (66.89 %) followed by separating the seeds operation (11.48 %).

Keywords: cherry, energy intensity, IQF Freezing

Introduction

Turkey is a rich country for having the advantage of different seasonal conditions to produce a large variety of fruits throughout the year. The geography and climate in many regions of Turkey are also appropriate for cultivation of sweet cherry. Turkey is ranked first in the world for sweet cherry production with the share of 12.83 %, and it comes second after USA in sweet cherry export with the share of 12.78 % in the world (Demircan et al., 2006). There is 7450000 sweet cherry trees yielding is approximately 230000 tons per year in Turkey (Vursavus et al., 2006).

Fruits of these species are not only consumed fresh but also used to produce jam, jelly, stewed fruit, marmalade, syrup and several types of soft drinks (Vursavus et al., 2006). Parallel to the global changes in food consumption habits, the extension of freezing technologies to households and having a considerable advantage in preparation time when compared with fresh foods; frozen food consumption also continues to increase. In 2009 the total production of frozen fruit was 22,000 tons in Turkey (İnci Selin Aydın, 2010).

As quality considerations and consumer satisfaction are important points for the frozen fruit and vegetable industry, most of the producer firms have ISO 9000, HACCP quality assurance systems that are certified by the Turkish Standards Institute, as well as internationally approved organizations.

There are many studies in the literature dealing with energy, exergy and economic analysis to determine the energy efficiency of food production processing operations, such as cashew nut (Jekayinfaa, Bamgboyeb, 2006), fruit juice (Waheeda et al., 2008), malt drink (Fadare et al., 2010), palm-kernel oil (Jekayinfa, Bamgboye, 2007), cassava-based foods (Jekayinfa, Olajide, 2007) in Nigeria, flavored yogurt (Sorgüven, Özilgen, 2012), raw juice (Tekin, Bayramoğlu, 2001), vegetable oil (Özilgena, Sorgüven, 2011) processing in Turkey. However, no studies have been published on the energy and economic analysis of frozen cherry processing operations in Turkey. This paper analyzes the whole system and illustrates energy and exergy losses in frozen cherry production.

Materials and methods

This study has been conducted in a factory produced frozen fruits & vegetables in Antalya. The process flow chart for production process is shown in Fig. 1.

The received cherries were weighed manually and loaded into process from the cold storage for precooling at 5 °C. Processing operations began by cleaning with a machine that was specially designed for washing fruits so as to get rid of dirt and other unwanted particles. There is a water pipe for water supply into the machine. The cherries are then carried by a conveyor to a machine for removing the stalks. The machine is incorporated with two motors and water pipes. The cherries without stalks were transported by conveyor to the machine to separate the seeds from cherries. Seedless cherries conveyed to the IQF to freeze up. Before and after the process of removing seeds, cherries were sorted out the bad cherries and unwanted particles manually. In IQF, each piece is frozen individually to very low temperature (-18 °C). The frozen charries are eventually packaged in the packaging unit manually.

The plant utilized electrical and manual energy for the frozen cherry production process. There is no use of steam in this process, so thermal energy was neglected in this study. The required parameters for evaluating energy consumption and exergy efficiency in each unit operation were measured directly or obtained from the factory's relevant department. All electric motors in the plant were identified, and the amperage and horsepower rating were measured to enable the calculation of electrical energy. The data were collected from the plant during a period of production.

Evaluation of electrical and manual energy

The electric energy input, E_p, was obtained by measuring the power of the electric motors by using the Qualistar C.A 8332B energy analyser. For three-phase system in the factory, volts RMS, amps RMS, power factor, instantaneous power in watts (W), instantaneous volt-amperes (VA), reactive volt-amperes (VAr), frequency (Hz), average and maximum powers (W), harmonic distortion, energy in watt-hours (Wh), reactive volt-ampere-hours (VArh), and phase angles were measured for determining how electrical power is consumed in the process with a view to reducing waste, calculate loads and costs.

Manual energy, E_m, in kW was estimated by using the following equation (1-5). The average physical power output of a normal human labour in tropical climates is 0.075 kW sustained for an 8-10 h workday (Fadare et al., 2010).

$$E_m = 0{,}075 * N * t \qquad \text{(kWh)} \qquad (1)$$

N is the number of persons involved in the operation and to is the useful time spent to accomplish a given task in hours (Fadare et al., 2010).

Energy intensity is the amount of energy required per unit output of production. The energy intensity was evaluated as the ratio of total energy input, E_t, in MJ and the mass of frozen cherry produced, m_p in kg:

$$E_i = \frac{E_t}{m_p} \qquad \text{(MJ/kg)} \qquad (2)$$

Exergy rates and exergy destructions for each process along with their exergy efficiencies were also determined by using following equations (Cay et al., 2009). The kinetic and potential energy effects and the physical and chemical exergies were neglected for the analysis.

The specific flow exergy is evaluated as

$$e_x = (h - h_0) - T_0 * (s - s_0) \qquad \text{(kJ/kg)} \qquad (3)$$

where h is the specific entalphy (kJ/kg), s is the specific entropy (kJ/kg K), and the subscript zero indicates properties at the reference state (T_0=303 K and P_0=100 kPa).

The specific exergy of the cherry material was calculated by

$$e_x = c_p * (T - T_0) - c_p * T_0 * \ln\left(\frac{T}{T_0}\right) + R * T_0 * \ln\left(\frac{P}{P_0}\right) \qquad \text{(kJ/kg)} \qquad (4)$$

The exergy rate is determined from

$$\dot{E}_x = \dot{m} * e_x \qquad \text{(kJ/h)} \qquad (5)$$

where m is the mass flow of the cherry (kg/h).

Results and discussion, energy expenditure of the system

The required parameters for evaluating energy and exergy in the operations are represented in Table 1 and Table 2.

Tab. 1 Required parameters for evaluating energy and exergy in the frozen cherry production operations

Unit operation	**Required parameters**	**Value**
Weighing and Loading	Number of persons involved in weighing and loading	1
	Time taken for weighing and loading	1.5
Prewashing	Electrical power (kW)	0.24
	Number of persons involved in prewashing	2
	Cherry inlet temperature (K)	287.9
	Cherry outlet temperature (K)	291
Removing the stalks	Electrical power (kW)	1.03
Separating the seeds	Electrical power (kW)	1.45
	Number of persons involved in separating the seeds	2
	Cherry inlet temperature (K)	291
	Cherry outlet temperature (K)	295.6

Unit operation	Required parameters	Value
Inspection/Sorting	Electrical power (kW)	2.03
	Number of persons involved in Inspection/Sorting	12
IQF Freezing	Electrical power (kW)	45.28
	Cherry inlet temperature (K)	295.6
	Cherry outlet temperature (K)	255
Packaging	Number of persons involved in packaging	6

* Time taken for the operations except weighing and loading is 8 h working shift.

Tab. 2 Operation parameters for cherry

Density of cherry (kg/m^3)	425
Mass flow rate of cherry (kg/h)	1011.87
Specific heat above freezing (kJ/kg K)	3.68
Specific heat blow freezing (KJ/kg K)	1.72

In process, two elevators and three conveyors, each has a motor, are used to convey the cherries. Inspection/sorting operations are carried out by the workers in the sides of the conveyors and elevators. For this operation unit, energy consumption was calculated by using total power of the electric motors of them and total number of the persons work in.

The total energy requirements for the seven defined unit operations and a diagram of an energy account and mass flow of the process stream based on symbols are given in Fig. 2. The total energy consumption per approximately 6 tons of frozen cherry production in a day was estimated to be 1,488.77 MJ while the average energy intensity was 0.25 MJ/kg. The proportion of the electric and manual energy in the total energy consumption is 96.78 % and 3.22 %, respectively. The energy intensity for manual energy is 0.0079 MJ/kg representing the least energy consumed. This was a result of the mechanization of the industry. Most energy consumed unit was IQF Freezing, which accounted for about 87.59 % of the total energy input. Weighing and loading unit consumed the least energy, which is about 0.03 % of the total energy input (Waheeda et al., 2008).

The factory works between 17th July and 3th August 2012 for the 99 tons frozen cherry production. Double shift also worked for 11 days of 16 working days. Total energy consumption for this production is 40,196.79 MJ. (11165 kWh). Daily average electric consumption for these dates is 2762.897 kWh. The proportion of the electric consumption for the production process of the frozen cherry in the total energy consumption of the factory is only 4.79 %. Energy intensity is 0.40 MJ/kg.

Exergy expenditure of the system

Exergy analysis has been applied to the overall production of frozen cherry by the evaluation of the unit processes involved in production. Table 3 presents exergy change in frozen cherry, useful work, entropy generated and inefficiency associated with each unit operation. There is no steam exergies, because there is no steam usage for these operations. The change in the frozen cherry exergy is only associated with operations where there is change in the inlet and outlet temperatures of the cherry. Consequently there is exergy change in the prewashing, separating the seeds and IQF Freezing operations. There is no exergy change in the weighing and loading, removing the stalks, inspection and sorting and packaging operations because these operations take place without any appreciable change in temperature between the inlet and the outlet of the processes.

Tab. 3 Exergy balance in the frozen cherry processing plant

Unit operation	Exergy change of the cherry (MJ)	Useful work (MJ)	Production of entropy (MJ/kg K)	Inefficiency (%)
Weighing and Loading	-	0.40	0.40	0.04
Prewashing	-53.03	11.23	64.26	7.25
Removing the stalks	-	29.66	29.66	3.35
Separating the seeds	-55.62	46.08	101.7	11.48
Inspection/Sorting	-	84.38	84.38	9.52
IQF Freezing	711.45	1,304.06	592.61	66.89
Packaging	-	12.96	12.96	1.47
Total	602.80	1488.77	885.92	100

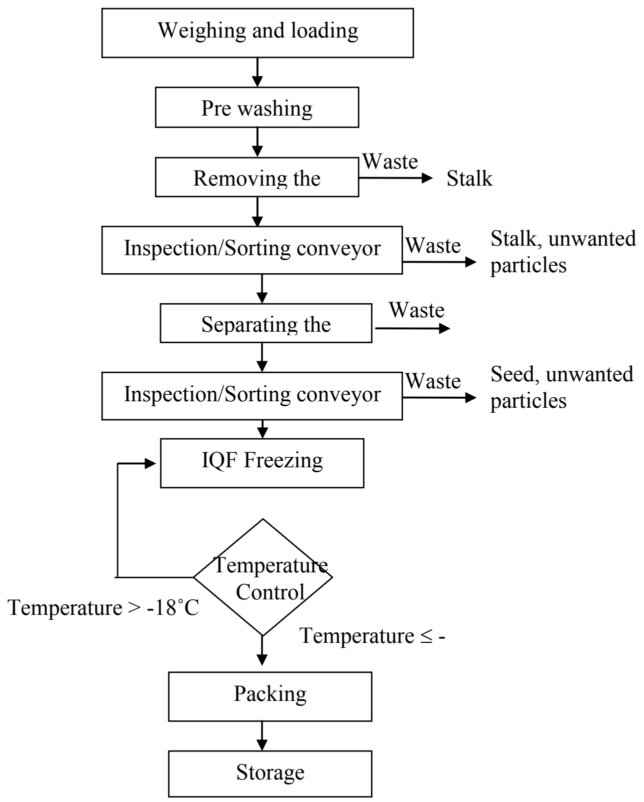

Fig. 1 Flow diagram of the frozen cherry processing operation

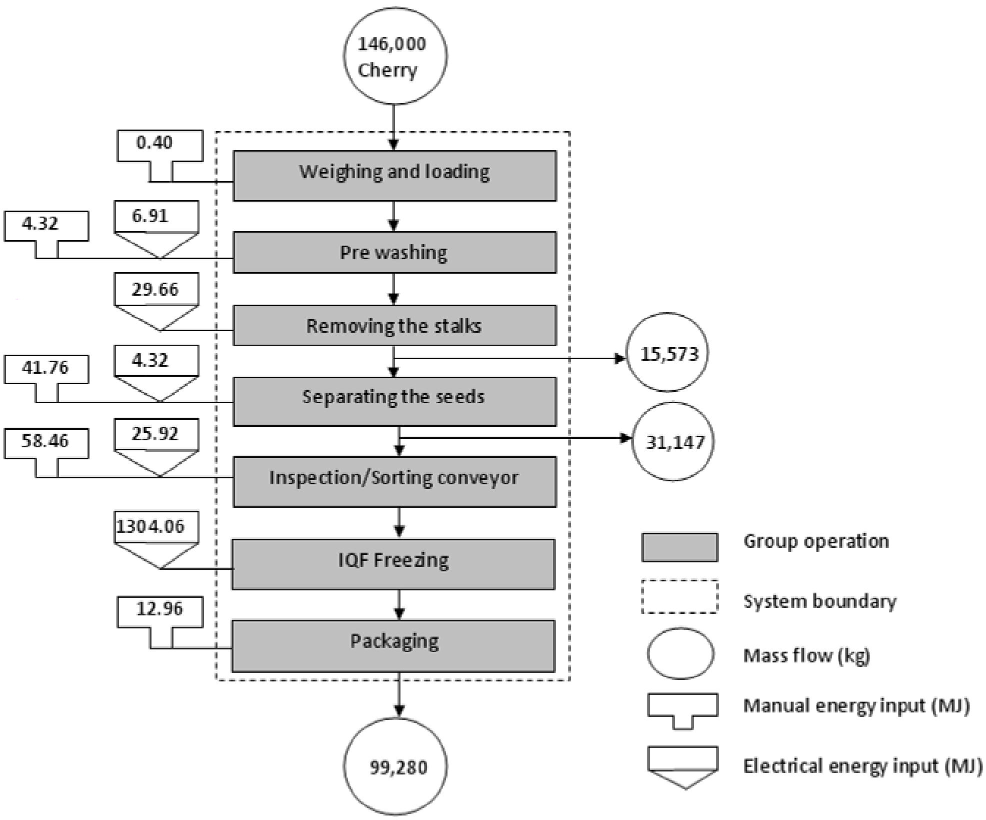

Fig. 2 Energy accounting and mass flow diagram for frozen cherry processing

Conclusion

The exergy efficiency and the irreversibility based on a combination of the first and second laws of thermodynamics are studied on production of frozen cherry produced in a factory in Turkey for a better understanding of energy flows in process. Seven basic unit operations were identified as weighing and loading, pre washing, removing the stalks, separating the seeds, inspection and sorting, IQF freezing and packaging. The average energy intensity for process was estimated as 0.4 MJ/kg. The types of energy used in the manufacturing of frozen cherry were electrical and manual with the proportion of 96.78 % and 3.22 % of the total energy, respectively. The results show that, the most energy consumed unit was IQF freezing, followed by inspection & sorting and weighing and loading unit consumed the least energy. The high entropy was generated in the IQF due to the irreversibility within the system as a result of high temperature difference between the inlet and outlet temperature of the cherry. The IQF freezing operation was also responsible for most of the inefficiency followed by separating the seeds operation. This result shows that freezing process is highly inefficient. To reduce the high exergy destruction in the IQF, pre-cooling before IQF freezing unit could be suggested.

References

Cay A., Tarakcıoğlu I., Hepbasli A., 2009. Assessment of finishing processes by exhaustion principle for textile fabrics: An exergetic approach. Applied Thermal Engineering, 29: 2554–2561.

Demircan V., Ekinci K., Keener H.M., Akbolat D., Ekinci Ç., 2006. Energy and economic analysis of sweet cherry production in Turkey: A case study from Isparta province. Energy Conversion and Management, 47: 1761–1769.

Fadare D.A., Nkpubre D.O., Oni A.O., Falana A., Waheed M.A., Bamiro O.A., 2010. Energy and exergy analyses of malt drink production in Nigeria. Energy, 35: 5336-5346.

İnci Selin Aydın İ.S., 2010. Frozen Fruits and Vegetables in Turkey. Report of Export Promotion Center of Turkey.

Jekayinfaa S.O., Bamgboyeb A.I., 2006. Estimating energy requirement in cashew (Anacardium occidentale L.) nut processing operations. Energy, 31: 1305–1320.

Jekayinfa S.O., Olajide J.O., 2007. Analysis of energy usage in the production of three selected cassava-based foods in Nigeria. Journal of Food Engineering, 82: 217–226.

Jekayinfa S.O., Bamgboye A.I., 2007. Development of equations for estimating energy requirements in palm-kernel oil processing operations. Journal of Food Engineering, 79: 322–329.

Özilgena M., Sorgüven E., 2011. Energy and exergy utilization, and carbon dioxide emission in vegetable oil production. Energy, 36: 5954-5967.

Sorgüven E., Özilgen M., 2012. Energy utilization, carbon dioxide emission, and exergy loss in flavored yogurt production process. Energy, 40: 214-225.

Tekin T., Bayramoğlu M., 2001. Exergy and structural analysis of raw juice production and steam-power units of a sugar production plant. Energy, 26: 287–297.

Vursavus K., Kelebek H., Selli S., 2006. A study on some chemical and physico-mechanic properties of three sweet cherry varieties (Prunus avium L.) in Turkey. Journal of Food Engineering, 74: 568–575.

Waheeda M.A., Jekayinfab S.O., Ojediranb J.O., Imeokpariaa O.E., 2008. Energetic analysis of fruit juice processing operations in Nigeria. Energy, 33: 35–45.

SHAKING FORCE MINIMISATION OF SLIDER-CRANK MECHANISMS VIA OPTIMAL MOTION CONTROL

Vigen Arakelian[1,2*], Sébastien Briot[1], Jean-Paul Le Baron[2]

[1]Institut de Recherches en Communications et Cybernétique de Nantes (IRCCyN)
BP 92101, 44321 Nantes Cedex – France
Phone: +33240376958, Fax: + 3324037690
E-mail: Vigen.Arakelyan@irccyn.ec-nantes.fr
[2]Institut National des Sciences Appliquées, France

Abstract

This paper deals with the problem of shaking force balancing of high-speed slider-crank mechanisms. The known solutions of this problem are carried out by an optimal redistribution of moving masses which allows the cancellation or the reduction of the variable loads on the mechanism frame. In this paper an innovative solution is developed which is based on the optimal motion control of the input crank. Such a solution allows the reduction of the translational acceleration and, consequently, the reduction in the shaking forces. The efficiency of the suggested method is illustrated by the numerical simulations that have been carried out via ADAMS software. The obtained results show that the shaking force reduction of translational motion reaches up to 35%.

Keywords: slider-crank mechanisms, bang-bang law, numerical simulations, ADAMS software

Introduction

In high-speed machines, shaking force, which are generated by an unbalanced mechanism brings about variable dynamic loads on the frame and, as a result, vibrations. The slider-crank mechanism is a common element in high-speed machines and many methods have been developed for their balancing (Lowen et al., 1983; Arakelian, 2000).

The known balancing methods can be arranged into the following groups:

- complete shaking force and shaking moment balancing (Berestov, 1978; Ye, Smith, 1994; Bagci, 1982; Arakelian,1993; Arakelian, 1998; Arakelian, Smith, 1999);
- complete shaking force and partial shaking moment balancing (Berestov, 1978; Shchepetilnikov, 1982; Arakelian et al., 2000; Artobolevskii, 1964);
- partial shaking force and shaking moment balancing (Shchepetilnikov, 1982; Artobolevskii, 1964; Dresig et al., 1994; Arakelian, Dahan, 2001);
- complete shaking force balancing (Kamenski, 1968; Balanced crank mechanism, 1979; Berkof, 1979; Arakelian, 1992);
- partial shaking force balancing (Shchepetilnikov, 1982; Gheronimus, 1968; Arakelian, 1995).

Problem statement

The shaking force of a slider-crank mechanism (Fig. 1) can be computed as the sum of two terms due to the rotational and translational motions:

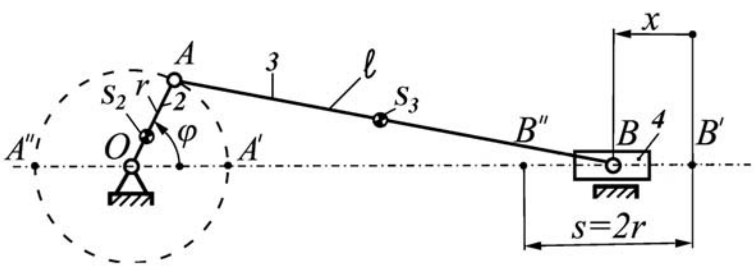

Fig 1 Slider-crank mechanism

$$F_{(rot)}^{\text{int}} = \left(m_2 l_{OS2} + m_3 r l_{BS3}/l\right)\left(\dot{\varphi}^2 \cos\varphi + \ddot{\varphi}\sin\varphi\right) \tag{1}$$

$$F_{(tr)}^{\text{int}} = -\left(m_4 + m_3 l_{AS3}/l\right)\ddot{x}_B = \left(m_4 + m_3 l_{AS3}/l\right)\left[r\left(\dot{\varphi}^2\cos\varphi + \ddot{\varphi}\sin\varphi\right) + l\left(\dot{\psi}^2\cos\psi + \ddot{\psi}\sin\psi\right)\right] \tag{2}$$

where φ is the crank rotation angle; $\psi = \sin^{-1}\left(-\sin\varphi/\lambda\right)$ is the connecting rod rotation angle $\left(\lambda = l/r\right)$; $\dot{\varphi}$ and $\ddot{\varphi}$ are the angular velocity and acceleration of the crank; $\dot{\psi} = -\dot{\varphi}\cos\varphi/\lambda\cos\psi$ is the angular velocity of the connecting rod;
$\ddot{\psi} = \left(\dot{\varphi}^2\sin\varphi - \ddot{\varphi}\sin\varphi + \dot{\psi}^2\lambda\sin\psi\right)/\lambda\cos\psi$
is the angular acceleration of the connecting rod; r is the distance between the centres of the joints O and A; l is the distance between the centres of the joints A and B; l_{OS2} is the distance of the center of the joint O from the center of masses S_2 of the crank; l_{BS3} and l_{AS3} are the distances of the centers of the joints A and B from the center of masses S_3 of the connecting rod; m_2 is the mass of the crank; m_3 is the mass of the connecting rod; m_4 is the mass of the slider.

The shaking force due to the rotational motion can be easily cancelled by adding a counterweight on the input crank. However, the balancing of the shaking force due to the translational rectilinear motion is much more difficult.

From expression (2), we can see that the shaking force due to the translational rectilinear motion is minimized, in terms of norm, if the norm $\ddot{x}_B$ of the slider acceleration is minimized during of a full rotation of the crank. This means that if the rotation of the input crank is optimally generated, the shaking force will be minimized. As a result, if the time interval $\left(t_0, t_f\right)$ for a full rotation of the crank is fixed, i.e. the time of the stroke is also fixed, the "bang-bang" (Fig. 2) (Khalil, Dombre, 2002) is law of the slider displacement that minimizes the value of the maximal acceleration $\ddot{x}_B^{\max}$ (Briot, 2012).

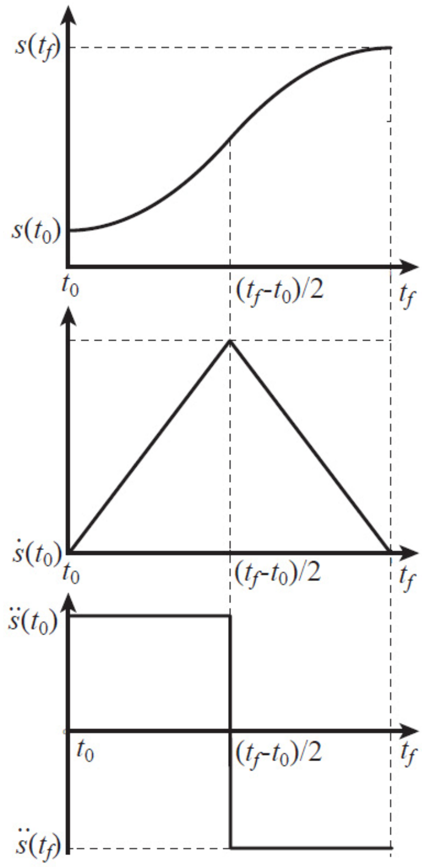

Fig. 2 "Bang-bang" law

Thus, in the present study we would like to reach the following condition $F_{(tr)}^{\text{int}} \to \min\limits_{\varphi(t)}$, i.e. to generate such an input rotation angle of the crank which leads to generation of an output acceleration $\ddot{x}_B$ that follows a 'bang-bang' motion law and thus minimizes the norm of $F_{(tr)}^{\text{int}}$.

Shaking force minimisation via optimal motion control of the input crank

The problem which has been mentioned above can be formulated as

$$\left(m_4 + m_3 l_{AS3}/l\right)\left[r\left(\dot{\varphi}^2\cos\varphi + \ddot{\varphi}\sin\varphi\right) + l\left(\dot{\psi}^2\cos\psi + \ddot{\psi}\sin\psi\right)\right] \to \min_{\varphi(t)} \tag{3}$$

It is obvious that in this form it is difficulty to find an explicit form of solution. Therefore, let us introduce an approximate expression of the slider displacement for solving the mentioned problem. The slider displacement can be represented by a Fourier series:

$$x_B = r\left[A_0 + A_1\cos\varphi + A_2\cos 2\varphi + A_4\cos 4\varphi + A_6\cos 6\varphi + ...\right] \quad (4)$$

where $A_0 = 1 + \frac{1}{4\lambda} + \frac{3}{64\lambda^3} + \frac{5}{256\lambda^5} + ...$; $A_1 = -1$; $A_2 = -\left(\frac{1}{4\lambda} + \frac{1}{16\lambda^3} + \frac{15}{512\lambda^5} + ...\right)$;
$A_4 = \frac{1}{64\lambda^3} + \frac{3}{256\lambda^5} + ...$; $A_6 = -\left(\frac{1}{512\lambda^5} + ...\right)$; etc.

Such a series has an infinite number of terms, each term representing a simple harmonic motion having a known frequency and amplitude. It turns out that higher-frequency amplitudes are so small that they can be neglected and hence only a small number of the lower-frequency amplitudes are needed. It is rarely necessary to consider the fourth or higher harmonics.

Thus the slider's displacement with a very higher precision can be represented as

$$x_B = r(A_0 + A_1\cos\varphi + A_2\cos 2\varphi) = r\left[A_0 + A_1\cos\varphi + A_2\left(2\cos^2\varphi - 1\right)\right] \quad (5)$$

From which we determine the crank rotation angle taking into account that the slider displacement x_B is generated by a "bang-bang" law:

$$\varphi = \cos^{-1}\left[\frac{-A_1 \pm \sqrt{A_1^2 - 8A_2\left(A_0 - A_2 - x_B/r\right)}}{4A_2}\right] \quad (6)$$

Let us consider an illustrative example.

Illustrative example

The parameters of the simulated slider-crank mechanism to be balanced are the following: $r = 0.05m$; $l = 0.2m$; $l_{OS_2} = 0.025m$; $l_{AS_3} = 0.1m$; $m_2 = 1$ kg $m_3 = 0.35$ kg; $m_4 = 2$ kg.

At first, let us determine from expression (5) the input angle φ taking into account that $x_B = 0.1m$ and $t_f = 0.1\sec$. The variations of the input angle φ and the input angular velocity $\dot{\varphi}$ are shown in Fig. 3 and Fig. 4.

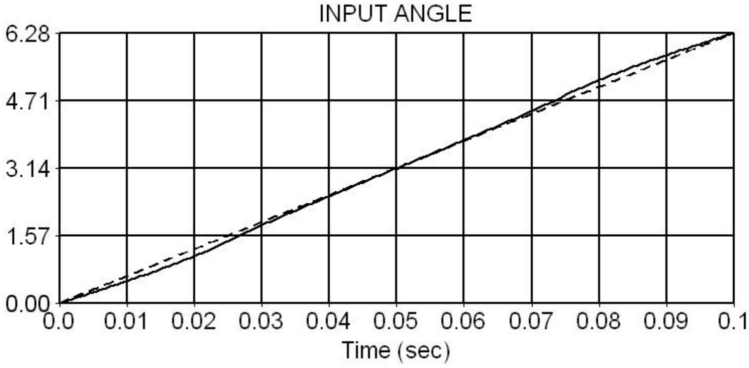

Fig. 3 Input angle φ (rad.)

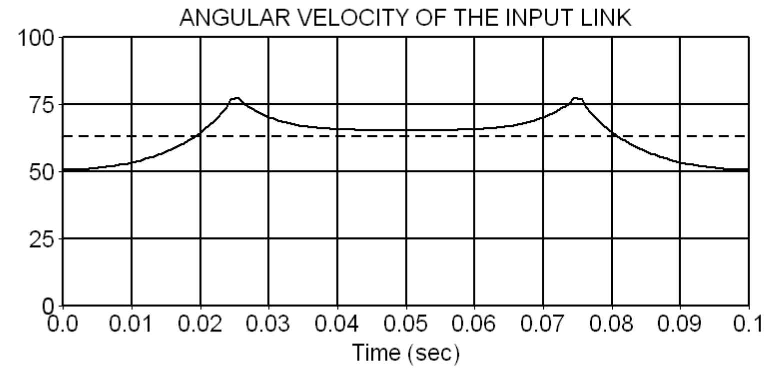

Fig. 4 Input angular velocity $\dot{\varphi}$ (sec.[-1])

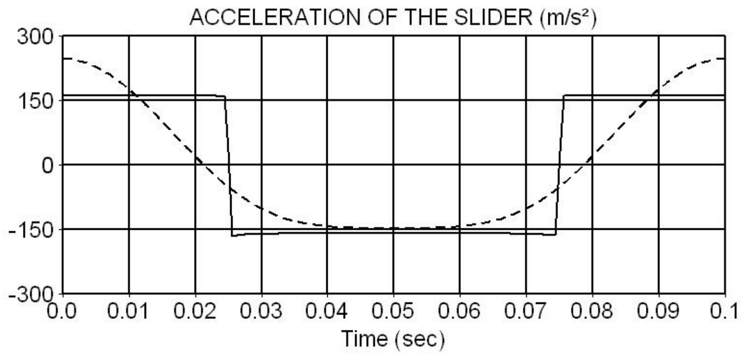

Fig. 5 Acceleration of the slider: $\ddot{x}_B$

In order to carry out a comparative analysis, a slider-crank mechanism with constant input speed ($\dot{\varphi} = 62.8s^{-1}$) has first been simulated. The variations of the parameters of the slider-crank mechanism with constant input angular velocity are shown in Fig. 4 and Fig. 5 by dashed lines.

Now we introduce in the software model the input angle calculated from (5), i.e. that minimize the norm of the acceleration $\ddot{x}_B$, In this case, as it was mentioned above, the linear acceleration of the slider should follow a "bang-bang" law. Indeed, the simulations carried out by using ADAMS software showed that the variation of the acceleration of the translational rectilinear motion is "bang-bang" law (Fig. 5). Thus, the maximal value of the linear acceleration $\ddot{x}_B$ is minimized and, as a result, the shaking force due to the translational motion of the slider is also minimized. For the given example the minimization of the linear acceleration (shaking force due to the translational motion of the slider) is 35 %.

Thus, only by optimal generation of the input crank rotation 35 % reduction of the translational component of the shaking force has been achieved.

With regard to the rotation component of the shaking force (see expression 1, it can be balanced by a counterweight with static moment:

$$m_{CW} r_{CW} = m_2 l_{OS2} + m_3 r l_{BS3} / l \qquad (7)$$

where m_{CW} is the mass of the counterweigh mounted on the input crank; r_{CW} is the rotation radius of the centre of mass of the counterweight. For the considered mechanism the balancing static moment will be equal to 0.03375 kgm.

It should be also noted that the rotation of the input crank by a variable input speed will lead to the increasing of the shaking moment of the input crank. However, it can be fully cancelled by using the counter-rotation motion technique (Berkof, 1973; Herder, Gosselin, 2004).

Conclusion

In this paper, we have presented a new approach, based on an optimal motion generation, which allows the reduction of the shaking force in slider-crank mechanisms. This simple and effective balancing method is based on the optimal control of the linear acceleration of the slider's centre of masses. For this purpose, a "bang-bang" law acceleration motion profile has been applied on the displacement of the slider. The aim of the suggested method consists in the fact that the slider-crank mechanism is controlled not by a constant input angular velocity but by an optimal law of rotation which leads to the minimization of the acceleration of the slider. Such a control approach allows the reduction of the maximum value of the slider acceleration and, consequently, the reduction in the shaking force. It should be mentioned that such a solution is also favourable from the point of view of mechanism design because it is carried out without adding any counterweight to the connecting rod of the slider-crank mechanism. The proposed balancing method has been illustrated via an example. The numerical simulations showed that considerable reduction in shaking force was achieved.

Reference

Arakelian V., 1992. Balanced slider-crank mechanism. Patent SU n°1779853.

Arakelian V.,1993. Balanced slider-crank mechanism. Patent SU n°1802244.

Arakelian V., 1995. Synthèse dynamique des mécanismes basée sur les méthodes d'approximation de la géométrie cinématique. Proceedings of the Ninth World Congress on the Theory of Machines and Mechanisms, Italy, August 29-September 2, Vol.1: 205-209.

Arakelian V., 1998. Equilibrage dynamique complet des mécanismes. Mechanism and Machine Theory, 33(4): 425-436.

Arakelian V., Smith M.R., 1999. Complete shaking force and shaking moment balancing of linkages. Mechanism and Machine Theory, 34(8): 1141-1153.

Arakelian V., Dahan M., Smith M.R., 2000. A historical review of the evolution of the theory on balancing of mechanisms. International Symposium on History of Machines and Mechanisms. Proceedings HMM2000, Kluwer Academic Publishers, Dordrecht / Boston / London, 291-300.

Arakelian V., Dahan M., Smith M.R., 2000. Shaking force and shaking moment balancing of slider-crank mechanisms. Abstracts of the 20th IUTAM Congress: ICTAM 2000, August 27 - September 2, 2000, Chicago, USA, 58-59.

Arakelian V., Dahan M., 2001. Partial shaking moment balancing of fully shaking force balanced linkages. Mechanism and Machine Theory, 36(11-12): 1241-1252.

Artobolevskii I.I., 1964. Theory of mechanisms and machines. Moscow, Ed. Nauka, 644.

Bagci C., 1982. Complete shaking force and shaking moment balancing of link mechanisms using balancing idler loops. Journal of Mechanical Design, Trans. ASME, 104: 482-493.

Balanced crank mechanism, 1979. Patent FR 2421103, October 26.

Berestov L.V., 1978. Shaking force and shaking moment balancing of planar linkages. Ph.D. dissertation, Alma-Ata, 203.

Berkof R.S., 1973. Complete fore and moment balancing of inline four-bar linkages. Mechanism and Machine Theory, 8(3): 397-410.

Berkof R.S., 1979. Force balancing of a six-bar linkage. Proceedings of the Fifth World Congress on Theory of Machines and Mechanisms, 1082-1085.

Briot S., Arakelian V., Le Baron J.P., 2012. Shaking force minimization of high-speed robots via centre of mass acceleration control. Mechanism and Machine Theory, 57: 1-12.

Dresig H., Naake S., Rockausen L., 1994. Vollständiger und harmonischer Ausgleich ebener Mechanismen. VDI Verlag, Düsseldorf, 73.

Gheronimus Y.L., 1968. On the application of Chebychev's methods to the problem of balancing mechanisms, Mechanisms, 3 (4): 235-281.

Herder J.L., Gosselin C.M., 2004. A counter-rotary counterweight for light-weight dynamic balancing. In Proceedings of ASME 2004 DETC/CIEC Conference, September 28 – October 2, Salt Lake City, Utah, USA, 659-667.

Kamenski V.A., 1968. On the question of the balancing of plane linkages, Mechanisms, 3 (4): 303-322.

Khalil W., Dombre E., 2002. Modeling, identification and control of robots. Hermes.

Lowen G.G., Tepper F.R., Berkof R.S., 1983. Balancing of Linkages - an Update, Mechanism and Machine Theory, 18(3): 213-230.

Shchepetilnikov V.A., 1982. Balancing of mechanisms, Moscow, Ed. Mashinostroenie, 256.

Ye Z., Smith M.R., 1994. Complete balancing of planar linkages by an equivalence method. Mechanism and Machine Theory, 29 (5): 701-712.

THE INFLUENCES OF DROPLET AND NOZZLE CHARACTERISTICS ON THE RELATIVE SPRAY DRIFT OF THE AIR INCLUSION NOZZLE USED IN JAPAN

Geng Bai[1]*, Kazuhiro Nakano[1], Shintaroh Ohashi[2], Tomomichi Mizukami[3], Sumihiko Miyahara[3], Haijun Yan[4]

[1] Graduate School of Science and Technology, Niigata University, Ikarashi 2-8050 Nishi-ku, Niigata 950-2181, Japan. Phone/Fax: +81-25-262-6657, E-mail: baigeng2010@gmail.com
[2]Faculty of Agriculture, Niigata University, Niigata, Japan
[3] Institute of Agricultural Machinery, 1-40-2 Nisshin, Kita-ku, Saitama 331-8537, Japan
[4] College of Water Resources and Civil Engineering, China Agricultural University, No. 17 Tsinghua East Road, Beijing 100083, China

Abstract

Compared with conventional nozzles, drift reduction nozzles with larger droplet diameters have been proven to significantly reduce the amount of spray drift. KIRINASHI ES nozzles have been widely used as drift reduction nozzles in Japan, especially in the Hokkaido region. However, the working parameters for the nozzles (henceforth referred to as nozzle parameters) being used on boom sprayers in Japan are different from those being used in Europe and America. The nozzle using in Japan was called high-pressure nozzles in this study due to the relatively higher nozzle pressure comparing with the nozzle pressure using in other regions. A wind tunnel test for spray drift was carried out before and a classification system was also established. In this study, a deeper analysis was used to investigate the relationship among nozzle parameters and the drift reduction performance of low-pressure nozzles after using a laser analyzer to obtain the droplet size characteristics. The results indicated that the droplet size characteristics were found to have little influence on the drift potential while nozzle height had the strongest influence, followed by nozzle size and nozzle pressure.

Keywords: spray drift, air inclusion nozzle

Introduction

Spray drift of pesticide not only causes environmental contamination, it also creates a health concern for nearby residents. Many countries have begun to pay increasing attention to the pollution produced by the spray drift of pesticides. The positive list system for pesticide residues, which was set in 2006, makes spray drift control a prominent issue in Japan. Compared with traditional pesticide nozzles, the application of air inclusion nozzles on boom sprayers could noticeably decrease the amount of spray drift due to the production of droplets with larger diameters (Japan Plant Protection Association, 2009). Therefore, the large scale application of such nozzles to boom sprayers could result in effective control of spray drift. Recently, the demand for air inclusion nozzles has been increasing in the market. KIRINASHI ES nozzles have been widely used as drift reduction nozzles in Japan, especially in the Hokkaido region (Miyahara, 2012). Currently, in the UK, air inclusion nozzles represent a high proportion of new agricultural nozzle sales (Miller et al., 2011).

However, the working parameters for the nozzles (henceforth referred to as nozzle parameters) being used on boom sprayers in Japan are different from those being used in the Europe and America. The most obvious difference is nozzle pressure. Therefore, the nozzles used in Japan are called as high-pressure nozzle and low--pressure nozzle used in Europe and America in this study. Table 1 shows the major differences in nozzle parameters between the two kinds of nozzles, such as the nozzle pressure and the recommended nozzle height. Therefore, the relationship between nozzle parameters and the drift reduction performance of high-pressure nozzles might differ from that of low-pressure nozzles.

Tab. 1 Comparison of the working parameters between high-pressure and low-pressure nozzles.

Nozzle parameters	Low-pressure nozzle (Hardi injet)	High-pressure nozzle (KIRINASHI ES)
Nozzle pressure, MPa	0.3~0.8(3~8bar)	1.0~1.5(10~15bar)
Nozzle size	Larger (ISO code)	Smaller
Droplet size, µm	>500 (nozzle size >015)	about 300
Recommended nozzle height, m	0.5	0.3~0.4
Nozzle flow rate, L/min	0.4~5.23	0.35~2.07

Measurement of droplet size characteristics, wind tunnel tests to determine the relative spray drift, and field tests of actual spray drift are the main approaches for evaluating the drift reduction performance of nozzles or the overall spray system. Measurement of the droplet characteristics is the fastest of the three and the droplet size distribution has proven to be one of the most important factors influencing the spray drift associated with certain some kinds of nozzles (Nuyttens et al., 2010a). However, this method cannot be used to investigate the influence of the nozzle height on the drift reduction performance. Additionally, it also neglects the influence of droplet velocity, density and trajectory, in addition to air entrainment (Nuyttens, 2007).

Although field tests can be used to evaluate the drift reduction performance of the overall spray system, variable weather conditions can lead to large differences among repetitions and the cost of such tests is relatively high. Additionally, it may be difficult to convince farmers to allow researchers to use liquids other than water, such as the soluble tracers that are often needed for quantitative measurements. Wind tunnel measurements have proven to be a reliable way of evaluating the influence of different nozzle parameters on the drift reduction performance of nozzles (Nuyttens et al., 2010a). Many studies have been done to evaluate the influence of nozzle parameters on the drift reduction performance of low-pressure nozzles (Herbst, 2001; Nuyttens et al., 2007). No study on the influence of the nozzle parameters on the drift reduction performance of high-pressure nozzles has been carried out.

Therefore, the goals of the present study were to (1) carry out laser-based droplet size measurements and determine the relative drift potential by wind tunnel tests; (2) evaluate the influence of the nozzle size, nozzle pressure, nozzle height, and droplet size characteristics on drift reduction performance.

Material and method

The droplet size characteristics were measured using a laser diffraction analyzer, LDSA-1400A (Nikkiso). Using the accessory software, the volume distribution of droplet sizes can be determined, in addition to parameters such as the volume median diameter (VMD) and the volume percentage of droplets smaller than a certain diameter. Previous research has showed that the latter parameter was the best prediction of spray drift, with the upper limits of droplet diameter set from 75 to 200 µm (Bode, 1984; Bouse et al., 1990; Combellack et al.,1996; Baetens et al., 2009; Nuyttens et al., 2010a; Nuyttens et al., 2010b; Donkersley, Nuyttens, 2011). The VMD and the volume percentage of droplet smaller than a certain diameter were evaluated for different nozzle size and pressure combinations in order to evaluate the influence of the droplet size characteristics on the drift reduction index.

Measurements were carried out on the entire series of KIRINASHI ES nozzles, with nozzle sizes from #05 to #11, where the number represents the nozzle diameter in millimeters. Compared with the ISO nozzle size of Hardi Injet nozzles, the size of KIRINASHI ES nozzles is clearly smaller. The reason for the smaller nozzle size may be to allow the flow rate to be controlled at higher nozzle pressures. From Table 1, although the nozzle pressure for KIRINASHI ES nozzles is much higher than that for Hardi Injet nozzles, it can be seen that Hardi Injet nozzles can achieve the same flow rate range as KIRINASHI ES nozzles. Additionally, the shape of the air inlet and the final orifice of KIRINASHI ES nozzles are square, while Hardi Injet nozzles have a circular air inlet and final orifice. For Hardi Injet nozzles, the inlet size increases with nozzle size, which is not the case with KIRINASHI ES nozzles.

For the relative drift measurements and index calculation, the measuring protocol and other information have been previously reported (Bai et al., 2013).

Results and discussion

First order linear regression was carried out to determine the relationship between the DIXRP and the nozzle height for nozzle heights in the range 0.3 to 0.9 m. It was found that nozzle height was inversely proportional to the DIXRP, with high coefficients of determination.

For two nozzle pressures, the droplet size characteristics under different nozzle sizes are shown in Fig. 1 and Fig. 2, respectively. Although the DIXRP increased with nozzle size, the VMD did not (Fig. 1 and Fig. 2). The VMD even exhibited a gradual decrease when the nozzle size was increased from #06 to #11. This suggests that the droplet size characteristics have little effect on the DIXRP for the conditions used in the present study. Thus, for KIRINASHI ES nozzles, nozzle height and nozzle size may be the most important parameters determining the DIXRP. The reason why the droplet size characteristics did not obviously influence the DIXRP may be that the droplet size did not vary much among the different nozzle sizes (Fig. 1 and Fig. 2). The VMD for all nozzle sizes was in the range 300 to 400 µm and 250 to 350 µm for nozzle pressures of 1.0 and 1.5 MPa, respectively. However, as mentioned above, the larger flow rate may lead to a thicker droplet sheet that could suppress the drift phenomenon.

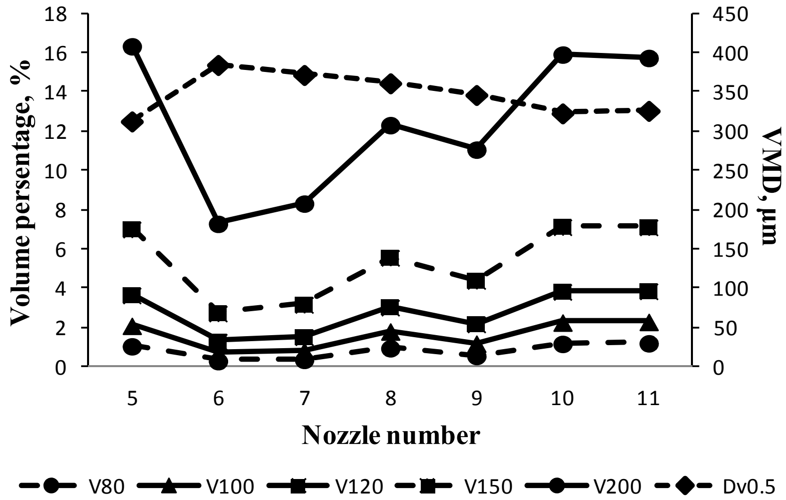

Fig. 1 Droplet size characteristics data under different nozzle sizes at 1.0 MPa nozzle pressure

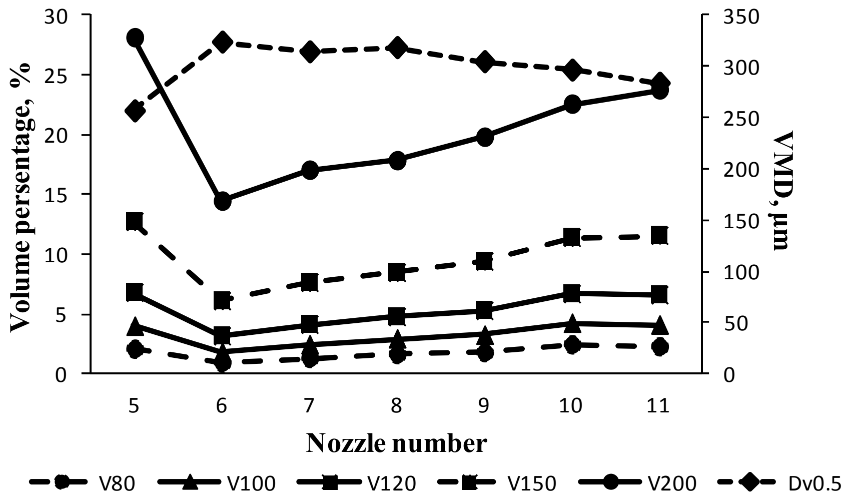

Fig. 2 Droplet size characteristics data under different nozzle sizes at 1.5 MPa nozzle pressure

Conclusions

For KIRINASHI ES nozzles, the influence of the nozzle parameters (nozzle height, size and pressure) on the drift reduction index (DIXRP) was evaluated in a wind tunnel test. Nozzle height was found to have the strongest effect on the DIXRP, followed by nozzle size and nozzle pressure. The droplet size characteristics had little influence. This may be because for the pressures used in the present study, droplet size was relative independent of nozzle size. However, for air inclusion nozzles at lower pressures, droplet size is often found to increase with nozzle size. The increase in the flow rate, which may lead to a thicker droplet sheet, could be the dominant factor causing an increase in the DIXRP for the investigated conditions. Linear and log functions were used to express the relationship between the nozzle parameters and the DIXRP.

Acknowledgements

The authors wish to personally thank Doctor David Nuyttens for the useful discussions about the experiment, the worksheet from Doctor Bradley K Fritz for the calibration experiment, Hypro company for the free nozzle samples and the China Scholarship Council for the scholarship supporting.

References

Baetens K., Ho Q.T., Nuyttens D., De Schampheleire M., Melese Endalew A., Hertog M., Nicolaď B., Ramon H., Verboven P.A., 2009. Validated 2-D diffusionadvection model for prediction of drift from ground boom sprayers. Atmospheric Environment, 43: 1674-1682.

Bai G., Nakano K., Mizukami T., Miyahara S., Ohashi S., Kubota Y., Takizawa K., Yan H.J., 2013. Characteristics and classification of Japanese nozzles based on relative spray drift potential. Crop Protection, 46: 88-93.

Bode L.E., 1984. Downwind drift deposits by ground applications. Proceedings Pesticide Drift Management Symposium, 50.

Bouse L.F., Kirk I.W., Bode L.E., 1990. Effect of spray mixture on droplet size. Transactions of the ASAE, 33: 783-788.

Combellack J.H., Western N.M., Richardson R.G., 1996. A comparison of the drift potential of a novel twin fluid nozzle with conventional low volume flat fan nozzles when using a range of adjuvants. Crop Protection, 15: 147-152.

Donkersley P., Nuyttens D., 2011. A meta analysis of spray drift sampling: drift in drift. Crop Protection, 30: 931-936.

Herbst A., 2011. A method to determine spray drift potential from nozzles and its link to buffer zone restrictions. ASAE International Meeting, Sacramento, California, Paper number: 01-1047.

Japan Plant Protection Association, 2001. Menu of technical countermeasures for spray drift. Japan Plant Protection Association.

Miller P.C.H., Ellis M.C.B., Lane A.G., Sullivan C.M.O., Tuck C.R., 2011. Methods for minimizing drift and off-target exposure from boom sprayer applications. Aspects of Applied Biology, 106: 281-288.

Miyahara S., 2012. Recent advances and future prospects on pesticide application equipment in Japan. Proceedings of 4th International Sympsium on Pesticides and Environmental Safety, Beijing, 253-254.

Nuyttens D., 2007. Drift from field crop sprayers: The influence of spray application technology determined using indirect and direct drift assessment means. Doctor thesis. Faculteit Bio-ingenieurswetenschappen, Katholieke Universiteit Leuven.

Nuyttens D., Baetens K., De Schampheleire M., Sonck B., 2007. Effect of nozzle type, size and pressure on spray droplet characteristics. Biosystems Engineering, 97: 333-345.

Nuyttens D., De Schampheleire M., Verboven P., Sonck B., 2010a. Comparison between indirect and direct spray drift assessment methods. Biosystems Engineering, 105: 2-12.

Nuyttens D., De Schampheleire M., Brusselman E., Dekeyser D., Verboven P., 2010b. Drift from field crop sprayers using an integrated approach: Results of a 5 year study. ASABE International Meeting, Pittsburgh, Pennsylvania, Paper Number: 1009.

NEW TRENDS IN CROPSTAND ESTABLISHMENT OF WINTER OILSEED RAPE

Vojtěch Bednář*, Ondřej Šařec, Petr Šařec

Czech University of Life Sciences Prague, 16521 Prague 6 – Suchdol, Czech Republic
Phone: +420 606632217, E-mail: vojtabed@volny.cz

Abstract

In recent years, substantial attention was given to winter oilseed rape in the field of plant genetics, protection and nutrition, but the field of machinery and technologies of cropstand establishment have not been considered thoroughly so far. Winter rape has become one of crops securing stable income to business and its production tends to intensification. Many agricultural businesses have not been so conservative and have been looking for more effective ways of oilseed rape growing. These trends and needs are recognized also by the manufacturers of agricultural equipment and new interesting solutions begin to emerge slowly. In addition to traditional plowing and reduced-tillage technologies, new implements for effective deep strip tillage with possibility of sowing and of depot fertilization have appeared recently. The merger of these operations requires profound knowledge on problems of cropstand establishment of winter oilseed rape, and new appropriate solutions of implements design.

Key words: oilseed rape, cropstand establishment, soil tillage, design

Introduction

In the modern world ruled by economy supported by technical development in all spheres, one cannot be satisfied in the long-run with the current state, but it is necessary to be on a watch for new ideas and the direction which will provide us with a lead and economic advantage in the competitive environment at all times. The situation is not different in agricultural sector, where it is necessary to follow the latest trends and to verify their suitability in various conditions. In agriculture, these economic influences are manifested by, for example, greater cut of machines, combination of operations, using more advanced technologies (e.g. GPS), changes in technological procedures, cultivated varieties, investment to post-harvest technologies, removing manpower, but also one’s own effort to sell commodities in foreign markets or an effort to obtain subsidies. Weather, however, remains a significant and unaffectable economic factor.

This work is devoted mainly to machines and technologies used when growing winter oilseed rape. This crop has a great economic potential, which starts to be perceived by farmers, and its further growth can be expected. One of the greatest questions in the issue of winter oilseed rape growing is cropstand establishment. This issue is addressed in more detail for its energy demand. The goal is not always to lower the expenses but also suitable water management, soil protection, limiting erosion etc. From the perspective of graduate of the Faculty of Engineering, the author perceives this issue with mechanizer´s eyes and has looked for savings especially in the above-mentioned operations of cropstand establishment while observing present findings, or needs and conditions for successful growing of winter oilseed rape. The goal was to collect the latest findings, possibilities, ideas and to try to find recommendations through them how to prepare a lot for winter oilseed rape growing in a most effective manner and at topmost quality.

Over the last three decades, there has been considerable research on the effects of conservation tillage on crop yield in many areas in Europe. Often, detailed reports were published both on the economic and environmental effects of conservation agriculture (Lopez, Arrue, 1997). However, the evidence from different studies often seems contradictory and is therefore difficult to interpret (Cantero-Martinez et al., 2003; Lopez, Arrue, 1997). This is to be expected: both the agro-environmental conditions as well as the type of conservation tillage applied vary greatly between individual studies.

According to the analysis of 563 observations carried out by Van den Putte et al. (2010), no significant yield effect of soil tillage practices was observed for fodder maize, potatoes, sugar beet and spring cereals. Only for grain maize and winter cereals a significant yield reduction occurred under conservation agriculture. For winter cereals the effect was limited but the yield reduction for grain maize was considerable. Tillage depth had a clear effect on relative crop yields. Reduced tillage resulted in crop yields that were similar to those of conventional ploughing, for all crops except maize. Particularly on sandy soils, grain maize was not performing well, and winter cereal yield was also slightly reduced. Deeper reduced-tillage to more than 0.15 meters though demonstrated similar (on sandy soils) or even higher (on clay-loam soils) winter cereal yields than conventional tillage. It seems therefore advisable that farmers starting with the implementation of conservation tillage use a sufficient tillage depth so that yields are maintained. In a later stage, tillage depth may be reduced as this may lead to a reduction of operational costs (Van den Putte et al., 2010).

A comparison of the different components of the total costs revealed that reduced-tillage required larger machinery and herbicide costs, but these costs were largely offset by reduced operating costs (Sanchez-Giron et al., 2004, 2007). In various other studies, it was concluded that slightly lower crop yields can be offset by the reduced fuel inputs and labour consumption (Bonciarelli, Archetti, 2000; Gemtos et al., 1998; Tebrügge, 2000). However, this may be dependent on local situation and farm-specific properties such as farm size (Sanchez-Giron et al., 2007), cropping system, etc.

Material and method

13 agricultural businesses growing winter oilseed rape in various production areas were chosen in the Czech Republic where different production technologies were monitored. At least one field was monitored in every business. Especially the following values were monitored:

- The nature of individual fields (area, type of soil cultivation, previous crop, the usage of crop residues, last application of organic fertilizers);
- The nature of soil (in particular bulk density - evaluated with the so called Kopecky sampling rollers for soil moisture constant determination, humidity, the degree of compaction – penetration resistance measurement by a penometer);
- The nature of growth (yield, the number of plants m^2, the weight of roots, hybrid / line variety);
- The data on conducted work operations (machinery, fuel consumption and work, expenses and other supplementary information)

After the completion of terrain experiments, there was evaluation of the obtained data and information, economic evaluation of the efficacy of money spent (with every business, the amount of expenses spent was evaluated regarding the achieved seed yield and the technology used for cropstand establishment), setting conclusions with a subsequent proposal for a suitable technology for effective growing of winter oilseed rape.

Results and discussion

The economic potential of growing winter oilseed rape has been lately attracting attention of not only growers but also development groups in the sphere of genetics, plant protection and last but not least the producers of agricultural technologies. It is where the space for technical innovation leading to savings in the expenses, time, increasing the crop and the overall efficacy in cropstand establishment can be sought. In cooperation with 13 agricultural businesses, technology-oriented operational monitoring and measuring for establishing the growth of winter oilseed rape were conducted. The goal of the experiments was to verify which of the technologies are advantageous from technological and economic perspective. When it comes to the results of operational monitoring, a significant difference in average expenses for a unit of production for the whole of monitored period in favour of minimization technology was found. Minimizing technologies also came out as more fertile in the monitoring period from the results of comparison of average seed crop. When growing winter oilseed rape, the best results were achieved in beet area. What is positive is that there was a significant drop of the soil compaction in the monitored businesses from 2009 – 2012. Fig. 1 displays a brief summary of results achieved by individual businesses. Based on these results it was further examined which of the measured and monitored values could have taken part in these results and whether there is any dependence between them.

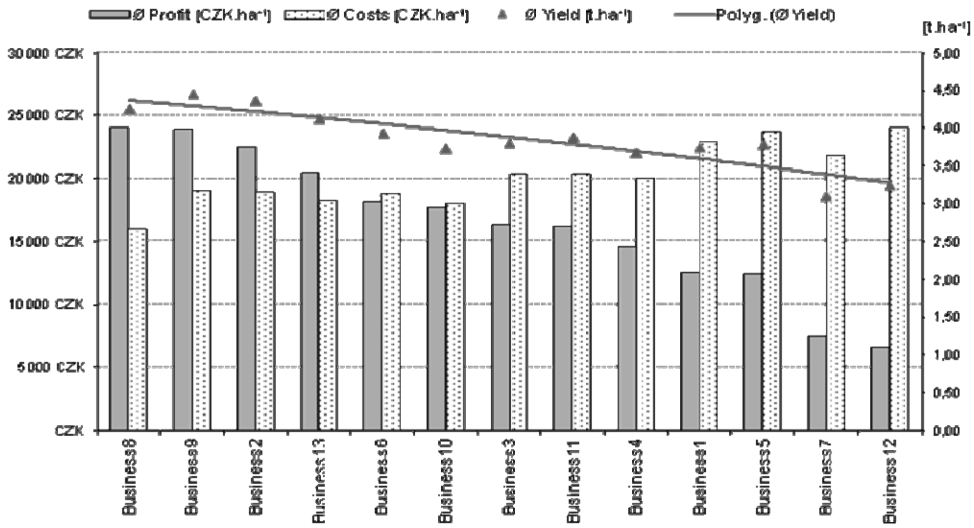

Fig. 1 Mean values of profit, expenses and seed yields for the monitored period in individual businesses

It is visible that seed yield has a significant influence on the final balance of a business. It must not be, however, forgotten that so does also a correct spending of expenses. It is also visible from the graph that the businesses with high expenses on a hectare, which were not effectively spent, had the worst results, which is also indicated by lower overall mean seed yield. Indirect costs, different in each of the businesses, were not considered in this work.

Minimization technology came as a technology with lower average costs from the obtained and measured data in the course of all the monitored years. This was for approximately CZK 3 000 per hectare, CZK 1 722 per tone respectively. Minimization technology also proved the one with higher average seed yield per hectare (by 0.54 t.ha^{-1}) and also the higher final average profit from one tone of seeds (by 1 722 CZK.t^{-1}) in the monitored businesses and years. Beet area came out as the area with the highest average yield for the time of our monitoring individual businesses in various production areas (3.99 t.ha^{-1}), followed by cereal area (3.94 t.ha^{-1}). The third position was occupied by both potato and maize area (3.81 t.ha^{-1}). The least suitable proved to be forage area (3.69 t.ha^{-1}). Furthermore, the dependence of seed yield on soil conditions was studied. It is visible from Fig. 2 that one can look for certain dependence between the reduced bulk density and the seed yield. It is therefore necessary to limit the number of travels on lots and to minimize soil compaction caused by machinery, in particular in areas with the occurrence of clayish soils prone to compaction.

The influence of soil compaction on the seed yield is shown in Fig. 3. It is visible that the dependence between the value of soil penetration resistance and the influence on seed yield can be found despite the tightness of measurement is small. Low soil penetration resistance has a beneficial influence on the root system growth which ensures better access to water and nutrients for its deeper rooting.

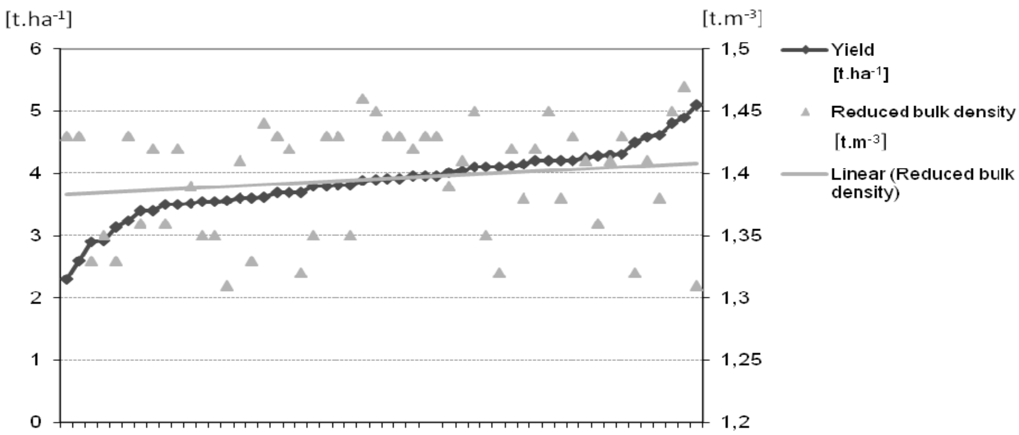

Fig. 2 The values of seed yield depending on the reduced bulk density

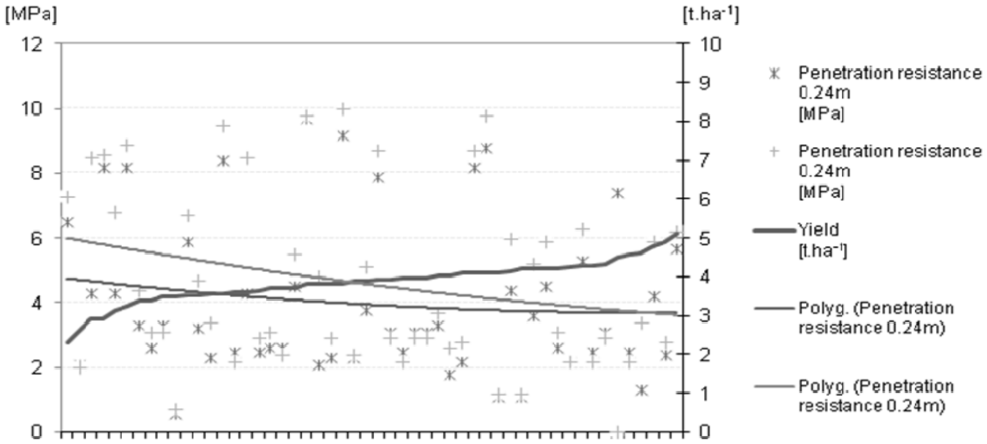

Fig. 3 The values of penetration resistance related to the achieved seed yield

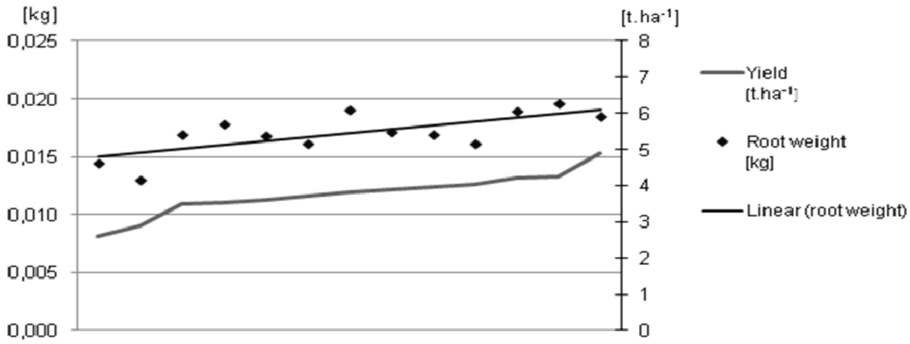

Fig. 4 The influence of root weight on seed yield

A lot without any greater signs of compaction is a requisite for fast and deep rooting of plants. It is visible from Fig. 4 how the maturity of root system (weight) gives evidence of the ability to supply plant with a sufficient water and nutrients intake, which is positively revealed in higher yield of seeds. The care for soil, or soil profile, and its structure is thus one of the necessary steps for achieving high yield of seed. Impenetrable compact soil layers preventing optimal function of water regimen and sufficient rooting of plant are totally inadmissible. The energy a plant has to exert for creating the root system in these difficult conditions is decisive when it comes to final yield.

Other factor that might have had an influence of the yield was the number of plants per 1 m^2. The links were not proved, unfortunately. It is, however, obvious that a higher number of plants was not always the guarantee of higher yield. On the contrary, it often had a negative influence on the increased nutrition competition of plants. When evaluating the results of yield of individual varieties grown in the monitored businesses and years, line variety came out better. The achieved values of mean hectare yield in hybrid and line varieties differed by 0.39 $t.ha^{-1}$.

Conclusions

- It is obvious from the study of the current state of affairs, the results of measurements, monitored data but also from the experience from abroad that the production of winter oilseed rape is heading towards intensification.
- The design of a new technology should follow the path of minimization. The new technology must create ideal conditions for the development of root system.
- One of the factors significantly influencing the development of the root system are compact soil layers. The new technology must ensure the disruption of these layers, loosening and the balance of water regimen in soil profile. When observing these requirements, the speed of cropstand establishment and expenses for this operation, the soil must be cultivated by Strip Till.
- It follows from domestic and foreign sources that the date of seeding winter oilseed rape is very demanding for timeliness, therefore all the operations for cropstand establishment must be done in one operation, if possible.
- Lately, there has been a gradual decrease of sowings and the number of plants per m^2 (35

and fewer), and the increase in between-the rows spacing (to 37.5 cm) which has a positive influence on the decrease of competition among individual plants. It is therefore way more important to ensure evenness of sprouting and the evenness of growth. This indicates that oilseed rape will be sown by precise sowing machine.

- To unify the operations of deep loosening and quality pre-sowing preparation together with sowing and fertilization requires special construction solution for this crop. On the basis of the evaluated data and findings, a new machine and a new technology of winter oilseed rape stand establishment is designed in cooperation with BEDNAR FMT - “Terra Rape” being the working name. The machine is currently in a phase of a prototype and it will soon be tested in operation conditions. The basic concept of the new machine is displayed on Fig. 5.

References

Bonciarelli F., Archetti R., 2000. Energy saving through reduction of soil tillage. In: 15th ISTRO Conference, Fort Worth, TX, USA.

Cantero-Martinez C., Angas P., Lampurlanes J., 2003. Growth, yield and water productivity of barley (hordeum vulgare l.) affected by tillage and N fertilization in Mediterranean semiarid, rainfed conditions of Spain. Field Crops Research, 84: 341–357.

Gemtos T.A., Galanopoulou S., Kavalaris C., 1998. Wheat establishment after cotton with minimal tillage. European Journal of Agronomy, 8: 137–147.

Lopez M., Arrue J., 1997. Growth, yield and water use efficiency of winter barley in response to conservation tillage in a semi-arid region of Spain. Soil and Tillage Research, 44: 35–54.

Sanchez-Giron V., Serrano A., Hernanz J., Navarrete L., 2004. Economic assessment of three long-term tillage systems for rainfed cereal and legume production in semiarid central Spain. Soil and Tillage Research, 78: 35–44.

Sanchez-Giron V., Serrano A., Suarez M., Hernanz J., Navarrete L., 2007. Economics of reduced tillage for cereal and legume production on rainfed farm enterprises of different sizes in semiarid conditions. Soil and Tillage Research, 95: 149–160.

Tebrügge F., 2000. Long-term no-tillage as a tool to protect the environment, results of 20 year field trials on different kinds of soil in different crop rotations. In: 15th ISTRO Conference, Fort Worth, TX, USA.

Van den Putte A., Govers G., Diels J., Gillijns K., Demuzere M., 2010. Assessing the effect of soil tillage on crop growth: A meta-regression analysis on European crop yields under conservation agriculture. European Journal of Agronomy, 33(3): 231-241.

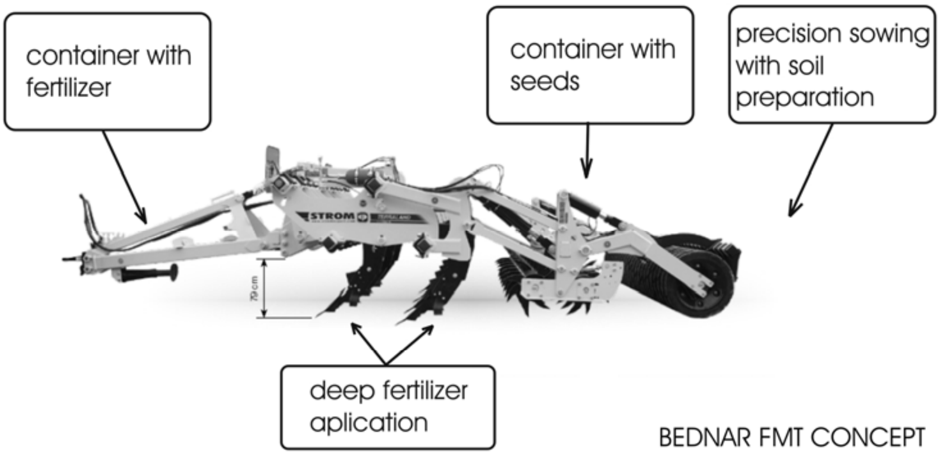

Fig. 5 Terra Rape concept

TEMPERATURE DEPENDENT ELASTICITY OF PLANTS INDICATED BY DMA

Jiří Blahovec

Czech University of Life Sciences, 16521 Prague 6 – Suchdol, Czech Republic,
Phone: +420-224384281, Fax: +420-220921361, E-mail: blahovec@tf.czu.cz

Abstract

DMA (Dynamic Mechanical Analysis) is used for thermal analysis (Haines, 2002) of few plant parts (pith and sprouts of two potato varieties, bean sprouts and carrot roots) during their heating from 30 °C up to 90 °C (heating rate 1 °C/minute). The results of the test are concentrated into the complex modulus of elasticity plotted versus the increasing temperature. Relations between the both components of elastic modulus form basis for discussions of the changes in elasticity of the heated products. It is concluded that decrease of elasticity starts to be important at some characteristic temperature different for different products (55-70 °C). The rate of decrease is comparable for many plants being appr. 0.2 %/K. In case of the bean sprouts there were observed values about one order higher.

Keywords: DMA, thermal analysis, modulus of elasticity

Introduction

The role of temperature as an important external parameter for living organisms is generally known. Even if the knowledge of the partial processes caused by temperature variation is relatively good (Garret, Grisham, 2010), there is still a lack of information on the details of the parallel processes taking part in living cells and tissues during their heating. As with tissues, the behaviour of cellular complexes has to be studied by indirect methods in which the characteristic states are indicated. For such purposes the methods of thermal analysis (Haines, 2002) can be used provided that tissue drying due to increasing temperature is prevented. In previous papers (Blahovec, Lahodova, 2012; Blahovec, Lahodova, 2012; Blahovec et al. 2012) we used one method of thermal analysis, dynamic mechanical analysis (DMA), for the detection of starch swelling in cells of potato parenchyma under conditions of high humidity. Characteristic peaks were observed at temperatures above 70 °C, i.e. slightly above the temperature of potato starch gelatinization in potato tubers (Karlsson, Eliasson, 2003; Karlsson, Eliasson, 2003). The existence of the observed peaks was explained (Blahovec, Lahodová, 2011) as due to the additional internal pressure caused by starch swelling in a manner analogous to turgor pressure, usually observed in cells at standard conditions. Turgor is an important source of the tissue toughness and its relationship to the potato modulus of elasticity was first theoretically expressed by Nilsson et al. (1958). The modulus of elasticity of a tested specimen is the main parameter that is recorded during controlled heating of the specimen in a DMA test (Haines, 2002). The DMA test makes possible the measurement of two components of the complex modulus: the real part (storage modulus, SM) expressing the elastic part of the material toughness, and the imaginary part (loss modulus, LM) describing the inelastic (fluid) part of the toughness.

The modulus of elasticity of cellular walls decreases with increasing temperature in the same way as the modulus of elasticity of other substances (Ward, 1983). This decrease, as well as the changes in the intracellular pressure during heating of the specimen, can be displayed in DMA's modulus-temperature plots. The intracellular pressure is controlled by the actual semi-permeability of the cellular walls which changes with temperature. A fundamental increase of the potato cell wall permeability at about 60 °C was observed (Personius, Sharp, 1938) as a result of the breakdown in the cell pore system separating parenchyma tissue into symplast and apoplast.

This behaviour is attributed to the changes in the pore protein conformation (folding), which can be caused by irreversible denaturation (Garret, Grisham, 2010; Personius, Sharp, 1938; Minetti, Remeta, 2006; Maule, 2008; Tsong, Su, 1999). The pores have very complicated structures; thus, for the structure of plasmodesma, Maule (2008) gave more than 20 components and different proteins including of cytoskeletal components, such as actin, and dynamic motor proteins such as myosin. The temperature stimulated folding in the conformed components can cause deep changes in pore function (Kubelka et al., 2004). The kinetics of folding can be extremely rapid with relaxation times in the order of μs (Kubelka et al., 2004) for simple proteins. On the other hand, for more complicated proteins and their complicated architectures such as plasmodesmata, the relaxation times are much longer, in the order of minutes or longer depending on temperature and other factors (Tsong, Su, 1999).

In this paper we applied our modified DMA method to few plant parenchyma with the aim of detecting details of the tissue softening especially at temperatures corresponding to the changes in the pore (protein) functions.

Material and Methods

Fresh potato tuber pith (variety Saturna), carrot root (*Daucus carota, subsp. Sativa*, diameter appr. 4 cm and length about 15 cm) was bought from the local market and stored in cold and wet conditions (4 °C, 85 % relative humidity). After a short storage (less than 2 weeks), the individual products were washed in cold water. The selected defect-free products of medium size were then left at room temperature for testing the next day. Rectangular specimens measuring 8 (width) x 3 (thickness) x 22 (length) mm with the long axis parallel to the root or tuber axis were cut from the myzoderma (outer part of the tested carrot roots) or tuber pith using special cutting jigs. Sprouts cultivated in laboratory from potato (variety Saturna) and beans were cut in the narrow parts into pieses appr. 2 cm long. Diameter of sprouts were 5.8 mm and 3.5 mm for potato and bean, respectively.

The DMA experiment was performed with a special DMA instrument, constructed by RMI Company (Pardubice, Czech Republic), model DX04TC. Each specimen was mechanically fixed in two points so that the longitudinal axis was perpendicular to the fixing jaws. The free length of the specimen between the jaws was 4.4 mm. The height of the fixed specimen was appr. 3 mm. One of the jaws was fixed, while the other moved up and down with a constant amplitude = 1 mm and a frequency = 1 Hz. The force connected with the oscillation was recorded, being the basis for the complex module determination (storage - SM and loss - LM). The moduli values (originally in Pa) sensitively depend on the form of the tested specimen. To prevent this source of variation we calculated the resulting SM and LM values as a ratio of the corresponding value obtained for SM at 30 °C. This method is suitable for the determination of peak positions and the slope analysis. Every experiment started at a temperature of 30 °C and 90 % air humidity in the test chamber. The humidity was kept constant during the whole experiment, while the temperature increased up to 90 °C at rate (A) 1 °C/minute. Every test was repeated ten times using fresh specimens.

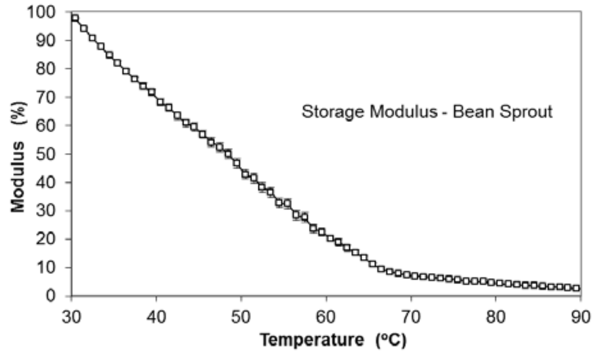

Fig. 1 Plot of storage modulus versus temperature for bean sprout. The bars denote calculated standard errors.

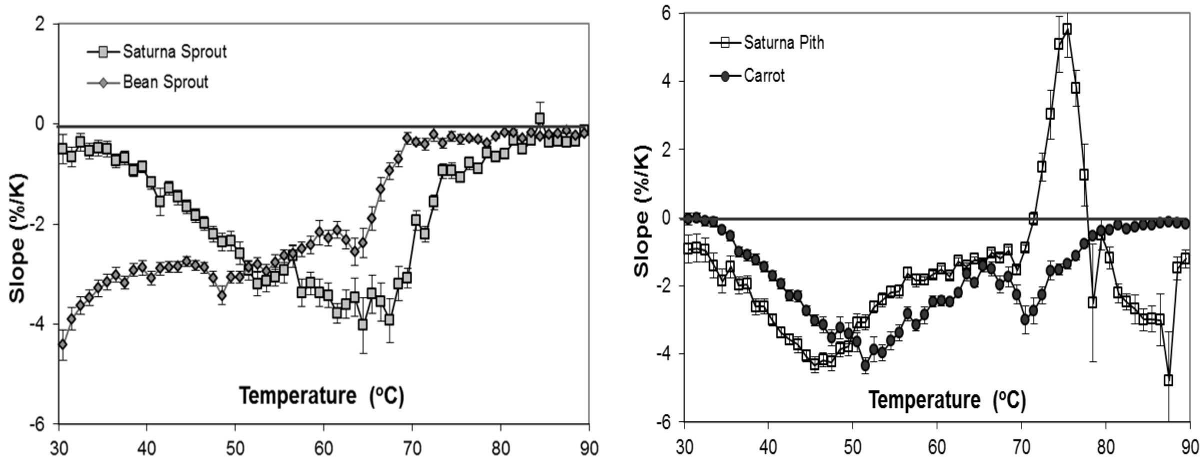

Fig. 2 Temperature derivative of storage modulus plotted versus temperature. In upper part sprouts, in lower part tissues of potato pith and carrot parenchyma. The bars denote standard error.

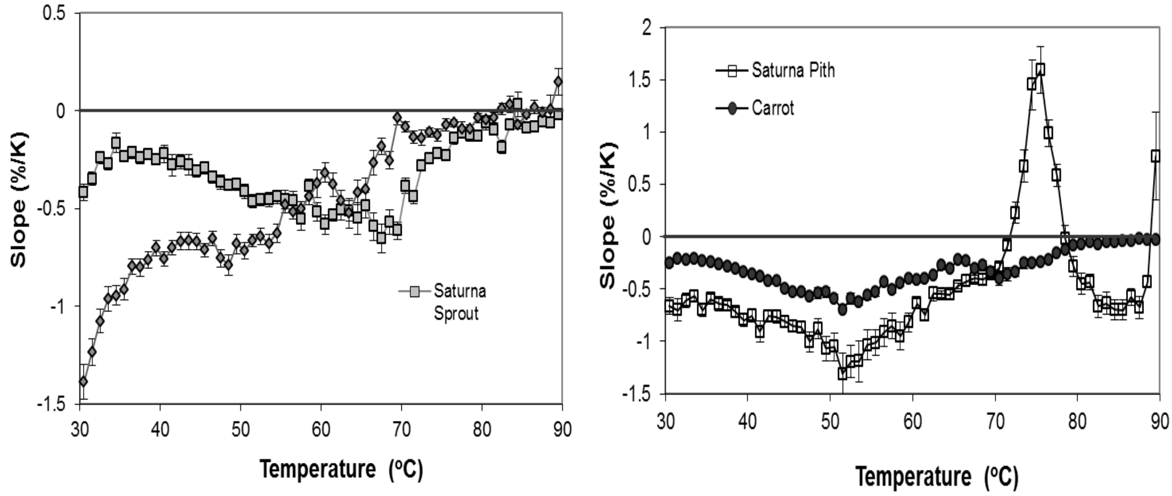

Fig. 3 Temperature derivative of loss modulus plotted versus temperature. In upper part sprouts, in lower part tissues of potato pith and carrot parenchyma.

Results and Discussion

Figure 1 shows that in the most simple case, the bean sprout, the obtain modulus-temperature plot is very simple. It is formed by two quasi-linear parts. The first one is formed by steep modulus decrease to values about one order lower at temperature between 60 and 70 °C. The second part is also quasi-linear similarly as the first part but its decrease is not so steep as the first one. The data are highly reproducible as is given by bars. The highest variability was observed at temperatures between 50 and 60 °C. Not simple are plots of the module of elasticity components for every specimen. It was reported previously (Blahovec, Lahodova, 2012; Blahovec, Lahodova, 2013; Blahovec et al., 2012) that at temperatures above 70 °C there were observed peaks for both modulus components. These peaks are less at potato pith (Blahovec, Lahodova, 2012; Blahovec, Lahodova, 2013), but some form of the peak is observed also in this case.

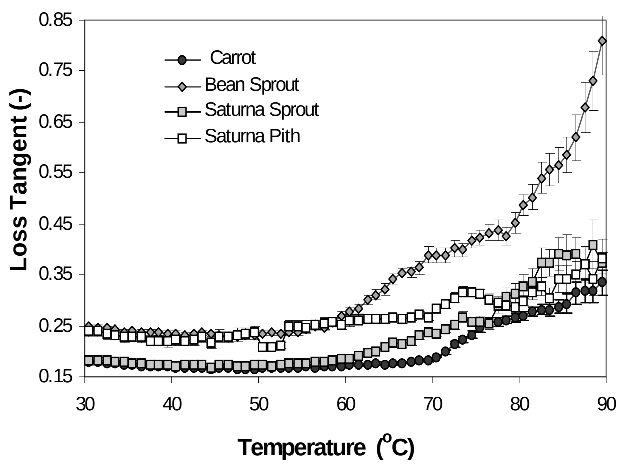

Fig. 4 Plot of loss tangent versus temperature

The details of temperature module plots are more visible when the temperature derivatives are analysed. It was done for the storage modulus in our data in Fig. 2, where data for different tissues (of sprout and or tubers) were separated. In sprouts one more important minimum was observed at temperatures 60-70 °C. This minimum corresponds to the point in Fig. 1, where the storage modulus versus temperature is separated into two quasi-linear parts. In sprouts are also observed smaller minima close to 50 °C. In the potato and carrot tissues the similar minima of the storage modulus versus temperature derivatives were observed. The difference between these two groups consists in depth of both minima. The minima at appr. 50 °C in potato and carrot tissues are much deeper than the minima observed at appr. 70 °C oppositely to the relation between both minima observed in the sprouts. The minimum at appr. 70 °C can be deformed by the starch peak located at temperatures above 70 °C, but in case of carrot this explanation cannot be applied. It seems that tissue structures differ from the simple cellular structures in the tested sprouts. Both minima should be related to the changes in the cell wall pores (Garret, Grisham, 2010; Maule, 2008; Tsong, Su, 1999).

The similar changes as for storage module were also observed for loss module. They are plotted in Fig. 3. The absolute values of the temperature derivatives comparing to the same plots for loss module are caused mainly by the absolute lower values of loss modulus comparing to the storage modulus. For the plots of sprouts, the depth of the minimum at appr. 50 °C is lower than that it was observed for storage modulus (Fig. 2). The slope increase at cca 70 ^{o} C is at loss modulus lower than the slope increase that was observed for the storage modulus (Fig. 2). Similarly to storage module the loss module in tissues (potato and carrot) had the deeper minima at temperature appr. 50 ^{o}C than at temperatures appr. 70 ^{o}C. Also indication of "starch" peak in potato pith at temperatures above 70 ^{o}C was observed.

The relation between loss and storage module can be easily expressed (Ward, 1983) by loss tangent tan δ:

$$\tan\delta = \frac{E_L}{E_S} \qquad (1)$$

where E_L is loss modulus and E_S corresponding storage modulus. The loss tangent is a formula expressing relation between dissipating and conserving processes participated in formation of toughness of the testing product. The participation of conserving processes in the toughness formation can be than expressed as elastic degree ED:

$$ED = \frac{E_S}{\sqrt{E_S^2 + E_L^2}} \qquad (2)$$

Eqs. (1) and (2) than gives the elastic degree as a function of loss tangent:

$$ED = \frac{1}{\sqrt{1+\tan^2\delta}} \qquad (3)$$

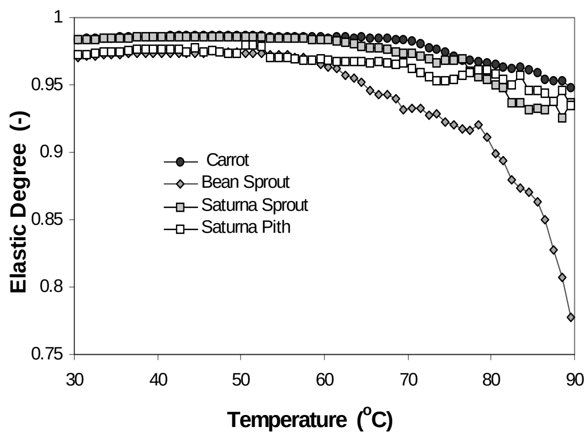

Fig. 5 Temperature plot of elasticity degrese for the tested plant tissues

Loss tangent values calculated from Eq. (1) are plotted versus temperature in Fig. 4. This figure shows that loss tangent increased with increasing temperature in all tested plant tissues. The elastic degree is than calculated and given in Fig. 5.

Figure 5 indicates that the observed decrease of elasticity degree is not homogeneous process and it has some parts with different rate of decrease. Slope analysis of the data with their smoothing (mean value with the 8 neighbours) is given in Fig. 6 (TSED means temperature slope of elastic degree). Even if the data plotted in Fig. 5 differ for different tested products, they have some common properties. The first one is slow increase of TSED with increasing temperature below about 55 ^{o}C. This trend is finished at some temperature denoted as T_1 (about 55 ^{o}C at sprouts and about 65 ^{o}C for potato and carrot) that is denoted by an arrow. The second arrow denotes the endpoint of the temperature range (T_2) where TSED is steeply higher than in the previous part. TSED forms between these two points peak at temperature T_3. The data for the characteristic temperatures and corresponding TSED for the tested plant tissues are given in Table 1. At temperatures higher than T_2 the TSED increased. The data for Saturna pith are influenced by the "starch" peak at high temperatures.

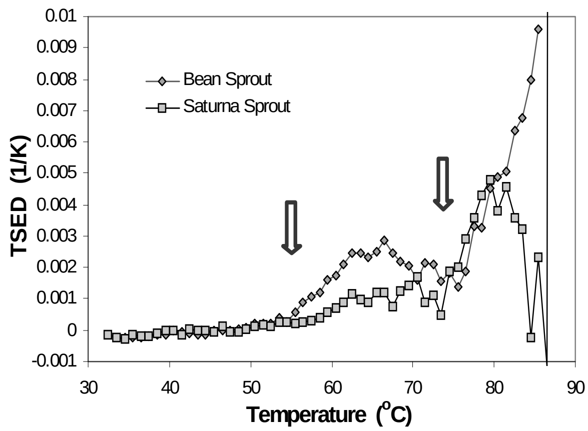

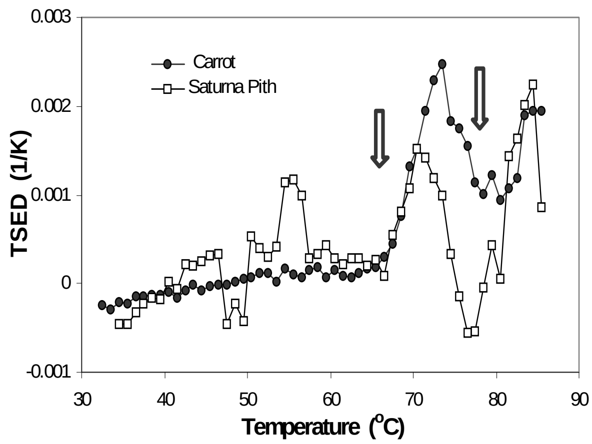

Fig. 6 Temperature slope of elastic degrese plotted versus temperature, upper figur efor sprouts, košer for plant tissues. The arrows determine the first area of higher slopes. The data were smoothed

Tab. 1 Characteristic points of TSDE-temperature plots

Tissue	T1		T2		T3	
	Temperature (°C)	TSDE (1/K)	Temperature (°C)	TSDE (1/K)	Temperature (°C)	TSDE (1/K)
Bean Sprout	55.5	0.00026	75.5	0.00138	66.5	0.00286
Saturna Sprout	57.5	0.00031	73.5	0.000473	70.5	0.00171
Saturna Pith	66.5	0.000084	76.5	-0.00056	70.5	0.00151
Carrot	65	0.000167	80.5	0.000936	73.5	0.00247

Conclusions

Elasticity of plant tissues toughness decreases with increasing temperature of heating. This decrease is not homogeneous and it has the first higher rate at temperatures higher than 55-65 °C (depending on tissue) and further one at temperatures above 75-80 °C.

Reference

Blahovec J., Lahodová M., 2011. DMA peaks in potato cork tissue of different mealiness. Food Eng. 103: 273-278.

Blahovec J., Lahodova M., 2012. DMA thermal analysis of different parts of potato tubers. Food Chem. 133: 1101-1106.

Blahovec J., Lahodová M., Zámečník J., 2012. Potato DMA analysis in area of starch gelatinization. Food Bioprocess Technol. 5: 929–938.

Blahovec J., Lahodova M., 2013. Storage induced changes of potato properties as detected by DMA. LWT - Food Sci. Technol. 50: 444-450.

Garret R.H., Grisham C.M., 2010. Biochemistry. 4th edition. Brooks/Cole, Boston.

Haines P.J., 2002. Principles of thermal analysis and calorimetry. Royal Society of Chemistry Cambridge, 220.

Karlsson M.E., Eliasson A.-C., 2003. Gelatinization and retrogradation of potato (Solanum tuberosum) starch in situ as assessed by differential scanning calorimetry (DSC). Lebensmittel-Wissenschaft und-Technologie 36: 735-741.

Karlsson M.E., Eliasson A.-C., 2003. Effects of time/temperature treatments on potato (Solanum tuberosum) starch: a comparison of isolated starch and starch in situ. J. Sci. Food Agriculture 83: 1587-1592.

Kubelka J., Hofrichter J., Eaton W.A., 2004. The protein folding ‘speed limit’. Curr. Opin. Struct. Biol. 14: 76-88.

Maule A.J., 2008. Plasmodesmata: structure, function and biogenesis. Curr. Opin, Plant Biol. 11: 680-686.

Minetti C.A.S.A., Remeta D.P., 2006. Energetics of membrane protein folding and stability. Arch. Biochem. Biophys. 453: 32-53.

Nilsson S.B., Hertz C.H., Falk S., 1958. On relation between turgor pressure and tissue rigidity. II. Theoretical calculations on model systems. Physiologica Plantarum 11: 818-837.

Personius C., Sharp P.F., 1938. Permeability of potato-tuber tissue as influenced by heat. Food Research 3: 525–541.

Tsong T.Y., Su Z.–D., 1999. Biological effects of electric shock and heat denaturation and oxidation of molecules, membranes, and cellular functions. Ann. N. Y. Acad. Sci. 888: 211-232.

Ward I.M., 1983. Mechanical properties of solid polymers. John Wiley & Sons New York.

UTILIZATION OF STALK MATERIALS AND THEIR MIXTURES WITH WOODEN SHAVINGS FOR BRIQUETTES PRODUCTION

David Blažej[1*], Jiří Souček[2], Martin Procházka[1]

[1]Czech University of Life Sciences Prague, Kamýcká 129 16521 Prague 6 – Suchdol, Czech Republic, E-mail: blazej@tf.czu.cz
[2]Research Institute of Agricultural Engineering, Prague, Czech Republic

Abstract

The article deals with the production of briquettes from reed canary grass and linseed stems and their mixtures with wooden shavings. Stems of both materials contain relatively high proportion of long solid fibres; therefore a disintegration of material by a cutting mechanism is necessary for further processing. In this case a cutting shredder Kovo Novák RS 650 was used. After this procedure, net calorific value was measured according to ČSN ISO 1928. The processed material was utilized for briquettes production at the Briklis HLS 50 production line. The basic parameters like dimensions and densities of the produced briquettes were measured. The samples of the production were also subjected to the mechanical durability test according to the ČSN P CEN/TS 15210-2. Measured and calculated research outputs were evaluated and compared to create an information overview. This can be used as a support tool to determine whether the briquettes produced from researched stalk materials fulfill the general demands on solid biofuels properties.

Keywords: reed canary grass, linseed, wooden shavings, briquettes, mechanical durability

Introduction

The yield of the linseed is usually between 2 – 6 tonnes of dry matter per hectare in the condition of the Central Europe. It is dependent on many factors like variety, place, weather in the area and, of course, utilized agro-technical methods (Rennebaum et al., 2002). The Amon variety of linseed was used for the purposes of this article.

Reed canary grass is a perennial grass with a yield of 4.5 – 8 tonnes of dry matter per hectare when the desired conditions are met (Lindh et al., 2009). The compaction of reed canarygrass was investigated by (Kronbergs et al., 2013).

Stalks of both materials contain a big amount of solid fibres. Desired parameters of stems for further processing can only be ensured by disintegrating the material by cutting mechanism. The aim of this article is to investigate the briquettes production from these material and their mixtures with wooden shavings.

Briquetting, the compression of the loose material, usually brings a lot of advantages, especially significant volumetric reduction, higher energetic density and more convenient manipulation. Briquettes are today made from a variety of wooden, stem or even metallic materials (Brožek, Nováková, 2010; Nováková, Brožek, 2008; Brožek, 2011; Stolarski, 2013).

Material and methods

Disintegration of the material was realized by the KOVO Novák RS 650 shredder. Its construction allows using sieves with different apertures diameters. Apertures diameters of used sieves were 12 mm. Input of the material was manual and in small doses to achieve continuous and balanced process.

The material obtained by dismantling of the bales was dosed manually and in small portions so as to ensure continuity of the process and that the input material does not contain impurities, which could damage the device or cause sparks and ignite the material. Compressed was clean material of the linseed, reed canary grass and mixture of one of each material with wooden shavings in the ratio of 1:1.

Briquettes were made on the Briklis HLS 50 piston hydraulic press. It has one compressing chamber with the 65 mm diameter and pressure varies from 0.4 to 1 MPa and is induced by the movement of piston against the outgoing briquettes. More detailed overview of the press attributes is in the Tab. 1. Net calorific value of the feedstocks was measured according to ČSN ISO 1928.

Tab. 1 Parameters of the briquetting press Brisktar HLS-50

performance	$kg.h^{-1}$	50.00
weight	kg	520
voltage	V	3x400
Power input	kW	4.3
Briquette diameter	mm	65
Briquette length	mm	30 - 50
Briquettes density	$kg.m^{-3}$	700 - 1100

Briquettes were tested on mechanical durability according to ČSN P CEN/TS 15210-2. The testing device schematics are on the Fig. 1. Samples are rotating in the drum and are exposed to shocks when hitting each other and walls of the drum. The mechanical durability is calculated from the remaining weight of the samples. This test is important for estimating behavior of pellets and briquettes during storage and manipulation.

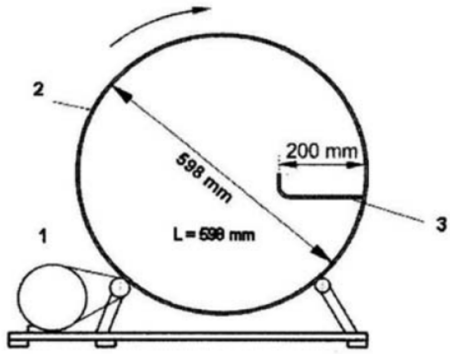

Fig. 1 Mechanical durability testing device
1 – engine; 2 – drum; 3 – shovel

Results

The results of the material disintegration are shown in the Tab. 2. Linseed has significantly higher material output. Reed canary grass shows slightly better results in energy consumption which can be caused by the lower solid fiber content.

Tab. 2 Parameters of the feedstock shredding

Material	Linseed Amon	Reed canary
Sieve apertures diameter (mm)	12.00	120
Output ($kg.h^{-1}$)	103.40	64.35
($MJ.kg^{-1}$)	0.17	0.12
($kWh.kg^{-1}$)	0.06	0.04

The net calorific values displayed in the Tab. 3, linseed's is noticeably lower.

Tab. 3 Net calorific value of the feedstock

Material	net calorific value [$MJ.kg^{-1}$]
Reed canary	17.41
Lineseed Amon	15.91

Linseed shows worse results even in the briquettes productions. The specific energy consumption is twice as high and the output per hour is 27.8 per cent lower. Results are in the Tab. 4.

The results of mechanical durability and other important parameters are shown in the Tab. 5. The results of reed canary grass and both mixtures are quite satisfactory. But the pure linseed briquettes are out of acceptable range. The density of reed canary grass briquettes is significantly lower than results reported by Kronbergs et al. (2013), were the maximum range is 899-964 kg m^{-3}.

Tab. 4 Important parameters of the briquettes production

	Linseed Amon	Reed canary	Amon + shavings	Reed canary + shavings
Specific energy consumed ($kWh.kg^{-1}$)	0.08	0.04	0.06	0.08
Output ($kg.h^{-1}$)	33.00	42.2	22.75	52.00
Volume (dm^3)	0.19	0.13	0.12	0.20
Density ($kg.m^{-3}$)	807.00	730.00	875.00	881.00

Tab. 5 Mechanical durability overview

	[%]
Linseed Amon	60.30
Reed canary	93.13
Amon+shavings	96.91
Reed canary + shavings	96.76

Conclusions

The problematic of using alternative feedstock than wood or wooden waste for solid biofuels production is a discussed topic.

1. The results show that the linseed, respectively its Amon variety, is not very suitable for this purpose (60.30 %). On the other hand the mixture with wooden shavings in a 1:1 ratio showed much better mechanical durability (96.91 %).
2. Results of pure reed canary grass (93.13 %) or its mixture with wooden shavings (96.76 %) were much more satisfactory and it can be recommended for this type of production.
3. The output of material from the production line per hour is lower, when linseed is used.
4. There is a noticeable difference between the briquettes from pure material and its mixture. In case of Amon the difference is 8.47 %, in case of reed canarygrass the difference is 20.68 %. There are only slight differences between the mixtures.

However, the utilization of alternative biofuels from stems materials is complicated due to the lack of compatible incineration devices on the market.

Acknowledgement

Supported by the Ministry of Agriculture of the Czech Republic, Project No. QI92A143.

Reference

Rennebaum H., Grimm E., Warnstorff K., Diepenbrock W., 2002. Fibre quality of linseed (Linum usitatissimum L.) and the assessment of genotypes for use of fibres as a by-product. Industrial Crops and Products 16(3): 201-215.

Lindh, T., Paappanen T., Rinne S., Sivonen K., Wihersaari M., 2009. Reed canary grass transportation costs - Reducing costs and increasing feasible transportation distances. Biomass and Bioenergy, 33(2): 209-212.

Kronbergs A., Kronbergs E., Repsa E., 2013. Evaluation of reed canary grass shredding and compacting properties. Agronomy Research, 11(1): 61-66.

Brožek M., Nováková A., 2010. Briquetting of chips from nonferrous metal. In.: 9th International Scientific Conference „Engineering for Rural Deve1opment“. Jelgava, Latvia University of Agriculture, Faculty of Engineering, 236 - 241.

Nováková A., Brožek M., 2008. Mechanical properties of pellets from sorrel. In.: 7th International Scientific Conference “Engineering for Rural Development”. Jelgava, Latvia University of Agriculture, Faculty of Engineering, 265 - 269.

Brožek M., 2011. Quality evaluation of briquettes made from biomass. In.: The Fifth International Scientific Conference “Rural Development 2011”. Akademija, Kaunas district, University of Agriculture (Aleksandras Stulginskis University), 308 - 313.

Stolarski M.J., Szczukowski S., Tworkowski J., Krzyzaniak M., Gulczynski P., 2013. Comparison of quality and production cost of briquettes made from agricultural and forest origin biomass. Renewable Energy, 57: 20-26.

THE PROPERTIES OF ELECTRODE CONDUCTIVITY MEASUREMENT METHODS OF BIOLOGICAL TISSUES

Zdeněk Bohuslávek

Czech University of Life Sciences in Prague, 16521 Prague 6 – Suchdol, Czech Republic, Phone: +42024383300, E-mail: bohuslavek@tf.czu.cz

Abstract:
This article analyzes properties of electrode conductivity measurement methods of biological tissues, which are one of the few able to measure the potentials of corresponding components of complex conductivity, thus real resistive component and an imaginary component reactive conductivity. The analysis was performed by computer modelling and experimental measurements. The publication describes modelling current and potential electrode methods for tissue phantoms using finite element method. Comsol Multiphysics v.3.4 program was used for calculations. Results are presented for 2D and 3D graphs. An experimental measurement with electrodes in the phantoms tissue with different conductivity was also conducted, and components of the complex conductivity were evaluated with RLC Bridge and most accurately by using the lock-in amplifier. The measured values of conductivity of the phantoms were used as reference values in the research of contactless methods of measuring conductivity.

Keywords: electrode conductivity, biological tissues, modelling, element method

Introduction

Based on monitoring conductivity (conductivity) of biological tissue with high precision can determine the quality and safety of meat. In addition, you can also use components of the complex conductivity to monitor the level of maturity of beef during maturation in cold storage and meat composition in terms of muscle and fat.

Conductivity extracellular environment and cytoplasm are approximately equally large and varies in the range of 0.2 to 10 $S{\cdot}m^{-1}$. In contrast, the conductivity of the cell membranes is 10^6-10^8 times lower, ie about $1{\cdot}10^{-6}$ to 10^{-8} $S{\cdot}m^{-1}$. The biological tissue can be very grossly present as a suspension (mixture) cells in interstitial fluid, which in the dc field appears as a suspension of non-conductive elements in the electrolyte solution (Hrazdira, Mornstein, 2001). In a simplified model of the biological tissue can be distinguished two types of electrical conductivity. The cytoplasm of cells and extracellular environment tissues behave as conductors of the second order, characterized by frequency-independent ohmic resistance, a resistance R. The membranes of cells of biological tissue to a capacitive properties, are therefore characterized by an impedance Z, in which in addition to resistance R also apply resistance Xc or capacitance, see (1) according to (Hrazdira, Mornstein, 2001).

$$Z = \sqrt{R^2 + X_C^2} \qquad [\Omega] \qquad (2)$$

Based on these facts, we can assess electrical properties of biological tissues embedded in an alternating electric field from two perspectives. This is either the evaluation of complex permittivity or complex conductivity. Permittivity of biological tissue in a complex shape is described by equation (2).

In the above equation represents the ε_0 vacuum permittivity and ε_r complex relative

$$\varepsilon = \varepsilon_0 \varepsilon_r = \varepsilon_0 (\varepsilon_r{}' - j\varepsilon_r{}'') = \varepsilon_0 (\varepsilon_r{}' - j\frac{\sigma}{\omega \varepsilon_0}) \cdots [F.m^{-1}] \qquad (1)$$

permittivity. Designation $\varepsilon_r{}'$ and $\varepsilon_r{}''$ describes the real and imaginary part of the complex relative permittivity and j expresses the imaginary unit, that $j^2 = -1$. Furthermore, σ denotes electrical conductivity of the tissue and ω is the angular frequency, ie $\omega = 2\pi f$ and f is the frequency of the alternating field.

Conductivity biological tissue can therefore be expressed in the form (3), in (Oppl et al., 2005).

$$\sigma = 2\pi f \varepsilon_0 \varepsilon_r'' \quad [S \cdot m^{-1}] \qquad (3)$$

The electric field induces in biological tissue polarization of ions and atoms and molecules. Moreover, it also causes the rotation of the molecules bound to the dipoles. As a result of these phenomena occurs in biological tissue conduction current whose density ***Jv*** is given by equation (4).

$$J_V = \sigma E = 2\pi f \varepsilon_0 \varepsilon_r'' E \quad [\mathrm{A \cdot m^{-2}}] \tag{4}$$

In addition, there is current or capacitive sliding J_o, whose density can be expressed by equation (5).

$$J_o = \frac{\varepsilon_0 \varepsilon' \partial E}{\partial t} = 2\pi f \varepsilon_0 \varepsilon_r' E \quad [\mathrm{A \cdot m^{-2}}] \tag{5}$$

Electrode method can measure the current real conductive and capacitive components folder and then calculated to determine resistance and capacitance (reactance) of complex conductivity.Contact methods are the simplest way of measuring the conductivity of biological tissues. The basic methods include two-and four-electrode method, a method of electrical impedance tomography. The simplest method for measuring conductivity is two-electrode (bipolar) measuring method. This method uses two electrodes for both excitation electric current I in the circuit and measure the voltage U between the two electrodes, see Fig. 1a. The resulting resistance R is given by the sum of the resistance R-tissue sample and parasitic resistances R1el-sample R2el- sample. These parasitic resistances are undesirable and arise due to the polarization or the formation of deposits on the electrodes, in (Zajíček et al., 2005; Zajíček, Vrba, 2005; Prance et al., 2000; Chi et al., 2010). One way to avoid this phenomenon is to generate zero current measuring circuit, which can be achieved using the four-electrode measurements. Four-electrode measurements introduces two outer current electrodes into the sample current I and voltage U is measured by the vector voltmeter connected to the inner two measuring electrodes, see Fig 1b. Due to the high input resistance voltmeter flows electrodes almost zero current, and therefore the resulting resistance R is not affected by the parasitic resistances and electrode polarization in (Yamashita, 1993; Schuetze, 2004; Griss et al., 2002).

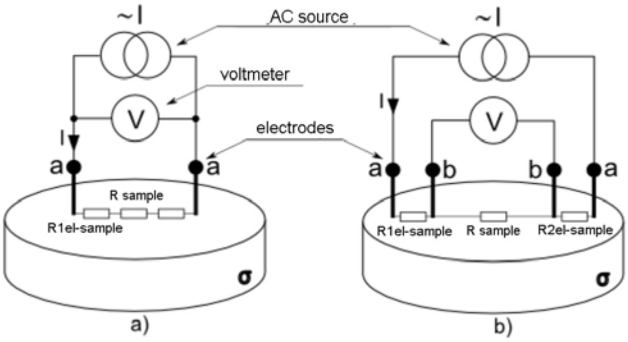

Fig. 1 Electrode measurements of conductivity a) a two-electrode method, b) the four-electrode method

The content and objective paper is to analyze the properties of electrode conductivity measurement methods complex biological tissues. The analysis was performed by computer modeling and experimental measurements. The publication describes modeling current and potential electrode methods for tissue phantoms using finite element method. The specific calculation program was used Comsol Multiphysics V.3.4. Results are presented for 2D and 3D graphs. It was also conducted experimental measurement electrodes to tissue phantoms with different conductivity, and with the evaluation components of the complex conductivity RLC bridge and accurately using the lock in amplifier. The measured values were used as reference for the research method of contactless measuring conductivity.

Materials and methods

Measuring phantoms

To measure the conductivity of biological tissues due to financial savings in initial tests implemented physical models, which are referred to as test measuring phantoms.To simulate the biological tissue with high water content such as the muscle tissue can be used agar or gelatin. The combination of various ingredients such as sodium chloride (NaCl) or aluminum powder can be changed dielectric parameters phantoms to meet the necessary tissue. For the initial test was created set homogenates phantoms which simulate biological tissue in terms of electrical conductivity σ. In order to prolong life of the phantoms for manufacturing was used the edible gelatine.The set of phantoms covered these values of conductivity: 3.7 $\mathrm{mS \cdot cm^{-1}}$; 6.7 $\mathrm{mS \cdot cm^{-1}}$; 10.3 $\mathrm{mS \cdot cm^{-1}}$; 32 $\mathrm{mS \cdot cm^{-1}}$ and 66.7 $\mathrm{mS \cdot cm^{-1}}$.

Comsol Multiphysics

Comsol Multiphysics to simulate and solve the multi-physical tasks that are described by partial differential equations using finite element method, known as FEM (Finite Element Method). Process modeling in Comsol Multiphysics consists of the following basic steps outlined in (Gerhardt, Kumar, 2009). In our case, the program Comsol Multiphysics is used to simulate the distribution of the electric field in two and four-electrode conductivity measurement of biological tissue. In both cases use the same virtual model phantom, which was identical conductivity and geometric dimensions. Geometric dimensions correspond to the dimensions of real phantoms, ie 11 cm x 11 cm x 3 cm. The value of conductivity chosen for the virtual phantom was value σ = 4 mS·cm^{-1}, which corresponds healthy biological tissue.

Dimensions of electrodes and their arrangement are identical to the natural placement during actual measurements. As the supply voltage has been selected value 1V, resulting in a streamlining of the resulting graphs. To build models of electrodes and the phantom was used CAD, Autodesk Inventor Professional 2010.

Conductivity measurement using electrodes

a) For the two-electrode conductivity measurement was used to sign EV-meter, designed to measure conductivity of the meat (by prof. Janál). This device allows to measure the conductivity directly without conversion, in the range 1-20 mScm^{-1}. For the four-electrode method was used RLC bridge type ESCORT ELC133A, which allows direct connection of the current and the electrode and makes possible to measure the impedance Z and phase angle.

b) For the calibration of the four-electrode method RLC bridge were used buffer solutions with values 450 uScm^{-1}, 4500 uScm^{-1} and 45000 uScm^{-1} Calibration of the two-electrode method with EV-Metro was only for the first two values. Calibration was carried out at a frequency of 10 kHz.

c) For the contact conductivity measurements was design and implemented the four-electrode method using a lock-in amplifier. The Lock-in amplifier to directly measure two voltages corresponding with the real and imaginary components allowed of the impedivity or conductivity of the sample. On Fig. 2 is a block diagram of the proposed method for the four-electrode conductivity measurement of tissue using a lock-in amplifier.

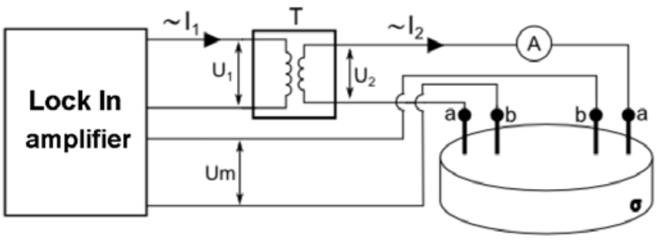

Fig. 2 Block diagram of the four-electrode measurement with Lock-in amplifier

Results and discussion

1) The simulation results electrode measurements COMSOL Multiphysics - are shown in Fig. 3. The voltage between the electrodes is also colorfully presented in 3D. From the 2D view is clearly visible non-linearity of the voltage between the power electrodes. These electrodes are simultaneously measuring electrodes, and therefore this method can be loaded error voltage at the electrodes. Perfect (almost linear) is the change in potential between the measuring electrodes in the four-electrode method. The electrodes in the graph were indicated by an arrow at the locations of short constant potential.
2) The results of electrode measurements on homogeneous phantoms
The bar chart in Fig. 4 illustrates the comparison of the results of the contact measurement. Made phantoms have a homogeneous structure, and therefore the capacitive component (reactance) was minimal. For these reasons, only resistance was evaluated and then calculated the real conductivity. The graph shows that the various contact methods give similar values results. The smallest deviations showed a method with Lock In amplifier.
3) Minor variations, the uncertainty of measurement that can be caused by inaccurate readings and the influence of small changes in temperature and calibration inaccuracies. Measurements using the two-electrode method with EV-meter was realized only for the first three test phantoms with low conductivity, due to the smaller scale of the measuring device. Conductivity is determined by measuring conductivity of meat where sufficient upper limit of the measuring range of 20 mS·cm^{-1}.

a) The electric potential at the two-electrode measurement

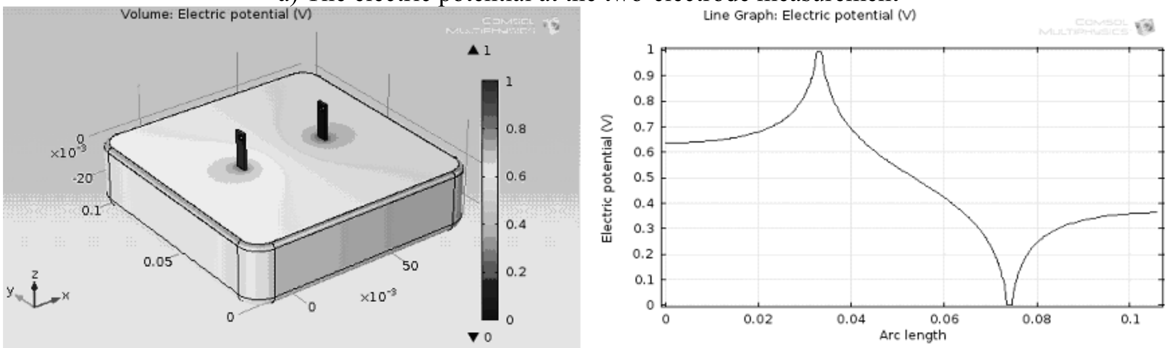

b) The electric potential during the four-electrode measurements

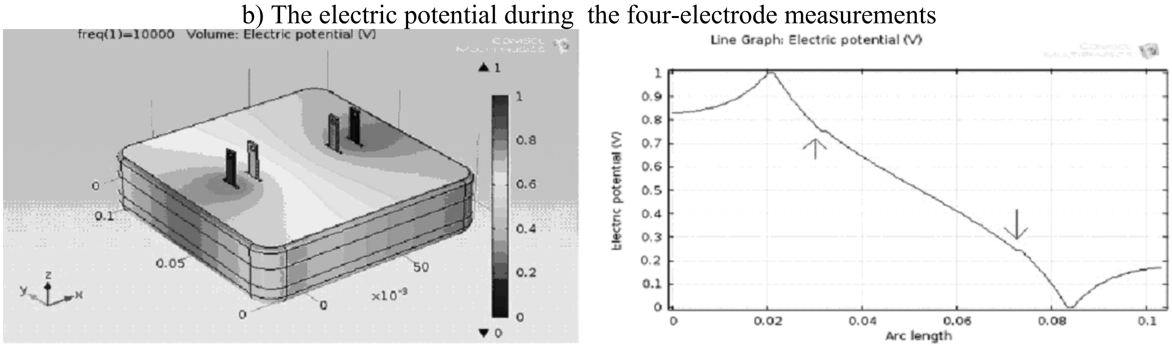

Fig. 3 a,b The potential distribution at the electrodes a) in 3D and b) 2D view (chart)

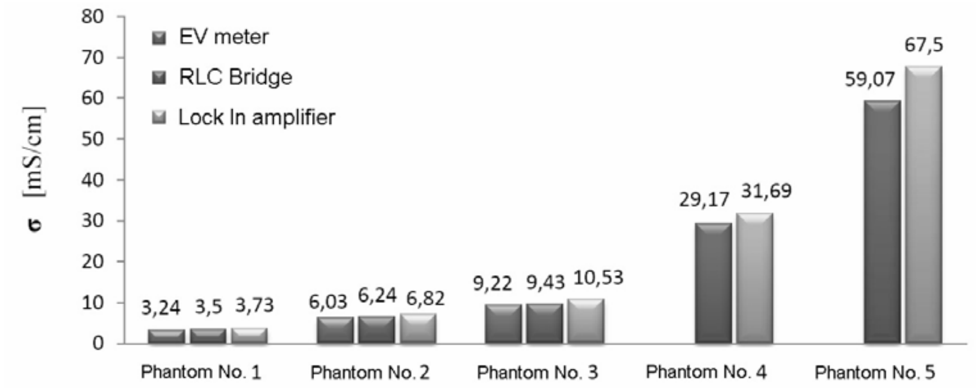

Fig. 4 Comparison of contact measurements on the test phantoms

Conclusion

The results of the study shows that:

• The four-electrode method is more accurate than the two-electrode

• The Finite Element Method implemented in the program Comsol can successfully simulate and analyze the progress and potential flow streams of the biological tissues

• It was verified that the implementation of gelatin phantoms as a first step towards the realization phantoms with heterogeneous structure is simulating actual dielectric properties of cellular tissue.

Results from the experiments enable the next phase of research, contact and for contactless inductive methods of measuring conductivity and dielectric properties of biological tissues, mainly in different forms of meat.

References

Gerhardt R.A., Kumar S., 2009. Numerical Study of the Electrical Properties of Insulating Thin Films Deposited on a Conductive Substrate, COMSOL Multiphysics®, COMSOL Conference, Boston, 105-110.

Griss P., Tolvanen-Laakso H., Merilainen P., Stemme G., 2002. "Characterization of micromachined spiked biopotential electrodes," IEEE Trans. Biomed. Eng., 49(6): 597–604.

Hrazdira I., Mornstein V., 2001. Lékařská biofyzika a přístrojová technika, Brno, Neptun, 396.

Chi Y.M., Tzyy P.J., Cauwenberghs G., 2010. Dry-Contact and Noncontact Biopotential Electrodes , IEEE Reviews in Biomedical Engineering, 3: 106-119.

Oppl L., Zajíček R., Vrba J., 2005. Measurement of Dielectric Properties of Biological Tissue. In ESHO 2005 - Book of Abstracts. Graz: Medical University of Graz, Department of Surgery, 90-92.

Prance R.J., Debray A., Clark T.D., Prance H., Nock M., Harland C.J., Clippingdale A.J., 2000. "An ultra-low-noise electrical-potential probe for human-body scanning," Measure. Sci. Technol., 11(3): 291.

Schuetze A.P., 2004. A laboratory on the four-point probe technice, Am. J. Phys., 72(2): 149-153.

Yamashita M., 1993. ''Resistivity correction factor for the four-circularprobe method,'' Jpn. J. Appl. Phys., 1(32): 246–251.

Zajíček R., Oppl L., Vrba J., 2005. Dielectric Properties Measurements of Biological Tissue. In: Abstract Book - Fröhlich Centenary International Symposim Coherence and Electromagnetic Fields in Biological Systems. Prague: Academy of Sciences of the Czech Republic, Institute of Radioengineering and Electronics, 156-159

Zajíček R., Vrba J., 2005. Measurement of Biological Tissue Dielecric Properties. In Radioelektronika 2005 - Conference Proceedings. Brno: VUT v Brně, FEI, Ústav radioelektroniky, 502-505.

THERMOPHYSICAL MEASUREMENT METHODS AND THEIR USAGE FOR DETECTION OF SELECTED FOOD MATERIALS THERMOPHYSICAL PARAMETERS

Monika Božiková*, Peter Hlaváč

Slovak University of Agriculture in Nitra, Faculty of Engineering, Department of Physics, 949 76 Nitra, Slovak Republic, Phone: +421376414711, Fax: + 421377417003,
E-mail: Monika.Bozikova@uniag.sk

Abstract

This contribution deals with theoretical parts of thermodynamics which can be applied in various types of thermophysical parameters measurement. Selected methods of measurement as Hot Wire method and Dynamic Plane Source method were used for detection of thermophysical parameters of selected bio-based materials. There were measured different samples of food materials. All results were obtained during experimental work at the laboratories of Department of Physics, SUA in Nitra. Contribution can be divided into two main parts. First part presents description of selected transient methods and also principles of the selected transient methods as: Hot wire method, Dynamic Plane Source method. Second part of contribution deals with selected results of thermophysical parameters measurements which are presented as graphs for each sample of measured materials. Presented results are dependencies of thermophysical parameters as: thermal conductivity and thermal diffusivity to the temperature. From obtained results is evident that thermophysical parameters are one type of physical parameters which can determine the status of the bio-based material. This fact is very useful in food and agriculture and industry for detection of materials quality. Thermophysical parameters are significant characteristics which can be used for improving of the technologic processes, thermal processing of bio-based materials and their storage conditions. Presented facts shows that thermophysical research applied on bio-based materials used in agriculture and food industry is very important because materials goes through the thermal manipulation during processing to final products and during their storage.

Keywords: Hot Wire method, Dynamic Plane Source method, food materials, thermophysical parameters

Introduction

Data reliability of the thermophysical parameters of materials is a crucial problem of measuring techniques. True values of thermophysical parameters can be obtained by different methods in various laboratories. Different type of experiments performed in various laboratories is a prerequisite for good data statistics. Therefore, the intercomparison of different measurements can improve the data reliability. Data analysis performed during intercomparison measurements helps to choose optimum experimental parameters of the individual methods. Therefore, the choice of the measurement strategy has a great influence on the data reliability.

The measurement process is usually influenced by a number of disturbing effects which shift the data from their true values. The experimenter has to include these effects into the underlying model of the method using appropriate parameters. As a result, additional unknown parameters have to be estimated during the experiment. Many of them are not independent, i.e. the possibility of founding correlation between the parameters is high. The analysis of the sensitivity coefficients gives the picture of the parameter correlations (Beck, Arnold, 2003). Therefore, the realization of the intercomparison measurements should carefully consider the measurement methods and measured parameters. Only the data can be intercompared which are independent of each other, i.e. which are not correlated.

Tab. 1 Description of the selected transient methods (Kubičár, Boháč, 2000)

<table>
<tr><th>Type of method</th><th>Temperature function</th></tr>
<tr><td>Hot wire method
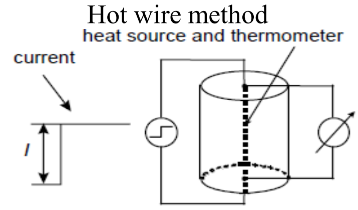
</td><td>$$T(r,t) = -\frac{q}{4\pi\lambda} E_i\left(-\frac{r_0^2}{4at}\right)$$
$$-E_i(-x) = \int_x^{\infty} \frac{\exp(-u)}{u}\,du\,; \quad q = R\,I^2$$
r_0 – diameter of the wire; m
R- electrical resistance of the wire; Ω</td></tr>
<tr><td>Pulse Transient method
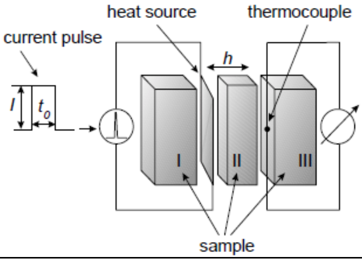
</td><td>$$T(x,t) = \frac{Q}{c\rho\sqrt{\pi\,a\,t}} \exp\left(-\frac{h^2}{4at}\right)$$
$$Q = R\,I^2 t_0$$
R - electrical resistance of the heat source; Ω</td></tr>
<tr><td>Step-wise transient method
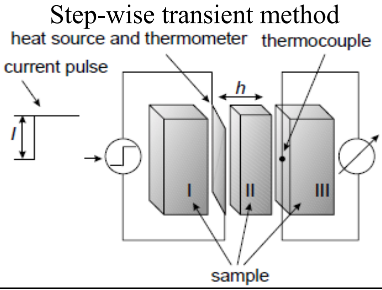
</td><td>$$T(x,t) = \frac{q}{a\,c\,\rho}\left[\sqrt{\frac{at}{\pi}} \exp\left(-\frac{h^2}{4at}\right) - \frac{h}{2} erfc\left(\frac{h}{\sqrt{4at}}\right)\right]$$
$$q = R\,I^2$$
R - electrical resistance of the heat source; Ω</td></tr>
<tr><td>Hot plate transient method
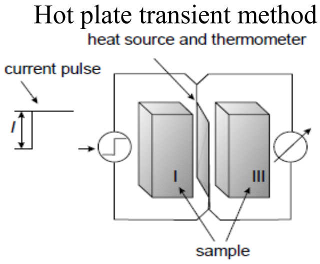
</td><td>$$T(t) = \frac{q}{\lambda}\sqrt{\frac{at}{\pi}}$$
$$q = R\,I^2$$
R - electrical resistance of the heat source; Ω</td></tr>
<tr><td>Hot disc Transient method
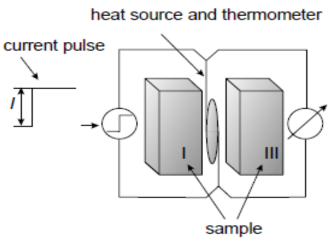
</td><td>$$T(t) = \frac{2q}{\lambda}\left[\sqrt{\frac{at}{\pi}} - \sqrt{\frac{at}{\pi}} \exp\left(-\frac{r^2}{4at}\right)\frac{r}{2} erfc\left(\frac{r}{2\sqrt{at}}\right)\right]$$
$$q = R\,I^2$$
R - electrical resistance of the disc; Ω
r - diameter of the disc; m</td></tr>
<tr><td>Gustafsson Probe
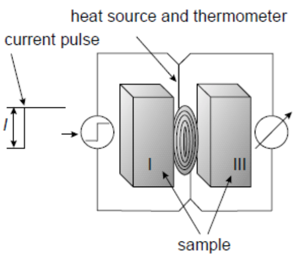
</td><td>$$T(\tau) = \frac{P_0}{\sqrt{\pi^3}\,d\lambda} D(\tau)$$
$$D(\tau) = \frac{1}{[m(m+1)]^2}\int_0^{\tau} s^{-2} ds \left[\sum_{n=1}^{m} n \sum_{k=1}^{m} k \exp\left\{-\frac{n^2+k^2}{4m^2 s^2}\right\} I_0\left(\frac{n\,k}{2m^2 s^2}\right)\right]$$
$$\tau = \frac{\sqrt{a\,t}}{r}\;;\; q = R\,I^2\;;\; R = R_0[1+\alpha\,T(\tau)]$$
R_0 - electrical resistance of the disc; Ω
r – diameter of the outer concentric circle; m
m – number of concentric circles
α – temperature coefficient of disc resistance; K^{-1}</td></tr>
</table>

Various techniques are used for thermophysical parameters measuring of materials (Kubičár, 1990; Maglić et al., 1992; Carslaw, Jaeger, 1959; Andersson, Backstyrom, 1996; Johns et al., 1998). Basic types of transient methods and their temperature functions are presented in Tab. 1.

In realised experiments were used mainly two methods – hot wire and dynamic plane source method which are described in the following text. This method was used for detection of basic thermophysical parameters of selected bio-based materials.

Materials and methods

Hot wire (HW) method - is a transient dynamic technique based on the measurement of the temperature rise of a linear heat source (hot wire) embedded in the tested material (Assael et al., 2008). Heat flux is generated for an appropriate time interval through a long thin uniform wire buried in a small groove or otherwise tightly sandwiched between two sample pieces and the temperature response is measured by the change in resistance of the wire or by the temperature sensor. The response is analysed in accordance with a model characterised by the particular formula found by solution of the partial differential equations using boundary and initial conditions corresponding to the experimental set up (Nagasaka, Nagashima, 1981).

Mathematical model requires ideal, infinitely long thermal source (hot wire) surrounded with infinitely homogenous and isotropic medium with constant starting temperature T_0. If in time $t = 0$ there starts radial heat flow q in measured material, so temperature $T(r,t)$ will have during time t increasing progress in distance r measured from hot wire. This time-temperature function can be described by equation (1) (Liang, 1995):

$$T(r,t) = T_0 - \frac{q}{4\pi\lambda} Ei(-u) \qquad (1)$$

Ei - is the exponential integral with function in argument $u = \frac{r^2}{4at}$, where a - is the thermal diffusivity. For values of function argument $u < 0.1$ we can approximate exponential integral by formula $-Ei(-u) = -\ln u - 0.577$ so, the final time-temperature function is (2):

$$T(r,t) = T_0 + \frac{q}{4\pi\lambda}\left(\ln\frac{4at}{r^2} - 0.577\right) \qquad (2)$$

and $\Delta T = T(r,t) - T_0 = \frac{q}{4\pi\lambda}\ln\frac{4at}{Cr^2}$ (3)

ΔT - is the temperature increment and $C = \exp(\gamma)$, γ - is the Euler constant.

From linear temperature increment ΔT can be calculated thermal conductivity λ (Eg. 4), thermal diffusivity a (Eg. 5)

$$\lambda = \frac{q}{4\pi A},\quad a = \frac{Cr^2}{4}\exp\left(\frac{B}{A}\right),\quad \Delta T = A + B\ln t \qquad (4), (5), (6)$$

where A, B are regression line coefficients obtained from function (6) (Karawacki et al, 1992). Hot wire method was used for detection of thermophysical parameters of selected food materials as: wheat, milk etc.

Dynamic Plane Source (DPS) method - is based on using an ideal plane sensor – PS. The PS sensor acts both as heat source and temperature detector. The plane source method is arranged for a one dimensional heat flow into a finite sample. The theory considers ideal experimental conditions – ideal heater (negligible thickness and mass), perfect thermal contact between PS sensor and the sample, zero thermal resistance between the sample and the material surrounding sample, zero heat losses from the lateral surfaces of the sample. If q is the total output of power per unit area dissipated by the heater, then the temperature increase as function of time is given by (7) (Beck - Arnold, 2003)

$$\Delta T(x,t) = 2\frac{q\sqrt{at}}{\lambda} ierf\left(\frac{x}{2\sqrt{at}}\right) \qquad (7)$$

where a - is thermal diffusivity, λ - is thermal conductivity of the sample and *ierfc* is the error function (Carslaw, Jeager, 1959). We consider the PS sensor, which is placed between two identical samples having the same cross section as the sensor in the plane $x = 0$. The temperature increase in the sample as a function of time (Eq. 8),

$$T(0,t) = \frac{q\sqrt{a}}{\lambda\sqrt{\pi}}\sqrt{t} \qquad (8)$$

which corresponds to the linear heat flow into an infinite medium (Karawacki, Suleiman, 2001). The sensor is made of a Ni-foil, 23 μm thick protected from both sides by an insulating layer made of kapton of 25 μm thick made on SAS. Several corrections have been introduced to account for the heat capacity of the wire, the thermal contact resistance between the wire and the test material, the finite dimension of the sample and the finite dimension of the wire embedded in the sample (Liang, 1995). DPS method was used for detection of thermophysical parameters of selected food and agricultural materials as: wheat, cheese etc.

Results and Discussion

Results for wheat samples - There were measured relations of thermal conductivity λ and thermal diffusivity a to temperature by HW method and DPS method. All samples were stabilised in cool box, where the temperature was approximately 2 °C during 24 hours before the measurements. Samples had moisture content 6.5 %. Wheat sample No1 had bulk density 791 $kg.m^{-3}$, thermal conductivity in range (0.123 - 0.179) $W.m^{-1}.K^{-1}$ and thermal diffusivity in range (0.232 - 0.240).10^{-8} $m^2.s^{-1}$. Wheat sample No2 had bulk density 805 $kg.m^{-3}$ and thermal conductivity in range (0.129 - 0.178) $W.m^{-1}.K^{-1}$ and thermal diffusivity in range (0.233-0.241).10^{-8} $m^2.s^{-1}$.

The values of thermophysical parameters which are presented in Fig. 1 – 2 were obtained as arithmetical averages from one hundred measurements for every sample. Relation of thermal conductivity λ and thermal diffusivity a declares linear increasing progresses $\lambda = f(t)$ and $a = f(t)$ in the temperature range (2 – 20) °C. The difference between characteristics obtained by both transient methods was insignificant.

Results for Unsmoked Tekov cheese - There were measured relations of thermal conductivity λ and thermal diffusivity a to temperature by DPS method. Tekov cheese includes: (53.5 – 58.5) % of dry mass, (43.0 – 47.5) % of fat content in dry mass and maximum 2.5 % of salt. Tekov cheese is made from pasteurized milk with admixture of acid milk cultures *Lactococcus* or *Streptococcus.* The samples of Tekov cheese were measured during the temperature stabilisation from minimal temperature 13.5 °C (temperature after 10 minutes from refrigerator removing) to maximal temperature 23.5 °C (laboratory room temperature).

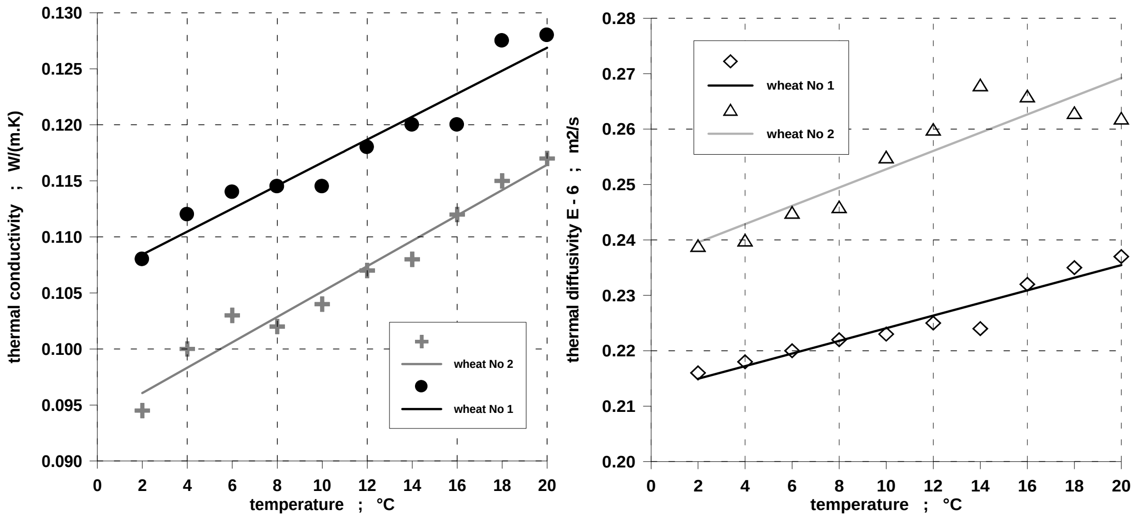

Fig. 1 – 2 Relations of thermal conductivity and thermal diffusivity versus temperature for samples of wheat No1 and No2

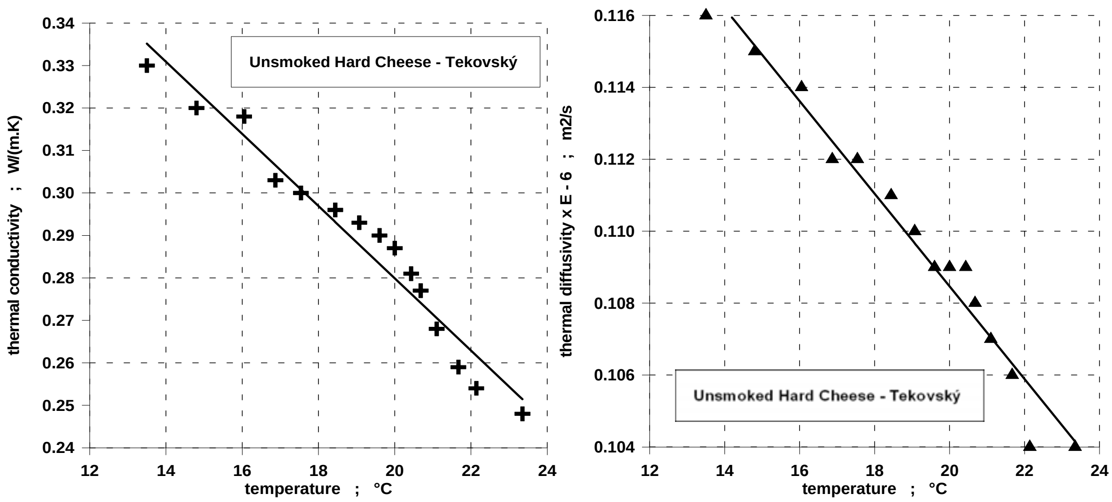

Fig. 3 – 4 Thermal conductivity and thermal diffusivity of cheese plotted versus temperature

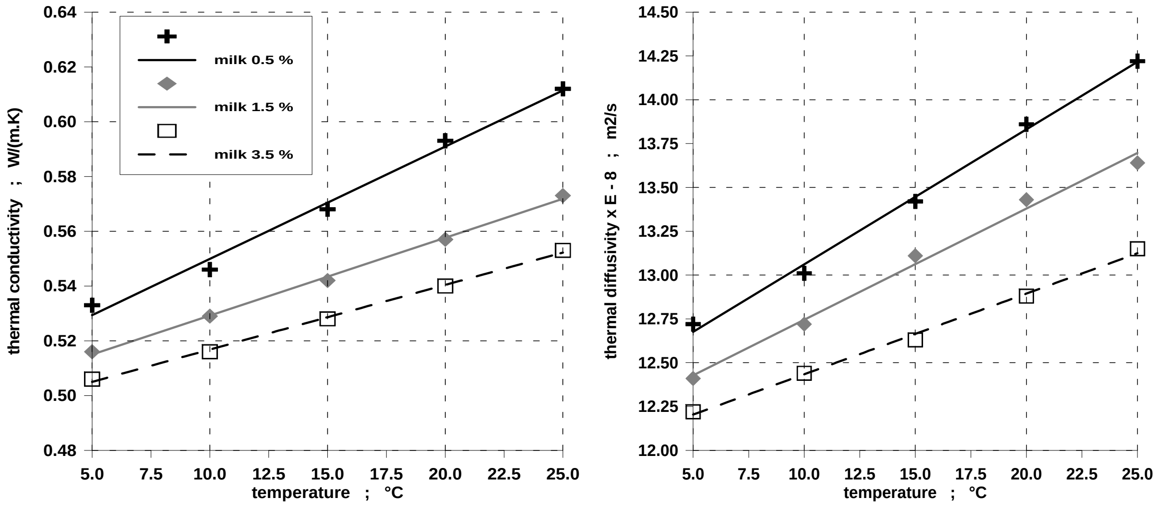

Fig. 5 – 6 Relations of thermal conductivity and thermal diffusivity versus temperature for samples of milk with fat content 0.5 %, 1.5 %, 3.5 % in temperature range (5 – 25) ºC

Presented graphic relations (Fig. 3 – 4) have linear decreasing progresses. Coefficient of regression for thermal conductivity is 0.957 and the average from measured values of thermal conductivity is 0.288 $W.m^{-1}.K^{-1}$. Relation of thermal diffusivity has also linear decreasing progress but with better coefficient of determination 0.966. Thermal diffusivity average of Tekov unsmoked cheese was $0.110.10^{-6}$ $m^2.s^{-1}$. All averages of thermophysical parameters were obtained from fifteen measurements for every sample and parameter. Thermophysical parameters of Tekov cheese are not known from literature, because Tekov cheese smoked and unsmoked is produced from 2001, so we can not do the comparison between obtained results.

Results for milk samples - Measured samples of milk were provided in storage boxes at the temperature from 4 °C to 5 °C and relations of thermophysical parameters to the temperature were measured during temperature stabilization of samples in laboratory settings. The measurement was performed for milk with relative fat content 0.5 %, 1.5 % and 3.5 % in temperature range (5 – 25) ºC. There were measured relations of thermal conductivity λ and thermal diffusivity a to temperature by HW method. Results of relationships study between thermal conductivity, thermal diffusivity and temperature which are showed on Fig. 5 – 6. Graphical dependencies demonstrate linear increasing progresses between thermophysical parameters and temperature. From graphical relations is evident, that increasing relative fat content has decreasing influence on milk thermal conductivity.

Conclusion

The selection of transient method depends on character of the sample, geometric design of the sample, chemical and physical stability of the sample and very important is analyzed parameter, because all transient methods are very convenient for thermal conductivity and thermal diffusivity measurements and we can calculate third parameter specific heat. For thermophysical parameter measurements of samples with compact structure (e.g. cheeses) are convenient methods with planar heat source – hot disc or hot plate. For granular and powder materials (grains, flours etc.) could be used method with planar heat source or hot wire method, for liquids and suspensoid materials (e.g. milk) is usually used hot wire method which was described in the text. All used methods are convenient for detection of thermophysical parameters of food materials or in generally bio-based materials. And obtained results are in good agreement with results presented in the literature.

Reference

Anderson P., Backstyrom G., 1996. Thermal conductivity of Solids under Pressure by Transient Hot Wire Method. In Review of Scientific Instruments, 47: 205.

Assael M.J., Antoniadis K.D., Wu J., 2008. New measurements of the thermal conductivity of PMMA, BK7, and Pyrex 7740 up to 450 K. In: International Journal of Thermophysics, 29(4): 1257–1266.

Beck J.V., Arnold K.J., 2003. Parameter estimation in engineering and science. John Wiley, New York, USA, 448.

Carslaw H.S., Jaeger J.C., 1959. Conduction of Heat in Solids. 2. edition, Oxford University Press, London (Great Britain), 510.

Johns A.I., Scotty A.C., Watson J.T.R., Ferguson D., Clifford A.A., 1988. Measurement of the Thermal Conductivity of Gates by the Transient Hot Wire Method. In: Bulletin of Transaction of Royal Society London, 325: 295.

Kubičár L., 1990. Thermal Analysis: Pulse Method of Measuring Basic Thermophysical Parameters. In: Comprehensive Chemistry, vol. XII, Part E, G. Svehla. Ed. Amsterdam, Oxford, New York, Tokyo Elsevier, 350.

Kubičár Ľ., Boháč V., 2000. A step-wise method for measuring thermophysical parameters of materials. In: Measurement Scientifics Technologies, 11, 252-258.

Liang X.G., 1995. The boundary induced error on the measurement of thermal conductivity by transient hot wire method. In Measurement Science and Technology, 6: 467-471.

Maglić K.D., Cezairliyan A., Peletsky V.E., 1992. Compendium of Thermophysical Property Measurements Methods, Recommended Measurement Techniques and Practices, New York, 2.

Nagasaka Y., Nagashima A., 1981. Absolute measurements of the thermal conductivity of electrically conducting liquids by the transient hot-wire method. In: Journal of Physics E, 14(12): 1435–1440.

TECHNICAL-ECONOMICAL EVALUATION OF PLYWOOD BONDING

Milan Brožek

Czech University of Life Sciences Prague, 165 21 Prague 6 – Suchdol, Czech Republic, Phone: +420 224 383 265, E-mail: brozek@tf.czu.cz

Abstract

The contribution contains results of bonded joints strength tests. The tests were carried out according to the modified standard CSN EN 1465 (2009). For bonding the pine three-ply plywood of 4 mm thickness was used. The test samples of 100 x 25 mm size were cut out from a semi-product of 2240 x 1220 mm size in the direction of its longer side (incline 0°), in the inclined direction (incline 45°) and in the direction of its shorter side (incline 90°). The bonding was carried out using seven different domestic as well as foreign adhesives according to the technology prescribed by the producer. All used adhesives were designated for wood bonding. At the bonding the consumption of the adhesive was determined. After curing the bonded assemblies were loaded using a universal tensile-strength testing machine up to the rupture. The rupture force and the rupture type were registered. Finally the technical-economical evaluation of the experiments was executed.

Keywords: bonding, adhesive, bonded joints testing, costs of bonding

Introduction

Increase in a technical level in the field of bonding of classic as well of modern materials led in the second half of the last century to the synthetic adhesives, binders and cements production rapid development and concurrently to the technology development, which enables their economical use.

Just as other technologies adhesive bonding is distinguished by many advantages, but by some negative and limiting factors, too. By the determining of the bonded joint type it is necessary except for the economical point of view to weigh not only advantages, but also disadvantages of bonding technology compared with conventional bonding ways (e.g. welding, soldering, riveting, and screwing). It is necessary to consider adhesive bonding for supplement of about mentioned methods, not for their substitution.

For the successful application of adhesives in practice the good knowledge of the bonding technology and of the used adhesives technological properties are important. The final quality of the bonded joint is actually influenced by many factors. Except for the bonded joint suitable design and the suitable adhesive choice for the concrete material it is above all the careful preparation of bonded surfaces. But the adhesive layer thickness (actually the glue joint between two bonded surfaces), roughness of adherends, load type (static or dynamic) and direction (radial, axial), way of curing, operation conditions of bonded structure etc. (Epstein, 1954; Cagle, 1973; Loctite, 1988; Pizzi, Mittal, 2003; Ebnesajjad, 2008) have the substantial influence on the bonded joint final strength.

In present bonding of plywood is still very topical. Many authors look at it from different angles. Sellers (1989), Olivares and Sellers (1994), Chen (1995). Yang, Kuo and Myers (2006), Cheng and Wang (2011), Fan, Qin and Chu (2011), Garcia Esteban, Garcia Fernandez and de Palacios (2011), He, Feng and Dai (2012) engaged intimately in the issues of plywood production in production plants, in research and development of adhesives new types or in plywood properties.

Brozek and Novakova (2009) engaged in pine plywood bonding using fusible adhesives. They proved that the final strength influences at most the angel of specimens cutting out from a semi-product (lengthwise, angle 0°, in the inclined direction, angle 45° or crosswise, angle 90°. At the same time they proved that the joints bonded using different fusible adhesives show different load capacity and that the influence of surface roughness is relatively small.

Materials and methods

For the tests seven types of domestic as well as foreign adhesives were bought (Tab. 1).

Tab. 1 Summary of tested adhesives

Adhesive	Designation in text	Adhesive symbol on the wrapping	Producer/supplier of the adhesive
1	DB	Den Braven, super glue	Den Braven Czech and Slovak, a.s.
2	HE	Herkules, univerzální lepidlo	Druchema družstvo
3	10	1001U, sekundové lepidlo	Den Braven Czech and Slovak, a.s.
4	PR	Pritt, gamafix bílý	Henkel ČR, spol. s r. o.
5	PW	Pattex Wood Standard	Henkel ČR, spol. s r. o.
6	TO	Glue Sticks	TOYA, S.A.
7	PA	Pattex 100%	Henkel ČR, spol. s r. o.

Adhesive	Amount of the wrapping, g	Price of the wrapping CZK	Price of the adhesive CZK/g
1	3	7.50	2.50
2	250	54.00	0.22
3	20	81.00	4.05
4	100	44.00	0.44
5	250	125.00	0.50
6	1000	308.00	0.31
7	100	154.00	1.54

Note: Index 0, 45 or 90 at the designation denotes the direction of the cutting out from a semi-product (lengthwise, in the inclined direction, crosswise).
For information: Exchange rate at 07.03.2013: 1 € = 25.765 CZK

Test specimens were cut out from a three-ply plywood sheet of size 2440 x 1220 mm and of 4 mm thickness in different directions – in the direction of the bigger semi-product size (declination 0°), in the direction of the smaller semi-product size (declination 90°) and in the inclined direction (declination 45°). Plywood was chosen because it is easily accessible and universally applicable material of low price.

For strength testing of plywood joints the test according to the modified standard CSN EN 1465 (2009) was used. Form and dimensions of specimens before and after bonding are evident from Fig. 1.

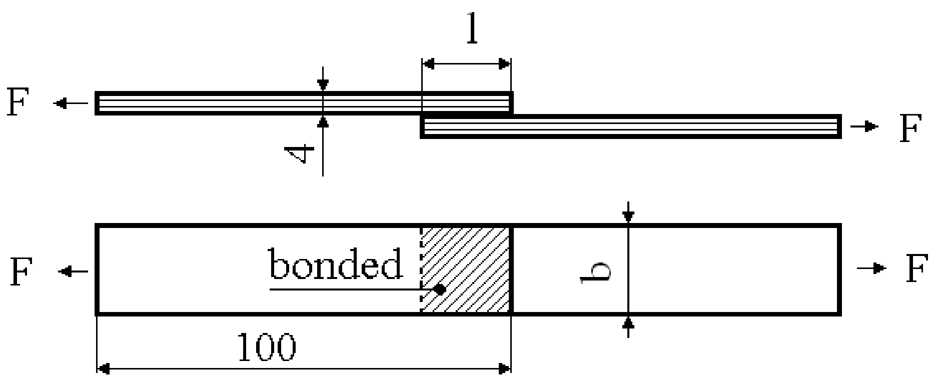

Fig. 1 Tested specimens form and dimensions

The bonding was carried out according to the recommendation of the relevant adhesive producer. From each adhesive type and from each direction of samples cutting out from a semi-product 12 bonded assemblies were tested. The amount of the adhesive needed for the bonding of each run was determined.

After the adhesive curing (min. 24 hours) the prepared bonded samples were fixed in jaws of a tensile-strength testing machine and loaded till to the rupture. The rupture force F (N) was determined. Then the overlapping width b (mm) and overlapping length l (mm) of each tested assembly were measured. From these values the bonded joint surface S (mm^2) was calculated

$$S = b.l \qquad (1)$$

Where:
S – Bonded joint surface (mm^2)
b – Overlapping width (mm)
l – Overlapping length (mm).

The tensile lap-shear strength of the bonded assembly (MPa) was calculated using the equation

$$\tau = \frac{F}{S} \qquad (2)$$

Where:
τ – Tensile lap-shear strength (MPa)
F – Rupture force (N)
S – Bonded joint surface (mm^2).

The aim of carried out tests was to evaluate the influence of the load direction (0°, 45° and 90°) on the bonded joints load capacity using different adhesives and to determine the costs for bonding.

Results and discussion

The test results are presented in Fig. 2 to Fig. 4.
The joint rupture occurred either in the bonded surface or in the bonded material. The bonded joint was damaged mostly (75%) at the specimens cut out lengthwise (0°) (Fig. 2a). At the specimens cut out in the inclined direction (45°) the rupture occurred sometime in the bonded joint (30%), sometime in the plywood (70%) (Fig. 2b). At the specimens cut out crosswise (90°) the rupture occurred almost always (98%) in the plywood (Fig. 2c).

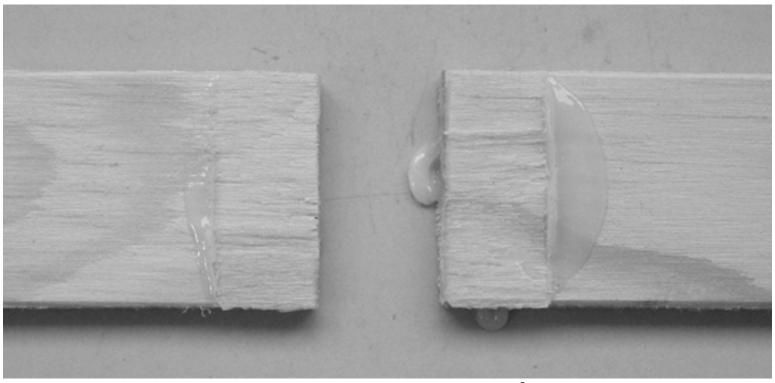

a) Herkules, specimen 0°

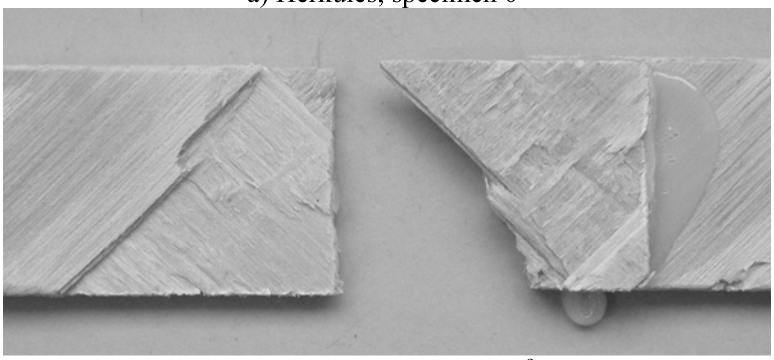

b) Herkules, specimen 45°

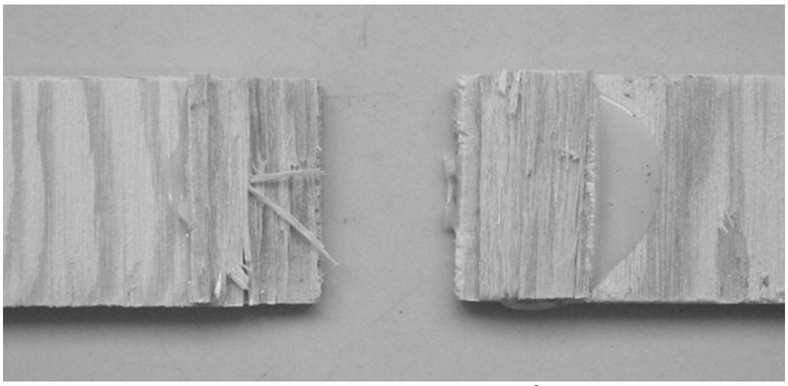

c) Herkules, specimen 90°

Fig. 2 Joints rupture

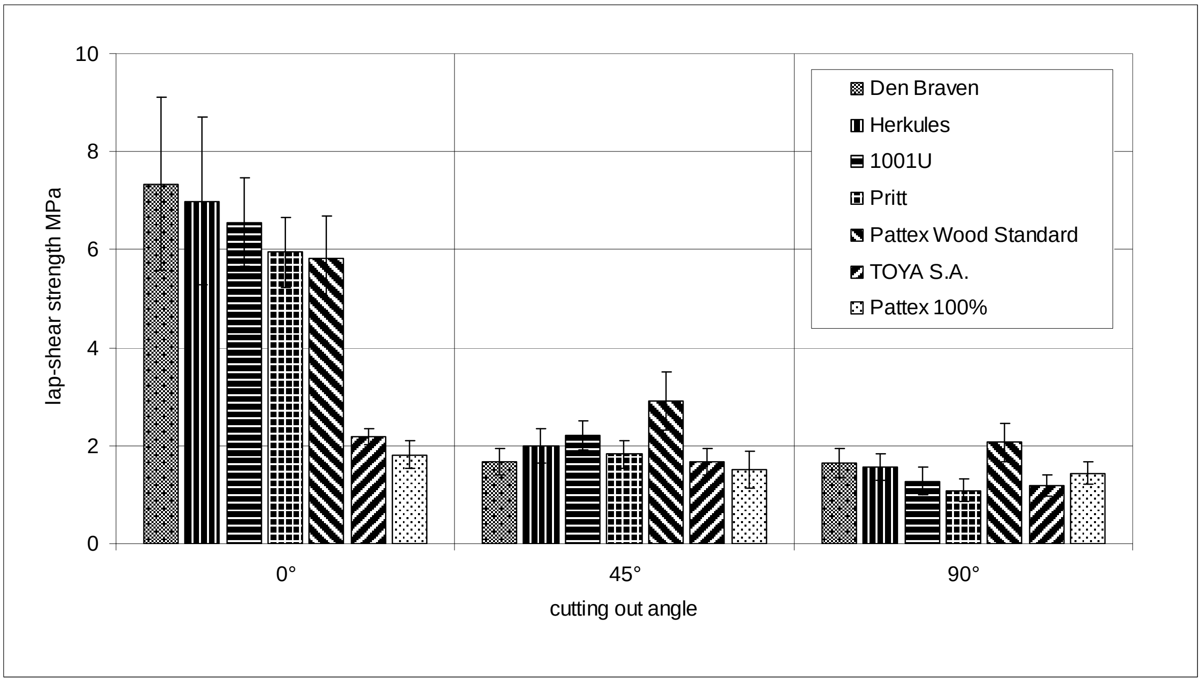

Fig. 3 Relation between the tensile lap-shear strength and the cutting out angle

In Fig. 3 the adhesives are arranged from the highest strength to the lowest strength at the bonding of specimens cut out lengthwise from a semi-product (angle 0°).

From the results (Fig. 3) it is evident that the load direction with regard to the plywood production influences the strength the most. In the longitudinal direction (0°) the joint rupture occurs in the adhesive layer, because the bonded material is more strong that the adhesive. On the contrary in next directions (45° and 90°) the plywood is less strong than the adhesive.

From Fig. 3 it is evident that for different adhesives very different bonded joint strengths were determined. The highest strength in the longitudinal direction (0°) was determined at the adhesive Den Braven (DB, 7.3 MPa), only mildly lower strength was determined at the adhesive Herkules (HE, 7.0 MPa). On the contrary the lowest strength was measured using the adhesive Toya (TO, 2.2 MPa) and Pattex 100% (PA, 1.8 MPa). In the longitudinal direction (0°) the strength values are not influenced by the plywood strength. The ratio of the highest to the lowest strength is about 4.0. In the inclined direction (45°) the order of joints strength was changed. It is caused by force of circumstance that the bonded joint strength is influenced by the strength of the used plywood. The bonded joint highest strength was determined by the use of the adhesive Pattex Wood Standard (PW, 2.9 MPa), the lowest at the adhesive Pattex

100% (Pa, 1.5 MPa). The ratio of the highest to the lowest strength is about 1.9. The lowest values of the bonded joints strength were determined at bonding of specimens cut out crosswise (90°). The highest strength was determined at bonding using the adhesive Pattex Wood Standard (PW, 2.1 MPa), the lowest at bonding using the adhesive Pritt (PR, 1.1 MPa). The ratio of the highest to the lowest determined strength is about 1.9.

From the statistical evaluation of the carried out tests it follows that the dispersion of values of the bonded joints strength (standard deviation) is relatively great.

The differences between prices of tested adhesives are very great (Tab. 1). The most expensive tested adhesive (1001U, 10) was almost 20 times more expensive than the cheapest one (Herkules, HE). At the same time the precondition was not confirmed that using the most expensive adhesive the joints will be of the highest strength.

The graphical representation of the relation between the bonded joint strength and the joint price is shown in Fig. 4. For the problem analysis it is fit to describe the results separately for each tested direction (0°. 45°, 90°). From the technical-economical point of view the most advantageous and so the strongest and at the same time the cheapest bonded joints are in the picture left on the top. On the contrary, the most expensive and the least strong joints are right at the bottom.

For the direction 0° the adhesives Herkules (HE), Den Braven (DB), Pritt (PR) and Pattex Wood Standard (PW) can be recommended. The keenly priced joints (from 0.11 to 0.34 CZK) made using these adhesives had relatively high strength from 5.8 to 7.3 MPa. On the contrary, the adhesive Pattex 100% (PA) had low strength at the relatively high price. The adhesive 1001U (10) defies a bit the foregoing evaluation, because using this adhesive the bonded joint had high strength but at high price.

For the direction 45° the considerable lower load capacity of bonded joints compared with the direction 0° was reached. Above all it is caused by the influence of the strength of the bonded material – plywood. The bonded joints were ruptured in the basic material. It is possible to recommend some of the group of five adhesives, shown in Fig. 4 left (HE, PW, PR, TO, DB). The adhesives PA and 10 can be not recommended, because at the same strength they are multiple more expensive.

For the direction 90° similar results were determined. The bonded joint strength was even lower than for the direction 45°. For bonding it is possible to recommend or not recommend adhesives mentioned in the previous paragraph.

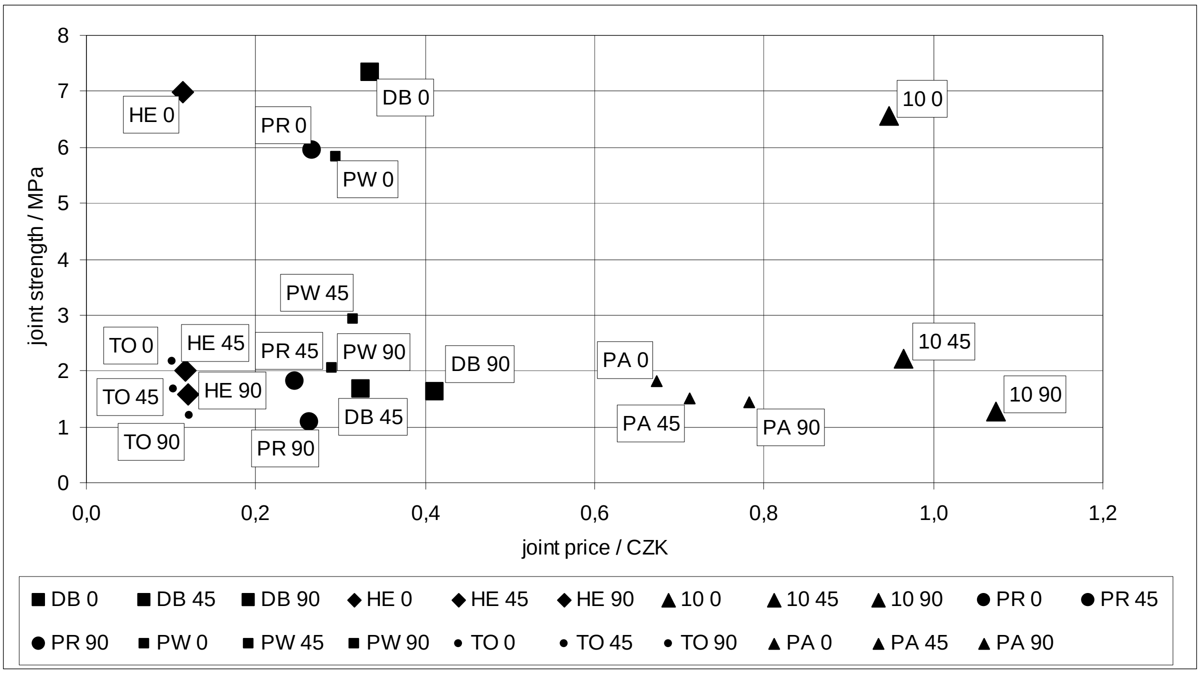

Fig. 4 Relation between the bonded joint strength and the joint price

Conclusions

The paper presents the strength results of the laboratory tests carried out according to the modified standard CSN EN 1465 (2009) using the specimens made from the three-ply plywood of 4 mm thickness. From the plywood sheet of size 2440 x 1220 mm the specimens were cut out lengthwise (0°), in the direction of 45° and crosswise (90°).

The bonded joints were made using seven different adhesives of domestic as well as foreign producers. The bonding was made exactly according to the producer recommendations. After bonding the assemblies were left in a laboratory till to the adhesive total curing. The specimens were loaded using the universal tensile testing machine till to the rupture. The maximum force was noted.
The part of the evaluation was the assessment of the specimens after the test.
From the test results it follows that from the point of view of the final strength not only the type of used adhesive but also the direction of the loading force is dominant. The joint rupture occurred either in the adhesive layer (load direction 0°) or in the basic material (load directions 45° and 90°).

In the contribution the methodology of technical-economical evaluation of tested adhesives and of bonded joints was published and checked. At the same time it was proved that between adhesives offered in the domestic market considerable differences exist. That is both in their price and in their quality, evaluated according to the bonded joint strength.

Acknowledgement

Supported by the Internal Grant Agency of the Czech University of Life Sciences Prague, Czech Republic, Project No. 31140/1312/3107.

Reference

Cagle, Ch. V., 1973. Handbook of adhesive bonding. New York, Mac-Graw-Hill.
Chen, C. M., 1995. Gluability of Kraft Lignin Copolymer Resins on Bonding Southern Pine Plywood. Holzforschung, 49: 153-157.
Cheng, R.-X., Wang, Q.-W., 2011. The Influence of FRW-1 Fire Retardant Treatment on the Bonding of Plywood. Journal of Adhesion Science and Technology, 25: 1715-1724.
Ebnesajjad, S., 2008. Adhesives technology handbook. 2nd ed. Norwich, William Andrew.
Epstein, G., 1954. Adhesive bonding of metals. New York, Reinhold.
Fan, D. B., Qin, T. F., Chu, F. X., 2011. A new interior plywood adhesive based on oil-tea cake**.** Advanced Materials Research, 194-196, 2183-2186.
Garcia Esteban, L., Garcia Fernandez, F., de Palacios, P., 2011. Prediction of Plywood Bonding Quality Using an Artificial Neural Network. Holzforschung, 65: 209-214.
He, G., Feng, M., Dai, C., 2012. Development of soy-based adhesives for the manufacture of wood composite products**.** Holzforschung, 66: 857-862.
Loctite, 1988. Der Loctite. München, Loctite.
Novakova, A., Brozek, M., 2009. Bonding of Non-metallic Materials Using Thermoplastic Adhesives. In.: Engineering for Rural Development. Jelgava, Latvia University of Agriculture: 261-264.
Olivares, M., Sellers, T., 1994. Resin-adhesive Formulations for Bonding Exterior-type Plywood Using Chilean Radiata Pine and 4 Hardwoods. Holzforschung, 48: 157-162.
Pizzi, A., Mittal, K. L., 2003. Handbook of adhesive technology. Dekker, New York.
Sellers, T., 1989. Diisocyanate Furfural Adhesive for Bonding Plywood. Forest Production Journal, 39: 53-56.
Yang, I., Kuo, M., Myers, D. J., 2006. Bond Quality of Soy-based Phenolic Adhesives in Southern Pine Plywood. Journal of the American oil chemistry society**,** 73: 231-237.
CSN EN 1465 (2009): Adhesives - Determination of tensile lap-shear strength of bonded assemblies. Czech office for Standards, Metrology and Testing, Prague, Czech Republic.

ANIMAL AND HUMAN THERMAL COMFORT IN POULTRY HOUSE IN BRAZILIAN SEMIARID

Cinara da C. S. Carvalho*[1], Ilda de F. F, Tinôco[2], Tatiany C. dos Santos[3], Geruza C. da Silva[4], Laize V. Santos[5], Sóstenes de J. M. Moreira[6], Luiz F. R. Botelho[7]

[1,3,4,5,6,7]State University of Montes Claros, Avenida Reinaldo Viana 2630 Bico da Pedra, Janaúba, MG,39440-000, Brazil, *cinarasiqueira@yahoo.com.br
[2] Federal University of Viçosa, Viçosa, MG, Brazil

Abstract

The remaining animals in hot or cold environments directly influence its growth performance, while the effects are noticeable for employees in the quality of work performed and future health problems. Therefore, the aim of this work was to evaluate the condition of thermal comfort for the animals and workers during the first 21 days of life of poultry reared in sheds in the semiarid region of Minas Gerais (Brazil), where the average annual temperature is around 27 ºC. The work was developed in two distinct phases (winter and summer) in a poultry farm in the Nova Porteirinha city (MG). To evaluate the thermal comfort of the animals, we used the Index Globe Temperature and Humidity (BGT) and to characterize the thermal environment for workers, adopted the Index and Wet Bulb Globe Thermometer (WBGT). The data collected revealed that regardless of the season, the values were above BGT, 74 featuring heat stress condition for poultry. With regard to workers it was found that the activity of farm management conducted during the winter does not expose people to thermal overload condition, however, in the summer, from 9am, the quality of work can suffer and have runtime due to reduced heat stress condition verified on site that leads employees to adopt frequent breaks for hydration and rest. During the first twenty days of the birds no need to hold daytime heating but a greater control over the movement of curtains and ventilation systems in order to provide the best thermal conditions for both animals and for humans inside the aviary.

Keywords: ergonomics, poultry production, thermal environment

Introduction

The control of the thermal environment inside the premises where the animals are housed must be greater during the first weeks of life of the birds and with greater precision during the winter (Menegali et al., 2010).

Thermal conditions outside the comfort range are also premises for the development of health problems in workers who perform activities that require attention and agility, and can be affected by the lack of concentration and fatigue resulting from heat (Carvalho et al., 2011; Damasceno et al., 2010). Although the climatic conditions in the North of Minas Gerais are theoretically favorable for creation of poultry during the initial phase, there is a concern on the part of the creators, since the temperatures are high and the range of thermal comfort can then be extrapolated for the area of hyperthermia.

The aim of this study was to evaluate the thermal comfort condition for poultry chicks during the first 21 days of life, as well as the condition of comfort for people working in these sheds during winter and summer in the northern region of Minas Gerais.

Material and method

The study was conducted in a poultry farm in the city of New Porteirinha (MG). The city has a latitude of 15°47'50" S, longitude 43°18'31" W, altitude 516 m, climate according to Köppen, the type AW (rainy tropical, savannah with dry winter).

Data were collected during the winter of 2011 and summer of 2012, the period of 21 days, which corresponds to the initial stage of life of poultry.

During the experimental period, daily measurements were made of the environmental variables through the use of two dataloggers brand EXTECH, RHT 10, with a resolution of ± 1ºC (temperature), ± 3.5% (humidity), and accuracy of ± 2nd to the dew point temperature. The equipment was programmed to collect data every 15 minutes, beginning at 8am and ending at 5pm.

Possession of the collected data, it was estimated initially IBGT through the following formula:

IBGT = Tgn + 0,36Tpo + 41,5 (1)
Where:
IBGT = Index Black Globe Temperature and Humidity; *Tgn* = Black globe temperature, (ºC); *Tpo* = Dew point temperature, (°C).

To characterize the thermal comfort condition for humans, was used WBGT which was calculated by the equation described below, suitable for assessing internal environments (sunlight without load) in accordance with the NR 15 (2004):

WBGT = 0,7tbn + 0,3tg (2)
Where:
tbn - Natural wet bulb temperature, (°C);
tg – Globe temperature, (ºC).

Ownership of the data collected was used descriptive statistics to compare the data with BGT hourly, depending on the weeks studied. WBGT values were confronted with the limits established by the Norms Regulamentory of Ministry of Labour and Employment (NR).

Results and discussion

According Menegali et al. (2010) the animals are in thermal comfort when BGT is analyzed between 74 and 77. Below 74, the chickens are exposed to low temperatures, while values above 77, bird performance is impaired due to high Temperatures.

During the winter period it was found that only the first and second weeks before 10am and 9pm respectively, the values of BGT were below 74. At other times and in the third week of BGT values were above the recommended, especially in the period at 12am and 3pm, reaching values of up to 83 in the third week, a condition characterized as dangerous.

The heating system operating only in the first week, the atmosphere was with high temperatures even in the wintertime. This result suggests that there is no need to keep the shed fully enclosed and the simple handling of curtain mainly during higher temperatures, associated with rapid activation of the fan would be interesting to help reduce the temperature inside the shed.

Second Baêta (1987) values above 84 represent requiring emergency intervention such as ventilation, for example to assist in thermal comfort of the animals. Values close to 84, were observed between 1pm and 3pm.

In the second experimental phase took place during the summer, it was found that starting from 8am, animals were exposed to values of the greater than 74 reaching the emergency condition from 11am, including the first week of life. The values of BGT above the comfort zone are limiting development and reproductive traits of poultry.

The activities of management in a poultry house, are considered heavy the according the NR 15 (2004), which refers to the understanding of the attendant exposure to thermal overload conditions, for an 8 hour workday. The job of handling this shed is done by two people and consists of manual filling the feeders, cleaning water fountains, manual revolving bed with the aid of hoe and removal of dead animals.

Where workers are exposed to thermal overload condition only from 12am in the third week of life of poultry. This reflects the need of adopting breaks only in accordance with the needs of workers due to the fact that the work be classified as heavy, and not with the adoption of scheduled breaks, as required by NR 15 (2004), since the thermal condition is not a factor in this case that exposes workers to stress.

Carvalho et al. (2012), evaluating the working condition in sheds for poultry house during the winter brood, found thermal overload condition and physics in the period around the 9am to 6pm, especially in the critical period between the 11am to 3pm, and recommended the adoption of rest breaks.

The surrounding landscaping was present around the shed evaluated, a condition associated with that time of the year, gave values of WBGT below the ceiling, which makes the management activity less stressful for the worker.

To Tinôco (2001), the possibility of existence of trees on the east side or west buildings open is very desirable (as partitions high damping) to prevent the incidence of direct solar irradiance within the areas of coverage. The vegetation in general, is promoting natural shade on the toppings, either by creating regions with mild microclimate, can completely reverse a situation of thermal discomfort.

Seeking to assess the contribution of tree shading to soften the sunlight in poultry facilities in two different directions, east-west and north-south. Alves and Rodrigues (2004) found that for both facilities with east-west orientation to north as south-using landscaping surrounding was very relevant.

However, during the summer season, when the repetition of work performed to characterize the thermal environment for animals and humans, it was found that the landscaping surrounding did not help in reducing the WBGT inside the shed, the values were above the recommended IBUTG by NR 15 for continuous during the three-week trial.

According to the Carvalho et al. (2011), the execution of works considered heavy in hot weather condition, deserve special attention regarding the ergonomic factors, work environment, food and breaks, as they are subject to greater physical stress at work.

The most common health problems in aviaries are related to musculoskeletal pain in the lower back due to manual activities cleaning drinkers and feeders (Alencar et al., 2006; Evangelista et al., 2012).

According Grandjean (1998), excessive heat in working environments results in fatigue and drowsiness, which reduces the prompt response and increases the tendency to fail.

The use of ventilation system, misting and scheduled breaks are measures that can be adopted to minimize heat stress condition evidenced inside the shed that compromise the efficiency of the work done by the employees and the health of ourselves.

Conclusion

For livestock, irrespective of season, it is concluded that there is no necessity to use heating system suitable for the first three weeks of life of the poultry, since the actual thermal condition site is sufficient to expose the animals to heat stress.

The winter season does not expose workers is most suitable for the realization of management activities, however, in summer, the climate condition is a factor that reduces the efficiency of the work.

Acknowledgement

CNPq (National Council for Scientific and Technological Development), the Foundation for Research Support of Minas Gerais (FAPEMIG), CAPES (Coordination of Improvement of Higher Level Personnel) and the State University of Montes Claros (UNIMONTES).

References

Alencar M.C.B., Nääs I.A., Salgado D.D.A., Gontijo L.A., 2006. Broiler mortality and human behavior at work. Scientia Agricola, 63: 529-533.

Alves S.P., Rodrigues E.H.V., 2004. Tree shading and orientation in poultry houses. Journal Agricultural Engineering, 24(2): 241-245.

Baêta F.C., Meadox N.F., Shanklin M.D., Johnson H.D., 1987. Equivalent temperature index at temperatures above the thermoneutral for lactating dairy cows. St. Joseph: American Society Agricultural Engineers, 87(4015): 21.

Carvalho C.C.S., Souza C.F., Tinôco I.F.F., Vieira M.F.A., Minette L.J., 2011. Safety, health and ergonomics of workers in poultry houses systems equipped with different feed supply Journal Agricultural Engineering, 31: 438-447.

Carvalho C.C.S., Souza C.F., Tinôco I.F.F., Vieira M.F.A., Menegali I., Santos C.R., 2012. Ergonomic conditions of workers in poultry houses during the heating phase. Brazilian Journal of Agricultural and Environmental Engineering, 16(11): 1243–1251.

Damasceno F.A., Yanagi Jr.T., Lima R.R., Gomes R.C.C., Moraes S.R.P., 2010. Evaluation of poultry well-being in two commercial climatized poultry houses. Journal Science and Agrotechnology, 34: 1031-1038.

Evangelista W.L., Tinoco I.F.F., Souza A.P., Minetti L.J., Baêta F.C., Silva E.P., Oliveira L.A., 2012. Postural analysis of workers in a typical meat processing company in Brazil. Work: A Journal of Prevention, Assessment and Rehabilitation, 41: 5392-5394.

Grandjean E., 1998. Ergonomics Handbook: adapting the work of man. Porto Alegre - Brazil: Bookman.

Mazza G., Jayas D.S, White N.D.G., 1990. Moisture sorption isotherms of flax seed. Trans. ASAE, 33: 1313-1318.

Menegali I., Baeta F.C., Tinoco I.F.F., Cordeiro M.B., Guimarães M.C.C., 2010. Poultry performance in different half-acclimatized facility systems in the south of Brazil. Journal Agricultural Engineering, 18, 461-471.

Tinoco I.F.F., 2001. Poultry industry: new concepts in materials, designs and construction techniques available for Brazilian broiler. Brazilian Journal of Poultry Science, 3: 2001.

STUDY OF PHYSICAL WORK LOAD THE SUPPLY CHAIN OF POULTRY

Cinara da C. S. Carvalho[1*], Ilda de F. F, Tinôco[2], Cecília de F. Souza[3], Maria de F. A. Vieira[4], Irene Menegali[5], Maria C. de C. Guimarães[6], Cláudia R. Santos[7]

[1*] State University of Montes Claros, Avenida Reinaldo Viana 2630 Bico da Pedra, Janaúba, MG, 39440-000, Brazil, Phone: +5503838211378, *cinarasiqueira@yahoo.com.br
[2,3,4,7] Federal University of Viçosa, Viçosa, MG, Brazil
[5] Federal Universtiy of Minas Gerais, Montes Claros, MG, Brazil
[6] Federal University of Vale do Jequitinhonha e Mucuri, Diamantina, MG, Brazil

Abstract

The work of managing the supply chain of poultry is associated with loading weight, repetitive movements and long working hours, which may expose employees to develop health problems. In this context, the aim of this study was to evaluate the physical burden of work that employees are subjected during the execution of management activities in a hatchery and slaughterhouse poultry, broiler breeding sheds and matrices. The physical work load was determined by the use of a heart rate meter label Polar Electro comprising a digital receiver, an elastic band and a transmitter of sensors placed on the chest of the worker. The Polar was placed on workers (men and women) at the beginning of the workday and removed at the end of the workday, remaining even during breaks hygiene, lunch and rest. In hatchery verified physical strain during unloading boxes of eggs, cleaning the metal boxes that come from incubation and loading boxes with chicks. At the slaughterhouse the physical burden was higher during evisceration, cutting pieces, hang the chicken in nória after leaving the chiller and the separation of little poultry. Sheds in creating the food supply system manually and revolving bed activities are more strenuous and demanding greater efforts to be performed. In sheds matrices loading egg cartons and sacks of feed, as well as the revolving bed, are linked to increased physical burdens. The adoption of scheduled breaks or whenever workers feel the need, rotation activities and gymnastics are measures that can minimize or even eliminate future problems health of these workers.

Keywords: ergonomics, physical effort, poultry production

Itroduction

The concern of the Brazilian poultry industry to maintain high levels of productivity while meeting the rigorous standards required of the national and international market with respect to environmental sustainability, animal welfare and human, has fostered the emergence of techniques and adoption of regulations governing the whole process of production of poultry (Tinôco, 2001; Menegali et al., 2010).

Thus, issues related to ergonomics of workers who work in the productive sector of broilers are also in process of modification in order to provide improvements in working conditions and thus provide welfare to those employees.

Knowing that the job of managing the supply chain of broiler chickens is associated with loading weight, repetitive movements and long working hours, which may expose employees to develop health problems, the aim of this work was to evaluate the physical burden of work to which employees are subjected during the execution of management activities in a hatchery and slaughterhouse broilers, broiler breeding sheds and dies in Brazil.

Material and method

This study was conducted at a commercial hatchery, representative of most of the poultry industry of Brazil, during the execution of management activities in a hatchery and slaughterhouse poultry, broiler breeding sheds and matrices.

Physical work load was analyzed using a heart rate meter of the brand polar eletro, composed of a digital receiver, an elastic band and a sensor transmitter placed at the height of the chest. At each stage analyzed, the Polar Electro was placed on the workers at the beginning of the workday and removed on completion of activities.

Using the data collected the physical work load was determined in each activity as well as the cardiovascular workload when performing the tasks. For the calculation of cardiovascular load, the following equation was used:

$$CVL = [(HRW - HRR)/(MHR - HRR)]x100 \quad (1)$$

Where:
CVL = cardiovascular load, in %; *HRW* = heart rate at work, in bpm; *HRR* = heart rate at rest, in bpm; *MHR* = maximum heart rate, (220 – age).
The physical load of work was classified according to the working heart rate (Tab. 1).

Tab. 1 Classification of the physical load of work through the heart work

Physical load	Heart rate in bpm
Lightweight	< 75
Light	75 – 100
Moderately heavy	100 – 125
Heavy	125 – 150
Very heavy	150 – 175
Extremely heavy	> 175

Source: Couto (1996)

Results and discussion

Hatchery

Upon possessing the data collected by the heart rate monitor, analyzed according to equation 1 and Tab. 1, one can observe that the physical work load in the hatchery ranged from light to moderately heavy. Here it was verified that all activities are performed in a standing position with no place for seating, therefore according to Fiedler et al. (2012) it is of utmost importance to encourage voluntary adoption of breaks for muscle rest and relaxation, especially in activities that require constant standing.

Activities such as grading of eggs, hatching, turning, sexing, vaccination, separation of eggshells and inspection of the incubator, although carried out almost exclusively by women, require little physical force. Additionally, the company adopts a system for rotation of activities to allow for variations in posture and movements, seeking to promote biomechanical aspects (Silva et al., 2010).

Activities including the loading of egg crates that arrive to be incubated, cleaning the plastic crates arriving from the egg grading, hatching and sexing (for both, the crates are constructed of metal), as well as loading of crates with chicks that will go to the farms, are considered light to moderately heavy and are therefore performed only by men.

Association of the incubation + turning activities were classified as light to moderately heavy, due to overloading resultant from the activity imposed on the physical condition of the employees. Even when performing these activities, an increase heart rate when at work was observed in the hatchery (121 bpm), with CVL of 30 %. It is believed that this condition is probably due to the force required to remove the carts with eggs inside the incubator and take them to the turning room. Furthermore, this situation was reported by the employees as the most tiring activity in the hatchery.

After incubation and turning, while loading the crates of chicks onto the truck, it was found that the heart rate at work was 118 bpm, with a CVL of 32 %; these values are related to the fact that the employee has to push, lift and carry several crates at the same time for a period of 40 minutes. According to Couto (1996), during a workday of 8 hours the heart rate should not exceed 110 bpm. Adverse conditions may compromise the health of the worker due to demands of the cardiac and respiratory systems.

Poultry House

With regard to physical work load checked in management activities in sheds equipped with automatic and manual feeder was found that in all the sheds where the food supply system was automatic, the physical workload was classified as mild and higher value was 28 %. These sheds, during the post-heating, workers were responsible for washing the bell drinkers, rolling all over the bed or only part of it, take dead chickens for compost, straw spread of coffee in bed to make more room in the shed , and check that all the equipment shed were working properly.

However, in the sheds where the power system was manual (tubular feeder), the physical load of work was classified as mild to moderately heavy. Comparing the two types of feeding system, it can be seen that the highest value of CVL was found in sheds with the feeder tube. It is believed that two other sheds where tasks are performed simultaneously by two people, the CVL could have been higher, because this way, the exercise was mitigated.

Furthermore, in the fourth sheds found that heart rate were equivalent workers and / or above 100 bpm which characterizes the working condition to be moderately heavy.

The sheds where the power system is manual, workers are responsible for filling the feeders with the aid of metal buckets (10 and 20 liters) and its trolley to load feed, wash troughs, roll the entire bed or only part it, take dead chickens for compost, straw spread of coffee in bed to make more room in the shed, and check the operation of other equipment shed. After the supply of feeders, other activity considered very tiring for most workers is the partial or total revolving bed.

Slaughterhouse

Based on the values of CVL verifies that all activities were below the limit recommended by Apud (1989) which is 40 %. Thus, it is not necessary to calculate the settling time for activities.

Activities performed only by men, such as unloading the truck with boxes of chicken, hanging, bleeding manual and mechanized plucking, although laborious and tiring, were classified as mild. It is believed that this condition may be due to the fact that man have a better fitness than the woman, which can be evidenced by CVL values are lower for these activities when compared to activities undertaken mostly by women.

According Defani (2006) which highlights the differences between men and women in the category strenght, has close relationship with anthropometric issues. Realizes that provision muscle, bone structures and systems enable lever man greater degree of strenght.

Therefore, women may be more susceptible to the demands imposed by work and, consequently, suffer more frequent problems related to repetitive strain injuries and work-related musculoskeletal disorder, and physical overload. This situation is observed in activities gutting the room, cutting room (national and export) and kids where the number of working women is higher than the number of men.

Matrices

Based on the values of CVL (cardio vascular load) it is verified that all the activities were lower than the recommended by Apud (1989) that is 40 %. Thus, it is not necessary to calculate the settling time for the activities. However, according to Fiedler et al. (2012) is extremely important to encourage the voluntary adoption of breaks for rest and muscle relaxation, especially in activities that are constant standing. In breeders, it was found that all activities are performed in the standing position and always in motion.

The staff of the breeders is formed by men and women and both perform almost the same activities. The classified as moderately heavy activities are performed by women and involve weight bearing postures and in most associated with age and physical condition of employees.

Conclusion

It was verified in this study that workers in the supply chain of poultry may be exposed to unhealthy working conditions, and some activities associated with weight and poor posture can result in bodily injury. However, meeting the safety standards, adoption of scheduled breaks, workplace gymnastics, facility improvements, use of personal protective equipment and training of employees to make them aware of how to properly perform tasks, can significantly contribute to reducing injuries and improving the quality of life of workers, thus increasing productivity.

Acknowledgement

CNPq (National Council for Scientific and Technological Development), the Foundation for Research Support of Minas Gerais (FAPEMIG), CAPES (Coordination of Improvement of Higher Level Personnel) and the State Universtiy of Montes Claros (UNIMONTES).

Reference

Apud E., 1989. Guidelines on ergonomic study in forestry. Genebra: ILO, 241.

Couto H.A., 1996. Ergonomics applied to work: technical manual of the human machine, 2.

Defani J.C., Xavier A.A.P., 2006. Maintenance program gymnastics: a case study in a slaughterhouse and meat packing plant. In: XXVI National Meeting of Production Engineering.

Fiedler N.C., Juvanhol R.S., Silva E.N., Goncalves S.B., Carmo F.C.A., Maziero R., 2012. Analysis of physical work load in deployment activities in forest hilly areas. Forest, 42: 241-248.

Menegali I., Baeta F.C., Tinoco I.F.F., Cordeiro M.B., Guimarães M.C.C., 2010. Poultry performance in different half-acclimatized facility systems in the south of Brazil. Journal Agricultural Engineering, 18: 461-471.

Silva E.P., Cotta R.M.M., Souza A.P., Minette L.J., Vieira H.A.N.F., 2010. Diagnosis of the health of workers involved in the activity manual extraction of wood. Tree journal, 34: 561-566.

Tinoco I.F.F., 2001. Poultry industry: new concepts in materials, designs and construction techniques available for Brazilian broiler. Brazilian Journal of Poultry Science, 3: 2001.

PREDICTING LIMIT DRAFT FORCE FOR A CHISEL TINE USING FEA BASED SIMULATION

H. Kursat Celik[1*], Allan E.W. Rennie[2], Ibrahim Akinci[1]

[1]Dept. of Agricultural Machinery, Faculty of Agriculture, Akdeniz University, Antalya, TURKEY
[*]Phone: +90-242-3106570, Fax: +90-242-2274564, E-mail: hkcelik@akdeniz.edu.tr
[2]Lancaster Product Development Unit, Engineering Dept., Lancaster University, Lancaster, UNITED KINGDOM

Abstract

In this study, a chisel tool's tines which were subject to plastic deformation during tillage operations are considered. Stress distributions on the tools tines have been simulated using finite elements analysis (FEA) considering operational draft forces which have been obtained from the experimental study. Experimental material properties are assigned into the FEA simulations and all analyses conducted with due consideration to geometric and contact non-linearity in order to obtain more realistic results. According to the findings from simulations, it is shown that there is no plastic deformation failure evidence for conventional operational conditions. Subsequently, the limit draft force has been explored with setting up 'What-If' scenarios. Simulated visual outputs have been compared with physical deformation cases considering overloading conditions. Finally, it is concluded that the tillage tool considered within this paper was operated with very high draft force values which do not correlate with the design aim of the tool.

Keywords: Agricultural machinery design, Finite Elements Analysis, Finite Elements Method, Chisel tine deformation

Introduction

Primary tillage of soil is mainly conducted for cutting and loosening to a depth of 150 to 900 [mm] (McKyes, 1985). However, the mouldboard plough is the most common primary tillage tool in the world, and nowadays it is possible to see that use of the chisel tool instead of the plough as an alternative primary tillage tool is because of its added benefits such as less energy consumption and reduced number of transactions when in use. In addition to these benefits, the chisel tool is also used in agricultural fields to avoid problems associated with the negative effects resulting from soil compaction (Yalcin et al., 1996; Celik et al., 2007). The chisel's tines have narrow shares (tine's tip) and it is operated deeper in the soil than conventional ploughs, especially when it is used for breaking the hard layer in the soil. The tines and tine tips are important functional components of a chisel tool. As a result of deep tillage operations, the chisel tine and its tips may meet with high reaction forces of the soil, which may be a cause of their failure. Consequently, due to the component(s) failure, the chisel cannot realise its tillage function. Here, the failure can be defined as permanent deformation or instant breaking on the structure when it is loaded beyond its constituent material's elastic limit (Risitano, 2011). Most of the chisel components are manufactured from ductile steel based materials. The failure case is seen in two steps in these types of ductile materials as it is explained through Hookes Law (Ugural, Fenster, 2003). Approaching the yield point of the material, the first failure occurs which is known as plastic deformation. With increase in loading, subsequently, breaking may occur if the load exceeds the fracture point of the material. Therefore, one of the key points is predicting limit draft force during tillage to avoid failure cases and for the structural optimisation procedures of the tillage tools. However, although prediction of the limit draft force of a tillage tool can be realised by conducting field experiments, this may not be a practical and economical way for the design and optimisation procedures of such tools, as designing and optimising procedures are highly iterative and repetitive processes. Recent decades have witnessed many developments for high technology computers and numerical methods integrated engineering design software. Hence, nowadays, a powerful method to predict physical behaviours of materials under different loading conditions is by using numerical method based engineering simulations. One of the most used numerical methods in the computer aided design and engineering applications is Finite Elements Method (FEM). The first development studies of FEM in the engineering field started in 1950's for stress analysis of complicated structures in the aircraft industry and the term FEM was first presented by Clough in his publication in 1960 (Clough, 1960; Rao, 2004; Chandrupatla, Belegundu, 2011). Nowadays, usability of the method has a wide spread in different engineering application areas such as structural, electromagnetics, fluid dynamics, heat transfer, chemical reactions etc. since its first application.

In this study, a chisel's tine, which had met a plastic deformation case has been considered and it is aimed to predict limit draft force of the chisel tool by using advanced computer aided design and engineering analysis applications. The study has been carried out into two parts: these are field experiment and computer aided engineering applications. The field experiment has been utilised on the same party manufactured chisel tool in order to observe conventional tillage operation and to determine draft forces experimentally for each of chisel's tine. Subsequently, FEM based stress analysis has been carried out to map out stress distribution on the tine. According to findings from FEM based simulations, visual outputs have been compared with physical deformation cases and What-If scenarios based FEA were set up to determine draft force for one tine which force is called as limit force at just before plastic deformation case.

Field Experiments

In the field experiments, a chisel with seven times, which was manufactured by a company in Turkey, were considered to determine its draft force in conventional tillage operation. Some technical properties of the chisel tool can be seen in Fig. 1. Two-tractor method and computer aided force measurement system with a dynamometer (HBM-U9A) were used to measure draft force of the chisel tool in the experimental study. The force transducer has a nominal force of 50 [kN] and a nominal sensitivity of 1.1 mV/V, the sensitivity tolerances being within ±0.5 % of pull force. The nominal range of supply voltage is 0.5-12 V. The nominal temperature range is 10-70 ºC. The mass of force dynamometer is 0.4 [kg] (Akinci et al., 2004). The study was carried out in a private agricultural field (in 25 [da] area with wheat stubble) at Serik/Antalya, located in the West-Mediterranean region of Turkey. The field consisted of clay-silt structured soil. The soil penetration magnitude was 2.53 [MPa] at 200-400 [mm] depth. Average moisture content of the soil was 16 % for dry conditions. In the tillage operations, a New Holland TD75D agricultural tractor was utilised and skidding in tires was measured as 19 %. All experiments were carried out in a soil depth of 300 [mm] with three different tractor speeds with three runs. Measured data were recorded throughout 45 seconds for each run.

Some of Technical Properties of the Chisel Tool

General Properties of the Tool			Properties of the Tine's Tip		
Full Lenght	850	[mm]	Type	Narrow	[-]
Full Width	2100	[mm]	Shear Angle	26	[º]
Full Height	1200	[mm]	Immersion Angle	8.4	[º]
Weight	280	[kg]	Length	280	[mm]
Tillage Width	2000	[mm]	Width	60	[mm]
Number of Tines	7	[-]	Thickness	10	[mm]
Distance Between Tines	280	[mm]	Hardness	380	[HB]

Fig. 1 Chisel tool and some of its technical properties

According to these variables, the maximum draft force values of the chisel tool were determined as 11.34, 14.98, and 15.19 [kN] based on the average force experienced for 3.0, 5.0 and 5.6 [km h^{-1}] tractor speeds respectively. Subsequently, draft force for each single tine was calculated by dividing total force values to the number of tines belonging to the chisel (Fig. 2).

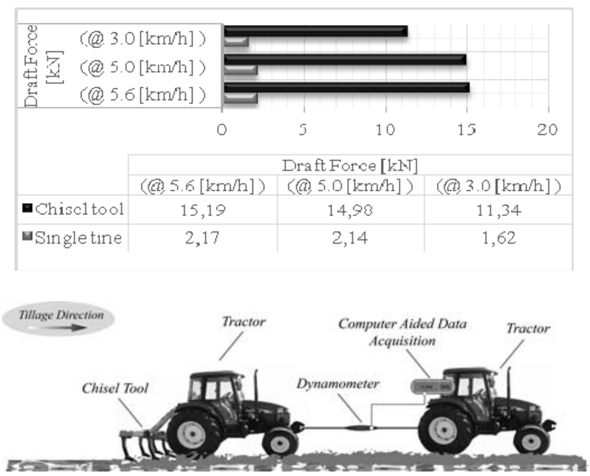

Fig. 2 Field experiment setup and chart supported numerical results for draft force

FEM Based Stress Analysis of Chisel's Tine Assembly Group

In this part of the study, FEM based stress analyses were carried out to investigate stress distributions on the single chisel tine for three different tillage speeds which are defined as conventional tillage operations in this study. This study focused on the deformation of a single tine of the chisel. Therefore, all components of the chisel were not used in the FEM based analyses. Three dimensional (3D) solid model of the tine group was created using SolidWorks 3D parametric design software. All Finite Elements Analyses (FEA) were set up in 3D-geometric and contact non-linearity, static, and isotropic material model assumptions. Ansys Workbench commercial FEA code was used for the FEA. Tillage conditions were set up in the FEA software to simulate the act of the chisel' tine under draft forces calculated in the experiments. Draft force was applied to the narrow share (tine's tip) through opposite of headway. The narrow share has a 20˚ tangent. Material properties used in the FEA were obtained from tensile tests which were conducted on the specimens taken from the chisel's related components during manufacturing operations. Assigned properties of the material are presented in Fig. 3. Mesh structure of the model was created in the FEA procedure. Meshing operations were generated by using the meshing functions of Ansys Workbench (Ansys Software Product, 2012). In the meshed structure, Quadratic Tetrahedron, Hexahedron, Quadrilateral element types were used and a total of 33973 nodes and a total of 24859 elements were obtained. After running the FEA process, deformation and stress distributions were obtained on the chisel's tine for three different draft forces at different tillage speeds. In the FEA post-processing step, output screens were displayed, which detailed that the maximum equivalent stress (Von Mises) occurred on the Chisel's tine assembly group as 64.884, 84.154 and 85.416 [MPa] for different draft forces at tractor speeds of 3.0, 5.0 and 5.6 [km h^{-1}] respectively. Boundary conditions, mesh structure and simulation screen outputs are presented in Fig. 4.

According to the simulation outputs, plastic deformation or breaking failure signs were not seen when the maximum stress magnitudes were evaluated according to the yield stress point (280 [MPa]) of the material. In addition to this, deformation values on the tine group were in a quite small range which did not lead to any negative effect on the aimed tillage function of the tool (Fig. 4). Therefore it can be said that the tool accomplished its tillage function within conventional tillage conditions as this was also observed in the experimental study.

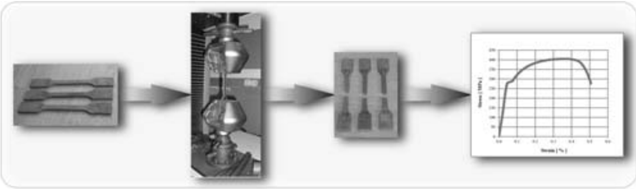

Material Properties		
Elastic Modulus	[GPa]	210
Poisson Ratio	[-]	0.3
Yield Strength	[MPa]	280
Tensile Strength	[MPa]	404
Fracture Strength	[MPa]	348
Density	[kg m^{-3}]	7850

Fig. 3 Tensile testing progress and material properties used in the FEA

Predicting Limit Draft Force

FEA based simulation results shows that the tine group compensates the draft forces in the defined conventional tillage operations. Here, another important point is predicting limit draft force magnitude which is the limit magnitude for current tine construction at just before a plastic deformation failure case. Subsequently, with having this knowledge, the tine's constructional design can be used for an optimisation study to determine optimum design parameters of the tool. Ansys DesignXplorer design exploration module was utilised and 'What-If' scenarios (Ansys DesignXplorer, 2012) were set up to predict the limit draft force. In the 'What-If' exploration, 34 design points in total (included conventional tillage draft forces) were prepared and all points were solved in the module. According to 'What-If' based solutions, the variations between draft forces and stresses have been obtained (Fig. 5). This solution (by considering material yield point) indicates that the allowable maximum draft force (Limit force) was able to reach a maximum 6.0 [kN] (Max. Stress of 273.858 [MPa]). In the 'What-If' scenario, over loading conditions were also considered. The tool was loaded step-by-step (with 0.25 [kN] intervals) until 10.0 [kN] that was the highest draft force in the setup. At this magnitude of the force, stress value was above the material failure points of the tine assembly group (Fig. 5).

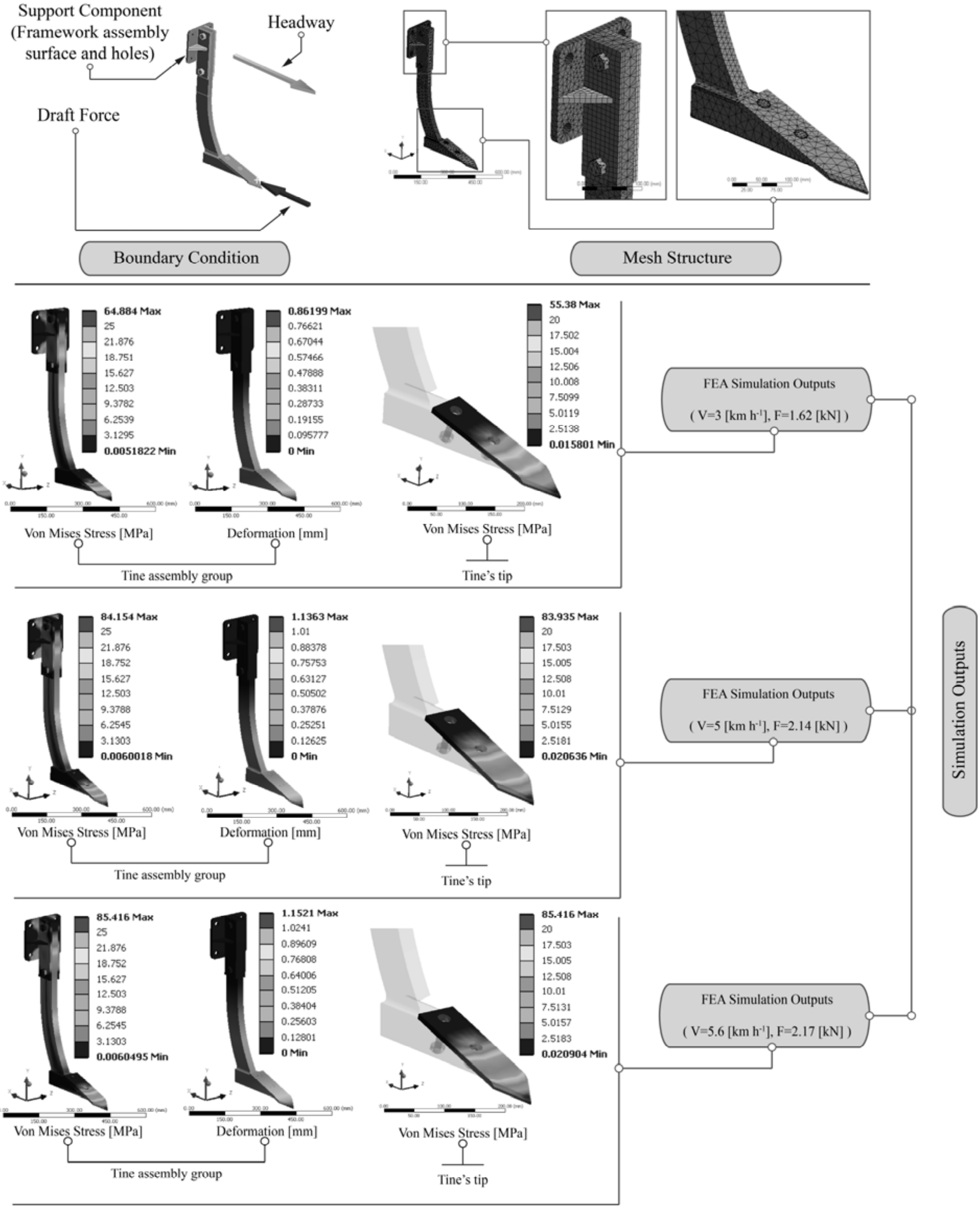

Fig. 4 FEA setup and simulation outputs

What-If Study Results			
Order No	Draft Force [N]	Maximum Eq. Stress (Tine Assembly Group) [Mpa]	Maximum Eq. Stress (Tine Tip) [Mpa]
1	1.62	64.884	55.380
2	2.14	84.154	83.935
3	2.17	85.416	85.416
4	2.50	101.965	101.965
5	2.75	114.336	114.336
6	3.00	126.429	126.429
7	3.25	139.107	139.107
8	3.50	151.476	151.476
9	3.75	163.788	163.788
10	4.00	176.095	176.095
11	4.25	188.630	188.630
12	4.50	200.910	200.910
13	4.75	213.078	213.078
14	5.00	225.188	225.188
15	5.25	237.857	237.857
16	5.50	250.051	250.051
17	5.75	261.764	261.764
18	6.00	273.858	273.858
19	6.25	285.568	285.568
20	6.50	297.010	297.010
21	6.75	308.991	308.991
22	7.00	320.270	320.270
23	7.25	331.165	331.165
24	7.50	341.687	341.687
25	7.75	352.890	352.890
26	8.00	363.918	363.918
27	8.25	373.640	373.640
28	8.50	385.480	385.480
29	8.75	395.993	395.993
30	9.00	406.644	406.644
31	9.25	417.564	417.564
32	9.50	428.126	428.126
33	9.75	438.265	438.265
34	10.00	449.006	449.006

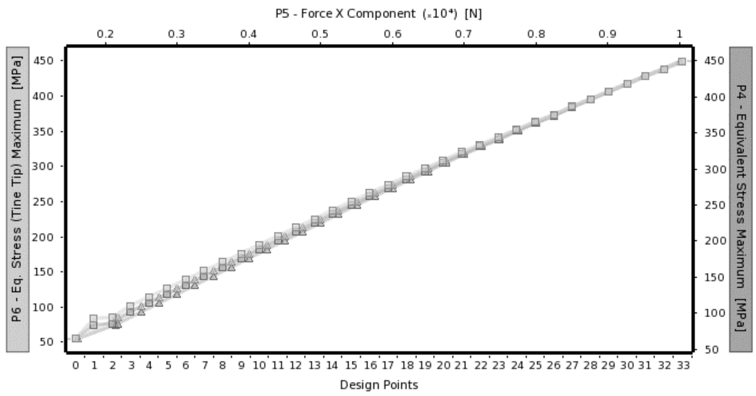

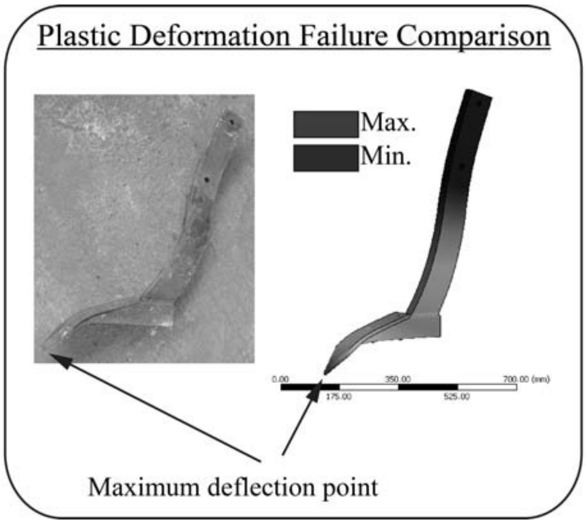

Fig. 5 Numerical results and chart display of the 'What-If' study and visual comparison between simulation outputs and physical plastic deformation cases

Discussion and conclusion

The knowledge acquired from 'What-If' scenario results have extracted the relationship between draft force and stress magnitudes on the chisel's tine assembly group. Increase in loading reflects an increase in stress magnitudes. By considering the material's yield point, the limit draft force appeared as 6.0 [kN] and plastic deformation case could be interpreted above this loading magnitude. Visual comparison between simulation outputs and the physical deformation case has also proved that the simulation was set up with success and deformation behaviour of the components could be seen clearly in the simulation output screen (Fig. 5). This plastic deformation case also highlighted that the tillage tool considered within this paper was operated with very high draft force values which do not correlate with the design aim of the tool. The limit draft force (6.0 [kN]) highlighted in exploration seem to be quite a high level. Therefore an optimisation study can be thought to deliver optimum material use for the related components. In addition to these results, where this study is focused on predicting limit draft force for a sample chisel tool by means of CAE applications, such applications can be used to prevent probable failures, design-material errors, and excessive time and costs for similar agricultural machineries. This study can also be used as a preliminary study for a structural optimisation of the constructional elements of the tool. In addition to these results, although failure was detected, a failure analysis study was not conducted exactly. This can be thought of as a subject for a future study.

Reference

Akinci I., Canakci M., Topakci M., Ozmerzi A., Yilmaz D., 2004. Development of draft and torque measurement system for agricultural machinery. Energy Efficiency and Agricultural Engineering Conference, EE&AE-04, June 3-5, Rousse, Bulgaria, 308-314.

Ansys Software Product, 2012. Overview of the meshing process in ANSYS Workbench. Release Notes for Ansys Workbench Release 14.5.

Ansys DesignXplorer, 2012. Design Exploration user guide release 14.5 documentation for ANSYS Workbench, ANSYS Inc. SAS IP, USA.

Celik H.K., Topakcı M., Yilmaz D., Akinci I., 2007. Strength Analysis on the Constructional and Operational Components of a Chisel Using Finite Element. Journal of Agricultural Machinery Science, 3(2): 111-116.

Clough R.W., 1960. Finite element method in plane stress analysis. Proceedings American Society of Civil Engineers (2nd Conference on Electronic Computation). Pitsburg, Pennsylvania, 23: 345-378.

Chandrupatla T.R., Belegundu A.D., 2011. Introduction to finite elements in engineering-4th Ed. Prentice Hall Publication, 448. ISBN:0132162741.

McKyes E., 1985. Soil cutting and tillage-Developments in agricultural engineering. Elsevier, 217.

Rao S.S., 2004. The finite element method in engineering-4th Ed. Elsevier Inc, 663. ISBN: 0750678283.

Risitano A., 2011. Mechanical Design. CRC Press, ISBN: 9781439811696, 650.

Ugural A.C., Fenster S.K., 2003. Advanced strength and applied elasticity-4th Ed. Prentice Hall, 544. ISBN: 0130473928.

Yalcin H., Demir V., Ucucu R., 1996. Functional efficiency (Its effect on soil) and running characteristics of the chisel at different order of its legs and working speeds. The Journal of Ege University Faculty of Agriculture, 33(2-3): 159-166.

MONITOR THE STATUS OF SIMULTANEOUS MALFUNCTION EGR AND DPF THE TDCI ENGINES POWERED EKODIESEL ULTRA DIESEL OIL AND B10 FUEL

Boguslaw Cieślikowski

University of Agriculture in Krakow, Faculty of Production and Power Engineering
ul. Balicka 116B, 30-149 Kraków, Poland
Phone: +48 12 662 46 82, E-mail: Boguslaw.Cieslikowski@ur.krakow.pl

Abstract

In the article was discussed the location faults in the agreements EGR (Exhaust Gas Recirculation) and DPF (Diesel Particulate Filter) using list of fault codes OBD II. The monitoring systems of vehicles with an engine DURATORQ TDCi was used as an example. Analyzing the processes of heat and mass transfer over a distance of the engine intake system, called attention to a number of simplifications in the formal description, leading to establish a temporary tolerance range of recirculation. Functional analysis system and knowledge of diagnostic procedures, using selected recording car operating parameters, is the appropriate focus in the damage location process. The aim of this study was to determine the influence of diesel oil Ekodiesel Ultra with biocomponents B10 used as a modern fuel to power diesel engines on the formation of deposits in the EGR and DPF. Analysis was performed in a certified laboratory by means of energy dispersive X-ray fluorescence and infrared spectroscopy methods. The subject of the study was the deposits formation in elements a EGR and DPF resulting from the use of diesel oil with biocomponents. The inference focused on the analysis of the content of unoxidised organic ingredients precipitated in the elements.

Key words: EGR, DPF, diagnostic procedures OBD II, X-ray fluorescence, infrared spectroscopy

Introduction

The optimization of the process of charge combustion in a multiple injected diesel engine using hydrocarbon and biocomponent fuels in a Common Rail system sets the main trends in the research and development works on diesel engines. Exhaust aftertreatment systems such a exhaust gas recirculation (EGR), catalytic converters and diesel particulate filters (DPF) are used increasingly.

The manufactures of diesel engines for modern farm tractors declare the compatibility of their engines with the B 100 biofuels provided the EN/PN 14213 quality standards is met (PN-EN 14214). Fatty acid methyl esters (FAME) is substantially different from diesel oil in that it has a different chemical construction, fractional composition, viscosity molar mass and the content of sulfur and oxygen. Higher fatty acids have a substantial impact on the operation of DPF because high content of unsaturated acids results in an increase of the soot emission. Additionally oils of low quality may contain more contaminants such as free fatty acids, phospholipids, colorants and water. One of the important quality parameters of FANE related to their chemical construction is the proneness to form deposits in the intake system and combustion chambers. A chemical composition of the FAME introduces a low thermal stability and susceptibility to polymerization.

Research experiments into innovative construction of DPF and EGR are convergent with the improvement of the physical and chemical characteristics of FAME biofuels containing certain selected conditioners (Cieślikowski, 2011). The application of the EGR systems is reduced to the benefit of the selective catalytic reduction (SCR) system using AdBlue. Sometimes a combined systems are applied in the case of JOHN DEERE heavy-duty farm tractors (Yokomura et al., 2003). In diesel engines of vehicles fueled of conventional hydrocarbon fuels with a growing content of FAME we can see an advancement of the EGR systems. The systems controls their operation, leads to a reduction of the combustion rate, this contributing to the reduction of the NO_x concentration in the exhaust gas (Jung et al., 2010).

However, an excess amount of exhaust gas in the charge fed to cylinder may result in a drop of the engine power in crease in the emission of particulate matter (PM), thus deteriorating other engine index (Bieniek et al., 2011).

Functional analysis o the EGR and DPF systems

The mass of the recirculated exhaust gas is calculated from the difference of the total mass of the charge and the mass of air in reference to the intake air temperature correction [9]. The opening of the EGR valve defines the mass of the exhaust gas to assure the instantaneous required recirculation rate XEGR.

$$X_E = \frac{m_E}{m_E + m_p} 100\% \qquad (1)$$

m_p – mass flow rate of air ($kg.s^{-1}$),
m_E – exhaust gas mass flow driven by the EGR valve to the intake system ($kg.s^{-1}$).

The error range is precisely determined and its excess results in an emission related malfunction signaled by a malfunction indicator light (MIL). The EGR system is distinguished by a great range of tolerance to momentary change of the recircula-tion rate, particularly in the interval of non-steady engine operating states.

The analysis of the energy balance of heat and mass exchange contains certain simplifications due to a lack of the possibility of unambiguous description of all the factors conditioning an accurate parameterization of the exhaust gas recirculation process.

A fundamental problem is proper determination of the specific heat of the recirculated exhaust gas based on the specific heat of all its individual components:

$$m_p c_p T_p + m_E c_{sp} T_{sp} = (m_p + m_E) c_m T_m \qquad (2)$$

$$c_{sp} = \sum_{i=1}^{n} \frac{m_{spi}}{m_E} c_{spi} \qquad (3)$$

c_{sp} – specific heat of the recirculated exhaust gas ($kJ.kg^{-1}.K^{-1}$),
T_{sp} – temperature of the exhaust gas (K),
c_m – specific heat of the all components ($kJ.kg^{-1}.K^{-1}$),
T_m – temperature of the exhaust gas and mass of air (K),
m_{spi} – the flow of the identified component in the exhaust gas recirculation ($kg.s^{-1}$),
c_{spi} – specific heat of the exhaust gas recirculation component identified ($kJ.kg^{-1}.K^{-1}$).

Besides, as a result of the use of biofuel conditioners there are more (as compared to regular hydrocarbon fuels) such components as: CO_2, CO, HC and NO_x (Cieślikowski, 2011). Another approximation of the actual state is contained in the notation of the Clapeyron equation of the state of the formed mixture of air and exhaust gas:

$$p_m (V_p + V_E) = m_m R_m T_m \qquad (4)$$

p_m – pressure of the of the exhaust gas and air (Pa),
V_p – air flow rate determined by the mass of data air flow meter ($m^3.s^{-1}$),
V_E – exhaust gas recirculation flow rate ($m^3.s^{-1}$),
R_m - solid, gaseous mixture of air and recirculated exhaust gas ($kJ.kg^{-1}.K^{-1}$).

The difficulty in the notation also results from the fact that feeding recirculated exhaust gas, irrespective of its prior chilling, results in a growth of the intake air temperature (SAE J2012 i ISO 15 031-6). A secondary temperature drop of the mixture takes place as a result of a heat exchange in the intake manifold. We can precisely determine the flow time of the mixture through the analyzed distance (taking the engine speed and the filling efficiency) but it is difficult to average the medium flow results having variable intake geometry in the zones of varied wall temperatures.

$$T_m = \frac{Q_E + Q_p}{m_m c_m}, \text{(K)} \qquad (5)$$

Q_E – heat flow is recirculated exhaust ($kJ.s^{-1}$),
Q_p – heat flow of air forced through the flowmeter ($kJ.s^{-1}$).

A simplification is, thus introduced consisting in that a circular cross section is assumed of the intake manifold for its replacement diameter, which leads to a simplification of the notation of the heat exchange area. The situation is aggravated by the fact that, due to tar deposits, there is no possibility of allowing for the variable flow resistance exhaust gas of the DPF and EGR in the zone of the valve controlling the exhaust gas flow.

EGR and DPF system diagnostics using a scan tool

The area of the unification of the diagnostic principles has been significantly extended by compliance of the controllers with the software according to the OBD II system meeting both the SAEJ1830 and ISO9141-2 standards. The coexistence of the diagnostic controllers was initiated when the ISO15031-3 standard was introduced allowing communication through the CAN standard (Controller Area Network). The skill of making multi-symptom diagnostic conclusions and the knowledge of technical solutions used in the functional system of a vehicle are a basis for the formulation of correct diagnostic decisions. An important step in the development of OBD was the notation and definitions of the trouble codes (SAE J2012). The pulling of the error codes from the controller is possible with a scan tool. Diagnostic scan tools (SAE J1978) and the description of the individual scan tool operating modes (SAE J1979) are also subject to standardization. A list of standardized error codes directly or indirectly related to the operation of the EGR and DPF systems has been shown in Tab. 1.

Tab. 1 Standardized diagnostic trouble codes directly or indirectly related to the malfunctioning EGR and DPF (SAE J2012 i ISO 15 031-6)

DTC	Circuit, system, parameter to which the error code is related	Type of malfunction
P0400	Exhaust gas recirculation flow	Malfunction
P0401-P0404	Exhaust gas recirculation flow	Range/performance problem
P0405-P0408	Exhaust gas recirculation sensors A/B	Circuit range performance problem
P0100	Mass or volume air flow	Malfunction
P0101-P0103	Mass or volume air flow	Range/performance
P0104	Mass or volume air flow	Circuit intermittent
P0470	Exhaust pressure sensor	Malfunction
P0471-P0474	Exhaust pressure sensor	Range/performance
P0475	Exhaust pressure control valve	Malfunction
P0476-P0478	Exhaust pressure control valve	Range/performance
P0479	Exhaust pressure control valve	Circuit intermittent

Besides, the P0100 to P0104 error codes shown in table 1 may provide additional information in the assessment of the EGR system operation (showing an incorrect recirculation rate). The stored error codes from the P0110 to P0114 group are assigned to the air intake temperature sensor. Usually problematic in the malfunction identification is the effect of simultaneous storage of the error codes in the turbocharger pressure circuit from the P0235 to P0242 group supplemented with the error code of the recirculated exhaust gas temperature sensor from the P0544 to P0549 group. Problematic in the malfunction identification is the effect of simultaneous storage of the error codes in the exhaust pressure sensor DPF from the P0470 to P0474 group supplemented with the error code of the recirculated exhaust pressure control valve from the P0475 to P0479 group.

The subject of the analysis as regards the identification of malfunctions in the EGR and DPF system is the intake manifold of a Common Rail DURATORQ TDCi engine. The ECU controller – J248 controls the stepper motor positioning the EGR valve. The process of fault identification is getting difficult if intermittent malfunctions occur at irregular intervals and unsteady engine operating states [PTNSS]. Upon connecting of the diagnostic interface of the TEXA Nawigator TXT (Fig. 1) scan tool to the vehicle error codes stored in the memory ECU were detected - P0402 and P0404. The analysis of the parameters pulled from the ECU and those given by the manufacturer did show deviations from the required values.

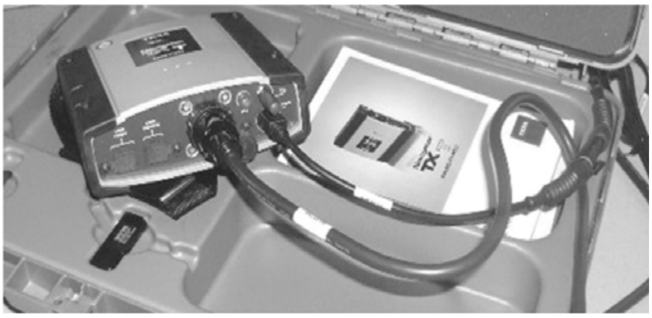

Fig. 1 TEXA Nawigator TXT scan tool

Parameter shown in this group of measurement blocks is the current signal of the mass airflow determined by the MAF sensor. An important parameter is the percentage value of the filling coefficient of the PWM signal confirming the setting of the EGR valve stepper motor. In the analyzed system, when the valve was closed the value of the filling coefficient did deviate from the admissible level i.e. above 70 % and when the valve was open the value was also in the 32 % limit. In the measurement block the values of the mass airflow changed as well and fell in the interval from 420 to 600 mg/cycle when the EGR valve was closed. When the EGR valve was opened in 130 mg/cycle of the mass airflow was also in the 130 mg/cycle limit. The mass airflow must changed as well and fell not in the interval from 180 to 340 mg/cycle. An important fact that has to be noted is the course of the changes of the mass airflow whose value should change stepwise from the moment of the setting of the EGR valve. An extended time of the expected change of the value in the mass airflow may indicate an excessive contamination of the actuators of the EGR valve leading to a delay in its positioning. No reaction of the air mass airflow to the opening and closing of the EGR valve may confirm a malfunction of the MAF sensor.

Spectral analysis of the deposits in the EGR and DPF zone

A spectral analysis of the deposits sampled in the surface of the EGR channel in the DURATORQ TDCi engines fueled with B10 biofuel and Ekodiesel Ultra (diesel fuel) was performed. Analysis was performed in a certified laboratory by means of energy dispersive X-ray fluorescence and infrared spectroscopy methods. The spectrums of the X-ray fluorescence with the XRF ED energy dispersion were recorded with the ED 2000 recorder made by Oxford Instruments, while the IR infrared spectrums (FTIR) were recorded with FTS 175 by BIO-RAD. The subject of the study was the deposits formation in elements a EGR and DPF resulting from the use of diesel oil with biocomponents – Fig. 2.

a) b)

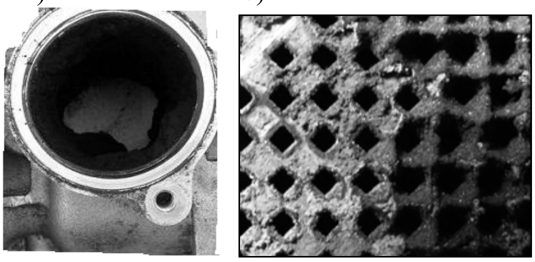

Fig.2 The deposits on the inner surface of the EGR channel: a) and DPF structure, b) in the DURATORQ TDCi engine

The recording of the XRF characteristics for deposits taken from the EGR valve zone of an engine fueled with Ekodiesel Ultra and B10 have been shown in Fig. 3. Based on the assessment of the changes of the intensity of the spectral bands for the identified elements a qualitative analysis was performed. In the analyzed deposits such metals were identified as: iron, zinc, chromium, nickel and copper. The presence of zinc, calcium and phosphorus results from the degradation of the engine lubricant, including the oil additives. Besides, depresators as part of the biofuel conditioners contain ions of iron (Cieślikowski, 2011). The contaminants results from the processes of corrosion of steel elements whose structure is more prone to FAME related corrosion.

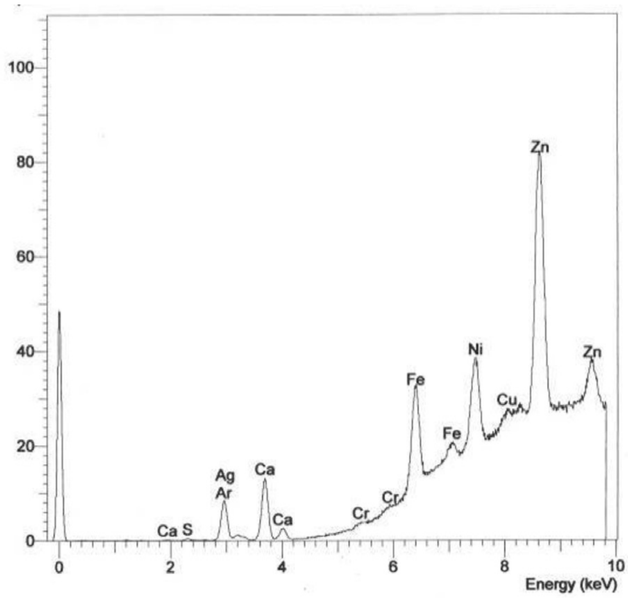

Fig. 3 The XRF spectrum for the deposits taken from the EGR valve zone of an engine fueled with Ekodiesel Ultra

Upon taking the deposit off the inner walls of the DPF and EGR with chloroform the samples were analyzed in the infrared spectrum – Fig. 4. The most intense is the spectral band of approx. 1655 cm^{-1} in the diagnostic area of 2000 cm^{-1} – 1600 cm^{-1} confirming the occurrence of processes of oxidation of organic compounds to carbonyl and carboxyl structures. The effect of the influence of these compounds on the nitric oxides is most likely related to the presence of the hydrated salts of carboxylic acids. We may observe an intense spectral band of 1747 cm^{-1} related to the presence of esters. We cannot unambiguously state whether these are undegraded FAME esters or the products of their degradation, d_i or trimerization. For the purpose of identification of the deposits of the ester group the relations of the carbonyl groups C=O (aliphatic) are representative with the corresponding spectral band in the wave number of 1750-1735 cm^{-1}. The presence of the ester structures is confirmed by the spectral bands in the „finger print" range (approx. 1240 cm^{-1} and 1160 cm^{-1}).

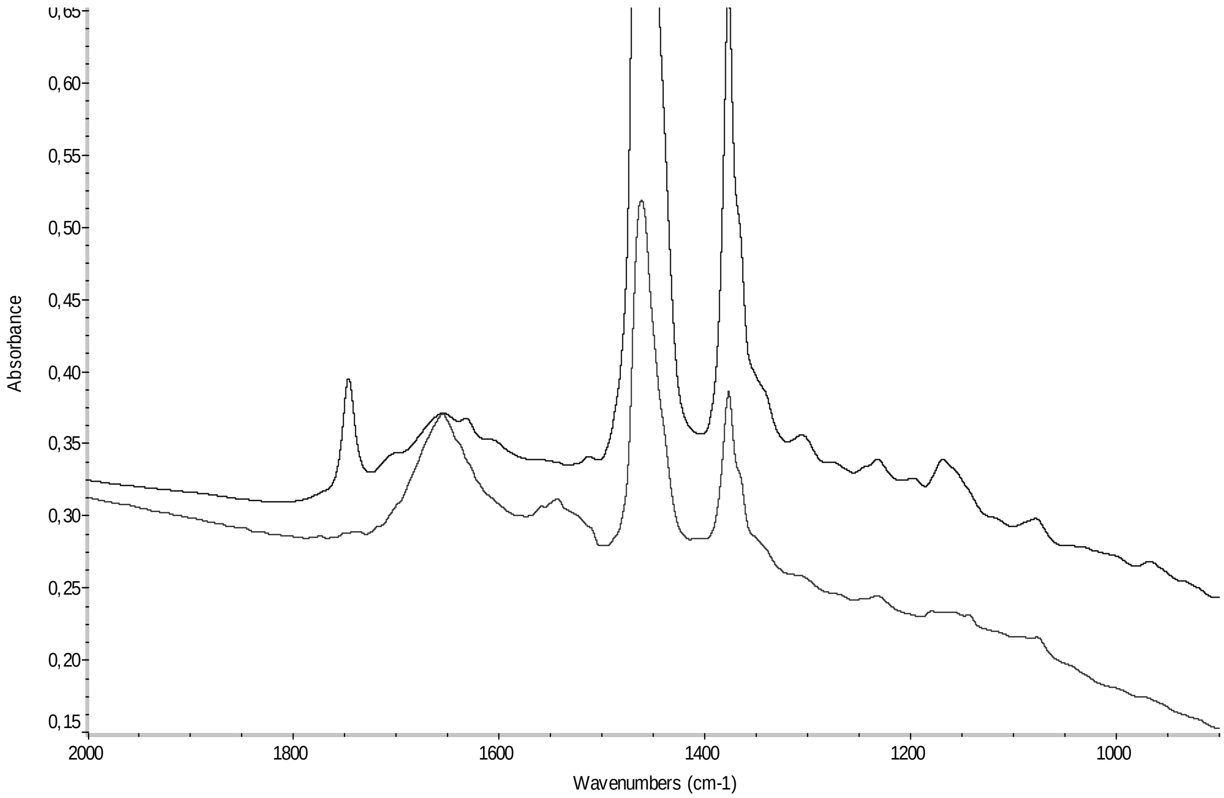

Fig. 4 IR spectrum (range 2000 cm^{-1}– 900 cm^{-1}) of the soluble fraction of the deposit from the DPF valve zone in the engines fueled with the fuels: diesel oil (lower curve) and B10 (upper curve)

Conclusion

- The fundamental problem of a diagnostic analysis appears in the need to explore complex phenomena of stored malfunctions of the analyzed system.
- The spectral analyses of the X-ray fluorescence with energy dispersion in relation to the determination of the share of the chemical elements forming the deposit in the EGR valve and DPF zone as well as the recording of the IR spectrum made after the extraction of the sample have confirmed a share of organic compounds in the solid deposit.
- The main sources of the deposit are FAME polymer groups coming from varied biofuel conditioners.

Reference

Bieniek A., Graba M., Lechowicz A., 2011. Adaptive Control Of Exhaust Gas Recirculation at Nonroad Vehicle Diesel Engine, Journal of KONES, 18(4): 11-15.

Cieślikowski B., 2011. Spectral analysis of deposits from a catalytic converter of Diesel engine. Kongres: Combustion Engines, 2011, Wyd. Silniki Spalinowe, 3(146): 17 - 26.

Excerpt from the standards: SAE J2012 i ISO 15 031-6.

Jung S., Ishida M., Yamamoto S., Ueki H., Sakaguchi D., 2010. Enhancement of NOx- PM trade off a diesel engine adopting bio-ethanol and EGR. International Journal of Automotive Technology, 11(5): 611–611.

PN-EN 14214: Paliwa do pojazdów samochodowych - FAME do silników o zapłonie samoczynnym (Diesla). Wymagania i metody, 37.(in Polish)

Yokomura H., Kohketsu S., Mori K., 2003. EGR systems in a turbocharged and intercooled heavy-duty diesel engine – expansion of EGR area with Venturi EGR system, Technical Review, 46-57.

OSMOTIC DEHYDRATION OF STAR FRUITS (*Averrhoa carambola*)

Lara Covre[1], Jadir Nogueira da Silva[2*], Silmara Almeida de Carvalho[1], Modesto Antonio Chaves[1]

[1]Estadual University South-west of Bahia, Itapetinga, Brazil
[2]Federal University of Viçosa, Av. P. H. Rolfs, University Campus, 36570-000 Viçosa, MG, Brazil,
Phone: +55 31 38991928, Fax: +55 31 38992734, E-mail: jadir@ufv.br

Abstract

Osmotic dehydration is a stage of pre-conservation treatment that has been widely used to reduce the water activity, to increase chemical stability and to improve of some nutritional, sensory and functional properties of fruit (Torreggiani, 1993; Torreggiani, Bertolo, 2001). This research was made aiming to study some effects of osmotic dehydration conditions on star fruits. The star fruits (Averrhoa carambola) from the variety Twaian were produced at Ouro Verde farm, located in Una town, Bahia, Brazil (15° 17' 36'' S and -39° 04' 31''W). The experiment was conducted with the solutions at two temperatures (40 to 50°C), three concentrations (40, 50 and 60%) and eight immersion times (1 to 8 hours) which were taken as independent variables seeking by multiple regressions analysis for responses of the following dependent variables: water activity (a_w), moisture content, weight reduction (WR), water loss (WL), solid gain (SG) and soluble solids concentration (SSC) of the star fruits. Fruit:solution ratio was 1:10. Regression models that explain the effect of the independent variables on each independent one were adjusted. Temperatures, sucrose concentration and time of osmotic dehydration significantly increased ($p < 0.05$) WL, WR and SSC and significantly decreased ($p < 0.05$) a_w and moisture content. Regarding SG, only osmotic dehydration time presented a significant effect increasing solid gain. The main changes expected in this type of process, greater water loss with lower solid gain, rushed in the first 4 hours of osmotic dehydration of study at the two temperatures, which are considered the maximum processing time for the evaluated conditions. It was obtained with 60% sucrose and 50ºC values more desirable in all parameters, mainly greater weight reduction and water loss and lower water activity and moisture content. Thus indicating that these are the concentration and the solution temperature more suitable for the osmotic dehydration of star fruits among the conditions studied.

Keywords: osmotic dehydration, water, solid gain, refractometer

Introduction

For the past years, due to the diversification and the interest for exotic fruits, the production of star fruits have reached an expressive volume in Brazil, especially in the state of São Paulo. The country is considered one of the biggest producers of star fruit in the world, having this kind of cultivation in almost all of the territory, except in cold regions or subjected to frost (Donadio et al., 2001; Natale et al., 2008; Teixeira et al., 2001).

The use of the star fruit have always been limited due to the perishable characteristic of the fruit and to the occasional loss because of the lack of suitable installations in some production places. Having in mind these problems, the development of a simple process and little expensive of preservation of this fruit becomes desirable (Abd Karim, Chee Wai, 1999).

The osmotic dehydration have been considered an important techniques of pre-treatment in order to develop new products derived from the fruits, with aggregate value and with functional properties. The process is composed of the immersion of food that can be as a whole or pieces in a hipper tonic solution of one or more solutes, originating two simultaneous flows and in concurrent: a water exit of the product to the solution and done migration out of the solution of the solutes to the food (Torreggiani, 1993; Torreggiani, Bertolo, 2001).

In this kind of process, the phenomenon of mass transfer that happens between the food and the osmotic environment is widely affected by the variables of the process, which are associated to the characteristics of the raw material and the operational conditions adopted (Dhingra et al., 2008).

The aim of this research was to evaluate the effect of the time of the immersion and of the sucrose solution concentration, submitted to different temperatures, in the osmotic dehydration process of the star fruit.

Material and Methods

Star fruits from Taiwan cultivare, produced in Ouro Verde farm, Una, BA, were used as raw material. The fruits were selected according to their size, shape, maturation stage (yellow with green end point) and lack of harm. The osmotic agent used was the commercial sucrose (refined sugar) diluted in distilled water.

The fruits, previously washed and sanitized in chlorinate water, were crosscut 1 cm thick. The seeds were removed and each slice was weighed on an analytical scale.

The star fruit slices were added, individually in a proportion fruit:ratio 1:10, to the dehidrating solution in glass recipient placed in thermostetic shower. As the programmed osmotic dehidration time had passed, the jars were removed and the samples drained, washed with distilled water, dried carefully with paper towel and weighed on an analytic scale.

The moisture content was determined through the direct drying in greenhouse at 105°C, even the constant mass and the soluble solids concentration, expressed in °Brix, was determined through the direct reading of a digital refractometer workbenchof DSA E-Scan (The ElectronMachine Corporation), according to the proposed method by Adolfo Lutz Institute (2004). a_w was done through direct measurement in digital device workbench of AquaLab 4 TEV (DecagonDevices, Inc.), with controlled temperature at 25 ºC and ± 0,003 precision. The water loss, weight reduction and solid gain were calculated through math equations according to what was described by Carvalho et al. (2006). All the analysis were done in third copy.

The outlining of random blocks were used with three repetitions for each treatment. The factorial scheme used was 3x8, being 3 concentrations of sucrose osmotic solutions (40, 50 and 60%) and 8 times of immersion (1, 2, 3, 4, 5, 6, 7 and 8 h) for the dependant variables water loss, weight reduction and solid gain. For the dependent variables water activity, moisture content and fruit soluble solids concentration, the experiment was conducted in a factorial scheme 3x9, being 3 concentrations of sucrose osmotic solution (40, 50 and 60%) and 9 times of immersion (0, 1, 2, 3, 4, 5, 6, 7 and 8 h), in which the time 0 h corresponded to the star fruit physic analysis *in natura*.

The data obtained were submitted to the analysis of multiple regression. The significance of the models was tested by the variance analysis (ANOVA) and F test ($p < 0,05$), being the coefficients estimatted by t test of Student. With the obtainment of regression equations were placed the graphs of answer surface by using a SigmaPlot versão 11.0 software. The SAS versão 8.0 (SAS Institute Inc., North Carolina, USA, 1995) statistic package was used for the data treatment.

Results and discussions

It was observed in the *in natura* fruits, average of 93,46% moisture content, soluble solids concentration of 5,60 °Brix and water activity of 0,9945. The low content of soluble solids and the high value of the star fruit water activity used in this experiment provide a picture of a small quantity of sugar presented in the *in natura* fruit, and that the most part of the water content of this fruit is possibly found distributed in free water form, this way, it is possible to apply the osmotic dehydration technique as an alternative of pre-treatment conservation of this fruit.

On both temperatures studied, the water activity (a_w), moisture content, weight reduction (WR), water loss (WL) and soluble solids concentarion (SSC) of the star fruit were affected significantly ($p < 0,05$) by the osmotic solution concentration and by the time of immersion of the fruits. The solid gain (SG) was affected significantly ($p < 0,05$) only by the immersion time (Fig. 1 and 2).

It was observed that a_w and the moisture content of the star fruit decreased as it had risen the concentration of the osmotic environment and the time of immersion of it. The WR, WL and SSC of the fruits were higher when it was used a higher concentration of sucrose and the time of immersion in the osmotic solution. It was also verified that there was an increase in solid gain in each interval of processing in all of the sucrose concentration.

Although the values of a_w and the moisture content of the star fruit had diminished after the osmotic dehydration, they were still very high, confirming the necessity of use of an additional conservation treatment in order to increase the chemical and microbiological stability of the final product.

The most elevated loss of water and mass was observed in most of the concentration of sucrose of the osmotic solution, considering that more concentrated solutions facilitate the water exit of the food due to the higher gradient of osmotic concentration.

The solid gain and the water loss promote the increase of the soluble solids concentration in the fruit, which can cause great alterations in the sensorial and nutritional characteristic when compared to the *in natura* fruit. What is ideal is if it occurs the maximum weight reduction and water loss with less solid gain with a result of reduction in the water activity. It was observed that this behavior and the highest variations in the mass trasfer rates happened during the first 4 hours of processing, this became the maximum time to get the most desirible alterations.

The highest temperature of the osmotic solution and the higher sucrose concentration at 50 ºC and 60 % respectively, promoted more expressive changes in all of the studied variables.

$\hat{y} = 0,99 + 7,41E\text{-}7C + 4,93E\text{-}4t – 3,86E\text{-}5Ct$
$R^2(\%) = 96,48$

$\hat{y} = 96,04 + 0,06C - 1,60t$
$R^2(\%) = 94,45$

$\hat{y} = 4,776 + 0,032C + 0,922t – 0,054t^2 + 0,016Ct$
$R^2(\%) = 96,75$

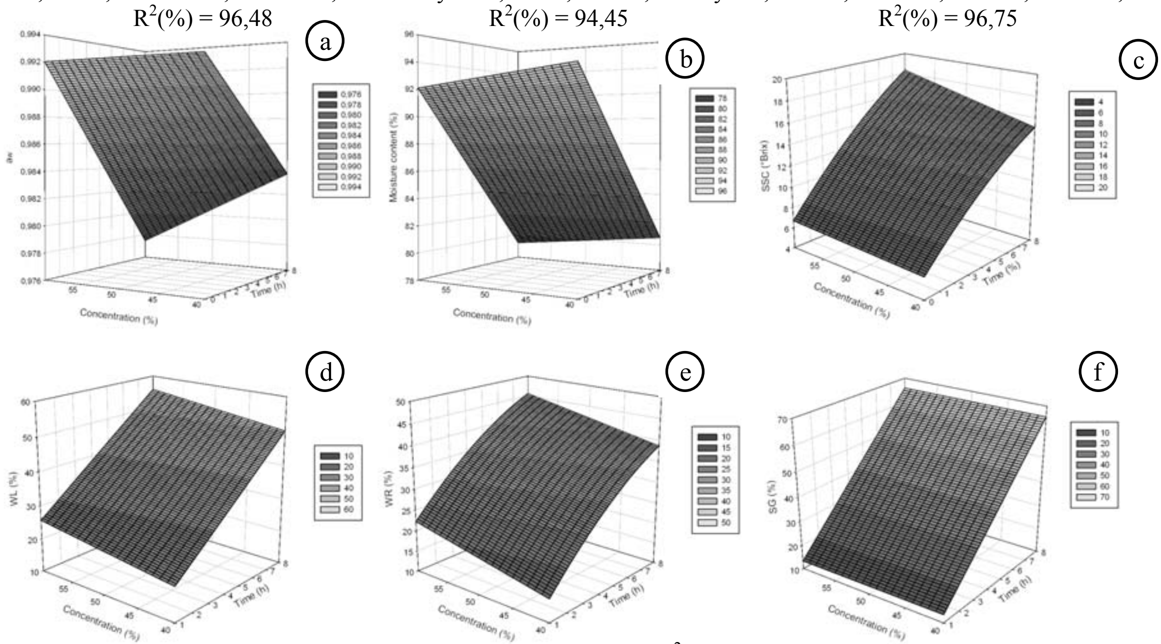

$\hat{y} = 4,66 + 0,28C + 4,30t$
$R^2(\%) = 96,63$

$\hat{y} = -3,42 + 0,34C + 5,20t – 0,21t^2$
$R^2(\%) = 97,09$

$\hat{y} = 5,792 + 7,512t$
$R^2(\%) = 87,86$

Fig. 1 The effect of the immersion time and the concentration of the osmotic solution in the water activity (a), moisture content (b), soluble solids concentration (c), water loss (d), weight reduction (e) and solid gain (f) of osmotic dehydrated star fruits at 40°C.

$\hat{y} = 0{,}99 + 8{,}15E\text{-}5C + 2{,}67E\text{-}3t - 1{,}14E\text{-}4Ct$
$R^2(\%) = 97{,}15$

$\hat{y} = 93{,}67 - 0{,}02C - 0{,}85t - 0{,}11t^2 - 0{,}04Ct$
$R^2(\%) = 98{,}13$

$\hat{y} = 4{,}86 + 0{,}03C + 0{,}94t - 0{,}14t^2 + 0{,}05Ct$
$R^2(\%) = 98{,}73$

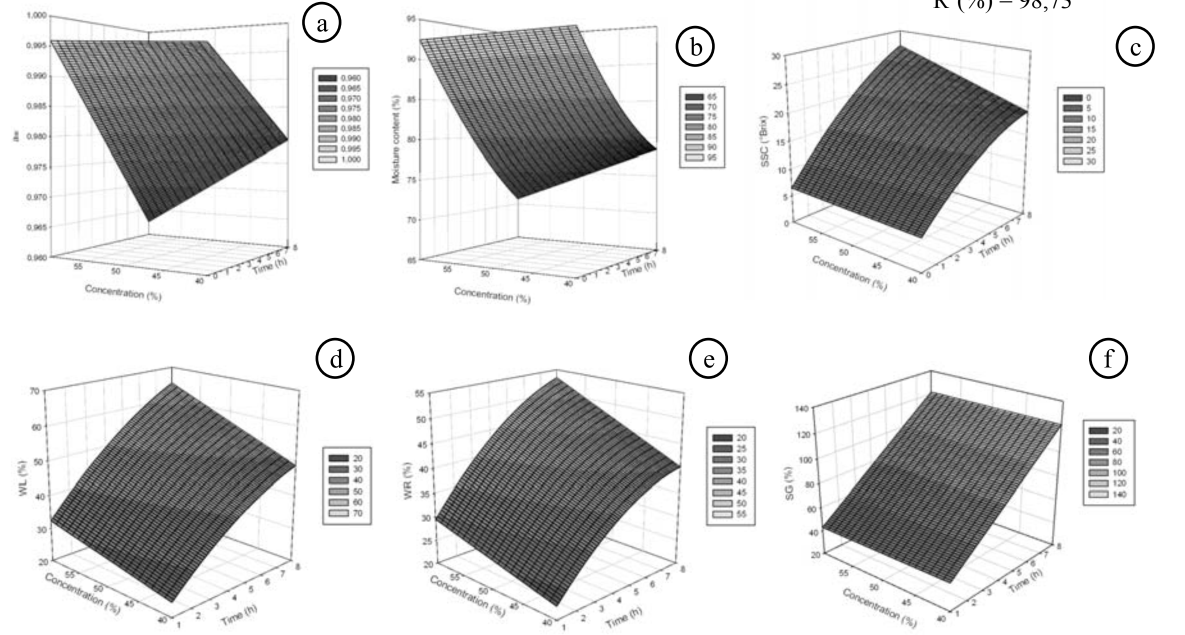

$\hat{y} = 4{,}68 + 0{,}35C + 3{,}53t - 0{,}27t^2 + 0{,}06Ct$
$R^2(\%) = 98{,}73$

$\hat{y} = 6{,}05 + 0{,}29C + 3{,}34t - 0{,}29t^2 + 0{,}04Ct$
$R^2(\%) = 97{,}38$

$\hat{y} = 31{,}771 + 11{,}24t$
$R^2(\%) = 95{,}11$

Fig. 2 The effect of the immersion time and the concentration of the osmotic solution in the water activity (a), moisture content (b), soluble solids concentration(c), water loss (d), weight reduction (e) and solid gain (f) of osmotic dehydrated star fruits at 50°C.

Conclusions

The weight reduction, water loss, water activity, moisture content and soluble solids concentration of the star fruits were influenced by the concentration of the osmotic environment and by the immersion time at both studied temperatures. The solid gain was affected only by the osmotic dehydration time. The mainly alterations that were desired in this kind of process, the highest loss of water and mass rates with lower solid gain, occurred in the first 4 hours of osmotic dehydration, this was considered the maximum time of processing in the evaluated conditions. It was obtained with a higher concentration of osmotic solution, that it, 60% of sucrose, more desirable values in all of the studied varieties, at both evaluated temperatures, in comparison to the other concentrations, indicating that this might be a possible concentration for the industrial process. At 50°C, it was obtained the best results in all of the variables when compared to 40°C, so this is the best indicated dehydrating solution's temperature for the osmotic dehydration among the studied conditions.

Acknowledgement

To CNPq, CAPES, FAPEMIG e FAPESB.

References:

Abd Karim,A., Chee Wai,C., 1999. Foam-mat drying of starfruit (*Averrhoa carambola* L.) purée. Stability and air drying characteristics, Food Chemistry 64: 337-343.

Carvalho,A.V., Moreira,D.K.T., Souza,L.Q., Vasconcelos,M.A.M., 2006. Osmotic dehydration of star fruit (*Averrhoa carambola* L.) followed by oven drying. Belém: Embrapa.

Dhingra,D., Singh,J.-Patil,R.T., UPPAL,D.S., 2008. Osmotic dehydration of fruits and vegetables: a review. Journal of Food Science and Technology 45: 209-217.

Donadio,L.C., Silva,J.A.A., Araújo,P.R.S., Prado,R.M., 2001. Star fruit tree (*Averrhoa carambola* L.). Jaboticabal: Brazilian Society of Tropical Fruits.

Adolfo Lutz Institute, 2004. Physico-chemical methods for food analysis. São Paulo: IAL.

Natale,W., Prado,R.M., Rozane,D.E., Romualdo,L.M., Souza,H.A., Hernades,A., 2008. Response of carambola tree liming. Brazilian Journal of Fruticulture 30: 1136-1145.

Teixeira,G.H.A., Durigan,J.F., Donadio,L.C., Silva,J.A.A., 2001. Characterization postharvest six cultivars of star fruit (*Averrhoa carambola* L.). Brazilian Journal of Fruticulture 23: 546-550.

Torreggiani,D., 1993. Osmotic dehydration in fruit and vegetable processing. Food Research International 26: 59-68.

Torreggiani,D., Bertolo,G., 2001. Osmotic pre-treatments in fruit processing: chemical, physical and structural effects. Journal of Food Engineering 49: 247-253.

TEMPERATURE DEPENDENCE OF PHOTOVOLTAIC CELLS EFFICIENCY

Vladimír Cviklovič*, Martin Olejár

[1]Department of Electrical Engineering, Automation and Informatics, Faculty of Engineering, Slovak University of Agriculture in Nitra, Tr. A. Hlinku 2, 949 76 Nitra, Slovakia, Phone: +421 641 5783, E-mail: vladimir.cviklovic@uniag.sk

Abstract

This contribution is oriented for analysis of the temperature influence to the photovoltaic cells efficiency in practiced conditions. Photovoltaic cells were monitored during one year in microregion Nitra, Slovakia. Cells are based on the monocrystalline silicon with surface 1,95 m^2 *and they are directed perpendicularly to the direction of the solar radiation during the time of meassurement. The tracking is provided by special two-axis tracker. Analysis of the results confirmed the temperature dependence of the efficiency of the solar energy conversion. The higher temperature causes the decreasing of the efficiency of the energy conversion about a 0,023368 % per Celsius degree.*

Keywords: solar cell, efficiency, temperature dependence, solar tracker, tracking systems

Introduction

Conversion of the solar energy to electric energy by photovoltaic cells is popular in this time. Photovoltaic cells are mostly based on monocrystalline and polycrystalline silicon. Theoretical efficiency of the monocrystalline cells is from 14% to 22 %. The polycrystalline cells have efficiency up to 14 %. Assuming that the collectors of the high quality based on the crystalline silicone are about 18÷20 % efficient (Libra, Poulek, 2012). Cells work on the base of the photovoltaic effect, firstly observed by physicist A. E. Becquerel in 1839. The voltage is created by the photovoltaic effect (Williams, 1960).

Our measurement system is located on the roof of RES laboratory DEEAI FE in Nitra. Obtained energy is used for heating of the laboratory and for illumination. The system is monitored for 24 hours a day. Various tracking algorithms were tested on the tracker. The output power differences between fixed and tracking system are shown in Fig. 1. The research is aimed to temperature dependence of the cells in this time.

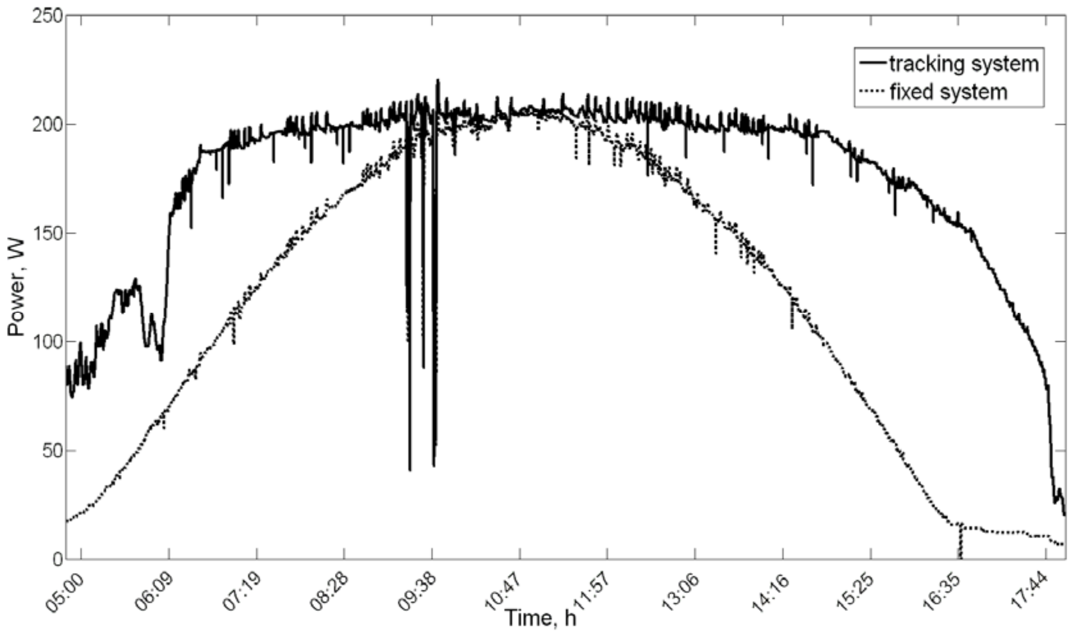

Fig. 1 The output power curves of the tracking and fixed system during a sunny summer day

Materials and Methods

The Measured cells are STP040S – 12/Rb developed by SUNTECH. Total efficiency 12.6 % with a 25 years warranty is specified in the manufacturer's datasheet. Optimal operating voltage is 17.6 V and optimal current is 2.56 A. Maximum power is 45 W_p (1000 $W.m^{-2}$) and operating temperature is from -40 to +85 °C. The cells based on monocrystalline silicon. Six cells are used in the combined serial-parallel connection as shown in Fig. 3. Active surface of cells is 1.95 m^2. The temperature coefficients declared by manufacturer are shown in Tab. 1.

The pyranometer SG002 was used for the measurement of global solar radiation intensity. The measurement is based on the principle of temperature difference, which is created on black and white surface. Thermocouples are used for temperature measuring of these surfaces. Pyranometer is situated on the tracker. Therefore, the value of the global radiation intensity is not distorted by azimuthal error. The pyranometer is thermally isolated from the metal construction and it is placed in the sufficient distance to minimize the thermal impact. Technical parameters of the used pyranometer are in Tab. 2 and its design is shown in Fig. 2.

Tab. 1 Declared temperature coefficients of PV module STP040S – 12/Rb

Nominal operating cell temperature	45 °C
Short-circuit current temperature coefficient	(0.055 ± 0.01) $\%.K^{-1}$
Open-circuit voltage temperature coefficient	-(78 ± 10) $mV.K^{-1}$
Peak power temperature coefficient	-(0.48 ± 0.05) $\%.K^{-1}$
Power tolerance	± 5 %

Tab. 2 Technical parameters of the pyranometer SG002

Measuring range	0 – 1200 $W.m^{-2}$
Spectral range	0.3 – 3 μm
Output voltage	0 – 2 V
Power supply	18 – 30 V
Response time	50 s
Operating temperature	-30 ÷ +60 °C
Minimal load impedance	500 Ω
Error	± 3 %

Fig. 2 Pyranometer SG002

The temperatures are measured by calibrated digital temperature sensors DS18B20. Communication between control microprocessor and sensors is realized by 1-wire protocol. Standard accuracy is ± 0.5 °C in temperature range from -10 to + 85 °C. The accuracy is better than 0.25 °C in temperature range from – 10 to + 100 °C. The temperature sensors were additionally calibrated for this range.

TriStarTM controller TS-45 is used for battery charging. The controller operates in one mode at the time. Rated solar current of the controller is up to 45 A and system voltage is set to 24 V in our case. The accuracy of the voltage measurement is lower than 0.1 % ± 50 mV. Modbus communication protocol was used. Communication is realized on the RS-232C physical layer.

The system is loaded by bulbs, which are switched by the module Load Control (Fig. 3). Output current of the system and the battery voltage is measured by this module. Converter resolution is 12-bit. The sine wave inverter AJ1300 was used. The company STUDER is the manufacturer. Maximum output apparent power is 1300 VA and the efficiency is up to 95 %. Input voltage is optimally 24 V. Inverter output voltage is sine waveform with effective value 230 V / 50 Hz, it is generated by the PWM principle with passive filtration.

The measurement system is controlled by the single-chip microcontroller modules. Data are loaded by the program in Labview via USB port as shown in figure 3. Measurements are saved to data files in Matlab structure (*.dat) for a better results evaluation.

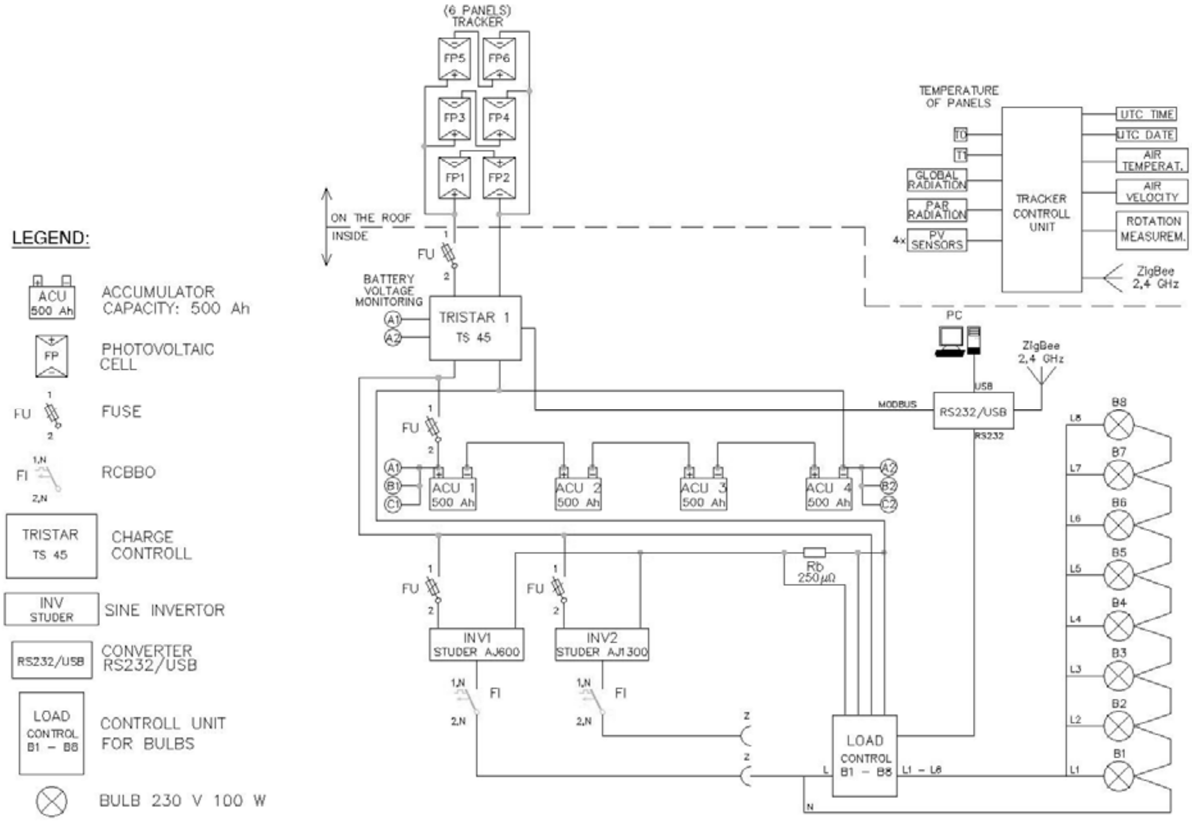

Fig. 3 Block wire diagram

Results and Discussion

Collected energy from the system was approximately equal to the supplied energy during the measurement. Therefore, battery voltage was regulated to 26 V. Constant battery voltage is controlled by the program in Labview. The basic role of load control module is the regulation of the output power. The system is based on the industrial single-chip microcontroller C8051F340, which is manufactured by Silicon Laboratories. All important parameters has been monitored and saved to the file. Namely they are: cells output voltage, cells output current, battery voltage and load current. These data are very important for energy relationship evaluation.

Days without wind were selected for measurements. Selected value of global solar radiation intensity was 760 W.m^2. Ambient air temperatures were selected in range from -7 to 25 °C during the measurement. The temperature of cells is not used, because its precise measurement is complicated. Selected days are 12.2.2012 at -7 °C, 1.2.2012 at -1 °C, 26.1.2012 at 1 °C, 27.1.21012 at 2 °C, 4.3.2012 at 8 °C, 16.3.2012 at 16 °C, 24.3.2012 at 20 °C and 6.4.2012 at 25 °C.

Solar cell efficiency is 11.655 % for solar radiation intensity 760 W.m^{-2} at ambient air temperature 0 °C. Manufacturer's specified efficiency is 12.5 % for solar radiation intensity 1000 W.m^{-2} at the temperature 20 °C. A lower value of efficiency is caused by the dust on the cell surface during the measurement. The measured temperature coefficient of cells is -0.023368 %.K^{-1} with norm of residual 0.0116859 %.K^{-1}. The graphical interpretation of the temperature dependence is shown in Fig. 4. The temperature dependence of selected solar photovoltaic cells can be written as:

$$\eta = \eta_0 - 0.023368 \, . \, t \tag{1}$$

Where: η is solar cell efficiency, %,
η_0 – solar cell efficiency at 0 °C, %,
t – air temperature, °C.

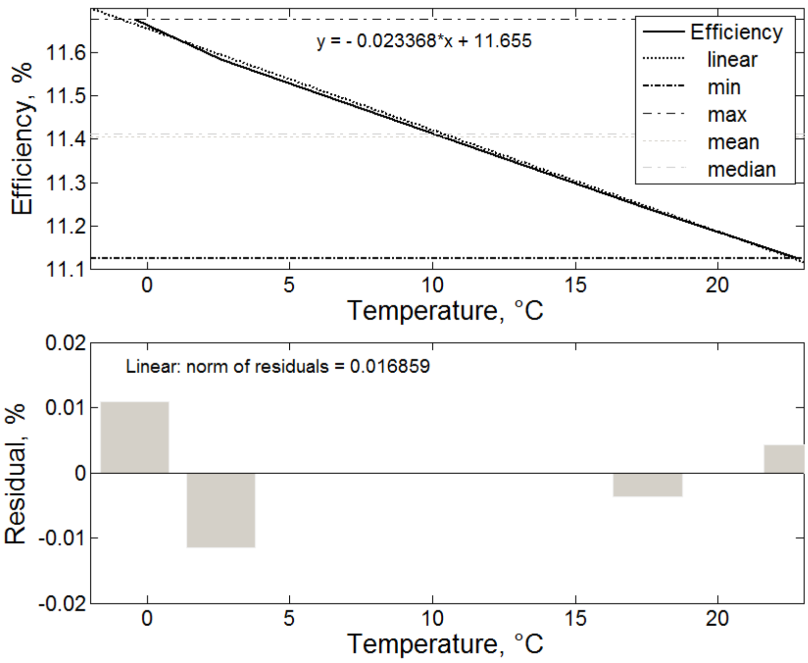

Fig. 4 Impact of ambient air temperature to the efficiency of the solar cells in practice

Conclusion

The temperature coefficient of the pyranometer has not been verified. The temperature impact to the measured solar irradiation is unknown. The results are in the range, which is declared by manufacturer. The results show that electric energy obtained from the tracking solar photovoltaic system is higher for equal solar radiation during the winter sunny day than in a summer sunny day. The temperature of solar cells is the key factor. The next measurements will be realised at a higher cells temperature.

Acknowledgement

This contribution was realized in the frame of VEGA 1/0696/11 Scientific Grant Agency of the Ministry of Education, Sport and Culture of the Slovak Republic and of the Slovak Academy of Sciences.

Reference

Libra M., Poulek V., 2012. Photovoltaic Solar Systems in the Czech Republic. In: Applications of Physical Research in Engineering. Scientific Monograph. SUA in Nitra, 2012. ISBN 978-80-552-0839-8

Williams R., 1960. Becquerel Photovoltaic Effect in Binary Compounds. In: Journal of Chemical Physics. American Institute of Physics, 32 (5). ISSN 1089-7690

COEFFICIENT OF THERMAL EXPANSION DETERMINATION METHOD USING FUNDAMENTAL FREQUENCY OF THE STRING

Oldrich Dajbych*

Czech University of Life Sciences Prague, 16521 Prague 6 – Suchdol, Czech Republic, Phone: +420 22438 3178, E-mail: dajbych@tf.czu.cz

Abstract

The coefficient of thermal expansion of guitar string material was obtained by its fundamental frequency measurement. Principle of the method is tension change caused by temperature change in statically indeterminate attachment of the string which results in change of its vibration fundamental frequency. The method is very simple and has better advantage compared to other possible methods of determining the coefficient of thermal expansion. Especially the need for advanced laboratory equipment. Such as push-rod dilatometer (Vikram et al., 1986), laser interferometric dilatometer (Okaji et al., 1997), capacitive dilatometer (Abe et al., 2012) and more (Kanagaraj, Pattanayak, 2003). Introduced method requires thermometer, frequency measuring device such as digital musical instrument tuner, rigid base for string attachment and different temperature environment provider such as fridge or oven. Steel electric guitar strings were used for method verification.

Keywords: string, termal, expansion

Introduction

Thermal expansion is an important parameter for characterization of different binding forces, lattice dynamics, band and crystal structure of any solids. It is one of the important properties of metals and its alloys, which helps to calculate the thermal stress (Kanagaraj, Pattanayak, 2003).

Most methods of determination of coefficient of thermal expansion require special equipment. Therefore simple method was derived for materials which are flexible enough to be processed as vibrating string. Depending on required accuracy of the result this method can be performed in simple laboratory conditions even at home.

Material and methods

Calculation

The method is based on statically indeterminate case of string attached on both ends to rigid frame. Changing temperature causes change of tension which results in vibration frequency shift. A guitar string provides vibrations loud enough to be measured by contactless device with microphone and frequency spectral analyzer. Relation between fundamental frequency of the string shift, temperature change and coefficient of thermal expansion can be derived from basic physical equations. These include the following: object elongation caused by temperature difference (1) (Halliday et al., 2004), elongation caused by tensile stress based on Hoocke's law (2) (Feynman et al., 1964) and fundamental frequency of string (3) (Raichel, 2006).

$$\Delta l = \alpha \cdot \Delta t \cdot l_0 \tag{1}$$

$$\Delta l = \sigma \cdot \frac{l_0}{E} \tag{2}$$

Where Δl is elongation in (m), Δ is coefficient of thermal expansion in (K^{-1}), Δt is temperature difference in (K), l_0 is initial length in (m), Δ is tensile stress in (Pa) and E is Young's modulus of elasticity in (Pa).

$$f = \frac{1}{2l}\sqrt{\frac{\sigma}{\rho}} \tag{3}$$

Where f is fundamental frequency of string in (Hz), l is length of string in (m), σ is tensile stress in (Pa) and ρ is density of string material in ($kg \cdot m^{-3}$).

Combining (1), (2) and (3) we obtain final formula for coefficient of thermal expansion (4).

$$\alpha = \frac{4 \cdot \rho \cdot l^2}{E} \cdot \frac{f_1^2 - f_2^2}{t_2 - t_1} \tag{4}$$

Where α is coefficient of thermal expansion in (K^{-1}), t_1 and t_2 are temperatures in (K or °C), l is length in (m), E is Young's modulus of elasticity in (Pa), ρ is density of string material in (kg · m^{-3}), f_1 and f_2 are fundamental frequencies in (Hz) of string for corresponding temperatures.

Strings

Lee Hooker steel electric guitar strings were used in experiment. Because wound strings outer layer would distort results and complicate calculation only plain strings (e, b, g) with diameters 0.009 in., 0.011 in. and 0,016 in. were used.

Initial measurement of strings material was carried-out to obtain basic physical parameters needed for calculation since string manufacturer did not provide such information. Material density was calculated from string weight measured on KERN ABS 120 weight and string length and diameter. Young's modulus of elasticity was obtained from tensile diagram provided by Shredding machine Labor Tech MPTest 5.050 connected to computer program LT Test&Motion. Acquired values are given in (Tab. 1).

Measuring device

For purpose of measuring in different temperatures a simple measuring device was built. It contained base of wood and several electric guitar parts used for string tightening and fixing. These parts were placed symmetrically as shown in Fig. 1 and Fig. 2. Vibrating length of the string between locks was 350 mm.

Tab. 1 Mechanical properties of strings materials

String	ρ (kg · m^{-3})	*E* (GPa)
e	7687	195.0
b	7701	194.4
g	7699	193.9
mean	7696	194.4

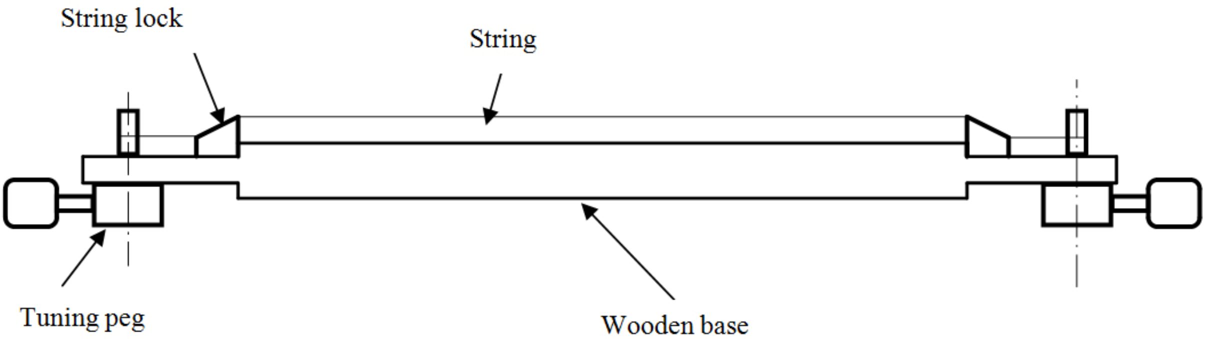

Fig. 1 Measuring device scheme

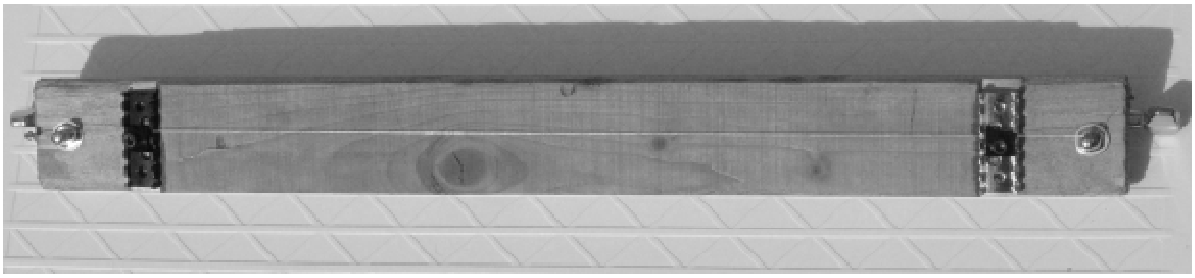

Fig. 2 Measuring device

Measuring instruments

Multifunctional measuring device UNI-T UT39C with temperature probe was used for temperature measurement.

Mobile phone Samsung Galaxy S2 i9100 with Android application *Tuner - gStrings Free* was also used. The string was hit with plastic guitar pick and the sound was transferred though phone microphone to analyzing software.

For lower temperature environments the fridge Calex R220 was used. For higher temperature EKZ KB-8 Standart G oven was used.

Measuring method

The string was tightened on a measuring device and it was left in thermally stable environment of room temperature. Then the string was tuned to initial frequency which was chosen by ear for good sound of given string and the device was exposed into another environment with different stable temperature. The temperature probe was put on the string and the device was left in given temperature for 60 minutes when the string was considered as fully tempered. Frequency measurement was carried-out and the device was allowed into room temperature again in order to stabilize the system again and to verify the initial frequency. After that the environment was subsequently changed again.

Results and discussion

Two measurement cycles for each string was carried-out which meant 10 frequency measurement for each string thus 30 altogether. An example of one cycle of tests of string e is given in (Tab. 2). Where □ is calculated for difference between current and previous measurement.

Tab. 2 Different test of steel string e measurement

t **(°C)**	***f*** **(Hz)**	***α*** **(K^{-1})**
22	445,4	-
9	452,1	0,90
22	445,2	0,92
42	433,8	0,97
22	444,8	0,94

For each string 8 values of coefficient of thermal expansion were obtained and averaged separately thus 24 values were averaged as final mean for the material. The results are given in (Tab. 4).

Tab. 4 Coefficient of thermal expansion

String	**, (K^{-1})**
e	$0.95 \cdot 10^{-5}$
b	$0.91 \cdot 10^{-5}$
g	$0.89 \cdot 10^{-5}$
mean	$0.92 \cdot 10^{-5}$

It was shown that equation (4) is suitable for determination of coefficient of thermal expansion of steel electric guitar string. It was also verified that it is possible to achieve it with relatively available equipment.

However the method as it was introduced and performed showed several problems, mainly regarding to accuracy. Obviously input values of physical properties accuracy has to be taken into account. Young's modulus of elasticity also vary with temperature (Ranawaka, Mahendran, 2009) thus it would be appropriate to use exact value for given temperature. The other problem is thermal expansion (retraction) of measuring device itself. Wooden material has approx. value of coefficient of thermal expansion 0.3 – 0.4 . 10-5 K-1 (Kolman, Cote, 1968). Which is about 30 % of final value for steel. This represents major part of estimated measurement error. We can assume that real value of coefficient of thermal extraction of measured material was higher. Obtained value for steel then corresponds in the range of estimated measurement error with (White, 1993; DeStrycker et al., 2010; Bower, 2010). It would be appropriate to use for the base a material with thermal expansion as low as possible such as special glass ceramics (Xia et al., 2012). And obviously there is measurement error of used instruments. Even if all mentioned problems were minimized this method in matter of its principle could not achieve such accuracy as high resolution methods using advanced equipment (Wallace et al., 2005).

Main goal of this experiment was not to obtain exact values of coefficient of thermal expansion of selected materials but to verify the possibility of its obtaining by chosen method. Which was confirmed. This experiment which was performed without specialized equipment can be used as educational illustration in Physics and related subjects which was secondary goal of this work.

Conclusion

A simple experiment was performed which confirmed possibility to measure the coefficient of thermal expansion of vibrating objects by measuring their fundamental frequency in statically indeterminate case. As example guitar string and its pitch change was introduced.

It also appeared that correct values of physical properties of the material, rigidity and thermal stability of the fixing device which represents the frame are critical for accuracy.

Reference

Abe S., Sasaki F., Oonishi T., Inoue D., Yoshida J., Takahashi D., Tsujii H., Suzuki H., Matsumoto K., 2012. A compact capacitive dilatometer for thermal expansion and magnetostriction measurements at millikelvin temperatures. Cryogenics, 52(10): 452-456.

Bower A.F., 2010. Applied Mechanics of Solids. CRC Press, Boca Raton, FL.

DeStrycker M., Schueremans L., VanPaepegem W., Debruyne D., 2010. Measuring the thermal expansion coefficient of tubular steel specimens with digital image correlation techniques. Optics and Lasers in Engineering, 48(10): 978-986.

Feynman R.P., Leighton R.B., Sands M., 1964. The Feynman Lectures on Physics. Addison–Wesley, Reading, MA

Halliday D., Resnick R., Walker J., 2004. Fundamentals of Physics. Wiley, Hoboken, NY.

Kanagaraj S., Pattanayak S., 2003. Measurement of the thermal expansion of metal and FRPs. Cryogenics, 43(7): 399-424.

Kollman P., Cote W.A., 1968. Principles of wood science and technology 1. Solid wood. Sringler Verlag, Berlin – Heidelberg - New York.

Okaji M., Yamada N., Kato H., Nara K., 1997. Measurements of linear thermal expansion coefficients of copper SRM 736 and some commercially available coppers in the temperature range 20–300 K by means of an absolute interferometric dilatometer. Cryogenics, 37(5): 251-254.

Raichel D.R., 2006. The science and applications of acoustics, Springer, New York.

Ranawaka T., Mahendran M., 2009. Experimental study of the mechanical properties of light gauge cold-formed steels at elevated temperatures. Fire Safety Journal, 44(2): 219-229.

Vikram C.S., Agrawal D.K., Roy R., McKinstry H.A., 1986. Application of dial-gage and laser speckles for ultra-low thermal-expansion measurements using push-rod dilatometers. Optics and Lasers in Engineering, 7(4): 221-226.

Wallace G., Speer W., Ogren J., Omar S.E., 2005. High-Resolution Methods for Measuring the Thermal Expansion Coefficient of Aerospace Materials. Mechanical Engineering Faculty Works, 9.

White G. K., 1993. Reference materials for thermal expansion: certified or not? Thermochimica Acta, 218: 83-99.

Xia L., Wang X., Wen G., Zhong B., Song L., 2012. Nearly zero thermal expansion of β-spodumene glass ceramics prepared by sol–gel and hot pressing method. Ceramics International, 38(6): 5315-5318.

DETERMINING OF OPERATIONAL PROPERTIES OF BLADELESS TURBINE

Lukáš Dlabal*, Martin Polák

Czech University of Life Sciences Prague, 16521 Prague 6 – Suchdol, Czech Republic, Phone: +420 22438 3183, E-mail: dlaball@tf.czu.cz

Abstract

Current hot issues include alternative energy sources. One of them is energy from streams and rivers. The potential of the smallest water sources has not yet been sufficiently exploited and is an opportunity for the bladeless turbine. This article describes its operating characteristics.

The experiment's objective was to analyse the parameters measured at the turbine and to determine its operating characteristics. The measurement was performed on the SETUR DVE 120 bladeless turbine running in a closed testing hydraulic circuit in a laboratory of the Department of Mechanical Engineering, Faculty of Engineering, Czech University of Life Sciences in Prague. The turbine's operating characteristics have been determined based on the measured values, such as dependence of efficiency on water stream power or water gradient dependence on flow rate, etc. From the user's point of view, the most important characteristics include the dependence of the machine set's electric output on flow rate.

Keywords: Setur DVE 120, characteristics, efficiency

Introduction

A water turbine constructed on the water turbulence or whirlpool principle is capable of utilizing very small sources even for untapped water, and it is highly suitable for the closed circuit production of electrical energy. (Beran et al., 2013)

Bladeless turbine characteristics have not yet been accurately specified. Users of currently operated sets tend to rely on empirically acquired experience. Yet it is important to know and to predict operating features of generating sets to design and size them. Similarly, users must be aware of the operating parameters to create conditions for efficient operation.

The experiment resulted in determining relations between the main and auxiliary operating/technical characteristics of a generating set.

Material and method

The measuring has been performed on a SETUR DVE 120 mini-turbine within a closed testing hydraulic circuit in a laboratory of the Department of Mechanical Engineering, Faculty of Engineering, Czech University of Life Sciences. The circuit design provides for the necessary measuring and modelling of different operating states of the tested turbine. The measuring circuit (see Fig. 1) consists of a reservoir, installed under floor level, from which the water is pumped with an impeller pump (1) into a feeding line (the horizontal part beyond the pump), thus simulating the water gradient and flow rate of a water source feeding the turbine. The feeding line has a control valve (2), which can change the flow rate and the water gradient height. In addition, it features measuring equipment – pressure gauges (4) and an ultrasound flow meter (5). The feeding line ends with a flexible hose (the vertical part prior the turbine) featuring an input diameter reduction and a flange for connecting to the turbo-set (i.e. this section has been built the same way as in real installations). The DVE 120 unit, i.e. the turbine (6) and a generator (7) on a concrete foundation is located in a plastic tank the purpose of which is to maintain the correct water level necessary for proper functioning of the equipment. There is an overflow chute (12) in the tank wall through which water returns to the reservoir. The generator generates a three-phase voltage. As it is equipped with permanent magnets, it is capable of running autonomously in "island mode". For the purpose of measurement the generator output has been connected to a fluently variable resistance load (10). Current in individual phases (9) and interfacial voltage (8) were measured in order to determine the output power, which was then calculated based on the applicable relations. In addition, turbine speed was measured with an infra-red contactless sensor (11) during the operation (Polák et al., 2013).

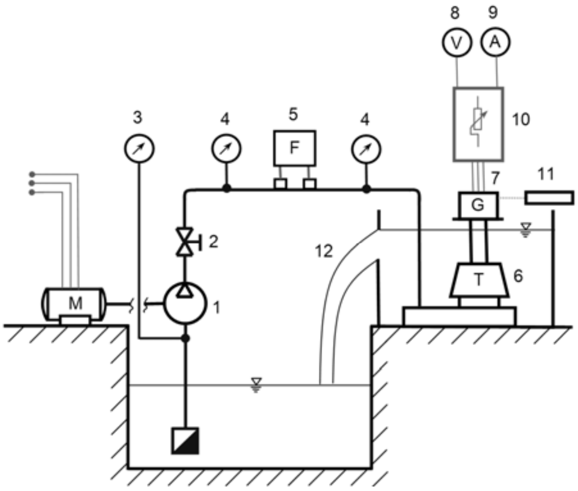

Fig. 1 Diagram of the hydraulic circuit for measuring the DVE 120 mini-turbine characteristics
1 – pump, 2 – control valve, 3 – vacuum gauge, 4 – pressure gauge, 5 – flow meter, 6 – turbine, 7 – generator, 8 – voltmeter, 9 – ammeter, 10 – resistance load, 11 – speedometer,12 – overflow discharge

Measuring took place at a defined water gradient, flow rate and load. The following parameters were recorded:

- pressure at the turbine input,
- flow rate in the feeding line,
- turbine speed,
- voltage and current at the generator output.

Based on these values, the following has been determined:

- water gradient,
- water flow power at the turbine input,
- generator electric output,
- generating set's overall efficiency.

Measuring was done at different water gradients, flow rates and loads. This resulted in graphically expressed relationships of different parameters, mainly as functions of the water gradient, the flow rate, the power, the speed and the load. The final characteristics are presented in the following text including brief comments (Polák et al., 2013).

Determining the Turbine's Input Hydraulic Power

The turbine characteristics were created based on the measured and calculated values. The values measured at the turbine include: pressure at the input, flow rate and speed. In addition, electric current and voltage produced by the generator were measured. The usable water gradient h_u has been calculated from the measured values by means of the Bernoulli's equation: (Munson et al., 2006; Bollrich 1989)

$$g \cdot h_u = g \cdot h_1 + \frac{p_1}{\rho} + \frac{v_1^2}{2} - e_z \quad (\mathrm{J \cdot kg^{-1}}) \quad (2.1)$$

where: $g{\cdot}h_1$ – specific potential energy,

$\frac{p_1}{\rho}$ – specific pressure energy, $\frac{v_1^2}{2}$ – specific kinetic energy, e_z – specific energy loss.

The v_1 speed has been calculated from the Q flow rate by means of the continuity equation:

$$v_1 = \frac{4 \cdot Q}{\pi \cdot d_1^2} \quad (\mathrm{m \cdot s^{-1}}) \quad (2.2)$$

where: d_1 = 0.08 m (diameter of feeding line, see above)

The specific energy loss is the sum of friction losses e_{zT} and local losses e_{zM}.

$$e_z = \sum e_{zT} + \sum e_{zM} \quad (\mathrm{J \cdot kg^{-1}}) \quad (2.3)$$

$$e_{zT} = \frac{v_1^2}{2} \cdot \lambda_1 \cdot \frac{L_1}{d_1} + \frac{v_2^2}{2} \cdot \lambda_2 \cdot \frac{L_2}{d_2} \quad (\mathrm{J \cdot kg^{-1}}) \quad (2.4)$$

$$e_{zM} = \zeta_K \cdot \frac{v_1^2}{2} + \zeta_R \cdot \frac{v_2^2}{2} + \zeta_Z \cdot \frac{v_2^2}{2} \quad (\mathrm{J \cdot kg^{-1}}) \quad (2.5)$$

where: ζ_K – coefficient of local losses in the bend, ζ_R – coefficient of local losses in the sudden broadening, ζ_Z – coefficient of local losses in the sudden narrowing

The v_2 speed has been calculated analogically to the speed v_1 (flexible hose, d_2 = 0.09 m).

Once these relationships for calculating energy losses are inserted in Bernoulli's equation, the equation for calculating the usable water gradient acquires the following form:

$$g \cdot h_u = g \cdot h_1 + \frac{p_1}{\rho} + \frac{v_1^2}{2} - \left[\frac{v_1^2}{2} \cdot \left(\lambda_1 \cdot \frac{L_1}{d_1} + \zeta_K \right) + \frac{v_2^2}{2} \cdot \left(\lambda_2 \cdot \frac{L_2}{d_2} + \zeta_R + \zeta_Z \right) \right] \quad (\mathrm{J \cdot kg^{-1}}) \quad (2.6)$$

The power of the water flow entering the turbine has been determined based on the usable water gradient calculated in equation (2.6): (Mays, 2001)

$$P = Q \cdot \rho \cdot g \cdot h_u \quad (\mathrm{W}) \quad (2.7)$$

where: Q – flow rate ($\mathrm{m^3 \cdot s^{-1}}$), ρ – density ($\mathrm{kg \cdot m^{-3}}$), g – acceleration due to gravity (Earth) ($\mathrm{m \cdot s^{-2}}$), h_u – usable water gradient (m).

Characteristics of turbine

From the operating parameters' point of view, the first characteristic is the relationship between the flow rate and the usable water gradient (Fig. 2). It clearly indicates that the flow rate increases together with the usable water gradient, which confirms the presumption. The curve is nearly linear.

It should be stressed that all the presented turbine parameters are at a constant speed of n = 200 min^{-1}.

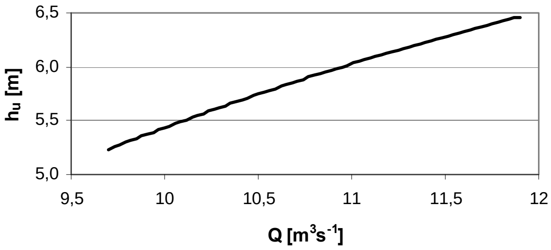

Fig. 2 Usable water gradient – flow rate relationship

From the user's perspective, output power and efficiency characteristics are more important. The electrical power supplied by the generator can be determined based on the measured current and voltage values.

The generating set efficiency is expressed as the ratio of the turbine's electric output power to its hydraulic input power (i.e. the water flow power):

$$\eta = \frac{P_{el}}{P} \qquad (-) \qquad (2.8)$$

where: P_{el} – electric power (W), P – water flow power (W).

Knowledge of the turbine's working characteristics is crucial for its proper operation. This concerns mainly the relationship between the power and the efficiency. The following diagram (Fig. 3) presents the dependency of the set's efficiency on the waterpower. Maximum efficiency is achieved at a certain value of power. Further increasing the waterpower reduces the efficiency.

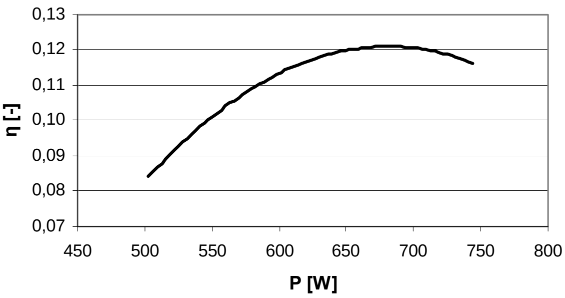

Fig. 3 Bladeless turbine working characteristics

This feature is typical also for conventional turbines. For illustration, Fig. 4 presents the Francis turbine's characteristics (Štoll et al., 1977).

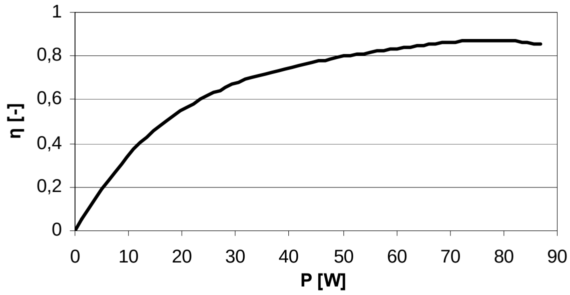

Fig. 4 Francis turbine operating characteristics

The following characteristic (Fig. 5) is useful for users of this system. It describes the dependence of the electric output power on the flow rate. This characteristic is beneficial especially for streams with variable flow rates during the year.

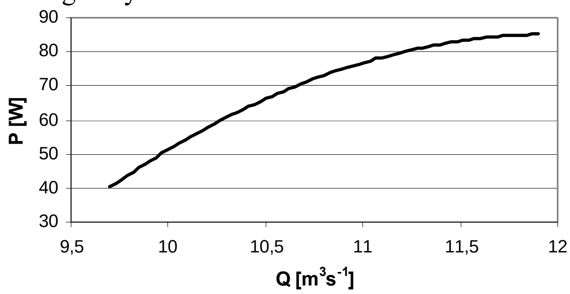

Fig. 5 Electric power – flow rate relationship

Conclusion

Following the experiment's evaluation, bladeless turbine parameters were defined determining its operating characteristics. These make it possible to predict its behaviour under different loads. The flow rate varied from 9.5 to 12 l/s at a water gradient height of 5 to 6.5 m during the laboratory tests. The overall system efficiency varied between 9 and 12 % during electricity generation. The greatest efficiency of 12 % has been achieved at the waterpower of 650 W, which corresponds to approximately 80 W of electric power generated. The electric power produced varied between 42 and 87 W. The ability to work in "island mode" is a significant benefit of the set, thanks to the generator type used.

Acknowledgement

This paper was supported by the IGA, Project 2013:31130/1312/3103 (Determining of operational properties of bladeless turbine).

Reference

Beran V., Sedláček M., Maršík F., 2013. A new bladeless hydraulic turbine. Applied Energy. Amsterdam: Elsevier, 978-983. ISSN 0306-2619.

Bollrich G., 1989. Technische Hydromechanik. Berlin: Verlag für Bauwesen, 78-79. ISBN 3-345-00245-0.

Munson B., Young D., Okiishi T., 2006. Fundamentals of fluid Mechanics. John Wiley & Sons, Inc., 290-291. ISBN 0-471-67582-2.

Mays L., 2001. Water Resources Engineering. Hamilton printing, 507-510. ISBN 0-471-29783-6.

Polák M., 2013. Bezlopatková miniturbína. Praha: Nakladatelství ČVUT, 57-59. ISBN 978-80-01-05233-4. (In Czech)

Štoll Č., 1977. Kratochvil, S. and Holata, M.: Využití vodní energie. SNTL Praha, 459. (In Czech)

ASSESSMENT OF RELEVANCE OF FUEL CONSUMPTION MEASUREMENT USING TELEMATICS

Jan Dovol*, Petr Šařec

Czech University of Life Sciences Prague, 16521 Prague 6 – Suchdol, Czech Republic,
E-mail: dovol@tff.czu.cz

Abstract

The objective of the work was to verify whether the accuracy of fuel consumption data provided by CAN-Bus is sufficient enough for a common evaluation of operation at a farm. In fact, CAN-Bus fuel consumption data accuracy depends on tractor engine load. Based on the comparison of data about fuel consumption provided by telematic system JDLink and by the records on tanked amount of fuel, the accuracy proved to be sufficient enough in the case of a tractor used primarily for soil tillage operations.

Key words: telematics, tractor, fuel consumption

Introduction

Telematics starts to be quite common on bigger farms and contractors uses it also very often. One reason could be better price than few years before and constant preasure to costs reduction. Telamatics systems have plenty of potential in costs reduction, but now lets focus on fuel. Fuel is significant costs part (Roebuk, 2012; Huang et al., 2010; Goel, 2007). Many systems provide data about the fuel based on CAN-Bus data (Goel, 2007). Accuracy of CAN-Bus data is a discussed theme. In fact, CAN-Bus fuel consumption data accuracy depends on tractor engine load (Sedlák et al., 2010). Theme is based on the comparasion of data about fuel consumption provided by telematics system JDLink and by the records on tanked amount of fuel, the accuracy proved to be sufficient enough in the case of a tractor used primarily for soil tillage operations.

Material and methods

Data was used from John Deere 8320R equipped by John Deere telematics system called JDLink. Ultimate version of this system was used. JDLink useses data from CAN-Bus. JDLink consist of standard devices like GPS a and GSM antenna, sim plug module and telematics-can-bus gateway. Fuel consumption data were compared to data from evidence of fuel from tank device.

This tractor was chosen because of its work structure – all of its works were soil preparing operations. This mean high overall engine load and probably accuracy of CAN-Bus data. Tractor worked together with 8 furrows plough Kverneland PW 100 (work width for 1 furrow 40 cm), seed bed preparing equipment from Farmet, type K 800 (8 m wide), soil cultivator Horsch Tiger 4 AS (4 m wide). This text focused on ploughing.

Results and discussion

General rule about CAN-Bus fuel consumption precision is shown at the (Fig 1). The graph was made by MENDEL UNIVERZITY from Brno and shows relation between fuel consumption from flow meter and ratio of fuel consumption from flow meter and from CAN-Bus. This was measured on another John Deere engine, smaller one 6,8 l powertech engine from CLAAS Axion. There is possible to see that in part where are high fuel consumption are also very good accuracy. Despite of this, in very low fuel consumption part of graph is accuracy very bad. When high engine load is supposed and also high fuel consumption for most of working time, is expected good total precision of all data.

Data from period of ploughing were processed. This period took 60 work days over whole year that corresponded to 792,5 ha. This amount of information is possible to considered as sufficient. Calculated average engine load was 64 % - this include engine load during idle and during transport. Only work engine load average is 80 %. Differences between tanked amount and fuel consumption from CAN-Bus are possible rate by two ways. First is possible to rate standard differences and second absolute value of differences. Results are in the Tab. 1.

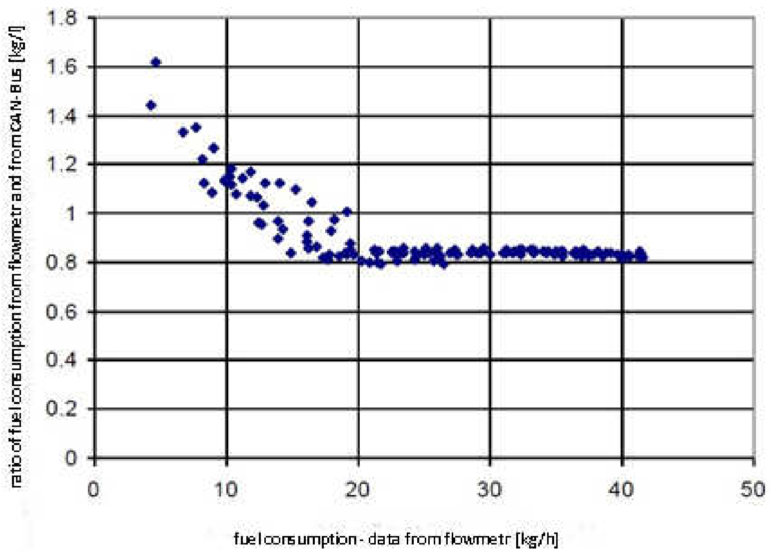

Fig. 1 Graph of fuel consumption and ration of fuel consumption from flowmetr and from CAN-Bus [Sedlák et al., 2010]

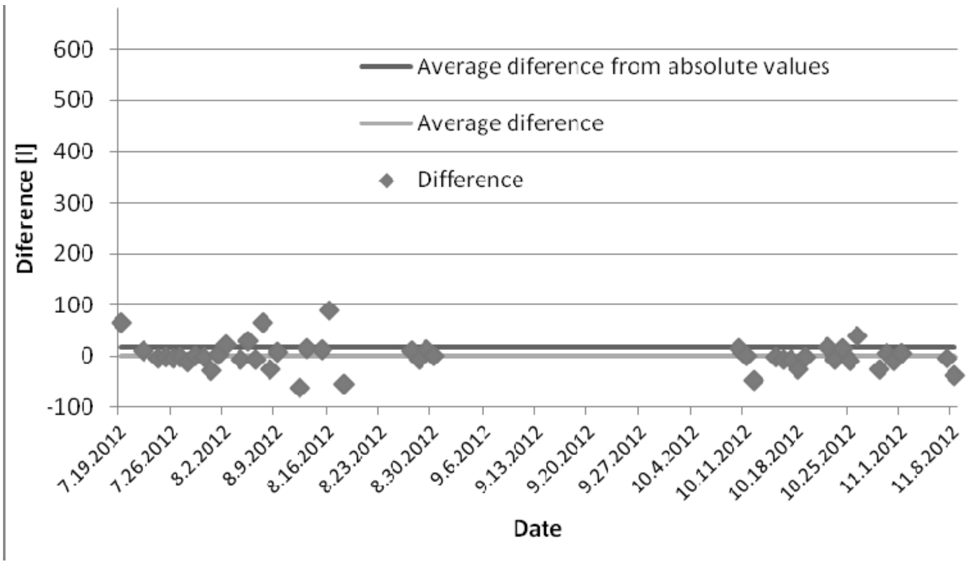

Fig. 1 Graoh of differences and statistc results

Tab. 1 Table of statistic results

	average	median	average deviatoin	dispersion
standard differences	0,9	-1,8	18,5	779,6
obsolute values of differences	18,4	10,0	15,7	433,5

For better projection of this result is in graph (Fig. 2) shown differences together with average values of differences from (Tab. 1).

During this period was tanked 16 055 l and JDLink shows 15 785 l, so total difference is 207 l and it means total mistake 1,7 %. Average fuel consumption was 20,3 l.ha^{-1}. When total amount of diesel for tank filling for year and fuel consumption data from JDLink for the same time are compared, there are even smaller difference. Tank filling volume is 32 195 l despite of 32 614 l from JDLink. Difference of 419 l means mistake of 1,3 %.

Conclusions

Standard mistake deviation was 18,5 l (15,7 l for absolute values) and average measurement mistake was 0,9 l (18,4 l for absolute values). Difference between sum of tanked amount (ploughing) from evidence and from JDLink was 207 l that is 1,7 %. Whole year difference was 419 l that is 1,3 %, so even more accurate. We can see that total numbers are relatively accurate despite of each measurements, it is probably given by inaccurate tank filling. Mistakes is also given by inaccuracy of CAN-Bus and inaccuracy of tank device. Main mistake was in tank filling and this is supported by increasing accuracy with more data. For tractors working with higher engine load is data about fuel consumption from CAN-Bus accurate enough.

Reference

Goel A., 2007. Fleet Telematics: Real-time management and planning of commercial vehicle operations (Operations Research/Computer Science Interfaces Series), Zaragoza, Zaragoza Logistics Centre, 200.

Huang C.M., Chen Y.S., 2010. Telematics Communication Technologies and Vehicular Networks: Wireless Architectures and Applications, Harshey, 412.

Roebuck K., 2012. Telematics: High-impact Strategies - What You Need to Know: Definitions, Adoptions, Impact, Benefits, Maturity, Vendors, Newstead, 93.

Sedlák P., Bauer F., Čupera J., 2010. Technofórum: Pokroky vo výskume poľnohospodárskej a environmentálnej techniky. Nitra : Slovenská poľnohospodárska univerzita v Nitre, 217-225. (in Slovak)

METHOD AND EQUIPMENT FOR PRODUCING BONELESS CARP FILLETS

Andrzej Dowgiałło*, Bogusław Pawlikowski

National Marine Sea Fisheries Institute, 81-332 Gdynia, Kołłątaja 1, Poland
Phone: +48 58 7356189, Fax: +48 58 7356110, E-mail: techmech@mir.gdynia.pl

Abstract

The main reason that demand for carp is limited is the danger to consumer health posed by the numerous bones in its meat. These can be eliminated effectively by cutting the bones into tiny pieces that are not detectable by the consumer and that pose no danger to consumer health. This can be done with portable or belt-system bone cutters for carp fillets. The only disadvantage of this method noted by some consumers is the esthetics of the fillets; after processing with portable bone cutters the fillets are no longer solid pieces of meat because of the deep cuts performed during processing. This problem can be solved with a process developed at the National Marine Fisheries Research Institute in cooperation with the Technical University in Koszalin to reconstruct deeply cut fillets to their original appearance thus producing boneless carp fillets. This is achieved by applying an enzymatic merging process to cut fillets, vacuum packing them in multilayers of plastic, and then deep chilling or freezing them. Thanks to this method, solid fillets are produced with tiny pieces of bone that are undetectable by the consumer. These frozen fillets have a shelf-life of more than 12 months, and the quality of the meat, in comparison to natural fillets, is juicier and more tender than it is following heat processing methods such as steaming or frying during which meat mass is lost to thermal drip.

Keywords: boneless, fillets, carp

Introduction

The stiff, sharply-pointed, branched intermuscular bones in carp muscles pose a serious choking hazard and can even be fatal to consumers, especially children. Because of this, carp is considered to be inedible in some countries. Intermuscular bones are not an issue in canned, minced, or boneless products such as fish burgers or fish sticks, and when the high temperatures of canned good sterilization softens intermuscular bones rendering them harmless to consumers. In minced meat, the intermuscular bones are crushed into such small pieces that they are no longer detectible.

The best solution to date for eliminating the choking risk from carp consumption is to cut the bones into tiny, safe, undetectable pieces approximately 3 mm in length (Dowgiałło, 2005). Machines for doing this were developed at the National Marine Fisheries Research Institute (NMFRI) in Poland and are pictured in Fig. 1 (Dowgiałło, Sikora, 2011) and Fig. 2. Thanks to theses machines, it is possible to mitigate the danger of these bones under industrial production conditions. Unfortunately, the integral structure of the fillets is destroyed during the operation (Fig. 3), and although this does not affect the organoleptic qualities of the meat, it does affect decidedly the appearance of the fillets and their physical properties.

Fig. 1 Table intermuscular bone cutter for fillets

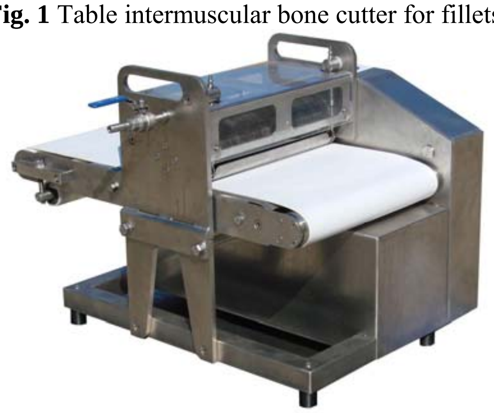

Fig. 2 Belt-system intermuscular bone cutter for fillets

Fig. 3 Cut carp fillet

Thanks to the availability of machines for cutting bones, fish fillets that have been processed through them are available commercially in Poland in some grocery retail chains. The availability of these fillets may increase significantly the demand for carp (Dowgiałło, 2005). The unusual, unattractive appearance of the cut carp fillets has not prompted consumers to purchase them. Consumers also remain unconvinced that these fillets can be prepared using traditional methods including frying, baking, and braising, and fear that the fillets will disintegrate during cooking. This is why the NMFRI developed technology for reconstructing the sliced fillets using the enzyme transglutaminase, which is produced industrially and used widely in foodstuffs (Motoki, Seguro, 1998; Kuraishi et al., 2001).

It was assumed that if the reconstruction problem could be solved it would be possible to produce a perfect market product in the form of intact carp fillets in which the bones are mitigated into tiny, safe, indiscernible fragments. The reconstructed and individually wrapped carp fillets are a product that would be suitable for sale throughout the year in large grocery retail chains.

Principles of fillet reconstruction technology

The technology of the cut and reconstructed carp fillets was based on the assumption that the starting material would be cut carp fillets without ribs. Thus, the technology was developed for use in fish processing plants capable of manual and mechanical processing of carp into fillets without ribs which are then processed with the bone cutting machine.

The initial concept of reconstruction technology for cut carp fillets included the following:

- preparing an aqueous solution of transglutaminase (TG) enzyme preparation,
- preparing precut fillets for the application of the preparation to the cuts in the meat, including excess water removal through draining, pressing, or blown air drying,
- applying the TG aqueous solution to the fillets in different ways, including aerosol application, spraying, actively painting, dipping, portion dispensing and stirring,
- removing excess TG solution from the fillets, for example, during a timed drip period or with a stream of compressed air,
- placing the reconstructed fillet on a stiff backing with the meat facing either up or down,
- placing the fillet and the backing in a plastic bag,
- vacuum packing the fillet on the backing in the plastic bag to achieve compression and the consolidation of the surface cuts of the fillet;
- vacuum packed fillets in a cooler at +8 °C in order to complete the transglutaminase fusion process of the surface cuts in the fillet.

In this version of the concept for realizing the task it is critical to choose the appropriate transglutaminase product that meets the following requirements:

- fuses the slices of carp fillets,
- has no adverse impact on the organoleptic characteristics of carp fillets,
- does not accelerate fillet spoilage during cold storage,
- is suitable for application as an aqueous solution under industrial conditions for mass production,
- allows for easy, precise application on fish fillets in amounts that are controllable and reproducible.

In order to select a transglutaminase product suitable for the technology under development, a preliminary review was performed of the various industrial TG products available, and the effectiveness of the transglutaminase enzyme in food technology was described and analyzed, as was this enzyme.

Choice of TG product

An important selection criterion for the transglutaminase product for carp fillet reconstruction was that it had negative impact on the natural organoleptic characteristics of the carp, i.e. its aroma, appearance, flavor, texture, and juiciness.

In order to determine the potential impact of the transglutaminase products selected for testing on the organoleptic characteristics of carp meat carp, the sensory properties of them were evaluated in both dry states and as in a 10 % aqueous solution.

The evaluations of dry products indicated that the tested transglutaminase products differed in organoleptic characteristics, and especially with regard to flavor. Activa EB and Saprona TG 2N, with casein bases, have weak, neutral smell and slightly soapy taste. Saprona TG 2N also had a notable but slight chemical smell reminiscent of urea. Both of these products have a fairly neutral, floury taste. Activa GS and Saprona TG F, with fish gelatin bases, have weak, neutral smell. The dominant flavors of both products are salty, and while Saprona TG F is has a clean flavor, that of Activa GS has a chemical, soapy-alkaline note.

The intense salty flavor of Saprona TG F was surprising since the product ingredients do not include sodium chloride. The analysis of Saprona TG F for sodium chloride content (NaCl) indicated that the share of it inn the product mass is about 20 %.

The evaluation of the organoleptic properties of 10 % aqueous solutions of the different products confirmed these differences. The greater salty taste of the Activa GS 10 % aqueous solution in comparison to that of Saprona TG F indicated that the share of sodium chloride in the base of Activa GS is probably higher than 20 %.

The results of the initial assessment of the organoleptic characteristics of the transglutaminase products selected for the study provided no grounds for excluding any of them from the study. They did indicate, however, that the products containing fish gelatin were more neutral in terms of potentially negative impacts on the organoleptic characteristics of the carp fillets. Therefore, it was decided to use Saprona TG F.

Coating fillets with transglutaminase

In addition to choosing a transglutaminase product, three fillet application methods were developed based on the results of tests:

- dipping;
- praying,
- transglutaminase curtain (e.g., as in wet coating).

One of the models used in the study is shown in Fig. 4.

Dipping

The simulation of this method, which consists of immersing the cut part of the fillet in a flat pan of transglutaminase solution for 2, 6, or 10 s, indicated that at an immersion depth of g = 7 mm and an immersion time of t = 6 s produces appropriately reconstructed fillets. However, the disadvantage of this method is the high consumption of transglutaminase solution removed from the reservoir on the mesh that covers the fillet transport conveyor belt. Therefore, this coating method cannot be recommended for use on an industrial scale.

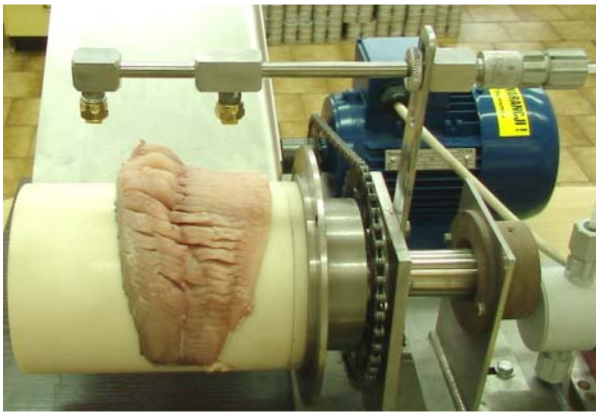

Fig. 4 Prototype station for transglutaminase spraying

Spraying

The set up for this method is illustrated in Fig. 4. Experiments indicated that this method not only ensures proper reconstruction, but it also uses small quantities of transglutaminase. However, the relatively quick gelling time makes spraying continually for longer periods difficult.

Transglutaminase curtain

Experiments have shown that when the nozzle in Fig. 4 is replaced with a transglutaminase curtain, this method produces smoother fillet gelling. This method was run for about 1 hour and it is suitable for use on an industrial scale. Therefore, in the present study the technology applied was the curtain method of coating carp fillets.

Summary

Reconstructed boneless carp fillets that are vacuum packed individually in plastic are modern products of the convenience food type and are suitable for sale in large grocery retail chains either refrigerated or frozen.

Studies that tested the quality of a sample lot of reconstructed fillets (Fig. 5 and Fig. 6) indicated that this product maintains its high quality even after one year of cold storage (Fig. 7).

Fig. 5 Appearance of reconstructed carp fillet after removing it from packaging

Fig. 6 Reconstructed carp fillet after cooking

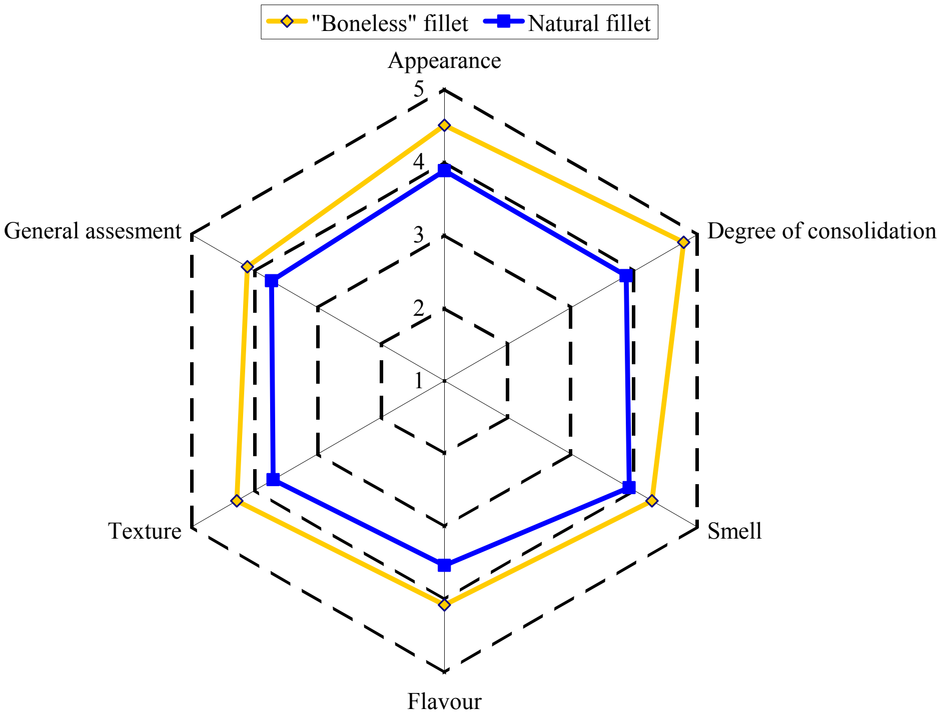

Fig. 7 Sensory quality of fried boneless carp fillets and natural carp fillets kept in cold storage for one year at a temperature of -20 °C

The technology for producing reconstructed boneless carp fillets is possible to be implemented in small fish processing facilities, and even directly at fish farming enterprises.

Reference

Dowgiałło A., 2005. Technological and technical conditions for increasing carp processing in Poland. Electronic Journal of Polish Agricultural Universities. Agricultural Engineering, 8(2).

Dowgiałło A., Sikora M., 2011. Table intermuscular bone cutter for fillets. Pl Patent 211040.

Kuraishi C., Yamazaki K., Susa Y., 2001. Transglutaminase: its utilization in the food industry. Food Reviews International, 17(2): 221-246.

Motoki M., Seguro K., 1998. Transglutaminase and its use for food processing. Trends in Food Science Technology, 9(5): 204-210.

THE NOISE MEASUREMENT AT THE UNIVERSITY CAMPUS ENTRANCE

František Dvořák*, František Lachnit

Czech University of Life Sciences Prague, 16521 Prague 6 – Suchdol, Czech Republic, Phone: +420 224 383 114, E-mail: dvorak@tf.czu.cz

Abstract

The paper deals with traffic noise at the entrance to the university campus. Further with the internal and external noise of motor vehicles and noise generating during driving of motor vehicles. Furthermore it is acquainted with the noise impacts on people and the noise hygienec limits. For the assessment the impact of transport on the acoustic situation in this locality are performed by corresponding measurements. The conclusion contains the evaluation of noise pollution from traffic in the monitored location.

Keywords: noise measurement, university campus

Introduction

Noise has been becoming one of serious current environmental problems and the total noise environment is constantly increasing. Development of transport entails in addition to positive also many negative effects, which include noise pollution in the road surroundings and protected outdoor areas of buildings. The issue of noise in protected outdoor areas of buildings and campuses is dealt among others in (Murphy, 2009; Zannini, 2013). Even though it is more a problem for cities, considering the topographical conditions it becomes a problem of open countryside as well.

The physical essence of the noise is vibration, which is transmitted most often in atmospheric environment and induces in a person the corresponding sensation. The basic characteristic of noise that impacts on person includes intensity, frequency and the time duration.

In common practice it is possible to meet, among others, a permanent broadband noise that is characteristic for ambient noise, the permanent narrowband noise, the impulsive noise, and finally an intermittent noise caused by the transport (Smetana, 1998).

The noise impacts on person

Noise acts through the organ of hearing on the nervous system of man. From a certain level and exposure time it may induce negative response to the psychical state of a person and also its fatigue. The human body is not able to disable hearing physiologically. Central nervous system processes the sounds capes during sleep, too (Muzet, 2007; Portera, 2010).

Adverse effects of noise on person health are generally defined as morphological or functional changes in the organism, which lead to a deterioration of functions of the organism, reducing stress resistance and increasing susceptibility to other adverse environmental effects. Stress affects neurohormonal and neurovegetative regulation, biochemical reactions, sleep, higher nervous functions such as learning and memory, motoric function, coordination, etc. In the complex form the noise manifests itself in the form of emotional and social disorders or disease. Noise can contribute to activating or accelerating the pathological process.

Negative effects of noise are manifested not only the recourse hearing, but also on other person systems, and in the psychological sphere. Noise is often underestimated, because its effects are manifested only after a longer period of time. Although operating on a large group of people, it does not cause mass occurrence of the disease, so nor any worry of its action. The effect of noise is individual according to the person to whom it operates.

Noise of motor vehicles

Interior noise of motor vehicles

Interior noise of motor vehicles acts on the driver or the crew of the vehicle. It has a direct effect on the fatigue or feeling of comfort or discomfort and affects traffic safety. Besides, it influences the attractiveness of the vehicle for any car buyer as it requires the simple voice communication, and of course there is connectivity between mobile phones and multimedia technology.

External noise of motor vehicles

External noise of vehicles interferes and burdens directly the environment. For this reason, the legislation strongly restricts it. Reducing levels of external noise of a motionless vehicle when the engine is idling is considered important in assessing the overall technical level of the vehicle.

Measurement conditions are specified in the regulations. These rules can be divided into international, national regulations and rules of producers. International regulations unify measurement and evaluation in a large number of countries such as the EEC and UNECE countries. The national exist then because of reasons such as tradition, a belief, etc., SAE, JASO, etc. Producers (manufacturers) often use their own measurement and evaluation methodologies which are not followed by international resp. national regulations, which are of a technical and sales perspective important.

These regulations include many measuring methods, such as noise measurement of a motionless vehicle, external noise of accelerating vehicle measuring, the noise of compressed-air brake systems etc. Achieving low levels of internal and external noise is necessity for vehicle manufacturers both in terms of the legislative and of sales.

Noise when driving vehicles

Sources of noise in the vehicle are components of the drive system, the engine with its auxiliary units, intake, exhaust resp. exhaust system, cooling system, transmission, brakes, tires, their construction and tread pattern, tire rolling on the road, noises of the body and of its extension, i.e. vibrations, turbulences and load fixing.

The formation of the noise is influenced by the driving style, i.e. driving speed, acceleration, deceleration, driving resistances etc. Furthermore the road resp. roadway, especially type of the cover and its condition, trace parameters, i.e. location in the terrain, climb, crossroads, etc. the traffic intensity, speed, track, traffic flow, passenger or cargo cars, tractors, special vehicles.

There are mainly rolling noise of tires at higher speeds and traffic outside the village, which is formed by contact tire surface with the road surface. Furthermore, it is aerodynamic noise vehicle, which is caused by the airflow and creates turbulences around the vehicle body and chassis.

Hygienic noise limits

Area of noise from road traffic is wide and includes many standards, regulations and guidelines. For a description of the acoustic conditions in the environment is used as a descriptor equivalent sound pressure level.

In addition to our regulations resp. standards, it is for example the EU Directive on the assessment and management of environmental noise. Directive has a tendency to unify the procedures of all Member States to provide the methodology for noise, recommendations for the introduction of noise mapping and improving public awareness about the noise situation.

It also introduces unified indicators of environmental noise and harmonized methodology for the evaluation.

At present our legislative regulations require a duty of not exceeding the prescribed noise limits that are the subject of government regulation of a health from the adverse effects of noise and vibration. According to the government regulation the hygienic limit in equivalent sound pressure level is equal to 50 dB and correction to the taking into account the kind of clearance during day and night. Hygienic noise limits resp. sound pressure level in a protected outdoor area buildings and protected outdoor space resp. external noise are listed in Tab. 1

Tab. 1 Noise limits

Limit L_{Aeq} [dB]	**1**	**2**	**3**	**4**
Day 6:00 - 22:00 hour	50	55	60	70
Night 22:00 - 6:00 hour	40	45	50	60

The rules for applying corrections in the table:
1 – applies to noise from traffic on purpose communications/ 4th. class roads
2 – applies to noise from traffic on the roads 3rd. class or local roads
3 - applies to noise from traffic on highways, roads of 1st. and 2nd. class
4 – applies in the case of former noise pollution from traffic on the roads with the exception of purpose communications/tertiary roads.

Noise measurements at the entrance to campus

Allocation of the measurement and description of the existing noise situation

The aim is to determine the equivalent sound pressure level for a given time of day and the share of road transport on the acoustic situation in the locality.

The existing noise situation in the area is primarily affected by traffic on the roads passing through this site. The primary source of noise here is the automobile traffic on Kamýcká road and the secondary source of noise is traffic on the communication Vysokoškolská and the noise of aircrafts landing at the airport Vaclav Havel in Prague.

Fig. 1 Map of the measuring point

Description of the area, topographic / geographic data, place of measuring

It is an outdoor area, the reference point of the measurement and location for evaluating noise nuisance is marked on the map. The place of measuring is located in Prague 6 - Suchdol at the entrance to the area of Life Sciences Prague in front of the entrance gate, the coordinates of this point are: 50 ° 7'57.139 "N, 14 ° 22'33 .703" E. There is lawn around, on one side at a distance of 40 m there are houses, on the opposite side at a distance of 50 m there is a building of health center facing grown broadleaved trees. The place of measuring is shown in Fig.1.

Traffic engineering data

Amongst these information traffic intensity, speed and composition of traffic flow, a description of the roads, slope, width configuration and communication type and quality of the road surface are included. Tab. 2 lists the detected hourly intensity at the entrance and exit of the campus.

Since the measurement was performed near the campus entrance gate, vehicle in front of the gate slowed down eventually stopped from the maximum speed of 50 km. h-1, behind the gate again they accelerated to a maximum speed of 30 km. h^{-1}.

Communication has a straight and hard surface, which is made up of cast bituminous material (asphalt) without bumps.

During the measurement 14 transport aircraft at an altitude of 600-800 m in the direction of the airport flew over.

Time of measurements and meteorological conditions

Daily measurements - Wednesday, the 24.4.2013 - (7:00 to 10:00) h,
Night measurement - was not done.

Temperature of the air - (8.4 to 15.9) ºC, air pressure (992 to 993) hPa, relative humidity of the air - (49.5 to 71.2) %, air velocity - (0.6 to 1.2) $m.s^{-1}$, clear, no rain, no snow.

Measuring devices and location of measuring point

The measuring point is marked in Fig. 1 Map of the measuring point, measuring microphone of the sound level meter was placed in the tripod at a height of 1.5 meters above the ground, the microphone was oriented to the bar gate.

For measuring was used - sound level meter - Frequency Analyzer - SC310 – 1st class of precision. It meets the international (IEC) and European (EN) standards and American standards ANSI, allows optional expansion modules for measuring other acoustic parameters, simultaneous measurements with A, C and Z, a condenser microphone was used.

Before the measurement and after the measurement sound level meter was checked by the calibrator equipment, no difference in values reading was noted.

Tab. 2 The traffic intensity - the number of vehicles

Time	Bicycle	Motorcycle	Passenger car	Truck	Summary
7:00 – 8:00	4	2	147	20	173
8:00 – 9:00	2	3	192	6	203
9:00 – 10:00	4	5	127	6	142

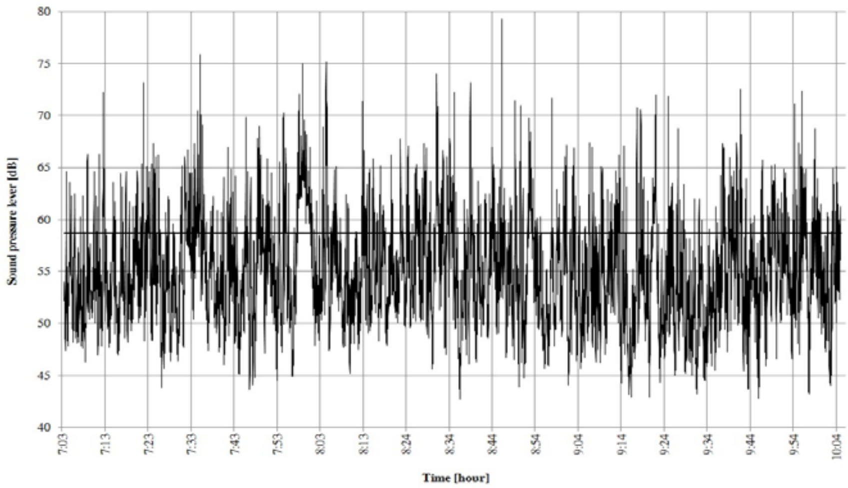

Fig. 2 Course of sound pressure levels

Measurement results and discussion

The results are shown in Fig. 2. The Figure shows considerable variation in sound pressure levels at the measuring point. Maximums were caused by the entrance of trucks supplying stores in campus and by accelaration of passenger cars with diesel engines and of motorcycles. Extreme values were achieved in combination in combination with the flight of transport planes landing at the airport Vaclav Havel.

Equivalent sound pressure level at the LAT measurements was 58.7 [dB] and is indicated in the Fig. 2 continuous thick line.

Conclusion

The purpose of noise measurement at the entrance gate to the university campus was to obtain objective information about the actual impact of road transport on the acoustic situation in the area, this information is necessary to evaluate the current situation.

Equivalent sound pressure level at the place and time of measurement exceeds the permitted value that is mainly due to the stopping and starting of older cars with diesel engines and motorcycles in combination with noise transport aircraft landing at the nearby airport Vaclav Havel. Surrounding localities owing to planted vegetation might not be affected by excessive noise of vehicles coming to campus. Mainly persons walking alongside the sidewalk that runs parallel to the access road are under impacts of increased exposure noise.

Acknowledgement

This work was supported by COST TU0902 „Integrated assessment technologies to support the sustainable development of urban areas“, Projekt MŠMT LD 11049: “Spotřeba energie dopravou v urbánních a suburbánních územích” *(The transport energy consumption in urban and suburban areas).*

Reference

Murphy E., King E.A., Rice H.J., 2009. Estimating human exposure to transport noise in central Dublin, Ireland Original Research artikle. Environment International, 35(2): 298-302.

Muzet A., 2007. Environmental noise, sleep and health Review Article. Sleep Medicine Reviews, 11(2): 135-142.

Pirrera S., De Valck E., Cluydts R., 2010. Nocturnal road traffic noise: A review on its assessment and consequences on sleep and health. Environment International, 36(5): 492-498.

Smetana C., 1998. Hluk a vibrace, Měření a hodnocení. Prague : Sdělovací technika, ISBN 80-90 1936-2-5. (in Czech)

Zannin P.H.T., Engel M.S., Fiedler P.E.K., Bunn F., 2013. Characterization of environmental noise based on noise measurements, noise mapping and interviews: A case study at a university campus in Brazil Original Research Artikle Cities, 31: 317-327.

ALTERNATIVE METHOD OF DETERMINING STREAM FLOW VELOCITY PROFILE

Šárka Dvořáková, Jiří Zeman

Czech University of Life Sciences Prague, 16521 Prague 6 – Suchdol, Czech Republic, Prague 6 – Suchdol, Czech Republic, e-mail: dvorakovas@tf.czu.cz

Abstract

The paper deals with the possibility of determination of distribution of the surface water flow velocity. This is an experimental method that develops the float method of water discharge measurement (Sargent, 1981). Improvement consists partly in a faster and more accurate acquisition of the experimental data and partly in setting new correction formulas for the water discharge calculation. The reference method used is the conventional method of measuring with hydrometric propeller. In comparison with this method, the float method allows the determination of the discharge profile even for a very small depth, because the velocity is determined photometrically from the velocity of the surface floating particles (Fig. 3). On the contrary a disadvantage of this method is the difficult determining of the vertical velocity profile. By comparing the results of these two methods in the stream channel of the Pryský brook (Dvořáková et al., 2012), the authors find the constraints and limits of applicability of both methods.

Keywords: floating method, velocity profile, brook, photometrical method

Introduction

With the fundamental task of hydrology, namely the channel discharge determination, we are in many cases limited to the determination from the current water level in the channel that has not shape defined by us. There are several approximate methods of setting out the relationship between the water level and channel discharge, for example Chezy's or Manning's equation. These formulas, however, always assume a known value of the channel roughness parameters, whose value is determined by estimation, and therefore with a relatively large error. For this reason, it is often necessary to determine the relationship between velocity and water level experimentally. To its determination a hydrometric propeller is usually used, which, if it is placed in the water flow, is able to determine the flow velocity at the site. It is thus possible to determine both deep velocity profile and horizontal velocity profile along the width of the channel and in some cases to determine relatively accurately the discharge trough the channel for defined water level (assuming that during the execution of the time series of measurements the water level is unchanged). One of basic requirements for the proper functioning of hydrometric propeller is that the entire propeller must be submerged with a margin on all sides. Just this fact is sometimes difficult to observe at shallow depths in some parts of the stream channel.

A possible alternative leading to a more accurate method of hydrometric propeller is the determination of the velocity of particles floating freely at the surface by photometrical method which we discuss below. The principle of this complementary method lies in determination of the relative displacement of macroscopic particles placed on the water level. In order to enable a simpler calculation, drifting particles are suitably located on the abscissa perpendicular to the axis of the stream channel and have a spherical shape. After passing a few meters through the stream channel, their position is repeatedly retained by a camera positioned above the stream channel. From the location of the centers of these particles, the horizontal velocity profile of the channel is then determined. A certain advantage is the fact that the measurement across the width of the stream channel takes place in one moment, and so the change of the water level and discharge does not take place during the measurement.

Material and method

Pryský brook discharge was determined by two experimental methods, in the closing profile with coordinates 50 ° 47'36 .629 "N, 14 ° 29'13 .440" E. Both measurements took place on 24th April 2013. Stream channel is paved with basalt blocks and is slightly overgrown by grass. The slope of the stream channel in the place of the measured profile is about 3.5 %, therefore the brook falls into the category of torrents. The cross-section is approximately trapezoidal and it is illustrated in Fig. 1.

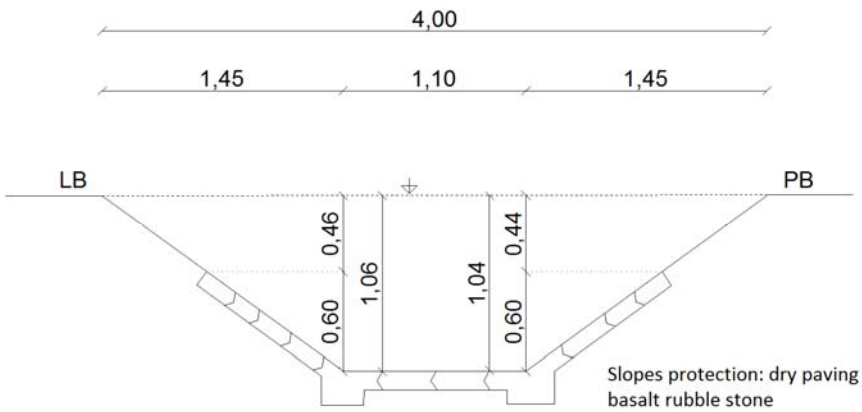

Fig. 1 Cross-sectional profile of Pryský brook (presented values are in meters)

As a reference method to determine the horizontal velocity discharge profile, measurement by the hydrometric propeller of type OTT-C-2 was used. A vertical profile was not determined because of the low water level. A comparative measurement was carried out at the water level of 110 mm. A horizontal profile was measured at three points along the width of the stream channel in the height of 44 mm from the bottom. The results of measurement are shown in Tab. 1.

The tested method was the above-mentioned method of photometric scanning of particles of spherical shape with a diameter of 40 mm and a density of 920 kg.m^{-3} floating on the surface. The thrower of the particles was placed above the stream channel perpendicularly to the axis. The camera with lens aimed askew upstream was placed about 4 m downstream above the centre of the brook. The situation is clear from Fig. 2, resp. Fig. 4.

An example of videorecording from measuring camera, which was submitted to analysis, we can see in Fig. 3.

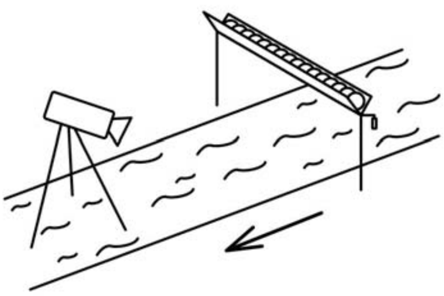

Fig. 2 Scheme of floating method measurement

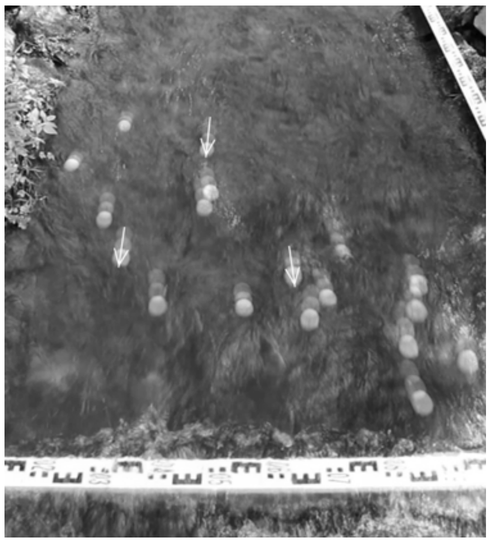

Fig. 3 Comparison of tree shot of analysed videorecord

The shot was at first aligned along the lines interlacing riparian water line in order that they were parallel on the transformed image. With the help of the measuring rod, also a longitudinal direction was calibrated. Thus we obtained a vertical projection of the scanned section of the stream channel. On the particular shots, the coordinates of released floats were found. Immediate float velocity was determined from the shift of positions between the shots after recalculation of pixels to centimetres.

Fig. 4 Real situation in the time of measurement

The snapshot rate was 50 frames per second. Videorecording resolution was 750x1334 pixels. Finally, in a series of 15 consecutive frames only every fifth frame was evaluated. From the 14 velocities acquired of each float, the mean value of velocity, its standard deviation and the distance from the axis of the stream channel was determined. The results are given in Tab. 2 and shown in Fig. 5.

Results and discussion

Tab. 1 shows the values measured by hydrometric propeller. From the measured velocity values, the average velocity 0.88 ms^{-1} was calculated. By multiplication with the cross-sectional area of 0.121 m^2 we got the discharge value 0.106 $m^3.s^{-1}$. The velocity calculation using the arithmetic mean was chosen due to the very small difference between the velocity in the middle of the channel and at its borders.

In the tested floating method, the velocity for each of the 12 floats was determined 14 times. Velocity values were averaged and together with their standard deviations they are given in the Tab. 2. In this table, the mean distances of floats from the axis of the channel and their standard deviations are also shown (Mošna, 2010). These values are also shown graphically in Fig. 5.

Tab. 1 Values measured by hydrometric propeller

vertical	number of turns N	measurement duration DT [s]	number of turns per sec. N/DT	velocity [$m.s^{-1}$]	note
I. measurement					
left bank	220	30	7.33	0.79	time:
axis	321	30	10.70	1.14	10.55 - 11.10
right bank	245	30	8.17	0.88	
II. measurement					
left bank	230	30	7.67	0.83	time:
axis	230	30	7.67	0.83	11.10 - 11.20
right bank	230	30	7.67	0.83	
III. measurement					
left bank	218	30	7.27	0.8	time:
axis	274	30	9.13	0.98	12.35 - 12.45
right bank	235	30	7.83	0.85	

Tab. 2 Velocity values measured by the floating method

Float	Distance from the stream channel axis [mm]	Distance standard deviation [mm]	Velocity of the float [m/s]	Velocity standard deviation [m/s]
1	358.4	11.1	1.023	0.170
2	169.8	13.4	1.028	0.165
3	-50.6	29.8	0.985	0.146
4	-231.8	21.8	0.983	0.207
5	433.1	6.4	0.917	0.141
6	332.7	35.2	1.035	0.118
7	-42.5	11.0	1.022	0.191
8	-267.0	9.9	1.019	0.139
9	395.3	16.4	0.980	0.322
10	299.7	27.7	0.981	0.208
11	-29.2	10.2	1.049	0.133
12	-352.5	22.2	1.016	0.217

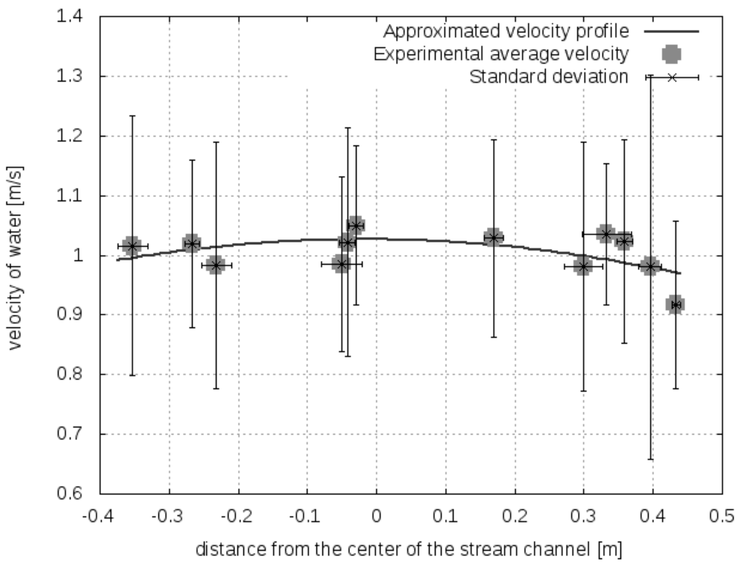

Fig. 5 Graphical representation of the velocity profile determined by the floating method. The abscissae show the size of the standard deviations of the data

The values of mean velocities in particular distances from the axis of the steam channel were approximated by the quadratic function $v(x) = ax^2 + bx + c$.The values of the coefficients a, b and c are shown in Tab. 3.

Tab. 3 Found values of horizontal velocity profile

coefficient	value	standard deviation
a [$m^{-1}s^{-1}$]	-0.28	0.18
b [s^{-1}]	-0.01	0.04
c [$m.s^{-1}$]	1.03	0.02

The coefficient c gives the mean water velocity in the channel, the coefficient b indicates how faster the water flows near the right bank than near the left bank and the coefficient a indicates how faster the water flows in the middle of the channel than near its border.

Comparing the mean velocity determined by hydrometric propeller and the mean velocity determined by the floating method, we come to the conclusion that the velocity determined by the floating method is about 20% higher, which may be due to the fact that floats determine the speed 6 cm higher above the bottom, where the higher water velocity can actually be expected. If we would want to measure in greater depth, it is necessary to furnish the floats with weights increasing its resistive surface in greater depths.

Large standard deviations of velocity are caused by unsteady flow in the channel, which is sometimes turbulent. In the case of using the tested method for flows with laminar, or at least steady flow, a much smaller variance of measured values can be assumed.

Conclusion

We were able to implement experimentally successfully a modification of the floating method and to provide it with such mathematical apparatus that allows determining photometrically the velocity of several floats spread over a greater or full width of the channel. In this way, we are (unlike the conventional methods) able to determine the horizontal velocity profile at the water level using a single measurement.

In this way some systematic errors of other methods are eliminated. These errors are caused for example by a non-parallel measurement along the entire width of the water channel, so it is not possible to avoid the error caused by the change of discharge between consecutive measurements.

Comparing the two methods in the water channel of the Pryský brook we also obtained the necessary calibration data, which we can use for evaluation of the dynamics of this watershed in which we have permanently installed the water-stage indicator. The dynamics of this watershed is especially investigated for verification of Linear Storage Model (Dvořáková, Zeman, 2010) and its application in flows with similar discharge.

Acknowledgement

This paper was supported by the Czech Technological Agency, Project TA02020402 (Water regime optimisation to mitigate impacts on hydrological extremes).

Reference

Dvořáková Š., Zeman J., 2010. Analysis of fluctuation in the stream water level during the dry season in forested areas, Scientia Agriculturae Bohemica, 41 (4). ISSN 1211-3174

Dvořáková Š., Kovář P., Zeman J., 2012. Implementation of conceptual linear storage model of runoff with diurnal fluctuation in rainless periods, Journal of Hydrology and Hydromechanics, 60 (4): 217-226.

Mošna F., 2010. Statistické zpracování dat na PC, příručka k projektu Alma Mater Studorium, UK Praha, Pedagogická fakulta. ISBN 978-80-7290-448-8

Sargent D.M., 1981. The development of a viable method of stream flow measurement using the integrating float technique, ICE Proceedings, 71 (1): 1-15. ISSN 1753-7789

QUALITY CHARACTERISTICS FOR AGRICULTURAL RESIDUES TO PRODUCE BRIQUETTES

Eissa A. H. A.[1,2], Gamea G. R.[2], El Saeidy E. A.[2], El Sisi S. F.[2]

[1]Department of Agriculture Systems Engineering, College of Agricultural and Food Sciences, King Faisal University, P.O. Box 420, Al-Hassa 31982, Saudi Arabia. aymanhafiz@kfu.edu.sa
[2]Agriculture Engineering Department, Faculty of Agriculture, Minoufiya University, Shibin El-Kom, EGYPT

Abstract

The agricultural crop residuals are considered one of the most important problems, which face the environmental life and farmers in the world. The mechanical treatment by cutting, crushing or chopping and briquetting processes are the primary step and the suitable solution for solving this problem and recycling these residuals to be transformed into useful products. So the aim of the present work to get a high quality for agriculture residues such as cotton stalks, rice straw briquettes. Chopped cotton stalks and rice straw having moisture content (8, 10 and 12%) and (8, 10 and 12.8% w.b.) were densified into briquettes without binder and with binder (Urea-Formaldhyde) using a screw press machine. Quality properties for briquettes were durability, compression ratio hardness, bulk density, compression ratio, resiliency, water resistance and gases emission. The optimum quality properties found for briquettes at 8 % moisture content and without binder. Where the highest compression stress and durability were 8.95, 10.39 MPa and 97.06 %, 93.64 % for cotton stalks and rice straw briquettes, respectively. The CO and CO_2 emissions for cotton stalks and rice straw briquettes were less than these for loose residuals.

Key Words: Residues, briquetting, quality properties

Introduction

Biomass is considered one of the main renewable energy resources of the future due to its large potential, economic viability and various social and environmental benefits. It was estimated that by 2050 biomass could provide nearly 38% of the world's direct fuel use and 17% of the world's electricity (Demirbas, 2000). The briquetting technology improves the characteristics of agro-residues for transportation, storage, feeding into furnaces, and combustion (Werther et al., 2000). The mechanical strength of the briquettes can be improved by adding some biomass samples. Water resistance of the briquettes can be augmented by adding olive refuse, cotton refuse, and pine cone or paper mill waste (Yamnan et al., 2001). To produce high quality pellets, the feedstock has to be dried to a moisture content of about 10% (raw weight). Since it is not possible to reach such low moisture contents by natural drying, the material has to be artificially dried. However, a wide range of temperatures and retention times can be used in the drying process (Stahl et al., 2004).To improve the quality of the briquettes and to have an economically competitive product at the same time, the esparto was partially pyrolyzed at temperatures between 160°C and 400°C, and the pressure of densification has been examined. The combustion profile of the samples has been studied by applying the derivative thermogravimetry technique and the mechanical properties of the briquettes were tested to evaluate the impact resistance and water resistance (Debdoubi et al., 2005). The low sulphur content of crop residues as compared to fossil fuels and their use as fuel does not add to the CO2 content of the atmosphere (Dubey et al., 2007). Densification process to create strong and durable bonding in densified products such as pellets, briquettes, and cubes can be determined by quality testes which include testing the strength (compressive resistance, impact resistance and water resistance) and durability (abrasion resistance) of the densified products These tests can indicate the maximum force/stress that the densified products can withstand, and the amount of fines produced during handling, transportation and storage (Nalladurai, Morey, 2009). The durability of briquettes is a measure of the ability of the briquettes to withstand the destructive forces such as compression, impact and shear during handling and transportation. In addition, the durability values represent the relative strength of the particle–particle bonding in the briquettes/pellets (Nalladurai, Morey, 2010). Pellet biomass fuels are compressed, homogenized and dried biomass fuels that possess several advantages during handling, storage and combustion when compared to unprocessed biomass fuels. Environmentally, pellet biomass fuels provide advantages of less ash, smoke and other compound emissions, including carbon particles, CO, NOx and SOx. Because the use of biomass pellets produces much fewer greenhouse gases when the biomass is sustainably harvested, there has been a recent push to replace fossil fuels with biomass fuels (Panwar et al., 2011).

Material and method

Material

The chopped materials were pressed in a screw press machine at the Shimada Company (Type SPMM-850 KS) at (8, 10, and 12 %) and (8, 10, and 12.8 %) moisture content for cotton stalks and rice straw with and without binder, respectively. The production capacity of the machine was 400 kg/h. The press machine is powered by 30 kW Electric Motor. It has 2 Electrical Ceramic heater bands each requiring 3 kW for operation and has an integrated "T" Stirrer with a 1.5 kW Motor. The chopped materials feeded from the container in to the machine by a belt which its velocity was 0.38 m/s.

Cotton stalks

Cotton stalks (Gossypium Barbadense) used at three different moisture content (8%, 10 % and 12 %). The stem length of cotton stalks ranged from 98 to 182 cm, stem diameter ranged from 7.3 to 15 mm, weight of one stalk ranged from 35 to 200 g and number of branches ranged from 6 to 27.

Rice straw

Rice straw (Oryza Sativa, Giza 101) used at three different moisture content (8%, 10 % and 12.8%). The stem average length was 80cm (from 70 to 90 cm), stem diameter ranged from 3 to 4.5 mm and number of branches ranged from 5 to 12.

Measurements

1. Briquettes durability

The durability (Du) of the briquettes was determined according to ASAE Standard S269.4 (2003). A 500 g sample of briquettes was tumbled at 50 rpm for 10 min, in a dust tight enclosure. A No. 5 US Sieve with an aperture size of 4.0 mm was used to retain crumbled briquettes after tumbling. Durability is expressed by the percent ratio of mass of briquettes retained on the sieve after tumbling (mpa) to mass of briquettes tumbling (mpb) according to with the following equation (1). (Fasina, 2008).

$$Du = \frac{mpa}{mpb} * 100 \qquad (1)$$

2. Compression test

The compression stress for each briquette was measured using a universal testing machine (UH-500KN, Shimadzu). The flat surface of the briquette sample was placed on the horizontal metal plate of the machine. A motorized screw slowly reduced the distance between this metal plate and a second one parallel to it. An increased load was applied at a constant rate until the test sample failed by cracking or breaking. The load at the fracture point and the maximum load were converted to compression stress using the following equation (2). (Gibiiz et al., 1996).

$$\text{Compression stress} = \frac{\text{Load at fracture}}{\text{Cross sectional area of plane of fracture}} \qquad (2)$$

3. Gases emissions

The emission was measured using analyzer (Rize 700 EIUK) as shown Fig. (2.4). Estimated emissions were carbon monoxide (CO), carbon dioxide (CO2), oxides of nitrogen (NOX), and sulfur dioxide (SO2) for each cotton stalks and rice straw (loose and briquettes) samples at moisture content (7.4, 8.57 and 10.35%) and (7.13, 9.21 and 10.98%) for cotton stalks and rice straw, respectively. The samples were burned in the stove and took the data of emissions from the chimney height of 180 cm. Ethyl Alcohol was used as an assistant at the start of the burning process and the readings taken during the samples ignition. Combustion efficiency (η) was calculated from the following equation: $\eta = CO2\ \%/(\ CO\ \% * CO2\ \%)$

Methods

The experiments were carried out in resistance of concrete Laboratory, Civil Engineering Department, Faculty of Engineering, Minoufiya Univ., and Biomass laboratory of the New and Renewable energy authority, Nasr City, Cairo. During years 2009 and 2010 to measured some quality properties for cotton stalks and rice straw briquettes such as the durability, compression stress, hardness, bulk density, compression ratio, resiliency, water resistance and gases emission.

Quality of briquettes

1. Bulk density (ρb)

Bulk density is an indicator of savings in storage, transportation space and cost of blocks.

The bulk density of the briquettes was calculated by Eq. (3), (Jha et al., 2008).

$$\rho_b = \frac{W}{L \times B \times T} \quad (3)$$

ρb = bulk density of cotton stalk briquette, kgm^{-3}
W = weight of cotton stalk briquette, kg
B = width of cotton stalk briquette, mm
L = length of cotton stalk briquette, mm
T = thickness of cotton stalk briquette, mm

2. Compression ratio (CR)

The compression ratio indicates volume reduction during compression. It was obtained from the ratio of bulk density of compact block to the initial density of the material being compressed. According to Eq. (4). (Jha et al., 2008)

$$CR = \frac{\rho_b}{\rho_{raw}} \quad (4)$$

CR = compression ratio
ρb = bulk density of cotton stalk briquettes, kgm^{-3}
ρraw = bulk density of loose cotton stalk, kgm^{-3}

3. Resiliency (R)

Resiliency was determined as the ratio of the increase in thickness to the initial thickness of the briquette according to Eq. (5). (Jha et al., 2008)

$$R = \frac{T - T_i}{T_i} \quad (5)$$

R = resiliency, %
T = thickness of stabilised cotton stalk briquette, mm
T_i= initial thickness of cotton stalk briquette, mm

4. Water resistance

The water resistance of the briquettes was tested by immersing them in a glass container filled with cold tap water and measuring the time required for onset of the dispersion in water (Yamnan et al., 2001; Debdoubi et al., 2004).

Result

Moisture content for cotton stalks and rice straw briquettes

Fig (1) shows that, after the pressing of the chopped cotton stalks and rice straw to briquettes, the moisture content decreased compared with before the pressing. Moisture content of cotton stalks briquettes were pressed at 8, 10 and 12 % decreased to 7.4, 8.57 and 10.35 %, respectively. While moisture content of rice straw briquettes were pressed at 8, 10 and 12.8 % decreased to 7.13, 9.21 and 10.98 %, respectively. The decrement percentages of moisture content were (7.5, 7.9 and 13.75 %) and (10. 87, 12.5 and 8.5 %) for cotton stalks and rice straw briquettes, respectively.

Effect of moisture content on compression stress and durability for cotton stalks and rice straw briquettes

The relation between compression stress and durability with moisture content for cotton stalks and rice straw briquettes are shown in Fig. (2a and 2b). It can be noticed that, increase of moisture content decreased the compression stress and durability. And show that, the values of the moisture content and compression stress for briquettes presented as contour (line dark) red on the horizontal plane. It shows the highest values for the durability (□ 90 %), (> 80 %) and (> 94 %), (> 94 %) for cotton stalks and rice straw briquettes, without binder and with binder, respectively.

Effect of moisture content on compression stress and resiliency for cotton stalks and rice straw briquettes

The relation between compression stress and resiliency with moisture content for cotton stalks and rice straw briquettes are shown in Fig. (3a and 3b). It can be noticed that, increase of moisture content decreased the compression stress and resiliency increased. And show that, the values of the moisture content and compression stress for briquettes presented as contour (line dark) red on the horizontal plane. It shows the highest values for the resiliency (>10), (>12) and (> 19), (>14) for cotton stalks and rice straw briquettes without binder and with binder, respectively.

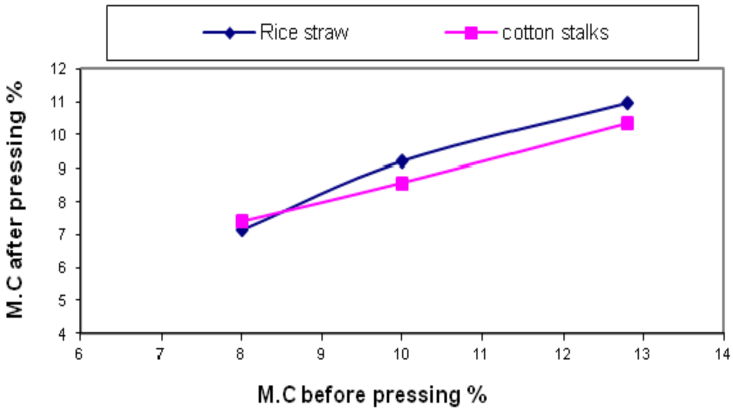

Fig. 1 The effect of pressing on the moisture content of cotton stalks and rice straw briquettes

Briquettes water resistance

The relation between water resistance and moisture content for cotton stalks briquettes and rice straw briquettes. It can be noticed that, increase moisture content decreased water resistance. The increment percentage of water resistance for cotton stalks briquettes was 16.17% and 73.53% during decreasing of moisture content from 8.57 % to 7.4% and from10.35% to 7.4%, respectively, at without binder. While the increment percentage of water resistance for rice straw briquettes 26.19% and 65.47% during decreasing of moisture content from 9.21% to 7.13% and from10.98% to 7.13%.

Effect of moisture content on gases emission of cotton stalk and rice straw

The relation between moisture content and gases emissions (CO, CO^2, NOx and SO_2) for cotton stalks and rice straw (loose and briquettes). It can be noticed that, by increasing of moisture content the gases emissions increase. The gases emitted from cotton stalks and rice straw briquettes were less than stalks loose. Increasing of moisture content from 7.4 to 10.35 % the CO2 emission increased from (2.2, 1.1and 1.6%) to (3, 1.6, and 2%) at cotton stalks (loose), cotton stalks briquettes without binder and with binder, respectively, the CO emission increased from (0.1197, 0.0098 and0.0175%) to (0.205, 0.015 and 0.0721%) at cotton stalks (loose) and cotton stalks briquettes without binder and with binder, respectively.

Resiliency% = -261.7925+39.5444*x+34.4434*y-1.2361*x*x-2.9141*x*y-0.8675*y*y

Resiliency% = -27.5969+7.2333*x+3.8013*y-0.2189*x*x-0.4643*x*y-0.051*y*

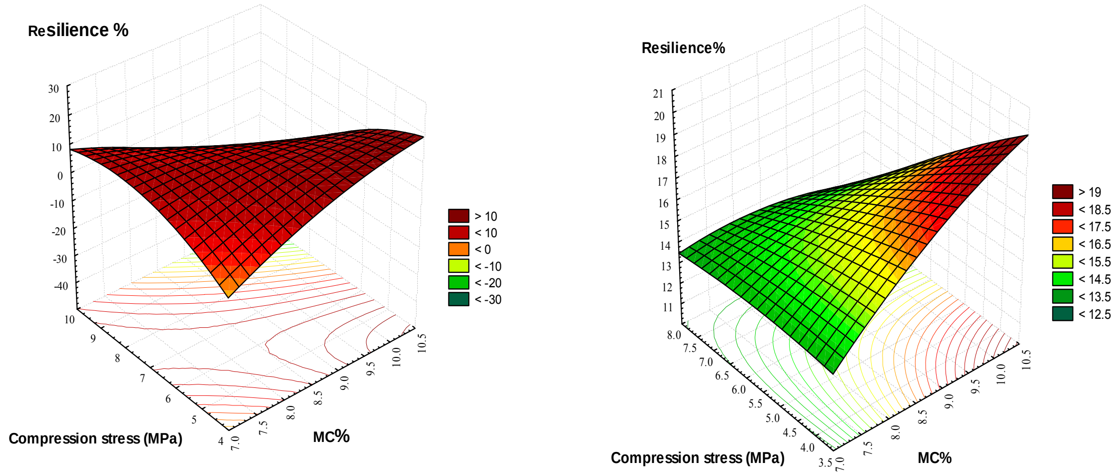

Without binder **With binder**

Fig. 3a Effect of moisture content on compression stress and resiliency for cotton stalks briquettes

Resiliency % = -155.2246+23.4389*x+13.6606*y-0.7622*x*x-1.0636*x*y-0.2461*y*y

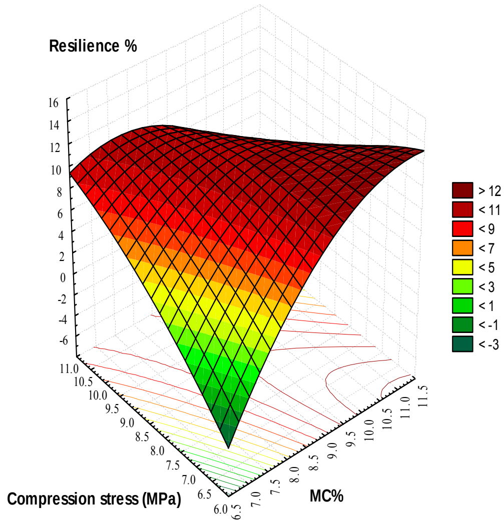

Without binder

Resiliency % = 33.9821-6.8295*x+2.8177*y+0.3892*x*x-0.0072*x*y-0.2373*y*y

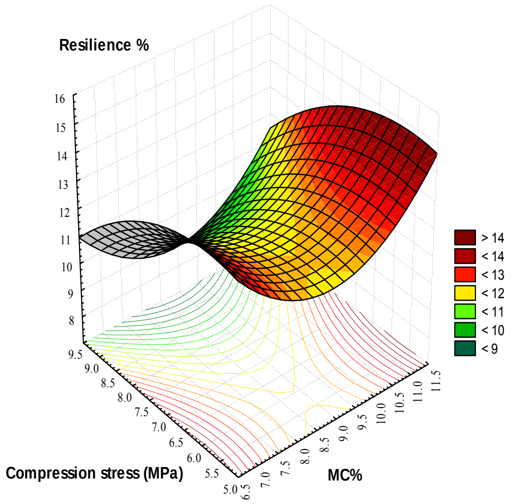

With binder

Fig. 3b Effect of moisture content on compression stress and resiliency for rice straw briquettes

Durability % = -192.6402+44.1899*x+31.6109*y-1.8471*x*x-2.4109*x*y-0.7676*y*y

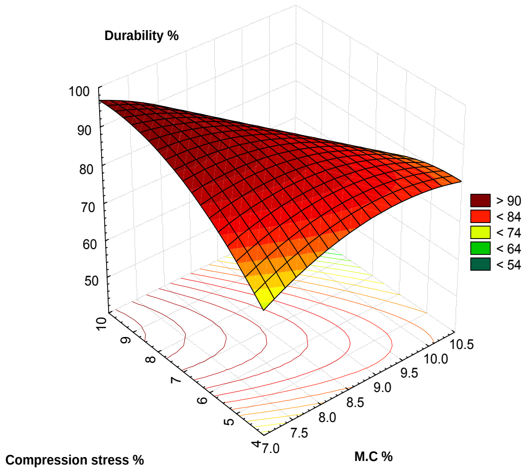

Without binder

Durability % = -378.5166+55.5382*x+101.6147*y-1.6143*x*x-7.2083*x*y-3.9764*y*y

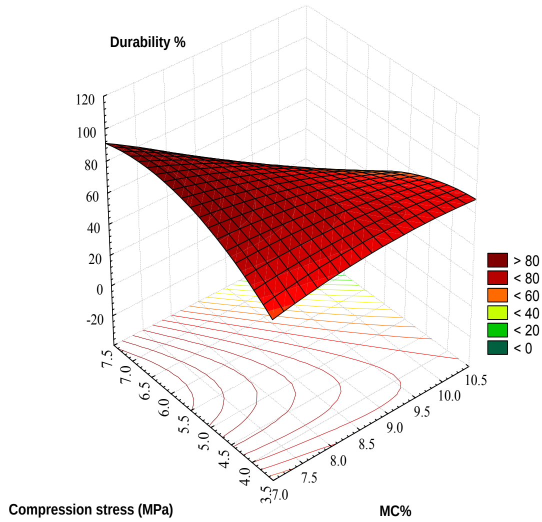

With binder

Fig. 2a Effect of moisture content on compression stress and durability for cotton stalks briquettes

Durability % = 135.2403-4.3794*x-5.6179*y+0.1247*x*x+0.1888*x*y+0.2565*y*y

Durability% = 678+5.2009*x+0.3272*y-0.1333*x*x-0.5945*x*y+0.4481*y*y

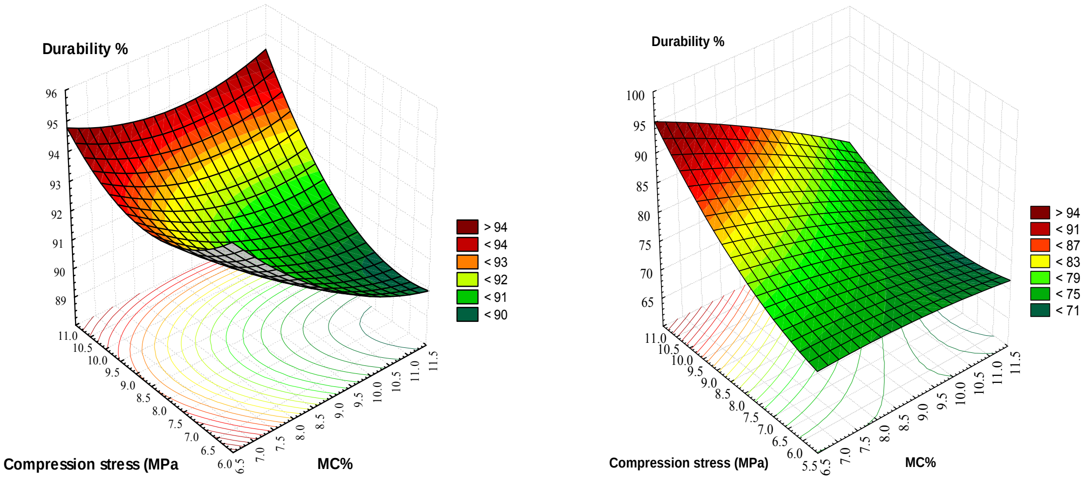

Without binder **With binder**

Fig. 2b Effect of moisture content of compression stress and durability for rice straw

Increasing of moisture content from 7.13 to 10.98 % the CO_2 emission increased from (3.2, 0.9and 1.6%) to (4.7, 1.6, and 2.3%) at rice straw (loose), rice straw briquettes without binder and with binder, respectively, and the CO emission increased from (0.324, 0.0105 and 0.018%) to (0.5681, 0.018 and 0.032%) at rice straw (loose), rice straw briquettes without binder and with binder, respectively.

Conclusion

Densification of biomass materials into briquettes could reduce costs and problems with handling, transportation, storage, and utilization of low bulk density biomass materials. And also, produce good quality (high strength and durability).

Moisture content of chopped residuals have a significant impact on the quality of the resulting briquettes the optimum quality properties of the briquettes were 7.4 and 7.13% moisture content of cotton stalks and rice straw, without binder, respectively. the highest compression stress, durability and bulk density were 8.95, 10.39 MPa, 97.06 %, 93.64 % and 1.18, 0.95 g.cm-3 for cotton stalks and rice straw briquettes, respectively Gases emission (CO2 and CO) during combustion reduced from cotton stalks and rice straw briquettes without binder than the briquettes with binder and cotton stalks and rice straw (loose) at each moisture contents.

Reference

Debdoubi A., El-amarti A., Colacio E., 2005. Production of fuel briquettes from esparto partially pyrolyzed". Energy Conversion and Management, 46: 1877–1884.

Demirbas A., 2000. Conversion of biomass to a pyrolytic oil for blending gasoline as an alternative fuel in internal combustion engines. Energy Sources; 23: 553–562.

Dubey A. K., Chandra P., Padhee D., Gangil S., 2007. Energy from Cotton Stalks and other Crop Residues. Cotton Advisory Board, 2007.

Fasina O.O., 2008. Physical properties of peanut hull pellets. Bioresource Technology, 99: 1259–1266.

Gibiiz B., Kucukbayrak U.S., 1996. Briquetting of Istanbul-Kemerburgaz lignite of Turkey. Fuel Processing Technology, 47: 111–118.

Jha S.K., Singh A., Kumar A., 2008. Physical characteristics of compressed cotton stalks. Biomass Engineering, 99: 205–210.

Nalladurai K., Morey R.V., 2009. Factors affecting strength and durability of densified biomass products. Biomass and Bio-energy, 33: 337–359.

Nalladurai K., Morey R.V., 2010. Natural binders and solid bridge type binding mechanisms in briquettes and pellets made from corn Stover and switchgrass. Bioresource Technology, 101: 1082–1090.

Panwar V., Prasad B., Wasewar K.L., 2011. Biomass Residue Briquetting and Characterization. J. Energy Eng.-ASCE 137: 108–114.

Stahl M., Granstrom K., Berghel J., Renstrom R., 2004. Industrial processes for biomass drying and their effects on the quality properties of wood pellets. Biomass and Bioenergy 27: 621–628.

Werther J., Saenger M., Hartge E.U., Ogada T., Siagi Z., 2000. Combustion of agricultural residues. Prog. Energ. Combust Sci, 26: 1–27.

Yamnan S., Sahan M., Haykiri-Açma H., Şeşen K., Küçükbayrak S., 2001. Fuel briquettes from biomass-lignite blends. Fuel Process Technol, 72: 1–8.

ENERGY CONSUMPTION OF MICROWAVE AND INFRARED DRYING OF LAUREL (LAURUS NOBILIS L.) BERRY

Tunahan Erdem[1], Serdar Öztekin[1], Sevil N. Karaaslan[2]

[1]Cukurova University Dept. of Agricultural Machinery in Adana, 01330 Balcalı, Turkey, Phone: +903386084-2230, Fax: +90-322-3387165, E-mail: terdem@cu.edu.tr
[2]Suleyman Demirel University, Faculty of Agriculture, Department of Agricultural Machinery, Isparta, Turkey

Abstract

In this research, drying characteristics and energy requirements for microwave and IR (infrared) drying of laurel berries. Infrared energy is very promising technology in drying procedure because of the low investment, maintain and energy consumption. Therefore microwave and infrared energy were compered in this study. During the experiments, Laurel berries were dried to the final moisture content of 7-9 % from 31.80-36.03 (w.b.). Drying by continuous microwave dryer three power levels were selected as 400, 600, 800 W. For infrared drying small scale drying room was constructed with 4 infrared heaters with maximum 20 kW heat power. The minimum and the maximum energy requirements for drying of laurel berries were also determined as 5.39-6.47 MJ/kg H_2O for microwave drying and 6.49-10.94 MJ/kg H_2O for IR drying.

The dried berries were subjected to the cold pressing to obtain the Laurel Berry oil. The max. oil yield was found 42.5 % (d.b.) at semi-ventilated mode of infrared drying .

Keywords: Laurel Berry, Drying, Microwave, Infrared

Introduction

Laurel (Laurus Nobilis L.) known as bay, daphne, bay laurel or sweet bay grows wild in the coastal areas of Mediterranean and the Black Sea. It is evergreen, large shrub tree and used since ancient times as medicinal and aromatic plant (Hafizoglu, Reunanen, 1993; Tuzlaci, Erol, 1999; Tuzlaci, Tolon, 2000; Longo, Vasapallo, 2005). The used parts of laurel are leaves and berries which are manually collected from wild flora. Locally this plant is evaluated as an important source to improve the income of indigenous people and contributes to the rural development. The fresh laurel leaves ripen in May-June. Main usages of laurel leaves are as herb or essential oil. For herbal production sun drying method is widely practiced. Essential oil from fresh laurel leaves is gained by steam distillation. The second used part of laurel plant is round, grape-sized berries with purplish black color. Laurel berries are manually picked up in November-December. Traditionally, laurel berry oil is extracted from fresh berries by boiling for several hours in an open drum of water using a wood fire. After the cooling the oil floating over the water is collected. The berry oil is also gained by organic solvent extraction or mechanical expression known as cold pressing. In practice oil yield by traditional method is about 10-12 % (w/w;).

The new post-harvest strategy for laurel berries suggested in this research is defined as follows;

1. Drying laurel berries till to 9 % of moisture (wet basis);
2. Cold pressing;
3. Extraction of oil cake gained from cold press.

The first step of new three stages processes is drying which plays a curious role. That means, as long as the laurel berries are not dried till to 9 %, cold press or extraction methods don't work. From the drying point of view three parts could be identified in single laurel berry, which are skin, flesh and an inner kernel (single seed). The whole berry, flesh, skin, and kernel contain 26, 38.8, and 18 % oil, respectively (Yazicioglu, Karaali, 1983). The outer skin and flesh with the 64.8 % oil content are actually very important morphological parts of berry with regard to drying. Because of the berry structure; any drying method applied to this crop should be sufficient to get the moisture from inside, but parallel to this it shouldn't cause any quality or quantity loss in the oil.

Therefore in this study microwave and infrared energy were applied to the Laurel Berry drying to achieve the low energy consumption and reduced drying time To compare the efficiency of energy electricity consumption of both applications were measured. Then the specific energy consumption was calculated.

Material and Method

Material

Laurel berries were provided from South-East Mediterranean cost of Turkey. They were washed and stored at 4 ± 0.5 ºC, at refrigerator for about one day equilibration of moisture. The initial moisture content of material was determined by standard oven method at 105 ºC for 24 h.

Drying equipment and procedure

For drying, microwave (MWD), and infrared (IRD) drying methods were used. Microwave drying were carried out by 11 kW microwave belt dryer with a maximum output of 8000 W at 2 450 MHz. The length and width of the belt were 5 m and 0.15 m, with 2.7 m active belt length respectively. The microwave power was generated by 10 magnetrons. To force the air on the belt two ventilators in inlet and outlet of the drying tunnel were used. The air speeds in drying tunnel were selected as 1.15 and 2.30 m/s, respectively. The crop density on the belt was 6 kg/m^2 which represent one layer of berries. Moisture losses for microwave drying were measured before and after drying by precision balance (Sartorius, precision: 0.01 g, maximum weighing capacity: 2 000 g). Three replications were carried out for each experiment.

Infrared drying procedure was selected to give the small entrepreneurs a possibility to build simple drying room that is heated by IR lamps (Fig. 2). Therefore a simple isolated room having a dimension of 3mx3mx3m and heated by IR lamps was build. Four IR heaters were mounted on the two opposite walls of room. Total capacity of heaters in drying room was 4x5 kW. The crops were dried on trays. For IR heating two operational modes could be selected where the drying air could be circulated in closed loop with or without mixing fresh air. The crop density on drying trays was 6 kg/m2. For IR, hot air and vacuum moisture losses were measured in every two hours until they reach the final moisture of under 10 % (w.b.).

Cold Press Procedure

Dried laurel berries were pressed by screw press having a nozzle diameter of 6.8 mm and a rotational speed of 47 rpm. Three replications were performed for each sample and oil yield was calculated as percentage in weight basis. After pressing, the remained oil in cakes was extracted by soxhelet apparatus.

Fig. 1 Microwave Belt Dryer

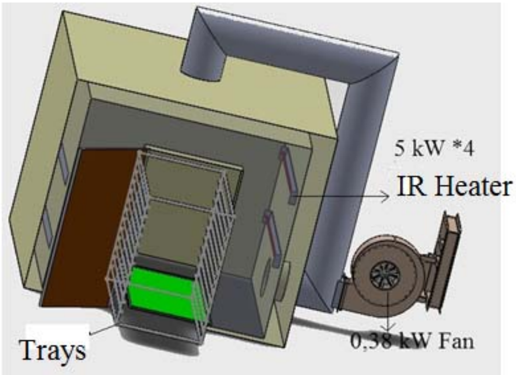

Fig. 2 IR drying room

Specific energy consumption

The drying of food material, a process of simultaneous heat and mass transfer, represents an energy intensive operation of some industrial applicaitons. The specific energy consumption was estimated, both in microwave and Infrared drying processes, considering the total energy supplied to dry Laurel Berries from initial moisture content of about 31.8-36.03 (w.b.) to a desired moisture content of 7.22 (w.b.). Energy consumption of microwave belt dryer and infrared drying room was measured by using an electrical power meter. Then specific energy consumption of microwave and infrared drying were calculated from the obtained data using the equations 2.1 and 2.2 below (Sharma, Prasad, 2006).

$$H_{ID} = \frac{h_1 + h_2}{W_e} \tag{2.1}$$

Where the H_{Id}; h_1; h_2 and W_e are the specific energy consumption of Infrared drying (MJ/kg), energy consumption of Infrared heater (MJ), energy consumption of fan (MJ), amount of evaporated water (kg) respectively.

$$H_{mw} = \frac{h_1 + h_2 + h_3 + h_4}{W_e} \tag{2.2}$$

Where the H_{mw}; h_1; h_2; h_3; h_4 and We are the specific energy consumption of microwave drying (MJ/kg), energy consumption of microwave generator (MJ), energy consumption of inlet and outlet fans (MJ), energy consumption of microwave fans (MJ), energy consumption of belt rotation motor (MJ), amount of evaporated water (kg) respectively.

Results and Discussion

Tab. 1and Tab. 2 shows drying time, kernel temperatures and initial and final moisture contents. These results shows, that it was possible to reach the final moisture content of under 10 % (w. b.) at the microwave level of 800 W and air velocity of 2.30 m/s.

Tab. 3 shows the oil yield of microwave and Infrared dried Laurel Berries. Form the data total oil yield was higher at Infrared drying. Because of the high temperature of microwave drying oil yield was decreased. During the microwave drying some explosion has been seen. Therefore the oil yield of microwave drying was lower.

Tab. 1 Microwave Drying (MWD) Parameters Used For Drying Of Laurel Berries

Air velocity (m/s)	Microwave power level (W) & belt speed (m/s)	Initial moisture content (w.b.)	Final moisture content (w.b.)	Surface temperature (ºC)	Internal kernel temperature (ºC)	Drying Time (min)
	400 W; 0,0062	31,80	14,36	111,80	88,80	8
2,30	400 W; 0,0068	31,80	16,01	106,40	78,90	7
	400 W: 0,0081	31,80	21,36	106,10	91,60	6,5
	400 W; 0,0062	30,82	17,28	181,10	91,30	8
1,15	400 W; 0,0068	30,82	21,86	147,40	87,10	7
	400 W: 0,0081	30,82	26,00	140,70	91,40	6,5
	600 W; 0,0062	31,80	13,87	114,60	89,40	8
2,30	600 W; 0,0068	31,80	18,70	116,80	85,40	7
	600 W: 0,0081	31,80	18,90	118,30	90,90	6,5
	600 W; 0,0062	30,82	16,06	159,90	83,30	8
1,15	600 W; 0,0068	30,82	14,02	157,50	85,60	7
	600 W: 0,0081	30,82	18,50	142,80	92,90	6,5
	800 W; 0,0062	30,82	7,22	193,30	96,20	8
2,30	800 W; 0,0068	30,82	7,63	155,90	103,20	7
	800 W: 0,0081	30,82	14,64	158,30	91,80	6,5
	800 W; 0,0062	30,82	10,65	194,40	178,00	8
1,15	800 W; 0,0068	30,82	10,80	255,00	125,70	7
	800 W: 0,0081	30,82	17,02	157,80	87,10	6,5

Tab. 2 Infrared Drying (IRD) Parameters Used For Drying Of Laurel Berries

Air flow type	Initial moisture content (w.b.)	Final moisture content (w.b.)	Surface temperature (ºC)	Internal kernel temperature (ºC)	Drying time (min)
Closed loop circulation	36.03	9.90	109.6	59.7	1 140
Circ. with fresh air mixing *	36.03	6.83	123.0	69.8	960
Closed loop circulation	20.28	6.43	83.0	58.1	480
Circ. with fresh air mixing	20.28	5.85	113.0	68.1	480

Tab. 3 Oil Yield from laurel berries after Pressing and Extraction by different methods

Drying Methods	Cold press (%)	Solvent extraction (%)	Total (%)
Microwave Drying (**MWD**)	25.4±0.024[a]	11.6±0.003[a c]	37.5±0.022[b]
Infrared Drying (**IRD**)	17.9±0.005[b]	24.6±0.007[b a]	42.5±0.012[a]

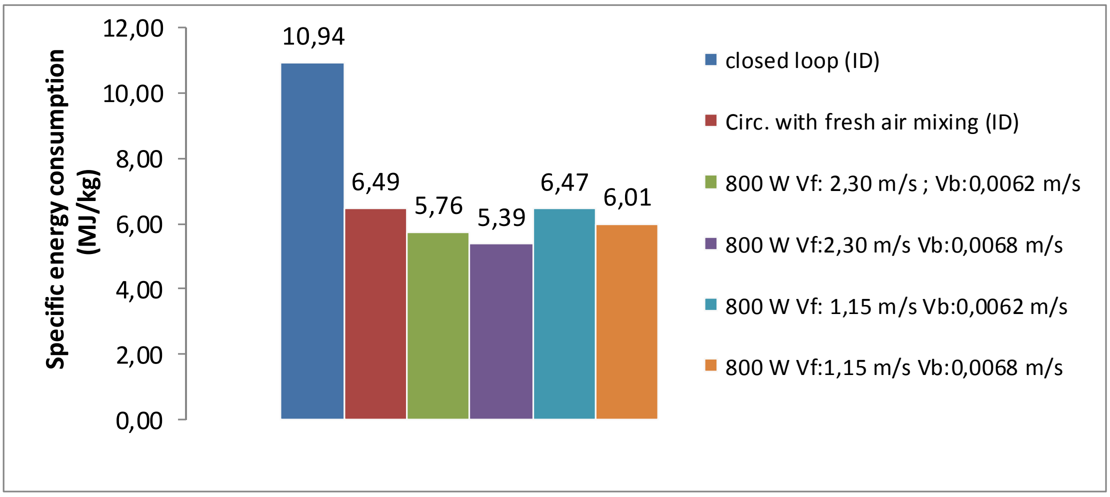

Fig. 3 Specific energy consumption of various application

The specific energy consumption of microwave and Infrared application is shown in Fig. 3. As we see from the illustrated figure as below the specific energy consumption of microwave and Infrared drying were close to each other when the circulation with fresh air mixing mode was applied for Infrared drying. The lower specific energy consumption was 5.39 MJ/kg for 800 W microwave drying (2.30 m/s Vb = 0.0068 m/s) and higher value was recorded at closed loop Infrared drying with 10.94 MJ/kg. The energy consumption of infrared drying was depend on the air circulation. For microwave drying the energy consumption was lower at 2.30 m/s air flow rate too. From this point to reduce the energy consumption air flow application must be optimized.

Conclusion

Drying is very important procedure to store the product and first step of many post-harvest applications. Nowadays microwave and infrared drying application is becoming widespread. Microwave energy has some advantages on drying issue, such as shorter drying time, lower energy consumption. From the data the microwave application consumed less energy than infrared application. On the other hand because of the high internal temperature the obtained oil yield was lower than Infrared drying. So that Infrared energy could be used oily products to preserve its oil yields and compositions. To reduce the energy consumption of infrared drying could be possible by optimizing the air flow rate. And most important factor to choose the infrared application is low investment and maintains cost.

Reference

Hafizoglu H., Reunanen M., 1993. Studies on the components of Laurus nobilis from Turkey with special reference to Laurel berry fat. Fat Sci Technol, 8:304–308.

Longo L., Vasapollo G., 2005. Determination of anthocyanins in Ruscus aculeatus L. berries. J.Agric Food Chem. 26, 53(2): 475-9.

Sharma G., Prasad S., 2006. Specific energy consumption in microwave drying of garlic cloves. Energy, 31: 1921–1926.

Tuzlaci E., Erol M.K., 1999. Turkish folk medicinal plants, part II: Eğirdir (Isparta), Fitoterapia, 70: 593–610.

Tuzlaci E., Tolon E., 2000. Turkish folk medicinal plants, part III: Sile (Istanbul), Fitoterapia, 71: 673–685.

Yazicioğlu T., Karaali A., 1983. Fette. Seifen Anstrichm, 85: 23-29.

SEPARATION OF SUNFLOWER SEEDS COMPONENTS BY PNEUMATIC SEPARATOR

Gamea G. R.

Agricultural Systems Engineering Department, Faculty of Agriculture and food sciences, King Faisal University, Saudi Arabia, E-mail: gamea_gamalrashad@yahoo.com , ggamea@kfu.edu.sa , Phone:00966501722535

Abstract

The first part of the present study deals with some physical and mechanical properties for sunflower seeds components (seeds, hulls and kernels) related to pneumatic separation which are evaluated as a function of change in moisture content from 8 % to 14 % (d.b.). Simple linear empirical equations were developed to predict sunflower seeds components properties according to moisture content. All dimensions, mass, angle of repose, coefficient of fraction, and terminal velocity increased linearly with the moisture content increased up to 14 %, while the bulk density decreased linearly with the moisture content increased. The second part was carried out on a series of experiments to specify the optimum conditions of separating operation which ensure the highest grade of separation efficiency with minimum losses. The combination of air velocity, feed rate, percentage of broken kernels and moisture content affected significantly the separation efficiency and kernel losses. Air stream velocity of 3.5 m/s combined with 30 kg/h feed rate, 10 % broken kernels and (10 – 12 %) moisture content can be considered the most favorable combination values of these variables to obtain the highest separation efficiency with minimum kernel losses.

Keywords: separation, sunflower, pneumatic separator

1. Introduction

Sunflower seed (*Helianthus annuus L.*) is an important oilseed crop because it contains a large quantity of highly nutritious oil. Sunflower considered as one of the most Egyptian leading oilseed crops; it could be planted in several soil types under varied climate condition.

EL-Shaer et al. (1993) mentioned that, sunflower seeds contained approximately 30 % hull and 70 % Kernels. The hulls contain the high fiber, low protein and high wax and only 2 – 3 % oil. Large proportion of oil is retained by the high percentage of hull of oil seeds. If the hulls are removed from the seed before processing, it would yield comparatively more volume of oil, decrease the production cost of edible oil and consequently increase the rate production of oil because removing of the hull from seeds decreased the mass of the used seeds.

Hulling is a process of removing hulls from the oil bearing seeds for obtaining high quality edible oil by the processing of kernels. This reduces fibrous content of the meal and increases the marketability as stock feed. About 99 % of oil is stored naturally in kernels and the hulls contain not more than 1 % oil. If the hulls are not removed they reduce the total yield of oil by absorbing or retaining oil in the pressed cake. In addition to this the wax and coloring matters present in the hulls get mixed with the expressed edible oil. After hulling of sunflower seeds, it is necessary to remove the separate hulls, therefore separating machine is needed. The separation of sunflower kernels from a hulled mixture is very difficult due to the slight difference of the properties of the mixture components and the lack of information about the methods of separation of this product. In handling and processing of several agricultural products, air is commonly used as a carrier for transport (Kilikan, Guner, 2006) or for separating the desirable products from unwanted materials (Khoshtaghaza, Mehdizadeh, 2006). In pneumatic separators, air is used for separation of products according to its differences in size, shape, density, and characteristics of surface air resistance. Air is supplied by a centrifugal fan with an adjustable inlet for controlling the flow. Air is moved through a separating duct into which the mixture dropped. Heavy materials (grains or kernels) drops on to a tray and collected. While the material carried by the air stream (unwanted material) is lifted to an air separator from which it is removed from the system. Gamea (2004) mentioned that, using the air as method of separating of rap-seed considered efficient to obtain satisfactory values of separation efficiency with minimum losses. Ilori et al. (2011) studied physical properties of Mexican sunflower seed, Gupta et al. (2007) evaluated the terminal velocity of sunflower seeds of three cultivars namely NSFH-36, PSF-118 and SH-3322 as a function of moisture content and concluded that the variation in moisture content as well as variety either individually or in combination influences terminal velocity and drage coefficient significantly.

The main objectives of the present study may be summarized as follows:

1. To identify the physical-mechanical properties of sunflower product components (seeds, hulls and kernels) and it is correlation with change in moisture content to predict the air velocity required for separation of kernel from hulls.

2. To carry out a series of experiments to specify the optimum conditions of separating process, which ensure the highest grade of separating efficiency with lowest kernel loss.

2. Materials and methods

2.1. Materials

Sample of the sunflower seeds (Vidoc variety) were taken from Oil Crops Institute, Ministry of Agriculture, and have been used in this study. Sunflower seeds were hulled by a prototype for sunflower seeds hulling (Gamea, Mohamed, 2011). Components of hulled product (full kernels, broken kernels and hulls) were separated manually. Kernels to hulls ratio was calculated as the ratio of mass of dry kernels to the mass of dry hulls. The shape and size of samples were determined by measuring the length (L), width (W), thickness (T), geometric diameter (Gd) , arithmetic diameter (Ad), flat surface area(Fs), transfer surface area(Ts) and sphercity (s %). The main dimensions of seeds, kernels and hulls (L, W, and T) under experiment were measured by digital calipers. The following equations (El-Raie, 1988) were used to calculate the values of the mentioned properties:

$Gd= (LWT)^{1/3}, mm$,

$Ad= (L+W+T)/3, mm$, $Fs = \pi/4\ LW, mm^2$,

$Ts = \pi/4\ TW, mm^2$, S= (Gd/l) x 100, %

The moisture content M.C.(d.b.) of the mixture, hulls and kernels was determined by a low constant temperature oven method . The static friction angle for samples (seeds, kernels and hulls) was measured against two structural materials (rough rubber and galvanized iron). (Mohsenin, 1986).The designed combined parallelogram and protractor was used to measure the angle of repose. The samples was conditioned to required moisture content level by adding the required amount of water, stirring occasionally and allowing it to achieve equilibrium, then the moisture content was checked again. The terminal velocity of the seeds, kernel and hull was obtained according to Awady and El-Sayed (1994). Dwyer Thermal Anemometer 470 was used to measure the air stream velocity (ft/min) then the readings were converted into m/s.

2.2 Experimental procedure

The pneumatic separating equipment as sketched in Fig. 1 was used in the present study.

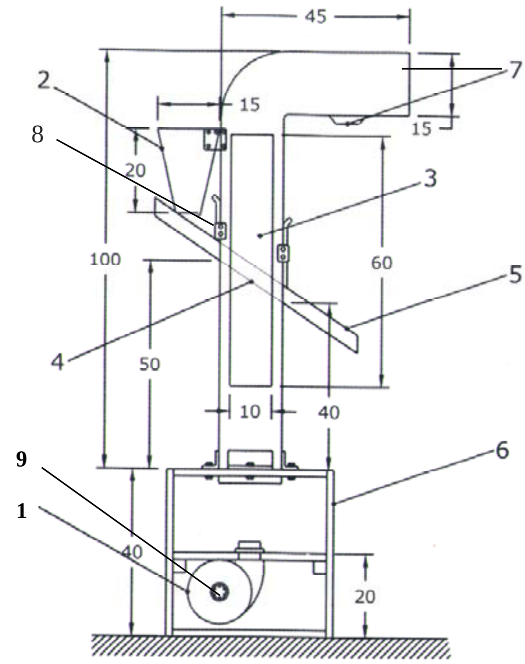

Fig. 1A sketch of the separating equipment
1- Centrifugal blower. 2- Feeding hopper. 3- Vertical separating duct. 4- First screen. 5- Kernel gate. 6- Frame. 7- Sediment chamber. 8- Feeding gate. 9- Second screen. Dims: cm

The main tested factors for separating unit were as follow:

1-Three different levels of mixture moisture content (d.b.) (8, 10, 12 and 14 %).

2-Three different quantities of broken kernel in sample (10, 20 and 30 %).

3-Three different velocities of air stream (3, 3.5 and 4 m/sec).

4-Two different feeding rates (30 and 50 kg/h).

The performance of the separating unit was evaluated from the point of view of separating efficiency and percentage of kernel losses.

The equations used for separating efficiency and kernel losses according to by (Ismail et al., 1994) as follow: $S.E\ \% = (M_2 - M_1)/(M_2) \times 100\ \%$

$S.E$ = Separating efficiency, %;

M_1 = the mass of hulls in the out kernel tank, g;

M_2 = the mass of hulls in feeding hopper, g.

$K.L = (M_4 - M_3)/(M_4) \times 100\ \%$

$K.L$ =Percentage of Kernel losses, %;

M_3 = the mass of kernel in the out kernel tank, g;

M_4 = The mass of kernel in feeding hopper, g.

The analysis of variance test (ANOVA) was used to test the effect of the experimented independent variables on separation efficiency and kernels losses percentage.

3. Results and discussions

3.1. Physical properties of seeds, hulls and kennels

All the dimensions were increased with moisture content up to about 14 %. The total average expanded was moving along its minor axis in comparison with its other two principal axes. This behavior was also observed by Dehspande (1993).

The results showed that the relationship between dimensional characteristics and moisture content of the studied samples suggested in trend with the results of Amer (2009).The surface area of both transfer and flat were increased with moisture content up to about 14 %.

As the moisture content increased from 8 to 10 % (d.b.), the bulk density decreased from 450.45 to 408.2, from 240.4 to 212.3 and from 690.6 to 615.1 kg/m^3 for seeds, hulls and kernels respectively.

A linear increase in angle of repose when the material moisture content increases has also been noted for sun flower seeds by Gupta (1997).

The mean value of angle of repose for. The mixture of hulls and kennels were 31.0, 32.8, 34.5 and 35.8 for mixture moisture content 8, 10, 12 and 14 % respectively.

The static coefficient of friction increased also linearly with respect to moisture content up to 14 %. As moisture content increased, the terminal velocity tend to increase linearly for seed, hulls and kernels. Similar increasing trend was observed for terminal velocity with increase in moisture content for edible squash seed (Paksoy, Aydin, 2004), for rapeseed (Calisir et al., 2005), for pin nut (Ozguven et al., 2005), for sunflower seed (Gupta et al., 2007) and for turgenia latifolia seeds and wheat kernels (Nalbandi et al., 2010). The terminal velocity was much lower for hull than that for seed and kernel at all levels of moisture content. However, the difference between the hull and the seed was more than with seed and kernel.

3.2. Evaluation of separating prototype

The performance of the prototype was defined by the separating efficiency % and kennels loss %. Fig. 2 show the relationship between the moisture content and separation efficiency at different values of air stream velocity (3, 3.5, 4 m/s), broken kennel percentage (10, 20 and 30 %) and feeding rate (30 and 50 kg/h). Fig. 3 show the relation between kernels losses % at different levels of all variables.

Generally, the results showed that, separating efficiency increased by increasing the air stream velocity. The minimum separating efficiency was 73.8 % at 3 m/s air velocity, 50 kg/h feed rate, 30 % broken kernel and 14 % moisture content. The maximum value of 100 % was obtained at 4.0 m/s, 30 kg/h, with all moisture contents and broken kennels. At all feeding rates, it was observed that, with increasing air stream velocity from 3 to 3.5 m/s, the increasing rate for separation efficiency was more than the increasing rate with increasing air stream velocity from 3.5 to 4 m/s. It may be due to that, air stream velocity 3.5 m/s was greater than the critical velocity for hulls. While, the lowest values of separation efficiency at lowest air stream velocities were due to the presence of some hulls with the kernel recovered because the airflow was insufficient to carry all the hulls out with it. On the other hand the results showed that, kernel losses percentage increased with the increase of air stream velocity. The highest mean percentage of losses was 20.0 % observed at 4m/s air velocity, 8 % moisture content, and 30 kg/h feed rate. While, the lowest mean percentage of losses was 0.0 % at 3.0 m/s air stream velocity, 10 % broken kernel and all feeding rates.

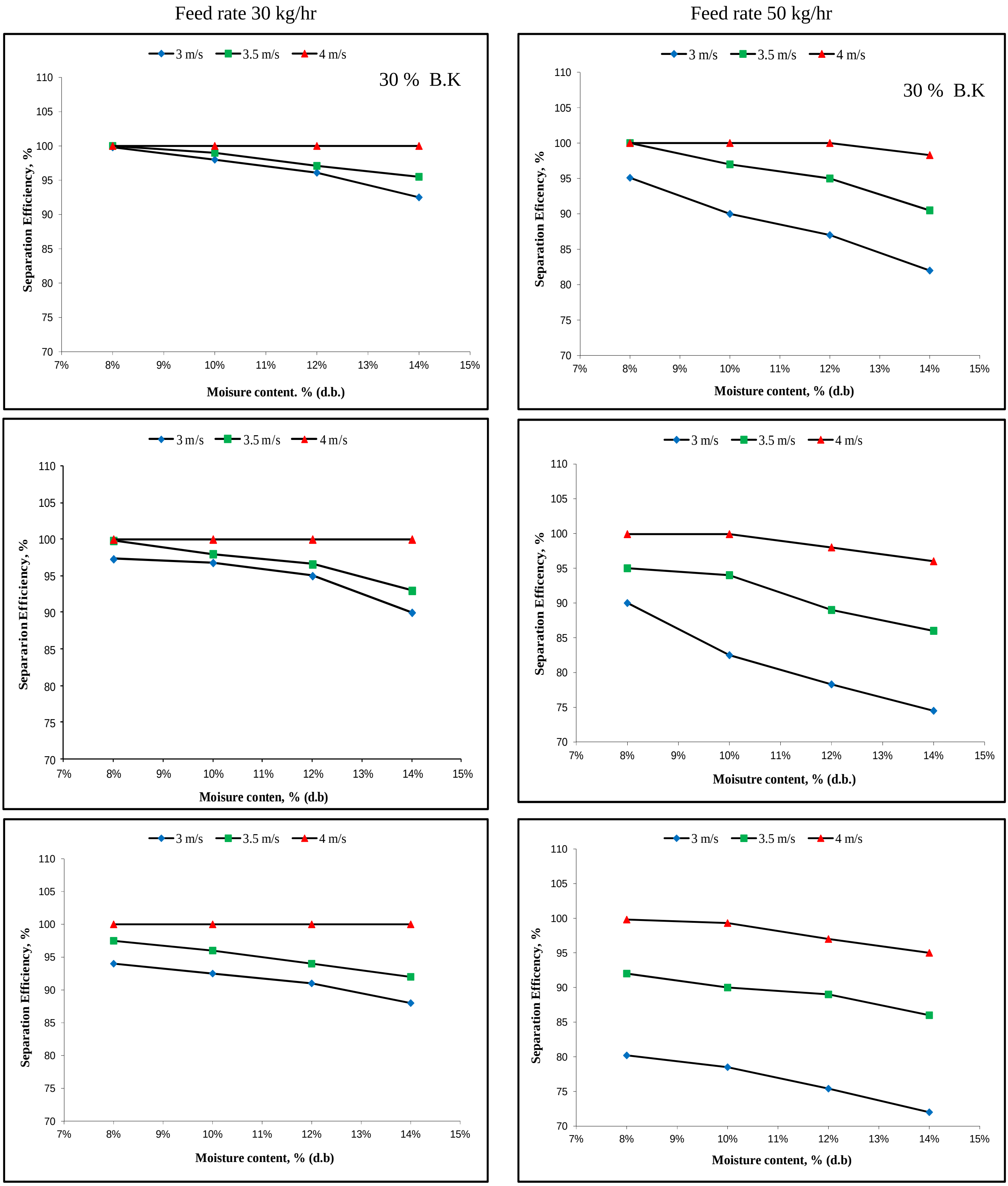

Fig. 2 Effect of moisture content on separation efficiency at different levels air stream velocity, broken kernels and feed rate

Feed rate 30 kg/hr   Feed rate 50 kg/hr

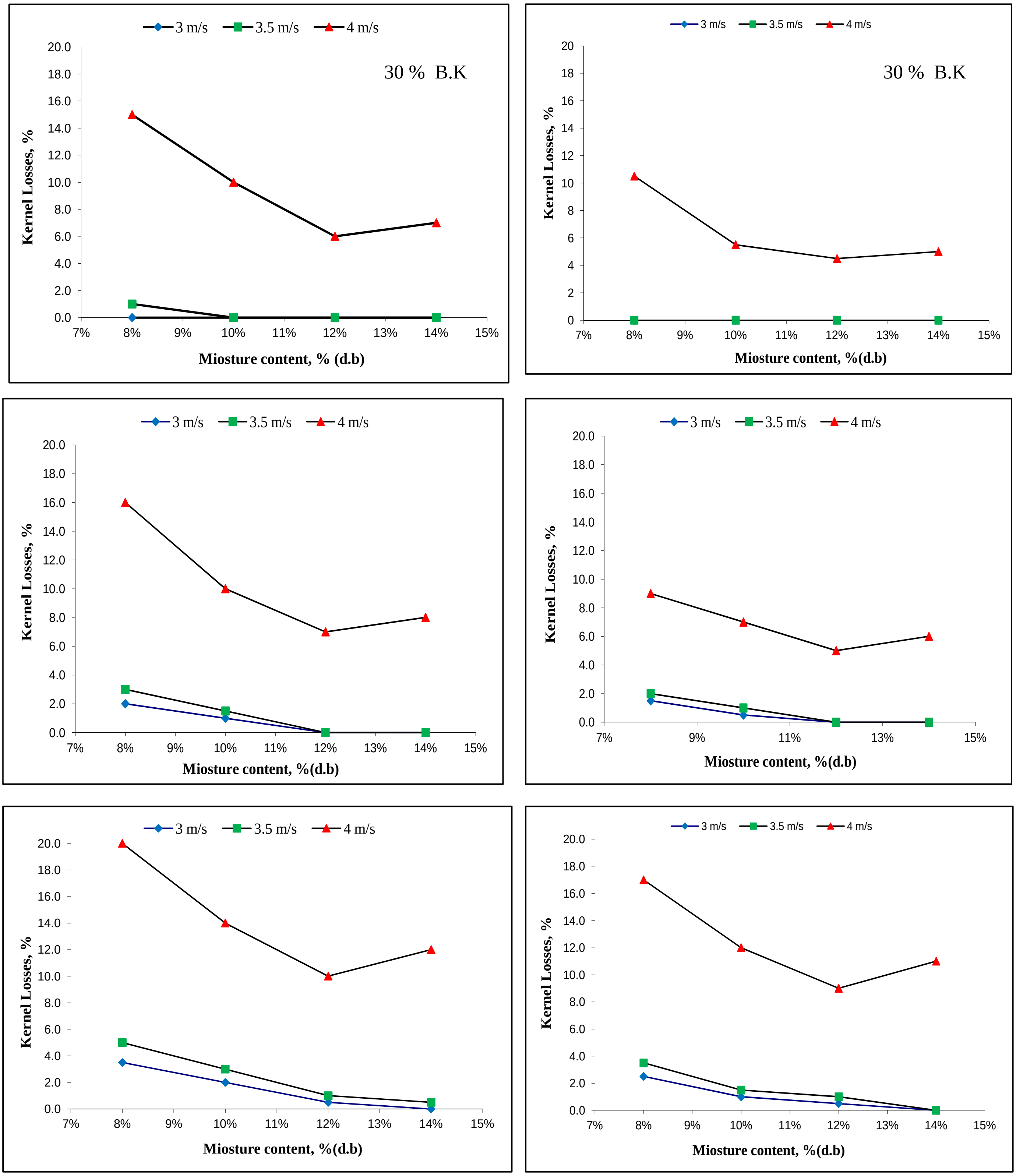

Fig. 3 Effect of moisture content on kernel losses (%) at different levels air stream velocity, broken kernels and feed rate

Conclusion

1-The physical properties of sunflower seeds, hulls and kernels varies linearly with moisture content

2-The average terminal velocity for sunflower seeds was 4, 4.5, 4.9 and 5.5 m/s, for sunflower hulls 1.9, 2.3, 2.7 and 3.1 m/s and for sunflower kernels was 5.4, 5.7, 6.1 and 6.5 m/s at moisture content 8, 10, 12 and 14 % (d.b.) respectively

3-The air stream velocity was a major controlling factor that affects the separating efficiency and kernel losses. The air stream velocity, which fulfilled the best results was 3.5 m/s.

4- The decrease of broken kernels percentage improved the separation efficiency and kernel losses

5- Air stream velocity of 3.5 m/s combined with 30 kg/h feed rate, 10 % broken kernels and (10 – 12 %) moisture content can be considered the most favorable combination values of these variables to obtain the highest separation efficiency with minimum kernel losses.

6- Using the air as the method of separating of sunflower kernel considered efficient to obtain satisfactory values of separation efficiency with minimum kernel losses at suitable levels of feed rate, broken kernels and moisture content.

References

Amer A.H., 2009. Aerodynamic and solid flow properties for flaxseeds for pneumatic separation by air stream. International Journal of Agricultural and biological Engineering, vol. 2. No 4: 31 – 45.

Awady M. N., El-Sayed A. S., 1994. Separation of peanut seeds by air stream. Misr J. Ag. Eng., 11 (1): 137-147.

Calisir S., Ozcan M., Hacisefergullari H., Yildaz M. U., 2005. A study on some physic-chemical properties of turkey okra seeds. Journal of Food Engineering, 68: 73 – 78.

Cumble L.O., Maina C., 1990. Friction coefficient of cereal seeds on varies surface agricultural mechanization in Asia. Frica and Latine America, 2 (4): 61 – 64.

Dehspannd S.D., Bal S., Ojha T.P., 1993. Physical properties of soybean. J. of Agric. Eng. Research 56: 89 – 98.

El-Raie A.E.S., Naser G.E.M., El-Ebaby F.G.I., El-Adawy W.M.I., 1998. Study of some physical and engineering properties for sunflower heads and seeds concerning the design of threshing devices. 6th conference of Misr society of Agr. Eng., 21-22 October 1998: 153-176.

El-Shaer M.S., Abdelazez A., Kandel M.H., Elsayed, 1993. Oil and suger crops book. Cairo University, Egypt.

Gamea G.R., 2004. Separation of rape seed by using air stream. Minufiya journal of Agricultural Research, 29 (4): 813-830.

Gamea G.R., Mohamed M.E., 2011. Design and manufacturing of prototype for sunflower seeds hulling. 28 (2): 468-486.

Gupta R.K., Das S.K., 1997. Physical properties of sunflower seeds. Journal of Agricultural Engineering Research, 66: 1–8.

Gupta R.K., Arora G.A., Sharma R., 2007. Aerodynamic properties of sunflower seed. Journal of Food Engineering, 79: 889-904.

Ismail Z.I., Hana K.F., Kassem M.A., 1994. Factors affecting grain cleaning efficiency. Part 2: Separating via vertical air streams, Misr J. Ag. Eng., 11 (1): 227-238.

Ilori T.A., Oradugba O.B., Raji A.O., 2011. Physical properties of Mexican sunflower seed. International Agrophysics, 25: 299-302.

Khoshtaghaza M., Mehdizadeh R., 2005. Aerodynamic properties of wheat kernel and straw materials. Agricultural Engineering International: The CIGRE journal, Vol. VIIII:5007.

Kilikan A., Guner M., 2006. Pneumatic conveying characterstics of cotton seeds. Biosystems Engineering, 95 (4): 537–546.

Mohsenin N.N., 1986. Physical properties of plant and Animal materials. Gordon and Breach Sc. Pub, N. Y.

Nalbandi H., Seiiedlou S., Ghassemzadeh H.R., 2010. Aerodynamic properties of turgenia latifolia seeds and wheat kernels. International Agrophysics, 24: 57–61.

Ozguven F.F., Vursavus K., 2005. Some physical, mechanical and aerodynamic properties of pine nuts. Journal of afood Engineering. 68: 191-196.

IRRIGATION IMPACT ON LEAF AREA AND NET PHOTOSYNTHETIC PRODUCTIVITY OF CANOLA

Antoaneta Gigova, Milena Moteva*, Totka Mitova, Georgi Kostadinov

Research Institute of Soil Science, Agrotechnologies and Plant Protection
3 Shose Bankya Str., Sofia 1331, Bulgaria
Phone: +359 2 89 29 305, Fax: +359 2 824 78 42, E-mail: milena_moteva@yahoo.com

Abstract

Crop productivity closely depends on the rate of leaf area development. The larger the leaf area is, the more photosynthetically active radiation is absorbed by plant, and the more dry-matter is accumulated. Water plays a key role to these processes. Since the climatic tendencies reveal future water scarcity in the Balkans, increasing irrigation water efficiency should be the main issue for the irrigated agriculture. The goal of the paper is to estimate the impact of different water supply on the rate of canola leaf area development and on the productivity of photosynthesis. Data of a field experiment with three varieties of was processed. The experiment was conducted in Sofia region, Bulgaria, on chromic luvisols. Three levels of soil moisturizing were applied – full irrigation (80 % of FC maintained), 50 % deficit irrigation and rain-fed conditions. Leaf area, biomass and dry matter were estimated five times during the spring vegetation period. The rate of leaf area index (LAI), photosynthetic potential, and net photosynthetic productivity (NPP) was calculated. The results show considerable impact of irrigation on those indicators, as well as on the final seed and oil yield. This investigation caters for the interests of Bulgarian canola production in the terms of the current EU strategy for climate change mitigation and energy assurance.

Keywords: leaf area, photosysthetic, canola

Introduction

Crop productivity closely depends on the rate of leaf area development. The larger the leaf area is, the more photosynthetic active radiation is absorbed by plant, and the more dry-matter is accumulated. Water plays a key role to these processes for it is responsible firstly, for the duration of the development stages, hence for leaf area formation and duration of leaf functioning and secondly, for the intensity of photosynthesis, hence for more assimilate accumulation, resulting in greater number of branches, flowers, siliques and seeds in a silique, greater seed mass and finally greater yield (Krogman et al., 1975; Mondul, Paul, 1995; Bonuelos et al., 2002). Winter canola is among the crops which are thought not to be irrigated in Bulgaria, because its vegetation period tallies with the soil water accumulation period and the crop avoids the dry period of the year. As to some recent establishments, Bulgarian climate is friendly to winter canola, but autumn and spring are risky for drought (Mitova, Moteva., 2011ab). Irrigation should be applied in order to ensure emergence and high yield. Local experiments show that irrigation has statistically significant effect on yield and yield components of canola. It contributes for 110-230 % seed yield increase and 100-220 % oil yield increase (Moteva et al., 2013). Some results from abroad reveal the impact of water stress conditions on some vegetative characteristics and accumulation processes in canola plant (Quaderi et al., 2012). When water is not readily available plants minimize the water losses by closing stomata, slowing down of the leaf area development and reducing it by throwing the leaves. Water deficit during the vegetative stage also slows down the stem and leaf development McKenzie (2009). Leaf area index (LAI) is smaller and sell concentration of CO_2 – lower than the optimal ones (Naderikharadji et al., 2008). But even a small deviation from a full water supply during flowering cause significant limitation of stomata conductivity and net assimilation rate (*NAR*) (Naderikharadji et al., 2008). This works for LAI and leaf area potential (*LAP*) decrease, because of wilting and falling of the leaves. Water stress conditions during flowering and siliqua formation causes 18-32 % less biomass and 19-39 % less seed yield (Gunasekara, 2003, 2006). Ahmadi, Bahrani (2009) and Moaveni et al. (2010) have established that water stress significantly impacts total dry matter (*TDM*), *LAI*, crop growth rate (*CGR*), relative crop growth (*RCG*) and *NAR*. During the initial stages *CGR* is slow (1.7–

5.2 g/m^2/d), it is maximal during the pre-reproductive and reproductive stages (6-25 g/m^2/d), and slowing down till harvesting time. The smallest values in their experiments are obtained under rain-fed conditions and the maximum ones – under full irrigation. RGR is greatest (0.077-0.120 g/g/d) during the initial stages and is maximal under full irrigation. *LAI*, *TDM* and *NAR* are also maximal (4.3 m^2/m^2, 1.8 g/m^2 and 5.88 g/m^2/d respectively) at full irrigation.

The goal of the paper is to estimate the impact of water supply on leaf area index (*LAI*), leaf area potential (*LAP*) and net photosynthetic productivity (*NPP*) of three varieties of canola. These data will be used for yield modeling and prediction.

Study Area

The field experiment was conducted in Sofia region, Bulgaria (42.6o N, asl 550 m) during the growing season 2011-2012. The climate according to Köppen Climate Classification System is temperate and humid continental. Freezing of plants in winter is practically insignificant. Rainfalls in September seeding period are of 61 % variability. In 75 % of the years, April-June rainfall totals are in the range of 150-300 mm, while reference evapotranspiration (ETo) is >300 mm. The atmospheric water supply cannot meet the potential evaporative requirements of the site. Irrigation is apparently needed (Moteva et al., 2012).

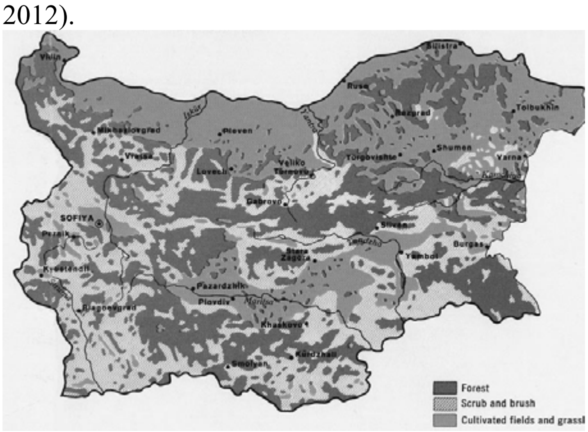

Fig. 1 Study area

Methods

The field experiment was put in a randomized complete block design as split-plot factorial arrangement in three replications. Irrigation was the main-plot factor. It consisted of three levels: full irrigation (a refill point (*RP*)=80 % of FC maintained), 50 % deficit irrigation and rain-fed conditions. Variety was the sub-plot factor: Triangle, PX100CL (Clearfield) and PR45D05 (Maximus). The soil was chromic luvisols. Irrigation was carried out by sprinkling technology. Leaf area of 10 plants in three replications for every variant was estimated by photographing and a follow-up processing in PHOTOSHOP environment. Leaf area index was calculated as: $LAI_i = \dfrac{LA_i}{F}$, m^2/m^2, where: LA_i – measured leaf area at *i*-moment, m^2; *F* – seeded area, m^2. Leaf area potential was calculated as: $LAP = \dfrac{LA_{i-1} + LA_i}{2} t$, m^2/m^2, where: LA_i и LA_{i-1} – leaf area in *i* and *i-1* moment, m^2/m^2; *t* – number of days between *i* and *i-1* moment. The rate of net photosynthetic productivity was calculated as: $NPP = \dfrac{B_i - B_{i-1}}{LAP}$ g/m^2/d/pl., where: B_i и B_{i-1} – plant dry matter *i* and *i-1* moment, g (Nichiporovich et al., 1961).

The weight of the plant components was determined using an electrobalance. Dry weight was obtained by drying the components at 60 °C for 72 hours in an isotherm oven and reweighning. The rainfall total of August-September 2011 was 62.6 mm and of March-July 2012 - 181.7 mm – both with 53.6 % and 38.7 % lower than the climatic values respectively. The periods August-September and March-July were very dry in the 1972-2011 statistical rows respectively. Analogously, the first one was very cool and the second one - extremely warm as to air temperature totals, and extremely dry, considering vapor pressure deficit totals (Tab. 1). Rainfall dis tribution within the vegetation period (Fig. 2) shows long dry periods in September and November 2011 and in April, June and July 2012. Two irrigation applications were given in the spring period – during pre-flowering and siliqua maturing.

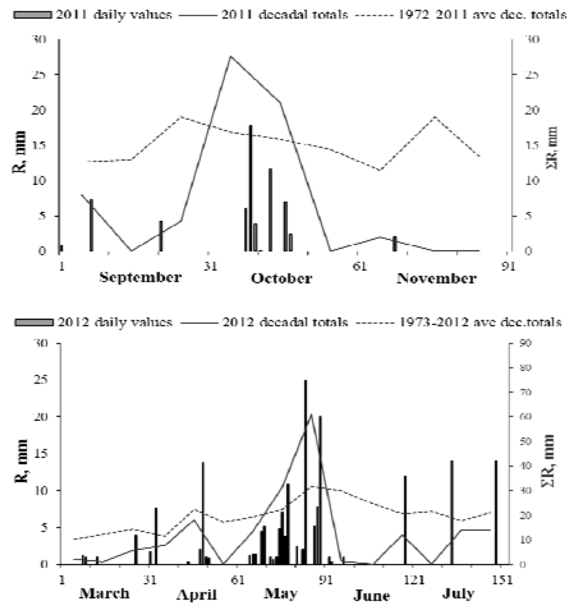

Fig. 2 Rainfalls: a) September-November 2010; b) March-July 2011

Results and discussion

Biomass

The leaf area potential of a variety and its sensibility to water predetermine the development of the biomass and the accumulation of the dry matter in plant organs. It is seen on Figs 3-5 that the stem had the greatest share in plant biomass. Under rainfed conditions the stems of Maximus were 53.4 g/pl., the leaves 29.1 g/pl., and the siliques - 42.1 g/pl. Triangle developed considerably greater biomass – 70.1 g/pl. stems, 36.2 g/pl. leaves and 67.1 g/pl. siliques. Irrigation contributed for prolonging the life of cells hence for prolonging photosynthesis and dry matter accumulation.

Tab. 1 Probability of exceedance

Meteorogical factor	Year	Probability, %	
		Sept.-Nov.	**Mar.-July**
Precipitation	2011	95.0	
	2012		92.5
Air temperature	2011	82.5	
	2012		10.0
VPD	2012		5.0

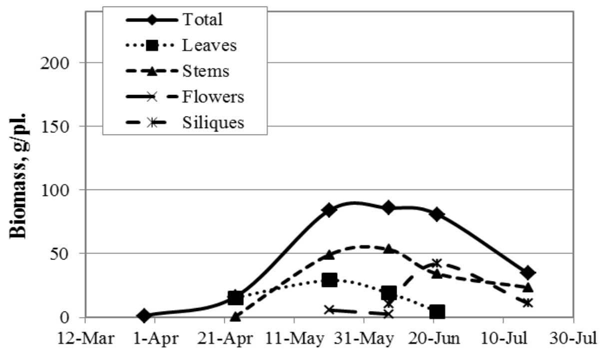

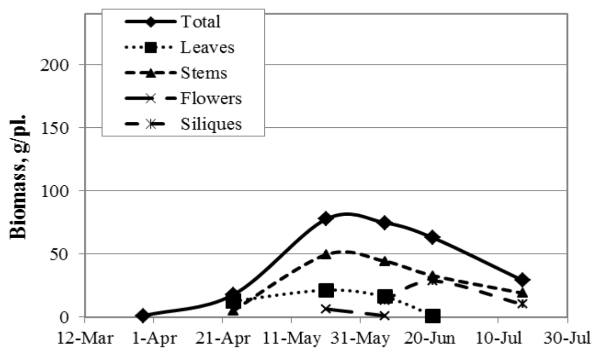

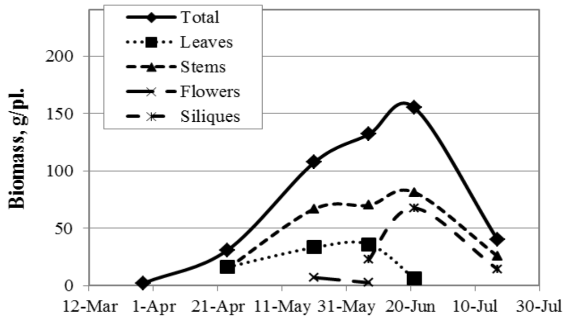

Fig. 3 Dynamics of biomass per plant under rainfed conditions. Left to right: Maximus; Clearfield;Triangle

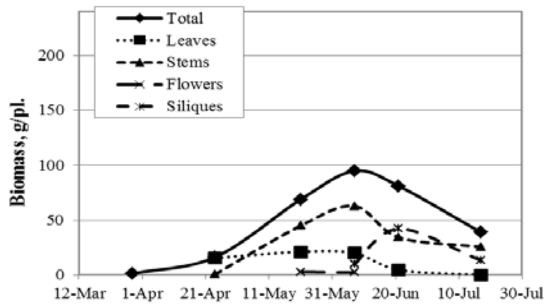

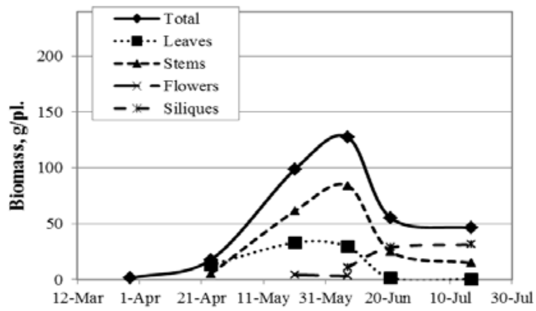

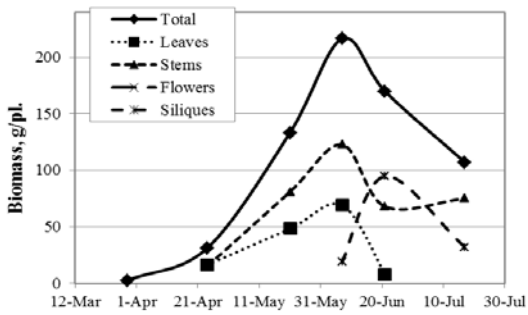

Fig. 4 Dynamics of biomass per plant under 50% deficit irrigation. Left to right: Maximus; Clearfield;Triangle

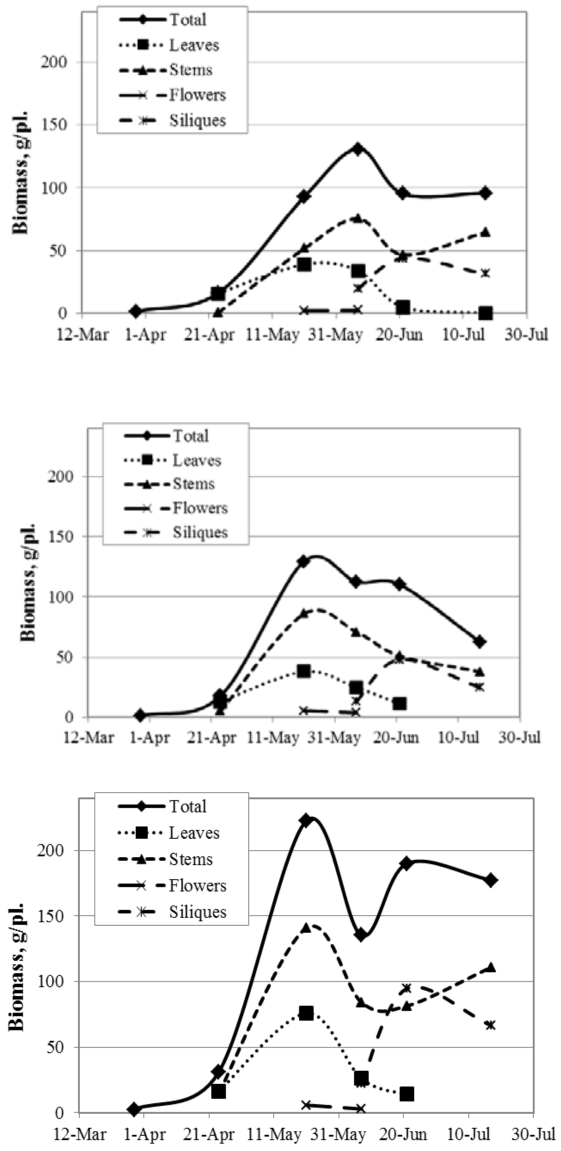

Fig. 5 Dynamics of biomass per plant under full irrigation. Left to right: Maximus; Clearfield;Triangle.

Under the conditions of full irrigation Maximus increased the mass of its components as follows: 75.1 g/pl. stems, 33.7 g/pl. leaves, and 43.7 g/pl. stems. Triangle developed 140.9 g/pl. stems, 75.9 g/pl. leaves and 94.6 g/pl. siliques. The course of the biomass under rain-fed conditions kept decreasing to the end of the vegetation season, but under full irrigation, it kept close to the maximum value, which was registered during flowering. These results are similar to those, obtained by Ahmadi and Bahrani (2009) and Moaveni et al. (2010).

Dry matter

Accumulation of dry matter gradually increased during the vegetation period. The average daily gain was small until the beginning of seed ripening, and was followed by an increase despite the biomass decrease (Figs 6-8). Under rain-fed conditions Maximus kept the rate of dry matter accumulation till the end of seed ripening. It was 24.9 g/pl. at the harvesting. During the same development stage Triangle increased its dry matter from 41.04 to 58.94 g/pl. The figures illustrate the potential of the varieties for yield under the impact of irrigation. Dry matter accumulation was high during seed ripening. Maximus reached 72.3 g/pl. and Triangle – 121.83 g/pl. It is obvious that the water amount of 50 % deficit irrigation did not contribute for much higher rate of dry matter accumulation. The results are in general agreement with Kage et al. (2001) and Kage et al. (2004).

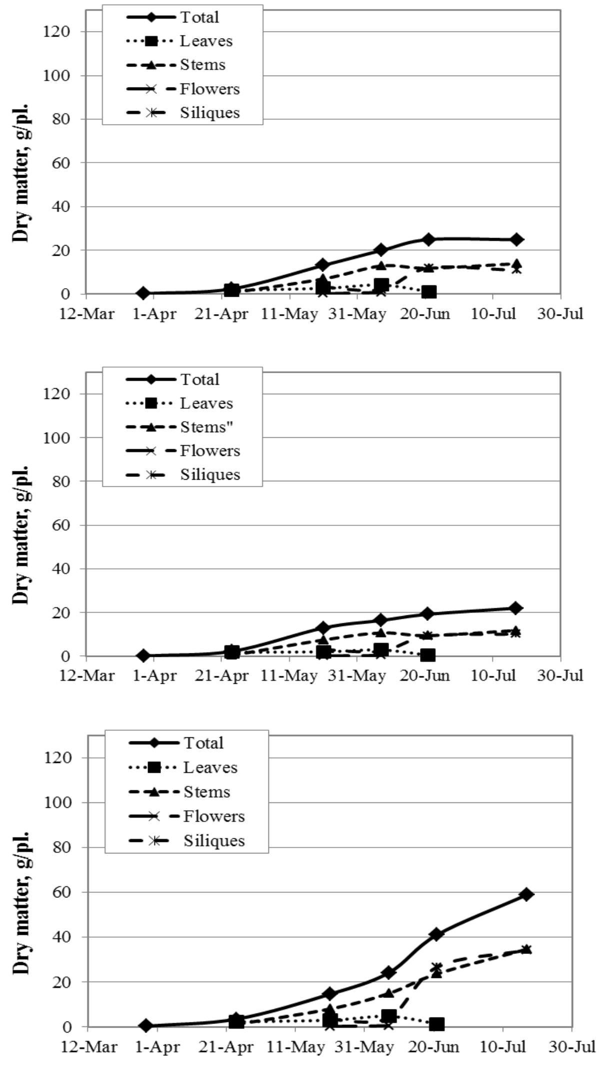

Fig. 6 Dynamics of dry matter per plant under rainfed conditions. Left to right: Maximus; Clearfield;Triangle

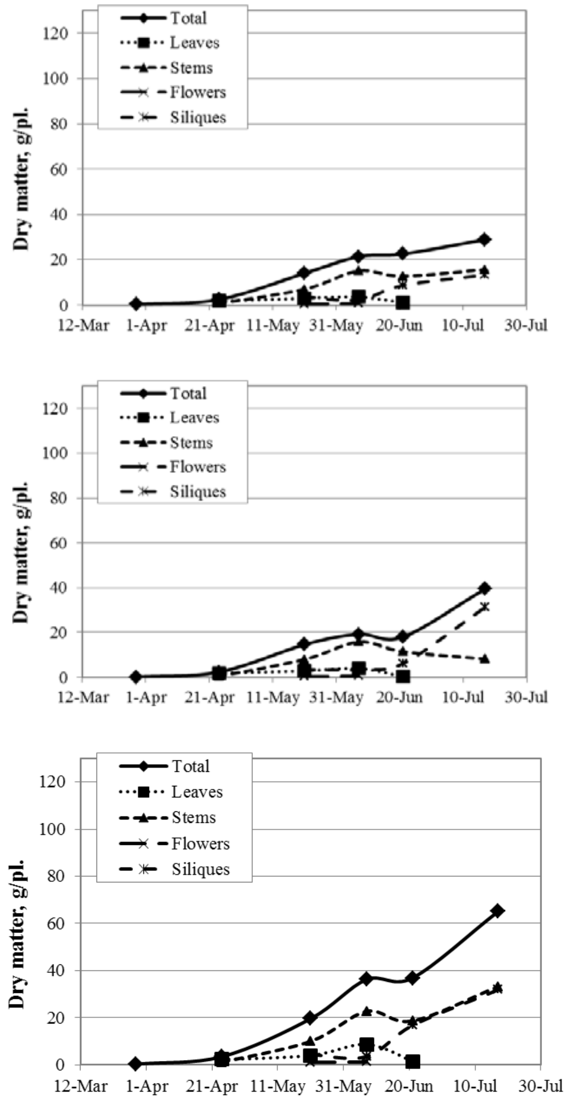

Fig. 7 Dynamics of dry matter per plant under 50% deficit irrigation. Left to right: Maximus; Clearfield;Triangle

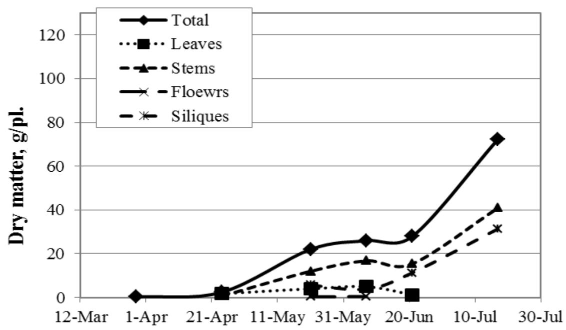

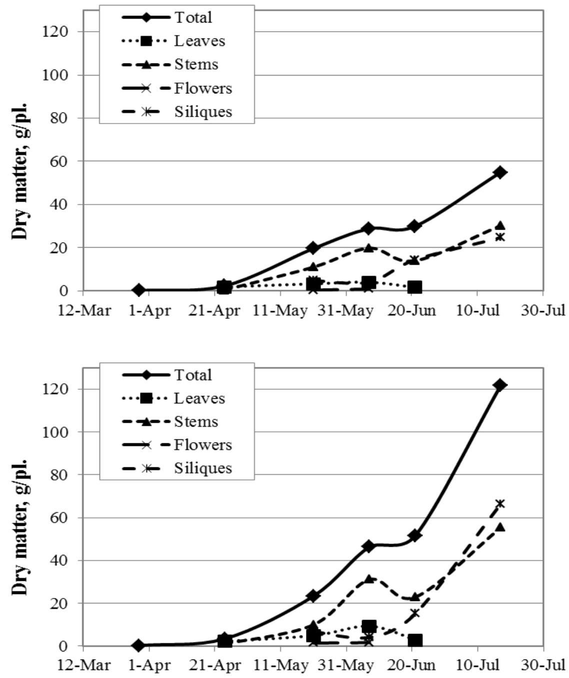

Fig. 8 Dynamics of dry matter per plant under full irrigation. Left to right: Maximus; Clearfield;Triangle

Leaf area index, leaf area potential and net photosynthetic productivity

LAI data show that Triangle has the greatest biological potential for leaf area development. Its *LAI* under rain-fed conditions is 4.9 m^2/m^2, which is much more than that of Maximus and Clearfield - 3.4 and 3.8 m^2/m^2 respectively. Leaf area is maximal at flowering (Fig. 9). There is a tendency for 21-50 % LAI increase with increasing of the level of watering. LAI of Triangle under full irrigation is 6.3 m^2/m^2, of Maximus – 5.1 m^2/m^2, and of Clearfield – 4.6 m^2/m^2. *LAI* under 50 % deficit irrigation is transitional, but the values of Triangle are close to the maximum ones.

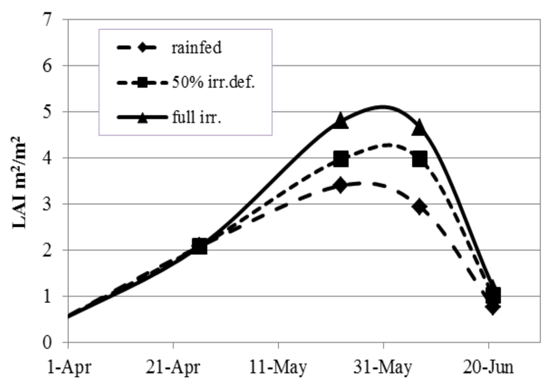

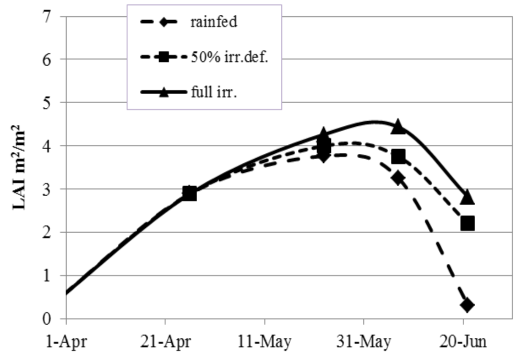

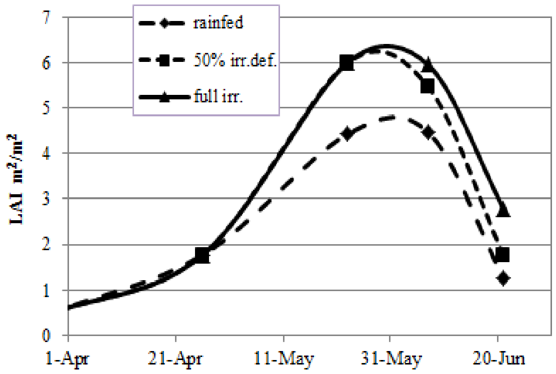

Fig.9 Leaf area index. From left to right: Maximus; Clearfield;Triangle

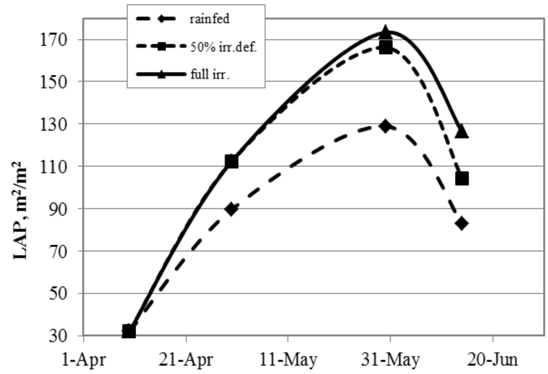

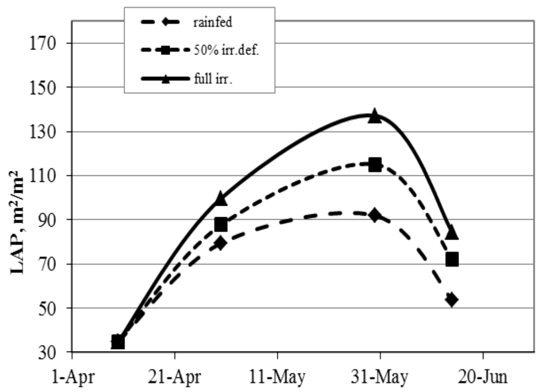

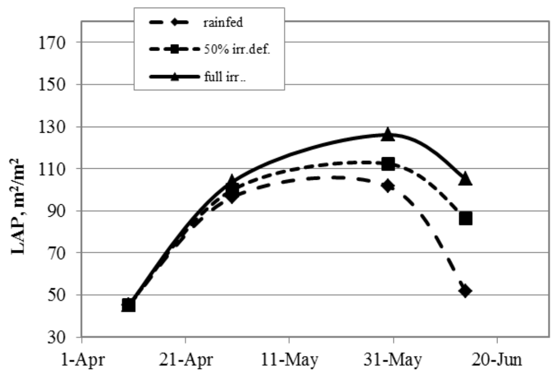

Fig.10 Leaf area potential. From left to right: Maximus; Clearfield;Triangle

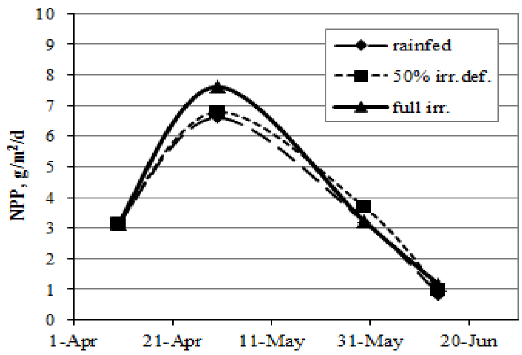

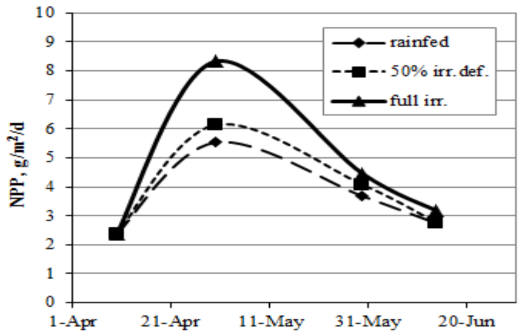

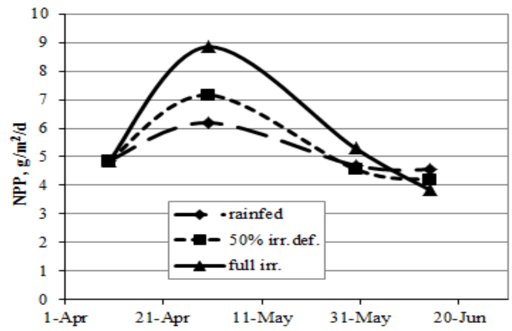

Fig.11 Net Photosynthetic productivity. From left to right: Maximus; Clearfield;Triangle

Tab. 2 Impact of the main factors on seed yield, Mg/ha

Factor	Seed Yield	Signif.	Seed Yield	Signif.	Seed Yield	Signif
	A1 - rainfed		A2 - 50% deficit irrigation		A3 – full irrigation	
B1 - Maximus	2.188		2.401		3.346	
B2 - Clearfield	2.120		2.343		3.070	
B3 - Triangle	2.833	+	3.838	+++	4.797	+++
$GD_{5\%}$=0.645 Mg/ha		$GD_{1\%}$=0.904 Mg/ha		$GD_{0.1\%}$=.1278 Mg/ha		
	B1 - Maximus		B2-Clearfield		B3 - Triangle	
A1 - rainfed	2.188		2.120		2.833	
A2 - 50% def. irr.	2.401		2.343		3.838	+
A3 – full irrigation	3.346	++	3.070	+	4.797	+++
$GD_{5\%}$=0.725 Mg/ha		$GD_{1\%}$=1.080 Mg/ha		$GD_{0.1\%}$=1.717 Mg/ha		

The annual course of the photosynthetic potential (i.e. leaf area potential) escalated till flowering, but afterwards it decreased, because of leaf senescence. The maximal leaf potential i.e. the maximal photosynthesizing area of Triangle was 130 m^2/m^2, of Maximus - 100 m^2/m^2 and of Clearfield - 112 m^2/m^2, which is considerably lower. Triangle increased its *LAP* with 72 % under full irrigation and reached 172 m^2/m^2; Maximus – with 40 % - 140 m^2/m^2 and Clearfield – with 16 % - 130 m^2/m^2 respectively (Fig. 10).

The rate of net photosynthetic productivity was maximal at the pre-flowering stage and varied among the different varieties from 8 to 9 $g/m^2/d$. Water stress considerably disabled the process which is seen on Fig. 11. By giving 50 % of the needed water, *NPP* was only 19-23 % reduced, while under rain-fed conditions - 30-32 %. Analogous results were obtained by Siddique et al. (1999) for wheat. *NPP* slowed down till the end of the vegetation period with the senescence of the leaves.

Seed yield

The intensity of the physiological processes, as impacted by the level of watering gives results in the seed yield (Tab. 2). Full irrigation has significant impact on all varieties, while only Triangle is significantly sensible to the deficit irrigation. Generally, the yield increase under full irrigation is 35-41 %. Triangle has obtained 26 % higher yield under 50 % deficit irrigation, but the other varieties – only 9-10 %. Triangle is also statistically different from the other varieties in all moisture conditions – from the rainfed to the full irrigated ones.

Conclusions

Bulgaria develops canola production, because of EU bio-fuels policy till 2020 (Directive 2003/30/EC). High market prices are also a good motivation for the farmers. Winter canola is among the crops which are thought not to be irrigated in Bulgaria, because its vegetation period shares the wet part of the year but the results from this study show that irrigation has considerable impact on canola physiological processes hence on seed and oil yield. When receiving as much water as its water needs are, canola develops considerable biomass and the dry matter accumulation is intensive. Leaf area, leaf area potential and net photosynthetic productivity under full irrigation develop to an unparalleled degree compared to those under rainfed conditions. Water stress suppresses the physiological processes, so that the indicators take transitional values. The most productive and water sensible hybrid is Triangle. If the latter is grown in water scarcity conditions, 50 % irrigation deficit is a good alternative, because the production indicators are close to those of full irrigation. The results obtained in this study can be used in simulation models for yield prediction purposes.

Reference

Ahmadi M., Bahrani M.J., 2009. Yield and yield components of rapeseed as influenced by water stress at different growth stages and nitrogen levels. Am.-Eurasian J.Agric.&Environ.Sci., 5(6): 755-761.

Bonuelos G.S., Bryla D.R., Cook C.G., 2002. Vegetative production of kenaf and canola under irrigation in central California,Ind.Crops Prod.,15: 137-145.

Gunasekara C.P., Martin L.D., French R.J., Siddique K.H.M., Walton G.H., 2006. Genotype by environment interactions of Indian mustard (*Brassica juncea*, L.) and canola (*Brassica napus*, L.) in Mediterranean-type environments: I. Crop growth and seed yield, Eu. J. Agron., 25: 1-12.

Kage H., Stützel H., Alt C., 2001. Predicting dry matter production of cauliflower (*Brassica oleracea* L. *botrytis*) under unstressed conditions: Part II. Comparison of light use efficiency and photosynthesis–respiration based modules, Scientia Horticulturae,87(3): 171–190.

Kage H., Kochler M., Stützel H., 2004. Root growth and dry matter partitioning of cauliflower under drought stress conditions: measurement and simulation European Journal of Agronomy, 20(4): 379–394.

Krogman K.K., Hobbs E.H., 1975. Yield and morphological response of rape (*Brassica campestris,* L.) to irrigation and fertilizer treatments,Can. J.Plant Sci.,55: 903-909.

Mitova T., Moteva M., 2011a. Abiotic stressing factors for rapeseed production in Bulgaria I part, Zemedelie plus, 2-3: 11-12.

Mitova T., Moteva M., 2011b. Abiotic stressing factors for rapeseed production in Bulgaria II part, Zemedelie plus, 4: 29-31.

Moaveni P., Ebrahimi A., Farahani H.A., 2010. Physiological growth indices in winter rapeseed (*Brassica napus,* L.) cultivars as affected by drought stress at Iran. J. Cereals and Oilseeds, 1(1): 11-16.

Mondul R.K., Paul N.K., 1995. Effect of soil moisture on growth attributes and yield, root characteristics of mustard (*Brassica juncea,* L.),Pak.J.Bot., 27: 143-150.

Moteva M., Mitova T., Gigova A., Georgieva V., 2013. Effect of irrigation on productivity of three cultivars of canola (*Brassica napus* l.). Proc. 2nd Int. Sym. on Kaz Mountains and Edremit "Human-Environmental Interactions and Ecology of Mountain Ecosystem", Edremit, Turkey, 379-388.

Naderikharaji R., Pakniyat H., Biyabani A.R., 2008. Effect of drought stress on photosynthetic rate of four rapeseed (*Brassica napus*, L.) cultivars, J.Applied Sci., 8(23): 4460-4463.

Nichiporovich A.A., Strogonova L.A., Chmora S.N., Vlasova M.P., 1961. Photosynthetic activity of plants in cropped fields.ANSSSR Ed.,M., 136.

Qaderi M.M., Kurepin L.V., Reid D.M., 2012. Effects of temperature and watering regime on growth, gas exchange and abscisic acid content of canola (Brassica napus) seedlings, Environ. and Experim. Bot., 75: 107–113.

Siddique M.R.B., Hamid A., Islam M.S., 1999. Drought stress effects on photosynthetic rate and leaf gas exchange of wheat, Bot.Bull.Acad.Sin., 40: 141-145.

VIBRATIONAL BEHAVIOR OF TRACTOR ENGINE HOOD

Ioannis Gravalos[1*], Spyros Loutridis[2], Theodoros Gialamas[1], Augoustinos Augousti[1]
Dimitrios Kateris[1], Panagiotis Xyradakis[1], Zisis Tsiropoulos[1]

[1]Technological Educational Institute of Larissa, School of Agricultural Technology,
Department of Biosystems Engineering, 41110 Larissa, Greece
Phone: +302410684216, Fax: +302410282209, E-mail: gravalos@teilar.gr
[2]Technological Educational Institute of Larissa, School of Technological Applications
Department of Electrical Engineering, 41110 Larissa, Greece

Abstract

The main source of vibration in agricultural tractors is the engine. Engine vibration results from the combustion process itself and the mass asymmetry in engine rotating elements. The vibration is transmitted from the engine to the tractor hood. The objective of this study is to record and analyze the vibration patterns on the hood under different operational engine speeds (800 - 2200 rpm). Two different wheeled tractors were used for the experiments. The hood of the first tractor was made from steel sheet. The new hood design of the second tractor was made from fiber reinforced plastic material. The following instruments were used: the PSV-400 scanning laser vibrometer (Polytec), and the 4500A piezoelectric accelerometer (Brüel & Kjaer) that served as reference accelerometer. The experimental data showed significant deflection of the hood surface. Vibration analysis between the two types of engine hoods showed that the steel sheet was indeed very stiff, in contrast to the fiber reinforced plastic hood, which better absorbed the mechanical vibration due to the increased damping.

Keywords: vibration, tractor, engine, noise

Introduction

Several tractors components do not have the ability to absorb noises, vibrations and harshness (NVH). Noise is an unpleasant sound created by vibrating objects, vibration is a rapid oscillation of a solid object back and forth across a position, and harshness is a perceived lack of suspension compliance (Volkswagen of America, 2005). The target of NVH engineering is to achieve maximum vibro-acoustic comfort.

The main source of vibration in agricultural tractors is the engine. Engine vibration results from cylinder firing, impacts due to piston clearances (piston slaps), fuel injection pressure, high rise of gas pressure during combustion and the impacts of admission and exhaust valves (Carlucci et al., 2006). These vibrations are transmitted from the cylinders (originator), through the engine block (conductor) on to the hood (reactor). As a result of this process the vibrating hood produces noise that ~~it~~ is heard by the driver. Noise is transferred directly from vibrating components or by the wind, turbulence, and air leaks to the driver (Ford Customer Service Division).

In the old types of tractors the engine hood was made from steel sheet. In modern tractors the engine hood is made from fiber reinforced plastic material. The engine hood is the main component of the front view of a tractor. It is used to cover the tractor engine, the radiator, and other sensitive components. Its shape is made as aerodynamic as possible. It is also used to decorate the tractor and add a luxurious look to it (Ganeshpure, Bhope, 2013). Accurate structural models are key to the optimization of the vibro-acoustic behaviour of engine hoods (Costi et al., 2011). Van der Auweraer et al. (2002) presented a vibration testing system based on pulse-laser holographic electronic speckle pattern interferometry measurements. The approach has been applied to several industrial case studies. Yamaguchi et al. (2007) presented a vibration analysis of automotive panels damped with sound-porous materials. The vibration was measured under the panel and on the PVC sheet. The vibration levels were small up to 200 Hz, and became increasingly greater at higher levels. The results from simulation were compared to the experimental results for validation.

The objective of this study is to record and analyze the vibration patterns of two types of engine hoods under a range of operational engine speeds (800 - 2200 rpm).

Materials and Methods

Two different types of wheeled tractors were used for the experiments. The hood of the first tractor (Renault 361) was made from steel sheet. The new hood design of the second tractor (Lamborghini R6) was made from fiber reinforced plastic material. The engine run-up tests are performed without any additional load, at engine speed range from 800 to 2200 rpm. The experiments help to locate the hood area that is sensitive to engine vibration. A total number of 109 points was used to cover the surface of the Renault 361 hood, and a number of 156 points to cover the surface of the Lamborghini R6 hood.

During the experimental process, the PSV-400 scanning laser vibrometer (Polytec), and the 4500A piezoelectric accelerometer (Brüel & Kjaer) are used to measure velocity and displacement of predefined points on the hood. The PSV-400 scanning laser vibrometer (Fig. 1) is a non-contact transducer for the vibration measurement of vehicles components. It is based on the laser-Doppler effect, and it is equipped with a computer-controlled orientation system. It is inherently a sequential procedure making a set of point measurements. A CCD camera is used to view the illuminated object. The second contact testing approach was based on the 4500A piezoelectric accelerometer (Brüel & Kjaer) and used as a reference set of measurements. The vibration measurement is performed at frequencies where maximal vibration occurs. The engine speed is accurately recorded with a tachometer.

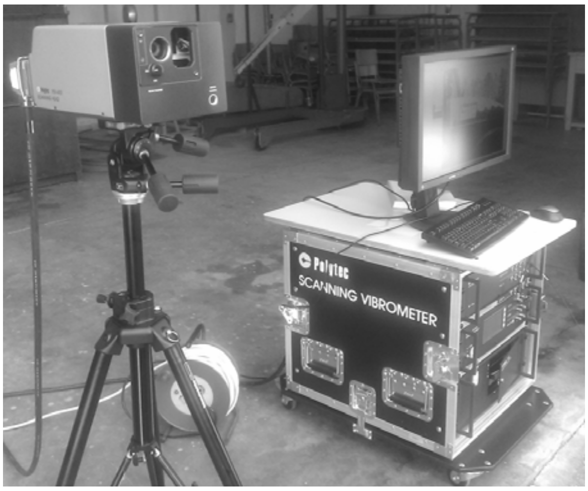

Fig. 1 The experimental setup including the PSV-400 scanning laser vibrometer

Results and Discussion

Fig. 2 and Fig. 3 depict examples of the engine hood vibration patterns for the two types of tractors tested with engine speed varying from 800-2200 rpm

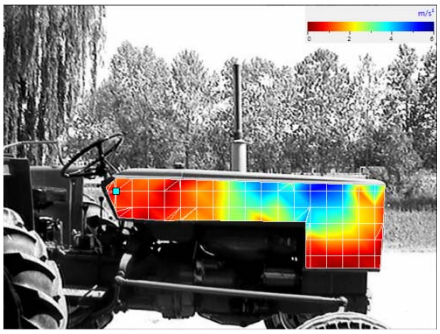

800 rpm

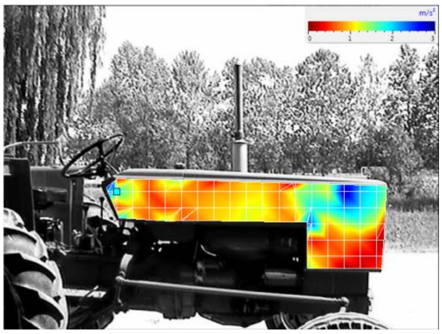

1000 rpm

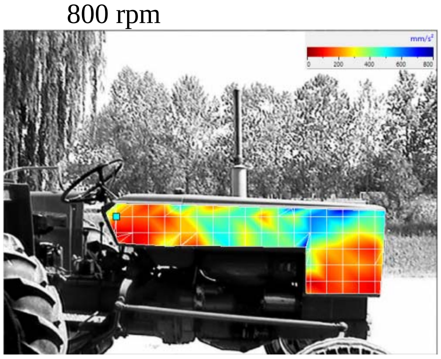

1200 rpm

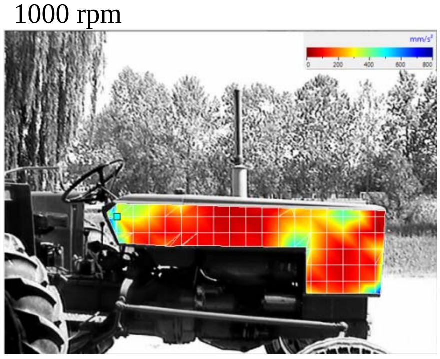

1400 rpm

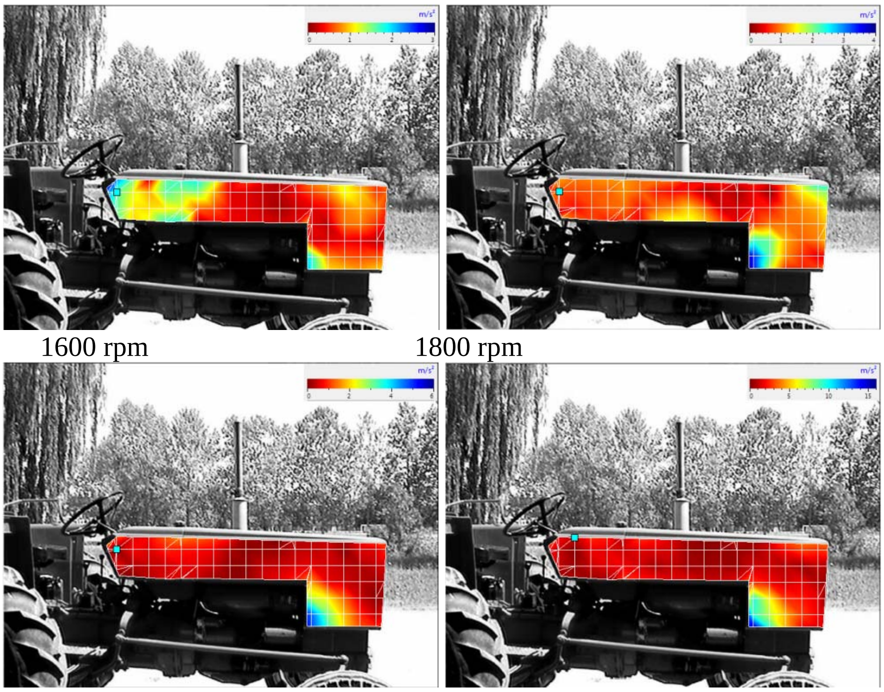

1600 rpm 1800 rpm

2000 rpm 2200 rpm

Fig. 2 Vibration patterns for the steel sheet hood

In Fig. 2, it can be seen that the steel sheet hood (Renault 361) shows significant variability in the vibration patterns up to the 1600 rpm. After 1800 rpm this variability is reduced. Fig. 3, presents measurements on the fiber reinforced plastic hood of the Lamborghini R6 tractor at various engine speeds. It is obvious that the vibration amplitude is highest when the engine rotates at 800 rpm. The variability in vibration patterns decreases as the engine speed increases from 1000 rpm to 2200 rpm. It is obvious that the fibre plastic hood better absorbs high frequency vibration.

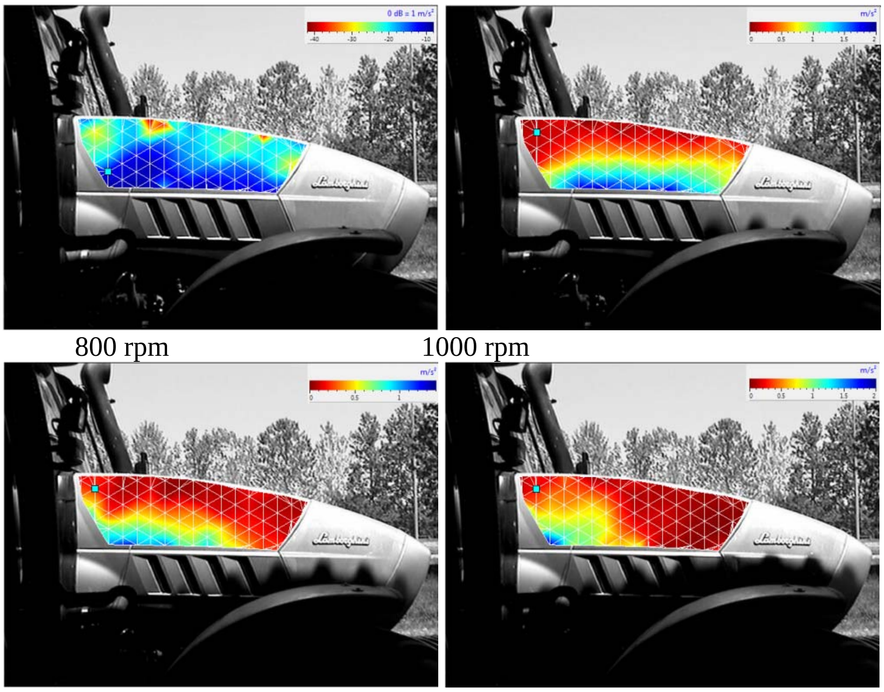

800 rpm 1000 rpm

1200 rpm 1400 rpm

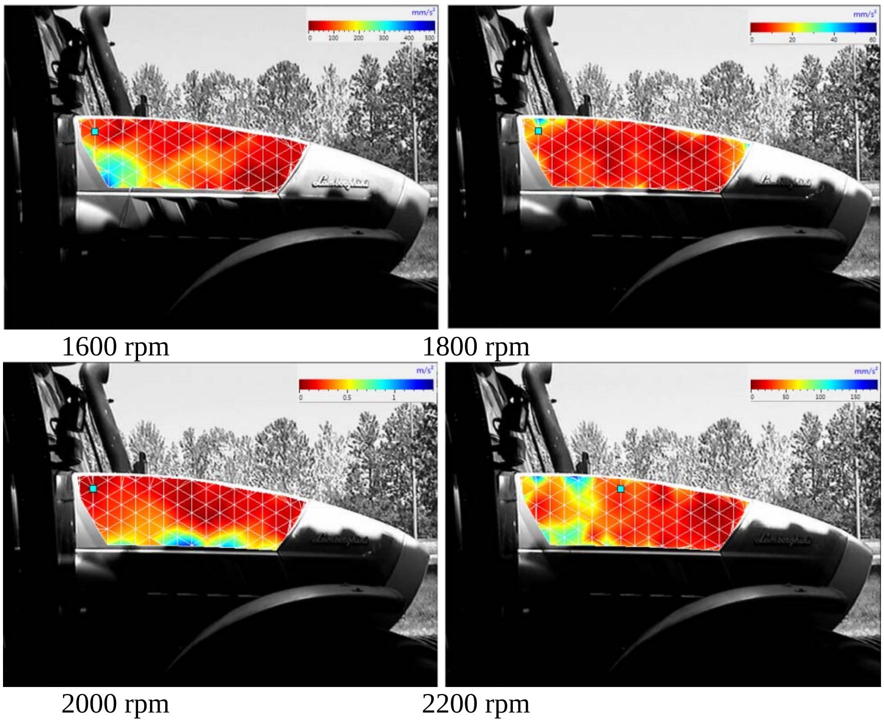

Fig. 3 Vibration distribution of hood surface made from fiber reinforced plastic material

In Fig. 4 the average values of hood surface acceleration in relation to engine speed for the two different types of tractors are presented. These averaged values are based on acquired values after the FFT process. The fiber reinforced plastic hood (Lamborghini R6) shows maximum vibration levels at 800 rpm, while above 1000 rpm the averaged acceleration values are greatly diminished. The steel sheet hood of the Renault 361 tractor has similar vibration behavior up to 1400 rpm. Above 1400 rpm tractor the steel sheet hood, shows high acceleration values in comparison to the fiber plastic hood.

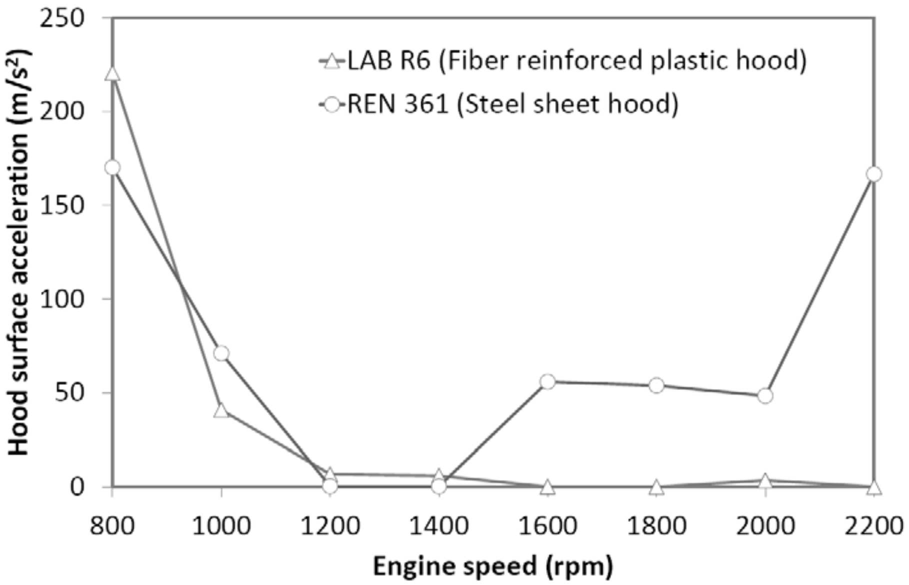

Fig. 4 Average values of hood surface acceleration in relation to engine speed for the two different types of hoods tested

Conclusion

Using a scanning laser vibrometer we have studied the vibration behaviour of two different types of tractor engine hoods. The main conclusions drawn from the vibration analysis are:

- The steel sheet hood shows increased vibration amplitude above 1600 rpm.
- The fiber reinforced plastic material hood shows minimal vibration above 1200 rpm.
- The steel sheet was indeed very stiff, in contrast to the fiber reinforced plastic hood, which better absorbed mechanical vibration due to increased damping.

Reference

Carlucci A.P., Chiara F.F., Laforgia D., 2006. Analysis of the relation between injection parameter variation and block vibration of an internal combustion diesel engine. J. Sound Vibrat. 295: 141-164.

Costi D., Torricelli E., Splendi L., Pettazzoni M., 2011. Optimization Methodology for an automotive Hood structure (Inner Panel). Proceeding on the world congress on engineering, II: 1-4.

Ford Customer Service Division: NVH principles and diagnosis. Student Reference Book (Course Code 30S03T0), 73-79.

Ganeshpure A.M., Bhope D.V., 2013. Static and free vibration analysis of a car bonnet. International Journal of Engineering Research & Technology, 2 (3): 1-8.

Van der Auweraer H., Steinbichler H., Vanlanduit S., Haberstok C., Freymann R., Storer D., Linet V., 2002. Application of stroboscopic and pulsed-laser electronic speckle pattern interferometry (ESPI) to modal analysis problems. Meas. Sci. Technol., 13: 451-463.

Volkswagen of America, 2005. Noise, Vibration, and Harshness. Self Study Program (Course Number 861503), 3-5.

Yamaguchi T., Nakamoto H., Kurosawa Y., Matsumura S., 2007. Dynamic analysis of dissipated energy for automotive sound-proof structures including elastic body, viscoelastic body and porous body using FEM in sound bridge phenomena. Journal of Environment and Engineering, 2(2): 315-326.

THE INFLUENCE OF TRAFFIC IN PERMANENT TRAFFIC LANES ON SOIL COMPACTION PARAMETERS

Dumitru Gutu[1], Josef Hula[2*], Frantisek Kumhala[2], Pavel Kovaricek[3]

[1]ZAS Podchotuci a.s., Krinec, Czech Republic,
[2]Czech University of Life Sciences Prague, 165 21 Prague 6 – Suchdol, Czech Republic,
Phone: +420-224383123, E-mail: hula@tf.czu.cz
[3]Research Institute of Agricultural Engineering, Prague, Czech Republic

Abstract

In a field trial in a field of 10 hectares all field operations were carried out by machine sets in the system of permanent traffic lanes at the module of 6-metre working width. The total area of machine tracks in the field accounted for 32 % of the field area, which represents a significant reduction in comparison with a conventional method of driving in fields, when the proportion of the track area is 75 up to 100 % of the total field area. The present paper contains results of measurement of soil physical properties in variants with traffic lanes and outside the traffic lanes. The results confirm a benefit from confining the wheel traffic to permanent traffic lanes aimed at protection of the most part of the field from soil compaction. Another advantage of the above-mentioned permanent traffic lanes is an improvement of soil tillage quality in the most part of the field.

Keywords: permanent traffic lanes, soil compaction, soil physical properties

Introduction

Modern technologies of field crop cultivation are connected with wheel traffic in fields that causes undesirable soil compaction. Soil compaction can result in a crop yield decrease, however, environmental consequences are particularly alarming. In the course of intensive rainfalls, decreased infiltration of precipitation water on compacted soils increases surface water runoff, implying a high risk of soil water erosion. Necessary water accumulation in the soil is diminished at the same time. Another consequence of soil compaction is an increase in energy requirements for soil tillage, impairment of soil tillage quality associated with the worsening of conditions for sowing.

In recent years intensive researches on problems of undesirable soil compaction have been conducted (Håkansson, 1995; Unger, 1996). The load of wheel traffic may cause different reactions in the soil profile during the year, first of all in relation with instantaneous soil moisture and degree of preceding soil loosening or compaction.

Proposals to confine the necessary wheel traffic of farm machines in fields to permanent tracks already appeared in the eighties of the last century. At that time no technical equipment was available that would allow using the system of permanent traffic lanes – reliable and precise navigation of machinery during its movement in fields was missing. Currently, there are great efforts to restrict the wheel traffic of farm machines in fields to defined tracks in order to maintain a major part of the area under crops without negative influence of wheel traffic (Chamen et al., 2003; Tullberg, 2007). The system of controlled traffic farming (CTF) is currently considered as promising also because satellite navigation systems are available that make it possible to ensure the required accuracy of passes during field operations including sowing.

In an agricultural enterprise possessing high-performance farm machinery a field trial was established in which besides the influence of wheel traffic restriction to permanent lanes on soil properties and on the quality of soil tillage a possibility of CTF technology realization in farming conditions was tested.

Material and method

A field trial on a land of 10 ha in size was established in the spring 2010. Soil conditions in the field: loamy soil (content of particles smaller than 0.01 mm in the topsoil layer: 38.3 % by weight). Content of combustible carbon in topsoil: 3.8 %.

In 2009 after winter wheat harvest the field was worked by a sweep cultivator to a depth of 80 mm, in autumn the soil tillage by a combined cultivator to a depth of 200 mm followed. After this medium-deep cultivation of soil the field remained without wheel traffic until spring 2010, when wheel traffic was organised within the CTF system using OutTrac (Chamen, 2006) – Fig. 1. It is typical of this wheel traffic system that the wheel tracks of a harvester-thresher that has a wider wheel gauge than tractors are on the outer side of common permanent traffic lanes.

Tab. 1 gives an overview of farm machines used for field operations in the field. Those machines were chosen whose working width corresponded to the basic module of 6 m. The field operations of soil tillage and sowing were performed at the working width of 6 m. The wheel rows established during sowing were used for the application of chemicals for plant protection while the working width of a sprinkler was 18 m. The same wheel rows were also used for the application of mineral fertilisers.

To evaluate the influence of wheel traffic of farm machines on the soil in a system of restricted wheel traffic four variants of traffic lanes were defined:

1. Traffic lanes of tractors during sowing, application of chemicals for plant protection, application of mineral fertilisers and during stubble breaking and other soil tillage.
2. Traffic lanes of dual wheels of a tractor during sowing, lanes of a combine harvester and lanes of a tractor during stubble breaking and other soil tillage.
3. Outside the traffic lanes.
4. Part of the field with uncontrolled wheel traffic (area of 3 ha).

In the particular variants of the field trial measurements were done with a PN 100 self-recording penetrometer and basic physical properties of soil were evaluated in the spring and autumn season. After soil tillage was carried out, the indicators of soil tillage quality were assessed. To measure the shearing strength of soil a CL-100 vane probe (Terratest) was used.

A GPS satellite system with the correction signal of RTK VRS was used for the navigation of farm machines during sowing, soil tillage, application of chemicals for plant protection and during harvest. An assisted steering system AgGPS EZ-STEER (Trimble) was used. The vehicles for grain transport during the operation of a harvester-thresher did not pass across the field, the grain tank of a harvester-thresher was emptied to a tractor semi-trailer on the edge of the field near the road.

The present paper contains the results of evaluation of wheel traffic impacts on the soil in a field trial in 2011 (the second year of the consistent application of controlled traffic farming in a field). In that year winter wheat was grown in the field concerned, after its harvest soil tillage for winter wheat sowing followed.

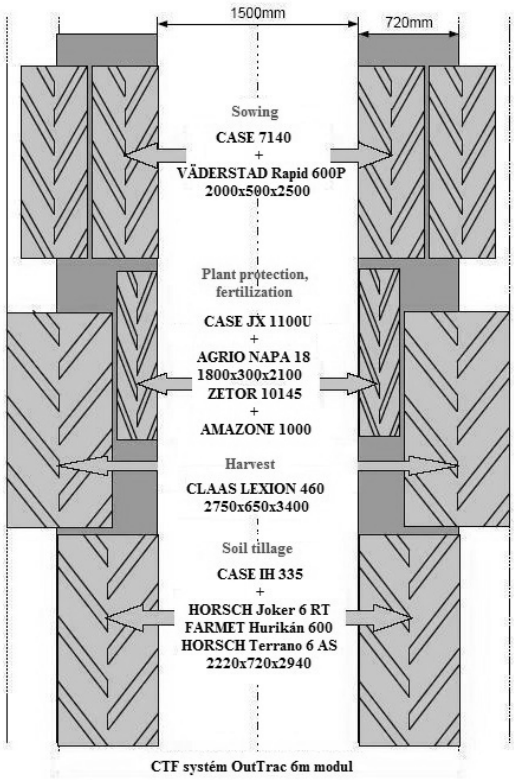

Fig. 1 Wheel ruts of tractors and combine harvester after their restriction to permanent traffic lanes – the area of lanes is enlarged by the wheel track of combine harvester that is larger than that of tractors and by dual wheels of tractor during sowing

Tab. 1 Field operations in 2011 and data of farm machines

Field operation	Time	Machines	Working width [m]	Distance of tracks [mm]	Tyre width [mm]
Sowing of winter wheat	12.10. 2010	CASE 7140 + VÄDERSTAD Rapid 600P	6	2000	500x2
Fertilization with mineral fertilizers	11.3. 2011	ZETOR 10145 + AMAZONE 1000	18	1800	300x2
Pesticide application	6.5. 2011.	CASE JX 1100U + AGRIO NAPA 18	18	1800	320x2
Fertilization with mineral fertilizers	9.5. 2011	ZETOR 10145 + AMAZONE 1000	18	1800	300x2
Fertilization with mineral fertilizers	30.5. 2011	ZETOR 10145 + AMAZONE 1000	18	1800	300x2
Pesticide application	13.6. 2011.	CASE JX 1100U + AGRIO NAPA 18	18	1800	320x2
Winter wheat harvest	18.8. 2011	CLAAS Lexion 460	6	2750	650x2
Shallow loosening (depth 80-100 mm)	3.9. 2011	CASE IH 335 + FARMET Hurikan 600	6	2220	720x2

Results and discussion

Fig. 2 shows the average values of some physical properties of soil after undisturbed soil samples were taken on 14th April 2011. At a depth of 50-100 mm the highest bulk density of soil was recorded in variant 1 – in this variant only one pass of machines across the field was done from wheat sowing in October 2010 (application of mineral fertilizer on 11th March 2011). The lowest values of bulk density of soil were found out on the land outside the wheel tracks. The values of minimum air capacity expressing the volume of pores that remain filled with air after capillary pores have been filled with water are a significant indicator of the degree of soil compaction (Fig. 3). The values of minimum air capacity lower than 10 % of the volume document undesirable soil compaction; the graph illustrates that these low values were measured at a depth of 50-100 mm in variant 4 (uncontrolled wheel traffic). A similar trend of differences in physical properties of soil was observed at a depth of 150-200 mm while at other evaluated depths (250-300 mm and 350-400 mm) there were no differences that would indicate a different degree of soil compaction in the particular variants.

Fig. 3 illustrates the values of soil penetration resistance measured on 12th April 2011. On that date statistically significantly higher penetration resistance was recorded in variant 1 compared to variants 2, 3 and 4 at measurement depths of 40, 80 and 120 mm, with the average soil moisture of 15.8 % of the weight at these depths. This difference can be ascribed mainly to soil compression by the tractor wheels during regeneration fertilization of winter wheat with mineral fertilizer (11th March 2011). These distinct differences were not recorded at other measured depths any more – penetrometer measurements were done to a depth of 500 mm.

Tab. 1 shows that in 2011, besides regeneration fertilization on 11th March, one field operation of chemical plant protection and two operations of production fertilization were performed in the course of May; these field operations necessitated tractor passes in wheel rows – variant 1. Measurements with vane probe on 29th June showed increasing differences between variant 1 (wheel rows) and the other variants. From these measurements values of the shearing strength of soil at a depth of 50 mm (in kPa) are presented (Fig. 4). Values of the shearing strength of soil in variant 1 were more than four times higher than in the other evaluated variants while the differences were statistically significant. Average soil moisture at the measurement depth was 11.3 % of the weight in variant 1 and 14.1 % of the weight in variants 2, 3 and 4. These results document the increasing soil bearing capacity within wheel rows as a consequence of wheel traffic in the spring 2011 and increasing differences in the degree of soil compression between variant 1 and the other variants. From the aspect of machine movement on the land repeated passes in the same tracks improve the “passability” of these tracks and conditions for a reduction of rolling resistance are created.

Using machinery of the ZAS Podchotuci, a.s. agricultural enterprise in Krinec, a system of controlled traffic farming with consistent separation of wheel tracks of machines from the production area of the field without traffic was realized on the land of 10 ha in area this agricultural enterprise is farming on. Although the wheels of tractors and harvester-threshers are not designed for their use in the CTF system (wider wheel gauge of harvester-threshers than the wheel gauge of tractors), a relatively good situation was reached when the total area of wheel tracks in the field (with the exception of headland) accounted for 32 % of the land area if the module of the 6-metre working width of machines was used. If the module of the 8-metre working width of machines were used, it would be realistic to decrease the area of wheel tracks to 20 – 25 % of the field area. It is a significant reduction of the wheel-tracked field area – according to Chamen (2006) the wheel-tracked area amounts to 75 – 100 % of the field area in a conventional system of machine passes. In conditions of the CR the monitoring of wheel traffic in fields showed that the proportion of wheel tracks accounted for 86 % of the field area in the production system of winter wheat with conventional soil tillage (Kroulik et al., 2011).

A decrease in the proportion of wheel tracks in the total area of fields could be reached by unification of the wheel gauge of tractors and harvesting machines. It is a costly approach, but these adaptations of machines for the CTF system are already implemented in other countries (Tullberg, 2010).

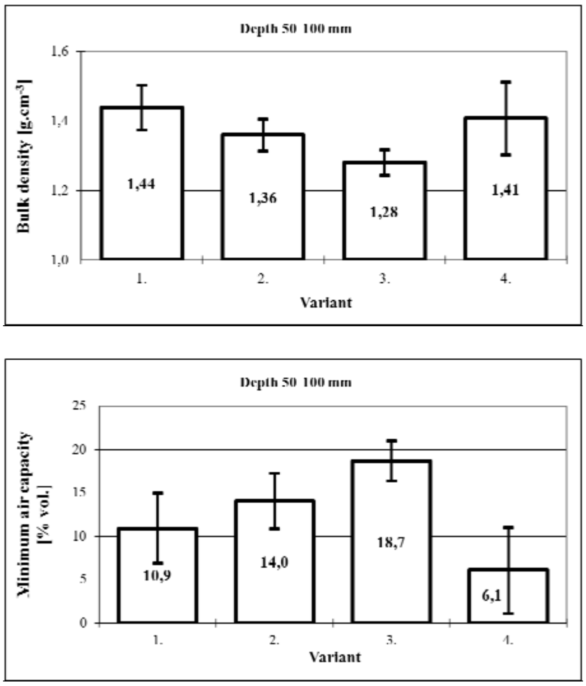

Fig. 2 Bulk density and minimum air capacity at a depth of 50-100 mm (14th April 2011)

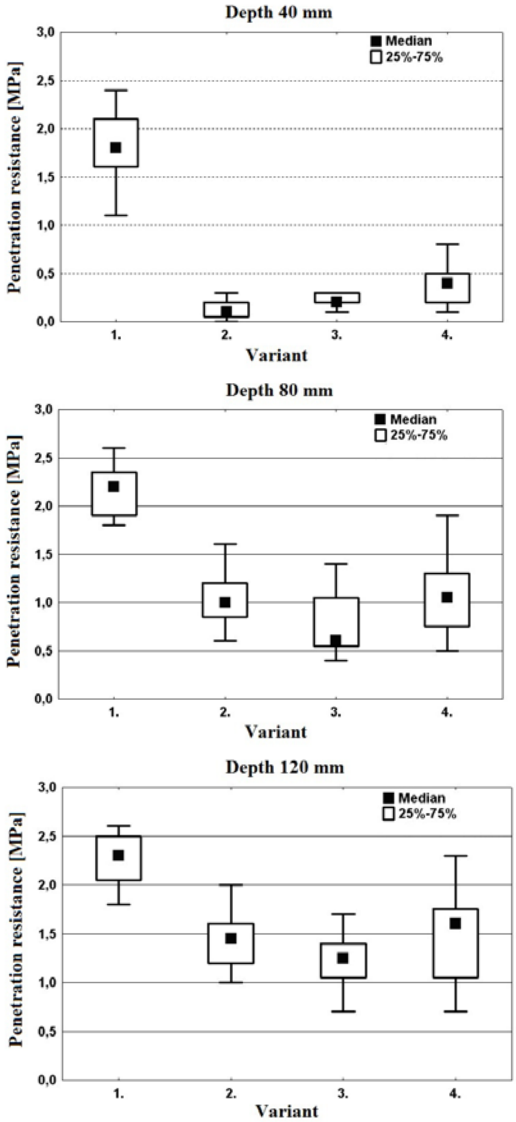

Fig. 3 Soil penetration resistance at a depth of 40, 80 a 120 mm (12th April 2011)

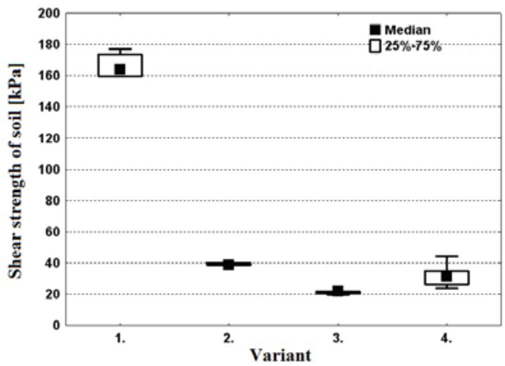

Fig. 4 Shear strength of soil at a depth of 50 mm (29th June)

Conclusion

The results of a pilot field trial obtained in 2011 demonstrate that the controlled traffic farming system can be realized in conditions of an agricultural enterprise. It should be based on the use of a precise navigation satellite system with the correction signal in connection with the assisted or automated steering of tractors and combine harvesters, and of course on the willingness to apply this non-traditional technology.

The findings from the assessment of machine work quality during soil tillage in 2011 did not confirm the impairment of the quality of soil preparation for sowing in a situation when the passes of machine sets were not diagonal to the direction of crop rows. Naturally, the controlled traffic farming system is not suitable for soil tillage with ploughing but it can be used in minimum tillage and soil conservation technologies for the production of crops harvested by combine harvesters.

Acknowledgement

Supported by the research project No. FR-TI3/069 and MZE0002703102.

Reference

Chamen W.C.T., Alakukku L., Pires S., Sommer C., Spoor G., Tijink F., Weisskopf P., 2003. Prevention strategies for field traffic - induced subsoil compaction: a review, Part 2. Equipment and field practices. Soil & Tillage Research, 73: 161–174.

Chamen W.C.T., 2006. Controlled traffic farming on a field scale in the UK. In: Horn R., Fleige H., Peth S., Peng X.H., (Eds.): Soil Management for Sustainability. Advances in geoecology, 38: 251-260.

Håkansson I., 1995. Compaction of arable soils. Uppsala, SLU Uppsala, 109: 153.

Kroulík M., Kvíz Z., Kumhála F., Hůla J., Loch T., 2011. Procedures of soil farming allowing reduction of compaction. Precision Agriculture, 12(3): 317-333.

Tullberg J.N., Yule D.F., McGarry D., 2007. Controlled traffic farming - From research to adoption in Australia. Soil & Tillage Research, 97: 272-281.

Tullberg J., 2010. Tillage, traffic and sustainability - A challenge for ISTRO. Soil & Tillage Research, 111: 26-32.

Unger P.W., 1996. Soil bulk density, penetration resistance, and hydraulic conductivity under controlled traffic conditions. Soil & Tillage Research, 37: 67-75.

ROBOTIC HANDLER INCRESES ROSELLE HARVESTING PRODUCTIVITY

Federico Hahn

IAUIA, University Autonoma Chapingo, km 38.5 Mexico Texcoco, Chapingo, 56230, Mexico,
e-mail: fhahn@correo.chapingo.mx

Abstract

Roselle is an important crop being cultivated in the tropical areas of Mexico. The bush produces red flowers and their calyxes are used to prepare beverage drinks, which are being consumed in the entire world. Roselle production on the field is costless, but its harvesting cost is too high. Calyx harvesting is done using two pair of rollers which turn in opposite directions in order to pull branches containing up to 15 flowers. Harvesting productivity depends on the worker ability to feed the branches to the harvester. A robotic handler was developed to increase harvesting productivity feeding two branches at the same time. A vision system cuts the branches,so that the robotic handler can feed them to the harvesting machine. Productivity increased from 50 kg/hr to 100 kg/hr with the robotic handler; if three branches are fed simultaneously productivity could increase more.

Keywords: Roselle, robotic handler, vision system.

Introduction

Roselle plants can be utilized almost everything and its importance lies primarily in the benefits obtained. It can be considered as a medicinal plant and contains several vitamins and minerals. Roselle cultivation is growing considerably in Mexico. Roselle does not have limitations in cultural practices such as planting or plant emergence. However, harvesting is hand done, requiring excessive labor. Considerable amount of economic resources are required during harvesting, drying and storage. Economic analysis (Caro et al, 2012) determined that harvest costs correspond from 40 to 60 % of the production cost. One of the current harvest tools is a fork with a 10 mm aperture, where the branch slips detaching the calyx. Calyxes fall and fill eighteen liter trays; each tray can manage 3.5 to 5 kg of fresh calyxes depending on the variety. A normal worker can harvest up to 80 kg fresh calyxes per day (Barragan et al., 2010; Reyes, Hahn, 2009).

Harvesting is done when the plant begins to mature in early December five months after planting; leaves color change from deep green to yellow, orange, coppery or brown. Leaves start to fall leaving the ground bare and red, only with the calyx and seeds in the cascalote (flower ovary). At this moment branches are cut with a machete and taken to the harvesting machine to detach the calyxes. The roselle harvester developed by Reyes and Hahn (2009) present a fresh calyx productivity of 37 kg/h, having a feeding height of 90 cm and a length of 100 cm.A new harvester presenting an improved transmission was developed to move four geared rollers getting a productivity of 62 kg/h (Poblano et al., 2013). Traction is maintained when rollers get wet as water is extracted from the branches when pressed.

This paper evaluates the branch selector which is the principal component of the robotic harvester. This selector increases the harvester productivity as well as it decreases human needs during roselle harvesting.

Methodology

The prototype built at the Mechanical department of the Universidad Autonoma Chapingo presents several new integrated systems as shown in Fig. 1. The complete roselle bush (bottom of the figure) is placed at the branch cutter and a vision system controls the saw inclination, ordering branch cutting. The vision system has two cameras placed orthogonally so that a 3D image can be acquired. A gripper takes the branch cut at the branch cutter and transports it towards the branch selector. Once the branches are cut the branch selector moves the branches towards the two section roller harvester.

The basic harvester prototype is operated by a 2 HP induction motor, with a 10:1 chain reducing transmission; rollers rotate at a speed of 170 rpm.

The paired rollers rotate in opposite directions in order to make the branches pass through them, Fig. 2. Two knives are fixed at the front of the machine with an automated adjustable spacing; branch size determines knife blade spacing. Adjusting screws change the separation between the blades according to the variety being harvested. As the branch enters, the upper roller pair gets up and exerts pressure through the tension system. The machine consists of eight toothed rollers adjusted by a pivoting system. Roselle branches pulled by the rollers are passed through a pair of adjustable steel blades damped with springs; these blades release the calyxes from the branches.

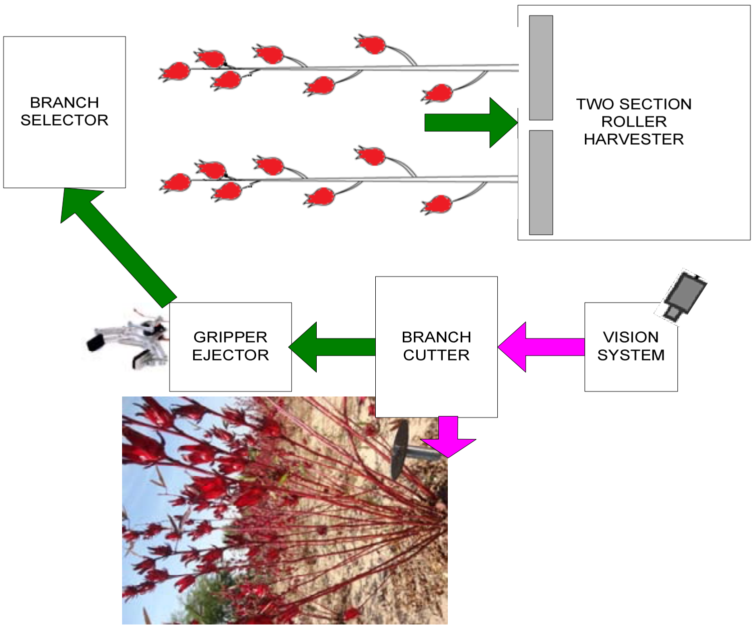

Fig. 1 Block diagram of the robotic system

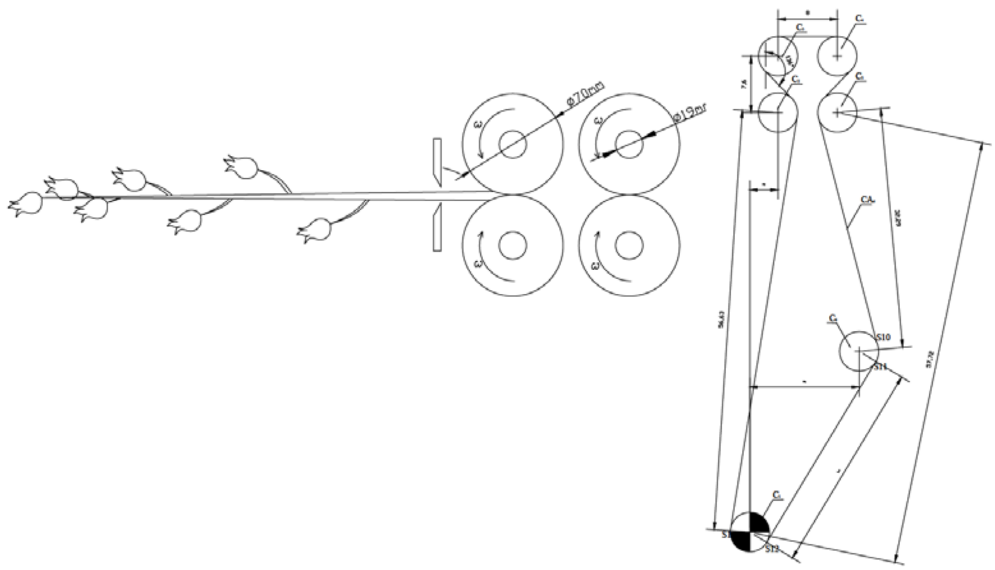

Fig. 2 Lateral view of the transmission system

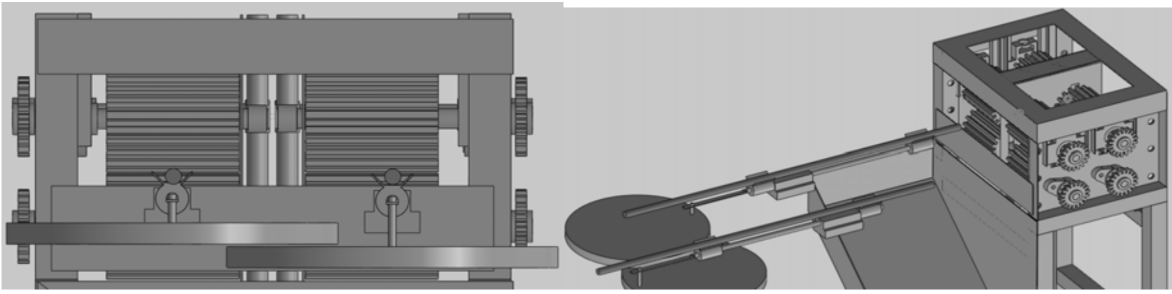

Fig. 3 Lateral and top view of the robotic handler

Robotic handler

The feeding system (Fig. 3) consists of two crankshaft rod devices which transform rotating movement into linear one. The linear movement transports the branch towards the pair of blades. A pair of ejectors in V-form avoid that the branch drops down. The circular cam rotates at 5 rpm and moves the steel shaft moving the branch toward the geared rollers. The base is soldered to the linear ball bearing giving the base a smooth movement to bring the branch to the harvester. A normal worker provides a branch every 5 seconds, while the gripper places a branch every 1.5 and 2 sec.

Result

The branch passes in middle of the gears lifting the upper one according to the branch diameter; transmission problems were observed in branches having diameters over 2 cm. As can be seen in Fig. 4 the upper and lower gear tooth are not in phase and as the branch is pulled the calyxes are separated.

Machine productivity depended on operator's ability to feed branches, flower maturity and uniformity, as well calyx turgor (Poblano et al., 2013). Tab. 1 shows that Nayarit variety presented the highest productivity of 64 kg/h as flowers are well distributed through the branch and the flower is big. Productivity is different due to the variety differences on diameters, flowers maturity state, turgor and calyxes' weight as well as the number of flowers in each branch. With the robotic handler productivity increased almost twice. Nayarit variety increased its productivity to 80 kg/h (Tab. 1) when the gripper placed every two seconds a branch, being more than what the operator can do.

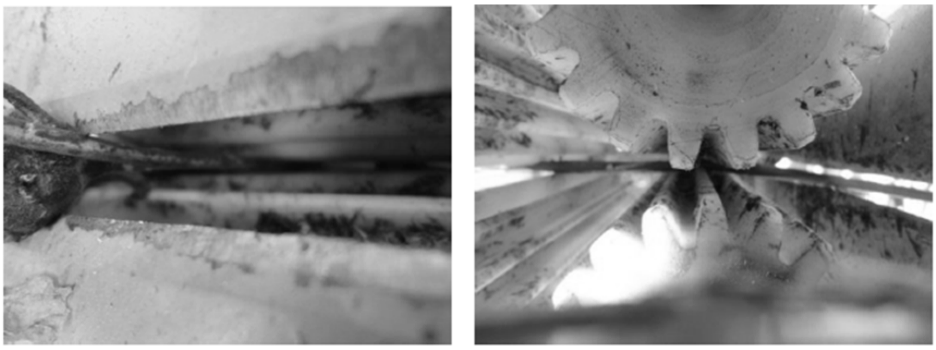

Fig. 4 Closer view of a branch being pulled by the roller gears

Tab. 1 Machine productivity per variety tested

	Productivity (kg/h)		
Manual/robotic	**Colima 5**	**Nayarit**	**Black Sudan**
Manual	43.2	64	62.5
Robotic	56	80	77

Tab. 2 Machine productivity whenthe robotic handler feeds branches at two different gripper placement times

Gripper placement, sec	Productivity (kg/h) Colima 5	Nayarit	Black Sudan
2	56	80	77
1.5	72	106	102

Tab. 3 Calyx quality obtained during manual and robotic harvesting

Variety	Manual feeding		Robotic feeder	
	Perfect calyxes, %	Calyx with cascalote, %	Perfect calyxes, %	Calyx with cascalote, %
Colima 5	85	10	80	15
Black Sudan	80	17.4	76	20
Nayarit	77	16	77	18

As the gripper placed one branch every 1.5 seconds over each arm of the robotic handler, better harvest productivity was achieved. The Black Sudan calyxes were harvested at 102 kg/hr, Tab. 2. A higher speed of one second could increase the productivity to 150 kg/hr but two grippers should be employed.

Productivity quality was affected by factors like flower turgor and maturation calyx differences throughout the branch. Several branches flowers containing cascalote were detached at the blades as flowers at the branches tip mature at last. The amount of green calyxes with green cascalote is considerable because the maturation of plants is not homogeneous. The better quality was obtained with Colima 5 variety and although Nayarit productivity is high its quality is not so high, Tab. 3.

Conclusion

It can be concluded that the gripper time required to place a branch over the robotic handler is the most important parameter to consider on harvest productivity. As it decreases to 1.5 seconds, productivity with Nayarit and Black Sudan varieties overpassed 100 kg/hr. A higher speed and number of gear rollers can increase harvest productivity even higher. Although more calyxes with green cascalote were harvested in the robotic system, total marketable calyxes by the robotic system overpassed by much the manual system. Productivity over time is very important during roselle harvesting.

Acknowledgement

I would like to thank CONACYT for the support for constructing the prototype.

Reference

Barragán S., Llamas S., Villalobos G., Mejías J., 2010. Diseño y análisis modal de una máquina despepitadora de jamaica. Ciencias Holguín, 16(2): 1-14.. (in Spanish)

Caro F., Machuca M., Flores E., 2012. El cultivo de Jamaica en Nayarit. [Roselle cultivation in Nayarit]. UAN, Nayarit, Mexico. Second Edition. ISBN: 978-607-7868-36-1. (in Spanish)

Poblano E., Hahn F., Hernández J., 2013. Geared rollers evaluation of roselle harvester. ASABE Technical Paper No. 1620291. St. Joseph, MI, USA.

Reyes A.A., Hahn F., 2009. Energy Optimization for a Roselle Harvester Machine. ASABE Technical Paper No. 097386. St. Joseph, MI, USA.

SILAGE MAIZE SIZE FRACTIONS EFFECTS ON BIOGAS PRODUCTION QUANTITY

Petr Hájek*, Petr Šařec, David Houška, David Hájek

Czech University of Life Science Prague, 165 21 Prague 6 – Suchdol, Czech Republic, Phone: +420 22438 3140, E-mail: hajekp@tf.czu.cz

Abstract

By the declaration of the EU-countries, the production of energy from renewable and sustainable resources to a certain percentage has given the biogas power plants a renewed attention. In this research project the focus is laid on the possibility to increase the efficiency of these power plants by optimizing a certain criterion. The knowledge of improvement of biogas production and the increase of its potential is also most crucial in an economical and sustainable way. This article specifically puts the attention to the crucial criterion of particle size in increasing efficiency and also the necessity of optimization of particle size. A specific influence has the fraction size of maize silage. In this research project one maize variety with different size particles were observed for the increase in efficiency of biogas production and thereby also their performances. This factor is firstly important for further development of efficiency and secondly for the identification of further factors which affect production and achieve higher utilization within biogas power plants. Identifying all the factors important for increasing the efficiency of biogas production will lead to a reduction in use of biological wastes and to an increase in utilization, as well as to a higher economic independency of power plant operating farms.

Key words: biogas utilization, particle size, maize silage

Introduction

Fraction size of maize is one of the essential properties of comminuted material. It is playing an important role in the utilization efficiency, and therefore it is necessary to define the most efficient fraction size. In order to use biological waste in the biogas production the most efficiently, it is necessary to know the rate of utilization of the fraction that would positively influence the biogas production. The research is focused on the material consumption and appropriate mix of chopped maize. The size can be influenced already during the harvest time for increasing the utilization and canned maize. At the moment of using maize with other raw materials, it is necessary to know how to prepare the substrate mixture. For calculating the dimension sizes, the ASAE Standards 1993 model was used.

Material and method

The method of size fraction determination has to be calculated by using ASAE standards. In a field, samples of the same maize variety differing only in harvesting machinery are chosen and taken afterwards from the harvesters in three different bags. After weighing, the geometric mean length needs to be calculated.

For this research one maize crops with the same FAO has been chosen. The maize crop has been chopped into three different particle sizes by the harvester JD 7050. Maize variety Ronaldinio was selected for this paper from the agricultural research farm in Czech Republic.

The whole shaking procedure was repeated for three samples, each 5 kg, from each of the harvesters using a screen shaker. The shaker was set to work for 120 second at the frequency of 2.4 Hz. After separation, the portions from individual screens were weighed. For the definition of silage maize quantity, it is necessary to calculate and measure the size of particles as geometric mean length Xgm (1) and standard deviation Sgm (2).(Lisowski, 2009)

Tab. 1 Harvesting characters of the silage maize Ronaldinio

Hybrid	FAO silage	The yield of green matter $t.ha^{-1}$	Solids %	The yield of dry matter $t.ha^{-1}$
Ronaldinio	250	66,67	34,93	23,29

Finally, the average mass from three different measurements left over on the screens is calculated and expressed also as percentage.

Analysis of mass distribution of all chopped forage materials is based on the assumption that these distributions are logarithmic normally distributed.

$$x_{gm} = \log^{-1}\frac{\sum(M_i \log[\bar{x}_i])}{\sum M_i} \tag{1}$$

For calculation of standard deviation, the following equation is used:

$$s_{gm} = \log^{-1}\left(\frac{\sum M_i (\log[\bar{x}_i - \log x_{gm})^2}{\sum M_i}\right)^{\frac{1}{2}} \tag{2}$$

where: X_{gm} - geometric mean length, M_i - mass on i^{th} screen, $\bar{\mathbf{x}}_{\mathbf{i}}$ – geometric mean length of particles on i^{th} screen, S_{gm} - standard deviation

The laboratory measurements were conducted according to DIN 38 414. The experiment was performed in a thermal water bath at mesophilic temperature conditions (35 ± 1 °C). For formulating series of dilution of experiments a mixture with 15 g of comparison mud (a sample of corn hybrid) and 385 g of inoculum, was used, the mixture totaling 400 g. The experiment for each corn hybrid was repeated four times. The control mixture was the comparison mud; it had a similar organic composition like mud in research. The control mixture was repeated four times as well. The self-standing bottle was filled with 400 g of mixture (385 g of inoculant and 15 g of comparison mud). The air in the bottle was displaced by nitrogen and the eudiometer was placed into the fermenter. With the help of layers of containers on the open tube of eudiometer a level of hydraulic fluid with sign 0 was placed. In this case the hydraulic fluid should not enter the connecting tube and sample of mud.

Before closing the tube, the standing bottle has been filled to circa one fourth of its volume and it was enclosed in Styrofoam to prevent the emersion of heat. The production of biogas peaked in the first week and decreases continuously during the experiment, which has lasted 35 days when the biological degradation was finished or until gas was still produced. The gas volume in the tube of the eudiometer is calculated by the temperature and air pressure in normalized state (273 K and 1013 mbar) (Cheng, 2009).

Results and discussion

The quality of energy crops used for biogas production is mainly determined directly in the field. The content and availability of substances which are able to produce methane are influenced by variety, cultivation, and stage of maturity during the harvest. Several relations between substrate biodegradability and substrate composition were found. An estimation of the potential of energy crops and animal manure to produce methane is essential. Maximum methane yield requires adequate and efficient nutrient supply for micro-organisms in the digester

Tab. 2 shows the weights of separated silage maize samples provided by the two harvesters. The average mass from three different measurements left over on the screens and expressed as percentage is also displayed in Tab. 1.

The results of geometric mean length are showed in Tab. 3. In this case, the results depend strongly on the harvesting machine and the pre-harvest preparation. The whole procedure affects quantity of maize silage for producing biogas. Nevertheless, the geometric mean length can influence only the quantity of produced biogas not its quality.

Through harvesting machinery and harvesting technology, the appropriate maize fraction for the usage in the biogas production can be prepared which would reduce the quantity required, as Tab. 1 describes.

Tab. 2 Mass distribution in percentage

Screen nr.	Nominal size opening (mm)	1. Ronaldinio		2. Ronaldinio		3. Ronaldinio	
		Average mass on screens (kg)	Percent of total mass on screens (%)	Average mass on screens (kg)	Percent of total mass on screens (%)	Average mass on screens (kg)	Percent of total mass on screens (%)
1	19.00	0.13	2.72	0.16	3.24	0.11	2.26
2	12.70	1.81	36.98	1.75	35.38	1.79	36.23
3	6.30	2.36	48.20	2.41	48.89	2.51	50.81
4	3.96	0.31	6.39	0.34	6.89	0.28	5.65
5	1.17	0.27	5.57	0.27	5.54	0.25	5.05
6	Pan	0.01	0.14	0.00	0.07	0.00	0.02

Tab. 3 Results of geometric mean length

Sample	Geometric mean length (mm)	Standard deviation (mm)
1. Ronaldinio	14.30	1.86
2. Ronaldinio	13.27	1.78
3. Ronaldinio	11.79	1.71

Tab. 4 Nutrient composition of the samples

Maize hybrid	XP	XL	XF	XA	ADL	Cel	Hem	C/N	Biogas Nl $(kg\ VS)^{-1}$	Methane Nl $(kg\ VS)^{-1}$
1. Ronaldinio	7.9	1.9	20.6	6.1	6.9	29.8	30.2	40.2	515	290
2. Ronaldinio	8.7	2.2	30.2	5.3	6.6	35.4	25.4	35.7	535	300
3. Ronaldinio	9.2	1.7	23.7	5.8	7.1	33.6	30.4	42.3	544	312

In Tab. 3 the results of the particle size measurements of the geometric mean length (mm) and Standard deviation (mm) are displayed of the three batches.

Tab. 4 gives the nutrient composition of the samples: XP = crude protein; XL = crude fat; XF = crude fibre; XA = crude ash; ADL = lignin; Cel = cellulose; Hem = hemi-cellulose and C/N = C:N ratio. Nl = norm litre (273 K, 1.013 bar).Biogas and methane yield per norm liter of volatile solids are listed as well. (Oechsner, 2003).

The maize varieties showed a characteristic methane production potential that was strongly dependent on their composition. The composition is mainly determined by the stage of vegetation and dry matter content. The nutrients crude protein (XP), crude fat (XL), cellulose (Cel) and hemi-cellulose (Hem) proved to have a significant influence on methane production. (Matjaz, 2010)

The C:N ratio rose from about 24 to >42. Anaerobic digestion requires a C:N ratio between 10 and 30. When the C:N ratio is too wide, carbon cannot optimally be converted to CH_4 and the CH_4 production potential is not fully achieved. When maize was harvested at high level of dry matter, the C:N ratio was outside the optimum range with regard to producing a maximum specific methane yield. Co-digestion of substrates with a narrower C:N ratio could help to overcome this disadvantage (Amon, 2007).

Conclusion

The biogas production is increasing its importance steadily within the energy sector throughout the European Union. The production of biogas is an environmental friendly procedure as well as a sustainable one, especially in the agricultural sector, as it bears the possibility to reduce the CO2 emissions. Therefore the knowledge of increasing efficiency and optimization of production processes gains on significance.

The research was focused on the heightening of efficiency in the biogas production and shows how important the particle sizes are to achieve this and it also opens the opportunity to further research in this specific topic. According to the results of the calculation and measurements, the smaller particle sizes are the one with the highest efficiency and have to be optimized during the harvest. As the size of the particles is one crucial criterion within the increase of efficiency of biogas production, this research topic has to be continued with the focus on other parts of the process of the production in order to achieve an even higher efficaciousness.

Acknowledgement

This proceeding originated within the project IGA TF nr. 2013:31180/1312/3120.

Reference

Amon T., Amon B., Kryvorchko V., 2007. Biogas production from maize and dairy cattle manure, Agriculture, Ecosystems and Environment, 118: 173-183.

ANSI/ASAE Standard 424.1 SEP92, “Part: Method of determining and expressing particle size of chopped forage materials by screening”.

DIN 38 414, 1985. Bestimmung des Faulverhaltens “Schlamm und Sedimente” Beuth Verlag GmbH, Berlin. (in German)

Cheng J., 2009. Biomass to Renewable Energy Processes, North Carolina State University USA, 517.

Lisowski A., Kostyra K., 2009. Efekty dzialania elementów wspomagajacych rozdrabnianie roślin kukurydzy a jakość kiszonki, Warszawa, 300. (in Polish)

Oslaj M., Mursec B., Vindis P., 2010. Biogas production from maize hybrids. Biomass and Bioenergy, 34(11): 1538–1545.

Oechsner H., Lemmer A., Neuberg C., 2003. Feldfruchte als Garsubstrat in Biogasanlagen; Landtechnik, 3: 146–147. (in German)

MODEL OF THE MECHANICAL BEHAVIOUR OF OIL BEARING CROPS SEEDS BASED ON THE TANGENT CURVE UTILIZATION

David Herák*, Abraham Kabutey, Monika Divišová, Risswanti Sigalingging

Czech University of Life Sciences Prague, Faculty of Engineering, Department of Mechanical Engineering, 16521 Prague 6 – Suchdol, Czech Republic, e-mail: herak@tf.czu.cz

Abstract

The article is focused on the description of the mechanical behaviour of oil bearing crops seeds under compression loading such as Jatropha curcas L., rape seeds and sunflower and also presents their related deformation characteristics. The article introduces mathematical model of their mechanical behaviour under compression loading which utilizes tangent curve function. The derivation and explanation of this mathematical model is an integrate part of article. The tangent curve function was used to describe the mechanical behaviour of oil bearing crops seeds at different pressing vessel diameters and seed pressing heights under compression loading. Based on the statistical analysis results, the tangent curve function was fitted by determining the force coefficient of mechanical behaviour and coefficient of mechanical deformation behaviour described the deformation behaviour of the seed pressing heights of oil bearing crops seeds with respect to the pressing vessel.

Keywords: mechanical model, crop seeds, pressing equipment

Introduction

To design suitable pressing equipment for processing oil bearing crops seeds with minimum energy performance, it is important to fully understand the mechanical behaviour of bulk material under compression loading (Sirisomboon, Kitchaiya, 2009). It is evident that determining the right pressing force could help achieve greater amounts of oil with minimum energy input (Herak et al., 2010; Singh, Kulshreshtha, 1996). Recently, some authors have also reported these deformation characteristics on oil bearing crops seeds using the tangent curve equation (Herak et al., 2010). The tangent curve equation was later modified to describe the mechanical behaviour of bulk seeds of jatropha, sunflower, rapeseeds and other materials such as spruce wood chips and paper chips (Herak et al., 2011; Herak et al., 2011a). The description of the mechanical behaviour and deformation characteristics using the tangent curve function has been verified by the finite element method (Petru et al., 2012). The aim of the study was to verify the general tangent curve equation was suitable for the description of mechanical behaviour of Rapeseeds, Sunflower seeds and Jatropha curcas seeds under compression loading for different pressing diameters and seed pressing heights.

Materials and methods

Sample

In this experiment, cleaned Rapeseeds (*Brassica napus* L.) and Sunflower seeds (*Helianthus annus* L.) both obtained from Czech Republic and Jatropha seeds (*Jatropha curcas* L.) obtained from Indonesia respectively, were used. The physical properties of the samples in terms of true and bulk densities, weight, moisture content and porosity (Blahovec, 2008) were also determined and have been presented in the Tab. 1.

Compression test

Compression devices namely ZDM 50 (VEB, Dresden, East Germany), pressing vessel with inner diameter D = 100 mm (Fig. 1) were used to determine the relationship between the magnitude of the pressing force and deformation of pressed mixtures initial pressing height of H = 80 mm. Also the pressing vessel has 16 holes at the bottom of diameter 3.5 mm where the oil passes. The pressing force was set between the range 0 kN and 250 kN to measure the deformation of the samples. The mixtures were pressed under the temperature condition of 20 °C and the pressing rate of 1 mm·s^{-1}. The experiment was repeated for each pressed mixture three times and averaged values were used in further calculations.

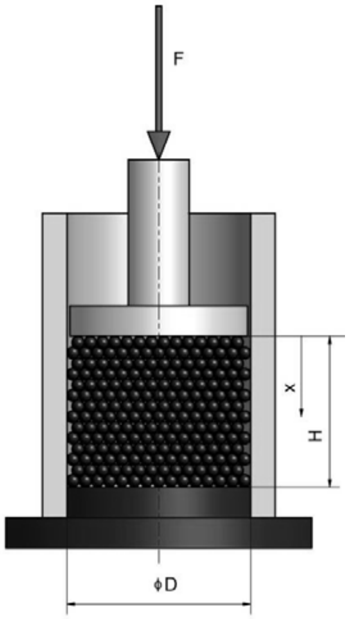

Fig. 1 Scheme of pressing equipment

Determination of general curve

The tangent curve equation can be described by Eq. 1 (Herak et al., 2011; Herak et al., 2011a)

$$F_D(x) = A \cdot [\tan(B \cdot x)]^n \qquad (1)$$

where $F_D(x)$ is the compression force (N) for deformation of bulk seeds, x (mm), A is force coefficient of mechanical behaviour (N) and B is coefficient of mechanical deformation behaviour (mm) in relation to the diameter of the pressing vessel. The deformation characteristic (Eq. 1) shows that the force coefficient of the mechanical behaviour A influences the slope of the deformation characteristic whereas deformation coefficient of the mechanical behaviour B also influences the range of deformation. The product of these two coefficients is essentially the initial rigidity of the system. Curvature of the curve is given by coefficient n (-) which is exponent of the compression curve.

The general tangent curve (Eq. 2) can be determined with aid of basic mathematical operations applied to the Eq. 1 (Herak et al., 2013)

$$F(x, D, H) = C \cdot D^2 \cdot \left[\tan\left(G \cdot \frac{x}{H}\right)\right]^n \qquad (2)$$

Where C (MPa) is stress coefficient is D (mm) is inside diameter of pressing vessel, G (-) is compression coefficient, x (mm) is bulk seeds deformation, H (mm) initial height of pressed bulk seeds, n (-) is exponent of the compression curve. The measured amounts of compressive force and deformation of jatropha seeds for different pressing heights and diameters of pressing vessels were analyzed with computer program Mathcad 14 (MathCAD 14, PTC Software, Needham, MA, USA), (Pritchard, 1998) uses Levenberg-Marquardt algorithm for data fitting (Marquardt, 1963; Lourakis, 2005) which is optimal for tangent curve approximation.

Tab. 1 Determined physical properties of seeds pressed mixture, data in the table are means ± SD

Crops seeds	ρ_t **(kg·m^{-3})**	ρ_b **(kg·m^{-3})**	***m*** **(g)**	M_c **(% d.b.)**	P_f **(%)**
Rapeseeds	1080 ± 2	716 ± 4	449.75 ± 1.12	6.8 ± 0.1	33.7 ± 0.5
Sunflower	885 ± 3	449 ± 4	282.25 ± 0.96	6.2 ± 0.2	49.2 ± 0.6
Jatropha	971 ± 3	386 ± 5	242.25 ± 1.01	5.7 ± 0.1	60.9 ± 0.6

ρ_t – true density, ρ_b – bulk density, m – mass of pressed mixture,
M_c – moisture content of the pressed mixture in dry basis, P_f – porosity of pressed mixture

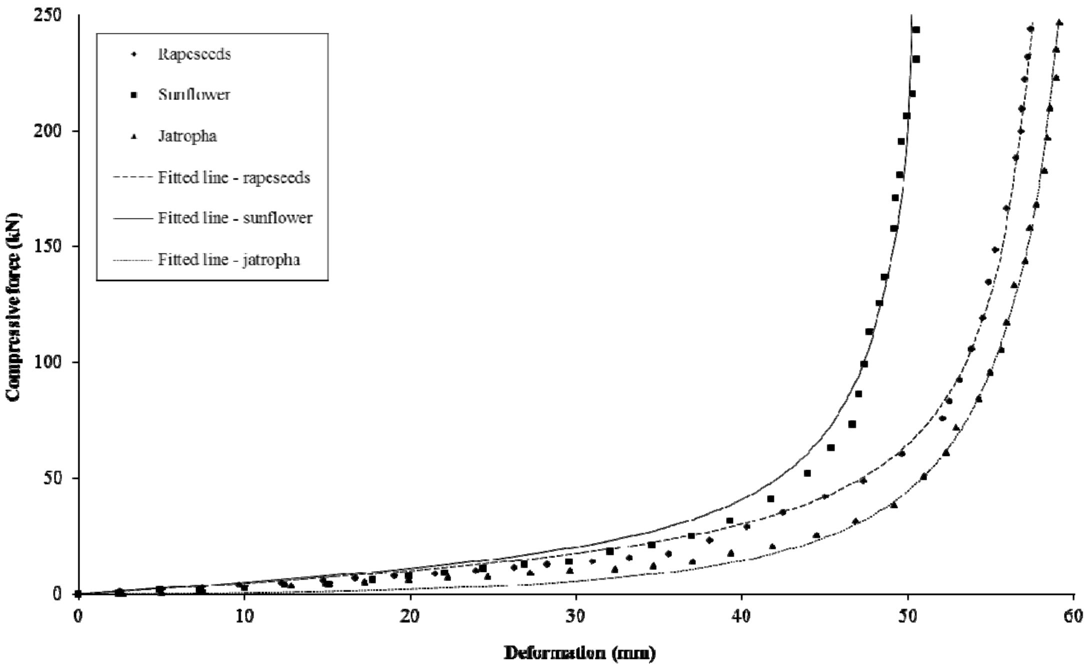

Fig. 2 Deformation characteristics

Tab. 2 Determined mechanical properties of seeds pressed mixture and data of statistical analyses for level of significance 0.05, data in the table are means ± SD

Crops seeds	*C* (MPa)	*G* (-)	*n* (-)	x_{max} (mm)	F_{crit} (-)	F_{ratio} (-)	P_{value} (-)	R^2 (-)
Rapeseeds	1.749	2.08	1	57.5 ± 1.2	3.978	$3.576 \cdot 10^{-3}$	0.952	0.998
Sunflower	1.624	2.40	1	50.6 ± 1.0	3.986	0.011	0.916	0.991
Jatropha	0.752	1.92	2	59.2 ± 1.8	3.967	$4.886 \cdot 10^{-3}$	0.944	0.998

C – stress coefficient, *G* – compression coefficient, *n* – exponent of the compressive function, x_{max} – maximal deformation, F_{ratio} - value of the F test, F_{crit} - critical value that compares a pair of models, P_{value} - the significance level at which it can be rejected the hypothesis of equality of models, R^2 – coefficient of determination

Results and discussion

The results of the pressed seed mixtures of rape, sunflower and jatropha from the dependency between compressive force and deformation characteristic are presented in Fig. 2. Tab. 2 also shows the measured parameters of maximal compression of the pressed bulk seeds. Statistical analysis of the determined amounts (Tab. 2) using software MathCAD 14 were significant where the values of F_{crit} were higher than F_{ratio} values and amounts of P_{value} were higher than significance level 0.05 and also high values of coefficients of determination R^2. These results are in accordance with already published study (Herak et al., 2012) in which the tangent curve equation has been solved and with aid of these results the tangent curve (Eq. 1) can be transformed in to general curve (Eq. 2).

From the results of this study, the tangent curve equation (Eq.2) (Herak et al., 2011; Herak et al., 2011a; Herak et al., 2013) comparing with the measured dependency, described accurately the dependency between the compressive force and deformation characteristic of the pressed bulk seeds (Herak et al., 2012) for different pressed volumes, it means different initial pressing heights and different inner diameter of pressing vessel. The physical properties of the bulk seeds of jatropha, presented in Tab. 1 shows that moisture content and porosity being constant can be substituted as means of M_c = (8.5 ± 0.2) % in dry basis (d.b.) and porosity, P_f = (59.98 ± 1.26) % respectively. Although the bulk seeds may vary biologically, the moisture content of the bulk seeds remained constant since a single batch of oil bearing crops seeds under the same temperature and storage conditions was used (Herak et al., 2013).

Conclusion

A general equation describing the mechanical behaviour of oil bearing crops seeds under compression loading was determined by tangent curve equation (Eq. 2) with stress constant of mechanical behaviour and compression coefficient. The general equation was statistically analysed and the results showed that measured amounts of deformation characteristic were statistically significant similar to the amounts determined from this general equation (Eq. 2) with its validity limited from zero to maximum deformation of the bulk seeds. The moisture content and porosity of the bulk seeds of jatropha were found to be constant but their changes could also influence the mechanical behaviour of oilseeds such as jatropha under compression loading. The tangent curve equation having been established in previous studies described accurately the deformation characteristics of the selected oilseeds.

Reference

Blahovec J., 2008. Agromaterials. CULS Prague, 102. ISBN 978-80-213-1784-0.

Herak D., Gurdil G., Sedlacek A., Dajbych O., Simanjuntak S., 2010. Energy demands for pressing Jatropha curcas L. seeds. Biosystems engineering, 106(4): 527-534.

Herak D., Kabutey A., Sedlacek A., 2011. Mathematical description of rape seeds' (Brassica napus L.) mixture mechanical behaviour under compression loading. Scientia Agriculturae Bohemica, 42(1): 31-36.

Herak D., Kabutey A., Sedlacek A., Gurdil G., 2011a. Tangent curve utilization for description of mechanical behaviour of pressed mixture. Research in Agricultural Engineering, 57(1): 13-18.

Herak D., Kabutey A., Divisova M., Svatonova T., 2012. Comparison of the mechanical behaviour of selected oilseeds under compression loading. Notulae Botanicae Agrobotanici Cluj – Napoca, 40(2): 227-232.

Herak D., Kabutey A., Divisova M., Simanjuntak S., 2013. Mathematical model of mechanical behaviour of Jatropha curcas L. seeds under compression loading. Biosystems engineering, 114(3): 279-288.

Lourakis M.I.A., 2005. A Brief Description of the Levenberg-Marquardt Algorithm Implemented by Levmar, ICS FORTH, Heraklion.

Marquardt D.W., 1963. An Algorithm for the Least-Squares Estimation of Nonlinear Parameters, SIAM. Journal of Applied Mathematics, 11(2): 431-441.

Petru M., Novak O., Herak D., Simanjuntak S., 2012. Finite element method model of the mechanical behaviour of Jatropha curcas L. seed under compression loading. Biosystems Engineering, 111(4): 412-421.

Pritchard P.J., 1998. Mathcad: A Tool for Engineering Problem Solving, McGraw-Hill Science Engineering.

Singh S., Kulshreshtha M., 1996. Mathematical modelling of juice expression from carrots under uniaxial compression. Journal of Food Engineering, 27(3): 323 -336.

Sirisomboon P., Kitchaiya P., 2009. Physical properties of Jatropha curcas L. kernels after heat treatments. Biosystems Engineering, 102(2): 244-250.

COMPARISON OF VARIANT SOLUTIONS OF HOP STRINGS AND ATTACHMENTS

Petr Heřmánek[1*], Ivo Honzík[1], Adolf Rybka[1], Bohuslav Jošt[1], Lubomír Vent[2], Jiří Mašek[1]

[1]Czech University of Life Sciences Prague, Faculty of Engineering, 165 21 Prague 6 – Suchdol, Czech Republic, Phone: +420, Fax: +420-24383122, E-mail: hermanek@tf.czu.cz
[2]CHMEL-Vent Ltd. Kněžice 18, 438 01 Žatec, Czech Republic

Abstract

The article deals with different variants of hop string hanging, a description of the measuring device and a measurement of the pulling force itself in a field test, and a realization of break tests in laboratory conditions with both new and used wires and twines. The field tests results proved advantageous the hanging variant combining a steel annealed wire of 1.00 mm in diameter and a polypropylene twine of strength designation 12 500 in the form of a simple attachment. Other tested variants included a steel annealed wire of 1.00 mm and 1.12 mm in diameter. Among the new trends in stringing is the use of a hemp twine with a factory designation 323 N, a jute twine with a factory designation 1700x3 and 2200x2, a paper twine with a factory designation 5000 and 1700x3, a galvanized clip of type VR16 and an attachment of a steel wire of 2.60 mm in diameter. The research dealing with issues of hop string hanging was carried out the third year in a row in a hop field CHMEL-Vent Ltd., Kněžice.

The field test monitored strength relations between a guide wire (hop string) and its attachment, or – with the variant of a direct attachment of a hop string to the supporting wire of the hop field trellis – the relation between a guide wire and the supporting wire. In the course of the test we carried out a measurement of the strength of the wires and twines when the hop bines were being pulled down. At the same time samples were taken from the hop field for the purpose of a laboratory measurement of both hop strings and attachments strength to find out about any changes in strength compared to new hop strings and their attachments.

After all the measurements had been processed, their analysis was performed. The break test revealed that wire strength is influenced by the microclimate of the hop field only minimally. In the case of twines it was confirmed that the size of the breaking force depends on the immediate twine moisture. That explains why the laboratory break test resulted in a higher breaking force than in the field measurement which had been done in rainy weather. In recent years laboratory testing proved that the breaking force with a moist twine decreases approximately by a half.

The results of pulling down the bines we got at the field measurement again proved the advantageousness of the hanging variant combining a black annealed wire of 1.0 mm and a polypropylene twine with a strength designation 12500 in the form of a simple attachment. When the given variant was being pulled down, 91 % of breakage occurred with the twine at zero spontaneous bines falling during the growing season. Approximately equal results showed other variants which combined black annealed wire 1.0 mm and hemp twine 323 N with a simple attachment, jute twine 2200x2 with a double attachment, and variants of wire 1.0 mm and paper twine 5000 with a simple attachment.

In the case of hanging by means of clips we used a type of thin clip, contrary to last year. In the course of the growing season spontaneous loosening and falling of bines occurred.

Key words: hops, hop string, twine, pulling down

Introduction

Purity of hops in the period of its overproduction is one of the chief indicators for quality of hops processing provided by grower. Nowadays, when a hop string – being a wire – is hung on the supporting structure by means of an attachment from polypropylene twine, it is possible to search for alternative solutions of hanging which would substitute the polypropylene twine. Thus any contamination of hops meant for further processing would be eliminated (Portner, 2007; Gobor, Fröhlich, 2010).

Material and method

A research dealing with alternative hanging of hop strings was carried out for the third year in a row in the hop field spreading between the towns of Oploty and Neprobylice nearby the town of Žatec. In 2012 we took over the attachment variant with only the most suitable combination of strength. The experiment was further extended by another variants. Besides hanging of hop strings by means of twines, we also tested other alternatives of hanging without using twines (Heřmánek et al., 2012).

The field experiment monitored strength relations between a guide wire (hop string) and its attachment, or –with the variant of a direct attachment of a hop string to the hop field supporting wire – a relation between a guide wire and a supporting wire. In the course of the test we carried out a measurement of the strength of wires and twines when the hop bines were being pulled down. At the same time samples were taken from the hop field for the purpose of a laboratory measurement of both hop strings and attachments strength to find out about any changes in strength compared to new hop strings and their attachments. The field experiment included seventeen variants of hop-string attachment to the supporting wire of the hop field (Fig. 1). In the experiment we worked with:

- steel annealed wire of 1.00 mm and 1.12 mm in diameter,
- polypropylene twine with factory designation 12 500,
- hemp twine with factory designation 323N,
- jute twine with factory designation 1700x3 and 2200x2,
- paper twine with factory designation 5000 and 1700x3,
- galvanized clip, type VR16,
- steel wire attachment of 2.60 mm in diameter.

During the growing season of hops we monitored any spontaneous falling of hop bines caused by the breakage of a hop string or an attachment. An attachment was broken at a drop in strength due to the impact of the hop-field microclimate on the used material. In the case of hop strings the problem lay mostly in breaking-off or fraying due rubbing against the supporting wire. Based on the total number of fallen bines we selected the perspective variants to put them to further testing. To measure the breaking force of a hop string or an attachment we used the device proven in years past.

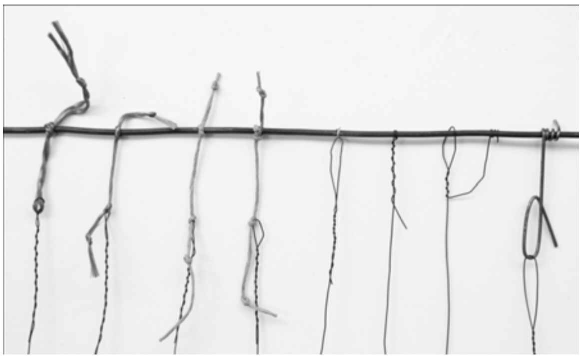

Fig. 1 Used variants of hop-string attachments
From the left: double attachment, simple attachment, simple attachment with simple knot, simple attachment with double knot, usage of clip, wire on wire, wire on wire with brake, fixed hanging

The device consists of a tractor with a connected semi-trailer which was supplemented with a frame for swing anchorage of the tensile sensor. The other side of the sensor was prolonged by the semi-trailer to catch hop bines when pulled down. The device dimension had been designed in a way to enable the same conditions for pulling down as with harvest pullers. This means that both the place of bine attachment at pulling down and the bine angle at pulling down were kept. The swing placement of both ends of the tensile force sensors ensured that at pulling down only the axial force in the hop string was measured. To measure the force itself we used a tensile force sensor supplied by HBM Brno company (exclusive representation by Hottinger Baldwin Messtechnik GmbH company) with type designation U9B and measuring range 0-1kN. The sensor output signal was further processed by means of MGC plus, a mobile central measuring station also supplied by HBM company and connected to a laptop. The central measuring station, sensor, and the measured data storage were secured by Catman Easy program, which is provided with the station (Rybka et al., 2011).

The measurement was always carried out in the course of an uninterrupted pulling of hop bines down in one row of the experimental hop field during which we recorded minimum of ten measuring values. Bines were cut off the ground at a height of app. 0.8 m and passed through the loop on the arm of the sensor. As the tractor was passing along they were stretched at an angle of 45° and due to a continuous pull a hop string or an attachment broke. After being pulled down, the hop bines were placed on the semi-trailer. In the course of pulling the bines down the sensor was measuring the tensile force at a time frequency of 50 Hz (Fig. 2).

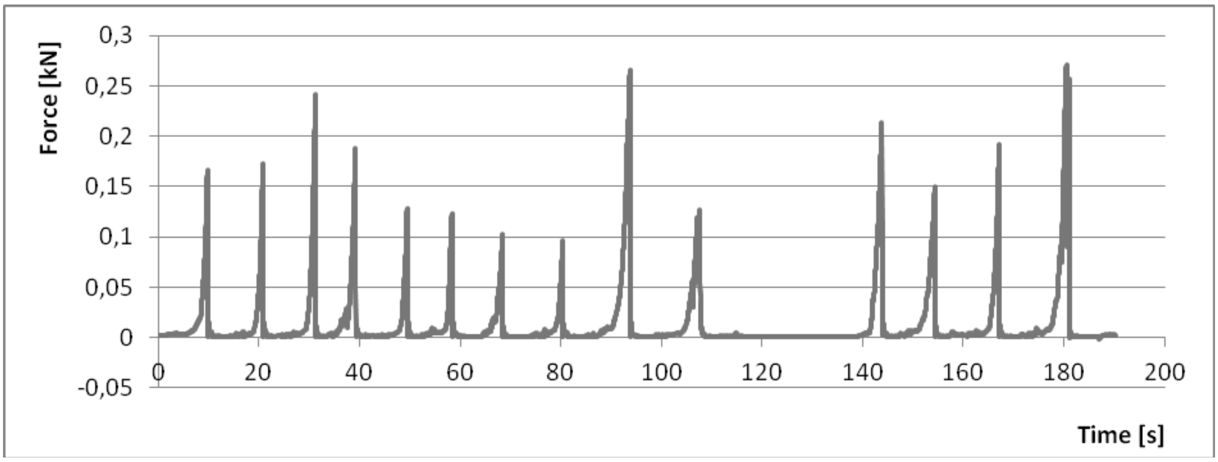

Fig. 2 Graph of progress of the tensile strength measured when pulling down hop bines
Variant of a hop string made of black annealed wire of 1.0 mm in diameter, and an attachment made of hemp twine 323N in the version of a simple attachment

Tab. 1 Results of the field measurement

	Polypropylene 12 500 Simple attachment	Hemp 323N Simple attachment	Jute 1700x3 Double attachment	Jute 2200x2 Double attachment	Paper 5000 Simple attachment	Paper 5000 Simple attachment, double knot	Paper 5000 Double attachment	Paper 1700x3 Double attachment	Fixed hanging 2.6 mm	Wire on wire with brake Ø 1.00 mm	Wire on wire with brake Ø 1.12 mm
	Breaking force										
Average [N]	212	173	297	256	245	301	303	309	345	270	396
Standard deviation [N]	38	54	39	39	59	42	43	40	54	25	22
Variation coefficient [%]	18	31	13	15	24	14	14	13	16	9	6

Tab. 2 Finding of the break point in one hop-field row for each measured variant

Description	**Total n^{o} of bines**	**Breakage in wire**		**Breakage in twine**	
	[pcs]	[pcs]	[%]	[pcs]	[%]
Polypropylene 12500 Simple attachment	180	16	9	164	91
Polypropylene 12500 Double attachment	186	87	47	99	53
Hemp 323N Simple attachment	181	19	10	162	90
Jute 1700x3 Double attachment	176	130	74	46	26
Jute 1700x3 Double attachment	186	160	86	26	14
Jute 2200x2 Double attachment	176	12	7	164	93
Paper 5000 Simple attachment	174	17	10	157	90
Paper 5000 Simple attachment, double knot	159	14	9	145	91
Paper 5000 Double attachment	168	162	96	6	4
Paper 1700x3 Double attachment	165	125	76	40	24

Results and discussion

The values measured in the course of pulling the bines down allowed us by means of a database program to get the values of breaking forces of a hop string or an attachment. The average values of all the measured variants are presented in Tab. 1.

For each measured variant with a twine attachment we chose a row in which we counted the number of hop strings. This was followed by pulling by means of a regular puller. After all the row of bines had been pulled down, we recorded the number of breakage in wire and the number of breakage in twine. Regarding the quality of work, breakage in wire proves to be more convenient, as the hop-string wire is completely removed and the attachment twine is partly or completely removed from the hop field (Tab. 2).

For the purpose of break tests we used a new material both with wires and twines before hanging and during the harvest samples of twine attachments and hop-string wires were taken. For each of the measured variants ten pcs of samples were taken in a way that the hop-string wire was cut app. 1 m off the upper end and then the twine attachment was cut off just below the supporting wire of the hop field. Thus when the samples were being taken, neither twines nor wires were strained by the tensile strength. Altogether we took samples of 6 twine types, 10 pieces of each, and 2 wire types, also 10 pieces of each. Then a break test was performed with Amsler-200 break test machine to record the breaking force. The break tests results of the 10 measurements are to be found in the graph (Fig. 3).

After all of the measurements had been processed, their analysis was performed. The break test revealed that the hop-field microclimate has only minimal influence on wire strength. In case of twines the breaking force proved to be dependent on the immediate twine moisture. That explains why the measured breaking force showed a higher value in the laboratory break test than in the field measurement which had been carried out in rainy weather. Over the past years the laboratory tests have already proved that with a moist twine the breaking force drops approximately by a half.
Bines began falling down from June 18th 2012. The worst proved to be the variants with paper twine 1700x3, wire on wire, and wire with brake, with a fall of more than 40 %. In the case of galvanized clip the bine fall reached 25 %. The other variants showed a zero fall or a fall of maximum 2 %.

Conclusion

The results of pulling hop bines down in a field measurement obviously indicate that the same as in 2011 the most convenient hop-string hanging proved to be the variant combining black annealed wire 1.0 mm and polypropylene twine of 12 500 strength designation, in the version of a simple attachment. When the given variant was being pulled down, it reached 91% breakage in the place of twine at a zero spontaneous fall of bines in the growing season. Similar results also showed other variants using black annealed wire 1.0 mm and hemp twine 323N with a simple attachment, jute twine 2200x2 with a double attachment, and the variants combining wire 1.0 mm and paper twine 5000 with a simple attachment.
In the case of hanging by means of clips, contrary to 2011 we used a thinner type of clip. In the course of the growing season spontaneous opening of clips and falling of bines occurred, but fixed hanging showed very good results as for both spontaneous bine fall during the growing season and pulling down the bines.

Acknowledgement

This article was written with the support of the Ministry of Agriculture of the Czech Republic as a part of NAZV QI101B071 research project.

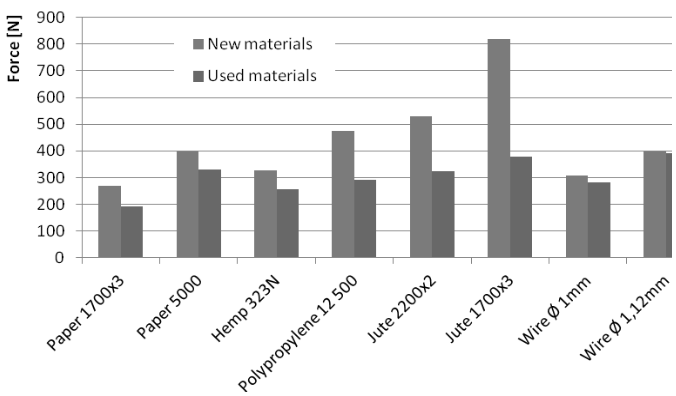

Fig. 3 Graph comparing the breaking force in laboratory measurement using new materials, and in field measurement during pulling down the hop bines

Reference

Gobor Z., Fröhlich G., 2010. Automated fastening of support wire in high trellis of hop. Landtechnik-Agricultural Engineering, 65: 283-285. (In German).

Heřmánek P., Rybka A., Honzík I., Vent L., Jošt B., Mašek J., 2012. Analysis of Strength Ratio of Different Hop Strings. Research in Agricultural Engineering (Zemědělská technika), 58 (4): 148-154. ISSN: 1212-9151.

Portner J., 2007. Einflussgrössen und produktionstechnische Massnahmen zur Verbesserung der Hopfenqualität für die Brauerei. Proceedings of the Technical Commission IHGC of the 51th International Hop Growers Congress, Yakima. (In German)

Rybka A., Heřmánek P., Honzík I., Mašek J., Vent L., 2011. Analysis of various implementations of hop strings during hop production. Plant, Soil and Environment, 57 (9): 441-446. ISSN: 1214-1178.

INFLUENCE OF TEMPERATURE AND STORING TIME ON SELECTED PHYSICAL PROPERTIES OF ROSE ACACIA HONEY

Peter Hlaváč*, Monika Božiková

Slovak University of Agriculture in Nitra, Faculty of Engineering, Department of Physics, SK-949 76, Nitra, Slovak Republic, Phone: +421376414749, Fax: + 421377417003, E-mail: Peter.Hlavac@is.uniag.sk

Abstract

This article deals with rheologic and thermophysical properties of rose acacia honey in Slovakia. Some physical properties of different kinds of honey are mentioned in literature. In generally physical properties of honey are influenced by various factors as: type of flowers, way of processing and most of all the area of origin, etc. Research of honey physical properties in Slovakia is in the beginning and particular properties are not known. The main aim of this contribution is to present selected rheologic and thermophysical properties of rose acacia honey, which quality is considered most highly in Slovakia. Our research was oriented on measuring of rheologic properties and thermophysical properties of honey. Measuring of dynamic viscosity was performed by digital rotational viscometer Anton Paar DV-3P, and measuring principle is based on dependency of sample resistance against the probe rotation. Thermophysical parameter measurements were done by instrument Isomet 2104, which uses for measuring Hot Wire method. Sample of honey was stored at laboratory temperature and was measured in different days during storage. Measurements were performed in temperature interval (20 – 43) °C. Dependencies of rheologic parameters as: dynamic and kinematic viscosity and fluidity on temperature and on storing time and dependencies of thermophysical parameters as: thermal conductivity and specific heat on temperature and storage are described. Temperature dependencies of dynamic and kinematic viscosity could be characterized by decreasing exponential function and temperature dependencies of fluidity by increasing exponential function. Relations between thermophysical parameters and temperature during the heating process had linear increasing shape. Values of dynamic and kinematic viscosity and thermophysical parameters were a bit higher after storing that can be caused by loosening of the water during storage. Values of fluidity were a bit smaller after storing, which is caused by loosening of the water, respectively by crystallization during the storage.

Keywords: temperature, storing time, rose acacia honey

Introduction

Automatically controlled processes at manufacturing, at handling and holding require exact knowledge about physical quantities of materials. Some physical properties of different kinds of honey are mentioned in literature. Komatsu et al. (2002) analyzed physical and chemical properties of wild flower honeys. Golob et al. (2002) were interested in sensory properties of Slovenian honeys. Bhandari et al. (1999) examined rheological properties of Australian honeys. They found out that rheologic properties of honey depend on the composition of individual sugars, and the amount and type of colloids presented in honey. Zaitoun et al. (2001) examined rheologic properties of selected light – coloured Jordanian honeys. They found out that the viscosity of honey decreases with water content. The water content is the major factor that influences the keeping quality or storability of honey. Chirife and Buera (1997) described simple model for predicting of viscosity of sugar and oligosaccharide solutions. They found out that disaccharides, made of two monomeric monosaccharides, give rise to a higher viscosity than monosaccharides when compared at the same mass fraction. Junzheng and Changying (1998) were interested in rheological model for natural honeys in China. They and many other authors had reported that honeys behave as Newtonian fluid. Honey viscosity was Newtonian, even in reduced-calorie varieties, and adhered to the Arrhenius equation, viscosity exponentially decreasing with temperature (Cohen, Weihs, 2010). White Jr. et al. (1964) examined the effect of storage and processing temperature on honey quality. In their investigation they found out that dark-coloured types of honey tend to be affected by heat faster than light-coloured types. It is natural for many types of honey to granulate or crystallize upon storage. Since the retail honey market largely favours liquid honey, some types of processing are necessary to maintain the liquid state. This is most commonly done by straining, heating, or filtration (White, 1999). In honey processing, heating is applied for the following reasons:

1. to warm it sufficiently to facilitate straining, handling, and packing;
2. to delay granulation.

Other reasons for heating of honey are to destroy yeast that may be present; hence, the keeping quality of the honey is assured (White, 1975).

In generally physical properties of honey are influenced by various factors as: type of flowers, way of processing and most of all the area of origin, etc. Research of honey physical properties in Slovak Republic is in the beginning and particular properties are not known. Our research was oriented on measuring of rheologic and thermophysical properties of honey.

In generally all food material during processing and storage goes through the thermal or mechanical manipulation, so it is convenient to know thermophysical and mechanical (especially rheologic for liquid materials) parameters. Measurement of thermal properties of selected food materials are described in publications Hlaváč and Božiková (2011) and Božiková and Hlaváč (2010).

Material and method

Honey is primary product of bees and it belongs between natural sweeteners, it is also known for its healthy effects. Main parts of honey are nectar and honeydew. Nectar is the secretion of the plant organs and it consists of concentrated solution of sugars (glucose, fructose, sucrose and maltose). Honeydew is plant juice, which passed through the part of bee digestive tract. Its main ingredients are also sugars, but in more varied compound. Honey is mixture of sugars, water and other components. Individual composition of honey depends mostly from mixture of flowers visited by bees producing the honey and it is different according to locations, terms and particular colony of bees. Honey in general consists from fructose (approximately 38 %), glucose (about 31 %), sucrose (around 1 %), other sugar (about 9 %), water (approximately 17 %), ash (around 0.17 %) and other substances (Hlaváč, Božiková, 2012). Honey is well appreciated in many places and its consumption has been increased either as raw material or as a food ingredient. Its use as food by the consumer, or even for exportation, implies safety inherent in its quality and processing control (Bera et al., 2008).

Viscosity as one of the most important rheologic parameters is defined as the resistance of a fluid to flow. Physical unit of dynamic viscosity in SI units is Pa.s. Viscosity changes with temperature. The difference in the effect of temperature on viscosity of fluids and gases is related to the difference in their molecular structure. Viscosity of most of the liquids decreases with increasing temperature. The effect of temperature on viscosity can be described by an Arrhenius equation .

$$\eta = \eta_0 \, e^{-\frac{E_A}{RT}} \tag{1}$$

where η_0 is reference value of dynamic viscosity, E_A is activation energy, R is gas constant and T is absolute temperature (Figura, Teixeira, 2007).

Liquid molecules are closely spaced with strong cohesive forces between them. The dependency of viscosity on temperature can also be explained by cohesive forces between the molecules (Munson et al., 1994). As temperature increases, these cohesive forces between the molecules decrease and flow became freer. As a result viscosities of liquids decrease as temperature increases. In liquids, the intermolecular (cohesive) forces play an important role (Sahin, Sumnu, 2006).

Between rheologic parameters can be also included kinematic viscosity and fluidity. Kinematic viscosity ν ($m^2.s^{-1}$) is defined by equation (2) as a ratio of dynamic viscosity to density of fluid at the same temperature. Fluidity φ (Pa-1.s-1) is defined by equation (3) as reciprocal value of dynamic viscosity.

$$\nu = \frac{\eta}{\rho} \quad , \quad \varphi = \frac{1}{\eta} \tag{2, 3}$$

Thermophysical parameters are one of the complex material characteristics. Thermal conductivity and thermal diffusivity could be counted into the thermophysical characteristics Thermal conductivity λ ($W.\ m^{-1}.K^{-1}$) is defined as ability of material to conduct heat and thermal diffusivity a ($m^2.s^{-1}$) is defined as velocity of temperature equalization in material during non stationary processes.

Rheologic and thermophysical measurement method

Measuring of dynamic viscosity was performed by digital viscometer Anton Paar (DV-3P). Principle of measuring by this viscometer is based on dependency of sample resistance against the probe rotation. Probe with signification R2 was used in our measurements. We have chosen frequency of probe rotation 200 min^{-1}.

The hot wire method is a standard transient dynamic technique. For dynamic techniques is typical that they are more comfortable than stationary techniques because of short measurement time. Hot Wire method (HW) is based on the measurement of the time - temperature relation in defined distance from the heat source (hot wire) (Davis, 1984). The heating wire as well as the temperature sensor (thermocouple) is encapsulated in a probe that electrically insulates the hot wire and the temperature sensor from the test material (Wechsler, 1992). Heat flux is generated for an appropriate time interval through a long thin uniform wire buried in the sample and the temperature response is measured by the change in resistance of the wire. The response is analysed in accordance with a model characterised by the particular formula found by solution of the partial differential equations using boundary and initial conditions corresponding to the experimental set up (Hlaváč, Božiková, 2011).

Temperature dependencies of dynamic and kinematic viscosity can be described by decreasing exponential functions (4, 5) and in the case of temperature dependencies of fluidity can be used increasing exponential functions (6). Temperature dependency of thermal conductivity can be described by linear increasing functions (7) and in the case of temperature dependency of thermal diffusivity can be used linear decreasing function (8).

$$\eta = A e^{-B\left(\frac{t}{t_o}\right)}, \nu = C e^{-D\left(\frac{t}{t_o}\right)}, \varphi = E e^{F\left(\frac{t}{t_o}\right)},$$

$$\lambda = G + H\left(\frac{t}{t_0}\right), \quad a = K - L\left(\frac{t}{t_0}\right) \qquad (4, 5, 6, 7, 8)$$

Where t is temperature, t_0 is 1 °C, A, B, C, D, E, F, G, H, K, L are constants dependent on kind of material, and on ways of processing and storing.

Results and discussion

Sample of rose acacia honey was stored at laboratory temperature and was measured in different days during storage. Measurements were performed in temperature interval from laboratory temperature till 43 °C. On honey sample were performed two measurements of rheologic properties and two measurements of thermophysical properties (at the beginning of storage and after one week of storing). Dependencies of dynamic viscosity, kinematic viscosity, fluidity, thermal conductivity and diffusivity on temperature and on storing time were examined. Results are shown on Fig. 1 – 5. Relations of dynamic viscosity to the temperature for sample of rose acacia honey are presented on Fig. 1. There are values from two measurements: first measurement (at the beginning of storage) and next measurement (after one week of storing).

It is possible to observe from Fig. 1 that dynamic viscosity of rose acacia honey is decreasing with increasing of temperature. The progress can be described by decreasing exponential function, which is in accordance with Arrhenius equation (1). It is also evident that values of dynamic viscosity were a bit higher after one week of storing and that can be caused by loosening of the water during storage. Relations of kinematic viscosity and fluidity to the temperature for sample of rose acacia honey are presented on Fig. 2 and Fig. 3. The dependency of kinematic viscosity on temperature can be also described by decreasing exponential function (Fig. 2). It is also evident that values of kinematic viscosity were a bit higher after one week of storing. That can also be caused by loosening of the water during storage. The temperature dependency of fluidity can be seen on Fig. 3. It is evident that fluidity is increasing with increasing of the temperature. The flow of the honey is better at higher temperatures. It is also evident that values of fluidity were a bit smaller after one week of storing. That can be caused by loosening of the water respectively by crystallization during the storage. All coefficients of regression equations and also coefficients of determination are presented in Tab. 1. In all cases were the coefficients of determination very high. It is also evident that storage time had effect on rheologic properties of examined sample of honey.

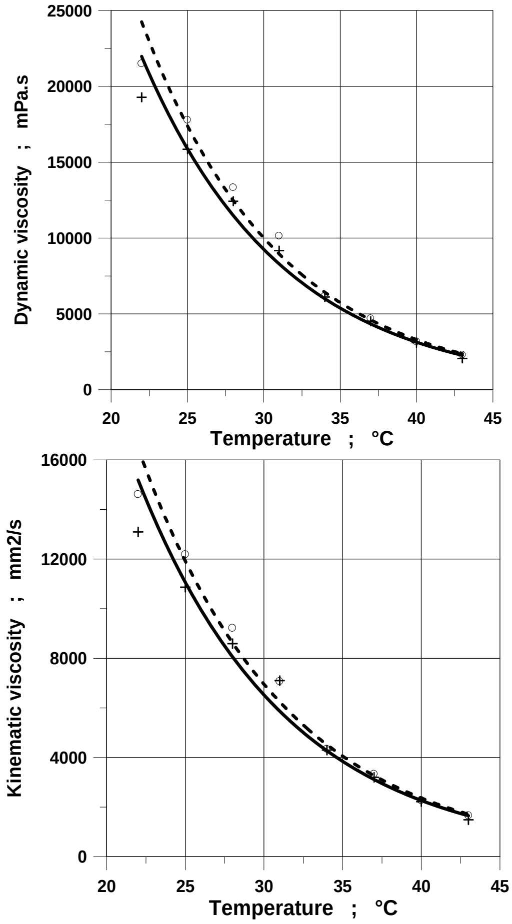

Fig. 1 – 2 Relations of rose acacia honey dynamic and kinematic viscosity, and fluidity to temperature: first measurement (+), next measurement (after one week of storing) (○)

Relations between thermal conductivity, thermal diffusivity and temperature are showed on Fig. 4 – 5. It demonstrates linear relations between thermophysical parameters and temperature during temperature stabilization of honey sample. Fig. 4 show that with increasing of the honey temperature the thermal conductivity increases linearly. But on the other hand thermal diffusivity of honey has linear decreasing progress during the temperature stabilisation process (Fig. 5). All obtained results are in good agreement with literature Figura and Teixeira (2007) and White (1975). It was showed that the thermal conductivity of high viscosity liquids or suspensoid materials can be measured with Hot wire method. For data reliability protection there were measured series of one hundred measurements for every point in presented graphic relations. Every point in graphics characteristics was obtained as average from measured values. All coefficients of regression equations and also coefficients of determination are presented in Tab. 1. In both dependencies were the coefficients of determination very high.

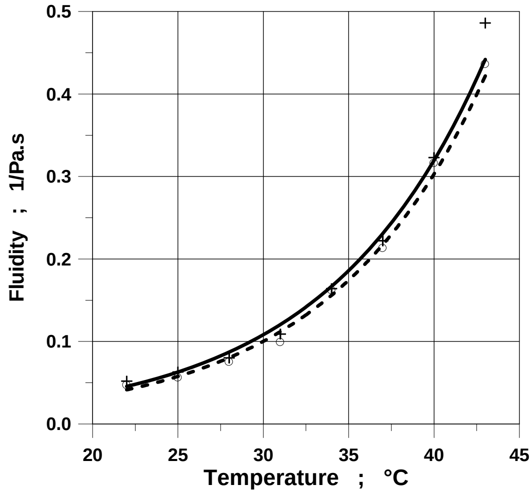

Fig. 3 Relations of rose acacia honey fluidity to temperature: first measurement (+), next measurement (after one week of storing) (○)

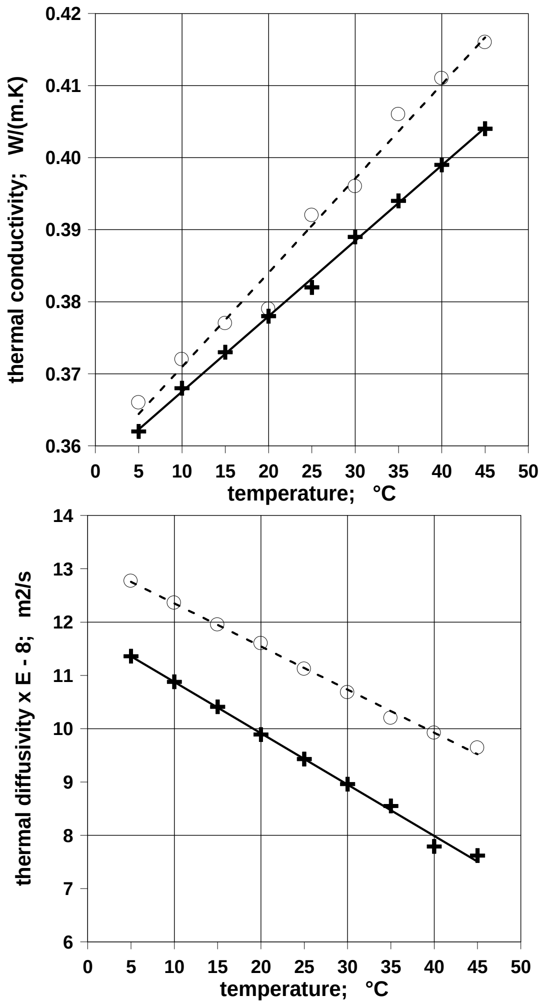

Fig. 4 – 5 Relations of rose acacia honey thermal conductivity and diffusivity to temperature: first measurement (+), next measurement (after one week of storing) (○)

Tab. 1 Coefficients A, B, C, D, E, F, G, H, K, L of regression equation (4, 5, 6, 7, 8) and coefficients of determinations

	Regression equations (4, 5, 6,7, 8)				
Rose acacia honey	**Coefficients**				
Measurement	**A [mPa.s]**	**B [1]**	**R^2**	**G[$W.m^{-1}.K^{-1}$]**	**K [$mm^2.s^{-1}$]**
First	237 655	0.108 231	0.990 000	0.357 056	0.118 389
Next	277 490	0.110 788	0.991 557	0.360 306	0.131 594
Measurement	**C [$mm^2.s^{-1}$]**	**D [1]**	**R^2**	**H [$W.m^{-1}.K^{-1}$]**	**L [$mm^2.s^{-1}$]**
First	155 260	0,105 675	0.982 558	0.001 046 67	0.000 966 3
Next	176 582	0.107 826	0.991 115	0.001 050 0	0.000 808 7
Measurement	**E [$Pa^{-1}.s^{-1}$]**	**F [1]**	**R^2**	**R^2**	**R^2**
First	0.004 199 7	0.108 285	0.989 684	0.998 609	0.995 742
Next	0.003 631 6	0.110 589	0.991 077	0.992 515	0.996 158

Conclusion

According to the main aim of this contribution rheologic and thermophysical properties of rose acacia honey were measured and analyzed. Effect of temperature and also effect of storage time on used honey sample was searched. Viscosity of honey depends mostly from its composition, mixture of flowers visited by bees producing the honey and it is different according to locations, terms and particular colony of bees. Temperature dependencies of rose acacia honey dynamic and kinematic viscosity had decreasing exponential shape and temperature dependencies of fluidity had increasing exponential shape for all measurements (Fig. 1 – 3). Coefficients of determination are very high in all measurements, approximately in the range (0.98 – 1.00) (Tab. 1). Arrhenius equation (1) has decreasing exponential shape, so the dependency of dynamic viscosity on temperature can be described by it. Same results were obtained by authors Cohen and Weihs (2010), Figura and Teixeira (2007), Sahin and Sumnu (2006). It can be seen from Fig. 1 – 3 that storing time had effect on rheologic properties. Dynamic and kinematic viscosity values were a bit higher after storing due to loosening of the water during storage. Values of fluidity were a bit smaller after storing, which is caused by loosening of the water respectively by crystallization during the storage. From presented results is clear that thermophysical parameters are influenced by temperature. Thermal conductivity of honey increases with increasing of temperature linearly. On the other hand thermal diffusivity of honey sample has typical decreasing linear shape. All obtained thermophysical results are in good agreement with literature.

In generally, on the base of previous research, is evident that rheologic and thermal parameters of rose acacia honey are the highest in comparison with all other honeys. On the base of presented results from rheologic and thermophysical measurements is clear that it is necessary to have knowledge about rheologic and thermophysical parameters during temperature changes, because temperature is one of the most important factor which determine quality of food stuffs including honey.

Reference

Bera A., Almeida-Muradian L.B., Sabato S.F., 2008. Study of some physicochemical and rheological properties of irradiated honey. Nukleonika, 53(2): 85 − 87.

Bhandari B., D'Arcy B., Chow S., 1999. Rheology of selected Australian honeys. Journal of Food Engineering, 41: 65–68.

Božiková M., Hlaváč P., 2010. Selected physical properties of agricultural and food products – scientific monograph, SUA in Nitra, 178.

Chirife J., Buera M.P., 1997. A simple model for predicting the viscosity of sugar and oligosaccharide solutions. Journal of Food Engineering, 33: 221–226.

Cohen I., Weihs D., 2010. Rheology and microrheology of natural and reduced-calorie Israeli honeys as a model for high-viscosity Newtonian liquids. Journal of Food Engineering, 100(2): 366 – 371.

Davis W.R., 1984. Compendium of Thermophysical Property Measurement Methods Vol. 1, Survey of Measurement Techniques, New York: Plenum Press.

Figura L.O., Teixeira A.A., 2007. Food Physics, Physical properties – measurement and applications, Springer, USA, 550.

Golob T., Bertoncelj J., Skrabanja V., 2002. Sensory characteristics of Slovenian honey. Zbornik Biotehniske fakultete Unniverze v Ljubljani, 79(2): 381 – 389.

Hlaváč P., Božiková M., 2011. Effect of temperature on milk rheologic and thermophysical properties. Journal on processing and energy in agriculture, 15(1): 17 – 22.

Hlaváč P., Božiková M., 2012. Influence of temperature and storing time on flower honey rheologic and thermophysical properties. Journal on processing and energy in agriculture, 16(2): 52 – 56.

Junzheng P., Changying J., 1998. General rheological model for natural honeys in China. Journal of Food Engineering, 36: 165–168.

Komatsu S.S., Marchini L.C., Moreti A.C. de C.C., 2002. Physical-Chemical Analysis of Honeys from Wild Flowers, Eucalyptus Flowers and Citrus Flowers Produced by Apis mellifera L. in the State of SÃO PAULO, Brazil. 2. Sugars and Protein Contents. Ciênc. Tecnol. Aliment., Campinas, 22(2): 143 – 146. (in Portuguese)

Munson B.R., Young D.F., Okiishi T.H., 1994. Fundamentals of fluid mechanics. New York, John Wilie & Sons.

Sahin S., Sumnu S.G., 2006. Physical properties of foods, Springer, USA, 257.

Wechsler A.E., 1992. The Probe Method for Measurement of Thermal Conductivity in Maglić K D, Cezairliyan A, Peletsky V E, (Eds.) Compendium of Thermophysical Property Measurement Methods, Vol. 2 Recommended Measurement Techniques and Practices, New York, London, Plenum Press.

White Jr. J.W., Kushnir I., Subers M.H., 1964. Effect of storage and processing temperatures on honey quality. Food Technology, 18: 153–156.

White Jr. J.W., 1975. Physical characteristics of honey. In E. Crane (Ed.), Honey, a comprehensive survey Heinemann, London, 207–239.

White Jr. J.W., 1999. Honey. In Dandant & Sons (Ed.), The hive and the honey bee. Hamilton, IL: Dandant & Sons, 491–530.

Zaitoun S.T., Al-Ghzawi A., Abu Jdayil B., Mallah K., 2001. Rheological properties of selected light colored honeys from Jordan. International Journal of Food Properties, 4(1): 139 – 148.

DESIGN OF HYDRAULIC CIRCUIT OF MECHANICAL PRUNER DRIVE USED IN LOW TRELLIS SYSTEM

David Hoffmann*, Adolf Rybka, Petr Heřmánek, Bohuslav Jošt

Czech University of Life Sciences Prague, 165 21 Prague 6 – Suchdol, Czech Republic, Phone: +4202, Fax: +420 224383160, E-mail: dhoffmann@tf.czu.cz

Abstract

A mechanical pruner serves to prune new hopvine shoots in the spring. On the right timing and quality of pruning depends later yield. That is why hop pruning is one of the most important agrotechnical procedures. A double-disc mechanical pruner used on high trellises cannot be used on low trellises due to its big size. Abroad, to prune hops on low trellises a specially adapted sprinkler is used (chemical pruning). With regard to the effort to minimize the chemical environmental burden, we opted for a design of mechanical pruner.

For low trellis systems the most effective proves to be the usage of a single-disc hop pruner with flat cutting disc. The introduction also contains a description of elements used in the design of hydraulic circuit.

The chapter dealing with material and methods describes the input requirements for the hydraulic circuit design as well as for the mechanical pruner design (such as cutting depth or e.g. its maximum structural height). The results include a description of an adapted inter-axle carrier used for the experimental model of hop mechanical pruner, a description of the effected field measurement, and an interpretation of the measured data. The chapter also describes in detail the designed hydraulic circuit supplemented with a one-way valve.

The conclusion summarizes the results and includes a recommendation for further research in mechanical hop pruner used in low trellises.

Keywords: hop, mechanical pruner, low trellis system.

Introduction

The system of hop growing in the low trellis system has brought new agro problems. Czech hops are currently offering three ways to perform this task. The first option is to inhibit sprouting of new shoots or to remove them through a chemical desiccant (chemical cut). The second way is to use manual hop cut, which is denied due to the labour and financial costs. The third method is performed by using mechanical pruners. A mechanical pruner is not currently mass produced (Křivánek, Ježek, 2010).

A mechanical pruner serves for spring pruning of new hop shoots. On its proper timing and quality depends later yield, which is why hop pruning is one of the most important agrotechnical operations (Kopecký, Ježek, 2008).

For low trellis systems the most effective proves to be the usage of single-disc hop pruner with flat cutting disc of 600 mm in diameter (Štranc et al., 2007). The disc is made of abrasion-resistant steel with cutting edge covered with wolfram-carbide coating 1 mm thick and 20 mm wide. In case the disc is coated on one side only, self-sharpening effect occurs when the disc in the soil is self-sharpened due to a different abrasion resistancy of the upper and lower part (Štranc et al., 2007). A flat disc may be further sharpened during the pruning by means of grinder which is mechanically pushed to the cutting disc edge by rectilinear hydraulic motor. The recommended disc rotational frequency is from 600 up to 750 min^{-1} (Štranc et al., 2007; Hoffmann, Rybka, 2010).

There are five principles that are important to follow in hydraulic circuit: (a) liquids have no shape of their own but will flow to acquire the shape of their container, (b) liquids can be considered at the pressures used in fluid power systems, (c) liquids transmit pressure equally in all directions, (d) the rate of flow from a positive displacement pump varies proportionally with pump speed but is virtually independent of system pressure, and (e) any flow of liquid through a pipe or orifice is accompanied by a reduction in liquid pressure (Srivastava et al., 2006; Mobley, 1999).

Equipment for hop cut in low trellis system must work in a relatively limited space (under the net, in the axis of hop plants and between the anchoring columns). For this reason, the design is challenge.

Material and methods

Basic requirements for mechanical pruner

The basic requirement is trimming the hopvine shoots (so called new wood) down to a depth of 50 mm below the terrain level. Thus the old hopvines are cut off their root part (rootstock). The cutting mechanism operates in the space under the low trellis anchoring rope, which is stretched at the maximum height of 250 mm above the terrain. Such height, however, is not the same for all low trellises due to which this limiting value cannot be relied upon. Generally we may say that the lesser the construction height of the rear transmission with cutting disc (Fig. 1) is, the more universal the mechanical pruner will be. On the anchoring rope of 6 mm in diameter there is usually hung a drop irrigation system which must not be damaged by the passing mechanical pruner. Some low trellises have the drop irrigation placed right on the ground in the axis under a plastic net. This type of low trellis excludes the usage of a mechanical pruner, where it is necessary to apply chemical pruning through a specially adapted sprinkler.

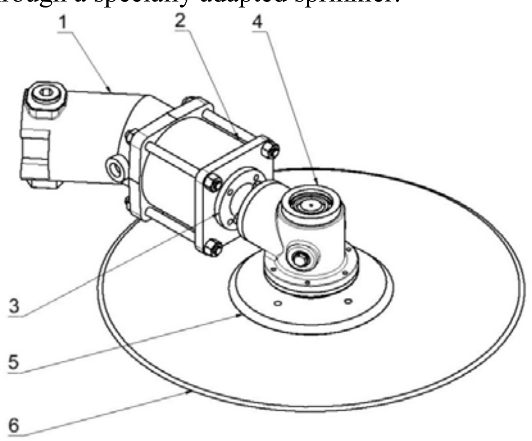

Fig. 1 Rear transmission with hydromotor
1 – axial piston hydromotor, 2 – coupler, 3 – extension,
4 – angular gear, 5 – carrier, 6 – cutting disc

Sharpening of the cutting disc when the machine is in operation improves the cutting and above all minimizes the idle time caused by disassembling, sharpening, and reassembling of the cutting disc. Without quality sharpening the cut would fray rendering the rootstock more prone to mildew and pest.

The drive is designed axial piston hydromotor A2FM (size 62) with a diagonal block. The hydromotor include a splined shaft 1 3/8 21T 16/32 DP (ANSI B92.1a- 1976), angle 30°, tolerance class 5^{th}. P_n = 40 MPa. M_t = 141 Nm. Weight 19.5 kg.

Hydraulic circuit

The hydraulic circuit (Fig. 2) contains 2 flowmeters (positions 2 and 3), a thermometer (position 4), and a revolution counter (position 5). The flowmeters measure the flow of hydraulic oil. They are placed on the pressure and waste branches. To measure the rotational frequency we used a Photo/contact speedometer, model DT-2268, in the mode of non-contact measurement. A reflective mark was placed on the cutting disc. The measurement was carried out this way – the revolution counter laser beam is set on the spot where the reflective mark was moving. After stabilization the actual value rpm (min^{-1}) could be read on the counter display.

Result

Field measurement

Field measurements were carried out through close cooperation with Chmelařství, cooperative Žatec, Mechanizace department in the low trellises.

After having verified the correct functioning of the experimental model of mechanical pruner and of the designed hydraulic circuit in laboratory conditions, it was installed on the inter-axle carrier placed on the tractor. The mechanical pruner model was connected to the source of pressure energy on the tractor represented by a hydraulic aggregate placed on the rear three-point linkage and driven from the tractor's rear outlet shaft. The last step before the field measurement was to ensure a precise automatic copying of the hop-field surface. That was achieved by adding a copying wheel and removing one rectilinear hydromotor of the inter-axle carrier which enables vertical motion of the carrier. The whole set is depicted in Fig. 3. Owing to this adjustment the copying wheel was then fully loaded, thus the copying effect was ensured. By moving of this rectilinear hydromotor (in copying wheel) we adjust the depth of the cut.

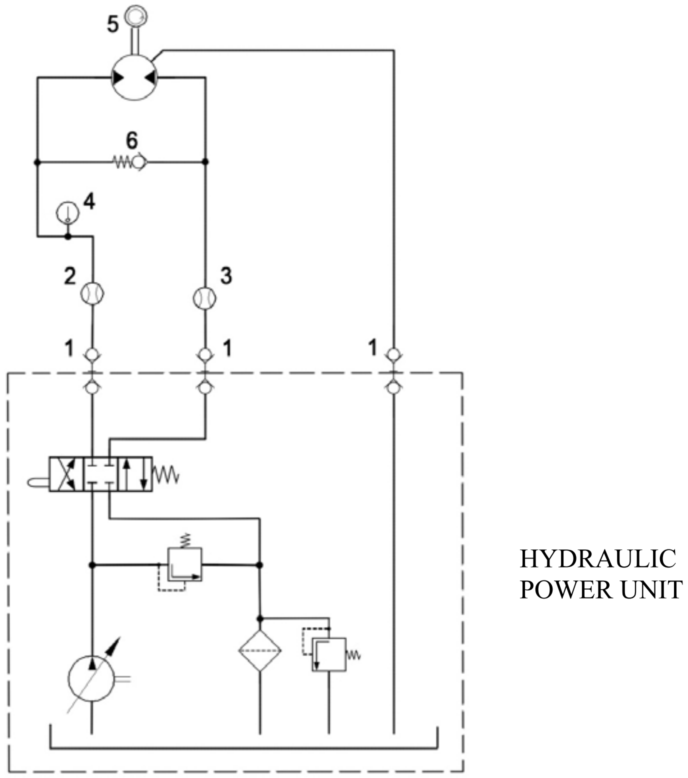

Fig. 2 Designed hydraulic circuit
1 – quick couplers, 2 – flowmeter on pressure branch, 3 – flowmeter on waste branch,
4 – thermometer, 5 – optical revolution counter of cutting disc,
6 – one-way valve with spring

Fig. 3 Experimental model of mechanical pruner

The measurement itself was carried out on a 10 m long low-trellis section where the tractor with connected mechanical pruner moved at a speed of 1 $km.h^{-1}$. The cutting disc in no-load conditions rotated at a maximum speed of 12.4 s^{-1} and the hydraulic oil temperature was kept at the value of 40 ± 2 °C.

During the first tractor's drive the cut height was set at 0, i.e. the cutting disc was moving on the surface level of the hop field. This way the hop-field surface was levelled. During the second drive through the same measured section, the cut depth was set at 50 mm (i.e. at maximum recess – see the agrotechnical requirements for mechanical pruner).

Values taken by sensors of pressure, flow and temperature were recorded only from the moment when the cutting disc reached the required depth and rotational frequency.

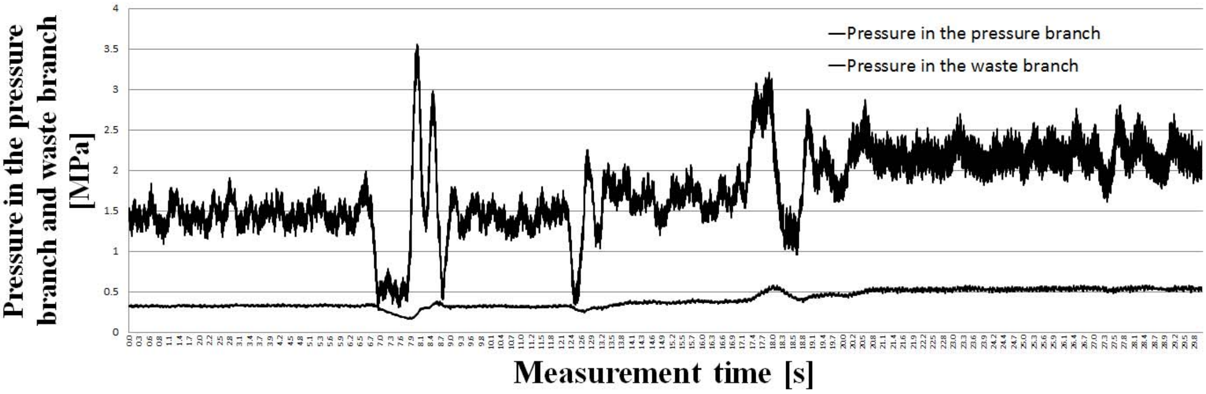

Fig. 4 Pressure at the input and output depending on time of the cut on the hop-field surface
upper black curve – pressure in the pressure branch, lower black curve – pressure in the waste branch

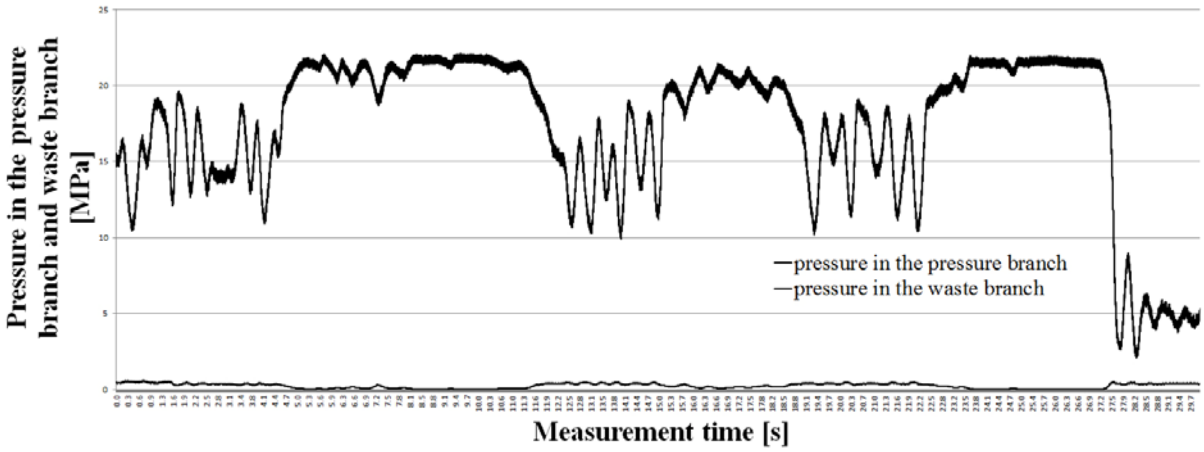

Fig. 5 Pressure at the input and output depending on time of recess 50 mm
upper black curve – pressure in the pressure branch, lower black curve – pressure in the waste branch

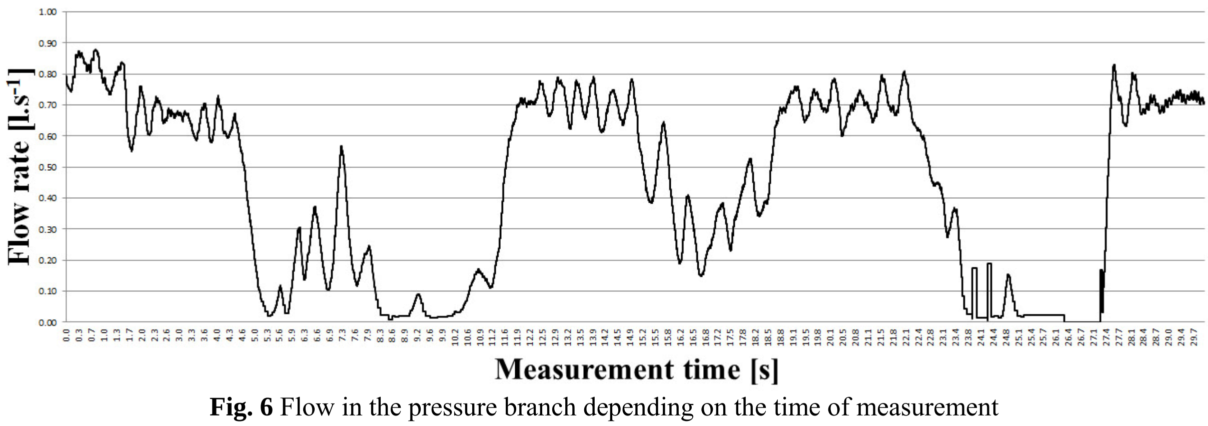

Fig. 6 Flow in the pressure branch depending on the time of measurement

The graph of Fig. 4 depicts data measured during the first drive through the measured section. The upper black curve shows the course of pressure in the pressure branch of the hydraulic circuit, while the lower black curve represents pressure in the waste branch. The graph clearly shows a drop in pressure and its immediate considerable rise in the interval between 6.6 and 9.5 s. This deviation was caused by the terrain unevenness (hollow). Subsequently occurred a repeated gradual recess of the cutting disc until the pressure in the pressure branch stabilized at a mean value of 2.2 MPa.

The graph in Fig. 5 shows data measured at the cut at a depth of 50 mm. The graph's upper black curve depicts the course of pressure in the pressure branch of the hydraulic circuit, while the lower black curve shows pressure in the waste branch. At such a big recess the cutting disc began to stop working due to the friction force. One part of the hydraulic aggregate was a safety pressure valve with a set value of 22 MPa. After the set pressure had been achieved, the safety pressure valve started letting the hydraulic oil flow back into the tank. In spite of that the rotation of the cutting disc did not cease, owing to the effect of friction forces. Due to the unevenness of the hop-field surface, the rotation of the cutting disc almost stopped two times in the measured section. Decrease in the friction force led to a repeated rotation of the cutting disc in the 11th second of the measured section. This was caused by lifting the cutting disc up slightly. From the 23.5 s the cutting disc rotation ceased again until the time when the cutting disc was dug out just below the hop-field surface. The hydraulic oil pressure in the pressure branch subsequently levelled off at the value of 5 MPa. To this development corresponds also the flow curve in the pressure branch, recorded in the course of the measurement (Fig. 6).

Conclusion

Fluctuating oil pressure in the hydraulic circuit is caused by unevenness of the hop-field surface.

The repeated measurements clearly show that a precise setting of the cut depth with a difference of 10 mm is practically impossible. The best results from the point of view of the hydraulic circuit power parameters (p, Q) were achieved by the experimental model of mechanical pruner at the cut on the surface and at the recess of a flat cutting disc at the maximum of 40 mm below the hop-field surface. A bigger recess of the cutting disc led to a decrease in or even cease of the cutting disc rotation due to friction forces.

The last step is adding the automatic deflection of the cutting disc when passing the supporting poles of the low trellis.

Acknowledgement

This article created as output of the project TA ČR TA03021046 and IGA 31160/1312/313112.

Reference

Hoffmann D., Rybka A., 2010. Technical project for hop cutting equipment in low trellis system. International student scientific conference - Recent advances in agriculture mechanical engineering and waste policy. 27 – 29 April 2010, Nitra, Slovakia (CD-ROM), 109 – 114.

Křivánek J., Ježek J., 2010. The importance of cut and verification German prototype machines for hop cutting designed for a low trellis system in ÚH Stekník. Chmelařství 83 (4): 45-48.

Kopecký J., Ježek J., 2008. Principles for quality mechanized cut. Chmelařství 81(1-2): 21-24.

Štranc P., Štranc J., Jurčák J., Štranc D., Pázler B., 2007. Cutting hop. CULS Prague, 42-43. ISBN 978-80-87111-03-1

Mobley R.K., 1999. Fluid Power Dynamics. Butterworth Heinemann, Hardbound, Knoxville, TN, USA. ISBN: 978-0-7506-7174-3

Srivastava A.K., Goering C.E., Rohrbach R.P., Buckmaster D.R., 2006. Engineering Principles of Agricultural Machines. 2nd Edition, ASABE, Michigan, USA. ISBN 1-892769-50-6

EFFECT OF NUMBER WELD DEPOSITS BEAD ON THE CHEMICAL COMPOSITION OF THE HARDFACING

Petr Hrabě, Jan Cidlina

Czech University of Life Sciences Prague, 16521 Prague 6 – Suchdol, Czech Republic, Phone: +42022438 3274, Fax: +4202-20921361, E-mail: hrabe@tf.czu.cz

Abstract

A hardfacing is used for creating layers which are meltingly connected with a base material. In practice it is used to various purposes, for a renovation of sires of parts and in the production for carrying out preventive overlays. At this metallurgical process it comes to melting – down the basic material by a source of the heat owing to which also a filler material (welding metal) is melted so it comes to a creation of a homogeneous layer. Owing to the melting – down of the welding metal and the basic metal it comes to the change of a chemical composition of an original overlay. From these reasons it is an effort to lower a depth of a full penetration as much as possible. At the hardfacing and by this also the portion of the basic material in the overlayed layer.

The hardfacing of worn areas or preventive overlays can be carried out as multilayer when it comes to further adding of alloying elements in further overlayed layers. At this change it comes not only to the change of the chemical composition which approaches to the composition of welding electrodes stated by a producer but it comes also to the change of mechanical qualities which are given by a microstructure of overlayed layers. The paper deals with the change of the chemical composition owing to the number of the overlayed layers and with change of the structure at the multilayer overlays.

Keywords: weld, chemical composition

Introduction

The hard facing is applied for creating homogenous layers which are meltingly connected with a base material. It is used to various purposes as a filling material of worn components or to create layers with different characteristics. The melting down of the basic material occurs during this metallurgical process by the heat source due to the filler metal is melted and the homogenous layer is created. Owing to the melting of the welding metal arises heat affected area (Houldcroft, Robert, 2009). In this area occurs to the changes in the structure and material properties owing to welding and subsequent cooling. For these reasons there is an effort to minimize the penetration depth and also participation of base material in the overlay. The amount of the input heat affects penetration depth and size of the resulting deformation and stress (Rabinowicz, 1964). The weldability of steels is affected mainly by carbon content and amount of the alloying elements, which has effect on the structure in the weld layer and in the heat affected area (Brožek, 2005). It is reason why in the case of poorly chosen technology or material, may become worse of the desired properties, in the worst case there is initiated creation of cracks owing to structural changes in the material (Ahmed, 2005; Ptáček et al., 2002).

The welding metal creates by melting of basic and filler material, which is melted from the electrode or welding stick. The proportion of the melted base material in the welding metal is called as a mixing. Grade of the mixing depends on the technology of welding. For the manual arc welding is mixing stage 10 – 40 % and for machine submerged-arc welding to the 85 % (Larsen-Badse, 1968). Sturdiness of the welding metal is usually lower than sturdiness of the base material. The properties of the welding metal are affected by type of microstructure, size of the grains, aging precipitation processes etc. The fatigue properties are worse in the compare with the base material. These characteristics are affected mainly by pouring structure of the weld, subaerial defects, a number of inclusions – clarity of the welding metal. In the consideration for lower carbon content in the welding metals are heat-strength properties also worse in the comparison with the base material (Hrivnak, 2009; Ochodek, 2000).

Tab. 1 Directive chemical composition

	C	Si	Mn	Cr	Mo	W	Co	Nb
UTP LEDURIT 61	3.5	1.0	0	35	-	-	-	-
UTP LEDURIT 65	4.4	0	0	23.5	6.5	2.2	1.5	5.5
CRC	3.8	1.2	0	33	0.5	-	-	-

Experimental arrangement

Nowadays are produce huge range of the material for welding with various properties, due to it is suitable for various components and in the different operation conditions. There is wide range of the filler material with difference chemical concentration as well as its form. It is produced as powders, wires with different diameters or tape with different thickness. Though there is wide range of the filler materials, the trend of these days is a use of powder filler materials (Posta et al., 1998).

In the experiment were used coated overlay electrodes UTP LEDURIT 61, UTP LEDURIT 65 and CRC with the directive chemical composition provided by manufacturer, as shown in Tab. 1. The basic material was used mild steel S235JR.

Weld deposit was made on the basic material with proportion 80 × 80 × 16 mm. The surfaces under the weld deposit were milled and then were plates marked by numbering die. The number code is characterized by electrode and a number of overlay layers on the basic plate. In the case of multi layer weld deposits were welded beads placed vertically on the previous layer.

After the welding of the weld deposit by welding source WTU 315-31, the deformation of welded plates occurred due to were aligned on the opposite side of the weld by milling. Afterwards the welds were grinded by surface-grinding machine to create a level surface with minimal material removal of the weld deposit.

From this plates for one-, two- and three-layers weld deposit were cut out specimens with proportion 25 × 25 mm. The specimens were used to find out the chemical composition by GD-OES method. GD-OES (Glow Discharge Optical Emission Spectroscopy) allows determining the chemical composition of the cubic electrically conductive materials. The outputs are not only the table values, but also the concentration depth profiles, which allows to document changes in the composition to the depth of 0,1 mm. All these values afford authentic information to identify the material and surface processes (Vnouček et al., 2011).

Results and discussion

Measurements were performed on three selected weld deposits materials. The chemical composition was ascertained on the surface layer of the weld deposit after the grinding on the magnetic-grinding machine. The results are shown in Fig. 1 for the UTP LEDURIT 61 hardfacing material; Fig. 2 for the UTP LEDURIT 65 hardfacing material and Fig. 3 for the CRC hardfacing material.

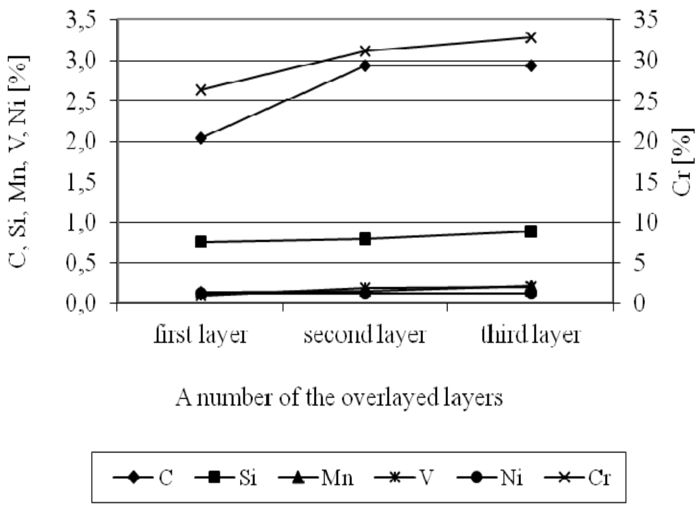

Fig. 1 Chemical composition changes of the UTP LEDURIT 61 hardfacing material

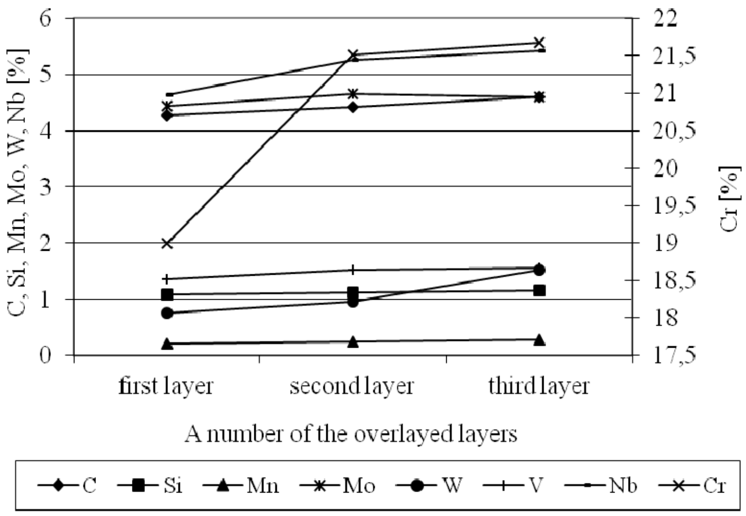

Fig. 2 Chemical composition changes of the UTP LEDURIT 65 hardfacing material

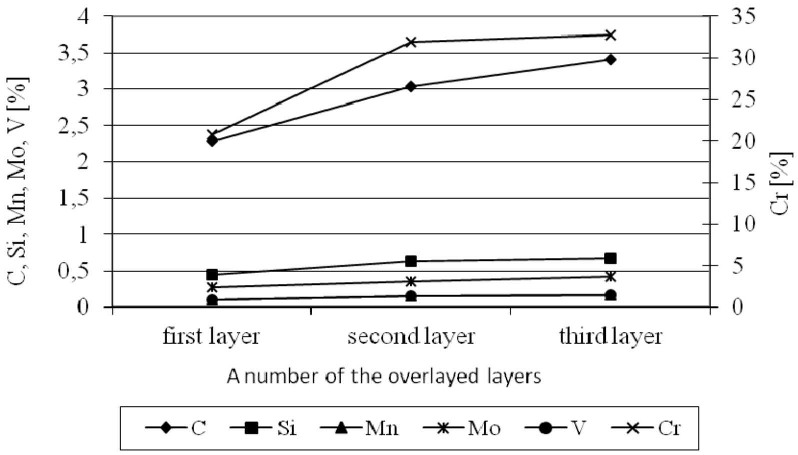

Fig. 3 Chemical composition changes of the CRC hardfacing material

From the Fig. 1, Fig. 2 and Fig. 3, it is clear that already in the third layer of the three lay weld deposits is chemical composition of the hardfacing material practically identical to the indicative chemical compositon gives by manufacturer. The percentage weight of individual alloying elements increases. Although during the hard facing occurs to burn of the alloying elements and the hard facing was performed on the mild steel, there was achieved the same chemical composition already in the third layer.

Conclusion

A hardfacing is still advantage although the high energy costs. Forasmuch as, even to very worm parts, it can weld back the original shape and mechanical properties (Müller, Hrabě, 2013). Another advantage is a possibility to hardface the shape and then hardface a surface layer of the material that has the desired properties. It markedly reduces the cost of the restoration.

Nowadays is interest about the hardfacing great, as it can be seen from the number of companies whose are dealing with this issues. Alien companies are aware of the benefits of the hardfacing, due to in the Czech Republic are the biggest companies, whose deal with hardfacing and other types of renovations, abroad.

The selected hardfaced materials were examined to found when the chemical composition of the material has the same or similar values as the manufacturer. The experiment showed that it is possible to achieve the same or similar chemical composition already in the third overlayed layer, even in the case of hard-facing on the mild steel.

Reference

Ahmed N., 2005. New Developments in Advanced Welding, Woodhead Publ. Ltd., Cambridge, England, 308. ISBN 1-85573-970-4

Brožek M., 2005. Abrasive wear resistant of overlays. Acta Mechanica Slovaca, Košice, 9: 51–60.

Houldcroft P., Robert J., 2004. Welding and cutting: A guide to fusion welding and associated cutting processes. Abington: Woodhead Publishing Limited, 100.

Hrivňák I., 2009. Zváranie a zvariteľnosť materiálov (Welding and weldability of the materials). Bratislava: Nakladateľstvo STU, 492. (in Slovak)

Larsen-Badse J., 1968. Influence of Grit Diameter and speciment size on wear duting sliding abrasion. Wear, 12: 35-53.

Müller M., Hrabě P., 2013. Overlay materials used for increasing lifetime of machine parts working under conditions of intensive abrasion. Research in Agricultural Engineering, 59(1): 16-22.

Ochodek V., 2000. Svařitelnost materiálu a praskavost (Materials and its weldability: Weldability of the material and crackability). Učební texty pro kurzy svářečských inženýrů a technologů. Ostrava: Zeross, 103-113. (in Czech)

Pošta J., Havlíček J., Černovol M.I., 1998. Renovace strojních součástí (Renovation of the machine parts), Praha: SVÚM a.s., 160. (in Czech)

Ptáček L., 2002. Nauka o materiálu II. (Material Science II.) Brno: Akademické nakladatelství CERM, s.r.o., 392. (in Czech)

Rabinowicz E., 1964. Practical uses of the surface energy criterion. Wear, 7: 9 – 22.

Vnouček M., Kříž A., Mišterová H., 2011. Porovnání vlastností duplexně připravených vrstev (Comparison of the properties of duplex prepared layers). Vrstvy a povlaky 2011. Trenčín: Miloš Vavrík - Knihviazačstvo, Trenčín, 181-187. (in Czech)

NEW GENERATION PORTABLE VERTICAL PENETROMETER DESIGN

Dušan Hrubý[1*], Jozef Bajla[2], Martin Olejár[1], Vladimír Cviklovič[1], Ladislav Tóth[1]

[1]Department of Electrical Engineering, Automation and Informatics, Faculty of Engineering, Slovak University of Agriculture in Nitra, TR. A. Hlinku 2, 949 76 Nitra, Slovak Republic
Phone: +421 37 641 4764, E-mail: dusan.hruby@uniag.sk
[2] Department of Machine Design, Slovak University of Agriculture in Nitra, Slovak Republic

Abstract

*This article describes the design of a new portable vertical penetrometer for the agricultural soil compaction measuring. The Department of Electrical Engineering, Automation and Informatics and the Department of Machine Design on FoE SUA in Nitra are currently preparing a new measuring system with modern electronic parts as well as application of new measuring principles for depth and force sensors. There is a design with a new arrangement of the elements in the body. Major innovation is the use of a colour touch screen which one allows real time monitor: the laboratory measurements, the measured data saved on SD card, Excel and *.csv formatted data, the ultrasound sensors values for the indirect ground depth measuring, the user friendly setup options of the device parameters and the incorporation of GPS into the device housing. Connection with personal computer remained unchanged from the previous type. Article describes the enhanced algorithm for penetration resistance measuring of a soil in dependence on place and on depth of the pushed sensing head.*

Keywords: portable vertical penetrometer, soil compaction, measurement of penetration resistance, cone index

Introduction

Sowing, harvesting, protection and mechanisms for tillage negatively affect soil compaction despite new design solutions, especially in extreme weather conditions.

There is necessary to have detailed and accurate information about the condition of land and constantly specifies those models of the soil particles spatial arrangement for finding appropriate solutions to minimize soil compaction. Monitoring of soil compaction is performed mainly by penetrating devices which are mainly used in mapping the immediate condition of the soil.

Soil compaction is most often defined by penetration resistance (Cone Index, CI), when measured cone and sensor measure the value of the resistive force exerted per unit area at the base of the cone (Hemmat, Adamchuk, 2008). To ensure comparability and reproducibility of results and objectively assess the changes of soil compaction it is used standard size cone by American standards ASAE S 313.3 (Raper, Kirby, 2006). This article describes the design of a new penetration device designed at DMD and DEEAI at FoE SUA in Nitra (Slovakia) and the first results in the implementation of this device.

Materials and methods

Research and development of microprocessor and computer technology influenced the development of penetration devices in positive direction due to which we can make the measurement quickly and results processed into more transparent and comprehensible form (Tekin et al., 2008). Through cooperation between DMD and DEEAI at FoE SUA in Nitra (Slovakia) was made P-BDH 3A penetrometer 15 years ago (Fig. 1).

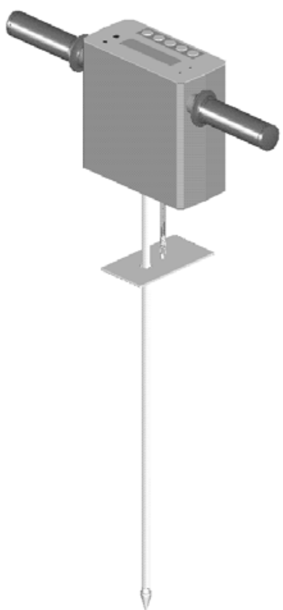

Fig. 1 P-BDH 3A penetrometer

Penetrometer was founded on the principle of sensing the force of soil resistance against solid shape (cone) pushed into the soil by capturing incremental value after pressing deeper every centimetre. For measurements were used optoelectronic measurement systems, digitization and record of measured values in memory, which were transported into a computer and processed further. The measuring device was very simple and reliable with over 10,000 possible record data. Through digital indicator can be adjusted input parameters, to calibrate the device and to check the measured data values. Wide application of penetration methods just for its benefits will likely continue in other areas (Sun et al., 2010). Increasingly sophisticated equipment available with electronics and modern processing methods and evaluation techniques can position the field tests keep at the forefront of scientific and agricultural interest. Author and his team have years of experience in the measurement and evaluation of measurement, therefore were prompted to upgrade the device so as to remove some of the shortcomings of the device in terms of measurement system, as well as increased measurement comfort and control. P-BDH 3A penetrometer at was not able to follow the course of the measured forces during the measurement depending on the depth and to locate measurement location by a GPS system.

Therefore, authors decided for technical and technological improving to meet the new requirements of the practice. The concept of the new device was based on the requirement of control options during the penetration resistance measurement and so extreme values (errors) can be immediately erased. It was also their aim to prepare a reliable measuring instrument with a low price that was unlike now commercially produced devices cheaper and more accessible for practice. There were applied into this new concept commercially produced force and depth ultrasonic sensors with modern electronic and microprocessor technology, including the use of a colour touch screen.

Results and discussion

Design of new variant of penetration device marked as PE90 consists of a steel casing, cut out and welded out of sheet metal which one is associated with the metal housing with countersunk screws. There is bolted carrying case with attached handles to this housing inside which is fixed force sensor. Bottom of the sensor is attached to the rod with cone probe. On the top of the metal cover is placed colour touch screen (Fig. 2). There was chosen sensor type EMS 20 for measuring the force of resistances with a measurement range up to 5 kN, which has minimal dimensions.

a)

b)

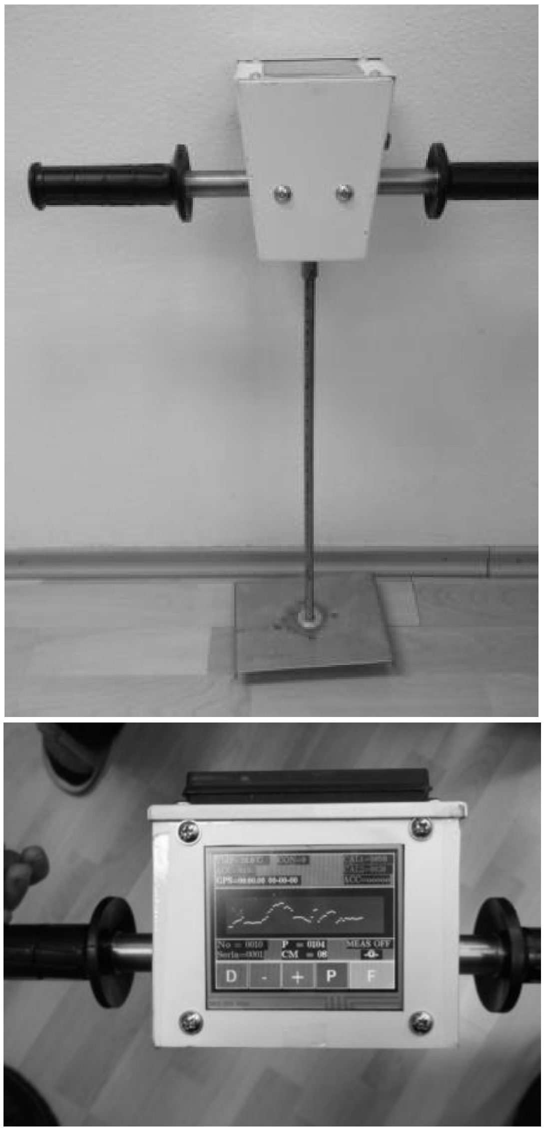

Fig. 2 Device view: a) body alignment, b) view on display unit

There were used current possibilities of modern electronic and microprocessor technology at the new concept. The device uses a colour touch screen for entering measuring conditions, parameter setting and control over the measurement on the display screen. There is mounted ultrasonic sensor for measuring of depth to the bottom of the housing, and is clamped sliding reflector plate to ensure a correct reflection of the ultrasonic signal to the measuring rod (Fig. 3).

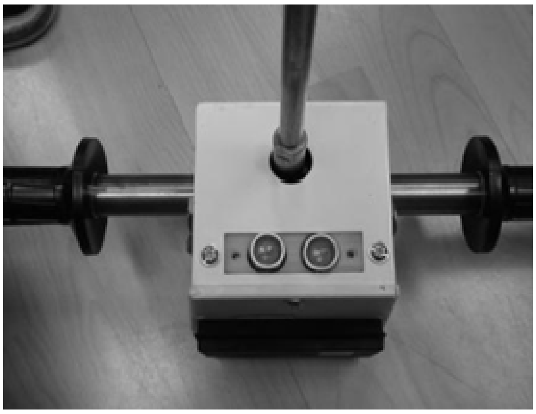

Fig. 3 Device view – location of ultrasonic probes

The device can be externally connected to a computer to export data and GPS position for their further process. It has the ability to connect to an external power source with controlled charging of Lithium-ion battery capacity. Handles, measuring rod and the GPS sensor is removable, which allows better storage-ability and its transfer.

Measurement algorithm of penetrometer resistance depending on the soil depth should take into account the following aspects:

- the measuring system has to do the calibration of sensors due to temperature after power on (1),
- penetrometer resistance measurement is performed depending on the depth of soil each 10 mm,
- it is necessary to determine start of the GPS signal activity,
- speed of recessed rod during the measurement has to be max. 0.01 ms^{-1},
- device has an audible alarm to warn the possible destruction of the force sensor under strong recessing,
- in case of the wrong methodology recessing irregular movements of measuring rod, for example impact on stone or finding an air gap, to beware for the possible incorrect results.

Built-in temperature sensor is implemented to calibrate ultrasonic sensor distance using a modified known equation:

$$s=(165.9+0.305.(T_S-273.15)).t \qquad (1)$$

where:

s - is sensed soil depth (m)
T_s - is air temperature (K)
t - is measurement time interval (s)

There were resolved in the new device after the first layout of the components other parts like battery, location of some controls, GPS sensor, battery charge and computer connection. New penetrometer has got GPS sensor with SiRFstar III chip, which in addition to determining the exact position of measurement also provides information about the current altitude and the time of measurement. Values of ambient and soil temperature is an additional indication of measurement. We expect that device will be supplemented by additional sensors to more precisely determine the properties of soil for sowing, especially humidity or conductivity (Hlavacova et al., 2001). The measured data are stored on the microSD card format in *.csv file that is readable in MS Excel or other spreadsheets.

Today a new variant of PE90 penetrometer is designed with the technical characteristics shown in Tab. 1:

Tab. 1 Technical characteristics of PE90 penetrometer

Measuring range	0 - 10 MPa (cone index)
	0 - 600 mm (measurement depth)
Measuring step depth	10 mm
Number of measurements	cca 100 000 on 256MB microSD card
File type	.csv (.txt, .bin)
GPS module	SirfStar III
Connectivity	USB, RS232C, SD card
Unit Dimensions	120 x 140x 90 mm (body)
Length of the rod	600 mm
Weight	2.6 kg
Size cone (diameter of base / top angle)	12.8 (20.3) mm/ 30°
Battery life	min. 10 hours

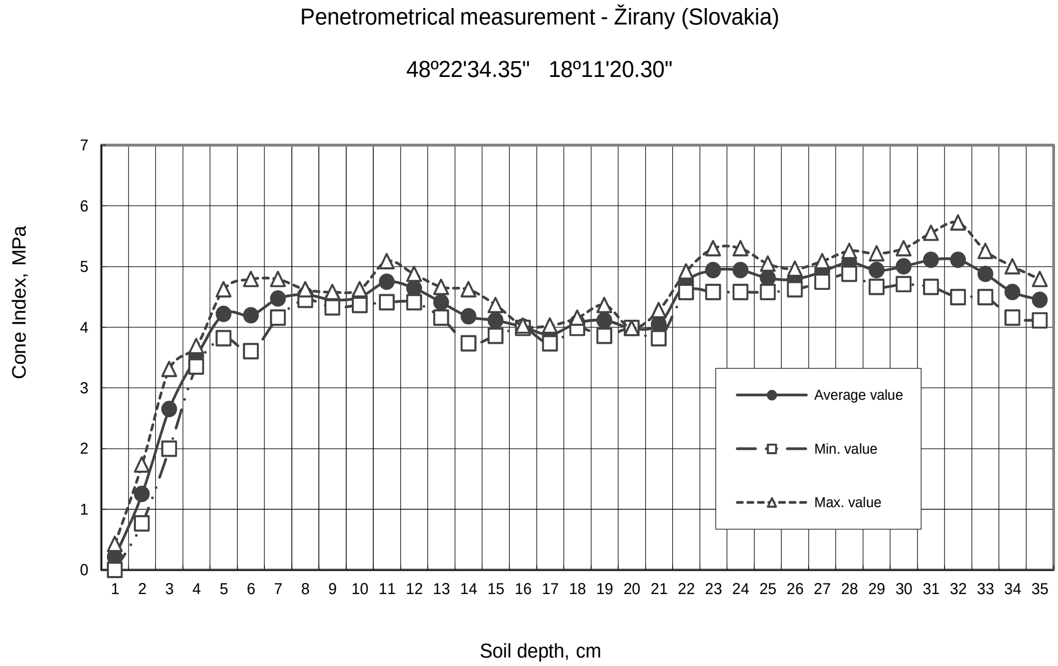

Fig. 4 Monitoring of heavy compacted soil

The graphic representation of penetrometrical measurements has the possibility of locating the measured data using GPS signal (Fig. 4).

Nowadays is well known companies Eijkelkamp Penetrologger that has a measuring range up to 10 MPa, measuring the depth in interval 10 or 20 mm, depth measurement is max. 800 mm. Cone used for measuring has got angle of 60° on special request also available with cone according to ASABE. The device can be added with GPS without connection to system memory.

ELE International Company offers Proving Ring penetrometer with ASABE cone, it has analogue pointer without electronic record of the measured resistance and depth and no GPS. They offer ELE CCP model with a measurement range up to 600N, depth measurement up to 450mm with a reading offer 15mm, 16-digit display with record up to 600 measurements a few years ago. Currently it is not in the catalogue.

Australian company AGRIDRY RIMIK PTY LTD in Toowoomba offers RIMIK CP 40 CONE, which one has advanced electronic components, display unit, strain gauge force transducer with a measuring range up to 5.5 MPa and depth measurements up to 600 mm at the rate 15, respectively 20 mm. It also has a built-in GPS. Measuring capacity is about 2047 measurements. This device appears to be the most advanced on the market.

It may be noted that the PE90 penetrometer has comparable properties with worldwide manufacturers. However, designed apparatus has improved the intuitive management and has bigger recording memory.

Conclusion

The purpose of the research and development of new penetrometers is not only to design lightweight, portable and reliable equipment, but also a consistent device enabling a wider usable and able to obtain data comparable to each other.

Current penetrometer devices except the new options (GPS, colour touchscreen, high memory capacity, autocalibration) must take into account the versatility and ease of use in a variety of conditions by affordable price. The new proposal penetration device can meet all these requirements and provide greater comfort and productivity.

Acknowledgement

This article was generated on the base of solving project VEGA 1/0816/11 (Production process of field crops at different tillage systems, application of fertilizers and plant residues to maintenance and increasing of soil fertility) of the Science Grant Agency MŠ SR a SAV.

Reference

Hemmat A., Adamchuk V.I., 2008. Sensor systems for measuring soil compaction: Review and analysis. Computers and Electronics in Agriculture, 63 (2): 89 – 103.

Hlavacova Z., Molnar L., Skovajova L., Lukac O., 2001. Electrical conductivity of different

modification of sugarbeet seeds. Czech Sugar and Sugar Beet Journal, 117: 15-17.
Raper R.L., Kirby J.M., 2006. Soil Compaction: How to Do It, Undo It, or Avoid Doing It. ASAE Distinguished Lecture Series, 30: 1-14.
Sun Y., Buescher W., Lin J., Lammers P.S., Ross F., Maack C., Cheng Q., Sun W., 2010. An improved penetrometry technique for determining bale density. Biosystems engineering, 105 (3): 273 – 277.
Tekin Y., Kul B., Okursoy R., 2008. Sensing and 3D mapping of soil compaction. Sensors 2008, 8: 3447-3459.

EFFECT OF DIE DIAMETER AND PRESSURE FORCE ON THE CHARACTERISTICS OF PELLETS

Affan Othman Hussein[2], Ladislav Nozdrovicky[1], Miroslav Macak[1]*, Juraj Maga[1]

[1]Slovak University of Agriculture in Nitra, Tr. A. Hlinku 2, 949 76 Nitra, Slovakia,
Phone: +421 37 641 43 66, E-mail: miroslav.macak@uniag.sk
[2]Khabat Agricultural Technical Institute, Erbil, Iraq

Abstract

Pellets made of biomass for energy purposes can be considered as a significant type of biofuel. The efficiency of the biopellets depends upon the many factors and therefore in our paper we have focused our attention on the measuring of physical properties of biopellets made from alfalfa hay and corn stover. The chemical composition of biomass materials is characterised. The biopellets were made on the hydraulic press and their durability were measured on the own instrument designed according to the ASABE S269.4 standard. As the biomass particle size plays an important role in the process of pellets producing the particle size distribution was determined. According to our experiments both the pressure and diameter had no effect on the durability of the pellets for both materials especially with pressure force of (100 and 125MPa), whereas with increasing the pressure force to 150MPa for the die diameter 20mm for both alfalfa hay and corn stover, a significant increment occurred in the durability of pellets.

Keywords: alfalfa hay, corn stover, biopellets, press, particle size distribution

Introduction

Increasing energy demand and decreasing oil reserves make it necessary to find alternative sources of energy. Cellulose materials are attractive as a sustainable source of fuels and chemicals because of their plentiful supply and relatively low cost. The world governments and petrochemical industry alike are looking at biomass as a substitute refinery feedstock for liquid fuels and other bulk chemicals. New large plantations are being established in many countries, mostly in the tropics, but also in China, North America, Norther Biomass, used for energy purposes, can have a different form, due to the fact that biomass is processed by different ways.

Technologies used for biomass processing are producing a very different final product what leads to very different energy efficiency. Barkoczi, Nozdrovicky and Macak (2012) have described a computer simulation model allowing determining the energy efficiency of the incineration of wooden chips. This model based on simulation can be considered as a tool suitable for optimization of the input parameters for the system using a wooden chips for energy purposes. Due to this fact the study of the physical properties of the biomass fuel is very important.

Cereal straw is usually considered as a by-product of the grain cropping systems and is often used for energy purposes. This material has very specific characteristics, which determine the using for energy purposes. Due to the low specific density straw the straw is harvested and baled by the straw balers. As mentioned by Zitnak and Korenko (2008), the efficiency of transport bales from a field depends upon the weight of the bales package and their shape in Europe, and in Russia (Samson et al., 2000; Patzek, Pimentel, 2006).

Material and method

In this study the durability of pellets was measured according to the ASAE S269.4 (2007) standard method of which is intended to assess the durability of Cubes, Pellets and Crumbles. A sample of about 5 pellets was placed in a dust-tight box. The box was rotated about an axis, which was perpendicular to the box and centered in the 300 mm side. A 230 mm long baffle was affixed symmetrically and diagonally to inside the box (300 × 300) mm. The samples were rotated for 10 min at 50 r.p.m. Fig. 1 shows the durability test instrument, 5 pellets of each treatment was tested with three replications for the durability measurement. The durability rating was expressed as the ratio of the original mass of the briquette to the briquette remaining on a 17 mm opening sieve after tumbling in accordance with the following equations,

$$Durability = \frac{mass\ of\ \ pellets\ or\ crumbles\ after\ tumbling}{mass\ of\ \ pellets\ or\ crumbles\ befor\ tumbling} \times 100 \quad (1)$$

Normally pellets will be tested immediately after cooling. When the temperature of the pellets falls within -5 °C of ambient, they are considered cool. If tested at a later time, the time, in hours after cooling, will be indicated as a subscript of the durability. For example, if the pellet durability tested 95 after a 4 h delay from the time of cooling, then the results will be expressed as (95)4. If pellets are tested before cooling, there will be a significant weight loss caused by water vaporization and the apparent durability will be decreased by this loss of water vapor. The loss of water vapor must be determined by making moisture content determinations before and after tumbling and compensating the final mass accordingly. When this procedure is followed, the durability would be expressed as (95)-1. In this study all briquettes which they made with preheating tested for durability after two hours from the point of extruding.

Pelleting procedure

A preliminary experiment conducted for selecting the proper die diameter and pressure for pelleting the biomass materials. Alfalfa hay and corn stover were used for the preliminary study, two die diameter were used 20mm (Fig.1-A) and 32 mm (Fig. 1-B) with three different pressure forces namely 100, 125 and 150 MPa, for the die diameter 20 mm all pressure forces completely were used, but for the die diameter 32 mm only the 100 and 125 MPa were used because the ability of the hydraulic press was limited. The pellets produced in this preliminary study all were in moisture content of 10% and the procedure done under room temperature. A known amount of 5 g and 12 g of each biomass feedstock was allowed to flow freely from a funnel and fills the cylindrical die of 20 mm and 32 mm respectively under room temperature without preheating. The pellets produced were divided to two parts, the first part their diameter, length and durability had measured immediately after ejection from the die, the second part had stored for three weeks under room temperature conditions approximately of 22 ^{o}C and relative humidity of 55 %. After the storage also the diameter, length and the durability of the pellets had been measured to determine the impact of storage on the characteristics of the pellets. The apparatuses consist of close fit cylinder and plunger die assemble with a hydraulic press for applying the mechanical pressure required for pelleting.

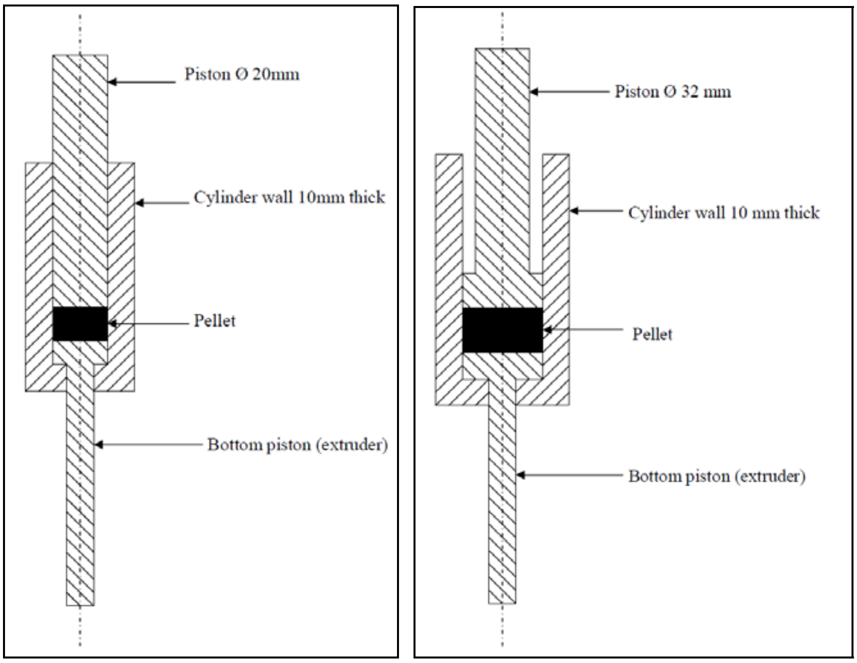

A **B**

Fig. 1 Side section view - cylinder and piston die assemble (a) 20mm, (b) 32 mm

Results and Discussion

Characteristics of the biomass materials

The results of chemical composition analyses of five biomass materials are given in Tab. 1. There are varieties between the biomass materials in the chemical composition; the alfalfa hay contains the highest amount of protein while the wheat straw contains the lowest, whereas the wheat straw contains the highest amount of lignin among the materials and prickly lettuce the lowest. Prickly lettuce has the highest amount of carbohydrate, while the corn stover and alfalfa hay has the lowest. Corn stover has the lowest amount of ash while the prickly lettuce has the highest.

There were big differences between the five biomass materials from the point of the rate of particle size distribution which remained on each sieve opening. These differences in geometric particle size of the grinds from different species are accounted for the difference in their morphology, physical structure and mechanical strength of the material.

Tab. 1 Chemical composition of biomass materials

Components, % DM	Biomass species	
	Corn stover	**Alfalfa hay**
Dry matter	94.7	93.4
Crud protein	5.3	16.75
Crud fiber	40.81	25.56
Carbohydrate	0.2	0.2
Lignin	6.71	6.46
Cellulose	40.59	26.99
Hemi-Cellulose	25.36	4.08
Ash	4.95	11.32

Particle size distribution of biomass grinds

Fig. 2 is showing the distribution of alfalfa hay particles on each sieve opening size, the highest rate of the chopped particles was 41 % on the sieve with 2 mm opening size whereas the lowest rate was 0.3 % on the sieve with 5mm opening size. The highest accumulation of the particles was on the sieves (3, 2 and 1) mm, it reached 83.6 % whereas the total rate on other five sieves was 16.1 %. The geometric mean diameter of the samples was 3.32 mm which was the finest particle size mean among the other biomass materials, the geometric standard deviation of the particles was 1.9.

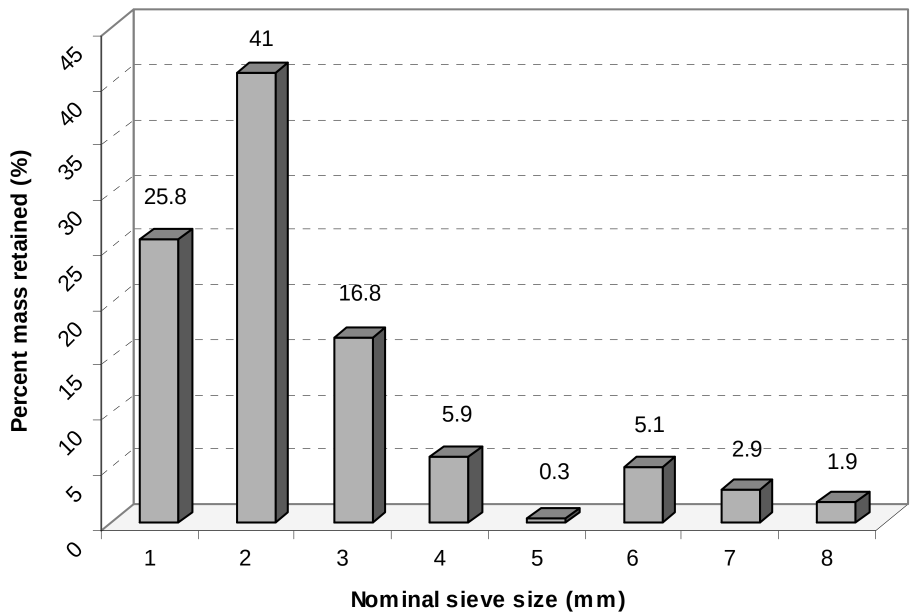

Fig. 2 Alfalfa hay particle size distribution

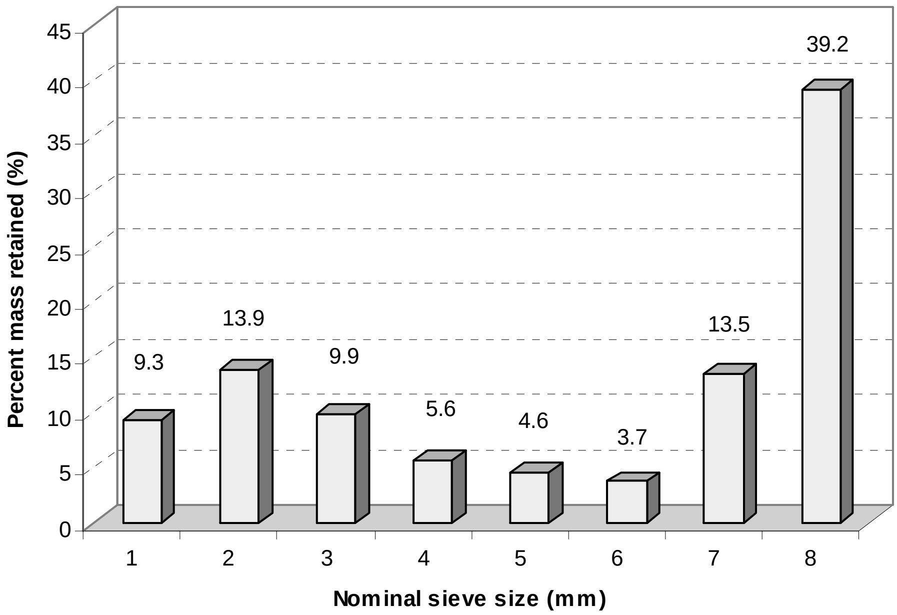

Fig. 3 Corn stover particle size distribution

Fig. 3 is illustrating the distribution of corn stover particles on each sieve opening size; the highest rate of the chopped particles was 35.6 % on the sieve with 8 mm opening size, whereas the lowest rate was 3.7 % on the sieve with 6mm opening size. The highest accumulation of the particles was on the sieves 7 mm and 8 mm. Among all the other materials corn stover had more than 50 % coarse shape particles, as we mentioned before it might be due to morphology, mechanical and physical properties. The geometric mean diameter of the samples was 8,5 mm which was the coarser particle size mean among the other biomass materials, the geometric standard deviation of the particles was 2,25.

The effect of die diameter 20 mm and 32 mm, pressure force of 100, 125 and 150 MPa and storing on the unit bulk density of pellets produced from alfalfa hay and corn stover in moisture content of 10% are shown in the Tab. 2. Generally it can be observed that with increasing the pressure force the bulk density increased for both die diameter pellets. The diameter had a significant difference on the bulk density of the pellets, with increasing the die diameter the bulk density had decreased and vice versa. The storage almost has a negative effect on the bulk density of pellets for all pressure forces and both diameters; although its effect was slightly in the case of alfalfa pellets made with 32 mm and pressure of 125 MPa.

Tab. 2 Bulk density of pellets made with different pressure and two diameters with moisture content of (10%) before and after storing

Biomass materials	**Bulk density of chopped particles, kg.m^{-3}**	**Pressure, MPa**	**Unit bulk density of pellets before storing, kg.m^{-3}**		**Unit bulk density of pellets after storing, kg.m^{-3}**	
			Pellets diameter, mm		**Pellets diameter, mm**	
			20 mm	**32 mm**	**20 mm**	**32 mm**
Alfalfa hay	97.4±1.4	100	1186.3±5.7	1023.8±5.9*	1141.3±5.2	972.5±5.6
		125	1202±6.9	1077.5±6.3	1179.2±5.9	1062.2±5.9
		150	1203.03±4.9	NA	1183.4±6.1	NA
Corn stover	*57.04±0.7*	*100*	1009.4±4.9	934.8±6.3	941.6±5.9	889.6±6.1
		125	1031.5±6.1	973.3±6.2	1067.6±6.2	939±5.9
		150	1045±5.7	NA	1005.3±4.8	NA

** Mean difference is significant at .01...*
#Mean ± standard deviation (n=5), NA: data not available

Tab. 3 is illustrating the effect of three different pressure forces and two die diameters on the mean durability of alfalfa hay and corn stover pellets before and after storing made with moisture content of 10 %. It’s obvious that with increasing the pressure force the durability of the pellets will increase for both kinds of materials and diameters before storing, but statistically this increment was not significant. Both the pressure and diameter had no effect on the durability of the pellets for both materials especially with pressure force of (100 and 125 MPa), whereas with increasing the pressure force to 150 MPa for the die diameter 20mm for both alfalfa hay and corn stover, a significant increment occurred in the durability of pellets where it were (60 %, 66 % and 75 %) and (65 %, 70 % and 82 %) for the pressure force of (100, 125 and 150 MPa) respectively.

The effect of storage on the durability was also investigated and is shown in the table, the durability has fluctuated between increasing and decreasing, in case of alfalfa hay pellets made with (20 mm) diameter and pressure force of (100 and 125 MPa) the durability of pellets increased form 60 % and 66 % to 63 % and 69 % respectively, while in the 32 mm diameter and 100 MPa pressure force the durability has decreased from 48 % to 41 % but it has increased from 56 % to 68 % when the pressure force increased to 125 MPa. These results agree with (Kaliyan, 2008); Franke, Rey, 2006; Saptoadi, 2006).

Conclusion

From the results of this study we can draw the following conclusions.

The die diameter affected on the unit bulk density of pellets made without preheating in moisture content of 10 %, by increasing the die diameter from 20 mm to 32 mm the unit bulk density of pellets made from alfalfa hay and corn stover had decreased.

Alfalfa hay and corn stover pellets recorded higher unit bulk density by increasing the pressure force from 100 to 150 MPa.

The durability of pellets made from alfalfa hay and corn stover increased with increasing compression pressure from 100 to 150 MPa, the pellets made without preheating with moisture content of 10 %.

According to the results we can suggest the following recommendation for the future work:

Comparing more diameters is for producing the pellets and observing the effect of each one on the durability of the produced pellets. With testing different pressure forces we can decide the best procedure for each type of biomass feedstocks.

Tab. 3 Durability of pellets before and after storing in moisture content of 10% made with different pressure forces and die diameters

Biomass materials	**Pressure, MPa**	**Durability of pellets before storing, %**		**Durability of pellets after storing, %**	
		Pellets diameter, mm		**Pellets diameter, mm**	
		20mm	**32mm**	**20mm**	***32mm***
Alfalfa hay	100 125 150	60±1.9 66±1.7 75±1.6*	48±1.7 56±1.2 NA	63±2.1 69±1.4 73±1.9	41±1.9 68±1.9 NA
Corn stover	100 125 150	65±1.9 70±2.2 82±2.3*	62±1.9 73±1.9 NA	63±1.9 74±2.1 78±1.8*	58±1.2 73±1.9 NA

** Mean difference is significant at .01...*

Acknowledgement

This paper has been prepared within the projects: “Application of the information technologies to increase the environmental and ecological sustainability of the production agrosystem”, project ITMS 26220220014, EU Operational programme RESEARCH and DEVELOPMENT.

“Development of International Cooperation for the Purpose of the Transfer and Implementation of Research and Development in Educational Programs” conducted by the Operational Program: Education, ITMS code: 26110230085

Reference

ASAE. Standards S269.4, 2001. Cubes, pellets, and crumbles-definitions and methods for determining density, durability, and moisture content. St. Joseph, Mich.: ASABE.

Barkoczi J., Nozdrovicky L., Macak M., 2012. Use of information technologies in the process of implementing the system of technological equipment for processing biomass for energy purposes : scientific monograph. 1. vyd. Nitra: Slovak University of Agriculture in Nitra, 178, ISBN 978-80-552-0874-9.

Fasina, O.O., Sokhansanj S., 2008. Storage and handling characteristics of alfalfa pellets. Powder Handling & Processing 8 (4): 361-365.

Franke M., Rey A., 2006. Pelleting quality. World Grain May 2006: 78-79.

Nalladurai K., 2008. Densification of biomass. Ph.D. Thesis. Faculty of the Graduate School, University of Minnesota. United States of America

Patzek T.W., Pimental, D., 2006. Thermodynamics of energy production from biomass. [Online], [cit. 2007-01-10] Available at: <http://petroleum.berkeley.edu/papers/patzek/CRPS-BiomassPaper.pdf>

Samson R., Duxbury P., Drisdelle M., Laponte C., 2000. Assessments of palletized biofuels. [Online], [cit. 2013-04-14] Available at: <http://www.reap-canada.com/online_b library/Reports%20and%20Newsletters/Bioenergy /15%20Assessment%20of.PDF

Harwin S., 2006. The best biobriquette dimension and its particle siuze. Proceedings of The 2nd joint international conference on "Sustainable Energy and Environment (SEE 2006)" 21-23 November, Bangkok, Thailand. [Online] 2006 [cit.2013-04-12]. Available at: http://www.jgsee.kmutt.ac.th /see1/cd/file/C-004.pdf

Zitnak M., Korenko M., 2008. Performance and energetic demandingness of vehicles during harvest and transport of straw bales. In VOZIDLÁ 2008: Nitra = VEHICLES 2008: new trends in construction and exploitation vehicles: International scientific conference. Nitra: Slovak University of Agriculture in Nitra, 181-185.

EVALUATION OF SPIKING ORCHID PRODUCTION IN ENVIRONMENTAL CONTROLLED CHAMBER WITH ARTIFICIAL LIGHT

Ming-Yih Chang[1], Chia-Chyi Wu[1], Hsin-Ying Chung[2], Wei Fang[2*]

[1]National Ilan University, Yilan, Taiwan
[2]National Taiwan University, 1, Sec. 4, Roosevelt Rd., Taipei 10617, Taiwan
Phone: +886-2-23671657, E-mail: Weifang@ntu.edu.tw

Abstract

Moth orchids can bloom year-round under a cool environment, normally inside air-conditioned greenhouses. The flower forcing of orchid is a time and energy consuming process. The commercial potted orchid growers in Taiwan usually entrust orchids to other greenhouses in mountain area for spike induction to reduce the electricity cost and to increase turnover rate of their own greenhouses near urban area. However, entrusting orchids to other greenhouses results in the management of inconvenience and inconsistence, loss in transportation, and the transportation cost, etc. The objective of this study was to investigate the effects of artificial light used during spike induction on the orchid spiking and flowering. Two experiments, light quality and lighting regimes, for 45-day spike induction were conducted in an environmental controlled chamber under the temperature of 26 ℃ day /18 ℃ night. The results show that the white light with color temperature 5000 K was better than the other two white light source, 2700 K and 10000 K, in days to anthesis and flower quality. Under the same daily light integral, the longer photoperiod with lower light intensity advanced the flower development compared with the shorter photoperiod with higher light intensity. Lower light intensity means less artificial light installation and less investment. The greenhouse turnover rate by using the proposed method of spike induction in environmental controlled chamber was 4.5 crops/year, which of the current method in air-conditioned greenhouse from spike initiation to anthesis was only 2.3 crops/year. This proved the practical potential to replace the entrusting spike induction in greenhouses by environmental controlled chambers with artificial light.

Keywords: orchid, artificial light environmental controlled chamber

Introduction

Moth orchids (*Phalaenopsis* spp.) had become worldwide ornamental plants in the past decade. The original sites of orchids are the tropical and subtropical areas of southern Pacific Asia. Winter and spring are the major flowering seasons. The key environmental factors to regulate orchid flowering are cool temperature and light (Lee, Lin, 1984; Lopez, Runkle, 2005). Due to the advancement in controlled-environment agriculture technology, orchids can bloom year-round under a cool environment. However, because of the slow growth rate of orchid, the flower forcing takes more than five months from spike induction to market, normally inside air-conditioned greenhouses. It is a time and energy consuming process. To increase the greenhouse turnover rate, the potted orchid growers in Taiwan usually entrust orchids to mountain greenhouses to use the cool natural environment for the spike induction. However, entrusting to mountain greenhouses may result in conflicts in management practices, increases plant damage risk due to long-distance transportation, and derives the transportation cost, etc.

The temperature tolerance for flower-forcing orchids is more critical during the spike induction than during the subsequent flower forcing. Lee and Lin (1984) suggested maintaining the cool temperature for the spike induction, but increasing the temperature a little higher to accelerate the flower development after the buds were visible. Using air-conditioned greenhouse to maintain the stable cool environment for spike induction has many advantages comparing with transporting plants to greenhouses in mountain area. However, a large amount of electricity is consumed to cool the space inside the entire air-conditioned greenhouse. To obtain a better environmental control and to increase energy efficiency, Liu et al. (2006) partitioned part of the greenhouse as an air-conditioned chamber for spike induction by an air-inflated double-poly envelope. Using the double-poly chamber inside an existing greenhouse has an advantage of reducing energy cost, but the double-poly films reduce the penetration of light available to plants, thus limiting the growth rate. A well-controlled chamber with artificial light may resolve this disadvantage. The objectives of this study were to use artificial light in an environmental controlled chamber for spike induction and to investigate the effects of light quality and lighting regime of white light on the orchid spiking and flowering.

Materials and Methods

The miniature moth orchids of *Phalaenopsis* 'PengBo Little Angel', with four leaves and leaves span around 22 cm, grown in 7.5 cm-diameter pots filled with sphagnum as the growing substrate, were cultivated in a spike-inhibitive greenhouse with the temperature set above 28 ºC. These orchids were moved into a cool environment to induce flower since the experiment began on 30 Aug. 2011 (day 0). The flower forcing process in this study was divided into two stages. The first stage was the 45-day spike induction in an environmental controlled chamber with different treatments of artificial lights. The second stage was the subsequent flower forcing in a commercial flower-forcing greenhouse reaching anthesis. The different treatments of artificial lights in the first stage included two experiments, described as followed.

Experiment 1. Various color temperature of white LED light on orchid spiking and flowering (Expt. 1)

The experiment had three treatments of various color temperature, 2700 K, 5000 K, and 10000 K, provided by white light-emitting diode (LED) lamps with the same photosynthetic photon flux (PPF) 200 μmol·m^{-2}·s^{-1} on the plant canopy. The light intensity was measured by the quantum sensor (LI-250A/LI-190, LI-COR, USA). The daily light integral (DLI) was equal to 8.6 mol·m^{-2}·day^{-1} under 12 h photoperiod. Fig. 1 shows the spectral distribution of the three experimental light sources. Tab. 1 lists the red, green, blue, and far-red fraction of these light spectra recorded by a spectroradiometer (USB4000, Ocean Optics, USA).

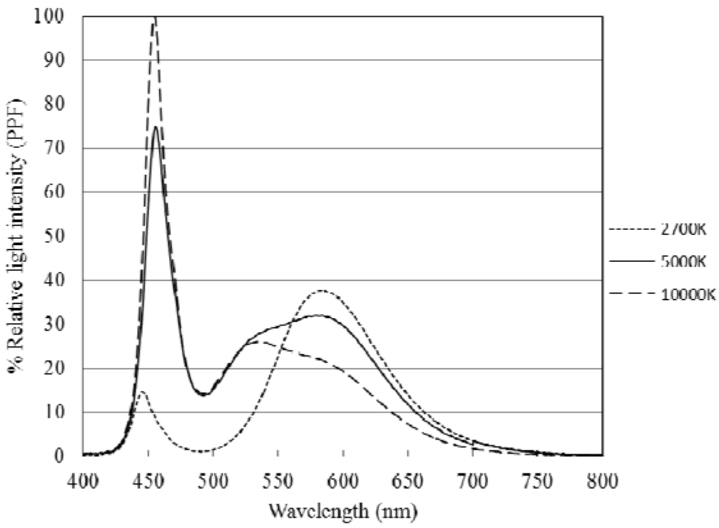

Fig. 1 The spectral distribution of the color temperature of white light used during the 45-day spike induction in the environmental controlled chamber

Tab. 1 The red, green, blue and far-red fraction of the various color temperature of white light with the same light intensity of 200 μmol·m^{-2}·s^{-1} used in Experiment 1

Treatment	PPF fraction (%)			Far red (FR) 700-800 nm	R/FR	B/R
	Blue (B) 400-500 nm	Green (G) 500-600 nm	Red (R) 600-700 nm			
2700 K	9.7	51.5	38.8	3.1	12.6	0.3
5000 K	35.1	43.4	21.5	1.9	11.4	1.6
10,000 K	45.8	39.3	14.9	1.1	14.0	3.1
FL WW^{z}	16.9	43.2	39.9	13.9	2.9	0.4

^{z}Warm white fluorescent tube used in Experiment 2

Experiment 2. Different lighting regimes on orchid spiking and flowering (Expt. 2)

Light intensity and photoperiod are two important factors affecting plant physiology. This experiment aimed at the effects of different lighting regimes during the 45-day spike induction. The lighting regimes of four treatments were conducted by the combination of two levels of photoperiod (12 and 16 h) and two levels of light intensity (120±10 and 160±10 $\mu mol \cdot m^{-2} \cdot s^{-1}$), provided by the warm-white (2700K) fluorescent lamps.

Cultivation during spike induction in environmental controlled chamber with artificial light

The environmental controlled chamber for 45-day spike induction was modified from a grafted seedling acclimatization chamber designed by Jou et al. (2005). The orchids were placed on the multi-layer cultivation beds with artificial light on each layer, which maximized the yield per unit area in the small chamber. The ambient temperature in this chamber was set at 26 ºC day /18 ºC night. The plants were irrigated using ebb-and-flow irrigation thoroughly for five minutes every three days and fertilized with the commercial fertilizer solution (Hyponex#2, 20N-20P-20K) in 2000-fold dilution every two weeks, accompanied with the regular irrigation.

Cultivation during subsequent flower forcing in commercial air-conditioned greenhouse with sunlight

The spike induction period in the environmental controlled chamber ended on 15 Oct. 2011 (day 45). All plants were moved to a commercial air-conditioned greenhouse with sunlight for the subsequent flower forcing to anthesis. This greenhouse was located at Bali, Taipei, Taiwan. The ambient temperature in this greenhouse was set at 26 ºC day /18 ºC night. The plants were watered overhead every one or two weeks and fertilized with the fertilizer solution (20N-20P-20K, electrical conductivity 0.8 mS/cm) accompanied with every two regular watering. Control orchids were transferred from the spike-inhibitive greenhouse directly into the flower-forcing greenhouse since day 0 and grown during the entire experimental period to anthesis.

Data collection and analysis

All orchids were inspected for the spike emergence every three days since day 21 after the beginning of the experiment. The number of spikes in each orchid was counted at day 45. The date to anthesis was also recorded when the first flower opened, defined by the two lateral petals completely extended. The size of the fourth flower (the longest distance between the edges of two lateral petals) in the first spike was measured when they fully opened. The number of spikes, the total number of flowers, and the first spike length were also recorded. In the experiment of color temperature (Expt. 1), fifteen orchids were selected for each treatment. The data were analyzed by the analysis of variance (ANOVA) with the means comparison by the Least Significant Differences (LSD at $P \leq 0.05$). In the experiment of lighting regimes (Expt. 2), twelve orchids were selected for each treatment. The data were analyzed by two-way ANOVA to verify the main effects of light intensity and photoperiod, and their interaction. Then, the means of data were compared by the Least Significant Differences (LSD at $P \leq 0.05$).

Tab. 2 Effects of color temperature of white LED light on orchid spiking and flowering

Treatment	Days to Spike (d)	Number of spikes		Days to anthesis (d)	Number of flowers	Size of flower^{z} (cm)	Length of spike^{y} (cm)
		Day 45	Anthesis				
2700 K	30.5 ab^{x}	1.6 b	1.8 ab	128.1 b	13.8 b	4.2 a	25.9 b
5000 K	28.9 b	2.0 a	2.1 a	125.9 b	20.0 a	4.1 ab	27.9 ab
10,000K	32.4 a	1.6 b	2.1 a	129.6 b	18.0 ab	4.1 ab	27.1 b
Control	-	0.5 c	1.6 b	155.7 a	14.4 b	4.0 b	29.8 a

^{z}Size of the fourth flower on the first spike
^{y}Length of the first spike
^{x}Means followed by the different letters in each column are significantly different at 5% level by LSD test.

Result and discussion

Effects of various color temperature of white LED lights on orchid spiking and flowering

Spike development. Tab. 2 shows the effects of color temperature on the orchid. The 28.9 days to spike in the 5000 K treatment, were significantly shorter than the 32.4 days in the 10,000 K treatment. The 5000 K treatment had the maximum spike number (2.0 spikes/plant) on day 45. The 5000 K spectrum seems helpful in inducing spike initiation. After being moved to the flower-forcing greenhouse for the subsequent flower forcing cultivation, the spikes continued to emerge. At anthesis, the numbers of spikes in the 5000 K treatment reach to 2.1 spikes/plant, which is significantly more than 1.6 spikes/plant in the control treatment. The control orchids grown in the flower-forcing greenhouse with sunlight from day 0 to anthesis did not fully result in double spikes, some orchids even had no spike at all. The stable and adequate light environment in environmental controlled chamber promotes not only the spike rate but also the uniformity of spike initiation. The spike length in all treatments ranged from 25.9 to 27.9 cm, and the 2700 K treatment produced significantly shorter spike length of 25.9 cm than the control treatment (Tab. 2).

Flower Development. Tab. 2 also shows the data of the orchid flowering after the two-stage flower forcing. The days to anthesis ranged from 125.9 to 129.6 days in all treatments under the two-stage flower forcing, which were significantly shorter than the 155.7 days in the control treatment. The 5000 K treatment had the shortest days to anthesis (125.9 days) among the treatments, which almost advanced 30 days to anthesis comparing with the control treatment. The numbers of flowers are also summarized in Tab. 2. The total flower number in the 5000 K treatment (20.0 flowers) was significantly more than that in the 2700 K and control treatments (13.8 and 14.4 flowers, respectively). The sizes of the fourth flowers are also shown in Tab. 2. The color temperature of light seems to have no significant effects on the size of the fourth flower.

Effects of different lighting regimes on orchid spiking and flowering

Tab. 3 lists the main effects and interactions of light intensity and photoperiod on orchid spiking and flowering by two-way ANOVA. The results show the effect of light intensity was not significant on the spike and flower development. However, the photoperiod significantly affected the orchids. The interaction between light intensity and photoperiod shows no significant effects on the plant, except the number of spikes on day 45, the days to anthesis ($p<0.01$) and size of flowers ($p<0.05$).

Spike development. The days to spike in the 16H and 16L treatments (34.3 and 34.0 days, respectively) of longer photoperiod are significantly earlier than that in the 12L treatment (44.4 days) by 10 days. The number of spikes in these treatments of longer photoperiod (2.2 spikes/plant) was significantly more than that in the 12L treatment (1.5 spikes/plant). Yoneda et al. (1991) reported the short daylength advanced the spike emergence. Our results seem not to draw the same conclusion. The length of spike in the 16H and 16L treatments (20.9 and 20.1 cm, respectively) of longer photoperiod are significantly shorter than those in the 12H and 12L treatments (24.1 and 23.9 cm, respectively).

Tab. 3 Effects of lighting regime on orchid flowering after the two-stage flower forcing

Treatment	Days to Spike (d)	Number of spikes		Days to anthesis (d)	Number of flowers	Size of flower[z] (cm)	Length of spike[y] (cm)
		Day 45	Anthesis				
12 L	44.4 a[x]	0.9 c	1.5 b	159.4 a	7.1 b	3.1 c	23.9 a
12 H	41.8 ab	1.3 bc	1.8 ab	145.9 b	8.5 b	3.6 b	24.1 a
16 L	34.0 b	2.0 a	2.2 a	130.3 c	14.5 a	4.2 a	20.1 b
16 H	34.3 b	1.6 ab	2.2 a	132.8 c	12.8 a	3.9 ab	20.9 b
Light intensity	n.s.	n.s.	n.s.	n.s.	n.s.	n.s.	n.s.
Photoperiod	**[w]	***	**	***	*	***	***
Light Intensity × photoperiod	n.s.	*	n.s.	**	n.s.	*	n.s.

[z]Size of the fourth flower on the first spike
[y]Length of the first spike
[x]Means followed by the different letters in each column are significantly different at 5% level by LSD test.
[w]*: $P < 0.05$ (significant); **: $P < 0.01$ (highly significant); ***: $P < 0.001$ (extremely significant)

Flower Development

The days to anthesis in the 16H and 16L treatments of long photoperiod (132.8 and 130.3 days, respectively) were significantly shorter than those in the 12H and 12L treatments of short photoperiod (145.9 and 159.4 days, respectively). The treatments of long photoperiod also show their superiority in the total number of flowers and size of flowers compared with the short photoperiod treatments. Under the same daily light integral (DLI), the longer photoperiod with lower light intensity (16 L) advanced the spike and flower development compared with the shorter photoperiod with higher light intensity (12 H). Lower light intensity means less artificial light installation and less investment. Lin and Lee (1998) found the light intensity in early stage of flower-forcing treatment would affect the time to spike and the number of spikes, and the light intensity in latter stage would affect the number of flowers. Our results correspond to the higher DLI, even in the early spike induction, enhanced the flowering quality. The total number of flowers and the size of flowers reached to maxima in the 16L treatment (14.5 flowers/plant and 4.2 cm). Although the 16H treatment had the maximum DLI among all treatment, its flowering performance was statistically the same as the 16L treatment. The temperature increase around the plants by installing more fluorescent lamps to provide high light intensity might retard the flower development in the 16H treatment.

Economical benefit evaluation for the proposed two-stage orchid production

The data of 5000 K treatment, the best performance among the treatments in both experiments, were calculated for the economical benefit evaluation. The days to anthesis were 125.9 days. Subtracting the 45 days of spike induction conducted in the environmental controlled chamber, the duration for cultivating the orchids in the air-conditioned greenhouse was only 80.9 days, significant reduction of 74.8 days comparing with the control treatment (155.7 days). The annual greenhouse turnover rate of 4.5 crops/year in the 5000 K treatment was almost doubled the rate of 2.3 crops/year in a conventional greenhouse.

Conclusion

The duration of the spike induction in the environmental controlled chamber was only one third of the entire duration of flower forcing. However, it proved that the proposed process in shortening the days to anthesis and in increasing flower quality offer business advantages to orchid growers. The cool white 5000 K LED light tube assured the shortest days to anthesis and the most number of flowers. The greenhouse turnover rate by using the proposed method reached to 4.5 crops/year, almost doubles the rate of the current method in air-conditioned greenhouse. This study also suggests that to extend the photoperiod was more effective than to increase light intensity in advancing the flower development under the same DLI. This proved the practical potential to replace the entrusting spike induction in greenhouses by environmental controlled chambers with artificial light.

Reference

Jou L.J., Liao C.M., Chiu Y.C., 2005. A boolean algebra algorithm suitable for use in temperature-humidity control of a grafted seedling acclimatization chamber. Comput.Electron.Agr.,48: 1-18.

Lee N., Lin G.M., 1984. Effect of temperature on growth and flowering of Phalaenopsis white hybrid. J. Chinese. Soc. Hort. Sci., 40: 223-231. (in Chinese)

Lin Y.Z., Lee N., 1998. Light requirement of Phalaenopsis during prior to and flowering cool-temperature forcing. J. Chinese. Soc. Hort. Sci., 44: 463-478. (in Chinese)

Liu Y.J., Huang C.N., Lin H.C., Fang W., 2006. Investigating electricity consumption and temperature distribution of air inflated double-poly Phalaenopsis flower forcing greenhouse. Proc. 2006 Symp. Biomechatronic Eng., 18-24. (in Chinese)

Lopez R.G., Runkle E.S., 2005. Environmental physiology of growth and flowering of orchids. HortScience, 40: 1969-1973.

Yoneda K., Momose H., Kubota S., 1991. Effect of daylength and temperature in juvenile and adult *Phalaenopsis* plants. J. Japan. Soc. Hort. Sci., 60: 651-657. (in Japanese)

MODELING OF DRYING OF SWEET MAJORAM (*Origanum vulgare* L.) LEAVES

Hossein Ahmadi Chenarbon[1*], Seyedeh Masoumeh Hasheminia[2]

[1]Department of Agronomy, Varamin - Pishva Branch, Islamic Azad University, Varamin, Iran.
Phone:+989123893145, E-mail: h.ahmadi@iauvaramin.ac.ir
[2]Department of Agronomy, Roudehen Branch, Islamic Azad University, Roudehen, Iran.

Abstract

It is important to store crops after harvest so that their quantity and quality properties maintained. Drying is the most common food preservation, particularly for medicinal plants and herbs because of reduction of essential oils and changes of qualitative properties such as color, which both of them influence on the economical value of the products. Drying process of Origanum vulgare L. leaves was studied and modeled in this investigation. Independent variables were temperature at three levels (50, 60 and 70°C), air velocity at two levels (1 and 2 m/s) and product depth at one level (1cm). The experimental data was fitted to a number of thin layer drying equation such as Yagcioglu, modified Page, Page, Henderson and Pabis, Lewis, two-term and Verma. Based on the results, the Page equation showed the best fit.

Keywords: drying, modeling, Origanum vulgare L.

Introduction

The main aims of drying of agricultural products are to increase the shelf life, to prevent from biological activities including microbial and enzymes, and to reduce the weight and volume of the materials in order to facilitate packaging, transporting and storing (Simal et al., 2005). During drying process it is important to preserve the texture, color, flavor, and nutritional value of the product. It means to reach moisture at safety level to minimize the quantity and quality losses during storage (Hall, 1980). In most developed countries many extensive studies have been conducted on native flora and medicinal herbs. The problems of research on medicinal herbs are indentifying and preserving the essential oils especially in different kinds of herbs. One of the most important advantages of the herbs is using a broad range of necessary elements for human body. *Origanum vulgare* L. has been known as having many therapeutic properties and its antimicrobial activity has currently received a renewed interest. *Origanum vulgare* L. appear particularly rich in volatiles mainly phenolic compounds such as carvacol and/or thymol. Arabhosseini examined drying of *Artemisia dracunculus* L. leaves at temperature range of 40 to 90°C, different relative humidities and air velocity of 0.6 m/s. Although the Diffusion approach equation showed the best fit, but Page model was chosen since it had almost a similar performance but the equation is simpler as it has only two parameters instead of three in Diffusion approach model (Arabhosseini et al., 2009). Doymaz assessed the drying behavior of mint leaves at temperatures of 35, 45, 55, and 65°C and air velocity of 1m/s. He reported that drying time reduced significantly at higher temperature. Four drying models were selected to fit the experimental data and the logarithmic model described satisfactorily the drying behavior of mint leaves (Doymaz, 2007). The present study was conducted to determine the best model for drying of *Origanum vulgare* L. leaves to preserve quality properties and effective chemical compounds.

Material and method

Drying equipment

Three experimental dryers of Kiln type were used for drying experiments (Fig. 1). This kind of dryer consists of two floors and usually use for drying of seeds, food stuffs, fruits and vegetables.
Data collection for thin layer drying experiments was performed through samples weighting at 5min time intervals using a digital balance (Sartorius, model PT210, Germany) with an accuracy of ±0.001g and then the results were recorded. Weighting of the samples continued until three consecutive readings showed the same value. Sample moisture was measured before and after drying experiment. The mean value of the samples dry weight was used for computations. The final moisture content of the samples was determined by drying in a vacuum dryer (model Galen Kamp) at 70°C, 150 mbar, for 8hours (Tsami et al., 1990).

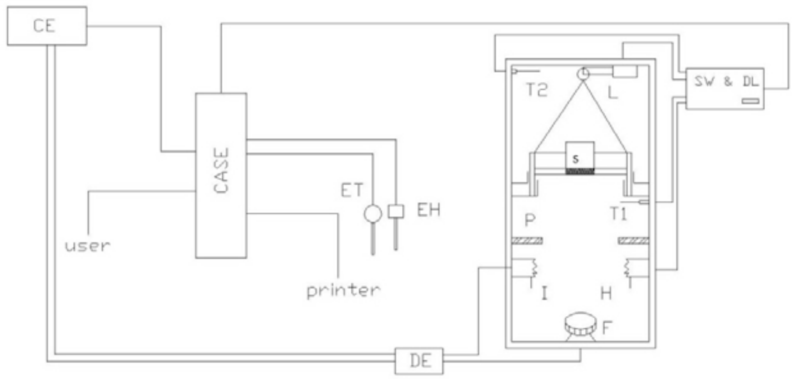

Fig 1. Experimental dryer
(F) fan, (H) heat generator, (S) sample – hold mesh, (T_1) thermometer before(s), (T_2) thermometer after(s), (Sw) switches, (DL) data logger, (CE) control electronic system, (DE) electronic driver, (EH) environment humidity sensor, (ET) environment temperature sensor.

Drying process

The used herb in the study was prepared by medicinal herb research collection of Jahad-e-Daneshgahi in May and June, 2012. The plants were harvested just before flowering and then the leaves were immediately removed from the stems. The separated leaves were cut and then the samples were stored separately in plastic bags and refrigerated at temperature of 4± 1°C to prevent from microbial spoilage. Moisture content of the leaves was found to be 61% db. In this study the independent variables were temperature at 50, 60, and 70°C air velocity at 1 and 2 m/s and bed depth of 1cm. A factorial experiment design was laid out in completely randomized design with four replications. All data were subjected to analysis of variance and the Duncans multiple range tests were used to compare the treatment means.

Mathematical modeling of drying

For modeling of thin layer drying of *Origanum vulgare* L., the moisture ratio was calculated using equation 1 initial moisture content of the sample (M_0), equilibrium moisture content (M_e), and sample moisture during the drying process using (Doymaz, 2007).

$$MR = \frac{M_t - M_e}{M_0 - M_e} \tag{1}$$

In which MR is moisture ratio (dimensionless), M_t is moisture content at time t (d.b%), M_0 is initial moisture content (d.b%), M_e is equilibrium moisture content(d.b%). For determining the final moisture content, the samples were placed in a vacuum oven at 70°C and 150 mbar for 8 hours. The samples were weighted before and after drying and their moisture was determined using equation 3 on the dry basis.

$$M_C = \frac{W_w - W_d}{W_d} \tag{2}$$

In which M_C is moisture content (d.b%) W_w is weigh of sample (kg) and W_d is dry matter weight (kg).

After drying, the drying models in table 1 were used to examine moisture variation during the drying process and to determine the best model.

Tab. 1 Mathematical equations used for modeling of drying process

Model name	Model equation	Reference
Lewis	*MR=exp(-kt)*	(Lewis, 1921)
Henderson and Pabis	*MR=a exp(-kt)*	(Westerman et al., 1973)
Page	$MR=exp(-kt^n)$	(Arabhosseini et al., 2009)
Modified Page	$MR=exp(-(kt)^n)$	(White et al., 1981)
Yagcioglu	*MR=a exp(-kt)+c*	(Yagcioglu et al., 1999)
Verma	*MR=a exp(-kt)+(1-a) exp(-gt)*	(Verma et al., 1985)
Two-term	$MR=a\ exp(-k_0t)+b\ exp(-k_1t)$	(Arabhosseini et al., 2009)

In the above equations, k, n, a, b, c, g, k_0 and k_1 are the model coefficients. Non-linear regression method was utilized to fit the data to the selected drying models. For evaluating the goodness of fit, three statistical indicators were used in addition to R^2 (Table 2). The model having the highest R^2 and the lowest Root Mean Squares Error (RMSE), χ^2, and P-value was thus determined as the best model.

In Table 2 M_i is moisture content of matter, M_{pre} is predicted moisture by the model, N is number of observations, n is number of model constants, MR_{exp} is moisture ratio of experimental data, MR_{pre} is predicted moisture ratio.

Results and Discussion

Tables 3 to 5 show the obtained statistical results of R^2, RMSE, P-value and for fitting the experimental data to selected drying models in order to determine the best model.

Tab. 2 Equations of indicators for evaluation of the drying models (San Martin et al, 2001)

Indicator	Equation
P- value	$P = \frac{100}{N}\sum\frac{\lvert M_i - M_{pre}\rvert}{M_i}$
χ^2	$\chi^2 = \frac{\sum_{i=1}^{n}(MR_{exp} - MR_{pre})^2}{N - n}$
$RMSE$	$RMSE = \sqrt{\frac{\sum_{i=1}^{n}(MR_{pre} - MR_{exp})^2}{N}}$

Tab. 3 Evaluation of the models at 50°C and air velocities of 1 and 2 m/s

Model	RMSE $\times 10^{-1}$	$\chi^2 \times 10^{-2}$	R^2	P- value (%)
v=1 m/s				
Lewis	19	6	0.97	8.32
Henderson and Pabis	24	38	0.99	22.32
Page	2	5	0.99	6.22
Modified Page	23	46	0.98	27.39
Yagcioglu	34	19	0.89	24.24
Verma	32	31	0.91	21.70
Two - term	43	14	0.87	19.46
v=2 m/s				
Lewis	18	6	0.97	7.35
Henderson and Pabis	37	40	0.98	17.23
Page	3	6	0.99	5.21
Modified Page	23	45	0.97	10.80
Yagcioglu	31	20	0.88	16.34
Verma	43	24	0.88	12.21
Two - term	24	13	0.90	15.12

Tab. 4 Evaluation of the models at 60°C and air velocities of 1 and 2 m/s

Model	RMSE ×10^{-1}	χ^2 ×10^{-2}	R^2	P- value (%)
v=1 m/s				
Lewis	13	10	0.89	8.14
Henderson and Pabis	24	52	0.98	10.70
Page	5	8	0.98	4.31
Modified Page	26	44	0.97	10.31
Yagcioglu	44	10	0.98	15.23
Verma	48	13	0.90	17.14
Two - term	43	15	0.91	17.34
v=2 m/s				
Lewis	12	12	0.97	7.54
Henderson and Pabis	58	34	0.98	12.15
Page	2	10	0.98	3.30
Modified Page	64	54	0.98	14.41
Yagcioglu	53	15	0.87	13.14
Verma	73	12	0.89	16.40
Two - term	66	14	0.84	14.31

Tab. 5 Evaluation of the models at 70°C and air velocities of 1 and 2 m/s

Model	RMSE ×10^{-1}	χ^2 ×10^{-2}	R^2	P- value (%)
v=1 m/s				
Lewis	10	5	0.98	5.31
Henderson and Pabis	55	23	0.97	16.40
Page	6	7	0.99	3.32
Modified Page	37	33	0.97	20.41
Yagcioglu	34	14	0.91	11.72
Verma	56	18	0.90	12.19
Two - term	45	20	0.94	10.23
v=2 m/s				
Lewis	11	10	0.98	5.21
Henderson and Pabis	45	37	0.87	9.79
Page	5	13	0.99	4.22
Modified Page	65	22	0.98	9.41
Yagcioglu	78	11	0.88	10.17
Verma	59	10	0.90	13.54
Two - term	55	16	0.90	16.39

Table 6 shows the fitness of obtained data from experimental treatments using the Page model. The R^2 values are above 0.99 and p-values are below 10% for all temperature and air velocities which statistically shows the good fit.

Tab. 6 Coefficient of the Page equation fitted to drying data

Temperature, °C	Velocity, m/s	k	n	RMSE ×10^{-1}	P- value (%)	χ^2 ×10^{-2}	R^2
	1	0.032	0.70	11.60	4.21	25.70	0.999
50	2	0.014	0.234	14.3	2.3	71.30	0.998
	1	0.21	0.564	32.12	5.4	19.15	0.998
60	2	0.35	0.423	52.21	3.6	12.61	0.999
	1	0.052	0.214	17.3	5.4	23.01	0.996
70	1	0.26	0.536	31.22	4.7	45.17	0.998

Conclusion

Among seven drying models, the Page equation showed the best fit for drying. Thus this model is suitable as a relevant equation for drying of *Origanum vulgare* L. The n and k parameters were estimated as functions of temperature for *Origanum vulgare* L. leaves. This model is suitable to estimate the moisture content during drying in order to determine drying time and energy consumption. It is also applicable for designing of relevant dryer for this type of medicinal plant.

Reference

Arabhosseini A., Huisman, W., van Boxtel, A. J. B., Mueller, J., 2009. Modeling of thin layer drying of tarragon (*Artemisia dracunculus* L.). Journal of Industrial Crops and Products 29: 53-59.

Doymaz, I., 2007. Thin layer drying behavior of mint leaves. Journal of Food Engineering 24: 370-375.

Hall, C. W., 1980. Drying and Storage of Agricultural Crops. The AVI Publishing Company, Inc, Westport.

Lewis, W. K., 1921. The rate of drying of solids materials. The Journal of Industrial and Engineering Chemistry 13(5): 427-432.

San Martin, M. B., Mate, J. I., Fernandez, T., Virseda, P., 2001. Modeling adsorption equilibrium moisture characteristics of rough rice. Journal of Drying Technology 19: 681-690.

Simal, S., Femenia, A., Garau, M., Rossello, C., 2005. Use of exponential, Page´s and diffusional models to simulate the drying kinetics of Kiwifruit. Journal of Food Engineering 66: 323-328.

Tsami, E., Maroulis, Z. B., Morunos-Kouris, D., Saravacos, G. D., 1990. Heat of sorption of water in dried fruits. International Food Science Technology 25: 350-359.

Verma, L.R., Bucklin, R.A., Endan, J. B., Wratten, F.T., 1985. Effect of drying air parameters on rice drying models. Transactions of the American Society of Agricultural Engineers 28: 296-301.

Westerman, P. W., White, G. M., Ross, I. J., 1973. Relative humidity effect on the high temperature drying oh shelled corn. Trans ASAE 16: 1136-9.

White, G. M., Ross, I. J., Poneleit, C. G., 1981. Fully- exposed drying of popcorn. Transactions of the American Society of Agricultural Engineers 24: 466-468.

Yagcioglu, A., Degirmencioglu, A., Cagatay, F., 1999. Drying characteristic of laurel leaves under different conditions. Proceeding of the 7th International Congress on Agricultural Mechanization and Energy: 565-569.

IMPACT OF MALT GRANULOMETRY ON LAUTER PROCES

Ladislav Chládek*, Petr Vaculík, Miroslav Přikryl, Michal Vaculík, Michaela Holomková

Czech University of Life Sciences Prague, Kamýcká 129, 165 21 Prague 6 – Suchdol
Phone: +420 224 383 192, Fax: +4202-34381828, e-mail: chladekl@tf.czu.cz

Abstract:

The preparation of beer consists of several important and closely interconnected steps. One of the essential steps is the preparation of sweet wort. The proper process of sweet wort preparation is created by mashing-in process, mashing process and finally by the lautering process. But also the preliminary operations, such as the malting or malt cleaning and milling, are necessary. The technology and technological equipment used for the preparation of sweet wort can significantly influence the final quality of the beer.

The precision of milling plays the crucial role in the last step of the sweet wort preparation – in the lautering process. The process of sweet wort separation can be provided either by the lauter tun, which is the most common, used sweet wort separation method in Czech breweries, or by mash filters. Both methods require slightly different dispersity of the crashed malt.

Keywords: beer, malt, desintegration, dispersity of crashed malt, lauter tun

Introduction

Sweet wort is prepared in the brew house („kitchen of the brewery“) from malt, eventually with partially substitute of unmalted cereals, starch adjuncts (maize, rice, unmalted barley, sorghum/millet, wheat, sugar surrogates, glucose syrup, coloring sugar) and water. Before the sweet wort preparation starts, the starch of the barley must be converted into the fermentable sugar, therefore the preliminary step should be malting process. The sweet wort preparation consists of following steps: malt cleaning, malt milling, mashing-in process, mashing process and sweet wort separation (Kunze, 2010; Basařová et al., 2010).

Before extraction into the wort, malt is crushed by milling to produce grist of an adequately reduced endosperm, an intact husk and embryo (that means with no adhering endosperm) (Sugden, 1998). The husks of malt are important contributors to beer flavour, providing body and bitterness (Bosewitz, 1957; Pollock, 1958).

That most commonly used for malt milling are dry milling processes. Dry mills can be roll, disk or hammer mills, but for malt milling the most used are the roller mills. There are many types of roller mills, and the general rule is, that the more rolls, the greater the flexibility and the capacity of the mill (Kunze, 2010; Hardwick, 1995; Chládek, 2007).

For dry milling there are used mills with smooth or fluted rollers. The composition of the malt grist is significantly influenced by the construction and the direction of the milling rollers and their rotating speed (Basařová et al., 2010; Hardwick, 1995).

Material and method

a) The determination of crushed malt dispersity

Crushed light barley malt samples were obtained from three breweries by using roller malt mills which were based on dry method of milling. Malt milling in the brewery 1 was performed by two-roller mill. The roller gap adjustment of this mill was 0.40 mm. In the brewery 2 there was used the four-roller mill with the gap sizes between the working roller pairs 1.60 and 0.70 mm. The milling of the third sample in the brewery 3 was realized by using the six-roller mill with gap settings 1.70 – 0.40 – 0.25 mm. The sieving analysis (grading test) was used for the consideration of crushed malt dispersity. Ten measurements were provided for each crushed malt sample.

For the test sieving analysis there was used the test sieve shaker (sieve analysator) HAVER EML 200 digital plus T. This test sieve shaker operates on the basis of dry sieving principle. This device offers the setting and storing of sieving time, interval and amplitude for reproductive sieving results.

Brassy analytical test sieves with woven wire screens and apertures square cross section were used. The test sieves, with aperture sizes of 5.00; 2.00; 1.60; 1.40; 1.25; 1.00; 0.80; 0.63; 0.50; 0.40; 0.315; 0.250; 0.200; 0.160; 0.125; 0.900 and 0.063 mm, were used for the sieving test. The weighing of crushed malt samples and test sieves was performed by a digital laboratory scale KERN PEJ 2200 – 2M.

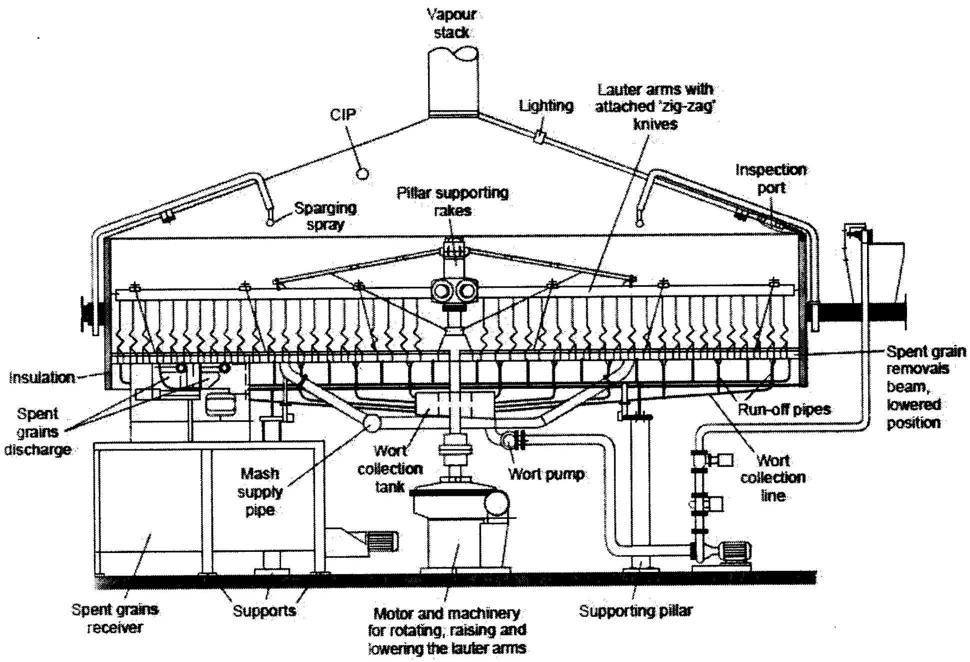

Fig. 1 The modern lauter tun (cross section) (Briggs, 2004)

b) The method of evaluation of the data

The method of evaluation of the test sieving data, are described by Maloun (Maloun, 2001). The data obtained from the sieve analysis is relatively difficult to evaluate in a reproducible way. Tabular data processing is not sufficient. Therefore a graphical interpretation of the data is often used as it helps to imagine the analytical form of the function (which describes the granulometric composition of the sample) more easily. From the analytical form of the function there is possible to obtain the essential characteristics of the bulk materials. There are important characteristics like „the co efficient of polydispersity“ and „the mean statistical size of the particle $\bar{x}$“ which determines the precision of milling. The probability curve of specific size particles presence moves the maximum into the range of small particles. This non-symmetry does not allow the standard distribution. RRSB distribution - an exponential relation by Rosin, Rammler and Sperling was invented for the fine grained materials. According to Bennett modification of this relation, there is a possibility to express the proportional evaluation of the relative residue on the sieve (Maloun, 2001):

$$R = 100\exp\left[-\left(\frac{x}{\bar{x}}\right)^n\right] \quad (\%) \qquad /1/$$

where R – is the relative residue on the sieve [%],

x – is the dimension of separate particle [mm],

$\bar{x}$ – is the main statistical size of the particle [mm],

n – is the material constant [1].

Because the shape of the curve is not suitable for the graphical expression, the distribution function can be linearised.

$$\frac{100}{R} = \exp\left[\left(\frac{x}{\bar{x}}\right)^n\right] \quad (\%) \qquad /2/$$

and there is obtained the relation

$$\log\left[\log\frac{100}{R}\right] = n\cdot\log x + C$$

where $C = \log(\log e) - n\cdot\log\bar{x}$ /3; 4/

which gives Y and X values

$$Y = \log\left[\log\frac{100}{R}\right]; \qquad X = \log x \qquad /5; 6/$$

The $\bar{x}$ value is defined by the inflexion point of the distribution function curve which is given by the particular value of the cumulative relative residue. This is possible to obtain from the equation:

$f''(R) = 0$ that means from

$$\left\{y = \log\left[\log\frac{100}{R}\right]\right\}'' = 0 \qquad /7; 8/$$

If the calculated second derivation is equated to zero, there is obtained the value of the relative residue which is corresponding with the point if inflexion:

$$R = \frac{100}{e} = 36{,}79 \ (\%) \qquad /9/$$

For the calculated value there is given $x = \bar{x}$. It is possible to locate the $\bar{x}$ value from the diagram by the point of intersection of the linearized distribution function and straight line Y = 36.79 %. The determination of the main statistical dimension of the particle on the logarithmic scale is not so precise, therefore this value can be evaluated analytically from the equation of the particular regressive straight line:

$$\log\left[\log\frac{100}{36{,}79}\right] = a + b \cdot \log x \qquad ;$$

$$\log \bar{x} = \frac{\log\left[\log\frac{100}{36{,}79}\right] - a}{b} = \frac{-0{,}36224 - a}{b} \quad /10;\ 11/$$

and therefore $\bar{x} = 10^{\log \bar{x}}$.

In the case of the data obtained from the sieve analysis, the mean statistical dimension of the particle, that means the determination of the precision of milling, was evaluated according to above-mentioned recommendation. The data obtained from the sieve analysis were noted into the protocol, while the initial data were "the weight of empty sieve (g), the weight of the sieve with the residue (g)", and "the sieve fraction (g)", that means the total residue. Then the values of the cumulative relative residue, and the Y , X values were calculated.

According to the regression line parameters from the graph there was possible to calculate the value of mean statistical dimension of the particle.

$Y = a + b \cdot \log x$ that means

$$Y = 0{,}3264 + 1{,}3295 \cdot \log x \qquad /12;\ 13/$$

Then parameter $\log \bar{x}$ was measured:

$$\log \bar{x} = \frac{\log\left[\log\frac{100}{36{,}79}\right] - a}{b} = \frac{-0{,}36224 - a}{b} = \frac{0{,}36224 - 0{,}3264}{1{,}3295} = -0{,}51797 \quad /14/$$

Then $\bar{x}$ was calculated:

$\bar{x} = 10^{\log \bar{x}}$ that means $\bar{x} = 10^{-0{,}51797}$ which is $\bar{x} = 0{,}30341$ mm.

c) The preparation of sweet wort

From crushed malt sample from the three types of roller malt mills, the sweet wort was prepared. The infusion mashing process was used for the sweet wort preparation and the used water/grist ratio was 1 litre of water and 0.20 kg of malt grit. A digital scale, a kettle with the volume of 5.0 litres and an electronic kitchen thermometer was used for the preparation of the sweet wort. The iodine test, using iodine tincture, was used for the determination of starch conversion in the mash.

The prepared mashes were filtered by using the small scale lauter tun apparatus. For the measuring of wort separated from the spent grains there was used laboratory beaker and stop clock. The small scale lauter tun apparatus constructed for this measurement was made by company: ZVU POTEZ a.s. from Hradec Králové. The body of the small scale apparatus was made from cast iron. The volume of the apparatus is 250 ml. The original false bottom from the lauter tun was mounted to the small scale lauter tun apparatus in order to separate the sweet wort from the spent grains.

Results and discussion

The precision of milling was determined with using RRSB distribution. The $\bar{x}$ value for particular samples was evaluated by average from 10 measurements.

The finest grist was obtained from the four-roll mill while the main statistical size of the particle, the $\bar{x}$ value was equal to 0.23 mm. The fine grist was obtained by two-roller milling with the main statistical size of the particle equal to 0.26 mm. The six-roller milling gave the coarser malt grist with the value of main statistical size of the particle 0.29 mm.

Tab. 1 The precision of milling of particular samples

Measurement	2-roll mill	4-roll mill	6-roll mill
1	0.29	0.28	0.28
2	0.28	0.19	0.29
3	0.28	0.27	0.30
4	0.25	0.25	0.31
5	0.23	0.25	0.30
6	0.25	0.19	0.30
7	0.24	0.20	0.27
8	0.26	0.25	0.29
9	0.23	0.25	0.27
10	0.26	0.21	0.26
Average	**0.26 mm**	**0.23 mm**	**0.29 mm**

Tab. 2 The report of lautering times for samples from two-roll mill

Date		18.3.2013	**Brewery 1**		Infusion mashing
Malt		Light barley malt	**Water/malt grist ratio**		1 liter/0.2 kg
Mill		2-roll mill	**Sample volume**		250 ml
Gap		0.40 mm	**Lauter tun**		
	Time (min)				
Volume	**Sample 1**	**Sample 2**	**Sample 3**	**Sample 4**	**Sample 5**
25 ml	00:09:04	00:09:12	00:11:53	00:09:58	00:10:14
50 ml	00:16:48	00:19:44	00:36:11	00:53:26	00:29:36
75 ml	00:35:21	00:39:81	01:33:37	01:59:93	01:33:61
100 ml	00:59:76	01:25:45	02:37:94	04:03:31	03:32:52
125 ml	02:03:92	01:59:06	04:00:58	06:42:46	06:59:15
150 ml	03:41:38	03:58:27	07:48:64	08:51:57	15:49:07
175 ml	12:07:73	12:46:26	15:41:39	18:02:29	34:06:13

Tab. 3 The report of lautering times for samples from four-roll mill

Date		25.3.2013	**Brewery 2**		Infusion mashing
Malt		Light barley malt	**Water/malt grist ratio**		1 liter/0.2 kg
Mill		4-roll mill	**Sample volume**		250 ml
Gap		1.60 – 0.70 mm	**Lauter tun**		
	Time (min)				
Volume	**Sample 1**	**Sample 2**	**Sample 3**	**Sample 4**	**Sample 5**
25 ml	00:09:43	00:10:27	00:09:52	00:11:02	00:11:24
50 ml	01:53:82	01:35:24	02:16:77	01:54:21	02:06:31
75 ml	05:49:56	04:57:13	06:42:09	06:10:87	05:47:65
100 ml	08:48:96	09:12:06	10:18:87	08:51:23	10:31:19
125 ml	15:28:43	15:43:76	17:27:09	14:43:56	16:52:31
150 ml	24:07:11	26:34:07	23:55:12	22:17:82	26:09:92
175 ml	35:27:75	42:58:07	39:37:94	36:47:82	39:21:17

Tab. 4 The report of lautering times for samples from six-roll mill

Date		2.4.2013	**Brewery 3**		Infusion mashing
Malt		Light barley malt	**Water/malt grist ratio**		1 liter/0.2 kg
Mill		6-roll mill	**Sample volume**		250 ml
Gap		1.7 – 0.4 – 0.25 mm	**Lauter tun**		
	Time (min)				
Volume	**Sample 1**	**Sample 2**	**Sample 3**	**Sample 4**	**Sample 5**
25 ml	00:10:95	00:11:24	00:07:58	00:09:63	00:09:52
50 ml	00:47:21	00:42:13	00:31:29	00:38:43	00:40:74
75 ml	00:59:28	01:23:24	01:12:89	01:48:13	02:07:23
100 ml	01:52:43	01:58:14	01:43:59	03:47:26	02:58:93
125 ml	02:31:27	04:06:51	02:29:71	06:13:28	04:58:19
150 ml	04:38:21	06:14:79	04:39:27	07:56:27	07:49:13
175 ml	12:03:91	11:23:06	15:17:81	17:48:32	18:07:42

The samples of particular mashes were filtered by using the small scale lauter tun apparatus. Prepared mash samples were filtered by five samples of volume 250 ml. The highest filterability showed the mash sample made from the six-roll mill. The samples from this mash were in average filtered in 14:56:26 min. The main statistical size of the particle obtained by milling in six-roll mill was 0.29 mm. The good filterability shoved also mash prepared from the malt grist sample, which was milled by the two-roller mill. The average lautering time was 18:33:00 minutes. The mean statistical particle size of the grist was 0.26 mm. Significantly longer lautering times shoved the mash, which was prepared from the grist obtained by milling in the four-roll mill. The average lautering time was 41:09:42 minutes. The mean statistical particle size of the grist was 0.23 mm.

Conclusion

Better properties of the grist sample from the four-roller mill were expected than of the ones from the two-roller mill. It can be explained by the selection of non-representative sample of malt grist. The time of lautering was lengthened during the measurement of the samples. That was influenced by the temperature decrease during lautering of particular samples. It caused the increase of the viscosity of the wort and therefore the filtration became more difficult. Malt grist samples from the six-roller mill showed different particle size distribution. The different particle size distribution occurred because there was a large amount of intact husks obtained in the malt grist sample. The above-mentioned husks were retained on the first two sieves with largest aperture sizes of 2.50 and 2.00 mm. In comparison to grist samples from the two- and six-roller mills the amount of fine particles retained on the sieves was lower, i.e. the mean statistical particle size was therefore higher. The presence of big amount of intact husk had a positive influence of the lautering process in the form of good loosening of the spent grain layer.

Reference

Basařová G., Šavel J., Basař P., Lejsek T., 2010. Pivovarství: Teorie a praxe výroby piva (Brewing: The Theory and Practice of Beer Production). 1st. edition. Praha: VŠCHT Publishing Praha, 904. (in Czech)

Briggs D.E., Boulton C.A., Brookes P.A., Stevens R., 2004. Brewing Science and Practice. Woodhead Publishing. ISBN: 978-1855734906

Bosewitz G., 1957. Die Nahrung. 1st. edition. J. Inst. Brew, 60.

Hardwick W.A., 1995. Handbook of Brewing. New York: Marcel Dekker, Inc., 714. ISBN: 0-8247-8908-3

Chládek L., 2007. Pivovarnictví. 1st. edition. Praha: Grada Publishing, a.s., 208. (in Czech)

Kunze W., 2010. Technology Brewing and Malting. 4th updated English Edition. Berlin: VLB, 1047. ISBN: 978-3-921690-64-2

Maloun J., 2001. Technologická zařízení a hlavní procesy při výrobě krmiv. 1st edition. Prague: Czech University of Life Sciences Prague, 201. ISBN 80-213-0783-8. (in Czech)

Pollock J.R.A., 1958. Barley and Malting. In: Malting, Brewing and Allied Processes Preece, I.A.). Literature Survey, Prepared for the Institute of Brewing. Surrey: Brewing Industry Research Foundation, 6-14.

Sugden D.T., 1998. Milling (Manual of Good Practice). UK: European Brewery Convention (EBC), 57.

MECHANICAL SURFACE TREATMENT FOR ADHESIVE BONDING TECHNOLOGY IN SANDWICH PRODUCTION

Petr Chocholouš*, Miroslav Müller

Czech University of Life Sciences Prague, 16521 Prague 6 – Suchdol, Czech Republic,
Phone: +420224383262, E-mail: chocholousp@tf.czu.cz

Abstract

The adhesive bonding technology is increasingly used process of material joining. The advantage of adhesive bonding is a possibility to join together two or more materials with different thicknesses or with different chemical and physical properties. This advantage is used in a production of sandwich materials, where various materials come into contact. The strength of bonded joint is influenced by many factors, where one of the most important factor is a surface treatment. The article deals with assessing bond strength depending on the surface treatment. The article also states dependence of resulting strength and hardness of adhesive on curing time. For experiment three metal materials with various surface treatments bonded with polyurethane adhesive were used. The experiment show that mechanical surface treatment can increase bonded surface and subsequently bond strength also.

Keywords: adhesive bonding, sandwich material

Introduction

The adhesive bonding technology is prospective method of joining materials. Science and research progress leads to producing new types of adhesives with improved properties. Using adhesive bonding technology eliminates the difficulty associated with having to create holes for screws or rivets or with heat-affected zone during soldering or welding. Adhesive bonding technology has many advantages, which include the possibility of bonding dissimilar materials or materials with different thicknesses. The disadvantage of bonded joints is less heat and chemical resistance due to using welding or screw joints.

The prospective example of using adhesive bonding technology is the production of sandwich materials. Sandwiches are usually made up of three or more layers, which considerably differ in thickness and used material. In the insulation sandwich material production various materials such as wood, plastic or metal, which are used as coatings, and materials with foam structure used as fillers are bonded together. The materials with foam structure have good insulating properties and by previous processing they have open structures, which absorb adhesive. For these materials it is appropriate to applied adhesive spraying angle to minimize volume of absorb adhesive.

However, there is not one universal adhesive that would be able to glue any material. The proper selection and application of adhesive is an important part of the chain that bonded joints properly fulfill their function under certain conditions. Designer must take into account many factors affecting joints when selecting adhesives. Main factors can be considered the kind of bonding material, environment that adhesive joint will be exposed to, type of loading and other properties such as look or vapor and liquid tightness. The aggressive environments such as high or low temperatures or aggressive chemical environments (fluids, salt) result in degradation of adhesive joints and it is associated with reduction of bond strength. (Müller, Valášek, 2012; Valášek, Müller, 2012; Müller, 2013).

For proper and safe behavior of bonded joints it is necessary to pay attention to respecting technologic procedure and to right choice of bonding surface treatment. Before each adhesive bonding it is necessary to degrease bonded surface. To increase the strength of bonded joints is it possible use mechanical surface treatment by scrubbing, grinding or blasting and subsequent degreasing. The mechanical surface treatment is closely related to surface roughness. By increasing material surface roughness functional surface for bonding increases also. With increasing size of abrasive particles roughness parameters grow when using blasting. When determining the optimal surface roughness the bond strength can be increased by up to 24 % as confirmed Müller et al. (2008) during their experiments. Other experiments carried out by Müller (2011) showed that in some cases mechanical treatment is redundant and it is possible to omit it, thereby reduce produce costs.

As it was described above adhesive bonding process is a difficult process depending on many factors and for the verification of suitability of bonded joint under specific conditions it is necessary to perform the testing. Producer's experience shows that the destruction of bonded joint usually occurs on surface of metal materials. The experiments were aimed at assessing bond strength depending on a surface treatment. The bonded joint does not reach the final maximum strength immediately, but this strength is achieved after a certain period. For this reason the experiments were also addressed at dependence of bond strength on curing time. With curing time the hardness of adhesive is also changing, so dependence between bond strength and hardness of adhesive was searched.

Materials and method

The selection of tested materials and adhesive was based on using these materials in production of thermal insulation sandwich materials for car bodies and additional insulation constructions.

To evaluate suitable surface treatment for adhesive bonding, three metal materials were selected (aluminum sheet thickness of 3 mm, galvanized sheet thickness 1.5 mm and stainless steel thickness of 1.5 mm). All these materials were subjected to three different mechanical surface treatments and one set was degreased only. The resulting strength of bonded joints was compared among each other and with material without mechanical surface treatment. Grinding and scrubbing was carried out on equipment (RWT, BSM 650 RB) for mechanical surface treatment of metal sheets. Grinding was performed using abrasive cloth P40 and scrubbing was performed with steel rotating brushes. Blasting was performed using artificial corundum grit of F80. Subsequently, bonded joints were degreased and according to the standard ČSN EN 1465 (Adhesives - Determination of tensile lap-shear strength of bonded assemblies) test specimens were made. Two component polyurethane adhesive SikaForce – 7723 L175 was used. After full curing (21 days according to the material sheets) specimens were tested in lap shear tensile strength on universal testing machine. After test the maximum load force was recorded and according to ČSN ISO 10365 (Adhesives - Designation of main failure patterns) type of destruction was identified.

For assessing bond strength depending on curing time same dimensions of specimen as for surface treatment assessment were made. Galvanized steel with scrubbing surface treatment were chosen. The series were prepared in accordance with the methodology for assessing the suitability of surface treatment and subsequently at intervals 1, 3, 5, 7, 14 and 21 days were tested in lap shear tensile strength on universal testing machine. After test the maximum load force and type of destruction was recorded.

To determine the dependence of hardness of adhesive on curing time, three specimens were made and subsequently in time intervals hardness Shore D was measured. The roughness of surface was assessing by parameter Ra (the arithmetic mean of the departures of the profile from the mean line (μm)) and measured using the profilometer Surftest 301. The roughness parameters were measured in five points of each specimen using the cut-off of 0.8 mm. For the evaluation of the material surface stereoscopic microscope with a camera with a PC output was used. The obtained values were statistically evaluated and graphically presented.

Result

Values of lap shear tensile strength are shown in Fig.1. The highest bond strength for aluminum is achieved by bonded joints with grinding surface treatment 5.81 ± 0.54 MPa, which is an increase of 21 % compared to degreased surface only. The optimal mechanical treatment for stainless steel in terms of bond strength is surface with scrubbing treatment. These bonded joints achieve values of 8.48 ± 0.93 MPa, which is an increase of 35 % compared to degreased surface only. Bonding strength of the galvanized metal sheet with blasted surface has increased by 29 % to 5.50 ± 0.77 MPa.

Type of the bond destruction differed according to applied surface treatment. In all cases of surface treatment by blasting only cohesive failure has occurred. In the case of stainless steel with scrubbing and grinding treatment combined destructions of bonded joints showed in the ratio of 15:85 (adhesion:cohesion). In all other cases, only adhesive destructions of bonded joints have occurred.

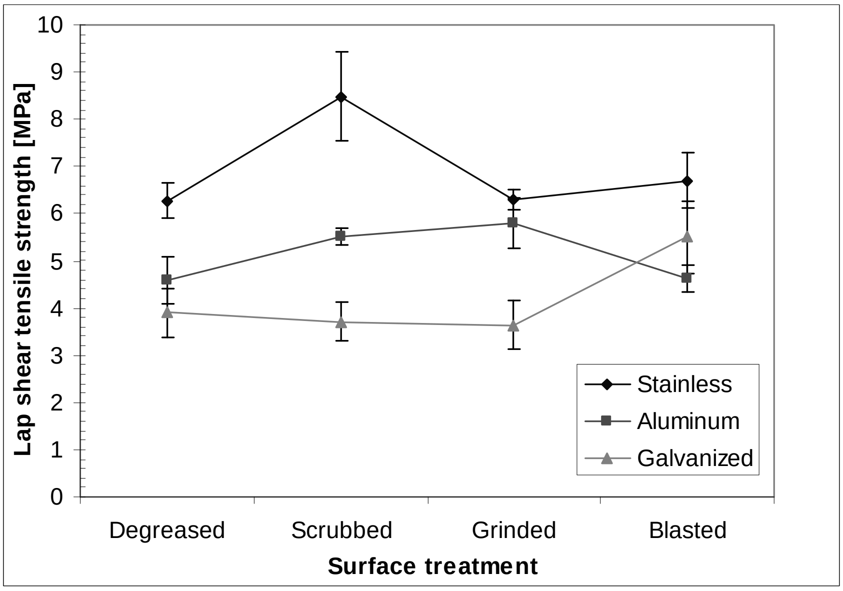

Fig. 1 Influence of bond strength on surface treatment

Tab.1 Values of surface roughness (Ra)

Ra	Aluminum	Stainless	Galvanized
Blasting	2,35 ± 0,61	0,99 ± 0,13	1,87 ± 0,46
Grinding	0,68 ± 0,44	0,23 ± 0,07	0,53 ± 0,07
Degreasing	0,24 ± 0,06	0,14 ± 0,07	0,48 ± 0,06
Scrubbing	3,19 ± 0,87	0,9 ± 0,21	0,91 ± 0,22

Measured values of surface roughness (Ra) are shown in Tab. 1. The highest values of roughness (Ra) for stainless and galvanized steel were achieved by blasting. In case of aluminum scrubbed surface had highest roughness.

The dependence of bond strength on curing time is graphically illustrated in Fig 2. The figure shows significant increase of bond strength during first 5 days. Bond strength after 24 hours reached 67 % (2.49 ± 0.25 MPa) of maximum strength. After 5th day of curing there has been no significant increase in lap shear tensile strength and after this period bond strength has stabilized.

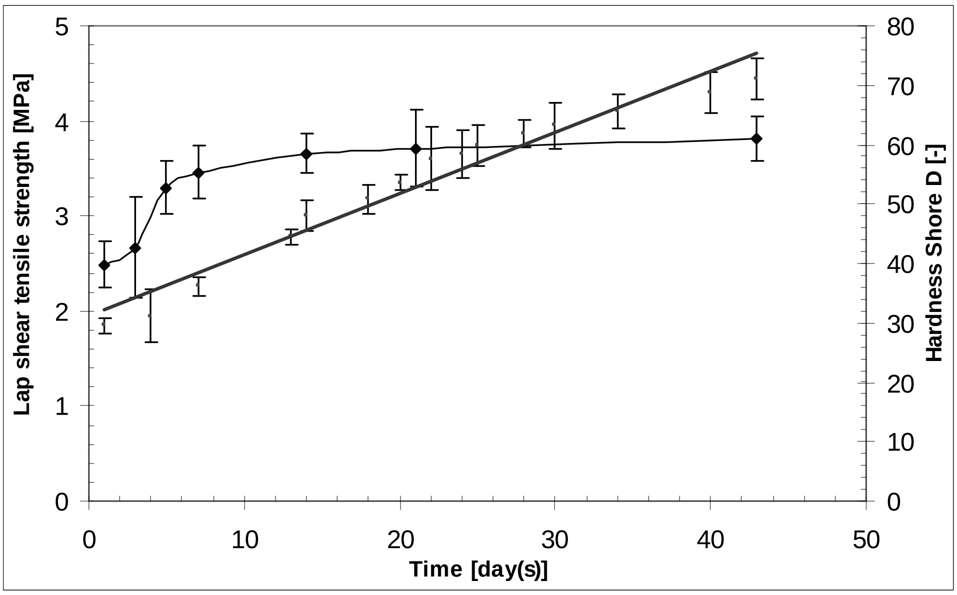

Fig. 2 Influence of bond strength and hardness on curing time

Fig. 3 Microscopic view on surface treatment

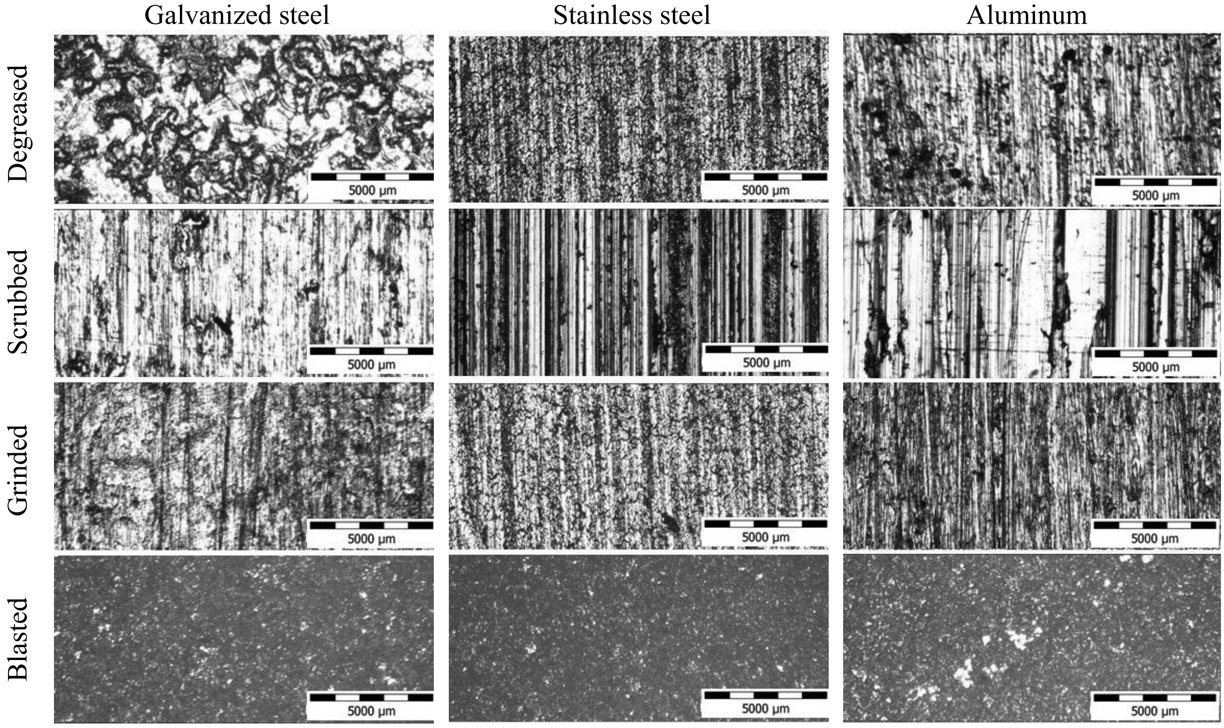

The dependence of the hardness Shore D on curing time is shown graphically in Fig.2. In the period 1--35 days hardness showed linearity, but then after 35 days there was a slight increase in hardness.

On Fig.3 the microscopic view on the bonded material surfaces is shown. The figure shows effect and differences of used methods on the final surface profile.

Conclusion

The adhesive bond strength is influenced by many factors such as curing time and surface treatment, which must be taken into account. Experiments clearly show that there is no universal optimum suitable surface treatment in terms of bond strength for various materials. For each material it is necessary to determine a different suitable surface treatment. The presumption of authors (Elbing et al., 2003; Habenicht, 2002) being related to the increasing function surface part thanks to increased values of surface roughness were confirmed. The presumption that the higher roughness leads to increase bond strength were not confirmed. Type of mechanical treatment and resulting surface profile has an effect on bond strength too. Experiments confirmed that with appropriate surface preparation by mechanical treatment, bond strength can be increased by up to 35 % (in case of the stainless steel with scrubbing surface).The most frequent destruction of bonded joints was adhesive destruction. Surface treatment improves adhesive properties and consequently combined or purely cohesive destruction has occurred. When selecting surface treatment the economic aspect must be taken into account. Surface treatment prolongs and complicates manufacture and thus final product is more expensive.

From curve tract of bond strength depending on curing time it is shown that after 24 hours after application the bond strength reaches 2/3 of maximum strength. This information is useful to know during production process. According to the time data production cycles can be planed. Long curing time (21 days according to the material sheets) in the presses used in the production very lengthened production and increased the price of the final product.

The manufacturer indicates that the maximum hardness is achieved after 21 days under compliance environment but hardness increases also after this period. The reason for this difference may be different curing conditions especially humidity (polyurethane adhesives are cured by ambient moisture).

From carried out experiments it was searched dependence of hardness and bond strength on curing time. These curve tracts show that longer curing time also increases hardness and bond strength. However, the hardness in the range 0-35 days increased linearly and bonding strength in the range 0-43 days had the general shape of the curve.

Acknowledgement

Supported by Internal grant agency of Faculty of Engineering Czech University of Life Sciences in Prague.

Reference

Müller M., Valášek P., 2012. Degradation medium of agrokomplex - adhesive bonded joints interaction. Research in Agricultural Engineering, 58 (3): 83-91. ISSN:1212-9151

Valášek P., Müller M., 2012. Vliv klimatických podmínek České republiky na pevnostní charakteristiky lepených spojů. Strojírenská technologie, 17 (5/6): 343-348. ISSN:1211-4162 (in Czech)

Müller M., 2013. Research of liquid contaminants influence on adhesive bond strength applied in agricultural machine construction. Agronomy Research, 11 (1): 147-154.

Müller M., Hrabě P., Chotěborský R., 2008. Optimization of surface treatment parameters in adhesive bonding technology. In 7th International Scientific Conference on Engineering for Rural Development, 29.05.2008, Jelgava, Latvia: Latvia University of Agriculture Faculty of Engineering, 214-219.

Müller M., 2011. Influence of surface integrity on bonding process; Research in Agricultural Engineering, 57 (4): 153-162. ISSN: 1212-9151

Elbing F., Anagreh N., Dorn L., Uhlmann E., 2003. Dry ice blasting as pretreatment of aluminum surfaces to improve the adhesive strength of aluminium bonding joints. International Journal of Adhesion & Adhesives, 1: 69–79.

Habenicht G., 2002. Kleben: Grundlagen, Technologien, Anwendung (Adhesive bonding: Principles, Technologies, Application), Springer, Berlin. Springer – Verlag.

STUDY OF THE QUASI-ISOTHERMAL PHASE TRANSFORMATION OF AUSTENITE BY ELECTROMAGNETIC SENSOR

Rostislav Chotěborský, Miloslav Linda

Czech University of Life Sciences, 16521 Prague 6 – Suchdol, Czech Republic, Phone: +4202 2438 3274, Fax: +4202-20921361, E-mail: choteborsky@tf.czu.cz

Abstract

The characterization of steel microstructures is an important tool for metallurgists as mechanical properties are controlled by microstructural parameters such as grain size, phase balance and precipitates. The majority of microstructural characterization tools are indirect (inference from measurement of temperature), destructive (optical metallography, SEM and X-ray) or require small samples and laboratory equipment (dilatometry and DSC). This paper describes an electromagnetic sensor that has been designed to detect changes in the relative permeability of steel. An overview of the instrument and measurements from a range of alloy tool steel samples are presented.

Keywords: quasi-isothermal phase, transformation, electromagnetic sensor

Introduction

Almost all commercial steels are produced using heat-treatment in which the austenite cools continuously through the transformation temperature range. This usually leads to a final microstructure which is a mixture of many transformation products, because the high temperature austenite can decompose into a large variety of ferritic transformation products which can be formed by different mechanisms. These reactions may overlap and interact with each other either by "hard"- impingement in which adjacent particles touch or by "soft''-impingement where their diffusion or thermal fields overlap. The interactions are known to be important in determining the final microstructure. Accurate process control is essential for the production of steel with single and multi-phase microstructures by hot working schedules and controlled cooling. Several techniques could be employed to monitor the microstructure evolution directly online including primarily X-rays, electromagnetics and ultrasonics (Dutta et al., 2013; Holzweissig et al., 2012; Kosec et al., 2013). Electromagnetic sensors work on the basis of detecting the difference in relative permeability, μ_r; conductivity, σ, between microstructural phases or due to changes with temperature. Below the Curie temperature ($T_c \approx 770$ °C for carbon steel), ferrite is ferromagnetic (μ_r =200+) and austenite is paramagnetic (μ_r =1). The conductivity difference between the two phases is much smaller (Liu et al., 2012; Peters, Manoli, 2008). The evolution of volume fraction during solid-state transformation is usually described using the classical Johnson–Mehl–Avrami theory (Jones, Bhadeshia, 1997; Kosec et al., 2013; Lan et al., 2013; Reti et al., 2001; Zagainov et al., 2012).

$$Y(t) = 1 - e^{-K \times t^n}, \quad (1)$$

where $K = \frac{\pi \times N \times G^3}{3}$ (N – nucleation rate, G – particle grow rate) and n=4.

Factors *N* and *G* depend directly on temperature. Their dependency is similar if temperature of the steel decreases then nucleation rate and particle growth rate also decreases. Due to these effects *K* decreases in relation to temperature. Therefore, equation (1) can be modified as:

$$Y(t,T) = 1 \quad e^{-K(T) \times t^n} \quad (2)$$

where *K(T)* is the temperature dependency coefficient which characterize changes of the nucleation rate and particle growth rate (Reti et al., 2001). Derivation of equation (2) shows that the maximum transformation rate is in the inflexed point equation. This precondition is significant for transformation of the austenite to bainite. If the real data shows more than one value as maximum limit, then the austenite transforms also to a value >1 of the transformation product. The changes of the derivation give information about the starting and finishing of austenite transformations.

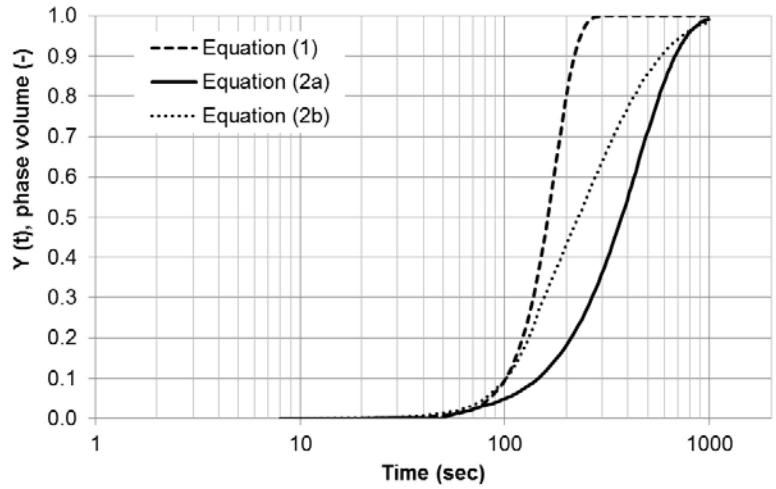

Fig. 1 Solution of equation (1) and (2), where $K = [K_{(1)} \times (T)_{max} - A \times t]$ for (2a) and $K = K_{(1)} \times (T)_{max} - A \times \log(t)$ for (2b)

Material and method

The selected steel CSN 19 436 (Tab. 1) was used for the analysis. Specimens with dimensions of 10 mm diameter and 40 mm length were used. Schema of measuring is presented in Fig. 2.

Tab. 1 Chemical composition of selected steel (wt. %)

	C	Mn	Si	Cr	Ni	P	S
19436	2.1	0.3	0.2	11.5	0.3	0.025	0.03

Temperature was measured by K-type of thermocouples which was connected to Nanodac data logger (co. Eurotherm). Inductivity of the samples was measured by Agilent U1731C LCR meter (accurancy 0.2 %) and data was saved online to PC. Next analyses were developed by an algorithm of synchronizing time from temperature datalogger and Agilent LCR meter in SciLab [15]. Austenizing temperature was 1000 °C for all samples. Inductance was measured after austenizing (30 min at 1000 °C) in measuring coil with 40 threads and 4 layers (Callegaro et al., 2003; Carullo et al., 2003; Constantinides, Angeli, 2012; Musioł et al., 2010; Musiol, 2006). The measured coil was tempered in furnace; conditions of the experiment are shown in Tab. 2. After tempering of the furnace, the furnace was turned off and sample was inserted into measuring coil. The cooling rate depended on thermal capacity of the furnace. Cooling rate at bainitic transformation was about 0.1 °C.min^{-1}.

Tab. 2 Measuring conditions

Sample No.	Temperature of the furnace
1	Room temperature
2	200 °C
3	300 °C
4	400 °C

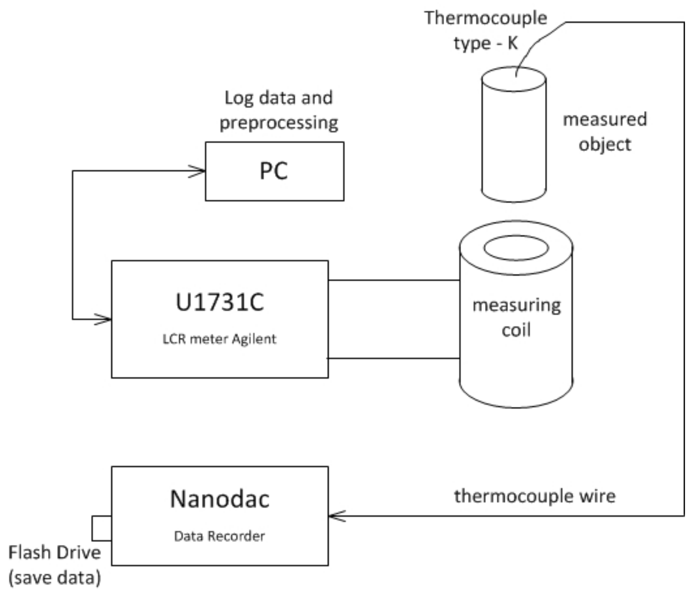

Fig. 2 Schema of measuring devices

Results and discussion

From measured data it was determined time and temperature for austenite transformation. The volume of transformation products was calculated by equation (3). Numerical solutions of equation (2) for a multiphase model are given in Tab. 3 and Fig. 5. In Fig. 3 and Fig. 4 are presented data of the sample 2.

$$V = \sum_{i=1}^{max} dV_i \times dt_i = \sum_{i=1}^{max} \frac{I_{min} + I_i}{I_{max} - I_{min}} \quad (3)$$

where I_{min} is the inductance of coil with a sample at austenizing temperature, I_{max} is the inductance of coil with sample at room temperature before austenizing (inductance of the base structure feritic-cementitic) and I_i is the actually inductance at measured temperature. These preconditions leads to fact that we can predict a volume of transformed phase in time but inductance of feritic-cementitic microstructure show a different value at room temperature than bainitic or martensitic microstructure as a transformation product at room temperature. This difference is lower than 2 % and this suggests that magnetic sensor should be used for an austenite transformation sensor measurement.

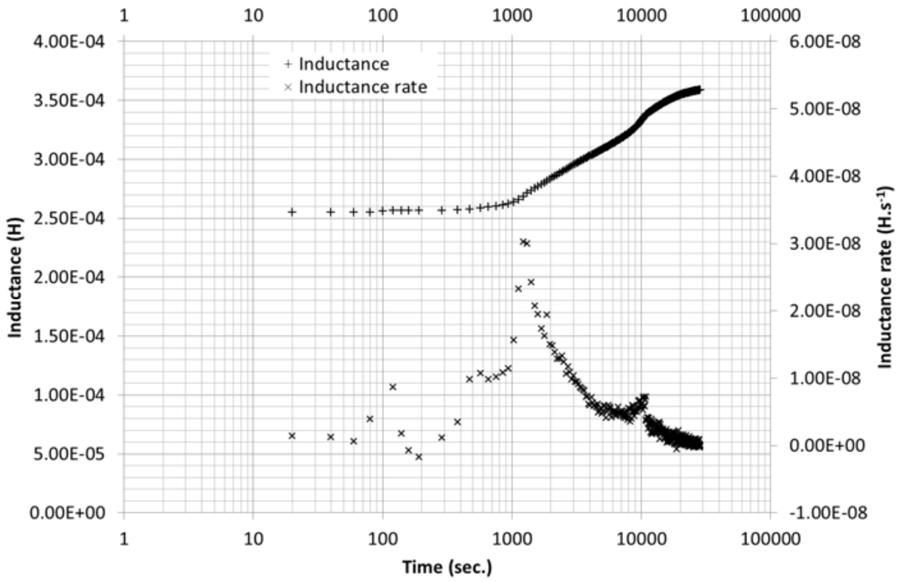

Fig. 3 Amounts of sample 2 showing the dependencies of inductance and inductance rate in relation to time

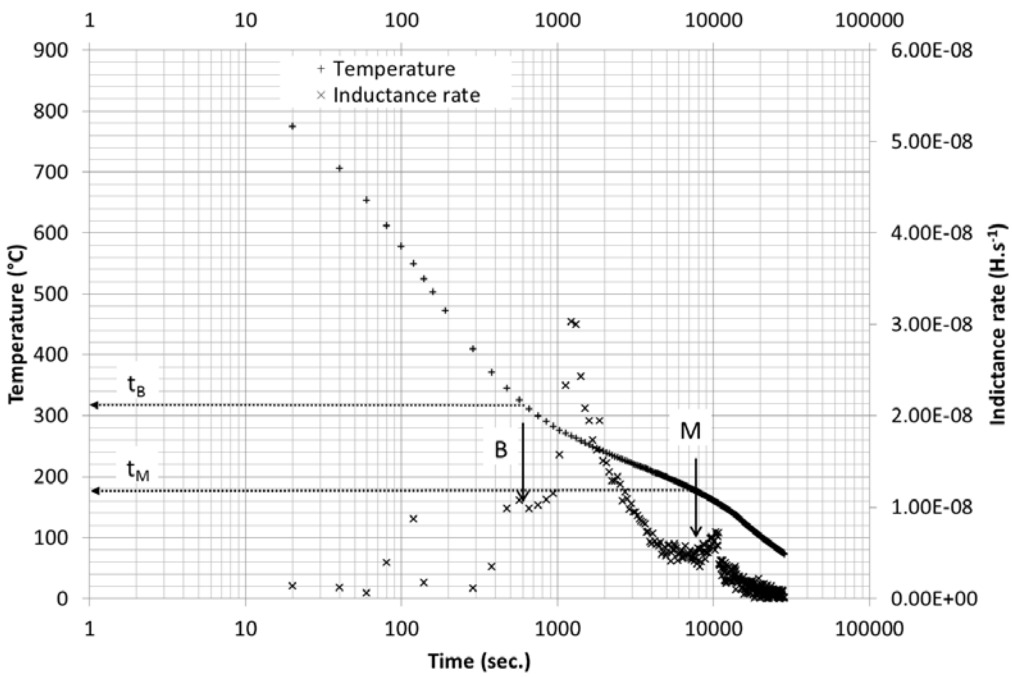

Fig. 4 Measured value of the sample 2 (dependence between temperature and time – left axis; dependence between inductance rate and time – right axis); B – start of the bainitic transformation at temperature t_B, M – start of martensitic transformation at temperature t_M

Tab. 3 Multiphase sample analysis

Sample no.	Time t_B (sec.)	Temperature T_B (°C)	Time t_M (sec.)	Temperature T_M (°C)	Volume of bainite (%)	Volume of martensite (%)
1	180	310	450	210	38	62
2	550	325	7100	180	62	38
3	1000	360	8000	180	86	14
4	4500	380	15500	180	94	6

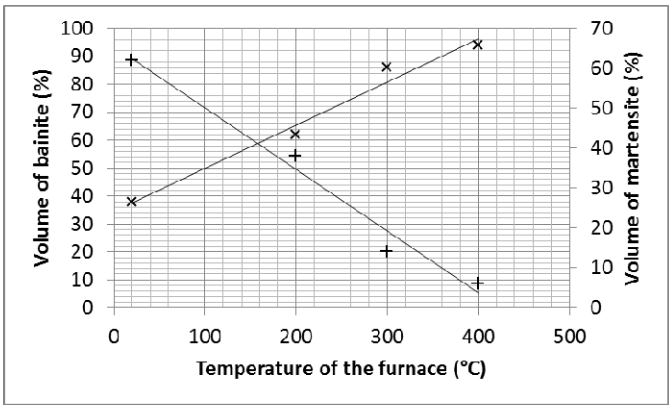

Fig. 5 Dependency between volume of austenite transformation product and temperature of the furnace

Conclusion

The results of the study shows that:

- electromagnetic sensor can be used for kinetic description of the austenite transformation,
- quasi-isothermal phase transformation leads to different volume of the austenite transformation product - bainite and martensite
- volume of the austenite transformation products can be controled by a range of temperature into the furnace.

Acknowledgement

The authors would like to thank Technology Agency of Czech Republic TA01010192 for a finical support.

Reference

Callegaro L., Galzerano G., Svelto C., 2003. Precision Impedance Measurements by the Three-Voltage Method With a Novel High-Stability Multiphase DDS Generator, IEEE Transactions on Instrumentation and Measurement, 52: 1195-1199.

Carullo M., Parvis A., Vallan L., Callegaro L., 2003. Automatic Compensation System for Impedance Measurement, IEEE Transactions on Instrumentation and Measurement, 52: 517-521.

Constantinides C., Angeli S., 2012. Elimination of mutual inductance in NMR phased arrays: The paddle design revisited. Journal of Magnetic Resonance, 222: 59-67.

Dutta R.K., Huizenga R.M., Amirthalingam M., Hermans M.J.M., King A., Richardson I.M., 2013. Transformation-induced diffraction peak broadening during bainitic and martensitic transformations under small external loads in quenched and tempered high strength steel. Metallurgical and Materials Transactions A: Physical Metallurgy and Materials Science (in Press), 1-4.

Holzweissig M.J., Canadinc D., Maier H.J., 2012. In-situ characterization of transformation plasticity during an isothermal austenite-to-bainite phase transformation. Materials Characterization, 65: 100-108.

Jones S.J., Bhadeshia H.K.D.H., 1997. Kinetics of the simultaneous decomposition of austenite into several transformation products. Acta Materialia, 45: 2911-2920.

Kosec L., Šavli Š., Kožuh S., Holjevac Grgurić T., Nagode A., Kosec G., Dražič G-Gojić M., 2013. Transformation of austenite during isothermal annealing at 600-900 C for heat-resistant stainless steel. Journal of Alloys and Compounds, 567: 59-64.

Lan H.F., Du L.X., Liu X.H., 2013. Microstructure and mechanical properties of a low carbon bainitic steel. Steel Research International, 84(4): 352-361.

Liu J., Hao X.J., Zhou L., Strangwood M., Davis C.L., Peyton A.J., 2012. Measurement of microstructure changes in 9Cr-1Mo and 2.25Cr-1Mo steels using an electromagnetic sensor. Scripta Materialia, 66: 367-370.

Musioł K., Met A., Skubis T., 2010. Automatic bridge for comparison of inductance standards.

Measurement: Journal of the International Measurement Confederation, 43(10): 1661-1667.

Musiol K., 2006. A digitally controlled switch for maintenance of inductance standards, in: 2006 Conference on Precision Electromagnetic Measurements. Conference Digest CPEM, Torino, 556–557.

Peters C., Manoli Y., 2008. Inductance calculation of planar multi-layer and multi-wire coils: An analytical approach. Sensors and Actuators, A: Physical, 145-146(1-2): 394-404.

Reti T., Fried Y., Felde I., 2001. Computer simulation of steel quenching process using a multi-phase transformation model. Computational Materials Science, 22: 261-278.

Zagainov A.V., Ulyanov A.I., Chulkina A.A., Zykina I.A., 2012. The effect of Cementite on the formation of the magnetic hysteresis properties of thermally treated carbon steels. Russian Journal of Nondestructive Testing, 48: 35-43.

OPTIMIZATION OF TECHNOLOGICAL PARAMETERS OF BIODEGRADABLE MUNICIPAL SOLID WASTE COLLECTION

Ondřej Chotovinský*, Vlastimil Altmann, Ondřej Tůma

Czech University of Life Sciences Prague
Prague, Czech Republic, chotovinsky@fzp.czu.cz, +420 224 383 862

Abstract

The article deals with the issues of biodegradable municipal solid waste (BMSW) management, focusing on its separate collection. The two locations are compared – rural area (Březník) and urban area (Náměšť nad Oslavou). The emphasis is put on evaluation of individual BMSW collections development from 2006 to 2010. Individual technological limitations of collection are also observed and evaluated (e.g. BMSW production, container quantity development and collection frequency). The observed data also verify the efficiency of BMSW management compared to relative representation of this waste in rest municipal solid waste (RMSW), which is produced in both locations. Also referential locations without separate BMSW collection are observed for evaluation. These are two urban area localities (Třebíč) and a rural area (Čichov).

Key words: Rest municipal solid waste, biodegradable waste, biodegradable municipal solid waste, separate collection, material analysis

Introduction

Any type of waste is considered biodegradable municipal solod waste (BMSW), providing it succumbs to aerobic and anaerobic decay, which is produced in municipal area. Table 1 shows an overview of each BMSW types of waste and also a biologic part ratio in individual types of this waste *(Altmann et al., 2010)*. The most important type of those species is biologically degradable waste from gardens and public green with catalog number 20 02 01. In this post is this waste evaluated.

Tab. 1 BMSW Overview

Index Number	Name of the Type of Waste	Ratio
20 01 01	Paper and cardboard with the exception of highly glossing paper and the wallpaper waste	1,00
20 01 08	Cafeteria biodegradable waste	1,00
20 01 10	Clothing	0,60
20 01 11	Textiles	0,50
20 01 38	Wood not included in 20 01 37	1,00
20 02 01	Biodegradable waste	1,00
20 03 02	Rest municipal solid waste	0,54
20 03 02	Marketplace waste	0,80
20 03 07	Bulky waste	0,50

The greenhouse gases production during BW and BMSW decay at landfills contributes to global greenhouse gases emissions with approximately 4 % *(Papageorgiou et al., 2009)*. In the current push to reduce greenhouse gas emissions is initiated efforts to reduce the landfill of BMWS. A directive which has a crucial value from this perspective and which is fully integrated with Czech legislation is called Council Directive on the landfill 1999/31/EC. The directive's requirement determines gradual decrease of BMSW stored at landfill to 2020. In 20200 there could be 35% of the whole BMSW mass produced in 1995 stored at landfill. In the Czech Republic, there were 1,530,000 tons of BMSW produced in 1995 and in 2010 there were 1.5 million tons of BMSW stored at landfill instead of admissible 1.15 million tons.The precautions of the directive should cover material and energetic use of the waste *(Vehlow et al., 2007)*. The basic presumption for further processing and subsequent use of the waste, considering the quality of compost or fertilizers, is the introduction of separate collection. *(Altmann et al., 2010)*. The action of waste collection is defined as a combination of a certain technology and a human labor *(Bilitewsky et al., 1997)*. This action corresponds not only with the waste collection from certain type of source, but includes the transport of this waste to the places where the waste management trucks are loaded *(Tchobanoglous, O'Leary, 1994)*. The method of BMSW collection and its organization significantly affect the quality and quantity of the obtained material and have an impact on the technical equipment requirements for collected BMSW treatment during subsequent processing *(Altmann et al., 2010)*. BMSW separate collection can be classified based on several aspects. Separate BMSW collection should be gradually introduced in EU member countries in places with more than 100,000 inhabitants and in places with more than 2,000 inhabitants afterwards. It is not recommended to organize separate collection in city centers and in areas with residential density below ten inhabitants / 1 km^2. And so, based on the population in each Czech municipality, the separate BMSW collection should gradually cover about 75 % of the population of the Czech Republic. However today, especially the small municipalities are involved in separate BMSW collection in the Czech Republic *(Altmann et al., 2010)*.

Methods and material

There is a long term BMSW collection established in the monitored sites. Area types are marked by letters (see abstract).
The individual steps are:

- Data collection about separate BMSW collection in A and B areas in 2006 – 2010.
- Analysis of monitored sites (number of containers and their volumes describing the frequency of collection in the reference period)
- Data collection about material composition of RMSW in all sites A, B, C, D1, D2 in 2006 – 2010
- Evaluation of acquired data

Separate BMSW collection data

Location A – rural area (Březník)
Location B – municipal area (Náměšť nad Oslavou)

There are 627 permanent residents living in 233 family houses (FH) and ten apartment houses (AH) in the village Březník(A). Most houses use gas as the heating energy. Population of Náměšť nad Oslavou is 4977. Municipal development consists of family houses and apartment houses. The collection in both areas is applied as combination of drop-off and pick-up systems.Better-arranged situation for village Březník (A) separate BMSW collection is seen in Tab. 2 and Tab. 3 and fort Náměšť nad Oslavou (B) in Tab. 4 and Tab. 5. In tables are only boundary years – 2006 and 2010.

Tab. 2 Separate BMSW collection data (20 02 01) site A in 2006

Month	Production [t]		Container ammount per month [p.month^{-1}]		Number of rides per month [number of rides.month^{-1}]	
	C_{BMSW} 0,24 m^3	LSC 18 m^3	C_{BMSW} 0,24 m^3	LSC 18 m^3	C_{BMSW} 0,24 m^3	LSC 18 m^3
April	1,36	-	18	-	2	1,36
May	1,79	16,82	18	4	2	1,79
June	3,802	-	18	-	2	3,802
July	2,07	20,06	18	4	2	2,07
August	2,77	19,08	18	4	2	2,77
September	2,18	-	18	-	2	2,18
October	2,12	24,73	18	4	2	2,12
November	1,85	25,24	18	4	2	1,85
December	0,55	-	18	-	1	0,55

**- number of containers (p)/month is a real number of containers available for one collection*
Source: Actual enquiry, ESKO-T s.r.o.

Tab. 3 Separate BMSW collection data (20 02 01) site A in 2010

Month	Production [t]		Container ammount per month [p.month^{-1}]			Number of rides per month [number of rides.month^{-1}]		
	C_{BMSW} 0,12 - 0,24 m^3	LSC 18 m^3	C_{BMSW} 0,24 m^3	C_{BMSW} 0,12 m^3	LSC 18 m^3	C_{BMSW} 0,24 m^3	C_{BMSW} 0,12 m^3	LSC 18 m^3
March	-	3,41	-	-	4	-	-	1
April	2,08	15,45	69	5	4	1	1	1
May	5,18	10,67	69	5	4	2	2	1
June	11,11	23,43	79	5	4	3	3	1
July	5,98	2,43	79	5	4	2	2	1
August	10,44	23,49	84	5	4	2	2	1
September	10,72	-	84	5	-	2	2	-
October	9,01	36,56	84	5	4	3	3	1

**- number of containers (p)/month is a real number of containers available for one collection*
Source: Actual enquiry, ESKO-T s.r.o.

Tab. 4 Separate BMSW data collection (20 02 01) site B in 2006

Month	Production [t]		Container ammount per month [p.month⁻¹]		Number of rides per month [number of rides.month⁻¹]	
	C_{BMSW} 0,24 m^3	LSC 18 m^3	C_{BMSW} 0,24 m^3	LSC 18 m^3	C_{BMSW} 0,24 m^3	LSC 18 m^3
April	1,750	-	80	-	1	-
May	6,290	15,450	80	1	2	3
June	5,778	-	80	-	2	-
July	7,750	4,240	80	1	2	1
August	4,810	4,530	80	1	1	1
September	7,990	8,020	80	1	2	2
October	6,210	4,830	80	1	2	1
November	5,220	2,270	80	1	3	1
December	1,400	-	80	-	2	-

**- number of containers (p)/month is a real number of containers available for one collection*
Source: Actual enquiry, ESKO-T s.r.o.

Tab. 5 Separate BMSW data collection (20 02 01) site B in 2010

Month	Production [t]		Container ammount per month [p.month⁻¹]		Number of rides per month [number of rides.month⁻¹]	
	C_{BMSW} 0,77 m^3	LSC 18 m^3	C_{BMSW} 0,77 m^3	LSC 18 m^3	C_{BMSW} 0,77 m^3	LSC 18 m^3
April	6,826	-	33	-	2	-
May	15,320	-	34	-	4	-
June	20,525	-	34	-	5	-
July	12,333	-	34	-	4	-
August	20,200	4,280	34	1	4	1
September	24,260	7,370	34	1	5	2
October	21,065	9,530	34	2	5	2
November	4,008	-	34	-	1	-
December	6,826	-	33	-	2	-

**- number of containers (p)/month is a real number of containers available for one collection*
Source: Actual enquiry, ESKO-T s.r.o.

RMSW analysis data
Site A, B, C, D1 and D2

The values given in tables 6 – 10 were provided by substance analysis of RMSW on landfill. Analysis were made once a month from May 2006 untill present. For the purpose of evaluating total amount of BMSW in RMSW only data from May to December of each year is used. RMSW was devided in 15 types of waste substances. Only monitored types of BMSW are listed in merged tables.

Tab. 6 Sample and merged data of RMSW analysis of the site A in 2006 and 2010

2006 (A)	May	June	July	.....	2010 (A)	October	November	December
	2,49 [t]*	**2,56 [t]***	**2,48 [t]***	**.....**		**5,08 [t]***	**4,82 [t]***	**5,02 [t]***
Code	**[kg]**	**[kg]**	**[kg]**	**.....**	**Code**	**[kg]**	**[kg]**	**[kg]**
.....								
20 02 01	17,6	7,2	12,8	**.....**	20 02 01	2,2	0,6	3,6
.....								
Total	**84,4**	**103,4**	**94,2**	**.....**	**Total**	**80,6**	**83,6**	**88,4**

* - Total amount of RMSW sample

Tab. 7 Sample and merged data of RMSW analysis of the site B in 2006 and 2010

2006 (B)	May	June	July	.....	2010 (B)	October	November	December
	8,24 [t]*	**8,28 [t]***	**7,26 [t]***	**.....**		**9,08 [t]***	**11,3 [t]***	**5,71 [t]***
Code	**[kg]**	**[kg]**	**[kg]**	**.....**	**Code**	**[kg]**	**[kg]**	**[kg]**
.....								
20 02 01	2,2	12,6	12,8	**.....**	20 02 01	12,2	4,2	7
.....								
Total	**93,0**	**95,6**	**107,8**	**.....**	**Total**	**101,6**	**96,0**	**97,4**

* - Total amount of RMSW sample

Tab. 8 Sample and merged data of RMSW analysis of the site C in 2006 and 2010

2006 (C)	May	June	July	.....	2010 (C)	October	November	December
	1,49 [t]*	1,28 [t]*	1,31 [t]*	.....		1,89 [t]*	1,42 [t]*	2,15 [t]*
Code	[kg]	[kg]	[kg]	.....	Code	[kg]	[kg]	[kg]
.....								
20 02 01	14,0	0,8	0,4	.....	20 02 01	5,8	2,6	0,8
.....								
Total	**81,4**	**59,0**	**72,2**	.....	**Total**	**87,0**	**84,8**	**82,6**

* - Total amount of RMSW sample

Tab. 9 Sample and merged data of RMSW analysis of the site D1 in 2006 and 2010

2006 (D1)	May	June	July	.....	2010 (D1)	October	November	December
	11,16 [t]*	10,67 [t]*	11,83 [t]*	.....		12,26 [t]*	11,40 [t]*	10,52 [t]*
Code	[kg]	[kg]	[kg]	.....	Code	[kg]	[kg]	[kg]
.....								
20 02 01	8,4	6,1	8,0	.....	20 02 01	12,3	4,6	1,2
.....								
Total	**70,8**	**79,1**	**74,7**	.....	**Total**	**104,3**	**92,6**	**99,2**

* - Total amount of RMSW sample

Tab.10 Sample and merged data of RMSW analysis of the site D2 in 2006 and 2010

2006 (D2)	May	June	July	.....	2010 (D2)	October	November	December
	7,96 [t]*	6,98 [t]*	7,26 [t]*	.....		7,55 [t]*	7,15 [t]*	6,45 [t]*
Code	[kg]	[kg]	[kg]	.....	Code	[kg]	[kg]	[kg]
.....								
20 02 01	7,4	20,4	12,8	.....	20 02 01	8,8	5,8	2,2
.....								
Total	**91,0**	**129,4**	**107,8**	.....	**Total**	**98,6**	**99,0**	**87,8**

**- Total amount of RMSW sample*

Methodology of BMSW production formulation

To evaluate separate BMSW collection, methodology based on relation (1) is used, where the total real collected production is shown in tons and years.

Production of BMSW [t.year^{-1}]

$$Q_{BMSW} = \sum_{1,n}^{n=nx} n_{C240} \cdot q_{C240} \cdot {}_r n_{j240} + \sum_{1,n}^{n=nx} n_{C120} \cdot q_{C120} \cdot {}_r n_{j120} + \sum_{1,n}^{n=nx} n_{LSC} \cdot q_{LSC} \cdot {}_r n_{jLSC} + \sum_{1,n}^{n=nx} n_{C770} \cdot q_{C770} \cdot {}_r n_{j770}$$

[t.year^{-1}] (1)

where:

Q_{BMSW}... production of BMSW [t.year^{-1}]

$n_{C240\ (120,\ 770)}$...number of collection containers (240, 120, 770 dm^3) [number]

n_{LSC}..... number of Large-sized containers (LSC) [number]

$q_{C240\ (120,\ 770)}$... amount of BMSW in containers (240, 120, 770 dm^3) [t]

q_{LSC}.....amount of BMSW in Large-sized containers (LSC) [t]

${}_r n_{j240\ (120,\ 770)}$.... number of rides to empty the containers (240, 120, 770 dm^3) [number]

${}_r n_{jLSC}$... number of rides to empty the Large-sized containers (LSC) [number]

Methodology of determining the average value of the RMSW composition in terms of BMSW distribution.

The determination of the amount of BMSW in RMSW is based on the results of composition analysis (Tab. 6 – 10). Average values of the content of individual MSW components are calculated by derived relation (2), where is adjusted formula for arithmetic mean from progressively performed RMSW analyzes in 2006 and 2010. For the considered calculations , the methodology also allow for relation (3) determining the relative amount of BMSW in RMSW.

Average relative content of type of waste in RMSW [%]

$$\overline{p_D} = \frac{\sum_{i=1}^{n}\left(\frac{m_{Di}}{m_{Ci}}\right)}{n} \cdot 100 \qquad [\%] \qquad (2)$$

where:

p_D ... Average relative content of type of waste in RMSW [%]

m_{Di} … content mass of type of waste in one RMSW sample [kg]

m_{Ci} ... one whole RMSW sample mass [kg]

n ... number of performed RMSW analyzes [-]

Relative amount of BMSW in RMSW [%]

$$p_{BMSW} = \frac{m_{BMSW}}{m_{sample}} \quad [\%] \qquad (3)$$

where:

p_{BMSW}... Relative amount of BMSW in RMSW [%]

m_{BMSW}... content mass of type of waste in one RMSW sample [kg]

m_{sample} ... one whole RMSW sample mass [kg]

Also methodology for descriptive statistics was used to process the RMSW composition results – standard deviation and coefficient of variation.

Result and discussion

The overall success evaluation of BMSW collection is shown in Fig. 1–4. It is a graphical representation of percentage of BMSW in RMSW with total amount of produced BMSW and the other RMSW in evaluated periods. Fig. 1–4 show that in all the sites, with the exception of site A, the process of RMSW production and total content of BMSW is steady and it has more likely increasing tendency. Percentage of BMSW in RMSW is also steady. The course is expected at sites C, D1 and D2 because there is not a separate BMSW collection. There has been no decrease of BMSW in RMSW nor of its total amount at site B (municipal area), despite the separate collection. The influence of separate BMSW collection on the total production of RMSW and the distribution of BMSW in RMSW, can be observed only at site A (rural area). There has been not only a significant decrease of percentage of BMSW in RMSW but also a slight decrease in RMSW production. Tab. 11 and Tab. 12 show the value of individual calculations of descriptive statistics (standard deviation and coefficient of variation) relating to average checked values of BMSW in RMSW.

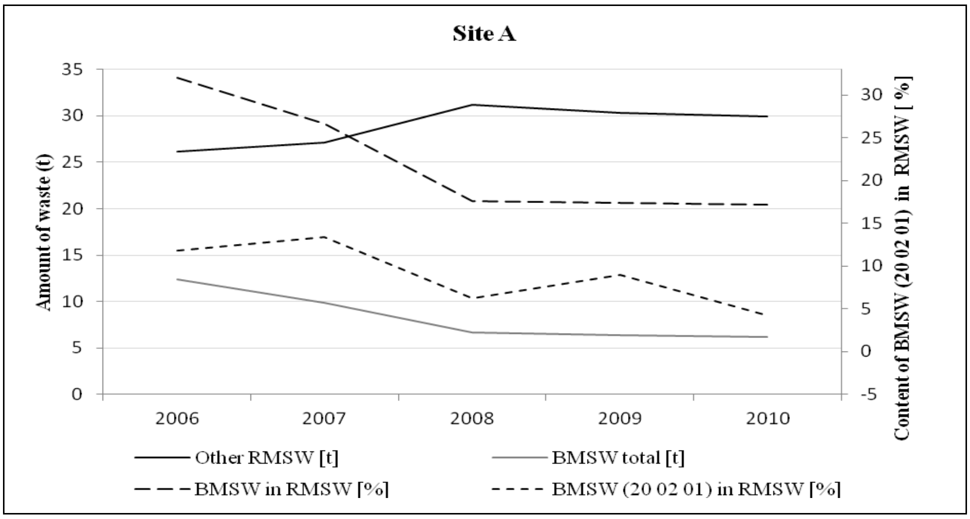

Fig. 1 Graphical representation of total BMSW and RMSW amounts and distribution of BMSW in RMSW (site A)

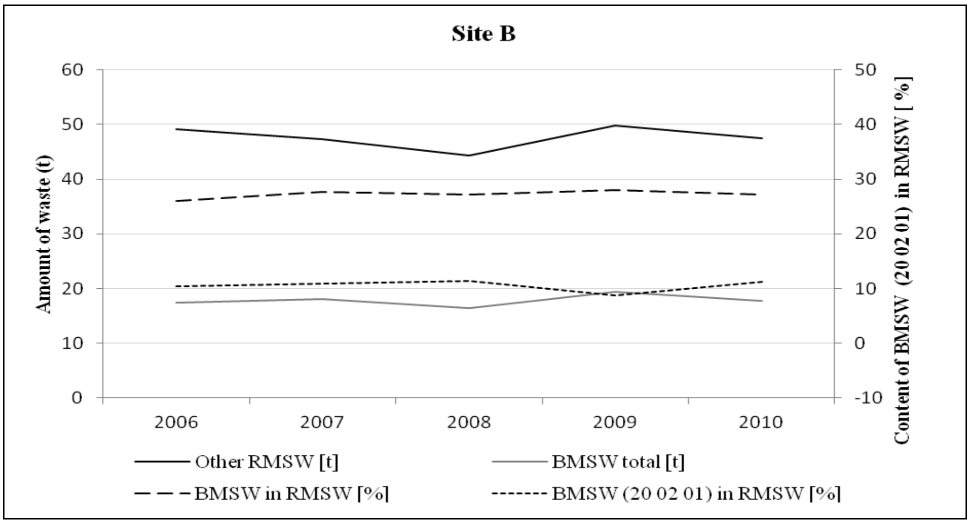

Fig. 2 Graphical representation of total BMSW and RMSW amounts and distribution of BMSW in RMSW (site

B)

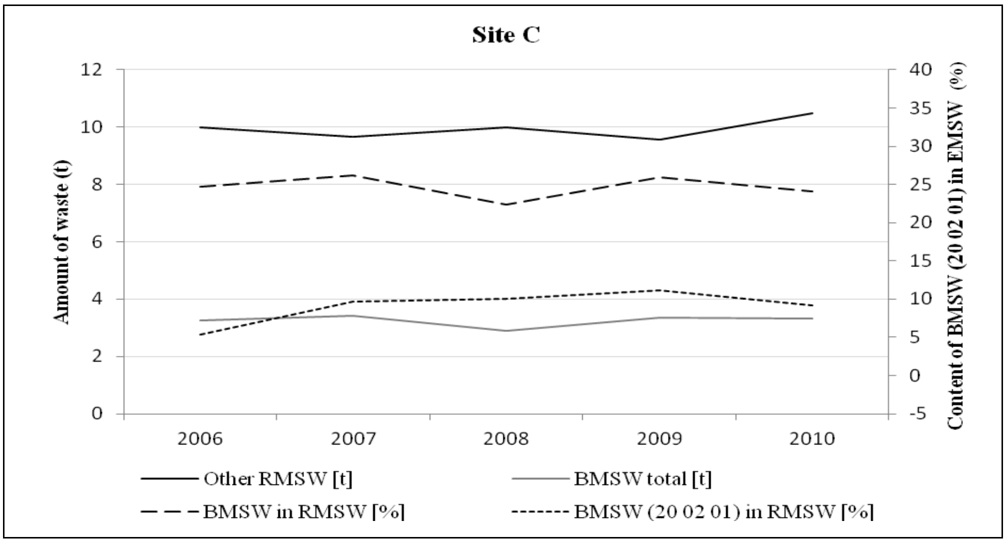

Fig. 3 Graphical representation of total BMSW and RMSW amounts and distribution of BMSW in RMSW (site C)

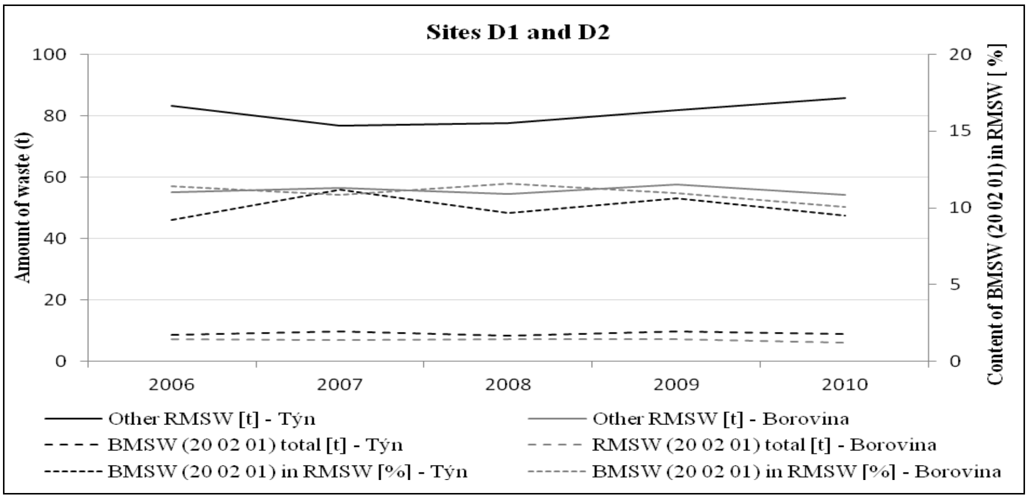

Fig. 4 Graphical representation of total BMSW and RMSW amounts and distribution of BMSW in RMSW (sites D1 and D2)

Tab. 11 Standard deviations (s) and coefficients of variation (V) of the sites A, B, C, D1 and D2 (BMSW values 20 02 01)

Year	A		B		C		D1		D2	
	s [-]	*V* [-]	*s* [-]	*V* [-]	*s* [-]	*V* [-]	*s* [-]	*V* [-]	*s* [-]	*V* [-]
2006	4,84	41,11	6,38	64,69	5,61	104,34	3,77	40,83	6,38	64,69
2007	4,93	36,82	3,81	34,99	4,04	41,98	3,02	27,03	3,48	30,52
2008	2,68	43,15	3,89	34,11	5,40	53,76	3,15	32,52	4,04	34,86
2009	4,12	45,89	4,15	47,72	4,24	38,14	3,51	33,00	4,26	38,89
2010	2,59	60,73	4,43	39,49	5,11	56,09	4,70	49,49	4,52	44,42

Tab. 12 Standard deviations (s) and coefficients of variation (V) of the sites A, B, C, D1 and D2 (BMSW values 20 01 08)

Year	A		B		C		D1		D2	
	s [-]	*V* [-]	*s* [-]	*V* [-]	*s* [-]	*V* [-]	*s* [-]	*V* [-]	*s* [-]	*V* [-]
2006	4,22	20,88	3,86	22,76	10,17	52,75	8,49	47,64	3,86	22,76
2007	1,93	14,54	1,74	10,40	2,61	15,84	2,59	14,99	1,98	11,48
2008	2,74	24,07	1,87	11,88	2,50	20,25	2,50	14,78	1,89	11,71
2009	2,38	28,23	3,29	17,01	2,23	15,00	2,10	11,72	2,04	10,57
2010	2,83	21,89	1,95	12,19	2,36	15,64	2,52	14,94	3,30	17,89

Conclusion

The basic aim of this paper was evaluation of separate BMSW collection at sites A and B (rural and municipal areas with separate BMSW collection). The work was based on assessing the effectiveness of separation in terms of relative BMSW representation in RMSW in monitored years of above mentioned sites and the values of relative BMSW representation in RMSW were available for referential sites C, D1 and D2 (without separate BMSW collection). The results of the article were based on two basic databases.

The first database has been related to information and features which lead to individual values of BMSW mass, number of containers and collection frequency.

The second database has described individual enquiries, which reflected RMSW analyzes at sites A, B, C, D1 and D2 in years 2006 – 2010. Relative BMSW value, indexed 20 02 01 and 20 01 08 in RMSW in given years, was expressed from the arranged data with the help of formulas. Individual calculations were supported from the perspective of descriptive statistics (standard deviation and coefficient of variation) relating to average BMSW values. In this part, fluctuations of BMSW in RMSW depending on the season were observed as assumed at all monitored sites. Whether or not there was separate BMSW collection in the area, had no influence on the fluctuations.

For other criteria, the influence of separate BMSW collection on its representation in RMSW was evident, but with the only positive effect at site A. There was a decrease of BMSW in RMSW approximately from 30 % to 18 % (BMSW 20 02 01 from 12 % to 1,5 %) here in monitored years 2006 – 2010 and these values remain. There was also a slight decrease in total amount of RMSW. This state is achieved by providing a sufficient number of containers and consequently shortening the delivery distance. On the other hand there was no reflection of separate BMSW collection in RMSW composition at site B. Representation of BMSW in RMSW still remains between 25 % and 28 % (BMSW 20 02 01 around 11 %) in monitored period. Stable values were also observed at referential sites C, D1 and D2 without separate BMSW collection. At site B, where separate system of BMSW collection has also been introduced, the collection did not have a positive effect, because there was an increased number of 0,24 dm^3 containers in exchange for a decrease in 0,77 dm^3 container numbers. Thus the delivery distance was extended above the tolerable limit which means higher efficiency of collection system.

The decrease of BMSW in RMSW at site A indicates that the directive on landfills can be followed with well-chosen technological parameters of separate BMSW collection at a given site. Improperly adjusted technological parametres at site B indicate that this site has total monitored results parallel to referential areas without separate collection. It means then, that the municipality has only an increase in costs for BMSW disposal without concrete positive effects of separate BMSW collection. Hence it is necessary to continually analyze the collection data, rigorously evaluate and carry out immediate remedial measures - optimize the biodegradable municipal solid waste technological parameters at given site.

This paper was supported by the GA Faculty of Engineering Czech University of Live in Prague "Analysis of the properties of sorted municipal waste" conducted under the number: 2013:31180 / 1312 / 3121.

Refference

Altmann V., Vaculík P., Mimra M., 2010. Technika pro zpracování odpadu. [Monografie].1st ed., Prague, The Czech Republic, Czech Univerzity of Life Sciences Prague, 120. ISBN 978-80-213-2022-2. (in Czech).

Bilitewsky B., Hardtle G., Marek K., 1997. Waste Management. 1st ed., Berlin, Germany, Springer – Verlag Berlin Heidelberg .

Papageorgiou A., Barton J.R., Karagiaannidis A., 2009. Assessment of the greenhouse effect impact of technologies used for energy recovery from municipal waste: A case for England. Journal of environmental management, *90*: 2999 – 3012.

Tchobanoglous G., O´Leary P.R., 1994. Handbook of Solid Waste Management. 1st ed., New York, USA, McGraw Hill, Inc.

Vehlow J., Bergfeldt B., Visser R., Wilén C., 2007. EuropeanUnion waste management strategy and the importance of biogenic waste. Journal of Material Cycles and Waste Management. 130 - 139.

SYSTEM FOR MONITORING OPERATING PARAMETERS OF VEHICLES

Jozef Chrastina, Ivan Janoško, Tomáš Polonec

Slovak University of Agriculture in Nitra, Tr. A. Hlinku 2, 949 76 Nitra, Slovak Republic,
Phone: +421 37 641 4114, E-mail: ivan.janosko@uniag.sk

Abstract

The paper deals with monitoring of selected technical - exploitative parameters of a municipal vehicle using newly developed recording system in operating conditions. The measuring system consists of a GPS module which records the time, location and travelling speed of the vehicle and two measurement cards scanning fuel consumption, engine RPM, operating temperatures of the fuel and hydro-generator's operation. The system according to the current mode of the vehicle also calculates the gear, approximate amount of CO_2 emissions, immediate and cumulative fuel consumption, etc. Post also describes the functions and characteristics of the detector elements, as well as their involvement and basic mathematical relationships. The proposed open measuring device is suitable for scanning arbitrary physical quantities (from sensors with electrical output) transport technology with immediate calculation of the required functionality and dependencies, which can be operatively created.

Keyword: municipal vehicle, GPS module, CO_2 emissions, fuel

Introduction

Technical-exploitative vehicle parameters characterize the efficiency of using selected vehicle and assess the vehicle construction in the given operating conditions. One of the basic technical and economic characteristics, in assessing the technical-exploitative characteristics, is the fuel economy of the vehicle. This indicator refers not only to the actual fuel consumption, but also indirectly to emissions produced. The electronic equipment of many modern cars provides its users with information on current fuel consumption. This information, however, has largely only informative character and therefore cannot be considered as exact measure of fuel consumption.

The aim of this paper is monitoring technical-exploitative parameters of municipal vehicle during operation. The monitored parameters will be operational deployment and load of the driveline of a vehicle, as well as the amount of fuel consumed in different operating modes using our proprietary recording and information system.

Materials and Methods

The measuring system is designed to inform the operator about the operating mode of the vehicle position, ground speed, current and cumulative fuel consumption, engine speed, vehicle working time, distance traveled, acceleration, current and recommended by the gear etc. Block diagram of the elements is shown in Figure 1. Measurement system consists of GPS device type Holux M 1000C and two measuring cards LabJack U12. Measuring cards sensed fuel consumption, operating temperature of the fuel, engine speed and hydraulic pump operation. Each sensed value is then converted by transmission constants, mathematical processes, graphically displayed and archived

Holux GPS device M100C

For continuous time measurement, position, slope and speed is used a GPS devise type M-1000C made by Holux. This device works at a frequency of 1 Hz while communication with the measuring computer runs the USB bus. The device sends so called Navigation sentences (sentence GPGGA, GPGSA, and GPGSV GPRMC) in format NMEA0183. Given the limited scope of the paper we mention just a sample of the patterns.

Formula (1) expresses the calculation of the cumulative distance traveled.

$$s_{KUMn} = \frac{v_n . T}{3,6} + s_{KUMn-1}, \quad \text{m} \qquad (1)$$

Where: s_{KUMn} – the cumulative total distance, m;
v_n – last known speed, km.h^{-1};
T - time period GPS data recovery, s.

Recorded the accuracy of the receiver:
- Location: normally in the range of <3 m without SA,
- Speed: from 0,1 m.s^{-1},
- Time: 0.1 ms synchronized with GPS time.

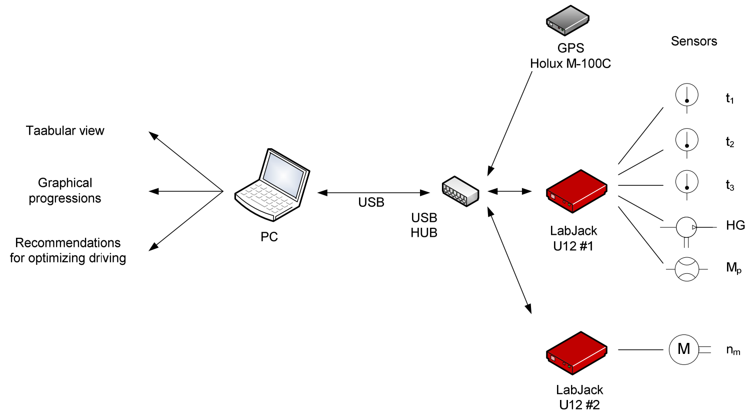

Fig. 1 Schematic diagram of measuring circuit

PC - recording computer; USB HUB - USB bus combiner of a single outlet; t_1 - temperature of oil in the suction branch; t_2 - temperature fuel injected; t_3 - oil temperature in the overflow pipe; HG - state variable hydraulic pump running, M_p - diesel consumption, n_m - engine speed.

Measuring card LabJack U12

It is an external peripheral device using the USB bus. It provides digitization of analog values and receiving digital signals such as operation of the hydraulic pump. As already mentioned, measuring cards to capture fuel consumption and speed, which use a 32 bit digital counter. Temperature sensors sensing the temperature of fuel is added to the differential involvement in analog inputs.

Basic technical specifications of the measuring card:

- Analog Inputs: 8x or 4x to ground differential with 12-bit resolution,
- 20 digital inputs or outputs,
- 1x 1 MHz digital counter with 32 bit resolution.

Flow meter Adast js6 8500.06

Adast Js6 is four-piston fuel flow meter, which is used for the direct measurement of the real fuel consumption. This meter was installed before the feed pump of low pressure fuel system. Output overflow pipe from the injectors was not fed back to the tank, but was connected with a three-way one-direction valve back into the low-pressure circuit for flow meter. This engagement prevents double mechanical loading fuel flow and requires the use of only one flow meter. During calibration measurements we recorded uneven fuel flow. According to Majdan et al. (2009) is the flutter caused by traffic surges from the conveyor pump itself and overcoming pistons friction on the wall in the flow meter. To avoid capture of these spurious effects is by itself treated with structurally flow so called wheel coupling and non-contact magnetic coupling. Temperature effect on fuel is monitored by temperature sensors Pt1000. Pulse volume caused by derived fuel spillage is modulated by flip-flop. The proposed utility program follows these signals that calculates the total cumulative and with help of time periods, instantaneous fuel consumption (2).

$$Q_{os2s} = V_{2s} . k \quad , \qquad dm^3.hod^{-1} \qquad (2)$$

Where:

Q_{os2s} – instantaneous fuel consumption calculated for 2 s, $dm^3.h^{-1}$;

V_{2s} – the amount of fuel spillage indicated flow meter for 2 s, dm^3;

K – conversion constant k = 1.8.

Features of the flow meter:

- Measuring range 1 – 100 $dm^3.h^{-1}$,
- Maximum momentary flow 130 $dm^3.h^{-1}$,
- The minimum deductive value 0,001 dm^3,
- Accuracy: 2% of the flow range 2–130 $dm^3.h^{-1}$, and 3% in the range Q = 1–3 $dm^3.h^{-1}$.

We performed the calibration of the flow meter on the bench for injection pumps and injection unit so that we compared the indicated fuel consumption with the flow meter with real overflow diesel fuel in a graduated cylinder at specified flow rates.

RPM sensor

RPM sensor is an inductive sensor based on the Hall phenomenon. If the flux passes around the sensing head, the sensor changes the magnetic flux and indicates the alternating voltage signal with amplitude U_{max} = 4.8 V. This AC voltage is further processed in the measuring LabJack card. The actual sensor is powered by a voltage of 5V.

Applying the formula to calculate the engine speed (3):

$$n = \frac{i_{imp}}{i_{n1}.T}.60 \quad , \quad min^{-1} \qquad (3)$$

Where:

N – engine speed, min^{-1};
i_{imp} – number of pulses counted;
i_{n1} – number of pulses per one rotation;
T – time period of data recovery, s.

To measure the operating temperatures of diesel fuel (in the suction, discharge and overflow pipes), we used a platinum resistance sensor Pt 1000 and to measure the hydraulic pump running, we used the relay connected to the electromagnetic clutch of hydraulic pump.

Characteristics of municipal vehicle

For the implementation of experimental measurements was chosen the vehicle Mercedes Benz 1828 Atego with the municipal extension with the type designation VarioPress 518 by Faun Eurotec manufacturer GmbH, Germany. Vehicle powertrain consists of diesel water cooled, turbocharged 6 cylinder of 6 374 cm^3 capacity with an output 205 kW at engine speed of 2200 min^{-1} and torque of 1100 Nm at rpm range 1 200 – 1 600 min^{-1}.

Due to the fact that we do not know the detailed map of emission engine OM 906LA III / 4 EURO 3, which is the fitted with, we will assume based on approximate production of CO_2 that 1 liter of diesel fuel produces about 2.8 kg CO_2 emissions. Defined operating modes selected municipal vehicles:

- Transit of the vehicle (speed is greater than zero),
- Vehicle downtime (idle RPM, the speed is zero),
- Combined hence lift and lower containers + pressing (run hydro, low variable rate, increased RPM),
- Emptying (run of the hydro generator, velocity is zero, increased RPM).

Results and Discussion

Meanwhile working gauging, public service vehicle was carrying on standard refuse collection schedule by bulk lorries. Preview harvested routes Dolné and Horné Krškany - corporate operation is shown in Figure 2. Table 1 contains the measured and calculated net time work as well as fuel consumption and CO_2 production in the different patterns of municipal vehicles. To illustrate in the following text there is more detailed processing of only one measuring day. From the measured values of 2 measurement date results that the greatest amount of fuel consumed is accounted for by the passage of vehicle. Average consumption during the passages value was 21.44 dm^3 of diesel fuel while measuring the total time passages was found that the vehicle takes about 2 h and 47 minutes to receive from temporary storage in bulk lorries turf and back, and in this time are also included crossings between each pass collection containers. The smallest share of total fuel consumption accounted for vehicle downtime. During the downtime was consumed 3.28 dm^3 of fuel and downtime lasted about 2 and 11 minutes. By that time are counted each non-working operations. During the combined operation of the vehicle is 6.73 dm^3 of fuel burned, the time of the operation lasted about 1 hour and 27 minutes. It's actually a total work time of the hydraulic system and includes operations such as lifting a container, flip it into the tray, run, and pressing, squeezing and emptying the tank transfer point. Figure 2 shows the percentage of fuel consumption during different modes of operation. Graphic demonstration of the record from the measuring apparatus from 2 measurement days is shown in Figures 3, 4, 5, 6 and 7.

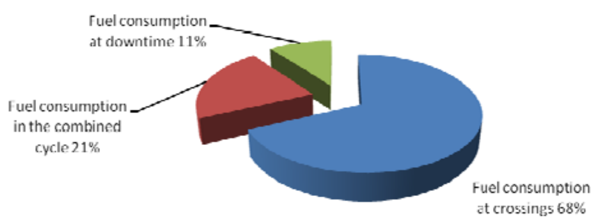

Fig. 2 Structure of working time municipal vehicles MB 1828, 2nd measuring day

Fig. 3 Sample of the harvested route from the 2nd measurement day on site in Dolné and Horné Krškany

Tab. 1 Measured and calculated values of operating parameters

	Parameter	1. day	2. day	3. day	4. day	5. day
Work time	Net when passing, h:mm:ss	1:20:36	2:11:44	2:40:56	2:32:44	2:42:22
	Net downtime, h:mm:ss	1:15:10	2:47:13	2:15:57	3:23:52	3:35:21
	Net combined operation time, h:mm:ss	0:50:07	1:27:55	0:56:33	1:52:15	1:28:54
	Total working time, h:mm:ss	3:25:53	6:26:52	5:53:26	7:48:51	7:46:37
Rou te	The total distance traveled by GPS, km	23.06	55.43	74.79	62.43	48.22
	The total distance traveled by tachometer, km	22.8	50.2	73.2	61.0	48
Fuel Consumpti on	When passing, dm^3	9.841	21.441	24.806	24.345	24.434
	In combined operation, dm^3	3.476	6.73	2.489	8.325	7.543
	Fuel consumption downtimes, dm^3	2.404	3.279	8.531	6.72	2.803
	Total fuel consumption, dm^3	15.721	31.45	35.826	39.39	34.78
Producti on of CO_2	When passing, kg	27.55	60.03	69.46	68.17	68.42
	In combined operation, kg	9.73	18.84	6.97	23.31	21.12
	during downtime, kg	6.73	9.18	23.89	18.82	7.85
	Total production CO_2, kg	44.02	88.06	100.31	110.29	97.38
Holding tanks	1100 l, peace	23	201	193	155	90
	120 l, peace	650	3	2	19	299
	240 l, peace	1	7	1	3	10
	Total containers, peace	674	211	196	177	399
	Mass of waste, t	14.58	11.6	11.09	13.34	18.02

Detailed examination of the values of instantaneous fuel consumption can be observed that during the work stoppage of the vehicle, the value of the instantaneous fuel consumption stabilized at about 1.08 to 1.8 $dm^3.h^{-1}$, the vehicle maintains a constant idle speed $n_m = 630$ min^{-1}. In combined mode of operation the vehicle maintains a constant operating speed in the range n_m = 1200-1220 min^{-1} necessary for running the hydraulic pump. These culminate speed under load hydraulic system. When passing the speed of the vehicle, as well as the travel speed of the vehicle and engaged gear ratio variable, which is reflected in the immediate household vehicle fuel consumption.

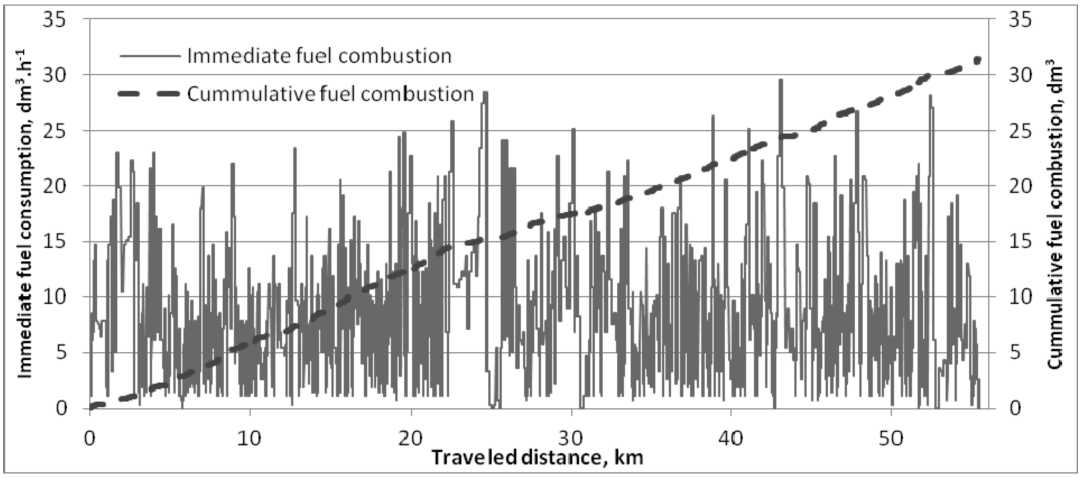

Fig. 4 Development of fuel consumption according to the path of the vehicle MB, 1828, 2nd measuring day

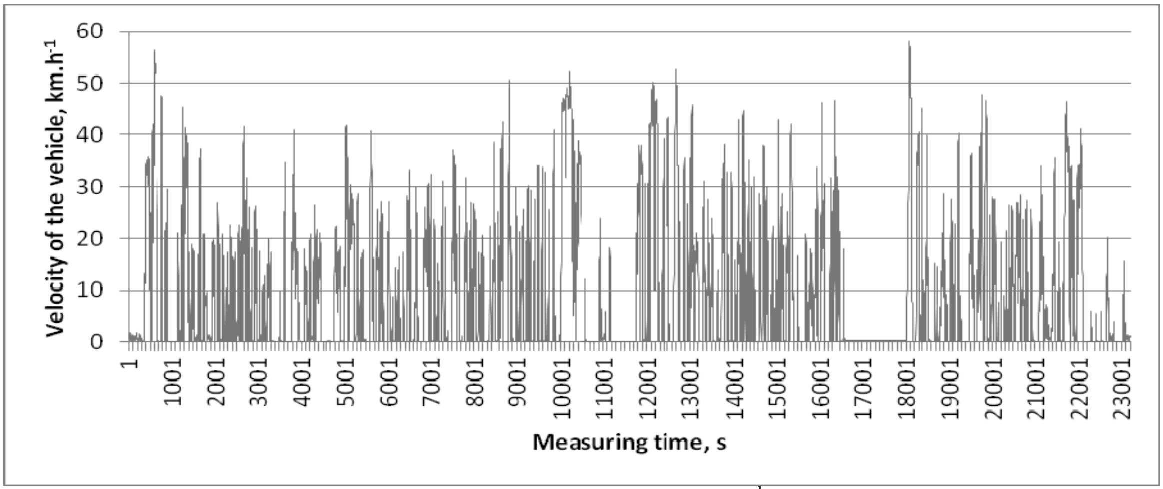

Fig. 5 speed vehicle during service 1828 MB, 2nd measuring day

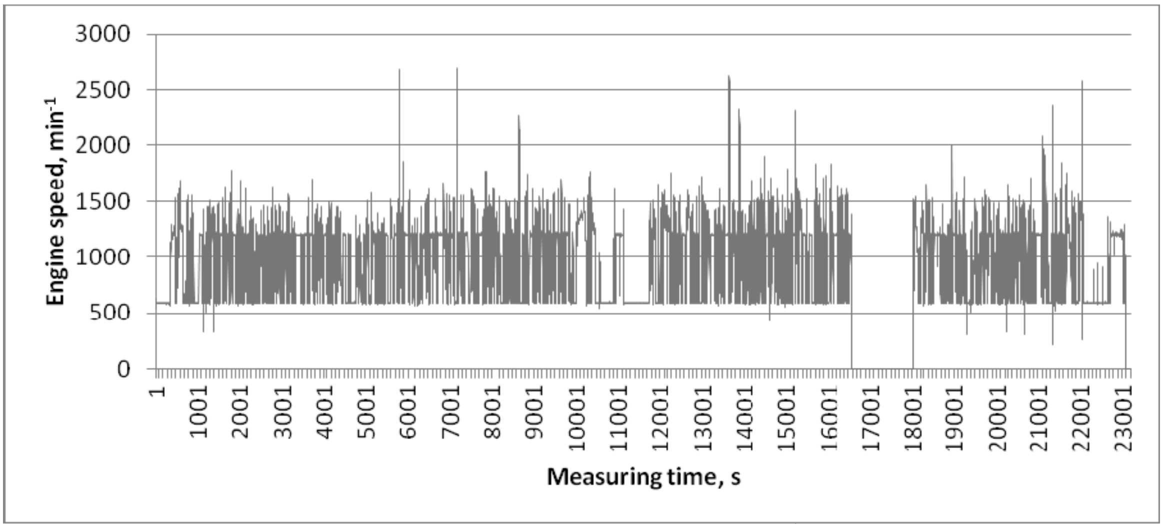

Fig. 6 speed motor vehicle during service 1828 MB, 2nd measuring day

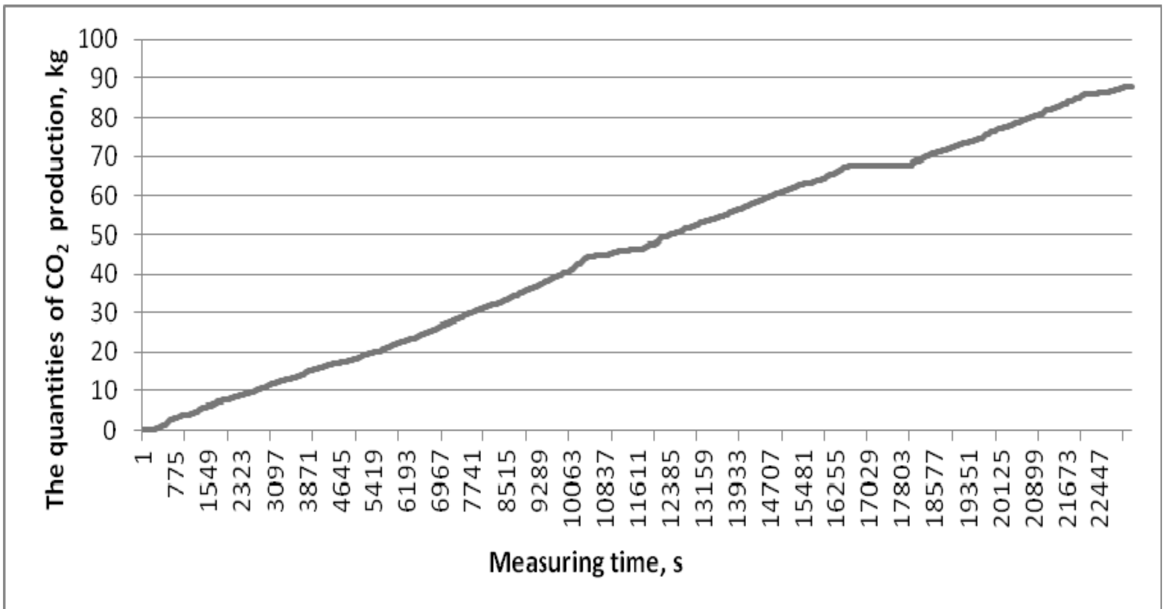

Fig. 7 The approximate amount of CO_2 produced municipal vehicle 2nd measuring day

Conclusion

Optimizing the operation of the vehicle by monitoring the drive, we can achieve a reduction in fuel consumption which is also undoubtedly directly related to the reduction of air pollutants. Kadleček et al. (2009) states that the driver, with the usual qualifications, has about 5 % higher fuel consumption than the minimum achievable. We can only confirm his argument. The motivation of drivers based the quality of work done and fuel savings, we can bring the desired effect reductions in fuel consumption and ultimately effect the reduction of operation cost of the entire vehicle fleet.

Optimizing time use bulk lorries car and fuel consumption by motivating employees to achieve the organization can increase the profitability of its operations, and simultaneously reducing the amount of carbon dioxide producing.

Acknowledgement

This paper was prepared with the support of Ministry of Education of the Slovak Republic, project VEGA No 1/0857/12 ‘Reduction of unfavorable impacts of agricultural and transport machinery on environment’.

Reference

Majdan R., Tkáč Z., Drabant Š., Tulík J., Zigiň P., Jablonický J., Abrahám R., Vozárová V., 2009. <The> damping of pressure shock for the hydrostatic circuit of agricultural tractor. Traktori i pogonske mašine, 14: 22-26.

Kadleček B., Růžička M., Pejša L., 2009a. GPS data processing used for measurement of vehicle´s drive dynamics. Nitra, Advances in automotive engineering, Volume II, Proceedings of scientific papers. Nitra: Slovak University of Agriculture in Nitra.

Kadleček B., Růžička M., Pejša L., 2009b. The dynamic of drive and fuel consumption. Nitra, Advances in automotive engineering, Volume II, Proceedings of scientific papers. Nitra: Slovak University of Agriculture in Nitra.

IMPACT OF LAND CROSSING ON SOIL PHYSICAL PROPERTIES

Jan Chyba*, Milan Kroulík, František Kumhála

Czech University of Life Sciences Prague, 16521 Prague 6 – Suchdol, Czech Republic,
E-mail: chyba@tf.czu.cz

Abstract

During the experiment were monitored values of soil bulk density and water infiltration rate. Appointed values were measured on experimental field where different soil treatment technologies and different compaction levels (inside and outside of the tracks of agricultural machinery) were applied. Different soil treatments were: loosening, loosening which was preceded by deep loosening (DL), ploughing, ploughing which was preceded by deep loosening (DL). Saturated hydraulic conductivity of the soil (K_{fs}) was measured at different soil treatments and compaction levels using the single-ring infiltration method (simplified falling-head method – SFH). The results showed statistically significant differences of K_{fs} between non-compacted and compacted parts of the soil. In the case of loosening technology the range of the results outside of the tracks was from 16.37 to 30.6 mm.h^{-1} and under the same condition of treatment the values was in the range from 4.88 to 8.58 mm.h^{-1} inside of tracks. Differences were observed between the different soil treatments however these differences were not statistically significant. In the case of the soil bulk density measurements were found that soil treatments and soil compaction level influences soil bulk density, but these effects are not statistically significant.

Keywords: soil bulk density, water infiltration rate, controlled traffic, soil treatments, soil compaction

Introduction

Soil compaction is an important factor that influences the water infiltration rate. Soil compaction is mainly caused by crossings of agricultural machinery. This compaction reduces the porosity and increase the density of the soil, thus reducing water infiltration rate in comparison with non-compacted soil (Liebig et al., 1993; Yuxia et al., 2001; Hamza et al., 2005; Raper et al., 2006). Non-compacted soil has 4-5 times higher water infiltration rate than run over soil. Yuxia et al. (2001) showed that the effect of agricultural machinery on soil has a greater influence on water infiltration rate than tillage.

Tillage is another factor influencing water infiltration rate. Kroulík et al. (2007) found that the highest average water infiltration rate was observed in ploughed soil and lowest values when the shallow tillage was used. It was also shown that loosened soil has a significantly higher water capacity in comparison with reduced tillage. For example controlled traffic farming (CTF) has a positive impact on the water retention, crop yields and also has economic benefits (Qingjie et al., 2009).

Soil compaction is dependent on the current state of the soil at the time when the agricultural machinery crossing the field. Soil compaction mainly depends on the soil type and current soil moisture. The soil water content is the most important factor that influences process of soil compaction. In other worlds, an increase of soil moisture causes a reduction of supporting stress ability of soil and thus reducing the permissible pressure on the ground. Knowledge that soil compaction depending on soil moisture can help in planning of field operations. Higher moisture and number of passes increases soil deformation (technogenic compaction), hence it is needed to perform operations according to the current soil moisture and thereby minimize soil compaction (Hamza et al., 2005).

Materials and methods

Measurements of soil bulk density and water infiltration rate were conducted on the school farm plot of Czech university of life sciences in Prague. On this plot is clayey soil type. Climatic area of the plot is slightly warm, slightly dry with mostly mild winter. Experiment area is 6.7 ha and modular width of tool is 4 m. Plot was divided into four parcels, namely: loosening, loosening which was preceded by deep loosening (DL), ploughing, ploughing which was preceded by deep loosening (DL).

Soil bulk density samples were collected at predetermined points. These points were determined inside of the traffic lines and outside of the traffic lines. To determine soil bulk density were collected soil samples to Kopecky´s steel cylinders with volume of 100 cm3. Samples were taken from the center of individual horizons (depth of 0.05 - 0.1 m). Cylinder with soil was dried at 105 ° C to constant weight and weighed after cooling, thus obtaining a dry weight (using the volume 100 cm3 of cylinder, dry weight is equal to bulk density).

The Simplified falling-head method (SFH) was used for assessment of water infiltration rate. The result of SFH method measurement is saturated hydraulic conductivity (Kfs). Kfs was measured using a ring of known diameter A. The ring was inserted into a small depth into the soil (encloses an area for application of water on the soil surface). SFH uses only a small amount of water volume V which is applied to the soil surface. The time ta was measured since pouring water on the soil surface till complete water absorption by soil. Also soil moisture content was measured before and after water application. The saturated hydraulic conductivity (Bagarello et al., 2004) was calculated based on the equation:

$$K_{fs} = \frac{\Delta\theta}{(1-\Delta\theta)t_a}\left[\frac{D}{\Delta\theta} - \frac{D+\frac{1}{\alpha^*}}{(1-\Delta\theta)}\ln\left(1+\frac{(1-\Delta\theta)D}{\Delta\theta\left(D+\frac{1}{\alpha^*}\right)}\right)\right] \quad (1)$$

where *Δ*□ is difference between the saturated water content and initial water content, *D=V/A* is the depth of water in the cylinder at the beginning of measurement and α^* is saturation potential coefficient for K_{fs} (Elrick, Reynolds, 1989).

For this measurement the ring diameter was 0.15 m. For all measurements was used the same volume (0.5 liters) of water. Five replications were conducted for each measurement. For potential coefficient was selected α*=12 m-1.

The statistical analysis was performed using the software STATISTICA Cz 9.1, ANOVA analysis tool.

Results and discussion

Fig. 1 shows relationship between different compaction levels, soil treatment on bulk density at the depth 0.05 - 0.1 m. This relationship shows the effect of soil compaction and soil preparation on the soil bulk density. Highest mean values of soil bulk density were observed on loosened and ploughed soil in the tracks however, the lowest values were observed on loosened and ploughed soil with deep loosening out of the tracks.

Fig. 2 shows relationship between different compaction levels, soil treatment on water infiltration rate on the surface of the soil. Also in this case non-compacted soil had better (higher) values than compacted soil. Aalthough it might seem that the lowest value of soil bulk density will correspond with the highest value of water infiltration rate, it is not so. Water infiltration rate measurements are supplemented by Tukey´s HSD test of homogenous groups (Tab. 1).

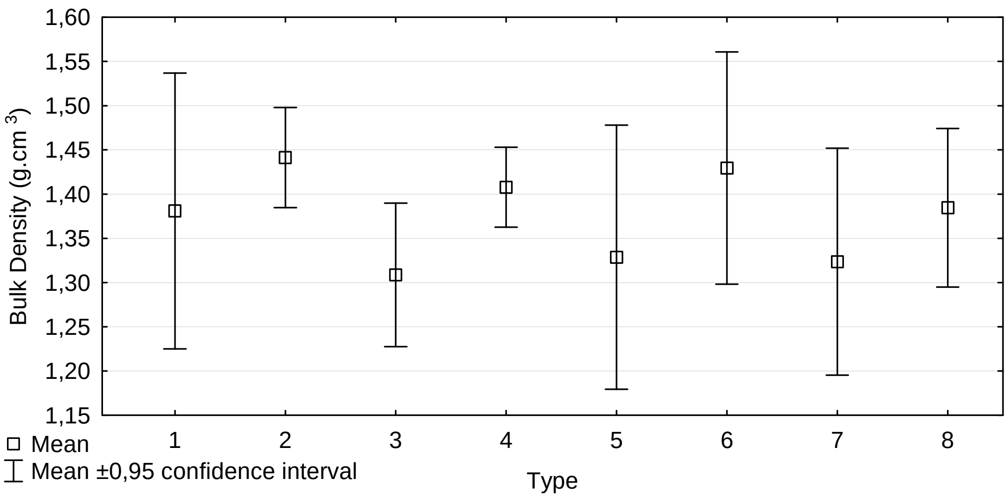

Fig. 1 Relationship between compaction levels, soil treatment and bulk density at the depth 0.05-0.10 m
1-Loosening (out of tracks), 2-Loosening (tracks), 3-Loosening+DL (out of tracks), 4-Loosening+DL (tracks), 5-Ploughing (out of tracks), 6-Ploughing (tracks), 7-Ploughing+DL (out of tracks), 8- Ploughing+DL (tracks), (DL-Deep Loosening)

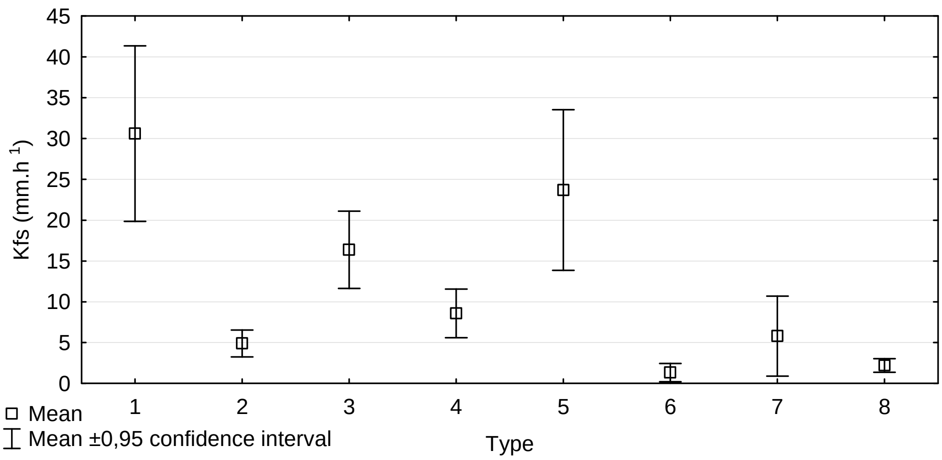

Fig. 2 Relationship between different compaction levels, soil treatment and water infiltration rate 1-Loosening (out of tracks), 2-Loosening (tracks), 3-Loosening+DL (out of tracks), 4-Loosening+DL (tracks), 5-Ploughing (out of tracks), 6-Ploughing (tracks), 7-Ploughing+DL (out of tracks), 8- Ploughing+DL (tracks), (DL-Deep Loosening)

Tab. 1 Tukey´s HSD test of homogenous groups for water infiltration rate

Type	Mean of K_{fs} (mm.h^{-1})	1	2	3	4
Ploughing (tracks)	1,34	****			
Ploughing + DL (tracks)	2,20	****			
Loosening (tracks)	4,89	****	****		
Ploughing + DL (out of tracks)	5,80	****	****		
Loosening + DL (tracks)	8,58	****	****		
Loosening + DL (out of tracks)	16,38		****	****	
Ploughing (out of tracks)	23,69			****	****
Loosening (out of tracks)	30,60				****

The measured values showed that the soil bulk density and water infiltration rate are dependent on the compaction level and on soil treatment. These results agree with conclusion of the literature (Liebig et al., 1993; Yuxia et al., 2001; Kroulík et al., 2007).

Conclusion

Water infiltration rate showed statistically significant differences between different compaction levels. Water infiltration rate were measured in the tracks 2-20 times lower than in the case of measured water infiltration rate out of the tracks. This result agrees with result of Yuxia et al. (2001), who found that compacted soil has 5 times lower infiltration rate than compacted soil. Also relationship between soil compaction levels and water infiltration rate were observed which corresponds to Liebig et al. (1993) and Yuxia et al. (2001).

Fig. 1 and Fig. 2 shows that water infiltration rate is dependent not only on soil compaction (soil bulk density) but also on soil treatment (Kroulík et al., 2007).

Acknowledgment

This paper was processed within the framework of the Research Project of CULS Prague, CIGA No. 20123006.

References

Bagarello V., Iovino M., Elrick D., 2004. A Simplified Falling-Head Technique for Rapid Determination of Field-Saturated Hydraulic Conductivity. Soil Science Society of America Journal, 68: 66-73.

Elrick D.E., Reynolds W.D., Tan K.A., 1989. Hydraulic conductivity measurement in the unsaturated zone using improved well analyses. Ground Water Monitoring & Remedition, 9(3): 184-193.

Hamza M., Anderson W., 2005. Soil compaction in cropping systems. Soil & Tillage Research, 82: 121-145.

Liebig M., Jones A., Mielke L, Doran J., 1993. Controlled Wheel Traffic Effects on Soil Properties in Ridge Tillage. Soil Science Society of America Journal, 57: 1061-1066.

Qingjie W., Hao Ch., Hongwen L., Wenying L., Xiaoyan W., McHugh A., Jin H., Huanwen G., 2009. Controlled traffic farming with no tillage for improved fallow water storage and crop yield on the Chinese Loess Plateau. Soil and Tillage Research, 104(1): 192-197.

Raper R., Kirby J., 2006. Soil compaction: How to do it, undo it, or avoid it, Agricultural Equipment Techonology Conference. - Louisville, Kentucky, USA, 1-14.

Kroulík M., Hůla J., Šindelář R., Illek F., 2007. Water Infiltration into Soil Related. Soil & Water Research, 2(2): 15-24.

Yuxia L.,Tullberg J., Freebairn D., 2001. Traffic and residue cover effects on infiltration. Australian Journal of Soil Research, 39: 239-247.

PROCESSING AND INTERPRETATION OF DATA OBTAINED FROM YIELD MONITORING SYSTEM

Martin Ingeli, Vladimír Rataj, Jana Galambošová*, Miroslav Macák, Lukáš Mesároš

Slovak University of Agriculture in Nitra, Tr. Andreja Hlinku 2, Phone: +420 37 6414344,
*e-mail: jana.galambosova@uniag.sk

Abstract

Implementation of site specific approach at large farm scale has to be based on decision process which uses reliable data on long term field variability. Beside other parameters (soil conductivity, aerial images, etc.) yield maps play an important role in field variability assessment. Their interpretation has to be as accurate as possible. The data obtained by the yield monitoring system are recorded to a memory card and are further processed with help of appropriate software. These are generally "user friendly", however, as the yield monitoring systems have limitations, their output cannot be automatically used. In terms of above mentioned limitations, there may be errors in the data due to the system, the operation conditions or due to the operator.

The aim of this paper is to assess the yield monitoring data obtained for different crops and in different growing conditions of Slovakia in terms of their further interpretation. The attention was paid to occurrence of extreme values. The paper points out the difference in obtained results compared to commercially used data processing software.

The importance of each raw dataset assessment in order to interpret the variability of given field correctly was proved.

Keywords: yield, monitoring, processing

Introduction

Nowadays, decision on implementation of precision agriculture technologies is based on robust data set analyses. First of all the variability of fields has to be assessed. Yield maps play on important role, as their gathering is relatively low cost and easy with detailed output information. Yield monitoring can be defined as a continual recording of actual yield, moisture and sometimes other parameters together with the corresponding geographical position A number of yield monitoring systems have been developed during the last two decades. Majority of the applications is in cereals production. However, yield monitoring systems for non grain crops have been developed recently. These are for sugar beet and potatoes (Ehlert, 2000; Elhert, Algerbo, 2000; De Hann et al., 1999; Kumhala et al., 2009), forrage crops (Kumhala et al., 2007; Kumhala et al., 2010;) hop (Kumhala et al., 2013) or balers (Godwin, 1999; Maquire et al., 2007).

In terms of grain crops monitoring, two groups of yield monitoring sensors are used for cereals yield mapping mainly, based on the principle of the measurement. These are: grain mass sensors, grain volume sensors (Galambošová, Godwin, 2013).

The data obtained by the yield monitoring system are recorded to a memory card and are further processed with help of propriety software. These now are generally "user friendly", however, the data have to be interpreted carefully as the yield monitoring systems have limitations. There may be errors in the data due to the system, the operation conditions or due to the operator. The main source of the errors is:

1. Not using the full width of cutterbar/header while harvesting some strips – then the harvested areas calculated by the program are not correct. This often appears as a strip of very low yield compared to the surrounding area.
2. The lag time. The time for crop to move from the head of the combine to the yield sensor is called "time delay" or "lag time." During the time delay, grain experiences conveying, threshing, separation, and cleaning processes (Arslan, Colvin, 2002). Also, the travel time of individual grain kernels from combine head to grain tank vary substantially (Blackmore, Moore, 1999). This is evident mainly at the headlands.

The GNSS errors, when some of the positions are not recorded or the positioning is wrong. This may happen to small number of readings and can be easily corrected. Blackmore et al. (2003) also pointed out the errors of grain flow through combine, grain losses due to combine and calibration errors. Pierce et al. (1997) reported that a sudden decrease in ground speed would result in a small estimated area at a given time. This might make the instantaneous yield estimation too large as the harvested grain keeps travelling in the combine. Ground speed variations cause fewer problems than sudden changes and/or stoppages but are still important since they influence the lag and crop redistribution issues. The solution was proposed Moore (1999), who suggest to exclude 12 values from the beginning of each pass. The commercial software excludes the zero values and extreme values as well, however, usually only 2 % of the data.

Yield maps play an important role in field variability assessment; their interpretation has to be as accurate as possible. The issues of the processing and interpretation of yield data are described in Griffin (2010). Ping and Dobermann (2005) proposed and validated an approach for processing multi - year yield map, where also the screening process of raw data is described.

Aim of this paper is to assess the yield monitoring data in terms of their further use for rapid evaluation of yield variability in practical crop production conditions. Attention is paid to filtering the data and removing the outliers in necessary extent.

Methodology

Yield data were recorded during seasons 2009 - 2012 with optical sensors mounted on combine harvesters Claas Lexion 480. Data were recorded to PCMC memory card, further processed in standard software AGROCOM AgroMap (© CLAAS Agrosystems, Germany) where the raw data file was exported as *.csv file.

Basic statistics was conducted and histogram of the data was created. The extreme values were displayed in Geographical Information System (GIS) (ArcGIS® software by Esri, United States of America) and the possible causes of error were estimated. The extreme values were removed in two steps:

1. exclusion of "zero values"
2. exclusion of outliers which were outside the user-defined minimum and maximum biological yield limits (Ping, Dobermann, 2005). While each step, the removed data were displayed in GIS, so important variability is not removed.

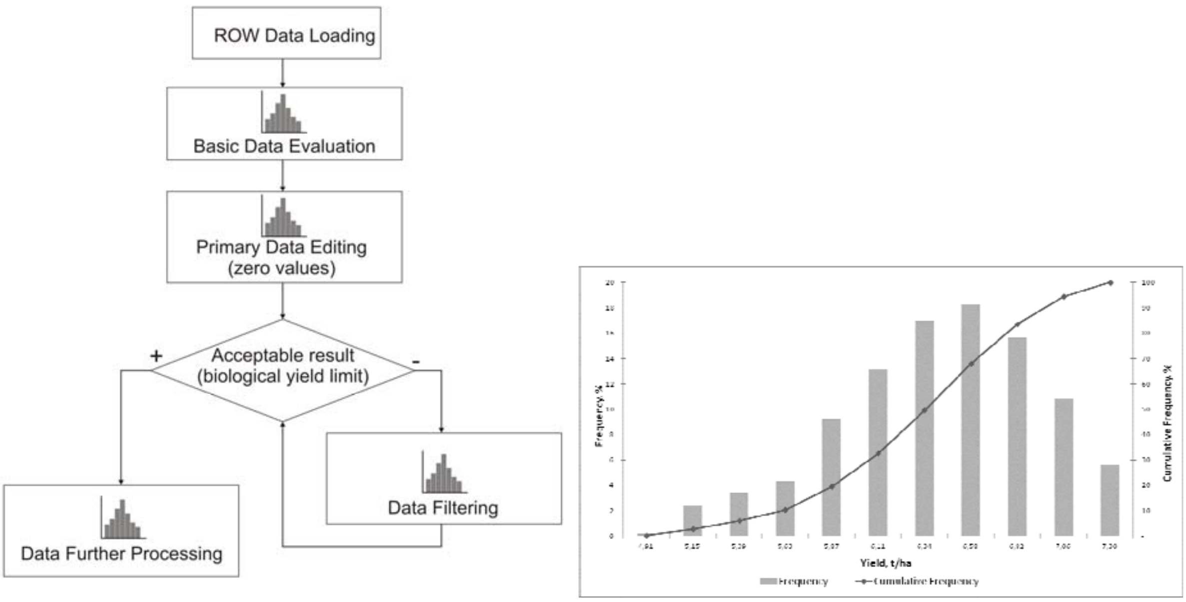

Fig. 1 Flowchart of data processing

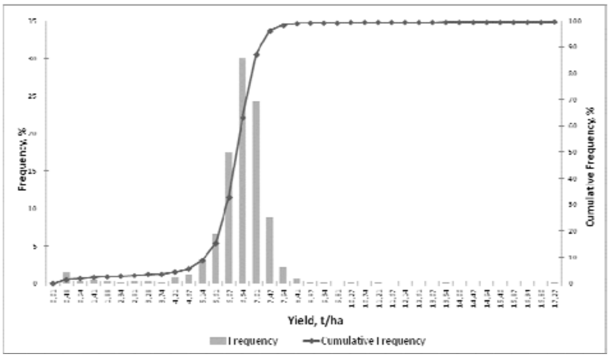

Fig. 2 Example of histograms during the process of data filtering, left- raw data, right - used-defined minimum and maximum

Dataset after each step was analysed with basic descriptive statistics and a histogram. Number and percentage of removed values was calculated.

Results and Discussion

First of all attention yield data from one field and four different seasons were analysed as follows: 2009 - spring barley, 2010 - oil seed rape, 2011 - winter wheat, 2012 - spring barley. In 2009 the average moisture content during the harvest was 11.65 % with variability of 16 %.The system enabled to gather 1465 of data. The average yield was estimated as 5.78 t.ha-1 with coefficient of variability of 33.07 %. The extreme data were plotted in geographical information system to validate their location and to justify their significance in term of further analyses. It was shown that their spatial location is at headlands. Location of extremely high values is random and is probably caused by the error of the system. After these analyses the minimum and maximum biological yield limits was set for 4.04 t.ha-1 as minimum and 8.24 t.ha-1 as maximum. After removing the outliers the average value has changed to 6.33 t.ha-1 and the coefficient decreased to 10.28 %. The extreme values represented 10.44 % of the raw data. In 2010 the same procedure was repeated with the data from oil seed rape harvest. The basic statistics of these data is given in Tab. 1. Average measured moisture content was 10.29 % and coefficient of variation of 5.78 %.When looking at these data, the yield up to 1 t.ha-1 was monitored at headlands at area of 10.5 % what is almost 1.5 ha. When further analysing the data, the extreme values in terms of maximum were targeted as errors of the system, the extremely high value is located in area of low yield. After removing these, the coefficient of variability decreased by 50 % (from 55.49 to 26.06 %). In 2011, the winter wheat was monitored while harvesting the field with 6.08 % average moisture content and coefficient of variability of 41 %. Here, the data do not include zero values; however, the headland effect is visible. Also, the extremely high values were recorded. In total 6.07 % of data was pointed out as outliers. In 2012 the spring barley was monitored at the experimental field. The pre processing data included reduction of 17 % of data. Again, the coefficient of variability decreased from 46.30 to 22.23 %. In general, the reduction of dataset was from 10.44 % to 20.54 %, these were mostly the extreme low values resulting from the lead effect (Fig. 3).

Tab. 1 Statistics of yield data of given field for different crops

Year	**2009**			**2010**			**2011**			**2012**		
Dataset	**a**	**b**	**c**	**a**	**B**	**c**	**a**	**b**	**c**	**a**	**b**	**C**
CV, %	33.07	21.38	10.28	58.4	49.28	24.64	50.11	38.18	17.57	46.3	34.88	22.23
Number of data in dataset	1 465	1 381	1 312	2 172	2 013	1 791	2 745	2 514	2 181	2 634	2 433	2 180
Mean values	5.776	6.127	6.33	1.825	1.969	2.09	6.399	6.986	7.64	5.063	5.481	5.51
Minimum	-	0.01	4.04	-	0.01	1.01	-	0.01	3.5	-	0.01	2.82
Maximum	17.27	17.27	8.24	28.41	28.41	3.56	30	30	10.9	30	30	8.49

a - raw data, b- data with removed zero values, c - user-defined minimum and maximum biological yield limits

Tab. 2 Statistics of winter wheat yield data for selected fields in one season

	Field	1	2	3	4	5
	CV, %	24.54	49.73	48.94	67.82	44.41
	Number of data	2330	1629	2161	3539	5071
	Average value, t.ha^{-1}	7.46	7.06	6.73	3.85	6.26
	Minimum, t.ha^{-1}	1.00	0.00	0.00	0.00	0.00
a	Maximum, t.ha^{-1}	14.84	30.00	30.00	30.00	30.00
	CV, %	24.54	37.32	37.22	55.88	36.99
	Number of data	2330	1488	1985	3181	4815
	Average value. t.ha^{-1}	7.46	7.73	7.32	4.29	6.59
	Minimum, t.ha^{-1}	1.00	0.01	0.01	0.01	0.01
b	Maximum, t.ha^{-1}	14.84	30.00	30.00	30.00	30.00
	CV, %	9.25	9.90	12.60	30.24	15.84
	Number of data	1283	1204	1196	2351	3602
	Average value, t.ha^{-1}	7.06	8.21	7.29	4.68	6.82
	Minimum, t.ha^{-1}	5.20	6.31	4.51	2.30	4.00
c	Maximum, t.ha^{-1}	8.00	10.00	8.50	7.50	8.60

a - raw data, b- data with removed zero values, c - user-defined minimum and maximum biological yield limits

This procedure was applied on yield data from the same combine harvester from different field, harvesting winter wheat in 2011. Statistics of the data is given in Tab. 2. The reduction of data is given in Fig. 4.

The results show that the modification of raw yield data and removing the outliers using the user-defined minimum and maximum yield limits caused that the coefficient of variability decreased by 55 – 80 %. With this data filtering, the data reduction of up to 44 % was achieved. These results were confirmed by other researchers reporting 10 – 50 % of (Sudduth, Drummond, 2007).

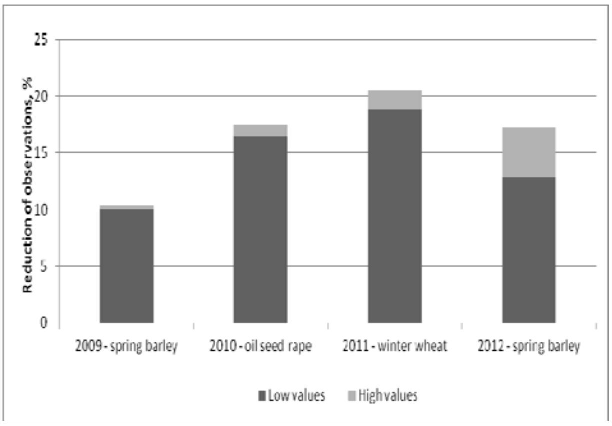

Fig. 3 Reduction of observations after final modification

Conclusion

Based on the above mentioned results it can be concluded that, when using the coefficient of variability as indicator, the yield monitoring data have to be pre-processed before the coefficient is calculated. The extreme values in the range of 12 – 45 % have to be removed. Filtering the data with the user-defined minimum and maximum proved to be appropriate, however, removed observations have to be plotted in map in order not to lose important dat. Considering the above mentioned conclusions. it has to be stressed that each dataset has to be assessed separately in order to interpret the field variability properly.

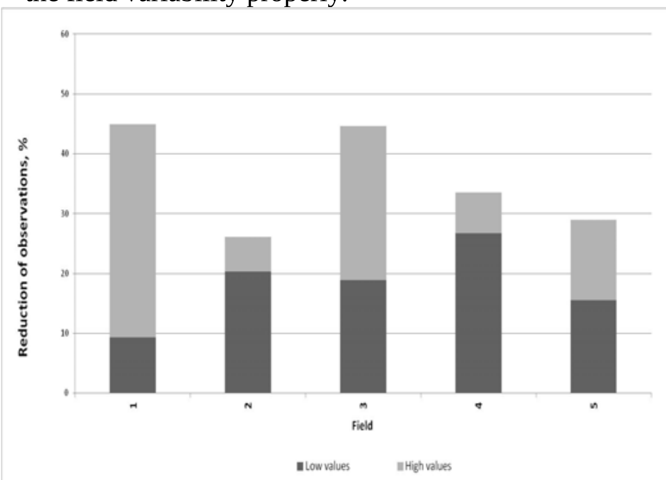

Fig. 4 Reduction of yield data observations after final modification (winter wheat, 2011)

Acknowledgement

This work was done in the frame of a research project funded from the European Union under the title: ITEPAg: Application of information technologies to increase the environmental and economic efficiency of production agro-system. ITMS 26220220014.

Reference

Arslan S., Colvin T., 2002. Grain Yield Mapping: Yield Sensing. Yield Reconstruction. and Errors. In Precision Agriculture, 3: 135–154.

Blackmoore S., 2003. The role of yield maps in Precision Farming. PhD thesis by papers. Cranfield University in Silsoe.

Blackmore B.S., Marshall C.J., 1996. Yield mapping: errors and algorithms. In Precision Agriculture.Proceedings of the 3rd International Conference on Precision Agriculture. edited by P. C. Robert. R. H Rust and W. E. Larson (MN. USA), 403–416.

Blackmore B.S., Moore M., 1999. Remedial correction ofyield map data. In Precision Agriculture, 1: 53–66.

De Hann K.R., Vessey G.T., Holmstrom D.A., MacLeod J.A., Sanderson J.B., Carter M.R., 1999. Relating potato yield to the level of soil degradation using a bulk yield monitor and differential global positioning systems. In Computers and Electronics in Agriculture, 23: 133-143.

Ehlert D., Algerbo P.A., 2000. Yield mapping of potatoes. In Landtechnik, 55: 436-437.

Ehlert D., 2000. Measuring mass flow by bounce plate for yield mapping potatoes. In Precision Agriculture, 2: 119-130.

Galambošová J., Godwin R.J., 2013. Elements of Precision Agriculture. Nitra: SPU v Nitre.

Godwin R.J., Wheeler P.N., O'Dogherty M.J., Watt C.D., Richards T., 1999. Cumulative mass determination for yield maps of non-grain crops. In Computers and Electronics in Agriculture, 23: 85-101.

Griffin T.W., 2010. The spatial analysis of Yield Data. In: Oliver.M.A. Geostatistical Applications for Precision Agriculture. Springer.

Kumhala F., Kavka M., Prošek V., 2013. Capacitive throughput unit applied to stationary hop picking machine. Computers and Electronics in Agriculture, 95: 92–97.

Kumhala F., Kroulík M., Prošek V., 2007. Development and evaluation of forage yield measure sensors in a mowing-conditioning machineComputers and Electronics in Agriculture, 58: 154–163.

Kumhala F., Prošek V., Blahovec J., 2009. Capacitive throughput sensor for sugar beets and potatoes. Biosystems Engineering, 102: 36 – 43.

Kumhala F., Prošek V., Kroulík M., 2010. Capacitive sensor for chopped maize throughput measurement. Computers and Electronics in Agriculture, 70: 234–238.

Maguire S.M., Godwin R.J., O'Dogherty M.J., Blackburn K., 2007. A Dynamic weighing system for determining individual square bale weight during harvesting.

Pierce F.J., Anderson N.W., Colvin T.S., Schueller J. K, Humburg D.S., McLaughlin N.B., 1997. Yield mapping. In Site-Specific Management for Agricultural Systems. Edited by P. C. Robert et al. (ASA.CSSA. and SSSA. Madison. WI), 211–243.

Ping J.L., Dobermann A., 2005. Processing of Yield Map Data. Precision Agriculture, 6: 293-212.

Kenneth A., Sudduth K.A., Drummond S.T., 2007. Yield Editor.Agronomy Journal, 99(6): 1471-1482.

AZIMUTHAL OPTIMIZATION OF STATIONARY SOLAR PANELS WITH RESPECT TO THE DISPERSED SUNLIGHT IN MIDDLE BOHEMIA REGION

Přemysl Jedlička, Jiří Zeman

Czech University of Life Sciences, 16251 Prague 6 – Suchdol, Czech Republic
email: jedlickap@tf.czu.cz, zeman@hydronet.cz

Abstract

When measuring the maximal energy output from solar panels over the year, we obtain, as optimal, the orientation to the south since the yield from the direct sun outshines the influence of the dispersed light form other directions. But there can be situations, like e.g. insular systems, where we do not look for the maximal output during sunny days since in these cases the storage batteries simply recharge and we cannot benefit of the additional power (Kacira et al., 2004; Bojić et al., 2012; Chen, Bai, 2011; Chang, 2009). We want rather to glean the sunlight during the days when we hardly recognize where the sun is since in these days we also want to power the instruments. Using the data from the direction intensity sensors installed on the roof of the CULS rectorate we figured out that over four years of observation during different seasons the maximum of the noon energy does not come from the south but from a direction 11 degrees to the west. Although it is currently, from the energetic point of view, a speculation, we would like to present the results of our several-year data collection about the direction of the emission, in hope that someone would verify the discovery directly on solar panels.

Keywords: solar panel, azimuthal optimalization, diffuse radiation

Introduction

The main source of the usable energy in solar panels is the direct sunlight. The direct sunlight is visible up to 1500 hours per year in middle Bohemia. The number of cloudless days is as many up to 50. These data do not correspond to the data we measured but they are not the object of our analysis. Nevertheless, let us recall that a cloudless day is such a day when the average cloud cover does not reach two tenths and vice versa. The number of days when the sun is not directly visible at all is more than 90. Consider an insular system where we need to produce a sufficient amount of energy every day to cover the energy consumption of a given electric device with a constant input power, e.g. an on-line camera or a creek surface measurement tool. In such a situation we need to mine the solar energy as regularly as possible. We do not care of the maximal integral over a year but we need the least daily standard deviation. Is the southern direction the optimal one as well? The arguments given before make clear that we have to consider the analysis of the dispersed radiation. Let us forget, for a while, the spectral sensitivity of the panels and the decreasing efficiency of the solar systems with increasing temperature. We have no data for the discussion about the near infra-red radiation intensity and, since the point of our efforts is to get over the winter season, we can postpone the care about overheating of the system. And we shall narrow the problem even a little bit more: we ask where to point the solar system to the sky, e.g. at the moment of the sun peak, so that the intensity of the sunlight is maximal in the specific season.

This task reduces, after a short consideration, into checking the axis symmetry coming from the average visible sunlight in an azimuthal direction and verifying the horizontal maximum given by the sun position. Or, we ask for the direction with most light coming from during some season and whether, except of this direction, the same amount of the dispersed light comes from the west as from the east.

Material and method

In 2007, we started to measure the dispersed light on the CULS rectorate roof with GPS coordinates 50°7'47.941"N, 14°22'24.202"E. Since this year we detect the intensity of the dispersed radiation coming from the sky and its spectral layout in the visible spectrum. The shot interval is 6 minutes. The device construction was described in (Sedláček et al., 2009). A picture scheme with angles needed for the computation is on Fig. 1. It consists of a camera and a mirror hemisphere. The angle θ is the altitude of the incoming beam which eventually comes into the camera under the angle α. The beam is reflected under the angle 2β. The axis of the impact intersects the axis of the device in the angle γ. The sphere has radius r and the lens of the camera is in the height h above the ground.

In order to correctly evaluate the intensity coming from a particular direction, we need to know the correspondence between the spots on the mirror and the celestial coordinates. We shall further on derive the formula:

$$\gamma = \arcsin(\cos\alpha \cdot (q \sin\alpha - (1-q^2\cos^2\alpha)^{1/2})) \quad (1)$$

where:

x is the horizontal coordinate of the beam impact spot on the sphere and $q=h/r$. Moreover, we shall find $\theta = 90° - \alpha - 2 \cdot \gamma$.

We need the inverse function which, however, probably impossible to compute explicitly. Hence we have to invert the formula (1) numerically.

We assembled four average shots of the noon sky (Fig. 2). Each of them was observed during one year season. The noon was considered to be the time UTC+1h, i.e. CET. Using the formula (1) we transformed the picture into a contribution of a given azimuth by integration over the altitude. The noon was considered because of two reasons: the yield is supposed to be maximal and the sun is always above the horizon. Nevertheless, the method allows to choose arbitrary hour. Each particular season was averaged between 2007 and 2011, always 200 randomly chosen images. For computing the intensity, we chose the 12-bits value of each color, corrected by the exposure time and aperture ratio. Every colour was considered separately as one can see on the graphs of Fig. 3.

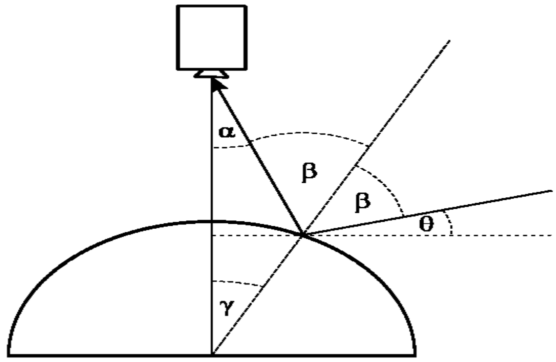

***Fig. 1** Scheme of the device for measuring the dispersed light*

Deriving the mathematical formula

We derive here the formulae for the computation of elevations. First we remark that the angles left of the impact axes are 90°−γ, 90°−α and β. They sum in 180° and therefore

$$180°-\gamma-\alpha+\beta=180° \quad \text{which means} \quad \beta=\alpha+\gamma. \quad (2)$$

The angles above the horizontal axis are 90°− α, β, β and θ and they sum again in 180°, giving

$$90°-\alpha+2\beta+\theta=180° \quad \text{and therefore} \quad 2\beta+\theta-\alpha=90°. \quad (3)$$

Substituting (2) into (3) we get

$$2\alpha+2\gamma+\theta-\alpha=90° \quad \text{and hence} \quad \theta=90°-2\gamma-\alpha. \quad (4)$$

In order to get the relation between α and θ, we need to express γ in terms of α. This is not going to be that easy and we have to use the algebraic geometry. Let us choose [0,0] to be the coordinates of the center of the sphere and $[x,y]$ the coordinates of the beam impact spot. The coordinates lie on a circle and hence they satisfy the equation

$$x^2 + y^2 = r^2. \quad (5)$$

Moreover, the spot lies on the line connecting it with the camera lens and the line has the equation

$$y = k\,x + h \quad (6)$$

where the slope $k = -\text{tg}\,\alpha$. Substituting y from (6) into (5) we get

$$x^2 + (k\,x + h)^2 = r^2$$

$$x^2 + k^2x^2 + 2kxh + h^2 = r^2$$

$$(1+k^2)\,x^2 + 2khx + h^2 - r^2 = 0$$

To solve the quadratic equation, we compute the discriminant

$$D = 4k^2h^2 - 4 \cdot (1+k^2) \cdot (h^2 - r^2) = 4k^2h^2 - 4h^2 + 4r^2 - 4k^2h^2 + 4k^2r^2 = 4r^2 \cdot (1 + k^2 - h^2/r^2).$$

It is useful to write $q=h/r$. With this we obtain

$$D = 4r^2 \cdot (1 + k^2 - q^2) \qquad \text{and} \qquad D^{1/2} = 2r \cdot (1 + k^2 - q^2)^{1/2}.$$

The quadratic equation has two solutions since the theoretical line intersects the theoretical circle in two points. In reality, only the smaller solution is valid.

Therefore $x = \dfrac{-2kh - 2r\cdot\sqrt{1+k^2-q^2}}{2\cdot(1+k^2)} = -r\cdot\dfrac{kq+\sqrt{1+k^2-q^2}}{1+k^2}$. Now we recall that $k = -\text{tg}\ \alpha$ and hence $1 + k^2 = \cos^{-2}\alpha$. Thus $x = -r\cdot\dfrac{-\dfrac{\sin\alpha}{\cos\alpha}\cdot q+\sqrt{\cos^{-2}\alpha-q^2}}{\cos^{-2}\alpha} = r\cdot\cos\alpha\cdot\left(\sin\alpha\cdot q-\sqrt{1-q^2\cos^2\alpha}\right)\cdot$

Finally, we use $\sin\gamma = x/r$ to obtain formula (1).

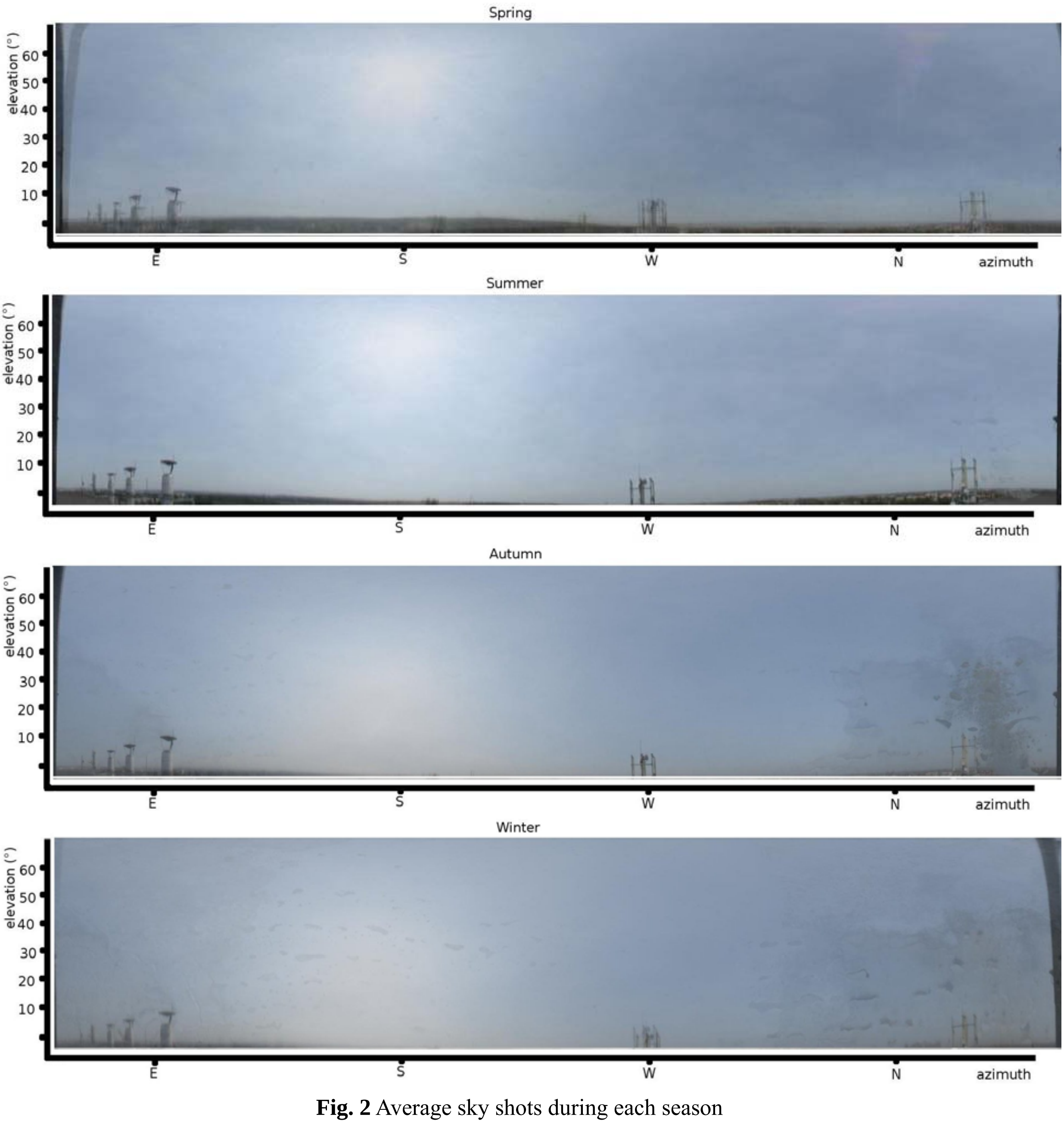

Fig. 2 Average sky shots during each season

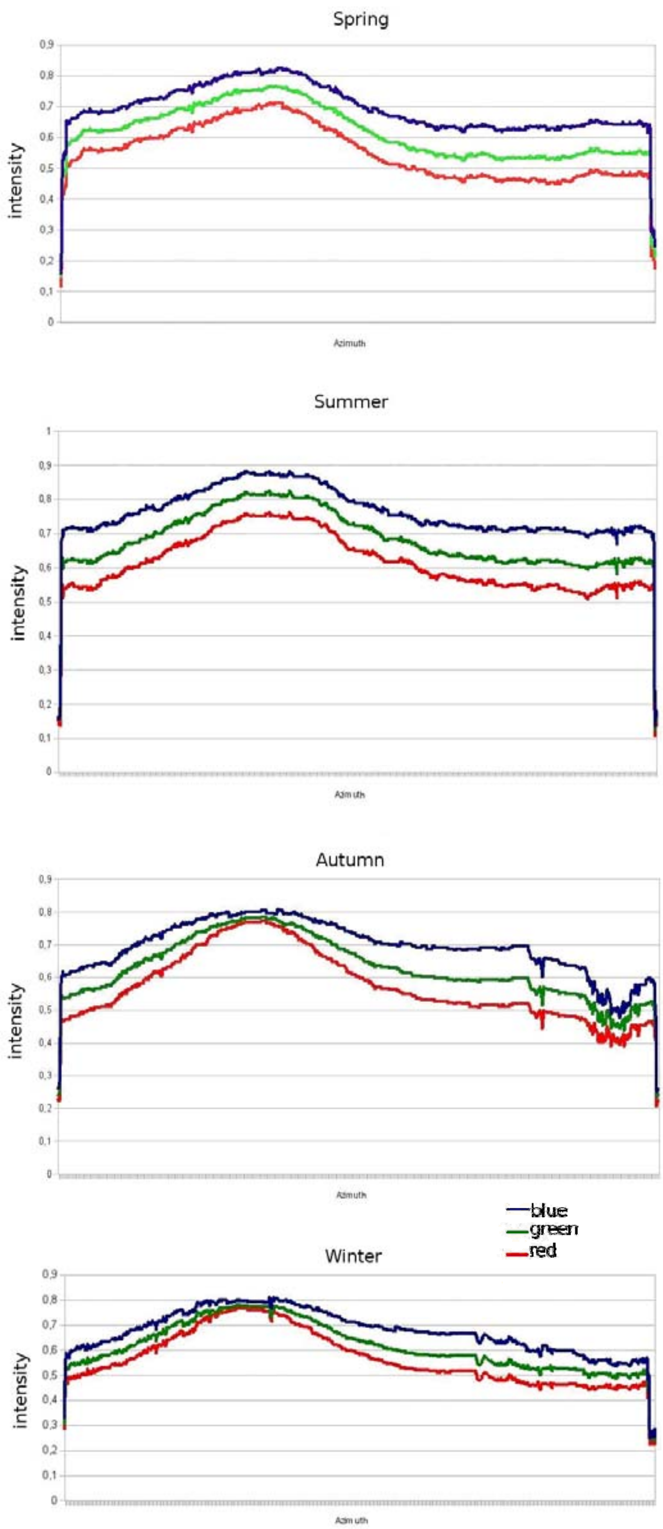

Fig. 3 Intesities of basic colours during each season

Results and discussion

Let us see first the averaged noon images of the year seasons on Fig. 2 and the graphs integrating the contribution of the azimuths on Fig. 3. The integral graphs show several fluctuations caused by growing number of telephone operators antennae. Another cause of the fluctuations is a progressive deteriorating of the mirror. Unfortunately, financial reasons prevent us to replace the mirror by a new one. We see also that the intensity is not symmetrical around the south – the intensity median is about 2° in winter, 5° in spring and in autumn and 7° in summer to the west.

Although it is a middle noon symmetry evaluation only, we consider the result interesting; it might be worth checking up on solar panels too. Moreover, we managed to do such measurements and their evaluations and hence the final goal, to map the dispersed sunlight, is a bit closer again. Although it is a middle noon symmetry evaluation only, we consider the result interesting; it might be worth checking up on solar panels too. Moreover, we managed to do such measurements and their evaluations and hence the final goal, to map the dispersed sunlight, is a bit closer again.

Conclusion

We succeeded in finding an experimental method enabling to study the intensities of all colour components coming from the entire sky, determining the direction where the light comes from. We managed to find a transformation of the image into a rectangle of detected azimuths and elevations. As an example, we computed average azimuthal and colour decomposition if the light intensities coming from the sky in different seasons. We show that the intensity is not symmetrical around the south direction but it is less steep to the west. This fact can have a consequence in some practical tasks considering the optimal directing of solar panels.

Reference

Kacira M., Simsek M., Babur Y., Demirkol D., 2004. Determining optimum tilt angles and orientations of photovoltaic panels in Sanliurfa, Turkey, Renewable Energy, 29 (8): 1265–1275. ISSN 0960-1481.

Bojić M., Bigot D., Miranville F., Parvedy-Patou A., Radulović J., 2012. Optimizing performances of photovoltaics in Reunion Island—tilt angle, Progress in Photovoltaics: Research and Applications, 20 (8): 923–935. ISSN: 1099-159X

Chen Z., Bai L., 2011. Design of dual-axis tracking control of photovoltaic based on position detection, School of Automation, Beijing Information Science and Technology University,Beijing 100192,China. ISSN 1867-5662

Chang T.P., 2009. The gain of single-axis tracked panel according to extraterrestrial radiation, Applied Energy, 86 (7–8): 1074–1079. ISSN 0306-2619

Sedláček J., Zeman J., Jedlička P., 2009. Apparatus for analysis of scattered solar radiation (utility model), Office of Industrial Property 20282. 26th November.

OPTIONS FOR REDUCING ENERGY DEMAND IN HEATING TECHNOLOGICAL PRODUCTION PLANTS

Tomáš Jehlička, Jan Sander*

Czech University of Life Sciences Prague, 165 21 Prague 6 – Suchdol, Czech Republic, Phone: +420 224383156, Fax: +4202-34381828, E-mail: sander@tf.czu.cz

Abstract

The present work deals with electromagnetic wave motion of high-frequency emitters used in industrial applications in the technological equipment of production constructions. Electromagnetic wave motion within 1 – 1000nm has been described as infrared radiation or heat radiation. It is the most efficient transfer of heat energy within a wide range of applications from primary agricultural production premises to processing industry or specific (health care) applications. Gas or electric construction systems, according to the source of the energy thus used, are the sources of electromagnetic wave motion of the given wave lengths. Electric systems prevail in industrial applications. Electric systems, according to their technical construction, are emitters with heated filaments (high-temperature systems with operation wave length around 1000nm) or emitters with planary carbon elements (low-temperature with operation wave length around 5000nm). Various operation properties stem from the construction difference of the two basic types of emitters. It is, for instance, the efficiency of the conversion of electric energy into radiation energy, the speed of reaching the efficient operation output, or the possibility of the output regulation related to the distance of the irradiated area or space.

Setting the basic operation parameters of the two construction emitter types has been subject to operation measurements. Experimental measurements were carried out on three standard-production emitters (on a high-temperature emitter with heated filaments at maximum power input of 1800W with a possibility of input regulation, and on two low-temperature planary carbon emitters with non-regulated input at 480W and 600W). The measured parameters were as follows: the efficiency of the radiated energy conversion into heat energy related to operation conditions of the emitter setting (e.g. the distance and the angle of the wave motion incidence, properties of the irradiated material), the speed of reaching the operation output and the efficiency of the conversion of electric energy into radiation energy and the following possibility of the emitter output regulation.

Evaluation of the emitters properties thus measured has proven that in the high-temperature emitters the intensity of irradiated energy at a certain distance from the source of radiation is not linearly dependent upon the emitter input, which means that reducing the emmiter input does not result at a certain distance in a considerable reduction of the conversion efficiency of the radiated energy into heat energy. The high-temperature emitters are characteristic of a relatively quick response to the input change. The low-temperature emitters have been proven to need a long time to reach the required operation output which has a considerable effect upon the output regulation. These results indicate basic options for the emitters´ output regulation and the possibilities of their application in technological production plants.

Keywords: heat radiation emitters, IR heating, regulation of heating, temperature, electric power

Introduction

Electric high-frequency heat radiation emitters have been increasingly applied in industrial and civil applications as heating systems. They provide a considerable advantage compared with conventional heating systems. It is, for instance, lower purchase costs, possibility of installation without a need of building heat-distributing systems (heat-carrying medium), or high efficiency of the electric energy conversion into the energy of heat radiation (Electric Infrared Heating Manual, 1998). A relatively high electric power input of the emitters is a disadvantage, mainly within the range of 500-2000W, and thereby a relatively high energy demand in operation (Barker, 2002).

The possibility of reducing the energy costs cannot be solved by increasing the efficiency of the transformation of electric energy into the energy of heat radiation, which can reach up to 98% in existing constructions, but by controlling the emmiter operation. With common operations, the emitters operation runs according to project calculation with no further control of their output. Possibilities of the emitters control depend on their type, construction (technical version), and a complex of concrete operation factors (Roth et al., 2007). It is expected that the technical version limits the possibility of the emitters operation control and thus even the possibility of reducing the total energy demand of their operation.

The technical version means a division of the emitters into high-frequency emitters (with heated filament and with the wave length around 1000nm), and low-temperature emitters (with flat carbon elements and wave length around 5000nm) (Dudkiewicz, Jezowiecki, 2009). The objective of the operation studies was to determine the primary operation parameters of both construction types of electric emitters and their suitability for output regulation. The data thus obtained can be used to determine the possibilities and efficiency of operation control of the two technical versions, i.e. emitters with heated filament and flat emitters. Parameters limiting the emitters´ operation were as follows: the time of the emitters´approach to stabilized temperature and the dependence of the irradiated area upon the distance from the emitters at the emitters´ set electric power input. Measurements were made using commonly available emitters characteristic of the given categories.

Material and method

The present measurements were aimed at the possibility of regulating the output of electric emitters´ infrared radiation. The measurements were made in a testing hall with the ceiling at 8m. The surrounding temperature was maintained at ca 20 °C. With all types of emitters the measurements were made in a vertical position with a fixed setting on a support construction using holders which were part of the product. A dull black area of 0.3 x 0.3 m placed in front of the white background was used for the measurement of the heat irradiation. The values thus measured were recorded using a contactless temperature measure TESTO 845. The emitters´electric energy input defined by the producer was checked using the calculation of the measured values of the electric current and voltage. The measurements were made using a laboratory ampere-meter and voltmeter.

Measuring the approach time to stabilized temperature

The high-temperature emitter with carbon infrared filament with nickel – VEITO CH 1800RW (Thermowell), 4 adjustable outputs (900W, 1200W, 1500W, 1800W), size 80x170x820 mm, weight 2.1 kg, coverage IP44, voltage 230V, frequency 50 hz.

The low-temperature emitter ITS 500/A. The heating element is based on carbon, a non-metal material - carbon plate. Input 480 W, voltage 230 V, frequency 50 Hz, surface temperature 90-105 °C, size 608 x 948 x 38 mm, weight 11.5 kg.

The low-temperature emitter IT-AG 600 (Thermowell). The panel is based on a carbon thermocouple covered with silicon grains on their surface with white surface treatment. Input 600 W, voltage 230 V, frequency 50 Hz, size 1200 x 600 x 50 mm, wight 14 kg.

The temperature in the middle of the emitter area was measured at two-minute intervals until the time of stabilized temperature. The measurements were made at perpendicular level and at constant distance using a contactless temperature measure TESTO 845.

Measurement of irradiation

<u>A high-temperature editor VEITO CH 1800RW</u>

A probe of 0.3 x 0.3 m was moved on a perpendicular level by 1 m from the maximum effective distance towards the emitter as declared by the producer. The temperatures were measured in the middle of the probe in front of the white background. Identical measurements were made at regulated input of 900, 1200, 1500 and 1800 W.

<u>Low-temperature editors ITS 500/A, IT-AG 600</u>

A probe of 0.3 x 0.3 m was moved on a perpendicular level by 0.5 m from the emitter. The temperatures were measured in the middle of the probe in front of the white background. Identical measurements were made on both low-temp. panels at 400 and 600 W.

Results thus measured and given in tables and diagrams were set as mean values each time from three repeated measurements at fully identical conditions.

Results and discussion

Tab. 1 shows mean values of operation temperatures of the low-temperature flat emitters ITS 500/A and IT-AG 600 measured in two-minute intervals. Fig. 1 shows values recorded in Table 1 in the form of a graph and a trend-connecting line. The curves thus obtained show the course of the emitters´ warming up to operation temperatures. The mutual shift of the two curves results from the difference in the operation outputs of the emitters (ITS 500A – 480W, IT-AG 600 – 600W). The time behaviour of the emitters´ temperatures is similar due to the same construction version. A characteristic feature is the fact that the operation temperature increase is very gentle and the optimum is reached after 15 minutes of operation. The optimum operation temperature in these emitters is between 70 and 80 °C.

The high-temperature emitters with heated filament, unlike the low-temperature flat emitter constructions, reach the operation temperature quickly, which is about 2600 °C (Borovec, 2012). Operation temperatures are reached within 60s of operation start. This fact has been verified experimentally for the high-temperature emitter with heated filament CH 1800RW. The values obtained experimentally and their plotting is not given due to the evident difference in comparison with low-temperature flat emitters.

Comparing the approach time up to the stabilized operation temperature for both construction types it is evident that the low-temperature flat emitters cannot respond quickly to a gradual energy input change and to the required operation temperature increase. That is why the low-temperature emitters are not suited for short-time operation nor for operations requiring a short-time operation temperature increase. On the other hand, high-temperature emitters with heated filament and with a possibility of a speedy reach of operation temperature can respond swiftly to the change of the surrounding operation conditions (surrounding temperature, persons present in the surroundings, etc.). This property makes it possible to regulate the operation, such as by energy input regulation or by controlled switch.

Tab. 1 Mean values of the emitters´ approach time to operation stabilized temperature (emitter ITS 500/A and IT-AG 600)

emitter ITS 500/A		**emitter IT-AG 600**	
time [min]	**temperature of the emitter [^{o}C]**	**time [min]**	**temperature of the emitter [^{o}C]**
0	21,5	0	21
2	36	2	27
4	48,5	4	35
6	52	6	39
8	59	8	47
10	63,1	10	49,3
12	68,5	12	52,7
14	70,3	14	66,7
16	72,6	16	69,2
28	76,7	18	72,6
20	78,8	20	73,3
24	80,3	24	73,8
25	81,5	25	75,8

The next parameter under study which regulates the emitter operation is the dependence of the temperature of the irradiated area upon the distance from the emitter at the set electric energy input. In the low-temperature flat emitters the temperature dependence of the irradiated area upon the distance from the emitter was studied under the constant construction electric energy input (ITS 500/A – 500W and IT-AG 600 – 600W). The temperatures obtained experimentally for emitters ITS 500/A and IT-AG 600 are plotted in Table 2 and Fig. 2. The temperatures of the irradiated area depending on the distance from the emitter show a very similar course in the low-temperature flat emitters for both electric energy inputs observed. The course of the curves (as a connecting line of the trend of the values measured) can be described as the same. The temperature shift is due only to the 120W difference in the electric energy inputs of the emitters.

In the high-temperature emitter with heated filament CH1800RW the dependence was studied with four set electric energy inputs (900W, 1200W, 1500W, 1800W). The temperatures were taken by one metre from the distance of 8 metres. The temperatures for the emitter CH18000RW obtained experimentally are given it Tab. 3 and they are plotted in Fig. 3.

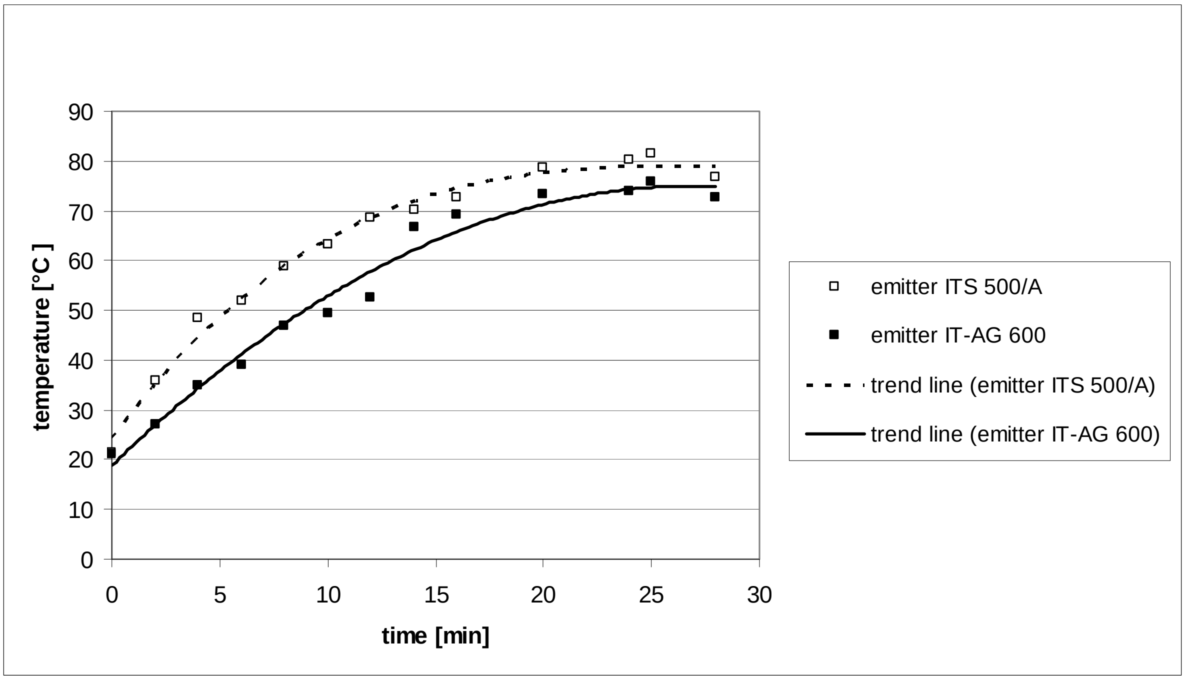

Fig.1 Emitters´ approach time up to the stabilized temperature (emitter ITS 500/A and IT-AG 600)

Tab. 2 Mean values of the irradiated area at a distance from the emitter with set electric energy input (emitter ITS 500/A and IT-AG 600)

distance [m]	temperature [°C]	
	emittor ITS 500/A	emittor IT-AG 600
	electric power 480W	electric power 600W
1	26,1	28,3
1,5	25,2	26,7
2	23,4	25,7
2,5	22,3	24,1
3	20,9	22,6
3,5	20,4	21,8
4	19,6	21
4,5	19,4	20,5
5	19,3	19,9
5,5	19,3	19,8
6	19,2	19,6

Temperatures of the irradiated area depending on the distance from the emitter show a similar course in a high-temperature emitter in all four electric energy input values. Like with the low-temperature emitters the mutual course of the curves is identical. With the inputs set at 1200 W up to 1800 W the temperatures are almost the same. There is a difference only with the input set at 900 W where the temperatures are less up to the distance of 4 metres from the emitter. The size of the buildings and the emitter´s electric energy input are limited by the space in which the effect of the infrared radiation can be used efficiently. This space is usually given at the distance of 2 – 4 m from the emitter. At this distance, the different emitter temperatures for different energy inputs are negligible. There is a slightly greater deviation in comparison of the minimum measured input at 900 W with the maximum measured input at 1800 W (at three metres from the emitter the difference is 2.4 °C). The values measured for the high-temperature emitter indicate a possibility of operation regulation by the surrounding conditions applying a time-limited decrease of the operation input.

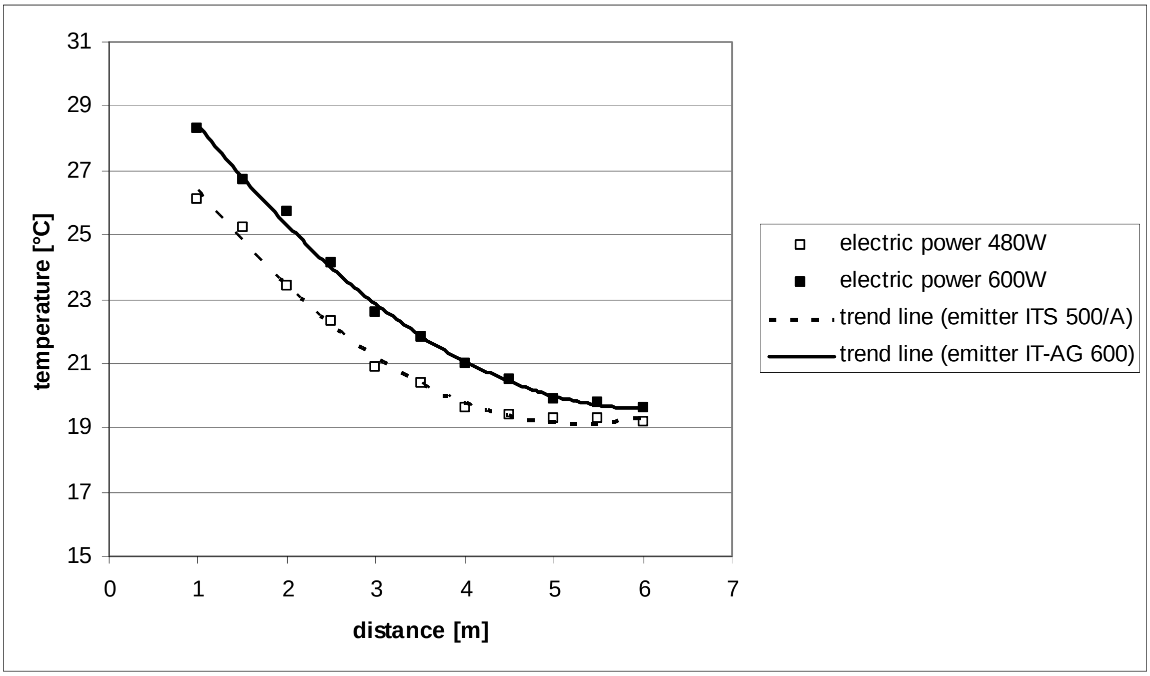

Fig.2 Course of temperatures of irradiated area at a distance from the emitter at emitter´s set electric energy input (emitter ITS 500/A and IT-AG 600)

Tab. 3 Mean values of irradiated area temperature at a distance from the emitter at emitter´s set electric energy input (emitter CH 1800RW)

distance [m]	**emitter CH 1800 RW**			
	temperature [°C]			
	electric power 900W	**electric power 1200W**	**electric power 1500W**	**electric power 1800W**
1	29,7	36,2	37,4	38,7
2	22,1	25,4	25,1	26,4
3	20,1	21,7	21,9	22,5
4	19,4	19,9	20,3	20,9
5	19,3	19,6	20	20,4
6	19,2	19,5	19,8	20
7	19,2	19,4	19,5	19,9
8	19,2	19,3	19,3	19,6

Coclusion

There has been a worldwide trend in the field of environment protection to reduce the energy demand of buildings and equipment. The EU has issued an instruction concerning the energy requirements of buildings.

The environment of technological plants is highly demanding of heating. The height of the heated space often reaches 3 and more metres. There are various changes in the heated space. Very often it is a matter of open spaces or spaces partly open to the outdoor environment. Indoor change of temperature can often be affected by the presence or non-presence of human service. The existing technological processes often produce excess of heat which affects the surrounding environment. Demands of heating are often changing in time as well as locally within the heated space.

Conventional heating systems based on convection must therefore be much too big, they are uneasy to regulate and they are excessively demanding of energy. There is a further load in the dusty environment due to air circulation. Such problems can be solved by the use of heating with infrared radiation emitters which are suitably located within the space of the technological plants.

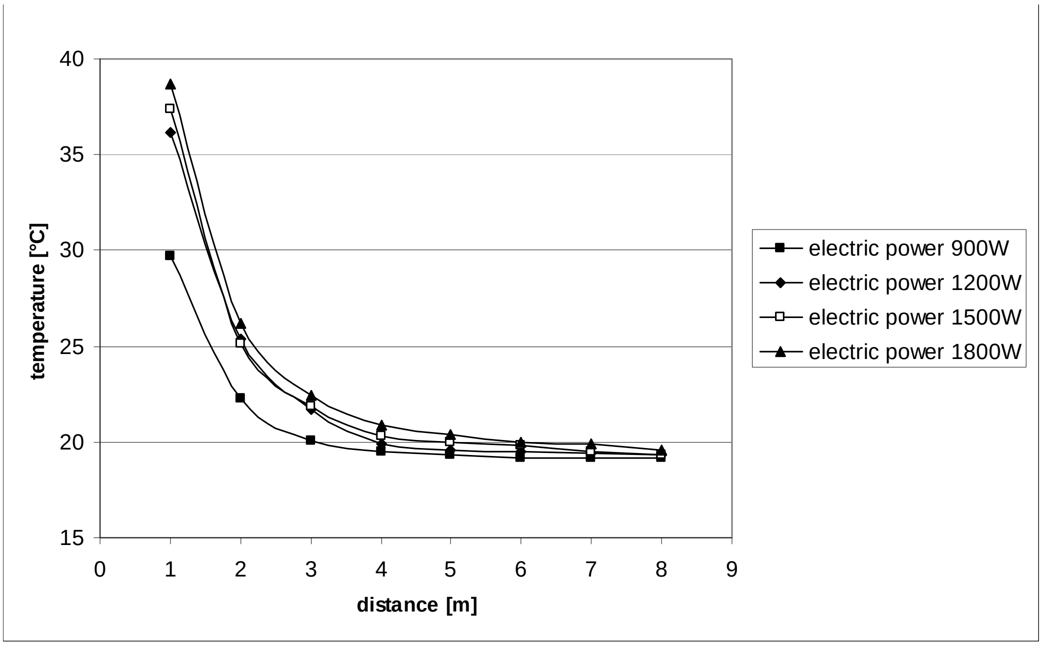

Fig. 3 Course of temperatures of irradiated area at a distance from the emitter at emitter´s set electric energy input (emitter CH 1800RW)

The values measured on selected emitters are characteristic of their technical and operational properties and they correspond with theoretical assumptions. The curves of the measured values indicate clearly the application of separate types of emitters based on their characteristics. Flat carbon emitters with a long time of approach up to the operation temperature are not suited for the regulation of electric energy input in real time required in technological processes. The low-temperature flat IR emitters are produced with fixed defined input given by their construction and size of the emission area. Input regulation in these emitters is thus impossible. They are suitable in households and offices with constant heat loss.

Measurements using gradual input regulation of high-temperature emitters ranging from 900 W to 1800 W have shown a temperature difference of 2.4 °C within three metres from the emitter. Input control can thereby bring considerable saving of electric energy while maintaining sufficient efficiency. A speedy reaction allows operation control by reducing the input or by controlled switch, e.g. using the workforce operating the equipment. Among the construction properties is, for instance, a possibility of zone heating using reflectors for more distant areas.

The high-temperature emitters, having their response time in dozens of seconds, having higher output, higher efficiency and better construction properties, fully satisfy the requirements of heating technological plants without unnecessary losses.

Reference

Barker M., 2002. Using infrared heating, Plant Engineering (Barrington, Illinois), 56(1): 34-36

Borovec I., 2012. Radiant heating on the principle of shortwave radiation. TZB Haustechnik 5(3).

Dudkiewicz E., Jezowiecki J., 2009. Measured radiant thermal fields in industrial spaces served by high intensity infrared heater, Energy and Buildings, 41(1): 27-35.

Electric Infrared Heating Manual, 1998. Fostoria Industries Inc, North Main, USA.

Roth K., Dieckmann J., Brodrick J., 2007. Emerging technologies: Infrared radiant heaters, 2007 ASHRAE Journal, 49(6): 72-73

THE ENVIRONMENTAL ASPECTS OF SUBURB AREAS' DEVELOPMENT

Boleslav Kadleček, Miroslav Růžička*, Martin Kotek

Czech University of Life Sciences Prague, 16521 Prague 6 – Suchdol, Czech Republic, Phone: +420 22438 3313, E-mail: kadlecek@tf.czu.cz

Abstract

The intensive and even chaotic development of the capital Prague's suburb areas was not performed usually in accordance with the transport infrastructure development and public facility construction. Traffic intensities doubled on the roads (of 2nd. or 3rd. class) on surveyed areas during the last five years, in extreme cases of the morning traffic peak vehicles spend about 50% of total drive in congestions. The offer of transit (public transport) has non adequate development in suburb areas as well. The passenger car transport has low average occupancy rate app. 1.3 persons per car. These conclusions result from long term traffic surveys carried out on the selected localities of suburb settlements up to 20(km) of radial distance from the Prague city centre. The quantification of transport environmental impacts of observed area requires not only accept the proportion of increased intensities but it is necessary to take into account a progressive influence of increased drive transience of traffic flows and congestions. That is why the traffic surveys were carried out simultaneously with experimental drives done by vehicles with measurement equipment to map emission production and fuel consumption in the suburb areas. Results confirm expectations that the higher rate of suburb populating increases vehicles' fuel consumption and consequently emission impacts. The important influencing factor is the quality of transport infrastructure and its control, including road horizontal and vertical profile shape.

Keywords: environmental aspects, suburb areas development

Introduction

The role of urban structure, at the strategic and local scales, would appear, intuitively, to be critically important in facilitating travel. Urban structure provides the framework for the location of housing, employment and other developments, such as health, education and leisure facilities. Urban structure thus provides the physical rationale for travel alongside socio-economic and cultural factors. It might be expected that different urban forms (say low density sprawl and high density, public transport orientated development) to be clearly associated with different travel behaviours on the ground. Some authors contend that certain land use variables, for example density, are strongly associated with energy consumption in travel (Newman, Kenworthy, 1989; Newman, Kenworthy, 1999). Some are more cautious and suggest that land use factors are, at most, only a small part of the picture, and that other factors, such as income, are more important in influencing the variation in travel (Gordon et al., 1997). Others add a further dimension in contenting that the suburbanisation of the labour force has actually led to reduced trip lengths, with both residences and jobs being located in the suburbs (Gordon, Richardson, 1989). Finally there are issues raised around the acceptability of various policy stances, particularly the public acceptability of compaction (Breheny, 1992); it is argued here that suburbanisation has been stimulated by lifestyle choice and that attempts towards urban compaction are futile.

The determination of fuel consumption per km can be affected through changes in the technological efficiency of cars or changes in driving habits. Urban density could have countervailing effects on fuel consumption per km.

Congestions could also affect both car ownership and the distances travelled, as well as fuel consumption per km.

According to the above cited references it is evident that the topic is arduous and it is influenced by many local aspects and questions e.g. is actually more non-work trips than those of work-related travel; do the most trips occur from suburb to suburb; is a decentralized concentration of cities very sustainable form etc.

The general aim of next described experiments is in detail to specify the range of traffic influences on the fuel consumption and emission production of personal cars under specific suburban (partly urban) conditions. The main purpose of this study is an attempt to create space characteristics of energy consumption by transport. This characteristic should serve as tool for current transport infrastructure evaluation, transport prognoses or it could help to control the traffic systems, finally to show the traffic environmental impacts that are caused by consumption of non renewable sources (fossil fuels), harmful emission production and further impacts.

Material and method

Simultaneously with carried out traffic surveys were conducted rides with the measuring car on radial roads oriented to the city centre. These roads are linked with ride origins (suburban estates) and destinations (the nearest P+R at the metro station). This study does not involve results of traffic surveys of higher class communications (motorways, speed roads) that are the topic of systematic surveillance of state authorities – results of traffic intensities are publicly accessible e.g. state-wide traffic census of the Czech Republic. Drives with special car were carried out on all these roads in the same days of surveys. The car was outfitted with measurement equipment that enabled data recording of:

1. Personal car was equipped with measuring technics (GPS unit, analyser of exhaust fumes). The vehicle was selected as represent of personal car according to analysis of vehicles' structure development (see statistics of vehicles' central register of the Czech Republic). The analysis proved that the number of vehicles with a bigger engine volume increases. There is expectation that these vehicles will be used in a majority under daily traffic commuting from the suburban areas (it includes population social aspects as well).
2. Experimental drives were conducted on routes during morning traffic peak on roads of II and III class (not motorways or international roads) in ordinary working day (Tue, We, Thu) in accordance with ministry of transport' standards (TP189)
3. The drives were carried out on routes located in space with a different level of the suburbanisation.
4. The length of drives from the origin to the destination was approximately the same. Drives were carried out within the radius up to 20 (km) from the city centre. The destination was the nearest metro's P+R lot.
5. The way of driving was fully subordinated to traffic conditions i.e. the vehicle did nor accelerate or decelerate purposelessly etc.

Measuring technics for experimental drives - communication with vehicle's onboard diagnostics was supported by diagnostic system SuperVag (see Fig. 1) made by Carsoft comp. The system enables to record and save instantaneous data provided by OBU as blocks of measured data (Tab.1.) According to number of recorded data (blocks) is changed recording frequency (the more data, the lower frequency). Three data blocks with 4 quantities were recorded i.e. total 12 values during experiments. Frequency of data saving app 0,28(s) was used for this choice.

Fig. 1 Equipment Super Vag (left) and example of computer screen (right)

Tab. 1 Structure of exported and saved data by Super Vag system (fragment)

Nb. row	Start time	Revol-ution	Required mass of air.	Real mass . of air	Valve	Speed	Position of pedal	Engine's torque	Consumption	Torque acc. pedal.
	s	min^{-1}	$mg.stroke^{-1}$	$mg.stroke^{-1}$	%	$km.h^{-1}$	%	Nm	$liter.h^{-1}$	Nm
1	0.2813	819	295	290	44	0	0	39	0.6	0
2	0.5626	819	295	295	44	0	0	39	0.6	0
3	0.8439	819	295	290	44	0	0	39	0.6	0

Tab. 2 Data structure from DEWE-VGPS-200C system (fragment)

Time	X absolute AVE	Y absolute; AVE	Z; AVE	Velocity; AVE	Velocity Z; AVE	Direction; AVE	Distance; AVE	satellites; AVE	Current sec; AVE
s	-	-	m	$km.h^{-1}$	$m.s^{-1}$	deg	m	-	s
0	0	0	0	0	0	0	0	0	0
0.5	857.132	3009.183	352.748	0.029985	0.009167	0	0	8	19733.65
1	857.132	3009.183	352.765	0.036114	0.0004	0	0	8	19734.23
1.5	857.132	3009.183	352.803	0.057412	0.00755	0	0	8	19734.73

System DEWE-VGPS-200C was used for experiments (Fig. 2) to determine precise vehicle's geographic positions and drive's dynamic parameters. The software records and continuously saves quantities of vehicle's position, direction, instantaneous speed, acceleration and number of reachable satellites. Frequency of recording and data saving is optional, frequency 2(Hz) was chosen to measure under traffic conditions

Fig. 2 GPS ‚DEWE-VGPS-200C system

Selected technical parameters:
Speed:
  Accuracy - 1,1 $km.h^{-1}$ ± 0.005% of range
  Min to Max – 0.1 $km.h^{-1}$ to 500 $km.h^{-1}$
  Resolution 0.01 $km.h^{-1}$
Absolute position:
  Accuracy < 40cm CEP
  Refresh rate 20Hz
  Resolution < 10cm

The mobile analyser of exhaust pollutants was installed into measuring vehicles (see Fig.3) It enabled to record emission CO, CO_2, HC, NO_x and O_2 in real time [with frequency 1 (Hz)] -Table 3 shows part of these records. The obtained data of instantaneous emission production and with GPS data are to assign emissions to specific locations (positions) and to compare stoichiometric calculations of fuel consumption.

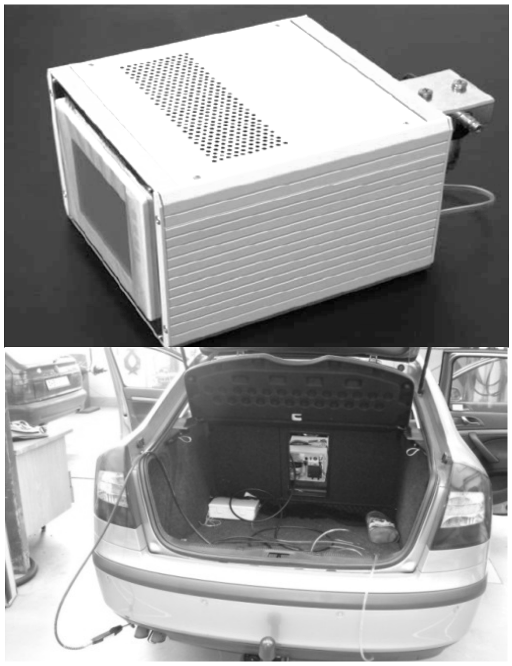

Fig. 3 Mobile analyser of exhaust fumes, installation into vehicle

Tab. 3 Exported data structure from mobile fume analyser (fragment)

Time	Mode	Time from midnight	CO	CO2 real.	Time hour	Time minute	Time second
S		s	%	%	hour	min	s
0	measurement	26938	-0.001	2.9	7	28	58
1	measurement	26939	-0.001	2.9	7	28	59
2	measurement	26940	-0.001	2.9	7	29	0

Data obtained from onboard diagnostics and emission analyser were synchronised and processed by formula (1) to calculate mass of air flow rate and as well it possible to calculate specific instantaneous mass production of observed emission according the formula (2):

$$Q_m = \frac{28{,}9 \cdot \left(p_s - \frac{p_{atm}}{\varepsilon}\right) \cdot V_Z \cdot \eta_d \cdot n}{1200 \cdot R \cdot T_{VZD}} \qquad (1) \quad ,$$

$$m_X = \frac{X}{100} \cdot \frac{Qm}{\rho_V} \cdot \rho_X \qquad (2)$$

- Q_m *($g.s^{-1}$)*…amount intake air by engine,
- *28,9 ($g.mol^{-1}$)*…molar mass of air,
- p_s *(mbar)*…intake pressure,
- p_{atm} *(mbar)*…atmospheric pressure,
- ε *(1)*… engines' compression ratio,
- V_Z *(1)*…engines' capacity (volume),
- η_d *(1)*… engines' transport efficiency,
- *n (min^{-1})*… engines' revolutions,
- *R ($J.K^{-1}\cdot mol$) $^{-1}$*…universal gas constant (for ideal gas R=8,314),
- T_{VZD} *(K)*…intake air temperature (K).
- m_x *($g.s^{-1}$)*…concentration of specific emission fraction,
- *X ($\%.s^{-1}$)*… concentration of specific emission fraction in exhaust pollutants
- ρ_v *($kg.m^{-3}$)*…density of air
- ρ_x *($kg.m^{-3}$)*…density of specific emission fraction.

Results and discussion

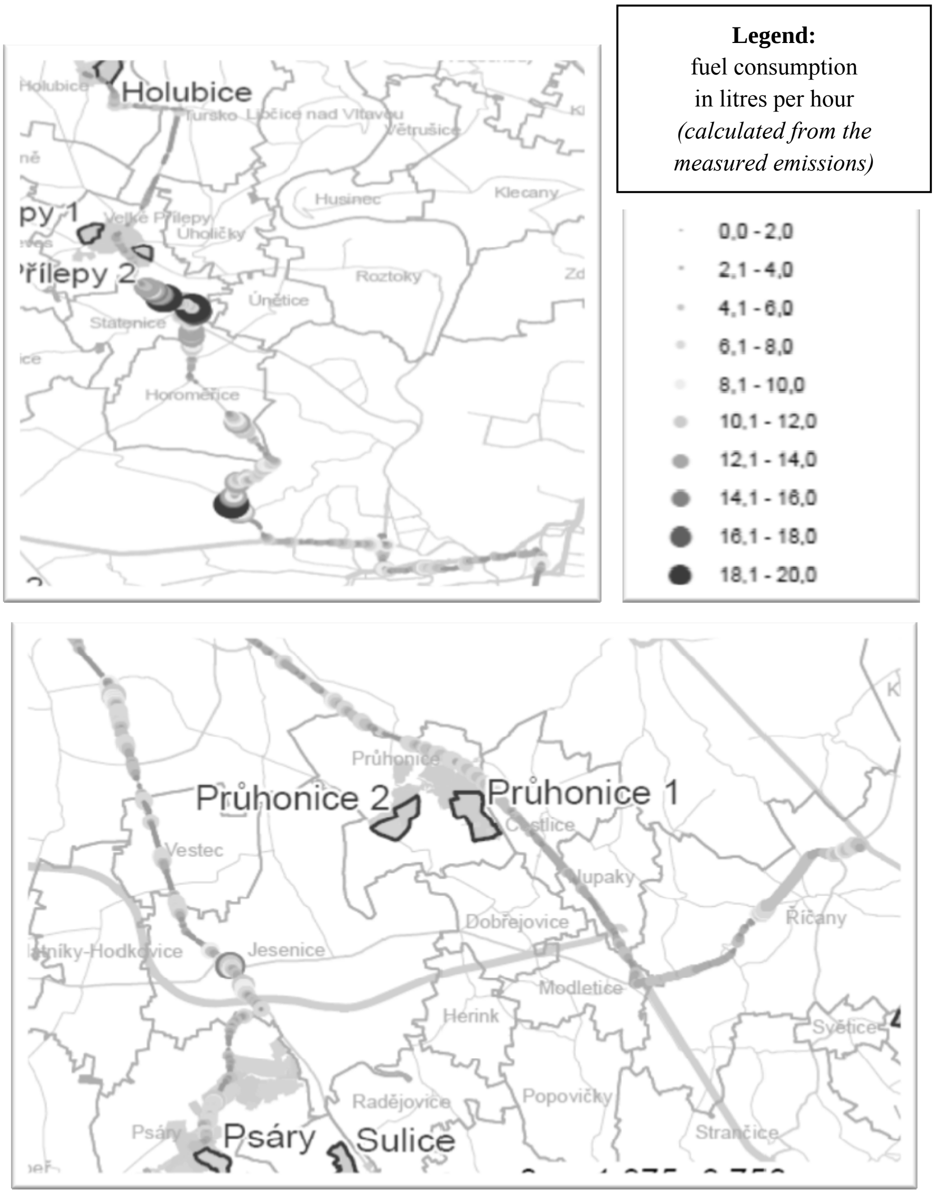

Fig. 4 GIS specialised map fragments of instantaneous fuel consumption in litre per hour

Some of experimental results were processed with software ARC MAP (i.e. GPS, Super-Vag and mobile analyser data record files were vectored) in a GIS specialised maps of fuel consumption (litre.h^{-1}). Fig. 4 shows graphical comparison of instantaneous fuel consumption on chosen parts of routes (zoomed). This part of route is located between villages Velke Prilepy and Horomerice. This part of route is specific by higher number of curves and alternating ascended/descended slopes of road longitudinal profile. These road attributes can significantly influence the instantaneous fuel consumption and emission production in comparison with straight and horizontal roads and usual traffic (e.g. Evropska street) and even significantly more then on routes with higher traffic intensities i.e. Říčany-Průhonice-Praha, Psáry-Jesenice-Praha shown in the lower part of Fig.4.

Conclusion

The process of suburban development is not possible to interrupt or even stop. Several attempts to do it usually failed and were futile. The process of suburbanisation has been stimulated by a choice of lifestyle. Research results prove and confirm the expected increase of energy consumption by transport. The scale of this increment is higher than usually published values based on the fuel consumption derived from homology tests. The results currently imply two basic ways of future development that could perform possible energy savings and decrease an emission production in the transport sector. The first way is the technical and technological development of vehicles' energy sources that decrease consumption by every possible different means. The second way is the space development that will be carried out to support every alternative transport modes i.e. transit (public transport), cycling and walking. Both these ways of development are closely linked with the sphere of transport management and politics. It should encourage and motivate public to prefer the use of these alternative transport modes. Another possibility is to reduce the use of personal cars (tolling etc.). This paper has limited number of pages and that is why the only example of results can be listed here. Who is interested in other results, complete list of maps, can visit the web page http://cost.mapovyportal.cz

Acknowledgement

This work was supported by COST TU0902 *„Integrated assessment technologies to support the sustainable development of urban areas“*, Projekt MŠMT LD 11049: "Spotřeba energie dopravou v urbánních a suburbánních územích" (*The transport energy consumption in urban and suburban areas)*

Reference

Breheny M., 1992. The Contradictions of the Compact City: A Review, in Breheny, M. (Ed) Sustainable Development and Urban Form. London, Pion, 138-159.

Ewing R., 1997. Is Los Angeles style sprawl desirable, J Am Plan Assoc, 63(1): 107–126.

Gordon I., Breheny M., Archer S., 1997. Urban Compaction Versus Higher Gas Prices: The Feasibility and Effectiveness of Alternative Approached to Securing Sustainable Levels of Urban Travel. Paper presented to Association of American Geographers, Fort Worth, Texas.

Gordon P., Richardson H.W., 1989. Gasoline Consumption and Cities: A Reply, Journal of American Planning Association, 55: 342-345.

Newman P.W.G., Kenworthy J.R., 1989. Cities and Automobile Dependence. An International Sourcebook. Aldershot: Gower.

Newman P.W.G., Kenworthy J.R., 1999. Sustainability and Cities: Overcoming Automobile Dependence. California: Island Press.

PRACTICAL EXPERIENCE WITH TREATMENT BIOGAS TO NATURAL GAS QUALITY

Jaroslav Kára[1*], Michal Pastorek[2], Zdeněk Pastorek[2]

[1]Research Institute of Agriculture Engineering in Prague, 16101 Prague 6 – Ruzyně, Czech Republic, Phone: +420-731 615 043, Fax: +420-233 312 507, E-mail: jaroslav.kara@vuzt.cz
[2] Czech University of Life Sciences Prague, 16521 Prague 6 – Suchdol, Czech Republic,

Abstract

In practice is the cogeneration of electricity and heat most commonly used method for the use of biogas. The most common alternative to cogeneration systems are now recommends the use of biogas to biomethane modified. Biogas is, however, need to clean and adjust to the commonly used forms of natural gas. Raw biogas from the digester is cleared of hydrogen sulphide, dried, and compressed. After the first stage of compression, the gas is cooled and then dries. Between the output of the first stage and entrance to second compressor stage is inherent separation of CO_2*, at a pressure up to 20 bars. For the final purification of biogas was used molecular sieves in the same pressure range, the carbon dioxide is then drained from the membrane system. After we got rid of* CO_2*, biomethane is ready for use or stored under pressure up to 250 bars. The device was tested on biogas plant in operating conditions with excellent results.*

Key words: treatment of biogas, biomethane, biogas plant

Introduction

For the afore-mentioned reasons, the European Union and its member-state environmental legislation support the development of biogas generation and exploitation in many fields. Biogas is commonly used for combined heat and power production (CHP) or upgraded into biomethane. Biomethane will henceforth be intended as a natural gas matching pipeline requirements obtained from biogas treatment.
The main objective of this contribution is to introduce a new technology for biomethane production and compression aimed at CNG vehicle refueling, or domestic purposes (e.g. heating or cooking).

In practice CHP is the most commonly adopted method for biogas exploitation. The method achieves a high energy utilization efficiency: about 80-90% of the energy is used, combining electricity and heat. Approximately 35% of biogas potential is transformed into electric power and 50% into heat energy. 1 kWh of electricity and 1.4 kWh of heat require about 0.6-0.7 $m^3.hour^{-1}$ of raw biogas with methane content of 55-60% (Pastorek, 2004). An important advantage of CHP is that in many EU countries there is a statutory obligation for public electricity network administrators to buy electricity from CHP at incentivized and guaranteed price, which is usually sufficient for a reasonable payback time of the initial investment. The most common alternative to CHP is biogas upgrading to biomethane, that can be compressed or liquefied and used as vehicle fuel, or injected into the natural-gas grid.

A few European firms deal with biogas upgrading. Biogas cleaning and refining is realized by elution in water or in other reactants like amines or carbonates. These methods exploit various adsorption properties of liquids, or activated charcoal, to separate carbon dioxide and methane. The efficiency of such methods is intensified by pressure and temperature modification during the adsorption or regeneration processes: typically the solvent is cooled down to absorb carbon dioxide, and heated up for regeneration after the maximum amount of CO_2 has been absorbed.

These technologies operate with high-efficiency and methane-recovery rates, yet their drawback is to be capital-intensive, therefore can be effectively operated for overall capacities higher than of 150 $m^3.hour^{-1}$. Moreover, the processes are quite complex, and very often need to be supervised and maintained. The appliances for the biogas utilization as fuel are operated in a few big biogas plants in Sweden, Switzerland and the Netherlands.

For medium-sized or small biogas plants, or for upgrading a small portion of the produced biogas, available technologies are not economically viable. Thus the need for developing cheaper and simpler technologies. Molecular sieves could be a good alternative. Molecular sieves select the contaminants (H_2O, CO_2, and H_2S) according to certain molecular characteristics, such as size or shape (Deublein, 2008). However, molecular sieves are quite expensive, and need periodic regeneration.

Material and method

The proposed upgrading and compression unit is supposed to be installed on an existing digester, and to operate along with a CHP generator. The basic scheme of the unit is shown in Fig 1. Raw biogas is taken from the digester, desulfurized, dried, and compressed. After a first compression stage, the gas is cooled down and dried again, then carbon dioxide is removed by a membrane system. After CO_2 has been got rid of, biomethane is ready to be boosted up to 250 bar and stored. Having removed all contaminants, the obtained biomethane is equivalent to natural gas, and can be used for domestic purposes or for vehicle refueling. The main adopted refining systems are described in the ensuing sections.

Desulfurization

Sulfur is indeed the most troublesome biogas contaminant. Hydrogen sulfide causes formation of sulfuric acid during biogas combustion, which causes corrosion whenever condensation occurs in combustion gases. Hydrogensulfide in biogas impairs the lifetime of pipelines and all installations, and might cause steel embrittlement at high pressure. Hydrogen sulfide is toxic and very dangerous for human and animal health. The limit for hydrogen sulfide concentration at 250 bar is 10ppm (NACE standard Mr0175-02:2002) for commonly used carbon steels, therefore this is the target concentration for the desulfurizer of the application at hand (Kára, Mužík, Paganelli 2010).

Biological desulfurization is the most commonly applied method for hydrogen sulfide reduction. Hydrogen sulfide is solved into water and then biologically decreased. Microorganisms of the species Thiobacillus and Sulfolobus, which are omnipresent and therefore do not have to be specifically inoculated, are capable of digesting hydrogen sulfide. Sulfur-attacking microorganisms are aerobic and need oxygen. Air is dosed directly into the fermenter or gasholder, at a rate of about 4-6%. Biological desulfurization can reduce hydrogen sulfide content down. to 200 - 500 mg m^3., which is usually enough for CHP utilization, but too high for high pressure compression. The decomposition of hydrogen sulfide to form sulfate and/or sulfur occurs according to the equation (Deublein, 2008):

$$2H_2S + O_2 \rightarrow 2S + H_2O \qquad (1)$$

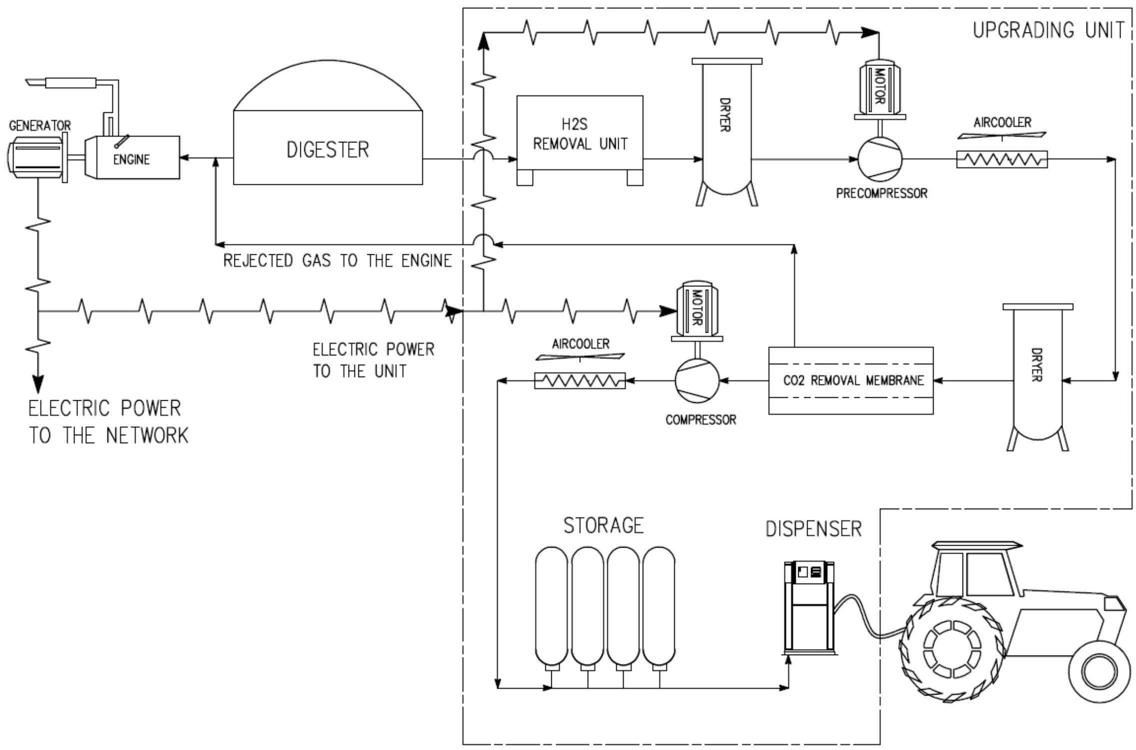

Fig. 1 Scheme of the upgrading and compression unit

Adsorption though iron-containing masses is a highly-efficient and relatively cheap method for desulfurization. In this process, hydrogen combines with iron (III) hydroxide ($Fe(OH)_3$) or with iron (III) oxide (Fe_2O_3). Both procedures run similarly and are dry desulfurization processes. Sulfur reverts the iron (III) hydroxide/oxide surface into iron (III) sulfide and water, according to the ensuing equations (Deublein, 2008):

$$2Fe(OH)_3 + 3H_2S \rightarrow Fe_2S_3 + 6H_2O \quad (2)$$
$$Fe_2O_3 + 3H_2S \rightarrow Fe_2S_3 + 3H_2O \quad (3)$$

Ferric oxide or hydroxide masses are stacked layer by layer in a desulfurization unit either as impregnated steel wool or as impregnated wooden chips or pellets. Biogas is fed at the bottom at low pressure and a temperature of 15-50°C. Biogas should be wet, but without suspension of water mist. This system should achieve reduction of the hydrogen sulfide content down to 5 $mg.m^3$, therefore is well-suited for CNG applications (Deublein, 2008):

Gas drying

Water is also a dangerous biogas contaminant. At the outlet of the digester, biogas is saturated with water, and during compression and aftercooling water condensates. Liquid phase along with CO_2 triggers carbonic acid formation and steel corrosion. Moreover, liquid water hardly reduces its volume during compression, thus jeopardizing the structural integrity of compressors. Therefore, it is important to remove liquid water as pressure increases. Many techniques are available on the market for this purpose: molecular sieves, membranes, chillers. The cheapest way is probably water absorption with anhydrous salts, that enables removal of about 70% of water content at a given pressure. By installing such a dryer after each compression stage, it is possible to prevent most of the problems due to water condensation.

Carbon dioxide removal

Membrane technology has been chosen for carbon dioxide removal. The working principle of membranes is the different permeation rate of different molecules through polymer films. The main advantages of membranes are:

1) The driving force for membrane separation is differential pressure on the two sides of the polymer film: since the gas has to be compressed anyway up to very high pressure for vehicle refueling, any desired pressure is available for membrane separation.

2) For very low capacities, membranes are probably the cheapest system.

3) Membranes operate like a filter, and do not need any kind of additional process for the separation (like washing, heating, or regeneration.)

The main drawback of membranes is the relatively low efficiency, for about 10% of methane contained in raw biogas is discarded together with carbon dioxide. However, as shown in Fig. 1, this wasted gas is collected and conveyed into the engine along with the normal feed flow of raw biogas. The amount of this rejected gas is negligible with respect to engine feed flow (usually about 5%), therefore average CO_2 increase in engine feed gas is also negligible, and engine operation remains unaffected. In this way, methane contained in the rejected gas is burnt into the engine, producing energy. From some preliminary calculations, this energy is more than enough to provide the required compression power for the unit, therefore the cleaning system is completely closed, and gets all needed power from biogas itself.

Result

Main features and operating data

The whole device is placed in a container, Fig.2, which makes it easy to manufacture and easy installation by the user. The proposed compressor unit is designed for biogas to natural gas quality of the input capacitance of about 200 $m^3.h^{-1}$ raw biogas. So far, the product of anaerobic digestion is used for cogeneration of electricity and heat in cogeneration units. For the purposes of biogas for the drive motor must first be removed from the biogas sulfide to prevent corrosion of the compressor. Biogas undergoes dehydration first tank anhydrous and then enters the compression system. Biogas is then cooled and the early stages of the compressor again significantly compressed to about 20 bar. After the first stage of treatment biogas is cooled and dried and then enters the membrane separators to remove more of CO_2, thereby forming an almost pure methane. At this point, the device is biogas to biomethane done and nearly pure biomethane to the pressures in the 250-bar refueling vehicles. The rest of the waste gas after deduction of membrane still contains CO_2 out small amounts of methane, so it is recommended to apply the residue gas stream led to the burning of biogas in cogeneration units. In this way it is possible to get enough energy to power all electrical devices compressor unit for biogas treatment. All main technical data are summarized in the following table 1.

Official analysis of purified biogas measured by an independent laboratory in Studio Alfa See Table 2.

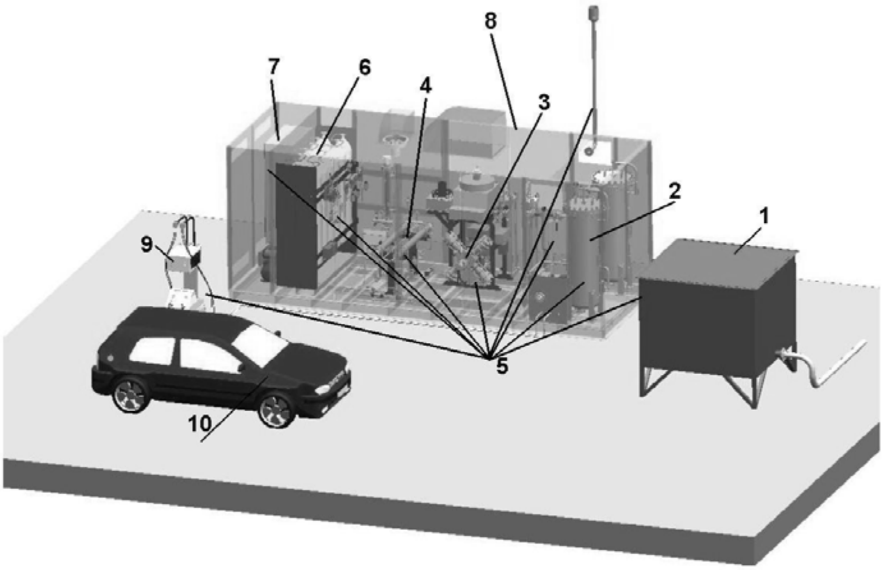

Fig. 2 Scheme of the compressor unit to adjust the biogas to natural gas quality
Legend: 1 - desulphurization, 2 - dryers and separators, 3 - major four-stage compressor, 4 - separator membrane (molecular sieves), 5 - sensor gas analyzer, sensor instrumentation, 6 - buffer consisting of cylinders 7 - control measurement and control panel, 8 - container, 9 - dispenser, 10 - car with a fuel system modified to operate in the CNG

Tab. 1 Main technical data compressor units for biogas treatment on the quality of the natural gas

Parameter	Value	Unit
The inlet pressure	0	bar
Inlet gas temperature	55	°C
Storage pressure	250	bar
Pressure for refueling vehicles	220	bar
Number of compressors	2	units
Input flow BIOGAS	200	$m^3.hour^{-1}$
Output flow biomethane (CNG)	100-120	$m^3.hour^{-1}$
Maximum inlet concentration of H_2S	10	ppm
Maximum inlet concentration of CO_2	50	vol %
The planned output of CO_2	2,5	vol %
Input humidity biogas	100	Φ, %
Output humidity biomethane	30	Φ, %
The installed capacity of the compressor	110	kW
The installed capacity of the auxiliary compressor	10	kW
The temperature range	-10/ +40	°C

Tab. 2 Composition of purified biomethane

Component	Value	Unit
Hydrogen sulfide	2,66	$mg.Nm^{-3}$
Methane	98,9	%
Oxygen	0,03	%
Carbon dioxide	0,19	%
Nitrogen	0,22	%
Mercaptans	0,006	%
Siloxanes	0,006	%
Other hydrocarbons	0,65	%

Fig. 6 Location of compressor units for biogas treatment in container for biogas

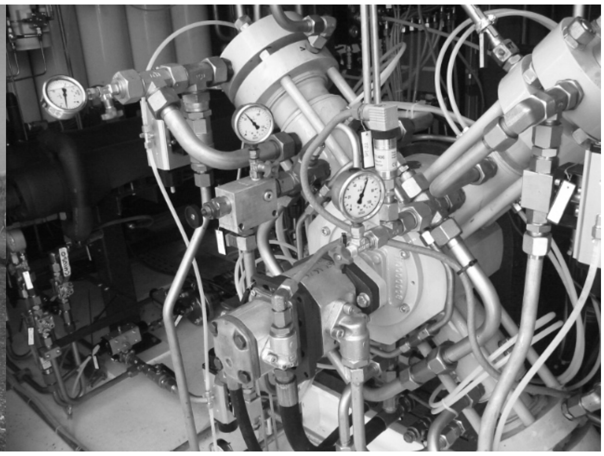

Fig. 7 The compressor section with compressor and storage section of cylinders

Tab. 3 Economic data compression unit on the performance of raw biogas 200 $m^3.hour^{-1}$

Performance of raw biogas per hour	$m^3.hour^{-1}$	200
Removing the share of biomethane from raw biogas	%	60
Biomethane per year (98% CH_4, calorific value of 35,16 $MJ.m^{-3}$)	m^3	1 036 800
Replacement of diesel fuel per year (calorific value 36,31 $MJ.l^{-1}$)	liters of diesel fuel	1 004 031
The cost of producing green biomass for biogas production	3,41 - 5,6	*Kč.m^{-3} biogas
The cost of biomass for biogas in a biogas plant	1,5 - 2,5	Kč.m^{-3} biogas
Department of biomethane from biogas with high pressure		
The processing costs for 1 m^3 of raw biogas production biomethane	2,2	Kč.m^{-3} biogas
The cost of processing 1 m^3 of biomethane	3,66	Kč.m^{-3} biomethane
The total cost of producing 1 m^3 of raw biogas to biomethane	7,11 - 10,30	Kč.m^{-3} biogas
The cost of producing 1 m^3 of biomethane	11,84 - 17,16	Kč.m^{-3} biomethane

*1€ = 25, 64 Kč

Conclusion

The prototype unit has been designed to process about 50 $m^3.hour^{-1}$ of raw biogas, and to produce 25-30 $m^3.hour^{-1}$ of clean, free, and green bio-CNG. However, there is in principle no limit for the size that could be reasonably increased up to 4-6 times with a less-than-proportional increase of the costs.

The designed unit is important for many reasons. First of all, according to the small and medium sized biogas plants have a better energetic balance than larger ones, but their higher relative investment costs influence negatively its economic efficiency. With regard to both parameters, medium sized biogas plants (500 - 2000 kW, or 300-1000 $m^3.hour^{-1}$) are the most effective. Therefore, the presented unit represents an interesting solution to diversify biogas exploitation of existing medium-sized digesters.

Eventually, biogas production of a digester often exceeds the amount used by CHP engine by some percents, in order to keep all engines properly fed at maximum power. For example, 50-100 $m^3.hour^{-1}$ over a production of 60-700 $m^3.hour^{-1}$ are likely to be continuously flared on usual digesters. The proposed unit can recover this exceeding gas, that is currently wasted, in order to obtain a clean arenewable fuel.

Pilot validation yielded successful confirmation of the expected results. Laboratory testing methods for separating components of biogas high pressure was effective but separation of CO_2 from CH_4 is only one of the phases of the biogas quality necessary for its use for gasoline engines under the requirements of IEC 65 6514th This stage must be preceded by the water vapor content (up to 32 $mg.m^{-3}$ biogas) and the amount of sulfur compounds (up to 10 $mg.m^{-3}$ biogas). The results of official analysis of purified biogas is clear that the model device has fully complied with both theoretical and practical assumptions about this new method of cleaning biogas to the natural gas fuel type. Its efficiency in the separation of CO_2 is 99.4%, which suggests that this device can be used for cleaning biogas volume concentration of CO_2 up to 60%, subject to the standard CSN 65 6514th

The attained parameters satisfy the reserve requirements of this standard, as in methane concentration and purity of the resulting gas with a minimum of pollutants, particularly hydrogen sulfide. Methodology The project envisaged under the project to address only the separation of CO_2 from biogas, with the existing methods of reducing the concentration of water vapor and H_2S will be sufficient for the needs of the project. This hypothesis proved to be unrealistic. We had to work on the project design and technical solutions to reduce the water vapor content and the amount of sulfur in the biogas, which has succeeded.

Acknowledgement

These results were obtained with the help of a grant project of the Ministry of Agriculture NAZV "QH81195 new technology systems for the efficient utilization of biogas" and of the "Research project MZE0002703102 effective use of technology systems for sustained management and use of natural resources in the specific conditions of the Czech agriculture".

Reference

DEUBLEIN D., STEINHAUSER A, 2008. Biogas from Waste and Renewable Resources. WILEY-VCH Verlag GmBh & Co. KgaA, Weinheim, ISBN 978-3-527-31841-4.

KÁRA J., MUŽÍK O., PAGANELLI D., 2010.: A cost effective solutionfor small-scale biomethane generation. In *NGV 2010, 12th World IANGV Conference and Exhibition, Rome 2010*.

PASTOREK Z., KÁRA J., JEVIČ P., 2004. Biomass – Renewable source of Energy (Biomasa – obnovitelný zdroj energie). Praha FCC Public, ISBN 80-86534-06-5.

DETERMINATION OF MINIMAL COSTS FOR TRACTORS OPERATION USING THE "BOUNDARY LINE ANALYSIS"

Miroslav Kavka*, Miroslav Mimra

Czech University of Life Sciences Prague, Faculty of Engineering,
Department of Machinery Utilization, 165 21 Prague 6 – Suchdol, Czech Republic,
Phone: + 420 224 383 145, E-mail: kvk@tf.czu.cz

Abstract

This article describes application of the so-called "Boundary line analysis method". This method is used to determine the optimal number of tractors owned in an agricultural company by assessing the minimal costs for the tractors' operation. A graph of total annual costs puts together data gained from observation of real usage of tractors in crop production during the year. The assessment of an optimal number of tractors is based on the calculation of operation costs of the owned as well as loaned tractors. To find out the optimal number of tractors owned, it is necessary to reach the minimum of total costs of all technological operations on all fields of the farm. This article works with the results from the analysis made in CULS Farm Estate in Lány. It presents some model solutions, describes the influence of changes of each variable on total costs, and shows how to determine the optimal number of tractors on a farm.

Key words: costs optimisation, fixed cost, variable cost, cost modelling, cost analysis, tractor

Introduction

Increasing prices of inputs oblige the agricultural companies to optimise production costs. This is mainly related to the mechanised works in the crop production. With regards to costs for tractors operations, it is necessary to look for the optimum between number of tractors owned and the possibility to attain some services via outsourcing. Such optimisation always needs to be considered from different perspectives. It is especially important to meet all the agricultural target dates so that the crop is harvested at its highest quality. Also, the failure-free tractor performance, as well as its availability, is essential so that all the activities are done in time. On the other hand, the costs related to the tractors' operation should be taken into account. The maintenance costs significantly affect the final costs as well as the total earnings. Hence the number of tractors must be considered with regards to the aspects of agro-technical deadlines, the quantity of the tractors in the company, and tractor-related maintenance costs.

Abrham et al. (2007) described a system AGROTEKIS used in the Czech Republic. Pulley and Chaplin (2008) developed a computer application called Common Agricultural Tractor Selection System (CATSS). Akarte and Askhedkar (1994) concentrated on calculations of economic effectiveness of tractors deployment in regard to a break-even point calculation of each operation as tillage, soil preparation, sowing etc. Audsley (1984) created another program to elaborate tractor-machine sets optimisation and costs calculation for autumn tillage followed by the soil preparations and sowing. Søgaard and Sørensen (2004) created a model for optimisation of tractor-machine sets that minimises costs.

Jannot and Cairol (1994) developed a model that allows designing the optimal layout of crops in the farm. Based on this, it is possible to calculate gross profit, demand for manpower, equipment requirements and the size of the machine managed land. Camarena, Gracia and Cabrera Sixto (2004) created a model for multiple farms that allows selection of machines from a database for each farm separately. This model allows calculating minimal costs for each of modelled farms based on its size, time working progress, possible combinations of machines, variable and fixed costs predictions including future changes. None of the above mentioned programs allows optimisation of the number of tractors owned by the farm with regards to tractors deployment according to works during the year and possibility to provide part of works through hired services in order to reduce costs related to tractors deployment.

Material and method

The University Farm in Lány operates on 2 955.29 ha of land of which 2 667.56 ha is arable. There are 23 tractors available: twelve tractors have the engine output up to 100 kW, six tractors up to 170 kW, five tractors above 170 kW and their average age is 18 years. The technical data was monitored during the whole year. The number of the tractors was observed for each pentad (meaning use of the tractor during five days) and at the same time, a number of working hours was monitored. This monitoring was performed in line with following operation groups: overheads, fertilisation, basic soil tillage, grain and fodder crops. The observed tractors were put into record according to this three output categories: up to 59 kW, 60 to 100 kW, above 100 kW and the data was consequently analysed. Also, the costs for operations of tractors owned plus outsourced services were monitored.

The costs analysis is done by a “Boundary line analysis”. This method summarised the costs of the owned tractors’ operation and the tractors which were being outsourced (secured by the services) in line with a formula (1). Subsequently the costs are shown in a graph according to the pentads. The graph shows the total costs, whereas the boundary line corresponds with the number of tractors owned by the company. It divides the graph into costs attributable to tractors owned (space under the line) and costs attributable to the operations secured by services (the space above the line).

The economically optimal number of tractors owned is determined as a minimum of total annual costs for the combined use of owned and outsourced tractors. For the assessment of the tractors’ operation costs, the number of tractors owned was between 0 to 30 pieces and number of outsourced tractors between 22 and 0. This model calculation was done for the following settings: where all works were performed by outsourced tractors only; or a combination where 30 owned tractors and none outsourced was used. The calculation of the analysis uses the maximum of 22 outsourced tractors which is the optimum able to do all necessary works in the company. Regarding tractors owned, a number exceeding the actual situation was chosen in order to incorporate the modelling cost flow when increasing the number of tractors owned. The cost modelling was done by using MS Excel functions and tools.

$$TAC = \sum AFC + \sum_{p=0}^{n} (T_{vp} \cdot UVC \cdot k_p) + \sum_{p=0}^{n} (T_N \cdot C_p \cdot k_p)$$

[CZK/year] (1)

where:

TAC – total annual costs of tractors operation in the company

AFC – annual fixed costs of owned tractor operation

T_{vp} – number of necessary owned tractors in the company in an interval

T_v – number of tractors owned by the company within a year

UVC – unit variable costs of owned tractor operation

p – pentad of tractors operation within a year (p = 0 to n)

C_p – price for service per hour

T_N – number of hired tractors in the company in an interval

C_p – price for service per hour

k_p – pentad parameter (k_p = 40)

Results and discussion

The bar chart (see Fig. 1) shows a number of necessary tractors in each pentad according to technological operations, whereas it can be seen from the chart that the tractors were used during the season. Fig. 2 indicates tractors according to their levels of performance shown in each pentad. It is clear from the Fig. 2 that the tractors from a lower level of performance are used during the whole year, especially for the “overheads” (meaning works that cannot be assigned to any working process section). Tractors from the higher performance level are used during some seasons mainly for basic working operations such as soil tillage (ZZP), fertilisation and operations related to crops, which is apparent from the Fig. 1 and Fig. 2.

In the Fig. 3, there are running costs of outsourced tractors which decrease quickly based on the growing number of tractors owned. The rapid decrease of these costs is caused by the fact that the outsourced tractors are used only for operations that cannot be secured by tractors owned. Therefore a greater number of tractors owned means a decreasing number of pentads, in which it is necessary to use outsourced tractors; thereby, the related costs decrease as well. The total costs curve shows the progress. The curve was calculated based on formula no. 1 for different combinations of owned and outsourced tractors. The total costs decrease first with an increasing number of the owned tractors and with their use. The minimal level of these total costs is achieved when nine owned tractors are used. This number appears to be economically optimal for the total annual costs of working operations. Subsequently, the curve grows due to the declining use of tractors owned.

[CZK/year]

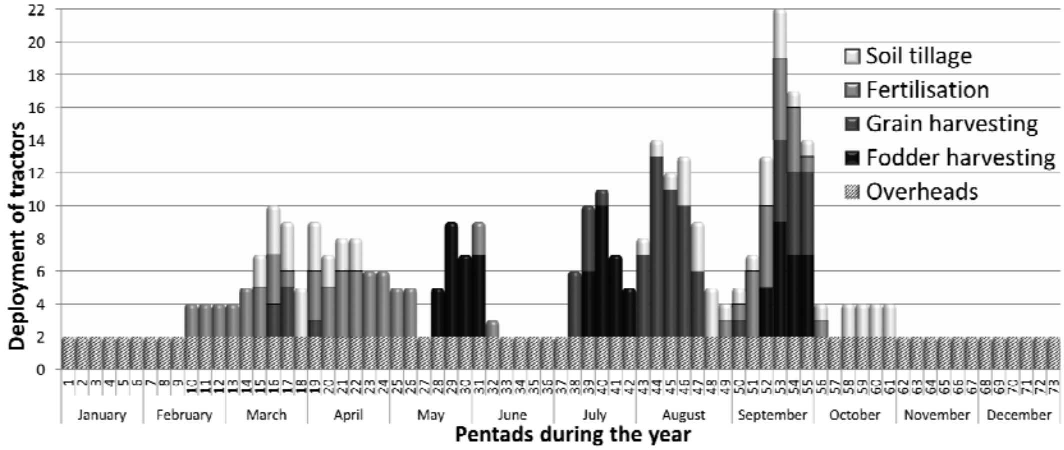

Fig. 1 Tractors used during a year according to working process

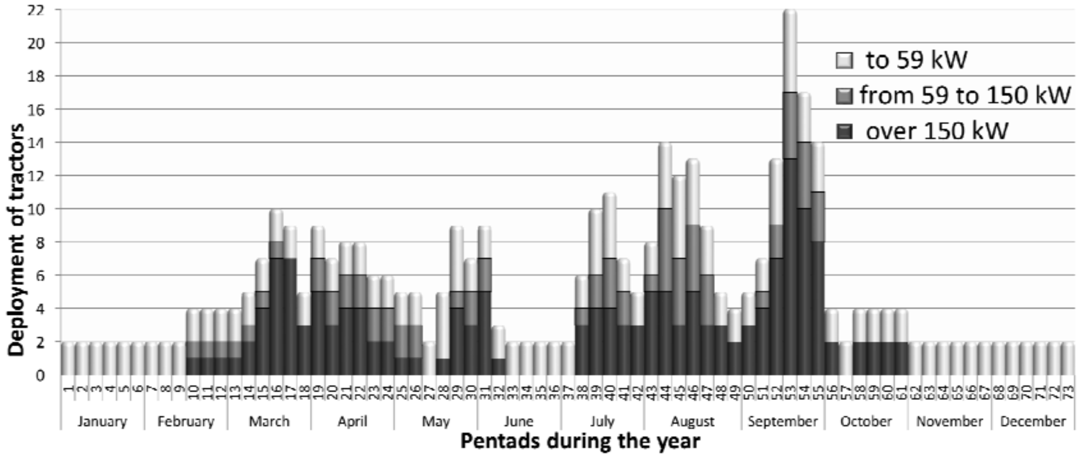

Fig. 2 The bar chart of tractors used during a year according to their performance level

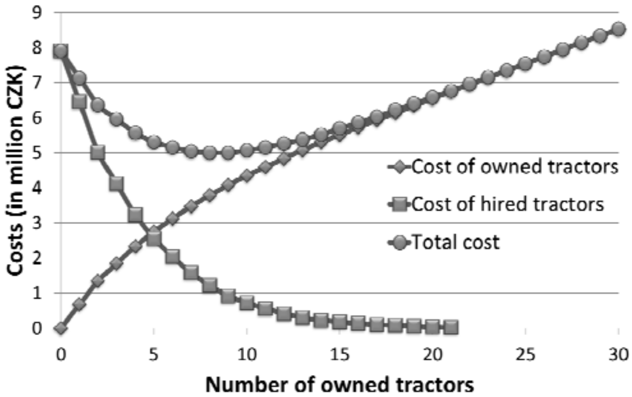

Fig. 3 The line graph of costs of owned tractors, outsourced tractors and annual total costs

The total costs of the tractors' operation (calculated under the formula no. 1 in relation with number of actually deployed tractors in each pentad) are shown as the space represented by the columns in the graph. As it is clear from Fig. 4, using the boundary line analysis divides the graph into two parts, whereas the line represents a number of tractors owned. The area under the line represents the costs of work secured by owned tractors. The area above the line represents the costs of works done by outsourced tractors, i.e. the owned tractors are insufficient for all works during the pentad. It is also apparent from the graph that higher number of tractors is needed only in ten pentads namely during the harvest time when different works are cumulating. From this perspective, it is possible to solve the optimisation by the organisational measures (e.g. to raise the number of tractor shifts, change the planted crop structure etc.).

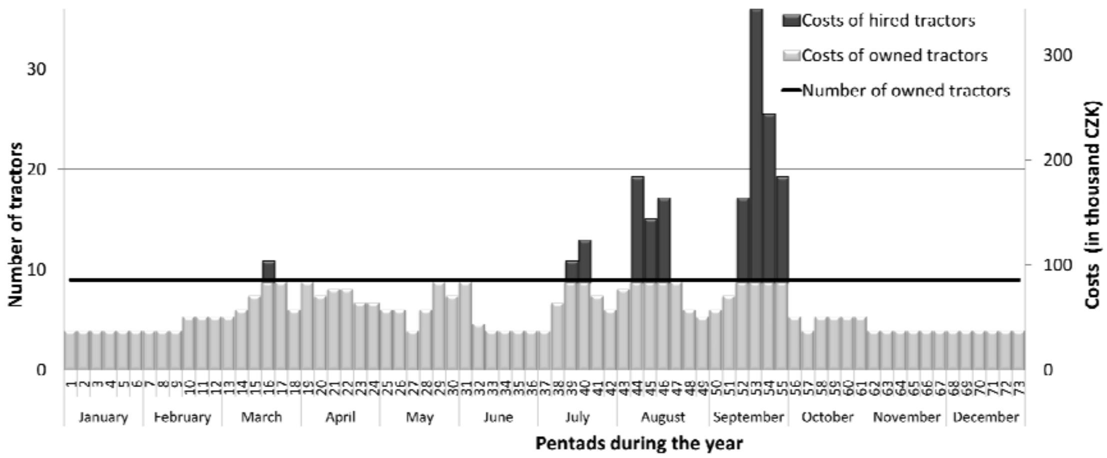

Fig. 4 The structure and timing costs of owned and outsourced tractors

One of the factors that must be taken into account for the calculation of the optimal number of tractors is the anticipated economic development (as the input price changes) which affects works done by both – owned and outsourced tractors. With the help of the “Method of boundary line analysis”, it is possible to model an impact of changed variables.

If there is a drop of prices of outsourced tractors, it will reduce the number of tractors, advantageous for a company to own, from an economical point of view. The curve of total costs will become flatter because the raising part of the curve is created mainly by the operational cost of the owned tractors.

If the hourly variables of owned tractors decrease, then the curve of total costs will become “deeper”, i.e. with an increase in the number of tractors owned, the decrease in total costs accelerates. From this it follows that by reducing variable costs of operating tractors (e.g. reduction of fuel consumption), the company’s total costs can be reduced significantly. Also, it will increase the number of tractors owned, whose operation costs equal the cost of outsourced working operations.

When considering the number of owned and outsourced tractors, the requirements given by agro-technical deadlines must be taken into account, i.e. for timely execution (the operations have to be executed timely in order to avoid further costs caused by delays). Also, it is necessary to keep in mind the operational reliability of the tractors so that the possible breakdowns do not affect the timeliness of execution of technological operations.

In many Czech farms, there are tractors with a high average usage time which often reflects their technical condition as well as fuel consumption. Similarly, the number of tractors owned by the companies is greater than the number of tractors needed to perform work operations. Thus, if the company wants to reduce its costs, it should assess the structure of its tractor fleet to get rid of the unnecessary machines. The optimisation cannot be solved only from an economical perspective but it is important to take into account the agro-technical requirements too.

Conclusion

As the results obtained by using the “Method of boundary line analysis” show, the annual total costs decline depending on the increase of tractors owned at a constant scope of the cultivated area. This decline, however, stops at the point where the tractors owned are not fully used because of an increase in the proportion of fixed costs to operating costs. At this moment, the agricultural company must start to solve the optimisation of the tractors’ usage. Another option is to increase the production scope by widening the cultivated area or to provide services to other companies. Also, it is possible to optimise technological processes (minimisation) or production structure (change of crop rotation or crop), as well as to amend them, so that some technological operations could be done in time when the tractors owned are fully used.

Recently, the University Agricultural Farm in Lány has a higher number of tractors than it would be optimal from the perspective of costs. This is due to the fact that some tractors are of a high average age; so in terms of security and compliance with agro-technical deadlines, it keeps some tractors “in reserve”. Therefore, it would be appropriate to replace older tractors with newer and more powerful ones. The number of tractors owned exceeds the actual need in most pentads. Thus, it is possible to analyse the pentads with a higher deployment of the tractors in terms of the structure of working operations carried out along with an assortment of services offered on the market.

Subsequently, some technological operations can be secured by a form of outsourced services. This measure would bring a significant decrease of annual total costs.

Acknowledgement

This paper is supported by the research project of Ministry of Education, Youth and Sports of the Czech Republic – Projects No. MSM 6046070905

Reference

Abrham Z., Kovářová M., Kocánová V., Herout M., Scheufler V., 2007. Technické a technologické normativy pro zemědělskou výrobu. (Technical and technological norms for agricultural production.) Research Institute of Agricultural Engineering, Prague, 29. (in Czech)

Akarte M.M., Askhedkar R.D., 1994. Economics of tractor utilization for agricultural operations. Modelling, Measurement & Control D: Manufacturing, Management, Human & Socio-Economic Problems, 10 (2): 1-16.

Audsley E., 1984. Use of weather uncertainty, compaction and timeliness in the selection of optimum machinery for autumn field work – A dynamic programme. Journal of Agricultural Engineering Research, 29 (2): 141-149.

Camarena E.A., Gracia C., Cabrera Sixto J.M., 2004. A Mixed Integer Linear Programming Machinery Selection Model for Multifarm Systems. Biosystems Engineering, 87 (2): 145-154.

Jannot P., Cairol D., 1994. Linear Programming as an Aid to Decision-making for Investments in Farm Equipment for Arable Farms. Journal of Agricultural Engineering Research, 59 (3): 173-179.

Pulley R.A., Chaplin J., 2008. A Program to Combine Climate, Soil, and Tractive Modeling Techniques to Predict Agricultural Field-Days and Optimize Tractor Selection. American Society of Agricultural and Biological Engineers Annual International Meeting. Providence, RI; 29 June 2008 through 2 July 2008, 3: 1369-1389.

Søgaard H.T., Sørensen C.G., 2004. A model for optimal selection of machinery sizes within the farm machinery system. Biosystems Engineering, 89 (1): 13-28.

INVESTIGATION OF EXPERIMENTAL FLAT PV THERMAL MODULE PARAMETRES IN NATURAL CONDITIONS

Valeriy Kharchenko*, Boris Nikitin, Pavel Tikhonov, Valentin Gusarov

Russian Scientific Research Institute for Electrification of Agriculture, Moscow, Russia
Phone: +7 (499) 171-96-70; Fax: +7 (499) 170-51-01, E-mail: viesh@dol.ru

Abstract

PV Thermal modules provide co generative producing simultaneously both electricity and heat. Such kind of devices looks to be perspective for use in agricultural householding for covering of consumer requirements in hot water and an electricity.
For heating systems the temperature of produced water is required to be as high as possible while heating up to high temperature negatively affect efficiency of photo-electric transformation of a sunlight, that results in lowering of electricity production. So the temperature of each PV Thermal modules part is very important parameters to be controlled among others during operation time. Results of investigation of PV Thermal module parameters in natural conditions are described and discussed in collation with simultaneously obtained meteorogical parameters.

Keywords: PV thermal modules, meteorogical parameter

Introduction

PV Thermal modules are the devices, uniting together PV modules and solar collectors for water heating, and thanks to that producing simultaneously both electricity and heat as well. This feature makes such kind of devices perspective for use in small scale agricultural householding for covering of consumer requirements in hot water and an electricity.

Despite rather recent beginning of application of PV Thermal (PVT) Technology it has gained considerable enough spreading at practice (Affolter et al., 2013). Water-type PVT technology plays important role in these processes.

The considerable number of works is devoted research of various complicated designs of important part of PT modules - heat collection systems (Chow, 2010; Swapnil Dubey, 2008). However it is represented to us, that flat heat receivers are the most effective in such systems as complication of their designs, causing their rise in price, does not lead to adequate efficiency increase of an overall performance of all module including as PV as well its thermal part.

The thermal and electrical yield of a PV - thermal collector both are very important (Zondag et al., 2003).

For heating systems the temperature of produced water should reach as high meanings as possible while heating up to high temperature negatively affect efficiency of photo-electric transformation of a sunlight, that results in lowering of electricity production. That's why the temperature of each PV Themal (PVT) modules part is very important parameters to be controlled during operation period.
And it is worth to mention that the choice of optimal water working temperature looks to be very important task.

Result and discussion

The scheme of module which was designed and manufactured for investigations is presented at Fig. 1.

Direction of incident solar radiation intake to PVT modules working surface and appearance of the investigated module are resulted on Fig 2.

Research of PVT module parameters was fulfilled by means of the installation which scheme is presented on Fig.3.

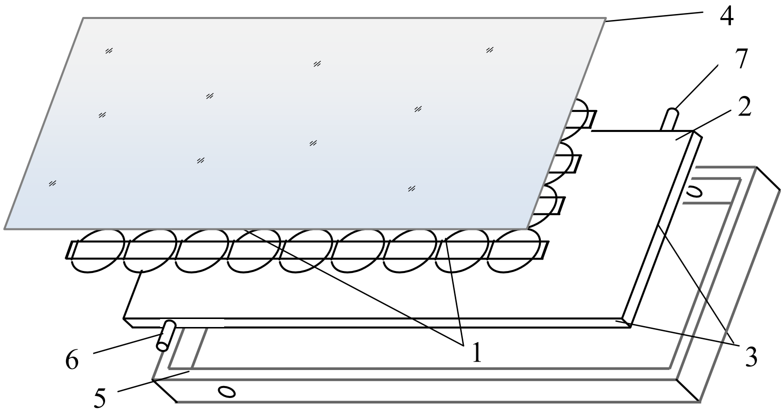

Fig. 1 The experimental PVT module design
1 - PV panel (solar cells battery); 2 - absorber; 3 - tank with a heat-carrier; 4 - transparent isolation (glazing); 5 - heat isolating case; 6 - filling branch pipe; 7 - drain branch pipe.

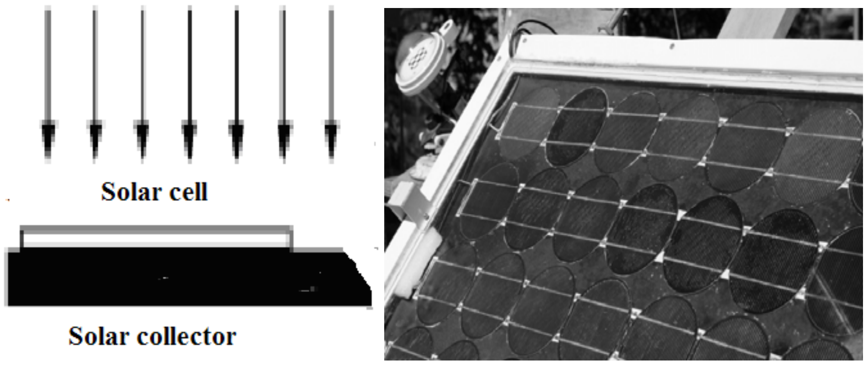

Fig. 2 Direction of incident solar radiation intake to PV Thermal modules working surface (left) and appearance of the investigated module (right). From this figure solar cells disposition on flat collector can be seen on the right.

We have carried out a cycle of researches, in which key parameters of module were considered in a context of simultaneously measured meanings of coming solar radiation. Special value was given to a constant estimation of temperature of various parts PV of the module.

For performance of researches has been used earlier developed (Zondag et al., 2003) complex for key parameters monitoring of solar power facilities with photoconverters.

There were obtained an abundant material concerning parameters of PVT module at different conditions of operation, which permit to identify an optimal mode of operation taking into account requirement of users. This file of the information demands long processing for development of strategy for PVT modules application in agriculture.

Below there are presented some results illustrating efficiency of use of the offered approach for PVT modules certifications and promotion of their penetration in the market of rural electrification.

On Fig. 4 it is visible, as decrease in level of the solar radiation, caused by cloudiness or overcast, influences temperature of PVT module working surface (surface of solar cells) and heat-carrier temperature in the module tank.

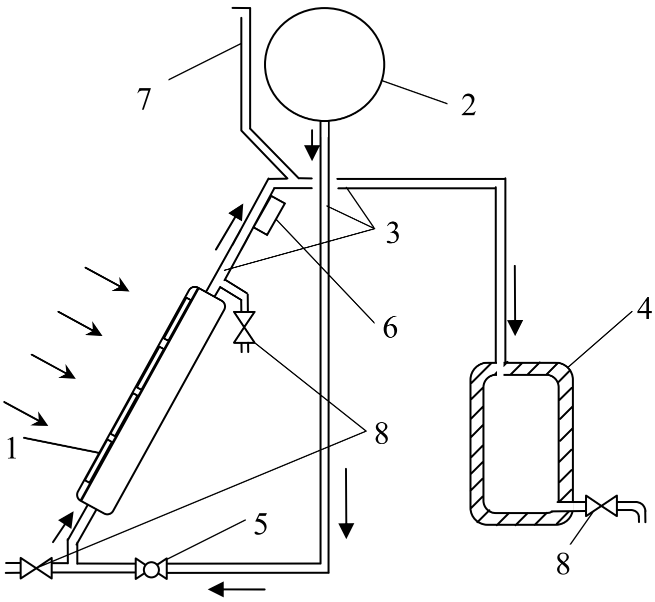

Fig. 3 Experimental installation for PVT module investigation
1-PVT module, 2- 1 – FET modul; 2 – pressure head tank; 3 - pipeline; 4 - storage container; 5 -solenoidal valve; 6 -thermorelay; 7 –air tap; 8 - gate

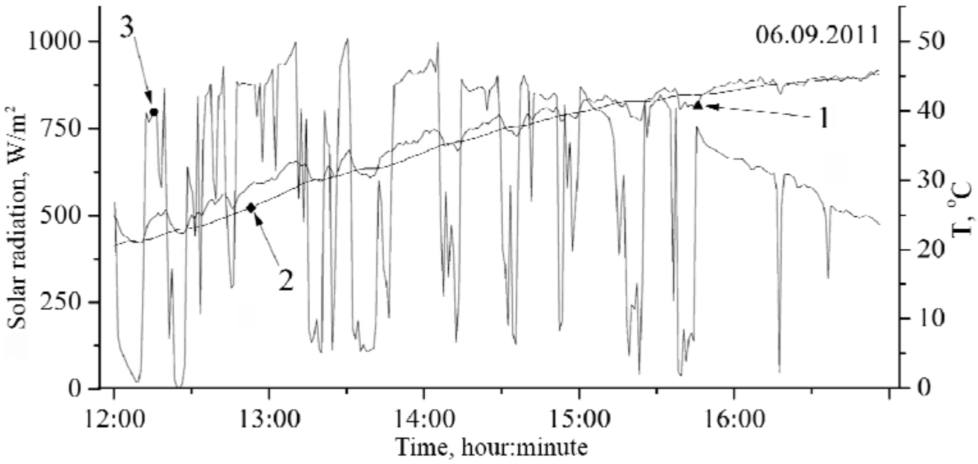

Fig. 4 Temperature of PVT module working surface (surface of solar cells) (1) and heat-carrier temperature in the module tank (2) vs level of solar radiation during operation time (3)

From Fig. 5 it is visible, as strictly PVT module electric capacity is connected with level of coming solar radiation.

On Fig. 6 the data received in rather another conditions, in other day and a lot of time later after the measurements presented on Fig. 5. It is easy to see, that PV panel parameters in accuracy follow all changes of solar radiation. And it is important, that these changes occur inertialessly.

At the same time from Fig. 4 consideration it is easy to notice, that temperature of PV cells surface and the more so heat-carrier temperature in the tank change a little differently. In this case monotonous growth of temperature which takes place and after 16.00 hours when level of solar radiation considerably decreases is observed.

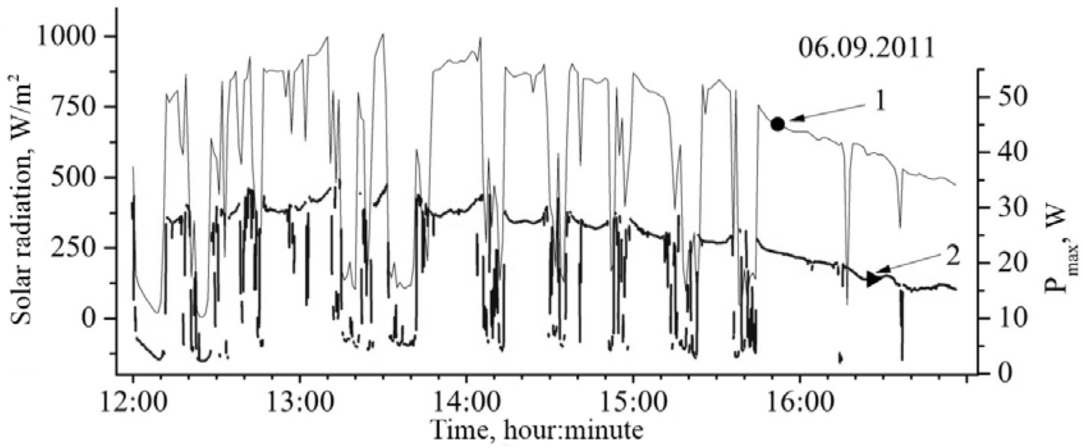

Fig. 5 Influense of solar radiation level on PVT module electric power
1-solar radiation level; 2-electric power of PVT module

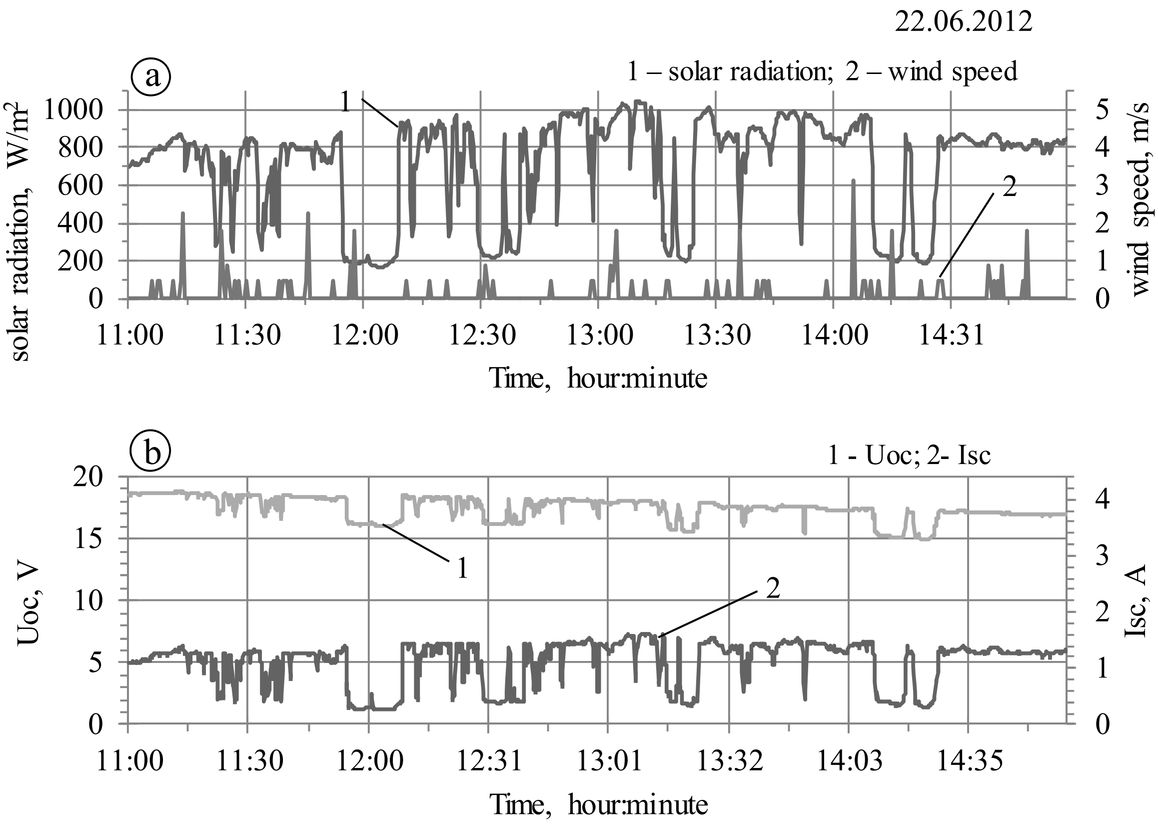

Fig. 6 Results of measurement of key parameters of PVT module photo-electric panel (Uoc and Isc) in comparison to obtained simultaneously results of an estimation of solar radiation level and wind speed
a-meteoparameters (1-solar radiation, 2-weend speed);
b-parametres of the photo-electric panel (1-open circuit voltage, 2-short circuit current

At the same time between changes of temperature of solar cells surface of and changes of temperature of water in the tank there is a distinction. The temperature of solar cells surface of all the same follows changes of solar radiation and it is possible to track some correlation between these changes, though and not such obvious, as for a case of photo-electric parameters.

Conclusion

In connection with inconsistent character of temperature influence on processes of thermal and electric energy generating we have established three possible modes of operation depending on wishes of the consumer.

Depending on consumer requirements it is supposed three basic operating modes of PVT modules:
- maintenance of peak efficiency of electricity production;
- maintenance of peak efficiency of thermal energy production, at warranting to the consumer of necessary temperature of the heat-carrier;
- maintenance of the PVT modules maximum general energy efficiency, at warranting to the consumer of necessary temperature of the heat-carrier.

Each of these purposes can be reached in two ways:
- Working out of special design PVT module
- Development and maintenance of the set mode of operation of modules of a uniform design

In the first case the module design will vary for each problem. While in the second case the problem can be solved at use of the module of the same design, maintained in different operating modes.

It is obvious, that small agricultural consumers use of one specially chosen design, modes of operation of which will be the optimum decision to get out according to inquiries of the end user.

Reference

Affolter P., Eisenmann W., Fechner H., Rommel M., Schaap A., Sørensen H, Tripanagnostopoulos Y., Zond H., 2013. PVT ROADMAP, A European guide for the development and market introduction of PV-Thermal technology // www.pvtforum.org

Chow T.T., 2010. A review on photovoltaic/thermal hybrid solar technology, Applied Energy, 87: 365–379.

Kharchenko V.V., Tikhonov P.V., 2013. Complex for key parameters monitoring of solar power facilities with photoconverters, ISJAEE, 2: 32-36.

Swapnil Dubey G.N., 2008. Tiwari Thermal modeling of a combined system of photovoltaic thermal (PV/T) solar water heater, Solar Energy 82: 602–612.

Zondag H.A., Vries D.W., Van Hendel W.G.J., Van Zolingen R.J.C., Van Steenhoven A.A., 2003. The yield of different combined PV-thermal collector designs, Solar Energy 74 (3): 253-269.

Zondag H.A., Vries D.W., Van Hendel W.G.J., Van Zolingen R.J.C., Van Steenhoven A.A., 2002. The thermal and electrical yield of a PV-thermal collector, Solar Energy 72 (2): 113-128.

SILENCERS FOR REDUCTION OF FAN NOISE

Pavel Kic

Czech University of Agriculture in Prague, 16521 Prague 6 – Suchdol, Czech Republic, Phone: +420 224 383 141, Fax: +420 234 381 828, E-mail: kic@tf.czu.cz

Abstract

To compare two different constructions of noise silencers is the aim of this paper. All buildings used for intensive animal production (poultry, pigs, rabbits breeding) are equipped by forced ventilation or air-conditioning. Food industry and wood processing industry need also intensive ventilation or air-conditioning to provide a suitable and comfortable indoor environment either for the people or for the technological processes.

Principle parts of ventilation system like fans, or air streams passing through air ducts, distribution elements and others components are the main source of noise. The most common air ducts are of round profile. The noise level can be reduced by use of silencers.

The noise control can be based on information provided by manufacturer of fans and on theoretical estimation including the calculation of aerodynamic noise generated by airflow through the air ducts and other air distribution components.

Cylindrical silencers are usually used as a part of ventilation equipment in conjunction with axial fans or installed together with round duct system. There are three main factors which are expected from the noise silencers: noise reduction, low hydraulic resistance a minimal dimensions. These parameters were used as criteria for tested silencers evaluation. In the case of direct installation near to the fan the special Spiral silencer has better results of noise reduction than the standard cylindrical silencer MAA. The other advantage is also minimal dimensions and easy installation into the air-duct. The high hydraulic resistance is the main disadvantage of tested Spiral silencer.

Keywords: noise silencers, animal production, ventilation, air-conditioning

Introduction

The sound is one of the principal features of our modern human civilization and of course of the operation of all machines and technological equipment performance. The undesirable sound is called a noise. The excessive noise endangers living environment and it is one of the more realized environmental factors controlled from the point of view of human health (Jokl, 2002).

The danger of the noise influence on human beings is above all in the small possibility of people to defend against that. That is the main reason why it is necessary to control the noise during the construction of machinery and technology in all production companies. The acoustic environment should be controlled like the other branches of living environment (Novy, 2001).

All buildings used for intensive animal production (poultry, pigs, rabbits breeding) are equipped by forced ventilation or air-conditioning. These buildings are very frequently equipped by axial fans. The most common air ducts are of round profile. Besides housed animals also principle parts of ventilation system like fans, air ducts, distribution elements, or others components are the main source of noise. Reduction of noise is important in these buildings for the suitable indoor environment of housed animals as well as because of the people working in it (Young et al., 2011). The influence of noise to the surroundings housing areas can also be one of the problems. Food industry and wood processing industry need also intensive ventilation or air-conditioning to provide a suitable and comfortable indoor environment either for the people or for the technological processes, which can cause on the other side the indoor noise problems (Novy, 1999).

The noise control can be based on information provided by manufacturer of fans and on theoretical estimation including the calculation of aerodynamic noise generated by airflow through the air ducts and other air distribution components. The noise level can be reduced by use of silencers (Szekyova et al., 2006).

Cylindrical silencers are usually used as a part of ventilation equipment in conjunction with axial fans or installed together with round duct system. To compare two different constructions of noise silencers is the aim of this paper. There are three main factors which are expected from the noise silencers: noise reduction, low hydraulic resistance a minimal dimensions. These parameters were used as criteria for tested silencers evaluation.

Method

All measurements were carried out in the experimental room of the Faculty of Engineering equipped with axial flow fan HCGT/2-315L and short duct for inlet – outlet connection to the outside air, with electric frequency convertor for control of air flow. The construction of fan enables to change position and direction of air flow for inlet and outlet. Measurements were therefore always carried out with both directions of air streams, as an inlet as well as for outlet flow.

The noise level was measured first without the noise silencers and later with two different types of noise silencers connected to the duct system. The influence of noise silencers on the air flow was also controlled by the measurements of air velocity. The influence of both arrangements without and with tube was tested by noise measurement in the rooms A and B. Two different arrangements of noise silencers were tested. In the first arrangement A were silencers installed directly in the room A with the fan in the wall (Fig. 1).

Fig. 1 Standard round silencer MAA connected to the fan (first arrangement A)

The second arrangement B was completed with the air-duct passing from the fan across the part of room A and through the wall into the room B, where the air-duct was finished by the silencers (Fig. 2).

Noise silencers used for the experiments were two types of absorptive silencers. First silencer is a standard industrial product MAA (Fig. 1) for a circular pipe with an inside diameter of 400 mm, outer diameter 620 mm and length 850 mm. The second tested silencer is a special Spiral silencer (Fig. 3), which is installed as a supplement to the ventilation duct of circular cross-section with diameter 400 mm and length 800 mm.

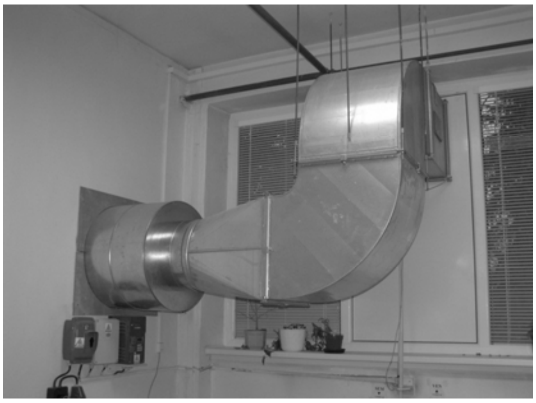

Fig. 2 Standard round silencer MAA connected to the air-duct (second arrangement B)

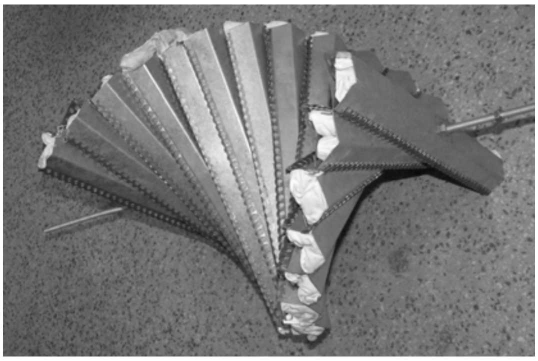

Fig. 3 Special Spiral silencer before installation into the air-duct

The instrument for the noise measurement was noise level measurement device Voltcraft SL – 400 VA. The technical data of this instrument are summarized in the Table 1. The measurements were focused to the equivalent level of noise A, respecting the whole noise exposition. The correction filter A is applied because of the needs of human sense of hearing which is also need according to the recommendations in the literature.

The instrument for the air velocity measurement was anemometer type CFM Master

8901 with rotating vanes with diameter 70 mm. Air velocity operative range is from 0.4 to 30 $m.s^{-1}$, resolution 0.01 $m.s^{-1}$and accuracy ± 2 %.

Table 1 Technical data of noise level measurement device Voltcraft SL – 400 VA.

Parameter	**Technical data**
Microphone	12.7 mm (1/2”) Electret condenser microphone
Sound level ranges	30 – 130 dB (auto range) 30 – 80 dB / 50 – 100 dB / 80 – 130 dB
Frequency weighting	A and C
Time rating	FAST (125 ms) / SLOW (1 s)
Frequency range	31.5 – 8 000 Hz
Resolution of sound levels	0.1 dB

Result

The average value of each noise measurement and also the air flow was calculated from the results of measurement according to the following equation:

$$\bar{x} = \frac{\sum_{i=1}^{n} x_i}{n} \tag{1}$$

where: x_i – value of the i-th measurement,
n – number of measurements.

The results of measurement were statistically evaluated first by F test of variances and according to the results by t-test or Welch test. The main statistical data from results of 10 measurements with silencers installed directly in the room A, just connected to the fan in the wall, are presented in the Tab. 2. The difference between both silencers in air outlet was statistically significant at level 0.05 ($t = 14{,}132 > t_{critical,\ 0.05} = 2.101$) and also for the air inlet was confirmed that the reduction of noise with Spiral silencer was better (statistically significant at level 0.05 ($t = 12.073 > t_{critical,\ 0.05} = 2.101$)).

The results of 10 measurements of noise in the room B with second type of arrangement of air duct with silencers are presented in the Tab. 3. In the case of air out let results were evaluated by Welch test because of results of F test of variances. The difference between measured values with silencer MAA and Spiral silencer in air outlet was statistically significant at level 0.05 ($t = 9{,}249 > t_{critical\ ,\ 0.05\ (10)} = 2.228$). But for the air inlet was confirmed by t test that the difference between the noise of both silencers was not statistically significant at level 0.05 ($t = 1.2327 < t_{critical,\ 0.05} = 2.101$).

There was measured with two directions of air streams (outlet and inlet), both typical for practical use. Table 4 contains the main statistical data of airflows, calculated from the results of 10 measurements of air velocity and cross section of the air-duct. There are obvious from these results differences in the air flows and influence of silencers on it.

Tab. 2 Statistical parameters of noise measurement in the room A (first arrangement)

-	Air Outlet			Air Inlet		
Value	**Without Silencer**	**Silencer MAA**	**Spiral Silencer**	**Without Silencer**	**Silencer MAA**	**Spiral Silencer**
-	dB(A)	dB(A)	dB(A)	dB(A)	dB(A)	dB(A)
Average	74.69	61.71	57.5	75.25	61.09	57.85
Minimum	74.2	60.5	57.1	74.9	60.7	56
Maximum	75.3	62.8	59.1	75.5	61.8	58.4
Stand. Dev.	0.348	0.662	0.6	0.172	0.423	0.685

Tab. 3 Statistical parameters of noise measurement in the room B (second arrangement)

-	Air Outlet			Air Inlet		
Value	**Without Silencer**	**Silencer MAA**	**Spiral Silencer**	**Without Silencer**	**Silencer MAA**	**Spiral Silencer**
-	dB(A)	dB(A)	dB(A)	dB(A)	dB(A)	dB(A)
Average	74.78	62.76	60.38	75.25	61.14	61.03
Minimum	74.2	61.8	60.2	74.8	60.8	60.7
Maximum	75.2	63.9	60.6	75.6	61.4	61.3
Stand. Dev.	0.358	0.803	0.132	0.272	0.196	0.183

Tab. 4 Statistical parameters of air flows in the room B (second arrangement)

-	Air outlet			Air inlet		
Value	**Without Silencer**	**Silencer MAA**	**Spiral Silencer**	**Without Silencer**	**Silencer MAA**	**Spiral Silencer**
-	$m^3.h^{-1}$	$m^3.h^{-1}$	$m^3.h^{-1}$	$m^3.h^{-1}$	$m^3.h^{-1}$	$m^3.h^{-1}$
Average	4,948.8	4,718.4	2,253.5	3,615.2	3,497.3	2,526.6
Minimum	4,445.3	4,127.8	1,927.8	3,084.5	3,220.6	1,905.1
Maximum	5,697.2	5,334.3	2,744.3	3,882.8	3,764.9	3,238.7
Stand. Dev.	320	279	236.2	221.8	182.7	358.1

Discussion

The first experiment with measurement of noise reduction by silencers installed directly in the room A showed that the Spiral silencer reduced the noise level better than standard round MAA silencer in the case of air outlet and also in air inlet. Different situation was in the second type of installation (second experiment). The bigger distance of the end of air-duct from fan and several fittings installed in the air-duct caused smaller reduction of noise by silencers and influenced the final level of noise in the room. There are obvious big differences of air flows in the air inlet as well as outlet in the case of air-ducts equipped by the special Spiral silencer. The average reduction of air flow in comparison with the air flow without silencer was for air outlet by MAA silencer to 95 %, by Spiral silencer to 46 %, and for air inlet by MAA silencer to 97 % and by Spiral silencer to 70 %.

Conclusion

According to three main parameters which were decided in introduction to be criteria for silencers evaluation we can make the following conclusions. In the case of direct installation near to the fan the Spiral silencer has better results of noise reduction than the standard cylindrical silencer. The high hydraulic resistance is main disadvantage of Spiral silencer. This principle and special construction of noise silencer was tested mainly because of minimal dimensions and easy installation into the air-duct. These are main advantages of this system. There should be paid more attention to the simplification of this type of silencer, especially to the reduction of its hydraulic resistance in the future research of these constructions.

Reference

Jokl M., 2002. Healthy living and working environment. Academia. Prague: 261. (in Czech)

Novy R., 1999. Noise in air-conditioning and its reduction. In: 14th Conference. Air-conditioning and ventilation for the next century. Prague: 180-182. (in Czech)

Novy R., 2001. Noise emissions of burning equipment. In: 16th Conference about heating. Praha: 147-150. (in Czech)

Szekyova M., Ferstl K., Novy R., 2006. Ventilation and air-conditioning. JAGA. Bratislava: 359. (in Czech)

Young M.T., French A.L., Clymer J.W., 2011. An Effective, Economical Method of Reducing Environmental Noise in the Vivárium. J. Am. Assoc. Lab. Anim. Sci., 50 (4): 513–515.

WATER QUANTITY AND QUALITY MONITORING FOR STREAM DEPLETION INVESTIGATION IN RURAL AREA

Sang Min Kim[1*] . Sung Min Kim[2] . Ye Eun Lee[2]

[1]Dept. of Agricultural Engineering (Inst. of Agric. & Life Sci.), Gyeongsang National Univ., Jinju 660-701, Korea, E-mail: smkim@gnu.ac.kr
[2]Graduate School, Gyeongsang National Univ., Jinju 660-701, Korea

Abstract

The purpose of this study was to monitor the stream flow of rural streams for investigating the status of stream depletion located downstream from irrigation reservoirs. The Bonghyun and Hai reservoirs, located in Hai-myeon, which is in the city of Gosung in the Gyeongnam Province, were selected for stream and watershed study. The stream flow monitoring was conducted seven times from March to September, 2011. The stream flow was measured in eight stations downstream from the two reservoirs. Stream depletion was found in most of the reservoirs downstream for the non-irrigation periods, and even in the irrigation periods when there were a lot of antecedent precipitation. The correlation analysis for water quality data indicated that the correlation between BOD and T-N was highest for the reservoirs. The correlation among BOD, T-N, and turbidity was high for both the Hai and Bonghyeon reservoirs. Continuous monitoring of rural streams located downstream from reservoirs are required to quantify the status of stream flow depletion, as well as to determine the amount of environmental flow.

Keywords: Environmental flows, Stream flow monitoring, Irrigation reservoir, Water supply

Introduction

Due to massive urbanization and industrial restructuring of Korea during its rapid economic growth period after 1970, Korea's waterside environment has been severely destroyed. In particular, the mass production and consumption from human activities released pollutants in excess of the self-purification systems in streams; consequently, the streams have lost their original functions (Yang, 2004). In recent years, interests about the environmental functions of streams as a buffer zone have increased as citizens' income levels and their quality of life improve. Also, a reassessment is being made actively about the ecological and environmental features in the cities of Korea. (Lim, 2001). Therefore, a need for the introduction of water used for environmental maintenance has been raised. The maintenance of stream flow is defined as the drought flow of streams in need to maintain the normal functioning of the streams (Kim, 2011). However, the natural and social conditions, while considering the possibility of using the supply capabilities of water for the maintenance of streams were calculated by considering the eight categories of water quality maintenance (KRCC, 2010). Currently, the many streams in Korea have lost their function as water sources. The drying out of medium-sized and small streams due to the lack of water in them will cause problems in irrigation, along with agricultural land shortages, with an increase in water pollution and a loss of function of the environment. As a result, the loss of economic aspects worsens every year. Hwang & Lee (2005) suggest that there is an urgent need to seek causes and implement preventive measures.

Most advanced nations have accumulated environmental technology and know-how about water management. By contrast, Korea has not yet achieved sustainable environmental water management, and knowledge about the hydraulic characteristics of streams and ecosystems has been very limited. Environmental water management with its unique environment of watersheds, having a constant flow like drought flow, was also thought to be limited. In the past, most studies were based on the habitat evaluative methods of fish for the environment with their optimal flows (KICT, 1995). The introduction of automated equipment is difficult and requires the participation of skilled ecology professionals. A few overseas examples are the IWMI (International Water Management Institute), the IBRD (International Bank for Reconstruction and Development), and the CRC (Co-operative Research Centre). They operate on-site monitoring systems adapted for specific purposes in environmental water maintenance. At the same time, thess systems are equipped with estimation procedures to determine appropriate environmental water levels according to the levels of the observed performance data. In other words, the previous case shows that on-site monitoring is extremely important (KRCC, 2010). It shows the importance of systematic on-site monitoring. Therefore, the purpose of this study was to monitor the stream flow of rural streams in order to investigate the status of stream depletion located downstream from irrigation reservoirs.

Material and method - Watershed Study

The Bonghyun and Hai reservoirs, located in Hai-myeon, which is in the city of Gosung in the Gyeongnam Province, Korea were selected for watershed and stream study. The Seokji stream has a length of approximately 2,600 m from the Hai reservoir spillway. The Seokji and Bonghyeon streams meet downstream. The flow goes into the southern sea. The Bonghyeon reservoir has a watershed area of 2.80 km^2 and the irrigation area is 0.38 km^2. The Hai reservoir has a watershed area of 13.42 km^2, and the irrigation area is 1.67 km^2. The scale of the land use data by the Ministry of Environment is 1:25,000 which indicates that paddies cover 62.3% of the total area or 4.40 km^2. Cropland has an area of 0.71 km^2 and the residential area is 0.75 km^2. The remaining area covers 17% of the total area. Stream water is released regularly from the reservoirs to use as irrigation water because most of the area is covered with paddies.

Meteorological data

It is important to have a steady water supply to prevent stream depletion. The outflow discharge, the amount of evapotranspiration, and reservoir flood routing should be considered in order to maintain stream environment. The weather data was collected from the Jinju weather station from 1970 through 2011. The rainfall data is divided into irrigation periods and non-irrigation periods (Fig. 1). The city of Jinju's annual average precipitation was 1,503 mm, higher than Korea's annual average precipitation. In 1989, Jinju's annual average precipitation reached a record high. It reached a low 784.9 mm in 1994. According to the weather data, the mean wind velocity in Jinju was the fastest at 2.9 m/s. The lowest was when the relative humidity was 45.2% in February, 2000. The mean wind velocity was lowest at 0.8 m/s in 1977, 2006, 2007, and 2008. 284 hours of recorded sunshine were the most recorded in July, 1994 and the lowest of 32.2 hours were recorded in July, 1984.

Reservoir Storage Capacity Assessment and Investigation

A selection of watersheds was made for the study after considering their accessibility, their storage amount, stream lengths, and the usages of riverbeds from the reservoirs. The Hai reservoir (Standard code, 4882010042), located in Hai-myeon, which is in the city of Gosung in the Gyeongnam Province, Korea was completed in 1971. Now it is managed and operated by the Goseong and Geoje offices of the Korean Rural Corporation. The Hai reservoir is a fill dam. It has 1,000 m^3 in volume, is more than 23.2 m tall and has a length that just reaches 394 m. The Hai reservoir can store $2,594\times10^3$ tons of water. The design frequency of droughts is 10 years, and the flood frequency is 200 years. The Bonghyun reservoir (Standard code, 4882010045) is also located in Hai-myeon but was completed in 1998. It is also managed and operated by the Goseong and Geoje offices of the Korean Rural Corporation. This reservoir is also a fill dam, as the Hai reservoir. The Bonghyun reservoir is 90,823 m^3 in volume, is more than 28.4 m tall and has a length that just reaches 246 m. The Bonghyun reservoir can store 910×10^3 tons of water, its design frequency of drought is 10 years, and its flood frequency is 200 years.

River Survey

The standard stations and periods were determined after considering the conditions that affected the changes in flow. Five stations were downstream: 750 m, 1,260 m, 1,730 m, 4,190 m, and 5,500 m from the Bonghyeon reservoir. Three stations were downstream: 30 m, 2,000 m, and 2,810 m from the Hai reservoir. A total of eight stations were selected to measure time-flow. The period under study was selected to compare with the irrigation periods and the non-irrigation periods from March through September, 2011. Stream monitoring was conducted regularly at the end of every month.

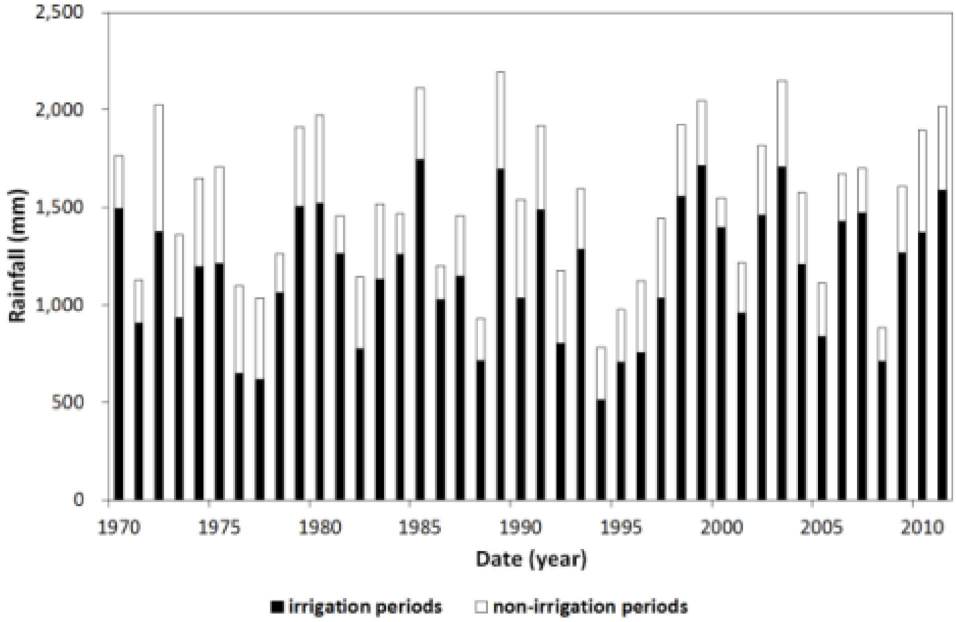

Fig. 1 Compared rainfall of irrigation periods (May-Oct.) and non-irrigation periods (Nov.-Apr.)

Statistical Analysis Method of River Water Quality Data

In this study, the water quality data at each station were statistically analyzed using the partial correlation coefficients. The control variable was the flow. The water quality factor was the independent variable. The commonly used Pearson's correlation coefficient r was the correlation coefficient of the two variables X and Y. The values for each case (x_1, y_1), (x_2, y_2), ..., (x_n, y_n) when the following equation (1) was calculated:

$$r = \frac{S_{XY}}{S_X \cdot S_Y} \tag{1}$$

S_X: The standard deviation of $X = \sqrt{\frac{\sum (x_i - \bar{x})^2}{n-1}}$

S_Y: The standard deviation of $Y = \sqrt{\frac{\sum (y_i - \bar{y})^2}{n-1}}$

Result and discussion, analysis of the Reservoir and River

From March to September, 2011 a total of seven field surveys were conducted to measure the water levels of the observed stream stations. The flow was calculated by measuring the flow speed of a cross-sectional area of stream. The changes in stream flow were analyzed according to five days of antecedent precipitation. According to Tab. 1, the low outflows of reservoir and rainfall were dry at all times from March to May. On June 29th, a large amount of antecedent precipitation was expected to create a large river flow. However, a stream flow did not occur downstream of the Hai reservoir. Also, the majority of the stations at Bonghyeon stream had little stagnant or no amount of water. It was presumed that the ground surface was dry before the start of rainfall. Relatively, the many outflows from the reservoir and rainfall had a flow of a fixed quantity from July to September. In Tab. 2, the average flow of each station from May to September during the irrigation periods is relatively larger than the average flow of each station from March to April during the non-irrigation periods. The flows of each station are shown to have a small difference, but the irrigation periods and the non-irrigation periods are shown to have large differences in flow.

During the actual field survey, some sections appeared to have a flow reduction due to the impact around the station from kiwi-fruit orchards, mills, and barns. At the Seokji stream, despite the rainy season in July, the flow appeared to have a significant decrease at the point of 2,000 m. This phenomenon was estimated to be from the result of the impact of plentiful grass, as well as the presence of beams and kiwi-fruit orchards located from the reservoir downstream. At the Bonghyeon stream, the flow appeared to have a significant decrease at the point of 4,000 m. This was estimated to be due to the pumping of water from the kiwi-fruit orchards to be used as irrigation water. The flow increases at several junctions of the stream was determined to be affected from the effluent coming from the inlets and drainage areas of Seokji stream.

Tab. 1 Stream discharge for each monitoring section with 5 days antecedent precipitation and reservoir storage (2011)

Date	Antecedent precipitation (mm)	Seokji Stream				Bonghyeon Stream					
		Storage in Hai reservoir (%)	stream discharge (m^3/s)			Storage in Bonghyeon reservoir (%)	stream discharge (m^3/s)				
			530 m	2,000 m	2,810 m		750 m	1,260 m	1,730 m	4,190 m	5,500 m
03/26	0.3	90	0.00	0.00	0.00	92	0.00	0.00	0.00	0.00	0.00
04/29	8.5	98	0.00	0.00	0.00	100	0.00	0.00	0.00	0.00	0.00
05/28	25.5	93	0.00	0.00	0.00	100	0.00	0.00	0.00	0.00	0.00
06/29	150.5	85	0.21	0.00	0.00	100	0.14	0.00	0.30	0.00	0.36
07/28	45.5	99	1.11	0.80	3.47	94	0.05	0.26	0.71	0.29	1.03
08/29	14.1	89	0.00	0.00	0.00	94	0.00	0.14	0.24	0.00	0.07
09/26	0.0	58	0.13	0.00	0.00	63	0.00	0.10	0.05	0.00	0.08

Tab. 2 Stream discharge for irrigation and non-irrigation periods (2011)

Period	Discharge of Seokji stream (m^3/s)			Discharge of Bonghyeon stream (m^3/s)					Average discharge (m^3/s)
	530 m	2,000 m	2,810 m	750 m	1,260 m	1,730 m	4,190 m	5,500 m	
Non-irrigation	0.00	0.00	0.00	0.00	0.00	0.00	0.00	0.00	0.00
Irrigation	0.29	0.16	0.69	0.04	0.10	0.26	0.06	0.31	0.24

Analysis of the Reservoir and River Water Quality

Using a portable water quality measuring device, the pH of the agricultural reservoirs and the rivers was measured a total of seven times to investigate the changes in water quality. The National Instrumentation Center for Environmental Management (NICEM) at Seoul National University was asked to analyze the following seven items of water quality: BOD, COD, TOC, SS, Turbidity, T-P, and T-N. The results in Tab. 3 show the analyses of each water quality item according to the survey period of watershed study. July was the only month in which the water samples were able to be collected. In all the other months, it was difficult to measure the water quality and flow due to the streams being dry.

Tab. 3 Water quality analysis of Seokji stream and Hai reservoir

Hai		pH	BOD (mg/L)	COD (mg/L)	TOC (mg/L)	SS (mg/L)	Turbidity (NTU)	T-P (mg/L)	T-N (mg/L)
03/26	Reservoir	7.54	0.27	2.80	1.74	0.0	0.42	0.003	0.412
	530 m	7.80	0.99	1.36	1.84	0.0	0.41	0.007	0.247
04/29	Reservoir	7.22	1.25	1.46	2.74	2.0	1.68	0.020	0.659
	530 m	7.19	0.52	1.84	1.90	2.0	0.79	0.009	0.576
05/28	Reservoir	7.06	0.24	1.16	2.12	16.0	0.32	0.022	0.000
	530 m	6.79	0.78	2.78	3.48	12.0	1.11	0.193	0.000
06/29	Reservoir	7.06	1.73	2.82	2.34	11.0	1.63	0.055	0.817
07/28	Reservoir	7.02	1.77	2.02	2.06	8.0	0.98	0.021	0.577
	530 m	7.12	1.17	1.60	1.75	8.0	0.25	0.080	0.796
	2,000 m	7.10	1.45	1.46	1.53	4.0	0.55	0.017	0.851
	2,810 m	7.08	0.85	1.60	1.36	3.0	0.33	0.028	1.510
08/29	Reservoir	6.72	0.66	2.18	1.90	3.0	0.96	0.020	0.577
	530 m	7.05	0.81	1.26	1.28	4.0	0.46	0.010	0.412
09/26	Reservoir	7.13	1.13	1.26	1.730	6.0	1.30	0.031	1.098
	530 m	7.35	0.23	0.72	1.070	0.0	0.32	0.029	0.000

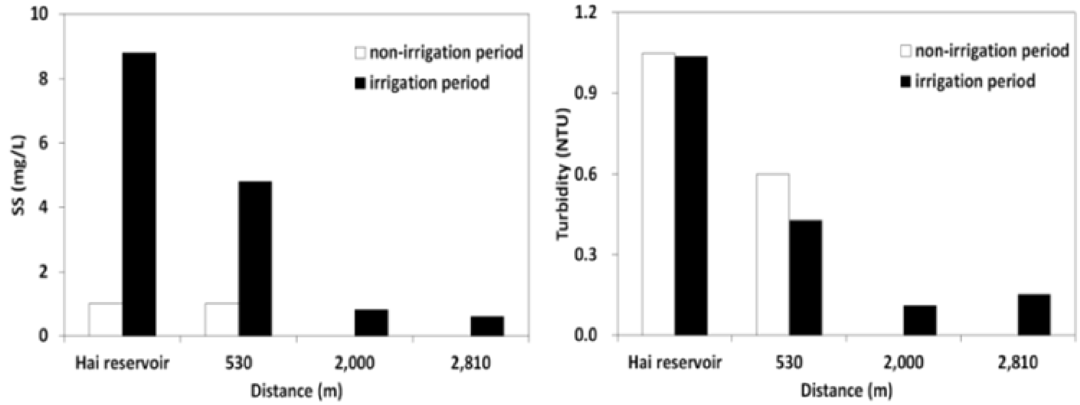

Fig. 2 SS and Turbidity variations for irrigation and non-irrigation periods of Seokji stream

Fig. 2 shows the SS and Turbidity variations of Seokji stream. The variations were divided into irrigation and non-irrigation periods to analyze the changes in water quality to the differences in the flow. The pollutant concentrations regarding COD, TOC, and Turbidity of the non-irrigation periods were slightly higher than the pollutant concentrations of the irrigation periods in the Hai reservoir. The pollutant concentrations of the regarding SS, COD, COD, TOC, Turbidity, T-N, and T-P of the non-irrigation periods were higher than the pollutant concentrations of the irrigation periods in the Seokji stream. The contaminant concentrations decreased nearer downstream. However, at the last station, there was a showing of an increase in concentration. This phenomenon was judged to be from the effects of ambient pollutants, like incinerated waste. The concentrations of SS were almost immeasurable during the non-irrigation periods. However, the concentrations of SS were judged to be high due to the inflow of ambient pollutants during the irrigation periods.

Correlation Analysis between Water Quality Parameters

The correlation of water quality items from the reservoir and stream studies were analyzed using the water quality data obtained in July. Water quality was the independent variable and the control variable was the flow. In the case of the station located 530 m of Seokji stream, the correlation coefficients between SS and T-P, and TOC and Turbidity were shown to be 0.925 and 0.960, respectively at a 0.01 level of significance. The correlation coefficients between COD and TOC, SS and TOC, SS and Turbidity, and TOC and T-P were shown to be 0.865, 0.854, 0.856, and 0.836, respectively at a 0.05 level of significance (Tab. 4). In the case of the station located 750 m of Bonghyeon stream, the correlation coefficient between COD and TOC was shown to be 0.887 at a 0.05 level of significance. At the station located 1,260 m of Bonghyeon stream, the correlation coefficients between the pH and COD, the pH and TOC, BOD and T-N, and COD and TOC were shown to be 0.920, 0.930, 0.938, and 0.932, respectively at a 0.01 level of significance. The correlation coefficients between the pH and T-P, BOD and COD, BOD and T-P, COD and T-P, TOC and T-P were shown to be 0.813, 0.814, 0.822, 0.866, and 0.818, respectively at a 0.05 level of significance (Tab. 5).

Tab. 4 Correlation analysis of water quality data at Seokji stream (530 m)

	pH	BOD	COD	SS	TOC	Turbidity	T-P	T-N
pH	1.000	0.649	0.672	0.294	0.631	0.578	0.229	0.535
BOD		1.000	0.594	0.777	0.743	0.777	0.534	0.467
COD			1.000	0.571	0.865*	0.744	0.530	0.449
SS				1.000	0.854*	0.856*	0.925**	-0.069
TOC					1.000	0.960*	0.836*	0.188
Turbidity						1.000	0.800	0.238
T-P							1.000	-0.343
T-N								1.000

* $p<0.05$, ** $p<0.01$

Tab. 5 Correlation analysis of water quality data at Bonghyeon stream

		pH	BOD	COD	SS	TOC	Turbidity	T-P	T-N
750 m	pH	1.000	0.335	0.652	-0.408	0.791	0.041	-0.185	-0.429
	BOD		1.000	0.756	0.104	0.710	-0.586	-0.144	0.004
	COD			1.000	-0.064	0.887*	0.033	-0.591	0.055
	SS				1.000	-0.366	-0.126	0.362	-0.350
	TOC					1.000	-0.057	-0.413	0.040
	Turbidity						1.000	-0.554	0.315
	T-P							1.000	-0.642
	T-N								1.000
1,260 m	pH	1.000	0.660	0.920**	0.158	0.930**	0.655	0.813*	0.503
	BOD		1.000	0.814*	-0.156	0.768	-0.070	0.822*	0.938**
	COD			1.000	-0.209	0.932**	0.452	0.866*	0.759
	SS				1.000	0.002	0.229	-0.044	-0.450
	TOC					1.000	0.429	0.818*	0.700
	Turbidity						1.000	0.417	-0.200
	T-P							1.000	0.727
	T-N								1.000

* $p<0.05$, ** $p<0.01$

Conclusion

In conclusion, this study shows that there was a low outflow from the reservoir during the survey period. Therefore, it can be concluded that these streams were heavily influenced by their surroundings. This phenomenon shows the necessity of environmental water maintenance. The continuous monitoring of rural streams located downstream from reservoirs is required to quantify the status of stream flow depletion and to determine the amount of environmental flow. Through continuous monitoring and observations, we will be able to discover some preventive measures to prevent the drying out of rural streams located downstream from reservoirs.

Acknowledgment

This study was sponsored by the Korea Research Foundation of the Ministry of Education, Science, and Technology (code number: 2011-0005297).

Reference

Hwang B.G., Lee J.S., 2005. Methods to Prevent Hongjechun Stream from Becoming Dry and Maintenance Discharge. Sangmyung University, Research Institute of Engineering and Technology, 2: 1-7. (in Korean)

Kim S.M., Kim S.J., Kim S.M., 2011. Streamflow Monitoring of Rural Small Streams for Environmental Flows Supply from Irrigation Reservoir. Journal of Agriculture & Life Science, 45: 237-249.

Korea Institute of Construction Technology (KICT), 1995. Development and Application of Instream Determination Methods. IPD-95-2. Korea Water Resources Corporation (K-water), 247-264.

Korea Rural Community Corporation (KRCC), 2010. The Study for Estimation of Environmental Flows in Rural Areas. Rural Research Institute.

Lim, H. M., 2001. "Restoration of Anyang - Focusing on Upstream of Anyang and Hagui Streams". Magazine of Korea Water Resources Association, 34, 65-74 (in Korean).

Yang, H. K., 2004. "Drying Stream and Hydrological Environment for Gwangjucheon". Journal of the Korean Association of Geographic Information Studies, 10, 568-578 (in Korean).

DEVELOPMENT OF A NONDESTRUCTIVE DETECTOR OF UNSUITABLE CHICKEN EGGS USING LED LIGHTS FOR INFLUENZA VACCINE PRODUCTION

Kohei Kimura[1*], Kazuhiro Nakano[1], Shintaroh Ohashi[2], Kenichi Takizawa[1], Takayuki Nakano[3]

[1]Graduate School of Science and Technology, Niigata University, 8050, Ikarashi Ninocho, Nishi-ku Niigata, 950-2181, Japan
[2]Faculty of Agriculture, Niigata University, 8050, Ikarashi Ninocho, Nishi-ku Niigata, 950-2181, Japan
[3]Kagoshima Immaculate Heart University, Kagoshima, Japan
corresponding author: Phone:+81-25-262-6648, Fax:+81-25-262-6648,
E-mail:knakano@agr.niigata-u.ac.jp

Abstract

In Japan, fertilized chicken eggs are used to produce influenza vaccines. However, some fertilized eggs do not develop after fertilization, develop late, or die during development. If these unsuitable eggs are overlooked and included with normal eggs in the vaccine production process, the manufacturer must dispose whole of the vaccine stock solution in a tank, which results in large economic losses and raises health concerns. Therefore, a nondestructive method that allows distinction of normal and unsuitable chicken eggs was developed, using visible and near-infrared (VNIR) spectroscopy and a light-emitting diode (LED) light source. Normal and unsuitable eggs were sampled from an egg farm, where an experienced farmer assessed the eggs by candling. Linear discriminant analysis was applied using wavelength absorbance data to distinguish between normal and unsuitable eggs, and all of the optical absorbance values of the normal eggs were found to be higher than those of unsuitable eggs. The rate of discrimination between the two types of eggs exceeded 95.8 % when LED board was used. To reduce the production cost, LED lights and photodiodes were used as the light source and light receptors, respectively. The discrimination rate when LED was used as the light source was lower than that when a halogen lamp was used, but was almost the same discrimination rate. LED should be used singly to prevent the adjacent LED light sources from affecting detection because the surrounding LED lights affected the photodiode, thereby reducing the discrimination rate.

Keywords: fertilized chicken egg, influenza vaccine, nondestructive detection, VNIR spectroscopy, linear discriminant analysis, LED

Introduction

Influenza is an infectious disease with global prevalence and is caused by the influenza virus. Seasonal variations in influenza are characterized by peak prevalence in winter worldwide. Additionally, a new strain of pandemic influenza, H1N1, caused 18,500 laboratory-confirmed deaths from April 2009 to August 2010 (Dawood et al., 2012). Influenza vaccination is often recommended to reduce the risk of contracting the disease, especially for children, pregnant women, and the elderly. Fertilized chicken eggs developing steadily (hereafter referred to as "normal eggs") are used to manufacture influenza vaccines through injection of strains of the virus into the eggs, followed by incubation for 12 days. However, some fertilized eggs do not develop after fertilization, develop late, or die during development. If these eggs (hereinafter referred to "unsuitable eggs") are overlooked and included with normal eggs in the production process, the manufacturer must dispose of the vaccine stock solution, which results in large economic losses and raises health concerns. Macroscopic inspection by candling is conventionally used to eliminate unsuitable eggs in shipping trays. However, this inspection method is labour intensive and cost intensive. Therefore, the development of an automated, nondestructive method that can replace macroscopic inspection is crucial.

In recent years, a nondestructive technique using visible and near-infrared (VNIR) spectroscopy has been found to be useful for nondestructive evaluation in various fields. In the field of agriculture, this technique allows the evaluation of the internal quality of vegetables and fruits. Nondestructive method has been applied for quantitative and discriminative analyses, such as the detection of external insect infestation in jujube (Wang et al., 2011). A previous study showed that this nondestructive technique could be used to detect unfertilized eggs containing blood spots or having cracked shells (Usui et al., 2003). In fertilized eggs, blood vessel formation indicates a more advanced stage of development and can be detected through absorption of light by haemoglobin in the blood vessels.

Light-emitting diodes (LEDs) are used as light sources in various agricultural fields. For example, LED-based fluorescence imaging is used for evaluation of plant seedling water stress (Hsiao et al., 2011). In contrast to other light sources such as fluorescent lamps and halogen lamps, LEDs can provide irradiation with specific wavelengths such as purple to red in the visible light region as well as wavelengths in the near-infrared light region. In addition, the cost of LED light sources is lower than that of other light sources such as halogen lamps, and cost is an important factor to consider, because nondestructive detectors require multiple light sources to concurrently measure one tray (36 eggs) during vaccine manufacture.

Thus, the specific objectives of this study were to (1) determine the wavelength of LED for use in VNIR spectroscopy, (2) discriminate between normal and unsuitable eggs by using LED light in a nondestructive detector.

Materials and method

Egg samples

In this experiment, the eggs purchased from a farm were white, fertilized chicken eggs that had been warmed for 12 days in a dark incubator under a controlled environmental temperature of 38 °C. Each egg had been selected as normal or unsuitable by farm workers using the candling technique. Unsuitable eggs were unequal with regard to the developmental stage. Normal and unsuitable eggs were divided into a calibration set and prediction set for evaluation.

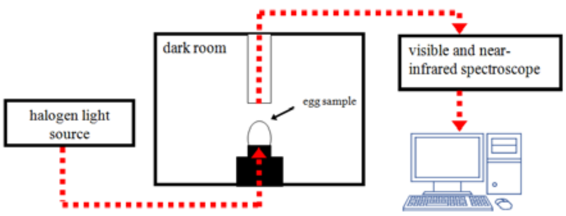

Fig. 1 Schematic diagram showing the near-infrared spectroscopy of the experimental apparatus

Experimental apparatus and measuring methods

The visible and near-infrared absorbance spectra of the eggs were measured using a compact spectroscope. A schematic diagram of the visible and near-infrared spectroscope is shown in Fig. 1. The device consisted of a compact diode array-type spectroscope (Handy-Lambda II, Spectra-scope) with a 150 W halogen light source (PICL-NEX-TWIN; NIPPON PI; 180,000 lx maximum illumination intensity), optical fibres supplying the light source and photoreception, a specimen table, a dark box, and a personal computer with exclusive software installed (Wave Viewer; Spectra Co., Ltd., Japan). The computer was attached to a near-infrared spectroscope. Reference data were obtained using a white reference plate with a thickness of 2 mm that was included with the compact diode array-type spectroscope. Egg samples were positioned vertically and were exposed to upward irradiation from the light source. After acquisition of light-intensity data from the reference and test egg samples by using software developed in-house, the absorbance data were calculated. The range of wavelengths that could be measured by the spectroscope was from 310 to 1100 nm, with a interval of 3.3nm. The light-intensity data acquired using the exclusive software were expressed as the relative intensity determined according to the electrical voltage of detection. The stepwise variable selection method to select a wavelength for LED was performed using statistical analysis software (JMP; SAS Institute Japan Inc., Japan).

The LED and photodiode (PDIO) incurred a markedly lower cost than the near-infrared spectroscope and halogen light source did. The equipment facilitated the simultaneous assessment of 1 tray of eggs (36 eggs), as illustrated in Fig. 2. The device consisted of yellow (585 nm; OSRAM, Germany) and red (635 nm; OSRAM, Germany) LED boards, PDIO (OSRAM, Germany) boards, a central processing unit (CPU) board, an analogue digital converter (ADC) board, an input/output (I/O) board, a specialized tray for the eggs, a dark box, and a personal computer. The LED boards and PDIO boards were set at the location of each egg. Exclusive software for egg discrimination developed in Microsoft Visual Studio 2008 was used to control LED irradiation and PDIO detection. The ADC board transduced the electrical voltage of the detector, which represented the intensity of the transmitted light, to digital data. The I/O board controlled the LED input-output processing. The CPU board controlled the ADC board and I/O board. The eggs were positioned vertically and were exposed to upward irradiation from the LED. Reference data were also obtained using the white reference plate with a thickness of 2 mm. In the present study, two types of LED configuration were compared: in one configuration, only one LED board just below egg sample was used, whereas in the other configuration, three LED boards, just below and both side of egg sample were used to generate ambient light to test whether ambient light from the three LED boards would affect the measurement (Fig. 3). The light-intensity data were converted to absorbance as log (1/[I/R]), where I is the intensity value and R is the reference value.

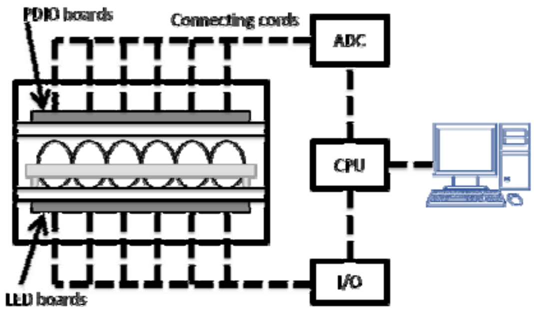

Fig. 2 Schematic diagram of the LED of the experimental apparatus

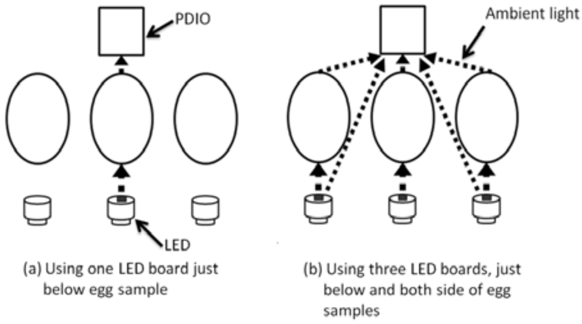

Fig. 3 Schematic diagram of Influence of ambient light when adjacent LEDs were used.

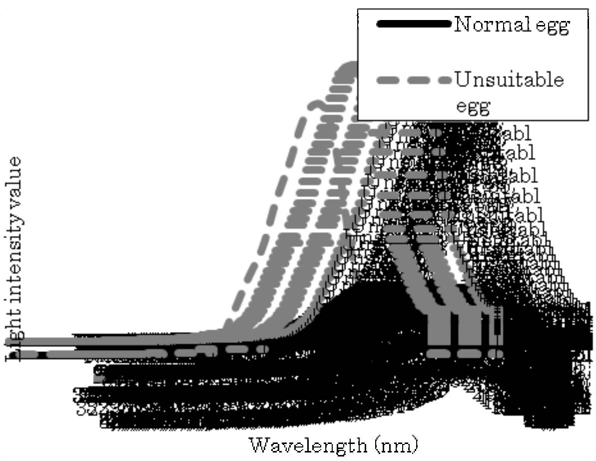

Fig. 4 Original light intensity spectra of normal eggs and unsuitable eggs acquired by near-infrared spectroscopy.

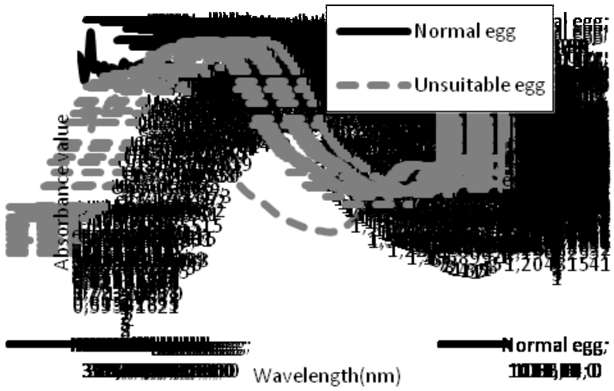

Fig. 5 Original absorbance spectra of normal eggs and unsuitable eggs calculated from light-intensity data.

Result and discussion

Visible and near-infrared spectra of normal eggs and unsuitable eggs

The intensity and absorbance spectra of normal eggs and unsuitable eggs are shown in Fig. 4 and Fig. 5. The intensity and absorbance spectra of normal eggs were lower and higher, respectively, than those of unsuitable eggs at 500–900 nm, because the blood vessels growing in the normal eggs intercepted the light. No signal was obtained outside the wavelength range of 500–900 nm when halogen lamp was used in this study. Therefore, visible wavelengths of 500–700 nm were selected for the LEDs. The stepwise selection method was applied to select 585nm and 635 nm by using statistical analysis software to discriminate normal from unsuitable eggs. 585 nm is the absorbance range of hemoglobin (Dover et al., 1999). 635 nm is the absorbance range of methemoglobin (Ohtake et al., 2010). These wavelengths were selected for use in the LED experiment.

LED and PDIO measurement

Unsuitable eggs were identified using one LED board just below egg sample or three LED boards just below and both side of egg samples from a total of 36 normal eggs and 36 unsuitable eggs. Fig. 6 shows the scatter diagram for the absorbance values obtained at 635 nm and 585 nm, in the presence of one LED board, on the x-axis and y-axis, respectively. To increase the speed of LED measurement, simultaneous multiple identification was also performed using three LED boards. Fig. 7 shows the scatter diagram for the absorbance values obtained at 635 nm and 585 nm, in the presence of three LED boards, on the x-axis and y-axis, respectively. The discrimination rate was calculated by introducing a linear discriminant function, and discriminant analysis was applied to determine the optimal line dividing the normal and unsuitable eggs. Table 1 shows the difference between using one LED board and three LED boards. A comprehensive discrimination rate of 95.8% was obtained when discrimination was performed using one LED board. By contrast, the comprehensive discrimination rate of 81.9 % obtained in the presence of three LED boards was much lower than that obtained using one LED board. When three LED boards were used, the surrounding LED lights affected the PDIO, thereby reducing the discrimination rate.

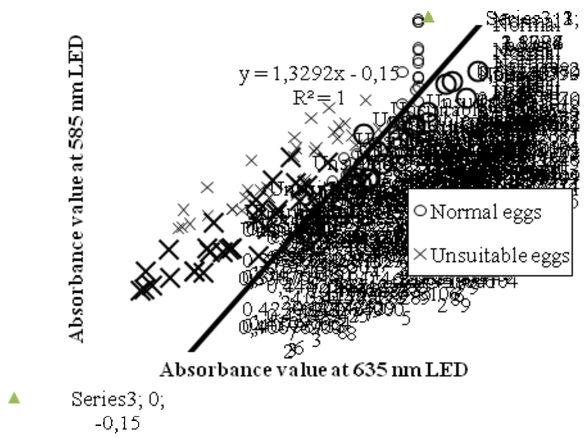

Fig. 6 Discrimination result using three LED boards, just below and both side of egg samples

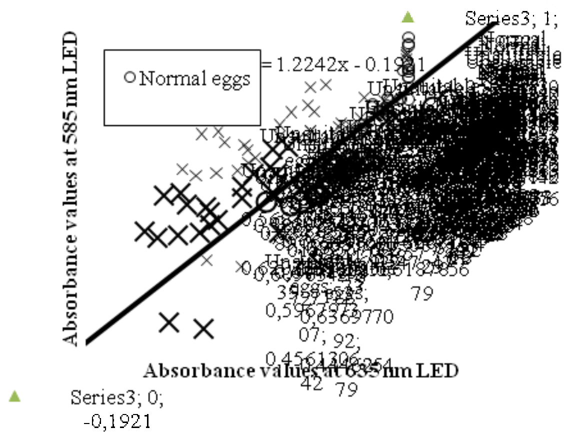

Fig. 7 Discrimination result using one LED board just below egg sample

Tab. 1 Detection results for egg samples using LED and PDIO measurement

	Detection rate (%)
Using one LED board just below egg sample	95.8
Using three LED boards, just below and both side of egg sample	81.9


Fig. 8 The automated, nondestructive detector of unsuitable eggs (Left: External structure; Right: Internal structure), Height : 1,800 mm
Length : 2,500 mm
Width : 750 mm

Automated, nondestructive detector of unsuitable eggs

The automated, nondestructive detector of unsuitable eggs consists of an LED, PDIO, embedded software device, conveyor, and application software. External and internal structure of this device is shown in Fig. 8. The conveyor controlled by a sequencer could move the tray containing the eggs to the measurement site. The embedded software device contained basal plates, including a CPU, ADC, I/O, 36 LEDs, and 36 PDIOs positioned appropriately for the assessment of 1 tray of 36 eggs. Additionally, the application software for detection could control the LED lighting pattern and speed. The maximum speed that the application software could apply to lighting the LED was 2 sec per 1 tray. The application software could also receive LED light by PDIO, calculate the absorbance, and detect the unsuitable eggs by using a linear discriminant function.

Conclusion

In this study, a high discrimination rate was obtained using visible and near-infrared spectroscopy to detect signals produced by LED light. LED and PDIO were able to discriminate normal from unsuitable eggs without requiring expensive visible and near-infrared spectroscopy or a halogen lamp. The differences in absorbance values at the two wavelengths contributed to the efficient discrimination between normal and unsuitable eggs. Furthermore, LED should be used singly to prevent the three LED boards light sources from affecting detection. Thus, in the future, an automated, nondestructive detector will be available to eliminate unsuitable eggs for vaccine production.

Acknowledgment

This work was supported by JSPS Grant-in-Aid for Scientific Research (B) Grant Number (23380148).

Reference

Armstrong P.R., 2006. Rapid single-kernel NIR measurement of grain and oil-seed attributes. Applied engineering in agriculture, 22: 767–772.

Dawood S.F., Luliano D.A., Reed C., Meltzer I.M., Shay K.D., Cheng P., Bandaranayake D., Breiman F.R., Brooks A.W., Buchy P., Feikin R.D., Fowler B.K., Gordon A., Hien T.N., Horby P., Huang S.Q., Katz M.A., Krishnan A., Lal R., Montgomery M.J., Mølbak K., Pebody R., Presanis M.A., Razuri H., Steens A., Tinoco O.Y., Wallinga J., Yu H., Vong S., Bresee J., Widdowson M., 2012. Estimated global mortality associated with the first12 months of 2009 pandemic influenza A H1N1 viruscirculation: a modelling study. The Lancet Infectious Diseases, 12: 687–695.

Dover S.J., Sadick S.N., Goldman P.M., 1999. The Role of Lasers and Light Sources in the Treatment of Leg Veins. Dermatologic Surgery, 25(4): 328-336.

Hsiao S., Chen S., Yang I., Chen C., Tsai C., Chuang Y., Wang F., Chen Y., Lin T., Lo M.Y.,

2010. Evaluation of plant seedling water stress using dynamic fluorescence index with blue LED-based fluorescence imaging. Computers and Electronics in Agriculture, 72: 127–133.

Ohtake K., Koga M., Uchida H., Sonoda K., Ito J., Uchida M., Natsume H., Kobayashi J., 2010. Oral nitrite ameliorates dextran sulfate sodium-induced acute experimental colitis in mice. Nitric Oxide, 23: 65–73.

Usui Y., Nakano K., Motonaga Y., 2003. A study of the development of nondestructive detection system for abnormal eggs. EFITA 2003(Hungary), 625-631.

Wang J., Nakano K., Ohashi S., Kubota Y., Takizawa K., Sasaki Y., 2011. Detection of external insect infestations in jujube fruit using hyperspectral reflectance imaging. Biosystems Engineering, 108 (4): 345-351.

THE USE OF RAW RAPESEED OIL TO POWER THE ENGINES OF AGRICULTURAL TRACTORS AND VEHICLES

Marek Klimkiewicz*, Remigiusz Mruk, Jacek Słoma, Janusz Wojdalski

Warsaw University of Life Sciences, Department of Production Management and Engineering, ul. Nowoursynowska 166, 02-787 Warszawa Poland,
Phone: (48 22) 59 34 572, E-mail: marek_klimkiewicz@sggw.pl

Abstract

The development of guidelines to the adaptation of the engine of agricultural tractor or car vehicle to the work on unprocessed rapeseed oil was the aim of investigations.The rapeseed oil properties were compared to the diesel oil properties, because of the possibility to use them to power diesel engines. The characteristics of rapeseed oil, which have an adverse effect on the operation of the engine have been identified. The research of combustion of rapeseed oil and its blend with diesel oil were carried out in a chamber of constant volume and on test benches on engines equipped with the conventional fuel equipment and the common-rail system. The operational tests were carried out on the car equipped with a diesel engine with indirect injection and on agricultural tractor equipped with a diesel engine with direct injection. The assessment of damageability of tractor power unit fuelled with rapeseed oil was also carried out.

Key words: agricultural tractor, diesel engine, rapeseed oil

Introduction

The use of raw rapeseed oil (RO) to power diesel engines can reduce the cost of biofuel production, the transport and the storage, especially when it is used for their own farms. The production process of RO is waste-free because after pressing rapeseed, expeller can be used for feeding cattle (Drosio et al., 2011). Energetic expenditures on the production of oil can carry out 3 % of his gross calorific value only in the case of the use of the simple technology of the production RO on the own use (Wojdalski, Bochenski, 2010).

In the literature, many examples are described of the use of a mixture of diesel oil (DO) with vegetable oil (VO) to power engines (Bocheński, 2003), as well as the use of the pure VO (Wcisło, 2003; Dzieniszewski, 2008). Engines specially designed to work on VO, as the Elsbett engine, are not popular. Currently, manufacturers of agricultural tractors (including Fendt, John Deere, Pronar Narew) indicate in their offers the possibility to provide models that can be fueled with diesel fuel or vegetable oil. Thuneke and Gassner shows that, according to research carried out on the tractor Deutz-FahrAgrotron TTV 1160 and Fendt Vario 412 series compatible with the control (ISO 8178) for emissions of hydrocarbons HC and particulate RO has better properties than DO. Only NOx emissions were higher (up to 10 %) when working on the rapeseed oil (Thuneke, Gassner, 2009). The fuel for combustion engines is regarded as an important element of design, so the range of variation of parameters of RO were included in the proposal standard DIN V 51605 (Remmele, Thuneke, 2007). A number of publications describes examples of the use of rapeseed oil or other vegetable oil to power the diesel engine after the modification of the properties of oil (mainly viscosity), by mixing it with a diesel oil or other combustible organic substances (Ambrozik, Kurczyński, 2006; Jakóbiec at al., 2011; Pilarski, Krysztofiak, 2009; Nwafor, Rice, 1996; He, Bao, 2003) or by heating oil (Wcisło, 2003; Dzieniszewski, 2006; Klimkiewicz, 2010).

Many authors have indicated problems resulting from engine powered with unprocessed rapeseed oil that are associated with the formation of carbon deposits in the combustion chamber and at the nozzles of injectors, and with other fuel system malfunctions (Dzieniszewski, 2006), and also linked to the need for more frequent replacement of engine oil (Thuneke at al., 2009). The high viscosity of rapeseed oil can be a source of problems in the supply system because of blocking the fuel filter (Klimkiewicz at al., 2010). Some researchers indicate problems such as the formation of carbon deposits on the nozzles, jamming the piston rings, rubber seals deformation and increasing the viscosity of the lubricating oil (Nwafor, Rice, 1996). During the combustion of VO, the spatial development of combustible mixture increases the ignition delay period compared to DO (Klimkiewicz, Bochenski, 2011). The high viscosity of rapeseed oil and its surface tension has a direct impact on spraying. RO droplets with Sauter diameter several times greater than that of the diesel oil cause an increase within a spray, which may cause the lack of combustion, may settle on the walls of the cylinder, and consequently penetrate of the engine oil in the crankcase (Sapiński, 1999).

Diesel engines in addition to the need for high-energy performance must comply with the applicable standards concerning exhaust emissions. Adherence to the limits of toxic gases enforces changing in the engine exhaust system (Exhaust Aftertratment) (Cieślikowski, 2011). These conditions should be considered in the effort to use rapeseed oil to power the diesel engines.

The quality of rapeseed oil

For the production fuel, rape varieties that contain 70-80 % oleic acid, about 10 % linoleic acid and about 10 % of linolenic acid are most useful. Contribution of individual fatty acids in the oil affects the physicochemical properties of the fuel. Rapeseed oil properties depend primarily on the chain length of fatty acids, the quantities of unsaturated fatty acids, and the number and position of double bonds.

Rapeseed oil in the comparison with diesel oil is characterized by: higher density, higher viscosity (almost 10 times at 20 °C), lower cetane number (RO - 39, DO - 50), the higher temperature of the distillation curve about 100 °C, more acidic causing corrosion impact on copper and its alloys; aggressive impact on some sealing materials, much higher temperature of cold filter blocking, content of phosphorus in the form of phospholipids, which cause the formation of deposits in the combustion chamber; susceptibility to oxidation and bacteriological contamination. Positive characteristics of rapeseed oil are as follows: low content of sulfur: content of about 10-12 % of the oxygen in the molecule, good lubricity - ensuring long-lasting of working parts of fuel equipment, flash point above 220 °C to ensure fire safety, and its renewability.

Material and methods

For the ***research conducted on the test bench***, a single-cylinder engine with direct fuel injection FARYMANN Diesel 18W with power of 5.2 kW was applied in investigations. The test bench was built to measure various parameters: the torque, the pressure inside the cylinder, the temperature of the cooling liquid, exhaust gas emissions, etc. The influence of the use of rapeseed oil and its blends with diesel oil on the parameters of the engine work was investigated.

Operational tests of diesel engine with indirect injection was conducted on a vehicle Ford Fiesta 1.8 D equipped with additional rapeseed oil tank and system consisting of a fuel filter, water separator and flow heater. The characteristics of the engine were determined on the chassis dynamometer SCHENCK.

Operational tests of diesel engine with direct injection was carried out using a farm tractor ZEFIR 85 of PRONAR Ltd., with the direct injection diesel engine with power of 62.5 kW. A two-tank system with heating of supplying rapeseed oil to 70 °C was used. The main fuel tank has been designed for rapeseed oil, and a second, smaller tank has been designed to supply diesel fuel to the engine during start-up and at the end of work, in order to flush the fuel system. Measurement of parameters of the engine, fueled with rapeseed oil, was performed on a chassis dynamometer PT 301 MES.

Within the ***assessment of damageability of tractor power unit fueled with rapeseed oil***, computation of reliability parameters have not been performed and the qualitative and quantitative methods, such as: Fault Tree Analysis (FTA), Event Tree Analysis (ETA), Failure Mode and Effects Analysis (FMEA) were used. The reason was the limited number of objects, such as tractors and vehicles fueled with rapeseed oil.

Results and discussion

The research of combustion rapeseed oil and its mixtures with diesel oil in a chamber of constant volume showed that the greatest impact on the combustion process of vegetable oils has the air temperature in the chamber. With increasing temperature of air in the chamber up to the maximum tested value, shorter the time of the ignition delay, faster increases of the combustion pressure and higher its maximum values were observed. At the highest tested temperature, keeping the optimum values of the other parameters, the combustion of investigated vegetable oils was similar to the process of the combustion of diesel fuel. The second factor that has a much greater effect on the combustion of VO than on burning of RO is the air pressure in the combustion chamber. As the temperature rises, the pressure in the chamber will reduce the time of the ignition delay of vegetable oil.

Research conducted on the test bench showed that increasing the amount of RO added to the DO significantly affected the energy performance and exhaust emissions. The highest values of maximum combustion pressure were obtained for the mixture of 30 % DO and 70 % RO for most of the configuration of parameters of the test. There was a positive effect of high injection pressures occurring in the test engine with the Common Rail (CR) system on energy performance and emissions, when the engine was powered with RO. At the highest value of fuel pressure in the CR system, equal to 150 MPa, the lowest specific fuel consumption was obtained for the pure DO, however for blends, it was obtained for the ratio of 50 % DO and 50 % RO.

The highest NOx emissions have been registered for the mixture of 30 % DO and 70 % RO. The influence of the kind of fuel on the content of CO and HC depends in the large stage on the parameters of the test and requires further study. The study confirmed the need to replace traditional fuel injection systems by CR systems. In each test, when no pilot dose was used (as in the conventional injection system) decreased in the engine parameters was observed.

Within the ***operational tests of diesel engine with indirect injection*** (Fig. 1), it can be concluded that the use of rapeseed oil to power diesel engine with indirect injection does not result in a reduction in power and torque.

The smoke measurement values were determined by free acceleration test. The average value of light absorption coefficient K for the engine powered with DO was 2.24 m^{-1}, and for the engine powered with RO, it was 2.27 m^{-1}. Final smoke measurement values do not exceed the maximum amount of specified rules, that is K = 2.50 m^{-1}.

The values of the noise level in dB at constant speed, which is equal to 75 % of the speed of the maximum power of the vehicle for both tested fuels, did not differ in within the error limits.

Verification the parts of the engine powered with RO after mileage of 80 thousand km has shown that the combustion process was proper, although an increased amount of the carbon deposits on the bottom surface of the pistons, the surface of the head, the valves, the exhaust gas ducts and the nozzles of the injectors were observed.

Compression test performed on the engine showed that the pressure was from 3.0 to 3.1 MPa. The manufacturer specifies the acceptable range of compression pressure 2.8 – 3.4 MPa.

The aim of the ***operational tests of an agricultural tractor with direct injection diesel engine fueled with unprocessed rapeseed oil*** was to investigate the effect of selected design parameters of the engine on: the power, torque and specific fuel consumption in direct injection diesel engine fueled with pure rapeseed oil.

The results confirmed the impact of design parameters on the value of power, torque and specific fuel consumption of an engine powered with rapeseed oil. Analysis of the results allows the following conclusions:

- Basic values that characterized the diesel engine when running fueled with rapeseed oil change compared to those fueled with diesel oil. The nominal output power is reduced by about 12 %, the torque is reduced by about 9 %, The hourly fuel consumption is reduced to the value of 7%, and the unit fuel consumption increases by about 15 %.

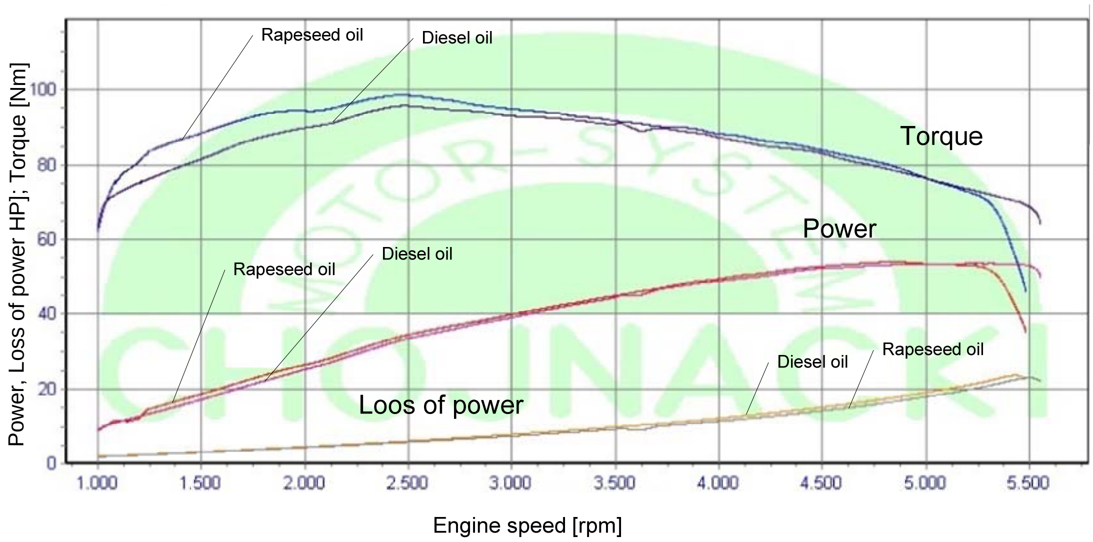

Fig. 1 Comparison of power, torque and power losses as a function of speed of diesel engine powered with rapeseed oil and diesel oil

- The most favorable value of specific fuel consumption across the range of tested angles of fuel injection, which was 329 g kWh^{-1}, was obtained for an angle of 15°. Engine oil was changed every 150 operating hours. Engine worked on rapeseed oil by 453 operating hours. After this period, the head of the engine was disassembled. The presence of carbon deposits on the surface of the combustion chamber and at the nozzles of the injectors was found. One of the nozzles of injectors was faulty. The cause of failure can be explained by the accumulation of excessive amounts of carbon deposits on the injector.

Thanks to conducted analysis of FTA within the ***assessment of damageability of tractor power unit fueled with rapeseed oil***, the basic events associated with the engine powered with rapeseed oil, which can cause damage of the drive unit were isolated. The analysis shows that the injector in the system is a weak link and the solution of the problem of the reliability of injectors should be undertaken in the first place.

By means of ETA, relationships occurring between the performance or unavailability, protective systems and systems of reducing the effects of faults caused by the occurrence of a single initiating event in a transparent manner were defined.

As a result of FMEA method, detailed recommendations how to operate the tractor with the engine that is fueled with rapeseed oil and how to deal with rapeseed oil in order to avoid the defects were given.

Conclusions

The study shows that rapeseed oil can be a substitute for diesel fuel. However, it is the fuel with special needs. Condition for the application this fuel is to keep the border properties of rapeseed oil as indicated by the proposed standards.

It is recommended to use the two-tank supply system of fuel with heating of rapeseed oil. Starting of the engine should be carried out on diesel oil with automatic switching to rapeseed oil after heating. However, before turning off the engine for a longer layover, it should be powered with the diesel fuel to flush the fuel system to prevent sticking precision components with rapeseed oil, in which occur a polycondensation reaction.

It is recommended to change engine oil more frequently in comparison with diesel oil powered engines, and more frequently perform maintenance of the fuel system. Problem of the nozzles contamination can be solved by introducing the additives to rapeseed oil to improve combustion and cleaning.

The study confirmed the need to replace traditional fuel injection systems by common rail systems also in engines powered with rapeseed oil.

References

Ambrozik A., Kurczyński D., 2006. Comparative evaluation of load characteristics of diesel engine fueled with diesel fuel and vegetable fuel mixture. MOTROL, 8A: 21-30. (in. Polish)

Cieślikowski B., 2011. Research trends and the latest trends in design and development of agricultural tractors. Expertise. Avaible at: www.agengpol.pl. (in. Polish)

Drosio A., Klimkiewicz M., Mruk R., 2011. Energetic and technical analysis of winter rapeseed production technology. MOTROL, 13: 100-110.

Dzieniszewski G., 2006. Analysis of potential to use raw rapeseed oil in diesel engine Inżynieria Rolnicza, 12(87): 117-125. (in. Polish)

Dzieniszewski G., 2008. Selected ecological and economic aspects of supplying diesel engines with vegetable fuels. Inżynieria Rolnicza, 10(108): 39-45. (in. Polish)

He Y., Bao Y.D., 2003. Study on rapeseed oil as alternative fuel for a single-cylindre diesel engine. Renewable Energy, 28: 1447-1453.

Jakóbiec J., Bocheńska A., Ambrozik A., 2011. Modification of the physicochemical and usable properties of rapeseed fuel. Inżynieria Rolnicza, 4(129): 85-92. (in. Polish)

Klimkiewicz M., Bocheński C., 2011. The use of crude rapeseed oil as a fuel for diesel engines of tractors and agricultural vehicles. The report on the implementation of a development project R10 037 03 Warszawa, WIP SGGW. Manuscript. (in. Polish)

Klimkiewicz M., Jobbágy J., Simonίk J., 2010. The analysis of the determinants of effective operation of diesel engines fueled with unprocessed rapeseed oil. (in) Modern aspects of the development of the energy and agriculture sector. Warsaw University of Life Sciences SGGW, 122-135. (in. Polish)

Nwafor O.M.I., Rice G., 1996. Performance of Rapeseed Oil Blends in a Diesel Engine. Applied Energy, 54(4): 345-354.

Pilarski K., Krysztofiak A., 2009. Effect of chemical additions on physical proprieties of rapeseed oil. Journal of Research and Applications in Agricultural Engineering, 54(1): 27-30. (in. Polish)

Remmele E., Thuneke K., 2007. Pre-Standard Din V 51 605 for Rapeseed oil fuel. 15th European biomass conference & Exhibition, Berlin.

Sapiński A., 1999. Spalanie olejów roślinnych w silniku o zapłonie samoczynnym. 25th International Conference on Combustion Engines. KONES'99. Zakopane, 194-204. (in. Polish)

Thuneke K., Gassner Th., Ember P., 2009. Is rapeseed oil still the alternative? Renewable energy. AGROmechanika, 3: 55-58. (in. Polish)

Wcisło G., 2003. Possibilities of rapeseed oil to supply diesel engines in agricultural vehicles. Inżynieria Rolnicza, 10(52): 43-49. (in. Polish)

Wojdalski J., Bocheński C., 2010. Studies of the combustion process rapeseed oil and its mixtures with additives in a test chamber with variable parameters of air and fuel intake (Common Rail) Report of the research project KBN N 502 007 31/0573. Manuscript. (in. Polish)

TRANSPORT EFFICIENCY OF STRAW BALES FOR ENERGY PURPOSES

Maros Korenko*, Miroslav Zitnak, Miroslav Macak

Slovak University of Agriculture in Nitra, Tr. A. Hlinku 2, 949 76 Nitra, Slovakia,
Phone: +421 37 641 4402, E-mail: maros.korenko@uniag.sk

Abstract

At the present, the world is increasingly used not only in the straw livestock, but also as a source of energy. Agriculture begins its role gradually enter into the sector of energy production (Libra, 2007). Agriculture and the new challenges are now not only in the EU but also the environment in a world increasingly supported (Van Stralen et al., 2013). Technology harvest straw pressing into giant bale features many advantages, the use of which is restricted by inefficient handling during transport from the field.

Currently used machines allow collection of all kinds of stalk material. Harvested material is in the press as needed chopped and pressed while pressing pressure can increase by up to 25%. It follows that the bales reach higher mass, thus increasing density bale and hence energy concentrated in it.

Pressing and transport bales of straw significantly affects the economic efficiency of heat production of this product (Lopez et al., 2010). Therefore, the transportation and handling of bales is advantageous to better utilize the capacity of vehicles (less shipping costs calculated per tonne of transported material). The aim of the paper was to evaluate the molding process, harvest, transport and stacking bales of straw. The result was to evaluate the individual components of the times, performance units and consumption of live work.

Keywords: transport, straw balles, energy

Introduction

Specific requirements for the design of transport technology is a technology of pressing stalky materials (straw and silage forage wilting) in bulk bales giant circle, respectively rectangular cross-section (Jensen et al., 1998). Modern brakes allow collection of all kinds of materials. Harvested material is in the press as needed chopped and crushed. New models of presses can squeeze up to 25% higher compression pressure. Therefore, the transport and handling of bales to better capacity utilization of vehicles (less expensive transport in per tonne of transported material). Technology harvest crops stalk (or straw) pressing into giant bale features many advantages, the use of which is restricted by inefficient at handling bale derives from the field.

For the collection, transportation and stacking bale, which remain under high pressure presses gatherers in the field using several approaches:

- Loading bales for tractor trailer tractor or self-propelled loader,
- Truck and trailer mounted hydraulic loader fitted in the rear of the hull for the collection and storage of bales,
- Collection, transport and stacking bales of different sizes special pantograph trailer.

Use of special pick-up trailer bale substantially streamlines technology collection and handling of straw bales at their place of storage.

Material and Methods

Measurements were made at the turn of July and August on the land (plains with a slope up to three degrees) on a plot of barley straw. The measurements are performed with a set of JCB Fastrac 3230 + Krone BIG pack (Fig. 1) and the set JCB Fastrac 3220 + ARCUSIN (Fig. 2).

Individual labor operation times were measured by a stopwatch. To monitor the work sets we used GPS navigation device Leica GS 20 with external antenna, whereby we recorded the distance between the bales and the traveled path sets. The average yield per hectare of land was determined by dividing the total weight of the harvested material and the number of hectares.

Fuel consumption was monitored for the entire work shift, and a method of refilling the fuel tank. Vehicle started with a full tank and the end of the day the tank refilled. At various times and determining the performance of the methods specified in the standard STN 47 0120.

Results and Discussion

The pressing of barley straw kit was used JCB Fastrac 3230 + BIG pack. After pressing the material continued to collect and bale stacking area at the edge set JCB Fastrac 3220 + ARCUSIN F 54.63 (Tab. 1).

Weather conditions were optimized by measuring, collecting straw moved and 2-3 weeks after harvesting grain. Although the yield of barley straw were low. The average transport distance of the harvested area was 3.2 km. Evaluating operative, productive and running time for series that followed compressed, collect and stack quality straw bales are in Tab. 2 and Tab. 3

The calculated coefficients of performance are high and so we can say that this is a high technology suitable for practice. This compression technology, collecting and stacking straw is characterized by low fuel consumption and live work. When harvesting and hauling straw special semi-gatherers, the loss of time due to technological downtime is very small, because the trailer merges several existing operations (loading and transport).

Fig. 1 Monitored machines JCB Fastrac 3230 + BIG pack

Fig. 2 Controlled machine JCB Fastrac 3220 + ARCUSIN

Tab. 1 Basic technical parameters of the vehicle

Parameters	Label	Units	Type of vehicle ARCUSIN F 54.63
Curb weight	m	kg	7540
The maximum length	l	mm	9850
Storage height	h	mm	5800-6400
The minimum working height		mm	6400-7000
The maximum total weight		kg	16800

Tab. 2 Summary of calculated parameters for JCB Fastrac 3230 + BIG pack

Label	Indicator	Units	The average of value
t_1	time main	h:mm:ss	0:03:05
t_2	By-time	h:mm:ss	0:00:18
t_3	time to prepare the machine for work activities	h:mm:ss	0:00:12
t_4	downtime caused Troubleshooting	h:mm:ss	0:00:00
t_8	Time Other Downtime	h:mm:ss	0:00:08
t_{02}	operative time	h:mm:ss	0:03:23
t_{04}	productive time	h:mm:ss	0:03:35
t_{08}	operating time	h:mm:ss	0:03:43
K_{02}	coefficient of utilization of operating time	-	0.91
K_{04}	coefficient of utilization of productive time	-	0.86
K_{07}	coefficient of utilization of operating time	-	0.83
W_{02}	performance per unit operating time	$ks.h^{-1}$	16.16
W_{04}	performance per unit of productive time	$ks.h^{-1}$	14.41
W_{08}	performance per unit operating time	$ks.h^{-1}$	13.39
v_p	average speed rigs	$km.h^{-1}$	9.40

Tab. 3 Summary of calculated parameters for JCB Fastrac 3220 + ARCUSIN F 54.63

Label	Indicator	Units	The average of value
t_1	time main	h	0:15:47
t_2	By-time	h	0:01:49
t_3	time to prepare the machine for work activities	h	0:01:00
t_4	downtime caused Troubleshooting	h	0:00:00
t_8	Time Other Downtime	h	0:00:45
t_{02}	operative time	h	0:17:36
t_{04}	productive time	h	0:18:36
t_{08}	operating time	h	0:19:21
K_{02}	coefficient of utilization of operating time		0,90
K_{04}	coefficient of utilization of productive time		0,85
K_{07}	coefficient of utilization of operating time		0,82
W_{02}	performance per unit operating time	$ks.h^{-1}$	43.40
W_{04}	performance per unit of productive time	$ks.h^{-1}$	41.07
W_{08}	performance per unit operating time	$ks.h^{-1}$	39.47
v_p	average speed rigs with costs	$km.h^{-1}$	12.90
L	transport distance	km	3.20
m_1	number of bales per cycle	ks	12.00
	fuel consumption	$l.ks^{-1}$	0.39

Conclusion

To achieve greater efficiency and productivity in the transport and handling operations should use the following steps:

- a comprehensive solution to every article covering the supply chain management, transportation, materials handling and unloading with respect to the alignment of stationary and mobile equipment,
- to increase payload vehicles while optimizing their design limitations in respect of delays in the implementation of auxiliary operations,
- material in the technical operations in order to achieve simplification of loading, unloading and handling of the overall material, while maintaining a high quality of the material transported.

When harvesting bale unit JCB Fastrac 3220 + ARCUSIN were found small technological and organizational downtime incurred due to low crop straw when set on pressing was not fast enough for a kit for collecting and stacking.

The resulting value of the average consumption of live work on a compressed bale was rigs at JCB Fastrac 3230 + BIG pack. 3.71 min. The resulting value of the average consumption of live work on a haphazard and stacked bale was in line JCB Fastrac 3220 + ARCUSIN 1.61 min and average fuel consumption per parcel was 0.39 liters. Consumption of live work with this technology was so low, because one person can be harvested and transported stacked as in reduced labor costs.

Acknowledgement

This paper has been prepared within the project:

"Development of International Cooperation for the Purpose of the Transfer and Implementation of Research and Development in Educational Programs" conducted by the Operational Program: Education, ITMS code: 26110230085

References:

Jensen J., Koch T., Parsby M., 1998. Straw collection and delivery system based on 70 m(3) tanks. In Proceedings BIOMASS FOR ENERGY AND INDUSTRY, 10th European Conference and Technology Exhibition on Biomass for Energy and Industry, WURZBURG, GERMANY: 1056-1058.

Libra M., Poulek V., 2007. Energy sources and their usage. Prague: Czech University of Life Sciences Prague: 141. (in Czech)

Lopez R. M., Hetz H. E., Maturana B. C., 2010. Economic Evaluation of Collection, Transport and Utilization of Straw in the Swath of Wheat Stubble. In Ama-Agricultural Mechanization in Asia Africa and Latin America, Vol.: 41, 3: 52 – 58.

STN 47 0120 (1993): Agricultural and forestry machines and tractors. Time measuring methods and operating indices determination. Slovak Standards Institute Bratislava. (in Slovak)

Van Stralen J. N. P., Uslu A., Dalla Longa F., Panoutsou C., 2013. The role of biomass in heat, electricity, and transport markets in the EU27 under different scenarios. In Source: Biofuels Bioproducts & Biorefining-Biofpr. Vol.: 7: 147 – 163.

EFFECTIVENESS OF DIFFERENT ROLLER/CRIMPER DESIGNS FOR COVER CROPS MANAGEMENT IN CONSERVATION AGRICULTURE

Ted S. Kornecki[1*]

[1]United States Department of Agriculture, Agricultural Research Service, National Soil Dynamics Laboratory, Auburn, Alabama, 36832, USA. Phone: 1-334-887-8596,
Fax: 1-334-887-8597, E-mail: ted.kornecki@ars.usda.gov

Abstract

In conservation agriculture, cover crops are utilized to improve soil properties and to enhance cash crop growth. A typical cover crop utilized in the Southern United States is cereal rye (Secale cereale. L.). Tall cover crops such as cereal rye if not properly managed will lodge in different directions and thereby create planting problems of a cash crop due to interference of residue with seed planting equipment. Rolling/crimping is a mechanical method used to terminate a cover crop three weeks prior planting a cash crop. Original rollers were not widely adopted in the US because of increased roller vibration associated with high operating speeds. Research using new roller designs has demonstrated effectiveness at cover crop termination without generating harmful vibrations. Since US farming encompasses large and small scale production systems, several types of roller/crimpers were developed to accommodate both large row crops and small vegetable no-till and organic farm systems. The spiral roller/crimper design did not generate adequate crimping force to sufficiently injure cover crops compared to other newer concepts. A roller/crimper for raised beds was formulated to manage cover crops on elevated row culture systems and terminate cover crops both on row-tops and in furrows. The smooth roller with crimping bar assembly and the two stage roller/crimper were developed to operate with various tractors and also designed to apply herbicide as a supplement to rolling. With these rollers, the crimping force can be adjusted by altering spring tension to obtain the proper crimping force for a particular cover crop. In no-till vegetable and organic production systems, field operations may be conducted on small beds. Because of this constraint a new powered roller/crimper for small walk-behind tractors was developed which allows growers to successfully manage cover crops. Generally, the new roller designs were very effective at terminating rye cover crops. These new roller/crimper concepts achieved termination rates exceeding 90% three weeks after rolling without the use of herbicides and in dry growing seasons conserved soil water due to the mulch effect of cover crop residue.

Keywords: roller, crimper, soil, spray, moisture

Introduction

There are many benefits associated with cover crops such as reduced runoff and soil erosion, increased infiltration and water holding capacity, increased soil organic carbon and decreased soil compaction (Reeves, 1994). To optimize these benefits, cover crops must be managed appropriately at the soil surface (Brady, Weil, 1999). Also cover crops must be terminated at an appropriate growth stage (Ashford, Reeves, 2003). If termination is done too early, this rolling technology is not effective because young plants have the capability to recover. There are several methods for cover crop management such as incorporation and burning, but potential cover crop benefits are lost with these methods. When incorporating a cover crop, the soil surface is fully exposed to detrimental rainfall impact, thus soil erosion and loss of nutrients with runoff can occur. Burning sometimes is still utilized, but toxic gases emitted to the atmosphere make this method environmentally unfriendly. Mowing of cover crops is a popular method used in no-till vegetable and organic systems to terminate covers before planting cash crops. If mowing occurs at early cover crop growth stages, re-growth can occur and cover crops will compete with the cash crop for nutrients and water which can negatively impact cash crop development. Another method is termination of cover crops with herbicides (e.g., glyphosate) since spraying is relatively fast, effective, and inexpensive. However, there are problems associated with effective herbicide application to tall covers such as rye. Tall cover crops can also lodge in different directions which impacts the effectiveness of cash crop planting units in high residue systems. This interference can result in frequent stops to clean the equipment, and increases the time needed to plant a cash crop. Another common problem is "hair-pinning", where residue is pushed into the soil rather than being sheared, which reduces seed-soil contact and thereby results in row skips that negatively impact desired stand establishment and yield. Rolling technology is a mechanical means of terminating cover crops with rolling done in the same direction as the planting direction of the follow-on cash crop in order to minimize residue cover build-up on planting units. The concept of rolling and crimping of a cover crop is to damage (injure) the plant without cutting stems with the crimping bars. Rollers typically consist of a steel drum with attached crimping bars equally spaced on the drum's perimeter. To maintain a roller's effectiveness in terminating different cover crops, the steel drum is filled with water to increase roller weight (Derpsch et al., 1991). Rolling technology which originated in Brazil was introduced to US producers in the past decade but excessive roller vibration at high operating speeds hindered roller adoption (Raper et al., 2004). As a result of vibration problems, research has been conducted with new types of rollers to maintain cover crop termination effectiveness, without generating vibration on the tractor frame and the operator (Kornecki et al., 2006). Ashford and Reeves (2003) indicated that due to accelerated rye senescence, rye termination rates above 90% are sufficient to plant a cash crop. A firm soil surface facilitates crimping; otherwise cover crop residue will not be properly crimped and will be pushed into the soil by crimping bars. Rolling of a cover crop should be done approximately three weeks before planting a cash crop assuring that there is no competition between cover crop and cash crop for water and nutrients. Cover crops must be terminated at the appropriate growth stage, and for rye the proper growth stage is between early milk and soft dough stage for mechanical termination without herbicide (Ashford, Reeves, 2003). Typically, a cover crop must be planted earlier in the fall (e.g., October and November in the northern hemisphere) to reach the appropriate growth stage.

Materials and methods

For each field experiment, rye (*Secale cereale*, L.) was planted in rows during the fall (middle of October to middle of November, depending on weather conditions) using a no-till drill. In the spring, rye was usually terminated during the month of April at the appropriate growth stage (early milk to soft dough) utilizing newly patented rollers/crimpers developed at the National Soil Dynamics Laboratory in Auburn, Alabama. The following rollers were evaluated: smooth roller with crimping bar (Kornecki, Raper, 2009), roller for elevated beds (Kornecki, 2009), two stage roller crimper (Kornecki, 2011), and powered roller crimper (Kornecki, 2012). Control was the original straight bar roller/crimper and standing rye. Before rolling, height and biomass data were collected. Termination rates on a scale of 0% (no injury symptoms) to 100% (complete death) were evaluated at rolling (zero day), 7, 14, and 21 days after rolling. Rye termination rates were evaluated weekly for three weeks after rolling utilizing a visual method (Frans et al., 1986) and optical method described by Kornecki et al. (2012). Soil volumetric moisture content (VMC) was also measured during the same period using a time domain reflectometry (TDR) moisture meter from Spectrum Technologies (Plainfield, Illinois). To evaluate different roller designs, several field experiments with appropriate experimental designs with 4 replicates were employed. New rollers were tested during 3 growing seasons to determine climatic effects on termination.

Results

Termination rates of a rye cover crop (%) by different roller designs (Figure 1) at 7, 14 and 21 days after rolling operation in 2004 are shown in Figure 2a (Kornecki et al, 2006).

Figure 1 Different roller types: a. original Brazilian type straight bar roller, b. curved bar roller/crimper and c. smooth roller with crimping bar (U.S. patent #7,604,067 B1).

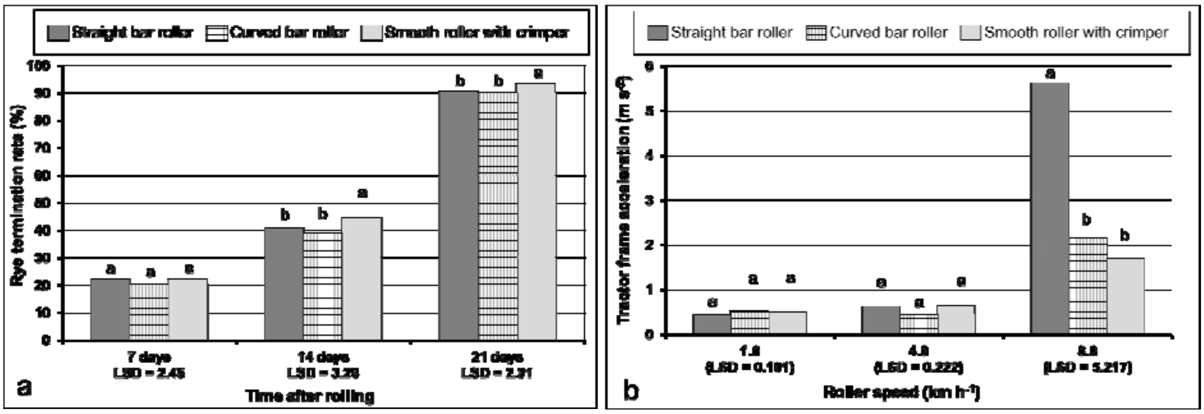

Figure 2 a. Termination rates for rye with respect to time after rolling/crimping for three different rollers in 2004, b. roller speed effect on vibration levels on tractor frame (2004 data).

Figure 3 Roller crimper for elevated beds (3a and 3b): a. one row and two furrows; b. two rows and three furrows (U.S. patent #7,562,517 B1); c. Two-stage roller/crimper (U.S. patent #7,987,917 B1).

Termination rates by newer roller designs were equivalent to or higher than termination rates obtained with the original straight bar roller. Three weeks after rolling, rye termination rates were 91%, 90%, and 93% for straight bar roller, curved bar roller and smooth roller with crimper, respectively. At 8.0 km h^{-1}, corresponding vibration levels for the smooth roller with crimper and curved roller were significantly lower than for the straight bar roller (Figure 2b).

Based on the success of new roller designs, new concepts of rollers/crimpers intended specifically for vegetable production were also developed. The first roller was for elevated beds to terminate cover crops on row-tops and in furrows. An example of this design (2.4 m wide roller) is shown in Figure 3: a. one row and two furrows, b. two rows and three furrows, Figure 3c shows a 1.8 m wide two stage roller/crimper designed to operate with smaller tractors (30 KW power source).

Rye termination rates obtained by the roller for elevated bed culture for different bed configurations as depicted in Figure 3a and Figure 3b were above 95% at 21 days after rolling. The two-stage roller crimper has been an aggressive device to successfully terminate different cover crops such as: rye, crimson clover and sunn hemp. It has been a roller of choice for small farm settings. Termination rates for the two-stage roller, 21 days after rolling were 99%, 97% and 98%, for 2006, 2007, and 2008, respectively (Kornecki et al., 2009a).

In conservation systems, rolling/crimping plus glyphosate application may be needed when there is a cold, wet, spring, because rolling/crimping alone may not be fast enough to efficiently and timely terminate a cover crop. Due to time constraints associated with cash crop planting, accelerating the termination process may be required to plant a cash crop without delays in the growing season that otherwise might have detrimental effects on cash crop yield. To determine an effective glyphosate rate in addition to cover crop rolling; an experiment was conducted with rye and glyphosate application. The idea was to spray glyphosate directly on crimped rye following crimping action (Kornecki et al., 2009b). Glyphosate was applied continuously while rolling, every second crimp, and every fourth crimp using a custom made boom with a high speed solenoid valve to momentary open and close herbicide flow to a flat stream discharge nozzle (Figure 4 a and b).

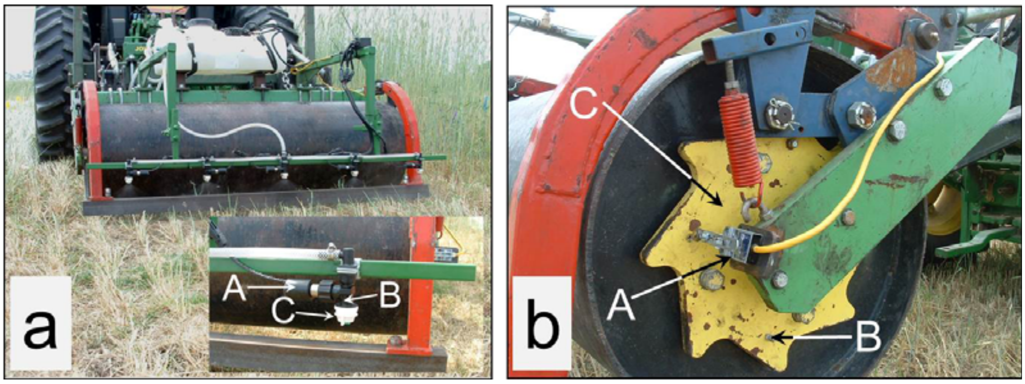

Figure 4 a. Back view of the smooth roller with crimping bar and the attached high speed solenoid valve: (A) solenoid valve, (B) nozzle body, (C) nozzle; b. Side view of the smooth roller with crimping bar. (A) Micro--switch, (B) engagement bolt with the micro-switch's arm, (C) eight-cam crimping bar control mechanism with clockwise rotation.

Table 1 Effect of treatment and amount glyphosate (Roundup™) used on average termination rates for smooth roller with crimping bar during 2006, 2007, and 2008 growing seasons.

Treatment	Glyphosate solution applied (L ha^{-1})	% glyphosate of continuous spray	Rye termination rate 7 days after rolling (%)
Continuous Spray	139.4	100	99
Spray every other crimp	40.2	29	96
Spray every 4^{th} crimp	17.8	13	93

Four engagement bolts (for every second crimp) and two bolts (for every fourth crimp), as shown in Figure 4b, were fastened to the cam mechanism at equal intervals 10.2 cm from the center of the roller's rotation. In operation, as the roller rotated, the engagement bolts also rotated. When the bolt was in contact with the micro-switch arm, the arm was rotated, which energized/de-energized the solenoid valves through the ON-OFF micro-switch and glyphosate was discharged through the nozzles for an instant (Figure 4a). Termination rates of rye and amount of glyphosate used are presented in Table 1.

The lowest glyphosate usage was measured for spraying herbicide every fourth crimp which reduced glyphosate usage 87% from the continuous spray treatment and caused 93% rye termination 7 days after rolling and spraying treatment application (Kornecki et al., 2009b).

As already indicated, to speed up cover crop termination, producers utilize herbicides to supplement rolling/crimping. However, in organic vegetable production, commercial herbicides cannot be used. Thus, terminating cover crops mechanically must be as efficient as chemical termination. In addition, on small farms, tractors are usually less powerful compared to large farms because of cost. To accommodate small farm operations, a powered roller crimper was developed and tested (Kornecki, 2012). The powered roller/crimper is a PTO-driven unit that is attached to a self-propelled walk behind a BCS 853 tractor powered by a Honda 9.7 kW gasoline engine (BCS Company, Milan, Italy). The potential energy stored in the springs when released, creates the downward acceleration of the crimping bar to crimp the cover crop (Figure 5). The crimping frequency can be manipulated both through the engine RPM and the forward speed of the tractor. To determine the roller's performance, a field experiment was established in 2010. The roller treatments were: Three different tractors' operating speeds and two different crimping bars: single-edge (Figure 5a) and double-edge (Figure 5b). A standing rye was a control and all treatments were replicated four times.

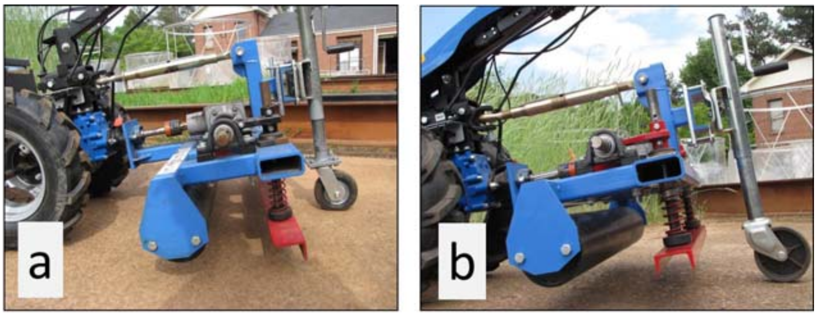

Figure 5 Powered roller: a. single edge crimper; b. double edge crimper (U.S. patent #8,176,991 B1).

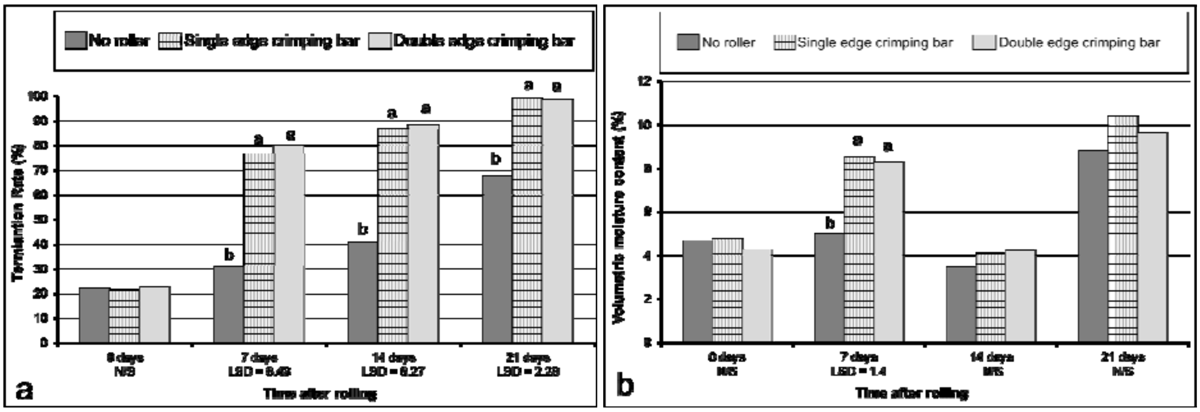

Figure 6 a. Effect of crimping bar type and forward speed on rye termination rate, b. treatment effect (crimping bar type and speed) on soil Volumetric Moisture Content during 2010 growing season.

Results have shown that the powered roller/crimper generated rye termination rates that are similar or higher compared with larger rollers. There were no significant differences between roller's operating speeds, and single and double edge crimping bar. Average termination rates were 87% and 98%, 14 and 21 days after rolling, respectively (Figure 6a), indicating that powered rollers are suitable for small farms where walk-behind tractors are used. Significant differences in soil VMC between all rolled rye (8.2%) and standing rye (5.0%) were observed one week after rolling indicating that rolled residue conserved soil moisture (Figure 6b).

Conclusion

Multi-year and multi-site research with many different roller developments showed that the new roller designs were very effective at terminating rye cover crops. Three weeks after rolling, these new roller/crimper concepts achieved termination rates exceeding 90% without the use of herbicides and in dry growing seasons conserved soil water due to mulch effects. This level of effectiveness is compatible with the original Brazilian design as termination rate by new rollers is maintained or exceeded. Vibrations generated by new roller designs were significantly lower compared with the original straight bar roller design. Filling the steel drum of the roller with water was not needed to increase the roller's weight, because the crimping energy was obtained from a spring system and the spring tension was adjustable to increase force to effectively terminate different cover crops with different biomass production. This family of new rollers was adopted to reduce the amount of herbicide required under cool wet spring conditions. Newly developed rollers were designed for different farm system scaling from large to very small. The powered roller crimper provided an effective solution for garden type and small vegetable no-till organic producers.

References:

Ashford D.L., Reeves, D.W., 2003. Use of a mechanical roller-crimper as an alternative kill method for cover crops. American Journal of Alternative Agriculture 18(1): 37-45.

Brady N.C., Weil R.R., 1999. The Nature and Properties of Soils, Twelfth ed. Prentice-Hall, Inc., Upper Saddle River, NJ.

Derpsch R., Roth C.H., Sidiras N., Köpke U., 1991. Controle da erosão no Paraná, Brazil: Sistemas de cobertura do solo, plantio directo e prepare conservacionista do solo. Deutsche Gesellschaft für Technische Zusammenarbeit (GTZ) GmbH, Eschborn, SP 245, Germany.

Frans R., Talbert R., Marx D., Crowley H., 1986. Experimental design and techniques for measuring and analyzing plant response to weed control practices. In Research Methods in Weed Science, 3rd ed., ed. N. D. Camper, Champaign, Ill.: Southern Weed Science Society: 37-38.

Kornecki T.S., Price A.J., Raper R.L., 2006. Performance of different roller designs in terminating rye cover crop and reducing vibration. Applied Engineering in Agriculture 22(5): 633-641.

Kornecki T.S., Raper R.L., 2009. Roller system for cover crop termination. U.S. Patent Number 7,604,067 B1.

Kornecki T.S., 2009. Rotary crimping apparatus for elevated crop beds. U.S. Patent Number 7,562,517 B1.

Kornecki T.S., Price A.J., Raper R.L., Arriaga F.J., 2009a. New roller crimper concepts for mechanical termination of cover crops. Renewable Agriculture and Food Systems 24(3): 165–173.

Kornecki, T.S., Price A.J., Raper R.L., Bergtold J.S., 2009b. Effectiveness of different herbicide applicators mounted on a roller/crimper for accelerated rye cover crop termination. Applied Engineering in Agriculture 25(6): 819-826.

Kornecki T.S., 2011. Multistage Crop Roller. U.S. Patent Number: 7,987,917 B1.

Kornecki T.S., 2012. Powered rolling and crimping device for crop termination. US Patent Number: 8,176,991 B1.

Kornecki T.S., Arriaga F.J., Price A.J., 2012. Evaluation of methods to assess termination rates of cover crops using visual and nonvisible light active sensors. The Transactions of the ASABE 54(4): 1213-1218.

Raper R.L., Simionescu P.A., Kornecki T.S., Price A.J., Reeves D.W., 2004. Reducing vibration while maintaining efficacy of rollers to terminate cover crops. Applied Engineering in Agriculture 20(5): 581-584.

Reeves D.W., 1994. Cover crops and rotations. In Advances in Soil Science: Crops Residue Management, eds. J. L. Hatfield and B. A. Stewart. Boca Raton, Fla.: Lewis Publishers.

CONVECTIVE AND MICROWAVE DRYING CHARACTERISTICS OF DILL LEAVES (*ANETHUM GRAVEOLENS* L.)

Turhan Koyuncu[1*], Fuat Lüle[2]

[1*]Faculty of Technology, University of Adiyaman, 02040 Adiyaman, Turkey
Phone: +90 416 2231775, Fax: +90416 2231774 E-mail: tkoyuncu@adiyaman.edu.tr
[2] University of Adiyaman, Vocational High School Kahta, Adiyaman, Turkey

Abstract

In this research, convective and microwave drying characteristics, energy requirement and color changes of dill leaves (Anethum graveolens L.) were reported. Dill leaves were dehydrated in a computer connected parallel air flow type dryer and in a microwave oven dryer. The convective dryer mainly consisted of an electric heater, temperature adjuster, centrifugal fan, air speed adjuster, corrosion resistant chromium mesh, corrosion resistant chromium sheet, glass wood insulator, a digital balance, RS232 connection, a PC, data processing software, drying air inlet and outlet channels as well as thermostat, hot-wire anemometer, humidity and temperature sensors, wattmeter and wheels. The microwave oven dryer mainly has a magnetron tube, oven cavity, filter, step-up transformer, power plug, wave guide, mode stirrer and oven tray. Samples of freshly harvested dill leaves were dehydrated under three air temperatures of 50 °C, 60 °C and 70 °C and at three microwave power levels of PL-1, PL-2 and PL-3. Selected drying air velocity was 0.30 m/s for all temperatures. This is coming from the fact that it was understood from the preliminary studies that the temperature less than 50 °C and the air speed more than 0.30 m/s increase the drying time and energy requirement, extremely for these products. Dill leaves were dehydrated from the initial moisture content of 735 (percentage dry basis) to a final moisture content of 8...10 %. During convective drying experiments, product were weighted automatically by the balance per 5...10 minutes. Data were transferred to the computer and processed by a software. During microwave drying, the product were weighted and data recorded manually per 15...60 minutes. The influence of drying method, drying air temperature and microwave power level have also been studied. Hunter L, a, b values system was also used to evaluate changes in total color difference (ΔE) on dried products. The results showed that convective drying air temperature and microwave oven power levels influenced the total drying time, total energy requirement, specific energy requirement and color difference for dill leaves. The minimum specific energy requirement were determined as 10.72 kWh/kg and 18.72 kWh/kg for 70 °C and PL-3 respectively. 70 °C drying air temperature and PL-3 was found to yield better quality product in terms of color retention of Hunter L, a, b and ΔE. As a result, to reduce drying energy consumption and to keep better color retention, convective drying can be recommended for this application.

Keywords : Dill leaves, convective drying, microwave drying, drying characteristics

Nomenclature

A Drying air flow surface area, m^2
c Specific heat of air under adiabatic conditions, kJ/(kg K)
D_t Total drying time, h
$E_{kg(c)}$ Energy requirement for drying 1 kg of product and for convective drying, kWh/kg
$E_{kg(m)}$ Energy requirement for drying 1 kg of product and for microwave drying, kWh/kg
$E_{t(c)}$ Total energy requirement for a charge of the convective dryer, kWh
$E_{t(m)}$ Total energy requirement for a charge of the microwave dryer, kWh
I Electric current, A
PM_{db} The moisture content on dry basis expressed as percentage, %
U Electric voltage, V
v Drying air speed , m/s
W_d Weight of dry matter in product, kg
W_o Initial weight of undried product, kg
ΔT Temperature differences, K
ρ Air density, kg/m^3

Introduction

The drying or dehydration is the oldest method in food conservation, and its object is to remove by evaporation most of the water present in the product. The reduction of moisture content inhibits or decrease microbial and enzymatic activity, which otherwise would produce food damage. Besides, dehydration makes food product handling easier owing to the volumetric shrinkage and weight losses products undergo during process (Ochoa et al., 2002). Natural open-air sun drying is practiced widely in hot climates and tropical countries. Considerable savings can be obtained with this type of drying, since the source of energy is free and renewable. However, this technique is extremely weather, dependent and has the problems of contamination, infestation, microbial attack, etc. Also, the required drying time for a given load is approximately 2-4 times longer than greenhouse, cabinet and parallel air flow type dryers (Koyuncu, Pinar, 2001; Koyuncu, Sessiz, 2002; Toğrul, Dursun, 2003). In addition, the drying methods and dryer types strongly affect the color retention of the product. In recent years, much attention has been paid to the quality of foods during drying. Both the method of drying and physicochemical changes that occur in tissues during drying affect the quality of the dehydrated product. More specially, the method used for drying affects properties such as colour, texture, density, porosity, and sorption characteristics of material (Krokida et al., 2001). Color plays an important role in appearance, processing, and acceptability of food materials. Color is perceived as part of the total appearance, which is the visual recognition and assessment of the surface and subsurface properties of the object (Ahmed et al., 2002; Termentziet al., 2009). The first quality judgement made by a consumer on a food at point of sale is on its appearance. Appearance analyses of foods (color, taste, odor, and texture) are used for the maintenance of quality throughout and at the end of processing. Color is, perhaps, the most important appearance attribute because abnormal colors, especially those associated with deterioration in eating quality or with spoilage, cause the product to be rejected by the consumer (Alarcao-E-Silva et al., 2001; Lopez et al., 1997).

Color deterioration has been studied by several researchers for a number of products. Studying the effects of five methods of drying: conventional, vacuum, microwave, freeze and osmotic drying on color of apple, banana, potato and carrot (Krokida et al., 2001), measured the color characteristics by Hunter Lab chromameter and reported that the changes in redness (a) and yellowness (b) followed a first order kinetic model. Lopez (1997) studied the influence of drying conditions on hazelnut browning, and evaluated the colour changes by CIELab system. The rate of pigment formation was determined from the total color values with zero-order kinetic model. Rocha et al. (1993) studied the effect of pretreatments on drying rate and color retention of basil. Negi and Roy (2000) studied about the effects of different blanching and drying treatments to establish the retention of β-carotene, ascorbic acid and chlorophyll in leaves of savoy beet (*Beta vulgaris* var *bengalensis*), amaranth (*Amaranthus tricolor*) and fenugreek (*Trigonella foenum graecum*).

Dill (Anethum graveolens L.), a biennial or annual herb of the parsley family (Apiaceae or Umbelliferae), is native to southwest Asia or southeast Europe and cultivated since ancient times. The leafy tops can be clipped and used in cottage cheese, potato salad, cream cheese, tomato soup and salads (Doymaz et al., 2006).

Dill grows up to 90–120 cm tall and has slender branched stems, finely divided leaves, small umbels (2–9 cm diameter) of yellow flowers, and long spindle- shaped roots. In general, dill leaves (dill weeds) and seeds (small fragrant fruits) are used as seasoning. The leaves could be used in eggs, meats, salads, seafoods and soups; the seeds could be used in bread, and flavouring pickles and soups. Dill essential oil, extracted from both leaves and seeds, could also be used in chewing gums, candies and pickles. The plant is native in Southwest Asia and is cultivated in Europe, India and the United States. It is also successfully cultivated in Taiwan. Literature demonstrates that dill leaf consumption could lower the risk of cancer and reduce the level of cholesterolaemia. Moreover, dill leaf, seed and their essential oil could provide good antioxidant activities (Shyu et al., 2009).

In recent years the demand for seasoning vegetables has grown, reflecting the increase in their consumption. The variety of dill classed as a seasoning vegetable is being applied more and more widely in modelling the flavour of numerous food products. It can be used as an ingredient in dried seasoning mixtures; in the production of cheeses, fish, and vegetarian dishes; as an admixture in ‘‘ready-to-eat’’ and—more recently—‘‘do-it-for-me’’ dishes; and also as a basic constituent of soups and sauces which are very popular in Central and Eastern Europe. The use of dill for various culinary purposes depends to a great extent on its vegetative development as measured by the plant height. The value of dill for processing also depends on the stage of growth. Young delicate plants can be used for drying, the older ones for freezing, while those at a more advanced stage of growth can be used for the preparation of stock or extracts. The intensity of colour and its shade—and hence the attractiveness of the raw material—depend on the level of chlorophyll pigments and their proportions. In green plants the chlorophyll pigments are accompanied by carotenoids, which affect the colour of the raw material and of products obtained from it and also enhance their vitamin content. The last statement chiefly concerns beta-carotene. Like vitamin C and polyphenol compounds, carotenoids are also classified among the basic constituents of the antioxidative effect. Green vegetables, including dill, are a rich source of these substances (Lisiewska et al., 2006).

In order to store dill leaves, it is possible to use different methods such as traditional method, cold storage and drying depending on the technical opportunities, food consumption and food processing ways (Slupski et al., 2005). In different literatures, it is possible to see some information about mathematical modelling and experimental studies of thin layer drying process of various vegetables such as garlic, red pepper, purslane, eggplant, broccoli, and onion. However, not enough report concerning the convective and microwave drying characteristics, heat energy requirement and color retention of dill leaves for during our literature survey (Doymaz et al., 2006). Therefore, fresh and cleaned dill leaves were dehydrated in a microwave oven dryer at different power levels and in a computer connected parallel air flow type dryer at various temperatures and selected most suitable velocity to determine the drying kinetics, energy requirement and color retention for drying in this experimental investigation. Besides, and other aim of this study was also to investigate the effect of various drying methods and drying temperatures on the color of dehydrated dill leaves.

Materials and Methods

Dill leaves grown in Black Sea Region of Turkey were freshly harvested manually and used for the investigation. Dill leaves were cleaned in an air screen to remove all foreign material such as dust, dirt, pieces of branches and foreign leaves. Dill leaves were dried in a computer connected parallel flow type dryer and in a microwave oven dryer. The convective dryer equipped with an electric heater (air heating duct), temperature adjuster, centrifugal fan (blower), air speed adjuster (regulator of variable transformer), corrosion resistant chromium mesh, corrosion resistant chromium sheet, glass wood insulator, a 0.01 g sensitive Precisa BJ 600 D digital balance, RS232 connection, a PC, specially designed Balint data processing software, drying air inlet and outlet channels as well as thermostat, temperature indicators, wattmeter and free wheels (Fig. 1). The microwave oven dryer mainly consists of magnetron tube (source of radiation), oven cavity, filter, step-up transformer, power plug, wave guide, mode stirrer and oven tray (Fig. 2). The products were placed on the chromium mesh as a thin layer. In order to produce different temperatures and fix up the velocity, the electric current of the heater and the rotation of the fan were adjusted manually. The system was also controlled by the thermostat automatically. To measure the power consumption, air speed, relative humidity and drying air temperatures at different points, several digital devices such as watt meter, hot-wire anemometer having in the measurement sensitive of 0.1 m/s, Testo AG 309 type relative humidity and temperature sensors and thermocouple were connected to the drying system. In addition, it must be noted that the experimental drying studies we conducted showed us that the maximum length of the drying chamber was approximately 1m depending on the drying air temperature distribution during the length of the dryer. Thus, the drying chamber was selected less than 1m long. During these studies, it was also seen that when the length of the drying chamber more than 1m, there were important temperature and relative humidity differences between the beginning and the end of the drying chamber (Koyuncu et al., 2003; Koyuncu et al., 2004). The moisture content (percentage dry basis) of fresh products, at harvest was approximately 735 % (Eq. 1) (Ekechukwu, 1999). Moisture content of the products were determined by using an air oven set at 105 °C, and kept until reaching constant weight (AOAC, 1984; (Ochoa et al., 2002). For safe long-term storage, the moisture content should preferably be less than 10 %. For that reason, the fresh products with moisture content of 735 % was dehydrated until the moisture content becomes 8…10 % in the dryer. During drying time, the mass of dill leave samples were weighted automatically by the balance per 5…10 minutes and all test were replicated three times. The dryer was installed in conditions that were a relative humidity of 60 % (±3) and a temperature of 20°C (±1). This air was heated by the heater and directed to the drying chamber. Three different temperatures such as 50, 60 and 70 °C and a selected air velocity of 0.30 m/s were used for experimentation. This is coming from the fact that it was understood from the preliminary studies that the temperature less than 50 °C and the air speed more than 0.30 m/s extremely increase the drying time and energy requirement for these products. In addition, three power levels (PL-1, PL-2 and PL-3) of microwave oven dryer were also used for products drying. The products were placed on the tray of the oven dryer that technical features given in Tab. 1 for drying. During experiments, drying characteristics, total drying time, total energy needed for drying of one charge of the dryer, total energy requirement for drying 1 kg of wet product (specific energy requirement) and color retention for different convective drying temperatures and for microwave drying power levels were found (Eq. 2, 3, 4 and 5) (Holman, 1994). When drying was complete, the average moisture content of each sample was analyzed according to the vacum oven method (AOAC, 1984) (Eq. 1) and the Hunter L, a, b values of dehydrated dill leaves were determined to study the color of the samples. Color was evaluated by measuring Hunter L (brightness, 100=white, 0=black), a (+, red; -, green) and b (+, yellow; -, blue) parameters by means of a reflectance colorimeter (CR 400, Chromometer, Minolta, Japan). A white tile (No: 19633162) was used to standardize the instrument. From the instrumental Hunter L, a, b values and the color difference (ΔE) were calculated according to the Eq. 6.

$$PM_{db} = \left[\frac{W_o - W_d}{W_d}\right] \times 100 \tag{1}$$

$$E_{t(c)} = A.v.\rho.c.\Delta T.D_t \tag{2}$$

$$E_{t(m)} = \frac{U.I}{1000}.D_t \tag{3}$$

$$E_{kg(c)} = \frac{E_{t(c)}}{W_o} \tag{4}$$

$$E_{kg(m)} = \frac{E_{t(m)}}{W_o} \tag{5}$$

$$\Delta E = \left[(\Delta L)^2 + (\Delta a)^2 + (\Delta b)^2\right]^{1/2} \tag{6}$$

Tab. 1 Technical features of microwave oven dryer

Data / Power Level (P-L) (Written on the oven by the manufacturer)	**(PL-1) 90 W**	**(PL-2) 160 W**	**(PL-3) 350 W**
Voltage (~V)	232	232	232
Current of fan and lamp (A)	0.23	0.23	0.23
Current of magnetron tube and tray motor (A)	6.92	6.92	6.92
Current of all components (A)	7.15	7.15	7.15
Power consumption of fan and lamp (W)	53.36	53.36	53.36
Power consumption of magnetron tube and tray motor (W)	1605.44	1605.44	1605.44
Total power consumption (for all components) (W)	1658.80	1658.80	1658.80
Active period time of Fan and Lamp, only (s)	17	15	12
Active period time of all components (s)	4	6	9
Total time of a period (s)	21	21	21
Real power consumption for different levels (measured) (W)	359.21	512.07	741.35

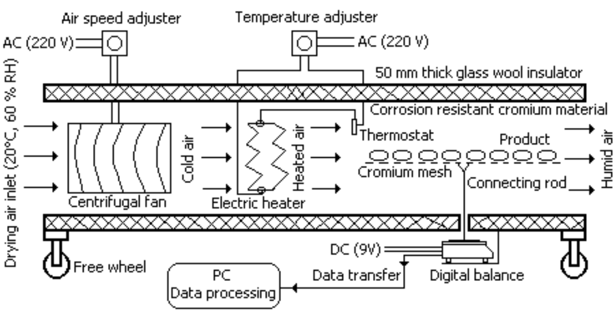

Fig. 1 Schematic presentation of the computer connected parallel flow type dryer

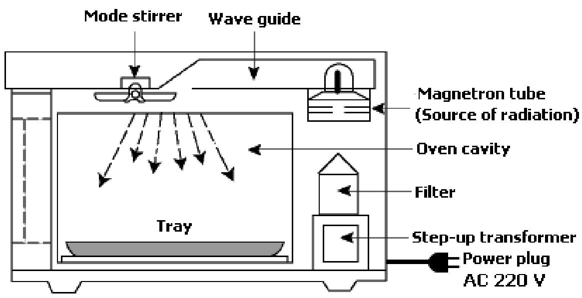

Fig. 2 Schematic presentation of the microwave oven dryer

Results and Discussion

During a drying process, two periods can be distinguished. The first is called constant drying rate period. The second drying stage is also called the falling drying rate period. During the first period, the surface of the product behaves as a surface of the water. The rate of moisture removal during this period is mainly dependent on the surrounding conditions and only affected slightly by the nature of the product. The end of the constant drying rate period is marked by a decrease in the rate of moisture migration from within the product below that sufficient to replenish the moisture being evaporated from the surface. The falling drying rate period is dependent essentially on the rate of diffusion of moisture from within the product to the surface and also on moisture removal from the surface. For agricultural products, the duration of each of the drying regimes depends on the initial moisture content and the safe storage moisture content. Especialy, for fruits and most vegetables, the drying would take place within both the constant and falling rate periods that can be seen easily. Both the external factors and the internal mechanisms controlling the drying processes in the two main rate regimes are important in determining the overall drying rate of products (Ekechukwu, 1999; Gigler et al., 2000). For these reasons, the changing of the moisture content of dill leaves must have two periods depending on the drying time. The moisture content of the products as a function of drying time are presented in Fig. 3 and 4 for different convective drying temperatures and for microwave power levels. As seen from these figures, all lines have two stages. The moisture content rapidly reduces and then slowly decreases with rising of the drying time. In addition, it is obvious from the figures that drying temperature and microwave power have an important role on the total drying time (Fig. 3, 4 and 5). The least drying time (0.42 h) was obtained at PL-3. The highest drying time (11 h) was also found at 50 °C temperature. The total energy requirement for a charge of each dryer and energy needed for drying 1 kg of products can be seen from Fig. 6 and Fig. 7, respectively. There is a strict correlation between these two figures. This is because of the fact that the values of Fig. 7 were obtained from value of Fig. 6 by calculation (Eq. 2, 3, 4 and 5). As it is understood from these figures, the minimum heat energy (10.72 kWh/kg) is needed for drying of 1 kg products at temperature of 70 °C for dill leaves. The maximum energy (61.68 kWh/kg) is needed at PL-1.

Colour is an important quality attribute in a food to most consumers. In addition, colour analysis is important of foods, especially quality criterion for the production and for the trade. It is an index of the inherent good qualities of a food and association of colour with acceptability of food is universal (Doymaz et al., 2006). L, a, b and ΔE values are commonly used as a index to report the colour quality.

The changes in color parameters of dehydrated dill leaves are presented in Fig. 8 and Fig. 9. Samples dried at 70 °C and PL-1 showed the highest Hunter L value, whereas the samples being dried at 60 °C and PL-2 gave the lowest L values. Different authors have reported that, decreases in L value correlated well with increases in browning of foods (Jimenes et al., 1994; Lozano et al., 1994). So the dill leaves dried at 60 °C and PL-2 experienced an extensive browning. The redness (a) value decreased in comparison to fresh samples and the highest decreases were found in the drying temperatures of 50 °C and power level of PL-2. The yellowness (b) value was highest for the samples dried at 60 °C and PL-3. The color changes in ΔE was also obtained for convective drying temperatures and microwave oven power levels. The color difference was relatively high for the samples dried at 50 °C and PL-2. Finally, the color changes in samples dehydrated at 70 °C and PL-3 were lower than the other drying temperature and power levels. No significant difference was found in color changes among the 70 °C temperature and PL-3. There were about 11 % and 5 % decline in Hunter b values, compared with the fresh products for 70 °C and PL-3, respectively. This may be caused by good retention of carotenoids in the samples dried at 70 °C and PL-3.

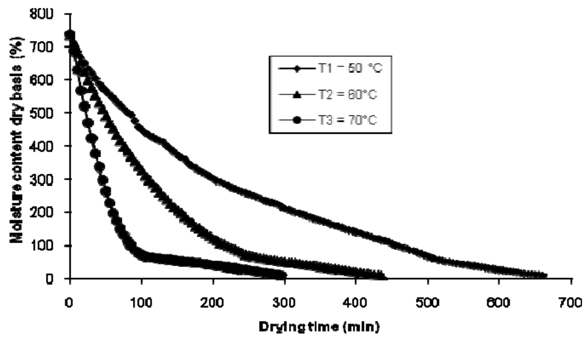

Fig. 3 Moisture content as a function of convective drying time for temperature of 50°C, 60°C and 70°C

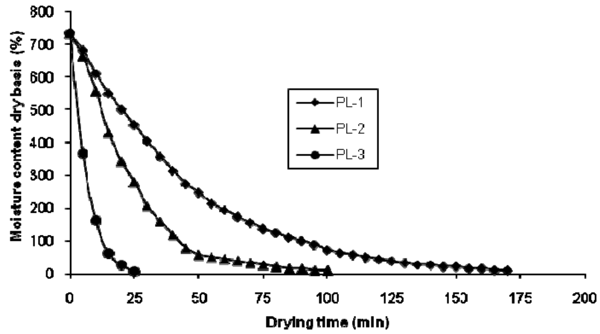

Fig. 4 Moisture content as a function of microwave drying time for power level of PL-1, PL-2 and PL-3

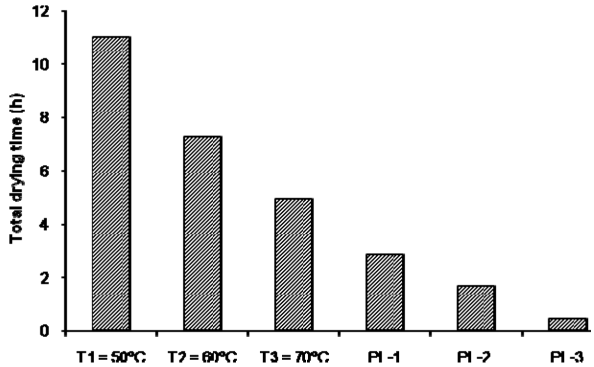

Fig. 5 Total drying time of product at different temperatures and power levels

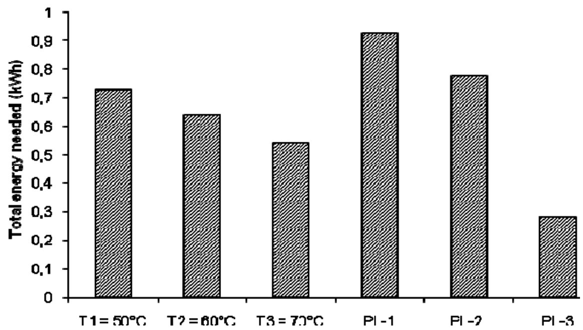

Fig. 6 Total energy requirement for a charge of convective and microwave dryers at different temperatures and power levels

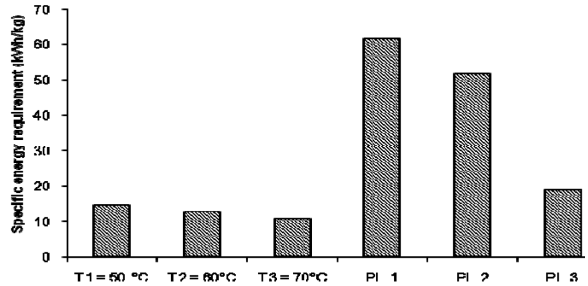

Fig. 7 Energy requirement for drying 1 kg of product for convective and microwave dryer

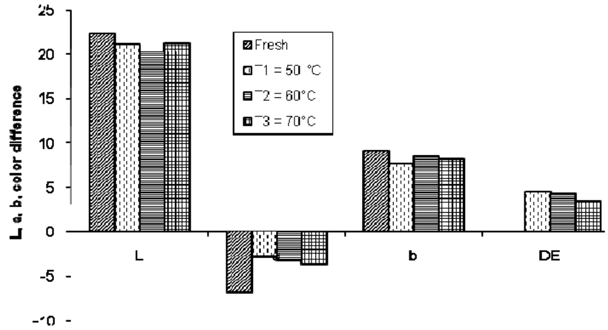

Fig. 8 Color changes in Hunter L, a, b and color difference (ΔE) of dill leaves dried at temperature of 50 °C, 60 °C and 70 °C

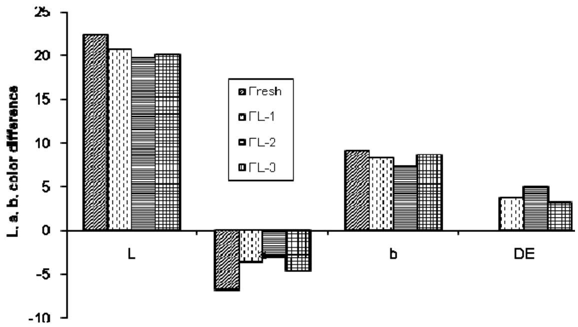

Fig. 9 Color changes in Hunter L, a, b and color difference (ΔE) of dill leaves dried at microwave power levels of PL-1, PL-2 and PL-3

Conclusions

Dill leaves were successfully dried in a computer connected parallel air flow type convective dryer and in a microwave oven dryer at different temperatures of 50, 60 and 70 °C, air speed of 0.30 m/s and power levels of PL-1, PL-2 and PL-3. It is found from the results of the experimental investigation that the drying air temperature and power levels has an important role on the total drying time, specific power consumption and dill leaves color changes. The main conclusion of this study is that dill leaves must be dried in convective type dryer at temperature of 70 °C and air velocity of 0.30 m/s to minimize the energy consumption and to keep the higher quality and color retention for drying of dill leaves.

References

Ahmed J., Kaur A., Shivhare U., 2002. Color egradation Kinetics of Spinach, Mustard Leaves, and Mixed Puree. Journal of Food Science, 67(3): 1088-1091.

Alarcao-E-Silva M.L.C.M.M., Leitao A.E.B., Azinheira H.G., Leitao M.C.A., 2001. The Arbutus berry : studies on its color and chemical characteristics at two mature stages. Jounal of Food Composition and Analysis, 14: 27-35.

AOAC, 1984. Official methods of analysis of the association of official analytical chemists. 14th Ed., Arlington : Virginia. 22.013, USA.

Doymaz I., Tugrul N., Pala M., 2006. Drying characteristics of dill and parsley leaves. Jounal of Food Engineering, 77: 559-565.

Ekechukwu O.V., 1999. Review of solar-energy drying systems I: an overview of drying principles and theory. Energy Conversion and Management, 40: 593-613.

Holman J.P., 1994. Experimental methods for engineers. McGraw-Hill, Inc; New York, USA.

Gigler J.K., Loon W.K.P., Seres I., Meerdink G., Coumans W.J., 2000. Drying characteristics of willow chips and stems. J. Agric. Engng. Res., 77(4): 391-400.

Jimenes M., Mateo J.J., Huerta T., Mateo R., 1994. Influence of the Storage Conditions on Some Physiochemical and Mycological Parameters of Honey. Journal of the Science of Food and Agriculture, 64(1): 67-74.

Koyuncu T., Pinar Y., 2001. Kırmızı biber için bir güneşli kurutucu tasarımı (Design of a solar dryer for red pepper). Tarımsal Mekanizasyon 20 Ulusal Kongresi; 13-15 Eylül, Şanlıurfa, Türkiye.

Koyuncu T., Sessiz A., 2002. Güneş enerjili kurutucular üzerine karşılaştırmalı bir araştırma (A comparative study on solar energy dryer). O.M.Ü. Ziraat Fak. Dergisi, 17(2): 53-60.

Koyuncu T., Tosun İ., Üstün N.S., 2003. Drying kinetics and color retention of dehydrated rosehips. Drying Technology, 21(7): 1369-1381.

Koyuncu T., Serdar U., Tosun İ., 2004. Drying kinetics and energy requirement for dehydration of chestnuts (Castanea sativa Mill.). Jounal of Food Engineering, 62: 165-168.

Krokida M.K., Maroulis Z.B., Saravacos G.D., 2001. The Effect of the Method of Drying on the Colour of Dehyrated Products. International Journal of Food Science and Technology, 36: 53-59.

Lisiewska Z., Kmiecik W., Korus A., 2006. Content of vitamin C, carotenoids, chlorophylls and polyphenols in green parts of dill (Anethum graveolens L.) depending on plant height. Jounal of Food Composition and Analysis, 19: 134-140.

Lopez A., Pique M.T., Boatella J., Romero A., Ferran A., Garcia J., 1997. Influence of Drying Conditions on the Hazelnut Quality: III. Browning. Drying Technology, 15(3&4): 989-1002.

Lozano J.E., Drudis R., Ibarz A., 1994. Enzymatic Browning in Apple Pulps. Journal of Food Science, 59(3): 564-567.

Negi P.S., Roy S.K., 2000. Effect of Blanching and Drying Methods on β-Carotene, Ascorbic acid and Chlorophyll Retention of Leafy Vegetables. Lebensmittel-Wissenschaft und-Technologie/FST., 33 (4): 295-298.

Ochoa M.R., Kesseler A.G., Pirone B.N., Marquez C.A., Michelis A.D., 2002. Shrinkage during convective drying of whole rose hip (Rosa Rubiginosa L.) fruits. Lebensm.- Wiss. U.-Technol., 35: 400-406.

Rocha T., Lebert A., Marty-Audouin C., 1993. Effect of Pretreatments and Drying Conditions on Drying Rate and Colour Retention of Basil (Ocimum basilicum). Lebensmittel-Wissenschaft und-Technologie/FST., 26(5): 456-463.

Shyu Y.S., Lin J.T., Chang Y.T., Chiang C.J., Yang D.J., 2009. Evaluation of antioxidant ability of ethanolic extract from dill (Anethum graveolens L.) flowers. Food Chemistry, 115: 515-521.

Slupski J., Lisiewska Z., Kmiecik W., 2005. Contents of macro and microelements in fresh and frozen dill (Anethum graveolens L.). Food Chemistry, 91: 737-743.

Termentzi A., Zervou M., Kokkalou E., 2009. Isolation and structure elucidation of novel phenolic constituents from Sorbus domestica fruits. Food Chemistry, 116: 371-381.

Toğrul T.T., Dursun P., 2003. Modeling of drying kinetics of single apricot. Jounal of Food Engineering, 58: 23-32.

ENERGY REQUIREMENT AND COLOR CHARACTERISTICS OF BLACK CABBAGE LEAVES (*BRASSICA OLERACEA* L.) DURING CONVECTIVE AND MICROWAVE DRYING

Turhan Koyuncu*, Fuat Lüle

University of Adiyaman, 02040 Adiyaman, Turkey
Phone: +90 416 2231775, Fax: +90416 2231774, E-mail: tkoyuncu@adiyaman.edu.tr

Abstract

In this research, convective and microwave drying characteristics, energy requirement and color changes of black cabbage leaves (Brassica oleracea L.) were reported. Black cabbage leaves were dehydrated in a computer connected parallel air flow type dryer and in a microwave oven dryer. The convective dryer mainly consisted of an electric heater, temperature adjuster, centrifugal fan, air speed adjuster, corrosion resistant chromium mesh, corrosion resistant chromium sheet, glass wood insulator, a digital balance, RS232 connection, a PC, data processing software, drying air inlet and outlet channels as well as thermostat, hot-wire anemometer, humidity and temperature sensors, wattmeter and wheels. The microwave oven dryer mainly has a magnetron tube, oven cavity, filter, step-up transformer, power plug, wave guide, mode stirrer and oven tray. Samples of freshly harvested black cabbage leaves were dehydrated under three air temperatures of 50 °C, 60 °C and 70 °C and at three microwave power levels of PL-1, PL-2 and PL-3. Selected drying air velocity was 0.30 m/s for all temperatures. This is coming from the fact that it was understood from the preliminary studies that the temperature less than 50 °C and the air speed more than 0.30 m/s increase the drying time and energy requirement, extremely for these products. Black cabbage leaves were dehydrated from the initial moisture content of 402 (percentage dry basis) to a final moisture content of 8...9 %. During convective drying experiments, product were weighted automatically by the balance per 5...10 minutes. Data were transferred to the computer and processed by a software. During microwave drying, the product were weighted and data recorded manually per 15...60 minutes. The influence of drying method, drying air temperature and microwave power level have also been studied. Hunter L, a, b values system was also used to evaluate changes in total color difference (ΔE) on dried products. The results showed that convective drying air temperature and microwave oven power levels influenced the total drying time, total energy requirement, specific energy requirement and color difference for black cabbage leaves. The minimum specific energy requirement were determined as 3.66 kWh/kg and 7.35 kWh/kg for 70 °C and PL-3 respectively. 70 °C drying air temperature and PL-1 was found to yield better quality product in terms of color retention of Hunter L, a, b and ΔE. As a result, to reduce drying energy consumption and to keep better color retention, convective drying can be recommended for this application.

Keywords: Black cabbage leaves, convective drying, microwave drying, drying characteristics.

Nomenclature

A Drying air flow surface area, m^2
c Specific heat of air under adiabatic conditions, kJ/(kg K)
D_t Total drying time, h
$E_{kg(c)}$ Energy requirement for drying 1 kg of product and for convective drying, kWh/kg
$E_{kg(m)}$ Energy requirement for drying 1 kg of product and for microwave drying, kWh/kg
$E_{t(c)}$ Total energy requirement for a charge of the convective dryer, kWh
$E_{t(m)}$ Total energy requirement for a charge of the microwave dryer, kWh
I Electric current, A
PM_{db} The moisture content on dry basis expressed as percentage, %
U Electric voltage, V
v Drying air speed , m/s
W_d Weight of dry matter in product, kg
W_o Initial weight of undried product, kg
ΔT Temperature differences, K
ρ Air density, kg/m^3

Introduction

The drying or dehydration is the oldest method in food conservation, and its object is to remove by evaporation most of the water present in the product. The reduction of moisture content inhibits or decrease microbial and enzymatic activity, which otherwise would produce food damage. Besides, dehydration makes food product handling easier owing to the volumetric shrinkage and weight losses products undergo during process (Ochoa et al., 2002). Natural open-air sun drying is practiced widely in hot climates and tropical countries. Considerable savings can be obtained with this type of drying, since the source of energy is free and renewable. However, this technique is extremely weather, dependent and has the problems of contamination, infestation, microbial attack, etc. Also, the required drying time for a given load is approximately 2-4 times longer than greenhouse, cabinet and parallel air flow type dryers (Koyuncu, Pinar, 2001; Koyuncu, Sessiz, 2002; Toğrul, Dursun, 2003). In addition, the drying methods and dryer types strongly affect the color retention of the product. In recent years, much attention has been paid to the quality of foods during drying. Both the method of drying and physicochemical changes that occur in tissues during drying affect the quality of the dehydrated product. More specially, the method used for drying affects properties such as colour, texture, density, porosity, and sorption characteristics of material (Krokida et al., 2001). Color plays an important role in appearance, processing, and acceptability of food materials. Color is perceived as part of the total appearance, which is the visual recognition and assessment of the surface and subsurface properties of the object (Ahmed et al., 2002; Termentzi et al., 2009). The first quality judgement made by a consumer on a food at point of sale is on its appearance. Appearance analyses of foods (color, taste, odor, and texture) are used for the maintenance of quality throughout and at the end of processing. Color is, perhaps, the most important appearance attribute because abnormal colors, especially those associated with deterioration in eating quality or with spoilage, cause the product to be rejected by the consumer (Alarcao-E-Silva et al., 2001; Lopez et al.,1997).

Color deterioration has been studied by several researchers for a number of products. Studying the effects of five methods of drying: conventional, vacuum, microwave, freeze and osmotic drying on color of apple, banana, potato and carrot, Krokida et al. (2001), measured the color characteristics by Hunter Lab chromameter and reported that the changes in redness (a) and yellowness (b) followed a first order kinetic model. López et al. (1997), studied the influence of drying conditions on hazelnut browning, and evaluated the colour changes by CIELab system. The rate of pigment formation was determined from the total color values with zero-order kinetic model. Rocha et al. (1993), studied the effect of pretreatments on drying rate and color retention of basil. Negi and Roy (2000), studied about the effects of different blanching and drying treatments to establish the retention of β-carotene, ascorbic acid and chlorophyll in leaves of savoy beet (*Beta vulgaris* var *bengalensis*), amaranth (*Amaranthus tricolor*) and fenugreek (*Trigonella foenum graecum*).

Brassica Oleracea is widely grown in all the East African countries and in many other parts of the world including Europe, Asia and Latin America. This leafy vegetable has high amounts of vitamins as well as other micronutrients and is well ranked in terms of nutrition among members of the cabbage family. However, it has a high moisture content at harvest and therefore cannot be preserved for more than a few days under ambient conditions of 20–25 °C (Mwithiga, Olwal, 2005). Therefore, it is necessary to use different methods for preservation of product.

In order to store black cabbage leaves, it is possible to use different methods such as traditional method, cold storage and drying depending on the technical opportunities, food consumption and food processing ways (Slupski et al., 2005). In different literatures, it is possible to see some information about mathematical modelling and experimental studies of thin layer drying process of various vegetables and fruits such as garlic, red pepper, purslane, eggplant, broccoli, onion, carrots, mint and grape. However, not enough report concerning the convective and microwave drying characteristics, heat energy requirement and color retention of black cabbage leaves for during our literature survey (Arslan, Özcan, 2010; Barnwal, Tiwari, 2008; Doymaz et al., 2006; Koca et al., 2007; Mo et al., 2006; Ozbek, Dadali, 2007; Volden et al.,2008). Therefore, fresh and cleaned black cabbage leaves were dehydrated in a microwave oven dryer at different power levels and in a computer connected parallel air flow type dryer at various temperatures and selected most suitable velocity to determine the drying kinetics, energy requirement and color retention for drying in this experimental investigation. Besides, and other aim of this study was also to investigate the effect of various drying methods and drying temperatures on the color of dehydrated black cabbage leaves.

Materials and Methods

Black cabbage leaves grown in Black Sea Region of Turkey were freshly harvested manually and used for the investigation. Black cabbage leaves were cleaned in an air screen to remove all foreign material such as dust, dirt, pieces of branches and foreign leaves. Black cabbage leaves were dried in a computer connected parallel flow type dryer and in a microwave oven dryer. The convective dryer equipped with an electric heater (air heating duct), temperature adjuster, centrifugal fan (blower), air speed adjuster (regulator of variable transformer), corrosion resistant chromium mesh, corrosion resistant chromium sheet, glass wood insulator, a 0.01 g sensitive Precisa BJ 600 D digital balance, RS232 connection, a PC, specially designed Balint data processing software, drying air inlet and outlet channels as well as thermostat, temperature indicators, wattmeter and free wheels (Fig. 1). The microwave oven dryer mainly consists of magnetron tube (source of radiation), oven cavity, filter, step-up transformer, power plug, wave guide, mode stirrer and oven tray (Fig. 2). The products were placed on the chromium mesh as a thin layer. In order to produce different temperatures and fix up the velocity, the electric current of the heater and the rotation of the fan were adjusted manually. The system was also controlled by the thermostat automatically. To measure the power consumption, air speed, relative humidity and drying air temperatures at different points, several digital devices such as watt meter, hot-wire anemometer having in the measurement sensitive of 0.1 m/s, Testo AG 309 type relative humidity and temperature sensors and thermocouple were connected to the drying system. In addition, it must be noted that the experimental drying studies we conducted showed us that the maximum length of the drying chamber was approximately 1m depending on the drying air temperature distribution during the length of the dryer. Thus, the drying chamber was selected less than 1m long. During these studies, it was also seen that when the length of the drying chamber more than 1m, there were important temperature and relative humidity differences between the beginning and the end of the drying chamber (Koyuncu et al., 2003; Koyuncu et al., 2004). The moisture content (percentage dry basis) of fresh products, at harvest was approximately 402 % (Eq. 1) (Ekechukwu, 1999). Moisture content of the products were determined by using an air oven set at 105 °C, and kept until reaching constant weight (AOAC, 1984; Ochoa et al., 2002). For safe long-term storage, the moisture content should preferably be less than 10%. For that reason, the fresh products with moisture content of 402 % was dehydrated until the moisture content becomes 8…9 % in the dryer. During drying time, the mass of black cabbage leaves samples were weighted automatically by the balance per 5…10 minutes and all test were replicated three times. The dryer was installed in conditions that were a relative humidity of 60 % (±3) and a temperature of 20 °C (±1). This air was heated by the heater and directed to the drying chamber. Three different temperatures such as 50, 60 and 70 °C and a selected air velocity of 0.30 m/s were used for experimentation. This is coming from the fact that it was understood from the preliminary studies that the temperature less than 50 °C and the air speed more than 0.30 m/s extremely increase the drying time and energy requirement for these products. In addition, three power levels (PL-1, PL-2 and PL-3) of microwave oven dryer were also used for products drying. The products were placed on the tray of the oven dryer that technical features given in Table 1 for drying. During experiments, drying characteristics, total drying time, total energy needed for drying of one charge of the dryer, total energy requirement for drying 1 kg of wet product (specific energy requirement) and color retention for different convective drying temperatures and for microwave drying power levels were found (Eq. 2, 3, 4 and 5) (Holman, 1994). When drying was complete, the average moisture content of each sample was analyzed according to the vacum oven method (AOAC, 1984). (AOAC, 1984) (Eq. 1) and the Hunter L, a, b values of dehydrated black cabbage leaves were determined to study the color of the samples. Color was evaluated by measuring Hunter L (brightness, 100=white, 0=black), a (+, red; -, green) and b (+, yellow; -, blue) parameters by means of a reflectance colorimeter (CR 400, Chromometer, Minolta, Japan). A white tile (No: 19633162) was used to standardize the instrument. From the instrumental Hunter L, a, b values and the color difference (ΔE) were calculated according to the Eq. 6.

$$PM_{db} = \left[\frac{W_o - W_d}{W_d}\right] \times 100 \tag{1}$$

$$E_{t(c)} = A.v.\rho.c.\Delta T.D_t \tag{2}$$

$$E_{t(m)} = \frac{U.I}{1000}.D_t \quad (3)$$

$$E_{kg(c)} = \frac{E_{t(c)}}{W_o} \quad (4)$$

$$E_{kg(m)} = \frac{E_{t(m)}}{W_o} \quad (5)$$

$$\Delta E = \left[(\Delta L)^2 + (\Delta a)^2 + (\Delta b)^2\right]^{1/2} \quad (6)$$

Table 1 Technical features of microwave oven dryer

Data / Power Level (P-L) (Written on the oven by the manufacturer)	**(PL-1) 90 W**	**(PL-2) 160 W**	**(PL-3) 350 W**
Voltage (~V)	232	232	232
Current of fan and lamp (A)	0.23	0.23	0.23
Current of magnetron tube and tray motor (A)	6.92	6.92	6.92
Current of all components (A)	7.15	7.15	7.15
Power consumption of fan and lamp (W)	53.36	53.36	53.36
Power consumption of magnetron tube and tray motor (W)	1605.44	1605.44	1605.44
Total power consumption (for all components) (W)	1658.80	1658.80	1658.80
Active period time of Fan and Lamp, only (s)	17	15	12
Active period time of all components (s)	4	6	9
Total time of a period (s)	21	21	21
Real power consumption for different levels (measured) (W)	359.21	512.07	741.35

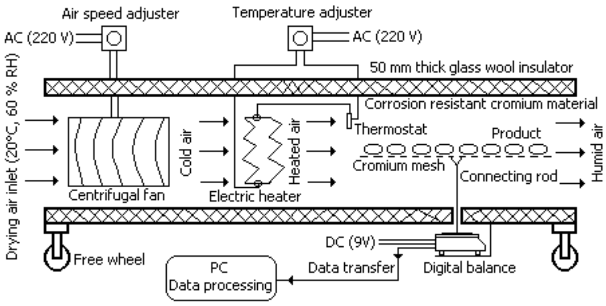

Fig. 1 Schematic presentation of the computer connected parallel flow type dryer

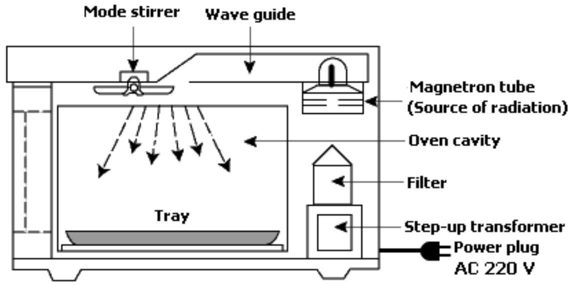

Fig. 2 Schematic presentation of the microwave oven dryer

Results and Discussion

During a drying process, two periods can be distinguished. The first is called constant drying rate period. The second drying stage is also called the falling drying rate period. During the first period, the surface of the product behaves as a surface of the water. The rate of moisture removal during this period is mainly dependent on the surrounding conditions and only affected slightly by the nature of the product. The end of the constant drying rate period is marked by a decrease in the rate of moisture migration from within the product below that sufficient to replenish the moisture being evaporated from the surface. The falling drying rate period is dependent essentially on the rate of diffusion of moisture from within the product to the surface and also on moisture removal from the surface. For agricultural products, the duration of each of the drying regimes depends on the initial moisture content and the safe storage moisture content. Especialy, for fruits and most vegetables, the drying would take place within both the constant and falling rate periods that can be seen easily. Both the external factors and the internal mechanisms controlling the drying processes in the two main rate regimes are important in determining the overall drying rate of products (Ekechukwu, 1999; Gigler et al., 2000). For these reasons, the changing of the moisture content of black cabbage leaves must have two periods depending on the drying time. The moisture content of the products as a function of drying time are presented in Fig. 3 and Fig. 4 for different convective drying temperatures and for microwave power levels. As seen from these figures, all lines have two stages. The moisture content rapidly reduces and then slowly decreases with rising of the drying time. In addition, it is obvious from the figures that drying temperature and microwave power have an important role on the total drying time (Fig. 3, Fig. 4 and Fig. 5). The least drying time (0.25 h) was obtained at PL-3. The highest drying time (25.83 h) was also found at 50 °C temperature. The total energy requirement for a charge of each dryer and energy needed for drying 1 kg of products can be seen from Fig. 6 and Fig. 7, respectively. There is a strict correlation between these two figures. This is because of the fact that the values of Fig. 7 were obtained from value of Fig. 6 by calculation (Eq. 2, 3, 4 and 5). As it is understood from these figures, the minimum heat energy (3.66 kWh/kg) is needed for drying of 1 kg products at temperature of 70 °C for black cabbage leaves. The maximum energy (22.81 kWh/kg) is needed at PL-1.

Colour is an important quality attribute in a food to most consumers. In addition, colour analysis is important of foods, especially quality criterion for the production and for the trade. It is an index of the inherent good qualities of a food and association of colour with acceptability of food is universal (Doymaz et al., 2006). L, a, b and ΔE values are commonly used as a index to report the colour quality.

The changes in color parameters of dehydrated black cabbage leaves are presented in Fig. 8 and Fig 9. Samples dried at 70 °C and PL-1 showed the highest Hunter L value, whereas the samples being dried at 50 °C and PL-3 gave the lowest L values. Different authors have reported that, decreases in L value correlated well with increases in browning of foods (Jimenes et al., 1994; Lozano et al., 1994). So the black cabbage leaves dried at 50 °C and PL-3 experienced an extensive browning. The redness (a) value decreased in comparison to fresh samples and the highest decreases were found in the drying temperatures of 70 °C and power level of PL-1. The yellowness (b) value was highest for the samples dried at 70 °C and PL-2. The color changes in ΔE was also obtained for convective drying temperatures and microwave oven power levels. The color difference was relatively high for the samples dried at 60 °C and PL-3.

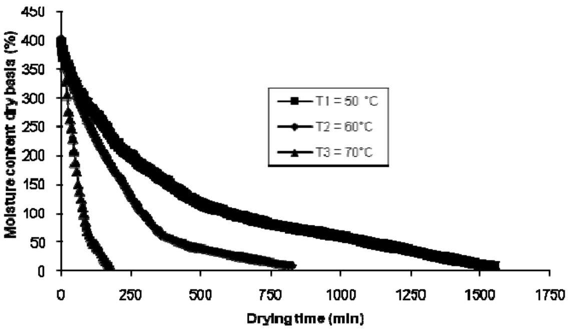

Fig. 3 Moisture content as a function of convective drying time for temperature of 50 °C, 60 °C and 70 °C

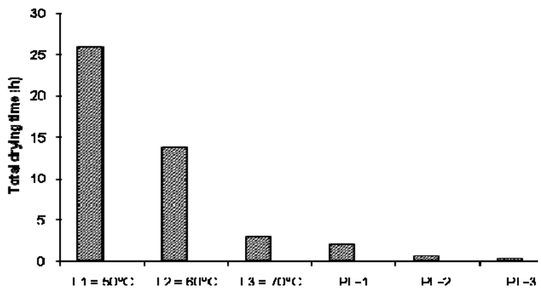

Fig. 5 Total drying time of product at different temperatures and power levels

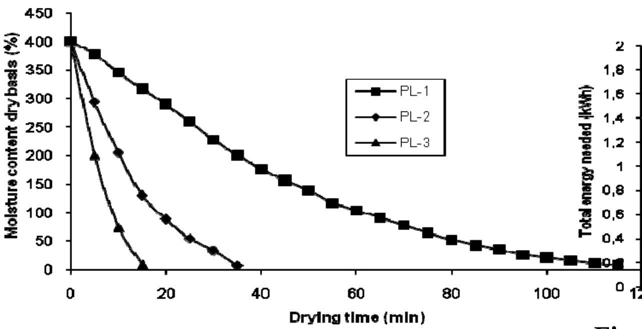

Fig. 4 Moisture content as a function of microwave drying time for power level of PL-1, PL-2 and PL-3

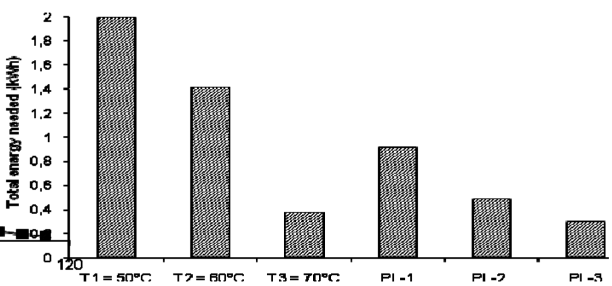

Fig. 6 Total energy requirement for a charge of convective and microwave dryers at different temperatures and power levels

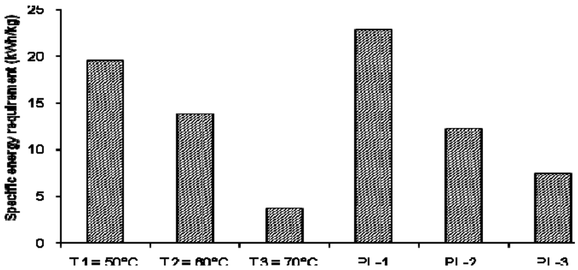

Fig. 7 Energy requirement for drying 1 kg of product for convective and microwave dryer

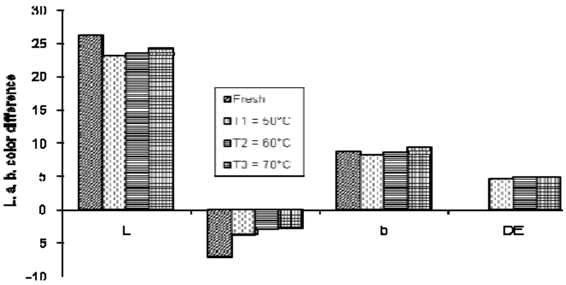

Fig. 8 Color changes in Hunter L, a, b and color difference (ΔE) of black cabbage leaves dried at temperature of 50 °C, 60 °C and 70 °C

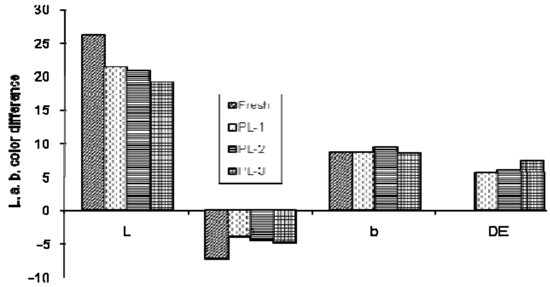

Fig. 9 Color changes in Hunter L, a, b and color difference (ΔE) of black cabbage leaves dried at microwave power levels of PL-1, PL-2 and PL-3

Conclusions

Black cabbage leaves were successfully dried in a computer connected parallel air flow type convective dryer and in a microwave oven dryer at different temperatures of 50, 60 and 70 °C, air speed of 0.30 m/s and power levels of PL-1, PL-2 and PL-3. It is found from the results of the experimental investigation that the drying air temperature and power levels has an important role on the total drying time, specific power consumption and black cabbage leaves color changes. The main conclusion of this study is that black cabbage leaves must be dried in convective type dryer at temperature of 70 °C and air velocity of 0.30 m/s to minimize the energy consumption and to keep the higher quality and color retention for drying of black cabbage leaves.

References

Ahmed J., Kaur A., Shivhare U., 2002. Color Degradation Kinetics of Spinach, Mustard Leaves, and Mixed Puree. Journal of Food Science, 67(3): 1088-1091.

Alarcao-E-Silva M.L.C.M.M., Leitao A.E.B., Azinheira H.G., Leitao, M.C.A., 2001. The Arbutus berry: studies on its color and chemical characteristics at two mature stages. Jounal of Food Composition and Analysis, 14: 27-35.

AOAC, 1984. Official methods of analysis of the association of official analytical chemists. 14th Ed., Arlington : Virginia. 22.013, USA.

Arslan D., Özcan M.M., 2010. Study the effect of sun, oven and microwave drying on quality of onion slices. WT - Food Science and Technolog, xxx: 1-7.

Barnwal P., Tiwari G.N., 2008. Grape drying by using hybrid photovoltaic-thermal (PV/T) greenhouse dryer: An experimental study, Solar Energy, 82: 1131–1144.

Doymaz I., Tugrul N., Pala M., 2006. Drying characteristics of dill and parsley leaves. Jounal of Food Engineering, 77: 559-565.

Ekechukwu O.V., 1999. Review of solar-energy drying systems I: an overview of drying principles and theory. Energy Conversion and Management, 40: 593-613.

Gigler J.K., Loon W.K.P., Seres I., Meerdink G., Coumans W.J., 2000. Drying characteristics of willow chips and stems. J. Agric. Engng. Res., 77(4): 391-400.

Holman J.P., 1994. Experimental methods for engineers. McGraw-Hill, Inc; New York, USA.

Jimenes M., Mateo J.J., Huerta T., Mateo R., 1994. Influence of the Storage Conditions on Some Physiochemical and Mycological Parameters of Honey. Journal of the Science of Food and Agriculture, 64(1): 67-74.

Koyuncu T., Pinar Y., 2001. Kırmızı biber için bir güneşli kurutucu tasarımı (Design of a solar dryer for red pepper). Tarımsal Mekanizasyon 20 Ulusal Kongresi; 13-15 Eylül, Şanlıurfa, Türkiye.

Koyuncu T., Sessiz A., 2002. Güneş enerjili kurutucular üzerine karşılaştırmalı bir araştırma

(A comparative study on solar energy dryer). O.M.Ü. Ziraat Fak. Dergisi, 17 (2): 53-60.

Koca N., Burdurlu H.S., Karadeniz F., 2007. Kinetics of colour changes in dehydrated carrots. Journal of Food Engineering, 78: 449–455.

Koyuncu T., Tosun İ., Üstün, N.S., 2003. Drying kinetics and color retention of dehydrated rosehips. Drying Technology, 21 (7): 1369-1381.

Koyuncu T., Serdar U., Tosun İ., 2004. Drying kinetics and energy requirement for dehydration of chestnuts (Castanea sativa Mill.). Jounal of Food Engineering, 62: 165-168.

Krokida M.K., Maroulis Z.B., Saravacos G.D., 2001. The Effect of the Method of Drying on the Colour of Dehyrated Products. International Journal of Food Science and Technology, 36: 53-59.

Lopez A., Pique M.T., Boatella J., Romero A., Ferran A., Garcia J., 1997. Influence of Drying Conditions on the Hazelnut Quality: III. Browning. Drying Technology, 15 (3&4): 989-1002.

Lozano J.E., Drudis R., Ibarz A., 1994. Enzymatic Browning in Apple Pulps. Journal of Food Science, 59(3): 564-567.

Mo H., Zhang M., Sun J., 2006. Effect of Drying Process Parameters on Dehydrated Cabbage Enriched with Selenium. Drying Technology, 24: 1657–1663.

Mwithiga G., Olwal J.O., 2005. The drying kinetics of kale (Brassica oleracea) in a convective hot air dryer, Journal of Food Engineering, 71: 373–378

Negi P.S., Roy S.K., 2000. Effect of Blanching and Drying Methods on β-Carotene, Ascorbic acid and Chlorophyll Retention of Leafy Vegetables. Lebensmittel-Wissenschaft und-Technologie/FST., 33 (4): 295-298.

Ochoa M.R., Kesseler A.G., Pirone B.N., Marquez C.A., Michelis A.D., 2002. Shrinkage during convective drying of whole rose hip (Rosa Rubiginosa L.) fruits. Lebensm.- Wiss. U.-Technol., 35: 400-406.

Ozbek B., Dadali G., 2007. Thin-layer drying characteristics and modelling of mint leaves undergoing microwave treatment. Journal of Food Engineering, 83: 541–549.

Rocha T., Lebert A., Marty-Audouin C., 1993. Effect of Pretreatments and Drying Conditions on Drying Rate and Colour Retention of Basil (Ocimum basilicum). Lebensmittel-Wissenschaft und-Technologie/FST., 26(5): 456-463.

Slupski J., Lisiewska Z., Kmiecik W., 2005. Contents of macro and microelements in fresh and frozen dill (Anethum graveolens L.). Food Chemistry, 91: 737-743.

Termentzi A., Zervou M., Kokkalou E., 2009. Isolation and structure elucidation of novel phenolic constituents from Sorbus domestica fruits. Food Chemistry, 116: 371-381.

Toğrul T.T., Dursun P., 2003. Modeling of drying kinetics of single apricot. Jounal of Food Engineering, 58: 23-32.

Volden J., Borge G.I.A., Bengtsson G.B., Hansen M., Thygesen I.E., Wicklund T., 2008. Effect of thermal treatment on glucosinolates and antioxidant-related parameters in red cabbage (Brassica oleracea L. ssp. capitata f. rubra). Food Chemistry, 109: 595–605.

QUANTIFYING POSTHARVEST LOSS OF CABBAGE IN THE SUPPLY CHAIN IN THAILAND

Somsak Kramchote[1,2*], Sirichai Kanlayanarat[1], Varit Srilaong[1], Thananya Wasusri[1], Chalermchai Wongs-Aree[1], Kazuhiro Nakano[2], Shintaroh Ohashi[2]

[1]Division of Postharvest Technology, King Mongkut's University of Technology Thonburi, Bangkok, 10140 Thailand. E-mail: peechote@hotmail.com
[2]Graduate School of Science and Technology, Niigata University, 8050 Ikarashi 2-no-cho, Nishi-ku, Niigata, 950-2181 Japan

Abstract

Cabbage is an important leafy vegetable in Thailand, providing income to many small farmers, processors, and other entrepreneurs, and serving as a health food for rural and urban people. However, cabbage is inherently perishable. During the process of distribution and marketing, substantial losses are incurred which range from a slight loss of quality to total spoilage. Postharvest losses may occur at any point in the marketing process, from the initial harvest through assembly and distribution to the final consumer. The causes of losses are mainly physical damage during handling and transport, water loss, or sometimes simply because there is a surplus in the marketplace and no buyer can be found. The objective of this research was to quantify the postharvest loss of cabbage during transport from the farm to the retail market in Thailand with the optimum remaining leaves and positioning of cabbage on the truck in order to improve the cabbage transport system. The cabbage heads were divided into 4 groups at the farm (0, 2, 4 and 6 wrapper leaves). In addition, the cabbages were also positioned on the truck in different locations (9 locations) and then transported to collection centers, wholesale markets and retail markets. The postharvest losses of cabbage were quantified along the supply chain. The results showed that the highest postharvest loss of cabbage from farm to retail market was found in non-wrapper leaves of cabbages (22 %) while cabbages with 2, 4 and 6 wrapper leaves maintained the postharvest quality by protecting the cabbage head from bruising during transport at about 6, 3 and 2 %, respectively. Moreover, the different locations of cabbages on the truck also affected the severity of postharvest loss. The most severe loss of cabbage heads was found on the top layer of the truck at about 25 % loss in non-wrapper leaf cabbages and a little physical damage in the middle or bottom parts on the truck. Interestingly, cabbages with at least 2 or more wrapper leaves were the most effective in maintaining the postharvest quality during transport from farm to retail market. In this research, we recommended that cabbage farmers keep at least 2 wrapper leaves after harvest to prevent bruising of the cabbage head during transport and fasten the top layer of cabbages on the truck to avoid severe postharvest loss.

Keywords: Cabbage, Postharvest loss, Quality, Transport system

Introduction

Cabbage is susceptible to injury from mechanical damage because of its structure and relatively soft texture associated with moisture content. This can occur at any stage of the marketing chain and can result from poor harvesting practices such as the use of dirty cutting knives, unsuitable containers used at harvest time or during the marketing process, e.g. containers that can be easily squashed or have splintered wood, sharp edges or poor nailing, overpacking or underpacking of containers and careless handling of containers. The resultant damage can include internal bruising, superficial grazing, and crushing of fresh produce. Poor handling can thus result in the development of entry points for molds and bacteria, increased water loss, and an increased respiration rate (Dixie, 2005). Occasionally, losses may be 100 %. For example, when there is a price collapse, it would cost the farmer more to harvest and market the produce than to plough it back into the ground. Thus, the use of the average loss figures is often misleading. There can be losses in quality, as measured both by the price obtained and the nutritional value, as well as in quantity. In addition, during harvest, the farmers trim or remove some cabbage leaves before selling to buyers. However, there is still no exact information on the estimation of postharvest loss of cabbage during transport in Thailand. Therefore, the objective of this study was to study the optimum number of wrapper leaves for transport and the effect of positioning on the truck on postharvest physical damage loss of cabbage during transport from farm to retail market in Thailand.

Materials and Methods

The study was conducted in the production season of 2010 in Petchabun Province, northern Thailand. The cabbage heads were harvested early in the morning at a commercial farm. 108 harvested cabbage heads were carefully tagged and packed into 9 plastic bags with holes. Each bag held 12 heads (3 heads for 0, 2, 4 and 6 wrapper leaves each). Data loggers were also put in the cabbage bags in order to record temperature and humidity data during transport. There were 2 kinds of trucks to transport the cabbages from the farm to the retail market, small truck (pick-up) and a bigger truck (6 wheels). The small truck was used from the farm to the collection center, the bigger truck for the collecting center to the wholesale market and another small truck from the wholesale market to the retail market. Moreover, the cabbage bags were positioned into different locations on the truck in order to test the transport system (Fig. 1). The percent of physical damage loss of cabbages at the farm and wholesale and retail markets were estimated.

Results and Discussion

Cause of postharvest loss of cabbage in the supply chain

The causes of postharvest loss of cabbage on previous survey in 2010 are described in Table 1. The harvest handling by cabbage farmers in the study area still involves traditional techniques without concern of contamination and food safety standards. Moreover, the transport and distribution systems of cabbages from farm sites to collecting center uses small trucks (pick-ups). However, there is a serious problem in the infrastructure from farms in the highlands to flat areas. At the collecting center, there were no cooling facilities to maintain the quality before selling to the wholesalers. Occasionally, cabbages might take 2 or 3 days without a cooling system at the collecting center. The packaging for cabbages only consists of polyethylene (PE) bags with holes. Cabbages are packed to about 10 kg per bag. In general, when the cabbages reach a wholesale market, some of the cabbages are distributed to retailers at the retail market and some of the cabbages are trimmed by wholesalers for consumers. In addition, there are a lot of damaged cabbage leaves at wholesale markets. Finally, they bring their waste to farms for animal feed.

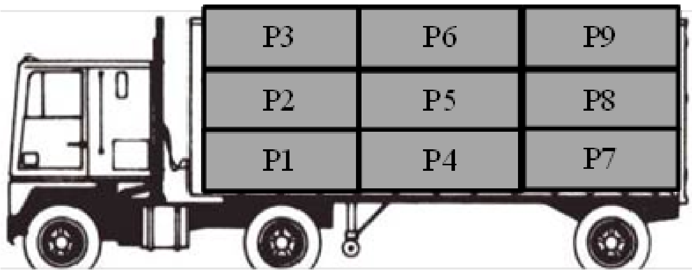

Fig. 1 The sketch of positioning of cabbages on the truck during transport from farms in Petchabun Province to wholesale and retail markets in Bangkok, Thailand

Table 1 Generic examples of cabbage loss in the supply chain.

Stage	Examples of cabbage loss characteristics
(1) Harvest handling	Poor handling techniques, crops damaged during harvest, edible cabbages left in the field
(2) Transport and distribution	Transport infrastructure, loss owing to spoiling/ bruising
(3) Storage	Pests, disease, spoilage, contamination
(4) Processing (trimming)	Contamination in the process causing loss of quality
(5) Packaging	Inappropriate packaging causing damage to produce
(6) Marketing, selling and distribution	Damage during transport: spoilage and poor handling in wet market losses caused by lack of cooling/cold storage
(7) End of life disposal of cabbage loss at different stages of the supply chain	Discarded food loss separately treated, fed to livestock/poultry, mixed with other wastes and landfilled

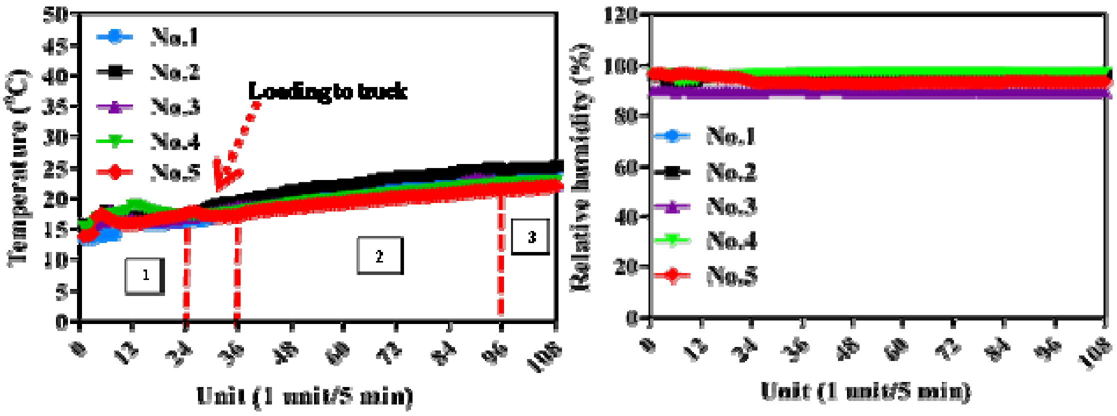

Fig. 2 Temperature (A) and relative humidity (B) of cabbages during transport from farms in Petchabun Province to wholesale and retail markets in Bangkok, Thailand

Transport system

The temperature and humidity data in the cores of cabbage bags during transport were recorded. The results showed that the temperature inside the cabbage bags at the cabbage farm site was about 13 ^{o}C with 96 % relative humidity (RH) (Fig. 2). After that, the small truck took only 2 hours from the farm to the collecting center in the provincial market. The temperature was gradually increased to 15 ^{o}C and 96 % RH. During transport of the cabbages to the wholesale market, the temperature was about 17-23 ^{o}C, while the temperatures of cabbage bags at the retail market were about 25 ^{o}C. However, the percent of RH was relatively constant during transport from the farm site to the retail market (96-98% RH) as shown in Fig. 2A.

Quantifying postharvest loss of cabbage in supply chain

After harvest, some farmers remove various numbers of cabbage wrapper leaves before packing into plastic bags while some farmers keep several wrappers in order to increase cabbage weight to improve their income. One problem is that several wrapper leaves are transported with only a small amount of edible cabbage which increases the cost of transport to the market. However, if farmers remove all wrapper leaves before transport, it results in the more serious problem of physical damage during transport (about 22-25 % loss at the retail market) (Fig. 3). Most of the physical damage to fruits and vegetables results from vibrations and impacts (Singh, Singh, 1992). These vibrations and impacts are caused from the irregularities of the road surfaces and are transmitted from the suspension systems of the vehicles to the produce. On the other hand, cabbages with at least 2 wrapper leaves were better protected during transport. The postharvest loss from physical damage of cabbage head with 2 wrapper leaves was only about 6 %. In addition, there were only 3 and 2 % losses in 4 and 6 wrapper leaves, respectively.

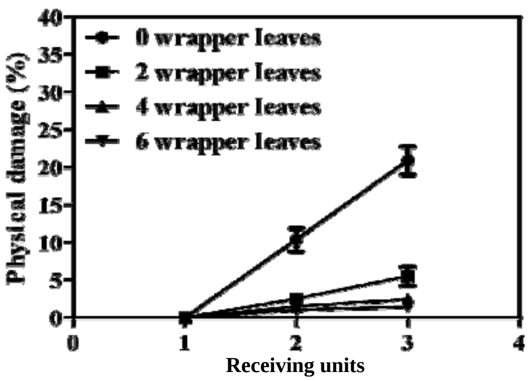

Fig. 3 Severity of physical damage of cabbages in different numbers of wrapper leaves during transport from farms in Petchabun Province (1), to wholesale market (2) and retail markets (3) in Bangkok, Thailand

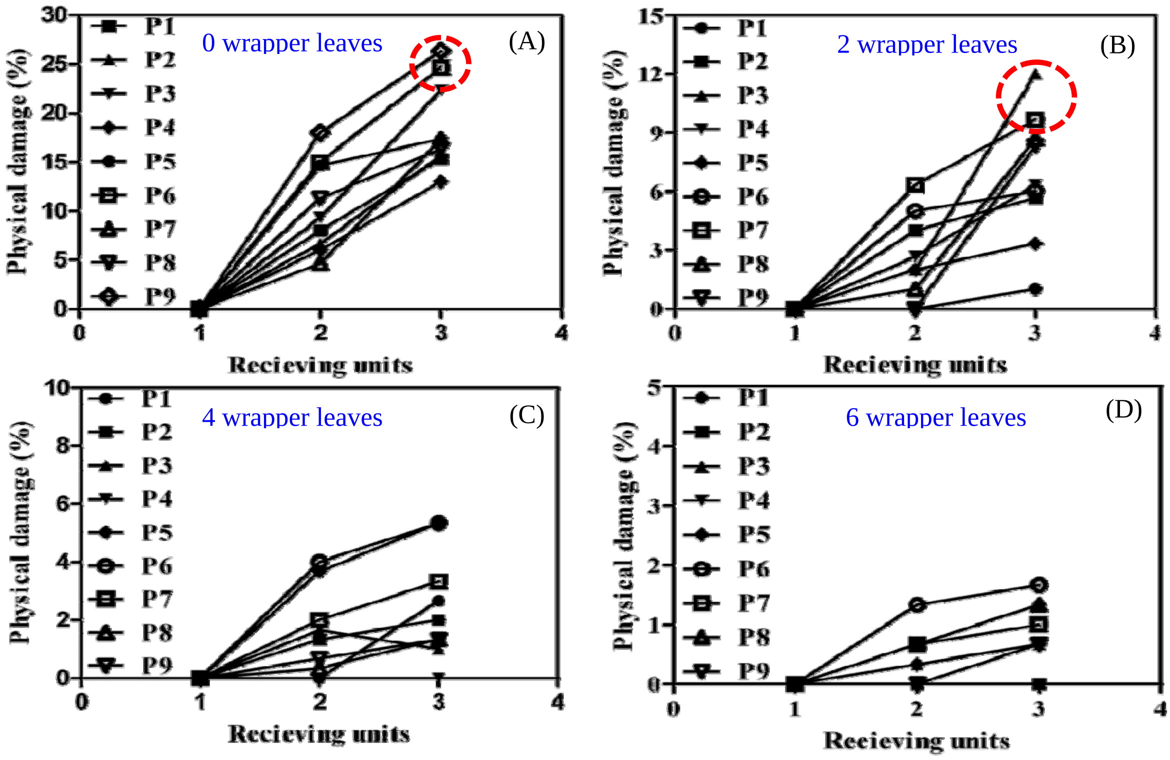

Fig. 4 Physical damage of cabbages with different numbers of wrapper leaves (0 wrapper leaves [A], 2 wrapper leaves [B], 4 wrapper leaves [C] and 6 wrapper leaves [D]) and positioning on the truck during transport from farms in Petchabun Province (1), wholesale (2) and retail markets in Bangkok, Thailand

The postharvest loss of cabbage due to physical damage during transport was estimated. The cabbage bags were positioned on the truck with 9 different locations (Fig. 1). The results showed that cabbages positioned on the top of truck (P3, P6 and P9) had the most severe symptoms from physical damage than the other positions (Fig. 4A&B). The physical damage percentages of cabbages without wrapper leaves were about 22, 24 and 25% in P3, P6 and P9 at retail market respectively. The cabbages at the bottom part (P1, P4 and P7) had less physical damage than other parts of about 14, 12 and 15%, respectively (Fig. 4A). However, cabbages with 4 or 6 wrapper leaves had less physical damage loss of only about 5% and 1.5 % at the bottom part of the truck (P1) (Fig. 4C&D). Losses directly attributed to transport can be high, particularly in developing countries (Kader, 2005). Moreover, damage occurs as a result of careless handling of packed produce during loading and unloading, vibration (shaking) of the vehicle, especially on bad roads, and poor stowage, with packages often squeezed into the vehicle in order to maximize revenue for the transporters (FAO, 1989). Overheating leads to decay and increases the rate of water loss. This can happen in transport as a result from using closed vehicles with no ventilation, stacking patterns that block the movement of air, and using vehicles that provide no protection from the sun (Dixie, 2005). Moreover, vehicle breakdowns can be a significant cause of losses in some countries, as perishable produce can be left exposed to the sun for a day or more while repairs are carried out (World Resources Institute, 1998).

Conclusions

Cabbage heads with at least 2 or more wrapper leaves were the most effective in maintaining the postharvest quality during transport from farms to retail markets. Interestingly, the most severe loss of cabbage heads was found on the top layer of the truck at about 25 % loss in non-wrapper leaves of cabbages and a little physical damage in the middle or bottom parts on the truck. In this research, we recommended that cabbage farmers keep at least 2 wrapper leaves after harvest to prevent bruising of cabbage heads during transport and fasten the top layer of cabbages on the truck to avoid severe postharvest loss.

Acknowledgment

This research was supported by a grant from the Thailand Research Fund (TRF) through the Royal Golden Jubilee Scholarship Ph.D. program (Grant No. PHD/0175/2551).

References

Dixie G., 2005. Horticultural Marketing. FAO, Rome.

FAO Prevention of post-harvest food losses, 1989. fruits, vegetables and root crops; a training manual FAO Training Series 17/2, Rome.

Kader A.A., 2005. Increasing Food Availability by Reducing Postharvest Losses of Fresh Produce, UC Davis.

Singh A., Singh Y., 1992. Effect of vibration during transportation on the quality of tomatoes. J. Agric. Mech. Asia, Africa and Latin America. AMA, 23: 70-72.

World Resources Institute, 1998. Disappearing Food: How Big are Postharvest Losses? Earth Trends.

POSSIBILITIES OF ENVIRONMENT AND SOIL PROTECTION BY MEANS OF GPS NAVIGATION USED IN AGRICULTURAL MACHINERY

Milan Kroulík*, Zdeněk Kvíz, Jan Chyba

Czech University of Life Sciences in Prague, Department of Agricultural Machines, Faculty of Engineering,16521 Prague 6 – Suchdol, Czech Republic, Phone: +420 224383130, Fax: +420 224383122, E-mail: kroulik@tf.czu.cz

Abstract

The article describes possibilities for soil protection and shows the technical means which can minimize the risk of soil degradation. This goal is possible to reach by means of very simple equipment based on GPS receiver which monitors and records vehicle trajectories. From the data gained about the vehicle movement the following facts and outcomes can be derived. The total area wheeled by the machinery tires, the map of soil exposure to machinery time-dependent presence, determination of places excessively loaded with traffic and deep loosening decision, counting benefits of Controlled Traffic Farming (CTF) usage for a particular field, possibility for combining more field operations into one machinery pass and last but not least planning of ideal machinery trajectory.

All of the above mentioned possibilities for soil structure protection, when talking about adverse effect of machinery passes on soil, are discussed and proposed as a tool for better farming with heavy machinery.

Key words: precision agriculture, soil protection, compaction, controlled traffic farming

Introduction

Passes within a field when performing farming activities are the necessity and are inevitable. Even passes by humans or animals can be considered as passes on soil which causes soil compaction. The most important phenomenon nowadays is agriculture machinery passes in fields. Machinery traffic monitoring and detailed analysis of machines passes across a field can be a tool for the field area determination which can be excessively loaded with tire contacts and therefore causes soil compaction followed by its unfavourable effects on next plant growth and final yield.

Soil compaction is defined as: “the process by which the soil grains are rearranged to decrease void space and bring them into closer contact with one another, thereby increasing the bulk density” (Soil Science Society of America, 1996) and is related to soil aggregates because it alters the spatial arrangement, size and shape of clods and aggregates and consequently the pore spaces both inside and between these units. Soil compaction is one of the major problems in modern agriculture and is a well-recognised problem in many parts of the world (Håkansson et al., 1988; Håkansson, 1990; Chan et al., 2006). The extent of the soil compaction problem is a function of soil type and water content and further vehicle weight, speed, ground contact pressure and number of passes, and their interactions with cropping frequency and farming practices (Ball, Ritchie, 1999; Chamen et al., 2003; Chan et al., 2006; Radford et al., 2007). Trafficking by wheeled heavy farm machines is common in most agricultural operations even in zero tillage systems (Tullberg, 2000) therefore the vast majority of arable land is endangered by soil compaction.

The development of precision agriculture at the end of the last century has opened new ways in the attitude to usage of mechanization for plant production. Mainly the due to expansion of GPS based satellite navigation it is possible to find new approaches for machinery passes. Machinery passes arrangement in fields is usually without any system and therefore random. Thus GPS with a particular traffic system, planning and optimization of machinery trajectories can minimize machinery passes and help soil protection.

Materials and Methods

Evaluation of the number and frequency of agricultural machinery passes across a field was realized by means of DGPS receivers with a position recorder and with a logging time of 2 s.

All field operations and all other machinery and vehicle passes across selected fields were monitored during one year. Also different tillage systems were evaluated, namely conventional tillage with ploughing and conservation tillage and also fields with perennial crops. Trajectories for every machine run in the field were defined from the data sets received from a GPS position recorder placed in the machine. Then the area covered by the machine tyres was calculated from the tyre type, tyre width and wheel spacing.

The measured values showed that the less intensity of field operations, the less is the load of soil by the machinery passes. Despite the fact that intensity of machinery passes decreases when using conservation tillage, the loading on the soil profile caused by machine tyres was still quite high. The results showed that 86.14 % of the total field area was run over with a machine at least once a year, when using conventional tillage, and 63.75 % of the total field area was run-over when using conservation tillage. A problem of intensive and random passes also affects other crops such as fodder grown on the arable land or perennial crops. Fig. 1 shows all machinery passes during harvest of grass for silage. In case of self-propelled forage chopper the total run over area was 63.8 % from the field area. In case of round baler it was 63.4 %.

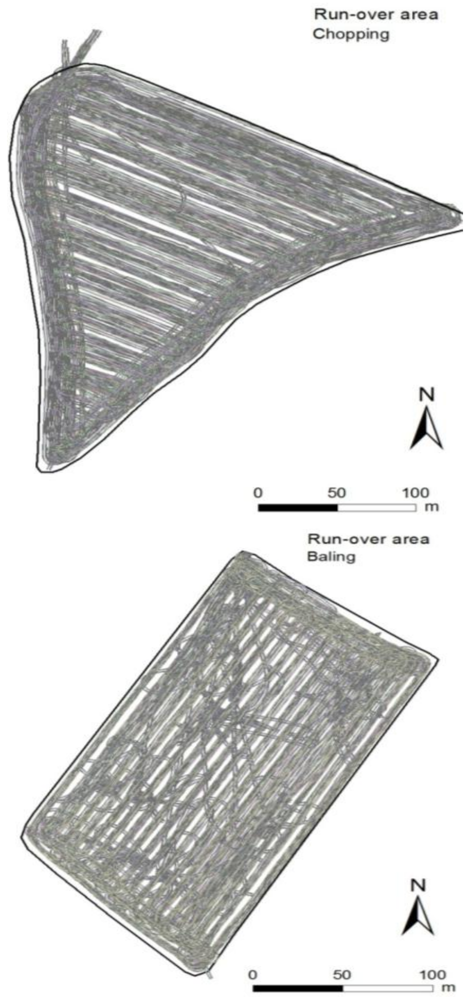

Fig. 1 Graphical representation of machinery passes for chopping and hay baling

From the data obtained it is possible to estimate the optimization of deep loosening operation. On the basis of machinery passes records it is also possible to determine how intensively the land is loaded by tyres of machines. Fig. 2 shows the oil compaction phenomenon which is connected with time exposure of soil surface to tyre contact pressure. The map was created from the sum of machinery position records in time at a particular place – in selected squares 6x6 m (the field was divided by square grid with the cells 6x6 m). It means, the more times a machine entered each square the more records for the square and also the more time a machine spent in the square the more records are there as well (dependence on working speed and even machine stops).

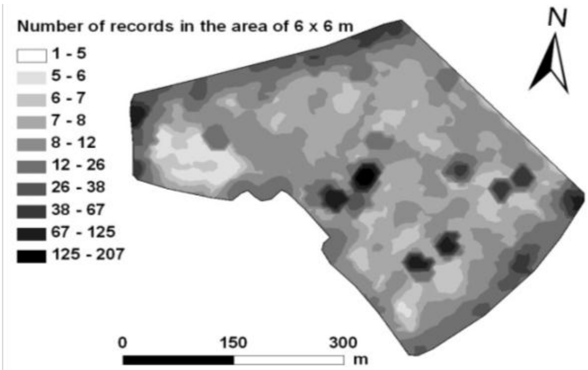

Fig. 2 Map characterising intensity of traffic and time spent at a certain area (in seconds)

Places which need deep loosening or sub soiling treatment against undesirable soil compaction can be calculated from this map. This extremely energy demanding intervention can be based on knowledge of the load intensity and the map to optimize the depth of loosening and exact place for loosening.

Another possibility how protect soil from compaction is a number of machinery passes reduction by means of combining of working operations and also adoption of fixed track system for machinery traffic. Tools combinations are quite commonly used in agriculture practice, such as tillers together with seeding machines, combination of more than one soil processing tools together with soil levelling etc. The results (Tab. 1) from the fixed track system for machinery traffic measurements on the experimental plots (only conservation tillage) revealed a significant decrease up to 31 % total run-over area by machinery tyres.

Tab. 1 Frequency of machinery passes across a field where fixed tracks were used

Conservation tillage 4 m working width	**Run-over area (%)**	**Conservation tillage 8 m working width**	**Run-over area (%)**
Number of passes repetitions		Number of passes repetitions	
1x	4.58	1x	10.38
2x	3.24	2x	0.00
3x	5.18	3x	8.46
4x	16.51	4x	7.65
5x	0.16	5x	1.36
6x	7.71	6x and more	3.03
Run-over area (total) (%)	37.38	Run-over area (total) (%)	30.88

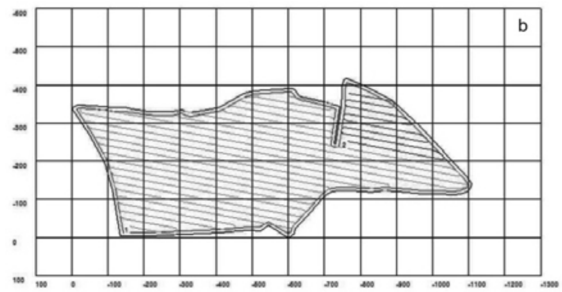

Fig. 3 Example of optimal trajectory of guidance line for the field

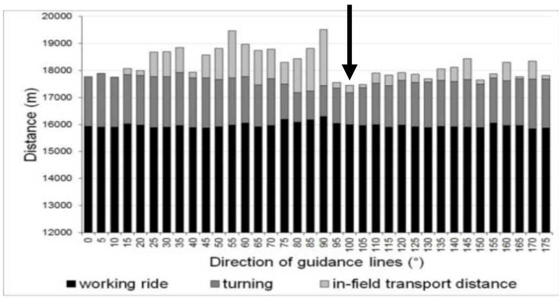

Fig. 4 Driving distance for the different directions of trajectories (an arrow shows the best direction angle)

Tab. 2 Parametric values the best variant for trajectories direction

Field	**Acreage (ha)**	**Opposite turns**	**Direction of ride (°)**	**Total (m)**	**Working ride (%)**	**Turning (%)**	**Ratio turning/working ride**
B	25.67	No	100	15090.54	94.89	5.11	0.05
		Yes	110	15526.77	92.75	7.25	0.08

Route planning and optimization of machinery trajectories is another possible point for better soil conditions achievement. At present, the machinery trajectories are based especially on the experience of drivers or usual habits of farmers. There are many factors that affect the efficiency of machine sets. Shape of the land, its size, slope, obstacles and working widths of machines play a significant role in this case. In our experiment, we have done the analysis of the direction of lines. The model with trajectories within a selected field in different directions with angle step of 5° was performed. It resulted in Fig. 3 and 4 which represent the real situation and the optimal trajectory which respects the shape of the field. A comparison of the lengths of driving distances, turnings and working times for different directions were taken into account. Exact values are shown in Tab. 2.

As illustrated in Fig. 4 even minimum deviation from optimal route (for example from 100o to 90o) can lead to a significant increase of non-working trips and passes. Trajectory model can be, quite easily, transferred into the navigation device. On the other hand, the model does not respect the slope of the land. The slope of the land is the essential prerequisite for the plan of erosion measure and has to be also taken into account.

Results and Discussion

Based on our measurements is possible to say that the mere tracking of machine sets and using the DGPS receivers or navigation will reveal a number of adverse effects of intensive farming and also show the ways and possibilities where to look for reserves. The possibilities how to use the position of the machines to reduce the passes risk factors with minimal additional cost of agriculture machine equipment have been discussed. There have to be also the possibility of data processing by external workplace and transfer to farmers through public portals in the form of prepared data and applications.

It was found out that there are several possibilities how to improve the soil conditions and minimize risk of soil compaction caused by machinery traffic.

- Accumulation of passes, especially during periods of increased soil moisture is a major source of unwanted soil compaction. Based on knowledge of passes can be organized and specifically identified remedial measures as is extremely expensive deep loosening.

- Reduction of redundant crossings by concentrating tracks to the permanent lines = an important element for reducing the intensity of passes during random motion of machine sets.
- The shape of the land is very variable. Any curvature of land increases the number of passes and turns. Machinery passes becomes less productive and results in more intensive and expensive land treatment. By selection of appropriate trajectories can significantly reduce non-working turns and passes. Combination of suitable trajectory and contour will contribute to time saving and to erosion measures in the form of contour farming. Route curves will be possible transmitted in a suitable format to save to the navigation through publicly accessible portals.

Conclusions

The GPS based systems and agriculture machinery guidance is very useful tool for minimizing risk of soil compaction caused by heavy machinery traffic. The simple equipment with data loggers and data recording can be a source of information for multidisciplinary analysis of different variables when evaluating machinery passes in fields and their effect on soil. Usage of such system is highly recommended in farms which use heavy machinery with wide working widths above 6 m and bigger fields with acreage above 20ha.

Acknowledgment

This paper was processed within the framework of the Research Project of CULS Prague, CIGA No. 20123006 and Research Project MPO FR-TI3/069.

References

Ball B. C., Ritchie R. M., 1999. Soil and residue management effects on arable cropping conditions and nitrous oxide fluxes under controlled traffic in Scotland 1. Soil and crop responses. Soil & Tillage Research, 52: 177 - 189.

Chamen T., Alakukku L., Pires S., Sommer C., Spoor G., Tijink F., Weisskopf P., 2003. Prevention strategies for field traffic-induced subsoil compaction: a review Part 2. Equipment and field practices. Soil & Tillage Research, 73: 161 - 174.

Chan K. Y., Oates A., Swan A. D., Hayes R. C., Dear B .S., Peoples M. B., 2006. Agronomic consequences of tractor wheel compaction on a clay soil. Soil & Tillage Research, 89: 13-21.

Håkansson I., Voorhees W. B., Riley H., 1988. Vehicle and wheel factors influencing soil compaction and crop response in different traffic regimes. Soil & Tillage Research, 11: 239 - 282.

Håkansson I., 1990. Soil compaction control - Objectives, possibilities and prospects. Soil Technology, 3(3): 231 - 239.

Radford B. J., Yule D. F., McGarry D., Playford C., 2007. Amelioration of soil compaction can take 5 years on a Vertisol under no till in the semi-arid subtropics. Soil & Tillage Research, 97: 249 - 255.

Tullberg J. N., 2000. Wheel Traffic Effects on Tillage Draught. Journal of Agricultural Engineering Research, 75 (4): 375 - 382.

MEASUREMENT OF ELECTRICAL CONDUCTIVITY OF LOVOGREEN FERTILIZER

Josef Krupička*, Petr Šařec

Czech University of Life Sciences Prague, 16521 Prague 6– Suchdol, Czech Republic
Phone: +420 224383127, E-mail: krup@tf.czu.cz

Abstract

Paper deals with the measurement of electrical conductivity of significant size groups of mineral fertilizer LOVOGREEN divided in the air stream. Samples of these groups were dissolved in distilled water and the values of electrical conductivity recorded. Measurements will be used to monitor the electrical conductivity of other mineral fertilizers and to create a standard for qualitative assessment of fertilizer solutions.

Key words: electrical conductivity, air flow, fertilizer solution, concentration, LOVOGREEN

Introduction

The concentration of fertilizers can be determined on the basis of the electrical conductivity (increasing the electrical conductivity). The value of the electrical conductivity can be used for precise application of fertilizers in liquid form. According to the electrical conductivity, the quality of the measured fluid can be assess accurately along with other data such as the level of pollution, the concentration of the various components of the solution, etc. (Kabeš, 1999). Electrical conductivity is the reciprocal of electrical resistance, is Indicated with the letter G and its basic unit is the Siemens (S).

The effectiveness of mineral fertilizers in crop cultivation depends on the particle stability and speed of their transformation to solution state to be acceptable by plants. This process depends on the particles dimensions, so that the dimension of particles is one of the main parameters that influence the fertilizer effectiveness.

Application of solid commercial fertilizers play important role in precision farming technologies. The application quality is depended on chemical composition and physical properties of fertilizer. Important from physical properties point of view is the grading of aggregate evaluation that is still performed by standard ČSN 01 50 30. The dimension of particulars only is characterized by this way.

In this paper we continue in the previous research program, in which the granulometric study mineral fertilizers were studied. In contrary to the similar study of other authors seat and airflow sorting were combined.

Experiments with particles can be designed differently. An elutriator was designed and constructed in which an airflow is supplied by a centrifugal fan (Csizmazia, 2000). Methods for measuring the coefficient of friction, the coefficient of restitution, the aerodynamic resistance coefficient, and the breaking force (particle strength) of fertilizers (Hofstee, 1992) were taken into account. The breaking force feature was skipped. The problem of particle destruction was overcome by fertilizer Superphosphate selection. The control of fertilizer discharge was studied for different designs of distributors and an experimental accurate fertilizer distributor with a rotary vessel type feeder was developed (Kudoh, 1989) what shows that dissolution of fertilizer also makes some problems. Consequent logistical problems are the same difficult for both pumping liquids, and transportation of particles by the air.

The size of particles makes the fertilizer's shelf life and stability of particulars behavior in the airflow more stable in storage, and better acceptable by the plant. Therefore, experiments studying motion of particles through the air were accompanied by grading of particles.

This paper contains results obtained for LOVOGREEN using the method developed previously.

Material end methods

Electrical conductivity was measured device Conductivity inoLab model WTW Cond 720. Instruments for the measurement of electrolytic conductivity, specifically electrical conductivity of liquids, consist of a measuring probe or conductivity sensor, transducer and evaluation unit. Most of the apparatus is adapted for measuring the resistivity and weight concentrations of some components of the solution, which can be derived from the electrical conductivity. They are very sensitive and allow you to measure the content of various substances from small to very high concentrations and is often used to control a wide range of industrial processes. (Kabeš, 1999). Measurement was carried out for mineral fertilizer LOVOGREEN, the composition of NPK 05.08.20 + 2MgO. Distribution of the air stream was carried out in the laboratory of the Department of Agricultural Machinery using the laboratory air sorting machine K - 293 (see Fig. 1).

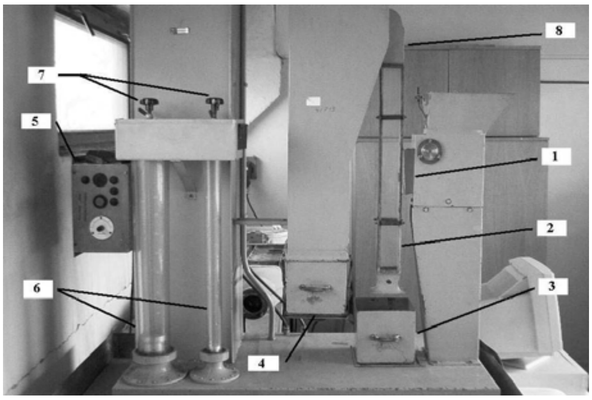

Fig. 1 Laboratory Air sorter K - 293
Labels: 1 - adjustable damper hoppers, 2 - vertical (aspiration) channel, 3.4 - tanks, 5 - control panel with buttons, 6 - small and large graduated cylinder, 7 - cylinder adjusting screws, 8 - fan

The measurement procedure was as follows. First the laboratory sorting machine K-293 determined ranges of required amount of air, i.e. the minimum amount of air in which the particles are carried, and in the opposite a maximum amount of air in which the sample is completely sorted. With the help of graduated cylinders, interval of gradually increasing speed of the air flow is selected so that the number of classes was 7 to 10. It is necessary to ensure the right plane for the weights to ensure accuracy. Scales are calibrated and set to zero. Fertilizer is mixed because of the measurement accuracy and a sample of fertilizer weighing 500 g removed. An appropriate, predetermined, air speed is set for the laboratory device using graduated cylinders and adjusting screws. A sample of fertilizer is poured into the tank (1) with pre-set for the damper. With the help of a vibrator, fertilizer gets into the air flow in a vertical channel (see Fig. 2). Here comes the separation. Granules with larger than the critical speed set fall through the channel into the container (3). Granules with lower critical speeds are vertically entrained in air stream and in the extended portion of the channel are falling into the tray (4). The amount of fertilizer separated using air flow into the tank (4) is then placed in a pre-labeled bowl for later use. Emptied tank (4) is placed back into the machine and the speed of the air flow is checked. Then the fertilizer from the tank (3) is filled back to the tank (1) and the graduated cylinder is set to the next value of air stream speed. In this way, the experiment continues until the entire sample of fertilizer gradually falls into the tank (4).

The whole process is repeated with eight different samples of fertilizers to maintain the accuracy and reliability of statistical data measurements.

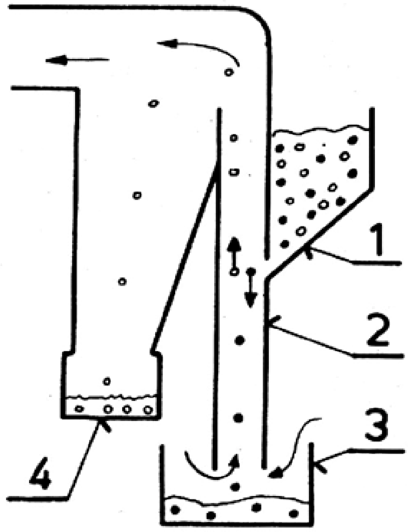

Fig. 2 The vertical channel (detailed view)
Labels: 1 - tray, 2 - vertical (aspiration) channel, 3 - stack, 4 - tray (particles of lower critical speed are carried into this tank)

Measurement was carried out in an air stream at a temperature of 22 °C and humidity of 22%. Electrical conductivity was measured on the machine Conductivity meter WTW inoLab model Cond 720

Results and discussion

From the samples measured in the air stream, samples weighing 5 grams were taken of significant proportions that were for the air stream 105, 115, 125 m3.h-1.

Therefore, these samples collected samples weighing 5 grams of six replications. Subsequently, 5 g samples were mixed and collected and then dissolved in distilled water to a volume of 50 ml. Table 1 shows the measured values. Conductivity measurements were performed after one hour. Electrical conductance G are given in units of electrical conductivity of G1, G2, G3 corresponding to granules of classes 105, 115, 125 (see Fig. 3).

Tab. 1 Measured values of electrical conductivity G of LOVOGREEN fertilizer

Time	**Temp. [°C]**	**G1 - for 105 $m^3.h^{-1}$ [$m^{-2}.kg^{-1}s^3.A^2$]**	**Temp. [°C]**	**G2 - for 115 $m^3.h^{-1}$ [$m^{-2}.kg^{-1}s^3.A^2$]**	**Temp. [°C]**	**G3 - for 125 $m^3.h^{-1}$ [$m^{-2}.kg^{-1}s^3.A^2$]**
0:0	25.8	12.9	26.7	17.6	26.7	19.5
1:0	25.9	15.1	26.9	18.2	26.9	20.4
2:0	26.8	29.9	27.2	29.9	27.2	32.3
3:0	26.9	38.7	27.4	43.4	27.3	39.7
4:0	27.0	52.0	27.3	56.2	27.4	49.5
5:0	27.0	56.9	27.2	59.3	27.3	57.6
6:0	27.0	59.2	27.8	62.4	27.7	61.2
7:0	27.8	75.8	28.1	77.4	28.2	73.3
8:0	27.9	87.1	28.3	87.2	28.3	80.4
9:0	28.0	89.9	28.3	92.3	28.4	92.4
10:0	28.1	95.2	28.4	98.3	28.9	106.5

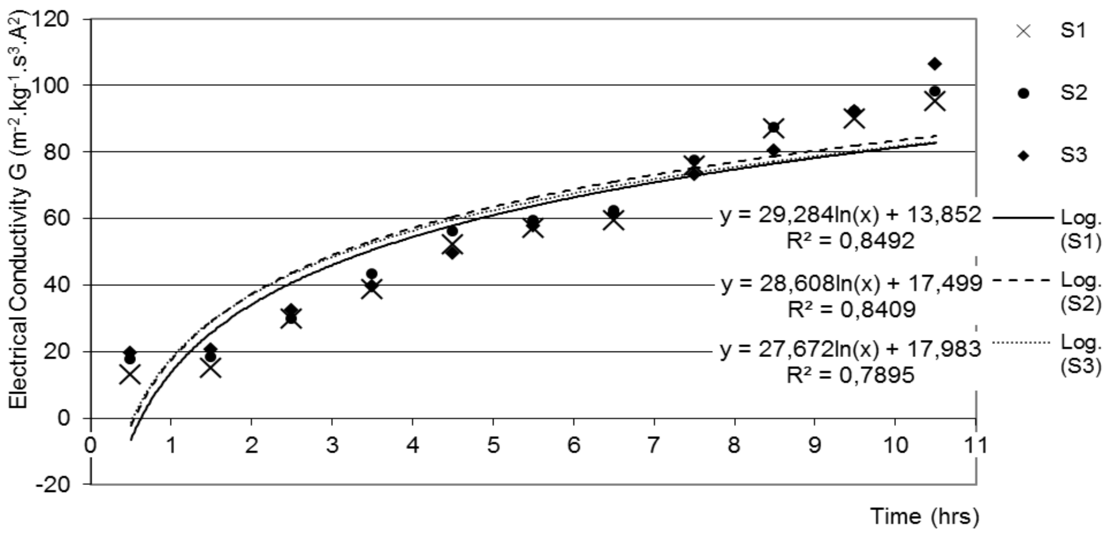

Fig. 3 Graph of time dependence of electrical conductivity

Undissolved residues were detected by using filter paper - the solution was filtered and the solids were weighed and dried in a dryer at a constant temperature of 105 °C to constant weight. These weights are not given here, because we can not determine the amount of undissolved fertilizer.

This measurement was performed as indicative, and following additional measurements based on it were done where the sample was dissolved until it stopped to change its electrical conductivity, i.e. ended its dissolution. The undissolved remains of fertilizer were weighed. You could determine using nutrient analysis whether undiluted sample contains nutrients, or it is a carrier roughage.

Conclusions

On the basis of the electrical conductivity, the concentration of dissolved mineral fertilizer can be determined. Figure 3 indicates that the values for the significant proportions are analogous. These values are crucial for the production of concentrated solutions of mineral fertilizers that can be applied by sprayers. Measurements are taken as the guidance for the methodology verification that will be used to measure other samples of similar fertilizers. These results will be used for the precise application of fertilizers and can be used as a reference for qualitative assessment fertilizer solutions.

Acknowledgements

This work was supported by Research Project of the Ministry of Education of the CR no. MSM 6046070905.

References

Csizmazia Z., 2000. Some physical properties of fertiliser particles. Department of Agricultural Engineering, Faculty of Agricultural Sciences, Debrecen University, Hungary. Aspects-of-Applied-Biology: 219-226.

Hofstee J. W., 1992. Handling and spreading of fertilizers: part 2, physical properties of fertilizer, measuring methods and data. Journal of Agricultural Engineering Research, Wageningen Agricultural University: 141-162.

Kabeš K., 1999. Market overview - equipments for the measurement of electrolytic conductivity. Automatization 42, no. 11: 826–832. (in Czech)

Kadlec K., 1999. Sensors of electrolytic liquids conductivity. Automatization 42, no. 11: 823–825. (in Czech)

Kudoh M., 1989. Flowability of fertilizers and development of an accurate fertilizer distributor. Department of Forestry & Landscape, Hokkaido College, Senshu University, Japan: 1-87.

EFFECTS OF CO_2 LASER IRRADIATION ON CHANGES IN COLOUR AND SACCHARIDES OF BEECH WOOD

Ivan Kubovský*, František Kačík

Technical University in Zvolen, T. G. Masaryka 24, 960 53 Zvolen, Slovakia,
Phone: +421455206462, E-mail: kubovsky@tuzvo.sk

Abstract

The paper deals with the influence of laser radiation energy on color changes and changes in carbohydrate complex of beech wood. Surface of beech wood (Fagus sylvatica L.) was irradiated with beam of CO_2 laser (wavelength 10.6 µm). With the growth of the dose of irradiation was observed brightness decrease (ΔL^*) and increase the total color difference (ΔE^*). At the irradiation of beech wood the amount of saccharides decreases in dependence of energy amount. The total decrease of saccharides at the highest dose of irradiation was 56.7 % from the initial amount of saccharides in the sample without irradiation. Hemicelluloses degrade more quickly, the changes take place also in cellulose. Good correlation between the increase of the total color difference and loss of hemicelluloses has been observed.

Key words: beech wood, laser irradiation, colour, saccharides, gas chromatography

INTRODUCTION

Beech is one of the most important tree species utilised in the wood industry. He is treated mainly for the production of bent parts of furniture, floor panels and staircases. One of the final steps in wood products is surface finishing. The most commonly process is applying of the various coatings for their aesthetic and protective roles. The colour of the wood may be changed also by action of heat, moisture, UV radiation and various chemicals, respectively. Thermal treatment helps to improve the mechanical, physical, chemical and optical properties of wood and increases resistance against biological pests (Bourgois et al., 1989; Mitsui et al., 2001; Mitsui et al., 2005; Esteves, Pereira, 2009; Reinprecht, Vidholdová, 2008; Chen et al., 2012). Those procedures are often targeted to change the colour of wood. Heat and electromagnetic radiation cause changes in the main components of wood (cellulose, hemicelluloses, and lignin) and extractives. Heating is usually done by an electric current, infrared or microwave radiation (Bourgois, Guyonnet, 1988; Kačík et al., 2006). As a novel source to achieve the colour changes of wood surface can be used CO_2 laser (which is primarily intended for cutting, drilling and engraving). Information about its use to change the colour of wood is relatively rare in the literature (Kubovský, Babiak, 2009). The aim of this paper is to show the effects of CO_2 laser irradiation on changes in colour and saccharides of beech wood.

MATERIAL AND METHODS

Experimental material

As experimental material was used beech wood (*Fagus sylvatica* L.). Sample sizes in the form of plates 140 × 500 × 15 mm (length x width x thickness) was obtained from strain tangential cut. Before starting the experiment, the surface was treated with sandpaper roughness "150", free of dust and dirt. Sample was dried to 12 % moisture.

Irradiation of samples

Irradiation was carried on a CO_2 laser machine LCS 400 (wavelength of 10.6 microns). Laser beam stroked on tangential surface of the sample perpendicularly and laser head carriage moved along the width (x-axis) at the selected scanning speed (Fig. 1). Range of speeds was chosen based on preliminary experiments under colouration after irradiation (Table 1). After irradiation across the entire width of sample was laser head shifted by 20 mm in the length direction of the sample (y-axis). The scanning rate was increased and the whole procedure was repeated. By changing the scanning speed of laser head have been created isolated parallel surface areas (stripes) on the wooden board. Each stripe was irradiated with different amounts of energy (Table 1), which is expressed as irradiation dose H (J.cm^{-2}). The output power of the laser and lens focal distance from the surface of the wood were constant.

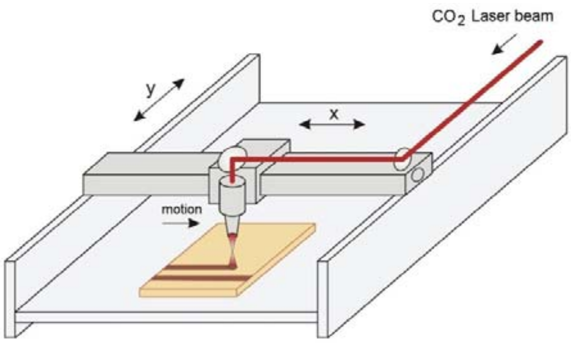

Fig. 1 Scheme of apparatus for laser irradiation

B10 B40

Fig. 2 Photo of beech surface after irradiation

Colour and colour differences

The colour was measured by spectrophotometer CM 2600d (MINOLTA-Konica). To quantify the colour was used colorimetric system $L^* \ a^* \ b^*$ (CIELAB). This colour space is based on the fact that a colour can't be simultaneously red and green (or blue and yellow), because these colours are opposite each other. Model of this system consists of three mutually perpendicular axes: axis L^* - determines the lightness, axis a^* - determines the ratio of red to green and axis b^* - specifies the ratio of yellow to blue (Fig. 1). To assess the difference of two colours is used total colour difference ΔE^*, expressing the distance between two points in the CIELAB system:

$$\Delta E^* = \sqrt{(\Delta L^*)^2 + (\Delta a^*)^2 + (\Delta b^*)^2}$$

where ΔL^*, Δa^*, Δb^* are differences in individual axes (difference between the value measured after heating the sample and the reference sample).

Analysis of changes in saccharides

Analytical materials for the analysis were taken of the irradiated stripes B10 to B30 and the non-irradiated part of the BREF (total 12 samples, in the range of radiation doses of from 19.1 to 57.3 J.cm-2). Cellulose was determined by the method of Kürschner and Hoffer (1929), the amount of glucose in the proportion of hemicelluloses was calculated as the difference between glucose and cellulose in wood. Analysis of carbohydrates in the samples was performed by gas chromatography (Kačík, Kačíková, 2009).

Preparation of carbohydrates aldonitrilacetates

A mixture of monosaccharides (L-Rhamnose, L-Arabinose, D-Xylose, D-Mannose, D-Glucose, D-Galactose) was dissolved in pyridine (0.05 cm^3 per 1 mg of a carbohydrate), and the addition of hydroxylamine hydrochloride (1 mg/1 mg of saccharide) the solution was heated for 30 min at 90 °C. After cooling to 20 °C was added to a mixture of acetic anhydride (0.15 cm^3 per 1 mg of carbohydrate) and the solution was heated an additional 30 minutes at 90 °C. The cooled solution was evaporated to dryness under vacuum at 60 °C. The dry residue was dissolved in ethyl acetate and injected into the chromatograph.

Hydrolysis of samples

Samples were hydrolysed by the method of Saeman (1954). In the first stage to the sample (100 mg) was added 1 cm^3 72 % H_2SO_4 and hydrolysis was carried out for 1 hour at 30 °C. Hydrolyzate was then diluted by adding 28 cm^3 of distilled water and secondary hydrolysis was carried out at 120 °C for 90 minutes. The resulting hydrolyzate was made up to 50 cm^3 of this solution was pipetted off aliquot (5 cm^3), to which was added 2 cm^3 of distilled water containing the internal standard (inositol) with concentration of the 1 $mg.cm^{-3}$. The sample containing the internal standard was evaporated to dryness under vacuum at 60 °C and the derivatized to the aldonitrilacetates as of the standard substances.

Analysis by gas chromatography

Aldonitrilacetates of saccharides were analyzed on a chromatograph type Fisons 8310 DPFC with Flame ionisation detector (FID). Separation was performed on a capillary column DB-5 (30 m × 0.32 mm ID, film thickness 0.25 mm) as a carrier gas was used helium (He 4.6) at a flow rate of 1.7 $cm^3.min^{-1}$. Oven temperature was 175 °C for 4 minutes, then increase for a rate of 4 $°C.min^{-1}$ to 220 °C. Injector temperature was 250 °C and detector 300 °C.

RESULTS AND DISCUSSION

Colour changes

Colour values measured before and after irradiation are in Table 2, colour differences are shown in Fig. 3.

Table 1 The reference values L^*_{REF}, a^*_{REF}, b^*_{REF} and the measured values of L^*, a^*, b^* depending on the dose of radiation to the beech

STRIP	B40	B38	B36	B34	B32	B30	B28	B26	B24	B22	B20	B18	B16	B14	B12	B10
L^*_{REF}	78,95	79,02	79,33	79,31	79,20	78,88	78,75	79,30	79,38	78,96	78,88	78,28	78,93	78,25	77,70	77,14
a^*_{REF}	5,95	5,91	5,82	5,82	5,88	6,04	6,13	5,87	5,90	6,06	6,17	6,42	6,12	6,41	6,60	6,79
b^*_{REF}	16,42	16,27	16,36	16,19	16,35	16,50	16,47	16,28	16,20	16,41	16,68	16,93	16,60	16,80	17,17	17,43
H (J.cm^{-2})	14,3	15,1	15,9	16,9	17,9	19,1	20,5	22,0	23,9	26,1	28,7	31,8	35,8	40,9	47,8	57,3
L^*	77,22	77,04	76,90	75,79	74,87	73,48	71,71	70,34	65,43	62,58	54,03	47,63	40,29	33,30	30,72	31,72
a^*	6,43	6,42	6,46	6,62	6,78	6,98	7,06	7,01	7,21	7,16	7,14	6,59	5,42	3,84	1,74	1,11
b^*	15,90	15,98	15,95	15,67	15,61	15,25	15,15	15,26	15,35	15,13	14,40	13,11	10,47	6,41	2,62	1,95

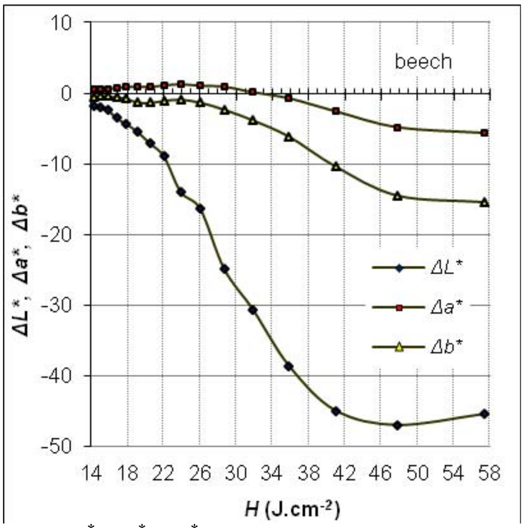

Fig. 3 ΔL^*, Δa^*, Δb^* with dependence of H

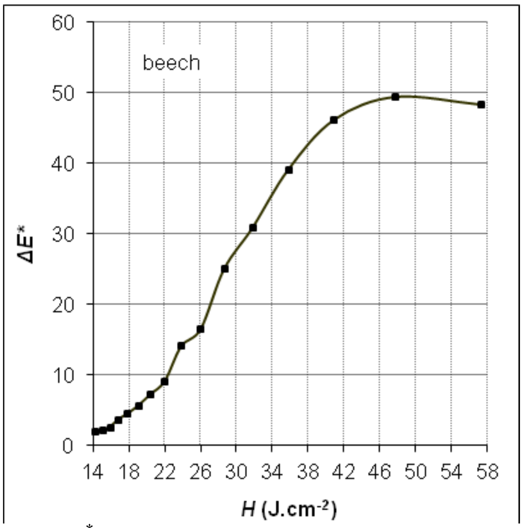

Fig. 4 ΔE^* with dependence of H

ΔL* decreased continuously (from -1.7 to 45.4) with the increase of the irradiation dose (Fig. 3). At lower dose levels was observed minimal changes and in the range of the 17-40 J.cm^{-2} was almost linear trend of decline. Above the 46 J.cm^{-2} is value of *ΔL**even reduced, which is probably due to the start-carbonisation of the wood.
Colour differences Δa^* and Δb^* are significantly changed above the dose of the 26 J.cm^{-2} when they began to fall. Decrease was stopped at the 47 J.cm^{-2}.

Total colour difference *ΔE** grew continuously up to a dose level of the 46 J.cm^{-2} (Fig. 4). Above this value decreased slightly due to severe degradation of the wood surface. The natural colour with a slight red hue gradually changed (through brown to dark brown shade).

Changes in saccharides

When exposed to various forms of energy in wood hemicellulose are considered the least stable part (Kačíková et al., 2006; Windeisen et al., 2009). Changes in chemical composition and structure of the components of the wood were observed in aging (Dadashian, Wilding, 2001), oxidation (Hon, 1989), hydrolysis (Laurová, Kúdela, 2008) and thermal degradation (Windeisen, Wegener, 2009; Rousset et al., 2009).

The results show that the irradiation surface of beech wood using CO_2 laser decreases the amount of saccharides depending on the size of the energy applied to the wood. Energy to the value of 26 J.cm^{-2} has little effect on the loss of saccharides (Table 2). With the growth of irradiation dose occurs by considerable decrease the amount of carbohydrates in the irradiated samples. This may be due to degradation of hemicelluloses and the amorphous content of cellulose, as evidenced by the ratio of cellulose to hemicellulose (Table 2). The thermal degradation of saccharides arise some volatile products - especially methanol, acetic acid, propionic acid, furan, carbonyl compounds and levoglucosan (Fengel, Wegener, 1984; Košík et al., 1968). More rapidly loss of hemicelluloses in comparison with the cellulose is also reported in (Turner et al., 2010). Above the dose of 32 J.cm^{-2} is already the ratio of cellulose to hemicellulose constant but their number is declining. This suggests inter degradation of hemicelluloses and cellulose degradation.

Table 2 Changes of beech wood saccharides in dependence of irradiation dose

H (J.cm^{-2})	RHA (%)	ARA (%)	XYL (%)	MAN (%)	GLC-hemi (%)	GLC-cel (%)	GAL (%)	Hemicel (%)	Yield of saccharides (%)
0	0.82	0.75	25.90	1.24	3.74	42.15	0.47	32,91	**75.06**
19,1	0.84	0.72	26.12	1.43	3.65	41.18	0.63	33,39	74.57
20,5	1.52	0.65	22.36	1.10	3.97	44.83	0.50	30,11	74.94
22,0	0.64	0.60	22.49	0.97	4.05	45.70	0.53	29,27	74.97
23,9	1.45	0.57	19.87	1.04	3.57	40.26	0.47	26,98	67.24
26,1	0.58	0.65	18.95	1.13	3.40	38.41	0.61	25,33	63.74
28,7	0.60	0.63	15.64	1.93	2.57	28.96	0.36	21,72	50.68
31,8	1.37	0.49	13.37	0.42	2.42	27.34	0.29	18,37	45.71
35,8	1.76	0.41	11.11	1.01	2.47	27.87	0.22	16,99	44.86
40,9	0.24	0.24	10.24	0.26	2.36	26.65	0.24	13,59	40.24
47,8	0.52	0.24	7.22	0.59	2.10	23.66	0.13	10,79	34.45
57,3	0.70	0.39	4.41	0.77	2.11	23.80	0.30	8,67	32.47

Legend: H – irradiation dose, RHA - L-Rhamnose, ARA - L-Arabinose, XYL - D-Xylose, GLC-Hemi - D-Glucose in Hemicelluloses, GLC-Cel - D-Glucose in Cellulose, GAL - D-Galactose.

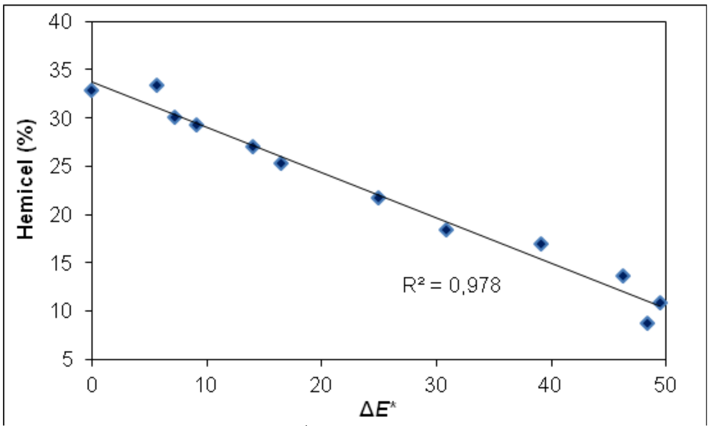

Fig. 5 Correlation between ΔE^* and decrease of hemicelluloses content

CONCLUSION

As follows from the experimental results the change of the irradiation dose causes changes in colour of the wood (mainly decreases its lightness). Analysis of saccharides shows the same trend in relation to the irradiation dose. Hemicelluloses degrade quickly but changes are also found in cellulose. Total loss of saccharides for maximum radiation dose was 56.7% of the amount of carbohydrates, compared with carbohydrates in the original sample beech wood. Very good correlation (R^2 = 0.978) is observed between the total colour difference (ΔE^*) and decrease in hemicellulose content of irradiated beechwood, which confirms the dependence of the wood colour on its chemical composition (Fig. 5) (Sunquist, 2004).

Acknowledgment: This work was supported by the KEGA agency of the Ministry of Education, Science, Research and Sport of the Slovak Republic (grant No. 011UMB-4/2012).

REFERENCES

Bourgois J., Bartholin M.C., Guyonnet R., 1989. Thermal treatment of wood: analysis of the obtained product. Wood Sci. Technol. 23: 303-310.

Mitsui K., Takada H., Sugiyama M., Hasegawa R., 2001. Changes in the Properties of Light-Irradiated Wood with Heat Treatment. Holzforschung, 55(6): 601-605.

Mitsui K., Tsuchikawa S., 2005. Low atmospheric temperature dependence on photodegradation of wood. Journal of Photochemistry and Photobiology B: Biology, 81: 84-88.

Esteves B., Pereira H., 2009. Wood modification by heat treatment: A review. Bioresources, 4(1), 370-404.

Reinprecht L., Vidholdová Z., 2008. Thermowood. Technická univerzita vo Zvolene, 89. ISBN 978-80-228-1920-6.
Chen Y., Fan Y., Gao J., Stark N.M., 2012. The effect of heat treatment on the chemical and color change of black locust (*Robinia pseudoacacia*) wood flour. BioResources, 7(1): 1157-1170.
Bourgois J., Guyonnet R., 1988. Characterization and analysis of torrefied wood. Wood Sci. Technol. 22: 143-155.
Kačík F., Kačíková D., Bubeníková T., 2006. Spruce wood lignin alteration after infrared heating at different wood moistures. Cellulose Chem. Technol, 40(8): 643-648.
Kubovský I., Babiak M., 2009. Color changes induced by CO_2 laser irradiation of wood surface. Wood Research, 54(3): 61-66.
Kürschner K., Hoffer A., 1929. Ein neues Verfahren zur Bestimmung der Cellulose in Hölzern und Zellstoffen. Techn. Chem. Pap. und Zellstoff. Fabr., 26: 125-129.
Kačík F., Kačíková D., 2009. Determination of carbohydrates in lignocellulosics by gas chromatography of aldonitrilacetates. Folia Forestalica Polonica, Series B, 40: 61-66.
Saeman J.F., Moore W.E., Mitchell R.L., Millett M.A., 1954. Technique for the determination of pulp constituents by quantitative paper chromatography. Tappi, 37: 336-343.
Kačíková D., Netopilová M., Osvald A., 2006. Drevo a jeho termická degradácia. Sdružení požárního a bezpečnostního inženýrství v Ostravě, 79. (in Czech). ISBN: 80-86634-78-7.
Windeisen E., Bächle H., Zimmer B., Wegener G., 2009. Relations between chemical changes and mechanical properties of thermally treated wood. Holzforschung, 63(6): 773-778.
Dadashian F., Wilding W.A., 2001. Photodegradation of lyocell fibers through exposure to simulated sunlight. Text. Res. J., 71(1): 7-14.
Hon N.S., 1989. Surface chemistry of oxidized wood. Cellulose and wood chemistry and technology. New York: John Wiley and Sons, Inc., 1401-1427.
Laurová M., Kúdela J., 2008. Analýza hydrolyzátov získaných po hydrotermickej plastifikácii jaseňového dreva. Acta Facultatis Xylologiae, 50(1): 5-14.
Windeisen E., Wegener G., 2009. Chemical characterization and comparison of thermally treated beech and ash wood. Materials Science Forum. Vol. 599: 143-158.
Rousset P., Lapierre C., Pollet B., Quirino W., Perre P., 2009. Effect of severe thermal treatment on spruce and beech wood lignins Ann. For. Sci., 2009, Vol. 66, p. 110-117.
Fengel D., Wegener G., 1984. Wood. Chemistry, Ultrastructure, Reactions. Walter de Gruyter, Berlin - New York, 613.
Košík M., Herein J., Domanský R., 1968. Pyrolyse des Buchenholzes bei niedriegen Temperaturen. IV. Grundlegende Angaben über die Bildung flüchtiger Produkte. Holzforschung und Holzvewertung, Heft 3, 20: 56-59.
Turner I., Rousset P., Rémond R., Perré P.,2010. An experimental and theoretical investigation of the thermal treatment of wood (*Fagus sylvatica* L.) in the range 200-260 °C. International Journal of Heat and Mass Transfer, 53: 715-725.
Sunquist B., 2004. Colour changes and acid formation in wood during heating. Doctoral thesis. Luleå University of Technology, 50. ISSN 1402-1544.

SHEAR STRESS AND KINEMATIC VISCOSITY OF AUTOMOTIVE ENGINE OIL

Vojtech Kumbar*, Petr Dostal, Stanislav Barton

Mendel University in Brno, Department of Engineering and Automobile Transport, Zemedelska 1, 613 00 Brno, Czech Republic, Phone: +420607670987, Fax: +420545132119,
E-mail: vojtech.kumbar@mendelu.cz

Abstract

The aims of this paper are shear stress and kinematic viscosity of engine oil. It was focused on automotive engine oil. Shear stress and kinematic viscosity are two of the most important behaviours of engine oil. There were observed two different engine oils – first from petrol engine and second from diesel engine. Service interval of change oil was 15,000 km and samples of used engine oil were taken after 1,500 km. The measured values were modelled.

Keywords: engine oils, passenger cars, kinematic viscosity, shear stress

Introduction

Shear stress is one of the most important behaviour of liquids. We can use it to describe flow behaviour of liquids. For Newtonians fluids increases shear stress with increasing shear rate (Batchelor, 1968).

Shear stress causes that the oil film is maintained at the lubricated parts of the engine. Then the all engine components are therefore good lubricated. With decreasing shear stress might wear engine parts and might come a follow failure in. Therefore it is important to continuously monitoring of engine oil's shear stress (Mang, Dresel, 2001).

Another important feature is viscosity (kinematic and dynamic). For liquids increase viscosity if temperature decreases. It is valid also for engine oils. If the temperature is under freezing-point engine oils might solidify. It is depend on viscosity class of engine oil. Oils with viscosity class 0Wxx or 5Wxx are designed for low temperatures, but we do not used engine oils with viscosity class 15Wxx or 20Wxx at cold temperature (-20 °C) (Maggi, 2006).

Materials and methods

There were observed two different engine oils in two different passenger cars. Specifications of engine oils are showed in Tab. 1 and specification of vehicles are showed in Tab. 2.

The Castrol engine oil was used in car Renault and the Shell engine oil was used in car Škoda. Samples of used engine oil were taken from engine after 1,500 km. Firsts samples are taken with raid 20 km, because after drain used (old) engine oil from engine a rest of old engine oil stay in engine and its parts. More of this problematic have written authors in their publication (Černý, Mašek, 2010). Delivery point was the oil dipstick for both cars.

The procedure of sample preparation for shear stress and viscosity measurements corresponded to a typical sampling procedure. The adequate volume (20 ml) of oil was put into the apparatus cuvette without previous heavy mixing or any other kind of preparation. There are several methods to measure shear stress and kinematic viscositz of fluid or semi fluid materials and different geometries may be utilized: concentric cylinders, cone and plate, and parallel plates.

Presented data have been obtained from measurements performed on laboratory digital reometer Anton Paar DV–3 P (Austria), which is designed to measure dynamic or kinematic viscosity, shear stress, and shear rate. The DV–3 P is a rotational reometer, based on measuring the torque of a spindle rotating in the sample at a given speed. Shear stress is expressed in [g.cm^{-1}.s^{-2}], shear rate in [s^{-1}], kinematic viscosity in [mm^{2}.s^{-1}], and speed of spindle in revolutions per minute [rpm]. The experiments have been performed with use of TR8 spindle with special adapter for a small amount of sample. Due to the parallel cylinder geometry shear stress and kinematic viscosity, except other values, can be determined (Kumbár et al., 2013). Schematic of the measuring geometry is shown in the Fig. 1.

Tab. 1 Specifications of engine oils

Producer	Designation	Viscosity Class	Performance Class
Castrol	Magnatec	10W-40	ACEA A3/B3/B4, API SL/CF
Shell	Helix Ultra Extra	5W-30	ACEA C2/C3 (A3/B3/B4)

Tab. 2 Specifications of passenger cars

Producer	Type	Engine	Turbocharger	Cylinder Volume, cm^3	Number of Cylinders	Engine Power, *kW*
Renault	Scenic I	Gasoline	No	1600	4	79
Škoda	Roomster	Diesel	Yes	1400	3	51

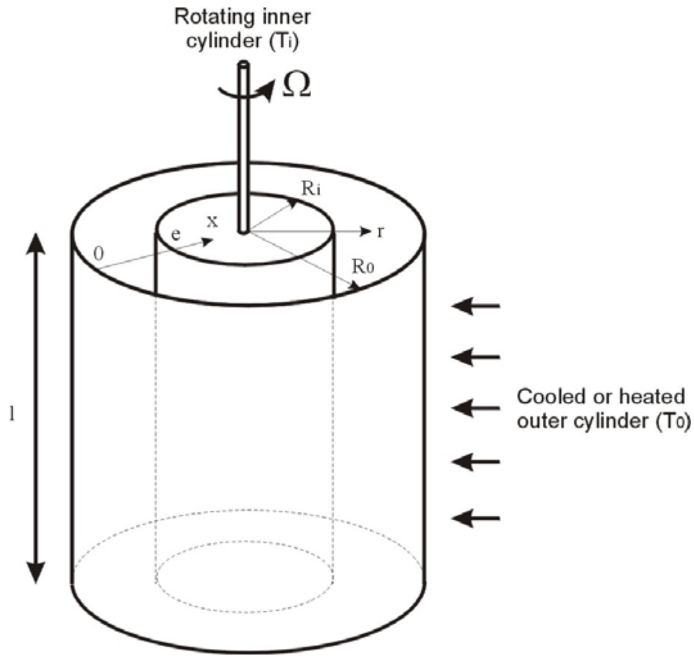

Fig. 1 Schematic of the measuring geometry (Kumbár et al., 2013)

Results and discussion

The result values of kinematic viscosity and shear stress of automobile engine oil taken from gasoline engine (Renault) are showed in Tab. 3 and Fig. 2.

Tab. 3 Kinematic viscosity and shear stress of engine oil (gasoline engine)

Raid, *km*	Kinematic Viscosity, $mm^2 \cdot s^{-1}$	Shear Stress, $g \cdot cm^{-1} \cdot s^{-2}$
0	214.96	172.33
20	212.80	170.59
1737	204.56	169.99
3097	201.79	161.76
4462	199.29	159.76
6053	198.12	158.82
7550	196.88	157.55
9104	196.40	157.45
11027	195.97	157.10
12079	195.06	156.37
13815	194.73	156.10
15108	193.59	155.60

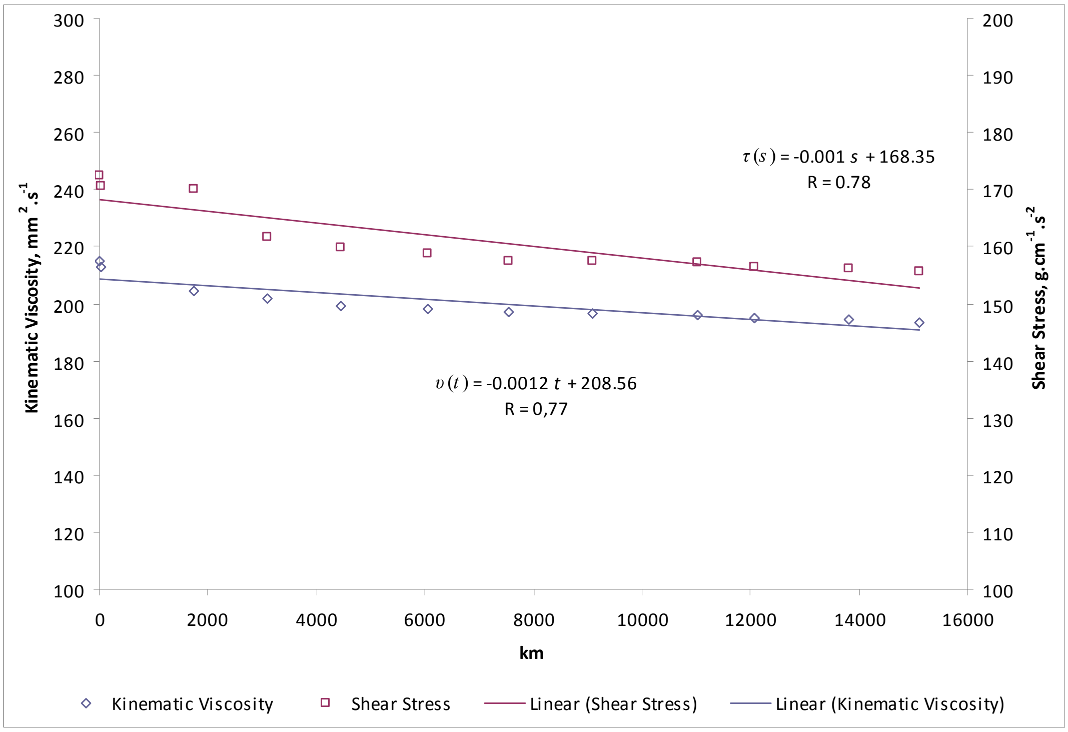

Fig. 2 Kinematic viscosity and shear stress of engine oil (gasoline engine)

Result values were modelled using linear function. The general formula of linear function is:

$$y(x) = k \cdot x + q\,. \tag{1}$$

For counting kinematic viscosity of automobile engine oil (gasoline engine) is valued formula:

$$\nu(s) = -0.0012 \cdot s + 208.56\left[mm^2 \cdot s^{-1}; km\right], \tag{2}$$

where ν is kinematic viscosity and s is raid.

For counting shear stress of automobile engine oil (gasoline engine) is valued formula:

$$\tau(s) = -0.00102 \cdot s + 168.35\left[g \cdot cm^{-1} \cdot s^{-2}; km\right] \tag{3}$$

where τ is shear stress and s is raid.

The values of correlation coefficients R were 0.77 and 0.78.

The result values of kinematic viscosity and shear stress of automobile engine oil taken from diesel engine (Škoda) are showed in Tab. 4 and Fig. 3.

Tab. 4 Kinematic viscosity and shear stress of engine oil (diesel engine)

Raid, *km*	Kinematic Viscosity, $mm^2 \cdot s^{-1}$	Shear Stress, $g \cdot cm^{-1} \cdot s^{-2}$
0	176.63	139.79
20	174.88	137.05
1475	170.85	135.22
2985	170.16	134.67
4436	165.87	131.27
6060	163.23	129.18
7820	162.89	128.99
9194	161.74	128.00
11653	160.20	127.12

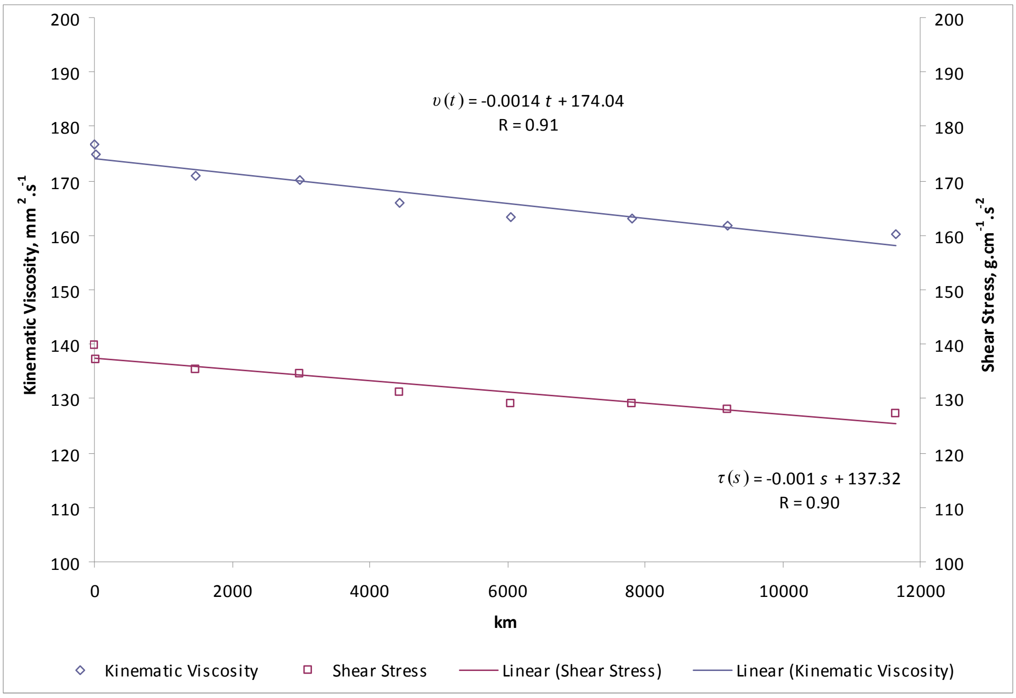

Fig. 3 Kinematic viscosity and shear stress of engine oil (diesel engine)

Result values were modelled using linear function (1). For counting kinematic viscosity of automobile engine oil (diesel engine) is valued formula:

$$\nu(s) = -0.0014 \cdot s + 174{,}04\left[mm^2 \cdot s^{-1}; km\right], \quad (4)$$

where ν is kinematic viscosity and s is raid.

For counting shear stress of automobile engine oil (diesel engine) is valued formula:

$$\tau(s) = -0.00101 \cdot s + 137.32\left[g \cdot cm^{-1} \cdot s^{-2}; km\right], \quad (5)$$

where τ is shear stress and s is raid.

The values of correlation coefficients R were 0.91 and 0.90.

With increasing count of kilometres the kinematic viscosity and shear stress of engine oil (both engines) decreased. These trends were compared with results of other authors (Barnes et al., 1998; Mann, 2007), and they achieved similar trends.

Conclusions

It was analyzed kinematic viscosity and shear stress of automobile engine oils. There were taken samples of used engine oil from two vehicles – with gasoline engine (Renault Scenic) and with diesel engine (Škoda Roomster). Engine oils were different too. First was Castrol Magnatec 10W-40 and second was Shell Ultra Extra 5W-30. The interval of taken samples was 1,500 km.

Kinematic viscosity and shear stress were decreased with increasing count of kilometers. The result values were modeled using linear mathematical model. Correlation coefficients R achieved high values.

Acknowledgement

The research has been supported by the project TP 5/2013 "Application of non-destructive methods of technical diagnostics in agricultural technology" financed by IGA AF MENDELU.

References

Batchelor G.K., 1968. An introduction to fluid dynamics. Nature, 217: 394.

Mang T., Dresel W., 2001. Lubricants and Lubrication. Weinheim: Wiley-vch, 759.

Maggi C.P., 2006.Advantages of Kinematic Viscosity Measurement in Used Oil Analysis.Practicing Oil Analysis Magazine, 5: 38-52.

Kumbár V., Polcar A., Čupera J., 2013. Rheological profiles of blends of the new and used motor oils. Acta Universitatis Agriculturae et Silviculturae Mendelianae Brunensis, 61(1): 115-122.

Černý J., Mašek P., 2010. Změna kvality nových náplní motorového oleje. Paliva, 2(1): 1-3. (in Czech)

Barnes H.A., Hutton J.F., Walters K., 1998. An Introduction to Rheology. Elsevier, Oxford, 200.

Mann D., 2007. Motor Oils and Engine Lubrication. Motor Oil Engineers, L.L.C., Detroit, 832.

MEASUREMENT OF HOP MATERIAL THROUGHPUT BY CAPACITIVE SENSOR

František Kumhála*, Miroslav Kavka, Jakub Lev, Václav Prošek

Czech University of Life Sciences Prague, 16521 Prague 6 – Suchdol, Czech Republic,
Phone: +420 224 383 135, E-mail: kumhala@tf.czu.cz

Abstract

The information about instantaneous hop material throughput could be used for stationary hop picking machine control which should bring higher harvesting efficiency with better quality of harvested product. In this research, a capacitive throughput sensor as a source of electronic control signal has been tested. Linear dependence of capacitive sensor output voltage on wet hop material throughput was found. Coefficients of determination R^2 ranged from 0.92 to 0.97. Nevertheless, the behaviour of capacitive sensor was necessary to explain by a mathematical model of the electric field intensity. This model was created by using of finite elements method. Based on the experiments carried out it can be concluded that the output voltage signal from capacitive sensor can be used for the aim of stationary hop picking machine throughput control with adequate precision under real harvesting conditions.

Keywords: capacitive sensor, material throughput, hop picking machine

Introduction

Enormous labour requirements of manual hop picking had led to the introduction of mechanized picking in the past. For example, in 1972, 92 per cent of the total area in Czechoslovakia was harvested mechanically (Rybáček, 1991). Nevertheless, just from the beginning of its development, the mechanization of hop picking has presented many problems connected to the efficiency and quality of the picking machines work (Rybáček, 1991). Nowadays in the Czech Republic, stationary hop picking machines with picking conveyer system are preferable (Podsedník, 2001).

Modern machines are equipped among others by control board with small computer unit for the supervisory of output, productivity, number of vines and stoppage time and also with control and operating units for continuous setting of basic parameters. Nevertheless, all basic important parameters of the machine (the speed of picking walls, feed track intake conveyer speed, belt conveyers speed etc.) are controlled manually according to machine operators' decision (Podsedník, 2001). In practice, these parameters are set by operator at the start of working day or at the beginning of different hop variety harvesting. It is almost impossible for the operator to adjust these parameters during machine operation because of two main reasons: (1) he is not able to react quickly enough to uneven material throughput and (2) he has visual information only about material throughput (Podsedník, J. Chmelařství družstvo Žatec, CR. Personal communication).

That is why one of the problems arising during stationary hop picking machines operation is related to uneven throughput of picked hop vines caused both by the differences in yield of individual vines and by machine operators' errors. This uneven throughput causes higher load of consequent hop cones separation mechanisms leading to increased impurity of the final product and higher harvesting losses (Podsedník, J. Chmelařství družstvo Žatec, CR. Personal communication).

A possible solution to this problem can be the implementation of throughput sensors to balance hop picking machine material throughput. However, finding a throughput sensor providing control signal with sufficient accuracy is a problem.

Immediate throughput of different plant materials, such as forage (Kumhála et al., 2007) potatoes and sugar beets (Kumhála et al., 2009) or chopped maize (Kumhála et al., 2010) can be measured by a capacitive throughput sensor. In our earlier papers mentioned above, theoretical considerations of the sensor function, advantages of capacitive sensor techniques as well as the influence of both material moisture content and volume density changes on capacitive sensor function were discussed. In 2011, we tested the function of capacitive throughput unit with wet hop cones under real harvesting conditions (Kumhála et al., 2013). Results showed suitable dependence of measured output voltage on wet hop cones throughput under both laboratory and harvesting conditions.

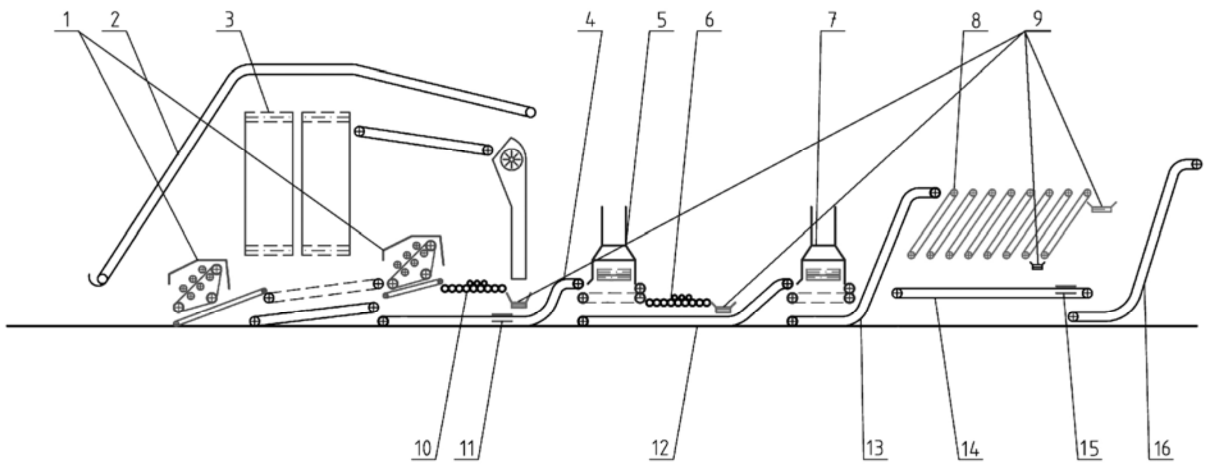

Fig. 1 Main parts of stationary hop picking machine PT-30
1-lateral pickers for secondary picking of long ends, 2-feed track intake, 3-picking walls, 4-belt conveyer to separation part, 5-primary air separator, 6-pinch rollers, 7-secondary air separator, 8-inclined separating conveyers, 9-waste conveyers, 10-pinch rollers, 11- location of capacitive sensor S1, 12-belt conveyer to secondary air separator, 13-belt conveyer to inclined separating conveyers, 14-horizontal elastic belt conveyer, 15-location of capacitive sensor S2, 16-belt conveyer to drying machine.

In this study, we applied the capacitive throughput sensor developed in our previous research to two different places of stationary hop picking machine with the aim to test its suitability as a source of electronic signal for machine throughput balancing.

Material and experimental methods

All harvesting experiments were done using a stationary hop picking machine PT-30 produced by Chmelařství družstvo Žatec, CR, and located in Stekník. This machine uses picking conveyer system. At the beginning of the picking process, hop vines are loaded into the picker manually using feed track intake. Then, hop cones are separated from the vine stalk by two picking walls (equipped with picking conveyers) along their entire length with subsequent secondary picking of long ends. Picked hop cones are then separated by air separators and inclined separating conveyers. At the end of the hop picking machine clean hop cones falling down from inclined separating conveyers are transported away from the machine by a horizontal elastic belt conveyer. Main parts of PT-30 can be seen in Fig. 1.

Two modified capacitive sensors (S1 and S2, please see Fig. 1) were made to be mounted on our PT-30 hop picking machine. The main difference was in capacitors dimensions. Dimensions of the bottom, grounding, and the upper, active plate of S1 were 890 mm in length and 300 mm in width. Both plates were made of 1.5 mm thick metal sheet. In order to increase the strength of the plates their edges were bent by 90 degrees. The upper plate was insulated from the rest of the machine by two 8 mm thick pertinax blocks with dimensions of 290 mm in length and 120 and 60 mm in width. The distance between the plates was 120 mm. The electronic measurement apparatus of S1 was mounted on the insulation block at the right side of the upper plate.

Dimensions of the bottom, grounding plate and of S2 were 1222 mm in length and 300 mm in width. Dimensions of the upper, active plate were 1170 mm in length and 300 mm in width. Both plates were again made of 1.5 mm thick metal sheet. The upper plate was also insulated from the rest of the machine in this case by two 15 mm thick pertinax blocks with dimensions of 290 mm in length and 80 mm in width. The distance between the plates was 80 mm. The electronic measurement apparatus of S2 was mounted on the insulation block at the right side of the upper plate again.

Capacitive sensor S1 was integrated to belt conveyer to separation part (please see position 4 and 11 in Fig. 1). S1 was used to measure immediate throughput of wet hop material exiting the picking part of the machine. The total transport width of the conveyer belt was 0.9 m and its velocity 0.44 $m.s^{-1}$.

For the purpose of wet hop cones immediate throughput measurement, capacitive sensor S2 was mounted towards the end of horizontal elastic belt conveyer transporting clean hop cones from the machine (position 15 in Fig. 1). The total transport width of the conveyer belt was 1.1 m and its velocity 0.64 $m.s^{-1}$.

Owing to changes in dimensions of the sensor, calibration of both capacitive sensors was necessary. The calibration was carried out repeatedly in August 21st and 29th and September 4th during 2012 harvesting season with different harvested material.

Saaz hop variety with 76.6 % hop cones and 77.3 % hop material moisture content (wet basis) was harvested on August 21st and then used for the calibration procedure. The same variety but from ecological production with 71.9 % hop cones and 75.8 % hop material moisture content (wet basis) was harvested on August 29th. Sladek variety with 75.5 % hop cones and 79.1 % hop material moisture content (wet basis) was harvested on September 4th. Wet hop cones and hop material moisture content was determined by ASABE Standard S358.2 (oven drying at 103 °C up to constant weight of the dry sample, wet basis).

The calibration was carried out in the late evening and night after the end of the harvesting day. At the beginning of each calibration measurement, a defined quantity of material was distributed as evenly as possible on clean conveyer belts, which were switched off. Only 1.85 m from the total transport length of the conveyer belt to separation and 3.84 m of horizontal elastic belt conveyer could be used for this purpose because of capacitive throughput sensors placement and difficult access to the conveyers. After switching on the conveyers, the material passed through the sensors and its output voltage was recorded every 0.5 s. The values were then averaged to obtain the final result for a particular calibration measurement.

Statistical evaluation and charting was done using MS Excell and Statgraphics. Finite elements method was made using Agros2D software (www.agros2d.org).

Results and discussion

Capacitive sensor S1

The measurement results of the dependence of measured output voltage on wet hop material throughput are shown graphically in Fig. 2. Freshly picked hop material is the mixture of wet hop cones, hop leaves and other rests from picking such as parts of stalks etc. Zero point of the calibration curves was set to 1.22 V. Linear approximation of the voltage/throughput dependence was considered in all cases up to app. 7 V. Then, upper limit of S1 measured range was already reached. Nevertheless, linear approximation of voltage-to-throughput dependence is just simplification of the problem. According to theory of capacitive throughput sensor (Kumhála et al., 2009) the filling of the sensor S1 was near to layer filling and shifted hyperbolic dependence would be obtained in this case.

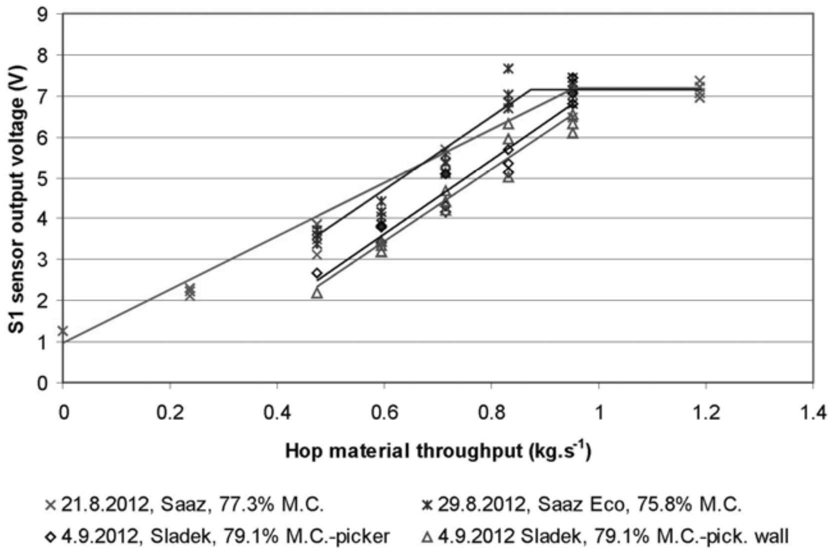

Fig. 2 Dependence of capacitive sensor S1 output voltage on wet hop material throughput under real harvesting conditions.

Linear dependence from 21.8.2012: y=6.37x+7.56, $R^2 = 0.97$; linear dependence from 29.8.2012: y=10.03x-1.56, $R^2 = 0.92$; Linear dependence from 4.9.2012-picking wall y=8.85x-1.88, $R^2 = 0.94$; Linear dependence from 4.9.2012-lateral picker y=9.13x–1.86, $R^2 = 0.94$. Horizontal lines indicate the reaching of the upper limit of S1 measurement range.

The problem was that the design of belt conveyer to separation part of stationary picking machine was different from those used in our previous tests. In this case, the conveyer was equipped with pockets made from metal sheets. Because metal sheet is a very good electrical conductor the presence of those sheets between capacitor plates influenced the behaviour of capacitive sensor significantly. In order to better understand sensor function, sensor behaviour modelling using finite element method was carried out. Mathematical model of capacitive sensor electric field intensity was calculated using higher order accuracy finite element method. Electric field intensity correlates well with sensor sensitivity. Results of the computes simulations are shown in Fig. 3.

Mathematical model showed the places with high electric field intensity on the tops of conveyer metal pockets. The sensitivity of capacitive sensor is the highest in those places. It was in good agreement with the results of our measurements. When the amount of hop material was so high that started to lie above conveyer metal pockets, upper limit of S1 measured range started to be reached quickly. This could be an advantage in operating conditions. Overloading of separation part started exactly when this situation occurred. Therefore it exist a good assumption that this moment can be indicated by capacitive sensor S1 with high reliability.

Another aim of the measurements with the sensor S1 was to determine the influence of different harvested material to sensor function. It is clear from Fig. 2 that here existed visual difference between approximated lines for different harvested varieties. Nevertheless, this difference was not confirmed statistically. It was probably because the variance of measured values was relatively high and the number of the measurements was not fully sufficient for statistical analysis in this case. Next measurements are scheduled for this reason.

Capacitive sensor S2

For the purpose of clean wet hop cones throughput measurement sensor S2 was mounted towards the end of horizontal elastic belt conveyer. Conveyer design was very similar with those used in our previous measurements in this case. Conveyer width was large enough not to allow the measured material to make layers between capacitor plates. According to the simple theory of capacitive throughput sensor (Kumhála et al., 2009) this was a typical example of filling by single particle and therefore linear dependence of sensor output voltage on wet hop cones throughput was anticipated.

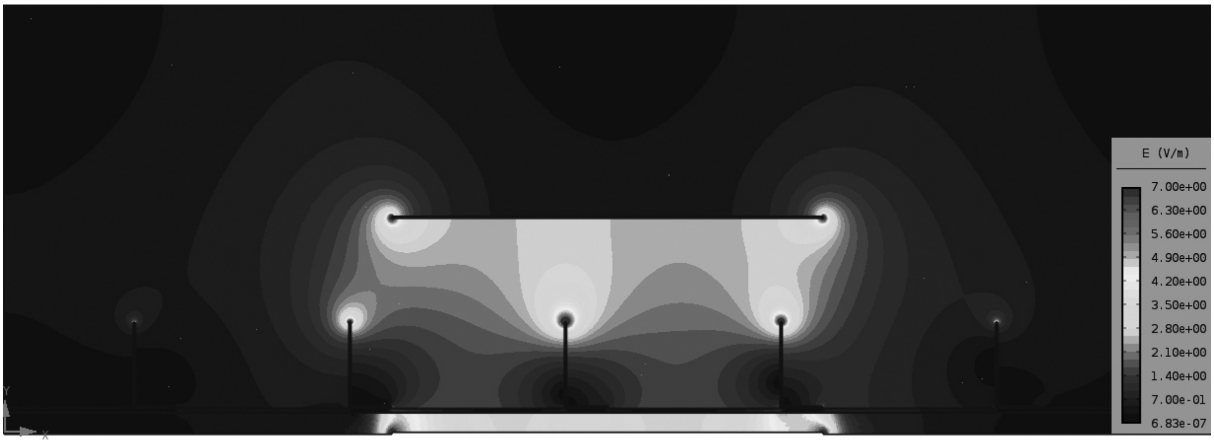

Fig. 3 Mathematical model of capacitive sensor electric field distribution when using belt conveyer with metal pockets calculated by Agros2D with higher order accuracy. Places with the higher electric field intensity are located on the tops of metal pockets.

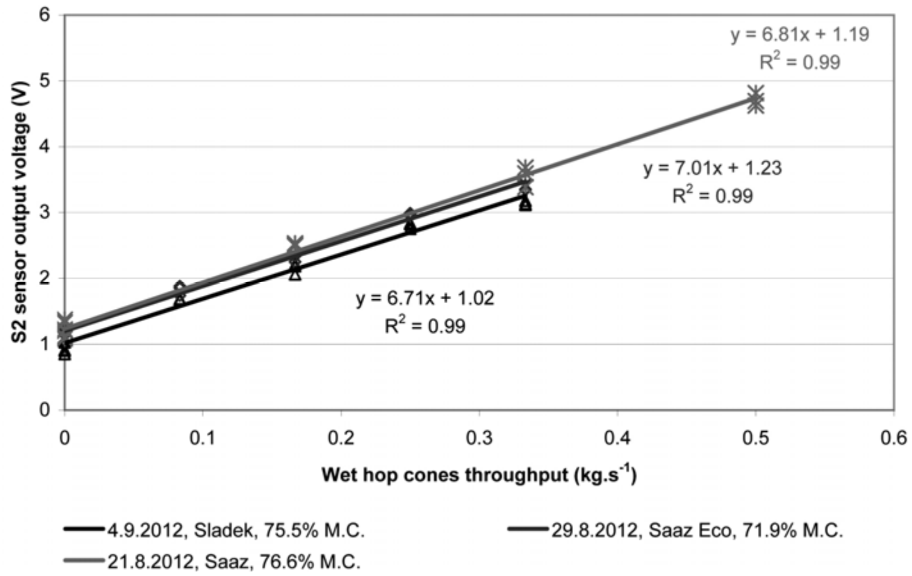

Fig. 4 Dependence of capacitive sensor S2 output voltage on wet hop cones throughput under real harvesting conditions with different hop varieties.

The results are shown graphically in Fig. 4. It is clear from the chart that this dependence was really linear one in all cases with a suitable coefficient of determination (R^2=0.99). Also the slopes of the lines from different days were very similar. It means that the influence of different type of measured material to the measurement results is very small. The main difference between the lines is in zero point, which varied from 1.02 to 1.22 V. It can cause problems in the case of using the sensor S2 to detect the yield of wet hop cones. The instability of zero point was caused by instability of measuring circuit. It means that it follows from presented results that measuring circuit stability needs to be improved in this case.

Conclusion

As the results showed, output voltage signal from capacitive sensors can be used for the aim of stationary hop picking machine throughput control with adequate precision under real harvesting conditions. Nevertheless the influence of differences in harvested material to sensor accuracy needs to be further verified and stability of measurements zero point needs to be increased.

Acknowledgements

This project was supported by TACR Project No. TA02010557 and by Research Project No. MSM 6046070905.

References

ASABE Standards, 2006. S358.2 Moisture measurement-Forages. St. Joseph, Michigan, USA.

Kumhála F., Kvíz Z., Kmoch J., Prošek V., 2007. Dynamic laboratory measurement with dielectric sensor for forage mass flow determination. Research in Agricultural Engineering 53(4): 149-154.

Kumhála F., Prošek V., Blahovec J., 2009. Capacitive throughput sensor for sugar beets and potatoes. Biosystems Engineering 102: 36-43.

Kumhála F., Prošek V., Kroulík M., 2010. Capacitive sensor for chopped maize throughput measurement. Computers and Electronics in Agriculture, 70: 234-238.

Kumhála F., Kavka M., Prošek V., 2013. Capacitive throughput unit applied to stationary hop picking machine. Computers and Electronics in Agriculture, 95: 92-97.

Podsedník J., 2001. Hop harvesting technology in the Czech Republic 1996-2000. In: Proceedings of the Technical Commission I.H.G.C. of the XLVIIIth International Hop Growers Congress, Canterbury, England. Agros, Žatec (CR), 9.

Rybáček V., 1991. Hop production. Development in Crop Science, 16. Elsevier, Amsterdam and SZN, Prague, 286.

EXPERIENCE GATHERED WITH THE PRAGUE NATIONAL THEATRE PV SYSTEM

Martin Libra[*1], Valentýn Avramov[2], Vladislav Poulek[3]

[1] Czech University of Life Sciences Prague, Faculty of Engineering 16521 Prague 6, Czech Republic,
E-mail: libra@tf.czu.cz
[2] ENESA a.s., U Voborníků 852/10, 19000 Prague 9, Czech Republic
[3] Poulek Solar, s.r.o., Velvarská 9, 16000 Prague 6, Czech Republic

Abstract:
Photovoltaic system on the National Theatre roof has been installed in the years 2008-2009. Due to the location in the urban conservation area in the historical quarters of Prague flexible photovoltaic foils have been used. In the paper the photovoltaic system is described and results of its test are presented. They are compared with the results of the previous tests of the foil as obtained in the Czech University of Life Sciences, Prague.

Keywords: alfalfa hay, corn stover, biopellets, press, particle size distribution

Introduction

Photovoltaic (PV) system on the National Theatre roof has been installed in the years 2008-2009. It was a period of photovoltaic's boom due to the Czech Republic's subsidiary policy and a number of larger or smaller solar PV power plants were built. This boom culminated in the year 2010 when already nearly 2000 MW_p of photovoltaic power plants were installed in the Czech Republic and a strict change of legislation has been adopted.

At that time, in connection with the reconstruction of the Service Building and New Scene Building roofs and within the framework of the EPC project, the National Theatre's management decided on the design and installation of a PV system that exhibits certain specific features and is thus interesting from several points of view. With respect to its location in Prague historical area and national heritage protection it was inapt to use a classical construction with southward inclined PV panels based on crystalline silicon. It was very imperative to decide for a construction that would fully rest on the roof with its entire surface and would thus not interfere with the roof's contour in this precious locality. The flexible photovoltaic foils based on thin semiconductor layers have been therefore used that in maximum measure conform to the modern outlook of the buildings mentioned above.

Our many years' experience in the field of photovoltaics was already summarized in the book (Poulek, Libra, 2010) and the tests of other types of PV power plants have been described elsewhere (Poulek, Libra, 2009; Libra et al., 2011). In this paper we shall describe a PV system of a completely different construction mentioned above and discuss our results of two-years monitoring of its functioning.

Experimental Arrangement

PV system on the New Scene Building roof of Prague National Theatre (see Fig. 1) was designed so that it comprises two identical PV systems on the southern and northern halves of the roof. The only difference is given by the fact that the southern part was inclined by about 3° southward and the northern part by about 3° northward. Flexible PV foils of the nominal output power

Fig. 1 PV system on the National Theatre New Scene roof

Fig. 2 PV system on the National Theatre Service Building roof

0.406 kW_p have been used. PV cells based on thin semiconductor layers are encapsulated in plastic material, they are mutually interconnected, and are directly integrated into the common roof PVC foils. Waterproof connectors are located on their back side. In both parts of this PV system four PV foils were connected in series, eight of these series were connected in parallel and via a three-phase convertor Fronius IG 150 Plus the generated electric power was supplied to mains (network). On the National Theatre New Scene roof altogether 64 foils with an overall rated output of 26 kW_p (in two independent branches per 13 kW_p) have been installed. A certain difference in the generated electric power can be expected, because one branch is slightly inclined southward and the other northward.

PV system on the National Theatre Service Building (see Fig. 2) was designed in the form of four independent branches. Flexible PV foils on an identical basis have been used, however with a somewhat lower nominal output power 0.203 kW_p. In two of these branches always six PV foils have been connected in series, these four series have been connected in parallel and via a single-phase convertor Fronius IG 40 the generated electric power was supplied into mains (network). In the other two branches six PV foils were connected in series, five of these series were connected in parallel and via a single-phase convertor Fronius IG 60 the generated electric power was supplied into mains (network). Altogether 108 foils with the overall nominal output power 22 kW_p (in four separate branches of 2 x 4.9 kW_p and 2 x 6.1 kW_p) have been installed on the National Theatre Service Building. From Fig. 2 it is evident that part of this PV system is inclined about 3° eastward a part of the PV system is inclined about 3° westward to allow draining of water and self-cleaning of dust. Because this small inclination is orientated in the east-west direction, it can be expected that it will not manifest itself significantly on the total electric power production.

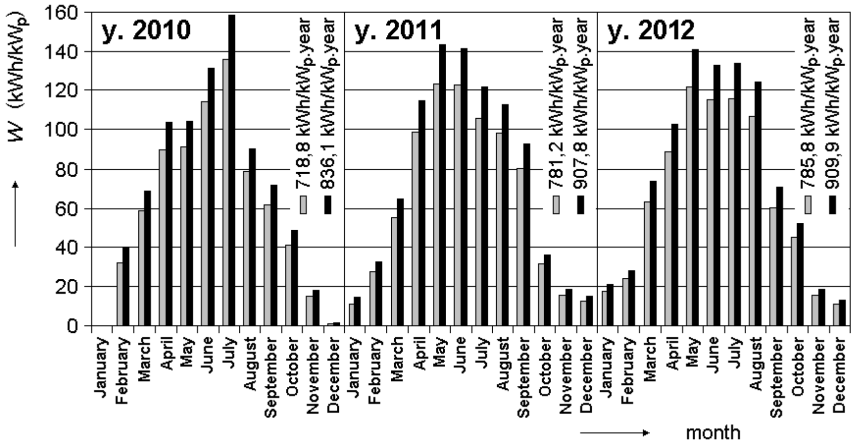

Fig. 3 Amount of electric power generated in the PV system on the National Theatre New Scene roof in the years 2010-2012

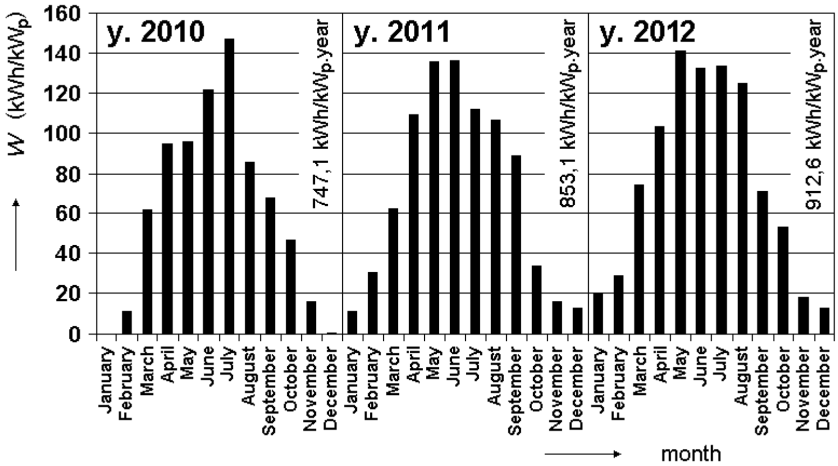

Fig. 4 Amount of electric power generated in the PV system on the National Theatre Service Building roof in the years 2010-2012

Fig. 5 Testing of the flexible PV foil in CULS Prague, Faculty of Engineering (measurements of the no load voltage)

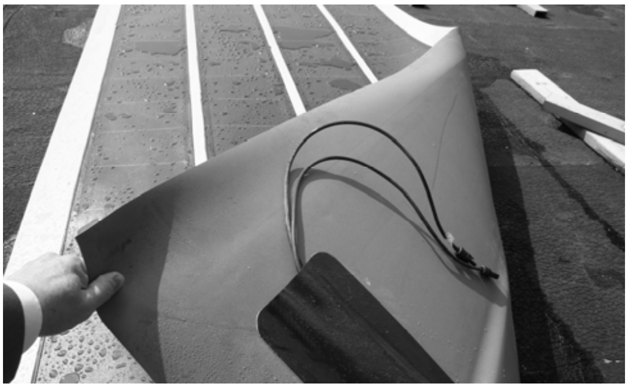

Fig. 6 Details of the waterproof connectors outlets from the flexible PV foil

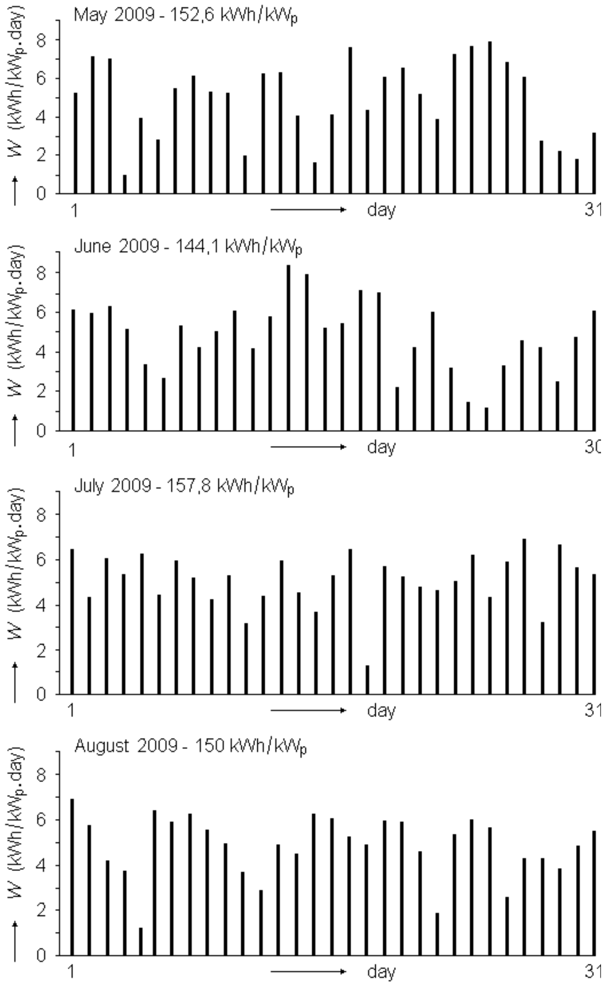

Fig. 7 Amounts of electric power generated in the flexible PV foil in the CULS Prague, Faculty of Engineering in the spring and summer months of the y. 2009

Results and Discussion

The results of three-year monitoring of the electric power production by the PV system described above are presented in the following diagrams. Fig. 3 presents the data from the PV system on the National Theatre New Scene roof,

Fig. 4 gives data from the PV system installed on the National Theatre Service Building roof. To make the results comparable the values are recalculated to 1 kW_p of installed output. It is evident that the year-round values correspond with the values expectable in Prague (50° north latitude) and that in winter months the amount of produced electric power is affected by the snow deposits on the roofs. Provided that snow would be regularly removed the amount of produced electric power will be somewhat higher, but this could not be proved. This is evident from the zero amount of produced electric power in January 2010 and from the minimum amount in December 2010. In 2011 there was nearly no snowfall in Prague.

From these diagrams (Fig. 3 and Fig. 4) it is also evident that on the New Scene Building there is always the amount of produced power higher in parts inclined southward in comparison with parts inclined northward. On the Service Building roof, inclined eastward and westward, the obtained values lay between the values from the New Scene Building. This fully complies with expectations. The PV panel area projection into the plane perpendicular to the Sun radiation is given by the incidence angle cosine ($S' = S_0 \cos\alpha$, where S_0 is the PV panel area and α is the incidence angle). The inclination of PV systems orientated northward and southward is approximately $\varphi = \pm 3°$. At a low Sun elevation of 20° at noon the incidence angle is 67° and 73°, respectively, and the difference in the panel area projection into the plane perpendicular to the Solar radiation amounts to about 33 %. At a high Sun elevation of 60° at noon the incidence angle is 27°and 33°, respectively and the difference of the panel area projection into the plane perpendicular to the Solar radiation amounts to about 6 %. Comparison of the results from the months in 2011 with a low Sun elevation, when the results were not distorted by snow deposits, reveals that the difference between the amount of produced electric energy was about 20 %, in January it was even 31 %. This difference is lower than the value of 33 % evaluated above as along to the direct Sun radiation a small part of power is also produced by the diffuse components, regardless of the incidence direction. In cloudy weather the difference between the produced electric power is negligible. On the other hand, in spring and summer months with high Sun elevation the difference between the amount of produced electric energy is about 15 %. This difference is higher than the value of 6 % evaluated above as the Sun is at high elevations only for few hours round noon and for majority of the day it is at lower elevations and it does not radiate precisely from south. However, the difference is lower than in the winter months.

Tests with a similar flexible PV foil were executed already in 2009 in the Czech University of Life Sciences Prague. Fig. 5 presents the no load voltage measurements and in Fig. 6 there is a detail of the waterproof connectors' outlets. The results of the produced power measurements in spring and summer months in the year 2009 are presented in Fig. 7. The results are also recalculated to 1 kW_p of installed nominal output power. Our PV foil had the nominal output power 0.5 kW_p and it was orientated practically horizontally on the roof of the Faculty of Engineering (the roof is slightly inclined by about 1° southward to allow water drainage). The values for individual months cannot be directly compared as they relate to months of another year but within the limits of differences between individual years the values comply. Fig. 8 presents examples of measurements of the instantaneous output power in dependence on the time during selected days in the year 2009. The amount of the produced electric energy is given by the area under the graph because the amount of the electric energy produced in the time period Δt is given by the equation $W = \int_{\Delta t} P \,\mathrm{d}t$, where P is the instantaneous output power and t is the time.

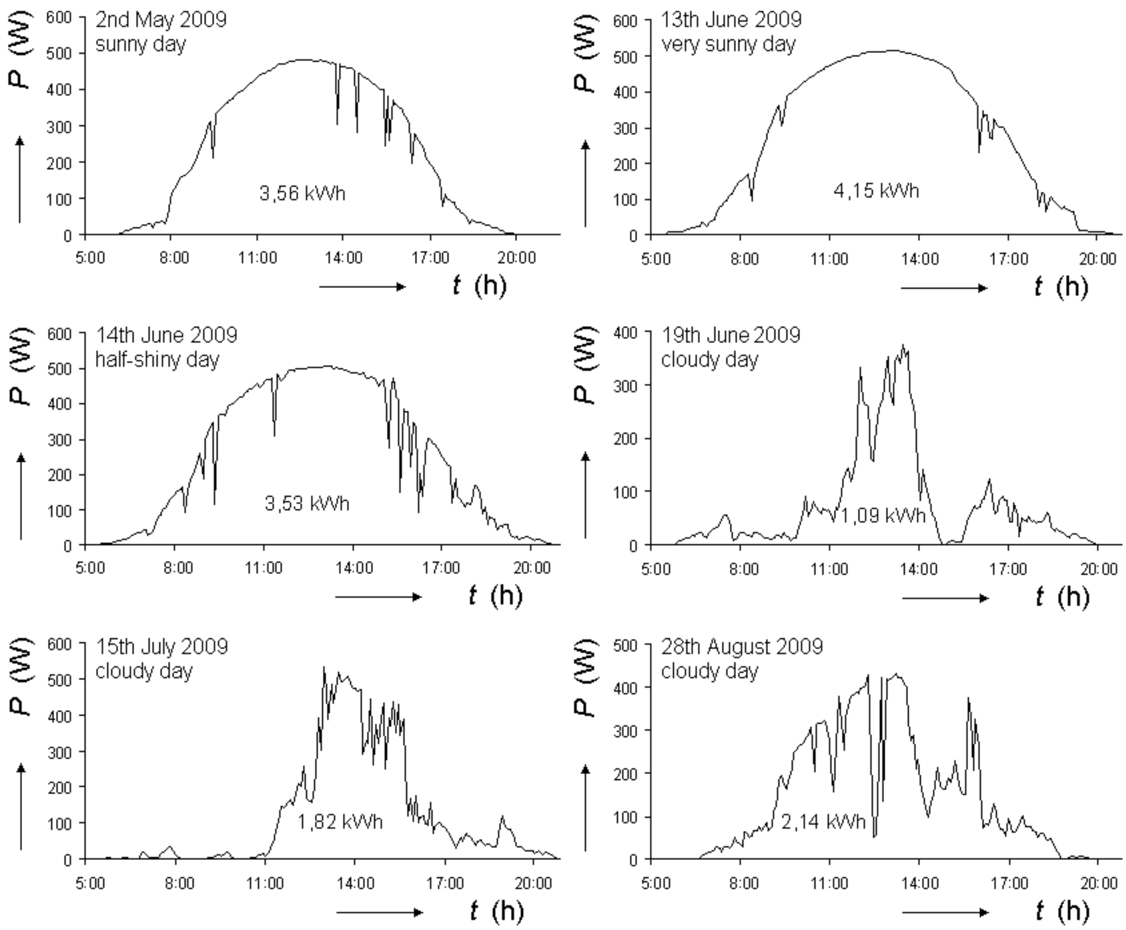

Fig. 8 Examples of the dependence of the instantaneous output measurements on time during selected days of the y. 2009 in the CULS Prague, Faculty of Engineering

Conclusions

We consider the reconstruction of the National Theatre roof with the incorporated PV system a suitable solution as the theatre management behaves thus ecologically ("green" solution) and, regardless of the fact that the PV system described above cannot by far cover the whole power consumption of the theatre, the roof is purposefully used. The PV system construction on the basis of flexible PV foils was the only acceptable alternative with respect to the Prague historical centre conservation requirements. The construction of flexible PV foils on other bases is dealt with in detail elsewhere (Tanenbaum et al., 2012; Larsen-Olsen et al., 2012).

Our tests proved that the PV system works so far perfectly and the amount of electric energy produced complies with the expectations. We intend to continue in the collection of data and it will be certainly interesting to observe how the measured values will change in connection with the whole construction ageing. These data will be of interest also for designers of other roof PV systems. We believe that in the nearest future it will be just the roof PV systems that will be of the highest importance as supplementary power sources.

References

Poulek V., Libra M., 2010. Photovoltaics. Prague: ILSA, 169.

Poulek V., Libra M., Novotný R., Mareš J., 2009. Testing of a photovoltaic system with a fixed stand in CULS. Prague, Elektro, 19, 7: 20-21.

Libra M., Beránek V., Sedláček P., Mareš J., Poulek V., Bican P., Korostenský T., 2011. Comparison of photovoltaic power plants of various design and location in the Czech Republic). Jemná mechanika a optika, 56 (5): 156-159.

Tanenbaum D.M., Dam H.F., Jørgensen R.R.M., Hoppe H., Krebs F.C., 2012. Edge sealing for low cost stability enhancement of roll-to-roll processed flexible polymer solar cell modules. Solar Energy Materials & Solar Cells, 97: 157–163.

Larsen-Olsen T.T., Andersen T.R., Andreasen B., Bőttiger A.P.L., Bundgaard E., Norrman K., Andreasen J.W., Jørgensen R.R.M., Krebs F.C., 2012. Roll-to-roll processed polymer tandem solar cells partially processed from water. Solar Energy Materials & Solar Cells, 97: 43–49.

CHANGING THE MOISTURE CONTENT OF THE TOPINAMBOUR, VIRGINIA MALLOW AND POLYGONACEOUS SHOOTS DURING STORAGE IN NATURAL CONDITIONS

Aleksander Lisowski*, Jacek Klonowski, Michał Sypuła, Jarosław Chlebowski, Krzysztof Kostyra, Tomasz Nowakowski, Adam Strużyk, Jan Kamiński, Małgorzata Powałka

Warsaw University of Life Sciences – SGGW, 02-787 Warsaw, Nowoursynowska 166, Poland, Phone: +4822-5934538, Fax: +4822-5934514, E-mail: aleksander_lisowski@sggw.pl

Abstract

The aim of this study was to determine the characteristics of the distribution of energy plant moisture content along the height of their shoots and the dynamics of moisture during storage in natural conditions. The shoots of topinambour, Virginia mallow and polygonaceous were used in the study. Entire shoots were cut into sections of 0.10 m and for each set moisture content was evaluated for six months in monthly cycles. The characteristics of moisture content distribution of energy plants along their height of shoots and the dynamics of changes in moisture content during a six-month storage in natural conditions differed significantly and depended on plant species. After a month's storage of freshly cut shoots the biggest decrease of content moisture in the shoots was recorded for topinambour and Virginia mallow , by 44 % and 37 % respectively, and the lowest in polygonaceous shoots (23 %). After six months of shoot storage the lowest moisture content (9 %) was reached in Virginia mallow, and for polygonaceous and topinambour it was recorded as 12 % and 14 % respectively. The dynamics of changes in the moisture of the plants during a 6-month storage in natural conditions under a roof were described by regression equations in the power function.

Keywords: topinambour, Virginia mallow, polygonaceous, moisture content, natural drying

Introduction

While harvesting energy plants with woody biomass: Sprint and Wodtur one-year willow and rose multiflora; semi-woody: Jerusalem artichokes, Virginia mallow, Japanese knotweed and Sakhalin knotweed, Silphium Perfoliatum; strawy: spartina prairie, sugar miscanthus, Chinese miscanthus, giant miscanthus at two periods, it was found that during harvest in November, moisture of semi-woody and strawy species ranged from 39.4 % for sugar miscanthus to 66 % for the Jerusalem artichoke, and in March from 16 % for sugar miscanthus to 26.2 % for prairie spartina. In both harvest periods willow and rose multiflora had a similar moisture content, 54.1 % and 49.8 %, respectively (Stolarski et al., 2008). The storage of willow was much more effective, because shoots harvested in November and stored without roofing reduced their moisture content to 50 %, and under roofing to 43%. Thereafter, the dynamics of plants drying changed and at the turn of June and July moisture content of plants was similar (22–23 %), regardless of the storage method.

The shoots of plants harvested at high moisture and chopped immediately after harvest create a problem in storage due to biological processes resulting in a decrease of the energy properties of biomass (Gigler et al., 1999; Nixon, Bullard, 2003; Clifton-Brown et al., 2004; Adler et al., 2006; Hayes, Hayes, 2009; Sevel et al., 2012).

Based on the available literature it can be said that we have very little information about changes in moisture content of energy plant shoots stored whole in natural conditions and how in these conditions the moisture content changes along the height of shoots, which affects the loads dynamics of working units of machines used to harvest and process biomass. The distribution of changes in moisture content along the height of shoots was pointed out by Igathinathane et al. (2006) in relation to maize plants, variety 743 DeKalb during their growing season. Prior to a harvest of silage maize, a sharp drop in the moisture occurs, especially in the lower region of the stem, followed by its stabilization and a fairly good alignment along the height of the stem. This coincides with a period of about 122 days after sowing, when the maize reaches the best maturity to harvest for silage. However, this depends on climatic conditions and maize varieties because our experience (Lisowski et al., 2010) shows that the harvest of Inagua variety at 127 days after sowing was slightly too early.

In previous studies (Lisowski et al., 2013) it was found that after a month's storage of freshly cut shoots the biggest decrease of content moisture in the shoots of spartina and miscanthus was recorded, by 31 % and 22 % respectively, and the lowest in willow shoots (12 %). After six months of storage of plant shoots the giant miscanthus shoots reached the lowest moisture content (10 %–12 %) and their moisture content was the most equalized along the height, which indicates that water is internally redistributed. The most uneven moisture content along the height was found in spartina shoots while the smallest drop in moisture content was found in willow shoots, and their final moisture content was 16 % and 23 % respectively.

The aim of this investigation is to explain the dynamics of moisture change of the topinambour, Virginia mallow and polygonaceous along their shoots during a six months storage in natural conditions.

Material and methods

The investigation was conducted for plant shoots of topinambour, Virginia mallow and polygonaceous. The material was harvested from plots at the Experimental Station in Skierniewice, which belongs to Warsaw University of Life Sciences. The harvest of plants was held on 13 October 2011 using hand secateurs and a petrol brush cutter. Plants were cut at a height of about 0.05 ± 0.03 m from the ground. After cutting, the plants were gathered in separate bundles of 30 shoots for each species. Shoots were arranged in a shed on wooden pallets in a horizontal position so as not to put them directly on the floor. The gap of 0.07 m between the ground and the upper surface of the pallet allowed for air circulation and natural drying.

The first measurement of moisture took place a day after the cut, and next measurements at regular monthly intervals for six months. Plants were cut into sections of 0.100 ±0.002 m along the shoot, then each section was cut and divided into three averaged samples and placed in measurement containers.

Moisture was determined by the dried-weight method according to the standard S358.2 ASABE (2011). For this purpose, three averaged samples of material from each section of the plant were weighed on the scales RADWAG WPS 600/C with an accuracy of 0.01 g and then dried to constant weight at 103 ± 2° C using a laboratory dryer SLW 115 for 24 hours. Because in each measuring monthly cycle approximately 270 samples were prepared, weighing of the moist material was carried out on one day and the drying of the whole lot of material of one cycle took about a week.

Plant shoot lengths were varied and ranged for Virginia mallow from 1.94 ±0.12 m, topinambour from 2.55 ± 0.8 m and polygonaceous from 2.89 ± 0.10 m. In order to compare the characteristics of the moisture change along such diverse shoot heights a normalized ratio was calculated, which is the relative height, expressed as a percentage. In this way, each plant shoot was divided into 21 parts, in increments of 5%. A statistical analysis was performed using a standard statistical package Statistica v.10.

Results and discussion

The results of statistical analysis (Tab. 1) indicate a statistical significance of the impact of the main factors: relative height of the shoot section, plant species and time of measurement of the moisture content of material, because the critical level of significance is lower than 0.0001. All double interactions and triple interaction also proved to be statistically significant.

Tab. 1 Results of variance analysis of moisture content in shoots of topinambour, Virginia mallow and polygonaceous for the main factors: relative height of the shoot section, plant species, time of measurement (period)

Source	Sum of squares	Degree of freedom	Mean square	F-ratio	p-value
Ratio	9724.7	12	810.4	256.82	<0.0001
Species	12012.1	1	12012.1	3806.78	<0.0001
Period	335345.9	2	167673.0	53137.47	<0.0001
Ratio×species	12111.0	32	378.5	119.94	<0.0001
Ratio×period	15008.1	108	139.0	44.04	<0.0001
Species×period	16386.2	8	2048.3	649.12	<0.0001
Ratio×species×period	15859.4	228	69.6	22.04	<0.0001
Residual	3635.1	1152	3.2		

A detailed statistical analysis was performed by using Duncan's test at a critical significance level $\alpha = 0.05$, an error between the groups of 3.15 and the number of degrees of freedom of 1152. It was found that the differences in the moisture of plant shoots along their length do not allow to establish homogeneous groups. For separate 21 relative sections 12 homogeneous groups were obtained. An average moisture content of polygonaceous was the highest (30.4 %), and although the average moisture content of topinambour and Virginia mallow shoots was similar and amounted to 22.6 % and 23.1 % respectively, all three plant species created their own homogeneous groups. Material moisture of energy plants were varied from period to period so significantly that for each of these periods homogeneous groups were separated.

During the harvest the largest and the most uneven moisture along the shoots was found in polygonaceous 77.0–60.8 % (Fig. 1). The moisture of topinambour shoots was in the range of 61.6–68.8 % and was higher at the top, due to a large share of leaves, and the moisture of Virginia mallow was the smallest and the most even (53.1–59.5 %).

After a month's storage of shoots in natural conditions the biggest difference in moisture content occurred in topinambour (43.7 %), followed by Virginia mallow (37.1 %) and the lowest in polygonaceous (23.0 %). The leaves of polygonaceous dried out very quickly, so the dynamics of a decrease of moisture content in the second half of the height shoot was significantly greater than in the lower part, which is built of thick stems of annular cross-section. Characteristics of moisture changes of polygonaceous shoots continued until the fourth month. In the fifth month of storage the characteristics of moisture of plant shoots practically overlapped.

In almost all cases, a characteristic feature of changes in moisture of the plant material was its lower value at the side of the shoot cut. This is logical, since a large cross-sectional area of the stem permitted the movement of water along the conductive tubes of plant tissues. This is particularly well visible in the polygonaceous shoots, for which in subsequent measurements, between the first and the fourth month, the moisture peak shifted accordingly from 10 % to 35 % of the height and amounted to 63.0 % and 27.1 % respectively (Fig. 1).

In subsequent monthly measurement cycles, it was found that the moisture content of plant shoots changed less intensively, especially for topinambour and Virginia mallow.

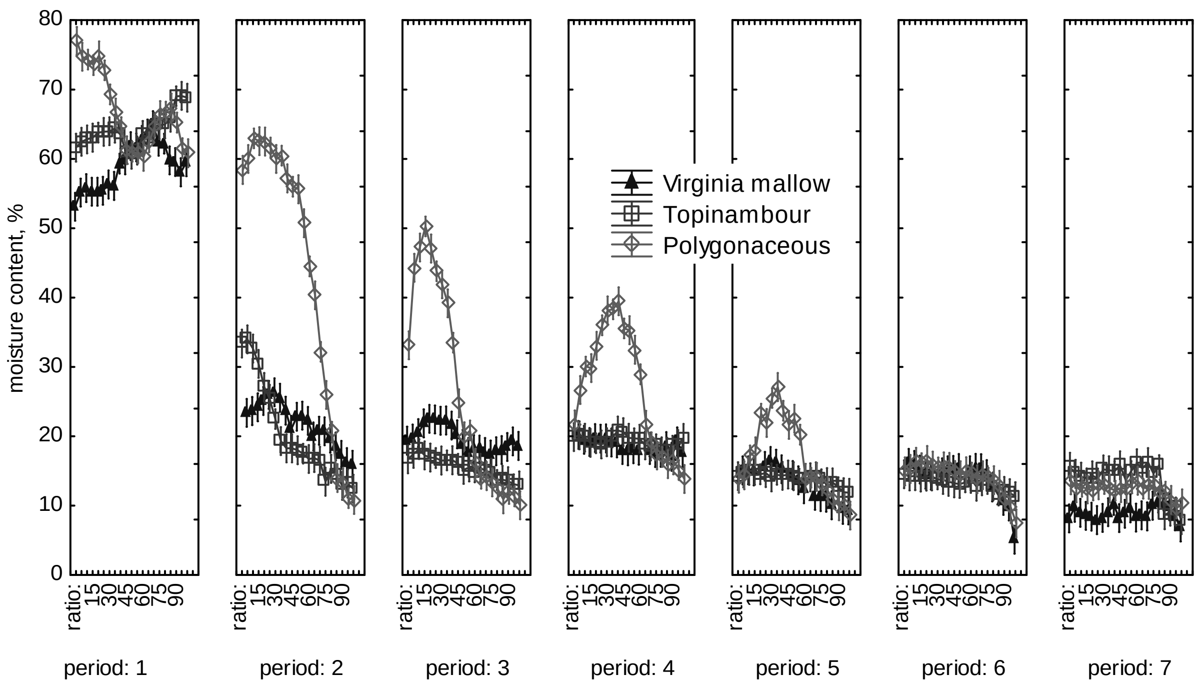

Fig. 1 Characteristics of moisture distribution along the relative height (ratio) of topinambour and Virginia mallow and polygonaceous shoots and the dynamics of changes in their moisture during a six-month storage in natural conditions

After six months of storage Virginia mallow shoots had the lowest moisture content (8.5–9.3 %), and topinambour shoots preserved the highest moisture content (13.4–14.2 %, Fig. 1). Moisture of polygonaceous shoots was 11.9–12.7 % and for this plant the biggest drop in moisture was recorded by an average of 54.7 % (percentage points). The decreases of moisture for Virginia mallow and topinambour were similar and amounted to 50.0% and 50.3 % respectively. In previous studies (Lisowski et al., 2013) after six months of storage miscanthus had a similar moisture (10–12%), whereas spartina shoots had about 16 % and woody willow stems up to 23 %. Frączek and Mudryk (2006, 2008) found that after spring storing willow shoots for 3–4 months their moisture content decreased to 22–23 %, irrespective of the harvest period, which in the studies was conducted in autumn and spring. For this reason, the harvest period should be based on other factors, especially weather and soil conditions of the plantation. These study findings from literature concern moisture content changes during storage, but without a detailed analysis of its distribution along the height of the energy plant shoots.

Based on the results of an analysis of variance a test was conducted to develop empirical models for the dynamics of moisture change of each plant species. By examining power and exponential functions it was found that the changes dynamics of moisture content during the six months of storing plants are best represented by the exponential functions given in Fig. 2, for which the coefficients of determination are the biggest, and for the equations of moisture content of the three plant shoots are in the range of 86.1–93.7 %. Similar considerations were assumed by Lisowski et al. (2013) for miscanthus and spartina and willow and by Gigler et al. (2000) for natural drying of willow shoots. The final moisture content of plant materials stored for six months was close to equilibrium moisture content. Diffusion of moisture inside the shoots is a long-term process, which is governed by the relation of air humidity and ambient temperature, but it can be recommended that a time of natural drying of topinambour and Virginia mallow and polygonaceous may be shortened to five months.

The estimated empirical models can be used to predict changes in moisture content for these plants stored under roofing. The decrease in the dynamics of moisture changes along the shoots of energy crops can be a factor in reducing the dynamics of changes in load working units of machines used to harvest and convert the material for energy purposes.

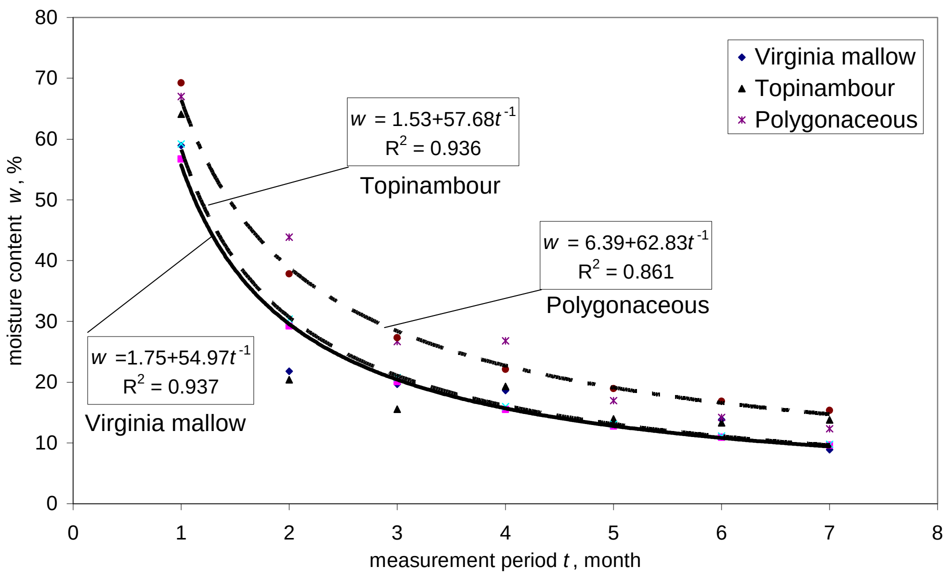

Fig. 2 Empirical models and average real values of dynamics of changes in moisture content of shoots of topinambour, Virginia mallow and polygonaceous during a six month storage

Conclusions

1. Characteristics of moisture content distribution of topinambour, Virginia mallow and polygonaceous along their height of shoots and the dynamics of changes in moisture content during a six-month storage in natural conditions differed significantly and depended on plant species and length of period storage.
2. After a month's storage of freshly cut shoots the biggest decrease in the moisture content of shoots was recorded for topinambour and Virginia mallow, by 44 % and 37 %, respectively and the lowest for shoots of polygonaceous (23 %).
3. After six months of storage Virginia mallow, polygonaceous and topinambour shoots reached moisture content, by 8.9 %, 12.3 % and 13.8 %, respectively, with a standard deviation of 0.2 %. The biggest difference in the reduction of moisture content was found for polygonaceous shoots 54.7 %, and for Virginia mallow and topinambour the differences were similar and amounted to 50.0 % and 50.3 % respectively.
4. The dynamics of moisture changes during the six-month storage of topinambour, Virginia mallow and polygonaceous shoots in natural conditions under roofing is described by the regression equations of power function. Empirical models can be used to predict changes in moisture content of these plants in experimental conditions.

References

Adler P.A., Sanderson M.A., Boateng A.A., Weimer P.J., Jung H.G., 2006. Biomass yield and biofuel quality of switchgrass harvested in fall and spring. Agron. J. 98: 1518–25.

ASABE Standards, 2011. Moisture measurement – forages ASABE S358.2 (R2008). In: ASABE Standards 2011, ASABE, St. Joseph, MI, USA, 780–781.

Clifton-Brown J.C., Stampfl P.F., Jones M.B., 2004. Miscanthus biomass production for energy in Europe and its potential contribution to decreasing fossil fuel carbon emissions. Glob. Chang. Biol., 10: 509–518.

Frączek J., Mudryk K., 2008. Changes in willow shoots moisture content of Salix Viminalis L. during seasoning. Agric. Eng., 10: 55–61. (in Polish)

Frączek J., Mudryk K., 2006. Measurement of moisture content of shoots and energy willow chips Agric. Eng., 12: 137–144. (in Polish)

Gigler J.K., Meerdink G., Hendrix E.M.T., 1999. Willow supply strategies to energy plants. Biomass Bioenerg., 17: 185–198.

Gigler J.K., Van Loon W.K.P., Van den Berg J.V., Sonneveld C., Meerdink G., 2000. Natural wind drying of willow stems. Biomass Bioenerg., 19: 153–163.

Hayes D.J., Hayes M.H.B., 2009. The role that lignocellulosic feedstocks and various biorefining technologies can play in meeting Ireland's biofuel targets. Biofuels Bioprod. Biorefin., 3: 500–520.

Igathinathane C., Womac A.R., Skohansanj S., Pordesimo L.O., 2006. Mass and moisture distribution in aboveground components of standing corn plants. T. ASABE 49: 97–106.

Lisowski A., Chlebowski J., Klonowski J., Nowakowski T., Strużyk A., Sypuła M., 2010. Energy plant harvesting technologies. Warsaw: WULS Press. (in Polish)

Lisowski A., Ciechacki A., Sypuła M., Klonowski J., Chlebowski J., Kostyra K., Nowakowski T., Strużyk A., Kamiński J., Powałka M., 2013. Changing the moisture content of the spartina and miscanthus and willow shoots during storage in natural conditions. Journal of Agricultural Science and Technology, 10. (in print)

Nixon P., Bullard M., 2003. Optimisation of miscanthus harvesting and storage strategies. Final report for DTI New and Renewable Energy Programme, 1–25.

Sevel L., Nord-Larsenb T., Raulund-Rasmussen K., 2012. Biomass production of four willow clones grown as short rotation coppice on two soil types in Denmark. Biomass Bioenerg., 46: 664–672.

Stolarski M., Szczukowski S., Tworkowski J., 2008. Biofuels from perennial energy crops. Energ., 51: 77–80. (in Polish)

ADDITIONAL FILTRATION OF UNIVERSAL OILS FOR ECOLOGICAL AND RELIABLE OPERATION OF AGRICULTURAL TRACTORS

Radoslav Majdan[1*], Zdenko Tkac[1], Jozef Chrastina[1], Rudolf Abraham[1], Milena Kurekova[2], Radoslav Paulenka[2]

[1] Slovak University of Agriculture in Nitra, Faculty of Engineering, Department of Transport and Handling, Tr. A. Hlinku 2, 949 76 Nitra, Slovak Republic
Phone: 00421 904 198 433, E-mail: radoslav.majdan@gmail.com
[2] Intertribodia Ltd., Francuzka 9, 935 21 Tlmace, Slovak Republic

Abstract

The agricultural tractors use the high volume of universal oils designed for hydraulic and transmission systems. These oils provide variety functions where the high cleanliness level is very important. This contribution presents the design and test operation of additional filtration to increase cleanliness level of universal oils. The excessively contaminated oil has to be change even though there was not reached the oil change interval. Such oil fill operation is fairly uneconomical mainly in case of high quality oils which are often used in agricultural machines on the present. The low contamination level of oil eliminates wear and creates conditions for reliable operation of tractor. Similarly, ecological oils require high cleanliness level because the contamination effects acceleration of degradation processes. The additional filtration was designed for external hydraulic circuit of tractor to clean oil continuously during the tractor operation. We realized the test operation of additional filtration by using a tractor type John Deere 8100 and an oil type Shell Donax DT. The test operation was evaluated on the basis of chemical elements concentration which represents contamination. The technical condition of oil was evaluated on the basis of kinematic viscosity, total acid number and chemical elements concentration which represents additives. The decrease of additive concentration reached only medium level (6.6 %) as well as physical and chemical parameters didn't overreach limits. During the test operation of tractor the concentration decrease of contamination chemical elements reached the values 25.53 % (Fe), 23.53 % (Si), 25 % (Al) and 5.5 % (Cu). The results of test operation mention import of additional filtration and suitability for using in agricultural tractors.

Key words: oil contamination, additives, biodegradable oil, spectroscopy, environmental protection

Introduction

Oils that are used in common transmission and hydraulic systems of tractors are exposed to specific conditions characteristic for agricultural production. These oils must perform all requires functions in the transmission and hydraulic system of tractor and they also must be resistant to oxidation and thermal degradation. Agricultural tractors often operate in dusty and humid environment which effects oil fill contamination. In addition, the oil fills are polluted by the amount of wear particles mainly from the transmission system, which carries the full power of the engine to the wheels of the tractor. Papers (Mihalčová, Dobránsky, 2008; Tóth et al., 2012; Tulík et al., 2013) dealt in detail with the oil fill contamination. Pollution causes a variety of adverse effects such as accelerated wear, corrosion of steel surfaces, oxidation of the oil and changes its physical and chemical properties. The pollution very harmfully affects manly on ecological fluid because accelerates the degradation processes.

The environmental protection forced the users and producers of a mobile technology to fulfill challenging requirements imposed on ecological hydraulic systems, which come into the contact with the environment (Drabant et al., 2010). There are required the use of ecological lubricants, especially in conditions of agricultural production. Tractors involve several hundred liters of various types of petroleum products, that causing contamination of soil and water by release into the environment. Alternative to petroleum oils are ecological liquids which present no risk to the environment. At present, ecological oils are commercially available and there are also suitable for use in the tractors. The test results of such oils were published in the contributions (Hujo et al., 2012; Janoško et al., 2004; Kučera, Rousek, 2008). Ecological oils are sensitive to contamination, such as metal wear particles, water or dirt from the environment. Therefore, the concept of additional filtration to raise cleanliness of tractor transmission and hydraulic oil fill was designed in Department of transport and handling.

Material and methods

The additional filtration of tractor transmission and hydraulic oils was designed as the second stage of filtration on the tractor. Tractor manufacturer standardly mounts filters of first stage filtration. These have filter ability 15 micron to 20 micron depending on the tractor type. The filtration device type FT-B68 (Filtration technology s.r.o, Czech Republic) with filter element made from pulp was used for additional filtration, Fig. 1. The filter ability of filter element is 1 micron and it is able to absorb 0.5 dm^3 of water, in contrast to the standard mounted filters. The maximum value of oil flow is 1.8 dm^3/min.

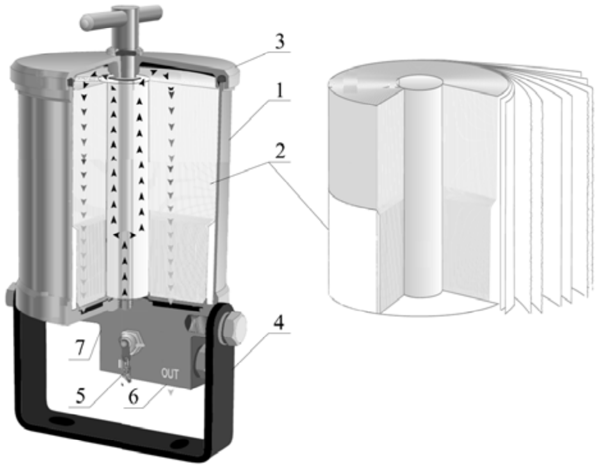

Fig. 1 Construction of filtration device which was used to additional filtration: 1 – filter housing, 2 – filter element, 3 – cover, 4 – console, 5 – oil inlet, 6 – oil outlet

Tractor worked 1,850 engine hours since the last oil change before installing additional filtration. This value corresponds to a total number of 12,693 tractor engine hours. External filter device was mounted on a tractor after completing 1,850 engine hours thus shortly before the prescribed oil change (2,000 engine hours). Operating of tractor fitted with an additional filtration took time 150 engine hours. During this time, the function of filtration was verified in the operating conditions of tractor. Function of filtration system has been evaluated on the basis of a content of chemical elements representing contamination of the oil. We used terminal of type mini-mess to sampling. Oil samples were taken before installing the filter and after completing 150 engine hours. There was collected representative sample of new oil before filling the transmission and hydraulic oil tractor. Oil samples were evaluated by ICP spectrometry (ASTM D 5185-05) at an accredited laboratory Wearcheck (Almásfüzitő, Hungary).

Decrease of chemical elements representing oil contamination is calculated on the basis of data of contaminated oil and after operating the tractor with filter. Decrease of chemical elements representing the oil contamination is calculated according to the formula:

$$\Delta_Z = \frac{Z_U - Z_F}{Z_U}.100\,,\% \qquad (1)$$

Where: Δ_Z – decrease in the concentration of chemical elements representing oil contamination, %

Z_U – concentration of chemical elements representing contamination before the filtration, mg/kg

Z_F – concentration of chemical elements representing contamination after the filtration, mg/kg

Additives concentration was monitored on the basis of content of the chemical elements (Ca, P and Zn) in the oil. Decrease in the content of these elements in a sample of oil is calculated using the following formula:

$$\Delta_A = \frac{A_N - A_U}{A_N}.100\,,\% \qquad (2)$$

Where: Δ_A – decrease in the content of chemical elements representing the additives, %

A_N – content of chemical elements representing the additives in the new oil, mg/kg

A_U – content of additives at the time of the oil change after 2,000 engine hours, mg/kg

In the tractor a fluid type Shell Donax DT was used during the test operation of additional filtration. This fluid is a high performance heavy-duty mineral oil-base transmission fluid suitable for use in combined transmission, hydraulic and wet-brake systems. Due to its low temperature properties it provides prompt and smooth operation of all hydraulic components during cold start-up conditions. Donax TD reduces wear and prevents corrosion, even if some water or moisture has entered the systems, while maintaining internal cleanliness. This type of universal tractor transmission oils (UTTO) was designed for use in transmissions, hydraulic systems, oil immersed brakes and other ancillary systems fitted mainly to agricultural tractors. Tab. 1 shows typical characteristics of fluid type Shell Donax DT.

Whilst production conforms to Shell's specification, variations in these characteristics may occur.

Tab. 1 Typical characteristics of fluid Shell Donax DT

Parameter	**Unite**	**Value**
SAE viscosity grade	-	5W - 30
API performance level	-	GL-4
Viscosity index	-	156
Kinematic viscosity at 40 °C	mm^2/s	55.4
Kinematic viscosity at 100 °C	mm^2/s	9.5
Density at 15 °C	kg/m^3	882
Flash point	°C	205
Pour point	°C	-39

Results and discussion

The scheme of designed additional filtration is shown in Fig. 2. The filtration device is connected to the external hydraulic circuit of tractor through hoses (4) and the quick couplings (9 and 10). Sockets terminate quick couplings which does not block the hydraulic circuit only for additional filtration. The filter housing (8) is sized for maximum flow rate 1.8 dm^3. min^{-1}, and therefore this filtering method is suitable only for tractors which allow to regulate the flow rate in external hydraulic circuit. The filtration device is placed in an area of the tractor three-point hitch so that it is easily accessible for replacement filter elements. Filtration is put into operation after the engine is started by setting the required flow of hydraulic oil. Filtering can also be operated at flow of hydraulic fluid through implements, because the filter is set up for maximum pressure of 30 MPa. Function of external hydraulic circuit is not limited by filtration because filtration system takes away only a small oil flow.

The designed filtration system is suitable for tractors which allow setting the flow rate in external hydraulic circuit. A tractor must be equipped with variable displacement hydraulic pump or throttle-valve which allows setting the specified flow rate through filter device (< 1.8 dm^3/min). The higher flow rate doesn't influences on a function of the filtration but uselessly loads the hydraulic system of tractor.

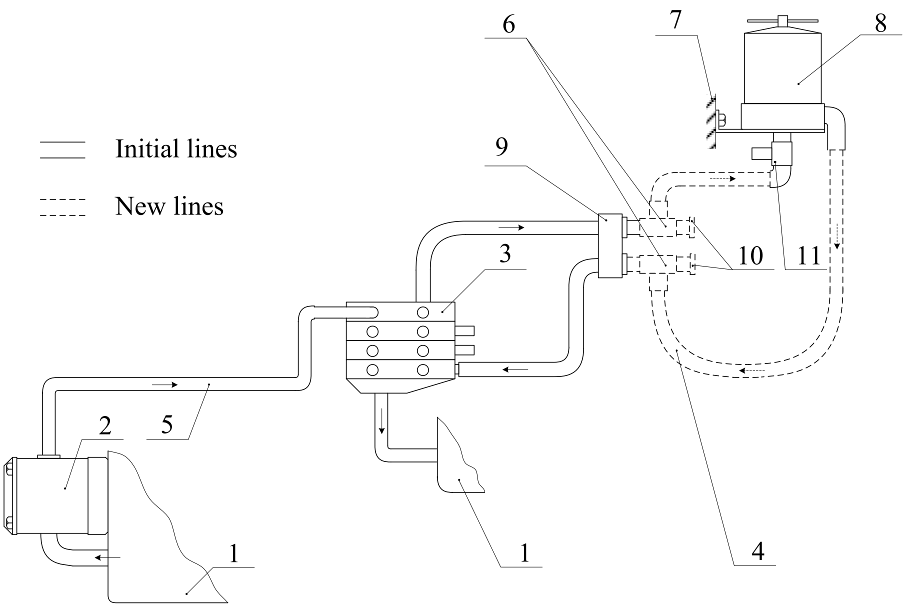

Fig. 2 Schematic diagram of additional filtration:
1 – tractor gearbox, 2 – hydraulic pump, 3 – hydraulic valve, 4 –hose, 5 – tube, 6 – T-tube, 7 – tractor frame, 8 – filtration device type FT-B68, 9, 10 – quick couplings of external hydraulic circuit of tractor 11 – terminal (minimess type) to sample fluids

The connection of additional filtration in tractor is shown in Fig. 3.

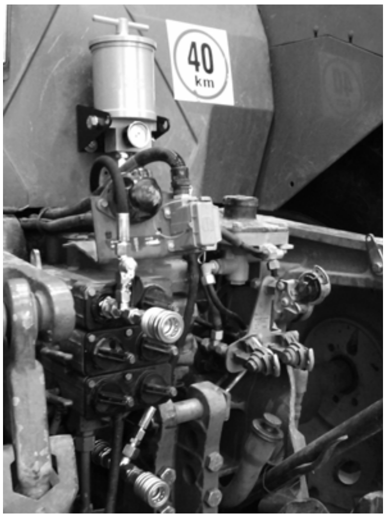

Fig. 3 Additional filtration system and its mounted on big tractors

Test operation of additional filtration was realized by using the tractor type John Derry 8100. This tractor has a variable displacement hydraulic pump. Therefore, it allows mounting the filtration device to the external hydraulic circuit. This hydraulic pump allows setting the minimal flow rate (0,5 $dm^3 . min^{-1}$) through the filter system.

Fig. 4 shows the concentrations of chemical elements such as silicon, aluminum, chromium, copper, iron, molybdenum and nickel, which represent fluid contamination. In Fig. 4 is possible to see an increase in contamination after completing 1,850 engine hours compared with new oil. This pollution originates in the normal operation of the tractor. We can observe the decrease in the concentration of chemical elements (representing the oil pollution) after mounting of additional filtration. For comparison, here are the values of the new oil.

Decrease of concentration of chemical elements representing oil contamination (Tab. 2) was calculated according to formula (1). Also, it was calculated on the basis of data before and after filtration. In the case of the most dangerous elements such as iron and silicon its decrease reached 25.53 % (Fe) and 23.53 % (Si).

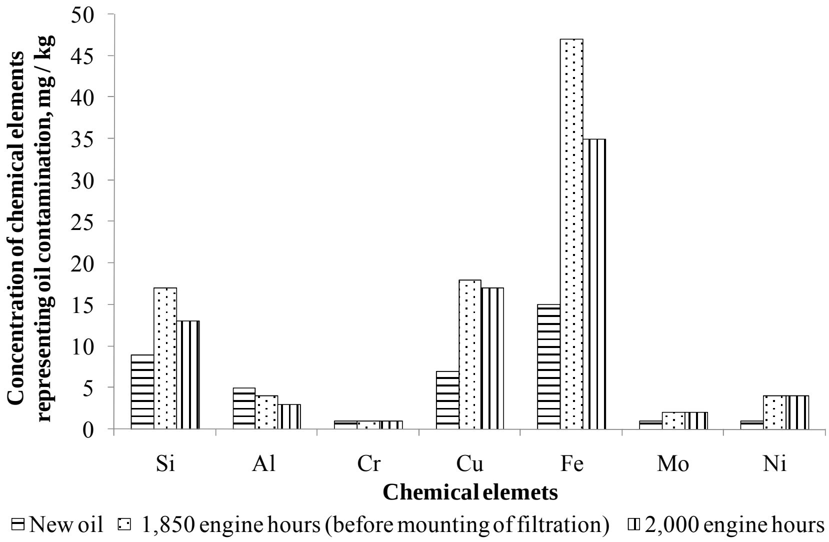

Fig. 4 Concentration of chemical elements representing the oil contamination

Tab. 2 Decrease in the concentration of chemical elements representing oil contamination

Chemical element	**Unit**	**Tractor operation, Engine hours**		**Δ_Z, %**
		1,850 (before filtration)	2,000 (after filtration)	
Fe	mg/kg	47	35	25.53
Cu		18	17	5.55
Si		17	13	23.53
Al		4	3	25.00
Ni		4	4	0
Mo		2	2	0
Cr		1	1	0

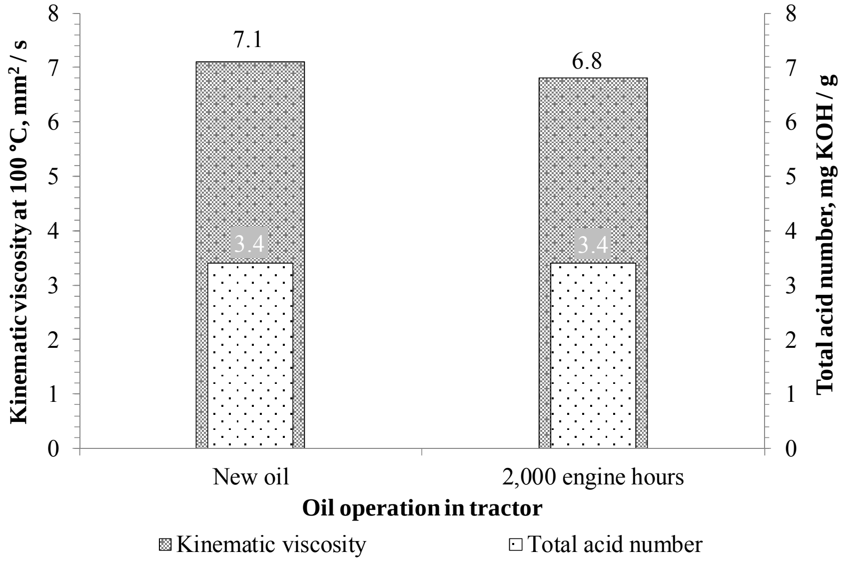

Fig. 5 Kinematic viscosity and total acid number of oil during the tractor operation

Tab. 3 Decrease in the concentration of chemical elements representing the additive

Chemical elements	**Unit**	**Tractor operation, engine hours**		**Δ_Z, %**
		0 (new oil)	2,000 (after filtration)	
Ca	mg/kg	3,593	3,398	5.42
P		1,314	1,287	2.05
Zn		1,647	1,539	6.55

The kinematic viscosity is one of the parameters which characterize the lubricating ability of oil and therefore it can be used to evaluate technical state of oil fill. During the oil fill operation the kinematic viscosity can decrease or increase. Limit value for kinematic viscosity is ± 10 % of new oil. The next parameter for determination of technical state of oil is the acid number which states the concentration of acid components in oil. The concentration of acid components increases when the oil degrades. Fig. 5 shows the kinematic viscosity and total acid number during the operation of tractor John Deere 8100 which was mentioned above. Both parameters were used to determine the oil technical state. The kinematic viscosity didn't overreach the limit value and acid number didn't change after the 2,000 engine hours (before oil fill change). Therefore, the main problem of oil fill in tractor John Derre 8100 is the contamination while the kinematic viscosity and acid number didn't overreach limit values.

Tab. 3 shows a decrease in the concentration of additives, which is calculated according to formula (2). The largest decrease was recorded at zinc 6.55 %. This value represents minimum decrease from view of oil operation in tractor during the exchange interval 2,000 engine hours.

Conclusion

The designed additional filtration of tractor universal oils take away contaminated oil from the external hydraulic circuit of tractor. The tractor owner can use different types of filtration devices from various manufacturers on the basis of chosen parameters of filtration. Filtration device is placed at the rear of the tractor above three-point hitch for easy installation and easy access. Oil is supplied into the filtration device through the hoses which are connected to the external hydraulic circuit of tractor through the quick coupling. Oil flow through the filtration device is provided turning on the given hydraulic circuit by the tractor operator. The designed filtration method is characterized by simple connection through the quick couplings, a high level of filtration, and continuous mode of operation. It removes contamination from the oil charge, which is not normally removed by the standard tractor filters. During the test operation of tractor (150 engine hours), there was a concentration decrease of iron at 25.53 %, silicon at 23.53 % and copper at 5.55 % in oil.

The use of ecological fluids requires a high cleanliness level of the oil fill and undetectable water concentration. Metal pollution particles act as catalysts for unwanted chemical reactions and water causes hydrolytic degradation of base oils and additives. Additional filtration system is designed to ensure reliable operation of the tractor using ecological fluid type UTTO. This system eliminates the wear particles concentration, oxidation products and water, thus pollution which endangers the durability and performance properties of ecological fluids, mainly. The designed filtration system creates the appropriate conditions for the extension of oil change interval. The high quality oils have superior oxidation resistance and thermal stability but the pollution is the reason for oil change also in case the physical and chemical parameters don't exceed limits.

Supported by the Ministry of Education of the Slovak Republic, Project VEGA 1/0857/12 „Reduction of unfavorable impacts of agricultural and transport machinery on environment".

Reference

ASTM D 5185-05. Test method for determination of additive elements, wear metals and contaminants in used lubricating oils and determination of selected elements in base oils by inductively coupled plasma atomic emission spectrometry (ICP-AES).

Drabant Š., Kosiba J., Jablonický J., Tulík J., 2010. The durability test of tractor hydrostatic pump type UD 25 under operating load. Research in agricultural engineering, 56: 116-121.

Hujo Ľ., Kosiba J., Jablonický J., Tulík J., 2012. Load characteristics of three-point tractor linkage. Naučni trudove : zemedelska technika i technologii, agrarni nauki i veterinarna medicina, remont i nadeždnosť, 51: 172-176.

Janoško I., Semetko J., Petrovič A., 2004. The degradable bio-oils in municipal engineering. Czasopismo techniczne, 45: 297-302.

Kučera M., Rousek M., 2008. Evaluation of thermooxidation stability of biodegradable recycled rapeseed-based oil NAPRO-HO 2003. Research in agricultural engineering, 54: 163-169.

Mihalčová J., Dobránsky J., 2008. Analyse of lubricant liquids in aircraft engines by tribotechnical diagnostics. Scientific Bulletin : Fascicle: Mechanics, Tribology, Machine Manufacturing Technology, 22: 281-286.

Tóth F., Rusnák J., Kadnár M., 2012. Monitoring of geometric cylindricity tolerance changes on a test sliding pair using the oils Madit PP 80 and Mobil Mobilube SHC. Acta technologica agriculturae,15: 100-102.

Tulík J., Kosiba J., Bureš Ľ., Šinský V., 2013. Analysis of synthetic oil samples during an operating test. Acta technologica agriculturae,16: 21-24.

ANALYSIS OF SELECTED WOOD BIOFUELS AND EVALUATION OF THEIR THERMAL EMISSION PROPERTIES

Jan Malaťák[1*], Jiří Bradna[2], Marian Kučera[3], David Černý[1], Luboš Passian[1]

[1] Czech University of Life Sciences Prague, Czech Republic, E-mail: malatak@tf.czu.cz
[2] Research Institute of Agricultural Engineering, p.r.i.
[3] Technical University in Zvolen

Abstract

This article describes the fuel properties of used biofuel samples in the form of pellets and subsequent thermal emission properties in the burner combustion plant with automatic feeding of fuel. There are four samples of spruce wood biomass and four samples mixed with spruce pine 1:1. On these samples is carried out elemental and stoichiometric analysis. The results of these analyzes show the same characteristics of used sample.

The samples are sequentially burned in the automatic burner combustion plant with automatic feeding of fuel. With the help of flue gas analyzer are set emission of carbon monoxide, oxides of nitrogen and flue gas temperature. The resulting values are statistically analyzed by regression analysis. Using the regression equation is backward assigned the coefficient of excess air and is set the average thermal emission concentration for samples from spruce and samples from wood mixture depending on the coefficient of excess air with the indicated scattering measurements. The results show increased concentration of carbon dioxide in the absence of combustion air during combustion of spruce samples. By reducing the combustion temperature there is no large increase in the emission of nitrogen oxides concentrations in spruce samples. For further use of combustion device based on the burner furnance can be improved combustion conditions by more balanced supply of fuel to the burner and better control of the combustion air.

Keywords: spruce, pine, pellets, elemental and stoichiometric analysis, burner furnance, flue gas

Introduction

The potential of organic waste is in the Czech Republic significant and their processing is problematic. The use of these materials as a fuel in small combustion plants faces many technical and economic challenges. Just more strict legislative conditions will increasingly take into account the quality of used biofuels and the operating conditions of the combustion devices. One of the ways is the use of high quality biofuels from wood material for small combustion plants and combustion plants with automatic feeding fuel into the combustion chamber.

Results obtained by foreign authors show good results during wood biomass combustion in small combustion plants. How present scientific papers from authors Johansson and Olsson, who show very good emission properties of biomass combustion in modern combustion devices, the basis is to know properties of used biofuels, which sufficiently characterized them.

High quality of pellets from biomass is required primarily for combustion in small combustion devices. For more combustion devices, that are equipped with gas cleaning and combustion process control is not critical fuel quality. It is important to divide two types of pellet fuel, for industrial or small residential combustion devices (Obernbergera, Theka, 2004).

Fuel quality is critical, as shown by the results of the author Olsson (2006), who tested at one combustion device the spruce pellets from several manufacturers, so there was found no large differences in exhaust gas production. From an ecological point of view it is better to use pellets made from wood for small home combustion devices and pellets from biomass can be used without difficulty for greater combustion devices.

The issue of emissions is very extensive and serious. This is particularly the case of biomass complete combustion. The options for reducing emissions of incomplete combustion include continuous dosing, enough high temperature in the combustion chamber, intake of secondary or tertiary air, choosing optimum moisture of biofuels. Parameters such as calorific value, water content and energy density, by the product of volume density or bulk weight and calorific value, affect design of the combustion device and its control in many ways. The water content in biomass has an influence on adiabatic temperature of the combustion chamber, on combustion conditions and amount of produced flue gas (Gürdíl et al., 2009).

The aim of this article is to define for wood raw material and mixtures their weight flows, emission factors and solid particles characteristics depending on the used combustion device. There will be made stoichiometric and elemental analysis, measured thermal emission parameters of the combustion device. Regression analysis will be used for statistical analysis of measurement results. In conclusion of this article there will be set out the problematic aspects of thermal and raw material use of selected solid biomass.

Material and methods

For research work are selected wood biofuels from forestry and waste sectors from different regions of Czech Republic. This is the raw material obtained from several timber processors. It is the wood chips and sawdust from spruce and pine. Samples are gradually acquired during the year 2012. Thus energetic exploitable biomass usually cannot be used in combustion devices directly, but must be modified into a suitable shape and size. Biomass is processed in the form of pellets for analysis. Pellets samples are pressed under the same conditions on the laboratory equipment CULS Prague (pellet press from manufacturer Kovo Novak). The resulting samples of pellets 6 mm in diameter and ratios are presented in Table 1.

Tab. 1 Samples of pellets

Number of sample	Samples of pellets 6 mm in diameter
1	spruce
2	spruce
3	spruce
4	spruce
5	spruce + pine in 1:1 ratio
6	spruce + pine in 1:1 ratio
7	spruce + pine in 1:1 ratio
8	spruce + pine in 1:1 ratio

Determining elemental analysis of samples is primary task to meet the objectives of the work. Elemental analyzes were performed by University of Chemical Technology in Prague, Faculty of Environmental Technology solved within internal projects of the Czech University of Life Sciences Prague. The elements carbon, hydrogen and nitrogen were determined by CHN analyzer Perkin-Elmer 2400.

For determination of chlorine and sulfur were samples burned in oxygen-hydrogen flame on Wickbold apparatus. Noncombustible fuel substances, i.e. ash and all water content were determined by combustion, respectively drying the sample. To determine the total water content was used certified moisture analyzer Ohaus MB 25. Measurements were carried out according to CSN EN 14 774-3 (2010).

Gross calorific value of examined biofuel samples was determined by measuring in the calorimeter IKA 2000 by CSN EN 14 918 (2010). Net calorific value was determined by calculation in the following equation, where are used the results of individual biofuel samples elemental analysis.

The relationship between gross calorific value Q_s and net calorific value Q_i was expressed in the following equation by CSN EN 14 918 (2010):

$$Q_i = Q_s - (0{,}02442 \cdot 1000) \cdot (W + 8{,}94 \cdot H),$$

(kJ.kg^{-1}, kJ.m$^{-3}_{N}$)

where: W .. the water content of test sample (%);
8,94 .. coefficient for the conversion of hydrogen to water;
H .. hydrogen content in test sample (%);
0,02442 .. value that corresponds to energy consumed in heating 1% of water at 25 °C.

The following stoichiometric calculations of combustion processes complement the characteristics of fuel and are the basis for any thermal calculation. They are especially important for solving of many problems in design practice, as well as for controlling the work of existing combustion devices. In these calculations is defined the amount of oxygen (air) required for complete fuel combustion, the quantity and composition of flue gas and the flue gas density.

Calculation of air consumption and flue gas amount was determined in this work by analytical method, i.e. according to information from elemental analysis using stoichiometric equations. Elemental analysis determination of samples and stoichiometric analysis determination are the basis for thermal-emission properties assessment. Stoichiometric calculations are converted to standard conditions (temperature t = 0 ° C and pressure p = 101.325 kPa) and for reference oxygen content in flue gas O_r.

Thermal emission measurements are carried out on the hot stove with automatic fuel feeding KNP by company KOVO NOVAK with burner furnace, in accordance with CSN 07 0240 (1993): Warm water and low-pressure steam boilers and CSN 12 4070 (1990): Dust collecting equipment. Measuring methods of quantity features. The nominal thermo-technical specifications of hot stoves are listed in Table 2.

Tab. 2 Thermo-technical specifications of hot stoves KNP
(Source: KOVO NOVAK Citonice, Hot stoves KNP – Operating instructions, installation and maintenance)

Parameter		Value
Nominal power [kW]		18
Controllable output [kW]		8 - 18
Fuel consumption [kg . h^{-1}]		1,5 – 4,9
Flue gas temperature	▪ at nominal power [°C]	210
	▪ at minimal power [°C]	110
Efficiency at nominal power [%]		88
Flue gas mass flow at the outlet	▪ at nominal power [kg.s^{-1}]	0,0138
	▪ at minimal power [kg.s^{-1}]	0,010

The fuel samples are sequentially burned at nominal thermal parameters of the combustion device, where is observed constant fuel supply and amount combustion air. Each sample is burned for three hours. Emission concentration measurement is done by measuring flue gas equipment Madur GA-60. This device Madur GA-60 is a multi-purpose flue gas analyzer. Its principle is based on the use of electrochemical converters. During measurement are measured values of surrounding temperature, exhaust temperature and chemical gases composition in the range of O_2, CO, SO_2, NO, NO_2. Signal of transducers is proportional to the volume concentration of the measured component in ppm. Average interval record of the individual components is set after one minute. Before the measurement is calibrated measuring device.

Emission concentrations are converted from ppm concentrations to normal conditions and transferred to concentration mg.m^{-3} and reference oxygen content 11% in flue gas. Subsequently are the results of thermal emission measurement processed by regression statistical analysis for mathematical expression of carbon monoxide, the flue gas temperature and nitrogen oxides depending on the excess air coefficient. Excess air coefficient is backward assigned in the regression equation in the range of 3-16 times the theoretical amount of air for complete combustion. The resulting average values of spruce samples and mixed spruce with pine are graphically displayed with expression scattering measurements. In conclusion of this article there will be set out the problematic aspects of thermal and raw material use of selected solid biomass.

Results and discussion

The resulting values of elemental analysis of selected pellets samples in their original state are shown in Table 3. From resulting table of elemental analysis is shown that the samples have few significant differences.

Problematic component in the fuel is sulfur in creation of emissions. Sulfur also goes out largely during combustion into gas phase as SO_2 or SO_3. Sulfur emissions in combustion devices using solid fuels from renewable resources are not as regards the limit values, generally no problem, as evidenced by the selected samples see Table 3.

Water and ash content is crucial for thermal use of each fuel. Range of all water contained in the samples is quite low, which has a positive contribution to the calorific value of individual biofuel samples. Ash content in the samples is also low, as can be seen from the elemental analyzes of selected samples in Table 3.

Tab. 3 Elemental analysis of selected pellets samples in their original state

Number of sample	Water Content (% Wt.)	Ashes (% Wt.)	Combustible matter volatile (% Wt.)	Combustible matter non-volatile (% Wt.)	Net calorific value (MJ.kg^{-1})	Carbon C (% Wt.)	Hydrogen H (% Wt.)	Nitrogen N (% Wt.)	Sulphur S (% Wt.)	Oxygen O (% Wt.)	Chlorine Cl (% Wt.)
	W	A	V	NV	Q_i	C	H	N	S	O	Cl
1	7,32	0,39	79,29	14,93	18,02	47,01	4,21	0,00	0,01	58,97	0,03
2	7,45	0,40	79,17	14,82	17,66	46,71	4,92	0,00	0,01	59,513	0,023
3	6,82	0,41	79,29	14,93	17,60	46,03	4,95	0,00	0,01	58,25	0,03
4	6,35	0,40	79,29	14,93	17,80	47,26	4,98	0,00	0,01	59,03	0,03
5	7,1	0,40	79,21	15,09	17,67	45,89	4,94	0,00	0,00	58,36	0,03
6	6,58	0,405	78,54	15,59	17,39	47,15	4,96	0,00	0,02	59,145	0,03
7	7,42	0,401	79,29	14,93	16,60	46,72	4,92	0,00	0,02	59,511	0,03
8	7,47	0,40	77,33	15,23	16,56	46,7	4,92	0,00	0,02	59,54	0,03

The amount of water and ash significantly affects thermal properties of the examined samples and subsequently affects both the selection and the adjustment of combustion device. First of all, the increased ash amount affects operation of the burner combustion plants, which is confirmed by further research authors Malatak, Passian, (2010); Olson et al., (2003).

The resulting values of stoichiometric analysis of combustion processes complement the sample characteristics and are the basis for any thermal calculation and controlling the work of existing combustion plants.

Thus performed analysis determines:

- The amount of oxygen (air) required for complete combustion of the sample ($kg.kg^{-1}$), ($m^3_N.kg^{-1}$)
- The quantity and composition of flue gas ($kg.kg^{-1}$), ($m^3_N.kg^{-1}$)

The resulting values of stoichiometric analysis point to a very good thermal emission parameters examined samples (see Table 4). From the examined samples biofuels stoichiometry based on the fact that the parameters calorific value, water content and energy density influence selection and design of combustion device. Concentration of elements in the examined samples, as confirmed by stoichiometric analysis of samples, is relatively uniform.

The resulting parameters of the stoichiometric analysis of selected biofuel samples are used to calculate the resulting emission parameters, in particular for the calculation of the excess air coefficient.

Thermal emission measurements based on previous elemental and stoichiometric analyzes of selected solid biofuel samples. There were eight thermal emission measurements on the hot stove KNP. Given the scale of measurement, the article shows only the resulting regression equation given in Table 5. The resulting graphs are based on regression equations compiled from single fuel samples measurements. The samples are divided into samples of spruce and mixed wood samples. The resulting values for each species of samples averaged and plotted in graphs in dependence on the excess air coefficient. The resulting graphs are assigned variances.

Tab. 4 Stoichiometric analysis of the original pellet samples for complete combustion

Number of sample	Theoretical amount of oxygen for complete combustion ($kg.kg^{-1}$)	Theoretical amount of air for complete combustion ($kg.kg^{-1}$)	Theoretical mass amount of dry flue gas ($kg.kg^{-1}$)	Theoretical mass concentration of carbon dioxide in dry flue gases (% Wt.)	Theoretical amount of oxygen for complete combustion ($kg.kg^{-1}$)	Theoretical amount of air for complete combustion ($kg.kg^{-1}$)	Theoretical mass amount of dry flue gas ($kg.kg^{-1}$)	Theoretical volume concentration of carbon dioxide in dry flue gases (% Wt.)
	O_{min}	L_{min}	m^s_{spmin}	CO_{2max}	O_{min}	L_{min}	m^s_{spmin}	CO_{2max}
	Mass combustion				Volume combustion			
1	1,18	5,09	7,56	22,79	0,82	3,92	3,93	22,17
2	1,23	5,32	7,73	22,16	0,86	4,10	4,07	21,30
3	1,24	5,36	7,77	22,20	0,87	4,13	4,09	21,30
4	1,25	5,39	7,80	22,23	0,87	4,15	4,11	21,30
5	1,24	5,39	7,75	22,18	0,86	4,12	4,08	21,30
6	1,25	5,37	7,78	22,21	0,87	4,14	4,10	21,30
7	1,24	5,32	7,73	22,16	0,86	4,10	4,07	21,30
8	1,23	5,32	7,73	22,16	0,86	4,10	4,07	21,30

Tab. 5 Regression analysis of relationship between carbon monoxide, flue gas temperature and nitrogen oxides into the excess air coefficient

Number of sample	Carbon monoxide ($mg.m^{-3}$)	Flue gas temperature (°C)	Nitrogen oxides ($mg.m^{-3}$)
1	$CO = 9{,}9303n^2 - 183{,}72n + 1112{,}6$	$T_{pl} = -0{,}6033n2 + 9{,}9949n + 170{,}94$	$NO_x = -0{,}241n^2 + 4{,}7434n + 179{,}33$
2	$CO = 0{,}3911n^{2,6959}$	$T_{pl} = 0{,}0918n^2 - 6{,}2779n + 254{,}97$	$NO_x = 131{,}22n^{0,357}$
3	$CO = 11{,}257n^2 - 385{,}16n + 4217{,}6$	$T_{pl} = -0{,}0722n^2 + 1{,}174n + 162{,}87$	$NO_x = 238{,}81n^{0,2999}$
4	$CO = -2{,}5646n^2 + 156{,}59n - 1067{,}2$	$T_{pl} = -1{,}7354n^2 + 26{,}463n + 129{,}48$	$NO_x = 605{,}6n^{-0,225}$
5	$CO = 0{,}2967n^{2,8022}$	$T_{pl} = 0{,}0489n^2 - 4{,}2867n + 241{,}71$	$NO_x = 246{,}55n^{0,0734}$
6	$CO = 0{,}0008n^{4,3239}$	$T_{pl} = 0{,}0346n^2 - 5{,}0977n + 274{,}43$	$NO_x = 492{,}1n^{0,3707}$
7	$CO = 0{,}4622n^{2,3137}$	$T_{pl} = 0{,}0067n^2 - 2{,}0239n + 209{,}05$	$NO_x = 478{,}38n^{0,261}$
8	$CO = 0{,}267n^{2,5417}$	$T_{pl} = -0{,}1976n^2 + 9{,}4687n + 62{,}958$	$NO_x = 202{,}66n^{0,5312}$

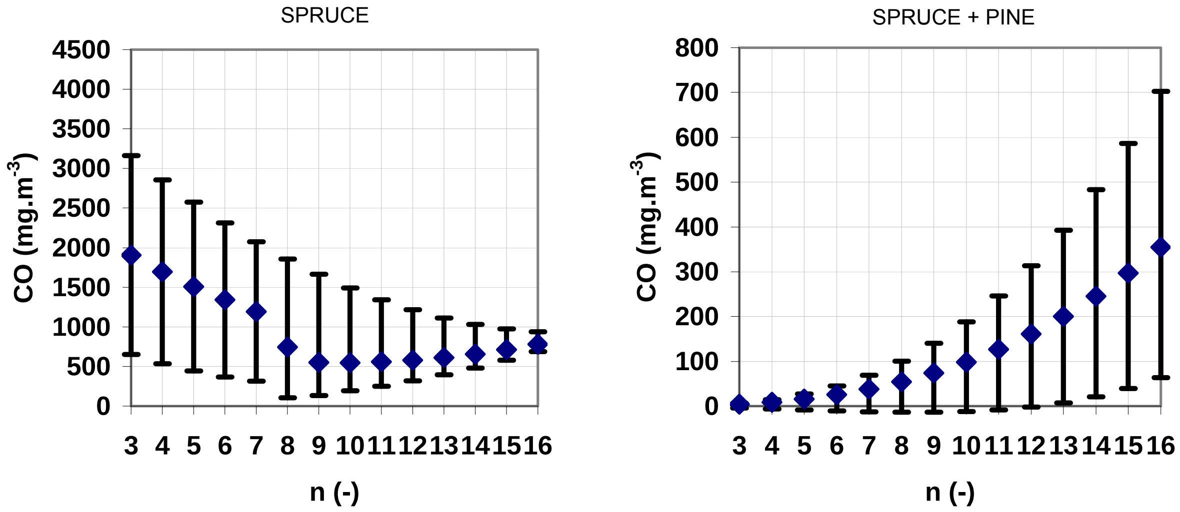

Fig. 1 Courses of carbon monoxide according to the excess air coefficient

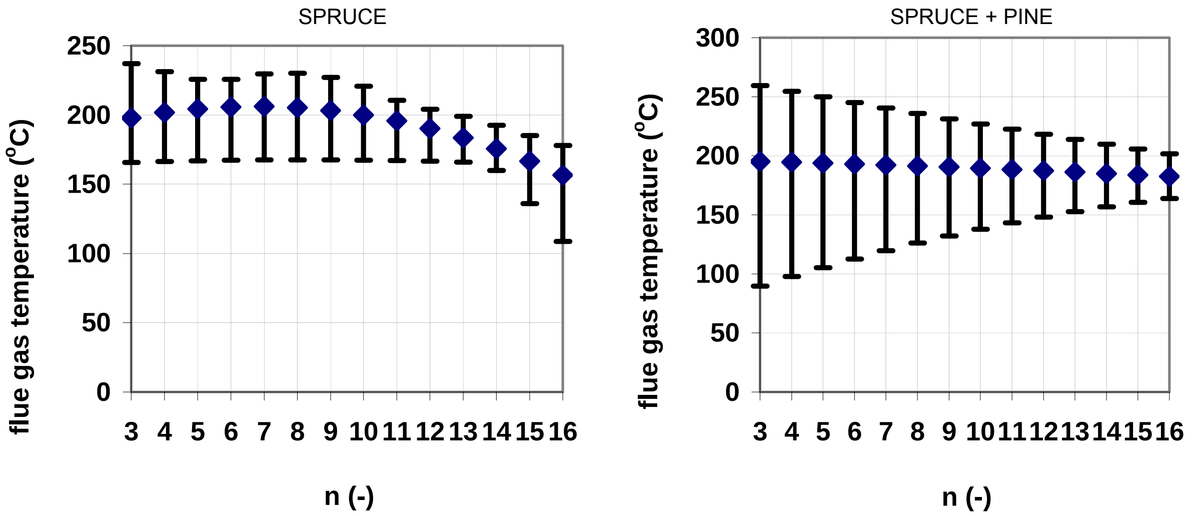

Fig. 2 Courses of flue gas temperature according to the excess air coefficient

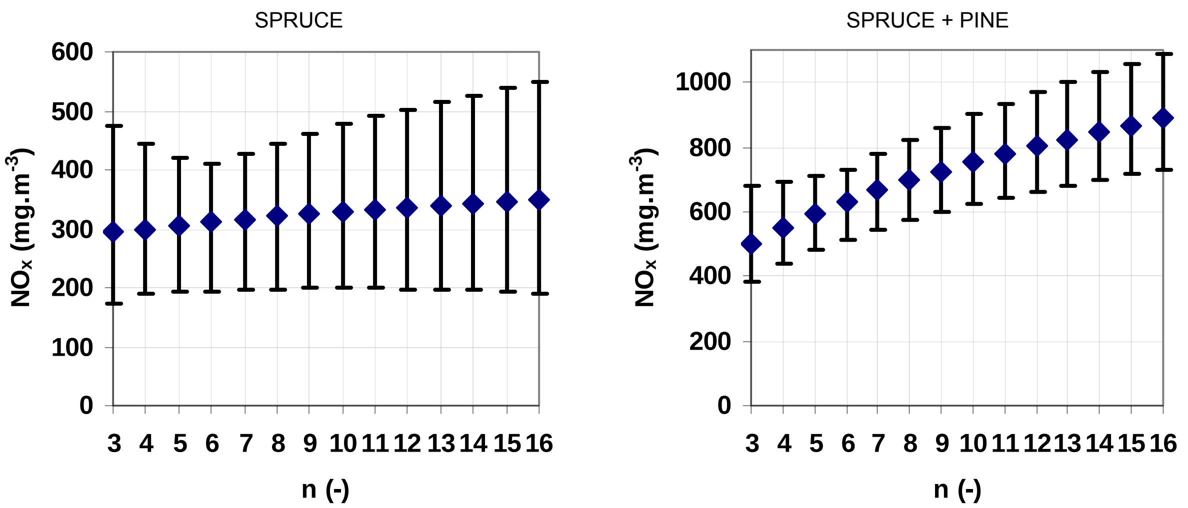

Fig. 3 Courses of nitrogen oxides according to the excess air coefficient

In Figure 1 have fuel samples opposite courses of carbon oxides emission concentrations. First of all the samples from spruce have high concentrations of carbon dioxide emissions in absence of combustion air. This course of combustion can also be seen in Figure 2, where temperature during spruce samples combustion are low at low excess air coefficient, then rise temperature and after crossing optimum amount of combustion air flue gases gradual cooling, different than occurs in combustion process in the case of samples with pine mixtures. The reason why rises another combustion process of carbon oxides in this fuel samples can look at several factors, such as the calorific value, the proportion of volatile matter in the sample and the amount of combustion air supplied into the combustion chamber. Also in the combustion device can lead to insufficient mixing of volatile flammable materials with combustion air and insufficient burn.

Figure 3 shows positive result during combustion of spruce samples on emission concentration of nitrogen oxides. There is no large increase in nitrogen oxides emission concentrations by reducing combustion temperatures, which is evident in the case of spruce samples mixed with pine. Thus expressed courses show the relationship between nitrogen oxides emissions and temperature on excess air coefficient (combustion air). There is cooling flame and thereby cooling flue gas in the course of excess air coefficient increasing.

The figures also show large variance of the resulting values. First of all samples from fuel mixtures with low excess air coefficient had different character. This can be seen particularly in Figure 2 during the flue gas temperature when the flue gases in one case falling to very low temperatures. The difference of flue gas temperature for each sample can be justified especially by amount of air supplied into the combustion device.

Conclusion

By continuously increasing the use of renewable raw materials is growing demand for high-quality biofuels for small combustion devices with automatic feeding of fuel. One of these fuels may be analyzed samples that have similar element and stoichiometric properties. These analyzes are not conclusive for good combustion. Thermal emission measurements show how the combustion device works with given fuel.

During measurement of emission concentration there was achieved great variances of measurement. Although the results of elemental and stoichiometric analyzes indicate similar characteristics, being implemented thermal emission measurements show large variance of the resulting parameters. One possibility why there was such large variance in measurements is the fact that during the combustion process has failed to achieve uniformity of pellets samples supply into the burner. This resulted in an irregular combustion. Used combustion device operates on the principle of periodic fuel feed by screw feeder after time intervals, so there were leap fluctuations in emission concentrations of all flue gas components. Supplying fresh fuel to the burner causing suppression of combustion processes. Another reason for large variances in measuring is the composition of spruce and pine mixture and their course release volatile inflammable.

The subsequent problem was supply of combustion air during periodic fuel supply. Amount of air during fresh fuel preheating was not regulated, resulting in high amount of combustion air. For further use of combustion devices based on burner furnace system can be improved combustion conditions by more uniform fuel supply to the burner and better control of combustion air, e.g. the lambda probe.

During the measurements were verified appropriate types of biofuels from further possibilities of their pre-treatment, such as Torrefaction technology. Determined elemental analyzes and stoichiometric characteristics can serve for further evaluation of energetic biomass use as a renewable energy source. The accurate determination of typical thermal emission properties is necessary in design practice for construction, but also controlling of combustion devices and heat using of solid fuels samples from wood examined in this research work.

Acknowledgments

The work was supported by the internal research project of the Faculty of Engineering IGA 2013: 31170/1312/3116.

References

Olsson M., Kjallstrand J., Petersson G., 2003. Specific chimney emissions and biofuel characteristics of softwood pellets for residential heating in Sweden. Biomass and Bioenergy 24: 51 – 57.

CSN 07 0240 (1993): Warm water and low-pressure steam boilers. Basic regulations. Czech Office for Standards, Metrology and Testing, Prague, Czech Republic. (in Czech)

CSN 12 4070 (1990): Dust collecting equipment. Measuring methods of quantity features. Czech

Office for Standards, Metrology and Testing, Prague, Czech Republic. (in Czech)
CSN EN 14 774-3 (2010): Solid biofuels. Determination of moisture content. Oven dry method, Part 3: Moisture in gen - eral analysis sample. Czech Office for Standards, Metrology and Testing, Prague, Czech Republic. (in Czech)
CSN EN 14 918 (2010): Solid biofuels. Determination of calorific value. Czech Office for Standards, Metrology and Testing, Prague, Czech Republic. (in Czech)
Gürdíl G., Malaťák J., Selví K., Pinar Y., 2009. Biomass utilization for thermal energy. AMA, Agricultural Mechanization in Asia, Africa and Latin America, 2 (40): 80 – 85.
Malaťák J., Passian L., 2011. Heat-emission analysis of small combustion equipments for biomass. Res. Agr. Eng., 57: 37–50.
Obernbergera I., Theka G., 2004. Physical characterisation and chemical composition of densified biomass fuels with regard to their combustion behaviour. Biomass and Bioenergy 27: 653–669.
Olsson M., Kjällstrand J., 2006. Low emissions from wood burning in an ecolabelled residential boiler. Atmospheric Environment, Volume 40, Issue 6: 1148-1158.

OFF-GRID PHOTOVOLTAIC SYSTEM WITH LED

Jan Mareš[1], Martin Libra, Vladislav Poulek[2]

[1]Czech University of Life Sciences Prague, Kamýcká 129, 16521 Prague 6, Czech Republic
[2]TRAXLE Solar, Ltd., Velvarská 9, 16000 Prague 6, Czech Republic

Abstract

The *small off-grid photovoltaic system for illumination was constructed and tested at the Czech University of Life Science in Prague. Light source with LED was used. Description of the PV system and results of the testing are presented in this paper.*

Keywords: photovoltaics, illumination, solar energy, PV system

Introduction

The off-grid photovoltaic (PV) systems are usually constructed for energy supply in locations where the network is missing. The combustion engines need fuels supply all the time. In this case, the off-grid PV system and energy accumulation into the batteries is more simple. Systems are suitable for energy supplying of various equipments or science instruments in the field. We constructed and tested various on-grid and off-grid PV systems in the past and our results were published regularly for example in the journal Solar Energy Materials and Solar Cells (Poulek, Libra, 2000) or in the book (Poulek, Libra, 2010). Recently, we realized the application with the off-grid PV system for illumination. The energy saving light source with light emitting diodes was used. In this paper we will describe the construction and the results of the testing.

Energy saving light sources

Incandescent lamps formerly used were discharging the batteries too fast. The filament inside the bulb emits the light according to Planck's law about radiation of the dark body. The efficiency of the energy conversion is only approx. $\eta \approx 3$ %. More energy saving discharge light sources have efficiency approx. $\eta = 18$ %. The most energy saving sources LED (light emitting diodes). LEDs producing yellow light have efficiency up to $\eta \approx 40$ %. LEDs producing white light have efficiency approx. $\eta \approx 30$ %. Also we used the light source based on the LEDs with white light.

Fig. 1 shows our measurement of the emission spectrum. The photometer has a long step and that is the reason that individual spectral lines on the figure are merging. But the spectrum is not continuous. Strong emission in blue part of the spectrum can be seen, as well as area of the transformed photons by luminescence. Because the efficiency of the energy conversion is approximately ten times higher in comparison with the incandescent lamp, the off-grid PV systems with such energy saving light source is discharging the battery approximately ten times more slowly. Moreover light sources with LED have the lifetime more than 50000 hours, fluorescent lamps have the lifetime approx. 5000÷8000 hours and the classic incandescent lamps have the lifetime about 1000 hours. The price of the LED light sources is few higher, but the massive production will decrease the price.

We did see few various off-grid PV systems. Fig. 2 shows an off-grid PV system in Shanghai, where PV panel is used for energy supplying of the traffic lights with LEDs (red, yellow, green).

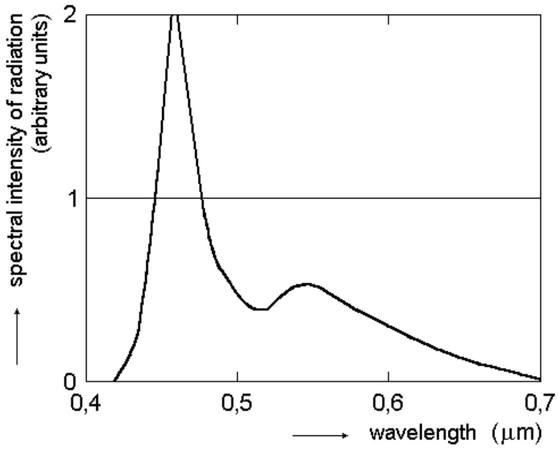

Fig. 1 Approximate measurement of the emission spectrum

Fig. 2 The off-grid PV system in Shanghai

Fig. 3 Outdoor part of the off-grid PV system. The PV panel is not far from the light source

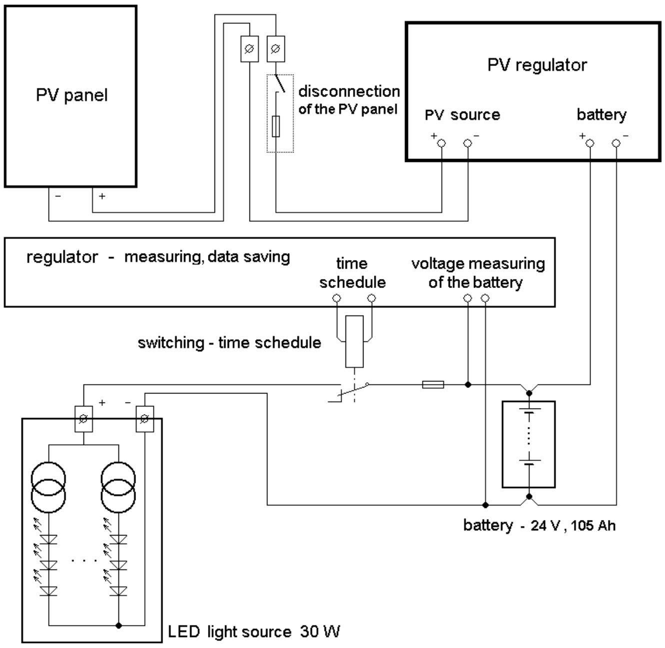

Fig. 4 Scheme of the off-grid PV system

Experimental Arrangement

We constructed the off-grid PV system designated for illumination on the Czech University of Life Sciences Prague. Fig. 3 shows the outdoor part. The batteries were located in the laboratory as well as the recharging unit and programmable unit (PLC). The data were collected and the visual supervision is possible cross the web interface. Fig. 4 shows scheme of the PV system. The nominal power of each diode was 1 W, the maximum total power was also 30 W during illumination. The recharging unit L2415 was used for the battery charging. This unit is controlling the recharging and it is also securing an overvoltage and under-voltage protection. The PV panel based on the monocrystalline silicon with maximum output power $P = 170\ W_p$ was used for the recharging of lead gel batteries EnerSys (12 V, 105 A.h). Two batteries were connected in series and the no load voltage was approx. $U_e = 28$ V if fully charged. Also the maximum amount of accumulated energy can be approx. $W_{max} = 2{,}5$ kWh.

The construction of the PV system was finished in summer of 2011 and the operation and the data collection started since August 2011.

Results and discussion

Fig. 5 shows the time behaviour of the battery voltage during few autumn days. The batteries were charged during the day by the PV panel and they were discharging during the night by the shining light source, the electric current cross the light source is seen as well. Till the 3rd November the charging and discharging was in balance. It is clearly seen that batteries were recharged during the day and discharged during the night. The illumination mode started at 21:00 and finished next day at 6:30. The daily illumination time was almost 10 hours. The voltage leap at the light source switching on and switching off is seen in the Fig. 5. The voltage oscillations during recharging are caused by a difference between measuring during the recharging pulse or otherwise. Smaller oscillations during the discharging are due to measurement accuracy.

The calculation according our previous measurements (Libra et al., 2010) show that during the whole year a PV panel is capable of supplying energy of more than $W_d > 150$ kWh. If the light source would be switched on for 10 hours per day, the energy of $W_s \approx 110$ kWh would be needed for a whole year, the efficiency of the battery is approximately 70 %. According to the theory, the PV system could be self-sufficient and it was self-sufficient during the summer period till autumn. No additional energy can be stored, if the batteries are fully charged. But during the winter period the time of sunlight is shorter and the angle of the solar radiation is lower (Libra et al., 2010). Ageing, energy losses and decrease of the batteries capacity must to be also taken into the consideration. After the November 2011 the illumination mode was changed, the light source was shining during the evenings and mornings with 50 % of the illumination capacity and during the night with 30 % of the illumination capacity. The illumination intensity was controlled by the ratio between switching on and switching off time at the higher frequency. The balance between the charging and discharging was restored and the PV system was operating reliably.

Fig. 6 shows the analogical case after the changing of the illumination mode. There the situation in the winter period and in the spring period is seen during the year 2013. No problems with the under-voltage protection were observed after the modification of the illumination mode (lower illumination intensity).

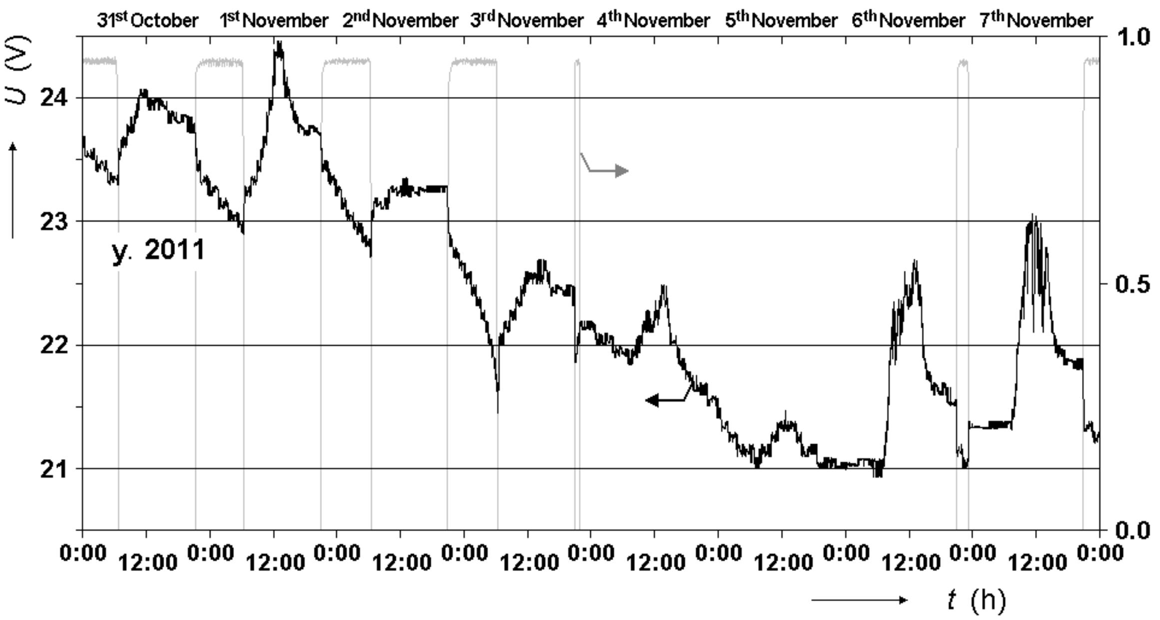

Fig. 5 Time behaviour of the battery voltage during few autumn days

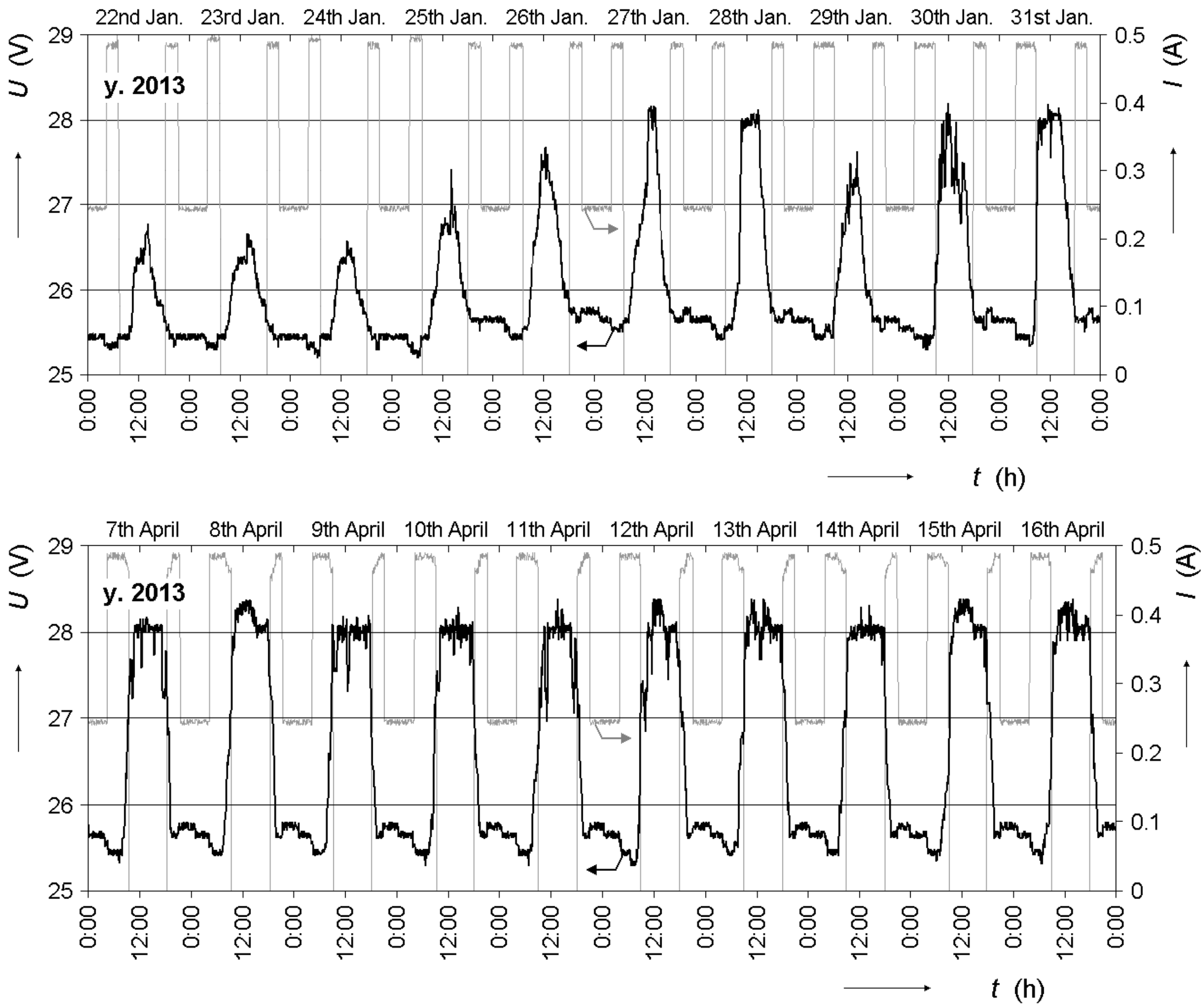

Fig. 6 Time behaviour of the battery voltage during few winter days and few spring days. The electric current cross the light source is seen as well.

Conclusion

We have constructed the above mentioned off-grid PV system for illumination, the testing was started in the spring 2011. The PV system was self-sufficient till the 3rd November 2011. Also since the November we modified the illumination mode. The illumination intensity was lowered, the discharging speed was decreased. Then the off-grid PV system was operating reliably during whole few years. Similar off-grid PV system was tested in the ref. (Sağlam et al., 2010).

The work was supported by the internal research project of the Faculty of Engineering IGA 2013:31120/1312/3102.

References

Poulek V., Libra M., 2000. A New Low Cost Tracking Ridge Concentrator. Solar Energy Materials and Solar Cells, 61, 2: pp.199-202.

Poulek V., Libra M., 2010. Photovoltaics, theory and practice of solar energy utilization, ILSA, Prague, 169. ISBN 978-80-904311-2-6

Libra M., Sedláček P., Mareš J., Poulek V., 2010. Porovnání PV systémů s pevným a proměnným sklonem PV panelů (Comparison of the PV systems with the fixed and adjusting inclination of PV panels). Jemná mechanika a optika (Fine mechanics and optics), 55, 10: 270-271 (in Czech).

Sağlam S., Ekren N., Erdal H., 2010. Controlling of grid connected photovoltaic lighting system with fuzzy logic. Solar Energy, 84: 256-262.

YIELD MONITORING SYSTEM FOR HAY AND STRAW

Jiří Mašek*, Milan Kroulík, Zdeněk Kvíz, Petr Novák

Czech University of Life Sciences Prague, Faculty of Engineering,
16521 Prague 6 – Suchdol, Czech Republic
Phone: +420 2 2438 3137, E-mail: masekj@tf.czu.cz

Abstract

Yield monitoring and mapping are one of the basic elements of precision agriculture system. Different sensors and systems are commonly used for yield mapping nowadays. Concretely for straw and forage crops yield mapping, the sensors are placed on mowing machines or choppers. The technical solution of described system for forage crops and straw yield measurement consists of a simple arrangement of a position sensor – potentiometer mounted on the belt tension roller on a chosen round pick-up baler with variable chamber. Press with variable chamber VICON RV1601 Opticut was used for measurement. Wheat straw and hay was pressed during trial measurement. Position of the belt tension roller was monitored by the potentiometer. Calibration of the measuring system showed a strong dependence of the tension roller position on the amount of pressed straw or hay (R = 0,99).

Key words: precision agriculture, yield mapping, harvest, round bale

Introduction

Mapping of crop yields is one of the fundamental elements of precision agriculture. For forage yield mapping is using sensors and systems that are placed directly on mowers or cutters. Several methods of determining the rate of mass-flow through hay and forage harvesting equipment have been explored. These sensors measure feedroll displacement, crop impact force, and torque, among others (Maughan et al., 2012). Yields mapping method suitable for various crops is proving to be a haul weighing devices or pick presses. The idea behind the principle of work of these methods is based, is relatively simple. Its practical applications, however, brings problems of technical and organizational nature.

Wheeler et al. (1997) described the basic requirements for the mapping system of crop yield based on continuous weighing of wagons. Goodwin (1999) continued research on the apparatus described based on continuous weighing trailer. Overall, the semi-continuous weighting in combination with the adoption of GPS (Global Positioning System) signal can be used for yield mapping. The same principle is founded the idea of mapping forage yield at harvest using the round baler.

Measuring system developed Behme et al. (1997) and Wild, Aurenhammer (1997, 1999). The system was based on load sensing axis wheels gauge sensors. The whole system can be supplemented with a GPS receiver to create yield maps. Weighing during stationary position of machine is very accurate, but the movement can achieve measurement errors greater than 20 %. The negative effect on measurement accuracy has impacts resulting from irregularities in the terrain crossing. The main content of the article is an introduction of measuring forage yield and straw using tape measure press with variable chamber, which is based on the measurement current location tension pulley bands of the pressing chamber (Kroulík et al., 2010).

Materials and methods

The technical solution consists in the arrangement of the tensioning mechanism for tracking a variable compression chamber of the press during molding of forage or straw into the bale. To measure was used Baler VICON RV1601 OPTICUT. During trial measurement was pressed wheat straw and hay. Location tensioning mechanism was monitored with the potentiometer. Location potentiometer is shown in Figure 1. Detailed description of the engagement and solution demonstrates the utility model CZ 19754 U1. The outputs from the potentiometer are pulses. A specially designed electrical circuit was connected with the potentiometer and DGPS receiver. The data were recorded each 2 seconds.

The system must be also calibrated. Before calibration line was created punctuated with 10 m line of straw with 10m break without straw (Fig. 2). Ten-lines were considered. Thus was gradually developed bale. For each line were pulses reading (Fig. 3), which corresponded to position the tensioning mechanism for the gradual implementation of the bale chamber.

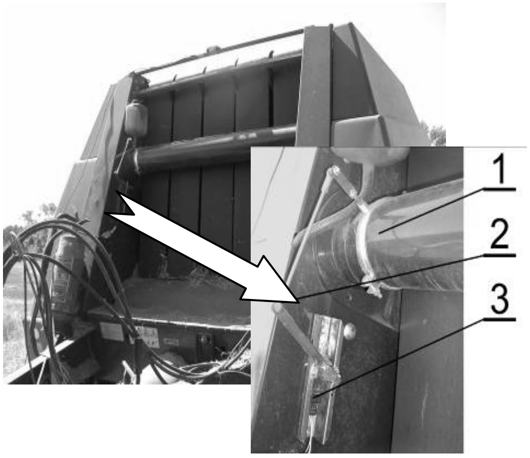

Fig. 1 Location potentiometer on the belt tensioning mechanism: 1 – belt tension roller mechanism, 2 – connecting rod, 3 - potentiometer

By monitoring these parameters can be determined by the immediate throughput of material and then harvested to create yield maps. To obtain spatially-related data throughput of material were recorded in data logger. Pulses of a potentiometer and machine position from DGPS receiver were at the same time recording to the data logger too.

Results and discussion

Trial measurement were carried out in the selected field and started by pressing arranged discontinuous row as it explained above. This step was taken as a calibration procedure. Based on the results of calibration potentiometer the calibration curve was obtained. Depending on the number of pulses during the potentiometer and net weight of the package best fit exponential curve with equation $y = 2745.1e^{-0,002x}$. Graph in Figure 3 shows the calibration curve. By pressing of forage with variable press chamber machine is achieved uniform compressibility of bale with the increased volume (diameter) of bale. Increased volume of bale recorded by potentiometer is proportional to the increasing of bale weight. Figure 4 shows the time series record of the measurement of growth package. For the subsequent processing of each set increases gradually yield t.ha^{-1}.

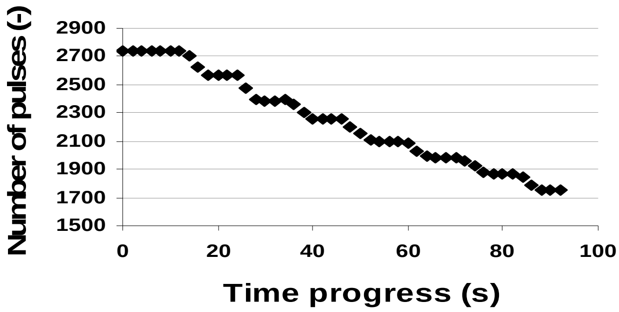

Fig. 3 Course of data record during discontinuous straw row pressing

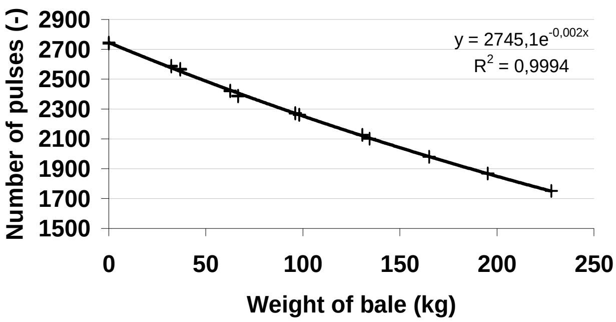

Fig. 4 Calibration curve

Prior to the processing of the data set was necessary to exclude values that were recorded during the tensioning mechanism for returning a package to the starting position and the value recorded on headlands. Also a point where the package is bound to be excluded from the data set. After processing, the record has been found in straw yield values ranging from 1.5 to 7.3 t.ha^{-1} with an average of 4.4 t.ha^{-1}.

Fig. 2 Calibration line – 10 m row + 5 m space

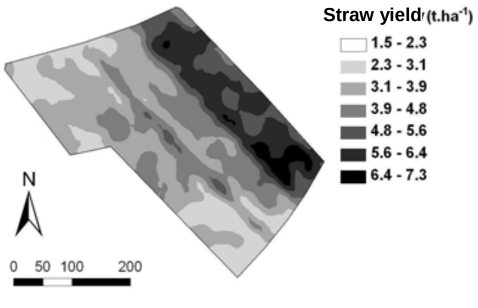

Fig. 5 Yield map of straw

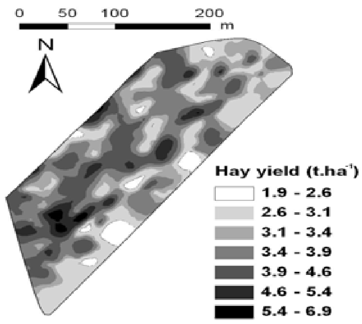

Fig. 6 Yield map of hay

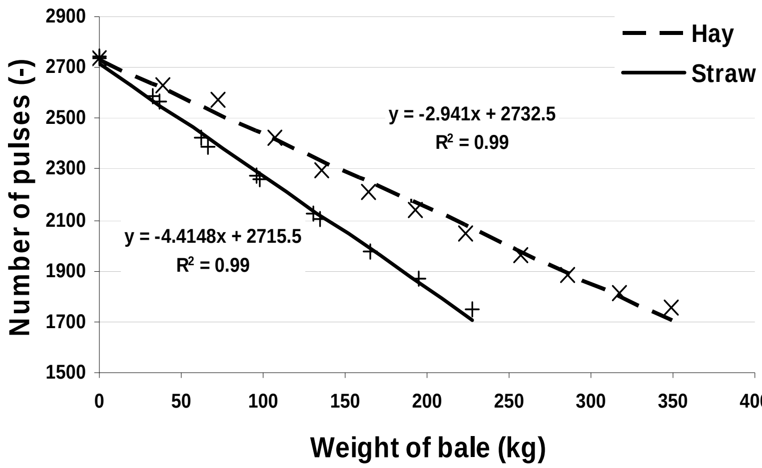

Fig. 7 Dependence of the number of pulses per bale weight for different materials

The course of calibration curves shown in figure 7 was proved according to our hypotheses that behaviour of calibration curves would be dependent on harvested material. Differences in bales density and material specific weight influenced angular coefficient of the curves. On the other hand, the value range of sensor output signal remained the same for different materials, because of the constant final volume of the bale press chamber.

Given the amount of pressed material may be information on forage yield is also beneficial. Although the literature review presented in some systems, there has not to extend any of these principles as is in the case of combine harvesters. One reason may be shortcomings in the systems which also derive from a literary analysis.

Conclusion

Measurement of position belt tensioning pulley of bale press with variable chamber is shown as a possible method of evaluating the yield pressed material. Calibration of the measuring system showed that the principle of measuring the position of the belt tensioning pulley is not sensitive to shocks. The big advantage of this solution is a simple construction. On the other hand, there is a limiting factor for the type of press, which is essential variable pressing chamber.

Acknowledgement

Supported by Ministry of Education, Youth and Sports of the Czech Republic, Project No. MSM 604 607 0905.

References

Behme J. A., Schinstock J. L., Bashford L. L., Leviticus L. I., 1997. Site-Specific Yield for Forages. ASAE Paper No. 97-1054. St. Joseph, Michigan, ASAE.

Goodwin, R. J., Wheeler P. N., O´Dogherty M. J., Watt C. D., Richards T., 1999. Cumulative mass determination for yield maps of non-grain crops. Computers and Electronics in Agriculture 23: 85-101.

Kroulík M., Mašek J., Kvíz Z., Prošek V., 2010. Sensor connection for yield determination on round balers with variable chamber. Landtechnik, VDI Verlag: Düsseldorf: 231 – 237.

Maughan J. D., Mathanker S. K., Grift T. E., Hansen A.C., 2012. Yield Monitoring and Mapping Systems for Hay and Forage Harvesting: A Review. ASABE Paper No. 12-1338184. St. Joseph, Michigan: ASABE.

Wheeler P. et al., 1997. Trailer Based Yield Mapping. Precision Agriculture, BIOS Scientific Publishers Ltd: 751-758.

Wild K., Auernhammer H., 1997. Dynamic Weighing in a Round Baler for Local Yield Measurement. ASAE Paper No. 97-1055. St. Joseph, Michigan, ASAE.

Wild K., Auernhammer H., 1999. A weighing system for local yield monitoring of forage crops in round balers. Computers and Electronics in Agriculture 23, Elsevier Sciences: 119-132.

ACHIEVEMENTS IN ENERGY VALORIZATION OF CEREAL STRAW IN BOILER MANUFACTURED IN ROMANIA

Mihaescu Lucian [1*], Enache Emil[2], Lazaroiu Gheorghe[1] ,Pisa Ionel[1], Berbece Viorel[1], Negreanu Gabriel-Paul[1], Pop Elena[1]

[1] University Politehnica of Bucarest,, 313 Splaiul Indepedndentei st. 060042 Bucharest, sector 6, Romania; tel: +404029158; fax:+404092224; E-mail: lmihaescu@caz.mecen.pub.ro
[2] S.C. Enache-Morarit S.R.L. Husi, Romania

Abstract

The paper presents the last achievement in hot water producing boilers, with a 150 kW power, which operates with straw briquettes. The boiler is developed in a flame tube construction and a mobile grate with water-cooled fixed bars, in order to reach a temperature, at the end of the furnace, under 850 °C (the limiting temperature above which the ash becomes adherent). The boiler is fully automated; it has an efficiency of 90-91 % and pollutant emissions under legal regulations.

Two such boilers are already manufactured until now, which, after a 28 months operation have not encountered problems in evacuating the ash. The convective heat exchanger is made with vertical pipes and has a cleaning system with mechanical drive, which required one cleaning for every 10-20 days of operation. The boiler is commercially available.

Keywords: cereal straw briquettes, hot water boiler

GENERAL ASPECTS

The 150 kW boiler is achieved following numerous research on burning for energy valorizing of briquettes from straw in the N-E region of Romania, but due to its technical and operational characteristics it can be used in all of the agricultural regions of Europe. In Romania the cereal straw production is very important, having an average value around 14 million tons per year. The prototype boiler was manufactured from 2011 to 2012.

The elemental calculations analysis for briquettes, made using the COSTECH ECS 4010 analyzer, shows:

$C^i = 42,6\%$, $H^i = 6,7\%$, $N^i = 0,6\%$, $O^i = 33,14\%$, $W^i_t = 11,97\%$, $A^i = 4,99\%$.

The lower heat value is:

$H^i_i = 17450$ kJ/kg.

The composition of the ash is:

$SiO_2 = 57,2\%$, $Al_2O_3 = 4,9\%$, $Fe_2O_3 = 1,1\%$, $MgO = 2,9\%$, $CaO = 3,9\%$.

The ash contains also phosphorus and potassium, so that it can be used as fertilizer.

By cooling intensely the furnace volume, the temperature at the ash evacuation was maintained below sub 850 °C, in order to avoid ash hardening (a phenomenon which inhibits the boiler construction for cereal straw).

For this purpose, the first successes were achieved by cooling the furnace chamber of the boiler by means of water chambers placed at the end of the furnace. The thermal power of this boiler was 150 kW, but subsequently constructions in the range of (80 .. 100) kW were tried. All these boilers were manufactured by the „E.Morarit" firm, in Husi, Romania (Mihaescu et al., 2011).

As the volume of the water chambers cooled furnace is bigger, the present generation of boiler was realized with burning into a flame tube immersed in water. The briquettes that were used had a very high density: 980 kg/m^3 to 1000 kg/m^3.

INNOVATIVE ASPECTS IN THE BOILER CONSTRUCTION

The boiler was designed to operate with 1.6 air excess and 125 °C temperature of flue gases at the stack. The efficiency reaches the value of $\eta = 91.6$ %, in that case. Values of up to 94 % were obtained for the efficiency, by lowering the air excess.

For a $\eta = 91.6$ % efficiency and 150 kW thermal power, the straw consumption is 33.7 kg/h. The measurements were made using the gas analyzer AFRISO Maxilize NG11, series 11.

The new boiler constructive variant is that of a flame tube and a vertical type convective heat exchanger placed above the furnace. In Fig. 1, a section through the boiler is presented.

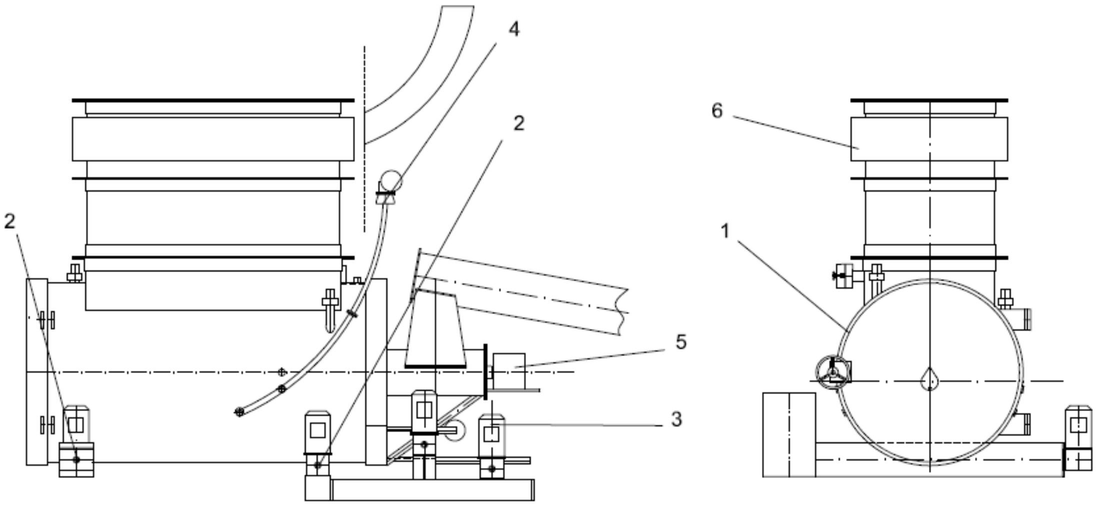

Fig. 1 The 150 kW boiler assembly
1- the cylindrical casing; 2 – ash removal system; 3 – moving grates system;
4 – secondary air pipe; 5 – briquettes feed system; 6 – the convective heat exchanger.

The boiler mantle has 850 mm in diameter and 1100 mm in length. The flame tube has a 600 mm external diameter.

The boiler constructive and dimensional design was made by the "Politehnica" University of Bucharest. The original elements were proposed for patenting, to the competent authority in Romania.

The boiler has fully automated governing, which comprises: constant load operation by adequate control for the fuel feeding, for the ash evacuation and for the burning efficiency by furnace temperature and air excess.

The convective heat exchanger has a system of steel screws, mounted in every pipe, having the role to increase the heat exchange by swirling the flue gases and also to clean the pipe walls from ash deposits for the duration of the boiler operation.

For that purpose a rod was welded to each of the steel screws, making thus possible an alternating translation movement or a rotation (corresponding to the desired constructive variant).

It was demonstrated in the boiler operation, that a cleaning for 2 to 10 minutes, is needed for every 24 hours period.

The area of the grate surface is 0.32 m^2, while the gravimetric load of the grate is 105 kg/(m^2h).

The fixed bars grate has water cooling from the boiler mantle, for an amplified heat extraction process from the burning area. The volume thermal load of the grate volume is 470 kW/m^3. In Fig. 2, a view to the fixed bars placed in the mantle is presented.

Fig. 2 The 150 kW furnace and mantle constructions

In Fig. 3, a view of the boiler is presented, with the convective heat exchanger placed above the boiler body. Under the convective heat exchanger a system of boxes is placed for the capture of the ash after the cleaning.

In order to decrease the temperature in the burning area the fixed part of the grate is water cooled. The mobile bars are made of gray cast iron and they have an alternating movement.

Fig. 3 The 150 kW boiler view

In Fig. 4 the systems for the fuel feed and the grate bars drive (by a electrical motor actuator and rack) are presented. After the grate, the burning installation has a fuel and ash pusher, which regulates the burning processes finalizing.

The moving grates are made of grey cast iron and they have an alternating movement.

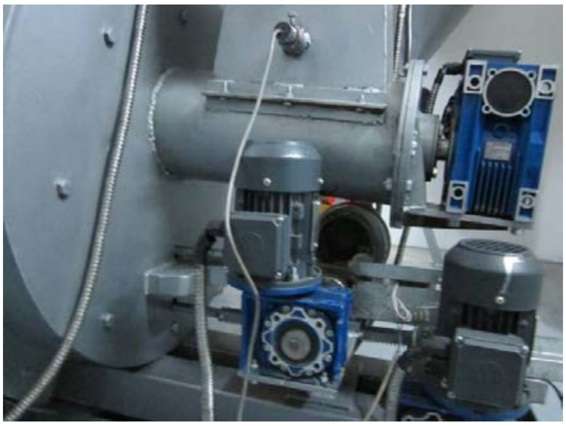

a.

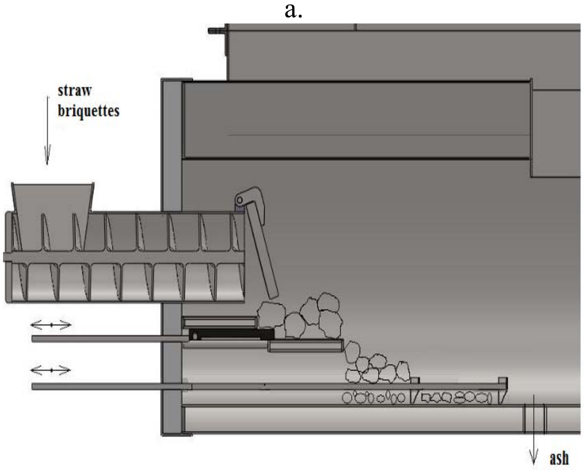

b.

Fig. 4 The fuel feed and grate drive systems
a – the view; b - the schematic drawing

The ash evacuation is carried out by two electrically driven worm systems that have automated sequential command. In Fig. 5 the worm system for the ash evacuation at the end of the flame tube is presented. The other worm system is placed under the grate.

The ash aspect, as seen in the Fig. 5, presents no agglomeration specific to reaching the melting temperature. The evacuated ash is deposited into a box; the ash evacuation deposit system is presented in the Fig. 6.

Fig. 5 View from the evacuation cover door

Fig. 6 The ash box view

The system of coupling helical worms for the cleaning the fume pipes of the convective heat exchanger to the actuator bars or racks is presented in the Fig. 7.

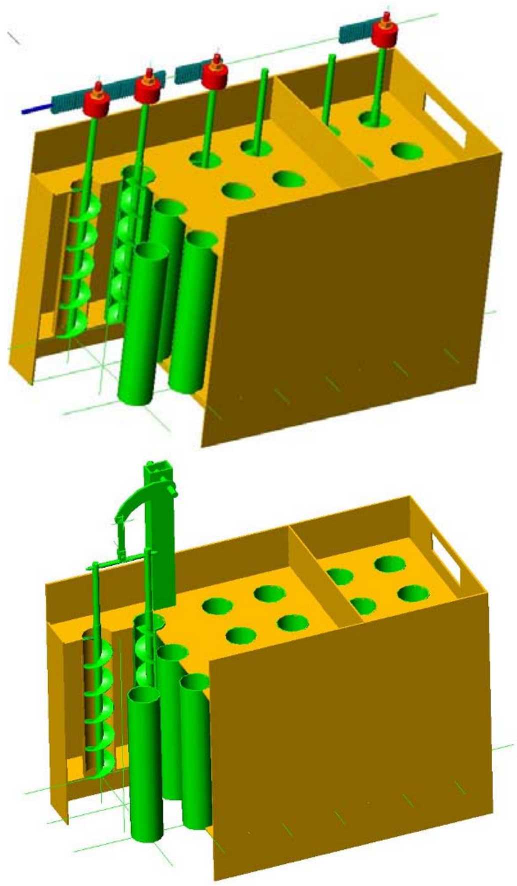

Fig. 7 Constructive variants for the mechanical drive of the ash cleaning worms

Overall boiler dimensions and mass are:

- length, 2900 mm;
- width, 1280 mm;
- height, 2000 mm;
- own mass, 1090 kg.

OPERATING RESULTS AND CONCLUSIONS

The load of the boiler was determined by measuring the water mass flow rate and the difference in temperature in the water network. The maximum efficiency was reached at the nominal load. The minimal accepted load for the boiler was imposed to be 40 % and the minimal efficiency value at the nominal load was 90-94 %.

The performances obtained during the winter season 2012/2013, permitted passing to fabrication of two more boilers. The delivery price for the fully equipped boiler (automated operation system included) is about 18,000 euros.

In Fig. 8 the aspect of burning in the fuel layer is presented.

Fig. 8 View of the straw briquettes burning in the boiler

Increasing the straw moisture up to 17 % did not influence considerably the efficiency of the installation. The decrease in the quality of the briquetting, with the density lowered to 650 kg/m^3, as a result of the higher moisture, lead to a decrease in the efficiency to (80-88) % values.

Admission of the primary air and the secondary air by separate ventilators creates advantages in the burning control, as well as the correlation with the speed of the fuel pusher.

The ash has a pulverulent aspect, being totally friable. For an operating period of 6 months, there were no situations of ash adherence to the furnace elements.

For an oxygen content of 11 % in the flue gases, the pollutant emissions were:

CO = 1300 - 2500 mg/m^3_N;

NO_x = 28 - 125 mg/m^3_N;

powders, under 30 mg/m^3_N.

The samples were taken at the gas exhaust before the cyclone separator, while the powder probing was made by a Bachart apparatus, placed after the separators.

The boiler endurance is characterized by these values:

- furnace cleaning of friable deposits, 7 to 10 days period;
- mechanical cleaning of the convective heat exchanger with boiler stopped, after 2 to 3 months period.

The paper presents especially the performance testing phase main measurements results and the original constructive features of this boiler, which is, so far, a singular development in cereal straw biomass energy valorization, in Romania, since all other boilers in the same thermal power range, use wooden pellets, briquettes and chips.

ACKNOWLEDGEMENTS

This work was supported by a grant of the Romanian National Authority for Scientific Research, CNDI – UEFISCDI, project number PN-II-IN-CI-2012 -1- 0259

REFERENCES

Mihaescu L., Bartha S., Enache E., Prisecaru T., Berbece V., Pisa I., 2011. Achievements in Biomass Valorization Using a Range of Boilers Made by Erpek-Romania and E-Morarit, HEEP 2011 Conference, Balatonfured, Hungary.

Pîşă I., Rădulescu C., Lăzăroiu G., Negreanu G., 2009. The Evaluation of Corrosive Effects in Co-Firing Process of Biomass and Coal, Environmental Engineering and Management Journal, 8(6): 1485-1490.

Rădulescu C., Lăzăroiu G., Pîşă I., 2010. Researches on the Negative Effects Asseessment (Slugging, Clogging, Ash Deposits) Developed at the Biomass-Coal Co-Firing. Enviromental Engineering and Management, 9(1): 17-25.

THE IMPACT OF USING COMPOST PRODUCED FROM BIODEGRADABLE WASTE ON SOME PROPERTIES OF SUGAR BEET

Miroslav Mimra*, Vlastimil Altmann, Miroslav Kavka

Czech University of Life Sciences Prague, Faculty of Engineering,
Department of Machinery Utilization, 165 21 Prague 6 – Suchdol, Czech Republic,
Phone: + 420 224 383 145, E-mail: mimra@tf.czu.cz

Abstract

This article presents the results of a four years' "small plot experiments", which verified the yields of sugar beets after fertilization using compost made from biodegradable waste; the compost was applied in doses of 25, 50, 75 and 100 t.ha^{-1}. The results were compared with experiments conducted without using compost. At the same time, the content of the following elements (K, N, P, Ca, Mg, Cu, Fe and Zn) was evaluated, as well as the content of polarized sugar. The effect of the compost application on biological hectare crop yield was statistically significant at level of α = 0.01 ($t_{0.1}$ = 2.897); what proved to be statistically non-significant was the effect of the compost application in connection with the content of polarized sugar. The best results of crop yield were achieved with the compost application in amount of 50 t.ha^{-1}. The plots of land with various rates of compost application showed a superior yield of sugar beet roots in comparison with the variant where no compost was applied.

Keywords: utilisation of biodegradable and organic waste, sugar beet, crop yield, sugar content

Introduction

Owing to decreasing numbers of livestock and thus a reduced production of manure, the utilization of composts may become a suitable mean for replenishing the organic substance of soil. Recently, an increasing number of cases have been reported which have shown that manure, non-composted plant residue, composts or their extracts reduced the occurrence of pests and diseases in crops. There have also been cases where these products (when added into the soil) had a positive impact on the condition of the soil which allowed for proliferation of beneficial microorganisms (Cayuela et al., 2005; Friend, 2004). The mechanism of plant residue action against pests is as follows: some plant residue secretes substances which are toxic to pests such as phenols, tannins, azadirachtins, and ricinin. Others release substances which are subsequently converted into toxic products, such as ammonia, nitrates, and hydrosulphides (Litterick et al., 2004).

The Kerner and Álvarez (2004) project focused on compost utilization testing as an alternative to chemical products. The results of the project confirmed the positive effects of compost obtained from bark and from biodegradable fraction of solid municipal waste against soil-borne diseases. Compost was used as a replacement for methyl-bromide which is normally used for soil disinfection and particularly for protection against Fusariumoxysporum, Phytophthora spp., Verticillium spp. as well as some other undesirable nematodes. Various amounts of additives were added to the tested composts. The compost pH was 6.5; during the composting process, temperatures of 60 °C were reached by a self-heating effect over a period of six days to remove micro-flora. Due to the higher pH level and lower accessibility of microelements, compost from the grapevine pulp demonstrated better effects against diseases compared with cork compost.

The results of research done by El-Nagdi and El Fattah (2011) showed that all plant residues, bio-fertilizer and organic compost alone (or in combination with biocides) significantly reduced the number of nematode juveniles in roots. All plant residues, bio-fertilizer and organic compost alone (or in combination with biocides) also significantly increased the studied sugar beet growth and the technological characteristics such as sucrose percentage, total soluble solids and juice purity. Moreover, there was a significant reduction in the number of juveniles, the galls and the eggmasses in sugar beet roots when plant residues, organic compost, nile fertile and biocides alone were added into the soil.

The positive effect of the application of vermi-compost was reported by Kopczynski et al. (1999): If it was applied together with fertilizer containing microelements, there was an increase in root yield as well as the sugar content of the beet. The compost was applied before and after sowing in the quantity of 60 tons per hectare. Vermi-compost applied before sowing improved the emergence rate of plants and reduced the amount of weeds.

Organic fertilization is the basis of the sugar beet fertilization system. Besides contributing to the supply of nutrients, it is the most significant factor for keeping the soil fertile. For sugar beet, all types of organic fertilization may be applied. Currently, 90 % of the sugar beet plantations utilize manure, making it the most highly used fertilizer. Amounts of manure differ according to the soil type. For medium-heavy and very heavy soils, preferable doses are 40 – 50 tons per hectare, while 30 – 35 tons per hectare will be sufficient for light soils with a good content of humus. Compost may also be used for fertilizing sugar beet. The advantage of using well-degraded composts is a possibility of subsequent under-ploughing.

Materials and Methods

The small-plot experiments have been established with three repetitions for each experimental alternative and five different treatments of compost application (see Tab. 1). All the experiments were repeated 3 times over a period of 4 years. The land used for the experiments may be characterized as flat with a loamy soil and pH of soil equal to 7.0; organic matter content 2.13 %, reduced bulk density 1.45 $g.cm^{-3}$, electric conductivity of soil 45 $mS.m^{-1}$ and compost 137 $mS.m^{-1}$. For more details see Tab. 2. The compost was made from biologically degradable waste – grass from permanent grass land maintenance took the main part of the compost material. Also leaves, wood chips etc. were used as well as soil and old compost (rate C:N – 33:1). In the autumn, the compost was applied onto the surface of the plot with subsequent under-ploughing every year. Each year, the same plot of land was used for each treatment. In spring, soil preparation and seeding took place.

During vegetative period, identical agrotechnical principles were applied within the complete experimental field. Apart from the application of compost, no fertilizer was used in individual treatments, both before seeding and during the vegetative period. A sufficient variety of sugar beet, “Impact”, was used for all combinations with a uniform seeding rate of 70 thousand plants per hectare. Twenty sugar beet plants were seeded on each 3 m^2 plot. Seeds were sown to the same depth of 30 mm in April. All treatments were regularly irrigated after sowing. Samples for analysing were taken every year. A summary of the combinations used during this experiment is given in Tab. 1. The plot where no compost was applied was used as a control and for comparisons.

Roots from each plot were harvested, cleaned, and counted. Leaves were cut away from the roots, which were then weighed. Biological yield of roots and leaves was recorded for all treatments. After completion of the harvesting from each treatment, a sample was taken to determine the polarized sugar content and other relevant parameters.

From each repetition of each treatment, three samples were taken (a total of nine samples per treatment). All samples of each treatment were mixed together and from this material, samples were taken for analysis. Samples of leaves were dried out at a temperature of 65 °C. The content of N by the Kjeldahl method was determined from those leaves:

P – colorimetric and K, Ca, Mg, Cu, Fe, Zn – spectrometric. From roots, the content of the polarized sugar yield was determined.

A comparison of the hectare yields was carried out using the one-sample t-test, which compares the sample mean and a certain constant value. The yield value for an alternative without the compost was used as a control constant.

Tab. 1 Scheme of the experiments – used alternatives for plant tests

Variants	Treatments
1	control, without compost
2	compost application in amounts of 25 $t.ha^{-1}$
3	compost application in amounts of 50 $t.ha^{-1}$
4	compost application in amounts of 75 $t.ha^{-1}$
5	compost application in amounts of 100 $t.ha^{-1}$

Tab. 2 Soil and compost properties (first year of experiment)

Properties	Soil	Compost
Texture	loamy soil	–
reduced bulk density ($g.cm^{-3}$)	1.45	–
pH – H_2O (1:5 v/w)	7.00	6.60
EC [$mS.m^{-1}$]	45.00	137.00
organic matter [%]	2.13	56.2
total N [%]	0.14	2.01
exchangeable Ca [me.100 g]	20.10	5.11
exchangeable K [me.100 g]	1.22	1.41
exchangeable Mg [me.100 g]	2.02	3.14
accessible P [$mg.kg^{-1}$]	12.00	23.00
accessible Cu [$mg.kg^{-1}$]	1.01	5.37
accessible Fe [$mg.kg^{-1}$]	12.10	23.40
accessible Zn [$mg.kg^{-1}$]	10.10	7.47

Results and Discussion

Tab. 3 and Tab. 4 show the obtained results – the average of all collected data each year after four year experiment periods. The effect of compost application on the yield of sugar beet roots and leaves, as well as the contents of nitrogen, phosphorus, potassium, were statistically significant. The highest biological yield of 105.5 tons (yield of roots plus top) per hectare was achieved for combination 3, where 50 tons of composts were applied per hectare. In contrast, the lowest yield was obtained for treatment 1 (control) without compost that provided biological yield of 72.3 tons per hectare.

The difference between the best and the worst alternative was 33.2 tons per hectare and the average biological yield for all treatments was 94.06 tons per hectare. Yields for treatments using compost were between 19.67 % and 31.47 % higher than the control treatments without compost.

The difference in biological hectare yield values in comparison with the control treatments without compost was shown to be statistically significantly higher ($t = 4.023 > t_{0.1} = 2.897$ upper-tailed test). Differences between combinations using compost were not statistically significant. The difference between the best and the second best result was only 1.03 %. The biological yield for sugar beet grew with an increasing amount of compost application.

If linear regression is used (R^2 = 0,512) for evaluation of applied amount of compost, then when increasing the fertilizer amount applied by 1 ton per hectare, biological yield of roots increased by 0.260 tons per hectare and yield of top leaves increased by 0.518 tons per hectare. The application of compost resulted in an increased biological yield of sugar beet. This explanation is only true to a certain extent because in nature, there is no linear influence for all range of values.

The difference of nitrogen, phosphorus, and potassium contents between control and others variants was also statistically significant. The content of polarized sugar, calcium and magnesium was reported as statistically nonsignificant (Tab. 3 and Tab. 4). Some authors describe the relation between phosphorus content and sugar content (Bremner, 1965; Cayuela et al., 2005), but during this experiment, the relation could not be confirmed. Nitrogen, phosphorus, and potassium contents rose with increasing compost amount. A statistically significant difference of calcium, magnesium, iron and copper contents in individual alternatives was not recorded (Tab. 4).

Various authors obtained differing results from their experiments. Some confirm the significant effect of compost upon sugar beet yield, but others did not detect such a significant influence. For example, Gaj and Gorski (2004) reported the effect of compost and nitrogen upon yield and technological properties of sugar beet roots with compost doses of 0, 10, 20 and 40 tons per hectare and nitrogen in a quantity of 0, 90, and 150 kg per hectare. The achieved yields of roots ranged from 68.7 up to 91 tons per hectare. The influence of compost and nitrogen fertilization was not proven in the first year, when experiments were established on light soils. On the other hand, it was proven for experiments established on heavy soils. The sugar content in roots was dependent upon the quantity of applied nitrogen, but the amount of compost applied did not have any influence upon the sugar content.

As published by Emmerling, Udelhoven and Schneider (2010) it was found that soil-quality parameters, such as soil organic matter and plant-available nutrient contents, microbial properties, aggregate stability, and the amounts of heavy metals can be improved by using of compost. This results were carried out in experiments done on arable soils of different rotation schedules applied with a total of 50 Mg dry mass ha^{-1} biowastecompost relative to an untreated control. Biowaste-compost application revealed an increase of plant-available P and K contents and aggregate stability in soil. The above mentioned results prove that biowaste compost can be useful as a source of some nutrients for plants and of some soil parameters' improvement. Also results of research by Kádar et al. (2009) prove that the yield and quality of sugar beet was decisively influenced by the available N quantity, provided the PK supplies satisfied crop needs. The maximum crude and pure sugar yields were obtained with a compost rate of 25 $t.ha^{-1}$.

Tab. 3 Analysis results of sugar beet plants from 5 variants – average of samples in a four year period

Variants	Beetroot yield	Leaves yield	Biological yield	Sugar content
	($t.ha^{-1}$)	($t.ha^{-1}$)	($t.ha^{-1}$)	(%)
1	51.5	20.8	72.3	19.9
2	59.9	30.1	90.0	20.3
3	69.2	36.3	105.5	20.4
4	65.1	37.2	102.3	20.5
5	66.4	37.8	104.2	20.4
Significance	*	*	*	N

Note: * – statistically significant α = 0.01, N – statistically non significant

Tab. 4 Analysis results of sugar beet plants from 5 variants – average of samples in a four year period

Variants	K	N	P	Ca	Mg	Cu	Fe	Zn
	(%)	(%)	(%)	(%)	(%)	(mg.kg^{-1})	(mg.kg^{-1})	(mg.kg^{-1})
1	4.38	4.44	0.54	1.38	0.86	14	84	33
2	5.51	5.71	0.71	1.40	0.84	11	88	36
3	5.27	6.32	0.78	1.35	0.85	13	85	43
4	5.43	6.73	0.77	1.33	0.87	14	91	59
5	5.50	6.88	0.80	1.39	0.86	14	86	50
Significance	*	*	*	N	N	N	N	*

Note: * – statistically significant $\alpha = 0.01$, N – statistically nonsignificant

Conclusion

The performed experiment compared the influence of applied compost upon the biological yield of sugar beet. With the increased compost amount, the biological yield rose; this has also been confirmed by other authors. The best results were achieved when 50 tons of compost per hectar was applied each year. When the increase of additional yield slows down, due to the lack of certain elements important for plant growth, the Liebig's Law of minimum fertilizer elements may play a role here. As stated by Montemurro et al. (2002), compost may be applied successfully to vegetation, especially when it is complemented and mixed with mineral nitrogen. Based on their statement, this leads to increased yield and better utilization of soil nitrogen by plants. Experiments performed in Italy, Tugnoli (2002) concluded that the sugar beet yield is influenced not only by the amount of compost used, but also the periods when it is applied to sugar beet. He also states that compost application allows reducing the mineral nitrogen dose.

Acknowledgments

This paper was processed within the framework of the Research Project of CULS Prague, No. 31900/1181/1818“, financed by Ministry of Education, Youth and Sports of the Czech Republic.

References

Cayuela M.L., Sánchez-Monedero M.A., Molina J., Roig A., 2005. Compost production from olive oil processing. BiocycleWorld, 46 (2): 64-65.

El-Nagdi W., El-Fattah A., 2011. Controlling root-knot nematode, meloidogyne inkognita infecting sugar beet using some plant residues, a biofertilizer, compost and biocides. Journal of Plant Protection Research, 51 (2): 107-113.

Emmerling C., Udelhoven T., Schneider R., 2010. Long-lasting impact of biowaste-compost application in agriculture on soil-quality parameters in three different crop-rotation systems. Journal of Plant Nutrition and Soil Science, 173 (3): 391-398.

Friend D., 2004. Using Compost to Reduce Irrigation Costs. Bio Cycle World, 45 (12): 33-35.

Kádar I.L., Petróczki F., Hámori V., Morvai B., 2009. Effect of communal sewage sludge and slaughterhouse waste compost on soil and crops in a field experiment. Agrokemiaes Talajtan, 58 (1): 121-136. (in Hungarian)

Kerner A., Álvarez J.M., 2004. Broadening Compost Use In Southern Europe. Bio Cycle World, 45 (10): 59.

Kopczynski J., Bury M., Denkiewicz J., 1999. The influence of surface application of vermicompost and calcium on the yield and quality of sugar beet roots. Folia Universitatis Agriculturae Stetinensis Agricultura. Akademia Rolnicza, Szczecin (Poland), Katedra Szczegolowej Uprawy Roslin, 78: 49-54. (in Polish)

Litterick A.M., Harrier L., Wallace P., Watson C.A., Wood M., 2004. The role of uncomposted materials, composts, manures, and compost extracts in reducing pest and disease incidence and severity in sustainable temperate agricultural and horticultural crop production – a review. Critical Reviews in Plant Sciences, 23 (6): 453-479.

Gaj R., Gorski D., 2004. Influence of compost produced from municipal solid wastes and of nitrogen fertilization on yields and technological quality of sugarbeet. Part I. Yields of roots and technological quality of sugarbeet. Biuletyn Instytutu Hodowlii Aklimatyzacji Roslin, 234: 145-154.

Montemurro F., Maiorana M., Convertini G., Ferri D., 2002: Effects of municipal solid waste compost on yield and nutritional status of the industrial crops. Attidel XX Convegno Nazionaledella Societa Italianadi Chimica Agraria, Padova, Italy 24-27. Septembre 2002, 287-294.

Tugnoli V., 2002. Quality compost: effective help for sugar beet. Rome, Italy: UNACOMA Service srl., Mondo Macchina., 11 (1): 26-29.

THE RELAXATION OF SPRINGS ON BELT-DRIVE SYSTEMS ON COMBINE HARVESTERS

Cestmir Mizera*, Vladimir Sleger

Czech University of Life Sciences Prague, 16521 Prague 6 – Suchdol, Czech Republic, Phone: +420 22438 3186, Fax: +420 234381828, E-mail: mizera@tf.czu.cz

Abstract:
The article discusses the problem with the use of compression springs on belt-driven tensioning components implemented on combine harvesters. Incorrect use of setting on the belt-driven tensioning component can cause the tension spring to be relaxed thereby causing a high temperature and lowering the effectiveness and lifespan of the entire drive system. The study concentrates on the main belt-drive system of the threshing system on the combine harvester using a quasi-static load on the compression springs. Tension strength on compression springs compressed at a length of 105 mm was used on a machine over a period of three, five, six, nine, and ten years. The reference value used to determine the drop of the tension force is a set of new springs with the average tension force of 1,445.8 N and a standard deviation of 16.4 N. The measurement results showed a 4 % decrease of the tension force when the machine was used for three years, 9.3 % (five years), 9.8 % (six years), 15.9 % (nine years), and 25.1 % (ten years). The article also shows a CAD model of the belt-drive system on the combine harvester and compression spring tensioner force ratios.

Keywords: combine harvesters, relaxation, springs

Introduction

We come into contact with the use of belt drives in the fields of agricultural technology more and more often. Ride control, easy maintenance, and especially protection of machines against overloading are just some of the benefits for which they are often used not only in the construction of modern combine harvesters. One of the very important elements of the belt transmission is the tensioning system. In order to allow belts to transfer peripheral force must be sufficiently pressed on the belt pulleys so that the tangential response was greater than the peripheral force. Tensioning system is for the transmission belt of agricultural machinery most often solved using tension springs. We make use of one of the important properties of a spring - it can accumulate supplied energy. Therefore it is often used just as a source of tension forces in belt drives and progressively replaces older systems, such as stretching by using weights. The principle is that the compression spring gets compressed by the screw and the nut to a certain value, and through mechanical transmission gear via connection rods and a two-arm lever using force on the tensioner pulley of the belt drive (Fig. 1). The spring is compressed to a specific value by using the dipstick and thus ensuring correct tensioning belt drive.

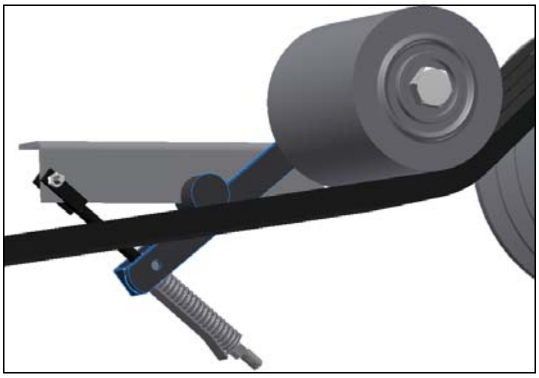

Fig. 1 A tensioner pulley of the belt drive with a spring

The problem lies in the fact that in long-term static weighted spring the pension forces are gradually reducing. It is not a new finding. Already in the mid-19th century, a famous physicist JC Maxwell said, that any weighted figure loses the ability to withstand the load over the time. It causes a reduction in voltage with time, relaxation.

Relaxation of springs is according to ČSN EN ISO 26909:2010 defined as the loss of the applied force at a constant deformation of the spring. Elastic deformation is gradually turning into a plastic one (Deda et al., 1997; Pothier, 1976). For the springs with the specified dimensions the loss of strength depends on temperature, time, voltage and material (Berry, 1961; Yu, Zhou, 2010; Dykhuizen, Robino, 2004).

Material and methods

Belt drive tensioning springs of combine harvester were used for the experiment. This is a medium power class tangential combine harvester with rated engine output of 270 kW. The purpose of these springs is to create sufficient tension forces for the main belt drive of the combine harvester (Fig. 2 and Fig. 3). The transfer is secured by a four-row V-belt and is used to transmit the power from the engine's gearbox and threshing mechanism. Tension springs of this transfer are cylindrical compression springs made of steel wire coated with corrosion treatment. Spring parameters are listed in Tab. 1. To create a tensioning force springs are permanently compressed to a length of 105 mm.

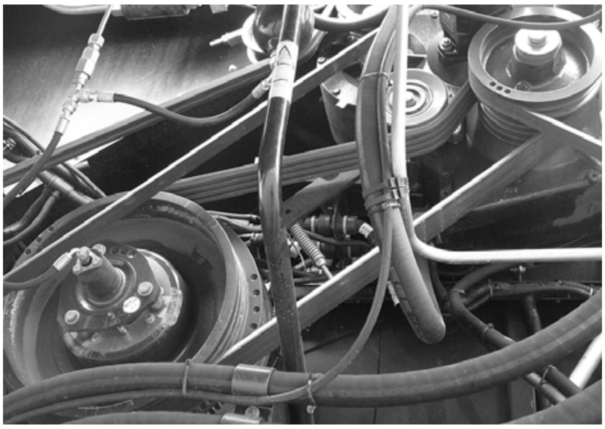

Fig. 2 Belt drive of a combine harvester with tensioning springs

For the experiment a total number of 10 pieces of tensioning springs, from combine harvesters with different times of operation of the machine, was selected. These are the periods of operations 3, 5, 6, 9, and 10 years, and each one was represented by two pieces of the tensioning springs. To determine reference values of the tensioning force of the new springs, 8 pieces of new springs as original spare parts from the manufacturer of the combine harvesters were purchased.

Tab. 1 Characteristic features of tension springs

Free length L_0 [mm]	Inner diameter D_m [mm]	Outter diameter D_v [mm]	Wire diameter d [mm]	Rigidity k [N/mm]	Number of threads n [-]
131	15	25	5	55,36	17

Before starting the experiment, dirt from the studied springs was removed to not affect the results. Subsequently, measurement took place using a pressure test, when the force depending on the deformation of the spring was recorded. Weighting speed was set at 30 mm/min. We run through three measurements for each spring, each with 24 hours interval between each measurement, and the average value was determined. Mainly the spring force, when pressing the length of 105 mm, which corresponds exactly to the value set in the machine, was observed.

All measurements were done on the MPTest 5,050 device from Labortech (Fig. 5a, 5b). The device allows us to perform tensile and compressive tests and store measured data in the control computer. Reported accuracy of the force of the measuring device is 0.1 N and sliding crosshead positioning accuracy is 0.001 mm.

Fig. 3 Drive model of a combine harvester in Autodesk Inventor 2012 environment

Power transferred by the V-belt depends also largely on the size of the tensioning force F_N (Švec, 1999). To determine the size of the transmitted torque, the components FN1 and FN2 (Fig. 4) from equation (1) are critical. These components will cause the desired tangential reaction between the belt and the pulley to transfer the necessary peripheral force. The decrease of tension force thus causes a corresponding decrease in the transmitted torque.

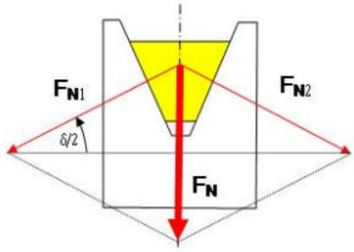

Fig. 4 Force ratios in the belt

$$F_{N1} = F_{N2} = \frac{F_N}{sin\left(\frac{\delta}{2}\right)} \quad \text{(N)} \qquad (1)$$

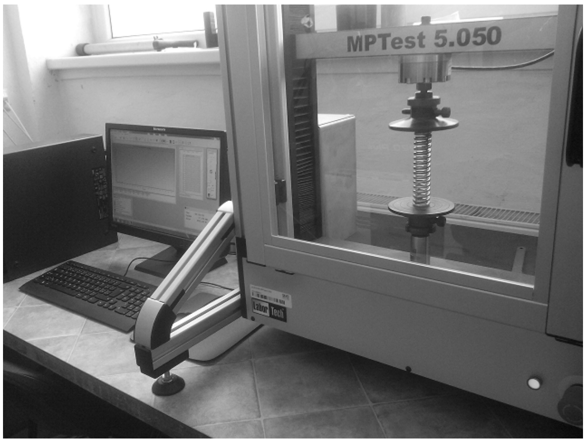

Fig. 5a Measuring device Labortech MPTest 5.050

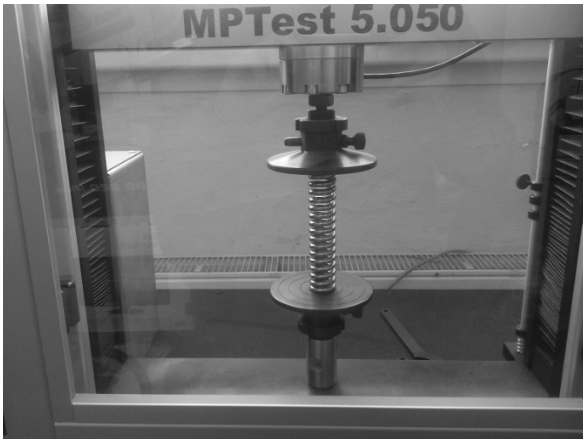

Fig. 5b Measuring device Labortech MPTest 5.050

Results and discussion

Of the eight pieces of new springs an average tensioning force for compressing the springs to the working length 105 mm, was determined. The average value of tensioning force for new springs was 1445.8 N with a standard deviation of 16.4 N.

Fig. 6 shows the measured values of the tension springs of combine harvesters. From Fig. 6 it is evident that there is significant reduction in the tensioning force in the belt transmission over a period of operation. The time of operation of 10 years causes the tension strength to decrease by 25.1 %.

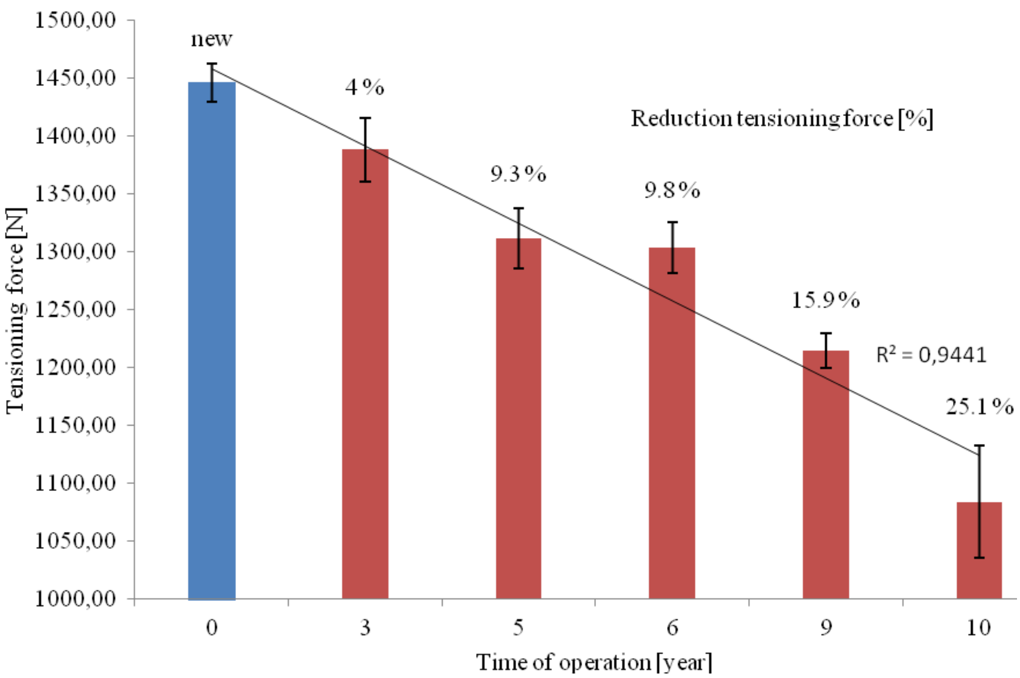

Fig. 6 The dependence of the tensioning force on the machine's time of operation

Conclusion

Improper tension of the belt transmission causes problems in power transmission. If there occurs a reduction of the tension force during the operation, for example due to relaxation of tension springs, an increased slip between the belt and the pulleys occurs, and thereby the efficiency of the entire drive is reduced. Increased slippage can also occur by increasing the temperature between the belt and the pulleys, and rapid wear-out of the drive and a faster degradation of the material properties of the rubber belt. On the contrary, when the belt tension is too large, there is a higher straining of the belt and the bearings of belt pulleys.

References

Berry W.R., 1961. *Spring design*. 1st ed. London: EMMOTT, 324.

ČSN EN 13906-1, 2003. Cylindrical helical springs made from round wire andbar-Calculation and design-Part 1: Compression springs. Czech Standards Institute, 36.

Deda S., Zhishou Z., Xinhua W., 1997. Research on Anti stress relaxational ability of helical compression springs made of austenitic stainless steel wires. Steel Wire Products, 2(5): 6.

Dykhuizen R.C., Robino C.V., 2004. Load relaxation of helical extension springs in transient thermal environments. Journal of Materials Engineering and Performance, 13(2): 151 - 157.

Pothier N.E., 1976. Observed load deflection characteristics of belleville springs under static loads at room and elevated temperatures. 1st ed. Chalk River: Atomic Energy of Canada Limited, 24.

Švec V., 1999. Parts of machines. Part 1. Praha: CTU, 174. ISBN 80-01-01934-9

Yu Y.Z., Zhou X.Y., 2010. Experimental research on stress relaxation of diskspring used for laser optical mounts. Advanced Materials Research, 129-131: 531 - 535.

ACTIVE LEARNING SENSOR FUSION SYSTEM FOR CROP DISEASE DETECTION

Dimitrios Moshou[1*], Xanthoula-Eirini Pantazi[1], Dimitrios Kateris[1], Ioannis Gravalos[2], Abdul Mounem Mouazen[3]

[1]Aristotle University of Thessaloniki, School of Agriculture, Laboratory of Agricultural Engineering, 54124, Thessaloniki, Greece,
Phone: +302310998721, E-mail: dkateris@agroauth.gr
[2]Technological Educational Institute of Larissa, School of Agricultural Technology, Department of Biosystems Engineering, Larissa, Greece
[3]Environmental Technology and Science Department, Cranfield University, Bedfordshire MK43 0AL, United Kingdom

Abstract

For sustainable intensification of production, inputs must be applied within recommended environmental constraints. The necessity of data fusion and active learning in the case of crop disease sensing emanates from the limitations of real-time crop monitoring due to the sole reliance on one crop measurement to indicate incidence of disease and the assumptions used for treatment strategy. However, in addition to nitrogen status, the spatial variation in a canopy colour could be due to a number of interrelated factors, such as other nutrients, drainage and diseases. This necessitates the need for information on crop to be fused in order to recognize the current context and aid decision support for management.

Feature level sensor fusion is accomplished through augmentation of features extracted from different sensors and joint consideration of the concatenated feature vector by data fusion techniques. The extracted fusion features are then used in the performance assessment and prediction modules. Intelligent fusion algorithms can produce reliable estimates related to crop health status based on sensory information from hyperspectral and fluorescence sensors. The context information regarding crop health status is extracted from mapping of categorical attributes resulting from spatial results of fusion classifiers. Spatially variable decisions are then inferred as consequents of combinations of sensor data.

In this paper, a new active learning method is proposed, which distinguishes between healthy and diseased crop (wheat) based on their different sensor fusion signatures. A method comprising novelty detection and incremental class augmentation was implemented. Novelty detection was based on one class classifiers.

Keywords: sensor, crop, autonomous robots

1. INTRODUCTION

The use of optical sensing through vehicle-mounted instruments provides a solution to the problem of automatic disease and stress detection. The difference in spectral reflectance between healthy and diseased wheat plants was investigated in order to use it as a means for automatic detection of plant stresses. Further, fluorescence kinetics measurements were used to gain extra information about the stress situation of the plant. The spectral reflectance was measured by means of an imaging spectrograph (Herrala et al., 1994) in order to detect different stresses as early as possible. Fluorescence Kinetics measurements were made in order to enhance stress discrimination through sensor fusion with the reflectance measurements. The fluorescence was recorded with the PEA (Plant Efficiency Analyser) fluorimeter. Multisensor fusion was used together with hyper spectral imaging.

1.2 Experimental Set up

During the experimental trials, the following simultaneous measurements were made on the same samples:

- Fluorescence kinetics on wheat plants (Hussar variety) infested by Septoria tritici;
- Spectral images obtained by a spectrograph.

The samples used for the tests consisted of "boxes" (60x40x23 cm; 60x40x15 cm) of wheat plants sown in four rows (approximately 20 plants per row) and grown in a suitably climate controlled greenhouse. The trials were carried out on four adjacent boxes (0.96 m^2 surface area) placed on trolleys, and the resulting density was in the order of 300-350 plants/m^2. All the measurements were conducted in such a way in order to simulate, to a good approximation, the conditions of crops in the open field. The experimentswere conducted on wheat (optimal level of nitrogen) infested by septoria [s+] or healthy [s-] in the presence [w+] or absence [w-] of water stress. The water supply in the soils of the investigated plants was measured by a Time Domain Reflectometer (TDR) and in addition pressure head measurements were performed. Water stressed plants were considered those that had a pressure head above 10^3 cm. Soil suction measurements were also used to verify the presence of water stress.

1.3 Optical instrumentation

Hyperspectral images were obtained through a visual spectrum of each point on a narrow linear stripe on the target surface (Heralla et al., 1994). It consists of three parts: an objective lens, an imaging spectrograph, and a camera. The system used was designed and made commercially available by Specim. Spectra from wheat leaves were obtained and normalised using ambient light based normalisation in order for the spectral magnitudes to become independent of lighting conditions as in Bravo et al. (2003). The fluorescence was recorded with the PEA (Plant Efficiency Analyser) fluorimeter of Hansatech. The fluorescence is excited by ultra-bright LEDs with a peak wavelength of 650 nm. Chlorophyll fluorescence signals are detected using a PIN photocell after passing through a long pass filter (50 % transmission at 720 nm). The recording time during the experiments was 1 s with a resolution of 10 µs during the first 2 ms and after that with a resolution of 1 ms. A leaf clip was used to avoid the entrance of ambient light into the photocell. The plants were dark-adapted in a room for at least 20 min. The upper side of a leaf was measured, roughly in the middle of the leaf, during one second with the PEA. On the septoria infected plants only the diseased leaves were measured on the healthy looking part of a diseased leaf (only the tip of the diseased leaves turned yellow-brown).

1.4 Fusion of optical sensing data

Multi-sensor data fusion systems combine data from multiple sensors to perform inferences that may not be possible from a single sensor alone (Hall, 1992), (Dam et al., 1996). Applications span military problems (target identification, threat assessment), remote sensing problems (location of mineral resources), medical diagnosis, control of complex machinery, autonomous robots and automated manufacturing. Data fusion is analogous to the ongoing cognitive process used by humans to integrate data continually from their senses to make inferences about the external world.

For fusion of different sensors, spectral features were integrated with fluorescence kinetics features. Four different treatments were produced in order to induce different stress situations that had to be detected. The four treatments were coded and performed according to the following list:

1. s-w-: control treatment, healthy and well supplied with water
2. s+w-: inoculated treatment with septoriatritici, well supplied with water
3. s-w+: healthy treatment, deficient water supply
4. s+w+: inoculated treatment, deficient water supply

Spectral data consisted of 21 features, each one representing 21 nm wavebands covering the spectral region of the spectrograph. The fluorescence data consisted of two features:

- F_0 : fluorescence at 0.05 ms
- F_V/F_M : efficiency of the primary photochemistry

Further, the spectral features were combined with two fluorescence features in order to try a fusion of the two sensors.

2 MATERIALS AND METHODS

2.1 One Class SOM

At first, a one class SOM (OCSOM) is trained with normal operation data. Then the feature vector corresponding to the unidentified measurement is compared with the weight vectors of all map units, and if the smallest difference exceeds a predetermined threshold, the process is probably in a fault situation (or deviation from normality).

This conclusion is based on the assumption that a large quantization error corresponding to the operation point belonging to the space not covered by the training data. Therefore, the situation is new and something is possibly going abnormal. Depending on how far away the current process is deviating from the normal operation state, a quantitative degradation index can be calculated.

In the plant condition monitoring application, the one-class SOM (OCSOM) builds a model from training on healthy plant data and then classifies test data as either normal or outlier based on its geometrical deviation from the healthy training data. During novelty recognition, the unseen exemplar from a vector consisting of a fusion of optical features of unknown health state forms the input to the network and the SOM algorithm determines the best matching unit. If the vector distance or quantisation error between the best matching unit (bmu) and new exemplar data ($\mathbf{x}^{\mathbf{NEW}}$) exceeds some pre-specified threshold (d) then the exemplar is classified as novel. Eq. 1 gives the minimum vector distance for the bmu and compares this to the threshold.

$$\min\left(\sum_{j=0}^{n-1}(\mathbf{x}_j^{NEW}-\mathbf{m}_i)^2\right) > d,\ i \in M \tag{1}$$

Where M represents the SOM grid of neurons $\mathbf{m}_i$.

There are many different heuristics to define a threshold depending on the utility of the threshold and the particular structure of the data set. A simple way to determine a threshold (d) relies on the distances between codebook vectors and target vectors in the training set that have selected them as bmu which is a measure of the quantization error. These distances have to be calculated first according to Eq. 2:

$$\text{distances} = \min\left(\sum_{k=0}^{N-1}(\mathrm{x}_k^{TARGET}-\mathrm{m}_i)^2\right),\ i \in M \tag{2}$$

The threshold is determined according to the Matlab code given here which is further explained below:

```
distances_sorted=sort(distances);
frac=round(fraction_targets*length(target_set));
threshold=(distances_sorted(frac)+distances_sorted(frac+1))/2;
```

By selecting the threshold to represent a fraction of the distances for the whole training set we can get distance values representing the most proximal to the codebooks data vectors when the distances are sorted. In this case the quantisation errors might be due to outliers so the fraction error would represent the distances that were calculated for a distribution of the distances including outlier values. By taking the 99 % fraction of the distances between data and codebooks as belonging to the dataset we define a description hypersphere that has a radius including the 99 % of the data. This leaves a 1 % outliers that will be classified as such since they exceed the target set description radius. In plain terms it means that by tightening the target data description we can afford to a number of false rejects in order to obtain a more accurate novelty detection which would be impossible with a very wide region of acceptance due to a very high threshold. In an explanatory schematic (Fig. 1) one can see the different areas defined by the threshold to the best matching units and the Voronoi polygons defining the domains of the OCSOM neurons. It can be seen that some data points that would be classified as belonging to a neuron now fall outside the threshold-defined polygon that delimits the target data from the novel data belonging to fusion signatures (combined hyperspectral and fluorescence features) from stressed plants (this is just an illustration, the actual data are high dimensional and cannot be visualized directly).

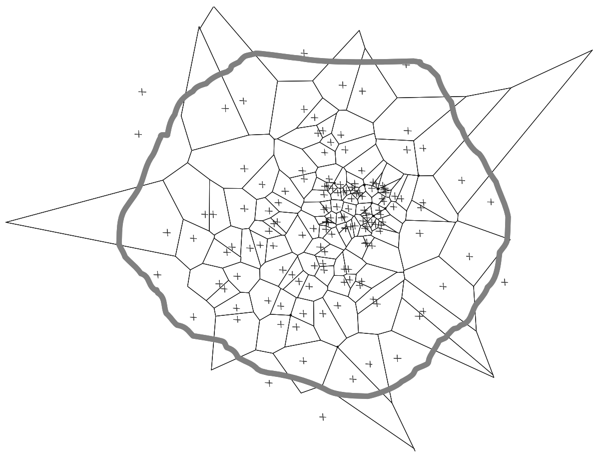

Fig. 1 Domains of target dataset and associated Voronoi polygons and threshold based classifier for OCSOM. The threshold defined target data fall inside the grey border line

An active learning method comprising of novelty detection and incremental class augmentation based on OCSOM, was implemented. A baseline set of fusion signatures from healthy plants were used as initial set. Then at each step, fusion signatures from plants that are exposed to different conditions such as water stress and Septoria infection were presented to the one-class classifier and after outlier detection, this condition type class was incrementally added in a multi-class classifier based on one-class binary classifiers. This step was repeated until all plant condition classes were augmented. In this way, the active learning scheme can achieve continuous incremental learning upon encountering new plant condition types (stressed plants).

3 RESULTS AND DISCUSSION

The detailed active learning scheme comprised the following steps:

1) The initial training set comprised of feature vectors which were consisting of 23 features (21 spectral bands and 2 fluorescence features)

extracted from the different plant conditions that were caused by water stress, Septoria infection or both. From each plant condition (4 types) a total of 894 vectors were used corresponding to 220 healthy plants, 235 water stressed, 228 with Septoria symptoms and 211 with both. The trained one-class SOM was tested with 235 vectors from water stressed plants. The criterion of success is the ability to classify the unknown plant condition as outlier in comparison with the healthy plants which are considered as the baseline set.

2) The initial target set was augmented with outlier values from the just detected outlier plant condition and the resulting set was considered as the new baseline set. The procedure of outlier detection is repeated but the criterion of success is the ability to classify new plant conditions as outlier a comparison with the newly augmented baseline set that includes the healthy plants and the incorporated plant conditions (healthy, water stress, Septoria infected).
3) In the case that the new sample belongs to a class that is already included in the target set the detection of outliers is executed per class internally in the baseline set and the sample is classified in one of the existent subclasses of the baseline set.
4) Steps 4 and 5 are repeated and more specifically, the detection of the outliers and the augmentation are executed for unknown data that could belong to the already existent plant condition categories or could concern new unclassified categories of plant conditions. In the current work the repetition of the steps terminated after the creation of 4 different classes that correspond to the healthy plants and the 3 plant conditions (water stress, septoria infection, or both) that were investigated.

It must be noted that the overall procedure from steps 1 to 6 does not require external intervention but relies solely on outlier detection and augmentation steps that are performed automatically.

The results of the active learning procedure are presented in Table 1.

Tab. 1 Performance of the active learning scheme based on One Class SOM (OC-SOM) for different stress conditions

	s-w-	s-w+	s+w-	s+w+	outliers
s-w-	97.73%	0%	1.36%	0%	0.91%
s-w+	4.39%	85.53%	9.21%	0%	0.88 %
s+w-	0%	0%	99.05%	0%	0.95 %
s+w+	0%	0%	0%	99.15%	0.85 %

The suggested Active Learning scheme has similar results for Septoria and combined Septoria infection-Water stress incidence reaching 99 %. In the case of water stress the performance was lower and reached 85 % while in the case of healthy plants it reached 97 %. A possible explanation for this behavior might be that the healthy group includes individual plants that show senescence symptoms that are independent of the stresses that have been imposed as part of the presented experiments. The lower performance in the case of water stress symptoms can be explained from the similarity of the symptoms between Septoria and water stress exhibiting both the their presence by affecting the same optical bands so that the proposed spectral and fluorescence methods and their fusion does not provide enough discriminant information.

4 COCLUSION

Disease (septoria) and water stress on winter wheat plants were successfully detected through the use of non-destructive sensing. The sensors were a spectrograph and a fluorimeter. The developed technique used a hybrid classification scheme consisting of a multisensor fusion system and Active learning algorithm based on one-class Self Organizing Maps (OCSOM). The proposed active learning procedure learns incrementaly to classify diffferent plant conditions based on novlety detection which is based on one class classification and builds a multiclass classifier which achives high performance in discovering new, unseen plant condition classes.The samples that cannot be clasified in existent classes are categorized as outliers in an extra class. The developed system can learn to discover new classes of plant stress and augment them in a continuously learning system.

REFERENCES

Bravo C., Moshou D., West J., Mc Cartney A., Ramon H., 2003. DetailedSpectralReflection Information forEarlyDiseaseDetection in Wheat Fields. Biosystems Engineering, 84(2): 137-145.

Dam J., Krösse B., Groen F., 1996. Neural network applications in sensor fusion for an autonomous mobile robot. In L. Dorst & M. van Lambalgen & Voorbaak, F. (Eds.) Reasoning with uncertainty in Robotics, 263-277.

Hall D.L., 1992. Mathematical Techniques in Multisensor Data Fusion. Artech House, Boston-London.

Herrala E., Okkonen J., Hyvarinen T., Aikio M., Lammasniemi J., 1994. Imaging spectrometer for process industry applications. SPIE, 2248: 33-40.

IDENTIFICATION AND COMPARISON OF STEROL AND TOCOPHEROL COMPOUNDS OF IRANIAN GRAPESEED OILS

Sara Movahed

Assistant Professor, Department of Food Science, Varamin-Pishva Branch, Islamic Azad University, Varamin, Iran. Phone: +989123502181, E-mail: movahhed@iauvaramin.ac.ir

Abstract

Three samples of Iranian grapeseeds (Red grapeseed(R), White grapeseed(W) and Mixed grapeseed (M)) with two samples of import grapeseed oils (Italian(C_1) and English(C_2)) as control treatment were prepared. At first grapeseeds dried at 50°C for two hours and were milled separately. Each sample was put into Leaching Extractor System (It acts as soxhlet) and its oil was extracted by normal hexane solvent. Extraction of oil was based on semi- industrial and has been done in pilot. Some of physical and chemical properties of the grapeseed oil were assessed including free fatty acid content, peroxide value, fatty acid composition, induction period, nonsaponifiable matters, specifically sterols and tocopherols content. Based on the results, the highest oil percent and the lowest percent of free fatty acid content were for (R) and had a significant difference with the other treatments ($P<0.05$). On the other hand, C_1 and C_2 had the highest amount of peroxide value and the highest and lowest rate for time stability were for M and C_1, respectively. Also results of fatty acids profiles percentage of grapeseed oils by Gas chromatography showed that linoleic and oleic fatty acids were the dominant fatty acids, respectively. M and W had the highest and C_1had the lowest nonsaponifiable matters included of sterols, 4- methylsterol, triterpene alcohols, delta, beta, and alpha tocopherols, dimer and hydrocarbons, that were separated by Thin Layer Chromatography (TLC) followed by spray reagent Rudamin 6G in %0.05 ethanol. Then the extracted sterol and tocopherol compounds on TLC plates were purified and identified by Gas Chromatograpy (GC) fitted by a capillary column. M and C_2 had the highest and lowest sterol but W and C_2 had the highest and lowest tocopherol, respectively. The research showed that β-sitosterol was the predominaut sterol present with smaller quantity of campesterol, stigmasterol and other minor sterols. Also there were three tocopherols (α, β, and Δ) in grapeseed oils with the most abundant one, alpha tocopherol accounted for more than 90%.

Keywords: Sterol, Tocopherol, Grapeseed oil, Thin Layer Chromatography

Introduction

Grape tree known as *Vitis vinifera* belongs to Ampelidaceae family and it has ten different genera, but only its vitis genus has dietary application (EL-Mallah et al., 1998). Grapeseed accounted for 2.5% grapes weight and 20-26% of the pomade by weight. This difference contributed to different varieties and ripening rate of grapes. Grapeseeds has commercial potential to produce oil so that *vitis vinifera* seeds contained 6-20% oil (Yoo, Min, 2000). Thus one of principle applications of grape pomades particularly the seeds may be industrial and dietary purposes. Also, grape pomades are considered of environmental pollutants, while as by-product they must be converted to valuable products such as grapeseed oil. Grapeseed oil may be used safety as oil. It can be used in anti cholesterol and low saturated fatty acid diets due to its composition (EL-Mallah et al., 2000). This oil because of high linoleic acid content (68-79%) which is an essential fatty acid for human body and desired ratio of PUFA: SAFA, and also it is well heat-resistant oil and then may be desirable for dietary and frying purposes (Yoo, Min, 2000). Grapeseed oil also contained tannins such oligomeric proantrocyanosids which act against cardio-vascular disease and cancer (Heyden, 2004; Tekin, Velioglu, 2003). In addition grapeseed oil contained vitamin E (60-120 mg/100g) which is of the most effective natural antioxidants; therefore there is no need to add synthetic antioxidants to the extracted grapeseed oil (Browne, 1999). Also grapeseed oil containes natural resources of tocopherols and tocotrienols which are very effective antioxidants, thus this oil is resistant to oxidative deterioration though it has a high unsaturation rate (Curro, Micali, 2002). In addition due to a low content of linolenic acid, this oil has a stable flavor compared to soybean oil (EL-Mallah et al., 1998). Crude grapeseed oil contained 30-120mg/100g tocopherol compounds which are fat- soluble due to their long chain hydrocarbons.

There are different kinds of tocopherols depending on the numbers and sites of methyl in their benzol structure. Reduced methyl numbers in the benzol ring binding results in lower biological effect of tocopherol, thus the biological effect of alpha tocopherol is more than gamma and delta tocopherols, but antioxidant function of delta tocopherol is more effective than gamma, beta and alpha. Tocopherol compounds are of dietary importance, so given high amount of fenol compounds (tocopherols) in grapeseed oil, this oil is oxidation resistant in addition to nutritional value, its shelf life also improved (Mattick, Rice, 1999). The objectives of this study were to determine and compare physical and chemical characteristics of Iranian grapeseed oils and with imported grapeseed oils and to identify different sterols and tocopherols compounds and their contents in the oil samples.

Materials and methods

Sample preparation

Three samples of grapeseed were obtained from three grape juice producing plant of Iran, and two samples of imported grapeseed oils (Italian and English) were prepared as compared to control compounds. Table 1 shows all the treatments in this research. First the samples of grapeseeds stabilized in an oven at 50°C for 2h till their moisture reach to 6-7 percent (EL-Mallah et al., 2000). Then the samples separately were milled. Each sample was put into Leaching Extractor System (It acts as soxhlet) and its oil was extracted by normal hexane solvent. Extraction of oil was based on semi-industrial and has been done in pilot. A rotary evaporator under vacuum condition in 65°C was used for separation of the solvent in micella. All the chemical materials used in the trials were made by Merck Co., Germany.

Table 1. The treatments have been used in this research

Samples	Code
Red grapeseed	R
White grapeseed	W
Mixed (Red – White) grapeseed	M
Importing – Italy	C_1
Importing - England	C_2

Chemical tests

At first, fat content measurement of grapeseed samples was performed in three replicates according to soxhlet method. The solvent was normal hexane and the extraction time was 5h. At least chemical and physical properties of Iranian grapeseed oils were compared with grapeseed oil of Italian and English. Free fatty acid percentage of grapeseed oil was determined according to AOAC No. 940.28 through oil titration using 0.01 and 0.1 soda normal adjacent to fenol fetalein in three replicates for each sample (AOAS, 1999). Peroxid value was measured for each sample according to AOAC No. 965.33 in three replicates (AOAS, 1999). In order to determine the compositions and amounts of fatty acids, grapeseed oil samples methylated according to ISO standard No. 5509 (AOCS, 1997). Then the methyl esters were identified by gas chromatography (model varian star 6890, England) according to AOAC No. 963.22 (AOAS, 1999). Induction period of the grapeseed oils against oxidation was determined according to Iranian standard No. 3734 at 110°C for 3g of oil sample that used rancimat metrohm system model 743 (AOCS, 1997). Non saponifiable matters were determined as AOAC method No. 933.08. Initially 5g of grapeseed oil was saponified using alcoholic potash, then non saponifiable matters were extracted by diethyl ether and their percentage was calculated for each sample (AOAS, 1999). Then, these components were divided into different parts through thin layer Chromatography (TLC) and spraying Rudamin 6G reagents in 0.01% ethanol. Each section separately was removed and extracted by solvent diethyl ether and their percentage separately was calculated. Non saponifiable matters of soybean oil were used as markers. Tocopherols were identified according to standard AOAC No. 970.51 using thin layer chromatography (AOAS, 1999). On the TLC plate, sterol bands, 4-methy sterol, triterpen alcohols, and tocopherols (delta, gamma, beta and alpha) were placed, respectively. To identify the presense of any tocopherols in grapeseed oil samples, spraying Rudamin 6G in 0.01% ethanol as a reagent was used, thus the related bands were removed from the TLC plate and tocopherols extracted by solvent diethyl ether. Tocopherol compounds were identified according to Gas Chromatography ISO method No. 6799-1983. The condition of Gas Chromatography was: Nitrogen gas velocity: 0.6mm/min, Pressure: 230kPa, Amount of injection: 1μlit, Temperature of injection point: 250°C, Temperature of column: 198°C, Temperature of detector: 250°C and length of CP sill 88, capillary column: 120mm and packed with DEGS. All data were subjected to analysis of variance and the Duncan's multiple range tests was used to compare the treatment means.

Results

Table 2 shows the mean percent of oil in Iranian grapeseed samples. Also table 3 shows the mean values of free fatty acids, peroxide value, Induction period and nonsaponifiable matters of Iranian and importing grapeseed oils.

Table 4 shows the composition of Fatty Acid profiles percentage of grapeseed oils and table 5 shows the nonsaponifiable matters percentage of grapeseed oils.

Table 6 shows RF values and nonsaponifiable components in seven areas of chromatography plate. On the other hand table 7 and 8 show percent of tocopherol compounds in different grapeseed oils and tocopherol percentage and their types in grapeseed oils, respectively.

Table 2 The mean percent of oil in Iranian grapeseed samples

Samples	Mean of Fat (%)
R	19.6^{a}
W	10.51^{b}
M	9.9^{b}

Table 3 The mean values of Free Fatty Acids, Peroxide value, Induction period and Non saponifiable matters of grapeseed oils

Treatment	FFA (%)	Peroxide value (meq/kg)	Induction period (h/110°C)	Nonsaponifaction (g value/100g)
R	0.1^{a}	7.00^{a}	4.5^{b}	3.4^{b}
W	0.16^{a}	7.03^{a}	4^{b}	5.3^{a}
M	0.16^{a}	7.3^{a}	15.4^{a}	5.3^{a}
C_1	0.16^{a}	10^{b}	3.3^{c}	1.3^{d}
C_2	0.16^{a}	9.33^{b}	2.9^{d}	2^{c}

In each column, means that at least one common letter are not significantly different according to Duncan's test at level 5%

Table 4 Composition of Fatty Acid profiles percentage of grapeseed oils

Fatty acid	Samples				
	R	W	M	C_1	C_2
C_{14}:o	0.14^{b}	0.48^{a}	0.53^{a}	0.12^{b}	-
C_{16}:o	9.94^{c}	13.93^{b}	16.28^{a}	7.18^{d}	6.93^{e}
C_{16}:1c	0.20^{b}	0.77^{a}	0.66^{a}	0.10^{b}	0.10^{b}
C_{17}:o	0.14^{c}	0.45^{a}	0.45^{a}	0.38^{b}	-
C_{18}:o	5.29^{a}	4.96^{a}	4.86^{a}	4.10^{c}	4.41^{a}
C_{18}:1c	19.55^{bc}	18.62^{c}	13.59^{d}	20.70^{a}	20.30^{ab}
C_{18}:2c	62.55^{c}	53.00^{d}	54.95^{d}	66.68^{b}	67.63^{a}
C_{18}:3α	1.04^{b}	4.01^{a}	4.18^{a}	0.37^{c}	0.24^{c}
C_{20}:o	0.54^{bc}	1.89^{a}	1.78^{a}	0.20^{c}	0.22^{c}
C_{20}:1	0.18^{c}	0.37^{b}	0.91^{a}	0.17^{c}	0.17^{c}
C_{22}:o	0.19^{b}	1.00^{a}	1.09^{a}	-	-
C_{24}:o	0.14^{c}	0.52^{b}	0.72^{a}	-	-

In each row, means that at least one common letter are not significantly different according to Duncan's test at level 5%

Table 5 The nonsaponifiable matters percentage of Iranian grapeseed oil

Treatment	Sterol	4-methyl sterol	Triterpen alcohls	Tocopherols	Hydrocarbons
R	17^{bc}	12.7^{d}	15.0^{ab}	14^{ab}	15.4^{a}
W	16.3^{c}	18.4^{a}	14.8^{b}	14.3^{a}	14.8^{ab}
M	18.1^{a}	15.6^{c}	14.5^{b}	13.4^{b}	13.1^{c}
C_1	17.5^{ab}	16.6^{b}	13.1^{c}	13.4^{b}	10.3^{d}
C_2	15.3^{d}	15^{c}	15.6^{a}	12.5^{c}	14.2^{b}

In each column, means that at least one common letter are not significantly different according to Duncan's test at level 5%

Table 6 RF values and nonsaponifiable components on seven areas of chromatography screen

Nonsaponifiable matters	Spot of color	*RF values	Treatment R	W	M	C_1	C_2
sterol	Gray	0.106	17^{bc}	16.3^{c}	18.1^{a}	17.5^{ab}	15.3^{d}
4- methyl sterol	Brown	0.206	12.7^{e}	18.4^{a}	15.6^{cd}	16.6^{b}	15^{d}
Triterpen alcohls	Orrange	0.290	15^{ab}	14.8^{b}	14.5^{b}	13.1^{c}	15.6^{a}
Delta tocopherol	Yellow	0.381					
Beta tocopherol	Yellow	0.500	14^{ab}	14.3^{a}	13.4^{b}	13.3^{b}	12.5^{c}
Alpha tocoferol	Yellow	0.584					
Hydrocarbons	Brown	0.956	15.4^{ab}	14.8^{b}	13.1^{c}	10.3^{d}	14.2^{b}

* Relative Friction= The distance from beginning line / The distance passed by solvent

Table 7 Percent of sterol compounds in different grapeseed oils

Sterol type	R (%)	W (%)	M (%)	C_1 (%)	C_2 (%)
Chlostrol	tr*	tr*	tr*	tr*	tr*
Campesterol	5.7^{d}	6.2^{cd}	2.8^{e}	9.3^{b}	11.2^{a}
Stigmasterol	4.9^{c}	5.2^{c}	2^{d}	9.2^{b}	10.2^{a}
Delta – 5- 23- stigmastadianol	tr*	tr*	tr*	tr*	tr*
Beta-Sitosterol	75.1^{c}	77.1^{b}	69.4^{d}	78.3^{a}	76.5^{bc}
Delta-5- avenasterol	9.0^{b}	5.5^{c}	19.1^{a}	tr*	tr*
Sitosterol	tr*	tr*	1.2^{a}	0.9^{a}	0.7^{a}
Delta-7- stigmasterol	3.9^{b}	1.2^{cd}	5.5^{a}	1.4^{c}	0.9^{d}
Delta-7-avenasterol	0.9^{a}	0.8^{a}	tr*	tr*	tr*

tr* < 0.5%. In each row, means that at least one common letter are not significantly different according to Duncan's test at level 5%

Table 8 Tocopherols percentage and their types in grapeseed oils

Treatment	Δ-tocopherol	β- tocopherol	α- tocopherol
R	5.7^{a}	4.2^{b}	90.1^{a}
W	5.4^{a}	4.5^{b}	90.1^{a}
M	0.9^{c}	8.0^{a}	91.1^{a}
C_1	1.7^{b}	8.3^{a}	90^{a}
C_2	6^{a}	4.0^{b}	90^{a}

In each column, means that at least one common letter are not significantly different according to Duncan's test at level 5%

Discussion

As it shown at table 2, R sample had the highest oil percent and a significant difference with other Iranian grape seed samples while M had the lowest oil percent ($p<0.05$). The Iranian grapeseed oils content is about 10-20% depending on grinding method, seeds freshness, oil extraction method, cultivation and growth conditions, the kind of solvent, and grapes variety (Gattuse, Cilluffo, 2001). It was due to use of different varieties of grape in this study which led to different amounts of oil extracted. Gattuse reported that the amount of oil extracted from grapeseeds varied with grape variety (Gattuse, Cilluffo, 2001). Based on table 3, no difference in FFA percent was observed between imported and Iranian grape seed oil samples; however R treatment showed the lowest percent of FFA with all samples exhibiting standard amounts of FFA. This index indicates hydrolysis of oil and edible fats and is used for evaluation of initial quality of lipids (Lovass, 1992). Also the highest amounts of peroxide value were related to C_1 and C_2 treatments, respectively, and the lowest were related to Iranian samples (without significant difference with each other). Peroxide value is a useful tool for evaluation of oxidant stability of oils under storage (Gattuse, Cilluffo, 2001). In addition the highest amount of induction period was related to M treatment ($p<0.05$) and the lowest amounts of this index were related to C_2 and C_1 treatments, respectively. Also M and W treatments showed the highest amounts of unsaponicable compounds (without significant difference with each other), and C_1 showed the lowest amount of this index. A significant difference was observed between treatments. The results shows that Iranian red grapeseed R had the highest fat content and contained the lowest free fatty acid and peroxide value and Italian grapeseed oil C_1 had the lowest nonsaponifiable matters. In addition, the mixed grapeseed oil M had the highest Induction period (15.4h/110°C), then can be considered as desirable frying oils. Also results of fatty acids profiles percentage of grapeseed oils showed that linoleic and oleic fatty acids were the dominant fatty acids, respectively. The difference in fatty acid values is due to the variety and geographic conditions (Prror, Novakvic, 2001). Iranian grapeseed oils may be categorized in suitable cooking and frying oils because of higher induction periods than importing oils. All fats and oils consisted of compounds known as nonsaponifiable matters. Based on table5 the nonsaponifiable matters of grapeseed oils included sterol, 4-methyl sterol, triterpene alcohols, tocopherols, dimer and hydrocarbons. These compounds were identified using Thin Layer Chromatography. On the chromatography, strol, 4-methyl strol, tritripene alcohols, delta, beta, and alpha tocopherols, dimer compounds that produced during oxidation and they formed hydrocarbons. As it shown at table 6, the nonsaponifiable matters of grapeseed oils had different RF values and color. According to table 7 all oil samples showed trace amounts of cholesterol. This holds true for all vegetable oils. Further the highest amounts of campestral and stigmasterol was related to C_2 and C_1 treatments, respectively the lowest amount was belonged to M sample. Regarding β- sitosterol of C_1 and M showed the highest and the lowest amounts, respectively. C_1 had a significant difference with other treatments. The highest amounts of Delta -5- avenasterol was belonged to M sample (with a significant difference with the other treatments) while W showed the lowest amount. M sample showed the highest amount of sitosterol however no significant difference was observed between these treatments with the other treatments. With respect to Delta -7- stigmasterol the highest and the lowest amounts were belonged to M and C_2 treatments, respectively. The highest amounts of Delta -7- avenasterol were related to R and W treatments while the other treatments showed trace amounts ($P<0.05$). As one can see from table 8, the highest amounts of Δ - tocopherol were related to C_2 followed by W and R treatments (no significant difference with each other) while the lowest amount was belonged to M treatment. Moreover the highest amounts of β- tocopherol were related to C_1 followed by M treatment (no significant difference) and the lowest amounts were belonged to other treatments (no significant difference). α- tocopherol was predominantly found at all treatments so that it accounted for 90% of total tocopherols. No significant difference was observed between treatments ($P<0.05$). Tocopherols act as natural antioxidants and their amounts are correlated with unsaturated fatty acid contents. These compounds are classified into different kinds based on position of methyl group against aromatic ring. They contribute to inhibition of oil oxidation at room temperatures and at moderate temperatures (Wanasundara, Shahidi, 2005). According to table 7, β-sitosterol was the prodominaut sterol present with smaller quantities of campesterol (2.8-11.2%), stigmasterol (2-10.2%) and the mean of delta 5- avenasterol (6.8%). One of the important nonsaponifiable matters in grapeseed oil samples are tocopherols which dietary importance. Since Iranian grapeseed oils contained high tocopherols value which act as antioxidants, it extends the oil shelf life and its stability against oxidative deterioration.

Conclusion

Fats and oils are important parts of the human diet. Nowadays given the lack of domestic production of oil seeds in Iran, extraction oil from the wastes of industrial operations such as grapeseeds may be profitable. Grapeseed is accounted for 2.5% of the grapes, and since its Iranian varieties contained about 10-20% oil it can be considered as a new vegetable oil resource. In addition, in this study the presence of different tocopherol compounds in Iranian grapeseed oil samples was identified. Thus, while Iranian grapeseed oils had a high unsaturation rate, like the other grapeseed oils in the other countries (Lang, 1999), the above tocopherol compounds in Iranian oils caused its stability against oxidative deterioration which was supported by the results obtained from oil induction period oxidation. As a result, Iranian grapeseed oils may be recommended as a new vegetable oil for cooking and salad purposes.

References

American Oil Chemist Society, 1997. Official methods of analysis (16th edition), Oven storage test for accelerated aging of oils, AOCS press Champion IL: 6-7.

AOAS, 2001. Archives, 92nd Aocs Annual Meeting and Expo. Aocs, Archives Meeting Abstract.

Associtation of Official Analytical Chemist. 1999. Official methods of analysis of the AOAC, Arlington, USA.

Browne F., 1999. The estimation of vitamin E. Biochemistry Journal 52: 523-526.

Curro P., Micali G., 2002. Determination of tocopherols in vegetable oil by HPLC-Rivista, Italiana-delle-sostanze, Grasse, 61C29: 95-98.
EL-Mallah M. H., Soukra L. M., Gad A. M., 1998. Fatty acid composition of seed oil of grapeseed, Seifen-Delo-fette-watches, 97(25): 956-961.
EL-Mallah M. H., Soukra L. M., Gad A. M., 2000. Fatty and composition of seed oil grapeseed. Seifen oelo fette watches 25: 50-96.
Gattuse A. M., Cilluffo V., 2001. Grapeseed. II. Characteristics and composition of the oil, Rivista- della – societa-di-scienza- almentazion 21(1): 47-54.
Heyden S., 2004. Poly unsaturated and monoun saturated fatty acids in the diet to prevent coronary heart disease via cholesterol reduction. Annals of Nutrition Metabolism 36(3): 117-122.
Lang W. J., 1999. Cholesterol, phytosetrol and tocopherol content of food products and animals tissues. A.O.C.S, 27: 414-422.
Lovass E. A., 1992. Sensitive spectrophotometric method for lipid hydroperoxide determination. Journal of the American Oil Chemists's Society 69: 777-783.
Mattick L. R., Rice A. C., 1999. Fatty acid composition of grapeseed oil from Native American hybrid grape varieties. American Journal of Enology and Viticulture 27(2): 88-90.
Prror W., Novakvic N., 2001. Composition of fatty acid and tocopherols in some grapeseed oils from the palatinate. Zeitschift-fuer- lebensm ittelunter swchung. Und – for schuny 144(4): 252-256.
Tekin A., Velioglu S., 2003. A research on some compositional properties of melon seed and bitter almond, Gida 18(6).
Wanasundara P. K., Shahidi F., 2005. Antioxidant: Science, Technology and Applications. In Baily's industrial oil and fat product, John Wiley & Sons, Inc. New Jersey.
Yoo J., Shin D. H., Min B., 2000. Composition of grapeseed oil. Korean Journal of Food Science and Technology 16(3): 257-260.

INFLUENCE OF LIQUID CONTAMINANTS ON STRENGTH OF ADHESIVE BOND ON BASIS OF TWO-COMPONENT EPOXY ADHESIVE

Miroslav Müller[1*], Petr Valášek[2]

[1]Czech University of Life Sciences Prague, 165 21 Prague 6 – Suchdol, Czech Republic, Phone: +420224383261, E-mail: muller@tf.czu.cz
[2]Czech University of Life Sciences Prague, Czech Republic

Abstract

Degradation processes exert on adhesive bonds strength usually in a negative way. These degradation processes have to be clearly quantified with an emphasis on a potential area of application of products which contain the adhesive bonds. The aim of the experiment was an experimental research of mechanical qualities of the adhesive bond created by means of the two-component epoxy adhesive of a top world producer depending on the cyclic degradation process. The running degradation processes were related to the given environment and time. Test specimens were subjected to the degradation process according to standard CSN EN ISO 9142. The specimens were tested in the cycles according to CSN EN ISO 9142 consisting in the application of the cycle D5. The laboratory tests results show a linear decrease of the strength owing to the exerting of the liquid contaminants.

Keywords: adhesive bond strength, agricultural machine, bonding technology, constructional adhesive, contaminants, cyclic degradation

Introduction

The adhesive bonds enable to substitute welding seams and mechanical connecting elements, help to decrease the material fatigue and failure around the heat-influenced area. An effective application is namely in an area of a construction of coach-works of traffic means and agricultural machines which are very stressed objects on which a range of unfavourable mechanical, chemical and weather influences exerts.

Influences exerting on the adhesive bond during the time of its usage are regarded as the outside conditions that means the conditions of environment. These are influences exerting e.g. at storing, transport and installation of the product. A breach of mounting and installation rules and directives for a trial run can show themselves at own operations. Also a great group of factors which are called the working environment in total belongs among the set of outside influences. The working environment encompasses all influences exerting on the bond during its operation, the climatic factors as well as the factors having their origin in the own activity of the adhesive bond. The working environment exerts on the adhesive bonds all the time of their technical life. A degradation of the equipment is a consequence of the working environment exerting on each technical equipment.

Degradation processes exert on adhesive bonds strength usually in a negative way (Doyle, Pethrick, 2009). These degradation processes have to be clearly quantified with an emphasis on a potential area of application of products which contain the adhesive bonds. The adhesive bond contamination by a degradation medium cannot be always defended by constructional design. The situation is made hard namely for a fact that the contamination is caused mainly by liquid contaminants (Herák et al., 2009; Müller, 2013; Müller, 2011).

The aim of the experiment was an experimental research of mechanical qualities of the adhesive bond created by means of the two-component epoxy adhesive of a top world producer depending on the cyclic degradation process. It was two-component epoxy adhesive is resistant to the influence of liquid contaminants.

Materials and methods

Experiments were made according to the standard CSN EN 1465, which determines the tensile lap-shear strength of rigid-to-rigid bonded assemblies. The substance of the test is the determination of the maximum force, which acts parallel with the bonded surface and with the principal axis of the assembly till to the failure. This method corresponds to the operational stress. The measured force at the adhesive bond failure is the test result. The test samples are prepared by bonding of two adherents of dimensions 100 ± 0.25 x 25 ± 0.25 x 1.6 ± 0.1 mm. The specific overlapping is 12.5 ± 0.25 mm. Laboratory tests were carried out using the standardized test samples made according to the standard CSN EN 1465 from the constructional plain carbon steel S235J0.

Before bonding the surface of bonded samples was blasted using the Al_2O_3 of F24 grain size. Using the profilograph Surftest 301 following values were determined: Ra 2.1 μm, Rz 12.3 μm. On one sample the adhesive was applied so that the whole surface in designated length (12.5 mm) was evenly coated.

Authors Müller and Valášek (2012) compared the adhesive bond strength at the comparative tests of 8 epoxy adhesives. They found out that the bonds reached their maximum strength in the range of 0.1 to 0.2 mm of the adhesive layer thickness. On the basis of their research the layer 0.14 ± 0.02 mm was applied. The adhesive bond cut is visible in fig. 1. Fig. 1 presents securing the constant layer of the adhesive.

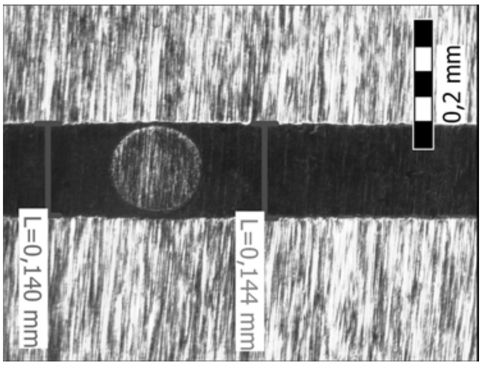

Fig. 1 Adhesive bond cut

In this layer two distance wires of 0.14 mm diameter were placed. The distance wires were laid down parallel to the load force direction of the tensile strength test. The assessment was left in the laboratory for in the instructions determined time (24 hours) for hardening at the temperature of 22 ± 2°C (temperature in the laboratory).

The running degradation processes were related to the given environment and time. Test specimens were subjected to the degradation process according to standard CSN EN ISO 9142. The specimens were tested in the cycles according to CSN EN ISO 9142 consisting in the application of the cycle D5.

The cycle D5 means hot-dry, hot-humid and cooling cycle (i.e. 48 ± 1 h in the conditioning chamber at temperature of 55 ± 2 ° C, 48 ± 1 h immersion in degradation medium, 24 ± 1 h in the cooling chamber at a temperature of -20 ± 2 ° C, 48 ± 1 h immersion in degradation medium). The samples were exposed to 0, 1, 2, 4, 6 and 10 cycles of the test. The testing cycle contained 10 test samples which were subsequently destructive tested. The number of test samples is visible from fig. 2.

Running degradation processes were related to the given environment at simultaneous regarding the time. At experiments focused on the influence of the environmental degradation, the samples were exposed to a cyclic operation of the water bath, the oil, the solution of the water with the mineral multi-component chloride free fertilizer NPK (Cererit) with sulphur, magnesium and trace elements (boron, molybdenum, copper and zinc), 33 % solution of halite and rain water, the diesel oil.

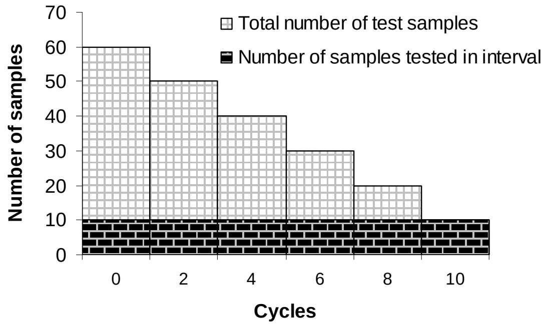

Fig. 2 Testing diagram – taking samples for destructive testing on universal testing machine

Each cycle was finished by the destructive testing of adhesive bond using the universal tensile-strength testing machine. After the bond rupture the maximum force was read, the overlapping length was measured with an accuracy of 0.05 mm and the failure type was determined according to ISO 10365 (1995).

Results and discussion

The common feature of the degradation environment is according to results a marked decrease of the adhesive bond strength, as it can be seen in that Fig. 3.

The variation coefficient ranged in the interval 4.7 – 11.5 % in single testing cycles. In laboratory environment the variation coefficient was 3.29 %. The water bath was distinguished for the variation coefficient ranged in the interval 5.1 – 11.1%, the solution of halite and water 5 – 10.2%, the diesel oil 5.8 – 9,6 %, the oil 4.7 – 11.5 % and the fertilizer 4.9 – 8.4%.

On the base of the evaluation of carried out experiments it can be said that the resultant adhesive bond strength decreases during the time with the environment action at the same time. The measure of the strength fall depends on the specific conditions of the environment.

The experimental results found out in 5 different environments/mediums confirm the statements of Kinloch (1987) and Court et al. (2001) about negative and harmful effects which the environment can have on the adhesive bond.

Conclusions released by Crocombe (1997) that the adhesive bond degradation depends on the degradation environment were confirmed by these experiments. This knowledge can be fully used in the elimination of the negative influence of the relevant environment.

At the experiments the failure area was of the adhesive type. The degradation environment had not an essential influence on the change of the failure area. The failure area change owing to the degradation processes is a function of the adhesive. Authors dealing with the change of the failure area state that it usually comes to the change of the failure area owing to the degradation process. Or to the increase of the adhesive failure area representation (Liljedahl, Armstrong, K. B. 1997, Kinloch, A. J. & Osiyemi, S. O. 1993, Müller talin 2013).

From the Fig. 4 (left) the adhesive failure area of the adhesive bond placed in the oil is visible. Fig. 4 (right) shows the corrosion of adhesive bonded material. The corrosive products penetrated also into the interface of the adhesive bond that means into the layer adhesive / adhesive bonded material.

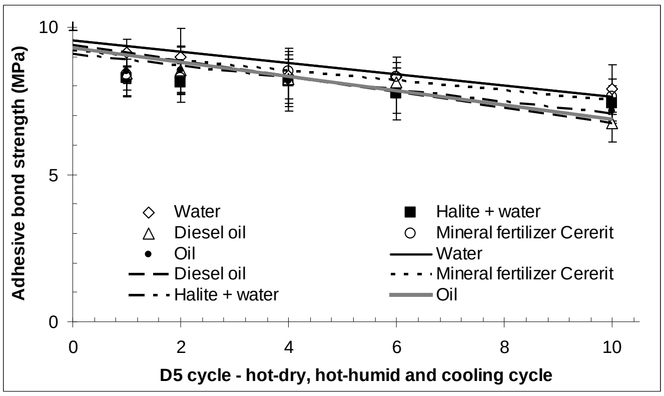

Fig. 3 Influence of degradation environment on adhesive bond strength

For the objective evaluation of the relation it is important to determine the dependence intensity. It is the task for the correlation analysis. The closeness of this relation is judged by means of the determination index, whose values can be from 0 to 1. When the values approach to 1, the relation is more intense. The closeness of the dependences among the adhesive bond strength and the degradation process is between 54 – 80%. By values introduction in equations presented in Tab. 1 it is possible to predict the further function course.

Fig. 5 shows the schematic presentation of the tensile shear strength results of adhesive bonds created by means of ANOVA by the lowest squares methods.

Tab. 1 Equations of regression functions and their determination index

Environment	Functional equations	Determination index $I^2_{\tau x}$
Mineral fertilizer Cererit	$\tau = -0.158x + 9.1322$	0.54
Diesel oil	$\tau = -0.2526x + 9.3185$	0.80
Water + halite	$\tau = -0.1886x + 9.0181$	0.59
Water	$\tau = -0.1827x + 9.4869$	0.80
Oil	$\tau = -0.2335x + 9.2449$	0.79

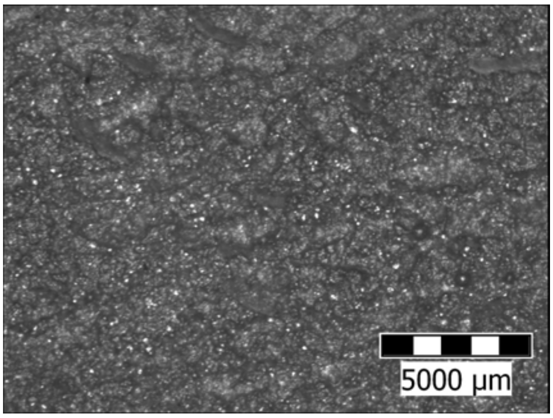

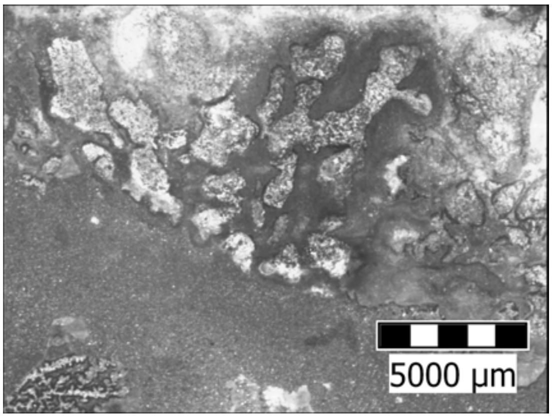

Fig. 4 Surface of bond – adhesive failure area – medium: oil, cycle 10 (in the left), corrosion of adhesive bonded material – steel S235J0 (in the right)

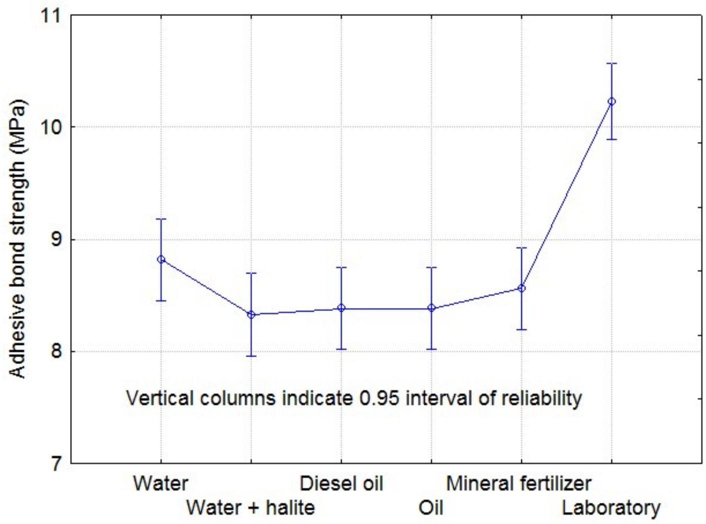

Fig. 5 Influence of environment on adhesive bond strength – arithmetical mean of values found out in cycles

Tab. 2 Statistical comparison of mean values – Tukey's HSD test

Environment	Arithmetical mean (MPa)	Agreement	
		1	2
Water + halite	8.29	****	
Diesel oil	8.38	****	
Oil	8.38	****	
Mineral fertilizer Cererit	8.56	****	
Water	8.82	****	
Laboratory	10.23		****

It was used Tukey's HSD test to compare statistical measured data sets. The pertinence of each average values to statistically homogeneous groups can be seen from Tab. 2, i.e. there are no statistically significant differences at a significance level of $\alpha = 0.95$ among data sets.

When comparing the mean values of the data sets of the adhesive bond strength it is visible the agreement among the degradation mediums. The laboratory environment is not identical with any other degradation environment.

Conclusions

On the basis of the carried out experiments it can be said that the resultant strength of adhesive bonds decreases during the time at simultaneous acting of the environment. The rate of the strength decrease depends on specific conditions of the environment. From the experiment results the hypothesis about the resistance of the two–component epoxy adhesives to the liquid contaminants was not certified.

These conclusions were set from the experiments:

- The laboratory tests results show a linear decrease of the strength owing to the exerting of the liquid contaminants.
- The change of the failure area does not depend directly on the degradation. The failure area was always of the adhesive type.
- The corrosion in the layer of the adhesive is one of the attributes having the influence on the decrease of the adhesive bond strength.
- According to Tukey's HSD test it was proved statistically homogenous groups at the degradation mediums. Various mediums have the same influence on the strength fall.
- The liquid contaminants diffuse into the layer of the adhesive and they lessen the functional area of the overlapping acting on the transfer of the loading force.
- The strength fall of the adhesive bonds is not direct proportional to the dispersion variance of the results of measured values.

Acknowledgement

Supported by Internal grant agency of Faculty of Engineering, Czech University of Life Sciences in Prague.

Reference

Armstrong K. B., 1997. Long-term durability in water of aluminium alloy adhesive joints bonded with epoxy adhesives. International Journal of Adhesion & Adhesives. 17(2): 89–105.

Court R. S. et al., 2001. Ageing of adhesively bonded joints – fracture and failure analysis using video imaging techniques. International Journal of Adhesion & Adhesive. 21(6): 455–463.

Crocombe A. D., 1997. Durability modelling concepts and tools for the cohesive environmental degradation of bonded structures. International Journal of Adhesion & Adhesives. 17(3): 229–238.

Doyle G., Pethrick R. A., 2009. Environmental effects on the ageing of epoxy adhesive joints. International Journal of Adhesion & Adhesives. 29(1) 77–90.

Herák D., Müller M., Dajbych O., Simanjuntak S., 2009. Bearing capacity and corrosion weight losses of the bonded metal joints in the conditions of Indonesia, North Sumatra province. Research in Agricultural Engineering 55(3): 94-100.

Kinloch A. J., 1987. Adhesion and adhesives – science and technology, 1st ed. London: Chapman and Hall, 425 pp.

Kinloch A. J., Osiyemi S. O., 1993. Predicting the fatigue life of adhesively-bonded joints. Journal of adhesion. 43(12): 79–90.

Liljedahl C. D. M. et al., 2009. Characterising moisture ingress in adhesively bonded joints using nuclear reaction analysis. International Journal of Adhesion & Adhesives. 29(4): 356–360.

Müller M., 2011. Influence of surface integrity on bonding process. Research in Agricultural Engineering, 57(4): 153 - 162.

Müller M., 2013. Research of liquid contaminants influence on adhesive bond strength applied in agricultural machine construction. Agronomy Research, 11(1): 147 - 154.

Müller M., Valášek P., 2012. Degradation medium of agrokomplex - adhesive bonded joints interaction. Research in Agricultural Engineering, 58(3): 83 - 91.

PRESENT ANT FUTURE COMBINED HEAT AND POWER IN CZECH REPUBLIC

René Neděla[1*], Radek Neděla[2]

[1]Czech University of Life Sciences Prague, Technical Faculty, 165 21 Prague 6 – Suchdol, Czech Republic, Phone: +4202, Fax: +4202-20923194, E-mail: nedela@tf.czu.cz
[2]University of Economics, Prague, Faculty of International Relations, 130 67 Prague 3, W. Churchill 4 SQ, Czech Republic, Phone: +420 224 09 5650, E-mail: xnedr01@vse.cz

Abstract

This paper describes the present and the future situation of the combined heat and power (CHP) in the Czech Republic. In first part of article are described principles of CHP from the viewpoint of the energy customer. Also there are presented cogeneration technologies that are covered by European Directives. In second part is described actual situation CHP in the Czech Republic and some information from past and future. Last part of this article is about future of cogeneration in the Czech Republic and heating industry.

Keywords: Combined heat and power, CHP, cogeneration, PES, primary energy savings

Introduction

CHP means combined heat and power (cogeneration); in Czech translation we are using combined power and heat; that is the simultaneous production of electricity and heat from single fuel source. The main advantage is that the CHP systems are able to recover waste heat produced from the generation of electricity. That's why cogeneration has higher efficiency (Flin, 2010) than separate production of electricity and heat. Best example how to explain the principle of CHP is to look at it from a viewpoint of the energy customer. See Fig. 1 where is described principle separate production of electricity and heat. As we can see energy customer needs 24 units of electrical power and 34 units of heat. For total 58 units of net energy (24 units of electrical power and 34 units of heat) required by the end user it is necessary to have 60 units for power plant and 40 units for boiler (total 100 units) for an overall efficiency of 58 %.

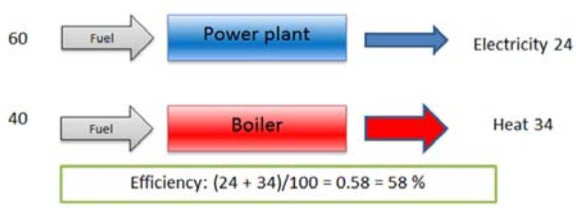

Fig. 1 Separate production of electricity and heat

For same customer (which needs 24 units of electrical power and 34 units of heat) by using CHP system is necessary just only 68 units see Fig. 2 for overall efficiency of 85 %.

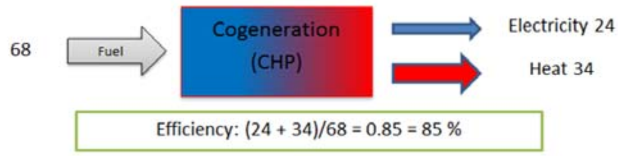

Fig. 2 Cogeneration (CHP) = simultaneous production of electricity and heat

As you can see in the both figures first advantage is that for same necessary units of energy (electrical energy and heat) for the end customer we will need less fuel units. Another advantage is to reduce losses. In separate production the losses are 42 units in CHP the losses are just only 10 units and we are not talking about losses that are caused by transport of energy (CHP is mostly decentralized source). If we have less fuel units and less distribution of production losses than we will have also lower emissions to the environment in particular CO2. So these are some of the advantages of CHP.

Cogeneration technologies:

- Combined cycle gas turbine with heat recovery
- Steam backpressure turbine
- Steam condensing extraction turbine
- Gas turbine with heat recovery
- Internal combustion engine
- Microturbines
- Stirling engines
- Fuel cells
- Steam engines
- Organic Rankine cycles

In the Czech Republic most popular are steam backpressure turbine, steam condensing extraction turbine and internal combustion engine (ERO, 2013). Fuel for turbines is mostly coal (because is cheaper than natural gas) and fuel for engine is mostly natural gas. But usually you can use a fuel such as bagasse, natural gas, coal, waste gas, biomass, liquid fuels and renewable gases.

Legislation

The basic legislation is anchored in Directive 2004/8/EC of the European Parliament and of the Council of 11 February 2004 on the promotion of cogeneration based on a useful heat demand in the internal energy market and amending Directive 92/42/EEC. At the end of 2012 came into force Directive 2012/27/EU of the European Parliament and of the Council of 25 October 2012 on energy efficiency, amending Directives 2009/125/EC and 2010/30/EU and repealing Directives 2004/8/EC and 2006/32/EC Text with EEA relevance (Ahner et al., 2012). The Czech Republic is the main legislation primarily in Act No. 458/2000 Coll., on business conditions and public administration in the energy sector and amending certain laws (the Energy Act), the Decree of the Ministry of Industry and Trade No. 453/2012 Coll., electricity from high-efficiency combined production electricity and heat and electricity from secondary sources and Price Decision of the Energy Regulatory Office No. 4/2012 of 26 November 2012 laying down support for electricity from renewable energy sources, combined heat and power production and secondary energy sources. Since 1st of January 2013, the conditions of CHP passes in the recently adopted Act No. 165/2012 Coll., on supported energy sources and amending certain acts. Along with the new act it was modified and the relevant implementing regulations are ready for a new implementing regulation.

The European Commission attaches great importance on CHP in achieving the primary energy savings and identified promotion of cogeneration as one of the necessary measures to reduce greenhouse gas emissions from power plants (EC, 1998). The promotion of cogeneration has been promoted document called the National Environmental Policy, which was approved by Government Resolution of 17 March 2004 (Schoots, Bouquet, 2009), (Hisham et al., 2013). It was also anchored in the document National Energy Policy of the Czech Republic approved by the Government on 10 March 2004 and updated in the new National Energy Policy of the Czech Republic approved by the Government 7 November 2012.

CHP in Czech Republic

Prevalence of CHP in the Czech Republic demonstrates the following map in Fig. 3, which shows the percentage of CHP in gross electricity production (Eurostat, 2013). Average in Europe in 2010 was 11.7%, Czech Republic reached the border of 14.2%, which is above the European average.

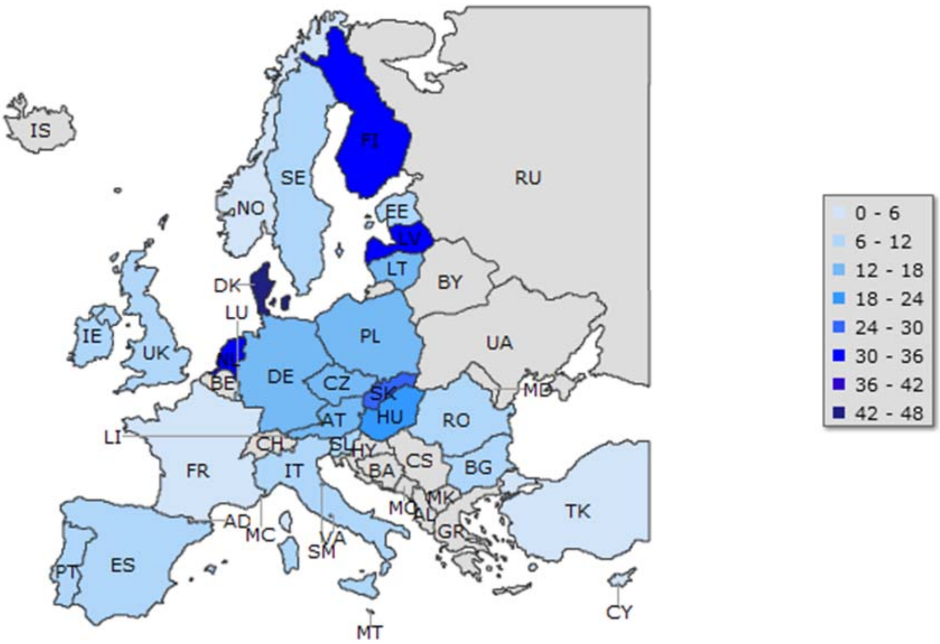

Fig. 3 Combined heat and power generation - % of gross electricity generation *(Eurostat)*

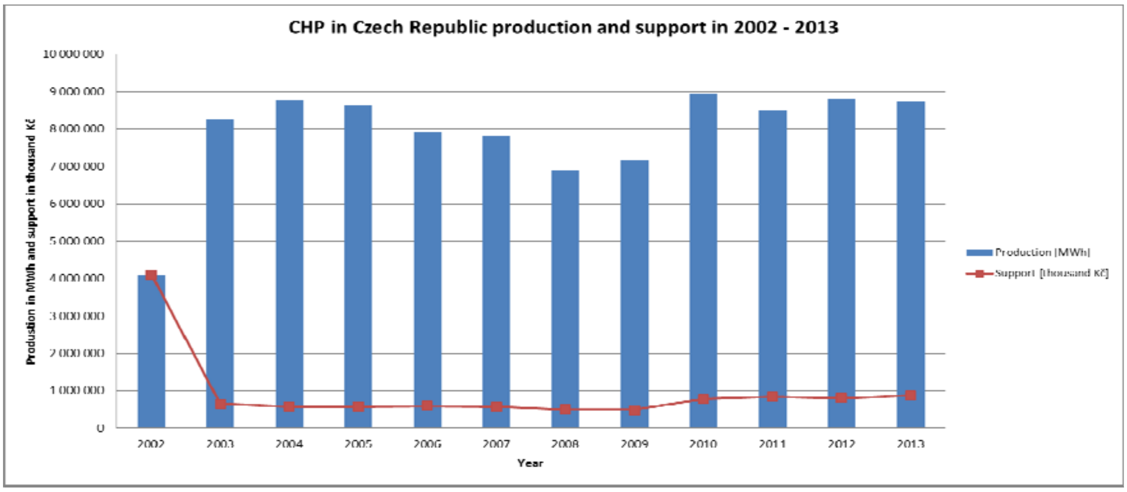

Fig. 4 Production and support CHP in Czech Republic in 2002 – 2013 *(ERO)*

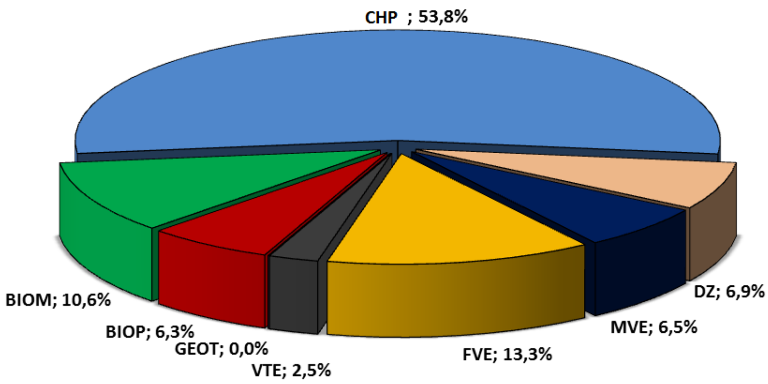

Fig. 5 Production structure from the supported sources 2011 *(ERO)*

Operational support in the Czech Republic since 2002, when it was gradually changing in relation to the change of input parameters, such as the cost of fuel, energy price inflation and the change in categories for which aid is paid from a simple division into two categories into a above 5 MW to more complex division to 1 MW, 1-5 MW over 5 MW, burning and renewable energy sources for five 10 MW natural gas combustion. Currently, the amount of operating aid divided on the basis of installed capacity, operating time, and primary energy savings. The amount of total aid paid in respect of the electricity produced is shown in Fig. 4 (ERO, 2013).

In 2011 production of electrical power from CHP was 8.5 TWh that is 54 % from all supported sources (supported sources = renewable sources, secondary sources and CHP) Fig. 5.

In Czech support scheme for CHP is Feed in Premium (in Czech we call it green bonus). Feed in premiums (FIP) is a premium paid to the producer on top of the electricity market price for MWh (Oberthur, Pallemaerts, 2010). In 2013 the support scheme for CHP has changed. Still there is FIP just conditions changed. Till this time the support scheme was just only up to installed capacity and day tariff (8/12/24 hours). In 2013 Energy Regulatory office changed this system to operating time and parameter primary energy savings (PES). Now producers at the beginning of the year the must choose how many hours per year they will operate. According operating time the FIP is lower or higher (less hours of operate higher support). This will cause that the producers will operate just only when they will have maximum efficiency. Second change – parameter PES, if your installed capacity is till 5 MW than your parameter PES must be positive (higher than 0 %), if installed capacity is higher than 5 MW than PES must be higher than 10 %, if you are below (0 % and 10 %) than you will not receive support. If your installed capacity is higher than 5 MW and your parameter PES is higher than 15 % than you will receive extra bonus because your device is extra high efficiency according to separate production. Last change is in new group small CHP with installed capacity maximum to 200 KW. This support scheme change is according to the European Commission and National Energy Policy of the Czech Republic.

Parameter PES:

PES parameter characterizes us what is the primary fuel savings compared to separate production. This parameter can also be a negative character and it would mean that the efficiency of cogeneration is less than the efficiency of separate production (ie the basic rule, why it supports the combined production would be suppressed). Parameter PES is calculated as the ratio of thermal and electrical efficiency of the specific production and is divided by the ratio of the reference efficiency separate productions (Ottinger et al., 2005). The basic relationship for production of one type of fuel and the equipment put into service in one year is:

$$PES = \left(1 - \frac{1}{\frac{CHP\,H\eta}{Ref\,H\eta} + \frac{CHP\,E\eta}{Ref\,E\eta}} \right) \times 100\%$$

Where:
PES is primary energy savings.
CHP Hη is the heat efficiency of the cogeneration production defined as annual useful heat output divided by the fuel input used to produce the sum of useful heat output and electricity from cogeneration.
Ref Hη is the efficiency reference value for separate heat production.
CHP Eη is the electrical efficiency of the cogeneration production defined as annual electricity from cogeneration divided by the fuel input used to produce the sum of useful heat output and electricity from cogeneration. Where a cogeneration unit generates mechanical energy, the annual electricity from cogeneration may be increased by an additional element representing the amount of electricity which is equivalent to that of mechanical energy.
Ref Eη is the efficiency reference value for separate electricity production.

Efficiency of production is certainly a very important parameter however, it is necessary to monitor the effectiveness of the whole system, ie from energy production through distribution to private delivery to the final customer. At present, the main measures aimed at reducing the energy consumption of appliances, the use of labels can choose energy efficient appliances. However, it is clear that the most significant impact on the effectiveness of the system have measures in production and distribution. For this reason, it is necessary to support the focus on highly efficient source of environmentally friendly and reducing losses in distribution systems. In the Czech Republic appears efficiency of resources by 25% (which is mostly condensing power) to power efficiency reaching 90% or more. The average loss in the distribution range 18.8% (ERO, 2013).

Conclusion:

As already mentioned the Czech Republic is among the countries where CHP and district heating systems have a long tradition and are attributed to high priority. Sources with higher output connected to the central heating system are a steam backpressure turbine and steam condensing extraction turbine, mainly for a coal. Small decentralized sources are combustion engines for natural gas. Due to the large resources of coal, the primary fuel is very necessary (with the increasing scarcity of coal) use this fuel as much as possible, which is certainly efficient CHP. At present, we are facing a major issue “What we will do now”? There are a number of important studies and analyzes that point to the fact that for resources with high capacity there is no longer any space - there is therefore a key priority must be directed to the modernization of these sources and to make best use compared with investment intensity relative to the modernization and reconstruction resources. For the Czech Republic is most important to have a reasonable mix as major sources and small decentralized sources, where both types have their advantages and disadvantages.

Currently, heating companies faces a fundamental decision which way to go, because there are many aspects that affect their viability. The main problem lies in the overall reduction of heat supply for households and industry, which is caused by the gradual destruction of the Czech industry and household insulation. Other problems are associated with the question of fuel base mainly for heating systems that burn brown coal. Here are primarily issues of mining, increasing fuel prices or substitute other fuels (which is also more expensive than brown coal itself), then it is the issue of emission allowances (the purchase), the introduction of new taxes and raising existing taxes and not least strict performance criteria and emission limits. Increasing efficiency, reducing environmental impact and improving the technical maturity of the individual devices is a clear direction where heating company must face, but it is clear that all of these improvements and modernization entail considerable investment, for which it is necessary to find sufficient funding. From 1st of June 2016 the European Union set new emission limits, anchored in European Parliament and of the Council 2010/75/EU on industrial emissions (integrated pollution prevention and control), which will have to meet any heating plant. All these facts lead to recall discussions about the future development of district heating system in the Czech Republic. Possibilities how to deal with this situation are numerous, and it is just a strategy of the company, which way you go.

Reference

Ahner N., Glachant J.-M., De Hauteclocque A., 2012. EU Energy Law and Policy Yearbook 2012, Claeys & Casteels, Brussels.

Energy statistics - Statistical Office of the European Union (ESTAT) 2013

Flin D., 2010. Cogeneration A user's guide. The Institution of Engineering and Technology, London: 5.

Hisham S. B., José M. P.-O., Mahmoud M. El-H, 2013. Multi-objective optimization of process cogeneration systems with economic, environmental, and social tradeoffs, Clean Technologies and Environmental Policy, 15: 185-197.

Internal data from Energy Regulatory Office Czech Republic, Prague, 2013

Oberthur S., Pallemaerts M., 2010. The New Climate Policies of the European Union. VUBPRESS: 121.

Ottinger R. L., Robinson N., Tafur N., 2005. Compendium of Sustainable Energy Laws, Cambridge University Press, New York: 377.

Resolution of European Council of 18 December 1997, Resolution of the European Parliament of 15 May 1998

Schoots K., Bouquet T., 2009. CHP-GO implementation and their integration with other policies, including policy recommendations (WP4 Report), ECN Policy Studies.

VERTICAL ROCK HEAT EXCHANGERS – SOURCES OF ENERGY TO HEAT PUMPS

Pavel Neuberger, Radomír Adamovský, Pavel Pauli

Czech University of Life Sciences Prague, 16521 Prague 6 – Suchdol, Czech Republic,
Phone: +420 224 383 179, Fax: +420 234 381 828, E-mail: neuberger@tf.czu.cz

Abstract

The goal of the article is to analyse the distribution and changes of temperatures in boreholes with the rock mass/fluid tubular heat exchangers used as an energy source for the heat pump. The quality of the regression model is evaluated using a determination index. Tables 2 and 3 show the values of this index for the individual dependencies obtained by non-linear regression. In most cases the figures were $I^2_{t_z\tau} > 0.8$*, indicating a very strong correlation dependency.*

Keywords: heat exchangers, heat pumps, temperature, borehole, depth

Introduction

In the agricultural sector, energy is obtained in heat pumps used mainly for heating greenhouses, aquaculture and for drying products. However, there are now energy systems which allow heat pumps to be used to heat barns used for breeding broiler chickens (Kharseh, Nordell, 2011). Air, water and ground mass may provide energy for heat pumps for farming activities or in rural areas. For small and medium-power heat pumps up to 100 kW the most optimal heat source for heating and ventilating barns is warm air from the stable. The use of surface water or groundwater is very limited due to availability, complicated legislation, water flow variability and unstable heating power. For pumps exceeding 100 kW the most suitable source of heat energy seems to be earth and rock mass, from which heat is transferred through horizontal or vertical heat exchangers. Factors limiting power generated by a horizontal earth heat exchanger include the size of the land the exchanger is to be placed on, limited possibility of growing crops and land that is unsuitable due to future building projects. The optimal low-potential heat sources for these thermal outputs in question are vertical heat exchangers installed to depths of 80 – 150 m. Vertical heat exchangers provide a stable heating factor compared to other sources, and thus stable heat pump output, regardless of the location climate and the changing of the seasons.

The aim of our work was to identify and analyse the distribution and changes of temperature in the rock mass with a vertical heat exchanger used as a source of energy for a heat pump. The results obtained will serve as a basis for mathematical models allowing the optimization of the design of vertical rock heat exchangers.

The article builds on the results of our validations presented in the publication (Adamovský et al., 2012). A detailed analysis of temperatures in the vicinity of the vertical exchanger is given in the fundamental publication by Banks (2012). It monitors temperature changes in relation to the heat output of the heating or cooling of the ground mass, the effects of the thermal characteristics of the rock mass on the heat transfer process, analogies between heat flux the flow of groundwater, initial and steady states in the ground mass. An analytical solution of heat transfer in the rock mass with a vertical heat exchanger taking into account groundwater flow and temperature changes along a linear source of heat is also a topic focused on by the University of Tübingen (Giraldo et al., 2011). The results of their tests have shown that these effects are significant with short boreholes and exchangers operating for a long time. U-shaped vertical heat exchangers, 30 m long and made from copper pipes, with R 134 as the working medium, are being tested in the Key Laboratory of Enhanced Heat Transfer and Energy Conversion at Beijing University of Technology in China (Xiaotao et al., 2009). This system, at a temperature of approx. 4 °C and a condensation heat of 53.41 °C in the vicinity of the exchanger, achieved a relatively high heating factor of 3.28 – 3.55. The German testing system in Schöffengrund-Schwalbach, near Frankfurt am Main (Rymbach, Sanner, 2000), actively monitored a borehole 50 m deep, surrounded by 9 monitoring boreholes at a distance of 2.5 m, 5 m and 10 m, also 50 m deep. Each monitoring borehole was fitted 24 temperature sensors spaced 2 m apart. The results of the experiment were used to create a numerical heat transfer model in the rock mass with a vertical heat exchanger.

Material and method

The research whose results are presented in this article was conducted at the experimental workplace of Veskom spol. s r. o. In Prague 10 – Dolní Měcholupy, which opened in September 2008. The source part of the energy system that supplies the complex with heat consisted of three heat pumps. Until 10 July 2012 these were two IVT GREENLINE HT PLUS E17 units (Industriell Värme Teknik, Tnanas, Sweden) with a heating capacity of 16.2 kW and one IVT PREMIUMLINE X15 unit with a heating capacity of 11.7 kW. On 10 July 2012 the IVT PREMIUMLINE X15 heat pump was replaced by an IVT PREMIUMLINE EQ13 with a heating capacity of 13.3 kW. The heating capacity is determined at a temperature of 0/35 °C. The heat pumps use earth and rock mass as a source of low-potential heat. In the energy system the heat pumps are connected to eight boreholes 113 m deep (V1 - V8), two linear horizontal earth heat exchangers (installed at a depth of 1.8 m) and two SLINK horizontal earth heat exchangers (installed at a depth of 1.5 m). Borehole V9 is not used for energy, and serves as a reference. These boreholes are used as sources of heat only to heat the administrative and service buildings and to provide hot water for social purposes. They are not used for cooling buildings.

Exterior air temperature was recorded by an ATF 2 KTY 81.210 sensor (GREISINGER electronic GmbH, Regenstauf) fitted at a height of 2 m on the eastern facade of the building.

The heat transfer medium used in the primary heat pump circuit is a mixture of 67 % H_2O and 33 % $C_2H_6O_2$.

Boreholes V1 – V4 and borehole V9 were fitted with Pt 1000A temperature sensors (GREISINGER electronic GmbH, Regenstauf). At each borehole the temperature was measured at a depth of 0.2 m below the soil surface. The temperature of the rock mass close to the vertical heat exchanger was monitored at depths of 9 m, 20 m, 50 m and 100 m. The sensors were placed during assembly between the ascending and descending branches of the heat exchanger. The borehole was then filled with bentonite. The temperature sensors were placed so as to best monitor the geological profile. The electrical signal is converted to digital form and saved on a recording device.

In 2012 the 2011/2012 heating season ended on 26 April 2012 and the 2012/2013 heating season commenced on 17 September 2012.

The results of the geological survey conducted by GESTEC, s.r.o. in collaboration with STAVEBNÍ GEOLOGIE – Geosan s.r.o. showed that the layers in the boreholes monitored were composed as follows:

VT2 – borehole equipment (PE 100RC pipeline (LUNA PLAST a.s., Hořín, Czech Republic), 4 pipes, pipe outer diameter 32 mm, pipe wall thickness 2.9 mm); 0.0–1.0 m: man-made ground, loamy-sandy gravel, brick chips and rubble; 1.0–2.0 m: man-made ground, sandy clay soil; 2.0–4.5 m: manmade ground sandy clay gravel; 4.5–7.5 m: manmade ground, clay loam with gravelly mixture and small brick chips; 7.5–9.5 m: man-made ground, sandy clay with small flint chips; 9.5–10.5 m: weathered wacke; 10.5–13.0 m: weathered clay shale, soft; 13.0–113.0 m: fresh clay shale with dust mixture.

VT4 – borehole equipment (PE 100RC pipeline, 4 pipes, pipe outer diameter 32 mm, pipe wall thickness 2.9 mm); 0.0–4.0 m: man-made ground, loam with gravel and brick chips; 4.0–5.5 m: manmade ground, sandy loam; 5.5–10.0 m: man-made ground, clay sandy gravel; 10.0–14.0 m: weathered clay shale; 14.0–113.0 m: fresh clay shale.

VT9 – without equipment; 0.0–3.5 m: man-made ground, coarse-grain gravel, crushed stones, brick chips; 3.5–7.0 m: man-made ground, sandy gravel with brick chips; 7.0–15.0 m: weathered clay shale, soft; 15.0–113.0 m: fresh clay shale.

The test of the temperature response of the rock mass showed the thermal conductivity coefficient of the rock mass to be $\lambda = 2.9$ W.m^{-1}.K^{-1} and the thermal resistance of the rock mass of borehole $R_b = 0.137$ K.m.W^{-1}. The groundwater level in all boreholes was detected at depths of 10-12 m below the surface.

In the temperate zone the land surface temperature alternates periodically during the calendar year. The dependence of temperature on time may be expressed at various depths using the equation:

$$t_z = t_z^* + \Delta t_{Az} \cdot \sin(\Omega \cdot \tau + \varphi_z) \qquad (1)$$

where:

t_z temperature of rock mass at depth z (°C),

t_z^* average temperature of rock mass at depth z (°C)

Δt_{Az} oscillation amplitude around temperature t_z^* (°C)

τ ordinal number of day in year (-)

φ_z initial oscillation phase (rad)

Ω angular velocity ($2 \cdot \pi / 366$) (rad·day^{-1})

A similar equation may be used to express the exterior air average temperature dependence t_e at time τ :

$$t_e = t_e^* + \Delta t_{Ae} \cdot sin(\Omega \cdot \tau + \varphi_e) \qquad (2)$$

where:

t_e average exterior air temperature at height of 2 m (°C)

t_e^* mean average exterior air temperature at height of 2 m (°C)

Δt_{Ae} oscillation amplitude around temperature t_e^* (°C)

φ_e initial oscillation phase (rad)

This is an equation based on the theory applicable for free undamped oscillation. *MathCAD* software was used to set the parameters of this function from the measurements, specifically the *sinfit* command for the non-linear regression function (Šleger, Vrecion, 1998).

Results

Tab. 1 Parameters of equation 1 for various boreholes and depths

Depth	Borehole V2			Borehole V4			Borehole V9		
	t_z^* (°C)	Δt_{Az} (°C)	φ_z (rad)	t_z^* (°C)	Δt_{Az} (°C)	φ_z (rad)	t_z^* (°C)	Δt_{Az} (°C)	φ_z (rad)
0.2 m	10.369	10.037	4.355	10.578	8.000	4.154	inoperative sensor		
9.0 m	9.124	4.236	4.254	9.789	4.231	4.214	10.962	0.606	1.294
20.0 m	8.912	3.701	4.271	9.056	3.647	4.271	10.312	0.178	1.186
50.0 m	8.785	2.472	4.289	8.658	2.88	4.319	10.227	0.190	0.983
100.0 m	8.510	2.514	4.333	8.750	2.565	4.346	11.013	0.290	1.150

Tab. 2 Values of determination index $I^2_{t_z\tau}$ non-linear regression t_z at τ

Depth	$I^2_{t_z\tau}$ (-)		
	Borehole V2	Borehole V4	Borehole V9
0.2 m	0.957	0.972	inoperative sensor
9.0 m	0.933	0.938	1
20.0 m	0.913	0.905	0.699
50.0 m	0.862	0.841	0.805
100.0 m	0.795	0.799	0.758

Tab. 3 Parameters of equation 2 and value of determination index $I^2_{t_e\tau}$ non-linear regression t_e at τ

Measurement point	Exterior			
Height	t_e^* (°C)	Δt_{Ae} (°C)	φ_e (rad)	$I^2_{t_e\tau}$ (-)
2 m	11.705	11.052	4.515	0.79

Discussion and conclusion

The dependence of t_z on τ resulting from non-linear regression is presented in equation 1. The parameters of equation 1 are given in Table 2. If we consider that at a depth of z = 0.2 m the temperature of the earth mass is affected by fluctuating air temperatures above the earth's surface and incident heat energy from the sun, the rock mass is cooled by the vertical heat exchanger to a state that characterizes the mean temperature of the rock mass t_z^*. Between depths of z = 9 m to z = 100 m the figure computed from the mathematical model for borehole V2 was $t^*_{z\,min}$ = 8.510 °C a $t^*_{z\,max}$ = 9.124 °C and for borehole V4 $t^*_{z\,min}$ = 8.658 °C a $t^*_{z\,max}$ = 9.789 °C. At depths of between z = 9 m and z = 100 the uncooled borehole V9 is characterised by m $t^*_{z\,min}$ = 10.227 °C and $t^*_{z\,max}$ = 11.013 °C, i.e. temperatures higher than those in the cooled boreholes, which is logical.

In the uncooled borehole V9 the size of the oscillation amplitude Δt_{Az} around the temperature t_z^* reaches the maximum at shallow depths (Table 1, Fig. 1). The cause is again the temperature of the air above the earth's surface and the amount of incident thermal energy from the sun. As the depth z increases, the oscillation amplitudes Δt_{Az} around the temperature t_z^* fall and are negligible, as expected.

The size of the oscillation amplitude Δt_{Az} around the temperature t_z^* in the cooled boreholes V2 and V4 varies considerably. At a depth of z = 0.2 m the oscillation amplitude Δt_{Az} around the temperature t_z^* follows the oscillation amplitude Δt_{Ae} around the temperature t_e^*. At greater depths the effect of the fluctuating temperature of the air above the earth's surface and the amount of incident thermal energy from the sun lessen and the oscillation amplitude Δt_{Az} around the temperature t_z^* is reduced. The cooling of the rock by the heat exchanger is the only factor with any significant effect at these depths.

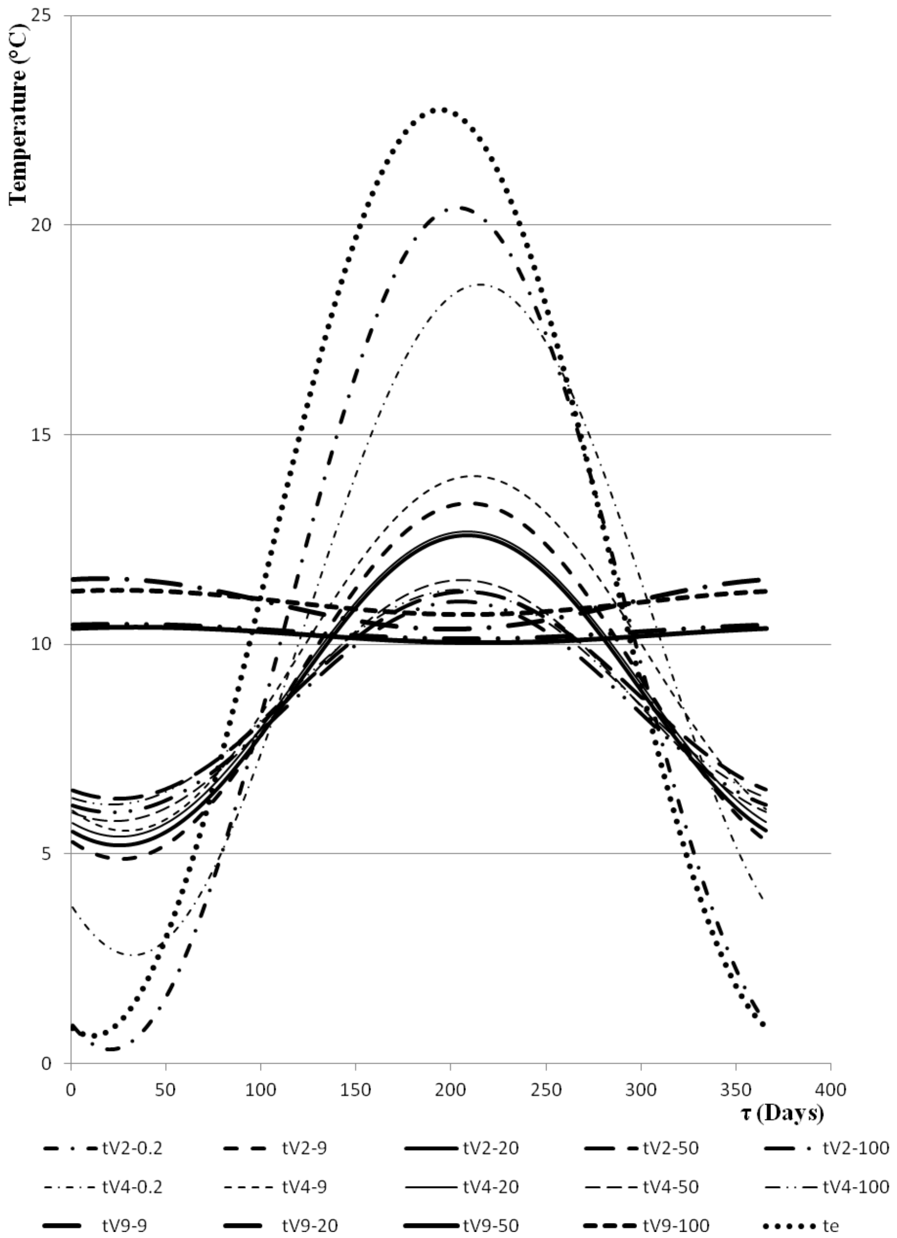

Fig. 1 Curves of calculated material temperature dependence close to the vertical heat exchanger and average air temperature at 2 m above ground level over time (tVx-z; t – temperature, V – borehole, x – borehole number, z – depth (m))

At depths of z = 9 m to z = 100 m the initial oscillation phase φ_z shows slight differences in boreholes V2 and V4. This is due to the fact that heat is evenly transferred into the vertical heat exchanger. In the case of the uncooled borehole V9, the greater variability of the initial oscillation phase ($\varphi_{z\,min}$ = 0.983 rad and ($\varphi_{z\,max}$ = 1.294 rad) is particularly due to the effect of incident sunlight and the impact of changes in the temperature of the air above the earth's surface on the temperature of the rock mass at a depth of 9 m. The conclusions stating the annual attenuation depth as 7.1 m as given in the literature [2] allow for a slight impact at the depth of 9 m. The cause of the variability of the initial oscillation phase of the uncooled borehole V9 at greater depths must be sought in another external source of cooling. The low oscillation amplitude shows that this source has a minimal effect and is therefore at a considerable distance. It is clearly borehole V4, which is 11 m away from borehole V9. However, this theory will have to be confirmed on the basis of further investigation. From experience it is also evidently recommended to build vertical heat exchangers that extend to depths of over 100 m spaced more than 10 m apart.

The parameters of the equation shown in Table 2 correspond to the parameters of equation 1 for a depth of 0.2 m. This fact proves that fluctuations in the temperature of the air above the earth's surface and the amount of incident thermal energy from the sun affect the temperature of the rock mass.

The quality of the regression model is evaluated using a determination index. Tables 2 and 3 show the values of this index for the individual dependencies obtained by non-linear regression. In most cases the figures were $I^2_{t_z\tau} > 0.8$, indicating a very strong correlation dependency.

Acknowledgement

Supported by the Czech University of Life Sciences Prague, Czech Republic, Project No. 31130/1312/3106.

Reference

Adamovský R., Mašek L., Neuberger P., 2012. Analysis of rock mass borehole temperatures with vertical heat exchanger. Research in Agricultural Engineering 58/2: 57-65.

Banks D., 2012. An Introduction to Thermogeology: Ground Source Heating and Cooling. 2nd Edition: 527.

Giraldo N. M., Blum P., Zhu Z., Bayer P., Fang Z., 2011. A moving finite line source model to simulate borehole heat exchangers with groundwater advection. International Journal of Thermal Sciences 50: 2506-2513.

Kharseh M., Nordell B., 2011. Sustainable heating and cooling systems for agriculture. International Journal of Energy Research 35: 415–422.

Rymbach L., Sanner B., 2000. Ground-source heat pump systems the European experience. Geo-Heat Bulletin 21/1: 16-26.

Šleger V., Vrecion P., 1998. Mathcad 7. Prague: Haar International: 157.

Xiaotao W., Chongfang M., Yuanwei L., 2009. An experimental study of a direct expansion ground-coupled heat pump system in heating mode. International Journal Energy of Research 33: 1367–1383.

QUALITY ASSESSMENT OF SELECTED TILLAGE MACHINES FOR DEEPER LOOSENING SOIL WITHOUT TURNING

Petr Novak*, Jiří Masek, Petr Knap, Stanislav Petrasek

Czech University of Life Sciences in Prague, 165 21 Prague 6- Suchdol, Czech Republic,
Phone: +420 224 383 133, E-mail: novakpetr@tf.czu.cz

Abstract

The aim of this paper is evaluate the quality of soil tillage with tillers for deep tillage without turning over the soil. Measurements were performed on July 2012 in Lužany near Jičín on sandy-loam soil at an altitude of 325 m. This evaluation is performed on three-row chisel tillers Strom Export Ecoland, Lemken Karat 9 and Horsch Terrano FX. Quality of soil tillage was assessed after crossing machine. The evaluated parameters of the quality of work are surface covering by crop residues, bottom profiles, surface profile and surface roughness.

The results confirm the similarity structure of all evaluated cultivators and similar quality soil tillage. These cultivators are suitable for technology mulch till and reduced till.

Keywords: soil tillage, chisel tiller, crop residue

Introduction

Tillage has long been linked to human effort to create the best conditions for the growth of desired plants. In the past, soil tillage has been limited by material possibilities of the time and also using only human or animal power. In recent years we can see an effort to optimize soil tillage technologies in terms of the needs of plants, maintenance of soil fertility, and last but not least energy consumption. It is also evident emphasis on the effects of tillage on soil erosion. For this reason, start developing of new soil tillage technologies and machines with the right tools for this process. These technologies are generally known as soil protection or conservation technologies.

Soil tillage is described as mechanical intervention into the soil or mixing of soil in order to create the best possible conditions for growth and nutrition of plants (Or, Ghezzehei, 2002). Tillage disrupts soil aggregates, soil compaction its structure and changing the size and distribution of pores and therefore forming a desirable environment for the movement of air and water in the soil (Titi, 2002). By soil tillage play important role soil physical properties such as density, porosity and penetration resistance (Titi, 2002). Some authors then describe the most important methods for measuring soil properties, such as measurement of density, pore size, the size of aggregates and the stability of aggregates (Titi, 2002; Dexter, 1988). Description and quantification of soil structure is very important because agronomic interventions are related to the arrangement of soil aggregates and clods and influence the stability of soil structure. Size of soil aggregates is related to the mechanical interference with the soil (Díaz-Zorita et al., 2002).

Cconservational and conventional soil tillage differently changing soil structure,which affects the soil's ability to absorb and displace water. The positive effect on the physical, chemical and biological soil properties described by many authors (Hubbard et al., 1994; Karlen et al., 1994). Among the machines that are suitable for soil conservation tillage includes a chisel plow, which leave a large amount of plant residues on the surface. The choice of the appropriate soil tillage system in that area is challenging process, which is required to apply deep theoretical knowledge of the subject but also long experience of the location. This process is also necessary to evaluate the quality of the machines for the soil and climatic conditions of the locality.

Material and method

The rating was done on machines Stromexport Ecoland EN3000R, Lemken Karat 9 and Horsch Terrano 3FX. Measurements were in the Lužany village near of Jičín town. Land for measurement is located at an altitude of 325 m above sea level. Measurements were carried out on the 10th July 2012. Crop on this land was winter barley, which has achieved an average yield 7.7 t.ha-1.Pulling vehicle for all cultivators was wheeled tractor New Holland T7050, which has a rated power output of 145 kW. Pulling device had sufficient power to meet with all machines identical conditions for measurement. A ground speed machine during work was 10 km.h^{-1} and working depth was set for all machines in the range of 18-20 cm. To determine the characteristics of the soil were removed unbroken soil samples to Kopecky cylinders. For the collection of samples was soil surface cleaned out of crop residues unbroken soil samples was carried out taking into Kopecky cylinders with a capacity of 100 cm^3 at depths of 5-10 cm, 10-15 cm and 15-20 cm. Sampling was conducted at two sites in four repetitions.

Measurement of land coverage by plant residues was performed immediately after crossing machine on site. On the surface plot is laid template with dimensions of 0.5 m x 0.5 m, which sets 0.25 m^2 plot. On this defined area is making a picture of surface by the camera and next step is using image analysis to determine the surface coverage by plant residues. Template plot is placed at an angle to the direction of travel so as to ensure the most representative picture possible layout of plant residues on the field. The selection is random.

Another parameter was measured furrow bottom profile. After crossing was refined profile loosened soil and the furrow bottom was excavated. The profile was measured after crossing machine on working width 3 m edge to edge. For the measurement of the profile was used wooden lath length of 3.5 m. The lath was placed on a plot of purified profile. Rod lying on the ends of the land and determine the zero height above the surface. She was then subtracted from the depth of the bottom slats. The values were measured each 2.5 cm (Fig. 1).

For each variant was also to measure the roughness of the soil after crossing machine. For roughness measurements were used chain method (Klik et al., 2002). The measurement was used roller chain of 1 m length when measuring the chain is randomly placed on the treated surface and then was measured in length.

Results and discussion

Coverage of the soil surface crop residues was not statistically significant between either one machine. In the box-graph in Fig. 2 is evident that the highest average land covering crop residues reached Stromexport Ecoland machine. The median value of this machine has reached 21.1 % and the average value was 22.67 %. Cultivator Lemken Karat 9 reached the lowest median value of 18.6 % and the lowest average coverage of 19.9 %. Ecoland machines and Karat 9 reached a similar variance and the difference between the minimum and maximum value is similar too. Cultivator Horsch Terrano FX had a median value of 21 % of the average value of coverage 20.19 %. This cultivator achieved the smallest variance and the smallest difference between the minimum and maximum value.

Fig. 1 Furrow bottom profile measurement

Soil tillage made by these cultivators cannot be described as soil protection technologies, because coverage of soil surface does not reach the ground surface plant residues over 30 %. The soil is still partially protected against erosion of plant residues, as for every increase of coverage of land plant residues by 10 % to reduce soil erosion by 20 % (Wischmeier, Smith, 1978). According to other authors' remains if the tillage covering the land surface from 20 to 30 % of plant residues, soil is protected against erosion and drying out in comparison to conventional technology. The percentage surface coverage of plant residues reduces the risk of erosion of 50-90 % (Hanna et al., 1995).

Cultivator Ecoland adheres well setting of the working depth. Groove width tillage in a place where drove chisel is relatively narrow. The narrow groove influenced processing the whole width edge to edge. Among the various chisels remained untreated surface, where it remained unbroken stubble after the previous crop(Fig. 3).

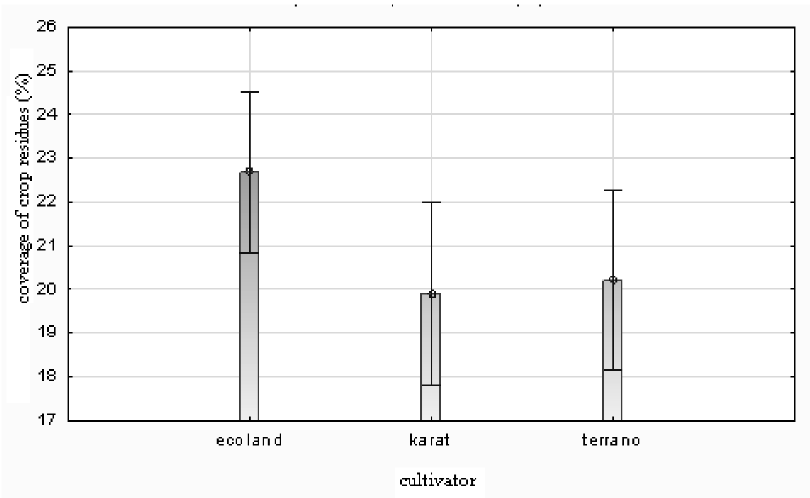

Fig. 2 Coverage of crop residues

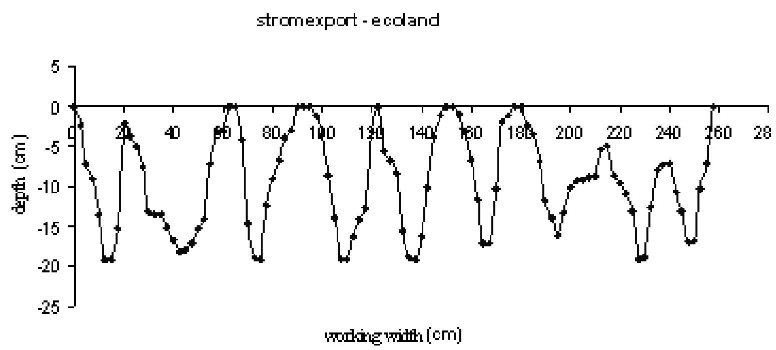

Fig. 3 Furrow bottom profile- Stromexport Ecoland

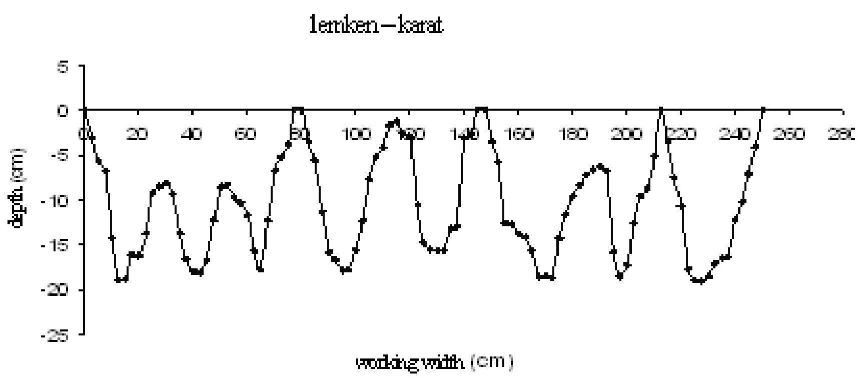

Fig. 4 Furrow bottom profile- Lemken Karat 9

Cultivator Karat 9 adheres worse setting of the working depth. In some cases, chisels was a lifting of the tine non-stop belay device to respond to an obstacle in the soil, or to increased local compaction, but rather was a lateral tilting of the machine, which allow setting of the floating position of tractors´ hydraulic hitch. Groove width tillage in a place where drove chisel is relatively sufficient. Width of grooves influenced processing the entire frame. Among the various chisels somewhere remained untreated surface, where it remained unbroken after the previous crop stubble(Fig. 4).

The graph in Fig. 5 shows that the Terrano cultivator relatively well respected setting depth. Groove width after passing is also comparatively sufficient. Cultivator worked in the wider context as well. The middle part between the tractors wheels were processed without leaving area. Skipped stubble stood at max 300 mm from the entire working width.

The difference in roughness of land after crossing by cultivators Ecoland and Karat 9 is statistically proven by Tukey HSD test. Cultivator Karat 9 reached the lower roughness of the soil than other machines, and the value of 21 mm, compared to machines Ecoland, which amounted to 35 mm and Terrano FX which amounted to 28 mm(Fig. 6). However cultivators Ecoland and Karat 9 in comparison to competitive machines Terrano FX have larger standard deviation.

Low soil roughness is important in the establishment of winter crops without further tillage seeders. Especially small seeds crops (eg. oilseed rape) dislike clods and uneven land surface is a problem meeting the drilling depth (Karlen et al., 1994). High roughness of the soil is important in the autumn soil preparation for spring crops to reduce soil erosion. In addition, you can successfully use the excitement created clods on the surface of the soil in winter, with the participation of frost and water in the soil.

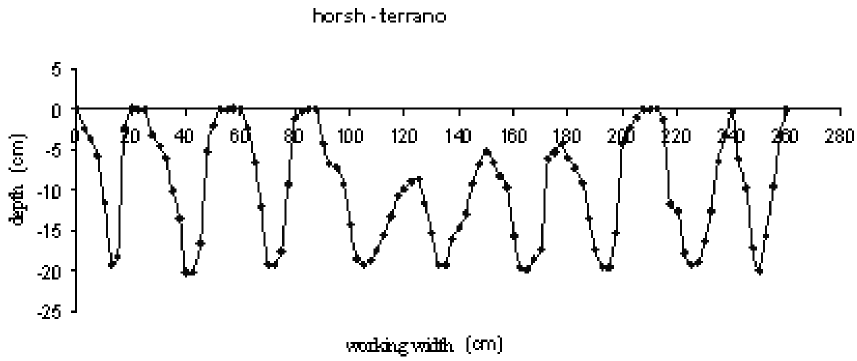

Fig. 5 Furrow bottom profile- Horsch Terrano 3FX

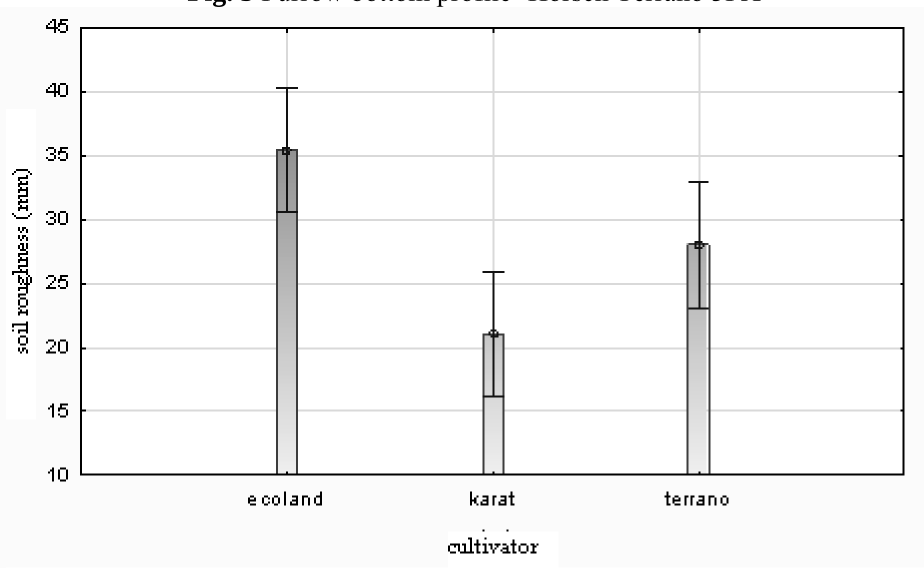

Fig. 6 Soil roughness

Conclusion

From results of the measured values we can probably see the similar construction of all evaluated machines and their tools. Coverage of the soil surface by plant residues had the lowest average value for cultivators Karat 9. The lowest coverage of land by plant residues may not be the desired outcome. Much depends on the user's perspective, what technology wants to use in the given conditions.

Processing of furrow bottom profile profile is very influenced by the width of the chisel. Cultivator Ecoland created narrow grooves and therefore it would be suitable to recommend casting machines by wider chisels. However, the cultivator kept setting of working depth very well. For Karat 9 and Terrano FX cultivators achieved very similar results; and it cannot be said which of these cultivators performed better loosening. From chosen cultivators Karat 9 has the lowest soil roughness.

References

Dexter A.R., 1988. Advances in characterization of soil structure. Soil Till. Res., 11: 199 - 238.

Díaz-Zorita M., Perfect E., Grove J.H., 2002. Disruptive methods for assessing soil structure. Soil Tillage Res., 64: 3 - 22.

Hanna H.M., Melwin S.W., Pope R.O., 1995. Tillage implement operational effects on residue cover. Applied Engineering in Agriculture, 11: 205 – 210.

Hubbard R.K., Hagrove W.L., Lowrance R.R., Williams R.G., 1994. Physical propertiesof a coastal plain soil as affected by tillage. J. Soil Water Cons, 49: 276 - 283.

Karlen D.L., Wollenhaupt N.C., Erbach D.C., 1994. Crop residue effects on soil qualityfollowing 10-years of no-till corn. Soil Tillage Res., 31: 149 - 167.

Klik A., Kaitana R., Badraoui M., 2002. Desertification hazard in a mountainous ecosystem in the High Atlas region, Marocco. Proc. 12th ISCO Conference, Beijing: 636 – 644.

Or D., Ghezzehei T.A., 2002. Modelling post-tillage soil structural dynamics: a review. Soil& Tillage Research, 64(1-2): 41 - 59.

Titi E.A., 2002. Soil tillage in agroecosystems. CRC press, U.S.A., 367.

Wischmeier W.H., Smith D. D., 1978. Predicting rainfall erosion losses: A guide to conservation planning. USDA Agric. Handb. U.S. Gov. Print. Office, Washington, DC., 79.

SUGAR-BEET VARIETAL FIELD TRIALS WITH HARVEST LOSSES ASSESSMENT IN 2011 AND 2012

Tomáš Novotný*, Ondřej Šařec, Petr Šařec

Czech University of Life Sciences Prague, 165 21 Prague 6– Suchdol, Czech Republic
Phone: +4202-24383140, Fax: +4202-24383151, E-mail: novotnyt@tf.czu.cz

Abstract

For assessment several years already, field trials on harvest losses of various sugar-beet varieties have taken place in Agro Slatiny (Šařec et al., 2009). There is a significant influence of the variety on root yield and sugar content (Radivojevic, Došenovic, 2006). This paper discusses the results from the years 2011 and 2012 that comprised 32, respectively 33 different sugar-beet varieties. For each variety, the following items have been measured and calculated: biological yield, plant number per 1 m², sugar content of beets, real yield harvested by HOLMER Terra Dos, polarization sugar yield, losses connected with not dug up beets and with beets left in the field and total losses. The weather in the year 2011 was characterized by remarkably warm April. On the other hand, May and June were below average in temperature, with frequent changes in weather. Precipitations in June and July were rich. Further weather development was more favorable. In 2011, total harvest losses ranged in general from 0.92 (IMPERIAL) to 3.59 % (APEL) with the average value 1.58 %. The harvest losses in 2012 were higher, with their top value 5.65 % (KEVIN) and the second highest 5.62 % (ST 12021). The average total harvest losses attained 2.83 % in 2012. In 2011, the highest yield at 16% sugar content reached by mechanized harvest was showed by the variety VÁCLAV (116.3 t.ha⁻¹). The average for all the varieties attained 106.20 t.ha⁻¹. In the year 2012, the highest yield at 16% sugar content was demonstrated by the variety KIRINGA (132.92 t.ha⁻¹). The average value of that year amounted to 116.68 t.ha⁻¹.

Key words: sugar beet, variety, harvest losses, biological yield, soil moisture, plant number per m^2

Introduction

There are many sugar beet varietal field trials each year, some of them focusing as well on other growing aspects, i.e. on soil tillage (Fecková et al., 2002), on pests infestation etc. but no studies are carried out that would assess varietal suitability in terms of mechanical harvest. Therefore, the field trials focused on harvest losses of various sugar beet varieties have been established at Agro Slatiny in the Czech Republic each year since 1994. Generally, more than 30 varieties are tested each year. Composition of the varieties changes from year to year considerably due to a high number of newly introduced ones. Mechanized harvest has been always done employing a six-row harvester by Holmer. In the year 2005, a new type of harvester, i.e. Holmer Terra Dos with better technological parameters (Šařec et al., 2009), was used for the first time. The field speed of the harvester thus increased to up to 9 to 10 km.h^{-1} according to soil moisture and sugar beet yield. For all the varieties, the following variables are measured or calculated: biological yield, plant number per 1 m^2, sugar content of beets, real yield harvested by HOLMER Terra Dos, polarization sugar yield, losses connected with not dug up beets and with beets left on the surface of the field and total losses. Harvester bunker is emptied into tractor trailers during harvester's turns at both headlands. The trailers commute between a field and a disposal site where they are weighed prior emptying. During harvest in a field, harvest losses due to not-dug-up beets and due to beets left on the surface of a field are measured. The sum of the both of them returns total harvest losses. Further on, assessment of beets harvested mechanically is done with respect to quality of cutting, degree of beet damage and gross to net weight ratio.

Material and method

All the varieties are sown, fertilized, sprayed and harvested in the same manner. A twelve-row drilling machine BECKER is used for sowing, a six-row sugar beet harvester Holmer Terra Dos is used for mechanized harvest. One variety takes most often a plot of 24-row width depending on the field size and shape. Individual plots are located side by side in the same field and growing technology is invariable for all the varieties within a year.

When evaluating harvest, biological yield of beets is measured first. In the same time, number of plants per 1 m^2 is measured as well. A rectangle of 10 m^2 is demarked. If there is a row spacing of 0.45 m, the rectangle takes six rows of 3.7 m length. Beets are dug up manually, then cleaned and counted, and beet leaves are cut off. Harvested beets and leaves are then weighed separately.

Evaluation of harvest losses, i.e. losses due to not-dug-up beets and due to beets left on the surface of a field, is carried out straight after the mechanized harvest. A rectangle of 10 m^2 is demarked again. Firstly, all beet material from the surface is collected, and then all beet remains are dug up from topsoil to the depth of 0.25 m. Both fractions are weighed and total losses enumerated as their sum. Measurements are repeated five times. Beet yield of mechanized harvest is determined by weighing the tractor trailers. Values found are converted to weight units per one hectare. Additionally, measurements of soil moisture and soil penetration resistance are done.

When evaluating sugar beet variety results, it is important to take into account not only beet yields (BY), but as well sugar content (SC). Beet yield at 16% sugar (CBY, see Eq. (1)) covers both above mentioned outputs and thus gives better possibility for comparing varieties. Moreover, higher sugar content requires less material handling relatively to sugar gained.

$$CBY = \frac{BY \cdot (SC - 3)}{13} \left[t \cdot ha^{-1}\right] \qquad (1)$$

Results and discussion

Harvest Conditions in the Years 2011 and 2012

Harvest conditions, e.g. soil moisture, soil compaction, belongs to the key factors influencing the extent of harvest losses. Therefore, the above mentioned variables are measured each year and Tab. 1 shows their values. Penetration resistance values can indicate soil compaction that decreases biological yield of sugar beet (Koch et al., 2008; Heuer et al., 2006). The field speed of the harvester Holmer Terra Dos reached from 9 to up to 10 $km.hour^{-1}$ in both years in question. During harvest in both years in question, soil moisture values were favorable in terms of harvest.

Harvest Yields in the years 2011 and 2012

Tab. 2 shows that the best results of the year 2011 in terms of mechanized harvest yield combined with sugar content were reached by the varieties Václav (116.32 $t.ha^{-1}$) and SyMarvin (114.60 $t.ha^{-1}$). From the same point of view, i.e. from the point of view of beet yield at 16% sugar, the varieties Halina (91.90 $t.ha^{-1}$) and Bering (96.14 $t.ha^{-1}$) proved the worst. In the year 2011, sugar content was generally lower, with an average at 17.74 %.

Tab. 1 Soil moisture and soil penetration resistance during the sugar-beet harvest in the years 2011 and 2012

Measurement Depth [m]	Soil Specific Moisture [%]				Penetration Resistance [MPa]		
	Beet Row		Harvester Track		Beet Row	Harvester Track	Headlands
	2011	2012	2011	2012			
< 0.01	21.2	19.3	21.4	19.1	0.2-1.4	0.7-1.1	0.8-2.0
0.01 – 0.02	22.3	20.2	22.5	19.8	1.4-1.6	1.1-1.4	2.0-2.6
0.02 – 0.03	22.8	21.3	22.8	20.7	1.6-1.8	1.4-1.6	2.6-3.5

Tab. 2 Yields and other indicators of sugar beet variety trials of manual and mechanized harvest in the year 2011

Variety	Plant Number	Manual Harvest		Machanized Harvest				Rating According to Yield at 16% Sugar
		Beet Yield	Beet Leave Yield	Beet Yield	Sugar Content	Palarized Sugar Yield	Beet Yield at 16% Sugar	
	$[10^3\ ha^{-1}]$	$[t.ha^{-1}]$	$[t.ha^{-1}]$	$[t.ha^{-1}]$	[%]	$[t.ha^{-1}]$	$[t.ha^{-1}]$	
Antilla	110	103.6	82.8	91.0	17.30	15.7	100.14	28
Imperial	120	95.2	100.8	89.6	17.90	16.0	102.68	25
Poseidon	140	98.0	98.4	88.1	17.36	15.3	97.37	30
Nancy	130	98.5	83.4	89.6	17.66	15.8	101.03	27
Xanada	70	105.5	83.1	96.8	17.37	16.8	107.02	14
Apel	110	108.0	65.4	94.2	17.88	16.8	107.79	13
Harley	110	105.5	69.6	92.7	17.50	16.2	103.37	24
MA 2034	110	107.0	88.2	94.2	17.61	16.6	105.84	18
Pohoda	140	120.1	111.0	97.2	17.71	17.2	109.94	10
Scorpion	110	110.7	66.0	97.5	18.02	17.6	112.69	5
Debut	130	105.5	74.4	92.9	18.12	16.8	108.04	12
Expert	130	87.0	57.0	86.7	18.71	16.2	104.77	20
Raptor	120	94.5	88.8	89.8	17.98	16.1	103.47	23
Danuška	120	104.8	60.3	96.2	18.12	17.4	111.84	7
Halina	130	88.5	75.0	80.5	17.84	14.4	91.90	32
Labonita	110	94.1	75.6	99.1	17.01	16.9	106.78	15
Danka	110	96.0	83.4	94.3	17.56	16.6	105.62	19
Kiringa	110	90.0	65.4	92.8	17.52	16.3	103.63	21
Esperanza	130	107.0	76.8	89.7	17.30	15.5	98.66	29
Alpina	130	99.0	53.1	98.7	17.74	17.5	111.86	6
Caruso	120	86.4	40.2	94.0	18.31	17.2	110.76	9
Victor	100	105.8	91.8	88.2	18.27	16.1	103.57	22
Merak	110	113.4	53.4	94.0	18.42	17.3	111.55	8
Václav	140	108.8	89.4	101.2	17.95	18.2	116.32	1
Bering	100	100.8	83.4	89.6	16.95	15.2	96.14	31
Charly	100	99.6	39.6	95.4	17.96	17.1	109.75	11
ST 12021	70	98.5	52.8	98.1	17.96	17.6	112.86	4
Marieta	110	99.0	63.0	100.9	17.67	17.8	113.88	3
Lucata	120	95.0	48.6	93.7	17.15	16.1	101.98	26
SYBelana	110	98.3	53.4	95.0	17.59	16.7	106.57	16
SyMarvin	120	118.8	64.5	103.0	17.47	18.0	114.60	2
Hi 0985	110	108.0	67.5	93.5	17.74	16.6	105.98	17
Average	**115**	**101.58**	**72.07**	**93.68**	**17.74**	**16.62**	**106.20**	

The difference in beet yields between manual and mechanized harvest yields were not too high, i.e. 7.77 % in average. Generally, the bigger the difference between manual and mechanized harvest, the less suitable a variety is for mechanized harvest by a beet harvester.

The next year 2012 in terms of beet yield at 16 % sugar, Kiringa (132.92 $t.ha^{-1}$) and again HI 0986 (131.54 $t.ha^{-1}$) varieties attained the best results (see Tab. 3). On the other hand, Kevin (93.43 $t.ha^{-1}$) and Xanadu (95.89 $t.ha^{-1}$) varieties showed the lowest results in this respect. The difference in beet yields between manual and mechanized harvest this year (2012) was reversed, i.e. mechanical harvest yield proved higher by 5.82 % in average. The sugar content demonstrated good values with an average of 18.18 %, i.e. almost a half percent higher than the previous year.

Tab. 3 Yields and other indicators of sugar beet variety trials of manual and mechanized harvest in the year 2012

Variety	Plant Number	Manual Harvest		Machanized Harvest				Rating According to Yield at 16% Sugar
		Beet Yield	Beet Leave Yield	Beet Yield	Sugar Content	Palarized Sugar Yield	Beet Yield at 16% Sugar	
	[10^3 ha^{-1}]	[t.ha^{-1}]	[t.ha^{-1}]	[t.ha^{-1}]	[%]	[t.ha^{-1}]	[t.ha^{-1}]	
Xanadu	101	87.2	79.6	94.8	16.15	15.3	95.89	32
Harley	99	112.0	74.0	104.0	17.60	18.3	116.80	22
SR - 546	97	84.2	67.0	97.5	19.00	18.5	120.00	12
MK 3006	99	86.0	84.2	95.4	18.00	17.2	110.08	27
Talenta	90	83.0	61.6	103.6	17.90	18.5	118.74	17
Vitalina	101	82.6	81.6	94.8	18.85	17.9	115.58	23
SY Marvin	99	105.4	96.8	101.9	18.25	18.6	119.54	13
Monsun	98	106.2	91.4	104.6	17.75	18.6	118.68	18
Sy Belana	89	99.8	66.2	101.6	17.35	17.6	112.15	26
Kevin	96	78.6	106.6	80.7	18.05	14.6	93.43	33
Vaclav	93	109.4	85.4	91.5	18.05	16.5	105.93	30
Apel	108	101.8	70.8	92.0	17.30	15.9	101.20	31
Poseidon	99	95.4	65.4	100.7	17.05	17.2	108.83	29
Pohoda	99	91.6	65.5	100.7	18.35	18.5	118.90	16
Expert	100	103.2	101.2	89.3	18.95	16.9	109.56	28
R 3401	101	131.6	119.8	109.3	17.35	19.0	120.65	10
Labonita	102	100.8	83.2	116.0	16.65	19.3	121.80	6
Lucata	101	100.7	83.4	102.0	17.65	18.0	114.95	25
HI 1140	100	82.0	55.2	96.6	18.85	18.2	117.78	21
HI 1133	101	78.6	51.4	100.5	18.45	18.5	119.44	15
ST 12021	102	71.2	63.6	100.4	17.90	18.0	115.07	24
Caruso	89	89.6	76.8	105.3	17.75	18.7	119.48	14
Gallant	102	92.6	80.4	101.8	18.10	18.4	118.24	19
Imperial	105	97.6	66.2	97.3	19.20	18.7	121.25	7
Raptor	111	88.6	82.0	101.8	18.85	19.2	124.12	4
Scorpion	104	97.6	79.0	106.4	17.70	18.8	120.31	11
Danka	96	106.6	71.4	105.3	17.90	18.8	120.69	9
Kiringa	104	95.4	55.6	108.0	19.00	20.5	132.92	1
HI 0986	112	84.4	85.4	102.7	19.65	20.2	131.54	2
Merak	107	99.0	101.2	100.6	18.60	18.7	120.72	8
Viktor	112	91.0	80.0	95.2	19.10	18.2	117.90	20
Debut	102	94.0	70.4	95.9	19.70	18.9	123.19	5
Katka	98	89.0	58.0	101.1	19.10	19.3	125.21	3
Average	**101**	**94.45**	**77.58**	**99.98**	**18.18**	**18.17**	**116.68**	

Tab. 4 Harvest losses of sugar beet variety trials in the years 2011 and 2012

Year 2011					Year 2012				
Variety	Harvest Losses [%]			Rating by Total Losses	Variety	Harvest Losses [%]			Rating by Total Losses
	Not Dug up Beets	Beets Left on Surface	Total			Not Dug up Beets	Beets Left on Surface	Total	
Antilla	0.86	0.67	1.52	15	Xanadu	0.63	1.01	1.65	2
Imperial	0.44	0.48	0.92	1	Harley	0.87	0.92	1.79	5
Poseidon	0.74	0.39	1.13	2	SR - 546	0.80	0.74	1.54	1
Nancy	0.58	0.82	1.40	8	MK 3006	1.45	3.02	4.47	29
Xanada	1.99	0.63	2.62	29	Talenta	2.03	1.97	4.00	26
Apel	2.26	1.33	3.59	32	Vitalina	1.20	2.03	3.23	19
Harley	2.25	1.12	3.37	31	SY Marvin	0.47	1.41	1.88	7
MA 2034	0.69	1.29	1.98	25	Monsun	1.09	0.69	1.78	4
Pohoda	0.80	0.67	1.47	14	Sy Belana	0.89	0.89	1.77	3
Scorpion	1.73	1.20	2.93	30	Kevin	3.12	2.53	5.65	33
Debut	1.26	0.56	1.82	22	Vaclav	1.84	1.44	3.28	21
Expert	0.75	0.65	1.40	7	Apel	0.78	1.24	2.02	9
Raptor	0.72	0.58	1.30	5	Poseidon	0.95	1.01	1.97	8
Danuška	0.92	0.54	1.47	12	Pohoda	1.55	1.67	3.22	18
Halina	0.97	0.70	1.67	19	Expert	1.14	1.14	2.28	11
Labonita	0.79	1.44	2.23	27	R 3401	1.37	1.04	2.42	12
Danka	1.06	0.41	1.47	13	Labonita	1.86	1.76	3.62	23
Kiringa	0.96	0.47	1.42	9	Lucata	1.12	1.88	3.00	16
Esperanza	1.57	0.72	2.30	28	HI 1140	2.36	1.99	4.35	28
Alpina	1.23	0.62	1.85	23	HI 1133	1.31	1.67	2.99	14
Caruso	0.55	0.74	1.29	4	ST 12021	4.24	1.37	5.62	32
Victor	1.08	0.79	1.87	24	Caruso	0.40	1.82	2.22	10
Merak	0.74	0.69	1.43	10	Gallant	1.12	3.06	4.18	27
Václav	1.11	0.26	1.37	6	Imperial	4.13	1.42	5.55	31
Bering	1.26	0.92	2.18	26	Raptor	2.18	1.18	3.36	22
Charly	0.80	1.00	1.80	21	Scorpion	1.75	1.24	2.99	15
ST 12021	1.19	0.40	1.59	18	Danka	1.88	1.31	3.19	17
Marieta	0.77	0.69	1.46	11	Kiringa	1.39	1.39	2.78	13
Lucata	1.18	0.51	1.69	20	HI 0986	2.40	2.22	4.62	30
SYBelana	1.19	0.37	1.55	16	Merak	1.79	1.91	3.70	25
SyMarvin	0.61	0.53	1.14	3	Viktor	2.21	1.07	3.28	20
Hi 0985	0.90	0.65	1.55	17	Debut	2.38	1.31	3.69	24
					Katka	0.83	1.01	1.84	6
Average	**1.06**	**0.71**	**1.58**			**1.65**	**1.54**	**2.83**	

Harvest Losses in the years 2011 and 2012

Tab. 4 shows harvest losses in the years 2011 and 2012. Harvest losses in the year 2011 were favorable compared to previous years of trials (Šařec et al., 2009).

Average total harvest losses, i.e. sum of losses incurred due to not-dug-up beets and beets left on the surface of the field, were 1.58 % in the year 2011 and 2.83 % in the year 2012. Average partial losses incurred in the 2011 year were 1.06 % due to not-dug-up beets, and 0.71 % due to beets left on the surface. The following year, the partial losses' values were 1.65 % and 1.54 % respectively. In the year 2011, Imperial (0,92 %) and Poseidon (1.13 %) attained the lowest total losses, whereas Apel (3.59 %) and Harley (3.37 %) demonstrated the highest ones. In the next year 2012, SR-546 (1.54 %) and Xanadu (1.65 %) total losses were the lowest ones, and on the opposite the ones of Kevin (5.65 %) and ST 12021 (5.62 %) the highest.

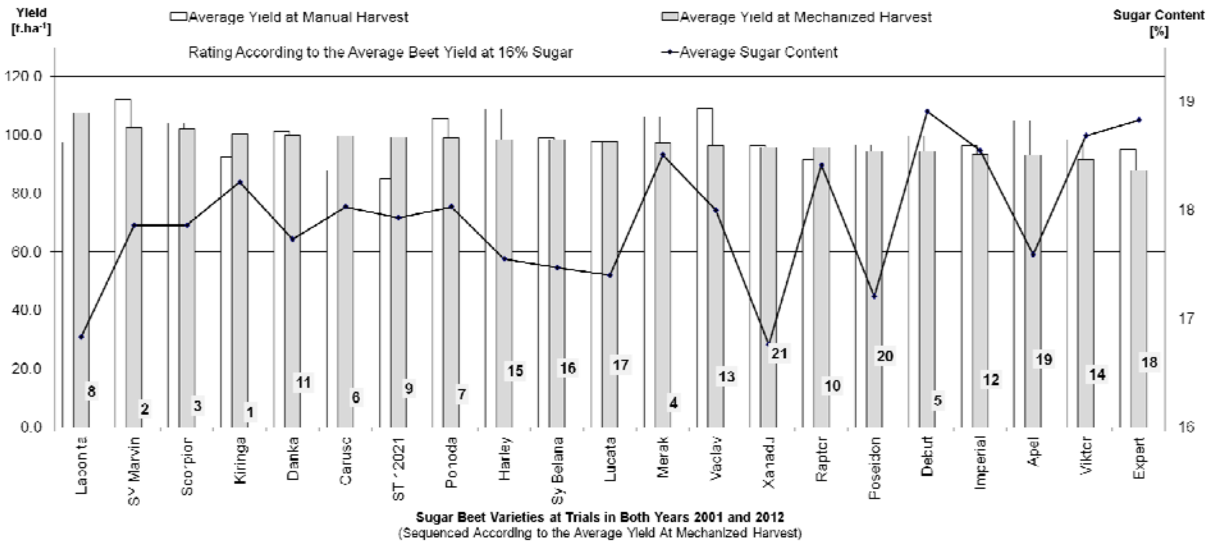

Fig. 1 Graph of sugar beet yields at manual and mechanized harvest, and sugar content for the varieties having occurred in both years 2011 and 2012

Conclusions

- The year 2011 was favorable for sugar beet growing in terms of moisture and temperature. The highest polarized sugar yield and yield at 16% sugar were demonstrated by the varieties Václav and SyMarvin. On the other hand, the varieties Halina and Bering showed the lowest yields. The highest yield gained by manual harvest was reached by the variety Pohoda (120.1 t.ha^{-1}). Differences between manual and mechanized harvest yields can be influenced by an uneven or high distance among plants in a row which may significantly affect the work of the cutting and lifting mechanisms.
- The year 2012 was also favorable for sugar beet growing in terms of moisture and temperature. The highest polarized sugar yield and yield at 16% sugar were demonstrated by the varieties Kiringa and HI 0986. On the other hand, the varieties Kevin and Xanadu showed the lowest yields. The highest yield gained by manual harvest was reached by the variety R 3401 (131.6 t.ha^{-1}).
- There were 21 varieties each year that were tested repeatedly in both years in question (Fig. 1). Kiringa and SyMarvin varieties proved best results in terms of yield and sugar content in both years in question, i.e. attained beet yield at 16% sugar 118.28 t.ha^{-1}, respectively 117.07 t.ha^{-1}. On the opposite, the varieties Xanadu (101.46 t.ha^{-1}) and Poseidon (103.10 t.ha^{-1}) demonstrated lowest yields.

Acknowledgement

This work was supported by the project NAZV QH72257.

Reference

Fecková J., Černý J., Pačuta V., 2002. Influence of different tillage systems on yield and selected qualitative parameters of sugar beet. Journal of Central European Agriculture, 3(1): 37 - 44. (in Slovak)

Heuer H., Tomanová O., Koch H.J., 2006. Preventive soil protection at sugarbeet harvest: Influence of repeated wheeling and different soil tillage systems. Sugar Ind, 131: 777 – 784. (in German)

Koch H. J., Heuer H., Tomanová O., Märländer B., 2008. Cumulative effect of annually repeated passes of heavy agricultural machinery on soil structural properties and sugar beet yield under two tillage systems, Soil & Tillage Research, 101: 69 - 77.

Radivojevic S., Došenovic I. S., 2006. Varietal and environmental influence on the yield and the end-use quality of sugar beet. Acta Periodica Technologica, 37: 27 - 35.

Šařec P., Šařec O., Przybyl J., Srb K., 2009. Comparison of sugar beet harvesters. Listy cukrovarnické a řepařské, 125(7/8): 212 - 216. (in Czech)

Šařec P., Šařec O., Srb K., Dobek T. K., 2009. Ocena plonów i strat przy zbiorze korzeni buraka cukrowego w latach 2005-2007. Inzynieria Rolnicza, 110(1): 281 - 288. (in Polish)

CURRENT TRENDS IN THE DEVELOPMENT OF AGRICULTURAL MACHINERY AND THEIR IMPACT ON THE KNOWLEDGE AND SKILLS OF THE HUMAN FACTOR

Ladislav Nozdrovický*, Miroslav Macák, Tomáš Šima

Slovak University of Agriculture in Nitra, 949 76 Nitra, Tr. A. Hlinku 2,
Phone: +421 37 6414366, Fax: +421 37 7417003, E-mail: ladislav.nozdrovicky@uniag.sk

Abstract

The aim of the paper is to present the main trends acting in the area of agricultural machinery that can be considered as a sector which significantly effects the efficiency of agrotechnical, agrobiological and agrochemical processes connected with the production of farm products and their processing. Function efficiency of this system being a part of the European agriculture depends upon technical and technological capability of the key factors. In the first part of the paper there are defined the main drivers affecting the development of sector of agricultural engineering. As main driver was considered the EU Common Agricultural Policy, its goals and principles and its implementation to the Vision 2020 and Strategic Research Agenda of the European Agricultural Machinery Industry. Based on general principles the trends in development of agricultural machines were characterised. As the combine harvester can be considered as a basic machine used in agricultural production the case of a new John Deere W Series Combine harvester was used to present the latest advances and improvements. The new John Deere W Series combine harvester is characterised from the point of engine power, and implementation of the intelligent solutions allowing to increase the performance, productivity, and fuel efficiency. The presented paper is focused on the key factors determining requirements on the operator and manager for the area of agricultural engineering.

Keywords: agricultural engineering; technology development; combine harvester; human resources;

Introduction

Branch of agricultural engineering can be considered as a sector with long term influence on the efficiency of agrobiological, agrochemical and agrotechnical processes connected with the processes of the farm products production and processing. Function efficiency of this system being a part of the European agriculture depends upon the technical and technological level of the key factors and also on the ability to respond to external effects of the competitive environment.

According to Frerichs (2006) in last years many factors have contributed to system of agricultural engineering. Reducing human drudgery, increasing productivity, improving timeliness of agricultural operations, and reducing peak labour demands are among the most compelling. The development of new techniques by research facilities and of new machinery by the industries is the driving force for the transfer of technology (Lammers, 1999). Agriculture is currently seeing the introduction of more advanced machinery (i.e., semi-autonomus machines) as well as information technologies (e.g., telematics, on-line remote diagnostic tools-, web-based monitoring and decision making tools) which enable the adoption of the analogous fleet management tools as seen in the industrial domain. However, the inherent dynamic nature of the bio-production systems together with an experienced smaller general user acceptance in terms of formalised planning tools have proven to inhibit the direct integration of current fleet management systems into the agricultural domain (Sørensen, Bochtis, 2010). From the point of adaption of new technologies and new machines it is very important to define the trends effecting the development in the sector of agricultural engineering and to identify the most drivers which are powering the trends.

Material and method

1. Definition of the main drivers affecting the development of sector of agricultural engineering

As main driver there was considered the EU Common Agricultural Policy, its goals and principles and its implementation to the Vision 2020 and Strategic Research Agenda of the European Agricultural Machinery Industry. Based on general principles the trends in development of agricultural machines are characterised.

2. Characterization of trends in machinery development (case of John Deere W Series Combine harvester)

As the combine harvester is considered as a very basic machine used in agricultural production the case new John Deere W 650 combine harvester was used to present the latest advances and improvements. The new John Deere W combine harvester was characterised from the point of engine power, working mechanism solutions, operator comfort and implementation of the intelligent solutions allowing to increase the harvest capacity, fuel efficiency, performance and productivity.

3. Specification of the requirements on the human resources arising from the use of combine harvester.

Results

Definition of the main drivers affecting the development of sector of agricultural engineering

The sector of agricultural engineering is an integral part of agriculture. In a first step we need to specifically describe the nature and function of the sector of agricultural engineering. Agricultural engineering is the branch of engineering that applies knowledge of biological science engineering science and technology to agricultural production and processing (Srivastava et al., 2006). Agricultural engineering combines the disciplines of mechanical, civil, electrical, chemical engineering with animal and plant biology. Basically there are four major specializations in agricultural engineering: farm machinery and power engineering, irrigation and drainage engineering, post harvest process and food engineering, soil and water conservation engineering.

Agricultural engineering has been accepted as one of the major disciplines which contribute significantly in increasing the productivity of agriculture in the country by way of increasing efficiency of inputs, conservation of resources and reducing post harvest losses besides value addition of agro-produce.

Functioning of the sector of agricultural engineering is substantially determined by the general agricultural policy implemented in the resort of agriculture. Agricultural policy in the Slovak Republic as well as in other EU member countries is heavily influenced by the EU Common Agricultural Policy and its goals and principles:

- to maintain and to strengthen the competitiveness of farming sector and food industry in the national and international markets,
- to provide health harmlessness and to increase quality of food in the interest of healthy public nutrition,
- to support agriculture in its role of protection and preservation of natural sources (especially soil and water) and to preserve bio diversity,
- to preserve use of land for agricultural purposes in areas with unfavourable production conditions, so that this process plays a landscaping, environmental and social role,
- to create conditions for permanent viability of rural areas.

EU Common Agricultural Policy can be considered as main driver effecting the function the sector of agricultural engineering and its development. Principles of the EU Common Agricultural Policy are implemented also into the development of the European agricultural machinery industry. Under the umbrella of the European Technology Platform MANUFUTURE the community of agricultural engineering in Europe has formulated, for the very first time, a common vision of how agriculture and its driving engineering technologies could look in 2020 and of the strategic technological necessities to translate this vision into reality.

In the year 2006 there was elaborated The Vision 2020 and Strategic Research Agenda of the European Agricultural Machinery Industry (Frerichs, 2006). Within this document there is clearly stated that the European agricultural machinery sector is a world leader in supplying enabling technology to the various businesses of crop and livestock farming. With this, the sector of agricultural engineering and technologies is part of the value-added chain for food production as well as for the increasingly important production of bio-materials and energy crops.

The implementation of the new technologies in the sector agricultural engineering will be effected by the rapid increase of the population, by global climate changes, by increased production and use of biofuels and growing demand for renewable raw materials. Due to this trends to the design of agricultural machines there will be significantly implemented the following systems:

- automation by using of GPS guidance and control systems for wide range of machines (section control and application rate control in case of planters, sprayers, etc.), headland management,
- implementation of the robotic systems on the autonomous vehicles used in the area of fertilizing, seeding, weeding and spraying with support of sophisticated sensors,

- electrification of the agricultural machines and vehicles with aim to obtain higher level of the fuel efficiency, automation and provide more efficient drive control.

The main purpose of implementing the above principles is to achieve:

- knowledge-based competitive machinery and process technology,
- food production with documented quality in conformity with the principles of traceability,
- production processes that are fully compatible with environment and animal welfare regulations,
- technology for production and utilization of renewable resources and efficient use of by-products,
- efficient machines to operate in optimized production systems (for example more automated tractors and harvesters, equipped with plug-and-play electronically-controlled implements, networked or autonomous or semi-autonomous, guided via telematic links with a control station).

Characterization of the technical and technological level and the implementation of the intelligent i-Solutions on the John Deere W 650 combine harvester

In John Deere W-series high-performance combine harvesters a classic technology of tangential threshing mechanism with straw walker is used, thanks to which the crop material is processed accurately and at the same time fuel consumption is sufficiently small. In the next part there are characterised the most important technical and technological parameters of the John Deere W 650 combine harvester.

<u>Parameters of engine</u> - As power unit on the John Deere W 650 combine harvester there is used PowerTech PSX Engine. The 6-cylinder turbocharged John Deere PowerTech PSX air-to air after-cooled delivers rated power up to 219 kW and meets the engine emission level Tier 3.

<u>Parameters of cutting platform</u> - John Deere W 650 combine harvester is equipped with the John Deere 600R Series platform having widths from 4,30 to 10,7 m, these platforms use stainless steel feed plates to help keep crop sliding smoothly into the 4-way adjustable auger.

<u>Parameters of the threshing mechanism</u> - Threshing cylinder diameter: 660mm; Threshing cylinder width: 1670mm; Cylinder speed range, standard: 450 – 980 rpm; Cylinder speed range, option: 220 – 480 and 450 – 980 rpm; Secondary Cylinder and Concave: Beater diameter - 400 mm.

<u>Parameters of the separation and cleaning mechanism</u>

Active Seperation Area: Cylinder concave area - 1,25 m²; Secondary concave area – 0,55 m²; Total active separation area - 1,80 m². Straw Walkers: Number of walkers – 6; Walker length- 4,6 m; Number of walker steps – 11; Walker area – 7,7 m². PowerSeparator: Drum diameter – 410 mm; No. of, type, pattern of fingers - 18 retractable, in-line.

Cleaning system Dual-Flo; adjustable Pre-Cleaner: Fan speed range 700 – 1525 rpm.

<u>Parameter of the grain tank</u> - Volume 9.000 L base; 11.000 L option.

Fig. 1 John Deere W 650 combine harvester as an example of modern farm machine equipped with the intelligent i-solutions based on information technologies

Implementation of the intelligent solutions - John Deere W 650 combine harvester is equipped with the spacious new Deluxe Cab with a CommandTouch armrest, a GreenStar 3 CommandCenter armrest display and digital corner post display. Digital corner post display gives operator complete information on combine's performance. This display provides a quick overview of all primary machine information such as forward speed, engine rpm, losses and warnings. This information is displayed permanently, avoiding confusion or the need to navigate multiple menus.

GreenStar 3 CommandCenter display puts vital machine and crop information within easy reach, making it simple to make quick adjustments to critical controls. Moreover, it supports AMS features such as AutoTrac. From one panel, operator gets quick access to:

- Combine harvester set-up; Remote shoe adjust;Automatic combine adjust system ACA;
- Harvest Monitor; Harvest Smart (automatic feedrate control); AutoTrac guidance system; AutoTrac RowSense; Warning alarms; Calibration "wizards"; On-board diagnostics; Set-point adjust; Video triggers.

John Deere W 650 combine harvester belongs to the group of modern combine harvesters which are equipped with the set of so-called intelligent solutions based on satellite guidance which allow significantly increase harvest performance and productivity. The integrated i-modules take the strain off of operators and owners alike and even help with the paperwork by recording and evaluating key data as you work. It is understandable that such solutions have much higher requirements on the knowledge and skills of the farm production managers, combine operators and technicians.

There are several powerful i-Modules which boost combine harvester productivity and significantly improve yield and throughput. They let operator make full use of the width of the header and maximise field speeds during work. The i-Package for John Deere W 650 combines contains:

- AutoTrac system: satellite controlled, automatic hands-free steering system.
- HarvestMonitor system: a sophisticated system to monitor harvest data.
- HarvestSmart system: system which optimises performance to give operator the choice between maximum throughput and minimum grain loss.
- HarvestDoc system: automatically records all key harvest data during harvest work.
- AutoTrac RowSense system combines the advantages of AutoTrac System and mechanical row feelers for the purpose of the corn harvesting.

We can pay attention to the modules which have direct effect on the harvest productivity.

HarvestMonitor system lets operator keep track of crops condition and performance during harvesting. From the comfort of the cab, operator can find out crop moisture content, dry yield and productivity on the CommandCenter system. Keep totals of crop yields and determine any crop variations in field on-the-go. With this information, it is possible to move towards minimizing inputs and maximising harvest productivity, even on marginal ground. There are three components of HarvestMonitor system:

1. A monitor integrated into the CommandCenter display helps you make machine adjustments as you go with user-friendly, one-touch adjustability.
2. Instant yield sensor calculates grain mass and converts it to a yield figure with ± 3% accuracy. Calibration is simple - simply weigh a reference trailer load and reconcile it against the measured value on the machine.
3. Advanced moisture sensor averages three measurements to give an accuracy of ± 1%. Response time is faster, too - critical when capturing accurate harvest data.

The HarvestSmart system gives combine harvester operator consistent feedrate control. It is the system which allows to get first-class feedrate in hilly terrain, different crop densities and changing field conditions. It is possible to do it manually and hope for the best. Or operator can do it automatically with John Deere's HarvestSmart feedrate control system.

HarvestSmart system can adjust to changing field conditions faster than just about any operator can. It works by calculating the best speed for any field condition, then automatically adjusts the combine speed on-the-go. That's critical to maintaining a consistent feedrate into the combine and achieving peak productivity. It's now standard equipment on all i-Series combines from John Deere.

With HarvestSmart system, operator can automatically control feedrate for either maximum throughput capacity or grain loss parameters. It is necessary to select "Capacity" or "Smart" modes and HarvestSmart system will continually adjust the combine's ground speed until combine harvester reaches either capacity limits (in Capacity mode) or loss limits (in Smart mode). Pulling back on the hydro lever and HarvestSmart system disengages, allowing operator to slow down for headland turns.

Since it automatically keeps the machine at its set maximum-capacity load, HarvestSmart system reduces fatigue and stress on the operator. Plus, combine harvester can get better grain quality and a cleaner grain sample due to more consistent crop loads.

HarvestDoc system can be considered as an efficient tool for documentation of the harvest data. By using of GreenStar 2600 display, located in the combine harvester cab, the HarvestDoc system automatically gathers raw yield, moisture and mapping information for every part of every field. The GreenStar 2600 display is used to operate HarvestDoc system, providing at-a-glance access to harvesting data and on-screen mapping on a large, touch screen, colour-coded display. At any given moment during the harvest, operator and production manager is able to know precisely crop yields, crop moisture levels and harvesting productivity.

Working seamlessly with the combine's HarvestMonitor hardware system, HarvestDoc system loads all this vital information onto a PC card. Production manager can take it to his home computer, download the data and create comprehensive yield and moisture maps along with productivity reports of each field. Precisely the information he need to better manage farming inputs and make informed planning decisions. Plus, harvest the crops that are proven to meet quality assurance requirements.

AutoTrac RowSense system represents the next step to pinpoint accuracy in corn harvesting. AutoTrac RowSense System combines the advantages of the AutoTrac System along with mechanical row feelers. This systems eliminates the limitations of a single system when harvesting corn. Productivity and precision in any conditions: down crop, curves and unevenly shaped fields. The AutoTrac RowSense system can be used in two modes: Down Corn mode and Curves mode.

In Down Corn mode when operating in AutoTrac RowSense mode, both systems - row feeler and AutoTrac - are active. As soon as the feelers are unable to deliver a reliable signal, AutoTrac System takes over control of the steering. The system switches immediately back to fused mode when a row signal is available.

In Curves mode when selecting "A-B curves" or "Adaptive curves" in the guidance settings, AutoTrac RowSense System reacts proactively when approaching curves in the field. The combine steers smoothly into the curve as the location and radius is already available from the last path.

AutoTrac RowSense system can be used also on the fields not planted using AutoTrac System. Until now it was not possible to utilize AutoTrac System in fields planted without the use of guidance assistance, because of the differing track spacings caused by manual steering. AutoTrac RowSense System is able to self-centershift using information from the mechanical row feeler. With this functionality the combine will still follow the rows accurately, even if the tracks in the field are not parallel.

System John Deere Machine Sync helps to increase the efficiency of farmer harvesting logistics. It begins with the grain trailer driver being able to see the grain tank levels of multiple combines in the field. Then he can either be “called” to a specific combine who wants to unload or drive to the machine with the fullest grain tank. Then with the push of a button, the combine operator can control the ground speed and steering of the tractor and grain trailer to ensure smooth unloading on-the-go while maintaining harvesting speed. This means the operator of the grain trailer is more productive as the combine operator loads the trailer to its capacity – no more stressful loading of large trailers or half loads being transported.

System JDLink allows for farm production manager to create the connection between his office and combine harvester. From the point of combine harvester function system JDLink Ultimate is advanced, web-based telematics solutions, which gives the farm production manager the possibility to track all of machines and applications from the convenience of his office or wherever he has an internet connection. Farm production manager can access the data on www.jdlink.com. System JDLink Ultimate offers the following functions: machine location, geofencing, recording of machine hours, maintenance planning, data characterizing fuel consumption, and machine utilization and allows machine diagnostics. Dealer who serves the farmer can use the JDLink infrastructure for additional monitoring services such as Service ADVISOR Remote. This is a new tool which enables dealer’s service manager to access farmer machine’s diagnostic system remotely to ensure his equipment is operating at peak performance.

Apex™ Farm Management software is a basic data management solution that plays a significant role both before a producer goes to the field and after each operation is complete. Just like a producer has to put money into their operation to get money out, they have to put data into the GreenStar™ system to get data out.

Before going to the field, producers can set up operational information in Apex and save the setup data to their USB drive.

Once the USB drive is inserted into the GreenStar display, all associated menus are pre-populated. This saves any downtime that would have been spent manually entering farm and field names while sitting in the field.

Additionally, setting up data in Apex ensures the consistency of such names when managing multiple operators or systems throughout the growing season.

After each operation is complete, the operator can unload the field data into Apex. After the data is unloaded, maps and reports can be generated, so the producer can easily visualize how previous management decisions impacted production and what improvements can still be made.

Apex offers producers the basics—the ability to organize and analyze both historical and current field data.

Apex™ Farm Management software is a basic data management solution that plays a significant role both before a producer goes to the field and after each operation is complete. Just like a producer has to put money into their operation to get money out, they have to put data into the GreenStar™ system to get data out.

Before going to the field, producers can set up operational information in Apex and save the setup data to their USB drive.

Once the USB drive is inserted into the GreenStar display, all associated menus are pre-populated. This saves any downtime that would have been spent manually entering farm and field names while sitting in the field.

Additionally, setting up data in Apex ensures the consistency of such names when managing multiple operators or systems throughout the growing season.

After each operation is complete, the operator can unload the field data into Apex. After the data is unloaded, maps and reports can be generated, so the producer can easily visualize how previous management decisions impacted production and what improvements can still be made.

Apex offers producers the basics—the ability to organize and analyze both historical and current field data.

Apex™ Farm Management software is a basic data management solution that plays a significant role both before a producer goes to the field and after each operation is complete. Just like a producer has to put money into their operation to get money out, they have to put data into the GreenStar™ system to get data out.

Before going to the field, producers can set up operational information in Apex and save the setup data to their USB drive.

Once the USB drive is inserted into the GreenStar display, all associated menus are pre-populated. This saves any downtime that would have been spent manually entering farm and field names while sitting in the field.

Additionally, setting up data in Apex ensures the consistency of such names when managing multiple operators or systems throughout the growing season.

After each operation is complete, the operator can unload the field data into Apex. After the data is unloaded, maps and reports can be generated, so the producer can easily visualize how previous management decisions impacted production and what improvements can still be made.

Apex offers producers the basics—the ability to organize and analyze both historical and current field data.

Apex™ Farm Management software is a basic data management solution that plays a significant role both before a producer goes to the field and after each operation is complete. Just like a producer has to put money into their operation to get money out, they have to put data into the GreenStar™ system to get data out.

Before going to the field, producers can set up operational information in Apex and save the setup data to their USB drive.

Once the USB drive is inserted into the GreenStar display, all associated menus are pre-populated. This saves any downtime that would have been spent manually entering farm and field names while sitting in the field.

Additionally, setting up data in Apex ensures the consistency of such names when managing multiple operators or systems throughout the growing season.

After each operation is complete, the operator can unload the field data into Apex. After the data is unloaded, maps and reports can be generated, so the producer can easily visualize how previous management decisions impacted production and what improvements can still be made.

Apex offers producers the basics—the ability to organize and analyze both historical and current field data.

APEX™ Farm Management software is a basic data management solution that plays a significant role both before a farm production manager goes to the field and after each operation is complete. Just like a producer has to put money into their operation to get money out, they have to put data into the GreenStar™ system to get data out. Before going to the field, producers can set up operational information in APEX and save the setup data to their USB drive. Once the USB drive is inserted into the GreenStar display, all associated menus are pre-populated. This saves any downtime that would have been spent manually entering farm and field names while sitting in the field. Additionally, setting up data in APEX ensures the consistency of such names when managing multiple operators or systems throughout the growing season.After each operation is complete, the operator can unload the field data into APEX file. After the data is unloaded, maps and reports can be generated, so the farm production manager can easily visualize how previous management decisions impacted production and what improvements can still be made. APEX offers farm production manager the basics - the ability to organize and analyze both historical and current field data.

Specification of the requirements on the human resources arising from the use of John Deere W 660 combine harvester

Combine harvesters John Deere W series are used for the harvest of the cereal crops as a part of production system. This production system includes also human resources operating at three levels as follows:

1st level: Farm production manager. Farm production manager makes decision about the ways of machine exploitation, about the organization of the work with regard to the weather condition, grain moisture content and other factors. He uses his knowledge, skills, information and experience to choose the appropriate combine harvester from the following point of view:

type of combine harvester and its price, combine engine power, header working width, type and capacity of the key mechanisms, type of options, expected annual use of the combine harvester, etc.

Farm production manager must be able to provide the activities focused on planning, management and organization of the farm machinery based on using of principles of precision farming. It means that he must be able to use in his work Geographic information system allowing him the processing of the geo-referenced data and preparing yield maps.

2nd level: Combine harvester operator. Combine harvester, which was acquired to the farm on the basis of decision of the production manager is allocated to a certain operator, who is responsible for the exploitation of the machine during the harvest operation. The operator has have knowledge, skills and training, which allows him to use the available technical and technological potential of the combine harvester, which represents some incurred capital costs. He must be able to control individual controllers, key-boards and TouchScreen displays to calibrate, set and regulate the function of individual mechanisms.

3rd level: Technician. Combine harvester as complicated machine needs technical maintenance, exchange of worn machine-parts, adjustments of different mechanisms, diagnostics of electronic units, repairs, etc. All these procedures require specific knowledge, skills, training and experience allowing to keep the function of all combine harvesters in adequate technical conditions.

The exploitation of the combine harvester during harvest is affected by different factors (organization of the harvest process, reliability of the machine, level of technical maintenance, availability of spare parts, weather conditions, etc.). All these factors depend upon the human factor, because it is the man who through his decisions affect the level of use of technical and economical potential of the combine harvester. As a result of the above mentioned factors there can be considered total machine cost and work rate. The more complex and sophisticated a combine harvester is, the higher demands are placed on knowledge, skills and experience of the farm production manager, operator and technician.

Inexperienced farm production manager, operator or technician can cause insufficient exploitation of the combine harvester capacity, with very negative economical consequences (high machinery costs, high fuel consumption, low grain quality, high maintenance costs, etc.). In general it means financial losses.

Conclusion

In the sector of farm machinery there can be observed a strong acceleration of the technical development and innovations. Design of the farm machines is permanently improved with the aim to increase the productivity of the machines, their capacity and fuel efficiency. Submitted paper is focused on presentation of main drivers of the development in sector of agricultural machinery. John Deere W 650 combine harvester was used as an example of modern machine used for harvest of grain crops in design of which there are implemented not only technical innovation but also a set of intelligent solutions based on APEX software and i-modules. Implementation of these intelligent solutions requires the higher level of knowledge, skills and abilities of the farm production managers, operators and technicians to control and operate computer-based applications.

Acknowledgement

This paper has been prepared within the projects:

- “Development of International Cooperation for the Purpose of the Transfer and Implementation of Research and Development in Educational Programs” conducted by the Operational Program: Education, ITMS code: 26110230085
- “Application of the information technologies to increase the environmental and ecological sustainability of the production agrosystem”, project ITMS 26220220014, EU Operational programme RESEARCH and DEVELOPMENT.

References

Frerichs L., 2006. Agricultural engineering and technologies. Vision 2020 and strategic research agenda of the European agricultural machinery industry and research community for the 7th Framework programme for research of the European community, Brussels: 26.

Lammers P. S., 1999. Transfer of technology. In: CIGR Handbook of agricultural engineering. Volume III. Plant production engineering. ASAE, St. Joseph, Michigan: 554-565.

Sørensen C. G., Bochtis D. D., 2010. Conceptual Model of Fleet Management in Agriculture. Biosystems Engineering, 105(1): 41-50.

Srivastava A. K., Goering C. E., Rohrbach R. P., Buckmaster D. R., 2006. Engineering principles of Agricultural Machines. 2nd Edition ASABE, St.Joseph, Michigan: 588.

THE ENVIRONMENT CONSCIOUS HEATING AND COOLING SYSTEM IN GREENHOUSE FOR USING RENEWABLE ENERGY IN COLD SNOWY REGIONS

Shintaroh Ohashi[1*], Kazuhiro Nakano[2], Naoya Kuroda[1]

[1]Faculty of Agriculture, Niigata University, Niigata, Japan
Phone: +81-25-262-6658, Fax: +81-25-262-6658, E-mail: sohashi@agr.niigata-u.ac.jp
[2] Graduate School of Science and Technology, Niigata University, Niigata, Japan

Abstract

It is possible to produce agricultural crops throughout the year using greenhouse horticulture in the cold snowy region. However, heating costs for creating the optimal cultivation environments are high - e.g. (Ohashi, Nakano, 2005). In addition, agricultural production in the greenhouse without oil consumption is desired for the realization of a low-carbon society. In order to reduce oil dependency, the heat pump for cooling and heating without oil consumption has aroused remarkably concern again in recent years, especially the water heat pump and air source heat pump which has been widely used in the agricultural field. On one hand, the heating efficiency of air source heat pumps decreases due to defrost on the heat exchanger of the outdoor unit in winter of the cold snowy region - e.g. (Furuno et al., 2009).

On the other hand, the water heat pump which uses groundwater heat is expected to have the ability of stable operation in winter. However, the problem remains in aspect of the initial investment such as the digging cost of the groundwater well, which restricts the development of water heat pumps. In this study, I focused on the use of the existing equipment which included the groundwater system for melting snow that is popular in the cold snowy region and the agricultural water that is popular in the agricultural areas. Those existing equipment were used as heat supplies and an environment conscious heating and cooling system was build in the greenhouse to reduce the initial investment cost. Comparison with the practices cultivated by oil boilers in winter, CO_2 emission was reduced by approximately 12 % by the present system. Furthermore, this system also created a cool environment in summer with a temperature of 20 ℃ in the greenhouse by using the agricultural water.

Therefore, the usefulness of the environment conscious heating and cooling system all year round by using the water heat pump was confirmed.

Keywords: heating, cooling system, renewable energy

Introduction

In the supply and demand structure of energy in Japan, 82 % of the primary energy supply is dependent on foreign countries, in which almost all (99.8 %) of the petroleum supply is dependent on import; this indicates that domestic production capacity of energy is extremely low. For this reason, reduction of dependency in energy import by establishment of stable energy supply is necessary.

In such circumstances with regard to energy, it is essential to reduce the consumption of fossil fuels and to shift toward safe and clean energy, which will lower environmental burden. Therefore, utilization of renewable energy, which exists in nature, is expected as an alternative to petroleum. Heat pumps (HPs), which allow us to effectively utilize natural energy, have undergone a remarkable improvement in their performance in recent years. In addition, due to the availability of smaller and lower-priced HPs, their use is increasing.

In the use of horticultural greenhouses in winter in cold snowy regions, a large amount of fossil fuel is used to maintain the cultivation environment, leading to an increase in production costs. For this reason, utilization of renewable energy is being attempted. With this background, this study aims to reduce the consumption of fossil fuel for heating greenhouses in winter through HP technology, which allows effective utilization of renewable energy. Currently, greenhouses are not used in horticulture in summer because the temperature inside the greenhouse becomes higher than the outside temperature, which may cause heat damage to plants. In this study, we attempt utilizing HPs for greenhouses throughout the year by creating a cultivation environment using the cooling function of HPs in summer (June through September) when greenhouses are not effectively used. The use of greenhouses in summer will allow planting of new crops, which may lead to an increase in profit.

Year-round utilization of HPs is expected to increase the total planting area in greenhouses and contribute to an early recovery of depreciation cost by increasing the profit.

Materials and Methods

The land for the experiment was Tsuchitaru, Yuzawa-machi, Minami-Uonuma-gun, Niigata, one of the areas that have heaviest snowfall in Japan, where greenhouses are used for crop cultivation in winter. The experiment was performed in an acrylic multi-layer snow-proof greenhouse equipped with a ventilator (facing North-South, 9.2 m wide and 15.5 m deep, with 5.5 m ridge height and 2.9 m eaves height) installed in this area. The greenhouse was heated by a warm water boiler using kerosene (SBG80s, Chofu Seisakusho Co., Ltd.). Flowers and ornamental plants were cultivated in the greenhouse. We installed two water source HPs (EC042, FHP) in this greenhouse, and the internal temperature was controlled within 15 °C –25 °C.

The water source HPs used groundwater in an existing well, used for collecting snowmelt in winter and agricultural water in summer. The use of groundwater in winter adopted an open loop to allow the water to be used for snow melting after heat collection by HP. The use of agricultural water in summer adopted a closed loop, with a heat exchanger installed in the agricultural waterway (Fig.1).

a. Measurement and analyses of the environmental data

To understand the environment-controlling status in the greenhouse, various types of sensors were placed inside and outside the greenhouse, and the data were recorded in a data logger. A thermocouple (type T, ϕ0.32 mm) was placed at four sites in the greenhouse at the height of 2 m above the ground to measure temperature. Near the centre of the greenhouse, thermocouples were placed at heights of 0.5, 1.0, and 2.0 m above the ground to measure temperature. A thermo-hygrometer (RTR-53, T&D) was also placed at the centre of the greenhouse. To understand the status of the conventional heating in the greenhouse, an oil meter (LM05ZAT-AR, HORIBASTEC) was installed on the kerosene pump to measure kerosene consumption (the investigation period of heating using the kerosene boiler was from 20 January to 25 March 2010, except the following investigation period of heating using HPs). In the cooling experiment in summer, a thermo-hygrometer was installed in a min greenhouse to conduct continuous measurement.

Temperature and flow rate (FD-50MY, KEYENCE) of ground water, used as a heat source, at the inlet and outlet of HPs were measured and recorded in a data logger.

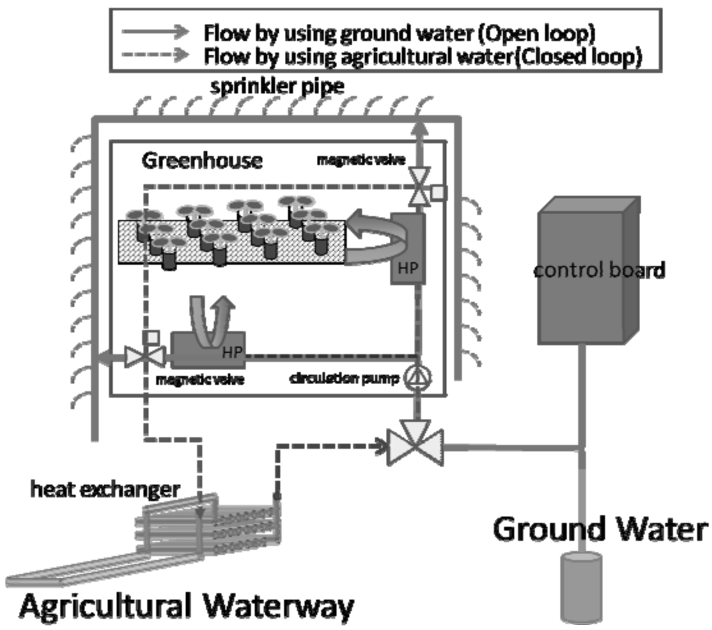

Fig.1 Heat pump system for using renewable energy

b. Analyses of calorific value and input energy through measurements

The heating experiment was conducted in the period between 2 December 2010 and 5 January 2011. Calorific values were calculated using the differences in temperature of snowmelt-derived groundwater between the inlet and outlet and flow rate when HP was in operation. In addition, in order to evaluate the effect of HP use, measurement data of electric power consumption and coefficient of performance (COP), which indicates operating efficiency, were obtained. Alternative kerosene volume was defined as the volume of kerosene that generated an equivalent calorific value by a HP, and calculated using 85% kerosene boiler efficiency and lower calorific values (9.47 kWh/L) of kerosene.

A cooling experiment was conducted from 18 August 2012 to 25 August 2012, in which the heat source was switched to agricultural water. Similar to winter, COP of HP was calculated. Changes in flow rate and the temperatures of agricultural waterway used as the heat source were measured to investigate their influences on the operating efficiency.

Moreover, CO_2 emissions of HP and kerosene were calculated based on the electric power consumed by HP and the alternative kerosene volume, respectively, and used to obtain the CO_2 emission reduction rate in the use of HP.

Results and Discussion

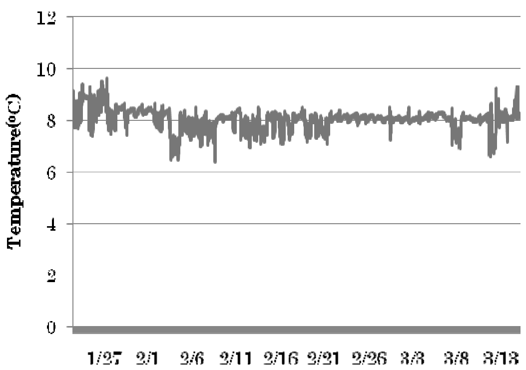

Fig. 2 The temperature change of underground water

a. Heat source in winter: Groundwater used for snow melting

Fig. 2 shows the result of continuous monitoring of the temperature change in the groundwater used for snow melting. During the investigation period, the temperature of the groundwater changed in the range of 6.4 °C–9.6 °C that was lower than expected for the source of heating by HP. This indicates that the volume of groundwater used is important for the improvement of COP of a HP.

Because the groundwater is originally utilized for snow melting, partition ratios of the water volume needs to be controlled when the water is used for both melting snow and HP. The HP system used by us stopped heating operation due to the function of its safety device when the outlet temperature of the ground water used as the heat source reached freezing temperatures. Trial-and-error testing to determine the minimum required flow rate of groundwater with average temperature at 8.5 °C used as the heat source resulted in 20 L/min per HP. In the present experiment, we operated HP at the minimum required flow rate to prioritize snow melting.

b. Heat source in summer: Agricultural water

Fig. 3 and Fig. 4 shows the results of continuous measurement of the flow rate and temperature of the agricultural water. The water temperature in the agricultural water way fluctuated between 0.8 °C and 22.8 °C during the investigation period. When the atmospheric temperature was highest in the investigation period of agricultural water, the water temperature was at 21.1 °C. Although we observed that temperature of the agricultural water was higher than outside air temperature in a period of time at night on and after 20 September, water temperature of the agricultural water was lower throughout the daytime, which confirmed its validity as a heat source for the cooling system of a HP. The temperature of the agricultural water was higher than that of the groundwater, but lower than average outside air temperature during the period when cooling was mainly required (June through September). Unlike groundwater, agricultural water shows seasonal fluctuations of temperature. However, the fluctuations remain within the range lower than the temperatures of outside air, which, suggest that HPs using agricultural water can achieve a higher efficiency operation than air source HPs. This also indicates that agricultural water can be effectively utilized as a heat source. Although rainfall may influence the flow rate of the agricultural waterway, a certain volume of water was observed at all times. Therefore, it was confirmed that agricultural water is available for cooling.

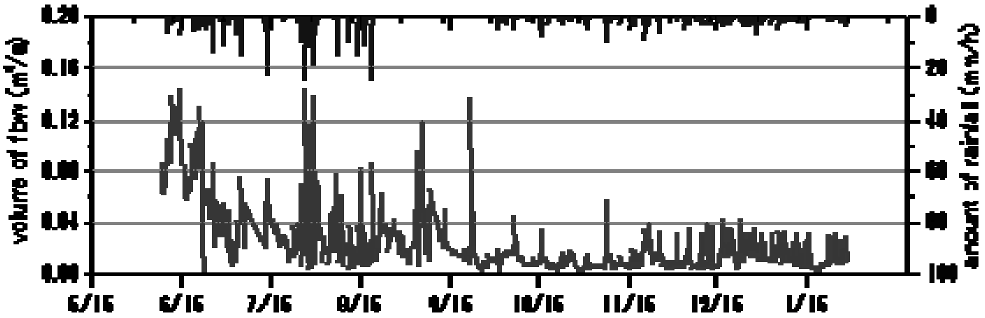

Fig. 3 Change of flow rate of the agricultural water and rainfall

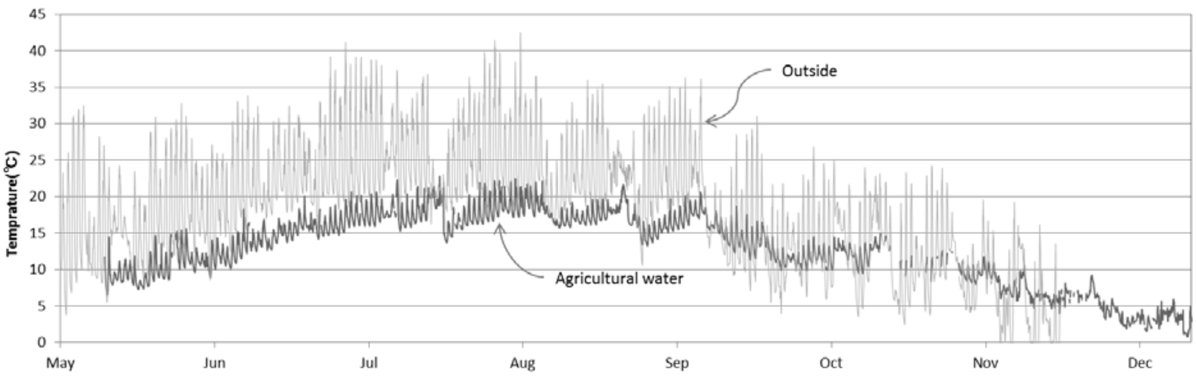

Fig. 4 Change of temperature of the agricultural water and outside

c. Operating efficiency of HP

Fig. 5 shows the temperature change inside the greenhouse during the heating experiment in winter. The average outside air temperature in this period was 1.8 °C. There were days when the temperature exceeded 20 °C in the daytime, when the weather was fine. The lowest temperature was −8.4 °C.

The temperature control by this system maintained the desired temperature range in the greenhouse. Although fluctuations of inside temperatures were seen, it was demonstrated that this system can create an equivalent cultivation environment in greenhouses to that by kerosene boilers.

In addition to electric power consumption, the rate of heat release into the greenhouse was calculated based on the measured data of flow rates and the differences in temperature between the inlet and outlet of the groundwater to obtain COP. The calculated COP of HP in operation in the experimental period was inversely proportional to the change of the air temperature inside the greenhouse. The groundwater at the inlet was 8.5 °C whereas it was discharged with a temperature difference of 3.6 °C. The average COP was 3.4 that is within 3.0–4.0, the level of practical use of water source HPs, showing the effectiveness of this system.

In the cooling experiment in summer, a desired control range of the temperature was maintained inside the mini greenhouse even on the day (20 August) when the highest outside air temperature was 40 °C. The temperature inside the mini greenhouse was 20.3 °C in average. Thus, it was possible to create a cool environment throughout the experimental period using this cooling system.

Although COP fluctuated along with the change in temperature of the agricultural water, it was showing that it was effective for cooling.

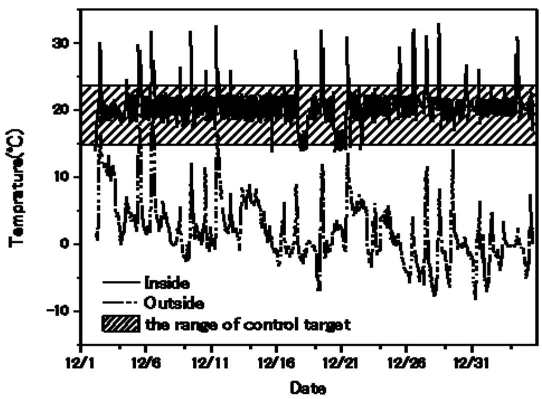

Fig. 5 Temperature change of inside and outside during the heating experiment

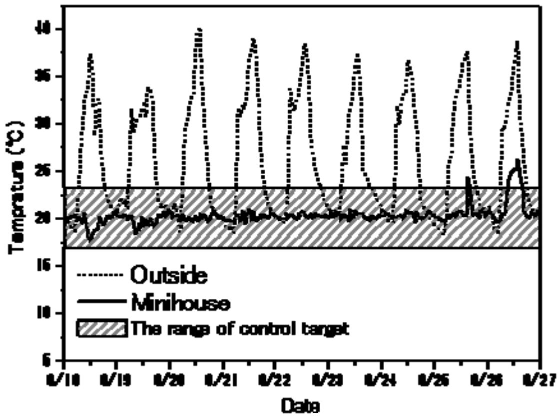

Fig. 6 Temperature change of inside the mini greenhouse and outside during the cooling experiment in summer

d. Alternative kerosene volume and CO2 reduction rate resulting from the introduction of the HP system

The kerosene volume saved by HPs was calculated to be 51.7 L/day during the experimental period. In addition, the reduction rate of CO2 emissions, which was calculated based on the electric power consumption of the whole system, was 12 %.

Future issues

For the improvement of COP of HPs, the system using groundwater needs to be improved to secure a stable flow rate of groundwater to a HP when the ground water is used for both snow-melting and heating a greenhouse. Additionally, in order to improve COP of the system, heating load needs to be reduced. For that purpose, we will investigate the use of supplemental equipment such as humidity-maintaining curtains. We also need to investigate the system's COP in long-term operation. Furthermore, we will investigate humidity control in future because not only temperature but also humidity is an important factor for the environment in crop cultivation.

Acknowledgment

The authors would like to thank Ministry of Agriculture, Forestry and Fisheries (Research and development projects for application in promoting new policy of Agriculture Forestry and Fisheries), The Uchida Energy Science Promotion Foundation, and Sasaki Environment Technology Foundation for supporting this study.

Reference

Furuno S., Sase S., Sato H., 2009. Measurements of the periodical heating load of commercial plastic greenhouses in a heavy snowfall winter. Journal of the Society of Agricultural Structures, 40(2): 113-120.

Ohashi S., Nakano K., 2005. Analysis of greenhouse heat-releasing mechanisms in snowy and cold areas, Journal of the Society of Agricultural Structures, 36(1): 37-45.

TACTILE SENSOR INDICATED GRIPPING FORCE AND SLIPPING

Jan Oliva[1], Jaromír Volf[2*]

[1]M. A. S. Automation, Kolín, Czech Republic, E-mail: olivaj@tiscali.cz
[2]Czech University of Life Sciences Prague, Faculty of Engineering, Kamýcká 129, 165 21 Prague 6, Czech Republic, Phone: +420224383203, Fax: +4202-20921361, E-mail: volf@tf.czu.cz

Abstract

This paper describes new construction of tactile sensor, which enables scanning and measurement of the normal and the tangential force of gripping subject by robot. Its advantage is automatic indication of slipping, too. All these functions are integrated in one sensor. The properties, design and electronic circles of this sensor are topic of this paper.

Keywords: Tactile, sensor, transducer, conductive elastomer, force, slipping.

Introduction

The idea of the using of the tactile information for the technical or biomedical purposes is found out the second part of the 20th century. The medicine development can give us better information of scanning, transmission and processing of tactile information. Similar problem is solved in robotics, too. The sensors, which are able measure force and slipping simultaneously, practically no exist. The sensor, described in this paper, has these properties.

The development of tactile sensor

The tactile information consists of some segments – the detection of mechanical suggestions, detection of pain and detection of the relative position of parts of the human body. We tried to detection of the strength and slipping. The scheme shows Fig.1.

Fig. 1 Block scheme of the sensor

We thought of nine sensors for the detecting of the forces for the Cartesian coordinate system [0, x ,y, z] – eight sensors in the plane xy (the angle 8x 45°) and the ninth sensor for the detecting of the force of the direction of z-axis. We reduced the number of the sensors in the plane xy - we use only four sensors (direction +x, +y, -x, -y) for the direction of the force. The system of the force sensors consists of two electrodes and a slice of conductive rubber between them. The conductive rubber changes its resistivity against the loading force. The output value of this type of sensor is analogue value of the voltage U_{2i} for each sensor. This analogue voltage is turned into the digital value by the analogue-digital converter, so we can obtain digital data.

Principle and construction of the sensor is shown on Fig. 2. All measure elements are placed in the case. The force transducer comprises from the five systems. The four systems are placed two by two in the axis x and in the axis y for measurement of the tangential force. The fifth system is placed on the top of the case and it measures the normal force. The optical head measures slipping.

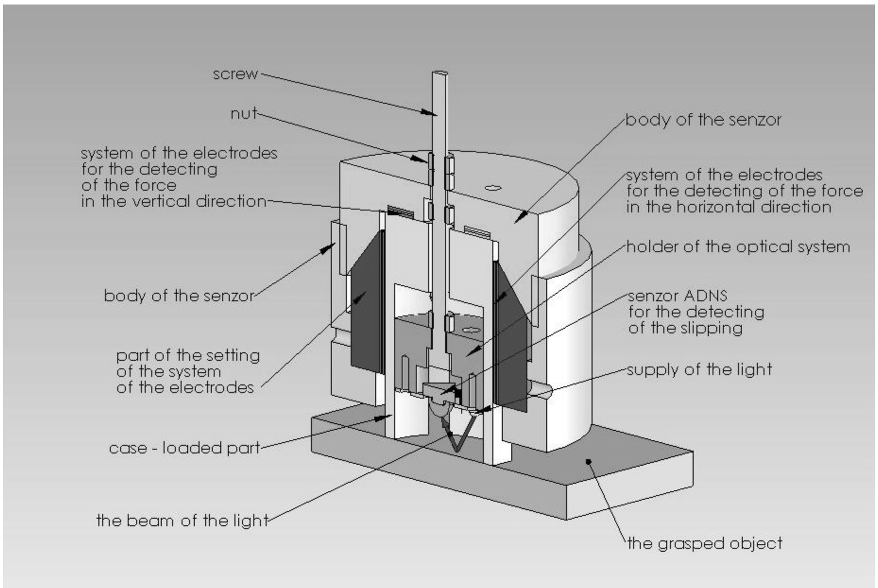

Fig. 2 Principle and construction of the sensor

Scanning part of sensor is evident on the Fig. 3 and Fig. 4. The moving octagon matches the tactile force transducer, which is placed inside of full transducer case.

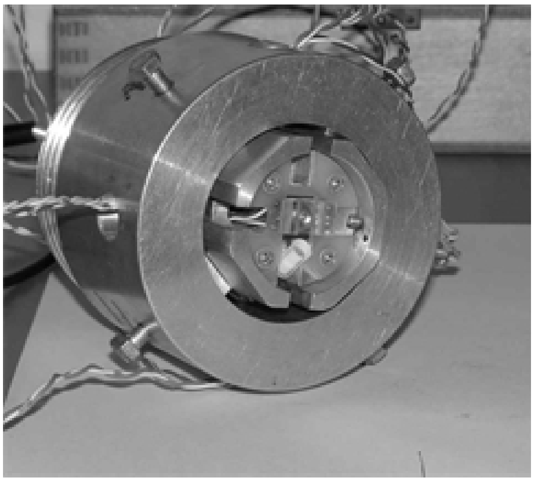

Fig. 3 Measure part of the sensor - bottom view

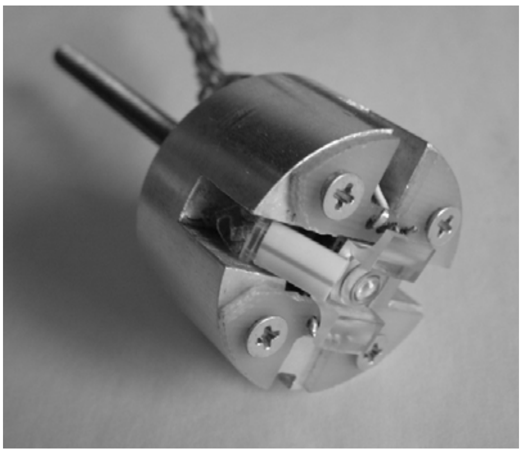

Fig. 4 Optical head for the detecting of the slipping

Slipping sensor (Fig. 4) – there is used an optical principle of the detection of the slipping. The advantage of this system is no contact between the sensor and the grasped object. The slipping can be detected unambiguously instead of mechanical detection. The LED diode (red light - wavelength λ = 639-835 nm) is used as a light supply. The sensor ADNS-2610 was used as a receiver of the red light.

This sensor can catch the beam of the reflected light from the surface of the touched part. This reflected light can turn into the picture. The reflected light is captured in the periods of the time. The sensor can compare the (k) and (k+1) picture and calculate the slipping. The sensor sends data of the motion of the direction x and direction y. The output value of this type sensor is data of the motion for the direction x and direction y.

All sent data is captured by microprocessor AT89C2051. This microprocessor can send the data in PC.

Testing of the assembled sensor

The functionality of an assembled sensor was tested after assembling of the sensor. Printed circuit board was completed. The test of the sensor was divided into four parts – test communication between microprocessor and PC, test of the sensors of forces, test of the conversion analogue voltage U_{2i} into digital value.

Test of communication – the program for AT89C2051 was very simple. Each register of microprocessor (register R0-R7) consisted of 8-bit value and this value was sent into PC. The master of this communication was set PC, the slave was a microprocessor. The principle of the communication was set a half-duplex communication.

Test of the force sensors – each sensor was loaded by weight. The range of the weight was <0;900>g and voltmeter shown the range of analogue voltage <0;1> V.

Test of A/D converter – The analogue value of the voltage was set and the data of A/D converter was sent to PC and the value was read. The analogue value was calculated too and the result was compared to PC value.

Test of the slipping – the Cartesian coordinate system [0,x,y] was drawn on the pad. The assembled sensor was moved in direction +x, +y, -x and –y and the data from the sensor of slipping was read. All measured data was in accordance of the datasheet (Agilent, 2010). All tests were successful.

The assembled sensor was calibrated after the tests. All adjustable parts were fixed and marked as "fixed setting". All sensors of force for each direction of the loaded force were individual loaded in accordance of the principle of superposition. The sensor was loaded by range of the weight <0;900>g and the analogue value U_{2i} was read. It is necessary to indicate the range of loaded force due to correct setting of the upper reference analogue value for the A/D converter, it is better to measure the analogue value U_{2i}. So this analogue value U_{2i} was set as output of the i-force sensor. Each force sensor was measured tenth for each value of the weight and the uncertainties for each force sensor were calculated

The sensor of the slipping was calibrated too, but only the direction. The measured values were the same like the values from datasheet (Agilent, 2010). We don't need calibrate the speed and the distance.

Conclusion

We assembled the prototype of functional model of the sensor for the tactile information. This sensor can detect tactile information – force information and information of the slipping. We resigned some parameters of the sensor due to capital intensity. This prototype of the tactile sensor consists of a lot of adjusting elements. These adjusting elements increased its volume (diameter D = 85 mm and the height H= cca 75 mm). If we use a nanotechnology, the dimensions of the sensor can be reduced into acceptable dimensions. Signal output can be determined for the human body in future. The output value of the forces sensors shows Fig. 5. The upper reference value can be set suitable on the basis of the range of values of U_{2i}. If the upper reference value is set unsuitable, the sensor will be not more sensible due to error of the discretization

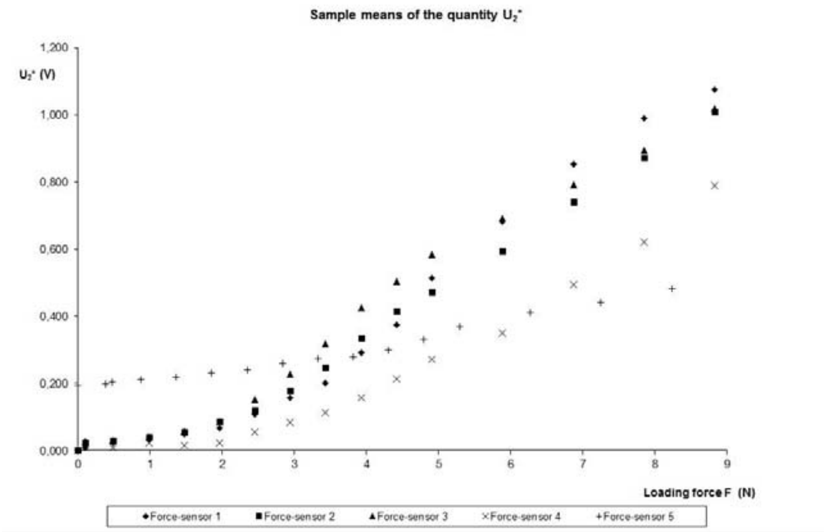

Fig. 5 Sample averages of the values of the force sensors

Acknowledgement

The measurements were carried out within the IGA project of the Faculty of Engineering, Czech University of Life Sciences in Prague, reg. no. IGA 31200/1312/3129, titled "Evaluation of contact surface of the tire using electronic pressure sensors".

Reference

Agilent. 2010. Agilent ADNS-2610 Optical mouse sensor. Datasheet. [online].

Baglio S., Muscato G., Savalli N., 2002. Tactile Measuring Systems for the Recognition of Unknown Surfaces. Instrumentation an Measurement, IEEE Transaction on

Instrumentation and Measurement. Vol. 51(3): 522 – 531.
Barman S., Guha S. K., 2006. Analysis of a new combined stretch and pressure sensor for internal nodule palpation. Sensors And Actuators A-Physical 125 (2): 210 – 216.
Chen G. H., Lu J. R., Lu W. et al., 2005. Time-dependence of piezo-resistive behavior for polyethylene/ foliated graphite nanocomposites. Polymer International 54 (12): 1689 – 1693.
Del Prete Z., Monteleone L., Steindler R., 2001. A novel pressure array sensor based on contact resistance variation: Metrological properties. Review Of Scientific Instruments Vol. 72(2): 1548 – 1553.
Girao P. S., Pinto R., Pedro M., Postolache, O. et al., 2013. Tactile sensors for robotic applications. MEASUREMENT, 46(5): 1771 – 1771.
Ishikawa M., Shimojo M., 1996. Tactile systems. In.: Yamasaki, H.: Intelligent Sensors, Elsewier: 165 - 176
Jiang M. J., Dang Z. M., Xu H. P., 2006. Significant temperature and pressure sensitivities of electrical properties in chemically modified multiwall carbon nanotube / methylvinyl silicone rubber nanocomposites. Applied Physics Letters 89 (18).
Job A. E., Oliveira F. A., Alves N. et al., 2003. Conductive composites of natural rubber and carbon black for pressure sensors. Synthetic Metals 135 (1-3): 99 – 100.
Králíček P., 2002. Introduction to Special Neurophysiology. Karolinum, Prague. (in Czech)
Liu H., Meusel P., Hirzinger G., 1998. A Tactile Sensing system for the DLR Three Finger Robot Hand. Institut of Robot and system Dynamics. German Aerospace Research Establishment.
Liu H., Meusel P., Hirzinger G., 2004. A Tactile sensing for the DLR Three-Finger Robot Hand. ISMCR 2004. Houston, USA.
Lu J. R., Weng W. G., Chen X. F. et al., 2005. Piezoresistive materials from directed shear-induced assembly of graphite nanosheets in polyethylene. Advanced Functional Materials 15 (8): 1358 – 1363.
Soares B. G., Amorim G. S., Souza F. G., et al., 2006. The in situ polymerization of aniline in nitrile rubber. Synthetic Metals 156 (2-4): 91 – 98.
Souza F. G., Michel R. C., Soares B. G., 2005. A methodology for studying the dependence of electrical resistivity with pressure in conducting composites. Polymer Testing 24 (8): 998-1004.
Tohyama O., Maeda S., Itoh H., 1999. Fiber-optic tactile microsensor for detecting the position of the tip of a fiberscope, IEEE J Sel Top Quant 5: 115 – 118.

MAIZE GROWTH AND DEVELOPMENT AS AFFECTED BY TILLAGE SYSTEMS UNDER MEDITERRANEAN CONDITIONS

Ali Ozpinar, Sakine Ozpinar

Plant Protection Department, Faculty of Agriculture, Canakkale Onsekiz Mart University Canakkale, Turkey.Tel:+902862180018, Fax:+902862180545, E-mail: aozpinar@comu.edu.tr

Abstract

Conservation tillage has proven to be very effective in reducing runoff and in increasing soil water storage. In semi-arid cropping situations, the later fact should result in a greater yield potential for conservation than for conventional tillage. The objective this study was to determine the influence of tillage on growth and yield of maize (Zea mays L.) under semi-arid Mediterranean conditions in the western Turkey. The experiment was conducted from 2005 through 2009 on a clay loam soil under shallow rototiller, chisel and mouldboard plough tillage systems. Results indicated that root biomass was higher in rototiller than in plough and chisel. Rototiller also provided higher plant biomass in all days after planting in three of the five years. The highest root dry matter by soil depth found at the 0 to 10 cm compared with the 10 to 20 cm and the 20 to 30 cm for all study years in three tillage systems. Rototiller also increased the plant height during the early part of the growing season when compared with plough and chisel, with the exception of the last part of the growing season that they showed similar. On the other hand, the highest root dry matter by soil depth found at the 0 to 10 cm compared with the 10 to 20 cm and the 20 to 30 cm for all study years in three tillage systems. Considering the tillage systems, the lowest root dry matter was found in plough, especially in 2008 of the 20 to 30 cm depth when compared with rototiller and chisel. Grain yield was also found higher in rototiller than in plough and chisel in two of the five years.

Key Words: Maize growth parameters, yield, tillage systems

Introduction

Tillage practices are sensitive to the physical conditions of the soil in the seedbed and on seedling emergence and plant stand establishment. In general, conventionally tilled soils tend to have lower water contents than conservation tillage at shallower depth (Unger, Fulton, 1990), but conservation tillage can reduce soil evaporation and offer a great potential to increase water available to the crop (Ozpinar, 2006a). In semi-arid cropping systems, water storage is increased in conservation tillage that it results in greater yield than in conventional tillage (Ozpinar, 2006a). On the other hand, conventional tillage known the traditional primary tillage practice led to a significant decline in soil quality. Therefore, there is need to add increasing amounts of nitrogen as chemical fertilizer to maintain maize yields or to add green manure to the soil to improve the soil quality. Green manuring is known to improve soil nitrogen fertility levels (Zentner et al., 2002) for the following crop and at the same time. It was reported that legume plowdown provides the equivalent of 90 to 125 kg nitrogen ha^{-1} to the following maize crop when maximum maize grain yields are achieved with 159 kg nitrogen ha^{-1} (Berenguer et al., 2009).

In this study, maize was planted after winter vetch (*Vicia sativa* L.) cover crop with three tillage systems. Objective was to evaluate the effects of two conservation or reduced tillage systems (including rototiller and chisel) by comparing them with the conventional tillage system using mouldboard plough and by studying some of the maize growth parameters and grain yield applying green manure instead of chemical fertilizer in the production of clay-loam soil conditions.

Experimental arrangement

A 5 year (2005-2009) tillage experiment was conducted in Canakkale, Turkey, where the soil is a clay-loam texture. The annual rainfall and temperature are 15.0 $^{\circ}$C and 609 mm, respectively, with partially cold winters and very hot dry summers. The experiment was conducted for 2005, 2006, 2007, 2008 and 2009 in winter vetch-summer maize rotation with three tillage systems. Two of these were conservation or reduced tillage systems in which rototiller (shallow) (ST) and chisel (CT) were used. The third was conventional tillage with mouldboard plough (MT) used traditionally in the region. All tillage treatments were performed following common vetch (*Vicia sativa* L.) in spring. Treatments were repeated on the same experimental area in successive years. The experiment consisted of a green manure-maize rotation from December 2004 until the end of the growing season in 2009. Maize (variety *Agromar MF 714*) was planted with 76 cm row spacing (eight rows) to have 68 000 seeds ha^{-1}.

The 20 meters length of the 4 inner rows of each plot was determined for the measurement of plant growth parameters. All plants in 5 meters of each row were marked at the beginning of the growing season and used throughout the season to measure plant growth parameters in three replications of each plot. Plant height was measured on 25 plants of the medium two rows of each plot from the ground level to the base of the last fully opened leaf from complete emergence to mature height. Biomass was determined by cutting aboveground plant from 5 plants in three replications of each plot on the same dates as the plant height measurements, with the exception of the 2008 which was done in different days. Biomass was oven-dried at 65 ºC to a constant weight to determine dry biomass matter content. Root dry matter was determined by excavating the entire root system and surrounding soil down to 1 meter, for the same 5 plants used for biomass weight measurements. Root and soil materials were saturated for 1-2 day prior to washing by use of a low pressure water jet. The roots were also oven-dried likewise biomass. Plant height above the ground and root biomass was measured until silking and pollination period. The daily crop dry matter production was calculated according to the dry matter production. For root weight by soil depths, samples were collected from each plot at depth of the 0 to 10 cm, 10 to 20 cm and 20 to 30 cm with a hand-operated soil core sampler. Crop growth rate was calculated using the following equation. W_1 and W_2 are total dry matter of plant at time of first (T_1) and second T_2 observations.

$$\text{Crop growth rate (kg ha}^{-1}\text{ per day)} = \frac{W_2 - W_1}{T_2 - T_1} \qquad (1)$$

The statistical analysis software MSTAT-C was used to analyze the data for a split-plot treatment arrangement. The ANOVA procedure was used to evaluate the significance of each treatment for parameters. Treatment means were separated by LSD test at the $P<0.05$.

Results and discussion

The biomass (stem and leaf) yield was determined higher in plough than in rototiller and chisel at the late part of 2007 (Table 2). Plough also increased the biomass weight in 2005 and 2009 in all the day after planting. In considering three tillage treatments, the highest rate of leaf and stem biomass weight increase was just before silking, apparently as a result of cell differentiation for ear production. It was reported that lags in the early growth and lower plant populations lead to less leaf and stem biomass in maize (Braim et al., 1992). In this context, it is likely that higher plant numbers and higher initial growth under rototiller for 2008 growing season were responsible for higher leaf and stem biomass. These findings are of paramount importance for the regional farmers because aboveground biomass production is a major quality factor in dry form for animal feed, and grain which is consumed as food. Similar to biomass, rototiller maintained higher plant heights than plough and chisel throughout the 2006 (Table 1), while rototiller provided similar plant height to plough throughout 2005. In 2006, the highest plant height occurred 20% and 14% at the 24 and 31 day after planting in rototiller and chisel, respectively, when compared with plough. In 2007, rototiller also increased the plant height during the early part of the growing season at the 20, 27, 34, 40 and 54 day after planting with rate of 0.05%, 0.08%, 11%, 12% and 10%, respectively, when compared with plough, with the exception of the last part of the growing season at the 60 day after planting (Table 2). The plant height found only higher in rototiller than in plough at the 45, 52, 57 and 65 day after planting, but it was similar in plough and chisel when chisel provided the highest plant height during the rest of 2008 season at the 71, 78, 86 and 93 day after planting (Table 2). In 2009, the plant height was similar in plough and chisel when rototiller was the lowest during the early part of the growing season at the 36, 43, 48, 54 and 62 day after planting (Table 3). In the same study year, plough provided more plant height than chisel and rototiller during the last part of the growing season at the 69, 76, 81 and 94 day after planting. When considering the five study years, the higher plant height of maize in rototiller and chisel compared with plough is inconsistent, but the maximum differences in plant height for rototiller occurred in the most of day after planting in all study years. This was similar to the results of several other studies (Kapusta et al., 1996). In this study, the higher water losses from increased air circulation in the cloddy seedbeds in plough may be responsible for lower plant growth in the early part of the growing season. It may be attribute lower final plant population in plough in comparison with rototiller. Field observations indicated that a more vigorous appearance of maize in rototiller, other growth promoting factors may also have contributed to faster growth in rototiller. The higher biomass growth in rototiller (Tables 1, 2, 3) could be attributed only in part to the higher leaf development (unpublished results). These results imply that the effect each treatment had on the plant height definitely affected the general growth of the plant. Measurements of penetration resistance indicated that it was lower in rototiller compared with that plough at the 20 to 30 cm depth (unpublished results). This suggested that lower water stress in rototiller was related to lower soil penetration resistance for root development (Table 1, 2, 3). Differences in the root dry biomass between tillage systems were generally significant, but significantly increased rooting for rototiller in all day after planting in 2006 (Table 1), while rooting was significantly higher for plough at the 32, 60, 80 and day after planting, except in the 49 day after planting with the highest rooting in chisel in 2005 (Table 1). Similarly, rototiller increased root dry matter only at the 60 day after planting in 2007 when chisel provided the highest root dry matter at the 40 and 47 day after planting following by plough (Table 2). In 2008, it was found significantly differences between tillage treatments, but the highest root dry matter was changed relative to day after planting for treatments (Table 2). Rototiller, for example, increased dry root at the 45, 57, 86 and 93 day after planting. On the other hand, plough increased root dry matter at the 52, 65 and 71 day after planting when chisel provided only higher value at the 78 day after planting. Similar results to 2006 for root dry mater were found in 2009 (Table 7).

Root dry matter weight by soil depth was measured out of 2005 in 2006, 2007, 2008 and 2009 and showed differences between tillage treatments at all soil depths (Table 4). It increased significantly for chisel at the 0 to 10 cm in 2006 and 2008, while plough increased the root dry matter in 2007 at the same depth. For 10 to 20 cm depth, rototiller had the highest root dry matter in 2008 and 2009 when chisel and rototiller provided the highest root dry matter in 2006. When considering 20 to 30 cm, chisel increased the root dry matter compared with plough and rototiller in 2007, 2008 and 2009, while chisel provide similar root dry matter to plough in 2006. Much of the root dry matter in all tillage treatments is determined at the topsoil followed by the 10 to 20 cm and the 20 to 30 cm for all study years when chisel showed higher root dry matter vertically than rototiller and plough. Lowest root dry matter for plough at the 20 to 30 cm depth in 2008 may be as a result of higher penetration resistance at this soil depth (unpublished results). After 5-year operation of three tillage systems, however, penetration resistance did not recorded any values that could affect root growth due to may be observing maximum value of resistance which is below the threshold of 2.5 MPa (Bengough, Mullins, 1990).

The grain yield with three tillage systems vary from year to year due to the fluctuations in weather and it significantly observed differences between tillage in all the study years (Table 5). Over the 5-year average, rototiller yielded 17% more than chisel, although there is slightly a yield differences by 0.08% between plough and rototiller.

Tab. 1 Tillage effect on maize growth under tillage systems for different dates in 2005 and 2006

Measurement	**Days after planting**										
	Tillage	**2005**					**2006**				
		25	40	60	80	126	24	31	39	52	67
Plant height (cm)	ST	22.0a[a]	51.3ab	77.7a	133.7a	154.3a	32.4a	53.9a	83.9a	156.9a	166.7a
	MT	24.7a	59.3a	82.0a	147.3a	170.2a	25.8ab	46.4ab	76.4ab	150.0ab	162.9a
	CT	17.0b	43.7b	71.0b	134.3a	170.8a	22.7b	38.6b	61.7b	119.3b	137.8b
	LSD[b]	4.3	9.5	5.7	NS	NS	6.1	10.6	18.2	37.9	31.3
		32	49	60	80	100	24	31	39	52	67
Biomass (leaf and stem) (kg ha^{-1})	ST	81.6b	179.5ab	4156.0ab	6789.0b	9234.3b	103.9a	184.3a	335.2a	3047.2a	10016.0a
	MT	115.3a	197.6a	5697.7a	8256.3a	10568.7a	70.8ab	159.0ab	351.7a	3305.6a	8067.1b
	CT	86.2b	159.3b	3984.7b	6997.7b	9227.0b	32.2b	73.0b	199.5b	1644.3b	5213.0c
	LSD	22.7	87.5	2245.0	2763.0	2707.0	46.8	104.5	108.2	1155.5	1390.0
		0-32	32-49	49-60	60-80	80-100	0-24	24-31	31-39	39-52	52-67
Crop growth rate (kg ha^{-1} per day)	ST	2.6b	5.8a	361.5b	131.7b	122.3a	3.4a	17.9a	16.0b	208.6a	464.6a
	MT	3.6a	4.8ab	500.0a	127.9b	115.6a	2.9a	12.6ab	24.1a	227.2a	317.4b
	CT	2.7b	4.3b	347.8b	150.7a	111.5a	1.3b	5.9b	15.8b	111.1b	237.9b
	LSD	0.7	6.9	209.9	179.3	NS	0.8	7.6	12.9	95.4	132.3
		32	49	60	80	100	24	31	39	52	67
Root biomass (kg ha^{-1})	ST	36.5b	92.0b	260.7ab	688.7b	895.3b	33.5a	45.1a	66.3a	427.6ab	2679.6a
	MT	44.8a	95.3b	526.0a	1024.7a	1325.3a	26.9ab	33.1ab	56.6a	452.6a	2021.5c
	CT	38.4b	101.8a	230.7b	644.7b	912.3b	13.6b	24.5b	31.4b	223.3b	2274.2ab
	LSD	25.1	36.5	282.8	115.2	533.7	16.0	20.5	23.9	207.4	819.8

[a] Values followed by the same letter in a column are not significantly different between tillage treatments at $P<0.05$.
[b] LSD between tillage treatments within a column ($P<0.05$).

Tab. 2 Tillage effect on maize growth under tillage systems for different dates in 2007 and 2008.

		Days after planting													
Measurement	**Tillage**	**2007**						**2008**							
Plant height (cm)		20	27	34	40	54	60	45	52	57	65	71	78	86	93
	ST	35.2a[a]	54.2a	71.5a	111.4a	205.1a	226.6b	86.7a	138.8a	142.3a	183.0a	187.1b	187.4c	201.8b	200.1b
	MT	33.6b	50.1b	64.0b	98.9b	186.3b	217.7c	64.5b	106.1b	120.8b	161.3b	175.3c	194.9b	202.9b	204.9b
	CT	35.9a	51.5b5.8	64.5b	105.1ab	198.4ab	235.9a	78.5a	125.4a	139.9a	184.4a	192.1a	211.7a	212.4a	214.3a
	LSD[b]	4.9	5.8	5.2	53.6	29.5	47.43	14.3	18.9	25.3	31.1	31.2	26.0	41.2	43.8
Biomass (leaf and stem) (kg ha^{-1})		20	26	34	40	47	60	30	45	56	61	78	80	100	107
	ST	52.9a	419.5a	473.6 a	834a	1512b	9525b	287.7a	480.0b	5065.4a	6395.1a	6622.8a	13485.8 a	20204.5 a	20410.9 a
	MT	51.8a	374.5ab	474.4 a	672b	2380a	10531a	214.6b	608.5a	5070.3a	6138.6a b	6222.5a b	11551.9 b	14031.2 b	14246.0 b
	CT	49.4a	3129a	412.5 a	797ab	1835b	9842ab	221.5a	457.7b	3893.9b	4825.5b	4994.8b	13647.3 a	14069.4 b	14615.0 b
	LSD	NS	93.7	NS	168.6	541.0	4326.0	196.6	219.0	1648.0	1444.0	1609.0	6301.0	5835.0	5453.0
Crop growth rate (kg ha^{-1} per day		0-20	26-20	34-26	40-34	47-40	60-47	30-0	45-30	56-45	61-56	78-61	80-78	100-80	107-100
	ST	2.6a	61.1a	6.8b	60.0a	52.2b	616.4b	6.8a	14.8b	764.2a	221.6a	119.8a	457.5b	959.8a	29.5b
	MT	2.6a	53.8ab	12.5a	32.9b	131.4a	627.0a	4.7b	30.3a	743.6a	178.0b	88.6b	355.3c	354.2b	30.7b
	CT	2.5a	44.9b	11.7a	64.1a	79.8b	615.9b	4.8b	18.2b	572.7b	155.3b	84.7b	576.8a	60.3c	77.9a
	LSD	0.2	15.7	16.2	41.9	48.2	309.0	4.4	25.2	260.9	416.6	192.7	387.6		121.5
Root biomass (kg ha^{-1})		20	26	34	40	47	60	30	45	56	61	78	80	100	107
	ST	15.6a	23.3b	1389.5b	1763.9c	2911. 8b	3440.7a	81.5a	53.8b	343.9a	323.1b	397.7b	1086.2b	111.45a	1198.5a
	MT	17.1a	26.1a	1952.4a	2521.2ab	3291.8 a	3362.8b	60.0b	112.3a	255.4c	502.3a	510.0a	722.3c	1027.7a	1087.0a b
	CT	14.8b	21.6b	1348.2b	2869.4a	3251.4 a	3313.5b	50.0b	4.5c	275.4b	308.5b	344.6b	1220.8a	925.4b	1038.5a b
	LSD	5.3	8.6	792.2	1224	994.5	194.3	66.1	89.8	346.4	197.8	220.7	516.9	513.6	279.3

Tab. 3 Tillage effect on maize growth under tillage systems for different dates in 2009.

Measurement	Tillage	Days after planting								
		36	**43**	**48**	**54**	**62**	**69**	**76**	**81**	**94**
Plant height (cm)	ST	57.9b[a]	83.7a	122.3b	171.3b	232.3b	266.2b	272.2b	269.6ab	277.2a
	MT	85.6a	126.5b	180.2a	238.0a	288.4a	300.4a	304.3a	289.9a	284.8a
	CT	94.9a	132.9b	180.7a	237.7a	271.8a	267.7b	271.3b	253.1b	256.3b
	LSD[b]	26.1	32.6	35.0	43.4	37.9	10.3	5.7	22.2	18.8
		36	50	75	81	100				
Biomass (leaf and stem) (kg ha^{-1})	ST	223.7b	362.3a	9310.1b	11483.8c	11937.0b				
	MT	230.0a	361.7a	13845.1a	15334.9a	15695.7a				
	CT	228.0a	323.3b	12601.5a	14298.4b	14821.0ab				
	LSD	10.7	115.7	5652.0	19.7	2892.0				
		36-0	50-36	75-50	81-75	100-181				
Crop growth rate (kg ha^{-1} per day)	ST	6.2a	9.90a	357.9b	362.3a	23.9b				
	MT	6.4a	9.40a	539.3a	248.3b	19.0c				
	CT	6.3a	6.81b	491.1a	282.8b	27.5a				
	LSD	NS	8.8	224.9	710.2	40.6				
		36	50	75	81	100				
Root biomass (kg ha^{-1})	ST	115.3a	311.7a	2220.0a	2610.1a	3139.7a				
	MT	103.7ab	286.7ab	1437.2b	2454.8a	2879.3ab				
	CT	95.7b	281.0b	2211.0a	2367.4a	2665.7b				
	LSD	18.8	29.2	1411.0	NS	439.3				

Tab. 4 Root dry weight (kg ha^{-1}) by soil depth at the maize flowering under tillage systems

Depth (cm)	ST	MT	CT	LSD[b]	ST	MT	CT	LSD[b]
	2006				**2008**			
0-10	441b[a]	439b	685a	203.5	5552a	2115b	7215a	2911.0
10-20	404a	246b	401a	121.5	2401a	525b	1764ab	1491.0
20-30	335b	437a	398ab	162.7	503a	168b	535a	289.0
	2007				2009			
0-10	1950b	2829a	2102a	1925.0	1885ab	2281a	2024a	2713.0
10-20	773b	470c	1225a	291.1	5774a	1996b	2584b	2675.0
20-30	893a	490b	960a	298.7	2194ab	1776c	3466a	4559.0

Tab. 5 Grain yield of maize under tillage systems in all years.

Tillage	Grain yield (Mg ha^{-1})						
	2005	**2006**	**2007**	**2008**	**2009**	**LSD**	**Mean**
ST	8.7bB[a]	12.0aA	9.9AB	9.9bB	14.6aAB	5.9	12.6a
MT	12.0aA	12.6aA	6.8B	13.5aA	12.2bA	3.9	11.4ab
CT	8.9bB	9.7bB	9.0B	10.6bAB	13.8abA	51.9	10.4b
LSD[b]	3.1	4.2	NS	3.8	6.2		1.2
Mean	9.9	11.4	8.6	11.3	13.5		11.5

The higher grain yield for rototiller in 2007 may in part be related to higher soil water content throughout soil profile (unpublished results). Also a higher penetration resistance registered in plough at the 20 to 30 cm soil depth may be cause grain yield decrease. This corroborates the notion of the longer-term suitability of this soil type for row crop production in rototiller, and the problems associated with spring plough tillage following vetch due to difficulties obtaining a suitable seedbed in the years of the experiment due to the seedbed's high plasticity. Similar results have been reported in other regions (Fabrizzi et al., 2005) under contrasting and similar rainfall availability conditions (Wilhelm et al., 1986). In contrast, several authors reported that chisel yielded more than plough (Raimbault, Vyn, 1991), while others reported no differences in maize yield between conservation and conventional tillage systems (Kapusta et al.,1996; Al-Darby, Lowery, 1996).

The higher average grain yield in rototiller suggests that surface soil in seedbed conditions improves the performance of rototiller on these soils, as was also concluded by Ozpinar (2006b) in the same region for cereal production.

Conclusion

Five years of study demonstrated that rototiller offers a high maize grain yield compared with plough for maize production which was planted after winter cover crop vetch in late spring. Crop growth was smaller in plough compared with rototiller. Rototiller significantly improved crop growth parameters after winter cover crop vetch. Much of the root dry matter in all tillage treatments is determined at the topsoil followed by the 10 to 20 cm and the 20 to 30 cm for all study years when chisel showed higher root dry matter vertically than rototiller and plough. In general, however, tillage treatments had no significant effect on aboveground biomass and crop growth rate during all study years, except the initial growing stage. Although economics were not considered in this study, considerable fuel and labour savings would be realized in rototiller because of at least two fewer trips over the field. Considering the higher cost of production and energy use combined with lower yields for plough (Ozpinar, Ozpinar, 2011), plough in this crop production could be replaced by rototiller in the spring seedbed preparation after cover crops.

Reference

Al-Darby A. M., Lowery B., 1996. Evaluation of corn growth and productivity with three conservation tillage system. Agron J 78: 901 - 907.

Bengough A. G., Mullins C. E., 1990. Mechanical impedance to root growth: a review of experimental techniques and root growth responses. J of Soil Sci.41: 341 - 358.

Berenguer P., Santiveri F., Boixaderac J., Lloveras J., 2009. Nitrogen fertilisation of irrigated maize under Mediterranean conditions. European J Argon 30: 163 - 171.

Braim A., Chane K., Hodgson D. R., 1992. Effects of simplified cultivation on the growth and yield of spring barley on a sandy loam soil. 2. Soil physical properties and root growth; root: shoot relationships, inflow rates of nitrogen; water use. Soil Till Res 22: 173 - 187.

Fabrizzi K. P., Garcia F. O., Costa J. L., Picone L. I., 2005. Soil water dynamics, physical properties and corn and wheat responses to minimum and no-tillage systems in the southern Pampas of Argentina. Soil Till Res 81: 57 - 69.

Kapusta G., Krausz R. F., Matthews J. L., 1996. Corn yield is equal in conventional, reduced, and no tillage after 20 years. Agronomy J 88: 812 - 817.

Ozpinar S., 2006a. Effects of tillage on productivity of a winter wheat-vetch rotation under dryland Mediterranean conditions. Soil Till Res 89: 258 - 265.

Ozpinar S., 2006b. Effects of tillage systems on weed population and economics for winter wheat production under the Mediterranean dryland conditions. Soil Till Res 87: 1 - 8.

Ozpinar S., Ozpinar A., 2011. Influence of tillage and crop rotation systems on economy and weed density in a semi-arid region. J. of Agricul. Science and Technology 13: 769 - 784.

Raimbault B. A., Vyn T. J., 1991. Crop rotation and tillage effects on corn growth and soil structural stability. Agronomy J 83: 979 - 985.

Unger P. W., Fulton L. J., 1990. Conventional and no-tillage effects on upper root zone soil conditions. Soil Till Res 16: 337 - 344.

Wilhelm W. W., Doran J. W., Power J. F., 1986. Corn and soybean yield response to crop residue management under no-tillage production system. Agronomy J 78: 184 - 189.

Zentner R. P., Lafond G. P., Derksen D. A., Campbell C. A., 2002. Tillage method and crop diversification: effect on economic returns and riskiness of cropping systems in a Thin Black Chernozem of the Canadian Prairies. Soil Till. Res 67: 9 - 11.

RAINFED WHEAT ENERGY BALANCE OF DIFFERENT TILLAGE SYSTEMS IN WESTERN TURKEY

Sakine Ozpinar, Ali Ozpinar

Farm Machinery Department, Faculty of Agriculture, Canakkale Onsekiz Mart University Canakkale,Turkey.Tel:+90 2862180018, Fax:+90 2862180545, E-mail:sozpinar@comu.edu.tr

Abstract

Data from a field experiment conducted in western Turkey over 3-year period (2001-2004) were used to determine the energy balance of continuous winter wheat as affected by three tillage systems under rainfed conditions in Mediterranean climate. Tillage systems included mouldboard plough, rototiller and tandem disk. As inputs, the factors supplied and controlled by farmers were considered. The energy balance was assessed by comparing the variables: net energy output (energy output minus energy input), energy output/input ratio, and energy productivity (wheat grain yield per unit energy input). According to 3-year mean, the grain yield ranking from the highest to the lowest was rototiller>disk> plough, indicating that grain yield increased as tillage decreased. The total energy inputs were 1.8 and 1.1 times greater in rototiller than in disk and plough, respectively. Rototiller required higher energy input for energy used in production of rototiller than disk (46.53% less) and plough (6.93% less). Energy output was highest in rototiller. Hence, the highest net energy was found in rototiller (26%) than in plough and disk while the difference between both was less. Output/input ratio and energy productivity was higher in disk than in plough and rototiller. This indicates that, in terms of energy efficiency, the viability of rototiller (low-input field practises, high yields and net energy) under rainfed conditions, compared to plough requiring high-input field practices (low yields and net energy), would appear more recommendable. In addition, both rototiller and disk systems improve the energy efficiency of wheat production compared with plough.

Keywords: Winter wheat, tillage systems, energy analysis, rainfed conditions.

Introduction

Management practices (tillage, pesticides, fertilizer, crop) used within a crop production system affect the energy balance of that system. The energy use for tillage is of concern to farmers. For farmers, the cost of fuel represents a major direct expense. High energy use for tillage is usually also associated with high machinery costs and labour inputs when 30% of energy in the field is consumed by tillage (Borin et al., 1997).

Many tillage systems are used in agriculture. The use of reduced is associated with lower energy inputs relative to conventional tillage such as mouldboard ploughing (Uri, 2000). The primary reasons for mouldboard ploughing are incorporation of straw residues, weed control and soil loosening, while reduced tillage provides the best opportunity for improving soil quality and enhancing crop productivity and it may also increase the amount of organic carbon in the soil (Etana et al., 1999; Arvidsson et al., 2009). Conventional tillage using mouldboard ploughing need more mechanical investment and labour when compared to reduced tillage. Reduced systems require almost half of field traffic compared to ploughing systems. These systems have clear economic advantages which are of increasing global concern, favourable water balance, significantly save the time with seedbed preparation and reduced energy cost.

There are a lot of researches on energy balances of crop production. However, the authors have not found a thorough publication comparative analyzing energy input and output on reduced tillage systems versus conventional tillage for continuous winter wheat under rainfed conditions in Mediterranean environments. The objective of this study was to determine the effects of tillage systems on the energy input, energy efficiency of wheat production using yield (grain and straw) results from a study in western of Turkey. The calculations were based on process analysis since this approach was considered to be the most suitable and accurate method for agricultural systems (Hülsbergen et al., 2001).

Experimental arrangement

A field experiment was conducted from 2001 to 2004 under rainfed conditions, western Turkey. The climate of the study area is semi-arid

Mediterranean, with a four-month drought period in summer coinciding with the highest temperatures. The average seasonal (1 October-31 September) rainfall during the experimental period was 625 mm, irregularly distributed annually in timing and amount. The highest rainfall was recorded in 2001 (705 mm), and the lowest in 2002 (566 mm), while it was recorded 603 mm in 2003. The annual rainfall ranging from 406.7 to 902.4 mm (1975-2004) of which about 94% of long-term rainfall is received from September to May during the growing of wheat. The mean annual temperature was 15.0 ^oC. The soil was clay loam in texture.

The experiment was carried out in a randomised complete block design with tillage systems, replicated three times. The tillage systems included conventional and reduced tillage. Conventional tillage involved the use of a mouldboard plough (CT), while reduced tillage involved rototiller (RT) and tandem disk (DT) (Table 1). All tillage operations were performed in autumn. The cultivation practices were similar to those employed by local farmers (Table 1). Wheat was hand harvested in early June from a 1 m x 3 m in each tillage plot at the 10.2% moisture content for grain. The energy balances were determined as reported by Hülsbergen et al., (2001) (Hülsbergen et al., 2001). This requires the identification of the inputs and the outputs involved and their conversion to energy values by means of corresponding energy coefficients or equivalents (Table 2).

Labour energy (Em) expended was determined using formula: Em= 1.96XMnXTm MJ, where Mn=number of labour spent on a farm activity; Tm=useful time spent by a labour on a farm activity (hours) using machines working speed and width for each tillage system. Mechanical energy input was evaluated by quantifying the amount of fuel consumed (Sharma et al., 2011). The fuel energy input was determined by Hülsbergen et al., (2001). These inputs were calculated from the amount of product used in each tillage system (kg ha^{-1}, L ha^{-1}) and the corresponding energy equivalents (MJ kg^{-1}, MJ L^{-1} (Table 2). The energy efficiency can be expressed in terms of net energy output (NE), and output/input ratio (O/I), which are derived from the energy input and the crop energy output, and energy productivity (EP) (wheat grain yield per unit energy input) (Table 3). The net energy (MJ ha^{-1}) is the difference between total energy output and total energy input. The dimensionless output/input ratio was determined by dividing the energy output by the energy input. Statistical assessment of this experiment for yield was performed by the analysis of variance (ANOVA). The Duncan's test was employed to compare the mean results (expressed with respect to one hectare and year for each tillage system), after a significant variation had been highlighted by ANOVA. The differences had been considered as significant if $P < 0.05$. Energy inputs were not analysed statistically since they cannot be considered random variables to be constant for each tillage system in every experimental year.

Tab. 1 Management practices for winter wheat production during the experimental period

Practices/operations	Wheat
1.Land preparation tractor used: New Holland TD 85 63 kW	RT; Rototiller CT; Mouldboard plough, disk harrow (twice) DT; Tandem disk (twice)
Land preparation period	September-November
Average number of tillage and seedbed preparation	RT; 1.0 CT; 3.0 DT; 2.0
2.Fertilizer	(a) N-150 kg ha^{-1} (b) P_2O_5-50 kg ha^{-1} (c) K_2O-0 kg ha^{-1} Application of fertilizers by tractor-drawn fertilizer spreader
Fertilization period	October-March
Average number of fertilization	3.0 (one starter and two top fertilizer)
3.Sowing	By tractor-drawn seed drill with a seed rate of 120 kg ha^{-1}
Sowing period	October-November
4. Weeding	Application of herbicides by tractor-drawn sprayer
5.Irrigation	Crop was grown as rainfed
6.Plant protection	Chemical control by sprayer of fenoxaprop-p-ethyl, bromoxynil, and 2,4-D
Plant protection period	March-April
Average number of spraying	2.0

Practices/operations	Wheat
7. Harvesting	Combine
Harvesting period	Mid-June
Average number of harvesting	1.0

Tab. 2 Energy equivalents for inputs and outputs and fuel consumption

Particulars	Unit	Equivalent energy	References
A. Input			
1.Labour (manpower)	MJ h^{-1}	1.96	(Mandal et al., 2009)
2.Diesel	MJ L^{-1}	39.60	(Hülsbergen et al., 2001)
3. Machinery	MJ kg^{-1}	62.70	(Mandal et al., 2009)
4.Mineral fertilizers			
(a)Nitrogen (N)	MJ kg^{-1}	35.30	(Hülsbergen et al., 2001)
(b)Phosphate (P_2O_5)	MJ kg^{-1}	11.10	(Mandal et al., 2009)
5. Herbicides[a]	MJ kg^{-1} a.i.	238.00	(Helsel, 1992)
7.Tractor	MJ kg^{-1}	93.61	(Hetz, 1992)
8.Combine	MJ kg^{-1}	87.60	(Hetz, 1992)
9.Transport	MJ Mg^{-1} km^{-1}	6.30	(Hetz, 1992)
10.Seed	MJ kg^{-1}	5.50	(Hülsbergen et al., 2001)
B. Output			
1. Grain	MJ kg^{-1}	18.60	(Hülsbergen et al., 2001)
1.Straw	MJ kg^{-1}	17.70	(Hülsbergen et al., 2001)

[a] Units of measure are active ingredient.

Tab. 3 Definition of energy variables

Variable	Definition	Unit
Direct energy input (Ed)	Input of fuel (diesel)	MJ ha^{-1} $year^{-1}$
Indirect energy input (Ei)	Machines+ mineral fertilizers + herbicides + seed	MJ ha^{-1} $year^{-1}$
Total energy input (EI)	EI= Ed + Ei	MJ ha^{-1} $year^{-1}$
Energy output (EO)	Energy in the harvested main product and by product	MJ ha^{-1} $year^{-1}$
Net energy output (NE)	NE=EI - EO	MJ ha^{-1} $year^{-1}$
Output/input ratio (O/I)	O/I=EO/EI	
Energy productivity (EP)	EP=Wheat grain yield/EI	MJ kg^{-1} $year^{-1}$

Results and discussion

Energy input

Differences were seen significant interaction between tillage systems and years for yields and, consequently, in energy output and the energy efficiency. These differences among years emphasizes the importance that weather has on the development and yield of wheat (Ozpinar, 2006) and in turn, on the energy output and energy efficiency. Yields were noticeably lower when rainfall was below normal or irregularly distributed throughout the season. The grain and straw yield, and energy input was given in Tables 4, 5 and 6, respectively, while the energy output and energy efficiency variables considered is summarized in Table 7. To facilitate and simplify the comprehension of the results, except yield and energy output, the year-to-year data are not shown; rather data across 3-year are provided. Over the 3-year period of the experiment, the yield was significantly higher in rototiller than in either plough or disk (Table 4). In a trend similar to that of straw yield, the highest figures occurred in rototiller, while plough and disk produced significantly the same values. This study grain yield results were similar to the findings of others (Arvidsson et al., 2009; Sharma et al., 2011) who reported on relative crop yield for reduced tillage compared with plough was highest on soils with a clay content of 15-25%.

Tab. 4 Grain and straw yield of winter wheat under three tillage systems from 2001 to 2004

Tillage	**Grain yield (kg ha^{-1})**					**Straw yield (kg ha^{-1})**				
	2002	**2003**	**2004**	**Mean**[a]	**LSD**	**2002**	**2003**	**2004**	**Mean**	**LSD**
Rototiller	5197a	4290	5685ab	5057a	NS	20448aA	22285aA	11031B	17921a	2450
M. plough	3496b	5210	5344b	4683c	NS	12704cAB	13544bA	10668B	12305b	2518
Tandem disk	3395bB	5138AB	5930aA	4821b	1747	14099bA	10997cB	10655B	11917b	2100
Year mean	4029B	4879AB	5653A	4854	1239	15750A	15608A	10785B	14048	2039
LSD	1598	NS	429	1041		1025	2534	NS	1213	
Tillage	1598	NS	429	128		1025	2534	NS	1213	
Year	-	-	-	1238					2039	
Tillage X year	-	-	-	554					8399	

[a] Means in the same row and columns followed by the same capital and lower case letters (for years and tillage systems, respectively) are not significantly different at $P<0.05$ as tested by LSD.

In this study, energy input of tillage systems was the same for each experimental year because of the same field operations and inputs were used for all tillage systems throughout experimental period (2001-2004). So, it was assumed that all inputs (direct and indirect) were applied uniformly across experimental years for each system. Thus, there is no difference between energy inputs of the experimental years. Both direct (fuel used on the farm) and indirect (expended beyond the farm for the production of machinery, fertilizers and plant protection agents, energy costs of seeds, etc.) inputs were determined for each field operation (Table 5 and 6). However, the energy input varied considerably for each tillage system due to using different machines and farm operations. Over the 3-year study period, for example, energy input of tillage systems per year increased in the order disk<plough<rototiller (Table 6). The total energy requirement was slightly higher in rototiller than in mouldboard plough and tandem disk, the result of the production machinery and, consequently, of energy input, even though the use of seed, fertilizer and herbicides were the same for three tillage systems.

Differences in total energy input between plough and rototiller were very small (Table 6). There was a difference in total energy input between plough and disk, while difference was 4.5% between plough and rototiller. This can be compared with a difference of 14% for similar systems in a study of maize-soybean production (Rathke et al., 2007). The overall energy use for the machinery production as a proportion of total non-operational energy use ranged from 83.81, 80.69, and 70.40% for rototiller, plough, and disk, respectively. Labour in this study was higher than developed countries (Borin et al., 1997). This ratio in only direct energy was calculated as 0.03% averaged over tillage systems (Table 5). Fuel consumption varied according to tillage systems, sowing, fertilization, spraying and harvesting. It was high in the plough, followed by disk and rototiller (Table 5). Fuel consumption accounted for the highest share of total energy input that the highest percentage occurred in disk system (5.90%) and the lowest in system with rototiller (2.86%), while plough required 6.36% of total energy input. In direct energy input, fuel consumption was highest percentage in plough (85.73%) and lowest in rototiller (80.76%), while it was occurred 85.09% in disk (Table 5).

Tab. 5 Mean energy input (MJ ha^{-1} year^{-1}) for labour and fuel in each field operation as affected by tillage systems over 3-year experiment

Operation	**Rototiller**		**Mouldboard plough**		**Tandem disk**	
	Labour	**Fuel**	**Labour**	**Fuel**	**Labour**	**Fuel**
Tillage	2.92(0.15)	507(25.20)[a](0.89)[b]	3.12(0.09)	1010(30.23)(1.86)	0.82(0.04)	368(16.90)(1.17)
Seedbed preparation			1.65(0.05)	737(22.05)(1.36)	0.82(0.04)	368(16.90)(1.17)
Sowing	0.98(0.05)	218(10.83)(0.38)	0.98(0.03)	218(5.52)(0.40)	0.98(0.04)	218(10.00)(0.69)
Fertilizer application	1.06(0.05)	42(2.07)(0.07)	1.06(0.03)	42(1.24)(0.08)	1.06(0.05)	42(1.91)(0.13)
Spraying	0.55(0.03)	137(6.83)(0.24)	0.55(0.02)	137(4.11)(1.33)	0.55(0.03)	137(6.31)(0.44)

Operation	Rototiller		Mouldboard plough		Tandem disk	
	Labour	**Fuel**	**Labour**	**Fuel**	**Labour**	**Fuel**
Harvesting	7.00(0.35)	721(35.83)(1.27)	7.00(0.21)	721(21.57)(1.33)	7.00(0.32)	721(33.08)(2.29)
Total	12.51(0.62)	1625(80.76)(2.86)	14.35(0.43)	2864(85.73)(6.36)	11.23(0.52)	1854(85.09)(5.90)

[a] Figures in parentheses indicate percentage of total direct energy input (Ed).
[b] Figures in parentheses indicate percentage of total energy input (Ed+Ei).
[c] Total direct energy input (labour+fuel+machinery uses) for field operations, except for transportation.

Tab. 6 Main energy input over the 3-year (2001-2004) as affected by tillage systems

Energy variable	Rototiller			Mouldboard plough			Tandem disk		
	Energy input (MJ ha^{-1})	**Percent of total (%)**		**Energy input (MJ ha^{-1})**	**Percent of total (%)**		**Energy input (MJ ha^{-1})**	**Percent of total (%)**	
Direct									
M. ploughing				1162 (33.70)	2.14				
Rototiller	649(30.11)[a]	1.15							
Disk harrow							408 (17.88)	1.30	
Seedbed	-			817(23.69)	1.51		408(17.88)	1.30	
Sowing	266(12.32)	0.47		266(7.70)	0.49		266(11.63)	0.84	
Fertilization	93(4.32)	0.16		93(2.70)	0.17		93(4.08)	0.30	
Spraying	164(7.61)	0.29		164(4.76)	0.30		164(7.19)	0.52	
Harvesting	839(38.92)	1.48		839(24.34)	1.55		839(36.73)	2.67	
Transportation	145(6.71)	0.26		107(3.10)	0.20		105(4.62)	0.34	
Total (Ed)	2156(100)		3.80	3448(100)		6.36	2284(100.0)		7.26
Indirect									
Seed	1155(2.12)	2.04		1155(2.28)	2.13		1155(3.96)	3.67	
Fertilizer	5850(10.73)	10.32		5850(11.52)	10.79		5850(20.06)	18.60	
Herbicides	18(0.03)	0.03		18(0.04)	0.03		18(0.06)	0.06	
Machines	47520(87.12)	83.81		42740(86.17)	80.69		29163(75.92)	70.40	
Total(Ei)			96.20			93.64			92.7
	54543(100)			50763(100)			29163(100)		4
Total (Ed+Ei)	56699	100	100	54211	100	100	31447	100	100

[a] Figures in parentheses indicate percentage of operational energy input.

Energy output

Energy output and net energy are crucial parameters when the availability of arable land is the limiting factor for plant production. Yields exhibited year-to-year variation due to weather variation (Ozpinar, 2006). Over the 3-year period of the experiment, energy output as a function of tillage system was the lowest for plough and the highest for rototiller (Table 7) in 2002. The energy output exhibited a similar pattern to tillage with the lowest values associated with plough tillage and highest values associated with disk tillage in 2004. In 2003, the lowest energy output occurred in disk; the highest energy output occurred in rototiller. The mean energy output was higher for rototiller than for plough or disk, a result of lower mean wheat grain and wheat straw yields.

The energy output increased with a reduction in tillage intensity, while mean energy output over 3-year were smaller between tillage systems, although the highest values were found in rotoiller followed by disk and plough, a result of lower wheat yields (Table 4). As mentioned above, energy inputs for disk and rototiller were 44 and 4% lower, respectively, than for plough, with reduction in energy output was not the same because reduction in energy output was 35 and 22% for plough and disk, respectively, over 3-year mean. Thus, the rototiller was the most productive system, about 26% higher than plough. In dry season (2003 with 493 mm) during growing period of wheat (October-May), this relationship was observed clearly: the highest energy outputs were obtained in this season (Table 7).

Tab. 7 Energy output and efficiency under three tillage systems for 2001-2004

Tillage	2001-2002	2002-2003	2003-2004	Mean
Energy output (MJ ha^{-1} year^{-1})				
Rototiller				
Grain	96664 (21.08)[a]	79794 (16.83)	105741 (35.13)	94066 (22.87)
Straw	361930 (78.92)	394445 (83.17)	195249 (64.87)	317208 (77.13)
Total	458594 (100.00)	474239 (100.00)	300990 (100.00)	411274 (100.00)
M. plough				
Grain	65026 (22.43)	96906 (28.79)	99398 (34.49)	87110 (28.57)
Straw	224861 (77.57)	239729 (71.21)	188824 (65.51)	217804 (71.43)
Total	289886 (100.00)	336635 (100.00)	288222 (100.00)	304914 (100.00)
Tandem disk				
Grain	74946 (21.19)	63147 (20.19)	90756 (24.73)	105146 (35.52)
Straw	278781 (78.81)	249552 (79.81)	276273 (75.27)	190889 (64.48)
Total	353727 (100.00)	312699 (100.00)	367029 (100.00)	296034 (100.00)
Year mean				
Grain	78878 (21.47)	79949 (21.35)	98632 (30.94)	95441 (28.29)
Straw	288524 (78.53)	294575 (78.65)	220115 (69.06)	241967 (71.71)
Total	367402 (100.00)	374524 (100.00)	318747 (100.00)	337408 (100.00)
Net energy (MJ ha^{-1} year^{-1})				
Rototiller	357173	417540	291811	355508
M. plough	228619	282424	277751	262932
Tandem disk	242631	258767	290629	264009
Year mean	276141	319577	286731	294149
Output/Input ratio(O/I)				
Rototiller	7.30	8.36	5.31	6.99
M. plough	5.22	6.21	5.32	5.58
Tandem disk	8.72	9.23	9.50	9.15
Year mean	7.08	7.93	6.71	7.24
Energy productivity (GJ^{-1} kg)				
Rototiller	92	76	100	88
M. plough	64	96	99	97
Tandem disk	108	163	189	176
Year mean	88	112	129	120

[a] Figures in parentheses indicate percentage of total energy output.

The energy ratio was 1.64 and 1.31 times higher in disk than those plough and rototiller, respectively (Table 7) since the reduction in energy inputs (Table 5) was more marked in disk (1.7 times) compared with plough. Thus, for 3-year mean, the disk produced 9.15 units of energy output for every one unit of energy input, while rototiller and plough returned 6.99 and 5.58 units, respectively. This has been observed in other studies (Rathke et al., 2007). Energy output/input ratio is measures of the environmental effects associated with the production of crops. They noted that the highest output/input ratio were achieved at low production intensities and declined with increasing production intensity and our results supported their findings. Some authors observed that the output/input ratio tended to increase when soil tillage operations were reduced, which are similar to this study results (Borin et al., 1997; Rathke et al., 2007).

Conclusion

The results of energy balance obtained in this 3-year study, considering as inputs the factors supplied and controlled by farmers, indicate that tillage systems requiring different inputs relation to tillage and seedbed operations under rainfed conditions in Mediterranean climate, whether plough appear to be little efficient regarding energy. Mineral fertilizer was the most important energy input, except machinery production and maintenance or fuel consumption, in plough and reduced tillage systems studied, but their use did not lead to an equivalent increase in yield because of the irregular distribution and the lack of opportunity of the scarce rainfalls in some seasons, for example for 2002-2003. Rototiller (low-input practices) appear to be suited better to the environmental conditions of Mediterranean under rainfed conditions, more than 1.5 times the energy efficiency (output/input) of the plough system and offering a sustainable production over time with a minimal energy input (12.34% less), with the exception of machinery production and maintenance.

Reference

Arvidsson J., Rydberg T., Etana A., 2009. Ploughless tillage in sweden–results from short and long-term field experiments. In: Proceedings of the 18th International Conference of ISTRO, Izmir, Turkey.

Borin M., Merini C., Sartori L., 1997. Effects of tillage systems on energy and carbon balance in north-eastern Italy, Soil Till Res 40: 209 - 226.

Etana A., HaÊkansson I., Zagal E., Bucas S., 1999. Effects of tillage depth on organic carbon content and physical properties in Swedish soils. Soil Till Res 52: 129 - 139.

Helsel Z. R., 1992. Energy and alternatives for fertilizer and pesticide use. In: Fluck. R.C. (Ed.). Energy in World Agriculture. 6, Elsevier Science Publishing, 177 – 210.

Hetz E. J., 1992. Energy utilization in Chilean agriculture. AMA 23: 52 - 56.

Hülsbergen K. J., Feil B., Biermann S., Rathke G. W., Kalk W. D., Diepenbrock W., 2001. A method of energy balancing in crop production and its application in a long-term fertilizer trial. Agric Ecosyst Environ 86: 303 - 321.

Mandal K. G., Hati K. M., Misra A. K., 2009. Biomass yield and energy analysis of soybean production in relation to fertilizer-NPK and organic manure. Biomass Bioenergy 33: 1670 - 1679.

Ozpinar S., 2006. Effects of tillage on productivity of a winter wheat-vetch rotation under dryland Mediterranean conditions. Soil Till Res 89: 258 - 265.

Rathke G. W., Wienhold B. J., Wilhelm W. W., Diepenbrock W., 2007. Tillage and rotation effect on corn-soybean energy balances in eastern Nebraska. Soil Till Res 97: 60 - 70.

Sharma P., Abrol V., Sharma R. K., 2011. Impact of tillage and mulch management on economics, energy requirement and crop performance in maize-wheat rotation in rainfed subhumid inceptisols, India European Journal of Agro 34: 46 - 51.

Uri N. D., 2000. Perceptions on the use of no-till farming in production agriculture in the United States: an analysis of survey results. Agric. Ecosyst Env 77: 263 - 266.

AUTOMATIC PREDICTION OF GASOLINE – BIOFUEL BLEND TYPE IN COMBUSTION FOUR-STROKE ENGINE BASED ON ONE CLASS SUPPORT VECTOR MACHINES

X. E. Pantazi[1], D. Moshou[1], D. Kateris[1], I. Gravalos[2], P. Xyradakis[1]

[1]Aristotle University of Thessaloniki, School of Agriculture, Department of Hydraulics, Soil Science and Agriculture Engineering, Laboratory of Agricultural Engineering, P.0 275 54 124, Thessaloniki, Greece, Phone: +30998264, Fax: +30-998729,E-mail: renepantazi@gmail.com
[2]Technological Educational Institute of Larissa, School of Agricultural Technology, Department of Biosystems Engineering, Larissa 41110, Greece

Abstract

Bio-fuels can be used for power generation in a number of ways. One possibility is to produce liquid or gaseous bio-fuels that can be burned in engines that normally burn fossil fuels. However, in practice, ethanol may do well as a fuel in spark ignition (SI) engines, either as pure ethanol, or when used as a blend with fossil fuels. Methanol can be blended with gasoline up to 15% by volume and used as fuel in SI engines without major modifications required. There is a considerable amount of literature regarding various ethanol and methanol blends with gasoline.The effects of using ethanol and methanol unleaded gasoline blends on emissions have been investigated by a number of researchers, but while the effects of using alcohols on spark ignition engine performance and emissions have been thoroughly investigated, very little research has been done on the engine vibrational behaviour.

In this study, unsupervised novelty detection was applied to determine automatically both the type of fuel and the blending ratio of the fuel mixture based on analysis vibrational signals during operation of a four-stroke combustion engine fueled with gasoline and gasoline blends with ethanol and methanol. Three types of fuel were utilized: unleaded gasoline as base fuel compared to the mixture of two alcohols, ethanol and methanol in admixture with gasoline, as a percentage ratio of around 10 %, 20 % and 30 %, respectively. The engine tests were performed at 1000, 1300, 1600 and 1900 rpm. The collections of measurements were conducted by a triaxial accelerometer. Features in time and frequency were calculated from the signals received. The classification of the type of fuel and fuel blend ratio was achieved using an active learning method based on incremental application of One Class Support Vector Machines (OC-SVM) for novelty detection.

Keywords: gasoline, biofuel, vector machine

1. INTRODUCTION

Bio-fuels can be used for power generation in a number of ways. They can also include alcohols, such as, ethanol and methanol. There is a considerable amount of literature regarding various ethanol and methanol blends with gasoline. The effects of using ethanol and methanol unleaded gasoline blends on emissions have been investigated by a number of researchers, but while the effects of using alcohols on spark ignition engine performance and emissions have been thoroughly investigated, very little research has been done on the engine vibrational behavior. Keskin (2010) investigated the effects of ethanol-gasoline-oil blends on spark ignition engine vibration characteristics, as well as, its noise emissions. The experimental results indicated that when fuel blends were used, vibration amplitudes and noise emission of the engine showed an increasing trend especially at 1500 and 2500 rpm. The author concluded that these results are probably due to oxygen content and higher latent heat of evaporation of ethanol, in which the increasing rate of pressure and peak pressure values in the cylinder rise during the combustion processes.

In this study, a detailed experimental investigation of the vibration behavior of a four-stroke internal combustion engine fueled with blends of gasoline, ethanol and methanol by developing utilizing One Class Support Vector Machine (OC-SVM). Three types of fuel were utilized: unleaded gasoline as base fuel so as to be compared with the mixture of two alcohols, ethanol and methanol in admixture with gasoline as a percentage ratio of around 10 %, 20 % and 30 %. The motor was tested at 1000, 1300, 1600 and 1900 rpm. Data acquisition was carried out by a triaxial accelerometer. Time and frequency domain features were calculated from the collected signals. Each of the three axes demonstrates a different degree of sensitivity to the used blend depending on its ratio due to the engine's different response to different blends of fuel, taking into account the nature of vibration. In the presented study, precise mixture identification resulted from vibration characteristics, by proposing One Class Support Vector Machine (OC-SVM).

1.2 Experimental set-up

The experimental test rig used in this study consisted of a SI engine, a hydraulic dynamometer and a vibration sensor connected to signal acquisition hardware. The experimental set-up is shown in Fig. 1. A single cylinder, carburetted, four-stroke, spark ignition non-road engine (type Bernard moteures 19A), was chosen. This engine had a 56 mm bore and a 58 mm stroke (total displacement 143 cm^3). Its rated power was 2.2 kW. The ignition system was composed of the conventional coil and spark plug arrangement with the primary coil circuit operating on a pulse generator unit. The engine was coupled to a hydraulic dynamometer through elastic couplings. The dynamometer was equipped with an instrument panel fitted with a torque gauge and switches for the load remote control.

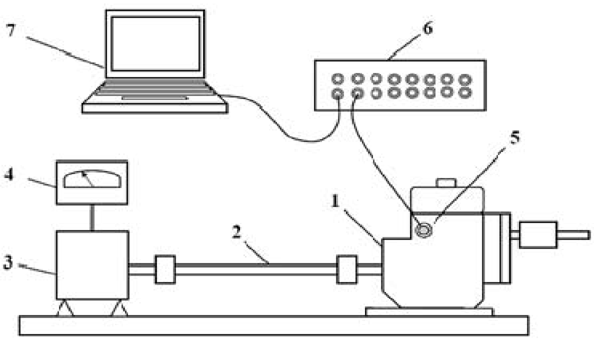

Fig.1 (1) Engine, (2) Shaft, (3) Hydraulic Dynamometer, (4) Dynamometer control unit, (5) Triaxial piezoelectric accelerometer, (6) Vibration analyzer, (7) Laptop PC

A series of experiments were carried out using pure gasoline, and various gasoline-ethanol and gasoline-methanol fuel blends, at different volume percentages namely: 10 %, 20 % and 30 %, reported for short as E10, E20, E30, M10, M20 and M30 respectively. The fuel blends were prepared just before starting the experiments to ensure that the fuel blend was homogeneous and prevent the reaction of ethanol with water vapour. The engine was started and allowed to warm up for a period of 20 up to 30 min. Before running the engine with a new fuel blend, it was allowed to run for sufficient time to consume the remaining fuel from the previous experiment. All the blends were tested under varying load conditions and at different engine speeds. The rotational speed of the engine in the series of runs was 1900, 1600, 1300 and 1000 rpm.

2 MATERIALS AND METHODS

2.1 Signal processing and feature extraction

The first and maybe the most important step in any fault diagnosis problem, is the feature extraction from the raw signal. The aim of this is to reflect the general changes of the machine operation conditions. However, though some features are closely related to the fault, others are not. In this paper, twenty four (24) features parameters, twelve (12) time-domain (T_1-T_{12}) and twelve (12) frequency-domain (F_1-F_{12}) were selected (Lei et al., 2008; Moshou et al., 2010).

2.2 Time-domain feature

The first eleven features were introduced by Lei et al. (2008). These were Mean value (T_1), Standard deviation (T_2), (T_3),Root mean square (T_4), Peak (T_5), Skewness (T_6), Kurtosis (T_7), Crest factor (T_8), Clearance factor (T_9), Shape indicator (T_{10}) and Impulse Indicator (T_{11}). The twelfth one was introduced by Moshou et al. (2010) and regards the linear integral of the acceleration signal (Line integral, T_{12}). All the used features provide statistical information about the nature of data, and were found to be reasonably good features for bearing fault detection. These features are shown in Table 1.

Tab. 1 Time-domain feature parameters

$$T_1 = \frac{\sum_{n=1}^{N} x(n)}{N} \quad (1)$$

$$T_2 = \sqrt{\frac{\sum_{n=1}^{N} (x(n) - T_1)^2}{N-1}} \quad (2)$$

$$T_3 = \left(\frac{\sum_{n=1}^{N} \sqrt{|x(n)|}}{N} \right)^2 \quad (3)$$

$$T_4 = \sqrt{\frac{\sum_{n=1}^{N} (x(n))^2}{N}} \quad (4)$$

$$T_5 = max|x(n)| \quad (5)$$

$$T_6 = \frac{\sum_{n=1}^{N} \left(x(n) - T_1\right)^3}{(N-1)T_2^3} \quad (6)$$

$$T_7 = \frac{\sum_{n=1}^{N} \left(x(n) - T_1\right)^4}{(N-1)T_2^4} \quad (7)$$

$$T_8 = \frac{T_5}{T_4} \quad (8)$$

$$T_9 = \frac{T_5}{T_3} \quad (9)$$

$$T_{10} = \frac{T_4}{\frac{1}{N}\sum_{n=1}^{N} |x(n)|} \quad (10)$$

$$T_{11} = \frac{T_5}{\frac{1}{N}\sum_{n=1}^{N} |x(n)|} \quad (11)$$

$$T_{12} = \int_a^b ds \approx \sum_{i=1}^{N} \vec{r}(t_i + T_s) - \vec{r}(t_i) = \sum_{i=1}^{N} \sqrt{\left(x(t_i + T_s) - x(t_i)\right)^2 + T}$$
$$\approx \sum^{N} |x(t_i + T_s) - x(t_i)| \quad (12)$$

where x(n) for the time-domain feature is a signal series for n=1,2,….,N, N is the number of data points. Especially for the line integral *N* is the number of sample points (equal to 500) in the non-overlapping windows used to calculate Kurtosis and the other features and the newly proposed line integral feature and T_s is the sampling period. Given the high sampling rate of 48 kHz and the domination of the signal from high frequencies (especially due to the presence of faults), the final approximation contains only acceleration values.

2.3 Frequency-domain feature

Frequency-domain is another description of a signal. This type of description includes some information that cannot be found in time-domain. In this study another twelve features (Lei et al., 2008) were used in order to feed the One Class Classifier with additional information with respect to the time domain features. These twelve features were based on the Fourier transform of the vibration signals. Feature F_1 may indicate the vibration energy in the frequency-domain. Features F_2-F_4, F_6 and F_{10}-F_{12} may describe the convergence of the spectrum power. Finally F_5 and F_7-F_9 give information about the position change of main frequencies.

Tab. 2 Frequency-domain feature parameters

$F_1 = \dfrac{\sum_{k=1}^{K} s(k)}{K}$	**(13)**	$F_7 = \sqrt{\dfrac{\sum_{k=1}^{K} f_k^2 s(k)}{\sum_{k=1}^{K} s(k)}}$	**(19)**
$F_2 = \dfrac{\sum_{k=1}^{K} \left(s(k)-F_1\right)^2}{K-1}$	**(14)**	$F_8 = \sqrt{\dfrac{\sum_{k=1}^{K} f_k^4 s(k)}{\sum_{k=1}^{K} f_k^2 s(k)}}$	**(20)**
$F_3 = \dfrac{\sum_{k=1}^{K} \left(s(k)-F_1\right)^3}{K\left(\sqrt{F_2}\right)^2}$	**(15)**	$F_9 = \dfrac{\sum_{k=1}^{K} f_k^2 s(k)}{\sqrt{\sum_{k=1}^{K} \sum_{k=1}^{K} f_k^4 s(k)}}$	**(21)**
$F_4 = \dfrac{\sum_{k=1}^{K} \left(s(k)-F_1\right)^4}{KF_2^2}$	**(16)**	$F_{10} = \dfrac{F_6}{F_5}$	**(22)**
$F_5 = \dfrac{\sum_{k=1}^{K} f_k s(k)}{\sum_{k=1}^{K} s(k)}$	**(17)**	$F_{11} = \dfrac{\sum_{k=1}^{K} \left(f_k - F_5\right)^3 s(k)}{KF_6^3}$	**(23)**
$F_6 = \sqrt{\dfrac{\sum_{k=1}^{K} \left(f_k - F_5\right)^2 s(k)}{K}}$	**(18)**	$F_{12} = \dfrac{\sum_{k=1}^{K} \left(f_k - F_5\right)^4 s(k)}{KF_6^4}$	**(24)**

2.4 One Class Support Vector Machine (OC-SVM)

One Class Support Vector Machines construct a model using data targets. In a second stage they classify test data which are based on deviation from normal training data which are classified either as targets or as outliers (Scholkopf et al., 2001). The effect of the spread parameter in the kernel $K(\mathbf{x},\mathbf{z}) = \exp\{-\|\mathbf{x}-\mathbf{z}\|^2 / \sigma^2\}$ can be estimated considering that a large spread demonstrates linearly separable classes while on the other hand, a large number of support vectors combined with small spread indicates highly nonlinear decision boundaries between classes.

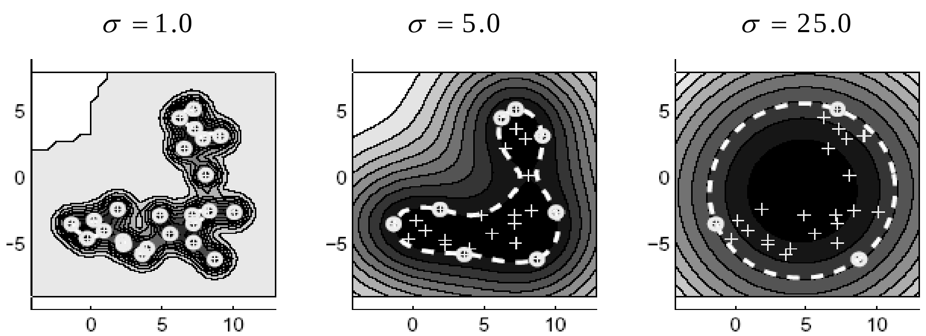

Fig. 2 The effect of spread parameter in the One Class Support Vector Machines behavior (Ypma, 2001).

Tab. 3 Successful fuel type identification performance corresponding to each technique that was employed in order to achieve 3-class OC-SVM classification

Classifier	Successful identification of unleaded gasoline (%)	Successful identification of methanol (%)	Successful identification of ethanol (%)
OC-SVM	53.69	39.19	52.35

3 RESULTS AND DISCUSSION

Concerning the different spreads, the best results are provided by the One Class SVM Classifier with spread equal to 2.5. Except of the mixture of unleaded gasoline-30 % methanol all the other classes corresponding to mixtures, are recognized with high percentages which reach 90 % and above. Concerning the different spreads, the best results are provided by the One Class SVM Classifier with spread equal to 2.5.

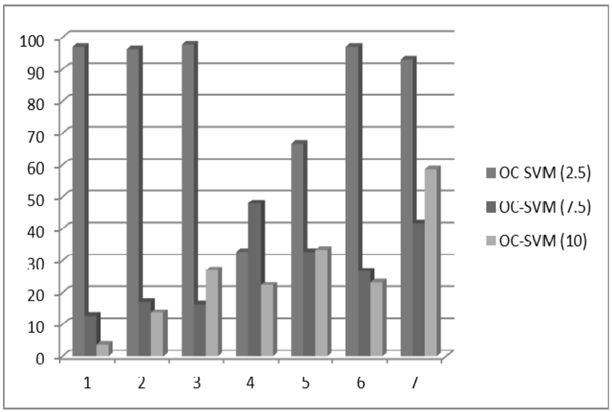

Fig.3 Graphical display of the success rates of blend ratio identification (7classes), utilizing the One Class Support Vector Machine (OC-SVM)

In the case of three classes corresponding to fuel type identification the spread doesn't play a crucial role in the recognition result due to fact that the decision boundaries are approximately linear. In the case of seven classes the situation is more complicated because the decision boundaries are highly nonlinear and the classification results are very sensitive to the spread parameter, reaching peak performance around a spread of 2.5.

CONCLUSION

In this study, a detailed experimental investigation of the vibration behavior of a four-stroke internal combustion engine fueled with blends of gasoline, ethanol and methanol by developing utilizing One Class Support Vector Machine (OC-SVM). The One Class SVM Classifier leads to the creation of a multiclass Classifier with high performance in recognizing biofuel mixture ratios from the behavior of vibration signals in internal combustion engines. This is explained from the nonlinear nature of the problem but shows also the flexibility of novelty detection schemes based on One Class Classifiers that can been combined from the solution of arbitrary classification problems.

REFERENCE

Keskin A., 2010. The influence of ethanol–gasoline blends on spark ignition engine vibration characteristics and noise emissions. Energy Sources, Part A, Recovery, Utilization, and Environmental Effects, 32: 1851-1860.

Moshou D., Kateris D., Gravalos I., Loutridis S., Sawalhi N., Gialamas T., Xyradakis P., Tsiropoulos Z., 2010. Determination of fault topology in mechanical subsystems of agricultural machinery based on feature fusion and neural networks. In Proc. 4th International Conference TAE 2010, Czech University of Life Sciences Prague, 448-453.

Lei Y., He Z., Zi Y., 2008. A new approach to intelligent fault diagnosis of rotating machinery, Expert Systems with Applications, 35: 1593-1600.

IS IT GOOD TO CHANGE THE COMPOSITION OF THE INPUT SUBSTRATE FOR BIOGAS PLANT OR NOT?

Luboš Passian[1*], Miroslav Andrt, Lenka Kačírková

[1]Czech University of Life Sciences Prague, 16521 Prague 6 – Suchdol, Czech Republic
Phone: +420224383204, Fax: +4202-20921361, E-mail: passian@tf.czu.cz

Abstract

In the submitted material there are shown some results gained by monitoring of the impact of consumption and composition of the substrate input into a biogas plant with regard to the quantity of biogas and electricity produced. The research was conducted on the biogas plant with a cogeneration (CHP) unit operated by the agricultural cooperative since year 2008. The data were collected during three years. The input substrate contained cattle slurry, corn silage, haylage, rye grain for 12 months and for 14 months the input substrate was without the rye grain content. The information associated to biogas unit – the quantity and composition of input material, temperature inside digester, outside temperature, operating time of the heat exchanger, stirrers, dispensers, solenoid valve, desulphurization, minimum and maximum level of the gas storage, and information about the cogeneration unit – operation time, gas consumption, and electricity output were collected.

The obtained results show that the portion of rye grains in the input substrate (feedstock) leads to a lower substrate amount consumption, due to a high energy yield from grains.

Valuable nutrients coming from digestate processing can be re-used as a substitute for artificial fertilizers and it can result in significant CO_2 emission and fossil energy savings, followed by cost savings.

Keywords: anaerobic digestion, biogas plant, biomass

Introduction

The choice and ensuring the optimal composition of the inputs into a biogas plant is one of the basic preconditions for its effective operation. Return on investments is conditioned by a smooth operation, a guarantee of sufficient resources of high-quality materials for fermentation and subsequent production of biogas. The ideal situation is when the agricultural entity is, at the same time; the owner and operator of agricultural biogas station and ensures the full amount of feedstock from its own resources - materials from plant and animal production.

The yield of biogas depends both on the roperties and quality of the input material (feedstock), as well as on the practical modalities of the biogas plant operation (method of operation, the operating temperature, and the residence time of the substrate in a digester), etc. The statistical analyses give very good results for the estimation of methane yields from the maize and cereals. Rye and triticale are very suitable as intercrops (Amon, 2007).

The digester in which the process of anaerobic decomposition takes place is likened to the rumen of a cow, where inputs are processed step by step into the final production of biogas with the help of several kinds of micro-organisms. It is therefore a very sensitive to the quality of the process, to the composition of the input material and to maintain a constant operating conditions (in particular the temperature, pH, C : N ratio and dry matter content). It is not recommended to unnecessarily experiment and it is better to follow the most common feedstock composition. If needed, possible changes should be applied slowly and over an extended period of time (Malaťák, Vaculík, 2008).

Products of anaerobic digestion are a biogas and a stabilized sludge (digestate). The biogas is a renewable energy source and provides a variety of options for energy recovery. The main components of the biogas are methane 55 - 70 % vol., carbon dioxide 27 - 47 % vol., hydrogen 1 % vol., hydrogen sulphide 3 %. Hydrogen sulphide is the major contaminant in biogas which is both poisonous and corrosive and has to be removed. In practice, biogas is most commonly used for combustion in cogeneration units (CHP) for the electricity and heat production. The advantage of this method is the possibility to sell electricity at the guaranteed price to the distribution network and the heat use for hot water, heating of office space, heating of stables, drying agricultural materials and wood.

The digestate is the second valuable product of a fermentation process in the biogas station. In general, anaerobic digestion in biogas plants seems an efficient way (thermophilic stage more efficient than mesophilic one) to treat organic farm wastes in a way that can totally eliminate weed seeds and animal parasites so that the digestates can be applied without risking spread of these pests (Johansen et al., 2013; Vaneeckhaute et al., 2013). The digestate can be directly used as a high quality organo-mineral fertilizer or as a raw material for the compost production. After reducing its moisture (separation), the separate can be used as bedding in lying boxes for dairy cows and liquid part for fertilizing. Substituting conventional fertilizers by digestate derivatives in different cultivation scenarios can result in significant economic and ecological benefits for the agriculturist (Vaneeckhaute et al., 2013). The separate can be used after drying as a solid fuel with an option to be combined with other kinds of biomass, but this option not common due to its high energy consumption and low cost-efficiency.

Materials and methods

The research was made on the biogas station located in Příbram district, which was put into operation in 2008 is operating on the principle of a wet anaerobic fermentation process. The agricultural cooperative is the owner and operator, which ensures the most effective use. The biogas station was designed by the FARMTEC a.s. In our case the main input materials for anaerobic digestion are cattle slurry, corn silage, haylage and under some instances cereal grain (especially rye, whose energy yield is 156 - 215 $GJ.ha^{-1}$). Produced biogas is burned in a cogeneration unit (CHP) with 526 kW electrical output and 558 kW thermal output. Approximately 8.1 % of the gained electricity is used for the biogas station itself and the rest is supplied to the national power distribution network. The heat produced by the CHP unit is used for heating of the anaerobic reactor (digester), heating for buildings and also for additional drying of grains and wood chips. The liquid digestate goes through a separator which divides the sludge in proportions 25 % of solid mass to 75 % of liquid substance. The separate is placed on a dung hill or used in stable for dairy cows as bedding, or possibly for the production of compost. Sludge liquor is stored in storage reservoirs and then used as a liquid fertilizer.

Input material consumption is estimated around 21 900 tonnes per year in the maximum possible quantity of usable raw materials:

- Cattle slurry 35.75 $t.day^{-1}$ ...13 050 $t.year^{-1}$ ...10 % of dry matter.
- Corn silage 16.16 $t.day^{-1}$ ...5 900 $t.year^{-1}$ ...32 % of dry matter.
- Haylage 8.08 $t.day^{-1}$ ...2 950 $t.year^{-1}$ ...35 % of dry matter.

A number of indicators is reviewed during biogas plant operation (quantity and composition of input material, temperature inside digester, outside temperature, operating time of the heat exchanger, stirrers, dispensers, solenoid valve, desulphurization, minimum and maximum level of gas storage) and information about cogeneration unit (operation time, gas consumption, electricity output). A stationary biogas analyser BC20 is used to determine concentrations of individual biogas components (methane, carbon dioxide, oxygen and hydrogen sulphide). On the bases of reviewed indicators comparison is made between the consumption and composition of the input substrate to maintain a constant amount of biogas produced, accordingly the amount of electricity generated. The change in the composition of the biogas station feedstock, where rye grain was temporarily used at the expense of the corn silage amount was made during a three-year reporting period due to a low redemption price of the rye. Because of better energy potential of grain arrived the reduction in the total amount of material used. Some months were excluded from the reporting period because the cogeneration unit was in operation less then 23 hours and 45 minutes per day on average. Other months were excluded due to broken measuring equipment. The following tables show, in the abbreviated form, monitored variables in pertinent periods.

Tab. 1 Entry substrate with rye grain…August 2010

Monthly report August 2010	Working time	CHP output	Biogas consumption	Green bonus	Average temp. in main digester	Average temp. in post-digester	Daily substrate consumption	Corn silage	Rye grain	Haylage
Date	[hh:mm]	[kWh]	[m^3]	[kWh]	[°C]	[°C]	[t]	[t]	[t]	[t]
1.8.2010	24:00	12590	6950	11534	40.1	42.3	18.16	11.62	1.09	5.45
2.8.2010	24:00	12600	7010	11553	40.1	42.2	17.27	11.05	1.04	5.18
3.8.2010	24:00	12600	6900	11564	39.4	42.2	17.97	11.50	1.08	5.39
4.8.2010	24:00	12600	6860	11558	39.9	42.2	17.84	11.42	1.07	5.35
5.8.2010	24:00	12600	6980	11578	39.6	42.2	17.99	11.51	1.08	5.40
6.8.2010	24:00	12600	6880	11593	39.9	42.2	17.68	11.31	1.06	5.31
7.8.2010	23:27	12210	6610	11187	39.9	42.2	17.03	10.90	1.02	5.11
8.8.2010	24:00	12600	6800	11600	39.8	42.1	18.07	11.57	1.08	5.42
9.8.2010	24:00	12600	6800	11604	39.5	42.1	18.47	11.82	1.11	5.54
10.8.2010	24:00	12600	6830	11566	39.5	42.1	18.05	12.03	1.13	4.89
11.8.2010	24:00	12600	6840	11587	39.6	42.1	18.63	11.92	1.12	5.59
12.8.2010	24:00	12600	6890	11589	39.9	42.0	18.90	12.10	1.13	5.67
13.8.2010	24:00	12600	6820	11575	39.8	42.0	18.43	11.79	1.11	5.53
14.8.2010	24:00	12600	6840	11568	40.0	42.0	18.96	12.13	1.14	5.69
15.8.2010	23:56	12570	6960	11560	40.2	42.0	19.00	12.16	1.14	5.70
16.8.2010	23:33	12340	6730	11287	40.5	42.0	18.27	11.69	1.10	5.48
17.8.2010	24:00	12600	6900	11593	40.5	42.0	19.64	12.57	1.18	5.89
18.8.2010	24:00	12600	6870	11597	40.3	42.0	18.15	11.62	1.09	5.44
19.8.2010	24:00	12600	6900	11582	39.9	41.9	19.50	12.48	1.17	5.85
20.8.2010	21:27	11080	6090	10183	39.4	41.9	17.57	11.25	1.05	5.27
21.8.2010	24:00	12600	6880	11578	39.7	41.9	18.83	12.05	1.13	5.65
22.8.2010	24:00	12600	6990	11563	39.4	41.9	18.28	11.67	1.10	5.51
23.8.2010	24:00	12600	7060	11589	39.8	41.9	19.44	12.44	1.17	5.83
24.8.2010	24:00	12600	6970	11600	39.6	41.9	18.71	11.98	1.12	5.61
25.8.2010	23:55	12520	6670	11532	38.9	41.9	19.36	12.39	1.16	5.81
26.8.2010	24:00	12600	6940	11586	38.9	41.9	18.61	11.55	1.18	5.88
27.8.2010	24:00	12600	6970	11604	39.8	41.9	19.40	12.42	1.16	5.82
28.8.2010	24:00	12600	6890	11560	39.4	42.0	20.10	12.86	1.21	6.03
29.8.2010	24:00	12600	6870	11597	39.1	42.0	19.47	12.46	1.17	5.84
30.8.2010	24:00	12600	6870	11582	39.6	42.0	19.60	12.54	1.18	5.88
31.8.2010	24:00	12600	6790	11600	39.4	42.0	19.47	12.46	1.17	5.84

Tab. 2 Entry substrate without rye grain…September 2011

Monthly report September 2011	Working time	CHP output	Biogas consumption	Green bonus	Average temp. in main digester	Average temp. in post-digester	Daily substrate consumption	Corn silage	Haylage
Date	[hh:mm]	[kWh]	[m^3]	[kWh]	[°C]	[°C]	[t]	[t]	[t]
1.10.2011	24:00	12600	6920	11902	39.8	41.4	20.91	14.64	6.27
2.10.2011	24:00	12600	6790	11941	39.8	41.4	19.66	13.76	5.90
3.10.2011	24:00	12600	6810	11942	39.5	41.4	19.86	13.90	5.96
4.10.2011	24:00	12600	6730	11962	39.0	41.5	20.01	14.01	6.00
5.10.2011	24:00	12600	6770	11982	39.8	41.6	21.36	14.95	6.41
6.10.2011	23:56	12560	6930	11859	38.4	41.6	20.00	14.00	6.00
7.10.2011	22:31	11780	6400	11107	39.5	41.6	16.23	11.36	4.87
8.10.2011	24:00	12600	6977	11838	38.4	41.6	18.80	13.16	5.64
9.10.2011	24:00	12600	6820	11850	38.2	41.7	20.40	14.28	6.12
10.10.2011	24:00	12600	6860	11884	38.0	41.7	19.03	13.32	5.71
11.10.2011	24:00	12600	6790	11859	39.2	41.8	16.86	11.80	5.06
12.10.2011	24:00	12600	6860	11885	39.8	41.8	19.77	13.84	5.93
13.10.2011	24:00	12600	6790	11892	38.6	41.8	20.24	14.17	6.07
14.10.2011	24:00	12600	6790	11889	37.9	41.8	21.90	15.33	6.57
15.10.2011	24:00	12600	6540	11897	37.5	41.8	19.93	13.95	5.98
16.10.2011	24:00	12600	6580	11904	38.2	41.8	18.89	13.22	5.67
17.10.2011	24:00	12600	6670	11912	38.9	41.8	19.43	14.30	5.13
18.10.2011	24:00	12600	5520	11888	37.9	41.8	21.43	15.00	6.43
19.10.2011	24:00	12600	6760	11887	37.4	41.8	19.36	13.55	5.81
20.10.2011	24:00	12600	6710	11818	38.5	41.8	20.00	14.00	6.00
21.10.2011	23:46	12440	6790	11693	39.3	41.7	18.76	13.13	5.63
22.10.2011	24:00	12600	6880	11825	38.0	41.7	19.94	13.96	5.98
23.10.2011	24:00	12600	6880	11869	37.5	41.7	20.46	13.30	7.16
24.10.2011	24:00	12600	6920	11859	37.0	41.7	20.83	13.54	7.29
25.10.2011	24:00	12470	6730	11781	39.0	41.8	21.20	13.78	7.42
26.10.2011	24:00	12600	6680	11900	37.3	41.8	20.61	13.40	7.21
27.10.2011	24:00	12600	6740	11879	38.1	41.9	20.46	13.30	7.16
28.10.2011	24:00	12600	6760	11851	38.5	41.9	21.55	14.01	7.54
29.10.2011	24:00	12600	6700	11861	37.9	41.9	19.87	12.92	6.95
30.10.2011	24:00	12600	6640	11815	39.3	41.9	19.55	12.71	6.84
31.10.2011	24:00	12600	6730	11816	38.4	41.9	20.40	13.26	7.14

Discussion and conclusion

Measurements of input substrate (feedstock) consumption were performed at the particular biogas plant in Central Bohemia Region with various feedstock compositions over a three year period of time. 26 months were selected with the fact that rye grains create part of the initial substrate for 12 months and substrate was without rye grains for 14 months. From the obtained data it appears that the total monthly consumption was in the first case, an average of 64 tonnes lower than in the other while maintaining the same average amount of biogas monthly produced. The data of composition and consumption of input substrate with and without rye grain are shown in the following Tab. 3 and Tab. 4 and Fig. 1 and Fig. 2.

The obtained data indicate that it is advisable to choose such a composition of the raw input materials that ensure high performance parameters of the biogas station at optimum consumption of inputs, resulting in an economic evaluation of the process.

The rye grain content in the input substrate combined with the cattle slurry can produce biogas with high methane content and a smaller amount of the substrate is used. Similar results were obtained in the work of Herout et al. which is focused on the biogas composition depending on the type of plant biomass used (Herout et al., 2011). From that point of view rye grains seem to be an advantageous energy source for biogas production in case that the price for rye grain drops under production costs.

Valuable nutrients coming from digestate processing can be re-used as a substitute for artificial fertilizers and it could result in significant CO_2-emission and fossil energy savings, as well as cost savings.

Tab. 3 Composition and consumption of input substrate with rye grain

Month		05/09	06/09	09/09	10/09	12/09	01/10	02/10	03/10	06/10	07/10	08/10	09/10
Consumption [t]		573.3	497.9	533.6	546.1	511.6	520.5	527.7	522.0	535.4	538.4	578.7	574.4
Substrate composition [%]	Corn silage	52	52	54	54	54	54	60	64	64	64	64	64
	Rye grain	6	6	6	6	6	6	6	6	6	6	6	6
	Haylage	42	42	40	40	40	40	34	30	30	30	30	30

Tab. 4 Composition and consumption of input substrate without rye grain

Month		10/10	11/10	12/10	01/11	02/11	03/11	04/11	05/11	06/11	07/11	09/11	10/11	11/11	12/11
Consumption [t]		590.8	610.3	618.7	623.0	590.5	584.0	580.3	572.0	568.7	591.3	623.4	631.3	631.3	613.4
Substrate composition [%]	Corn silage	70	70	70	70	70	70	70	70	70	70	70	70	70	70
	Rye grain	-	-	-	-	-	-	-	-	-	-	-	-	-	-
	Haylage	30	30	30	30	30	30	30	30	30	30	30	30	30	30

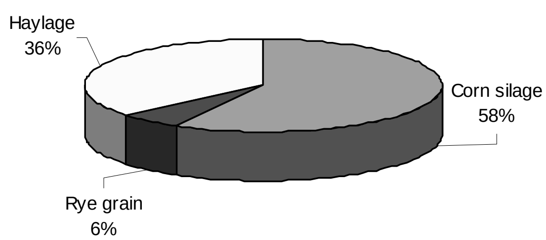

Fig. 1 Substrate composition with rye grain - average consumption 538 $t.month^{-1}$

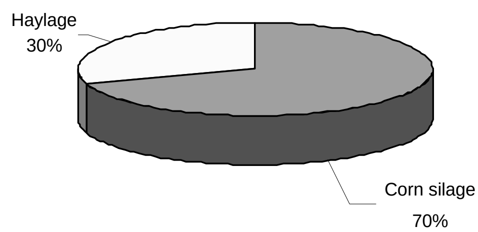

Fig. 2 Substrate composition without rye grain - average consumption 602 $t.month^{-1}$

Reference

Amon T., Amon B., Kryvoruchko V., Machmuller A., Hopfner-Sixt K., Bodiroza V., Hrbek R., Friedel J., Pötsch E., Wagentristl H., Schreiner M., Zollitsch W., 2007. Methane production through anaerobic digestion of various energy crops grown in sustainable crop rotations. BIORESOURCE TECHNOLOGY, 98(17): 3204-3212.

Herout M., Malaťák J., Kučera L., Dlabaja T., 2011. Biogas composition depending on the type of plant biomass used. Res. Agr. Eng., 57: 137–143.

Johansen A., Nielsen H.B., Hansen Ch.M., Andreasen Ch., Carlsgart J., Hauggard-Nielsen H., Roepstorff A., 2013. Survival of weed seeds and animal parasites as affected by anaerobic digestion at meso- and thermophilic conditions. Waste Management, 33(4): 807–812.

Malaťák J., Vaculík P., 2008. Technologická zařízení staveb odpadového hospodářství: zpracování biologicky rozložitelných odpadů. Praha: ČZU, 180. (in Czech)

Vaneeckhaute C., Meers E., Michels E., Buysse J., Tack F.M.G., 2013. Ecological and economic benefits of the application of bio-based mineral fertilizers in modern agriculture. BIOMASS & BIOENERGY, 49: 239-248.

UTILIZATION OF PLANT MATTER FOR BIOGAS PRODUCTION

Michal Pastorek[1], Jaroslav Kára[2], Zdeněk Pastorek[1*]

[1]Czech University of Life Sciences Prague, 165 21 Prague 6 – Suchdol, Czech Republic
Phone: +420 224383171, (+420 604 678 645), E-mail: pastorekz@tf.czu.cz
[2]Research Institute of Agricultural Engineering, 160 01 Prague 6 – Ruzyně

Abstract

Agriculture and municipal sphere produce a lot of waste materials that can be used for anaerobic fermentation as an energy source.

What are the main purposes of agricultural biogas plant construction?

1) *additional source of energy (e.g. biogas or biomethan)*
2) *improvements in organic fertilizer management in agriculture or in municipal sphere*
3) *support of environmental aspects of organic waste management*

This research focuses on effect of phytomass on agricultural biogas plant operation. Furthermore, the conditions being changed by using of the mixture of organic materials in agricultural biogas plant are presented. Most of the agricultural biogas plants process farm animal waste mixed with phytomass.

This research discussed the following problems:

- *advantages and disadvantages of different agricultural biogas plats regarding to the phytomass utilization*
- *raw material processing (before fermentor loading)*
- *effective utilization of outputs (e.g. biogas and fermented materials)*

In addition, recommendations for operators and investors of agricultural biogas plants have been summarized.

Keywords: plant matter, anaerobic fermentation, biogas

Introduction

Production of biogas from organic materials is very known processing technology for a long time. Many farmers and other entrepreneurs or investors take interest in anaerobic processing of wet biomass (more than 70 % w.b.). They decide by following EEE system points of view at the present time (Fig.1.):

1) **E**nergy profit (profit of power)
2) **E**cological contribution
3) **E**conomical profit

The sustainability of biogas production is determined by many materials, operating, economic and other parameters (Straka, 2003).

Quality and quantity of dosage material influence quantity and quality of biogas , that is biogas produced in 1 m^3 of utility fermentor volume per day.

The most of biogas plants are processed mixtures of domestic animals excreta (manure,slurry,urine,…) and plant biomass from fields and water (Plochl, 2008; Lehman, Friedrich, 2012; Wang et al., 2012; Zehnsdorf et al., 2011).

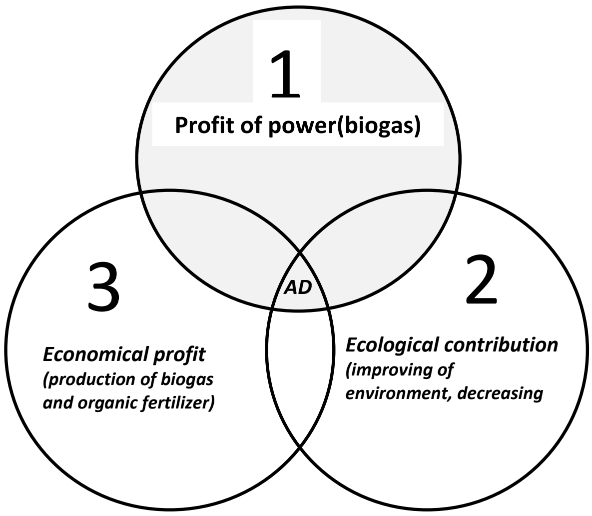

Fig. 1 Utilization of anaerobic fermentation in agriculture and municipal sphere (Pastorek et al., 2004), (AD –anaerobic digestion)

There are technological problems with processing of high content of lignocellulosic material (Lehman, Friedrich, 2012). Reason is high content of lignin. We obtain too much residues (Fig.2.).

One method, increasing rate of biogas production, is preprocessing and mixing of plant materials before fermentor input. (Plochl, 2008; Lehman, Friedrich, 2012; Vintiloiu et al., 2009; Weisbach, 2009; Baaboukani et al., 2012; Bohrsen, 2011).

Many researchers vere interested in investigation of various crops for energy purposes, especially for anaerobic fermentation . Therefore we focused our interest on unusual crops and plant matter. (The maiz varieties Banicia, Fixxif, Saxxo and alternative crop sorghum.)

Material and methode

The experiments took place in the laboratory of RIAEng Prague. We used apparatus for anaerobic fermentation of liquid material. This one is described in literature reference (Pastorek et al., 2004).

The apparatus consits of nine small fermentors (3 l volume) and two big fermentors (100 l volume), gas meter and analyzer of biogas.

We investigated various varieties of maiz and mixture maiz and sorghum (Fig.3, 4, 5.). Maiz and sorghum vere crushed befor anaerobic fermentation. Retention time was 29 days in all experiments.

Results and discusion

The best results had maize variety „Benicia“ and „Fixxif“ (Fig.5, 6). There are certain differences in investigated varietes of maize and in comparison with other material. It depends on yield of dry matter (Dohler et al., 2006; Dlabaja, Malaťák et al., 2013). But results are not the same in all regions in case of maize. Soil conditions, altitude and local environmental conditions are very important for successful growing of maize.

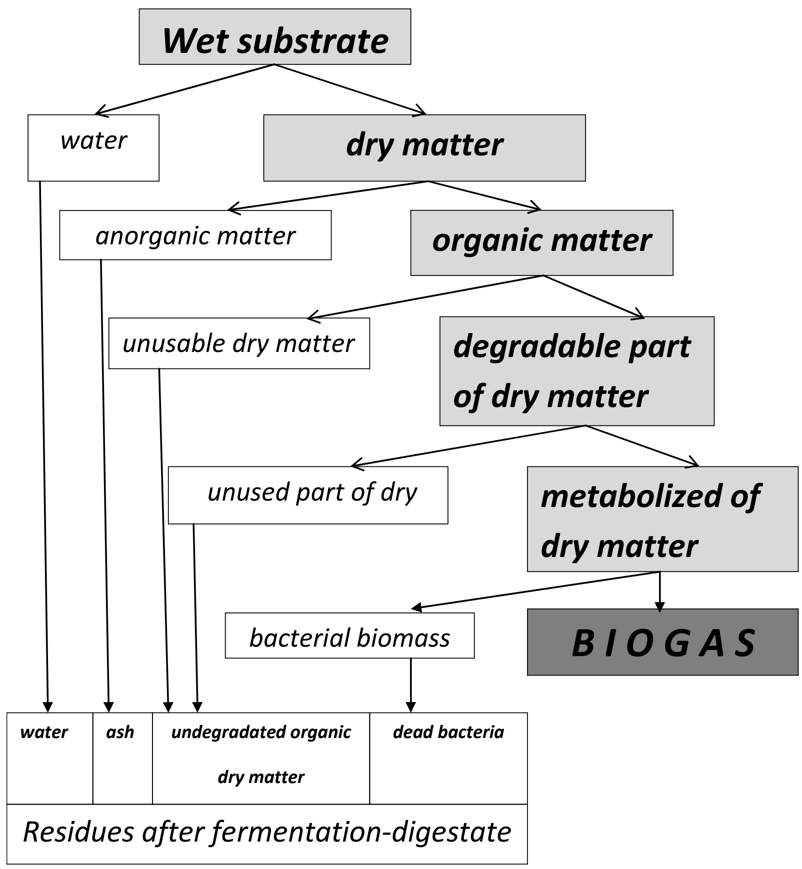

Fig. 2 Fractionation of wet material in the fermentor

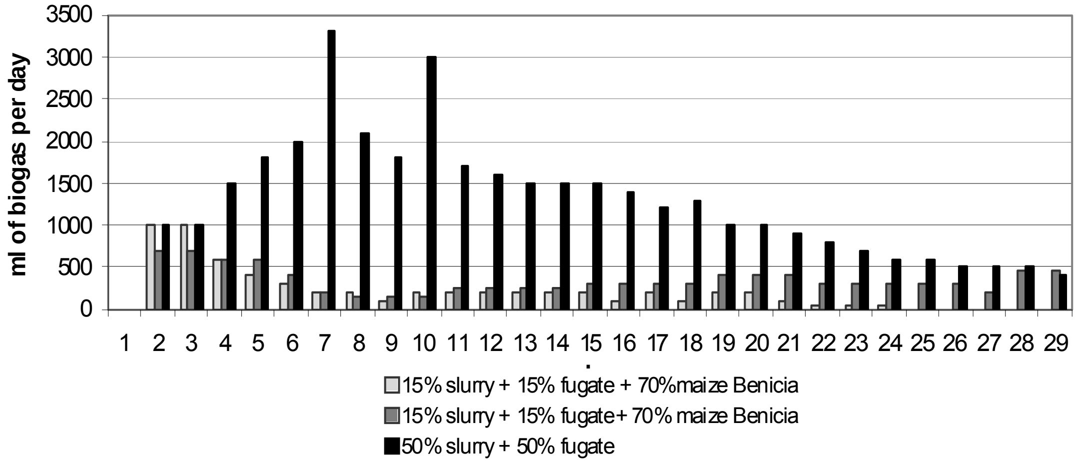

Fig. 3 Daily production of biogas (fugata + crushed maize Benicia)

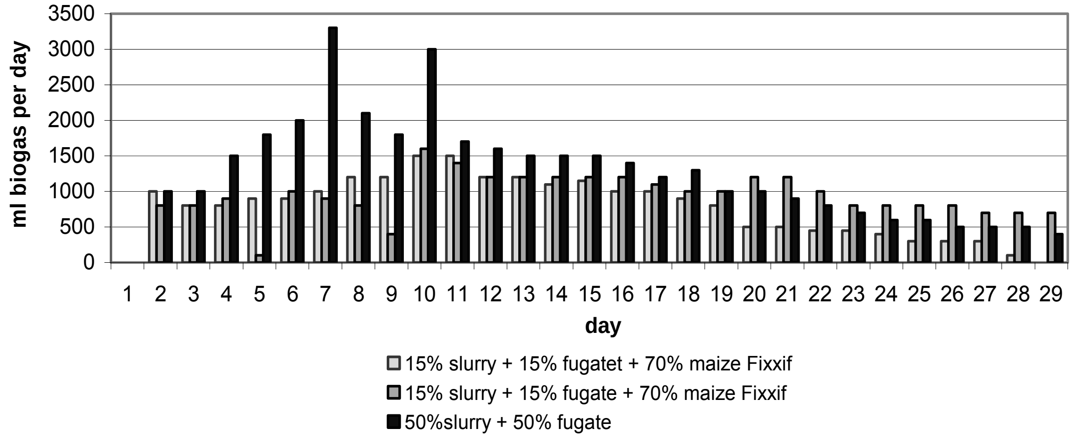

Fig. 4 Daily production of biogas (fugata+crushed maize Fixxif)

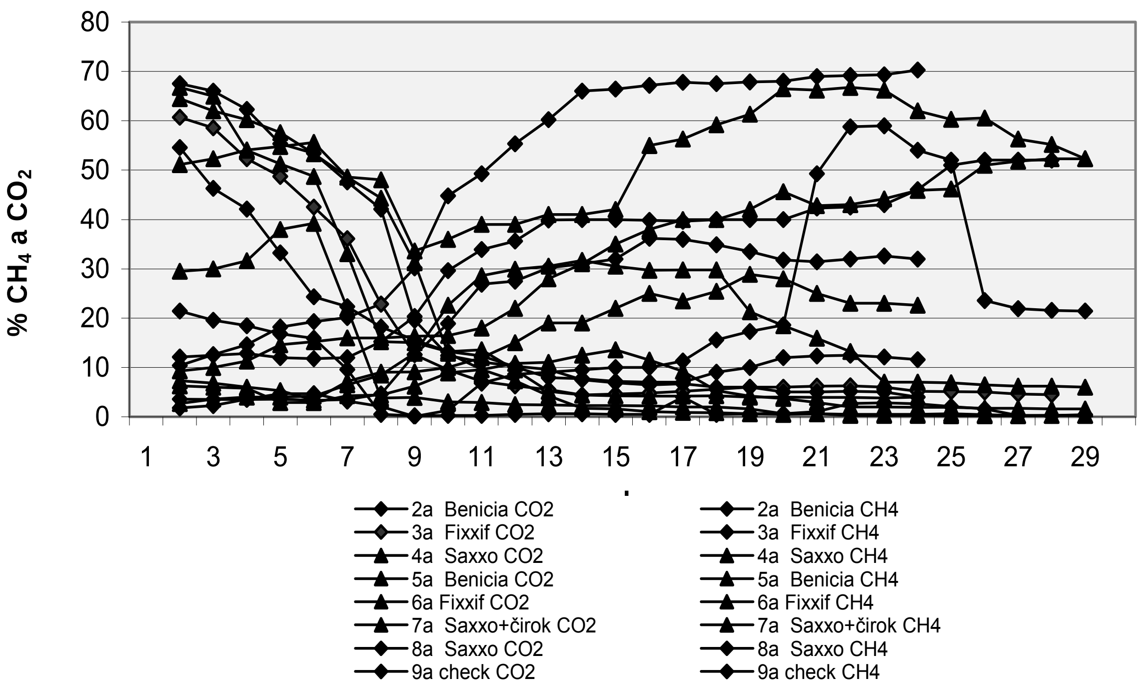

Fig. 5 Quantity of CH_4 and CO_2 in biogas from various varieties of maize + sorghum

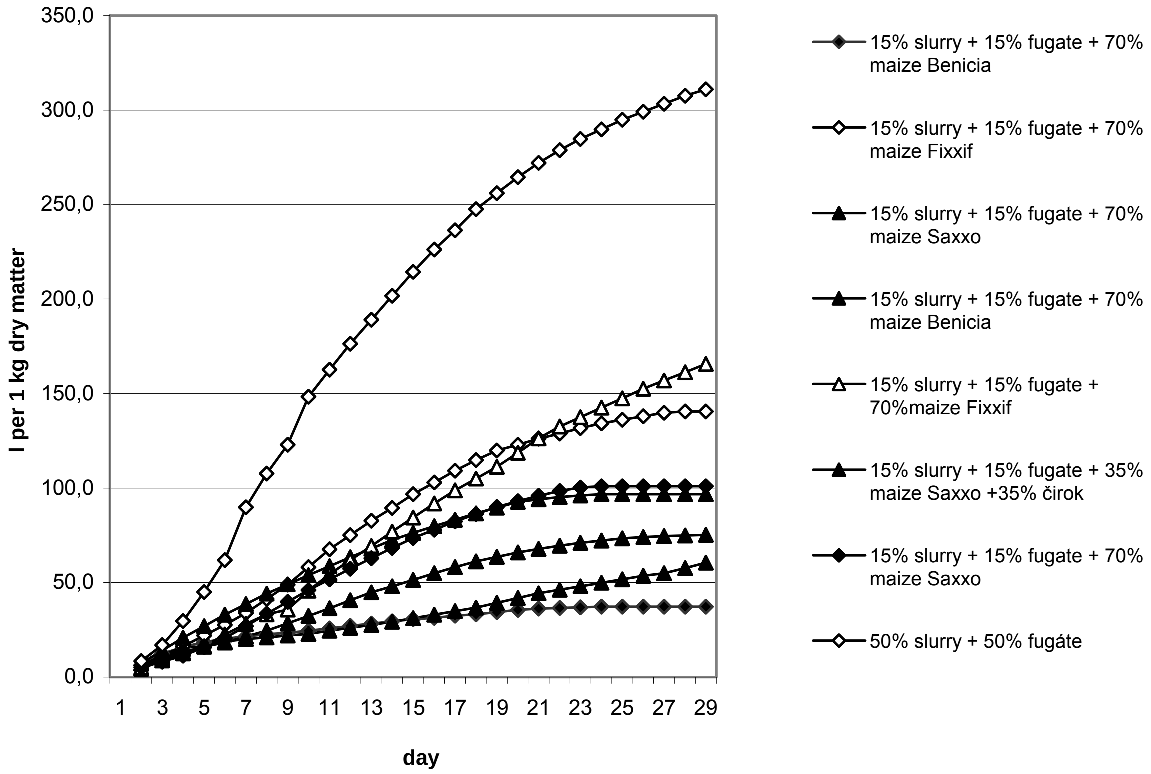

Fig. 6 Cumulative production of biogas (digestate+crushed maize and sorghum)

Conclusion

Maize is main crop for anaerobicc fermentation in Czech Republic. There are more varietes of maiz for growing as energy plants. Suitable maiz varietes exist for all regions of Czech Republic. The best results had maize varietes Benicia and Fixxif in our experiments. Optimal results of biogas plants we can reach when we use mixture of various organic materials. Alternative plants can be for example sorghum.

Reference

Baaboukani B.S., Nossoughi M., Alemzadeh I., 2012. Optimization of dilute-acid pretreatment conditions for enhancement sugar recovery and enzymatic hydrolysis of weat straw. Biosystems engineering 111, 166-174.

Bohrnsen A., 2011. BioCrack of Vogelsand: High voltage in tube. Profi, No 5., 76-78

Dlabaja T., Malaťák J., 2013. Optimization of anaerobic fermentation of kitchen waste, Res. Agric.Eng., No 1, 9-15.

Dohler H.,at all.,2006. Energy plants, KTBL Darmstadt, ATB Bornim

Lehman T., Friedrich E., 2012. Lignocellulosic substrates – not a problem for biogas plants? Landtechnik, No 2., 114-117.

Pastorek Z., Kára J., Jevič P., 2004. Biomass-renewable source of energy. FCC Public, Prague. (in czech)

Plochl M., 2008. Mixture is working! DLZ, No 11, 68-72.

Vintiloiu A., Brulé M., Lemmer A., Oechsner H., Jungbluth T., 2009. Influence of temperature and pH value on enzyme aktivity in the biogas process. Landtechnik, No.1., 22-24.

Straka F., 2003. Biogas, Říčany, Gas s.r.o. (in czech)

Wang L., Wang Q., Cai W., Sun X., 2012. Influence of mixing proportion on solid-state anaerobic co-digestion of distiller´s grains and food waste., Biosystems engineering 112, 130-137.

Weisbach F., 2009. Degree of utilization of renewable primary products in biogas production. Landtechnik, No 1., 18-21.

Zehnsdorf A., Korn U., Proter J., Nauman D., Seirig M., Ronicke H., Pieper B., 2011. Western waterweed (Elodea nuttallii) as a co-substrate for biogas plants. Landtechnik, No 2., 136-139.

UTILIZATION OF SATELLITE MONITORING FOR DETERMINATION OF OPTIMAL MAINTENANCE INTERVAL OF AGRICULTURAL MACHINES

Jindřich Pavlů, Zdeněk Aleš*, Vladimír Jurča

Czech University of Life Sciences Prague, Faculty of Engineering
16521 Prague 6 – Suchdol, Czech Republic, Phone: +4202, Fax: +4202- 24383254
E-mail: pavlu@tf.czu.cz, ales@tf.czu.cz, jurca@tf.czu.cz

Abstract

Standard component of today's modern mobile machinery in general is GPS/GPRS technology. Situation in agricultural sector is similar and most of current machinery is equipped with a lot of electronic devices for measuring all kind of parameters. GPS/GPRS technology allows us to monitor a number of operational parameters of mobile machinery in real time. Collected data obtained from the operation can be used for decision-making of maintenance activities. To ensure machinery it is important to determine the optimal maintenance interval. The authors propose new method for using data from satellite monitoring. Furthermore, authors designed algorithm using the criterial function in order to determine the optimal interval for performing preventive maintenance.

Keywords: GPS/GPRS technology, mobile machinery, fuel consumption, operational time

Introduction

There are two basic maintenance systems for ensuring preventive maintenance of vehicles and mobile machines - maintenance by the technical state (result of diagnostics) or maintenance according predetermined operating time intervals (distance travelled (km), operated hours (hrs) measured by hour meter, etc.) (Drożyner, Mikołajczak, 2007). Amount of the specific fuel consumption is mostly used as an overall diagnostic signal in the maintenance system according to technical state of mobile machines (Jin et al., 2009). This system faces several problems - a relatively accurate measurement of the roller bed test is very expensive, and furthermore, there are problems with the measurement of combustion engines with high power and some engines of construction machinery. Significantly cheaper acceleration methods are not without problems too, especially when measuring the nowadays conventional turbocharged engines, where delay of turbocharger during engine acceleration must be eliminated by various correction methods. For these reasons, second system (i.e. maintenance according predetermined operating time intervals) is mostly applied in this group of machines (Westerkamp, 2006).

Maintenance intervals are often determined only by a qualified estimate of the machine manufacturer or maintenance manager, which results in costs increase of operating machines - if the intervals are too short, it leads to unnecessary increase in maintenance costs, oppositely, it also leads to increase of costs resulting from the poor technical condition of machines (Wiest, 1998). In addition, predetermined intervals do not reflect operational utilization of a particular machine; the interval is set for the entire group of machines of the same type. Attempts to use known methods of mathematical optimization of preventive maintenance is problematic - known stochastic models are based on knowledge of the probability of failure in different periods of an object's life - it would presumed using statistical methods and monitoring of a number of other indicators of machine operation (dependability characteristics). The required stochastic model of renewal could be described and formulated after analysis of the history of machine operation (Eti et al., 2006; Jurča, Aleš, 2007).

One of the other options how to determine the optimal preventive maintenance interval is the application of renewal theory using data from satellite monitoring equipment. Satellite monitoring of mobile machinery is now relatively common, but companies use it in a very limited way - practically only for monitoring of machines. Transmitted data allow utilization of whole monitoring in more sophisticated way. In order to achieve such a goal, authors propose to set up and apply proper algorithm for data processing. Based on data of fuel consumption it is possible to determine the optimal maintenance interval of a particular machine and determine the losses which result from not complying with optimal maintenance interval.

Algorithm of determination of optimal preventive maintenance interval is based on the known value of preventive maintenance costs and slope of linear trend of specific fuel consumption, which is obtained by processing data from a satellite monitoring of machinery. Calculated optimal maintenance interval is corrected according to increasing operating time. In addition, it is possible to verify if previous maintenance interval was chosen correctly and how effectively operator of machinery contributes to production efficiency and effect of change in operating conditions, etc. (Jurča et al., 2008)

Material and method

Principle of operational monitoring using GPS/GPRS of machinery is widely known, therefore there are only briefly described issues related to this paper (Kans, 2008). After turning on the ignition system, control unit starts up from sleep mode, it will start to measure and store data into memory and connects to the server. After connecting the control unit sends quickly the recorded data, clears the memory and subsequent data sends at specified intervals, such as 120 s. Data is processed in the device according to the configuration file. Obtained data is in a various form: immediate values, maximum or minimum for the recorded period, the average, statistical parameters and it is also possible to apply various filters, and all data is conveniently available from user web application.

The digital data is converted to physical data (on the server); this level is called "measured data". User application calculates "calculated data" from stored "measured data". Measured and calculated data allows according user's algorithms to calculate pivot tables and "summed data". Pivot tables represent computed data tracked over the certain period of time according the user's requirements.

Summed data are usually categorized into three groups:

1. Mileage / service

This category provides information about: date and time, fuel tank START MODE (l), fuel tank STOP MODE (l), mileage from fuel tank (l), driven distance (km), time of idle running (hrs), time of trip (hrs), specific fuel consumption (l/100 km, 1/ha, l/hrs), over consumption of fuel, distance to repair shop (km), overall distance of tachograph (km).

2. Re-fuelling

This category provides information about: date and time, fuel tank START MODE (l), fuel tank STOP MODE (l), losses during break (l), losses during operation (l), probe check, re-fuelling off the record (l), re-fuelling on the record (l), overall re-fuelling (l), entry data about re-fuelling (l), differences between entered and measured data (l), relative deviation between entered and measured data (%).

3. Time utilization

This category provides information about: date and time, position – start of shift, start time of shift, position – finish of shift, finish time of shift, duration of operation time / shift (hrs), breaks (hrs), utilization per day (%).

In order to use the theory of renewal to determine the optimal maintenance interval of machinery it is important to measure fuel consumption with sufficient precision. Use of the CAN-BUS information is not suitable because the accuracy is determined by the fuel float up to 10 % according to CAN-BUS standard. For this reason, capacitance probe CAP04 (Partner mb.) were mounted into fuel tank.

Capacitive probe CAP04 consists of two tubes of different diameter, which are the electrodes of capacitor. The dielectric is composed of electrically non-conductive material, specifically with a fuel and air. The relative permittivity of air is $\varepsilon_r = 1$, during re-fuelling the air is replaced with diesel which has relative permittivity $\varepsilon_r = 2$ and due to this fact the capacity of the capacitor increases. The capacitive sensor measures the position of the boundary between air and diesel fuel.

The probe is also equipped with thermometers to sense temperature of fuel and the surface temperature of the fuel tank. The processor evaluates data according to the actual capacity of the probe to match the measured volume of diesel at a reference temperature 15 °C. This method ensures that the reported amounts of fuel are not distorted by thermal expansion of diesel. Furthermore, the probe measures the tilt of the tank in two axes. While driving terrain when the level of diesel fluctuates rapidly and strongly, the probe indicates stable signal by means of appropriate filters of the signal.

Before installing the fuel probes the accuracy of measurement of the probe was tested at temperatures from -15° C to + 55° C. Samples of diesel from three different fuel suppliers (Shell, and Slovnaft OMW) were used for testing. The highest deviation of measurement was measured on a sample from Shell at 13 °C - deviation was 0,21 %. In operation the accuracy of fuel capacity probe is slightly worse (about 0,5 %), which is fully satisfying for the purposes of measurement.

General criterial function of renewal (replacement) seeks the minimum of mean unit costs of renewal and operation – the minimum of the function marks the optimum time for renewal (see Equation 1). It is obvious, that the costs of maintenance itself act in the way of prolonging the standard preventive maintenance period. Conversely, the costs of operation, which rise due to worsening technical condition when extending the maintenance period, make the preventive maintenance period as short as possible. The sum curve *u(t)* must have a local minimum, which needs to be found in order to determine the optimum period of preventive maintenance. Specific fuel consumption is a comprehensive diagnostic signal indicating instantaneous extent of wear of machine (Legát et al., 1996).

$$u(t) = \frac{N_O + N_P(t)}{t} \rightarrow \min \tag{1}$$

Where: N_O - Costs of renewal (CZK)
t - mean time of operation (w)
$N_P(t)$ - Costs of operation (CZK), $u(t)$ - mean unit costs of renewal and operation ($CZK.w^{-1}$)

Author's proposed method for optimizing maintenance intervals of machinery uses information about fuel consumption that is assessed for each day of machine's operation in unit l/100 km or l/hrs.

For the calculation of the local minimum of a function of mean unit costs, its first derivative set equal to 0, thus:

$$\frac{\partial u(\bar{t})}{\partial \bar{t}} = \frac{\frac{\partial N_P(\bar{t})}{\partial \bar{t}} \cdot \bar{t} - \left[N_O + N_P(\bar{t})\right]}{\bar{t}^2} \tag{2}$$

$$\frac{\partial N_P(\overline{t_O})}{\partial \bar{t}} \cdot \bar{t}_O - \left[N_O + N_P(\overline{t_O})\right] = 0 \tag{3}$$

$$\frac{\partial N_P(\overline{t_O})}{\partial \overline{t_O}} = \frac{N_O + N_P(\overline{t_O})}{\overline{t_O}} \tag{4}$$

The right side of equation (4) equals to the intermediate mean unit costs $u(t_O)$ at optimum of operating time for renewal. The left side of the equation (4) equals to the intermediate immediate operation unit costs $v_P(t_O)$ at optimum of operating time for renewal. The equation describes that the optimal moment of renewal, i.e. a local minimum of the criterial function when immediate operation unit costs equal to the mean unit costs of operation and renewal.

Consequently, in order to find the minimum of sum function *u(t)* it is necessary to know two basic values - renewal costs N_O (the costs of performed maintenance) and mean unit costs of operation $u_p(t)$, which are based on the tracking of specific fuel consumption (therefore, it is necessary to determine the equation of growth trend of specific fuel consumption).

Results and discussion

Proposed algorithm for determining the optimum of maintenance interval is using MS Excel. Imported data on specific fuel consumption of the machine are listed in the table by date and time of their recording and from these data it is necessary to select only the data which characterize the utilization of agricultural machinery. The algorithms for data filtering are different according to different groups of agricultural machines and their utilization (tractor aggregated with different tool, combine harvesters, sprayers, etc.). For example, when filtering data on fuel consumption of combine harvester the algorithm filters out data on fuel consumption at idle mode of engine - the engine consumes fuel, but the driven distance is zero - the value of specific fuel consumption (l/ha) is reaching the infinity. Specific fuel consumption most of agricultural machinery is evaluated in litres per hectare or litres per operating hour – data collected during on-site position of the machine cannot be used for calculations, on the contrary for some machines (e.g. excavators and loaders), data collected during on-site position has to be included for data processing because machinery does perform intended work. A properly designed algorithm for filtering data affects the entire primary data processing and results of optimal maintenance interval of a particular machine.

After selection, the mean specific fuel consumption is calculated for each day and linear trend is constructed, as shown in Fig. 1.

Relatively simple and universal data filtering can be done by setting the certain level of engine speed (motor revolution). This certain level of engine speed is critical point when include specific consumption for further calculation. Furthermore, for each group of machines second condition is applied for data filtering (particular machinery has its own operating state: agricultural machinery (tractor) – aggregation with different working tool and move forward, combine harvesters and sprayers – move forward and operating mode, heavy trucks – position change, excavators and loaders – on-site, etc.). Correct adjustment of the raw data filtering algorithm provides more accurate processing procedure and consequential optimal maintenance interval of a particular machine.

Specific fuel consumption is a comprehensive diagnostic signal and depends on many operational factors and therefore there is large variance in monitored specific fuel consumptions. Linear trend is chosen because of very large dispersion of specific fuel consumption for each working day. Linear trend is characterized by an increase in specific fuel consumption depending on the operational time.

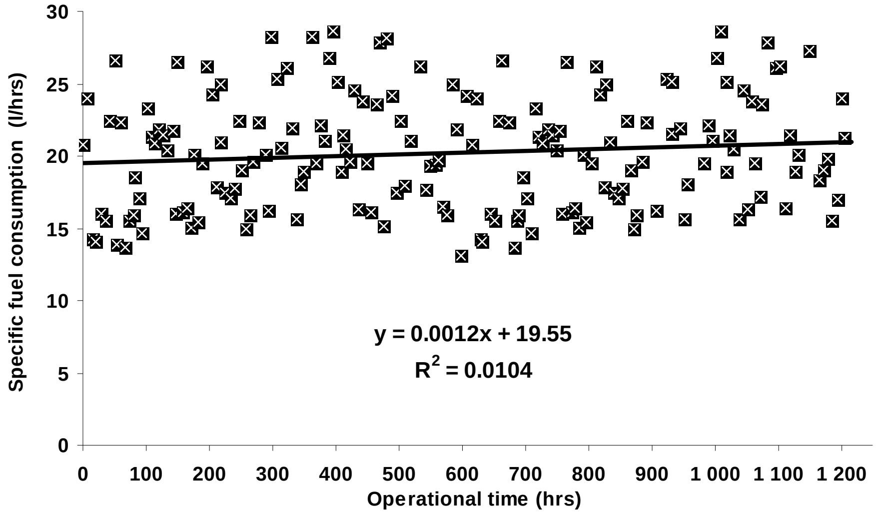

Fig. 1 Correlation of specific fuel consumption and operational time of tractor John Deere 6930

The unit costs of operation $u_P(t)$ are determined by a linear trend, which is set by slope of specific fuel consumption trend and the average price of diesel fuel (32,84 CZK.l^{-1} - February 2011) during agricultural machinery operation.

The function of the mean unit costs is determined by the sum of two functions - unit operational costs function and unit costs of replacement function. The optimal maintenance interval is determined by a local minimum of the mean unit costs function. In this case, the function $u_P(t)$ is linear, the local minimum of the function $u(t)$ located at the same spot as intersection of both forming curves $u_O(t)$ and $u_P(t)$. The specific examples of the graphic solution are shown in Fig. 2.

The costs of renewal (maintenance) for tractor John Deere 6930 are estimated at 50 000 CZK. In this particular case, the amount of 50 000 CZK represents costs of diagnostic maintenance of motor tractor John Deere 6930. Maintenance is performed within one working day and during this day the maintenance costs are calculated as follows:

1) The driver generates a financial loss during the day when the maintenance is carried out because transport of vehicle to the service shop and back does not generates any profit, but the driver has to be paid anyway. The financial loss can be calculated as follows: 25000 CZK / month (driver's salary) x 1,35 (deductions from wages) / 20 (working days) = 1 688 CZK.

2) The financial loss due to downtime of the vehicle is calculated: 1 000 CZK / hrs (the price of processed material) × 8 hrs / day (the average hrs per day) = 8 000 CZK

3) The financial loss occurred due to fuel consumed on a journey into and back: 40 l/100 km (average specific consumption of the vehicle) × 30 km (average distance to the maintenance service and back) × 32,84 CZK / l (average price of fuel at the date February 2011) = 394 CZK.

4) Costs of diagnostic maintenance = 15000CZK

5) The price of labour after diagnostic maintenance and the average price of spare parts (e.g., fuel, air and oil filter, injector, pump alignment, oil change, etc.) = 25 000 CZK.

Tab. 1 Calculation of maintenance interval of tractor John Deere 6930 for the increase in specific fuel consumption depending on the operational time with linear trend equation y = 0,0012x and fuel price 32,84 CZK per liter

Operational time (km)	Increase in specific fuel consumption (l/hrs)	Unit costs of operation $u_P(t)$ (CZK/hrs)	Unit costs of renewal $u_O(t)$ (CZK/hrs)	Mean unit costs of renewal and operation $u(t)$ (CZK/hrs)
1124	1.3488	44.294592	44.48399	88.778577
1125	1.3500	44.334000	44.44444	88.778444
1126	**1.3512**	**44.373408**	**44.40497**	**88.778381**
1127	1.3524	44.412816	44.36557	88.778388
1128	1.3536	44.452224	44.32624	88.778465

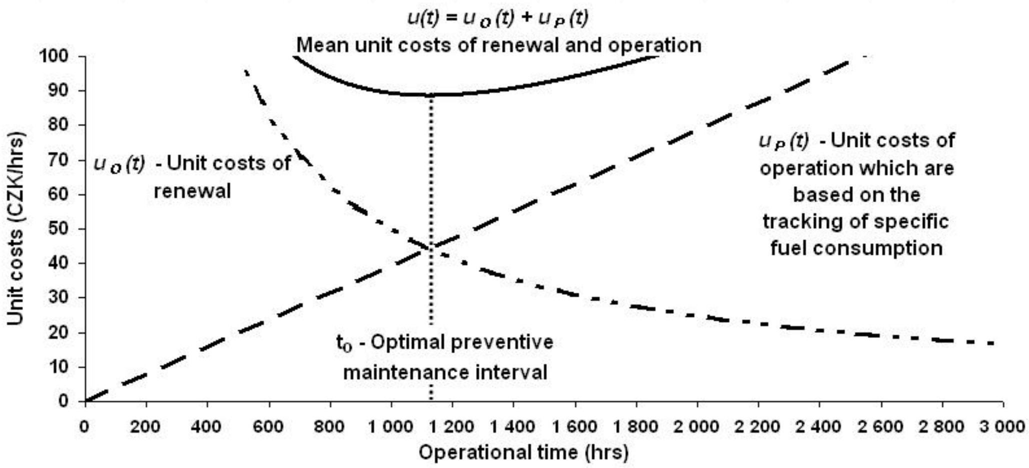

Fig. 2 Determination of engine maintenance intervals for the increase of specific fuel consumption – graphic interpretation of Table 1

Tab. 2 Determination of the mean maintenance interval for different agricultural machinery

Agricultural Machine type	Gcom number	Operated time (hrs)	Average (hrs/day)	Trend of slope of specific fuel consumption	Determined maintenance interval t_O (hrs)
John Deere 6930	680	1 216	8,2	0,0012	1 126 → 1 100
John Deere 6830	684	1 457	7,9	0,0095	1 253 → 1 300
Fendt Vario 500	1 030	1653	6,8	0,0013	1 082 → 1 100

This practical example shows that the optimal preventive maintenance interval is 1126 hrs for vehicle tractor John Deere 6930 (see Table 1 and Fig. 2). For better labour planning it is useful to round this number to 1100 operated hours.

For the calculated procedure, it is clear that the maintenance interval is variable and can be influenced by:

- maintenance costs,
- function of mean unit operational costs (influenced by fuel costs).

Specific fuel consumption is influenced by the conditions of operation of the machine and therefore determined maintenance interval has to be continually updated. Data analysis of plenty same types of vehicles will help determine the intervals for maintenance for a particular type of machine and use it for simple long-term maintenance planning of mobile machines in the enterprise (see examples below in Table 2).

Table 2 provides data on agricultural machine, number GCOM (the unit of remote control monitoring), monitored time of operation (hrs), the average operated hours per day, slope of linear trend of specific fuel consumption and data of specified maintenance intervals t_O (hrs). Slope of linear trend of specific fuel consumption is different for each particular vehicle. Such a fact is due to different operational conditions of certain vehicles and also due to different style of driving of drivers. Slope of trend for agricultural machinery ranged from 0,0095 to 0,0013. Determined optimal intervals were calculated with N_O = 50000 CZK and average fuel costs 32,84 CZK per litre.

Conclusion

The paper presents proposed methodology for optimization of planned preventive maintenance, which is based on the use of data from satellite monitoring - data collection, their final selection and algorithmic processing and therefore finding optimal preventive maintenance interval for a particular machine or group of machines. Algorithm of determination of optimal preventive maintenance interval is based on renewal theory and its modification for solving particular problem. Principle of this algorithm is based on minimization of operational and renewal costs.

The proposed methodology for determining the optimal maintenance interval is particularly suitable for companies that already use satellite monitoring, but mostly in its elementary form for the current position of the vehicle, construction equipment downtime monitoring, etc. It is obvious that the observed specific fuel consumption relatively largely varies, which is influenced by variability of operating conditions, load weight, driver's driving style, nature of extracted material within construction machinery, etc. This variance is eliminated by large quantities of raw data and therefore processing of raw data allows for a precise determination of the optimal preventive maintenance interval for a specific machine, its current operational conditions and the changes of their technical state during deterioration.

Algorithm of data processing from satellite monitoring provides timely reports on individual machine maintenance requirements and enables continuous refinement of maintenance intervals during operational time. Suspiciously different maintenance interval of particular machine (calculated optimal maintenance interval deviates from the average) might be followed by detailed diagnostics in order to determine the causes of short maintenance interval. Proposed algorithm may contribute to better maintenance planning and consequently to economical operation of machinery.

Acknowledgement

Grant project of the Ministry of Industry and Trade of the Czech Republic No. FR-TI2/202 "Information system of effectiveness and performance monitoring of production equipment – OEE-DTM".

Reference

Drożyner P, Mikołajczak P., 2007. Maintenance of vehicles, machines and equipment in view of the ISO 9001 requirements. Eksploatacja i Niezawodność - Maintenance and Reliability 4: 55-58.

Eti M.C., Ogaji S.O.T., Probert S.D., 2006. Reducing the cost of preventive maintenance (PM) through adopting a proactive reliability-focused culture, Applied Energy, 83: 1235–1248.

Jin G.Y., Xiang Z., Lv F., 2009. Semantic Integrated Condition Monitoring and Maintenance of Complex System. In: IEEE 16th International Conference on Industrial Engineering and Engineering Management. Beijing, PRC: 670-674.

Jurča V., Aleš Z., 2007. Maintenance Management Efficiency Evaluation. Eksploatacja i Niezawodnosc – Maintenance and Reliability, 1: 13-19.

Jurča V., Hladík T., Aleš Z., 2008. Optimization of Preventive Maintenance Intervals. Eksploatacja i Niezawodność - Maintenance and Reliability, 3: 41-44.

Kans M., 2008. An approach for determining the requirements of computerized maintenance management systems. COMPUTERS IN INDUSTRY, 59: 32-40.

Legát V., Žaludová A.H., Červenka V., Jurča V., 1996. Contribution to optimization of preventive replacement. Reliability Engineering and System Safety 51, Elsevier Science Limited. ISSN 0951-8320

Westerkamp T.A., 2006. Maintaining maintenance - How smart managers plan and execute successful CMMS implementations. INDUSTRIAL ENGINEER, 38: 37-42.

Wiest W., 1998. Improvement of the availability through quality control and preventive maintenance of self-propelled vehicles. In: Conference on Agricultural Engineering, VDI BERICHTE vol. 1449: 351-356.

STATISTICAL EVALUATION OF DATA OBTAINED BY PARTICLE COUNTER USING NON-REFERENCE FLUIDS

Bohuslav Peterka[1*], Zuzana Novotná[2], Petr Jindra[1]

[1] Department for Quality and Dependability of Machines, Czech University of Agriculture in Prague (CULS Prague), 16521 Prague 6 – Suchdol, Czech Republic, Phone: +420224384334, E-mail: peterka@tf.czu.cz
[2]Department of Statistics, CULS Prague, Czech Republic,

Abstract

Machine condition monitoring based on oil analysis is one of commonly accepted diagnostics methods. Some of standard methods of oil analysis are based on particle counting and particle shape classification. The LaserNet Fines-C (LNF-C) is analytical tool that combines both of those methods in one instrument. Relevant results of the analysis are conditional on the use of appropriate methodology and main characteristics of the diagnostic tool. In this paper are discussed the results of repeated measurements on the same sample normal type of oil. The results were subjected to statistical processing to determine the repeatability of the measurement without the use of conventional but very expensive standard calibration fluid.

Keywords: wear, maintenance, LaserNet Fines-C, hydraulic oil, shape clasification, normality test, statistics

Introduction

Service of every machinery is closely connected with function deterioration and wear. Wear is related to interactions between surfaces and more specifically the removal and deformation of material on a surface as a result of mechanical action of the opposite surface. Wear debris is typically carried to the lubricating or hydraulic oil. Size, count and type of particles are significant diagnostic signals which are commonly used within evaluation of technical condition of the machine.

During normal machine operation small wear debris particles in range of 1-10 µm are generated. When abnormal wear begins, large debris particles in the range of 10-150 µm microns are produced. The particle size and concentration will increase gradually until machine failure. It also leads to deterioration of lubricating ability and deterioration of both physical and chemical properties of the oil. With the use of modern diagnostic methods and appropriate instrumentation we can prevent these undesirable changes and significantly reduce machine downtime and significantly extend the physical life of the machine.

Quality product is dependent on reliable and serviceable manufacturing facility, which is influenced by effective and timely performed maintenance, including checking and refilling of lubricants and other vital fluids. For assessing the state of lubricants and parts of manufacturing machinery, it is possible to use a series of analysis including, for example particle counter and particle shape classifier LaserNet Fines-C, flash point, kinematic viscosity, water content, determination of solid particles, wear metals, etc. (Ales at al., 2010),

Automatic particle counters (APC) usually use blocking or scattering of light while oil sample flow through sensing chamber. Light intensity is measured using sensitive photodetector. Size of particles corresponds to voltage peaks on the output of the photodetector and quantity of particles corresponds to the width of those impulses. The influence of the measurement results is mainly due to different calibration method, particle shape, transparency and reflectivity and different flow rate during measurement. Lastly, errors may occur in automatic particle counters when the particle concentration becomes so high that 2 or more particles are present in the sensing chamber simultaneously. These smaller particles are interpreted as one larger particle. This so-called “coincidence error” causes the number of small particles to be under-reported and the number of large particles to be over-reported. Depending upon the specific particle counter being used, coincidence errors begin around 10^3 particles/ml or at an ISO code of 21 according ISO 4406. The coincidence error gets worse as particle concentration goes up.

Automatic particle counting is very often applied to new or "clean" oils (hydraulic fluids). Less often, these methods are applied to the motor and gear oils, where the character of their operational stress causes an increase in the number of wear and contaminant particles present. The main reason is that the APC are unable to work with oils with a high proportion of soot (diesel) or oil with a high concentration of particles.

Author's oil laboratory is equipped with a laser particle analyzer and classifier LaserNet Fines (LNF-C). This unit is specific in that it uses direct imaging of particles. Therefore, it is not necessary to perform calibration using a reference liquid. Reference fluid is used only for to verify the accuracy of the measurement. The authors have raised the question whether it is possible to check some parameters of particle counters without need of use of calibration fluid. One possible way is to use any oil sample and perform the repeatability test. This is done so that it is carried out repeated analysis of the same sample of oil, and then statistically processed rate variability, and other statistical characteristics of each measurement.

In the past, a similar study was done by Spectro, Inc. to determine the reproducibility and repeatability of several manufactured LNF instruments. This study summarizes the results of measurement of five samples of the same test liquid to five devices LNF (total of 25 runs) and was performed with a liquid PartiStan, which is a commercial version of NIST SRM 2806 calibration fluid. Results from the two randomly chosen instruments are presented on Tab. 1.

Since the data was evaluated only a few basic statistical methods. The authors have attempted to extend the data processing using other statistcal method and modern software such as SPSS and Statistica.

Graphical presentation is essential to assess the data distribution. The distribution must also be assessed quantitatively. These approaches will determine if the data is Normal or not. Finally the results of these tests of Normality must be shown to be free of sample size effects. The preferred graphical techniques are the histogram and the box-and-whisker plots that may be supplemented, with advantage, by quantile–quantile or probability–probability plots. Classical tests of skewness and kurtosis can produce conflicting and often confusing results and, as a consequence, the alternative use of the newer L-moments is advocated. Normality tests included the Kolmogorov–Smirnov (Lilliefors modification), Crame´r-von Mises and Anderson–Darling tests (empirical distribution function statistics) and the Gan–Koehler, Shapiro–Wilk, Shapiro–Francia, and Filliben tests (regression/correlation techniques). Of these only the Anderson–Darling, Shapiro–Wilk, and Shapiro–Francia tests correctly classified all four test samples (Handerson, 2006).

In our case, there we assuming that results will be free of sample size and also that the samples are homogeneous and contained particles are well dispersed. For purpose of normality test in our study, it was used Shapiro-Wilk test also known as W test. The Shapiro-Wilk W is the ratio of the best estimator of the variance to the usual corrected sum of squares estimator of the variance (Shapiro and Wilk 1965). The statistic is positive and less than or equal to one. Being close to one indicates normality.

For purpose of repeatability test it was used basic statistic, particulary the Coeficient of variation. In probability theory and statistics, the coefficient of variation (CV) is a normalized measure of dispersion of a probability distribution or frequency distribution. It is also known as unitized risk or the variation coefficient. The absolute value of the CV is sometimes known as relative standard deviation (RSD), which is expressed as a percentage.

Tab. 1 Repeatability of individual LNF instruments for particle counting. Source: Spectro, Inc. –LNFC-08

Bottle	LNF S/N	Run #		>4 µm	>5 µm	>6 µm	>10 µm	>14 µm	>15 µm	>20 µm	>21 µm	>25 µm	>38 µm	>50 µm	>70 µm
1	21	1		73646	44431	28957	8663	2584	2018	708	596	292	74	14	0
2	21	10		75907	45561	29508	9036	2806	2180	801	663	315	39	8	2
3	21	14		78449	47124	30390	9060	2696	2153	791	652	366	77	18	3
4	21	18		70252	43042	28397	8524	2410	1899	719	571	257	51	12	3
5	21	22		74094	44591	28859	8582	2476	1939	698	603	302	51	8	2
			Average	74470	44950	29222	8773	2594	2038	743	617	306	58	12	2
			Standard Deviation	3021	1511	763	256	161	125	48	39	40	17	5	1
			% RSD	4.1	3.4	2.6	2.9	6.2	6.1	6.5	6.4	13.0	28.4	37.7	69.7
1	77	5		74295	45196	29476	8624	2223	1733	638	541	273	45	8	0
2	77	9		78763	45951	29133	8685	2286	1774	668	582	310	46	14	0
3	77	13		73934	45471	29841	8485	2107	1648	624	524	271	43	11	2
4	77	17		74869	45561	29957	8850	2256	1773	725	600	305	46	6	2
5	77	21		75997	46210	30314	8663	2281	1789	679	564	268	34	9	0
			Average	75571	45678	29744	8661	2231	1743	667	562	285	43	10	1
			Standard Deviation	1948	402	454	131	73	57	39	31	20	5	3	1
			% RSD	2.6	0.9	1.5	1.5	3.3	3.3	5.9	5.5	7.0	12.0	31.0	136.9

Experimental arrangement

Evaluation of data was obtained by repeated measurements of the same sample of hydraulic oil Mobil DTE Excel 46. Operating time of this oil on the machine was 8000 hours. The oil was sampled from sinking line Salvagnini according to methodology ČSN 656207.

Oil sample (50 ml) was removed for analysis after thorough shaking (approx. 5 min) storage containers. Prior to each sample analysis carried out was deprived of air bubbles by inserting in ultrasonic bath. The procedure was repeated for 31 cycles in the same conditions using same oil sample. In this way it was obtained 31 data sets including overall particle counts, particle counts for specific size range and particle type classification for particles >20 μm.

Measurements were performed using by laser particle counter and classifier LNF-C S/N:0288 made in 2008 by Lockheed Martin Defense Systems.

The data obtained from the measurements were processed using the software Statistica and SPSS. Descriptive statistic and data normality testing using Shapiro-Wilk test were performed. Almost all calculations including graphical output were done by using Statistica or SPSS software.

Results and discussion

Processing oil sample using the analyzer LNF-C was obtained 31 data sets. These data contain information about the overall particle counts, particle counts for specific size ranges (5÷10 μm, 5÷10 μm, 10÷15 μm, 15÷20 μm, 20÷25 μm, 50÷100 μm a >100 μm) and particle shape classification for particles >20 μm. Furthermore, the particles 20> μm are classified according to their shape. The algorithm of LNF-C utilizing neural networks sorts particles in these categories: cutting, fatigue, severe sliding, nonmetallic and fibers. LNF-C software is also able to test circularity, so water bubbles and air bubbles are excluded from results of particle counting.

Fig. 1 shows overall average particle count for each particular size range. This is actually Particle Size Distribution (PSD) chart of observed hydraulic oil. It is obvious that particles in range of 5÷15 μm are the most represented.

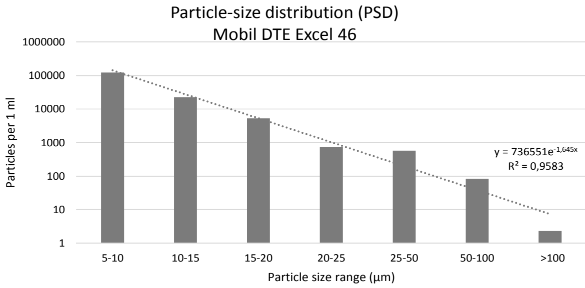

Fig. 1 Particle size distribution (PSD) of tested oil

In addition, calculation of statistical indicators for each size range was performed. Obtained data can be compared to the results of the research mentioned above (Tab. 1). Tab. 2 shows repeatability of observed LNF-C instrument. The percent RSD (Relative Standard Deviation) is about 4,8 % for particles 5÷10 μm and about 186,8 % for particles greater than 100 μm. As expected as particles become larger the RSD increases.

Normality was tested using Statistica and Shapiro-Wilk test for each of 31 datasets for each particularly size range. It was found that the Normal distribution correspond practically only to observations in size range of 5-10 μm (Fig. 2). However, other size categories from 10 μm to more than 100 μm exhibit Non-normal distribution (Fig. 3).

Tab. 1 Descriptive statistics for LNF Repeatability test

Variable	Descriptive Statistics - LNF Repeatability test												
	Valid N	Mean	Median	Minimum	Maximum	Lower Quartile	Upper Quartile	Variance	Std.Dev.	Confidence SD -95,00%	Confidence SD 95,00%	Coef.Var. % RSD	Skewness	Kurtosis
5÷10 μm	31	122176,2	123551,9	108668,8	135358,7	118045,6	126618,0	34989558	5915,197	4726,905	7906,686	**4,8415**	-0,337458	0,09232
10÷15 μm	31	22445,3	21570,0	20340,2	30547,7	21085,4	22460,8	5726589	2393,029	1912,298	3198,699	**10,6616**	2,452251	5,80189
15÷25 μm	31	5263,0	5163,9	4524,7	6836,5	4950,9	5328,1	306248	553,397	442,226	739,711	**10,5148**	1,631799	2,53109
20÷25 μm	31	731,5	717,2	601,9	1016,6	684,1	759,0	7944	89,128	71,223	119,135	**12,1836**	1,320526	2,69919
25÷50 μm	31	576,6	562,4	482,3	749,8	528,0	626,6	4405	66,371	53,038	88,716	**11,5114**	1,083551	0,87312
50÷100 μm	31	83,0	66,7	43,4	159,8	55,9	99,1	1412	37,582	30,032	50,234	**45,2702**	1,152972	-0,04206
>100 μm	31	2,3	0,0	0,0	20,7	0,0	3,1	18	4,273	3,414	5,711	**186,8436**	3,161135	11,59878

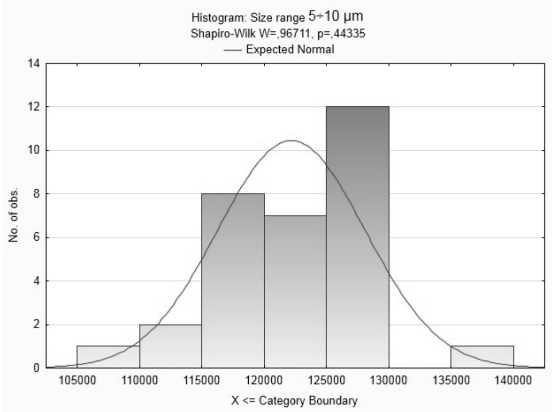

Fig. 2 Size range 5-10 µm – Normally distributed

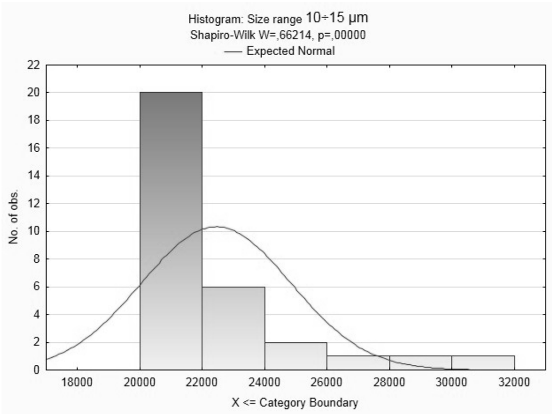

Fig. 3 Size range 10-15 µm – Non-normally distributed

Differences between two of size ranges is easier to find using Box-plot. Results are depicted on Fig. 4 and Fig. 5.

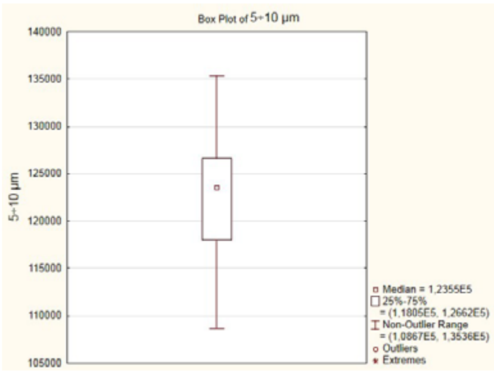

Fig. 4 Box plot – Normally distributed

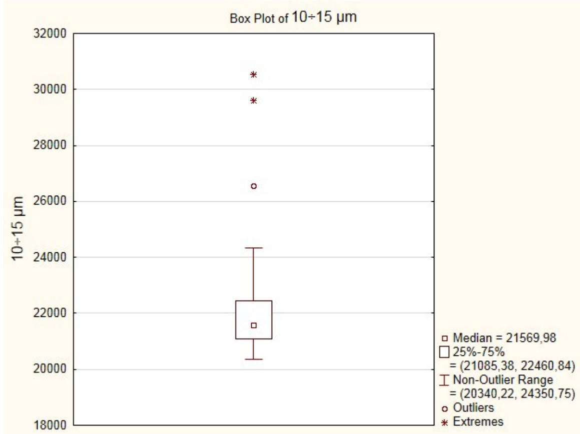

Fig. 5 Box plot – Non-normally distributed

The same tests as mentioned above was done for each of 31 datasets of shape classification results. Tab. 2 shows results of repeatability test of shape classification.

Shape clasification normality test show that non-metallic particles are Normal distributed (Fig. **6**). Similar results was observed within sliding particles category. Other particle shapes category are Non-normaly distributed i.e. fatigue particles observations (Fig. 7).

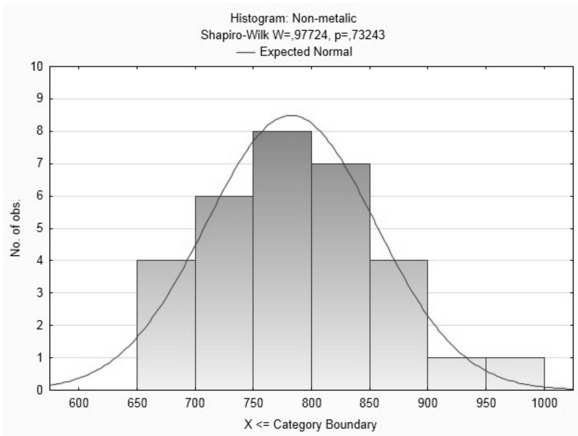

Fig. 6 Non-metallic particles – Normally distributed

Tab. 2 Descriptive statistics for LNF Repeatability test – shape classification results

Variable	Valid N	Mean	Median	Minimum	Maximum	Lower Quartile	Upper Quartile	Variance	Std.Dev.	Confidence SD -95,00%	Confidence SD 95,00%	Coef.Var. % RSD	Skewness	Kurtosis
Cutting	31	146,6	144,6	102,4	218,6	123,4	158,3	974	31,21	24,94	41,72	**21,29**	0,873	0,304
Sliding	31	194,9	191,8	146,2	267,9	175,6	204,7	713	26,71	21,34	35,70	**13,70**	0,648	0,693
Fatique	31	235,2	228,1	181,4	421,6	194,3	242,1	2978	54,57	43,61	72,94	**23,20**	2,045	4,480
Non-metalic	31	782,3	778,9	655,7	964,9	718,5	828,6	5305	72,83	58,20	97,36	**9,31**	0,466	-0,054
Other	31	49,6	34,0	18,5	131,1	25,2	68,5	1055	32,48	25,96	43,42	**65,54**	1,346	0,844

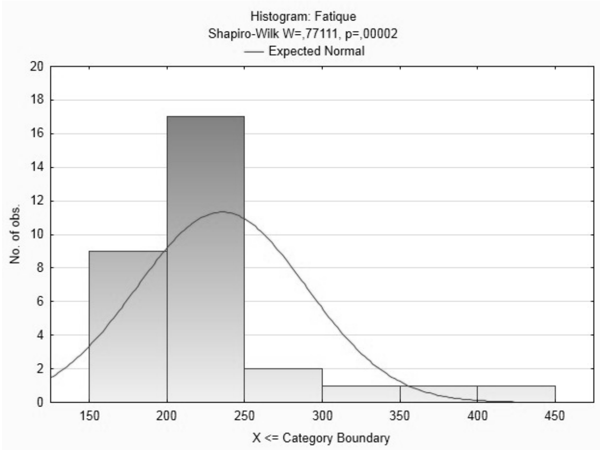

Fig. 7 Fatigue - particles – Non-normally distributed

Conclusions

According to the results of repeatability test it can be inferred that used LNF-C instrument have comparable repeatability as similar instruments of his kind. Variance of measurement results of individual measurements is negligible according to needs of assessment of cleanness code of hydraulic oil. In the field of predictive maintenance observed variability can be also omitted. Repeatability test of LNF-C instrument can be done with any kind of appropriate hydraulic fluid. There is no need to use expensive calibration fluids for this kind of test.

During statistical evaluation of obtained data it was observed that only few particular particle counting and clasification categories of realized measurements falls in to Normal distribution. Graphical methods provide easy way to a qualitative assessment of a Normality. From numerical methods for evaluation normality it can be used Shapiro-Wilk test.

Acknowledgment

This paper was prepared under grant IGA 2013/1022 "Methods and techniques of research project focusing on different forms of output presentation."

Reference

Aleš Z., Pexa M., Peterka B., Holek M., 2010. Compressor maintenance supported by tribodiagnostics. In: Manufacturing Technology, 1: 88 - 96.

Henderson A. R., 2006. Testing experimental data for univariate normality. In: Clinica Chimica Acta, 366: 112 – 129.

Shapiro S. S., Wilk M. B., 1965. An Analysis of Variance Test for Normality (CompleteSamples). In: Biometrika, 52: 591 - 611.

Spectro Inc. LaserNet Fines Reproducibility Test with Medium Test Dust. LNFC-08 Bulletin.

IMPACT OF BIOFUELS ON PERFORMANCE AND EMISSION CHARACTERISTICS COMBUSTION ENGINE - ZETOR 8641 FORTERRA

Martin Pexa[1], Jakub Mařík[1*], Karel Kubín[2]

[1]Czech University of Life Sciences Prague, 16521 Prague 6 – Suchdol, Czech Republic, Phone: +420 224 383 278, E-mail: pexa@tf.czu.cz
[2]VUZT-Research institute of Agricultural Engeneering. p.r.i, Prague, Czech Republic,

Abstract

The European Union currently pays great attention to the possibilities of the use of biofuels to power mobile machinery. The main reasons for the promotion of biofuels is the effort of Member States to reduce dependence on oil imports, efforts to reduce emissions from internal combustion engines and also efforts to support agriculture. The best substitute of diesel promote fatty acid methyl ester, namely in the Czech conditions rapeseed methyl ester (RME - Rapeseed Methyl Ester). Requirements for diesel fuel are the norm EN 590 (CSN EN 590, 2010) and prescribes requirements for RME standard EN 14 214 (CSN EN 14 214, 2010). At present, based on the requirements of EU directives made mandatory addition of methyl ester in diesel of a maximum volume fraction of 7 %. This blended fuel complies with EN 590 (CSN EN 590, 2010) and can be used without any modification existing diesel engines. Production of methyl ester of fatty acids is energy intensive and therefore offer, with allowance made for the structural adjustment of the engine, the possibility to use a mixture of diesel fuel and oil directly. In this paper are compared engine performance parameters (torque and engine power) and minimum specific fuel consumption. Based on standardized test NRSC (non-road steady cycle) (97/68/EC, 1997, 2004/26/EC, 2004, 2000/25/EC, 2000, 2005/13/EC, 2005) are compared also carbon monoxide and carbon dioxide of the internal combustion engine tractor Zetor 8641 Forterra (tractor engine has worked less than 100 hours). The fuel is a mixture of different ratios of selected diesel with rapeseed oil, jatropha curcas oil and rapeseed oil methyl ester.

Keywords: biofuels, carbon monoxide, carbon dioxide, total engine charakteristic

Introduction

As the best substitute for diesel fuel, which covers most of the energy consumption of agricultural equipment, the fatty acid methyl esters (FAME) are currently being promoted. Specifically in the Czech Republic, the most common substitute for diesel oil is Rapeseed Oil Methyl Ester (RME). Although the RME is chemically different from petroleum products, its fuel properties such as density, viscosity, calorific value and combustion process, the diesel is very close (Table 1). Requirements for the diesel fuel are specified in the standard ČSN EN 590 (2010) and the RME requirements prescribes the standard ČSN EN 14214 (2010).

Another option is to use vegetable oil (rapeseed oil). The idea is to use it to drive machines originated in 1895 when Rudolf Diesel invented the diesel engine. Currently, mainly two views on propulsion engines using vegetable oil are widespread. Engine engineers and technicians refuse to address this issue (damage to both the pump and the motor). In their opinion, they are supported by enthusiasts who pour vegetable oil into the tank without any modifications or they use an unprofessionally rebuilt diesel engine. The vegetable oil is denser than the oil and its viscosity is higher (Table 1). There are basically two ways to reduce the viscosity:

- chemically – so do the manufacturers of the RME,
- by heating – by heating the vegetable oil a large increase in its fluidity can be achieved. (Gabrielová, 2010).

Similar to the rapeseed oil is the oil from the African plant Jatropha Curcas. Jatropha Curcas has the advantage that it is grown on agriculturally unsuitable soils, meaning it produces little or no carbon deficiency of the soil and thus provides an immediate advantage. The biodiesel made from Jatropha Curcas is very close to the biodiesel satisfying the ČSN EN 14214 standard. Properties of the oil, particularly its quality and density, are important for production of the biodiesel (Table 1). Generally, it is necessary to reach small oil contamination, low acid number, low levels of phosphorus, water and ash particles and to increase its oxidative stability. (Achten et al., 2008; Mazancová, Panáčková, 2011; Liu et al., 2012).

The raw oil can be poured directly into the diesel engines without major modifications. It has a higher viscosity than normal petrol, which doesn't cause a real problem when it is used in areas with a higher temperature. Thanks to the higher oxygen content, the engine has got more power under full load than that of diesel. Some systems can be divided into two fuel tanks. The motor is started and stopped using the mineral oil. There may be used a specially modified engine. Unlike the diesel, the biodiesel is very biodegradable (within 21 days the degradation is around 90 %), contains almost zero of sulfur and heavy metals, and generally is low in emissions. (Huang et al., 2010; Chauhan et al., 2010; Mazancová, Panáčková, 2011; Varatharajan et al., 2011).

Tab. 1 Comparison of basic parameters of the diesel fuel (ČSN EN 590), RME (ČSN EN 14214), rapeseed oil and the oil from Jatropha Curcas

Request	Diesel	Jatropha oil	Rapeseed oil	RME
Density at 15°C (kg m^{-3})	820 to 860	919	915	860–900
Kinematic viscosity at 40°C (mm^2 s^{-1})	2.0–4.5	50	35	3.5–5.0
Flash Point (°C)	over 55	240	246	over 120
Cetane number	min. 51	51	38	min. 51
Calorific value (MJ kg^{-1})	42,5	39.6	36	37.1–40.7

Tab. 2 Dynamometer AW NEB 400 - parameters

Parameter	Value
Maximum torque on PTO (Nm)	2,850
PTO - Maximum speed (min^{-1})	3,200
Maximum braking power (kW)	343
Maximum braking power at a speed of 540 min^{-1} PTO (kW)	149

Fig. 1 Dynamometer AWNEB 400

The aim of this paper is to compare the influence of different types of fuels containing bio-characteristics on the tractor engine (they were chosen different mixing ratios of the biofuel and the diesel). These characteristics were measured for carbon monoxide (CO) and carbon dioxide (CO_2). As fuel for the engine of the Zetor 8641 Forterra tractor (less than 100 mth) blends of the diesel fuel with the bio fuel were used (the percentage indicates the proportion of the biocomponent and the rest is complemented by a clean diesel) – 5.5 %, 19.7 %, 33.9 %, 48 % and 100 % RME, 5.5 % and 19.7 % of the oil from Jatropha Curcas, 5.5 % and 19.7 % of the rapeseed oil.

Materials and method

The fuel system of the tractor was not constructed for fuels containing FAME, Jatropha oil, canola oil. To the rear PTO of the Zetor 8641 Forterra tractor (Fig. 1) to, turbo-blower supercharged engine with direct-injection, engine capacity 4,156 cm^3, max. power 60 kW, max. torque 351 Nm, min. specific fuel consumption 253 g (kW $h)^{-1}$, rated speed 2,200 min^{-1} a hydraulic dynamometer AW NEB 400 was attached (Table 4 and the Fig. 1). To the fuel system was added a tractor fuel measuring device, which contains two flowmeters Macnaught MSeries FLOWMETER M2ASP-1R (1 % accuracy). For smoke measurement purposes, was used the Brain Bee analyser (accuracy of opacity – 2 %, temperature 2.5 °C (Pexa, Kubín, 2012).

At first, the external rotation speed characteristic was measured. Some external speed characteristics were selected as measuring points for the NRSC tests that can be used in addition to assessing the technical condition of the internal combustion engine, also to examine the impact of emissions on human health. (Topinka et al., 2012) The NRSC test (2005/13/EC, 2000/25/EC, 2004/26/EC, 97/68/EC) consists of a series of eight modes of speed and torque measurements (Table 3).

Tab. 3 Measuring points NRSC test

Mode number	Engine speed	Load (%)	Weighting factor
1	Rated	100	0.15
2	Rated	75	0.15
3	Rated	50	0.15
4	Rated	10	0.10
5	Intermediate	100	0.10
6	Intermediate	75	0.10
7	Intermediate	50	0.10
8	Idle	–	0.15

After determining the measuring points of the NRSC test, the measurements of the fuel consumption and the smoke in the individual sections of the test were carried out. The specific fuel consumption or specific emissions (g (kW h)$^{-1}$), respectively, for the whole NRSC test were calculated according to the equation (1).

$$m_{NRSC} = \frac{\sum_{i=1}^{8}\left(M_{P,i} \cdot VF_i\right)}{\sum_{i=1}^{8}\left(P_{PTO,i} \cdot VF_i\right)} \qquad (1)$$

m_{NRSC} – the specific fuel consumption and the specific emissions over the NRSC test (g (kW h)$^{-1}$);
$M_{P,I}$ – the weight of the hourly fuel consumption or emissions produced in the i (g h^{-1});
VF – the mode weighting factor i (–);
$P_{PTO,I}$ – the engine power to the PTO in the i (kW).

Furthermore, based on the external speed characteristic, the eligible measuring points for building a complete motor characteristic were chosen. The measuring points (about 35–40) are determined so that most of them belong to the engine working space. Measuring of the individual points is carried out in a similar way as in the case of the NRSC test.

The torque values measured on the dynamometer PTO are converted – by using the appropriate gear ratio (3.543) – into the torque of the engine. To compare the impact of the fuel on the engine characteristics, the losses of the engine don't influence the PTO shaft, and therefore these are not considered. The resulting values of the specific fuel consumption and smoke therefore correspond to the engine power at the PTO shaft.

The measured values were then processed by using the MathCad program functions into the form of continuous surfaces. To create the continuous surfaces, the functions *REGRESS* and *INTERP* were used. The function *REGRESS* in conjunction with the interpolation function *INTERP* approximates the preset polynomial fits of the measured points in the fuel consumption. The *PlochaZ* in the coordinates of the *PlochaXY* represents the coordinates of the rotation speed *om* and the torque *TM*. The result of the fitting is a continuous variable *Plocha(om,TM)*. From this surface, the 41x41 square matrix (1,681 points) is created to be used for further processing. This matrix of the 1,681 points is then further processed using the interpolation function *SPLINE*, which interleaves the area precisely defined by the points in the 41x41 matrix.

Results

In Table 4 the values of output parameters. We can say that with more biofuel output parameters values are falling.

In Fig. 2 is a complete example of the characteristics of the engine and on the basis of the processed NRSC test (Table 5), which can be observed decrease in CO and CO2 with the share of biofuels as well as increased fuel consumption.

Table 6 shows the number of points with a minimum specific fuel consumption, which are found in the complete characteristics of the engine and confirm that the increase in the share of biofuels and fuel consumption increases.

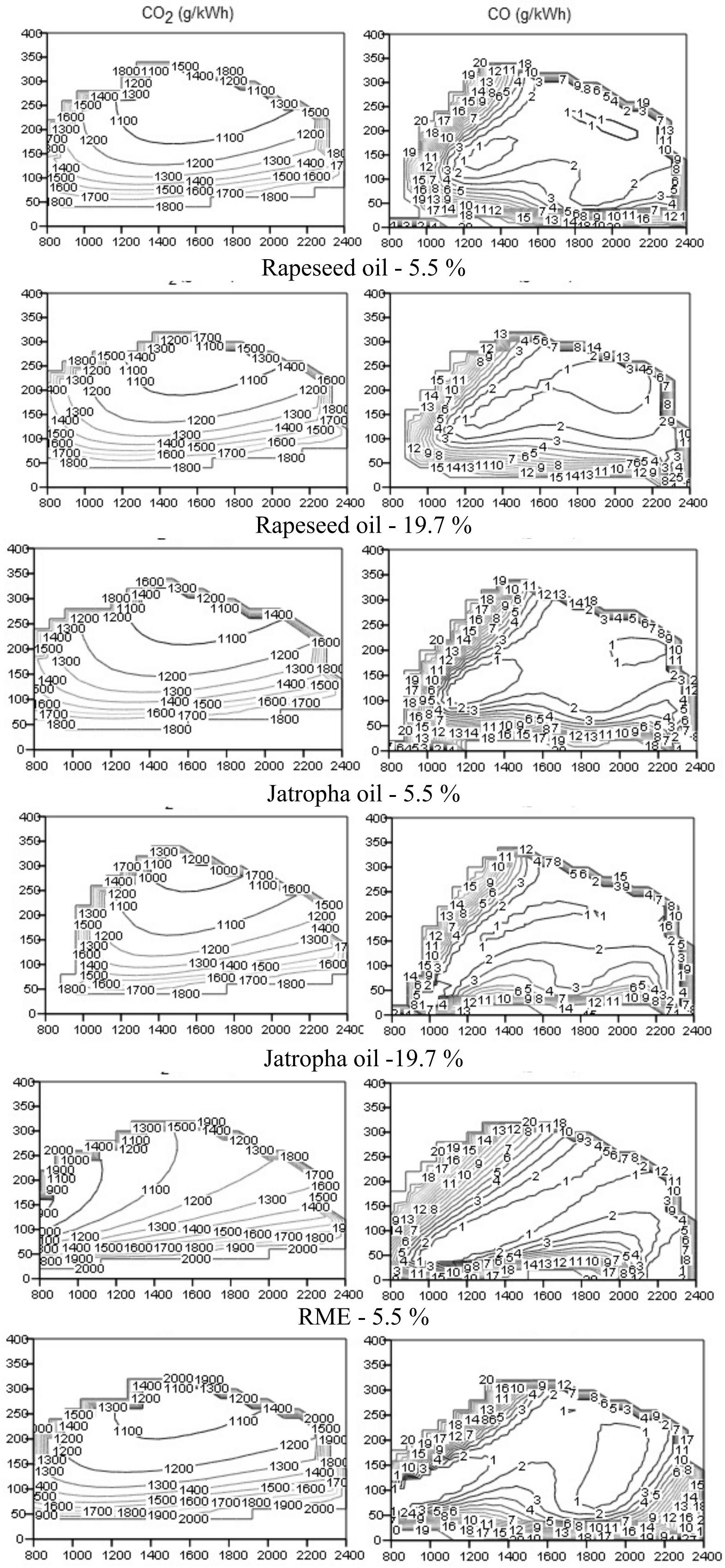

Fig. 2 Example of complete characteristic engine for selected fuels.(x-axis - engine speed (rpm) axis y –torque (Nm)

Tab. 4 The values of maximum torque and engine power - Zetor Forterra 8641

	Maximum values				Values at rated speed (2200 1/min)	
	Torque		Power			
Fuel	**Torque** (Nm)	**Speed** (1/min)	**Power** (kW)	**Speed** (1/min)	**Torque** (Nm)	**Power** (kW)
5.5 % RME	318.3	1449	55.1	1868	225.0	51.8
19.7 % RME	318.0	1446	55.8	1945	232.8	53.6
33.9 % RME	306.2	1441	52.9	1945	216.9	50.0
48 % RME	292.5	1549	52.2	2025	212.0	48.8
100 % RME	299.5	1505	53.2	2101	222.0	51.1
5.5 % Jatropha	324.7	1455	56.9	2086	234.4	54.0
19.7 % Jatropha	323.7	1470	56.1	1945	234.0	53.9
5.5 % Rapeseed oil	326.0	1525	57.1	1919	237.7	54.8
19.7 % Rapeseed oil	315.3	1470	55.3	2096	230.7	53.1

Tab. 5 NRSC test results for the selected fuel type - Zetor Forterra 8641

Fuel	**CO** (g/kWh)	**CO_2** (g/kWh)	**Fuel consumption** (g/kWh)
5.5 % RME	3.5	1345	325.6
19.7 % RME	3.0	1359	324.8
33.9 % RME	3.4	1349	339.7
48 % RME	2.0	1355	337.6
100 % RME	1.9	1309	367.0
5.5 % Jatropha	3.2	1288	319.3
19.7 % Jatropha	2.6	1154	337.3
5.5 % Rapeseed oil	2.5	1235	312.7
19.7 % Rapeseed oil	2.4	1286	318.8

Tab. 6 Minimum Specific Fuel Consumption

Minimum specific fuel consumption (g/kWh)	**Engine speed (1/min)**	**Torque (Nm)**
259.7	1564	298
262.6	1612	311
268.6	1524	303
274.0	1548	289
286.6	1581	285
254.6	1578	304
255.4	1624	312
250.6	1570	320
256.6	1552	296

Conclusion

For the measurements of the engine of the Zetor 8641 Forterra tractor with the attached PTO was used hydraulic dynamometer AW NEB 400. By using the dynamometer, the individual points arising from the 8-point NRSC test points were fixed to create a complete engine characteristics. For recording the carbon monoxide and carbon dioxide level, was used the emission analyser BrainBee. To record the fuel consumption the fuel box with two fuel gauges was explored Macnaught MSeries FLOWMETER M2ASP-1R .

Results processed NRSC test for carbon monoxide, carbon dioxide and fuel consumption are shown in Table 5. Increasing the proportion of biofuel is manifested by reducing the content of carbon monoxide and carbon dioxide, and conversely an increase in fuel consumption. In terms of performance parameters of the internal combustion engine tractor can be stated (Table 4), the higher the share of biofuels decreases the maximum torque and power.The disadvantage of the use of the fuels with a higher proportion of biofuels are mainly due to the higher maintenance demands put on the fuel system, lower engine power and greater fuel consumption. In contrast, the advantage of using biofuels is higher lubricity and reduction of emissions and very good biodegradability against the diesel.

Acknowledgment

The research carried out was supported by the grant project CZU 2013:31190/1312/3122 – Impact of biofuels and the operating mode at the smoke.

Reference

Achten W.M.J., Verchot L., Franken Y.J., Mathijs E., Singh V.P., Aerts R., Muys B., 2008. Jatropha bio-diesel production and use. Biomass and Bioenergy, 32(12): 1063-1084.

Bauer F., Sedlák P., Šmerda T., 2006. Traktory (Tractors). Prague. Profi Press. (in Czech)

ČSN EN 14214+A1. 2010. Automotive fuels – Fatty acid methyl esters (FAME) for diesel engines – Requirements and test methods. ČSNI. 20. (in Czech)

ČSN EN 590+A1. 2010. Automotive fuels – Diesel – Requirements and test methods. ČSNI. 16. (in Czech)

Commission directive 2005/13/EC of 21 February 2005 amending Directive 2000/25/EC of the European Parliament and of the Council concerning the emission of gaseous and particulate pollutants by engines intended to power agricultural or forestry tractors. and amending Annex I to Directive 2003/37/EC of the European Parliament and of the Council concerning the type-approval of agricultural or forestry tractors.

Directive 97/68/EC of the European parliament and of the Council of 16 December 1997 on the approximation of the laws of the Member States relating to measures against the emission of gaseous and particulate pollutants from internal combustion engines to be installed in non-road mobile machinery.

Directive 2000/25/EC of the European parliament and of the Council of 22 May 2000 on action to be taken against the emission of gaseous and particulate pollutants by engines intended to power agricultural or forestry tractors and amending Council Directive 74/150/EEC.

Directive 2004/26/EC of the European parliament and of the Council of 21 April 2004 amending Directive 97/68/EC on the approximation of the laws of the Member States relating to measures against the emission of gaseous and particulate pollutants from internal combustion engines to be installed in non-road mobile machinery

Gabrielová H., 2010. Consumer issues, contributors, "Can a car run on vegetable oil?" Available at: www.ekoporadna.cz/wiki/doku.php?id=energie:muze_automobil_jezdit_na_rostlinny_olej&rev=1305581252 (accessed July 13, 2011). (in Czech)

Huang J., Wang Y., Qin J., Roskilly A.P., 2010. Comparative study of performance and emissions of a diesel engine using Chinese pistache and jatropha biodiesel. Fuel Processing Technology, 91(11): 1761-1767.

Chauhan Bhupendra S., Kumar N., Jun Y.D., Lee K.B., 2010. Performance and emission study of preheated Jatropha oil on medium capacity diesel engine. Energy, 35(6): 2484-2492.

Liu K., Gao S., Chung T., Huang C., Lin Y., 2012. Effect of process conditions on the removal of phospholipids from jatropha curcas oil during the degumming process. Chemical Engineering Research and Design, 90(9): 1381-1386.

Mazancová J., Panáčková B., 2010. Využití jatropha sp k energetickým účelům. Studie, Institut tropů a subtropů, Česká zemědělská univerzita v Praze. 24. (in Czech)

Topinka J., Milcova A., Schmuczerova J., Mazac M., Pechout M., Vojtisek-Lom M., 2012. Genotoxic potential of organic extracts from particle emissions of diesel and rapeseed oil powered engines. Toxicology Letters, 212(1): 11-17.

Varatharajan K., Cheralathan M., Velraj R., 2011. Mitigation of NOx emissions from a jatropha biodiesel fuelled DI diesel engine using antioxidant additives. Fuel, 90(8): 2721-2725.

SYSTEM VIBRATION OF ROLLER BEARINGS

Josef Pošta

Czech University of Life Sciences Prague, 16521 Prague 6 – Suchdol, Czech Republic, Phone: +4202-224383266, E-mail: posta@tf.czu.cz

Abstract

Support with roller bearing is one of the most widely used construction groups of machines. During the long development of rolling bearings became standard precise design features that with the proper design and operation achieve high reliability and durability, but also require appropriate operating conditions and maintenance. Bearing damage occurs in the majority of cases gradually, due to the accumulation of defects microstructure and macrostructure of materials that lead to wear, clearance increase, influence of impacts. This damage affects the external behavior of bearings and might be indicated and monitored by tools of condition based monitoring. This paper deals with the vibration of rolling bearings resulting from the characteristics of their design.

Key words: bearings, roller bearing, bearing vibration, contact pressure

Introduction

Rolling bearings are precision components of machines their good conditions influences reliable operation. However, bearings are sensitive and can be easily damaged, damage can have various causes. Generally, in operation, it is necessary to ensure proper clearance bearings, cleanliness and lubrication. Bearing space must be protected against dirt and grease leakage. Bearings should be protected against overload, which easily occurs due to misalignment of bearings and shafts, caused either by incorrect installation or poor geometric alignment of bearings, bearing housings, rotors, clutches and complete machines. The undesirable parasitic forces may also result from the effect of operating influences, particularly the operating forces of the connected equipment, piping, etc. that can be designed or assembled incorrectly, or not properly compensated dimensional changes caused by thermal expansion during temperature fluctuations. Bearings can also be exposed to electrical currents and discharges, especially when operating motors by frequency converters in the presence of high-frequency fields, (Posta, 2012). All of these factors may result in damage to the bearings, which usually appear as wear, such as cracking the surface layers of bearing material, such as curling or wrinkling of functional surfaces such as brakes or seizure. In practice, there is a combination of those types of wear that appear simultaneously or sequentially in time, (Huang et al., 2013).

Bearing damage occurs in the majority of cases gradually, due to the accumulation of defects of microstructure and macrostructure of materials caused by mentioned potential negative effects. The consequence may be an breakdown of the bearing support, often with serious dependent failures, (Cann et al., 2001).

Gradually increasing damage has necessarily consequences in bearing behavior and therefore behavior of entire machine. These symptoms, which are gradually increasing damage may be therefore influenced by appropriate methods to monitor, analyze and evaluate them and predict their future evolution in time. These facts allow preventive actions, which prevents the origin of more serious problems.

The paper shows one of the less significant and yet somewhat neglected sources of vibration of rolling bearings, which is a manifestation of emerging fault, but is caused by direct structural system of rolling bearings.

Material and method

There are numerous diagnostic methods for monitoring and evaluating the bearings. One of these possibilities is vibrodiagnostics which is based on the fact that each mechanism in the work emits vibrations that appear by:

- movement, i.e. changing the position of the vibrating between elastic deformation of contact points, or
- pressure, i.e. by changing the contact pressure,
- or impacts (in the case of clearance, which allows greater freedom of movement than the elastic deformation of the contact points).

It is possible to record and analyze vibration and consequently evaluate measured data in order to obtain conclusions of the technical condition and its foreseeable trend. Current state of measuring and sensor technology has no problems with vibration measuring and recording. It is necessary (for proper evaluation of the obtained data) to know as much as possible factors and influences that cause vibration emission, (Nikolaou, Antoniadis, 2002).

The most common design with support bearings, which not always transmit axial load, use ball or roller or needle bearings.

The most frequent case of rolling bearing under load is such that the outer ring is securely mounted and the inner ring rotates. The surfaces of the inner ring (orbital track) and rolling elements, the surfaces of the rolling elements and the outer ring (orbital track) surfaces and rolling elements and the cage gradually come into contact. Any contact with a source of pressure pulse or impact appears as vibrational motion (real or virtual). Real and virtual movements of the inner ring are generated by changing the position of the loading force against the rolling bodies moving under load bearing inner ring (Fig. 1 and Fig. 2). This case is applicable for source of vibration of flawless and properly installed and properly operated bearings. These vibrations can therefore be considered as a "system" and such a state is characterized according to condition monitoring as "vibrating noise" or "vibrating background". On the other hand, the incorrectly installed or improperly operated bearing characterised as vibrational noise increases rapidly, indicating the development of emerging failure.

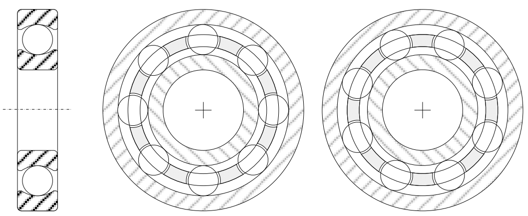

Fig. 1 Ball bearing loaded only with radial forces

For examination the vibrating noise it is primarily assumed that the outer ring is securely mounted, external force imposes only the inner ring and has constant direction and size. Furthermore, there is no axial force, bearing has zero radial clearance and zero clearance between the rolling elements and cage, zero radial pre-stress, there is no defect anywhere in the bearing surface, and relative motion is only rolling without slipping.

Schema of this case is shown in Fig. 2. In this simple case, it can be determined what will be the amplitude and frequency of movement of the inner ring.

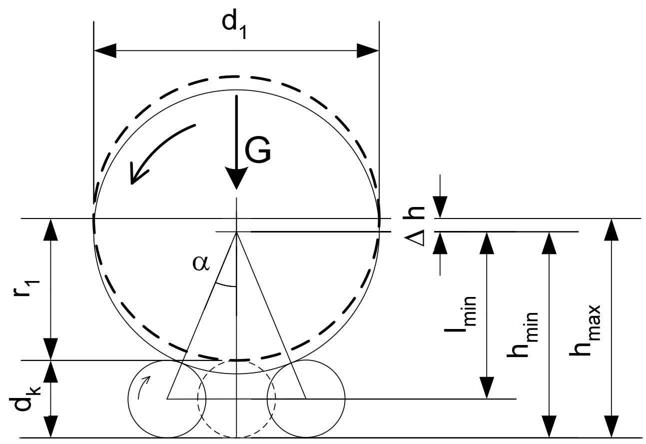

Fig. 2 Scheme for derivation of amplitude and frequency of system vibrations of bearing

Amplitude of vibrating noise

Legend:

$d_1 = 2r_1$ inner ring shoulder diameter

$d_k = 2r_k$ rolling element diameter

2α rolling element pitch angle, $\alpha = \frac{360}{k} = \frac{2\cdot\pi}{k}$

k number of rolling elements

Δh amplitude of inner ring (virtual) movement in the y-direction

f_1 frequency oscillatory movement of the rotor (inner ring) in the y-direction

n_1 inner ring (rotor) revolutions

n_k ball revolutions

According to Fig. 2, it can be written:

$$\Delta h = h_{max} - h_{min} \tag{1}$$

$$h_{max} = r_1 + d_k = \frac{d_1}{2} + d_k \tag{2}$$

$$h_{min} = l_{min} + r_k = l_{min} + \frac{d_k}{2} = \frac{d_1 + d_k}{2}\cdot\cos\alpha + \frac{d_k}{2} \tag{3}$$

$$l_{min} = (r_1 + r_k)\cdot\cos\alpha = \frac{d_1 + d_k}{2}\cdot\cos\alpha \tag{4}$$

$$\Delta h = h_{max} - h_{min} = \frac{d_1}{2} + d_k - \frac{d_1 + d_k}{2}\cdot\cos\alpha - \frac{d_k}{2} = \frac{d_1 + d_k}{2}\cdot(1 - \cos\alpha) \tag{5}$$

Frequency of vibrating noise

Assuming zero slipping then track s_{c1} is circumference of ring (arc length) corresponding to one cycle as shown in Fig. 2 and is equal to the track around balls circumference of (arc length) s_{k1}

$$s_{c1} = \frac{\pi \cdot d_1}{k} = s_{k1} = \widehat{\alpha_k} \cdot \frac{d_k}{2} \qquad (6)$$

and the angle of rotation of balls corresponding to one vertical cycle is equal to

$$\widehat{\alpha_k} = \frac{\pi \cdot d_1}{k} \cdot \frac{2}{d_k} \qquad (7)$$

Assuming zero slipping then circumferential velocity of ring v_1 and circumferential velocity of ball v_k is the same in the contact point

$$v_1 = \frac{\pi \cdot d_1 \cdot n_1}{60} = v_k = \frac{\pi \cdot d_k \cdot n_k}{60} \qquad (8)$$

then $d_1 \cdot n_1 = d_k \cdot n_k$ (9)

and then the ring revolutions (rotor) n_1 and ball revolutions n_k are equal to:

$$n_1 = n_k \cdot \frac{d_k}{d_1} \qquad n_k = n_1 \cdot \frac{d_1}{d_k} \qquad (10)\ (11)$$

Consequently, it is possible to define the frequency f_1 of oscillatory motion in the vertical axis of the duration of the cycle:

t_{c1} duration of one cycle of inner ring (rotor)
s_{c1} track moved for one cycle
v_1 circumferential velocity in the contact point of ring and ball

Then applies:

$$s_{c1} = v_1 \cdot t_{c1} \Rightarrow t_{c1} = \frac{s_{c1}}{v_1} \qquad (12)$$

Substituting from (6) and (8) is derived

$$t_{c1} = \frac{\pi \cdot d_1}{k} \cdot \frac{1}{\frac{\pi \cdot d_1 \cdot n_1}{60}} = \frac{60}{k \cdot n_1} \qquad (13)$$

Because (definition) applies: $f = \frac{1}{t}$ it is also

$$f_1 = \frac{k \cdot n_1}{60} \qquad (14)$$

Conclusion

Assuming that the rolling bearing has zero radial clearance without pre-stress and rolling bearing inner ring after rolling elements has no slipping (Fig. 2), then at positions shown in Figure 1 there is present varying contact pressure at the contact of rolling elements and tracks of bearing rings. Size of the contact pressure varies from zero to values based load force G (Fig. 2). In the event that this variable contact pressure is acting repeatedly in the same places in the tracks of bearing rings, then it appears as a gradual development of fatigue damage, ripple surface, formation of pitting. This damage will have the character of so-called high-cycle fatigue - number of cycles (formation of external symptoms) of bearing damage depends on the load torque and rotational speed.

If the rolling bearing has a radial clearance and a rolling bearing inner ring with rolling elements has no slipping, and the inner ring is in real oscillating motion in the vertical axis, then amplitude Δh is calculated by the equation (5) and the frequency f_1 according to equation (14). These vibrations occur in otherwise flawless, properly operated and lubricated bearings and are accompanied by shocks at each change of movement direction. These shocks act repeatedly in the same places on track of rings. This again leads to fatigue damage, depending on the particular circumstances, it is likely to be a so-called low-cycle fatigue. The resulting shocks are externally presented more significantly and become noticeable for normal vibrodiagnostics methods.

It is evident that the vibrations of roller bearings, virtual or real, are already formed from their structural arrangement. These vibrations can therefore be considered as a "system" and such a state is characterized according to condition monitoring as "vibrating noise" or "vibrating background" and not a the "unwanted vibrations". Proper design, installation, operation and maintenance of rolling bearings cannot exclude these system vibrations, but it is possible to achieve state when consequences of system vibrations are revealed as high cycle fatigue with such a large number of cycles, that it will have no practical importance during machine operation.

Acknowledgement

This paper was prepared under grant IGA TF 2012/3121 "Possibilities of using ultrasound to improve the properties of fluids machines."

Reference

Cann P.M., Doner J.P., Webster M.N., Wikstrom V., 2001. Grease degradation in rolling element bearings. Tribology Transactions, 44 (3): 399-404.

Huang Z., Li Q., Zhou Y., Jing S., Ma Y., Hu W., Fan Y., 2013. Experimental research on the surface strengthening technology of roller cone bit bearing based on the failure analysis. Engineering Failure Analysis, 29: 12-26.

Nikolaou N.G., Antoniadis I.A., 2002. Rolling element bearing fault diagnosis using wavelet packets. NDT and E International, 35(3): 197-205.

Pošta J., 2012. Poškození ložisek elektrickým proudem. In: Proceedings "Maintenance 2012", Liblice, 6-7 November 2012, 124-128. (in Czech)

NEW WAY IN THE PHOTOVOLTAIC PANELS CONSTRUCTION

Vladislav Poulek[1], Martin Libra[2], Persic I.S.[3], Strebkov D.S.[3],

[1] Traxle Solar s. r. o., Eliasova 12, CZ 16000 Prague, Czech Republic
[2] Czech University of Life Sciences Prague, Faculty of Engineering, Prague, Czech Republic
[3] VIESH, Moscow, Russia

Abstract

The new way in the photovoltaic panels construction has been developed. New silicone gel encapsulation was compared with the standard EVA lamination of photovoltaic panels. Negligible corrosion of silicone gel laminated PV panels was observed in comparison with EVA laminated panels. Silicone gel laminated c-Si PV panels were prepared and tested at 3.5 times concentrated solar radiation. In contrast to EVA-laminated panels the transparency reduction induced by UV radiation in silicone gel lamination is very small. The lifetime of silicone gel laminated photovoltaic panels could be up to 50 years.

Keywords: Silicone gel, photovoltaics, solar energy

Introduction

The economic competitiveness of solar PV energy compared with traditional technologies can be achieved ether by reducing the cost of PV modules or by increasing the solar energy conversion efficiency, as well as by increasing the PV modules lifetime at least 1.5÷2 times.

Thus, development of materials with high light and thermal stability for use in PV panels (including CPV) is urgently needed. The main factor determining the operational life of PV modules is the encapsulation material (encapsulant). Encapsulant is a protective material completely enveloping and isolating the photovoltaic cells from moisture, heat and mechanical damage and providing good optical contact between the surface of the PV cells and the protective outer coating. The chemical composition of standard thermoplastic encapsulant based on EVA copolymer has many drawbacks (Paretta et al., 2005) inherent in all known modifications of the films:

- corrosiveness,
- instability of optical characteristics for long-term operation and under the effect of concentrated solar radiation,
- fundamental limits of lamination process performance due to the need of peroxide induced crosslinking of the encapsulant material,
- creation of volatile chemicals in the process of thermal–vacuum lamination, complicating the vacuum apparatus application (active oxygen, carbon oxides, acetic acid, etc.),
- high power consumption during lamination process (46 kW of standard laminator).

The corrosiveness of recent EVA encapsulant films is among the main sources of PV panels failures (i.e., reduced lifetime). Tab. 1 gives the main sources of PV panel failures (Wohlgemuth, 2003).

From the standpoint of optical transparency, operational temperature range and absence of corrosive impurities (e.g., acetic acid in EVA), silicone polymers (polysiloxanes) are the most attractive candidates. Polysiloxanes have been proved and used for decades as adhesives and sealing materials for space solar cells. Properties of EVA and silicone gel are compared in Tab. 2.

Conventional silicone encapsulants are two-component systems, where one component is a polymer matrix (low molecular weight silicone rubber reacting by hydroxyl end groups) and the other one is a mixture of curing agent and a low molecular weight crosslinking agent (usually based on tetraethoxysilane derivatives). Thus, crosslinking is carried out by short bridges. This feature contributes to the low physical–mechanical properties of curred polymers and to the low adhesion to common surfaces without special treatment.

Moreover, toxic catalysts of vulcanisation and formation of aggressive condensation products (alcohols, acids) are the main constraints of using cold vulcanized rubbers of low molecular weight siloxane in terrestrial photovoltaic modules.

Tab. 1 Types of EVA laminated PV panel failures (Wohlgemuth, 2003)

type of failure	**total failures (%)**
corrosion	45.3
cell or interconnect break	40.7
output lead problem	3.9
J-box problem	3.6
delamination	3.4
overheated wires or diodes	1.5
mechanical damage	1.4
defective bypass diodes	0.2

Tab. 2 Comparison of EVA and silicone gel properties (Sobolevski, 1975)

	EVA	**silicone gel**
long term operational temperature	(-40 , +80)°C	(-60 , +250)°C
UV radiation resistance	low	high
operational lifetime	25 years	50 years
laminator energy consumption per hour	49 kWh	4.5 kWh
refractive index	1.482	1.406
transparency for solar radiation	8% (λ=360 nm)	90% (λ=360 nm)
transparency for solar radiation	62% (λ=400 nm)	92% (λ=400 nm)
transparency for solar radiation	91% (λ=600÷1000 nm)	93% (λ=600÷1000 nm)
corrosive agents - lamination	acetic acid	none
corrosive agents - ageing	acetic acid	none
modulus of elasticity	10.0 N/mm^2	0.006 N/mm^2
linear coefficient of thermal expansion	$4.0 \times 10^{-4} K^{-1}$	$2.5 \times 10^{-4} K^{-1}$
thermal conductivity	0.13 W/m.K	0.18 W/m.K

Silicone gel

From the nineties there is positive experience with semiconductor devices encapsulated in so-called polysiloxane gels.

Gels belong to a special class of ultrasoft encapsulants and are represented by a soft structure formed during hydrosilylation – the reaction of low molecular weight polysiloxanes containing dimethylmethylvinylsiloxane links with crosslinking agent based on a mixture of different cyclic and linear hydrosiloxanes in the presence of platinum catalyst. Fig. 1 shows the scheme.

Thus, the vulcanization is carried out on a “polymer–polymer” base without separation of by-products of the reaction with the formation of long cross-bridges, giving vulcanizate a number of unique properties.

Analysis of available data (Sobolevski, 1975) allows us to formulate the following advantages of polysiloxane gels over low molecular weight siloxane rubbers:

- Good dielectric properties, even at low temperatures,
- the possibility of regulation of the crosslinking density and, thus, regulation of the viscoelastic characteristics in a wide range,
- the high degree of purity on the content of ionic impurities (10^{-4}÷10^{-6}% of Na, K, Ca impurities),
- the absence of a gel internal stresses,
- effective vibration absorption,
- the effect of “self-healing” of defects inherent in liquids, along with the dimensional stability characteristic for crosslinked elastomers,
- resistance to temperature, UV and ozone degradation,
- very high adhesion to semiconductors, glass and most other materials through the mechanism of “stickiness” – the physical adhesion without the use of sub-layers,
- environmental safety.

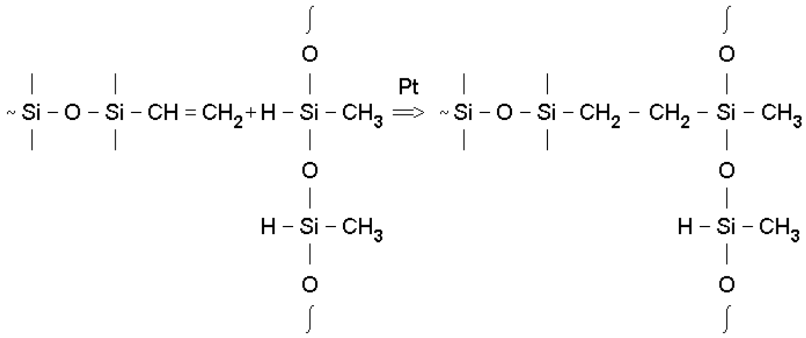

Fig. 1 Hydrosilylation reaction scheme (Sobolevski, 1975)

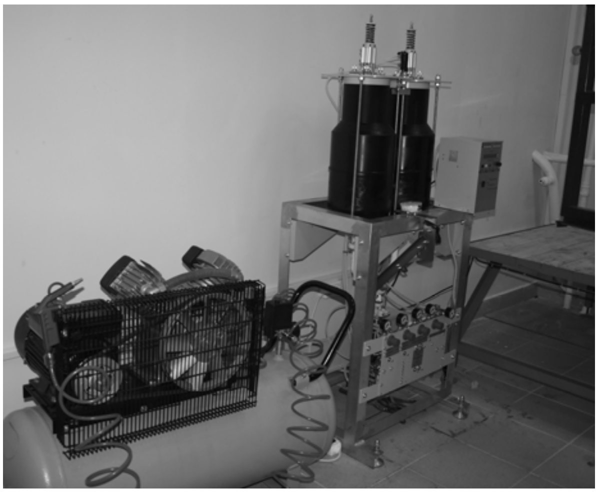

Fig. 2 Mixing unit including vacuum dosing unit

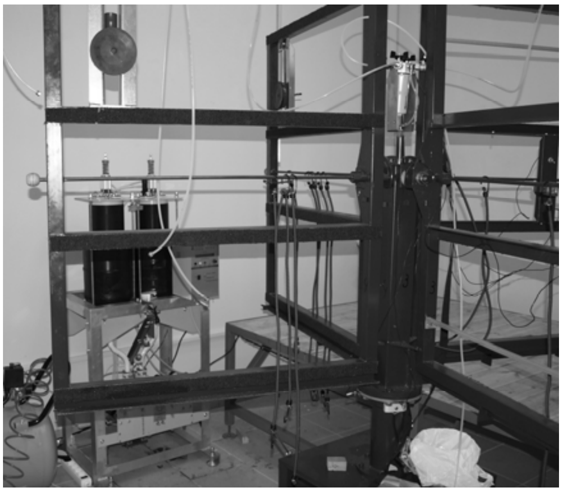

Fig. 3 Vibrating stand

Experimental arrangement

The silicone gel encapsulation machine (Persic et al., 2005; Persic et al., 2010 shown in Fig. 2, Fig. 3 and Fig. 4 consists of two basic units, i.e., mixer with vacuum dosing and vibrating stand.

The device parameters:

- Voltage – 220 V, 50 Hz,
- power consumption – 5.5 kW,
- compressed air pressure – 8 to 10 atm (compressor must be equipped with air, moisture, oil and solid particles filter),
- overall dimensions – 1.0×1.0×2.0 m^3,
- tanks on the gel part – 30 l,
- control E (semi automatic).

Dosage specifications:

- synchronous feed of ingredients to the pump cylinder – 5 to 6 ml/s,
- volume mixing ratio of ingredients – 01:01 ± 5%,
- pouring time of the full panel lamination – approx. 5 min,
- consumption of gel per 1 m^2 panel approx 1.5 kg.

Maximum PV panel size: 1050×2000 mm^2. Performance: max. 6000 panels/year (250 W panels sized 1000×1650 mm^2).

Parts of encapsulation equipment (see Fig. 4):

- A1, B1 – tanks for the supply of components and their evacuation,
- B – vacuum generator powered by compressed air,
- A2, B2 – piston pumps valves,
- A3, B3 – piston pumps – dosing of components,
- PP – synchronous transmission – piston pumps,
- A5, B5 – mixing valves to mix ingredients,
- V1 – mixing equipment,
- V2 – removable static mixer,
- V3 – implementation probe ready mix,
- V4 – unit injector,
- SM – solar module,
- VU – microprocessor electronic control unit.

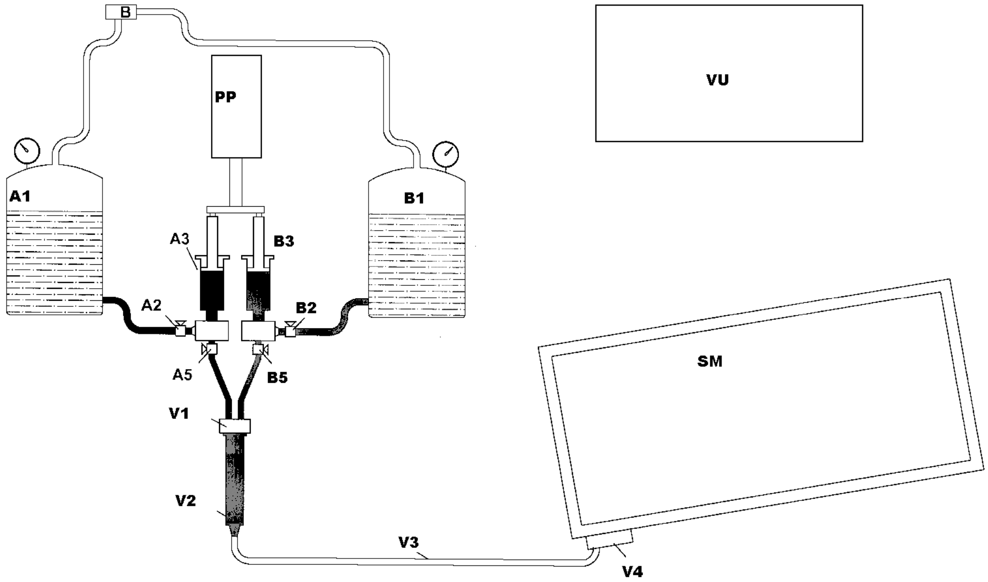

Fig. 4 Scheme of the lamination equipment

Results and discussion

The study of the siloxane compound optical characteristics stability was carried out both in the mode of accelerated laboratory tests (UV radiation intensity 140 W/m^2, sample temperature 85°C, test duration 1000 h) and in field conditions as a part of the installation with a concentrated (3.5 times higher) solar radiation (see Fig. 5). These are initial tests which will be followed by complete IEC61215 PV panel tests set. Photodegradation of some components of PV systems was observed in the past (Daliento, Lancellotti, 2010; Reda, 2007).

The comparative tests were performed with "glass–encapsulant–glass" samples by applying polysiloxane compound with optimized formula and a standard thermoplastic encapsulant based on copolymer of EVA as encapsulants. The results of the spectral transmittance measurement before and after radiation exposure in laboratory and field tests performed under the influence of concentrated light beam are shown in Figs. 6÷8 and in Tab. 3.

Experimental conditions (both EVA and gel laminated panels):

- Time 1000 h, $T = 85$°C,
- UV radiation ($\lambda < 385$ nm), intensity = 140 W/m^2.

The comparison of Fig. 6a and 6b shows some silicone gel transparency reduction in the $\lambda = 350÷550$ nm wavelength range only, but substantial transparency reduction of the EVA encapsulant transparency in the whole $\lambda = 350÷1100$ nm wavelength range. Moreover, the silicone gel transparency is always substantially better in the $\lambda = 350÷900$ nm wavelength range, in good accordance with data publisher by other authors (Ketola et al., 2008) – see Fig. 6c.

Experimental conditions (both EVA and gel laminated panels):

- Time 1000 h, $T = 85$°C,
- UV radiation ($\lambda < 385$ nm), intensity = 140 W/m^2,
- total UV radiation dose = 140 kWh/m^2.

While tin plated bus bars in the gel encapsulant remain shiny (Fig. 8), the bus bars in EVA encapsulant are matt with visible sign of corrosion (Fig. 7b) after 1000 h exposure to UV radiation at elevated temperature of 85°C. The results of the test module installed at the parabolic concentrator 3.5 times focus, made during the 4 summer months, are shown in Tab. 3. There is negligible change of parameters within the test period.

Fig. 5 The solar PV concentrator using bifacial cells laminated in silicone gel encapsulant was used for the gel encapsulant test under concentrated solar radiation

Tab. 3 Effect of concentrated solar radiation (3.5 times) on the main electrical parameters of the experimental module with gel lamination

number of samples	experimental conditions	test duration (months)	electrical characteristics				
			U_{max} (V)	I_{max} (A)	P_{max} (W)	U_{oc} (V)	I_{sc} (A)
2	3.5 times solar concentrator, Moscow	0	4.44	1.74	7.54	5.73	1.86
		4 (May-August)	4.44	1.70	7.54	5.71	1.86

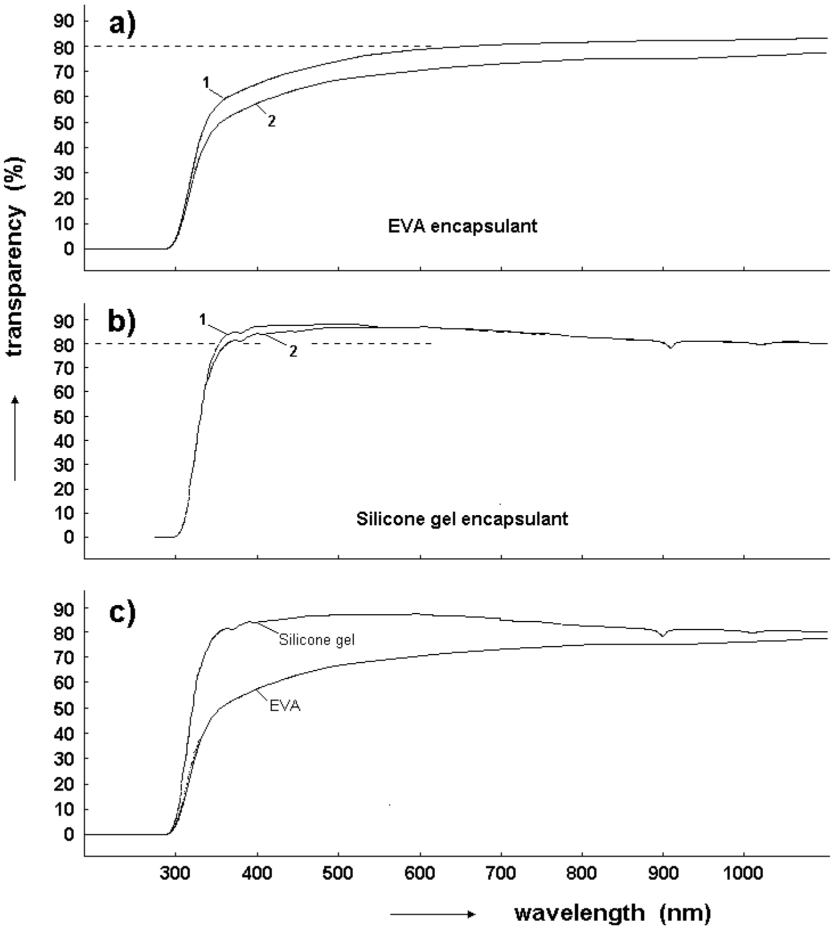

Fig. 6 (a) EVA encapsulant transparency before and after UV radiation exposure, line 1 - initial, line 2 - after 1000 h of exposure to UV radiation, (b) silicone gel encapsulant transparency before and after UV radiation exposure, line 1 - initial, line 2 - after 1000 h of exposure to UV radiation and (c) transparency of EVA solid film and silicone gel after exposure toUV radiation

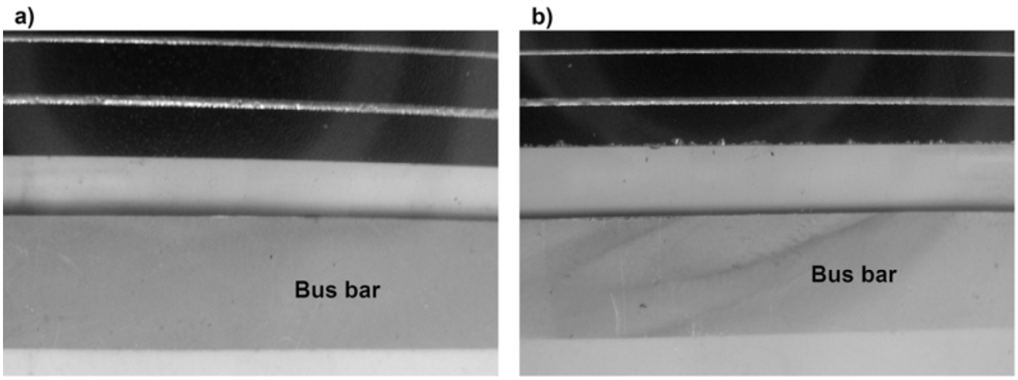

Fig. 7 Tin plated bus bar in the EVA laminated PV panel. a) initial, b) after the test

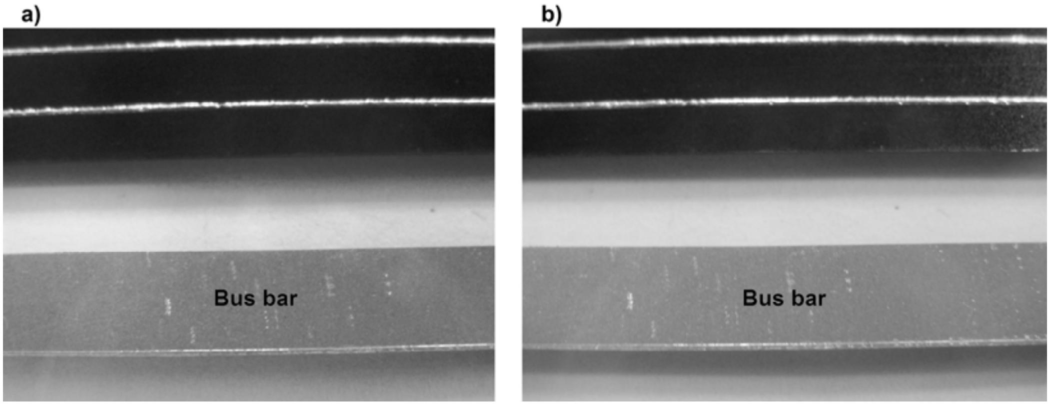

Fig. 8 Tin plated bus bar in the silicone gel laminated PV panel. a) initial, b) after the test

Conclusions

It has been found that corrosiveness of silicone gel encapsulant of PV panel, at elevated temperature of + 85 °C and UV radiation, is negligible compared to standard EVA film. This finding is in accordance with negligible (5 %) power reduction observed in polysiloxane laminated panels after 25 years of environmental exposure (Wohlgemuth, 2003). In contrast to EVA, the transparency of the silicone gel is substantially better, namely in the wavelength range 350 ÷ 700 nm. The transparency reduction of silicone gel caused by UV radiation is very small compared to EVA. The standard IEC61215 certification of the silicone gel laminated PV panel will be completed in the year 2012. The design of silicone gel laminated PV panel with power reduction about -15 % over 50 years service life is possible because of strongly reduced silicone gel corrosiveness which is the main source of failures in EVA laminated PV panels (Wohlgemuth, 2003). Using silicone gel encapsulant we expect also substantial cell and interconnect break reduction because the very soft silicone gel encapsulant allows better stress relaxation during thermal cycling of PV panels, compared to solid EVA encapsulant. The cell and interconnect break is the second main source of PV panels failures – see Tab. 1. The thermal cycling comparison tests between EVA and silicone gel laminated panels commenced already in our laboratory.

References

Paretta A., Bombace M., Graditi G., Schioppo R., 2005. Optical degradation of long-term, field-aged c–Si photovoltaic modules. Solar Energy Materials & Solar Cells, 86: 349–364.

Wohlgemuth J.H., 2003. Long Term Photovoltaic Module Reliability. NCPV and Solar Program Review Meeting, NREL/CD-520-33586.

Sobolevski M.V., 1975. Properties and areas of exploitation of silicone organic products. Chemistry, 296 (in Russian).

Persic I.S., Strebkov D.S., Cechunina G.S., Potapov V.N., 2005. The Solar Photovoltaic Panel Design. Russia Patent 2.284.075.

Persic I.S., Strebkov D.S., Cechunina G.S., Cirkov A.V., Poulek V., 2010. The Solar Photovoltaic Panel Design. Russia Patent 2.431.786.

Daliento S., Lancellotti L., 2010. 3D Analysis of the performance degradation caused by series resistance in concentrator solar cells. Solar Energy, 84: 44–50.

Reda S.M., 2007. Stability and photodegradation of phthalocyanines and hematoporphyrin doped PMMA as solar concentrators. Solar Energy, 81: 755–760.

Ketola B.M., McIntosh K.R., Norris A., Tomalia M.K., 2008. Silicones for photovoltaic encapsulation. In: 23rd European Photovoltaic Solar Energy Conference, 1–5 September 2008, Valencia, Spain, 2969– 2973.

BP Solar, 2010BP. Solar Sees Proven Performance Over 25 Years Using Silicone Encapsulant from Dow Corning. Case Study. Available at: www.dowcorning.com/content/publishedlit/06-1030-01.pdf

METHODS FOR ENHANCING THE EFFICIENCY OF ENERGY PRODUCTION FROM BIOMASS

Roksana Rama

University of Technology and Life Sciences in Bydgoszcz
Faculty of Mechanical Engineering, Institute of Machine Operation and Transport
ul. Prof. Kaliskiego 7, 85-789 Bydgoszcz, Poland
Phone: +48523408208, Fax: +48523408462
e-mail: roxirama@tlen.pl

Abstract

One of the main elements of assessment of the biomass generation is this process's efficiency. In the article, the selected stages of cultivation and acquisition of biomass of agricultural origin, as well as the manners of their energy-consuming reduction have been presented.

It is possible to design weak soils of low agrarian usability for energy purposes' cultivation. The caloric value of oats cultivated on light soils, does not change substantially depending on the level of fertilization. Similarly, there looks the caloric value of barley, which changes only at a very high level of fertilization.

There exist constructional solutions of cutting units characterized by a high energy-consumption of the cutting process. Within the frames of realization of the research works aiming at identification of the power consumption of the cutting process.

Also the harvesting of biogas works' substrates with the use of additives may be the source of savings. Application of specialist additives during crops harvesting unfortunately is a costly treatment which may be rationalized.

Keywords: energy production, biomass

Introduction

One of the main elements of assessment of the processes of biomass acquiring is the efficiency of that process. As it results from the definition, efficiency of each process is lower than unity. However, in case of biomass, the biggest part of energy put in is the solar power. So, biomass is the solar power's battery. However, in order to acquire biomass possibly in the best manner, one should decrease power outlays connected with its production.

For European farming, apart from food production, production of plants for power purposes has becoming the necessity. Possibility to design products of plant origin for these purposes, in particular products of worse quality and acquired at low outlays, as well as looking for sources of power alternative for minerals, contributes to the increase of interest in the use of commonly cultivated plants for power purposes.

Cultivation of plants for power purposes

With reference to perennials typically used for power generation (ie. sida hermaphrodita rusby, basket willow or miscanthus) there appear many essential difficulties in their cultivation – very often they require application of special technologies, non-typical equipment, and establishment and displacement of a plantation is often troublesome (miscanthus, sida hermaphrodita rusby). There also occurs the problem connected with application of many pesticides (sida hermaphrodita rusby or sorghum), as in the climate conditions of the Middle Europe, there are no accepted efficiently protecting plants' formulations to be used.

That is why, more and more common there has been becoming designation for power purposes of plants produced so far exclusively for food or fodder purposes. There belong most of all cereals, designed both for direct combustion as well as for biogas and bioethanol production, or sugar beets constituting most of all substrate for a biogas works.

Oats, traditionally used for direct combustion due to high content of fat, may successfully be replaced with other cereals of admittedly lower power value but yielding on a higher level especially during drought. As mentioned by Kaszkowiak and Kaszkowiak (2009) both oats as well as spring and winter barley or rye, may successfully be used for direct combustion. Even at low-outlay technology of cultivation (level of fertilization with nitrogen 40 kg ha-1, and even without fertilization with nitrogen) both the heat of combustion, as well as energy efficiency per 1 ha, reach comparable values.

Satisfactory energy effects may also be obtained in case of rye and barley, even in case of cultivation of both the species on very light soils, very often set aside, also at low levels of fertilization (Kaszkowiak, Kaszkowiak, 2011). Weather conditions of the vegetation period are the factor that influences yielding to a significant level. Light soils, in particular in years of low precipitation or unfavorable their distribution, expressly react at water shortages reducing yielding at simultaneous slightly decreasing energy value.

In case of combustion of only cereals' grain, the unfavorable phenomenon of soils depletion from organic substances is avoided as both straw as well as ash remaining after combustion of grain may be used as multicomponent fertilizers. Grain is easier to be combusted, both in unprocessed form as well as briquettes or pellets. It makes it possible to combust grain in furnaces used for combustion of pellets, eco-pea coal or wooden briquettes. Studies conducted concerning briquetting grain in mixtures with wooden sawdust (of different percentage content of grain) expressly confirm such a possibility of its use for furnace purposes.

Corn's grain may be used universally for power generation (biogas, bioethanol, corn for direct combustion). As there mention Niedziółka and Zuchniarz (2006), and Kaszkowiak and Kaszkowiak (2013) lowering of outlays for nitrogen fertilization for 50% (from 160 kg ha-1 to 80 kg ha-1) results in the drop of biogas efficiency from 1 ha only for 5-6%)

Low-cost technologies of cultivation and the use of soils of low soil capability for annual grain crops, may constitute an alternative for set-aside fields on which production of plants for nutritional purposes in ineffective.

Biomass harvest

The technological process of plant material's cutting is one of the most important processes realized within the frames of plant material's harvesting for power purposes. One of the basic working assemblies, the task of which is cutting of plant material is the shear-finger cutting unit.

The existing constructional solutions of shear-finger cutting units is characterized by high energy-consumption of the cutting process, what as is connected with that as an effect, their power transmission systems are equipped with motors of relative big power (Zastempowski, Bochat, 2010; Zastempowski, 2010).

Within the frames of realization of the research works timing at identification of energy-consumption of the cutting process Bochat and Zastempowski conducted the analysis of efficiency of the shear-finger cutting unit's functioning efficiency. Studies were conducted towards determining the power demand.

Within the frames of the cutting process's realization, the impact of the knife strip's speed vnśr, speed of feeding the material for cutting vm and the angle of cutting unit's setting in relation to cut stalks on the total cutting operation Lc . Exemplary results of the studies are presented in Fig. 1.

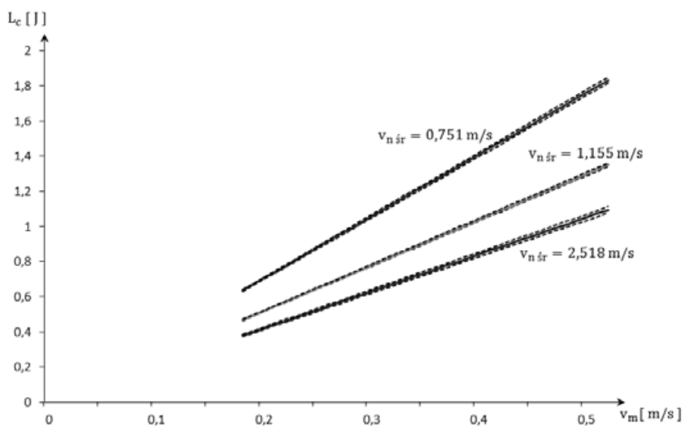

Fig.1 Impact of the knife strip's speed $v_{n\,śr}$, speed of feeding the material for cutting v_m and the angle of cutting unit's setting in relation to cut stalks on the total cutting operation L_c

The results of the studies presented by Zastępowski and Bochat unequivocally show, that an essential impact on energy-consumption on the process of cutting of stalk plants realized with the use of a shear-finger cutting unit there have the following: speed of the knife strip of the cutting unit and the speed of feeding of material for cutting (Bochat, Zastempowski, 2011). However, the lack of significant impact of the angle of cutting unit's setting in relation to cut stalks on the total cutting operation Lc was shown (Zastempowski, Bochat, 2011).

The maximum value of the cutting operation Lc=1,784 J was obtained for the speed of knife strip vcśr = 0,751 m s^{-1} and the speed of feeding material for cutting vm = 0,50 m s^{-1}. However, the lowest value of cutting operation Lc=0,330 J was obtained for the knife strip's speed vnśr = 2,58 m s^{-1} ad the speed of feeding material for cutting vm = 0,18 m s^{-1}.

The second one from the basic working units the task of which is to cut plant material into chaff, is the drum cutting unit. It is widely used in field chaff cutters. Similarly like in case of a shear-finger cutting unit, constructional solutions of cutting units are characterized by high energy-consumption of the cutting process.

There were conducted studies described by Zastempowski and Bochat. The purpose of these studies was to determined functional characteristics of a cutting drum. Within the frames of the experiment's realization, the impact of the cutting speed vc, thickness of knife's blade δ, degree of plant material's concentration h/ho and the angle of plant material's feeding θ on the unit cutting resistance pc and the unit cutting work Lj. Selected results of the studies are presented in Fig. 2.

The presented results of the studies conducted by Zastempowski and Bochat unequivocally show, that the essential impact on resistance and energy-consumption of the cutting process with the drum cutting unit there have the following: type of cut material, mode of cutting (lateral or oblique), cutting speed, thickness of knife's blade, degree of cut material's concentration (Zastempowski, Bochat, 2011).

Preservation and storage

Losses connected with storage of biomass are the big source of power losses occurring in biomass processing. One of the manners of counteracting these harmful processes is adding of appropriate preservatives resulting in the decrease of power losses during storage (Borowski, 2012). It is particularly important in case of harvesting corn for substrates for biogas production. On the market there are available many preservatives adjusted for preservation of green fodder from corn for feed purposes. However in ensiling of green fodder for power purposes in piles, there should occur processes leading to acetic fermentation (Dorszewski, 2009; Kalač, 2011).

However, application of preserving additives is not a cheap process. Due to that, farmers tend to reduce the dosages of preserving additives. Such proceedings may, in case of occurrence of variable collecting machines' throughputs, lead to forming of places of lower volume of additives in siloes (Borowski, 2012; Dulcet at al., 2006).

As mentioned by Borowski (2010) and Dulcet at al. (2006), the knowledge on its distribution in a silo is a very important issue allowing to lower the volume of applied formula. Studies conducted by them so far focused mainly on mini-silos that is on bales received in rolling presses. Described studies concerned wet hay harvested with the application of microbiological additives. However in case of silos with silage from whole corn plants, these processes according to preliminary studies conducted by the author are different and connected with transportation of silage juices. That is why, conducting of further studies concerning his issue is necessary.

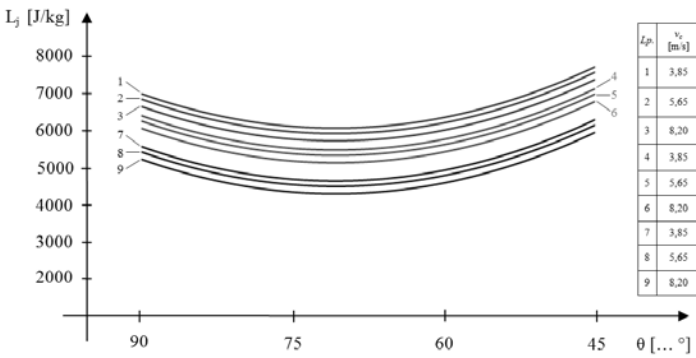

Lp.	v_c [m/s]	h/h_o	δ [μm]
1	3,85	0,47	40
2	5,65		
3	8,20		
4	3,85	0,54	
5	5,65		
6	8,20		
7	3,85	0,65	
8	5,65		
9	8,20		

Fig. 2 The angle of material feeding's angle θ on the unit work of rye straw's cutting work L_j for the value of cutting speed v_c, degree of concentration h/h_o and blade's thickness δ.

Conclusion

Acquiring of biomass for power purposes requires input of power connected with cultivation, production of fertilizers, harvesting and other applications used during a technological cycle. Excessive number of power inputs at that stage results in lowering of efficiency of the process of biomass conversion. Additionally there is the risk of the loss of a considerable volume of power during storage of biomass to be further processed. So, that is why one should tend to draw up technologies that would allow to earn the highest financial profits at simultaneous low financial, power but also environmental outlays.

References

Bochat A., Zastempowski M., 2011. Selected simulation analysis for use in designing of shear-finger cutting sections. Journal Research and Applications in Agricultural Engineering, 56(1): 6 - 10.

Borowski S., 2010. Analysis of distribution of additives in round bales of moist hay. Journal of POLISH CIMAC, 5(3): 9 - 13.

Borowski S., 2012. Controlling Rate Of Delivery Of Applicators At The Harvest Of Substrates Biogasworks - Preliminary Issues, Journal of POLISH CIMAC, 7(3): 17 - 22.

Dorszewski P. A., 2009. The effectiveness of the use of additives in silage preservation of green fodder legume-grass mixtures, and the whole plant corn. Rozprawy nr 136. Wyd. Ucz. UTP, Bydgoszcz. (in Polish)

Dulcet E., Kaszkowiak J., Borowski S., Mikolajczak J., 2006. Effects of microbiological additive on baled wet hay. Biosystems Engineering, 95(3): 379 - 384.

Kalač P., 2011. The required characteristics of ensiled crops used as a feedstock for biogas production: a review. J. Agrobiol., 28: 85 - 96.

Kaszkowiak E., Kaszkowiak J., 2011. Influence of crop production on their energy efficiency. Chemical Engineering and Equipment, 50(3): 33 - 34.

Kaszkowiak E., Kaszkowiak J., 2013. Yield and efficiency of bioethanol from maize in sandy soil conditions. Chemical Engineering and Equipment, 52(2): 56 - 57.

Kaszkowiak J., Kaszkowiak E., 2009. The use of cereal grains grown in simplified technology for energy production purposes. Chemical Engineering and Equipment, 48(2): 62 - 63.

Niedziółka I., Zuchniarz A., 2006. Energy analysis of selected types of plant biomass. MOTROL, 8A: 232 - 237.

Zastempowski M., 2010. The work efficiency analysis of scissor-fingers type cutting unit in selected type of mower. Chemical Engineering and Equipment 5: 144 - 145.

Zastempowski M., Bochat A., 2010. Analysis of the knife-bar dynamics movement in cutting unit. Journal of Polish CIMAC, 5(3): 257 - 263.

Zastempowski M., Bochat A., 2011. The research of energy-consuming in plant material cutting process. Parts I and II. Chemical Engineering and Equipment, 3: 89 - 92.

ASSESSMENT OF HYGIENIC CRITERIA OF A BUILDING ENVELOPE IN POULTRY HOUSING

Tímea Reichstädterová*, Jana Lendelová, Štefan Mihina, Štefan Pogran, Matúš Bošanský, Miroslav Žitňák

Slovak University of Agriculture in Nitra, Trieda A. Hlinku 2, 949 76 Nitra, Slovakia
Phone: +421 37 641 4621, E-mail: timeareichstadterova@gmail.com

Abstract

The aim of the study was an analysis of operational and energy risks associated with the assessment of hygienic criteria of envelope structures of insulated production hall buildings for poultry. By using the standard calculation procedure of heat demand for heating and by continuous measurements of temperature during three winter periods in years 2011, 2012 and 2013, it was found that the total energy required for heating is affected by the length of waiting times between periods, reduced quality of ceiling or ceiling-roof insulation, and disharmony in operational tasks. By a close examination of the development of temperatures in three thirds of every period, it was found that in the second third of the period, there was a changed trend in floor and bedding temperature with respect to the first and last third of the period in comparison with internal air temperature and the inside surface temperature of the ceiling and wall. In the first two weeks, there was also observed a positive correlation dependence (r = 0.924) between inner wall surface temperature and indoor air temperature. The surface temperature of the wall and ceiling surface temperature are also positively correlated (r = 0.905). Negative correlation at p <0.05 was found between straw bedding temperature and air temperature (r = - 0.715), wall surface temperature (r = - 0.662) or the ceiling (r = - 0.721). In the second third of the period, the development of floor temperature and bedding temperature was changed. Between inner wall surface temperature and the temperature of bedding, correlation coefficient was r = 0.142 in the middle third of the period. In the last third of the period, there was confirmed only a positive correlation between the surface temperature of the wall and ceiling surface temperature (r = 0.772) and a negative correlation between air temperature and bedding (r = - 0.495). However, in the middle third of the period, under a normal decrease of required internal temperature, there was an excessive soak of bedding due to the amount of condensate falling down from the ceiling to the floor. The consequent of increase in heating during the period with the required decreasing temperature of air causes higher energy consumption, lower profitability of farming, and breeding environment degradation.

Keywords: hygienic criteria, poultry housing, building

Introduction

The welfare and very good health and productivity of broiler chickens can only be achieved by ensuring optimum thermal conditions in the living area of the birds (Nawalany et al., 2010). Over the years of poultry house research, studies have been conducted by major universities, concerning the heat delivery systems and the heated air stratification common in poultry houses. After chicken feed the cost of energy is a close second and the long term price projections are only up. The farmers try to detect the inadequacies of the housing and understood the necessity for well designed and isolated buildings maybe with an alternative heating solution. According to the (Directive 2012/27/EU) Directive of the European Parliament and the Council 2012/27/EÚ on the energy efficiency improves the Union's security of energy supply by reducing primary energy consumption and reducing of energy imports. That regulation is to reduce greenhouse gas emissions by cost-effective manner, thereby mitigating climate change.

Energy severity of large-scale production facilities for poultry can be optimized only in cases where we can provide accurate sensing environmental parameters, the software evaluation and subsequent response to operation systems enabling control of heating and ventilation, respectively. Ventilating heat loss - in a veterinary and sanitary term - is the necessary loss for heat of the equivalent amount of incoming air to maintain optimal microclimate conditions (humidity, concentration of manure gases, dust and bacterial contamination of air) as specified (Tittl et al., 2012).

There is the internal air temperature control paramount in the initial stages of broiler production and involves the use of an external heat supply for the first four weeks of the production cycle. Usually, in the later stages of the cycle, the requirement for heat is reduced. Rising energy costs in occurrence of deficiently isolated buildings have led to some farmers reducing ventilation of the sheds as a cost saving measure. This can be detrimental to bird health as it can increase the moisture content of the litter, leading to hock burn and dermatitis and can also lead to the buildup of harmful emissions such as ammonia and carbon monoxide, increasing bird mortality (Defra, 2002; Nagaraj et al., 2007).

The aim of the study was an analysis of operational and energy risks associated with the assessment of hygienic criteria of envelope structures of insulated production poultry houses.

Material and Methods

The research was carried in the poultry house for 20,000 broiler located in southwestern Slovakia at an altitude of 250 m above the sea level. Raising ground area was 1257.5 m^2, with length of 100.6 m, width of 12.5 m, a height of the side walls 2.725 meters and height of the roof ridge 3.815 m (Fig. 1). Stable floor formed layer of 20 mm cement screed, 150 mm thick of concrete, 100 mm of cinder sub base placed on 150 mm thick layer of gravel. External walls were made of sandwich panels (composition: 7 mm Ezalit plate, 50 mm of thermal insulation and 7 mm of Ezalit plates). Ceiling-roof structure consisted of ceiling sandwich panels too, also of 7 mm Ezalit plates, 50 mm of thermal insulation, 10 mm of slag-cement boards, 7 mm of Ezalit plates and roofing from steel sheeting. Poultry raising was carried out on deep litter of chopped straw (3.5 kg.m^{-2}), the thickness of which was from 100-150 mm.

During the three winters of 2011, 2012 and 2013 year were studied indoor and outdoor climatic parameters, while DT 100 sensors were detected with 5 minute interval recording surface temperature of concrete floors and inside bedding temperature, surface wall temperature and temperature of ceiling surface. Using STN EN 730540 (2012) and STN EN 12831 (2003) were evaluated the basic characteristics and thermal-calculated of heat loss of the building. Statistical results were processed using the software STATISTICA 2007.

Results

There was analyzed the time course of all measured temperatures after calculation of the basic thermo-technical characteristics (Uwall = 0.631 W.m^{-2}.K^{-1}, Uceiling= 0.609 W.m-2.K-1 a Ufloor = 1.123 W.m^{-2}.K^{-1} and other) and thermal balance of the building (Tab. 1). There were processed average weekly records of internal and external environment parameters for each measured with order quantity of 10,000 values (Fig. 2). In poultry house for fattening broilers was also at decreasing demands for the internal air temperature during the 6-week winter batch found increased energy consumption not only in the first third of the fattening period, but in the last two weeks, too (Tab. 1).

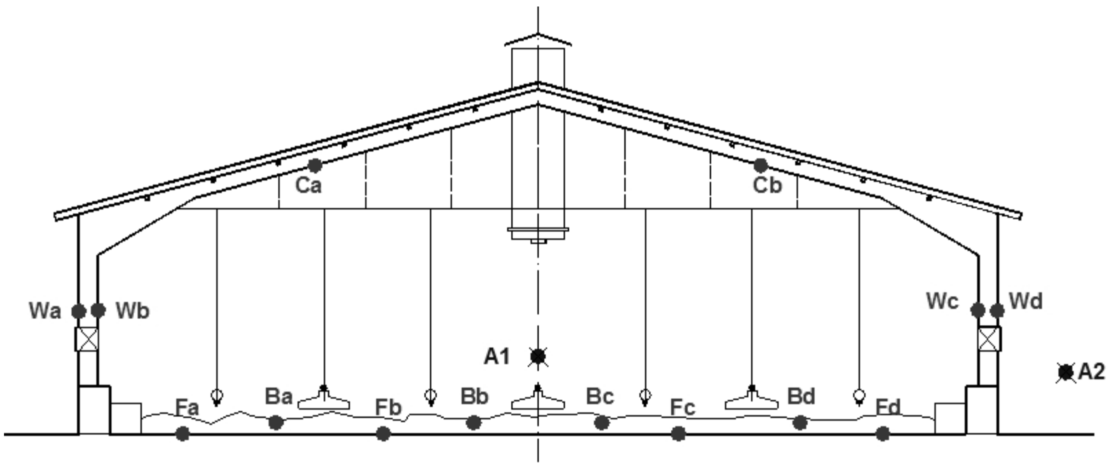

Fig. 1 Position of points for measurement places

A_1 – internal place for measuring for air temperature and relative humidity, A_2 – external place for measuring for air temperature and relative humidity, C_a, C_b – places for measuring of ceiling surface temperature W_a, W_b, W_c, W_d – places for measuring of external surface wall temperature, F_a, F_b, F_c, F_d – places for measuring of floor surface temperature, B_a, B_b, B_c, B_d – places for measuring of bedding temperature

Tab. 1 Heat balance of poultry house according standard calculating technique

Heat balance						
	1. week	2. week	3. week	4. week	5. week	6. week
Production of sensible heat, $\dot{Q}_c$ (W)	6966.1	24232.9	52196.6	87761.9	122643.6	151438.1
Output of heater, $\dot{Q}_t$ (W)	321950	325340	308390	265100	257500	287010
Heat loss by transfer $\dot{Q}_p$ (W)	76065.3	71157.8	66627.9	62286.7	60399.2	60399.2
Heat loss by ventilation, $\dot{Q}_v$ (W)	252847	278419	293958.9	290570.9	319741.7	378047

There was in detail analyzed the course of construction and surface temperatures and air temperature as well as operating faults. Despite of the decrease of air temperature, surface temperature of the ceiling and walls - recorded throughout the fattening period – the floor temperature, and the litter temperature increased in all measured turn (Fig. 2).

The temperature state of structures and floor temperature was harmonized after removal of the animals and floor constructions behaved like standard concrete structure on the ground. Produce of the animal sensible heat and probably also the process of straw fermentation in the bedding that also affected the concrete floor temperature by conductive heat transport helped with the gradual heating of the floor structure layers and the litter during the heating season.

According to results of the correlation matrix – there was observed the positive correlation (r = 0.952) between the inside air temperature and the internal wall surface for p <0.05 and the positive correlation for p <0.05 between the internal air temperature and the internal surface temperature of the ceiling (r = 0.953). The most pronounced positive correlation dependence was found between the interior surface temperature of the ceiling and interior wall surface temperature (r = 0.983). Other relationships were in negative correlation.

But there were detected anomalies during weekly search of the temperature development in comparison with the evolution of temperatures in the transitional period. In the first and second week - between the internal wall surface temperature and internal air temperature – was also observed positive correlation dependence (r = 0.924), both in the positive correlates the surface temperature of the walls and ceiling surface temperature (r = 0.905). The negative correlation (p <0.05) was found between the temperature and the air temperature of litter (r = - 0.715), the wall surface temperature (r = - 0.662) and floor (r = - 0.721). There was some development of disharmony in the third and fourth week in the floor temperature and in the litter temperature. This was the consequence of the recurrent phenomenon, which in the winter due to the lack of ceiling thermal insulation caused the water condensation on its surface. The condensed water drips into the litter, increasing its moisture, increasing its thermal conductivity, inherent reducing a floor temperature.

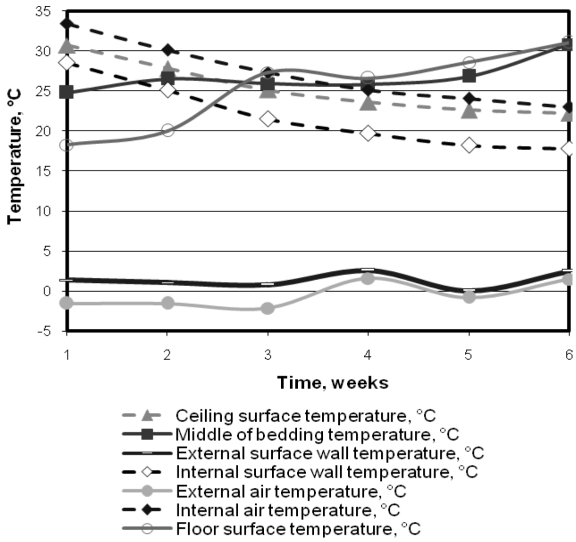

Fig. 2 The time course of measured temperatures in the poultry house processed with weekly averages of 5 minute records from the internal and external environment

In the middle of the turn, the positive correlation between the internal wall surface temperature and indoor air temperature and the positive correlation between the internal surface wall temperature and ceiling surface temperature was again confirmed (p <0.05), although with a partial damping of the Pearson coefficient (r = 0.658, respectively r = 0.903), but the negative correlation of air and surfaces with bedding from the first 14 days changed into low or no positive correlation dependence, respectively. For example, the inner wall surface temperature and the temperature of litter was found in third and fourth week of the turn correlation coefficient r = 0.142 (compared to the previous value of r = - 0.662). At the same time, it was even a period with a slight increase of outdoor temperature (Fig. 2). Between indoor air temperature and the air temperature outside was negative correlation with a correlation coefficient of r = - 0.519.

There was necessary to modify the heat output and at least partially dried wetted litter, and there was necessary to increase the ventilation performance in the fifth and the sixth week. During this period, the only confirmed a positive correlation between the surface temperature of the wall and ceiling surface temperature (r = 0.772) and a negative correlation between air temperature and litter temperature (r = - 0.495).

The actual temperature development of the indoor and outdoor environment was analyzed by measurement in addition to the computational evaluation in terms of the evaluation of sanitary criteria. In time of the 6 week period evaluating as a whole, the inner surface temperature of the wall and ceiling dew point positively correlated at $p < 0.05$, but the value of the Pearson correlation coefficient was very low (r = 0.196).

The consequent increase in heating during the period with the required decreasing temperature of air causes the higher energy consumption, lower profitability of farming, and breeding environment degradation.

Discussion

In big modern broiler houses there is often a significant heat loss due to conduction and ventilation while the price of fuel for heating is rising notably. Thus, it is profitable to secure an optimum heat recovery in poultry production facilities. In older production buildings, it is necessary to consider the degradation of the thermal-insulating function by increasing the thermal conductivity coefficient of 30-50 % (Jandásek, Rubinová, 2012). If the thermal insulation of building envelope inadequately protect against the heat loss, a undesirable risk of reduction of surface temperature below its dew point, respectively below the critical value for the formation of mold (Chmúrny, 2003). The subsequent formation of condensate and the incidence of microscopic filamentous fungi in stables are undesirable not only in terms of energy. Negative phenomenon is the increase in humidity of structures and bedding, as well as health risks. A dryer litter means a healthier environment for the birds and less ammonia. Dryer environment also mean the chicken sheds will have a longer structural life. A dryer environment with less ammonia means reduced electrical costs from reduced fan time for ventilation which obviously will pull heat out of the chicken house. Wet bedding and mouldy structures with hygienic problems may represent risks through the impact with a human food web.

Cold weather management of broilers is a challenge for many producers. Rising costs of fuel complicate the issue even more. The key is to choose ways to reduce fuel usage that do not have negative impacts on bird performance. The major source of heat loss in a broiler house is through the ventilation system. Ventilation is needed to bring fresh air into the house to maintain good air quality and to keep the floors dry. The results of the metering and calculations of the efficiency have proven that the heat exchanger reaches the operational efficiency of 10–47 % and thermal efficiency of 20–80 % even during the most demanding operational first twenty days of the breeding cycle of broiler (Adamovský et al., 2008).

Another research of broiler production practice shows that daily mean litter temperature is the lowest (as much as a dozen or so degrees lower than the required air temperature optimal air temperature). Cold bedding favours the incidence of avian mycoplasmosis, infectious bronchitis, gallinarum infections, coccidiosis, retarded growth and body weight decline. The measurements of bedding temperature from real operating conditions indicated that thermal conditions in the living area of birds, especially at the early and late stages of growth, are by far insufficient. Next analysis of the results led the authors to conclude that optimized thermal conditions in the living area of chickens throughout the production cycle can be expected when using a floor heating and cooling system (Nawalany et al., 2004; Nawalany et al., 2006). The improvement of thermal conditions in the living area of chickens increased weight gains by approx. 3 %, reduced feed consumption by approx. 3% and mortality by approx. 50 % compared to the control part of the production facility (Nawalany et al., 2010). Next idea show that poultry litter is a useful biomass source where produced locally. Using the litter for heating reduces waste to 10 % of original mass, mitigates environmental pollution caused by land spreading and concentrates nutrients in a sterile and easily transportable ash (Lynch et al., 2013). But the moisture content of poultry litter impacts on the lower heating value of the fuel, which can range from 9 GJ. t−1-13 GJ. t−1(Dagnall, 1993). Using the dry litter in the manner described by Lynch (Lynch et al., 2013) reduces waste to 10 % of original mass, mitigates environmental pollution caused by land spreading and concentrates nutrients in a sterile and easily transportable ash.

Conclusion

Insufficient heat protection of poultry houses is not only the risk of increased the power consumption. It causes wetting structures and their durability decreasing, health problems and increase of litter moisture. Also in the case of further litter processing as a biofuel, and pellet - the bedding with high moisture content have to be modified at first. The wet litter causes increased production of emissions, which raise of need the increased electrical cost from necessary fan time for ventilation which obviously will pull heat out of the chicken house. The consequent increase in heating period with desired decreasing temperature of air causes lower profitability of farming and breeding environment degradation.

Reference

Adamovský R., Adamovský D., Kára J., Neuberger P., 2008. Verification of the effects of the secondary heat recovery from ventilation air in an animal house for the fattening of broiler chickens. Infrastructure and Ecology of Rural Areas, Polska Akademia Nauk, Oddział w Krakowie, 6: 51 – 61.

Chmúrny I., 2003. Thermal protection of buildings. Bratislava : Jaga group: 214.

Dagnall S., 1993. Poultry litter as a fuel. Worlds Poult. Sci J, 49: 175 – 177.

Defra, 2002. Meat chickens and Breeding chickens - Code of Recommendations for the Welfare of livestock Department for Environment, Food and Rural Affairs, London: 28.

Directive 2012/27/EU of the European Parliament and of the Council of 25 October 2012 on energy efficiency, amending Directives 2009/125/EC and 2010/30/EU and repealing Directives 2004/8/EC and 2006/32/EC.

Jandásek M., Rubinová O., 2012. Energy self-sufficient farm. In : Current Issues Bioclimatology animals 2012: ČHMU Brno. Praha : Czech Bioclimatological Company, 1(124).

Lynch D., Henihan A. M., Bowen B., Lynch D., McDonnell K., Kwapinski W., Leahy J. J., 2013. Utilisation of poultry litter as an energy feedstock. Biomass and Bioenergy, 49: 197 - 204.

Nagaraj M., Wilson C. A. P., Saenmahayak B., Hess J. B., Bilgili S. F., 2007. Efficacy of a litter amendment to reduce pedodermatitis in broiler chickens. J. Appl. Poult. Res., 16: 255 – 261.

Nawalany G., Bieda W., Radon J., 2004. Thermal and moisture parameters of broiler house litter in light of research. Annals of Animal Science, 1: 193 - 196.

Nawalany G., Bieda W., Radon J., 2006. Effect of floor thermal insulation in broiler houses. Acta Scientiarum Polonorum Architectura, 5, 111-117. (in Polish)

Nawalany G., Bieda W., Radon J., 2010. Effect of floor heating and cooling of bedding on thermal conditions in the living area of broiler chickens. Arch. Geflügelk., 74 (2): 98 – 101.

STN EN 730540-2, 2012. Thermal protection of buildings. Thermal performance of buildings and components. Part 2: Functional requirements

STN EN 12 831, 2003. Heating systems in buildings. Method for calculation of the design heat load

Tittl K., Novák P., Malá G., 2012. Protection of animals against the spread of dangerous infections In: Current Issues Bioclimatology animals 2012 : ČHMU Brno. Praha : Czech Bioclimatological Company, 1(124).

EVALUATION OF HYDRAULIC BRIQUETTER MECHANISM

Edgars Repsa*, Eriks Kronbergs

Latvia University of Agriculture, J. Cakstes bulv. 5, Jelgava, LV-3001, Latvia,
Phone: +37163080674, Fax: +37163020762, E-mail: edgars.repsa@llu.lv
Faculty of Engineering, Institute of Mechanics

Abstract

The purpose of presented investigation is the theoretical and experimental evaluation of rhombus linkage pressing mechanism comparing with direct pressing mechanism. Necessary electrical motor power and power losses in hydraulic drive system were determined.

Briquettes from grinded common reed (Phragmites Australis) and peat (30%) mixture were produced with designed experimental briquetting press with density (958÷1085) ± 43 kg.m^{-3}.

Necessary electric motor power for hydraulic pump was N_{ER} = 0.813 kW (rhombus linkage pressing mechanism) and N_{ED} = 2.641 kW (direct pressing mechanism). Difference between necessary electric motor powers is 1.828 kW. Results of calculations show that energy losses in hydraulic drive system were 3.3 times greater for direct pressing mechanism.

Keywords: hydraulic mechanism, briquette

Introduction

Biomass compacting represents technology for the conversion of biomass raw material into a solid biomass fuel in shape of briquettes and pellets. Previously chopped stalk biomass is material of low bulk density (80 – 150 kg.m^{-3}), therefore compacting of biomass is one of the important processes for effective handling, transport and storage of this biomass fuel material.

There are several methods available for compacting biomass. Pelleting, briquetting, and extrusion processing are methods commonly used to achieve densification. Hydraulic piston presses are commonly used as briquetting machines for densification of biomass. The energy to the piston is transmitted from an electric motor via a high-pressure hydraulic system. The output of a hydraulic press is lower, since the movement of the cylinder is slower compared to mechanical processes (Neethi-Manickama et al., 2006).

The hypothesis of this investigation is that the energy requirement in compacting process can be reduced when pressing mechanism is provided with nonlinear force – displacement characteristic.

The presented paper deals with theoretical and experimental evaluation of piston press type briquetter with rhombus linkage pressing mechanism and hydraulic drive. Necessary electrical motor energy and energy losses in hydraulic drive system were compared for rhombus linkage pressing mechanism and direct pressing mechanism.

Materials and Methods

Experimental briquetter with rhombus linkage pressing mechanism (Fig. 1) for experimental investigation was used. Rhombus linkage mechanism link size was 200 mm, drive hydraulic cylinder piston diameter 60 mm and rod diameter 40 mm. Hydraulic drive scheme is shown in Fig. 2. Open end tapered pressing die diameter was 25 mm and pressing piston stroke 175 mm. During briquetting experiments hydraulic pressure was measured with calibrated pressure sensor. For data collection was used Data Logger Pico and computer. For briquetting experiments grinded common reed and peat (30 %) mixture was used. Grinding of common reed was realized with hammer mill using 6 mm sieve screen opening size.

Moisture of experimental material was less than 10 %. The moisture content was determined according the standard BS EN 14774-2:2009, where oven drying of the samples was carried out at 105±2 ºC (BS EN 14774-2, 2009). The briquettes with different density were obtained. Briquettes density was determined from the ratio of the mass to the volume of the briquette. The weight of briquette was measured on electronic scales Sartorius GM312 with division 0.01 g and size of briquettes was measured with sliding callipers (division 0.1 mm).

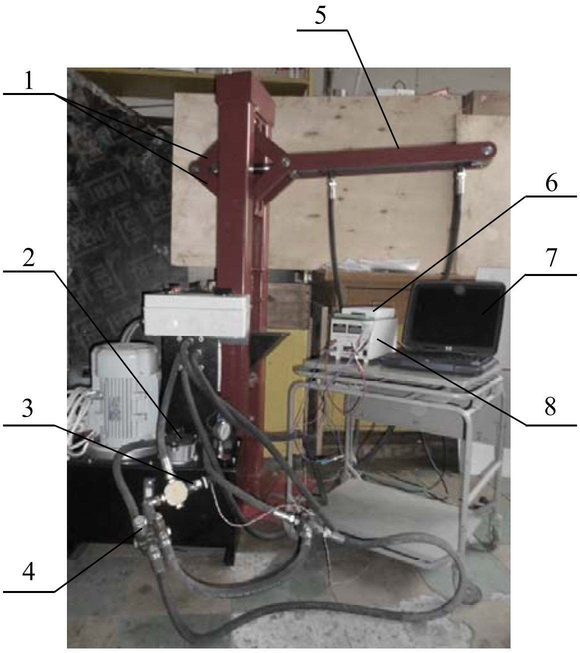

Fig. 1 Experimental briquetter:
1 – rhombus linkage mechanism; 2 – power station; 3 – pressure sensor; 4 – flow control valve; 5 – drive cylinder; 6 – Data Logger Pico; 7 – computer; 8 – power supply

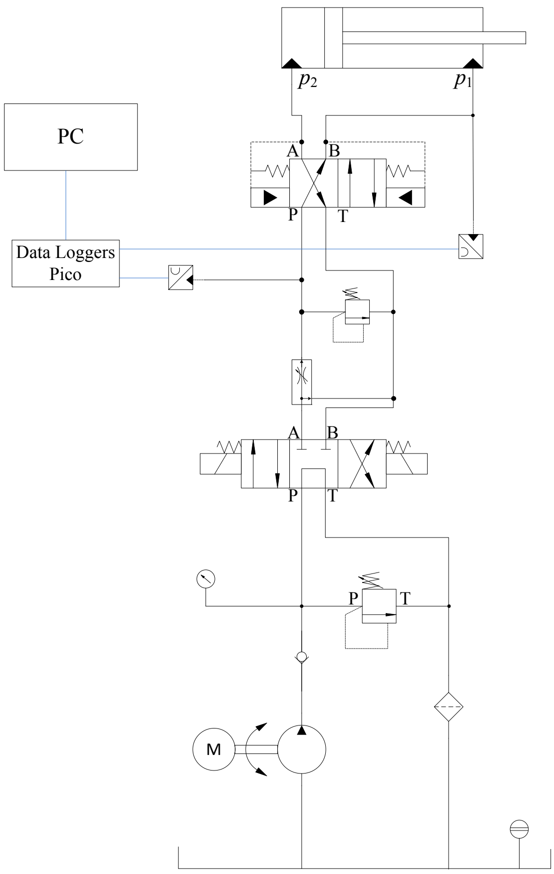

Fig. 2 Hydraulic drive scheme

Hydraulic cylinder loading force can be calculated by equation (1) and for unloading force equation (2).

$$F_L = \left(p_1 \frac{\pi \left(D^2 - d^2 \right)}{4} - p_2 \frac{\pi D^2}{4} \right) \eta ; \qquad (1)$$

$$F_{UL} = \left(p_2 \frac{\pi D^2}{4} - p_1 \frac{\pi \left(D^2 - d^2 \right)}{4} \right) \eta , \qquad (2)$$

where F_L – loading force, N; F_{UL} – unloading force, N; p_1, p_2 – pressure (Fig. 2), MPa; D – piston diameter, mm; d – rod diameter, mm; η – mechanical losses.

Equation (3) can be used for rhombus linkage mechanism pressing force (Repsa et al., 2013) calculation

$$F_P = \frac{F_L}{\tan \alpha} \eta_f , \qquad (3)$$

where F_P – briquetting force, N; α – rhombus linkage mechanism linkage position (Fig. 3), deg; η_f – coefficient of mechanical losses in pins. The evaluation of presented experimental briquetter can be realized comparing necessary drive power for rhombus linkage pressing mechanism (Fig. 3) and direct piston pressing mechanism (Fig. 4). Power of pressure losses in hydraulic drive system can be used as other criterion for evaluation of presented mechanisms.

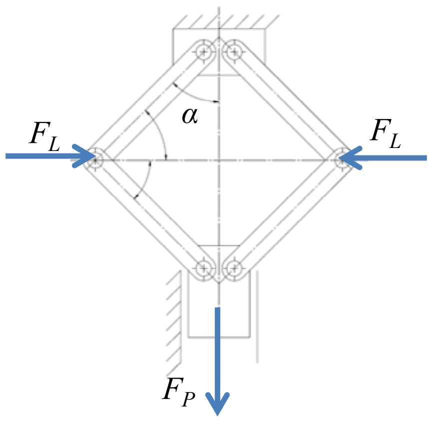

Fig. 3 Rhombus linkage mechanism scheme

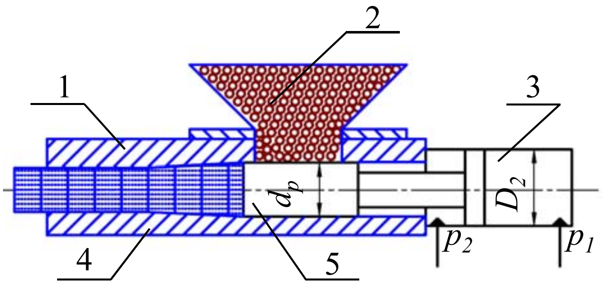

Fig. 4 Direct pressing mechanism scheme:
1 – conical die; 2 – pressing material feeder;
3 – hydraulic cylinder; 4 – briquettes;
5 – pressing piston

Before evaluation it is necessary to calculate hydraulic drive parameters.

For rhombus linkage mechanism necessary pump flow rate:

$$Q_R = v_H \frac{\pi\left(D^2 - d^2\right)}{4}, \tag{4}$$

where Q_R – flow rate (rhombus linkage mechanism drive), $m^3.s^{-1}$; v_H – rod velocity, $m.s^{-1}$.

Necessary hydraulic cylinder piston diameter of direct pressing mechanism:

$$D_2 = \sqrt{\frac{4F_{L\max}}{\pi\, p_{1\max}}}, \tag{5}$$

where D_2 – hydraulic cylinder piston diameter, mm; $F_{L\max}$ – necessary maximal pressing piston force, N; $p_{1\max}$ – maximal pressure, MPa.

Pump flow rate for direct pressing mechanism hydraulic drive:

$$Q_D = v_P \frac{\pi D^2}{4}, \tag{6}$$

where Q_D – flow rate (direct pressing drive), $m^3.s^{-1}$; v_P – rod velocity (equal with rhombus linkage mechanism pressing piston average velocity), $m\ s^{-1}$.

Necessary electric motor power for both mechanism hydraulic pumps:

$$N_{ER} = \frac{p_{\max} Q_R}{1000\ \eta_P};\ N_{ED} = \frac{p_{\max} Q_D}{1000\ \eta_P}, \tag{7}$$

where $p_{\max}$ – maximal pressure of hydraulic drive, Pa; N_{ER} – power of electrical motor (rhombus linkage mechanism), kW; N_{ED} – power of electrical motor (direct pressing mechanism), kW; ηP – coefficient of pump efficiency (0.87) (Chapple P., 2003; Наземцев, Рыбальченко, 2007).

Hydraulic drive effectiveness can be evaluated comparing pressure losses in hydraulic drive. Allowable pressure losses in hydraulic drive systems cannot exceed 6 % (Наземцев, Рыбальченко, 2007).

$$N_{ERL} = \frac{\Delta p Q_R}{1000};\ N_{EDL} = \frac{\Delta p Q_D}{1000}, \tag{8}$$

where N_{ERL} – power losses of rhombus linkage mechanism, kW; N_{EDL} – power losses of direct pressing mechanism, kW; Δp – pressure losses – 6% of maximal pressure value, Pa.

Results and Discussions

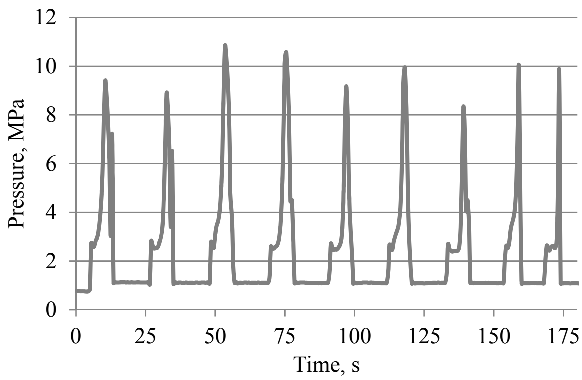

Fig. 5 Briquetting pressure diagram

During briquetting experiments with experimental briquetter (Fig. 1) hydraulic pressure was measured with calibrated pressure sensor.

Example of briquetting pressure dependence on time is shown in Fig. 5.

Results of experiments show that maximal pressure values do not exceed 11 MPa. During briquetting experiments average velocity of hydraulic cylinder rod during loading was 0.041 $m.s^{-1}$ and average velocity of pressing piston 0.022 $m.s^{-1}$, respectively.

Fig. 6 Common reed and peat mixture briquettes

The density of produced briquettes changes (958÷ 1085) ± 43 kg.m^{-3}. Average diameter of briquettes was 25±0.05 mm and length (12÷30) ± 0.05 mm. Example of produced common reed and peat (30%) mixture briquettes with experimental briquetter are shown in Fig. 6.

For presented rhombus linkage mechanism and direct pressing mechanism evaluation following assumptions were introduced (according experiments):

- equal hydraulic drive schemes;
- equal die diameter (25 mm) and pressing piston maximal force (Fp = 108 kN);
- unloading force ignored;
- equal hydraulic pressure maximal value (pmax = 11 MPa) and loading time (8 s).

Pressing piston force was calculated by equation (3). To provide on mentioned assumptions rhombus linkage mechanism necessary velocity hydraulics pump flow rate calculated by equation (4) was QR = 6.43•10-5 m^3.s^{-1}. Necessary hydraulic cylinder piston diameter of direct pressing mechanism calculated by equation (5) was D2 = 111.8 mm. Nearest standard hydraulic cylinder piston diameter for future calculation – 110 mm. Pump flow rate for direct pressing mechanism hydraulic drive calculated by equation (6) was QD = 2.09•10-4 m^3.s^{-1}.

Necessary electric motor power for hydraulic pump calculated by equation (7) was NER = 0.813 kW (rhombus linkage pressing mechanism) and NED = 2.641 kW (direct pressing mechanism). Difference between necessary electric motor powers is 1.828 kW.

Energy losses depending on pressure losses in hydraulic drive system can be calculated by equation (8) NERL = 0.0424 kW and NEDL = 0.1387 kW. Results of calculations show that energy losses in hydraulic drive system were 3.3 times greater for direct pressing mechanism. Therefore it can be concluded that the energy requirement in compacting process can be reduced when pressing mechanism is provided with nonlinear force – displacement characteristic. In Fig. 7 is shown calculated hydraulic cylinder force – displacement curves for one pressing cycle.

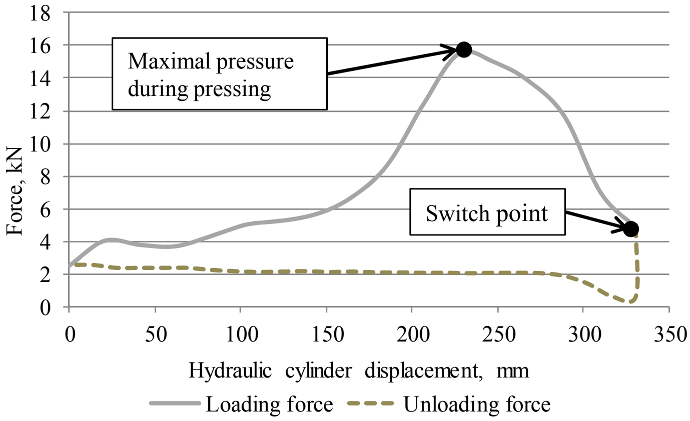

Fig. 7 Hydraulic cylinder force – displacement curves for one pressing cycle

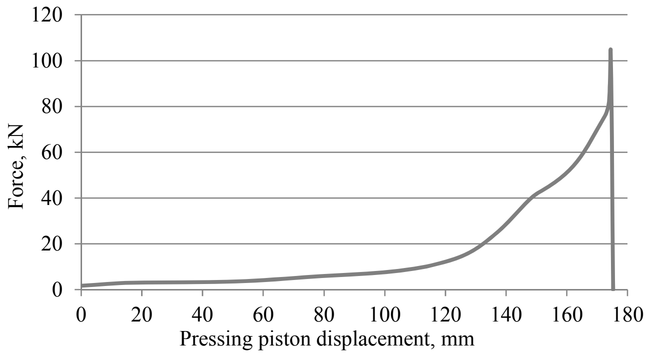

Fig. 8 Pressing mechanism force – displacement curve

Pressing cycle consists of two parts – loading and unloading. Forces were calculated by equations (1) and (2). Hydraulic cylinder piston changes moving direction in switch point.

Rhombus linkage pressing mechanism force – displacement curve of loading was calculated by equation (3) (Fig. 8). Results of evaluation of hydraulic cylinder force – displacement curve and pressing mechanism force – displacement curve show that maximal hydraulic cylinder force and pressing piston maximal force were achieved with some time delay. It is possible because presented rhombus linkage mechanism have nonlinear characteristic. The designed rhomb pressing mechanism can be recommended for biomass briquetting with drive from tractor hydraulic system with pressure < 20 MPa in rural conditions.

Conclusions

Results of experiments obtained during compacting with rhombus linkage pressing mechanism show that values of hydraulic drive maximal pressure are less than 11 MPa. Calculated pressing piston maximal force is 108 kN.

The density of experimentally produced common reed and peat (30%) mixture briquettes is (958÷1085) ± 43 kg.m^{-3}. Results of calculations show that necessary electric motor power for hydraulic pump was N_{ER} = 0.813 kW (rhombus linkage pressing mechanism) and N_{ED} = 2.641 kW (direct pressing mechanism). Difference between necessary electric motor powers is 1.828 kW. Energy losses in hydraulic drive system were 3.3 times greater for direct pressing mechanism. The energy requirement in compacting process can be reduced when pressing mechanism is provided with nonlinear force – displacement characteristic.

The designed rhomb pressing mechanism can be recommended for biomass briquetting with drive from tractor hydraulic system with pressure < 20 MPa in rural conditions.

Acknowledgment

This publication has been prepared within the framework of the ERAF Project „Development of mechanization equipment for energy crops conditioning”, contract Nr.2010/0306/2DP/ 2.1.1.1.0/10/APIA/VIAA/128.

References

BS EN 14774-2,2009. Solid biofuels Determination of moisture content – Oven dry method – Part 2: Total moisture – Simplified method.

Наземцев А.С., Рыбальченко Д.Е., 2007. Пневматические и гидравлические приводы и системы. Часть 2. Гидравлические приводы и системы. Основы. Москва: Форум, 297. (In Russian)

Chapple P., 2003. Principles of Hydraulic System Design: First Edition. Great Britain: Coxmoor Publishing Company, 274.

Neethi-Manickama I., Ravindrana D., Subramanianb P., 2006. Biomass Densification Methods and Mechanism. In: Distributed Generation & Alternative Energy Journal, 21(4): 33 – 45.

Repsa E., Kronbergs E., Kronbergs A., 2013. Evaluation of biomass briquetting mechanism. In: Environment. Technology. Resources: Proceedings of the 9th International Scientific and Practical Conference June 20-22. Rezekne.

THE EFFICIENCY OF THE HEAT PUMP INCLUDED IN THE GREENHOUSE HEATING SYSTEM

Kazimierz Rutkowski*[1], Anna Krakowiak-Bal[1], Patrik Burg[2]

[1]University of Agriculture in Krakow, Balicka 116 B, 30-149 Krakow, Poland,
Phone: +48 12 6624629, E-mail: Kazimierz.Rutkowski@ur.krakow.pl
[2]Mendel University in Brno, Czech Republic

Abstract

Objects with the horticultural production have a specific heat demand that is mostly dependent on the solar conditions. With low outdoor temperatures but high solar radiation intensity a large heat surpluses in greenhouses are generated. They are released into the atmosphere through ventilation system (Rutkowski, Wojciech, 2009).

Simultaneously, if the gardening production is carried on there is a high heat demand for process water heating.

Therefore, the goal of the study was to measure and exploit heat excess directly in the production process. To better use the heat surpluses the heat pump was integrated into the recovery system. Inclusion a heat pump into the system allows wider use of the effect, which is higher water temperature.

Water with a higher temperature after mixing can be used for fertigation or as a heat accumulator in the greenhouse heating process.

In specific outside climate conditions the object's energy balance was carried and the energy amount loses through ventilation system were determined. A heat exchanger installed in the ventilation system was the lower heat pump source, which supplied hot water tank.

The energy excess that occur on the upper source of heat pump, allows at the same time the energy accumulation and heating an object at the period of the increased demand (Rutkowski, Wojciech, 2009). The heat pump as an auxiliary energy source allows covering partially the heat demands during rush periods and in large part solves the energy problems for process water heating. An important factor in combined heat and power system is the proper selection of system components.

An adequate heat pump power, a matched buffer tank capacity and the way of use the energy stream from ventilation system have a significant impact on the energy and economic efficiency of the system.

Keywords: heating system, pump, greenhouse

Introduction

The use of renewable alternative energy sources in terms of environment and energy is very important. However, this issue still requires prudence and a broad perspective. Due to the high investment costs of the installation of renewable energy sources, their wider use should be considered. In many economy sectors, such a comprehensive approach is used and the return on investment is reduced to a few years. In the under cover objects i.e. greenhouses and foil tunnels, with a large heat demand and sensitivity to changing external conditions reaching for renewable energy seems justified.

Another argument for renewable energy is the ability to use a various energy forms (heat and cold) throughout the year. Furthermore, there is the greenhouse effect in these objects causing periodic heat gain, which in current practice is wasted. Considering the high heat demand in the greenhouse facilities overnight and large amounts of waste heat arising during the day a multifaceted use of heat pumps in the energy system of under covered objects should be consider.

Many authors undertook research in this area. In most cases, the scope of the research included the restricted range of energy sources use.

Garcia at al. (1998) have conducted the analysis of the effectiveness of renewable energy equipment in greenhouses on various latitudes. In their study cogeneration systems were evaluated. Due to the large differences in heat demand during the day in the greenhouse objects, many researchers are trying to implement heat accumulators into the greenhouse energy system (Santamauris et al., 1994; Chinese et al., 2005). In these studies, there are a number of valuable suggestions regarding energy storage in liquid accumulators, rock-beds, diaphragm heat exchangers to air heating, and the phase transition.

The use of various renewable energy sources in horticultural production is the main purpose of Hepbasli's publications (2011). To increase the efficiency of the heat pump, heat raises the temperature of the lower heat source by blowing warm air from the solar collectors.

Bayer et al. (2012) and Ozenger (2005) are dealing with similar problems concerning increasing the heat pump efficiency.

A literature review shows that the use of heat pump for heating systems has a high efficiency if the stable temperature of lower heat source will be ensured and low temperature at the output (upper heat source) is accepted. For this reason, many scientists are looking for technologies where the combined heat and power can be applied using various energy streams.

On that assumption Panwi et al. (2011) has presented an overview of mathematical models having regard streams from both the heating and cooling as well.

The above mentioned works and processes can be widely used in under cover objects. Combining the utilization of heat excess from the greenhouse effect accumulated in various accumulator types with heat pump a high efficiency rate of the system can be achieved (Adamowský et al., 2011).

Using a heat pump for air-conditioning in the greenhouse also the physical quantities of lower heat exchanger should be considered. According to the Research Center for Energy and Environment in Lecce, Italy (UNILECCE-DII-CREA), significant impact on the heat efficiency of lower heat exchanger have: the thermal conductivity coefficient, the flow rate of the heating medium and the orientation in the substrate.

Examining the above presented research reports, greenhouse's energy analysis for the correct selection of the heat pump seems appropriate.

Purpose and methods

For the heat pump operation analysis, an experimental object located at the Faculty of Production and Power Engineering of the University of Agriculture in Krakow was used. Study was carried out in two periods with different heat demands.

The whole tunnel is covered with polycarbonate panels. The object is equipped with a heat pump of 9.7 kW, and the system of automatic data acquisition and archiving. There is possible a measurement and archiving of following parameters:

- ambient temperature,
- temperature of heating water at the flow and return from the heat exchanger,
- wind speed,
- solar radiation, etc.

Inside the tunnel a microclimate was registered: temperature, air humidity and electricity amount used in respective circuits. Measurement frequency was set at 30 sec. The buffer exchanger with variable volume from 120 to 360 liters powered the upper heat source.

As the second, lower heat source was used the exchanger powered by waste heat, gained from the upper part of horticulture tunnel.

The connected system allows for monitoring and archiving the temperatures of circulating heating medium and ground.

Results and discussion

High heat demand in the study object at night results the high value of heat transfer coefficient. The substitute heat transfer coefficient *k'* (*μ'*), for the assumptive tunnel coverage ranged from 3.8 - 4.2 ($W.m^{-2}.K^{-1}$). Differentiation was due to the wind speed and direction. Heat transfer coefficient was determined on the night's measurements.

The internal temperature inside study object was established at 10 °C. There was not production inside the tunnel but the proper microclimate condition, appropriate quantity and temperature of the process water were guaranteed. The balance sheet includes constant process water demand in an amount of 8 ($liters.m^{-2}$) regarding crops area, with initial temperature of 4 °C and finish of 12 °C. Process water was heated by the heat exchanger supplied from the heat pump. During the day, there was a large amount of waste energy from the greenhouse effect. Despite unfavorable weather conditions (April 2013) the amount of waste energy, which is the lower power source of heat pump heating the process water was sufficient. In 94 % of the research period (1.5 months), the amount of sun energy was enough to secure a temperature above 16 °C on the heat exchanger.

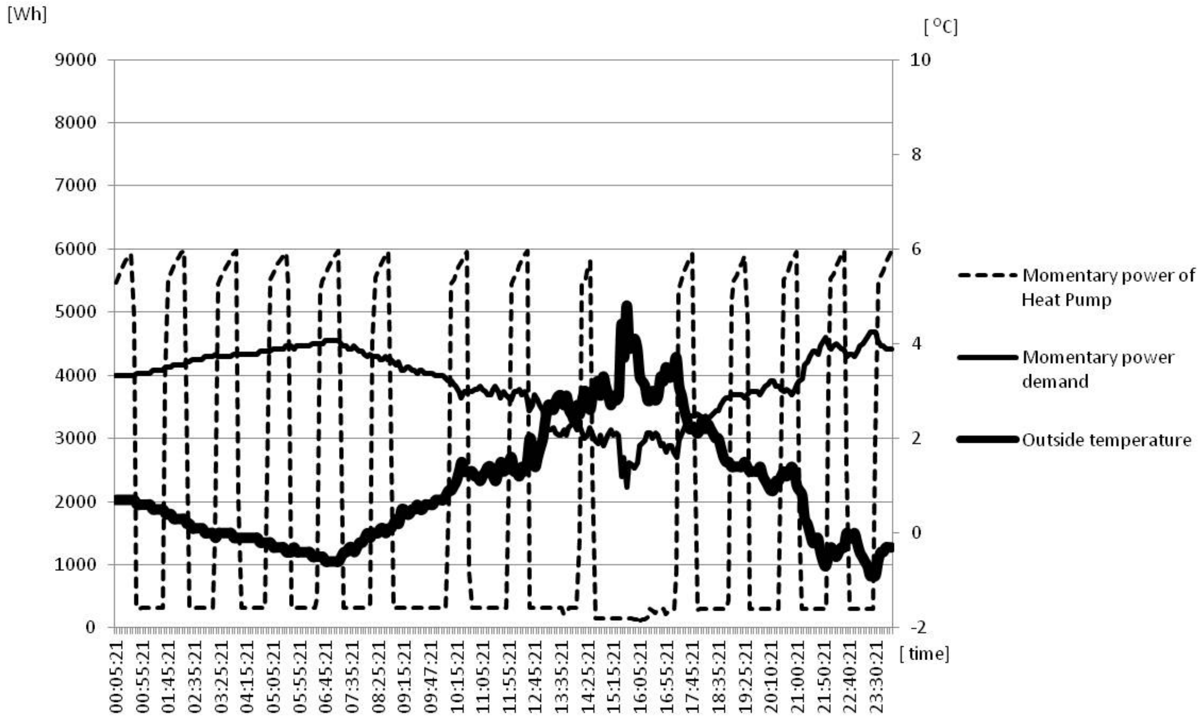

Fig. 1 Power consumption demand and power coverage for the surveyed object with low outside temperature (average temperature 0.51 °C)

Thanks to the high temperature of lower heat source and low temperature in the heat exchanger for water heating, high coefficient of energy performance (COP) was obtained. Its average value (during wastewater heating) equals 3.0. From the whole research cycle 2 days were choose, and they were detailed analyzed. Fig.1 shows the external temperatures on day with solar energy inside the tunnel at 1,66 $kWh.m^{-2}$.

Following the heat pump power supplying the object, it is noted that it is stabilized and peak value reaches 6 kW. Work periods and night breaks have similar values. Daytime ratio of the pump working time to pump breaks decreases. It depends on solar conditions. Following the power changes dynamic, there should be remembered that, in the morning when the temperature in the upper tunnel exceeds 25 °C, the ground lower heat source switches to exchanger powered by waste heat. The Fig. 2. shows this switching moment (about 8.45).

Following the times of heat pump operation, regarding external temperature, a significant correlation is visible. The values shown on Fig.1. were obtained while the upper heating circuit included a 300 l buffer tank. There can be stated, that dynamic of heat pump operation is established and fully logic.

The second day, which was selected for detailed analysis, has a higher outside temperature relatively stable at night. Simultaneously, there must be added, that selected day, was one of the few with very low solar irradiance, and daily energy amount was 0.42 $kWh.\ m^{-2}$. Despite of this low value, the heat pump has worked with lower exchanger powered by waste energy (by airing). It has an excellent coefficient of performance (COP = 2.9) and it has provided heating of necessary process water amount.

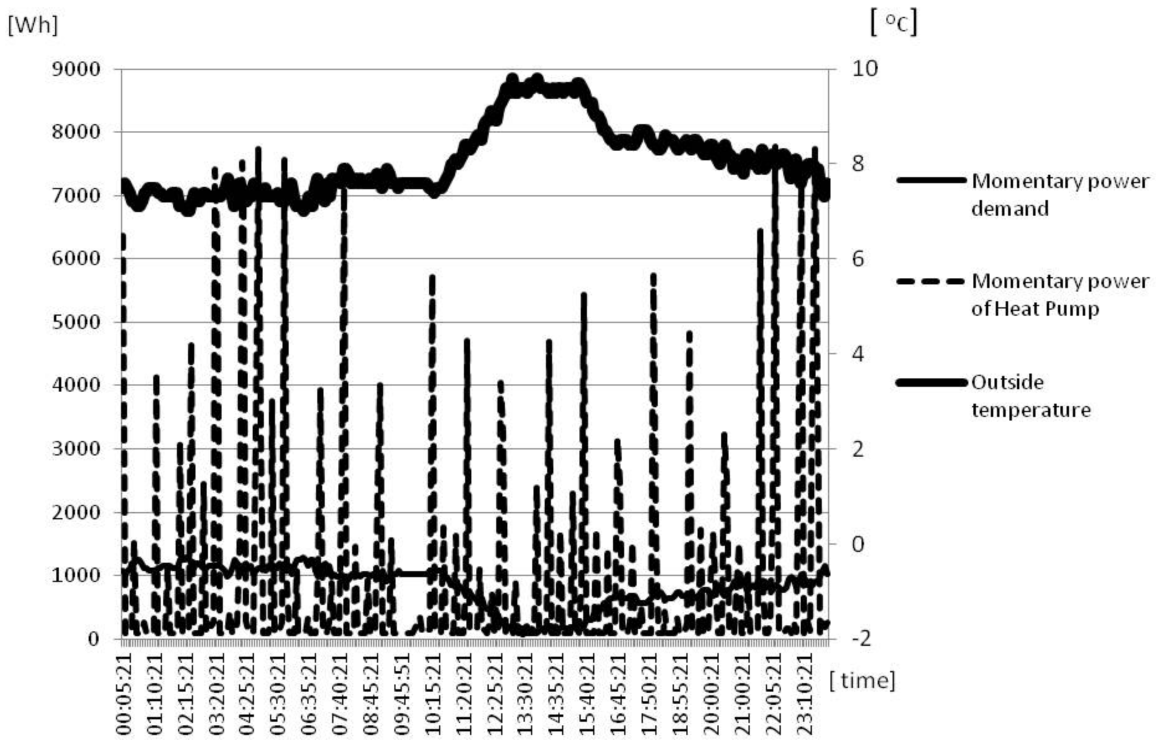

Fig. 2 Power consumption demand and power coverage for the study object with high outside temperature (average temperature 8.21 °C)

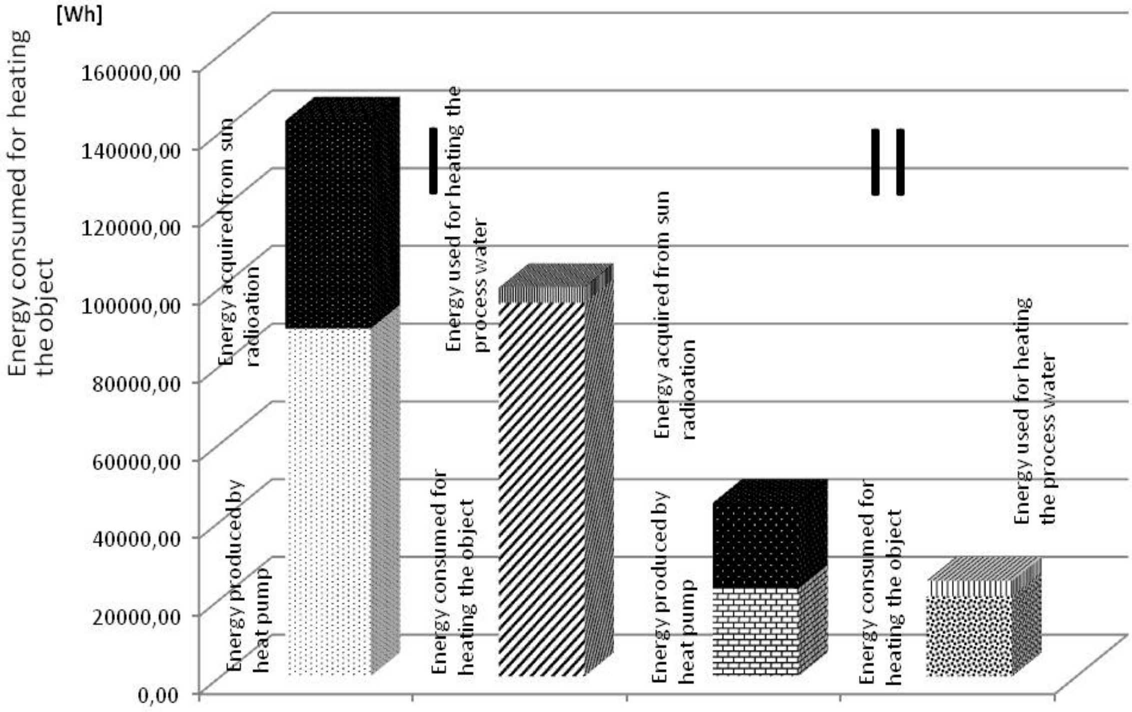

Fig. 3 Energy balance of the technology process by analyzed climate conditions

Following the dynamic of power changes (on the Fig. 2), there is a significant difference comparing with Fig. 1. The difference is too frequent heat pump switching and short operation times. These noticeable differences are probably due to the different research conditions on analyzed days. The condition difference consisted in including into the circuit the buffer tank of small capacity i.e. 120 l (the other conditions were not changed). Low buffer tank capacity has caused very frequent pump switching, short operation time and high peak power values (with daily high diversity).

Assessing the heat pump dynamics there can be concluded that heat pump operation was unsettled.

These conditions result of significantly higher electricity consumption in relation to the thermal energy supplied (COP = 2.9) and clearly reduced compressor durability (high compressor due to frequent switching off).

Fig.3 shows useful power amount delivered to the object as energy from the heat pump powered from the ground and by energy from the greenhouse effect. Comparing power amount possible to use and used at I and II days, still a considerable energy amount unused is noticeable. In a further research stage the balance with heat excesses to ground heating will be carry out.

Summarizing the study results, there can be concluded that, during early spring, even by low solar radiation intensity, use of waste heat to process water heating is energetically justified (after energy balance).

Conclusions

1. Using a heat pump as an energy source in the greenhouse heating system it is justified to include energy from the greenhouse effect.
2. Double-suction heat pump allows to obtain higher average COP value (from 2.2 for 3.0).
3. Energy Surpluses generated by the greenhouse effect (spring period) cover fully the energy needs of process water.

This work is financed by research project No. N 313 445137 National Science Centre Poland.

References

Adamovský R., Masek L., Neuberger P., 2011. Analysis of rock mass borehole temperatures with vertical heat exchanger. Research in Agricultural Engineering, 58(2): 57 - 65.

Bayer P., Saner D., Rybach L., Blum P., 2012. Greenhouse gas emission savings of ground source heat pump systems in Europe: A review. Renewable and Sustainable Energy Reviews, 16(2): 1256 -1267.

Chinese D., Meneghetti A., Cardin G., 2005. Waste-to-energy based greenhouse heating: exploring viability conditions through optimisation models. Renewable Energy, 30(10): 1573 - 1586.

Congedo P.M., Colangelo G., Starace G., 2012. CFD simulations of horizontal ground heat exchangers: A comparison among different configurations. Applied Thermal Engineering, (33-34): 24 - 32.

Garcia J.L, Plaza S.D., Navas L.M., Benavente R.M., Luna L., 1998. Evaluation of the Feasibility of Alternative Energy Sources for Greenhouse Heating. J. Agric. Engng Res., 69: 107 - 114.

Hepbasli A., 2011. A comparative investigation of various greenhouse heating options using exergy analysis method. Applied Energy, 88(12): 4411 - 4423.

Ozenger O., Hepbasli A., 2005. Experimental performance analysis of a solar assisted ground-source heat pump greenhouse heating system Energy and Buildings, 37(1): 101 - 110.

Panwai N.L., Kaushik S.C., Kothari S., 2011. Solar greenhouse an option for renewable and sustainable farming. Renewable and Sustainable Energy Reviews, 15(8): 3934 - 3945.

Rutkowski K., Wojciech J., 2009. Horizontal temperature profile in selected glasshouses. Media4u Magazine, 11: 32 - 37

Santamouris M., Balaras C.A., Dascalaki E., Vallindras M., 1994. Passive solar agricultural greenhouses: A worldwide classification and evaluation of technologies and systems used for heating purposes. Solar Energy, 53(6): 511 - 426.

THE TRANSPORT CHARACTERISTICS OF SUBURB AREAS

Miroslav Růžička*, Boleslav Kadleček, Martin Kotek

Czech University of Life Sciences Prague, 16521 Prague 6 – Suchdol, Czech Republic, Phone: +420 224 383 106, E-mail: ruzicka@tf.czu.cz

Abstract

Characteristics of suburb areas from the point of generated transport is determined by many attributes (density of settlement, balance of job opportunities and accommodation, mix of areas use, public facilities, parameters of transport accessibility, centrality, transport speeds etc.). Presented attributes were find out and determined on the base of several years traffic and household surveys. These surveys were carried out in 15 chosen localities, suburb settlements, within radial distance from Prague's city centre up to 20 (km). Some of these localities are part of former municipalities but other ones are newly built in the open space of countryside. The traffic surveys were carried out during time of morning peak. Traffic intensities per quarter of hour, vehicles' occupancy, structure of traffic flow, number of public transit passengers, frequency of bus lines, number of households per square and other variables were been finding out there. The results do not prove generally accepted expectation that larger suburb settlements have lower density of households. The study has proved as well that the spatial development of chosen suburb municipalities is not in accordance with the public transit supply. Concurrently the occupancy of passenger cars was app. 1,3 person per vehicle. Morning peak traffic intensities has increased twice from the year 2005 to 2010 on surveyed radial roads to city centre and duration of drive, in several special cases, is in from 50% of time in congestion.

Keywords: suburb areas, transport characteristics

Introduction

The process of urban sprawl, which commonly describes physically expanding urban areas, is a major issue for sustainable development (European Environment Agency, 2006). Urban sprawl is known to represent a significant contribution to the overall energy consumption of a territory for energy needs in buildings and for transport. In fact, for the same standard of insulation, detached houses need more energy for heating than terraced houses (Marique, Reiter, 2010). In suburban residential neighbourhoods mainly composed of detached houses and often located far away from city centres, car ownership is often high and public transport is generally less available, which tends to favour the use of private cars (Marique, Reiter, 2011). An evaluation on the sustainability of these suburban neighbourhoods is necessary and requires appropriate methods and tools, especially as far as the private transport is concerned. In fact, transport energy consumption is rarely taken into account when the sustainability of these suburban structures is studied. Based on data from 32 big cities located all over the world, (Newman, Kenworthy, 1989 and 1999) have highlighted a strong inverse relationship between urban density and transport consumption, but their work is only valid for certain conditions and is often criticized by other works (Mindali et al., 2004; Owens, 1995) mainly for methodological reasons. Banister (1992) applied the same kind of approach to British cities and highlighted, on the basis of statistical data obtained from a national survey, that transport energy consumption is slightly higher in London than in smaller cities, which refutes Newman and Kenworthy's observations. Boarnet and Crane (2001) are also sceptical on the relationship between urban design and transport behaviours. On the basis of several case studies, they estimate that if the use of the soil and the urban form impact transport behaviours, it is through the price of travel (public transport prices are reduced in dense areas). Gordon and Richardson (1997) demonstrated that if fuel prices are included in the analysis, urban density only plays a limited role on energy consumption in transport. Ewing and Cervero (2001) on the basis of a number of case studies, concluded that the impact of urban density on car travel reduction stays marginal. Elasticity is evaluated at−0.05, which means that if the density of a district is multiplied by two, private car commutes are only reduced by 5% because of the rise of congestion. Finally, (Breheny, 1995) has emphasized minor reductions in transport energy consumption thanks to the compact city model. His experiments show that, even under very strict conditions that are difficult to reproduce, energy used in transport could only be reduced by 10 to 15%. There are issues raised around the acceptability of various policy stances, particularly the public acceptability of compaction (Breheny, 1992); it is argued here that suburbanisation has been stimulated by lifestyle choice and that attempts towards urban compaction are futile.

Above cited references provides overview that the topic is really arduous and it is influenced by many local aspects and questions e.g. are there actually more non-work trips than those of work-related to travel; do the most trips occur from suburb to suburb; is a decentralized concentration of cities very sustainable form etc. The increase of suburban settlement, mainly number of inhabitants, surrounding large cities in the Czech Republic was already proved by many studies.

Methods

There were chosen 15 localities within Prague's suburban space; in a radial distance up to 20(km) from the city centre. (see Fig. 1). Some of these suburban settlements are part of the former municipalities (or close to), but some of them were built solitary under the open space of countryside. Built-up area consists of different buildings as family houses (54 % of total square), semi-detached houses (2 %), row houses (8 %) and apartment houses (2 %). Next squares are unfinished constructions (3 %), civic facilities (2 %), plots of land (13 %) and other squares (18 %). The measurement of squares was done by "Geoprohlížeč" see "http://geoportal.cuzk.cz/geoprohlizec". The preciseness of square measurement was app ±1,5% in dependence on the individual's endeavour; but it is possible to say that the preciseness is acceptable for this research purpose. These selected suburbia and survey organisation enabled a surveillance of all generated rides. The traffic surveys were carried out during morning traffic peak (from 6 to 9 a.m.) in ordinary working days (Tues, We, Thu). The aim of the traffic survey was to find out a number of generated rides by passenger cars or by public transit.

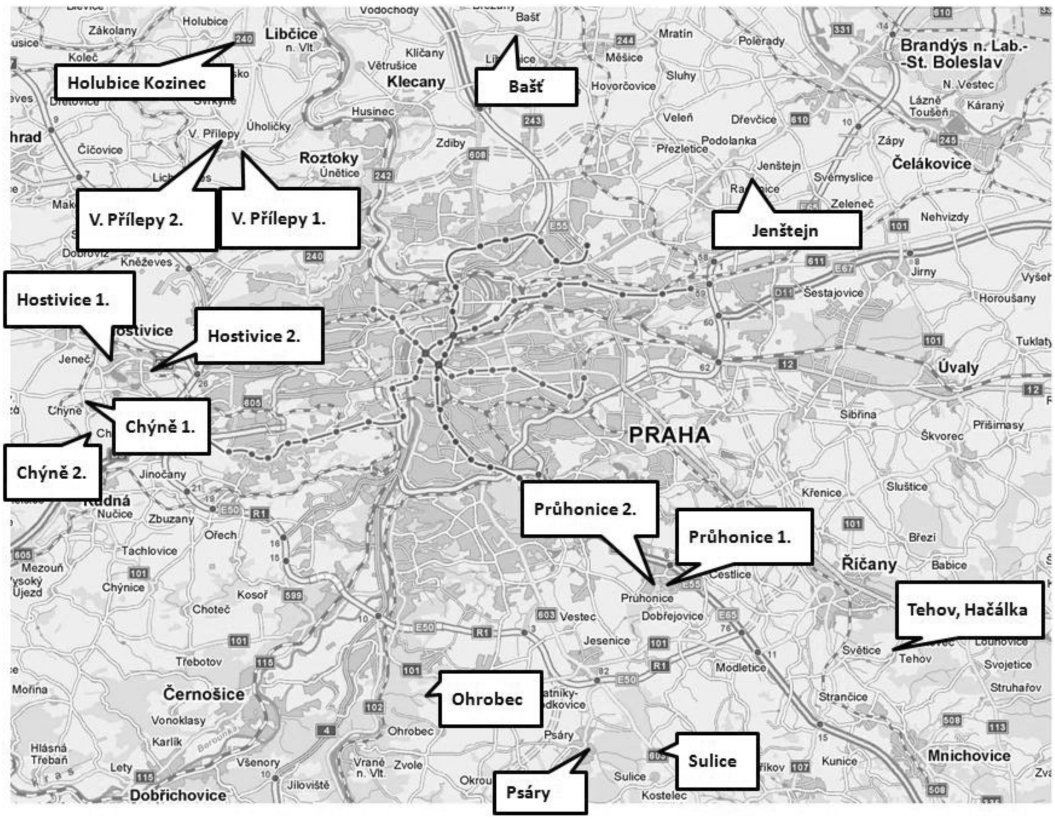

Fig. 1 Map of suburban localities

Further obtained information after the survey processing was: peak hour intensity, occupancy of passenger cars, vehicle categories, distribution of passenger cars according to guessed engine power, number of passengers commuting by public transit, frequency of transit (buses), squares (see above) and other. Simultaneously traffic surveys were conducted on radially oriented roads for several years. These roads have links with ride origins of suburban estates. This study does not involve results of traffic surveys of higher class communications (motorways, speed roads) that are the topic of systematic surveys of state authorities – results of traffic intensities are publicly accessible e.g. state-wide traffic census of the Czech Republic. Drives with the measuring car were carried out on all these roads in the same days of traffic surveys. The car was outfitted with measurement equipment that enabled data recording of: fuel consumption, GPS, time, emission production, speed and others.

Results and discussion

The built-up areas and surrounding building plots of chosen suburban estates are shown on Fig. 2. These suburban estates are distinguished according the total square of plots from small up to 10 (ha), prevailingly in number are middle up to 10 – 25 (ha) and large above 25 (ha). The number of households was found out in these estates. This indicator was found more important than a probable number of official inhabitants. The presented data proves that relation between the total square of estate and households density is not really significant, coefficient of determination R^2 = 0,16. The presumption that suburbia (larger in square) should have lower household density was not confirmed in these selected estates. The type of buildings (see above) significantly influences the relation. Partly it is possible to confirm the presumption at selected suburbia with land square above 40 (ha) but these large estates are not commonly widespread in the Czech Republic.

The Fig. 3 shows a proportion in usage of transit (public transport) and passenger car. Total number of commuting persons was app. 15,460 during three surveyed days. The use of transit reaches from minimum (transit is not supplied there) to the maximal transit use i.e. 48 % for all persons leaving this suburban estate by transport means.

The use of transit is not influenced by the offer of bus departures from the specific locality – coefficient of determination R^2 = 0.16. It is evident that people, who everyday commute, prefer passenger cars regardless number of offered buses and it causes problems linked with congestions, negative environmental impacts, car's costs etc. It is evident that decision to use transit is influenced by many other aspects that should be researched.

Fig. 2 Squares of suburban estates

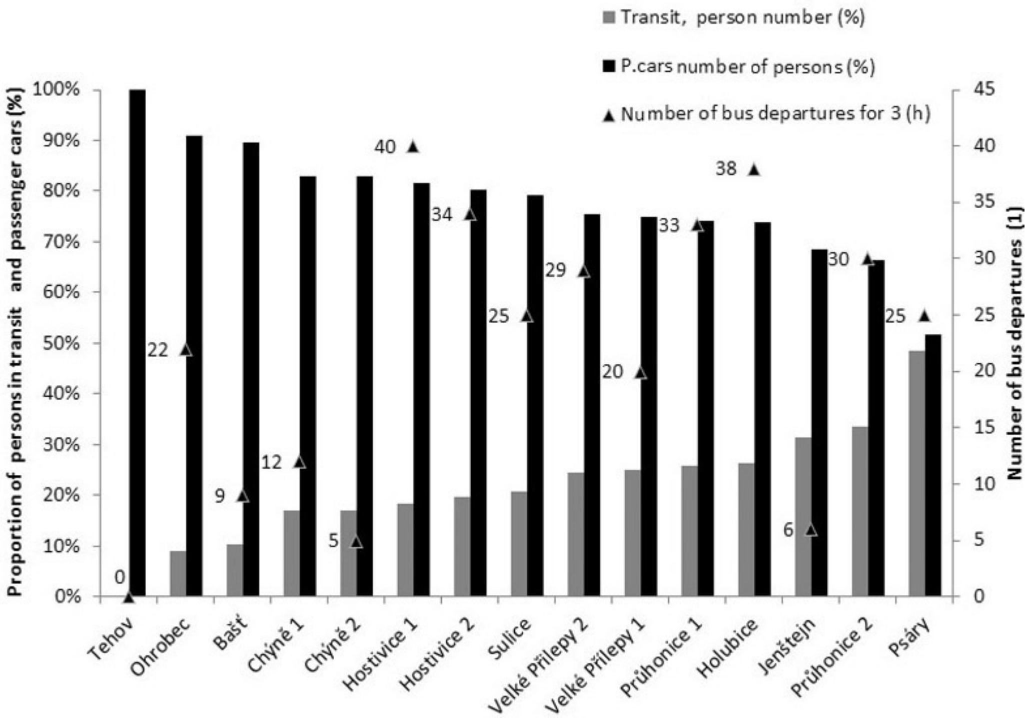

Fig. 3 The comparison of transit or passenger car usage

The occupancy of passenger cars could be taken as another view of transport characteristics. Results of performed surveys point out on a low occupancy i.e. 70 % of cars is occupied by one person only; 23 % occupancy is for two persons and cars with three and more passengers are in proportion 6 %. The average occupancy under carried out survey was 1.37 of passenger per one car.

Results of long term traffic surveys confirmed these expectation - lower class roads (motorways or first class road was not surveyed) radially oriented from the suburban estates to the city centre, have to carry forward the increasing number of vehicles' drives during the last years - as an example can be used the result of traffic surveys carried out on the north-west border of Prague (2nd class roads, duration of survey 3 hours, morning peak, ordinary working day) see Fig. 4.

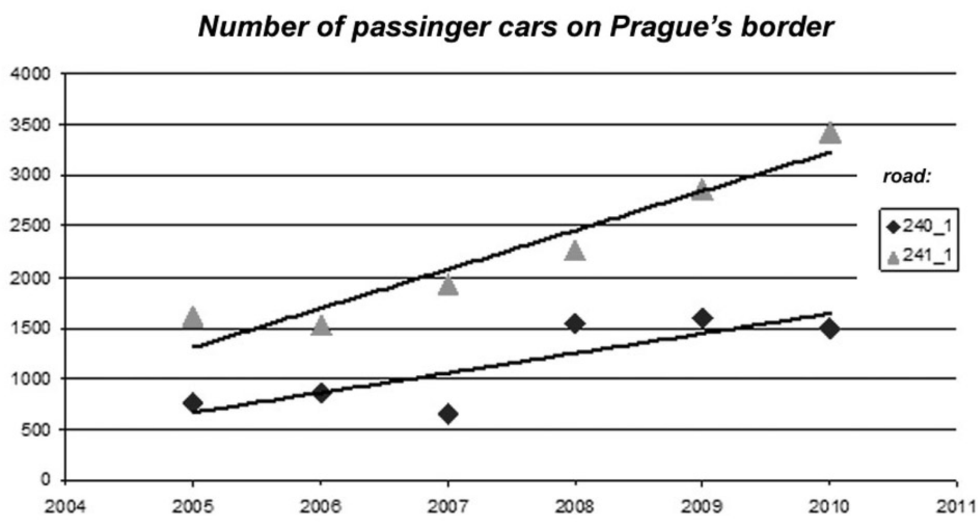

Fig. 4 Increase of passenger car number in years

Conclusion

The process of suburban development is not possible to interrupt or even stop. Several attempts to do it usually failed and were futile. As it was above mentioned the suburbanisation has been stimulated by choice of lifestyle. This paper points out that a way of uncontrolled development brings higher consumption of energy used within a transport. Survey results prove that the decrease of energy consumption and emission production is not possible to reach by the improvement of combustion engine design only (e.g. in a simplified way, number of cars doubled in several localities but energy and emissions are not on the half value). A sense of the paper should be in a recommendation for future transport development. The future passenger car design should involve specific requirements for suburban traffic to save energy and reduce emission production (e.g. Stop and Go systems, alternative energies). Contemporary it is very important to apply and impose strict rules on spatial planning in case that urban sprawl occurs there with all its negative impacts. The suburban development should be conditioned by the simultaneously applied construction of a new transport infrastructure and the high quality offer of public transit.

Acknowledgement

This work was supported by COST TU0902 *„Integrated assessment technologies to support the sustainable development of urban areas“*, Projekt MŠMT LD 11049: “Spotřeba energie dopravou v urbánních a suburbánních územích” *The transport energy consumption in urban and suburban areas*

References:

Banister D., 1992. Energy use, transport and settlement patterns. In: Breheny M., editor. Sustainable development and urban form. London: Pion Ltd, 92: 160–81.

Boarnet M., Crane R., 2001. Travel by design. The influence of urban form on travel. New-York: Oxford University Press.

Breheny M., 1995. The compact city and transport energy consumption. Trans Inst Br Geogr, 20(1): 81-101.

Breheny M., 1992. The Contradictions of the Compact City: A Review, in Breheny, M. (Ed) Sustainable Development and Urban Form. London: Pion, 138-159.

European Environment Agency, 2006. Urban sprawl in Europe. The ignored challenge Final report, 1. Copenhagen: European Environment Agency.

Ewing R., Cervero R., 2001. Travel and the built environment: a synthesis. Transp. Res Rec, 1780: 87-114.

Gordon P., Richardson H.W., 1997. Are compact cities a desirable planning goal? J Am. Plan. Assoc. 63(1): 95-106.

Marique A.F., Reiter S., 2010. A method to assess global energy requirements of suburban areas at the neighbourhood scale. Proceedings of the 7th International IAQVEC Conference on Indoor Air Quality, Ventilation and Energy Conservation in Buildings; 2010 Aug 15–18; Syracuse, New York, USA.

Marique A.F., Reiter S., 2012. A method for evaluating transport energy consumption in suburban areas, Elsevier, Environmental Impact Assessment Review, 33: 1–6.

Mindali O., Raveh A., Salomon I., 2004. Urban density and energy consumption: a new look at old statistics. Transp Res Part A, 38: 143–62.

Newman P., Kenworthy J.R., 1989. Cities and automobile dependence: a sourcebook. Aldershot: Gower Publishing Co.

Newman P., Kenworthy J.R., 1999. Sustainability and cities: overcoming automobile dependence. Washington DC: Island Press.

Owens S., 1995. A response to Michael Breheny. Trans Inst Br Geogr, 20: 381–386.

EVALUATION OF DIFFERENT SOIL TILLAGE TECHNOLOGIES OF GRAIN MAIZE PRODUCTION

Ondřej Šařec, Petr Šařec*, Petr Hájek

Czech University of Life Sciences Prague, 165 21 Prague 6– Suchdol, Czech Republic
Phone: +4202-24383147, Fax: +4202-24383155, E-mail: psarec@tf.czu.cz

Abstract

Several years already, field monitoring and measurements focused on technological and economic comparison of conventional and reduced-tillage technologies of soil cultivation and drilling of grain maize have been carried out in around 10 farm businesses located in sugar-beet and maize production areas of the Czech Republic. The paper presents seven-year results starting from the production year 2005/06, where almost 80 fields were monitored over the period in question. In general, reduced-tillage technology prevailed, and was even solely employed in the maize production area. In each of the years in question except the production year 2007/08, average wheat yield produced by the reduced-tillage technology slightly surpassed the yield of the conventional technology. The seven-year average difference in grain yields amounted then to 11 %, i.e. to 1.02 t.ha^{-1}. Higher yields were reached in the maize production area. Over the period in question, reduced-tillage technology demonstrated by 19 % lower fuel consumption, by 17 % lower labour consumption and by 2 % lower total direct costs. The average unit costs per ton of production gained using conventional technology thus surpassed those gained using reduced-tillage technology by approximately 10 %., i.e. by 236 CZK.t^{-1}.

Keywords: grain maize, conventional technology, reduced tillage, costs, fuel consumption, labor consumption

Introduction

In spite of its tropical origin, maize is a crop that is grown nowadays in various climatic conditions. This practice has been enabled by evolvement of breeding, which resulted in the fact that solely hybrid seed is applied at the present time. Maize growers are thus wholly dependent on specialized seed improvers. Maize grown for grain plays an important role in alimentation of population, but as well in livestock feeding where it ranks among the most important feeding crops (Vrzal, 1995).

In the Czech Republic, maize cultivation area increases yearly, e.g. from around 40 thousand hectares in the year 2000 to 121 thousand hectares in 2012. In the conditions of the Czech Republic, a range of varieties starting with very early hybrids with 200 FAO, i.e. 120 days of vegetative period, to late hybrids with 600 FAO, i.e. 142 to 148 days of vegetative period, is used (Petr, Húska, 1997). Moth-resistant Bt maize is one of the few genetically modified crops allowed for growing in the Czech Republic at the moment. Its acreage had increased gradually up to the year 2008, when it was 8 380 ha, but decreased since then to 3 053 ha in the year 2012. The seed price and strict regulations concerning GM grain handling are the key reasons of the decline (Kůst, Potměšilová, 2012).

From the point of view of maize stand establishment, it is clear that ploughing is still widely used in the Czech Republic. Long-time experience shows that no technology of soil cultivation should be left out or prioritized, because each has its pros and cons (Šařec et al., 2008). The most important is always the way of implementation of a chosen technology. Especially farmers producing in prone fields must give an increased attention to agronomical practices, because there is a higher erosion danger with nutrient downwash related to it than on the flat.

Soil erosion is a major environmental problem. Recent estimates put the total soil loss from agricultural land in Europe between 3 and 40 t.ha^{-1}.yr^{-1} (Verheijen et al., 2009). In the intensive agricultural systems generally used in Europe the effects of erosion on crop yields mainly occur due to the reduction of the amount of water the soil can store and make available to plants. If soil depth is sufficient, yield losses may be very small as the nutrient losses due to erosion can be compensated for by the increased application of fertilizers (Bakker et al., 2004, 2007). However, the implementation of conservation agriculture and conservation tillage is clearly lagging in Europe in comparison to other continents (Holland, 2004; Lahmar, 2010; Wauters et al., 2010).

Over the last three decades, there has been considerable research on the effects of conservation tillage on crop yield in many areas in Europe. Often, detailed reports were published both on the economic and environmental effects of conservation agriculture (Lopez, Arrue, 1997). However, the evidence from different studies often seems contradictory and is therefore difficult to interpret (Cantero-Martinez et al., 2003; Lopez, Arrue, 1997). This is to be expected: both the agro-environmental conditions as well as the type of conservation tillage applied vary greatly between individual studies.

According to the analysis of 563 observations carried out by Van den Putte et al. (2010), no significant yield effect of soil tillage practices was observed for fodder maize, potatoes, sugar beet and spring cereals. Only for grain maize and winter cereals a significant yield reduction occurred under conservation agriculture. For winter cereals the effect was limited but the yield reduction for grain maize was considerable. Tillage depth had a clear effect on relative crop yields. Reduced tillage resulted in crop yields that were similar to those of conventional ploughing, for all crops except maize. Particularly on sandy soils, grain maize was not performing well. Deeper reduced-tillage to more than 0.15 meters on clay-loam soils though demonstrated comparable grain maize yields as conventional tillage. It seems therefore advisable that farmers starting with the implementation of conservation tillage use a sufficient tillage depth so that yields are maintained. In a later stage, tillage depth may be reduced as this may lead to a reduction of operational costs (Van den Putte et al., 2010).

The reasons for the crop effect of the tillage technology are not entirely clear. Swiss scientists did experiments on rooting behavior of winter cereals and maize. For maize, conventional ploughing resulted in more and finer roots than no-tillage, likely due to the lower soil strength, the higher soil temperature during early growth and a more uniform phosphorus availability with soil depth (Qin et al., 2006). Birkas and Gyuricza (2000) carried out experiments on grain maize from 1977 to 1981 and from 1992 to 1996. They conclude that in the second period, differences in soil conditions indeed resulted in significant yield differences, with the best results for conventional ploughing and other techniques that thoroughly loosened the soil over a large depth.

A comparison of the different components of the total costs revealed that reduced-tillage required larger machinery and herbicide costs, but these costs were largely offset by reduced operating costs (Sanchez-Giron et al., 2004, 2007). In various other studies, it was concluded that slightly lower crop yields can be offset by the reduced fuel inputs and labour consumption (Bonciarelli and Archetti, 2000; Gemtos et al., 1998; Tebrügge, 2000). However, this may be dependent on local situation and farm-specific properties such as farm size (Sanchez-Giron et al., 2007), cropping system, etc.

Material and method

During seven production years from 2005/06 to 2011/12 at eleven farm businesses located in the beet production region and two located in the maize production region of the Czech Republic, field monitoring and measurements focused on different maize for grain production technologies from the viewpoint of conventional an reduced-tillage technologies were carried out. The total number amounted to 37 monitored fields.

The key aim of the work is to verify which technologies of maize for grain stand establishment are profitable.

The following items were monitored or measured:

- characteristics of individual fields (acreage, cadastre, preceding crop, plant residue treatment, year of last manure application ...),
- soil characteristics (bulk density, penetration resistance ...) - not analysed in this paper,
- crop stand characteristics (number of plants per square meter ...) - not analysed in this paper,
- data on every field operation performed (date, machinery used, its workrate, fuel consumption, age and purchasing price, material used, its application rate and price, and other supplementary information)

The latter enabled to calculate machinery and material costs. Subsequently, total costs of a field operation are the sum of the two above mentioned. The total costs could be as well increased due to possible manure application two or three years prior to the maize. Accordingly, for the operations of manure and lime treatment of the maize, only 40 % of the machinery and material costs are calculated in the first year. The total costs do not include costs of lease or ownership of land, and overhead costs.

Results and discussion

During four production years starting in 2005, trials were set up in 77 fields of the beet and maize production regions. Reduced-tillage technology of maize for grain growing was employed in 52 cases, conventional in 25 cases. In each production year, the total average yield gained from the trial fields exceeded the average of the Czech Republic by 21 to up to 60 %.

Prior to maize sowing, manure was applied in more than 30 % of trial fields managed by conventional technology and in mere 15 % of trial fields within reduced-tillage technology. Winter wheat preceded maize in more than 70 % of the trial fields. Concerning the types of maize varieties, those of lower FAO, i.e. maturing very early or early, prevailed.

The most frequent tillage procedures within the reduced-tillage technology consisted of two soil cultivations followed by one or two operations of seedbed preparation. Deeper soil loosening to more than 0.15 meters was performed in only in one fifth of the cases.

Within the conventional technology, the most frequent tillage procedures consisted of a stubble cultivation followed by ploughing and one or two operations of seedbed preparation.

Disc cultivators prevailed within conventional technologies, whereas within the reduced-tillage technologies, where two stubble cultivations were common, tine cultivators were more frequent, particularly for the second cultivation.

Over the period of four production years, the average grain yield of all 77 fields was 10.27 $t.ha^{-1}$. Tab. 1 shows average maize grain yields at 14 % moisture according to several criteria. Reduced-tillage technology reached yields exceeding those of conventional technology in all of the monitored production years except the year 2007/08. The overall difference between the average yields of the technologies in question amounted to 10.6 %, i.e. 1.02 $t.ha^{-1}$, and was statistically significant ($p=0{,}01356$) Concerning regionalization, solely reduced-tillage technology was employed in the more arid conditions of maize production area, where the average yield surpassed significantly the one given by beet production area by 13.1 % ($p=0{,}01313$). Fig. 1 combines both above mentioned criteria, i.e. tillage technology and production area. Within reduced-tillage technology, yields in maize production area generally surpassed those of beet production area. Within beet production area, reduced-tillage technology displayed higher grain yields than conventional technology except the production year 2007/08.

With fertilizer application during maize sowing, which was generally the case of reduced-tillage technology, the average yield at 14 % moisture slightly exceeded the yield produced when no fertilizers were applied while sowing, i.e. by 3.0 %. Small frequencies and uneven distribution of cases in individual categories may have influenced the results and have impeded to draw conclusions.

Tab. 1 Average maize for grain yields at 14 % moisture and frequencies of cases according to the tillage technology and other criteria over the whole monitored period

	Tillage Technology				**Aggregate**	
	Reduced		**Conventional**		**Yield* [$t.ha^{-1}$]**	**Frequency**
	Yield* [$t.ha^{-1}$]	**Frequency**	**Yield* [$t.ha^{-1}$]**	**Frequency**		
Production Year						
2005/06	9.10	6	8.54	4	**8.87**	**10**
2006/07	10.60	6	9.80	4	**10.28**	**10**
2007/08	9.45	7	9.97	4	**9.64**	**11**
2008/09	11.45	8	9.75	4	**10.88**	**12**
2009/10	10.43	9	9.62	3	**10.23**	**12**
2010/11	11.17	9	9.47	3	**10.74**	**12**
2011/12	11.61	7	10.05	3	**11.14**	**10**
Production Area						
Beet	10.37	40	9.59	25	**10.07**	**65**
Maize	11.39	12	—	—	**11.39**	**12**
Fertilizers at Sowing						
No	10.71	16	9.64	20	**10.11**	**36**
Yes	10.56	36	9.38	5	**10.42**	**41**
Aggregate	**10.61**	**52**	**9.59**	**25**	**10.27**	**77**

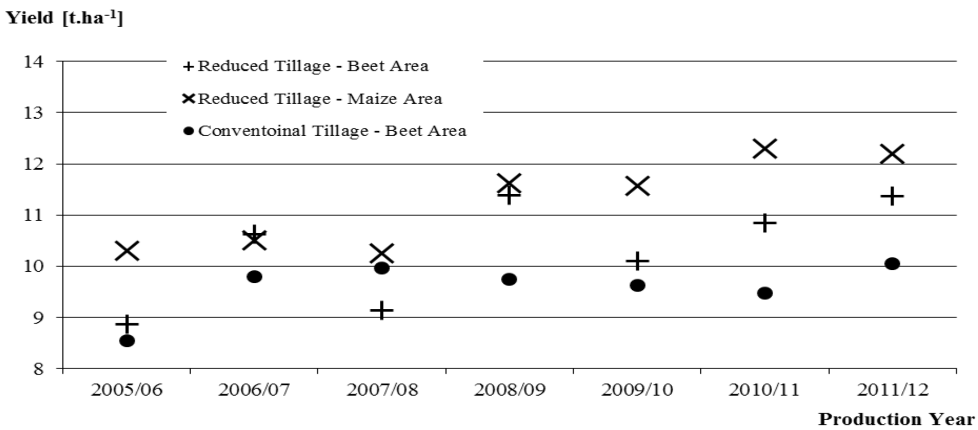

Fig. 1 Graph of averages of maize grain yields according to tillage technology and to production area in individual production years

Tab. 2 Average fuel and labour consumption, average total costs, and average costs per ton of maize grain production at 14 % moisture according to the tillage technology and other criteria over the whole monitored period

	Fuel Consumption [$l.ha^{-1}$]	Labour Consumption [$hrs.ha^{-1}$]	Average Costs	
			Total [$CZK.ha^{-1}$]	Unit [$CZK.t^{-1}$]
Tillage Technology				
Reduced	73.01	5.24	21174.42	2057.48
Conventional	90.27	6.30	21646.24	2293.84
Production Area				
Beet	81.27	5.85	21363.48	2184.13
Maize	64.21	4.14	21133.33	1863.86
Fertilizers at Sowing				
No	77.60	5.76	21209.89	2139.05
Yes	79.50	5.43	21430.98	2129.98
Aggregate	**78.61**	**5.58**	**21327.61**	**2134.22**

Among technological and economic indicators, the following were monitored or calculated (see Tab. 2): fuel consumption, labour consumption, total costs composed of machinery and material costs, and unit costs per ton of production at 14 % moisture.

With respect to the tillage technologies, the average fuel consumption of the reduced-tillage technology was by 19.1 % lower than the one of the conventional technology, and the overall labour consumption again lower by 16.9 %. The average total costs of the reduced-tillage technology were then demonstrated by 2.2 % lower value than those of the conventional technology. Together with the higher grain yield at 14 % moisture, the reduced-tillage technology costs per ton of production at 14 % moisture were by 236 $CZK.t^{-1}$, i.e. by 10.3 %, lower than using conventional technology. The differences according to the tillage technology were statistically highly significant in the cases of fuel (p=0,000000004) and labour (p=0,00004) consumptions, and unit costs (p=0,00969). The results rendered by the conventional technology may have been adversely influenced by uneven distribution of application of organic fertilisers, which is cost and time consuming, and by uneven distribution to production areas. Also evaluation of the results according to the other criteria, such as production area or fertilizer application at sowing etc., is only informative due to small frequencies and uneven distribution of cases in individual categories. Concerning production areas, maize production area returned more favourable results than beet production area. The differences were statistically highly significant in terms of labour (p=0,0000001) and fuel (p=0,00002) consumption and also unit costs (p=0,00650), particularly due to reduced-tillage technology being the only one used in maize production area. The cases of fertilizers applied at sowing showed slightly lower value of unit costs compared to common sowing due to slightly higher grain yields and total costs higher by only 1.0 %. No difference, e.g. in labour or fuel consumption etc., was statistically significant.

Conclusions

- The average fuel consumption of the reduced-tillage technology was by 10.6 % lower than that of the conventional technology, the labour consumption was lower by 16.9 %, and the total costs by only 2.2 %. Yields reached by reduced-tillage were higher by 10.6 %, and thus the unit costs lower by 10.3 %. All the mentioned differences according to soil tillage except for the total costs were significant.
- From the point of view of economics as well as of labour and fuel consumption, the reduced-tillage technology proved to be more than an adequate alternative to the conventional technology.

Acknowledgment

This work was supported by the project NAZV QH72257.

Reference

Bakker M. M., Govers G., Rounsevell M. D. A., 2004. The crop productivity-erosion relationship: an analysis based on experimental work. Catena, 57: 55 – 76.

Bakker M. M., Govers G., Jones R. A., Rounsevell M. D. A., 2007. The effect of soil erosion on Europe's crop yields. Ecosystems, 10: 1209 – 1219.

Birkas M., Gyuricza C., 2000. Results of long-term trials on the direct drilling of maize in Hungary. Bodenkultu, 51: 19 – 34.

Bonciarelli F., Archetti R., 2000. Energy saving through reduction of soil tillage. In: 15th ISTRO Conference, Fort Worth, TX, USA.

Cantero-Martinez C., Angas P., Lampurlanes J., 2003. Growth, yield and water productivity of barley (hordeum vulgare l.) affected by tillage and N fertilization in Mediterranean semiarid, rainfed conditions of Spain. Field Crops Research, 84: 341 – 357.

Gemtos T. A., Galanopoulou S., Kavalaris C., 1998. Wheat establishment after cotton with minimal tillage. European Journal of Agronomy, 8, 137 – 147.

Holland J., 2004. The environmental consequences of adopting conservation tillage in Europe: reviewing the evidence. Agriculture Ecosystems and Environment, 103: 1 – 25.

Kůst F., Potměšilová, J., 2012. Situation and Outlook Report - December cereals 2012. Prague: MZe CR, 107. (in Czech)

Lahmar R., 2010. Adoption of conservation agriculture in Europe lessons of the KASSA project. Land Use Policy, 27: 4 – 10.

Lopez M., Arrue J., 1997. Growth, yield and water use efficiency of winter barley in response to conservation tillage in a semi-arid region of Spain. Soil and Tillage Research, 44: 35 – 54.

Petr J., Húska J., 1997. Special plant production – I. Prague: CULS, 193. (in Czech)

Qin R. J., Stamp P., Richner W., 2006. Impact of tillage on maize rooting in a cambisol and luvisol in Switzerland. Soil and Tillage Research, 85: 50 – 61.

Sanchez-Giron V., Serrano A., Hernanz J., Navarrete L., 2004. Economic assessment of three long-term tillage systems for rainfed cereal and legume production in semiarid central Spain. Soil and Tillage Research, 78: 35 – 44.

Sanchez-Giron V., Serrano A., Suarez M., Hernanz J., Navarrete L., 2007. Economics of reduced tillage for cereal and legume production on rainfed farm enterprises of different sizes in semiarid conditions. Soil and Tillage Research, 95: 149 – 160.

Šařec P., Šařec O., Gil K., 2008. Field trials on grain maize cultivation technologies in 2004, 2005 and 2006. Annales UMCS, Sec. E-Agricultura, 63, no. 2: 21 - 27.

Tebrügge F., 2000. Long-term no-tillage as a tool to protect the environment, results of 20 year field trials on different kinds of soil in different crop rotations. In: 15th ISTRO Conference, Fort Worth, TX, USA.

Van den Putte, An et al., 2010. Assessing the effect of soil tillage on crop growth: A meta-regression analysis on European crop yields under conservation agriculture. European Journal of Agronomy, 33: 231 - 241.

Verheijen F. G. A. et al., 2009. Tolerable versus actual soil erosion rates in Europe. Earth-Science Reviews, 94: 23 – 38.

Vrzal J., Novák D. et al., 1995. Basics of maize cultivation and annual forage. Prague: MZe CR, 32. (in Czech)

Wauters E., Bielders C., Poesen J., Govers G., Mathijs E., 2010. Adoption of soil conservation practices in Belgium: an examination of the theory of planned behaviour in the agri-environmental domain. Land Use Policy, 27: 86 – 94.

EVALUATION OF DIFFERENT SOIL TILLAGE METHODS OF WINTER WHEAT PRODUCTION

Petr Šařec*, Ondřej Šařec

Czech University of Life Sciences Prague, 165 21 Prague 6– Suchdol, Czech Republic
Phone: +4202-24383147, Fax: +4202-24383155, E-mail: psarec@tf.czu.cz

Abstract

Several years already, field monitoring and measurements focused on technological and economic comparison of conventional and reduced-tillage technologies of soil cultivation and drilling of winter wheat have been carried out in around 40 farm businesses located in all of the districts of the Czech Republic. The paper presents six-year results starting from the production year 2006/07, where around 240 fields were monitored over that period. In general, reduced-tillage technologies prevailed. Conventional technology was more frequent only in potato production region. In each of the years in question, average wheat yield produced by the reduced-tillage technology slightly surpassed the yield of the conventional technology. The six-year average difference in yields amounted then to 7.7 %, i.e. to 0.52 t.ha^{-1}. Over the six years, the highest yields were reached in sugar-beet production area, the lowest on the other hand in potato production area. But the difference in average yield among the latter mentioned and the forage and wheat production areas were minor. Over the period in question, reduced-tillage technology demonstrated by 20 % lower fuel consumption, by 19 % lower labour consumption and by 5 % lower total direct costs. The average unit costs per ton of production gained using conventional technology thus surpassed those gained using reduced-tillage technology by 11 %., i.e. by 314 CZK.t^{-1}.

Key words: winter wheat, conventional technology, reduced tillage, costs, fuel consumption, labor consumption

Introduction

Long term field trials as well as farming experience in the Czech Republic show that cereals in general respond favourably to reduction of depth and intensity of tillage, i.e. the measures of conservation agriculture. Conservation tillage is primarily used as a means to protect soils from erosion and compaction, to conserve soil moisture and to reduce production costs (Holland, 2004). Soil erosion is, also in Europe, a major environmental problem. Recent estimates put the total soil loss from agricultural land in Europe between 3 and 40 t.ha^{-1}.yr^{-1} (Verheijen et al., 2009). In the intensive agricultural systems generally used in Europe, the effects of erosion on crop yields mainly occur due to the reduction of the amount of water the soil can store and make available to plants. If soil depth is sufficient, yield losses may be very small as the nutrient losses due to erosion can be compensated for by the increased application of fertilizers (Bakker et al., 2004 and 2007). However, the implementation of conservation agriculture and conservation tillage is clearly lagging in Europe in comparison to other continents (Holland, 2004; Lahmar, 2010; Wauters et al., 2010).

Over the last three decades, there has been considerable research on the effects of conservation tillage on crop yield in many areas in Europe. Often, detailed reports were published both on the economic and environmental effects of conservation agriculture (e.g. Lopez, Arrue, 1997). However, the evidence from different studies often seems contradictory and is therefore difficult to interpret (e.g. Cantero-Martinez et al., 2003; Lopez, Arrue, 1997). This is to be expected: both the agro-environmental conditions as well as the type of conservation tillage applied vary greatly between individual studies.

According to the analysis of 563 observations carried out by Van den Putte et al. (2010), no significant yield effect of soil tillage practices was observed for fodder maize, potatoes, sugar beet and spring cereals. Only for grain maize and winter cereals a significant yield reduction occurred under conservation agriculture. For winter cereals the effect was limited but the yield reduction for grain maize was considerable. Tillage depth had a clear effect on relative crop yields. Reduced tillage resulted in crop yields that were similar to those of conventional ploughing, for all crops except maize. Particularly on sandy soils, grain maize was not performing well, and winter cereal yield was also slightly reduced. Deeper reduced-tillage to more than 0.15 meters though demonstrated similar (on sandy soils) or even higher (on clay-loam soils) winter cereal yields than conventional tillage. It seems therefore advisable that farmers starting with the implementation of conservation tillage use a sufficient tillage depth so that yields are maintained. In a later stage, tillage depth may be reduced as this may lead to a reduction of operational costs (Van den Putte et al., 2010).

The reasons for the crop effect of the tillage technology are not entirely clear. Swiss scientists did experiments on rooting behavior of winter cereals and maize. For winter cereals, no significant effect on root development was found (Qin et al., 2004).

For winter wheat production, reduced-tillage technology of soil cultivation and stand establishment are frequently employed in the Czech Republic. When choosing tillage technology, it is necessary to respect agricultural and ecological conditions. At large, the most suitable conditions for tillage depth and intensity reduction are on medium-textured soils with higher natural fertility in drier conditions of maize and beet production regions (Procházková, Dovrtěl, 2000; Horák et al., 2007).

Reduced-tillage technology of soil cultivation and winter wheat stand establishment are often applied to heavy-textured soils, where soil environment frequently impede quality stand establishment using conventional soil cultivation technology including ploughing. In such case, reduced-tillage technology is practically the only way of stand establishment. Replacing ploughing with a shallow soil loosening followed by winter wheat sowing using no-till drills is a suitable alternative (Hůla, et al., 2008).

A comparison of the different components of the total costs revealed that reduced-tillage required larger machinery and herbicide costs, but these costs were largely offset by reduced operating costs (Sanchez-Giron et al., 2004 and 2007). In various other studies, it was concluded that slightly lower crop yields can be offset by the reduced fuel inputs and labour consumption (Bonciarelli, Archetti, 2000; Gemtos et al., 1998; Tebrügge, 2000). However, this may be dependent on local situation and farm-specific properties such as farm size (Sanchez-Giron et al., 2007), cropping system, etc.

Material and methods

During six production years from 2006/07 to 2011/12 at around 40 farm businesses in all of the districts of the Czech Republic, field monitoring and measurements focused on different winter wheat production technologies from the viewpoint of conventional an reduced-tillage technologies were carried out. The total number amounted to 243 monitored fields.

The key aim of the work is to verify which technologies of winter wheat stand establishment are profitable.

The following items were monitored or measured:

- characteristics of individual fields (acreage, cadastre, preceding crop, plant residue treatment, year of last manure application ...),
- soil characteristics (bulk density, penetration resistance ...),
- crop stand characteristics - not analysed in this paper,
- data on every field operation performed (date, machinery used, its workrate, fuel consumption, age and purchasing price, material used, its application rate and price, and other supplementary information)

The latter enabled to calculate machinery and material costs. Subsequently, total costs of a field operation are the sum of the two above mentioned. The total costs could be as well increased due to possible manure application two or three years prior to the winter wheat. Accordingly, for the operations of manure and lime treatment of the winter wheat, only 40 % of the machinery and material costs are calculated in the first year. The total costs do not include costs of lease or ownership of land, and overhead costs.

Results and discussion

During six production years starting in 2006/07, trials were set up in 243 fields located in all of the districts of the Czech Republic. Reduced-tillage technology of winter wheat growing was employed in 172 cases, conventional in 71 cases, i.e. approximately two times less frequently. In each production year, the total average winter wheat yield gained from the trial fields exceeded the average of the Czech Republic by 26 in 2007/08 to up to 48 % in 2011/12.

Prior to winter wheat sowing, manure was applied only in 28 out of 243 trial fields, i.e. in ten fields managed by reduced tillage and in eighteen managed by conventional technology. Winter rape preceded winter wheat in more than a half of the trial fields.

The most frequent tillage procedures within the reduced-tillage technology consisted of two soil cultivations, followed in some cases by a seedbed preparation.

Tab. 1 Average winter wheat seed yields and frequencies of cases according to the tillage technology and other criteria over the whole monitored period

	Tillage Technology				Aggregate	
	Reduced		Conventional		Yield [t.ha^{-1}]	Frequency
	Yield [t.ha^{-1}]	Frequency	Yield [t.ha^{-1}]	Frequency		
Production Year						
2006/07	7.23	31	6.69	14	**7.07**	**45**
2007/08	7.60	30	6.92	14	**7.39**	**44**
2008/09	7.01	30	7.00	13	**7.01**	**43**
2009/10	6.81	32	6.75	11	**6.79**	**43**
2010/11	7.91	33	7.09	11	**7.70**	**44**
2011/12	7.06	16	5.89	8	**6.67**	**24**
Production Area						
Forage	6.90	20	6.32	5	**6.78**	**25**
Potato	6.60	9	6.55	26	**6.56**	**35**
Cereal	6.91	50	6.33	13	**6.79**	**63**
Beet	7.72	77	7.28	27	**7.61**	**104**
Maize	7.28	16	—	—	**7.28**	**16**
Organic Fertilisers						
No	6.99	38	7.34	9	**7.06**	**47**
Yes	7.38	134	6.69	62	**7.16**	**196**
Fertilizers at Sowing						
No	7.31	111	6.77	71	**7.10**	**182**
Yes	7.26	61	—	—	**7.26**	**61**
Aggregate	**7.29**	**172**	**6.77**	**71**	**7.14**	**243**

Within the conventional technology, the most frequent tillage procedures consisted of stubble cultivation followed by ploughing, and seedbed preparation done once or twice.

Disc cultivators prevailed within conventional technologies, whereas within the reduced-tillage technologies, where two stubble cultivations were common, tine cultivators were more frequent, particularly for the second cultivation.

Over the period of three production years, the average wheat yield of all 243 fields was 7.14 t.ha^{-1}. Tab. 1 shows average wheat yields according to several criteria. Reduced-tillage technology reached yields exceeding slightly those attained by conventional technology in all of the production years in question. Concerning regionalization, the highest average yield demonstrated beet production area, followed by maize production area where only reduced-tillage technology was used. Potato production area, where conventional technology only prevailed, showed the less favourable. Concerning organic fertilisers, if those were applied, which was the majority of cases (81 %), the average yield attained by merely 1.4 % higher value. With fertilizer application during winter wheat sowing, which was solely the case of reduced-tillage technology, the average yield exceeded the yield produced when no fertilizers were applied while sowing by 2.3 %. Relatively small frequencies and uneven distribution of cases in individual categories may have influenced the results.

Among technological and economic indicators, the following were monitored or calculated (see Tab. 2): sowing rates, penetration resistance at the depth of 0.2 m, fuel consumption, labour consumption, total costs composed of machinery and material costs, and unit costs per ton of production.

Tab. 2 Average sowing rates, penetration resistance at the depth of 0.2 m, fuel and labour consumption, average total costs, and average costs per ton of winter wheat production according to the tillage technology and other criteria over the whole monitored period

	Sowing Rate [kg.ha^{-1}]	Penetration Resistance at 0.2 m [MPa]	Fuel Consumption [l.ha^{-1}]	Labour Consumption [hrs.ha^{-1}]	Average Costs Total [CZK.ha^{-1}]	Average Costs Unit [CZK.t^{-1}]
Tillage Technology						
Reduced	193.4	4.04	58.7	3.69	18 744.85	2 655.88
Conventional	202.5	2.74	74.0	4.56	19 652.38	2 970.02
Production Area						
Forage	194.9	4.72	62.8	3.90	17 203.60	2 580.87
Potato	193.7	2.34	67.1	4.36	19 468.57	3 039.79
Cereal	193.4	3.71	63.6	4.02	18 172.00	2 789.80
Beet	196.5	3.57	63.0	3.85	19 577.52	2 638.43
Maize	210.9	5.20	54.7	3.39	20 440.38	2 913.41
Organic Fertilisers						
No	180.2	3.92	61.3	3.66	18 380.04	2 664.13
Yes	199.9	3.59	63.6	4.01	19 161.08	2 767.70
Fertilizers at Sowing						
No	202.4	3.41	64.9	4.05	19 319.25	2 808.44
Yes	177.2	4.39	58.2	3.60	18 087.38	2 566.36
Aggregate	**196.1**	**3.66**	**63.2**	**3.94**	**19 010.02**	**2 747.67**

With respect to the tillage technologies, the average fuel consumption of the reduced-tillage technology was by 20.7 % lower than the one of the conventional technology, and the labour consumption was lower by 19.2 %. The same can be stated about the total costs that were also lower with the reduced-tillage technology, namely by 4.6 %. Together with the higher wheat yield, the reduced-tillage technology costs per ton of production were by 314 CZK.t^{-1}, i.e. by 10.6 %, lower than using conventional technology. The forage production area demonstrated the lowest unit costs per ton of production thanks to its lowest average total costs. Evaluation of the results according to the other criteria, such as organic fertilizer application etc., is only informative due to small frequencies and uneven distribution of cases in individual categories.

The fuel and labour consumption as well as the value of total costs were influenced by organic fertilizer application. Also due to almost the same average yield, the unit cost per ton of production exceeded by 3.9 % the average of the cases where no organic fertilisers were applied. Average sowing rates did not differ among tillage technologies and production areas. When fertilisers ware applied at sowing though, sowing rates were by more than 12 % lower. The cases of fertilizers applied at sowing showed by 8.6 % lower value of average unit costs compared to common sowing due to higher yields and slightly lower total costs. Soil penetration resistance at 0.2 m depth was higher by 47 % higher in the fields where reduced-tillage was employed. Concerning production areas, the highest soil resistance was measured at maize production area, the lowest at potato one.

Fig. 1 shows the average values of soil penetration resistance at 0.2 m depth and of winter wheat seed yields in individual production years. Reduced-tillage technology showed higher values than conventional technology. The highest overall penetration resistance values were measured in the production year 2009/10 where average resistance reached 4.26 MPa. On the opposite, substantially smaller resistance values were found in the year 2011/12 with an average of 1.7 MPa, particularly due to the black frost in February 2012. Difference between reduced and conventional tillage soil penetration resistances was minor in that year.

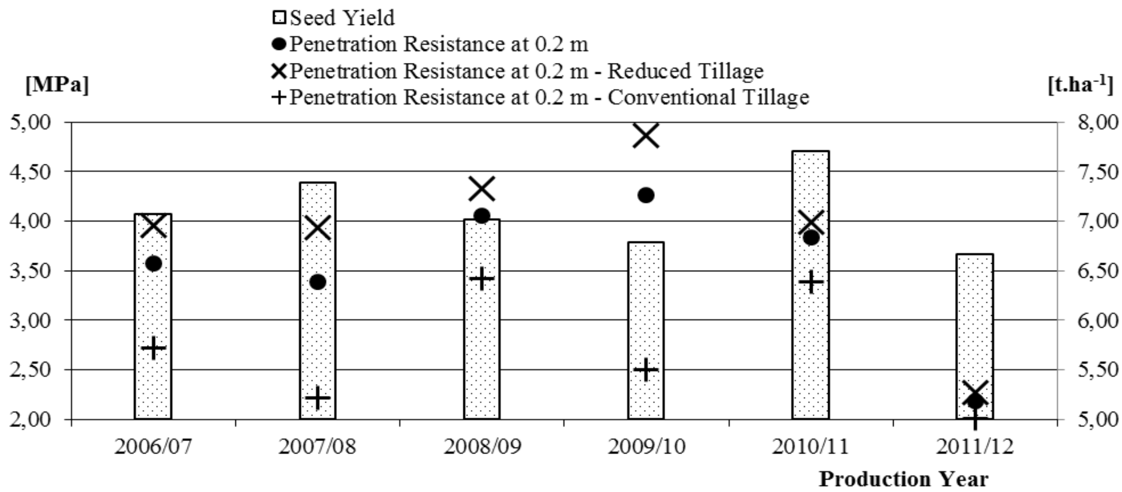

Fig. 2 Graph of soil average penetration resistances at the depth of 0.2 m and of overall winter wheat seed yields according to production years

The production years with high penetration resistance, i.e. the years 2009/10 and 2008/09, attained lower values of winter wheat seed yields. When the penetration resistance values decreased, seed yields increased generally. The year 2011/12 is an exception, probably because of the black frost and resulting freezing of winter crops.

Conclusions

- The average fuel consumption of the reduced-tillage technology was by 20.7 % lower than that of the conventional technology, the overall labour consumption again lower by 19.2 %, and the total costs lower by 4.6 %. Yields reached by reduced-tillage were higher by 7.7 % and thus the unit costs lower by 10.6 %. All the mentioned differences according to soil tillage were significant.
- The beet production area proved to be the most favourable in terms of winter wheat yields.
- From the point of view of economics as well as of labour and fuel consumption, the reduced-tillage technology proved to be an adequate alternative to the conventional technology.

This work was supported by the project NAZV QH72257.

References

Bakker M.M., Govers G., Rounsevell M.D.A., 2004. The crop productivity-erosion relationship: an analysis based on experimental work. Catena, 57: 55–76.

Bakker M.M., Govers G., Jones R.A., Rounsevell M.D.A., 2007. The effect of soil erosion on Europe’s crop yields. Ecosystems, 10: 1209–1219.

Bonciarelli F., Archetti R., 2000. Energy saving through reduction of soil tillage. In: 15th ISTRO Conference, Fort Worth, TX, USA.

Cantero-Martinez C., Angas P., Lampurlanes J., 2003. Growth, yield and water productivity of barley (hordeum vulgare l.) affected by tillage and N fertilization in Mediterranean semiarid, rainfed conditions of Spain. Field Crops Research, 84: 341–357.

Gemtos T.A., Galanopoulou S., Kavalaris C., 1998. Wheat establishment after cotton with minimal tillage. European Journal of Agronomy, 8: 137–147.

Holland J., 2004. The environmental consequences of adopting conservation tillage in Europe: reviewing the evidence. Agriculture Ecosystems and Environment, 103: 1–25.

Horák L., Šařec P., Vozka P., 2007. Porovnání klasického a půdoochranného způsobu založení porostu pšenice ozimé. Agromanuál, 2(8): 56-59. (in Czech)

Hůla J., Procházková B., 2008. Minimalizace zpracování půdy. Prague: Profi Press, 248. (in Czech)

Lahmar R., 2010. Adoption of conservation agriculture in Europe lessons of the KASSA project. Land Use Policy, 27: 4–10.

Lopez M., Arrue J., 1997. Growth, yield and water use efficiency of winter barley in response to conservation tillage in a semi-arid region of Spain. Soil and Tillage Research, 44: 35–54.

Procházková B., Dovrtěl J., 2000. Vliv různého zpracování půdy na výnosy ozimé pšenice. Plant Production, 10(46): 437–442. (in Czech)

Qin R.J., Stamp P., Richner W., 2004. Impact of tillage on root systems of winter wheat. Agronomy Journal, 96: 1523–1530.

Sanchez-Giron V., Serrano A., Hernanz J., Navarrete L., 2004. Economic assessment of three long-term tillage systems for rainfed cereal and legume production in semiarid central Spain. Soil and Tillage Research, 78: 35–44.

Sanchez-Giron V., Serrano A., Suarez M., Hernanz J., Navarrete L., 2007. Economics of reduced tillage for cereal and legume production on rainfed farm enterprises of different sizes in semiarid conditions. Soil and Tillage Research, 95: 149–160.

Tebrügge F., 2000. Long-term no-tillage as a tool to protect the environment, results of 20 year field trials on different kinds of soil in different crop rotations. In: 15th ISTRO Conference, Fort Worth, TX, USA.

Van den Putte A., Govers G., Diels J., Gillijns K., Demuzere M., 2010. Assessing the effect of soil tillage on crop growth: A meta-regression analysis on European crop yields under conservation agriculture. European Journal of Agronomy, 33: 231-241.

Verheijen F.G.A., Jones R.J.A., Rickson R.J., Smith C.J., 2009. Tolerable versus actual soil erosion rates in Europe. Earth-Science Reviews, 94: 23–38.

Wauters E., Bielders C., Poesen J., Govers G., Mathijs E., 2010. Adoption of soil conservation practices in Belgium: an examination of the theory of planned behaviour in the agri-environmental domain. Land Use Policy, 27: 86–94.

THE DEPENDENCE OF THE SPEED MOVEMENT OF THE FOREST ANT (FORMICA RUFA) ON THE TEMPERATURE

Jan Sedlacek*, Josef Zeman

Czech University of Life Sciences Prague, 16521 Prague 6 – Suchdol, Czech Republic, Phone: +420-224383286, Fax: +420-234381850, E-mail: sedlacek@tf.czu.cz

Abstract

Our paper deals with the influence of temperature on the movement activity of the ant – Formica rufa species. Because this kind of ant belongs to the ectotherms, i.e. the body temperature depends on the ambient temperature; its physical activity and biorhythm depend on temperature changes of the environment. The thermo box with adjustable temperature was used for this experiment. The high-speed camera, thermo sensor and shining prisms were in this box. The ant movement was recorded at temperatures of 10 °C, 15 °C, 20 °C, 25 °C, 30 °C, 40 °C and 50 °C. The observed ant was placed in an enclosed area of the visual field of the camera. The ant movement was recorded in this area at different temperatures after a five-minute acclimation. The speed of the ant was calculated by determining the number of frames between the start and the end of the selected limb movement. The software of Gimp was used for this job. The resulting values indicate that the speed of the ant is exponentially dependent on the temperature up to 40 °C. The ant starts moving at about 6.5 °C. The growth of speed is 8.7 $mm.s^{-1}.K^{-1}$. The speed of the ant begins to decrease when the outside temperature increases above 40 ° C.

Key words: Ants, Formica rufa, speed of movement, temperature, thermo box, video of movement.

Introduction

The most of authors are satisfied only with the phenomenological description in describing the behavior of insects depending on the temperature, but from the viewpoint of mathematical propagation models of different kinds is far more efficient to know analytical curve describing the dependence of the speed of movement on the temperature. This curve is surprisingly known only for very few species. The speed of movement is then vaguely defined by the minimum temperature at which the movement is already possible and by the maximum temperature at which the insect dies (Heinrich, 1999). This information is sometimes together with an indication of the temperature optimum (Vacha et al., 2004). There are several studies dealing with the mechanism which is used by individual species of insect for thermoregulation and a shift in the internal temperature to the optimum. Some species are capable of thermoregulation only in the group Drosophila (Dillon et al., 2009). Other species like moths, cockroaches or crickets are able to get their body temperature to some extent adjusted individually. Ants in our measurements lie on the edge of the first group.

Our measurements were made on isolated individuals who have been forced upon the desired temperature using the thermostat and the speed of the ends of the limbs was determined photometrically. The ants were not observed in the entire temperature range the effort to regulate body temperature. Neither excessive motion that would cause an increase in body temperature at low ambient temperatures nor saving energy by motion that would cause no increase in temperature at high ambient temperatures. Thereby these insects differed from cockroaches, crickets and ladybirds. For this reason, we can describe the greater part of the curve (see Graph 1), like with Drosophila, as an increasing exponential dependence of the extremities of the temperature. This type of dependence can be explained by an increased rate of chemical reactions allowing the dependence of movement on the temperature.

Methods and materials

An adult forest ant (Formica rufa) was placed in a thermostat chamber with dimensions of 20x30x8 mm. The upper chamber lid is made of aluminum – it provides good heat transfer between chamber and thermostat. The lower lid is made of clear plastic through which the movement of individual is captured by camera Festo SBOC - M.

Thermo box in Fig. 1 is equipped, in addition to the temperature controller, with two cameras and lighting prisms which bring light but not heat from external sources. Furthermore, two thermometers are installed in the thermo box. The first thermometer is the contact one – it reads the temperature of the casing chamber of biological object and the second one is non-contact – it can be used to accurate determining ant body temperature, if it just moves in the center of the chamber. With this second thermometer it was determined that the temperature of ant never differs by more than 1 °C from the chamber temperature.

Fig. 1 Thermo box to achieve the predefined body temperature of ant

Camera images are calibrated by capturing of the image of graph paper, which is temporarily placed in the measuring chamber. After a 15-minute acclimatization at the set temperature few sequences are recorded at a frequency scanning 190 frames per second. There is a record of the time of acquisition with microsecond precision for each frame. By comparing individual pictures it can be determined (due to the abovementioned calibration), how long distance the end of the right back leg of ant has traveled and hereby to estimate the maximum speed of its movement at a given temperature.

The total number of measured ants was 25. The ants were caught in the woods (by attracting at a sugar cube). In terms of actual measurement, for each of the measured temperatures, the ants were taken from their space with room temperature of 25 °C and air relative humidity 40 %, they were available water and food there. Three different ants were measured at each temperature. Number of measuring the speed of the legs of each ant was five. We observed motion for the lowest temperature 10 °C. Following temperatures were 15, 20, 25, 30 and 40 °C. Higher temperatures were not patently good for ants and they were threatened with death. For the determination of the speed the first hind limb was chosen for each ant. For each ant its speed was measured ten times. For all the measurements of the given temperature the mathematical average and standard deviation were determined. The entire experiment was repeated twice, therefore, two values for every temperature are given on the Graph 1. Averaged values obtained for each temperature were fitted curve, which is described by equation (Treherne, 1974)

$$v(t) = A e^{-\frac{E}{R(t+t_0)}}, \qquad (1)$$

where:

v (t) is the speed of limb, depending on the temperature t,

A is a geometric coefficient,

E is effective activation energy,

R is the universal gas constant, R = (8.3143 ± 0.0012) J.mol^{-1}.K^{-1},

t_0 is the temperature when the reactants cease to move (usually 273.15 K or 0 ° C).

The temperature t_0 was considered here as completely terminating the movement of nutrition in the body of the ant (Jones, 1977). We did not use the thermodynamic scale of temperature but the temperature in degrees Celsius. It was found that t_0 = 0 °C after all experiments with the shape of the function (1). We get the best agreement with experimental data for this parameter value t_0. The coefficient of determination (2) and the correlation coefficient (3) were determined for the resulting function.

$$R^2 = \frac{\sum_{i=1}^{6}(u(t_i) - \tilde{v})^2}{\sum_{i=1}^{6}(v(t_i) - \tilde{v})^2}, \qquad (2)$$

$$r^2 = \frac{\sum_{i=1}^{6}\left[(u(t_i) - \tilde{u})(v(t_i) - \tilde{v})\right]}{\sqrt{\sum_{i=1}^{6}(u(t_i) - \tilde{u})^2 \sum_{i=1}^{6}(v(t_i) - \tilde{v})^2}}, \qquad (3)$$

where:

$u(t_i)$ are calculated values of speed at temperatures t_i,

$\tilde{u}$ is the mean value of calculated speeds,

$v(t_i)$ are measured values of speed at temperatures t_i,

$\tilde{V}$ is the mean value of measured speeds.

Results and discussion

Graph 1 shows all mean values with their standard deviations, it was measured in two series of measurements. This graph contains also the fitted function of type (1); the values of fitted coefficients are listed in Tab. 1.

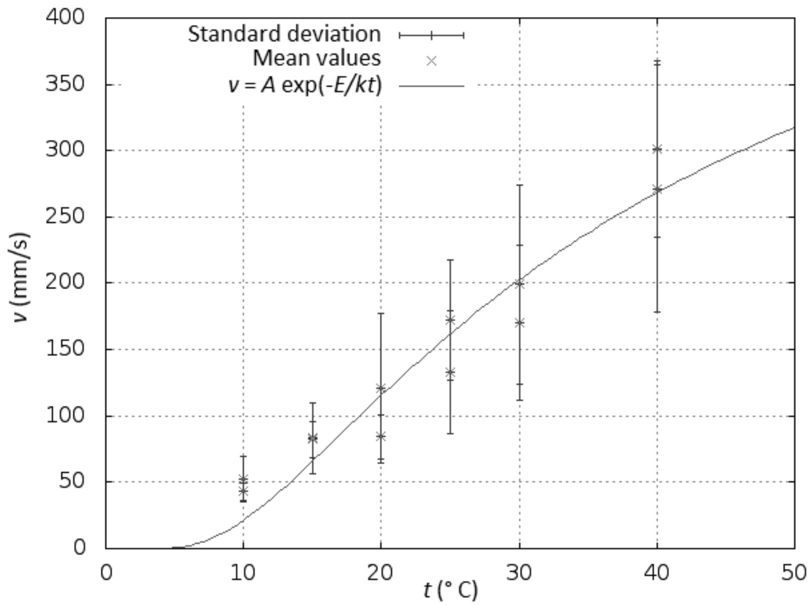

Fig. 1 The temperature dependence of the speed of movement of ants

Tab. 1 The resulting parameter values of the fitted function of the temperature dependence of the speed ant for the temperature range 0 - 40 ° C.

Quantity	**Mean value**	**Standard deviation**
A (mm/s)	623	92
E (J)	280	35
t_0 (°C)	0	0,8

While the correlation coefficient (3) gives the agreement of function (1) (for the parameters listed in Tab. 1) with the measured values 0.96, so the coefficient of determination (2) is slightly lower - only 0.92. Nevertheless, it seems that the proposed function describes good agreement with the temperature dependence of ants for the temperature range of 0 – 40 °C. It is suitable for the area of starting movement, before plateau, which have some kinds of the insects in this dependence, and for all kinds of insects before the area, when destructive thermal effects on proteins become dominant. The importance of the coefficient E is not yet entirely clear - we call it effective activation energy of the reaction, which allows movement, despite the fact that we are very clear that this is a complex system of reaction processes, which are also spatially distributed. Nevertheless, we think it is appropriate to specify the movement of insects in this field using coefficients of function (1), as it enables to characterize well the changes that occur, such as through acclimatization, or through different incubation temperatures within a species. Comparison of coefficients of function (1) allows also a mutual comparison among the different species of insects, since these parameters, unlike the previously used constants, describe a functional dependence relatively accurately.

Conclusion

We have constructed a device, what is possible to use for determination of the temperature dependence of the speed of movement of insect specimens. Nevertheless, it is not a native environment and acclimatization therein is limited in time, we hope that the device together with the proposed mathematical description of the dependence will enrich the categorization of different insect species and they will enable better to explore their physiology.

References:

Abdullah M., 1961. Behavioural effects of temperature on insects. The Ohio Journal of Science, vol. 61, 4: 212-219. ISSN 0030-0950

Bennett A.F., 1985. Temperature and muscle. The Journal of Experimental Biology, 115: 333-344. ISSN 0022-0949

Bodenheimer F.S., Klein H.Z., 1930. The Dependence of Activity in the Harvester Ant, M. semirufus, on Temperature and other Factors. Zeitschrift für Vergleichende Physiologie, 11, 3: 345-385. ISSN 0044-362X. (in German)

Dillon M.E., Wang G., Garrity P.A., Huey R.B., 2009. Thermal preference in Drosophila. Journal of Thermal Biology, 34, 3: 109-119. ISSN 0306-4565

Harrison J.F., Fewell J.H., Roberts S.P., Hall H.G., 1996. Achievement of Thermal Stability by Varying Metabolic Heat Production in Flying Honeybees. Science Magazine, 274, 5284: 88-90. ISSN 0036-8075

Heinrich B., 1971. Temperature regulation of the sphinx moth. The Journal of Experimental Biology, 54: 141-152. ISSN 0022-0949

Heinrich B., 1999. The Thermal Warriors. Harvard University Press, London, 221. ISBN 0-674-88341-1

Herreid II C.F., Full R.J., 1984. Cockroaches on a treadmill: Aerobic running. Journal of Insect Physiology, 30, 5: 395-403. ISSN 0022-1910

Jones J.C., 1977. The Circulatory System of Insects. Charles C Thomas Publisher, Springfield, 255. ISBN 0-398-03636-5

Porter S.D., Tschinkel W.R., 1993. Fire ant thermal preferences: behavioral control of growth and metabolism. Behavioral Ecology and Sociobiology, 32, 5: 321-329. ISSN 0340-5443

Treherne J.E., 1974. Insect Neurobiology. North-Holland Publishing Company, Amsterdam, Oxford, 450. ISBN 0-7204-7136-2

Vacha M., Bicik V., Petrasek R., Simek V., Fellnerova I., 2004. Comparative Animal Physiology. Masaryk University, Brno, 166. ISBN 80-210-3379-7 (in Czech)

TEMPERATURE PROCESS OF GROUND MASSIF WITH SLINKY HEAT EXCHANGER

Michaela Šeďová, Zuzana Štěrbová

Czech University of Life Sciences Prague, 165 21 Prague 6 – Suchdol, Czech Republic, Phone: +420 734 170 854, E-mail: sedova@tf.czu.cz

Abstract

The article is describing a ground massif with Slinky heat exchanger as a heat source for a heat pump, which is used for cold water warming and a heating an administration building. The object of the research is to analyse the influence of the heat exchanger on ground massif temperature while extracting heat energy at the beginning and during the heating season, as well as beyond it. Based on executed measurements the process of ground massif temperatures near the exchanger is described.

Key words: Slinky heat exchanger, ground massif, heat source, heat pump

Introduction

We live in a time when the use of alternative energy sources gets more and more into the foreground. Heat pumps are devices that can effectively use these resources. It can draw a heat from land, air and water, but it can also utilize a secondary heat. These heat sources for heat pump evaporators are used in both residential and civil construction and in agriculture. They can be used for heating of stables for breeding sows with piglets, fattening of broiler chickens to heat water for technological purposes, drying crops, etc.

In Korea at Seoul National University the cost of heating greenhouses were solved. (Ha et al., 2011) The Saint Mary's University in Halifax and at Hokkaido University addresses the issue of heating water in production ponds, grain drying and pasteurization of milk. (Tarnawski et al 2009) The University Geriz and Arge University in Turkey has been verifying a heat pump driven by a gas engine during drying of medicinal and aromatic plants. (Gungor et al., 2011)

Heat pumps ground - water use two sources of low potential heat energy witch is drawn by heat exchangers. There are called rock massif and ground massif (the rock to a depth of 2 m). Exchangers are installed vertically or horizontally. It consists of polyethylene pipes of different diameters and lengths. This depends mainly on the required performance.

Vertical heat exchangers are using the internal performance of the Earth using polyethylene pipe in the shape of "U" in which a cooling medium is flowing. (Petráš et al., 2008) The space in the borehole around the pipes is filled with a suitable material to provide good contact between the pipe and the massif and to reduce thermal resistance. (Florides et al., 2007)

Horizontal heat exchangers are mainly using thermal energy that is naturally accumulated in the surface ground massif as a result of the incident solar radiation. (Petráš et al., 2008) With horizontal exchanger the flow of heat is used. Heat comes from above and it is received by upper layer of the Earth from direct and indirect solar energy (radiation, rain, etc.). 98 % of the energy draws horizontal heat exchanger from a layer of ground massif that is above it. Only 2 % of the energy is taken from the ground massif under the exchanger. This heat exchanger can be considered as a sizable solar collector with low efficiency, which is complemented by a huge heat accumulator (surface) with an annual cycle of charging and discharging.

Material and method

Experimental measurements were carried out in Prague - Dolní Měcholupy within the company Veskom spol. s r.o. Slinky heat exchanger was made of polyethylene pipes PE 100 RC 32 x 2.9 mm. Slinky with a total length of 200 m is installed at a depth of 1.5 m, 53 coils rolled in a circle. Exchanger was put into operation in August 2008. It is not stored in the bed of sand. Ground massif to a depth of 2 m is dark brown sandy - clay loam. In the heat exchanger a cooling liquid mixture of 33 % ethanol and 67 % water is used. Fig. 1 shows in placement scheme of sensors that measure the temperature of the ground massif.

Temperatures of ground massif and ambient air were recorded from 1 March 2011 every 15 minutes.

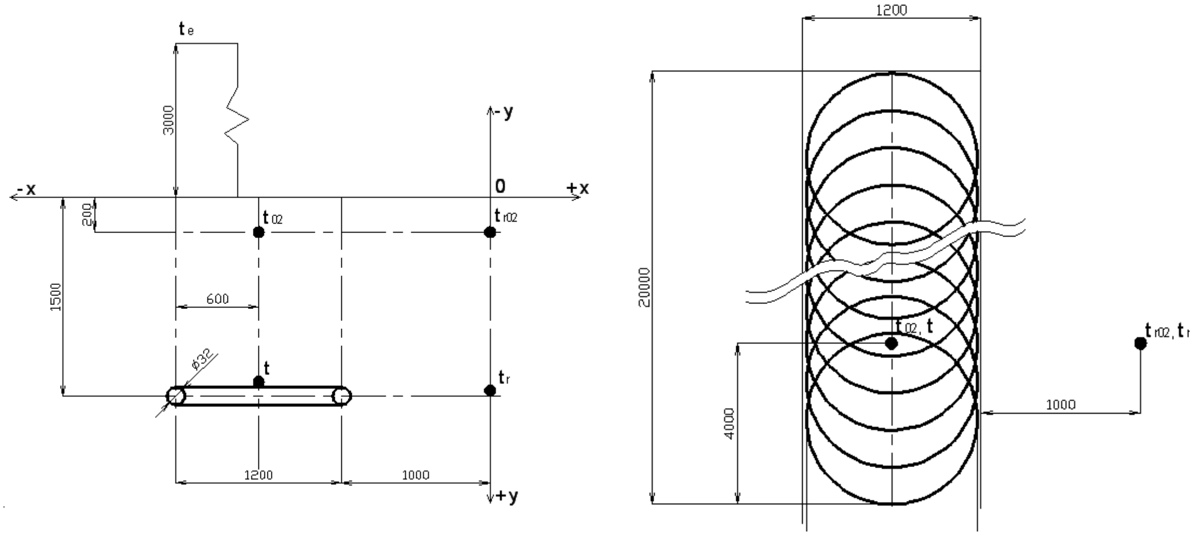

Fig. 1 Scheme of Slinky heat exchanger and location of the temperature sensors
t – temperature sensor located at a depth of 1.5 m near the pipe
t_r - referential temperature sensor located 1.0 m from the heat exchanger at a depth of 1.5 m
t_{02} - temperature sensor located at a depth of 0.2 m above the heat exchanger
t_{r02} – referential temperature sensor located 1.0 m from the heat exchanger at a depth of 0.2 m
t_e – sensor located at a height of 3.0 m above the surface

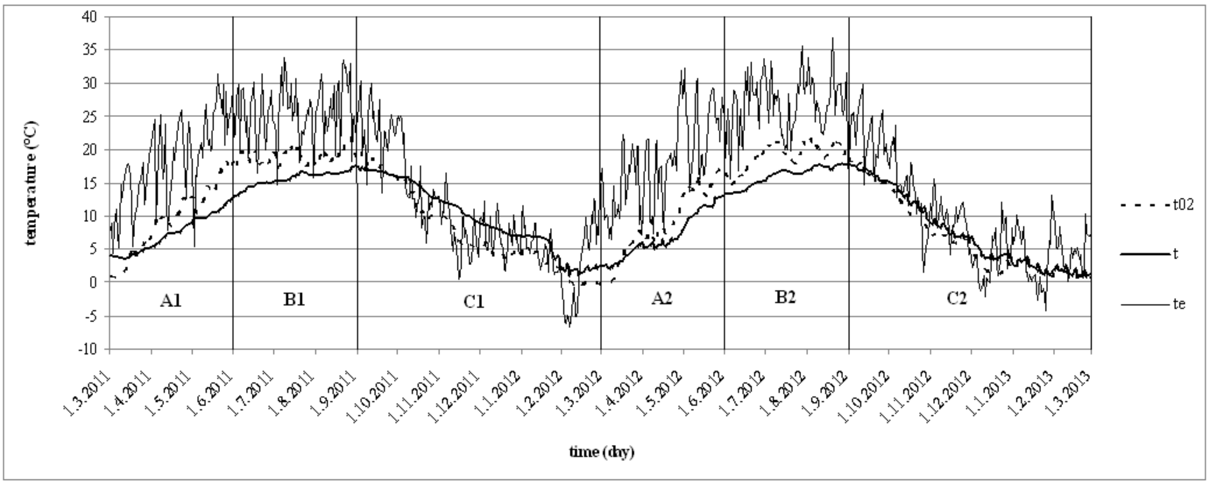

Fig. 2 Course of mean temperature of the ground massif with Slinky heat exchanger in the period from 1 March 2011 to 28 February 2013

Result and discussion

Measurements were carried out from 1 March 2011 to 28 February 2013. Fig. 2 shows the progress of the average temperature of ground massif with Slinky in the time period around the 3 p.m. It can be divided into 6 phases.

In phase A1 (1 March 2011 – 31 May 2011) a gradual increase in the temperature of the ground massif occurred at the end of the heating season 2010/2011. The average temperature t of ground massif with Slinky was 7.33 °C. Its maximum value was 12.57 °C, minimum 3.51 °C. The course of the temperature t can be written in the form:

$$t_{A1} = -10^{-5} \cdot d^3 + 1.9 \cdot 10^{-3} \cdot d^2 + 9.9 \cdot 10^{-3} \cdot d + 3.54 \quad (°C) \qquad (1)$$

(R^2=0.99)

where: d – number of days from the beginning of the measurement, ie from 1 March 2011

The second phase of the temperature in the ground massif, called B1, ran from 1 June 2011 to 31 August 2011 (92 days) during the stagnation heat exchanger. Temperature of the ground massif t ranged from 12.86 °C to 17.46 °C. Its average value was 15.61 °C. For this phase the equation of temperature t has the form:

$$t_{B1} = 10^{-5} \cdot d^3 - 2.2 \cdot 10^{-3} \cdot d^2 + 14.47 \cdot 10^{-2} \cdot d + 12.68 \quad (°C) \qquad (2)$$

(R^2=0.958)

where: d – number of days from the beginning of the measurement, ie from 1 June 2011

The beginning and course of the heating season 2011/2012, phase C1, lasted from 1 September 2011 to 29 February 2012 (182 days). The temperature of the ground massif with the Slinky declined from 17.31 °C to 1.13 °C. The average value in this period was 9.67 °C. The equation of the temperature *t* has the form:

$$t_{C1} = 10^{-6} \cdot d^3 - 3 \cdot 10^{-4} \cdot d^2 - 6.82 \cdot 10^{-2} \cdot d + 17.96 \quad (°C) \qquad (3)$$

(R^2=0.98)

where: d – number of days from the beginning of the measurement, ie from 1 September 2011

In the same way, the temperature of the ground massif *t* was processed at the end of the heating season 2011/2012, phase A2, (1 March 2012 - 31 May 2012), during the stagnation of heat exchanger, phase B2, and at the beginning and during the heating season 2012/2013, phase C2.

In phase A2 (92 days) is the increase of the average temperature of the ground massif from 2.05 ° C to 13.09 ° C. The average value during this period is 6.93 ° C. The equation of the temperature of the ground massif with Slinky has the following form:

$$t_{A2} = 10^{-5} \cdot d^3 - 6 \cdot 10^{-4} \cdot d^2 + 9.92 \cdot 10^{-2} \cdot d + 2.04 \quad (°C) \qquad (4)$$

(R^2=0.966)

where: d – number of days from the beginning of the measurement, ie from 1 March 2012

During the stagnation of the heat exchanger, which lasted from 1 June 2012 to 1 September 2012 (92 days), the temperature *t* ranged from 13.29 °C and 17.84 °C. During this period, the average value was 16.01 °C. The course of the temperature has the following form:

$$t_{B2} = 2 \cdot 10^{-6} \cdot d^3 - 9 \cdot 10^{-4} \cdot d^2 + 12.03 \cdot 10^{-2} \cdot d + 12.63 \quad (°C) \qquad (5)$$

(R^2=0.951)

where: d – number of days from the beginning of the measurement, ie from 1 June 2012

The last phase, phase C2, is at the beginning and during the heating season 2012/2013, from 1 September 2012 to 28 February 2013 (181 days). The temperature of ground massif decreased from the value of 17.81 °C up to 0.86 °C. On average, however, it reaches 7.59 °C. For this phase, the equation is:

$$t_{C2} = 3 \cdot 10^{-6} \cdot d^3 - 3 \cdot 10^{-4} \cdot d^2 - 13.63 \cdot 10^{-2} \cdot d + 18.78 \quad (°C) \qquad (6)$$

(R^2=0.989)

where: d – number of days from the beginning of the measurement, ie from 1 September 2012

In order to judge the ground massif in terms of energy potential, it was necessary to analyze the temperature at the beginning and the end of each heating season. The following table (Tab. 1) shows the recorded temperatures of the ground massif with Slinky in the period 2011/2012 and 2012/2013.

These temperature differences show that ground massif, under the climatic conditions and the quantity of heat can be considered as a stable energy source for the heat pump.

Conclusion

The result of our findings is the verification of temperature in ground massif with Slinky heat exchanger. The temperature development in massif is described by equations (1) through (6).

From the results of temperature in ground massif t at the beginning and the end of each heating season (Tab. 1) the ground massif has sufficient potential energy and can be considered as a stable energy source for heat pump.

Tab. 1 Temperatures of ground massif near the Slinky heat exchanger at the beginning and the end of the heating season

heating season	date	temperature of ground massif *t* (°C)	temperature difference *Δt* (K)
2011/2012	14 September 2011	16.83	the beginning of heat season -0.25 K
2012/2013	14 September 2012	17.08	
2011/2012	28 February 2012	2.29	the end of heating season 1.02 K
2012/2013	28 February 2013	1.27	

Reference

Florides G., 2007. Kalorigou, S. Ground heat exchangers : A review of systems, models and applications. In *Renewable Energy*. Elsevier, 2461 - 2478.

Gungor A., Erbay Z., Hepbasli A., 2011. Exergoeconomic analyses of a gas engine driven heat pump drier and food drying process. In Applied Energy, 88/8, Elsevier, 2677 – 2684.

Ha T. et al., 2011. Development of an assessment model for greenhouse using geothermal heat pump system. In American Society of Agricultural and Biological Engineers Annual International Meeting 2011, Louisville, Kentucky, USA, 2105 - 2114.

Petráš D. et al., 2008. Low temperature heating and renewable energy. JAGA group. 216. (in Czech)

Tarnawski V. et al., 2009. Analysis of ground source heat pumps with horizontal ground heat exchangers for northern Japan. In Renewable Energy, 34, Elsevier: 127 – 134.

DETERMINING THE AMOUNT OF BIOGAS DERIVED FROM COSUBSTRATE ON BASE EXECUTED CORN SILAGE AND WASTES OF AGRICULTURAL INDUSTRIES

Jakub Sikora*, Kazimierz Rutkowski

University of Agriculture in Krakow, Institute of Agricultural Engineering and Computer Science, 30-149 Krakow, Balicka street 116B, Poland, Phone: +48126624660, Fax: +4812-6624660, E-mail: jakub.sikora@ur.krakow.pl

Abstract

The XXI century is a time of great need for energy and the many environmental problems. Developed countries produce more waste vegetable and animal origin, which causes the first human non-utilization of energy, and secondly there is an increasing danger for the environment. The resulting biogas poses a major threat to humans, water, soil, and above all the atmosphere causing the increase of the greenhouse effect (Kacprzak et al., 2012).

Even in the twentieth century noticed a huge increase in organic waste and pollution from agriculture and the food industry. Wastes include the essential elements of the development of carbohydrate, protein, fat, biogenic elements, microelements and vitamins. In the fermentation under aerobic and anaerobic conditions, bacteries break down the organic compounds and consequently take place the emission of gases into the atmosphere. Gases produced in the metabolism is mainly NH_3, CH_4, H_2S, CO_2, NOx and nitrogen compounds, phosphate and potassium. Compounds could enter the atmosphere and surface water alters the balance of the ecosystem and contribute to the eutrophication. Anaerobic fermentation can play a significant role related to produce bioenergy (methane). More specifically, this method transforms the energy contained in agricultural crops, the fuels such as biogas, without any contraindications that may be collected and transported. It is also a way of recycling organic wastes and the removal of oxygen from the wastes, which aims to reduce the adverse impact on the environment (Kacprzak et al., 2012).

The study determined amount of biogas from organic materials which were in apple pomace silage corn in cosubstrate. Two control batches were made from apple pomace (100 %) and corn silage (100 %). Additionally, measurements of gas from maize silage and apple pomace were performed in the ratio of 50/50 % 75/25 % and 25/75. The number and composition of the evolved biogas, the pH and temperature of the feedstock were also examined. The highest total yield of biogas was presented in the sample in which the value of corn silage substrates and apple pomace was 50 % to 50 %. The efficiency of the feedstock reached 210 $Ndm^3 \cdot kg_{s.\,m.}^{-1}$. Apple pomace is used to produce pectin, spirits and as a feed for cattle. The study showed that apple pomace is also a good substrate for biogas production.

Keywords: biogas, waste, agricultural industries

Introduction

New opportunities for the development of the biogas market offers EU Directive, 2009/28/EC of 5 June 2009 on the promotion of renewable energy sources, which obliges Poland to achieve a 15 % share of renewables in final energy consumption in 2020. Design of a new quantitative target in relation to "energy consumption" provides opportunities for the development of biogas industry that can find the direct and indirect use in all three markets of final energy carriers (electricity, heat and transport). According to the Institute of Renewable Energy in the implementation are currently hundreds of agricultural biogas projects in various stages of development, and soon you can expect to be put into service next objects.

Despite the clear trend towards increased interest in biogas production, are still knowledge of the parameters process and the technology is not sufficient. This is due to different, relative to the standard, substrates and the possibilities of using the products from the production of biogas for other purposes (resulting from for example development of manufacturing technology called fuel compact). So far, national knowledge of commercial processes in biogas installation is mainly based on the experience of Germany, where the meaning of previously implemented a number of procedures in practice (Jędrczak, 2007). Successful implementation of the maximum amount of innovation solutions for the production of biogas installations, requires the development of a laboratory scale results that will be implemented by the economy subjects. Implementation of the results to commercial energy technologies must take into account not only the procedural aspects, but also legal issues, environmental, administrative, organizational and logistical (Sikora, 2012).

At the present time, the development of the market has led to a number of different technical solutions adapted to the diverse needs of users, but the used technology are often include cutting problem. This applies to both solutions on the Polish market as well as globally. Issues of alternative (compared to the commonly used) biogas plants were also subject of research in the world's scientific centers. As the substrate tested were: wastes yeast (Merwe, Britz, 1993), wastes from sewage treatment plants (Sharma et al., 1999), the wastes from the pharmaceutical industry (Yapa et al., 1999), the wastes from the processing of fish (Koutinas et al., 1991). However, quoted the research work described the findings in the laboratory.

Germany and the United Kingdom is currently in the process of biogas production are at the forefront, together produce almost 70 % of the total production of biogas in the European Union. Then, in the biogas production there are leading countries such as: Italy, Spain, France, Netherlands, Austria, Denmark, Belgium. In Poland and other EU countries, this energy represents a small percentage. In the coming years, in all EU countries because of the growing market for energy crops, such as: corn, sunflower seeds and wheat, increased agricultural biogas can become more dynamic. Small share of the total production of biogas in Poland is due to the fact that operating a biogas plant is only a few (Londo et al., 2009). In Germany, the current moment there are about 4,000 biogas plants that provide power at 1.1 gwel. Germany produces more than 23 % of the resulting manure into biogas. In Sweden, operates 22 large biogas plants that produce 500 m^3 of methane per hour, allowing the delivery of electricity to about 2,000 households (Londo et al., 2009).

The aim of the study was to determine the amount of harvested biogas from organic material on base of corn silage and apple pomace. In order to compare and illustrate the amount of emitted biogas performed batch mixes made with the parameters shown in Tab. 1.

Material and methods

Research was carried out in the biogas laboratory of the University of Agriculture in Cracow placed in the Department of Production Engineering and Energy Power. Material for the research was obtained in 2012 from the individual diary farm in Goleszów municipality. Moreover, organic fractions of municipal waste were obtained from the area of Cracow municipality. The following fractions were accepted for the research:

- organic plant mass: maize silage, cattle manure,
- apple pomace.

Fractions were fragmented and five samples were collected from each. Samples were weighed in order to determine their weight before drying. The fragmented material was hydrated to approx. 90 % moisture forming optimal conditions for development of mesophile bacteria. Six mixtures of batches of parameters presented in Tab. 1 were accepted for the research. Fermentation was carried out in the digester of 20 dm^3 volume with regulated temperature environment. The following are controlled in this fermentor: pH, redox potential and the batch temperature. The produced biogas was collected in the container of a variable volume. A schematic representation of the stand with a digester is presented in Fig. 1.

Tab. 1 Characteristics of batches for Digesters

Name	Fractions	
	Maize silage [%]	**Apple pomace [%]**
Batch 1	100	0
Batch 2	0	100
Batch 3	50	50
Batch 4	25	75
Batch 5	75	25

Source: Own

Batch 1, accepted as control material was proved and introduced to the digester. Batch 1 was placed in the digester (2) in which by means of sondes (5) fermentation parameters, such as temperature, redox and pH are controlled. These parameters are automatically saved with time interval on the hard disc of a computer of the measuring system. In the digester, the batch was mixed with a mechanical mixer (4) to avoid delamination. The mixer may be smoothly regulated within 0 to 400 rot./min. is equipped with three blades of regulated spacing, which enables the change of intensity of mixing zones in the fermentor.

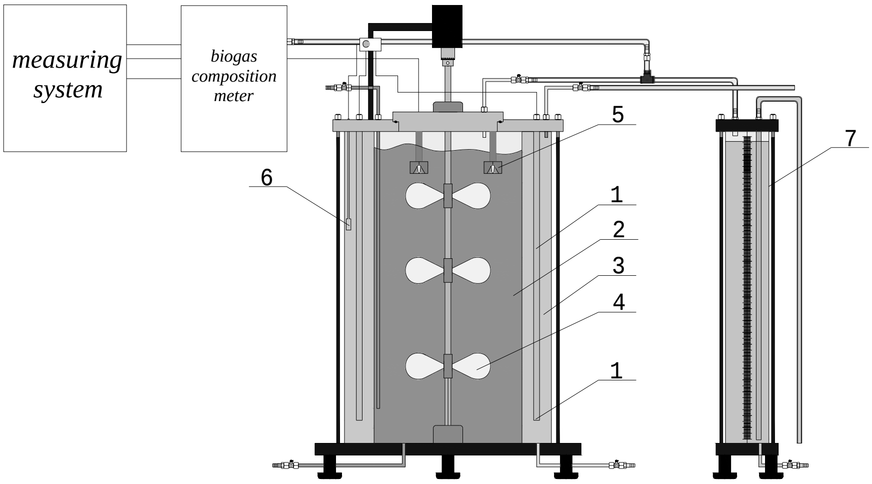

Fig. 1 A schematic representation the of the test stand with 20 litre fermenter *Source: Own*

The digester of the fermenter is equipped with a water jacket (3) where three cartridge heaters are placed (1), which are responsible for heating liquid. The measuring system equipped with a thermometer (6) PT100 is responsible for controlling the process temperature. The produced biogas is collected over the surface of the batch in the fermentor and in the container (7) of variable volume from which it is sucked in by the biogas composition measuring meter. This meter analyses the following parameters: moisture, temperature, pressure, methane CH_4, oxygen O_2, carbon dioxide CO_2 and hydrogen sulphide H_2S. Biogas composition parameters which are measured are automatically saved on the computer disc of the measuring system.

Determination of the intensity of the biogas production in the remaining batches was carried out according to standard DIN 38414. Batch mixes were fermented in static conditions consisting in a single introduction of fraction to digesters and conducting the process to the end of fermentation.

Fermentation devices were installed in a container with regulated temperature forming a part of the test stand, which was additionally composed of a switch panel and the measuring system. Schematic representation of the test stand was presented in Fig. 2. Devices for maintaining a constant temperature environment were mounted to a rack (1) located next to the container (2). Controlling took place by means of electronic thermostat ESCO ES-20 (unit switch 16A) with precision up to ± 0.2 °C resulting from hysteresis of a sensor. Temperature decrease by value exceeding 0.1 °C caused switching on a heater of 1500 W (3) power with a simultaneous start of the water pump Hanning DPO 25-205 (4) in order to ensure a uniform distribution of temperature in the whole chamber. After heating water to the temperature exceeding the set temperature by 0.1 °C the heater switched off and with a 30 seconds delay of then pump.

Separators combined in a row along with cut-off valves (6) and a manometer (7) which measures pressure in particular measuring branches constituted a switch board (5). Due to the use of such system for service of all fermenters, only one measuring system was enough. The system of measuring volume (8) was composed of two columns filled with water with drain valves and a container for filling up the liquid level in columns (9). Measuring system was combined with a switchboard and a biogas composition meter by means of a conduit (10) which was presented in Fig. 1.

A chemical analysis was carried out for all the researched batches before the commencement of fermentation. Dry mass of fraction and reaction were determined. For each researched batch, fermentation was carried out simultaneously. The amount of the produced gas was read out twice daily at the same time.

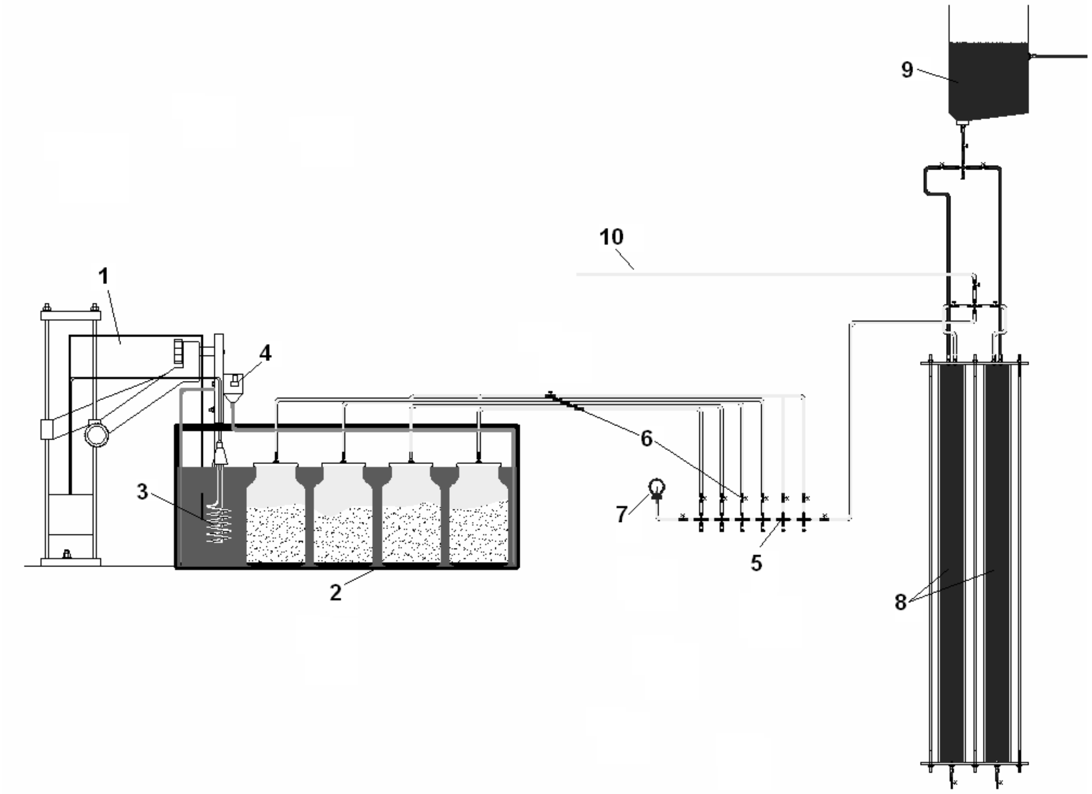

Fig. 2 A schematic representation of the test stand with 2 litre fermenter *Source: Own*

Results and a discussion

In the processing of fruit and vegetables produced annually about 377 thousand tonnes of wastes, which is a good substrate for biogas plants. Polish agriculture produces 80,750 thousand tons of manure and about 35 million m^3 of slurry of which about 30 % can be used for biogas production. In Poland, the production of biogas for energy purposes is 12.5 %. The used plants are: corn, grass, clover, fodder and sugar beet, oats, wheat, barley and sunflower. These plants may be used in whole, in the form of fruit, leaves, seeds or as a plants processed in the form of silage or straw.

In Fig. 1B, we see that in the first three days of fermentation occurred hydration period, until the next day there was a decomposition of organic matter and began to evolve biogas. The increase in the yield of biogas ran gently and gradually which proves to no disruption during the course of fermentation. The first stage of fermentation of corn silage (Fig. 1A) ran successfully on 12 day fermentation is slightly disturbed due to the different thickness of the fraction, which has a negative effect on the process. Then again work correctly.

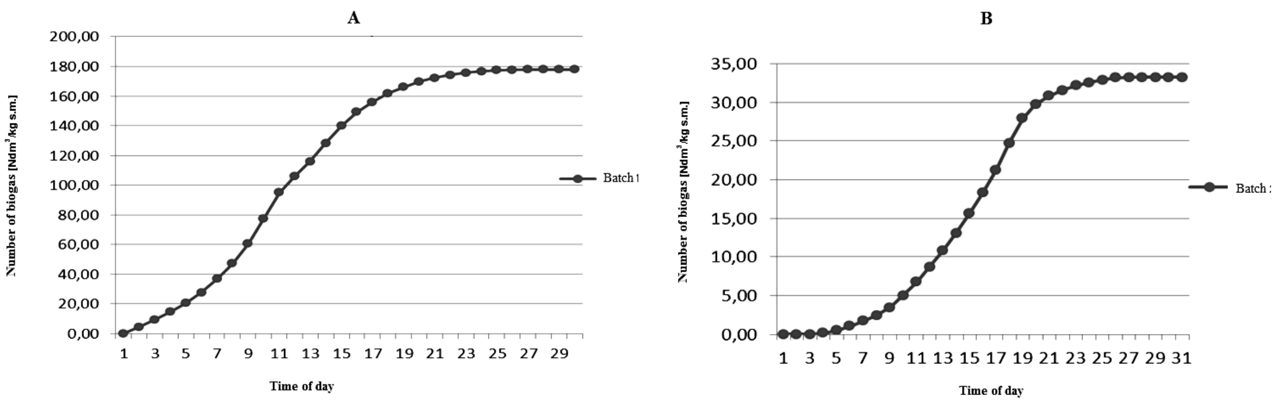

Fig.1 The total yield of gas: A – corn silage B – apple pomace *Source: Own*

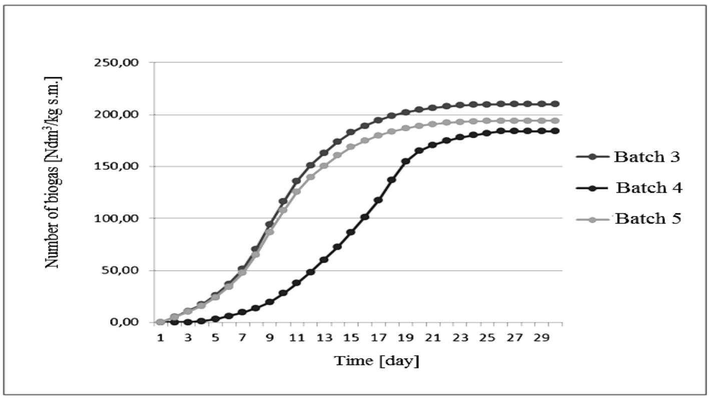

Fig. 2 The total gas yield of silage corn and apple pomace *Source: Own*

The total gas yield of corn silage and apple pomace in a ratio of 50 % to 50 % is shows a taking place properly fermentation process. The increase in the yield of gas is intense and reaches the highest value of the three batches. The graph showing the silage corn and apple pomace in a ratio of 25 % to 75 %, in the first stage of the fermentation showing 4 day hydration followed by appropriate fermentation. In the following days the process runs smoothly without any interruption. Biogas yield is smaller, the process occurred more slowly than in the two previous batches and biogas yield was lower. The bath in which corn silage and apple pomace was in the ratio of 75 % to 25 % for several days the yield of biogas was gradual. Only after 5 days of the trial can be seen larger and more violent yield biogas emitted.

Conclusions

Results of the analysis shows that the greatest release of methane occurred in the batch, which is made of corn silage and apple pomace in a ratio of 50 % to 50 %. The resulting biogas contains about 65 % methane. A lower but also has a satisfactory yield biogas obtained from the sample in which the ratio of corn silage substrates and apple pomace was 75 % to 25 %. The yields of methane was 54 %. The highest levels of carbon dioxide was observed in the sample in which the ratio of corn silage substrates and apple pomace was 25 % to 75 %. The yield of carbon dioxide was 57 %. Visible distortion amounts of oxygen and carbon dioxide was caused by opening the chamber and adding the bacteria to ferment.

The largest daily biogas yield activity occurred in the sample in which the ratio of corn silage substrates and apple pomace was 50 % to 50 %. Performance of the test reached 4700 Nml. Yield second trial, in which the ratio of corn silage and apple pomace was 75 % to 25 %, was slightly lower. Received in the capacity range of 4350 Nml. The variety of substrates had a very positive influence on the process, because the food industry wastes are a cheap raw material for the plant. Biogas production of this type of wastes contributes to food and agriculture wastes whose disposal in many cases it is very expensive. Wastes food is available all year round.

Reference

Jędrczak A., 2007. Biologiczne przetwarzanie odpadów, Wydawnictwo Naukowe PWN, Warszawa, 27-181. (In Polish)

Kacprzak A., Matyka M., Krzystek L., Ledakowicz S., 2012. Evaluation of biogas collection from reed canary grass, depending on nitrogen fertilisation levels. Chemical and process engineering, 33(4): 697-701. (In Polish)

Koutinas A.A., Toutoutzidakis G., Kana K., Kouinis I., 1991. Methane fermentation promoted by alumina pellets. Journal of Fermentation and Bioengineering, 72(1): 648- 665.

Londo M., Lensink S., Wakker A., Kupczyk A., 2009. The REFUEL EU road map for biofuels in transport: Application of the project's tools to some short-term policy issues. Biomass and bioenergy, 34(2): 244-250.

Merwe V.M., Britz T.J., 1993. Anaerobic digestion of baker's yeast factory effluent using an anaerobic filter and a hybrid digester. Bioresource Technology, 43(2): 169-174.

Sharma V.K., Testa C., Castelluccio G., 1999. Anaerobic treatment of semi-solid organic waste. Energy Conversion and Management, 40(4): 369-384.

Sikora J., 2012. Badanie efektywności produkcji biogazu z frakcji organicznej odpadów komunalnych zmieszanej z biomasą pochodzenia rolniczego. Infrastruktura i ekologia terenów wiejskich, 11: 120-130. (In Polish)

Yapa M.G.S., Nigh W.J., Chuaa H., 1992. Performance of an anaerobic biofilter for 2-ethylhexanoic acid degradation. Bioresource Technology, 41(1): 458- 471.

EFFECT OF THE VERTICAL AND HORIZONTAL SOIL TILLAGE TECHNOLOGY TO NITROUS OXIDE FLUX FROM SOIL

Tomáš Šima[1*], Ladislav Nozdrovický[1], Koloman Krištof[1], Monika Dubeňová[1], Josef Krupička[2]

[1]Slovak University of Agriculture in Nitra, Tr. A. Hlinku 2, 949 76 Nitra, Slovak Republic,
E-mail: tomasko.sima@gmail.com
[2] Czech University of Life Sciences Prague, Czech Republic,

Abstract

The aim of the paper was to compare of the amount of nitrous oxide (N_2O) emissions released from the soil to the atmosphere and its dependence on soil tillage technology. Monitoring points were selected in parts of a field characterised as clay-loam soil type. The N_2O emissions were analysed before soil tillage, straight after soil tillage, 24 hours and 7 days after soil tillage. Three variants of the experiment were conducted: no tillage, vertical tillage by deep loosening (Terraland TD 4000 with working width 4 m) and horizontal soil tillage technology by plough (LemkenEuroDiamant 8 with 3.5m working width). Both machines were aggregated with tractor JOHN DEERE 8230. The used laboratory method of measuring N_2O emissions released from the soil to the atmosphere consists of collecting soil samples from the field and their subsequent analysis in the laboratory. There were used INNOVA devices which consist of a photo-acoustic field gas monitor INNOVA 1412 based on the photo-acoustic infrared detection method, a multipoint sampler INNOVA 1309 used for gas sampling transport to the gas analyser INNOVA 1412, and a notebook with operation software used for the control and setup of the analysis. The effects of soil tillage technology on nitrous oxide flux were not found. There were found effect of time interval after soil tillage technology. The maximum values of N_2O flux were observed straight after tillage with decreasing trend in time after tillage. The horizontal tillage technology caused the greater soil respiration and therefore the higher amount of N_2O emissions from soil.

Keywords: nitrous oxide, vertical soil tillage, horizontal soil tillage, soil emission

Introduction

Agriculture, especially soil tillage and the usage of fertilizers, contributes to nitrous oxide (N_2O) emissions significantly. Nitrogen is an essential element for plant growth (Ambus et al., 2011). Nitrous oxide is one of the most important greenhouse gases (Šima et al., 2013a) contributing 6% to global warming (Loubet et al., 2011; Ranucci et al., 2011) and N_2O directly affects the stratospheric ozone layer (William et al., 1992; Ravishankara et al., 2009). Nitrous oxide is produced in soils during nitrification and denitrification (Davidson, 1991; Ambus et al., 2006) and chemical denitrification at low pH<5.5 (Van Cleemput, Samater, 1996). The most important factors affecting the amount of N_2O and CO_2 released from soil to the atmosphere are soil compaction and crop residues (Šima et al., 2013b; Šima , Dubeňová, 2013 in press), soil organic matter content (Hayakawa et al., 2009); fertilization (Verma et al., 2006; Jones et al., 2007; He et al., 2009; Pang et al., 2009; Lin et al., 2010; Šima et al., 2012a; Šima et al., 2013 in press); temperature (Kesik et al., 2006); soil texture (Ruser et al., 2006; Beare et al., 2009); soil pH (Mørkved et al., 2007) and cropping system (Petersen et al., 2013).

The aim of the study was the comparison of the amount of nitrous oxide emissions released from soil to the atmosphere depending on soil tillage technology. In the paper is compared vertical tillage by deep loosening by Terraland TD 4000 with working width 4 m and horizontal soil tillage technology by plough LemkenEuroDiamant 8 with 3.5m working width.

Experimental arrangement

Monitoring points were selected in parts of a field characterised as clay-loam soil type. The soil moisture content was measured by a gravimetric method. Soil properties (table 1) were analysed at the Department of Soil Science and Geology at the Slovak University of Agriculture in Nitra, Slovakia.

Tab. 1 Soil properties of experimental site

Soil parameter	
Soil	Haplic luvisoil
Texture	Clay loam
Clay content	45-60 %
pH	7.3-8.5
Organic matter	3.00 %
Humus	4.99 %
Moisture (*by Volume*)	11.42-18.29 %

The N_2O emissions were analysed before soil tillage, straight after soil tillage, 24 hours and 7 days after soil tillage. Three variants of the experiment were conducted: no tillage, vertical tillage by deep loosening (Terraland TD 4000) and horizontal soil tillage technology by plough (LemkenEuroDiamant 8). Basic technical parameters of machines are show in table 2. Both machines were aggregated with tractor JOHN DEERE 8230.

Tab. 2 Basic technical parameters of Strom Terraland TD 4000 and LemkenEuroDiamant 8

Technical parameter	**Strom Terraland TD 4000**	**LemkenEuroDiamant 8**
Working width	4 m	3.5 m
Working depth	0.65 m	0.25 m
Weight	2640 kg	2272 kg
Number of working bodies	7	6
Pull force recommended	183-220 kW	110-170 kW

There were used laboratory method (Šima et al., 2012b) of measuring N_2O emissions released from the soil to the atmosphere consists of collecting soil samples from the field and their subsequent analysis in the laboratory. This method is possible to use for measuring N_2O (Šima et al., 2012b) and CO_2 (Šima et al., 2012c) emissions flux. There were used INNOVA devices (LumaSense Technologies, Inc., Denmark) which consist of a photo-acoustic field gas monitor INNOVA 1412 based on the photo-acoustic infrared detection method, a multipoint sampler INNOVA 1309 used for gas sampling transport to the gas analyser INNOVA 1412, and a notebook with operation software used for the control and setup of the analysis.

Results and discussion

Nitrous oxide emissions released from soil into the atmosphere is affected by time interval after soil tillage. Similar results was published for carbon dioxide emissions (Krištof et al., 2012), however, there were found statistically significant difference between time interval right after soil tillage and other time interval (before soil tillage, 24 hours after soil tillage and 7 days after soil tillage) in the vertical tillage by Strom Terraland TD 4000. Analysis of data of horizontal tillage by Lemken EuroDiamant 8 also showed effect of time interval after soil tillage. There were found statistically significant difference among the time intervals right after soil tillage and other time intervals and also were found difference between time interval before soil tillage and 24 hours after soil tillage. As it was anticipated (Krištof et al., 2012), there were also not found differences between before soil tillage and 7 days after soil tillage and also between the 24 hours after and 7 days after soil tillage.

Table 3 – Summary statistics and Multiple Range test LSD at 95.0% confidence intervals of N_2O emissions flux

Time	**Variant**								
	No tillage			**Strom Terraland TD 4000**			**LemkenEuroDiamant 8**		
	Mean, ppm	**Max., ppm**	**Min., ppm**	**Mean, ppm**	**Max., ppm**	**Min., ppm**	**Mean, ppm**	**Max., ppm**	**Min., ppm**
Before (n = 23)	0.5539_a	0.6098	0.4966	-	-	-	-	-	-
Right after (n = 21)	-	-	-	2.2030_b^x	3.6353	1.1017	2.6836_c^x	4.2308	1.5235
24 hours after (n = 19)	-	-	-	0.7638_a^y	1.2524	0.5827	0.8173_b^y	1.4103	0.5912
7 days after (n = 24)	-	-	-	0.6289_a^z	0.7759	0.5190	0.6713_{ab}^z	0.8316	0.5625

*Different letters in the columns ($_{a,b,c}$) mean the effect of the time interval and different letters in the rows (xyz) mean the effect of the tillage technology on the nitrous oxide emissions. It indicates that means are significantly different at P<0.05 according to the LSD multiple-range test at the 95.0% confidence level.

In addition, there were not found effect of tillage technology on nitrous oxide emissions released from soil into the atmosphereas demonstrate the data of summary statistics and Multiple Range test LSD at 95.0% confidence intervals shown in table 3. Simultaneously, this results are in agreement with our previous results where were also found statistically significant effect of time interval after soil tillage on nitrous oxide emissions flux (Šima et al., 2013b) and also on carbon dioxide emissions flux (Šima, Dubeňová, 2013 in press).

Conclusion

The aim of the study was to compare of the amount of nitrous oxide (N_2O) emissions released from the soil to the atmosphere and its dependence on soil tillage technology. There were compared vertical tillage by deep loosening (Terraland TD 4000 with working width 4 m) and horizontal soil tillage technology by plough (LemkenEuroDiamant 8 with 3.5m working width). The N_2O emissions were analysed before soil tillage, straight after soil tillage, 24 hours and 7 days after soil tillage. The used laboratory method of measuring N_2O emissions released from the soil to the atmosphere consists of collecting soil samples from the field and their subsequent analysis in the laboratory by INNOVA device with photo-acoustic infrared detection measuring system. The effects of soil tillage technology on nitrous oxide flux were not found although there were found the effect of time interval after soil tillage technology for both tillage technologies. The maximum values of N_2O flux were observed straight after tillage with decreasing trend in time after tillage. The horizontal tillage technology caused the greater soil respiration and therefore the higher amount of N_2O emissions from soil. However, to a deeper understanding of the effect of soil tillage on the amount of released N_2O emissions released from soil into the atmosphere is desirable to extend the area of experimental studies in other soil tillage technologies.

Acknowledgements

This paper has been prepared within the projects:
"Development of International Cooperation for the Purpose of the Transfer and Implementation of Research and Development in Educational Programs" conducted by the Operational Program: Education, ITMS code: 26110230085 "Application of the information technologies to increase the environmental and ecological sustainability of the production agrosystem", project ITMS 26220220014, EU Operational programme RESEARCH and DEVELOPMENT.

References

Ambus P., Zechmeister, Boltenstern S., Butterbach, Bahl K., 2006. Sources of nitrous oxide emitted from European forrest soils. Biogeosciences 3: 135-145.

Ambus P., Skiba U., Butterbach, Bahl K., Sutton M., 2011. Reactive nitrogen and greenhouse gas flux interactions in terrestial ecosystems. Plant and Soil 343: 1-3.

Beare M. H., Gregorich E. G., Georges P. S., 2009. Compaction effects on CO_2 and N_2O production during drying and rewetting of soil. Soil Biology and Biochemistry 41: 611-621.

Davidson E. A., 1991. Fluxes of nitrous oxide and nitric oxide from terrestial ecosystems. Rogers and Whitman (eds.), Microbial production and comsumption of greenhouse gases: Methane, nitrogen oxides and halomethanes. The American Society for Microbiology: 219-235.

Hayakawa A., Akiyama H., Sudo S., Yagi K., 2009. N_2O and NO emissions from Andisol field as influenced by pelleted poultry manure. Soil Biology and Biochemistry 41: 521-529.

He F. F., Jiang R. F., Chen Q., Zhang F. S., Su F., 2009. Nitrous oxide emissions from an intensively managed greenhouse vegetable cropping system in Northern China. Environmental Pollution 157: 1666-1672.

Jones S. K., Rees R. M., Skiba U. M., Ball B. C., 2007. Influence of organic and mineral N fertiliser on N_2O fluxes from a temperate grassland. Agriculture, Ecosystems & Environment 121: 74-83.

Kesik M., Blagodatski S., Papen H., Butterbach, Bahl K., 2006. Effect of pH, temperature and substrate on N_2O, NO and CO_2 production by Alcaligenes faecalis p., Journal of Applied Microbiology 101: 655-667.

Krištof K., Findura P., Nozdrovický L., Turan J., Šima T., Kuruc O., 2012. Effect of tillage technology on carbon dioxide emissions released from soil into the atmosphere. Naučni trudove 51: 182-186.

Lin S., Iqbal J., Hu R. G., Feng M. L., 2010. N_2O emissions from different land uses in midsubtropical China. Agriculture, Ecosystems & Environment 136: 40-48.

Loubet B., 2011. Carbon, nitrogen and Greenhouse gases budgets over a four years crop rotation in northern France. Plant and Soil 343: 109-137.

Mørkved P. T., Dorsch P., Bakken L. R., 2007. The N_2O product ratio of nitrification and its

dependence on long-term changes in soil pH. Soil Biology and Biochemistry 39: 2048-2057.
Pang X. B., Mu Y. J., Lee X. Q., Fang S. X., Yuan J., Huang D. K., 2009. Nitric oxides and nitrous oxide fluxes from typical vegetables cropland in China: Effects of canopy, soil properties and field management. Atmospheric Environment 43: 2571-2578.
Petersen S. O., Ambus P., Elsgaard L., Schjonning P., Olesen J. E., 2013. Long-term effects of cropping system on N_2O emission potential. Soil Biology and Biochemistry 57: 706-712.
Ranucci S., 2011. The influence of management and environmental variables on soil N_2O emissions in a crop system in Southern Italy. Plant and Soil 343: 83-96.
Ravishankara A. R., Daniel J. S., Portmann R. W., 2009. Nitrous oxide (N_2O): the dominant ozone-depleting substance emitted in the 21st century. Science 326: 123-125.
Ruser R., Flessa H., Russow R., Schmidt G., Buegger F., Munch J. C., 2006. Emission of N_2O, N_2 and CO_2 from soil fertilized with nitrate: Effect of compaction, soil moisture and rewetting. Soil Biology and Biochemistry38: 263-274.
Šima T., Krupička J., Nozdrovický L., Krištof K., 2012a. Effect of nitrogen fertilizer consumption in the Czech Republic on N_2O flux during the years 1990-2011. Technics in Agrisector Technologies 2012: 188-191.
Šima T., Nozdrovický L., Krištof K., Dubeňová M., Krupička J., Králik S., 2012b. Method for measuring of N_2O emissions from fertilized soil after the using of fertilizer spreader. Poljoprivredna tehnika 37: 51-60.
Šima T., Nozdrovický L., Krištof K., Dubeňová M., Macák M., 2012c. A comparison of the field and laboratory methods of measuring CO_2 emissions released from soil to the atmosphere. Poljoprivredna tehnika 37: 63-72.
Šima T., Dubeňová M., 2013. Effect of crop residues on CO_2 flux in the CTF system during soil tillage by a disc harrow Lemken Rubin 9. Research in Agricultural Engineering.
Šima T., Nozdrovický L., Krištof K., Dubeňová M., Krupička J., 2013a. Effect of the nitrogen fertiliser rate on the Nitrou oxide flux from haplic luvisol soil in the laboratory experiment. Agronomy Research 11: 97-102.
Šima T., Nozdrovický L., Dubeňová M., Krištof K., Krupička J., 2013b. Effect of crop residues on nitrous oxide flux in the controlled traffic farming system during the soil tillage by Lemken Rubin 9 disc harrow. Agronomy Research 11: 103-110.
Šima T., Nozdrovický L., Krištof K., Krupička J., 2013. Impact of the size of nitrogen fertiliser application rate on N_2O flux. Research in Agricultural Engineering.
Van Cleemput O., Samater A. H., 1996. Nitrite in soils: accumulation and role in the formation of gaseous N compounds. Fertilizer Research 45: 81-89.
Verma A., Tyagi L., Yadav S., Singh S.N., 2006. Temporal changes in N_2O efflux from cropped and fallow agricultural fields. Agriculture, Ecosystems & Environment 116: 209-215.
Williams E. J., Hutchinson G. L., Fehsenfeld F. C., 1992. NOx and N_2O emissions from soil. Global Biogeochemical Cycles 4: 351-388.

DETERMINATION OF DIFFERENT ANIMAL SPECIES HAIR VISCOELASTIC PROPERTIES

Lucie Šimková[1], Marie Skřontová[1], Karel Jelen[1], Bohumil Chalupa[2]

[1]Department of Anatomy and Biomechanics, Faculty of Physical Education and Sport, Charles University in Prague, Jose Martiho 31, 162 52 Prague 6 – Veleslavin, Czech Republic
[2]Department of physics, Faculty of Engineering, Czech University of Life Sciences Prague, Kamycka 129, 165 21 Prague 6 – Suchdol, Czech Republic
e-mail: LucikSimik@seznam.cz

Abstrakt

The paper deals with the analysis of deformation curve of the hair of different species and with determining of basic viscoelastic parameters thereof. From the data obtained authors come to inter-species differences of particular parameters, influencing of viscoelastic parameters' values by the pigmentation, and most importantly, they determine the dependence between the diameter and the Young's modulus of particular animal species. Among the basic parameters evaluated in this work, hair diameter, Young's modulus in tension, yield strength, ultimate strength and fracture strain are discussed. Animal species studied include human (Homo sapiens sapiens), domestic cat (Felis silvestris f. catus), domestic dog (Canis lupus f. familiaris), ferret (Putorius putorius furo), Guinea pig (Cavia aperea f. porcellus), horse (Equus caballus f. caballus), domestic goat (Capra aegagrus hircus), domestic rabbit (Oryctolagus cuniculus f. domesticus), dromedary (Camelus dromedarius). Essential findings are 1) black coloured pigmentation increases the Young's modulus, 2) outdoor breeding increases the hair diameter, 3) the value of hair diameter decreases with increasing Young's modulus. Minimum Young's modulus from the animal species studied has been found in domestic cat.

Keywords: viscoelastic parameters, hair, animal species, deformation curve.

Introduction

The paper deals with comparison of mechanical properties of different mammals' species hairs.

Hair kinds

Mammals' hairs are of very different kinds. Most often they are cover hairs and underfur hairs.

Cover hairs are coarse and long and they always contain medulla. They grow out of the skin individually and overlap other coat. They grow up slantwise from the skin and they keep common direction over large regions. Thus hair streams and vortices are formed, the latter being either convergent or divergent. They are often colored and changed continuously (Reece, 1998).

Underfur hairs are thin and soft hairs, that don't contain medulla, or it is reduced in them. They grow perpendicularly from the skin (Reece, 1998). They participate in thermoregulation. They are the shortest, most thin, finest hairs and their diameter is constant over their whole length.

The hair maintains itself constantly by its hairs renewal. After their growth completion, the hairs start ageing, they become worn out and eventually they fall out from the skin. Underfur hairs fall out usually twice a year, in the spring and in the autumn. Large scale underfur hair loss is denoted as moulting (Reece, 1998). The pattern of human hairs is changing continually from prenatal development up to the old age and the same follicle creates different hair types successively even in physiological conditions. Since the hair growth cycle takes at least 1000 days in adult humans, about 100 hairs a day can fall out even in physiological conditions (Bartosova et al., 1984).

Hair characteristics

Hairs *(pili)* are threadlike corneous structures of mammals' skin. They protect the skin against adverse environment effects like water, sunshine, mechanical and other actions. Coherent air layer built near the skin surface and within the fur is important for thermoregulation. The hairs' pigmentation implicates both general fur coloration and its changes with the age and the season (Reece, 1998).

Hair composition

Macroscopically, one can distinguish between the root and the shaft on a single hair. Microscopically, the hair consists of three layers, them being medulla, cortex and cuticle.

Medulla is found in the hair centre and it is formed through the whole hair length in the coarse terminal hairs only (Benzarti et al., 2011). In thin hairs, it is reduced or it doesn't develop at all (Reece, 1998). In fine hairs, it can be fragmented, or present in particular segments only, or missing completely (Bartosova et al., 1984). In animals, medulla is fond more often and it serves as thermoregulation. In humans, this demand has become secondary.

The *cortex* is the main cellular hair layer, which gives it its strength and overall character. Pigment is embedded in the cells and according to its distribution the hairs display either dark or light colour. In case of air penetration of the intercellular space, the hairs are gaining grey colour (Reece, 1998). This applies also in humans. There, the cortex accounts for up to 90 % of the hairs' mass. It comprises a complex fibrous system influencing mechanical properties of the hair (Benzarti et al., 2011).

The cuticle, formed from a single layer of transparent cells without pigment, display signs of keratinization (cornification). Free edges of the hair cuticle cells are formed diversely and they are oriented to the free hair end (Bartosova et al., 1984; Reece, 1998). The cuticle protects inner parts against external environment and the damage from daily treatment. Cuticle's thickness is 3–5 μm and it accounts for up to 10 % of the hair mass (Benzarti et al., 2011).

Objective

Our objective has been determining of the dependence between particular mechanical parameters and determining this parameters' dependence on the species.

Materials and methods

Mechanical properties of the hairs depend (besides hair length and thickness) also on the keratin molecules being soaked with water, thus on relative humidity and temperature, at which the hair samples are examined (Bartosova et al., 1984).

Samples of the hairs had been obtained from various species of mammals. The samples had been snipped from equal place with sharp scissors just above the skin surface. From animals, they had been taken from the shoulder area, except of the horses (tail horsehair) and at humans from the occiput

Using an optical microscope equipped with a digital camera, diameter was determined for each sample. It was measured 15 times in the first 3 cm of the sample, i.e. at each 2 mm of its length. From values taken this way, average has been calculated for each sample.

Thereafter, thus measured part of the sample had been fixed in the jaws of the testing machine Deform type 2 (Fig. 1). This equipment is suitable for measuring of small slow changes in biological materials. With 20 N load cell range, and special jaws for measuring of fibres, the machine allows for both determining classical deformation curve and relaxation or even cyclic load measurements. The travel of the jaws is max. 215 mm, that's why we're using samples of up to 5 cm length. The machine is controlled through an Ethernet connection by a multiplatform client Trhey!. The sensitivity is 5 mN. The testing machine can be moved around easily thanks to its relatively low mass of 38 kg.

Particular samples had been tensioned with the jaws motion speed of 2 mm/min up until the specimen breakage. From recalculated deformation curves (Fig. 2), i.e. the dependence of true stress on the true strain, mechanical parameters of particular samples (Young's modulus, yield strength, ultimate strength and maximal elongation) have been established.

Fig. 1 Testing machine Deform type 2

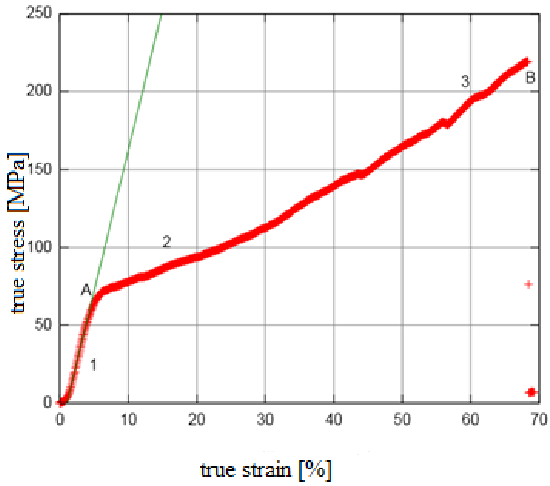

Fig. 2 Typical deformation curve

Deformation curve splits into three parts:

- First – elastic part (the part in which the deformation is so small that as long as external forces stop act, the sample returns to its original shape and dimensions) contains in case of both human and animal hair also the Hookean area (1), where the stress is directly proportional to the deformation. The constant of this proportionality and hence the slope of the fitted straight line gives the Young's modulus. Second part is non-linear and it ends with the yield strength (A), which defines maximum elastic deformation. Deformation past this point on the curve are plastic already and after stopping external force action the specimen remains deformed permanently. In this point, the curve passes into so called plastic area of deformation.
- Second part (2) is the area past the yield strength. It is characterized by viscoplastic deformation. The shape of the curve is affected significantly by deformation velocity in this area.
- Third part (3) is the area of the hardening before breakage (B). At constant stress increase, sample breakage appears (Benzarti et al., 2011). Dawber, Messenger (1997) state that in the area of 30 – 70 % elongation, irreversible changes occur and elongation of 80 % causes hair breakage. Our experience though moves the beginning of the irreversible changes in front of the area (2), past the 5 % relative deformation boundary. Maximum elongation, i.e. the B point position on the deformation axis is situated at 48 – 52 % in most nations and at about 40 % in Czechs according to our observation.

Young's modulus (E) is determined from the Hookean (linear) area of the deformation curve approximated with a linear function. Yield strength is defined by the coordinates of the cross-section of linear approximations of the deformation curve in the Hookean area and in the beginning of the plastic area. Ultimate strength is the maximum stress before the sample breakage. It is determined together with maximum elongation as the coordinate of the terminal point of the deformation curve. The coordinate on the independent variable axis presents maximum elongation [%], and the coordinate on the dependent variable axis gives the ultimate strength [MPa].

The data obtained have been processed and afterwards interpreted in graphic form.

Results and discussion

All material parameters of the hairs except of diameter have been determined from the deformation curve, a typical representative if which can be seen in fig. 2. These material parameters have been investigated: hair diameter, Young's modulus in tension, yield strength, ultimate strength and maximum elongation. Not all parameters could have been determined for all animal species from the deformation curve. They are listed in Table 1.

Tab. 1 Overview of mechanical parameters in view

	Diameter [μm]	E [GPa]	MS [MPa]	MS [%]	MP [MPa]	MPr [%]
Ho	88 ± 13	1,3 ± 0,3	72 ± 30	6,8 ± 3,9	265 ± 91	108 ± 21
Fe 1	55,6 ± 2,8	0,153 ± 0,018	2,33 ± 0,25	2,03 ± 0,61	5,5 ± 1,1	16,2 ± 5,2
Fe 2	69,2 ± 6,4	0,194 ± 0,056	2,77 ± 0,46	1,43 ± 0,34	7,0 ± 1,9	9,2 ± 6,1
Ca 1	133 ± 22	1,9 ± 0,5	48 ± 28	2,32 ± 0,31	119 ± 53	25,4 ± 1,8
Ca 2	57 ± 18	5,0 ± 1,3				
Put A	37 ± 12	4,9 ± 2,5	7,2 ± 4,3		85 ± 37	
Put B	91,6 ± 7,6	1,9 ± 1,2	6,8 ± 4,4		63 ± 44	
Cav	74 ± 18	2,6 ± 1,3	57 ± 31	2,8 ± 1,1	138 ± 79	29 ± 12
Eq FJ I.	142	2,5		4,7		13
Eq FJ II.	145	2,3		3,8	110	24,9
Eq PH I.	140	6,2		7,8		18
Eq PH II.	137	3,6		3,9		19,3
Eq SH I.	126	3,8		5,8		26
	Diameter [μm]	**E [GPa]**	**MS [MPa]**	**MS [%]**	**MP [MPa]**	**MPr [%]**
Eq SH II.	166	2,4		6,4		8,7
Cp	94 ± 25	2,9 ± 1,3	82 ± 30	3,9 ± 1,5	166 ± 14	27 ± 10
Cu I.	72 ± 25	10,7 ± 9,0	26 ± 20	14,8 ± 1,6	45 ± 36	13,7 ± 3,3
Cu II.	68 ± 21	7,5 ± 5,7	19 ± 13	18,6 ± 8,6	35 ± 22	18,5 ± 8,1
Cam	62,5 ± 3,9	1,1 ± 0,1	38,4 ± 8,9	4,0 ± 1,6	80 ± 15	53,3 ± 6,6

Glossary to Table 1:
E [GPa] – Young's modulus in tension in GPa
MS [MPa] – yield strength in MPa
MS [%] – yield strength in %
MP [MPa] – ultimate strength in MPa
MPr [%] – maximum elongation in %
Ho - human (*Homo sapiens sapiens*)
Fe 1 - domestic cat (*Felis silvestris f. catus*), kept outdoor
Fe 2 - domestic cat (*Felis silvestris f. catus*), kept indoor
Ca 1 - domestic dog (*Canis lupus f. familiaris*), kept outdoor
Ca 2 - domestic dog (*Canis lupus f. familiaris*), kept indoor
Put A - ferret (*Putorius putorius furo*), underfur
Put B - ferret (*Putorius putorius furo*), guard hair
Cav - Guinea pig (*Cavia aperea f. porcellus*)
Eq FJ I. - horse (*Equus caballus f. caballus*), Fjord horse, dark horsehair
Eq FJ II. - horse (*Equus caballus f. caballus*), Fjord horse, light horsehair
Eq PH I. - horse (*Equus caballus f. caballus*), Paint horse, dark horsehair
Eq PH II.- horse (*Equus caballus f. caballus*), Paint horse, light horsehair
Eq SH I. - horse (*Equus caballus f. caballus*), Shetland pony, dark horsehair
Eq SH II. - horse (*Equus caballus f. caballus*), Shetland pony, light horsehair
Cp - domestic goat (*Capra hircus*)
Cu I. domestic rabbit (*Oryctolagus cuniculus f. domesticus*), dark haired
Cu II. - domestic rabbit (*Oryctolagus cuniculus f. domesticus*), light haired
Cam - dromedary (*Camelus dromedarius*)

When looking for dependence between the parameters, dependence of the Young's modulus on the hair diameter seems most significant. This dependence is always indirectly proportional. It's thus described by a hyperbolical dependence. It is interesting that generalization of the power coefficient yields no accuracy improvement of the approximation and the coefficients obtained always differ only slightly from one. Illustration of this dependence with the fitted function is shown in Chart 1.

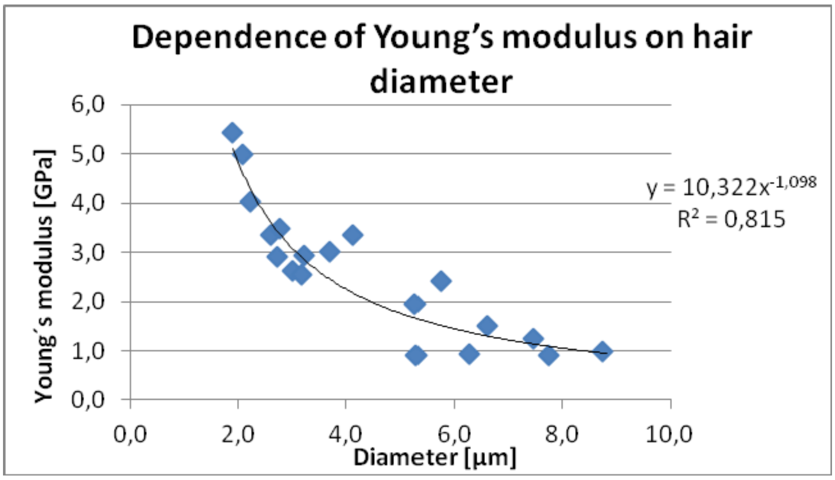

Fig. 1 Dependence of Young's modulus on hair diameter

Explanation of the dependence may be as follows: The hair cuticle has high Young's modulus and it is of the same thickness in all hairs, both thick and thin ones. Young's module of the cortex is at least one order of magnitude lower and its relative representation in the hair cross-section decreases with decreasing hair thickness. While the cuticle, its thickness being constant, is contained by higher percentage in thin hairs and the hair as whole thus appears more solid. However, verification of this hypothesis is not the aim of this work; it's necessary to combine mechanical testing of the hair with microscopic examination of their morphology.

As can be seen in Table 1, it is evident that the black pigment increases Young's modulus. It is lower in animals (cat, dog) kept outdoor than in animals kept in the household.

Conclusion

We have succeeded in finding material parameters of the hairs of several species of mammals. We have shown the dependence of Young's modulus on the fur pigmentation and on the rearing method of particular species and described the dependence of elasticity module on the hair diameter.

References

Bartosova L., Jorda V., Stava Z., 1984. Diseases of the Hair and the Scalp. Farmington, Connecticut, U.S.A.: 256.

Benzarti M., Tkaya M. B., Mattei C. P., Zahouani H., 2011. Hair Mechanical Properties Depending on Age and Origin. World Academy of Science, Engineering and Technology 74: 471-477.

Dawber R. P. R., Messenger A. G., 1997. Hair follicle structure, keratinization and the physical properties of hair. In: R. Dawber (ed). Diseases of the Hair and Scalp. 3rd edn. Oxford: Blackwell science: 23-50.

Reece W. O., 1998. Physiology of domestic animals. Grada: 456.

INFLUENCE OF AUDIOSTIMULATION ON MILKING INTERVAL ON DAIRY FARMS EQUIPPED BY AUTOMATIC MILKING SYSTEM

Josef Simon[1*], Miroslav Prikryl[1], Antonin Machalek[2]

[1]Czech University of Life Sciences Prague, 16521 Prague 6 – Suchdol, Czech Republic, Phone: +4202-33022301, E-mail: josef.simon@vuzt.cz
[2]Research Institute of Agricultural Engineering, p. r. i., Prague, Czech Republic

Abstract

On the farm with Holstein dairy cows, where are installed single stall automatic milking robots, was experimentally verified device for audio stimulation of cows to visit the automatic milking machines. There were chosen 10 cows for the experimental group and 10 cows for the control group. Cows were selected in order to age and stage of lactation. There was used the specially developed programmable audio device, which allows to play sound of pouring the pellets into feeder inside the robot in the preset interval and time duration. Device was attached on the collars of cows in the experimental group, placed directly behind the cow ears. The playing interval was set to 8 hours, with 10 second time duration. There was 10 minute execution time offset for individual cows, which represents the time spent in the robot including time reserve. Obtained data from the herd management program of automatic milking system, which observes and saves details about the herd and individual dairy cows, confirmes positive effect of controlled audio stimulation on number of visits in the robot, count of milking, shortening of interval between milking, which results in increasing the daily milk production and improving mammary gland health of dairy cows. After application of audio device there was shortened maximum interval of milking almost by 15 minutes compared to control group, average interval of milking was shortened approximately by 21 minutes. Number of visits in milking robot by cow per day was increased by 0,44 compared to the control group, number of milkings per cow and day was increased by 0,33 and daily milk production per cow was increased by 1 liter compared to the control group. This results indicates, that is possible to use audiostimulation to normalize milking interval of dairy cows on farms equipped by automatic milking system.

Keywords: dairy cows, robotic milking, audio stimulation

Introduction

Technology of milking using the milking robots has some spefics in relation to animals compared to a conventional milking in parlour, which especially lies in free movement of dairy cows and their access to the milking apparatus. It is decision of individual cow when will be milked. But it is desirable, that the milking interval was regular with a certain minimum frequency, to maximize the milk yield. The same opinion refers to the interval of milking and its frequency has also Hulsen (2008), who says, that the objective is that all cows went to the robot spontaneously, regularly and often enough. Regarding the milking frequency, for example, dairy cows with higher yield (more then 35 kg of milk) which are milked two times per day, after the transition to the three times milking per day has increased milk yield by 18,9 %. (Doležal et al., 2002). Except the direct stimuli, such as the pressure inside the filled udder, tension, uncomfortable walk or desire for the hormone oxytocin, the desire for pleasant stimulation of teat receptors and the pleasant feeling of mammary glands after the milking, cows can be stimulated to the visit the milking robot indirectly using the feeding concentrate in the feeder inside the robot. Regarding the intervals between the milking, in practice there is a large variance of individual cows during the day (De oning, 2010; Machalek et al., 2011). At present time is about 160 robotic milking stalls in operation on Czech farms and their number is still increasing. Developments in the Czech Republic follows the global trend. There are a further installations of automatic milking systems. To take a full advantage of the genetic material of high yield cows, it should be used the principle of voluntariness and freedom of movement of animals, it is necessary to provide them the suitable breeding environment and search the further possibilities for higher effectiveness of the system. One option to bring the higher effectiveness of the system is the normalization of milking interval and its frequency using the dairy cow audio stimulation with audio device placed near the ear of cows (Machalek et al., 2011). There was realized an experiment for the verification of this hypothesis in the stable with 4 milking robots.

Materials and methods

The experiment was realized in a new free stall dairy barn with 2 x 3 rows of beddings with mattres. Barn is divided into four sections of milked dairy cows and two calving pens. In each of sections is installed one single stall milking robot. For the experiment purposes was chosen one sections with fourty Holstein dairy cows of different age and stage of lactation. In this section was chosen in lottery 10 cows for the experimental group and 10 cows for the control group. So that in the both groups was the same number of cows according to its age and stage of lactation. There was used the specially developed programmable audio device, which allows to play sound of pouring the pellets into feeder inside the robot in the preset interval and time duration. Device was attached on the collars of cows in the experimental group, placed directly behind the cow ears. The playing interval was set to 8 hours, with 10 second time duration. There was 10 minute execution time offset for the individual cows, which represents the time spent in the robot including time reserve. View inside the audiostimulator is shown in Fig.1. Led diod signalize the operating status. For connection to computer is used USB port. In the Fig.1 is also shown the simple user interface for programming the audio device which allows setting the current time, day and time of execution, number of repetitions and record audio.

As a source of the information about the experiment and detailed data of individual cows provides the herd management program, which is a part of the milking robot equipment, in which is simultaneously created and stored database of whole herd. Obtained data was processed and evaluated in the MS Access and MS Excel.

Fig. 1 Inside view of the audiostimulator, connection via USB, programming interface and audiostimulator attachment on cow collar

Results

The measured data of the interval of milking during the experiment and before the experiment show, that the interval of milking was increased in the both groups, but after application of audio device there was shortened maximum interval of milking almost by 15 minutes compared to the control group. Before the experiment was the maximum interval of milking in the experimental group 9h37m24s and in the control group 10h06m33s. After the application of audiostimulator the maximum interval in the experimental group was changed to 10h20m25s and in the control group to 11h04m24s. In the experimental group was difference 43m01s and in the control group 57m51s. If we look at the average interval of milking, the difference between the experimental and the control group is approximately 21 minutes. Details are shown in the graphs in Fig. 2 and Fig. 3.

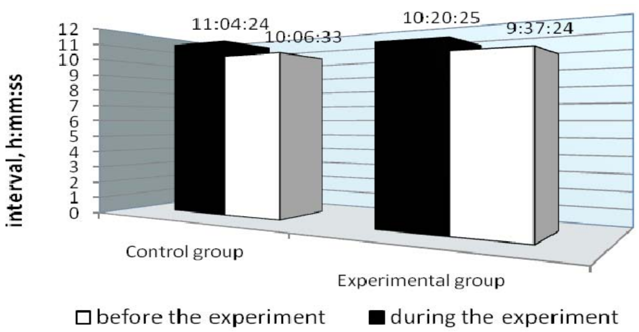

Fig. 2 The average of the maximum interval of milking on the Czech dairy farm equipped by automatic milking system before and after the application of audiostimulator

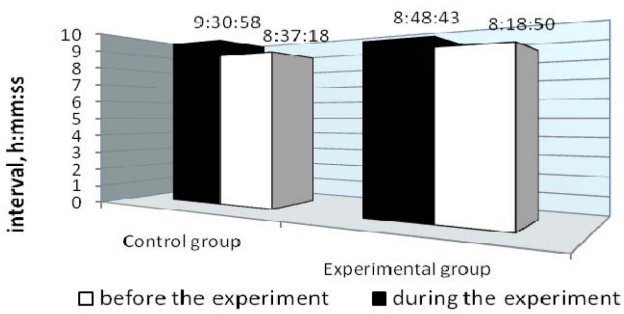

Fig. 3 Average interval of milking on the Czech dairy farm equipped by automatic milking system before and after the application of audiostimulator

During the experiment was the number of visits in the milking robot per day decreased compared to period before application of audiostimulator. In the experimental group was the number of visits per day decreased by 0,64 and in the control group by 1,08, it means, that difference between the experimental and the control group was 0,44. The same situation was in the number of milking per day. There was the difference between the experimental and the control group 0,33 milking per day. Details are shown in the graphs in Fig. 4 and Fig. 5.

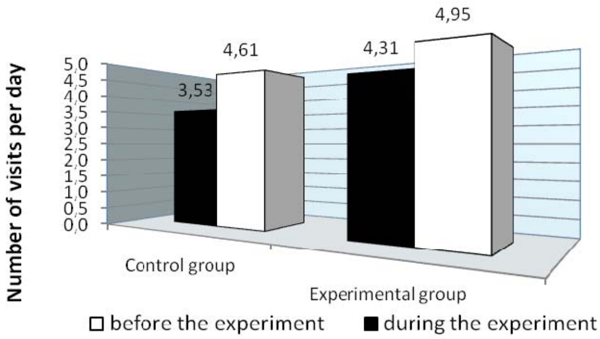

Fig. 4 Average number of visits in milking robot on the Czech dairy farm equipped by automatic milking system before and the after application of audiostimulator

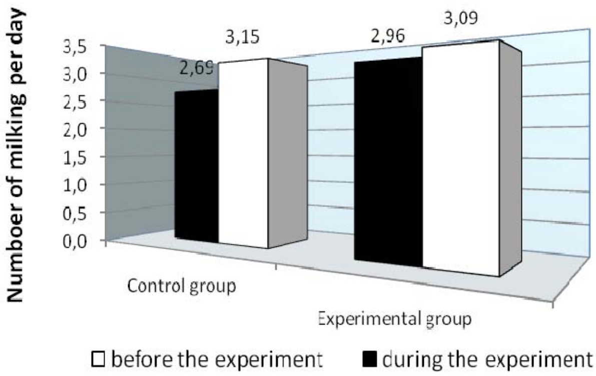

Fig. 5 Average number of milking on the Czech dairy farm equipped by automatic milking system before and after the application of audiostimulator

In both groups there was the decline in milk production. In the experimental group was the decline approximately 0,2 l of milk per cow and day and in the control group was the decline approximately 1,2 l of milk per cow and day. In the daily milk production there was the difference between both groups 1 l of milk per cow. Details are shown in the graph in Fig.6.

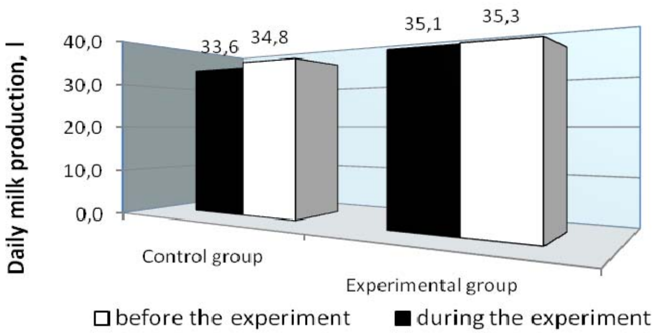

Fig. 6 Average daily milk production per cow on the Czech dairy farm equipped by automatic milking system before and after the application of audiostimulator

Discussion

Although there was worsening of selected parameters in the both groups during the experiment compared to period before the experiment, difference between experimental and control group is noticeable. In the experimental group due to application of audiostimulation was worsening significantly less compared to control group, so positive effect of audiostimulation on dairy cows willingness to visit the milking robot is demonstrable. Worsening of the parameters may be caused by many factors. One of the most important is heat stress. During the experiment period was average daily temperature higher than in period before experiment. Generally, it is important to minimize all disturbances in the stable. Setting the propper execution time of audiostimulation, according to individual requirements of the animals within a group, their habits and hierarchical status, could increase effectiveness of the system.

Conclusion

The results show possibility of use an audiostimulation to normalize milking interval of dairy cows on farms equipped by the automatic milking system. Next research should solve optimalization of time period between milking in context to a herd management and individual requirements of each cow due to its health condition, age and stage of lactation.

References:

De Köning C.J.A.M., 2010. Automatic milking: management and milk quality, International workshop: The future of the quarter individual milking, Bornimen Agrartechnische Berichte, heft 76, Potsdam –Bornim, 81- 98.

Dolezal O., Bilek M., Cerna D., Dolejs J., Gregoriadesova J., Knizkova I., Kudrna V., Kunc P., Toufar O., 2001. Komfortní ustájení vysokoprodukčních dojnic. Praha: Výzkumný ústav živočišné výroby. ISBN 80-86454-23-1 (in Czech)

Hulsen J., Rodenburg J., 2008. Robotic Milking, Zutphen: Roodbond Publishers, 52. ISBN:978-90-8740-043-9

Machalek A., Vegricht J., Simon J., Fabianova M., 2011. Utilization of audiostimulation for control of tima period between milkings on farms equipped by automatic milking machines. In: Ecology and farming technologies:agro-engineering aproaches: Proceedings of the 7th Internacional Scientific and Practical Conference. Saint-Petersburg: SZNIIMESH Publisher, 3: 98 – 103.

METHODS FOR DETECTION OF OBJECTS IN AGRICULTURE

Filip Skerik*, Jaromir Volf, Miloslav Linda , Tomas Martinek

Czech University of Life sciences in Prague, 16521 Prague 6 – Suchdol, Czech Republic, Phone: +420 22438 3193, E-mail: skerikf@tf.czu.cz

Abstract

Recognizing the size and type of the object in agriculture is important in moving the machinery and the material and their classification. Any material that is moving along a vibrating conveyor belt, or only after the conveyor can be detected and evaluated using a program created in a development environment Visual basic.net. The sensing element is Kinect sensor which senses the space in the direction of its rotation and transmits the data to a computer for further processing. After detecting the individual elements of the system evaluates this information and transmit signal actuators.

Keywords: Pattern recognition, objects detection, edge detection, Kinect sensor, laser measure system, actuator

Introduction

In agriculture, we do not only recognize small objects such as stones in the field, seed plants, straw bales, but also agricultural machinery. Other detectable things are obstacles that may make it more difficult work or crossings of agricultural machinery. They detect and use several methods. Each method uses sensors in the front area or in the vicinity of agricultural machinery and evaluates this information and process.

Edge detection

Edge detection is used in facilitating the crossing of agricultural machinery. The program is variously definable. The system can watch one or more of the white lines crossing on the road and by them to determine the direction of travel. The line monitors the real-time evaluation of the information takes place immediately. Custom application contains GUI (graphical user interface) for more comfortable for users. There are three buttons Open, Start and End. Furthermore, we can set one of the five methods of the edge detection (Sobel, Prewitt, Roberts, Canny and LoG) and the ability to determine the number of search lines. To coordinate the right is drawn loaded image. After you run the application and view the GUI interface and click on the Open button a menu will appear with a selection of the path to the image (allowed formats are *. Jpeg and *. Bmp). When you press the Start button then start the main part of the program. It is very important part of working of images and search for objects, their pre-processing. Our loaded colour image is first converted to grayscale and then adjusts the contrast. All these processes take place automatically according to the program.

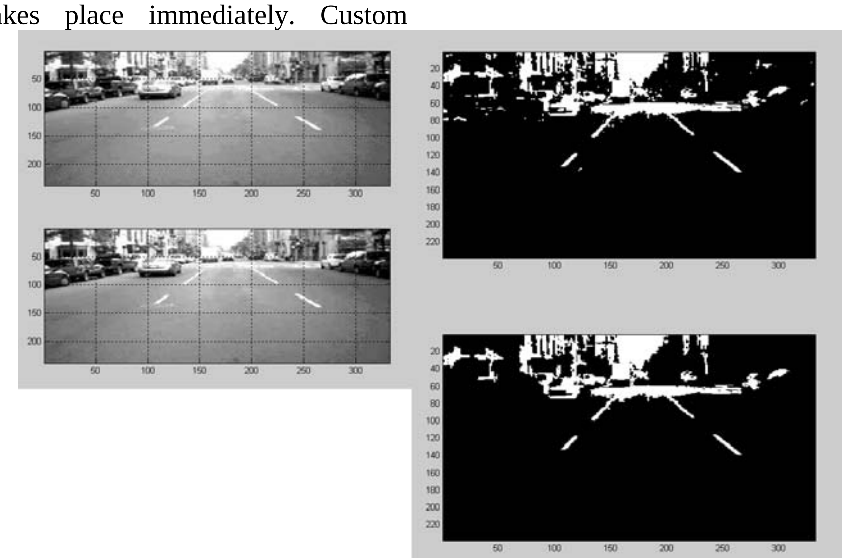

Fig. 1 Edge detection

Laser measuring system

Laser measuring system can detect objects of various sizes, from small stones on the field to large agricultural machinery. The advantage is the possibility of vertical for horizontal mounting.

The device consists of a laser sensor space, a control unit and controls. Laser measurement system LMS 100/111/151 an unconventional broadband detection system that allows the reflected optical beam control almost circular area with a diameter of over 20 meters. Typically used angular width of the space 270 degrees with a precision of 0.25 or 0.5 degrees in the scanning frequency of 25 or 50 Hz. LMS is used for operation up to 20 W. The laser measurement system for normal operation operates fully automatically without operator intervention. Interactive communication takes place using the supplied configuration software soaps ET. Wavelength of the beam is in the range 892 nm to 915 nm, the beam is safe even if accidentally hit the eye. The laser sensor does not work only as a transmitter / receiver reflected beam to a conventional diffuse optical sensors, but there is also directly measure the distance of objects from the sensor by measuring the time of flight. The sensor does not transmit light beam still, but at regular intervals generated from a laser light pulse and internal electronics expects his arrival at the optical receiver and calculates the elapsed time. If the reflected pulse arrives, time is deducted, which evaluates the distance. Where to send another pulse reflection comes, there is no sensor in the range of object. This mode is also gradually made throughout the scanned area at angles up to 270 degrees incrementally to 0.25 degrees, which is sent to 1080 pulses. The width of the scanning area can be adjusted freely, so you can scan a well-defined space. The sensor is fixed on the front page of agricultural machinery, so it will be possible to accurately determine the direction in which the single pulse send and receive, which can accurately detect the obstacle and the sensor itself will determine its distance. All data will be transported from the sensor to the control unit which processes the data and evaluate exactly in what direction and how far away an obstacle. After evaluating the results of the control unit sends a single pulse output control and manage specific present active element.

Fig. 2 Laser measuring systém

Scanning the area with Kinect sensor

Using the Kinect sensor, you can remove any items, but we are limited by the distance of the sensor from the subject. Kinect sensor reads the premises or equipment, and using Visual basic.net evaluates this information and process. The colour range we find the distance of the objects. The colour spectrum we convert the unit of distance, which is further processed and output actuator. Unfortunately the Fig. 3 is only in the gray scale and colour spectrum isn´t showed (the left figure of Fig. 3). The mask of the car is blue, the windscreen is green and the background is red in our colour range. The colour of floor continuously turns from blue through green, yellow to red colour.

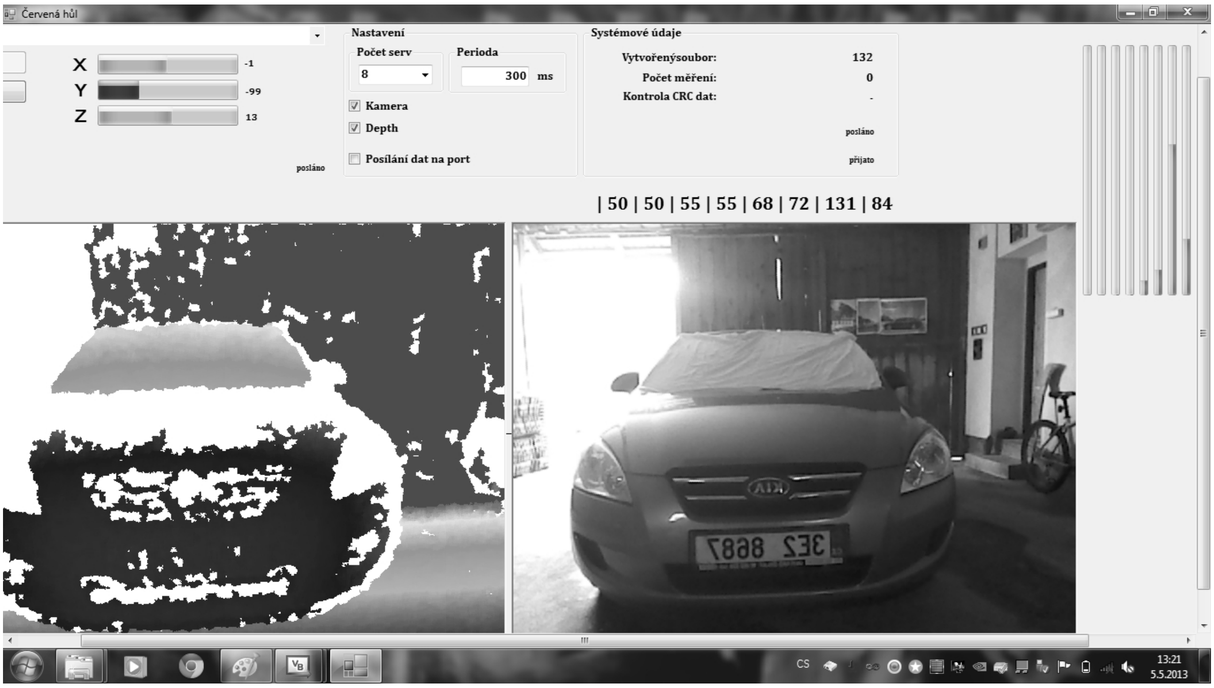

Fig. 3 Scanning the area with Kinect sensor

Conclusion

In this paper were described different methods for determine objects and their distance from the observer. The hardware and the software methods ware in this paper short described. Each object detection method has its advantages and disadvantages. We need to know what objects we want to detect in which environment and with what accuracy. You can then select a suitable method to implement the operation. The application of each method we have to consider the financial and technological demands. The using of the Kinect sensor sounds like very perspective.

Acknowledgment

This paper was supported by the Grant Agency of the Faculty of Engineering. The project "Collection and use of tactile information in agriculture through tactile activator" number: 31200/1312/3126.

Reference

Liang J., Yang J., Zhang C., Sun J., Zhu D., Shi L., Yang J., 2013. An object-oriented binary change detection method using nearest neighbor classification, IFIP Advances in Information and Communication Technology, 393(2): 394 - 406.

Lin T. T., Tsai A. C., Chuang K. C., Chen Y. C., Chen Y. S., 2012. A real-time stereo vision system for obstacle detection and recognition, American Society of Agricultural and Biological Engineers Annual International Meeting, 6: 4943 - 4959.

Ma J., Li D., Chen Y., Li L., Gao F., Zhang L. A collision detection-based wandering method for equipment deploy scene in land reclamation area of mining dump, IFIP Advances in Information and Communication Technology, 368(1): 455 - 460.

Wu J., Peng B., Huang Z., Xie J., 2013. Research on computer vision-based object detection and classification, IFIP Advances in Information and Communication Technology, 392(1): 183 - 188.

THE RELAXATION OF STATICALLY LOADED COMPRESSION SPRINGS

Vladimir Sleger, Cestmir Mizera*

Czech University of Life Sciences Prague, 16521 Prague 6 – Suchdol, Czech Republic,
Phone: +420 22438 3186, Fax: +420 234381828, E-mail: mizera@tf.czu.cz

Abstract

The article presents the measurement results of the relaxation of long-term loaded compression springs manufactured out of non-alloy steel. During the relaxation test that lasted one year in a laboratory with a temperature of 22 ºC, initial shear stress set at a value of 30 % of the ultimate tensile strength of the material, decreased the strength of the springs with a wire diameter of 1 mm by 4.0 %, springs with a wire diameter of 3.15 mm by 3.1 %, and springs with a wire diameter of 5 mm by 1.6 %. By lowering the initial shear stress to a value of only 14 % of the ultimate tensile strength of the material, no relaxation greater than 1.1 % was recorded in any of the springs during measuring. This initial shear stress value is recommended as a maximum in applications where the relaxation of statically loaded springs manufactured out of carbon steel has a significant impact on the operation of the device.

Keywords: relaxation, spring compression

Introduction

In the case of statically loaded springs, the permissible operating torsional stress is limited by the relaxation which can be tolerated, depending on the particular application concerned. Relaxation is the loss of the applied force (stress) in the long-loaded element when the strain is constant. The decline in force depends on the initial stress, temperature, and time (ČSN EN 13906-1:2003).

The measurement of statically loaded elastic elements and the influence of various parameters described eg Pothier (1976), Chang and Steckel (2003), Yu and Zhou (2010). The publications deal with disc springs. Relaxation of tension springs measured as Idermark and Johansson (1979), Dykhuizen and Robino (2004). Compression springs examined in detail Batanov and Petrov (1953). Examined the effect of the size of the initial stress, wire diameter, free height and pitch of the spring. According to the authors, the relaxation of springs is mainly during the first hours of compression, then it is very slow. The longest test lasted 816 hours. Deda et al. (1997) described the relaxation of compression springs made of stainless steel. Berry (1961) recommended applications sensitive to relaxation, the initial stress in the compression springs made of carbon steel does not exceed 25 % of yield. Restriction relaxation of statically loaded springs can also overload them before use, using the prestressing. Prestessing is a process of compression springs used in manufacturing or assembly to create a residual stress in the spring. The spring is produced longer by about 10 % to 30 % and then is temporarily compressed to a length which is exceeded by at least 10 % of the yield strength in shear (Shigley et al., 2010). The result is very rapid compression deformation, thereby achieving the desired spring length in a free state. When strain occurs in the section of the desired residual stress, it has an opposite orientation than stress generated during operation of the spring. Data on the relaxation after 48 hours of compression springs made from round wire specified in EN 10270, preset at ambient temperature, as a function of the torsional stress prior to relaxation at various temperatures and for several diameters are plotted in the Standard ČSN EN 13906-1:2003. So influence of time is not given. The relaxation values after 48 hours are regarded as characteristic values, despite the fact the relaxation is not fully completed at this point in time.

This article presents the results of measurements of relaxation at room temperature for a long time (one year) once-preset compression springs made common practice of non-alloy steel.

Material and methods

The relaxation test was made with 30 pieces of new uncoated helical compression cylindrical springs from the same manufacturer. Their basic characteristics are listed in Tab. 1. They are made from a patented circular wire of non-alloy steel in accordance with EN 10270-1 class SH. Tensile strength R_m (MPa) was determined from empirical relationship $R_m = 2330 - 900\ \ln(d)$, where d (mm) is the wire diameter (Shigley et al. 2010). The ends of the springs are closed and ground. All springs have 8.5 active coils and 2 reverse coils.

The forces in the springs and the corresponding deformation, i.e. the characteristics of the springs, were measured on a calibrated testing machine MPTest 5050 Corporate LaborTech, CR. Electromechanical servo driven machine complies to EN 7500-1 requirements for class 0.1. Accuracy force sensor is 0.5 %, the measurement start position and the track cross beam is 0.1 %. The testing machine at the start of each measurement was set to a known starting position and the force sensor and track were cleared. The selected initial distance plates were always greater than the free length of the spring measured. Set compressing speed was 0.5 mm/s. Free length L_o unloaded springs were determined from the position of the machine cross-member when the compression start rising force in the spring, a pusher plate was touching the sample.

The course of the relaxation test was as follows:

1. All springs are progressively using test equipment squeezed in length L_9 (1), ie almost fit coils.

$$L_9 = (n_t + 1)\ d\ \text{(m)}, \qquad (1)$$

where n_t = 10.5 is the total number of coils (-) and d (m) diameter wire. After pressing followed immediately relieving springs back to the free length.

2. The measured characteristics of the first compression were detected for each spring free length L_o and length L_8, which corresponds to the maximum permissible power F_8 stated by the manufacturer (Tab. 1). Force F_8 induces shear stress of about 50% of the yield strength in shear R_{se}. Also deducted was the length L_1 corresponding to the force F_1,

$$F_1 = \frac{\pi d^3}{8D}\tau_1\ \text{(N)}, \qquad (2)$$

where d (m), D (m) are the dimensions of the spring (Table 1) and τ_1 (Pa) is selected shear stress in the spring corresponding to 25% yield shear R_{se}. In accordance with the manual Shigley et al. (2010) has a yield strength in shear R_{se} considered value of 65% of the tensile strength R_m, ie including the correction factor (EN 13906-1:2003) 1235 MPa (size springs I) 1290 MPa (II), 1335 MPa (III), 1075 MPa (IV) and 975 MPa (V).

3. For each size spring I to V were determined average lengths L_8 and L_1.

4. Set A of springs, resp. B (Tab. 1) were in the test machine pressed on the calculated average length L_8, resp. L_1. The measured characteristics were determined by reducing the free length L_o and deduct the corresponding new force F_8 and F_1 at the beginning of the relaxation test. Then it was possible from (2) to calculate the corresponding actual uncorrected shear stress τ_8 and τ_1 (ČSN EN 13906-1:2003).

5. After unloading and removal of the test machines, they immediately re-compressed the springs to the same length L_8, resp. L_1 used a special product made from nuts, bolts and washers. The required length was monitored using a digital caliper with a resolution of 0.01 mm and an accuracy of ± 0.03 mm. The tube of appropriate length was also inserted into spring size IV and V (see Fig. 1). Springs were left at room temperature of 22 ºC ± 3 ºC.

Tab. 1 Basic properties of the springs and labeling of samples

size of the spring	wire diameter d (mm)	mean diameter spring D (mm)	free length L_o (mm)	max. permissible force F_8 (N)	stiffness spring R (N·mm^{-1})	set	number of pieces i (-)
I	1.00	6.3	24	41.6	4.734	A	3
						B	3
II	1.00	8.0	30	34.8	2.312	A	3
						B	3
III	1.00	10.0	42	29.4	1.148	A	3
						B	3
IV	3.15	31.5	105	231.0	3.730	A	3
						B	3
V	5.00	50.0	150	490.0	5.920	A	3
						B	3

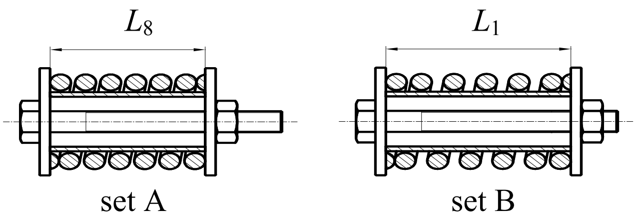

Fig. 1 The preparation for the relaxation test

6. At times of 3 hr, 6 hr, 9 hr, 24 hr, 48 hr, 100 hr, 260 hr, 430 hr, 600 hr, 770 hr, 1000 hr, 1500 hr, 2000 hr, 2500 hr, 3500 hr, 5000 hr, 8760 hr (1 year), the endurance test is interrupted and the test machine is measured by a new characteristic. The springs are compressed in the machine to the appropriate length L_8, L_1 respectively. Recorded are the changed values of forces F_8, resp. F_1. After relieving, the springs were immediately placed back into the test preparation (Fig. 1).

Results and discussion

Before starting the relaxation test it was verified by actual free length L_o purchased springs and attempted to short-term prestressing (stabilize) springs at room temperature. Due to single extreme compression length L_9 (1) to shorten the free length of springs ΔL_o which the stiffness R in Table 1 is the reduction of forces in the spring compressed to a certain length of $\Delta F = R \cdot \Delta L_o$. A significant change in stiffness preload does not (Šleger et al., 2012). The calculated values of each of the six measurements are in Tab. 2.

Purchased springs were therefore the first compression reduced by 0.1 % to 1.1 %. In order to preload we need a greater shortening (Shigley et al., 2010). Springs without the addition of stabilization are usually designed and constructed so that even when completely compressed to fit, not to exceed the yield strength. When it comes to large deformation, for example during assembly, then there can be no substantial changes to their properties. For effective preload recommended Shigley et al. (2010) stress limit state at least 1.1 times the yield strength.

Tab. 3 presents the findings of springs five sizes (see Tab. 1) set A (L_8) and set B (L_1) corresponding to the forces F_1 and F_8 at the first compression. The average lengths were chosen for long-term (8760 hr) test relaxation springs. Spring set A was the beginning relaxation test exhibited shear stress of about 50 % of the yield strength in shear, ie around 30 % of the ultimate strength R_m. Springs in the set B are weighted only 25 % yield, about 14% of ultimate strength R_m. Specific values uncorrected shear stress τ_8 and τ_1 at the beginning of the test (time t = 0 h) in the springs of various sizes are also listed in Tab. 3.

Tab. 2 Actual free length L_o and the influence of extreme compression springs to reduce ΔL_o, resp. decrease in force ΔF

		size spring				
		I	**II**	**III**	**IV**	**V**
L_o (mm)	average	24.04	30.38	42.16	106.50	151.44
	standard dev.	0.07	0.07	0.14	0.27	1.09
ΔL_o (mm)	average	0.27	0.33	0.45	0.34	0.20
	standard dev.	0.02	0.02	0.06	0.06	0.04
ΔF (N)	average	1.28	0.76	0.52	1.27	1.18
	standard dev.	0.09	0.05	0.07	0.22	0.24

Tab. 3 Determine length springs for relaxation test and shear stress at the beginning of the test

set			**size of springs**				
			I	**II**	**III**	**IV**	**V**
A	L_8 (mm)	average	14.62	15.20	16.30	45.47	71.71
		standard dev.	0.08	0.13	0.17	0.24	0.94
B	L_1 (mm)	average	19.57	22.87	29.95	77.30	110.24
		standard dev.	0.06	0.13	0.12	0.30	0.75
A	$\tau_{8\ (t=0)}$ (MPa)	average	644	688	738	595	499
		standard dev.	5	4	6	7	7
B	$\tau_{1\ (t=0)}$ (MPa)	average	285	311	317	270	243
		standard dev.	3	2	2	3	4

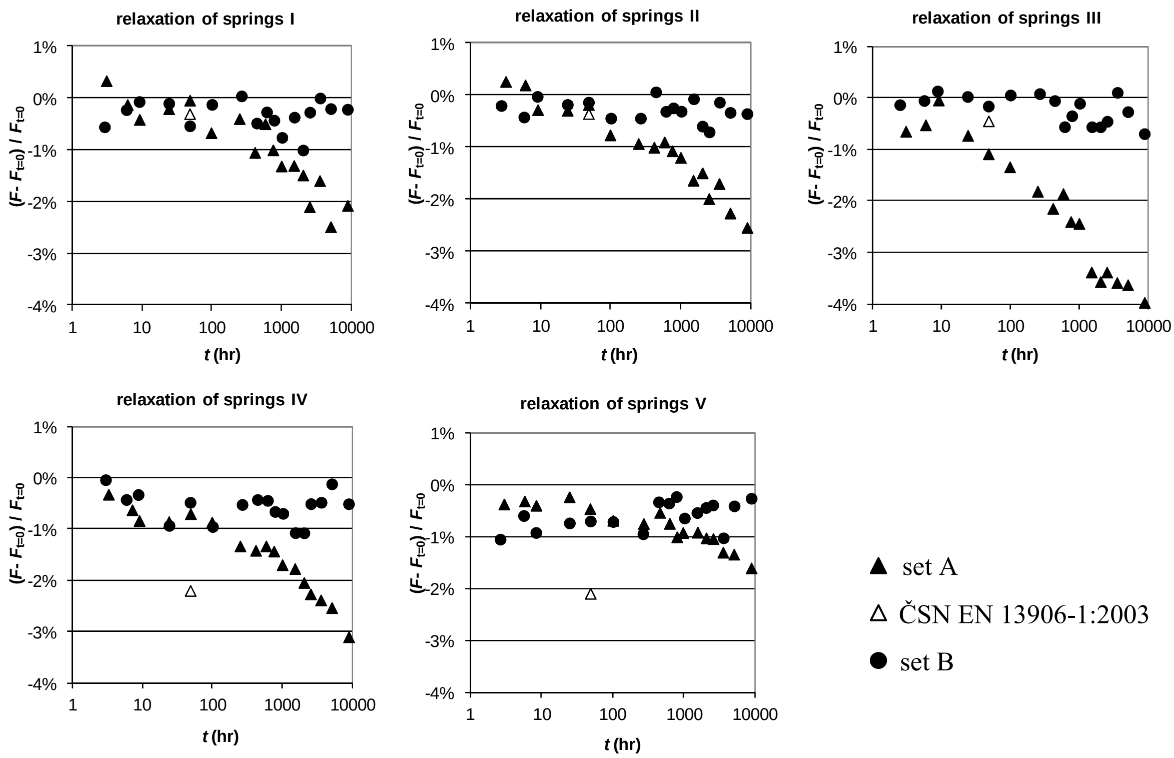

Fig. 2 Relative change of force (stress) in the springs of various sizes depends on time

Relative change of the force (or shear stress - dependence is the same) during the relaxation test in spring sizes I to V in Fig. 2. The spring set A of switching force F_8 relative to the value at the beginning of the test ($t = 0$ hr), the set B is the same for the force F_1.

Points in the graph show the average value of the measurement is always on the same three springs. Standard deviations of the measured values are in order of tenths of a percent. This error corresponds to the load cell used. Other causes are probably different material properties. Although they are all made of the same spring steel according to EN 10270-1, the composition of the material varies in a certain range. From the experiences of producers that have identical characteristics are guaranteed even with springs made in rapid succession on the same wire. The differences in relaxation may be due to different amounts of lattice defects in material identical springs, which have a significant impact on permanent deformation during relaxation.

The requirement for high accuracy measurements and time-consuming tests are among other reasons why the relaxation of statically loaded springs at room temperature, is a little researched phenomenon. Long-term static or quasi-static load springs occur in the measuring instruments, but the security devices also provide the necessary position of the various elements, etc. An unexpected change in the functional properties of the spring, the loss of stored energy could have serious consequences in some cases.

Reduction of shear stress in the statically loaded springs 25% yield by preventing the relaxation recommends Berry (1961) proves to be efficient (see Fig. 2, the set B), especially for smaller springs I to III. The question remains whether this will also apply during prolonged loads. Some springs even have negative relaxation. Preset and lightly loaded springs have a tendency to return to their original lengths, which they had before they were prestressed.

On Fig. 2 is displayed in addition to the measured results and the value of relaxation spring after 48 hours, obtained from the standard ČSN EN 13906-1:2003. The initial stress corresponds to a set A, the set B values are not available in the standard. The springs size IV are made of wire with a diameter 3.15 mm, the springs V with a diameter of 5 mm (Tab. 1). The standard, however, is only available close to the value of 3 mm and 6 mm. This does not explain the substantial difference between the measured and standard values for larger springs IV and V. The problem is that the standard is not specified length springs used and the number of coils. More detailed data do not contain the German DIN 2089-1:1984, which were the results for the European standard completely taken over. It is likely evidence of a significant influence of the size of the coil pitch on relaxation, which also points to Batanov and Petrov (1953).

The spring size I to III (wire diameter 1 mm), the values of standards agree with the measurements, but it is obvious that the standard does not provide information about the size of relaxation after prolonged loading. Value at 48 hours in the standard increased to relax during 8760 hr 6.9 x (size I), 7.3 x (II) and 8.8 x (III).

Batanov and Petrov (1953) reported a relative decrease in strength springs from wire with a diameter of 1 mm order of magnitude higher: after 264 hr it 13 %, after 816 hr it 15 %. Springs in their experiments to compress the touchdown coils in the cross section exceed allowable stress. The test thus provides a qualitative view of the relaxation provides a comparison of the influence of various parameters of the spring. The advantage is faster during the test.

Conclusion

The springs are usually designed so that even when completely compressed, not exceeded the yield strength of the material. With large deformation, for example during assembly, there cannot be significant changes in their properties. When you try to preload a spring, it has been shortened by a maximum of 1.1 % and had a decrease of force in the spring compressed to a certain length by a maximum of 1.3 N.

During the relaxation test lasting 8760 hr when the initial shear stress around 30 % of ultimate tensile strength of the material decreased the strength of the springs with a wire diameter of 1 mm by 4.0 %, springs with a wire diameter of 3.15 mm by 3.1 %, and springs with a wire diameter of 5 mm by 1.6 %. When reducing the shear stress at 14 % of ultimate strength was measured during the test in the spring relaxation no higher than 1.1 %. This stress is recommended as a limit in applications where the relaxation of statically loaded springs made out of carbon steel has a significant impact on the operation of the equipment.

The characteristic value of relaxation after 48 hours specified in ČSN EN 13906-1 of designing static and quasi-statically loaded springs is inadequate. In the standard is not described a pitch of coils of tested springs, which have a significant effect on the relaxation. Long-term load relaxation also increases significantly. Springs with a wire diameter of 1 mm after 8760 hr characteristic value are exceeded up to 8.8 x.

Current research focuses more on the dynamically loaded springs, usually at elevated temperatures. Variable load causes more pronounced, more measurable parameter changes in springs. This article is a contribution to the knowledge of the relaxation of statically loaded springs at room temperature. It is a phenomenon that is not sufficiently explored due to time-consuming tests and the necessity of high precision measuring instruments.

References

Batanov M.V., Petrov N.V., 1953. Steel springs. 1st ed. Praha: SNTL, 228. (in Czech)

Berry W.R., 1961. Spring design. 1st ed. London: EMMOTT, 324.

Chang D.J., Steckel G.L., 2003. Stress relaxation and stiffness of 17-7PH belleville springs in a stacked configuration. TR-2003(3901)-1. 1st ed. El Segundo: The Aerospace Corporation, 27.

ČSN EN 13906-1, 2003. Cylindrical helical springs made from round wire and bar-Calculation and design-Part 1: Compression springs. 1st ed. Praha: Český norm. institut, 36.

Deda S., Zhishou Z., Xinhua W., 1997. Research on Anti stress relaxational ability of helical compression springs made of austenitic stainless steel wires. Steel Wire Products, 2(5): 6.

Dykhuizen R.C., Robino C.V., 2004. Load relaxation of helical extension springs in transient thermal environments. Journal of Materials Engineering and Performance, 13(2): 151-157.

Idermark S.U.V., Johansson E.R., 1979. Room-temperature stress relaxation of high-strength strip and wire spring steels - procedures and data. In Stress Relaxation Testing, ASTM STP 676. 1st ed. Baltimore: American Society for Testing and Materials, 61-77.

Pothier N.E., 1976. Observed load deflection characteristics of belleville springs under static loads at room and elevated temperatures. 1st ed. Chalk River: Atomic Energy of Canada Limited, 24.

Shigley J.E., Mischke C.R., Budynas R.G., 2010. Mechanical engineering design. 1st ed. Brno: VUTIUM, 1186. (in Czech)

Šleger V., Herák D., Mizera Č., Divišová M., 2012. The change of the tension spring properties due to their prestressing. Agritech Science, 6(2): 1-6.

Yu Y.Z., Zhou X.Y., 2010. Experimental research on stress relaxation of diskspring used for laser optical mounts. Advanced Materials Research, 129-131: 531-535.

CALCULATION OF STRUCTURAL AND HEATING COSTS IN MODERN GREENHOUSES

Ahmet Tezcan*, Kenan Buyuktas

Department of Farm Structure and Irrigation, Faculty of Agriculture, University of Akdeniz, Post Box 07059, Antalya, Turkey, Phone: ++90 (242) 310 65 21, Fax: ++ 90 (242) 227 45 64,
E-mail: atezcan@akdeniz.edu.tr

Abstract

In this study, structural and heating costs of modern greenhouses in different sizes were determined by using "MS Excel Package Program". Three kinds of roof types such as gable, arc and gothic style, covered with plastic or glass were selected and three kinds of fuel types such as coal, fuel-oil and natural gas were used for water heating system commonly used in modern greenhouses for Mediterranean region. Users can determine structural and heating costs defining greenhouse sizes, heating time and fuel type by the package program. This developed program is easy to use, user friendly and has an interface used by everyone and it calculates the total costs according to the user preferences.

It is calculated that, when the modern greenhouses having same area compared according to the total costs, gable roofed greenhouses were more expensive 1.27 times than gothic and 2.64 times than arc-roofed greenhouses. Besides, gothic roofed greenhouses were also more expensive 2.09 times than arc-roofed greenhouses.

In addition, when the greenhouses evaluated by cover materials and fuel types, fuel-oil was more expensive 1.90 times than solid fuel and 2.48 times than natural gas. Furthermore, solid fuel was more expensive 1.31 times than natural gas. So, modern greenhouses which have same area and covered with different materials can be heated at the lowest cost by natural gas.

As a result, it is possible to calculate structural and heating costs according to the desire of the greenhouse investors in a wide range of different sizes, cover and roof types and also fuel types for modern greenhouses.

Keywords: Greenhouse, construction, climate, calculation, cost

Introduction

Current agricultural production needs to optimize cheaper and more effective in order to supply foods requirements in the future of countries considering the population growth. Nowadays, the profitability of agricultural production has decreased due to not enlarging of agricultural areas, dividing of lands, misusing of agricultural areas, decreasing of crop quantity and quality per unit area. Therefore, the importance of practices which increased profitability obtained from per unit area is increasing day by day (Coskun, Filiz, 1997).

Additionally, when considering the great majority of current greenhouses are build without project and automation, modern greenhouses built as fully automated in recent years have an important role in yield increase. However, structural and climating costs in fully automated modern greenhouses change according to greenhouse size and materials used in greenhouse. Due to this reason, manufacturers cannot determine the initial investment and climating cost of greenhouse which will be built by them.

In this study, users will be able to calculate structural costs, heat requirements and fuel costs according to fuel type for hot water heating system which is most widely used in greenhouses for different sizes greenhouses with *"MS Excel Package Program"*. Users can determine structural and heating costs the defining type, sizes, heating time and fuel type of greenhouses which they want to build to the program. Besides the program both can determine annual fuel cost for currently greenhouses and can help to choose the cheapest fuel type.

Materıal and method

Material

The structural and automation properties belong to greenhouses used in calculations were given in Table 1 and in Table 2, respectively (von Elsner et al., 2000; Critten, Bailey, 2002; Hakgoren, Kurklu, 2007).

Table 1 Greenhouse structural properties

Roof Type	Cover Material Type	Base Type (m)	Column Profile Type (mm)	Purlin Profile Type (mm)	Rafter Type (mm)	Gutter Type (mm)
Gable	Glass	0.5x0.5x0.6 rectangular	80x80x3 Box	40x60x2 Rectangular	30x30x2 Box	400 aluminum
Arch	Polyethylene	0.5x0.5x0.6 rectangular	80x80x3 Box	40x60x2 Rectangular	$\varnothing_{60}$ pipe	400 aluminum
Gothic	Polycarbonate	0.5x0.5x0.6 rectangular	80x80x3 Box	40x60x2 Rectangular	$\varnothing_{60}$ pipe	400 aluminum

Table 2 Greenhouse automation properties

Roof Type	Cover Material Type	Heating Type	Fuel Type	Irrigation System	Cooling System
Gable	Glass	Hot water	a. Solid fuel b. Liquid fuel c. Natural gas	Drop irrigation	Fogging
Arch	Polyethylene	Hot water	a. Solid fuel b. Liquid fuel c. Natural gas	Drop irrigation	Fogging
Gothic	Polycarbonate	Hot water	a. Solid fuel b. Liquid fuel c. Natural gas	Drop irrigation	Fogging

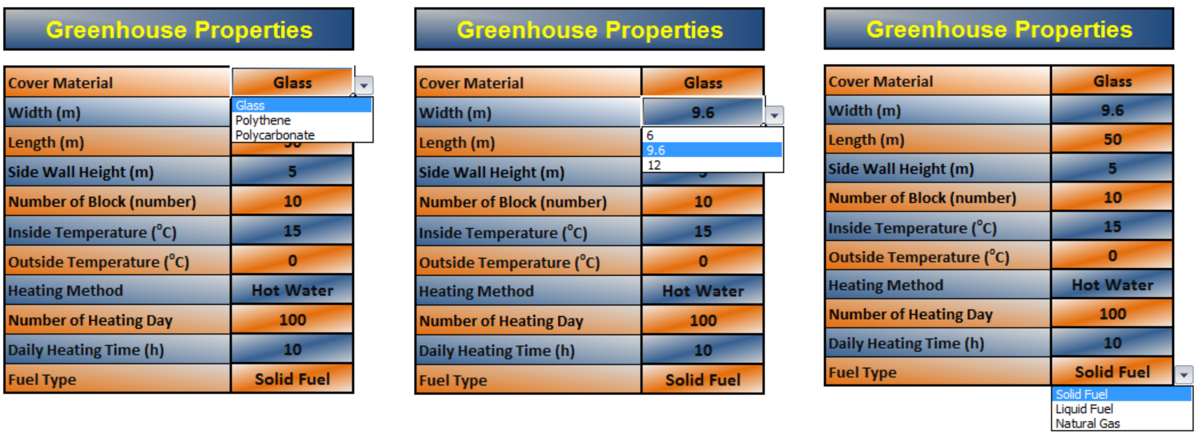

Figure 1. Screenshots for defining computational procedures regarding greenhouse properties

Method

Structural and climating cost of greenhouses can be calculated with the help of the properties defined in Figure 1 using “MS Excel Package Program”. The program has been designed as simple and user-friendly to use for people from every sector. In the program, users can determine total cost belonging to a modern greenhouse by choosing step by step physical properties and heating requirements. Thus, they will decide the most suitable and the cheapest greenhouse type and size trying approximately 4 million alternatives.

Results and discussion

Users can simply determine amount of greenhouse elements and materials (Figure 3), heat requirement and climating cost (Figure 4) and structural cost (Figure 5) of a fully automated modern greenhouse according to greenhouse properties given in Table 1 and Table 2. For this process, they will define structural properties such as cover material, length, width, side wall height, block number and automation properties such as inside and outside temperature, annual heating day number, daily heating time and fuel type from properties given in Figure 1.

For the better understanding of the program, a sample cost calculation was made according to properties defined in Figure 2.

Greenhouse Properties	
Cover Material	Glass
Width (m)	9.6
Length (m)	50
Side Wall Height (m)	5
Number of Block (number)	10
Inside Temperature (^{o}C)	15
Outside Temperature (^{o}C)	0
Heating Method	Hot Water
Number of Heating Day	100
Daily Heating Time (h)	10
Fuel Type	Solid Fuel

Figure 2 Screenshot of determining greenhouse properties

Greenhouse Elements	
Number of columns (number)	221
Base Area (m^2)	4800
Greenhouse Volume(m^3)	30000
Covered Area (m^2)	7112
Excavation Volume (m^3)	71
Amount of Mold (m^2)	557
Concrete Volume (m^3)	77

Amount of Material		
80*80*3 mm Rectengular Profil (Column)	(m)	1296
	(t)	9.2
Box Profile (Rafter)	(m)	7306
	(6m)	1219
Ø60 Pipe Iron Profile	(m)	Empty
	(t)	Empty
40*60*2 mm Box Profile	(m)	2584
	(t)	7.8
Ø32 Pipe Iron Profile	(m)	Empty
	(t)	Empty
$L_{50,50,5}$ Profile	(m)	3904
	(t)	14.7
Gutter	(m)	550
	(6 m)	93
$L_{30,30,3}$ (Window Frame)	(m)	3540
	(t)	4.8

Figure 3 Screenshots of calculating material amounts

Heat Requirement and Climating Cost Table		
S. No	Works	Value
1	Total Heat Requirement of Greenhouse	597789
2	Boiler Capacity (W)	663546
3	The annual heat consumption (KJ)	2400307982
4	Amount of Fuel (Kg)	135114
S. No	Works	Cost (€)
5	Fuel Cost	91878
6	Irrigation System (Drop Irrg. System)	9600
7	Cooling System (Fogging)	7680
8	TOTAL	109158
9	Other Charges (%10)	10916
10	OVERALL TOTAL	120074

Figure 4 Screenshot of Heat Requirement and Climating Cost Table

Structure Cost Table		
S. No	Works	Cost (€)
1	Volume of Excavation	97
2	Amount of Mould	4129
3	Volume of Concrete	3020
4	Total Profile Weight	58269
5	Cover Material (Glass)	53767
6	Cover Material	Empty
7	Cover Material (Polycarbor	Empty
8	TOTAL	119281
9	Other Charges (%10)	11928
10	OVERALL TOTAL	131210

Figure 5 Screenshot of Structure Cost Table

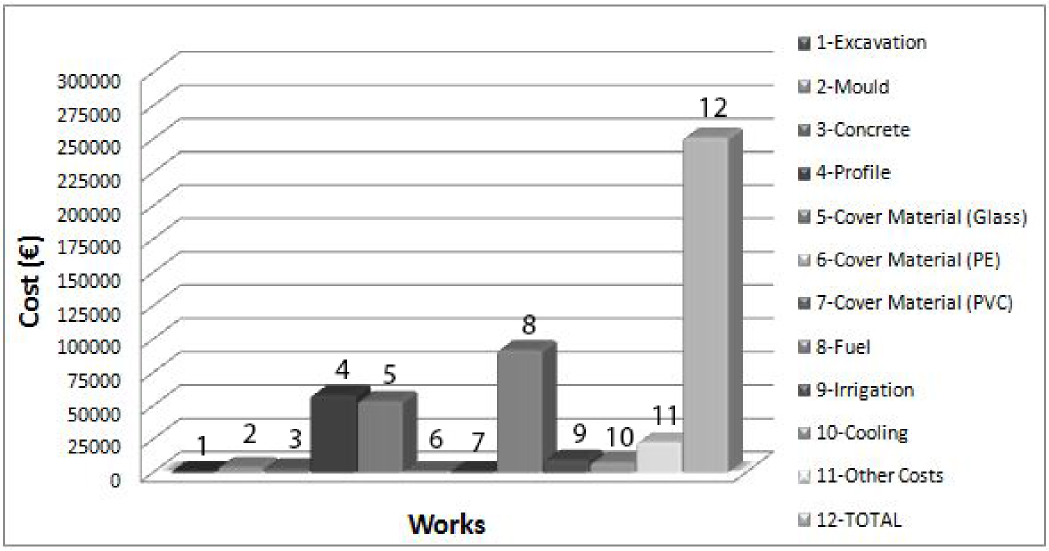

Figure 6 Cost of glasshouse heated with solid fuel

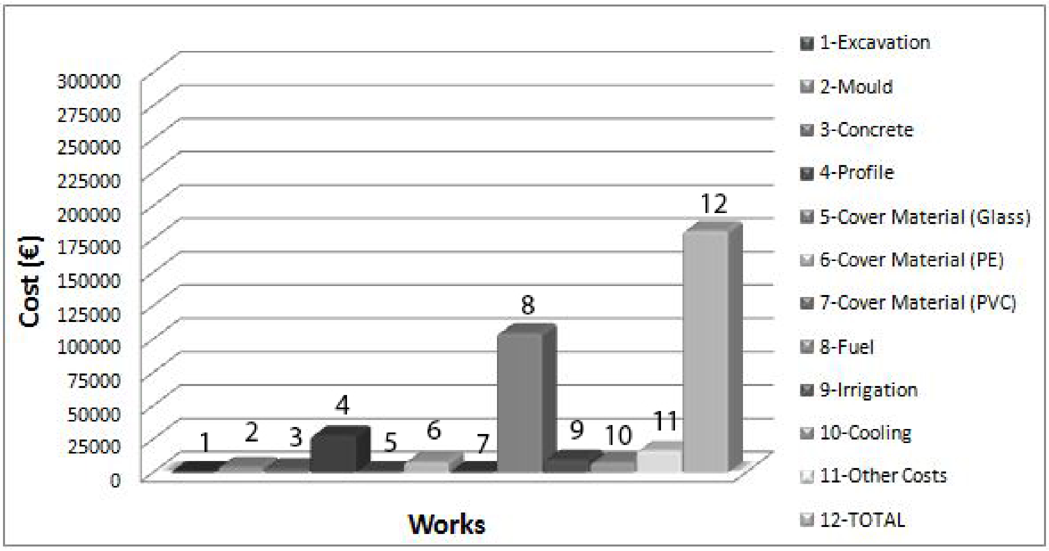

Figure 7 Cost of polyethylene greenhouse heated with natural gas

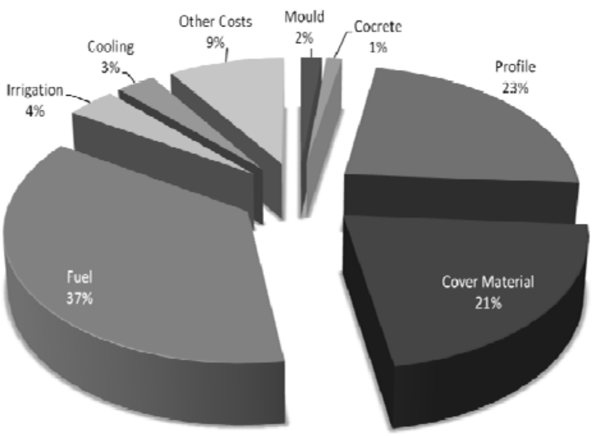

Figure 8 Cost proportion of glasshouse heated with solid fuel

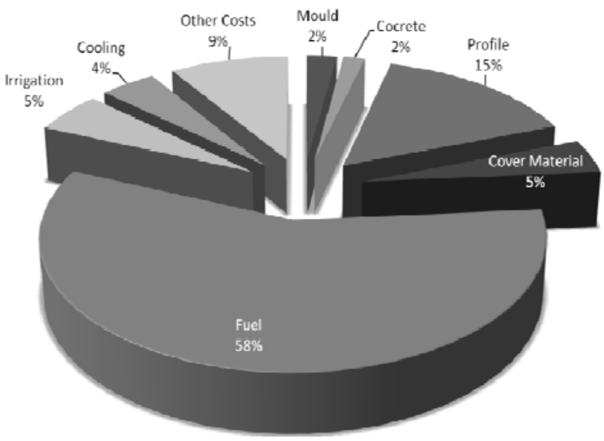

Figure 9 Cost proportion of polyethylene greenhouse heated with natural gas

When structural (Figure 4) and automation (Figure 5) cost in selected sample shown as graphic (Figure 6), it is clearly seen that heating, profile and cover material costs have the biggest amounts in totally, respectively.

When same sizes apply to arch-roofed greenhouse and fuel type is chosen as natural gas, cost change will be as in Figure 7. It is clearly seen that heating, profile and irrigation costs have the biggest amounts in totally, respectively.

As a result, users can easily and quickly calculate costs of greenhouses which have different type, size and automation properties using this program changing selected properties in Figure 1.

As shown in Figure 8, for selected sample glasshouse, fuel cost has the biggest proportion (37%) followed by profile (23%), cover material (21%), other costs (9%). Compared to glasshouse, proportion of fuel cost is almost doubled, whereas cover material cost has decreased about four times for polyethylene greenhouse (Figure 9).

Acknowledgement

The authors would like to thank the Administration Units of Akdeniz University for their support.

Reference

Coskun M., Filiz M., 1997. The Regulation Principles of Climate of Greenhouse’s inside and Research Technologies Developing on this Subject. 6th National Culturtechnic Congress. 5-8 June 1997 Bursa. (in Turkish)

Critten D. L., Bailey B. J., 2002. A Review of Greenhouse Engineering Developments During The 1990s. Agricultual and Forest Meteorology, 112: 1-22.

Hakgoren F., Kurklu A., 2007. Greenhouse Planning. University of Akdeniz, Faculty of Agriculture 6: 87-103. (in Turkish)

Von Elsner B., Briassoulis D., Waaijenberg D., Mistriotis A., von Zabeltitz C., Gratraud J., Russo G., Suay-Cortes R., 2000. Review of Structural and Functional Characteristics in European Union Countries, Part I: Design Requirements 75(1): 1-16.

KEY POINT FOLLOWING CONTROL ALGORITHM DESIGN FOR THE MOBILE ROBOT

Ladislav Tóth*, Dušan Hrubý, Martin Olejár, Vladimír Cviklovič

Slovak University of Agriculture in Nitra, TR. A. Hlinku 2, 949 76 Nitra, Slovak Republic
Phone: +421 37 641 4763, E-mail: ladislav.toth.laxy@gmail.com

Abstract

This work deals with design of an algorithm for the mobile robot guidance in the direction of known key point (significant point) in space. VGA camera and computer image processing algorithms are used to find the xy-coordinates of the key point on captured pictures. After manual cross calibration of the Microsoft Kinect VGA and depth sensor an algorithm was created for evaluation the depth information, obtained from the depth sensor, based on found xy-coordinates from VGA camera. The proposed control algorithm uses the theory of fuzzy logic due to continuous control of the output actuating units, and due to easier implementation of process control logic for multiple inputs and outputs of the mobile robot system. The resulting algorithm is able to autonomously control the direction and the speed of the mobile robot and also can maintain the desired distance between the mobile robot and the key point (coloured object). The accuracy of the mobile robot direction guidance to the key point depends on the resolution of the VGA chip and depth camera system, and the type of chassis unit construction has impact too.

Key words: image processing, depth measuring, fuzzy, algorithm, key point, mobile robot

Introduction

In areas of economy and industry increasingly higher requirements are asked for the quality and the productivity. In recent decades, research has been highly increased in the field of mobile robotics. But the problem is partially or fully autonomous robot navigation in a space. Mobile robots should have the ability to move in an environment without a physical connection with a control (navigator) object. From mobile robots are required a particular autonomy, and for this reason, they must be equipped with devices that are capable of providing an initial input navigation information. VGA cameras, laser systems, GPS and other sensors could be applied for this purpose. Currently, research is focused on the navigation systems that are using a complex system of image analysis and depth information, due to a higher degree of adaptability and application of these systems in various branches of industry and agriculture. Over the last years, several robotics research groups have developed techniques for image analysis tasks, based on visual and depth information.

Environment, where the mobile robot will move, may contain objects of different shapes and colours that can be used to obtain the necessary information useful for the mobile robot guidance or navigation. Objects could be created also artificially and therewith define the significant resp. the key reference points in space. In agriculture, it would be perspective to utilize camera systems together with algorithms for image processing for the purpose of autonomous control and navigation of the agricultural machinery.

The VGA camera and the new technology of laser depth measuring systems allow not only two-dimensional colour image (RGB), but also capture the depth image (D) i.e. are able to return information about the distance from an object at each pixel (point) in image. With using this system, it can be relatively easy to obtain a sufficient amount of input data for subsequent processing and evaluation of action hits for the driven autonomous system.

Materials and methods

The aim of work is to design an algorithm for image and depth information processing received from the Microsoft Kinect sensor system, with using C-Sharp programming language and MS Kinect SDK v1.6. Motion control algorithm design is focused to control an autonomous mobile robot assembled on the Ackerman's chassis type, and it will be able to follow a key point (coloured circle or elliptic object / ball) in space, and keep the set distance between them. The communication and the control system design for the mobile robot is provided by LabVIEW 2010 graphical programming language and with its additional module called Fuzzy System Designer. The RGB colour model usage is assumed in this article.

Multiple methods and procedures can be selected for a digital image processing and for purpose of obtaining information that will be served to the mobile robot navigation system. The environment has the biggest impact wherever the mobile robot will move. Under this condition, the image processing algorithms should be chosen carefully. In addition, a fast image processing is required with correct output information. As the environment and the objects in it contained characteristic features such as edges, different colours or surface topography, it is possible to use these features.

The Canny edge detector is useful at first step of the image processing. In principle, it is composed of several elements that are used in image analysis. These include, for example: noise suppression, application of a convolution operator with a mask, calculate the direction and intensity of edges and others. Combine multiple steps can be considered as an advantage of this detector, although more time is required to perform operations. Minor drawback may be the sensitivity; unwanted edges can be obtained on the output image in addition to the necessary edges. This could be eliminated by threshold intensity. The Hough transform is a standard method for shape recognition in digital images (Yuen et al., 1990). It was first applied to the recognition of straight lines and later extended to circles and ellipses (Duda, Hart, 1972). Its advantages include robustness to noise, robustness to shape distortions and to occlusions/missing parts of an object. Its main disadvantage is the fact that computational and storage requirements of the algorithm are increased as the power of the dimensionality of the curve (Ioannou et al.,1999).

One of the ways to control more than one input and output variable is using fuzzy control algorithm. The fuzzy control is a qualitative control based system on qualitative description of real systems. We do not need to know the exact equation of control system. One of main benefits of fuzzy logic system is intuitiveness of design that allows control system designing too, where is not available a mathematical model of the system or it is hardly determinable. The advantage of fuzzy control versus conventional methods is the ability to synchronous control of multiple independent physical variables.

A characteristic feature of the fuzzy control is the possibility of immediate use of a posteriori knowledge about the human controlled process, which is referred as base of data. The base of data consist information about invariant states and intervals where input and output variables move with their limits. The most important segments of base of data are verbally defined control rules by which the complex control algorithm of the system is written up.

The fuzzy sets are described by linguistic variables which could be any expression of any language. For example, the fuzzy set "distance from obstacle" contains the linguistic variables {Near (N), Middle (M), Far (F)}. Implemented verbal quantification of the distance from obstacle (e.g. "Near") refers to diffused fuzzy set defined by the characteristic function of membership. Example of three input fuzzy membership functions which are represented by linguistic variables and they are shown in Fig. 1.

Decision rules represent the body of experiences, knowledge and key information of fuzzy control algorithm. Example of decision rules has the following form:

IF (x belongs to Far) **AND** (y belongs to Right) **THEN** (motor$_1$ belongs to Go forward) **ALSO** (motor$_2$ belongs to Turn left)

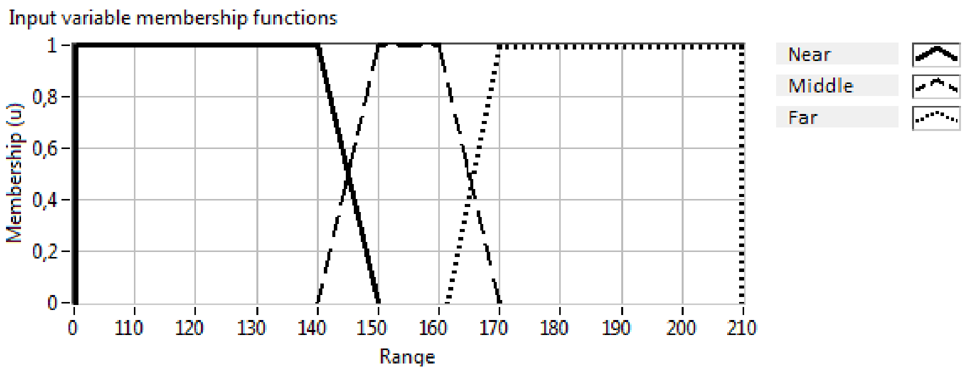

Fig. 1 Input functions of membership for input variable *"Distance from obstacle"* is represented by linguistic variables "Near" (N), "Middle" (M) and "Far" (F)

Results and discussion

The both, the colour camera and the depth sensor of the Kinect dispatch images in resolution 640x480pixels at 30fps. The colour and the depth sensor capture angle aren't the same, the depth camera has smaller capture angle, so an image calibration process is needed. Colour image sequence (video) captured by VGA camera is calibrated manually, the original width and height of the colour images are reduced (deleted) in relation to image captured from depth sensor. The calibration is described next; a rectangle object is moved in front of camera, from one side of depth image to another side. When the object on the depth image touches the border of the depth image, the colour image from that side is deleted up to the border of rectangle object on the colour image. These steps are repeated on each side on colour image. A new colour image was created with new width and height, so the size of image will be smaller.

After calibration process, ratios are needed to be calculated between depth image and new colour image width and height, because the new colour image size is reduced, the depth image wasn't. The colour and the depth image do not need to have the same resolution, but they need to have the same aspect ratio. The calculation of the ratio for each dimension is shown next in formula (1) for width and for height formula (2):

$$R_x = \frac{x_{org}}{x_{calib}} \qquad (1)$$

$$R_y = \frac{y_{org}}{y_{calib}} \qquad (2)$$

where: R_x – calibration ratio for width (x line);
R_y – calibration ratio for height (y line);
x_{org} , y_{org} – width and height of the depth image;
x_{calib} , y_{calib} – width and height of the new calibrated colour image from VGA camera.

The calibration ratio will be used at final calculation of x_{final},y_{final} co-ordinates for determining the distance at (x_{final},y_{final}) pixel on the depth image.

The main part of the key following algorithm is the pattern recognizing algorithm. The algorithm should be able to recognize a red circle or elliptic object on image, and determine the x_{circle},y_{circle} co-ordinates of the circle centre. Ali Adjari Rad (2003) says: "the Circle Hough transform (CHT) is one of the best-known algorithms and aim to find the circular shapes with a given radius r within an image. In spite of its popularity owning to its simple theory of operation, the CHT has some disadvantages when it works on a discrete image." Chiu ShihHsuan (2010) and Ali Adjari Rad (2003) think that the large amount of storage and computing power required by the CHT are the mayor disadvantages of using it in real-time applications. In case of video, or image sequence at speed 30fps CHT seems not enough fast. The solution could be the Fast Randomized method for Efficient Circle/arc Detection (FRECD) usage described by Chiu ShihHsuan (2013) or Sun's (2012) the real-time and robust multi-circle detection method based on randomized Hough transform algorithm. The storage and computing power decreasing is able with Chen's (2001) efficient randomized algorithm (RCD) for detecting circles, which is not based on the Hough transform. The shape recognition is the key factor of the whole key point following algorithm. In addition, the key point (ball or round object) could be colour painted, as additional information. Correct and definitive key point recognition could be made by the fusion of colour and shape information.

Information about the key point's (object's) distance is allocated at x_{final},y_{final} co-ordinates of depth image pixel. x_{final},y_{final} co-ordinates is necessary to calculate (3)(4) for correct pixel identification in depth picture:

$$x_{final} = R_x * x_{circle} \qquad (3)$$

$$y_{final} = R_y * y_{circle} \qquad (4)$$

where: x_{final}, y_{final} – corrected x and y co-ordinate of the circle centre pixel in depth image;
R_x , R_y – calibration ratio for width and height (x, y co-ordinate ratio);
x_{circle}, y_{circle} – x and y co-ordinate of the recognized circle centre;

The pixel's co-ordinate calculation result must be integer value, so these values will be rounded and converted to data type Int32. The space between camera and the object is directly characterized in millimetres by pixel's depth information.

The easiest way to ascertain the direction of the mobile robot according to key point is using the x_{circle} co-ordinate value. A simple algorithm could be used to determine the direction and the intensity of turn.

If the x_{circle} co-ordinate value is bigger than half of the new calibrated colour image width value (x_{calib}), i.e. the boundary vertical row at centre of horizontal line, then the key point (object) is more on the *right side* and the intensity (5) *"I"* will have positive sign of number:

$$I = x_{circle} - \frac{x_{calib}}{2} \qquad (5)$$

else the object is more on the *left side* and the intensity *"I"* will have negative sign of number. So bare, the sign of the intensity *"I"* indicates on which side of the colour image the object is situated on.

The last part of the main algorithm is to design a fuzzy regulation control system for multiple inputs and outputs. Two input fuzzy sets are needed to be created:

1. for the *"Distance from key point"*;
2. for the *"Turn intensity"*.

Output fuzzy sets are needed to be created for two actuators (electric motors):

1. for the *"Direction"*;
2. for the *"Accelerating"*.

An example input membership functions are showed on Fig. 1 for input fuzzy set *"Distance from key point"*, where the required distance is set to 1,55m from the key point (object), by the linguistic variable *"Middle"*. The *"Turn intensity"* fuzzy set input membership functions could be set from negative to positive values too, for left and right direction, and control the mobile robot direction and the intensity of turn with one variable at the same time.

Output membership functions could be set in the range from -100 to +100. The output (PWM) power can be represented by these numbers in percentages for two separate electric motors (turning and accelerating). Sign means direction of rotation. In this case is not usable PID regulator, which principles are better applicable to the one parameter systems (Nagy et al., 2012).

The final control algorithm is illustrated on Fig. 2 below:

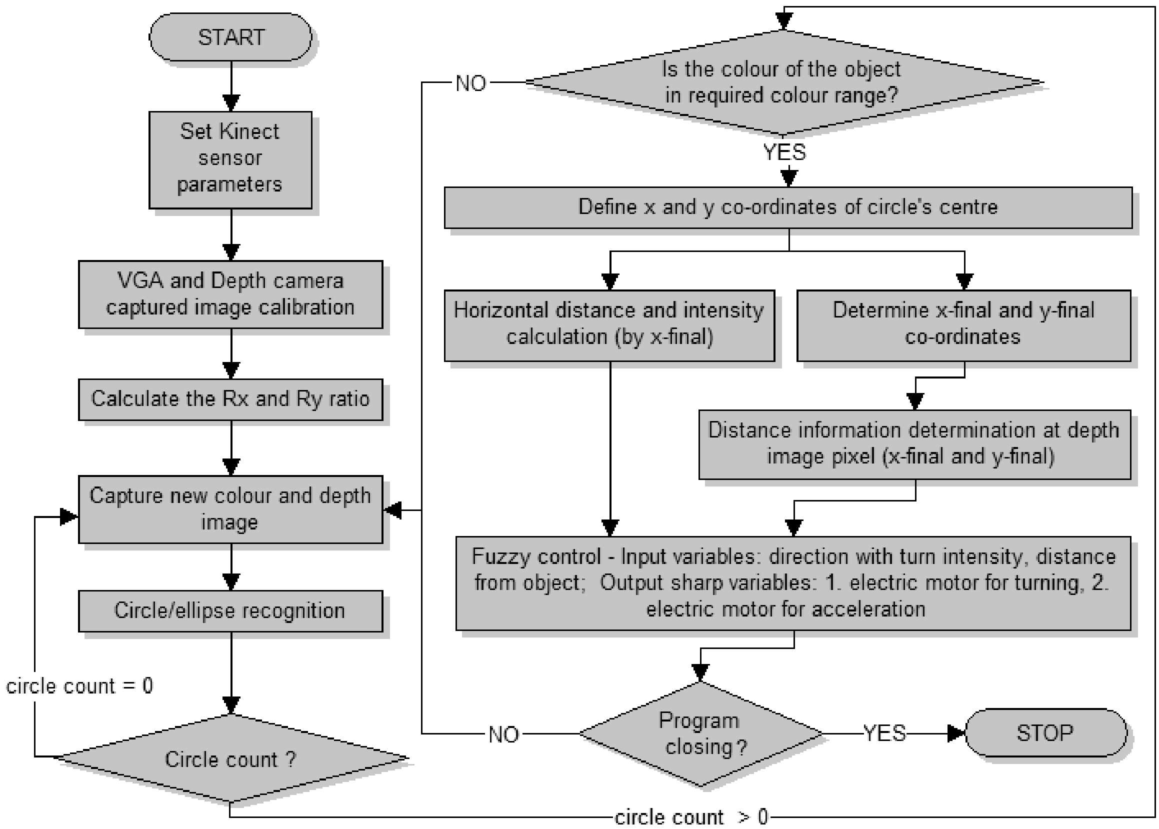

Fig. 2 Designed key point following algorithm for a mobile robot using Kinect sensor

Relatively large computational power is needed for image processing, communication and computing the fuzzy output crisp values, so a powerful computer will be placed outside of the mobile robot chassis, and will be powered from electrical power network due to limited battery capacity of the mobile robot.

Conclusions

The Microsoft Kinect sensor system is suitable for development and research in image processing area and mobile robot systems; because the depth measuring system directly creates 30 times per second a depth image without need of complicated algorithm or system. Every pixel data on the depth image characterize the distance from object that has been captured (measured). The Kinect sensor disadvantage is only the measurable distance range from 0,8m up to 4,1m indoor. The depth sensor cannot measure reliable distance outdoor on direct sunlight.

The actual process of the image processing can be completed by using the efficient randomized algorithm for detecting circles, which is not based on the Hough transform Fast Hough Transformation as Chen (2001) described. This technique is applicable where it is necessary to detect objects with known shape boundaries such as circles or ellipses. In contrast, good results could be achieved even in noisy objects with Sun's (2012) real-time and robust multi-circle detection method based on randomized Hough transform algorithm technique or with Ioannou's (1999) method. The Fuzzy control algorithm usage is effective and could be easily modified by changing fuzzy input/output membership functions resp. by modifying the decision rules (base of data) intuitively. At all, the computing power requirements are increased extremely with adding of various filters, pattern recognizing or control algorithms into process. In some cases, this problem can be solved by multi-threading application design or with parallel data processing in network.

Methods and algorithms proposed in this paper can be further used in complex systems navigation such as mobile robots in industry and agriculture. Implementation of image sensors creates a possibility to increase the productivity and efficiency of different parallel or serial mould work in agriculture sector, such as: ploughing, sowing, spraying, harvesting, mowing and more. These activities can be automated and thus unload agricultural machinery workers-drivers from the repetitive work.

Reference

Adjari A.R., Faez K., Qaragozlou N., 2003. Fast circle detection using gradient pair vectors, proceeding VIIth digital image computing: techniques and applications, 10-12.

Duda R.O., Hart P.E., 1972. Use of the Hough transformation to detect lines and curves in pictures. Comm. Assoc. Comput. Mach. 15, 11–15.

Chen T., Chung K., 2001. An efficient randomized algorithm for detecting circles. Computer Vision and Image Understanding, 83(2): 172-191.

Chiu S., Liaw J., Lin K., 2010. A fast randomized Hough transform for circle/circular arc recognition. International Journal of Pattern Recognition and Artificial Intelligence, 24(3): 457-474.

Chiu S., Lin K., Wen C., Lee J., Chen H., 2012. A Fast Randomized method for Efficient Circle/arc Detection. International Journal of Innovative Computing, Information and Control, 8(1A): 151-166.

Ioannou D., Huda W., Laine A.F., 1999. Circle recognition through a 2D Hough transform and radius histogramming. Image Vision Comput, 17: 15–26.

Nagy L., Palkova Z., Valicek J., Kiedrowicz M., Rokos K., Kovac P., 2012. Identification of Model Lightening System and Design of PID Controllers for the Purpose of Energy Savings by Using of MATLAB and Their Functionality in LabVIEW. Rocznik Ochrona Srodowiska, 14: 247-261.

Sun H., Mao Y., Yang N., Zhu D., 2012. A real-time and robust multi-circle detection method based on randomized Hough transform. International Conference on Computer Science and Information Processing, 2: 175-180.

Yuen H., Princen J., Illingworht J., Kittler J., 1990. Comparative study of Hough Transform methods for circle finding. Image and Vision Computing, 8(1): 71-77.

THE DURABILITY OF A TRACTOR GEAR-HYDRAULIC CIRCUIT

Juraj Tulik[1*], Ján Kosiba[1], Ľubomír Hujo[1], Juraj Jablonický[1], Vladimír Šinský[2]

[1]Slovak University of Agriculture in Nitra, Tr. Hlinku 2, 949 76 Nitra, Slovakia,
E-mail: juraj.tulik@gmail.com
[2]Biolife, Inc., Galanta, Slovakia

Abstract

This paper presents the results of exploration of the gear-hydraulic circuit durability of a tractor CASE IH Magnum 315. Mineral oil MULTAGRI PRO TEC has been applied in a tractor. The exploration on the basis of a ferrographic analysis and cleanliness code by ISO 4406 of oil samples was carried out. These oil samples from 5 tractors of the same types at different phase of operations (count of engine hours) were detract. The following oil samples were studied: oil samples after completing 500 engine hours, oil samples after completing 1,500 engine hours, oil samples after completing 2,000 engine hours, oil samples after completing 3,500 engine hours and oil samples after completing 5,000 engine hours. Based on the inducted analysis it is possible to determine of the degradation processes in the tractor gear-hydraulic circuit. These tests were realized in cooperation at the Department of Transport and Handling, SUA in Nitra and a BIOLIFE company, Inc and supported by the Scientific Grant Agency of the Ministry of Education, Science, Research and Sport of the Slovak Republic – VEGA, Grant No. 1/0857/12

Keywords: viscosity, oil, tractor, ferrography, cleanliness code

.

Introduction

Hydraulic equipment is widely used in powerful mechanisms of agricultural and forest machines as well as in many other areas. The development of modern hydraulic components is aimed at increasing the transmitted power, reducing the energy intensity, minimizing the environmental pollution and increasing the technical life and machine reliability (Tkáč et al., 2008a). Agricultural machinery has a negative impact on all elements of the environment. The air is influenced by means of exhaust emissions and oil or fuel components. As regards hydraulic fluid utilisation in machines, the most important is to know the running properties of a fluid, i.e. to know the effect of the fluid on the technical condition of hydraulic system parts.

In working device the fluid transfers the energy and also carries the information about process in it. Into the fluid during the device operation entrance metal particles through which is possible to evaluate a wear process and predict the next operation of the device. Particle contamination in hydraulic fluid accelerates wear of system components. Therefore is very important to pay attention to purity of hydraulic fluid which is used. The fluid should be replaced if the value exceeds the limits, which are specified by manufacturer. The most common hydraulic fluid contaminants are water and air, along with particles of metal, rubber or dirt.

At the present time, hydrostatic systems are widely dispersed in industry. They provide various types of motion. Power transmission is performed by means of hydraulic fluid. Hydraulic fluid needs service and the monitoring of operating parameters. From the viewpoint of hydraulic fluid utilisation in a machine, it is important to know the operating characteristics of a fluid, i. e. to know the effect of fluid on the technical condition of hydraulic system components (Tkáč et al., 2008b).

Materials and methods

In articles is presented the durability analysis of gear-hydraulic circuit of tractor CASE IH Magnum 315. It is a high-power tractor with a six cylinder engine, maximum engine power 260 kW. All forward and reverse gears are shifted under load (Full PowerShift and PowerShuttle). The hydraulic axial piston pump with maximum operational pressure 21 MPa, create the pressure load in hydraulic circuit.

The durability analysis was realized on the basis of analyzing samples of gear-hydraulic oil. These samples were from five the same type tractor at different operational time: after: 500 engine hours, 1,500 engine hours, 2,000 engine hours, 3,500 engine hours and 5,000 engine hours.

These samples were collected during the oil change of tractor.

In gear-hydraulic tractor circuit of CASE IH Magnum 315 was applied universal oil MULTAGRI PRO TEC. The basic characteristic of oil gives the table 1.

Tab. 1 Specifications of the oil MULTAGRI PRO TEC

Properties	Base value	Amount
Kinematic viscosity at 40°C	$mm^2.s^{-1}$	89
Kinematic viscosity at 100°C	$mm^2.s^{-1}$	13.5
Viscosity index		155
Pour point	°C	-36

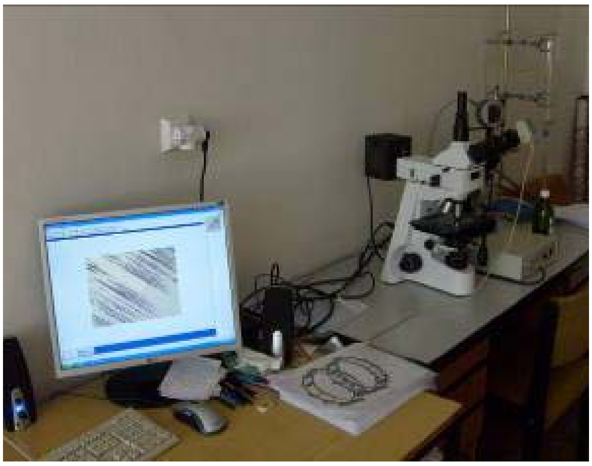

Fig. 1 KAPA 6000 Microscope connected to the computer

Ferrographic analysis of oil

The aim of a ferrography study is to identify the quantity and size of wear particles in oil samples. Wear particles have a significant effect on the abrasive wear of friction pairs in gear-hydraulic circuits of tractors. These contaminants degrade the hydraulic oil used. Pollution particle, despite oil filters located in the tractor gear-hydraulic circuit, should continue to grow during the operating. These particles tend to agglutinate during the operating and aggregate into large particles. The technological procedure of ferrography analysis was carried out in the laboratory of the Department of Transport and Handling, Faculty of Engineering, University of Agriculture in Nitra. The MA 1 magnetic analyzer and KAPA 6000 Microscope were used for the ferography analysis of samples oil. The MULTAGRI PRO TEC was diluted before ferrography analysis in proportion of 2:1 with tetrachlorethylene to better highlight of pollution particles in the oil.

Cleanliness code of oil

The fluid contamination is evaluated according to cleanliness code. The cleanliness code can be determined by standards: ISO 4406 – 1999, SAE AS 4059 or NAS 1938. The cleanliness code of hydraulic fluid per ISO 4406 is determined by counting number and size of particles in the fluid. The old ISO 4406 – 1987 defines the cleanliness code of particles lager than 5 µm and 15 µm according to two numbers X1/X2. X1 defines number of particles lager than 5µm and X2 defines number of particles lager than 15 µm. In 1999 both, the definition for particle counting and the definition of ISO code was changed. ISO 4406 - - 1999 defines cleanliness code according to particle sizes larger than 4 µm, 6 µm and 14 µm.
The CS 1000 states cleanliness code by continual method i.e. the device is connected to hydraulic circuit during its work. Device uses optical detection of counting number and size of particles. Results of measurement are recorded by PC connected to device by analog interface RS 485. The basis conditions for connection of CS 1000 device to hydraulic circuit are as follow:

- connection to suction or pressure pipe of circuit,
- flow rate of fluid must be from 30 ml . rpm to 300 ml . rpm,
- kinematic viscosity max. 1000 $mm^2. s^{-1}$,
- fluid pressure max. 10 MPa.

Diameter of inlet pipe must be smaller than 4 mm and output pipe lager than 4 mm.

Fig. 2 Measurement of cleanliness code of oil samples

Results and discussion

Figure 3 shows the ferrography images of oil samples. These images were created 400 times magnification with camera Moticam 1000 and microscope Kappa 6000.

a

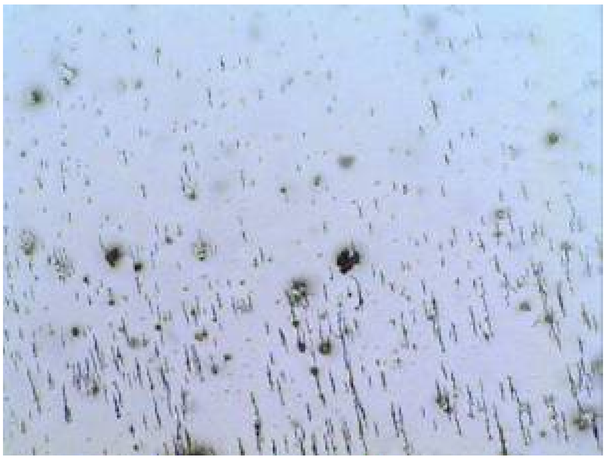

b

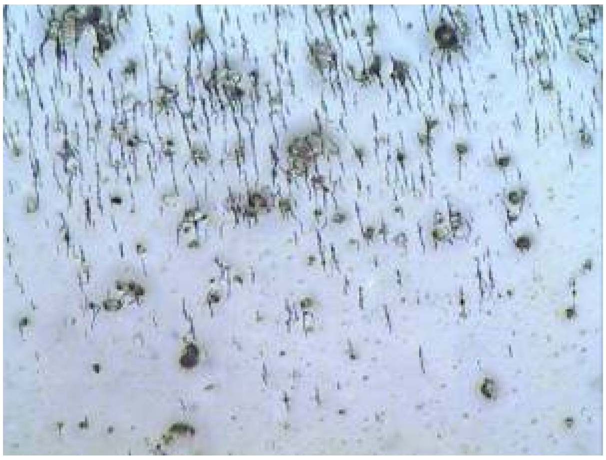

c

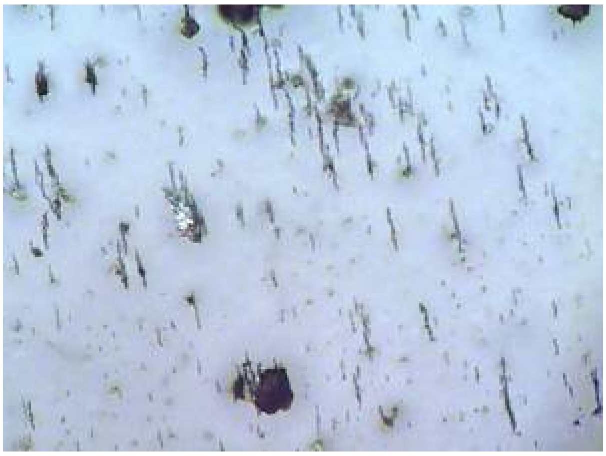

d

e

Fig. 3 Wear particles in the oil samples (a – 500 engine hours, b – 1,500 engine hours, c – 2,000 engine hours, d – 3,500 engine hours, e – 5,000 engine hours)

From the ferrography images of oil samples result that the samples after 500 engine hours 1,500 engine hours and 2,000 engine hours are not virtually visible wear particles. In the oil samples are only small chains of particles.

The tractors after 3,500 a 5,000 engine hours again show the small chains of particles, but in oil samples were found visible wear particles. The comparison with catalogue of wear particles we have found that their are particles of adhesives wear, which means that the gear-hydraulic circuits of tractors CASE IH Magnum 315 after completing defined engine hours are in running state of wear.

Table 2 shows the results from measuring of cleanliness code according to ISO 4406 with CS 1000 device.

Tab. 2 Evaluation of measurements cleanliness code

	Cleanliness code by ISO 4406		
	> 4 µm	**> 6 µm**	**> 14 µm**
500 engine hours	20	18	12
1,500 engine hours	18	16	13
2,000 engine hours	17	15	13
3,500 engine hours	17	15	13
5,000 engine hours	17	15	14

The evaluation of cleanliness code shows that in samples of oil from tractor after 500 engine hour is highest contents of particles > 4 µm and > 6 µm. From other samples is the cleanliness code in defined intervals lower and after 2,000 engine hours, 3,500 engine at 5,000 engine hours show the number of > 4 µm particles the value 17 and the number of > 6 µm particles the value 15.

The tractor after 500 engine hours showed the number of > 14 µm particles the value 12. The highest value of the number of particles 14 was detected in a tractor after 5,000 engine hours. The biggest production of wear particles in intervals > 4 µm and > 6 µm was at tractor after 500 engine hours because his gear-hydraulic system was in running. In interval of > 14 µm is in all tractors higher the number of particles, what indicating the operational wear.

Conclusion

The presented paper is focused on durability analysis of gear-hydraulic circuit of tractor CASE IH Magnum 315. Analysis was performed on five tractors in various stages of operational wear: after 500 engine hours, 1,500 engine hours, 2,000 engine hours, 3,500 engine hours and 5,000 engine hours. During the test were performed the ferrography analysis and measurement of cleanliness code of oil samples. The oil samples were collected during the oil change intervals (the change interval of oil is 500 engine hours). The universal oil MULTAGRI PRO TEC is applied in gear-hydraulic circuits of defined tractors.

From the findings resulting that the gear-hydraulic circuits of analysing tractors show no the technical or technological failing. On the basis of measurements of cleanliness code it can by stated that the tractor after 500 engine hours is in running state of wear because was determined the higher amount of wear particles in intervals > 4 µm a > 6 µm.

During ferrography analysis was not discovered the large particles. In tractor after 5,000 engine hours were detected the particles that were smaller than 20 µm. That speaks about the operational wear of gear-hydraulic circuit of tractor CASE IH Magnum 315 after completing 5,000 engine hours.

Acknowledgement

Supported by the Ministry of Education of the Slovak Republic, project VEGA 1/0857/12 “Reduction of unfavorable impacts of agricultural and transport machinery on environment”.

Reference Example:

Tkáč Z., Drabant Š., Majdan R., Cvíčela P., 2008a. Testing stands for laboratory tests of hydrostatic pump of agricultural machinery. Agricultural Engineering, Research in Agricultural Engineering 54: 183-191.

Tkáč Z., Drabant Š., Majdan R., Cvíčela P., 2008b. Testing stands for laboratory tests of hydrostatic pump of agricultural machine. In Research in Agricultural Engineering 54: 183-191.

INVESTIGATION OF ENGINE PERFORMANCE OF WASTE COOKING OIL AS A FUEL IN DIESEL TRACTOR ENGINES

Yahya ULUSOY[1*], Rıdvan ARSLAN[1], Cafer KAPLAN[1], Alper BOLAT[2]

[1]Uludağ University, Vocational School of Technical Sciences, Bursa, Turkey,
Phone: +44 224 2942307, Fax: +44 224 2942303, E-mail: yahyau@uludag.edu.tr
[2]Türk Traktör ve Ziraat Makinaları A.Ş. Ankara, Turkey.

Abstract

In this study; the availability of waste cooking oil (WCO) is experimentally examined whether it can be used as an alternative fuel in 3-cylinder, 4-stroke, direct injection and 48 kW power tractor engine. Test engine is operated at full load conditions by using diesel fuel and waste vegetable oil from 2400 to 1100 cycle and performance values are recorded. Tests are performed in two stages in order to evaluate the effect of the waste oils on engine life cycle. When the test engine is operated with diesel fuel and waste cooking oil; engine torque has decreased between 0,09 % and 3 % according to the cycle and average smoke opacity ratio has remained at the same ratios. However in the tests performed at the end of 100-hour operation; while no significant difference occurs in the diesel fuel, significant reduction is seen in the engine torque of WCO between 4,21 % and 14,48 % according to the cycle and an increase in average smoke opacity ratio is seen. The results obtained from the studies, it is determined that the engine performance values of waste cooking oil show similar properties with the diesel fuel but in long-term usage, performance losses have increased.

Key words: Biofuel, waste cooking oil, alternative fuels

Introduction

One of the significant results of increasing energy demand and the usage of this energy, greenhouse gases emission quantities, requires revising the energy scenarios in the world continuously. Especially the EU countries, most of the countries accelerate studies oriented to increase the usage opportunities of renewable energy sources. Issuance of the legislations that encourage the popularization of biofuel usage has provided the application of technological innovations. Within the biofuels; especially the investigations regarding to the agriculture-based biodiesel generation methods, usage ratios and emission values have gathered speed. As an environmentally friendly fuel, biodiesel can be used in diesel engines without requiring any modification (Ulusoy et al., 2004; Kaplan et al., 2006; Çetinkaya et. al., 2005). In the production of biodiesel; it is possible to use alternative products such as the raw oils obtained from different plants such as coleseed, soybean, safflower that are used together with cooking oil and animal based oils (tallow oil). Various studies have shown that bio-diesel from waste cooking oil can be used in different types of diesel engines with no loss of efficiency (Hamasaki et al., 2001) and significant reductions in particulate matter (PM) emissions (Lapuerta et al., 2008; Çanakçı, VanGerpen, 2003; Mittelbach, Tritthart, 1988; Payri et al., 2005), carbon monoxide (CO) emissions (Payri et al., 2005) and total hydrocarbon (THC) emissions (Mittelbach, Tritthart, 1988; Aakko et al., 2002) with respect to those obtained with conventional fossil diesel fuel. Also because biodiesel production is limited; it is a widely preferred application to mix particular ratios with petroleum fuel. Especially usage of the waste oils causing environmental pollution in the municipalities, in biodiesel production and significant added values from such sources will be provided (Ulusoy et al., 2010; Arslan, 2011). In Germany, where biofuel usage is common, when the biofuel ratios in 2010 fuel consumption is observed; we can see that pure biodiesel, vegetable oil and their mixture has 7,1 % and the case in which they are completely mixed with the diesel fuel has 8,2 % and bioethanol has a ratio of 5,6 % (UFOP ,2013).

Altın et al. (2001) had studied the effects of vegetable oil fuels and their methyl esters on a diesel engine performance and exhaust emissions. The results show that from the performance viewpoint, both vegetable oils and their esters are promising alternatives as fuel for diesel engines. Because of their high viscosity, drying with time and thickening in cold conditions, vegetable oil fuels still have problems, such as flow, atomization and heavy particulate emissions (Altın et al., 2001).

The objective of another research was to produce and test an economic and high quality non-esterified rapeseed oil suitable for use as a diesel fuel extender. This was achieved by acidified hot water degumming combined with filtration to five microns. This rapeseed oil, designated as a Semi Refined Oil, has a high viscosity in comparison with diesel. Hence Semi Refined Oil fuel can only be used as a diesel fuel extender, with inclusion rates of up to 25 %. When Semi Refined Oil was used to fuel diesel engines, power was considerably reduced mainly due to inadequate air/fuel mixing (McDonnel et al., 2000).

Waste vegetable oil is an important source for alternative fuels because of their low prices and ecological properties. For directly usage of waste oils in engines or usage by mixing together with diesel fuel; miscellaneous investigations are being performed. In a study (Isa et al., 2009) WCO that has been used several times for frying purposes is investigated for the utilization as an alternative fuel for diesel engines. It was found that blending WCO with diesel reduces the viscosity and different previous uses of WCO significantly affected the properties of the blended fuels. Blending of WCO with diesel has been shown to be an effective method to reduce engine problems associated with the high viscosity of WCO. The experimental results also show that the basic engine performance such as power output and fuel consumptions are comparable to diesel and the emissions of CO and NOx from the WCO/diesel blends were also found slightly higher than that of diesel fuel. In another study (Bari et al., 2004) examines the changes in the behavior of waste cooking oil with changes in injection timing of a direct injection diesel engine, compared with those of diesel. The aspects taken into consideration were the effects of injection timing on combustion, performance and emissions. The results reveal that WCO and diesel responded identically to injection timing changes. In a review (Naima, Liazid, 2013) gives a brief review about using waste oil of these three types of oil as a fuel for diesel engines. The conversion process of each type of waste oil is presented. Results from using waste cooking oil as fuel for diesel engines showed that the fuel obtained has a higher viscosity and lower calorific value; this will have a major bearing on spray formation and initial combustion.

In 2012; when the distribution of the automobiles registered to the traffics are observed in terms of their fuel types, it is seen that benzene has the ratio of 34 %, motorine 24 % and unknown fuel (No. 10 oil, vegetable oil) has 1 %. The ratio of unknown fuel varies between 1 % and 5 % according to the years (TUİK, 2013). In this study; the effect of the usage of waste cooking oils as a diesel engine fuel that is the final target in the name of providing recycling on the engine performance is experimentally examined.

Material and Methods

Test Fuels

Diesel fuel and waste cooking oils are used as the test fuel. Waste cooking oils have been obtained from a Civil Society Organization ALBİYOBİR, which performs the collection organization of waste oils nationally (Fig. 1).

Fig. 1 Waste Oil Sample used in the tests

Test and Measurement System

The properties of the engine used in the measurement of performance tests of the biofuel that is obtained from waste cooking oils is given in Table 1. Engine tests are performed by using a N J Froment Sigma 5 model A/C dynamometer. Smoke opacity measurements are performed by using Wager 6500 Model Smoke (Opacity) Meter. Tests are performed in two stages in order to examine the effect of waste oils on the engine life cycle by restoring the engine and fuel system settings to the factory settings. After the first stage of diesel and WCO performance tests; the tests are repeated after 100-hour operation.

Tab. 1 Properties of the Engine of the Test Tractor

Tractor Model	Case IH - JX70
Engine	TTF 8000s Engine
Type	4 Stroke In line
Cylinder	3-cylinder
Combustion space	Direct-Injection (DI)
Diameter x Course	104mm x 115 mm
Cylinder volume	2930 cm3
Compression ratio	18:1
Nominal cycle	2500 d/d
Max. Power	48,47 kW
Max. Torque	261 Nm (1400 d/d)
Fuel pump	Bosch In-line
Emission Level (tier)	TIER3A

Results

Loading tests in which the engine performance of WCO is examined directly on the diesel engine are obtained with the torque and power values given in Fig. 2 and Fig. 3. The torque curves in Fig. 2 consists of the 2-stage first test (Diesel-, WCO) and the tests performed after 100-hour operation (Diesel-2;WCO-2).

As seen in Fig. 2, in the first tests, diesel fuel and WCO torque values give similar ve approximate values. When the test engine is operated by diesel fuel and waste cooking oil; engine torque has decreased between 0,09 % and 3 % as expected according to the cycle. However in the tests performed at the end of 100-hour operation; while no significant difference occurs in the diesel fuel, significant reduction is seen in the engine torque of WCO between 4,21 % and 14,48 % according to the cycle and an increase in average smoke opacity ratio is seen. In the power curves in Fig. 3; we can see that the difference occurred at the end of 100-hour operation gets deep.

As given in Table 2; although the average alteration of smoke viscosity is at equal levels in the first tests, a significant increase in WCO can be seen in the final test. In this case, when they are matched with the performance changes; it is shown that serious combustion problems occur at the end of 100-hour operation of the engine.

Tab. 2 Average Smoke Opacity % at two stages

	Average Smoke Opacity %	
Test/Fuel	Diesel	WCO
First Test	19,9	19,9
Last Test	16,6	19

This performance loss in the engine performance that has occurred at the end of 100-hour operation shows that the combustion in the engine progressively deteriorates. This situation indicates the fuel system problems that arise during the usage of WCO. Deformations given in Fig. 3 that are formed on the injectors removed at the end of the test indicates that further analyses should be done regarding to this matter.

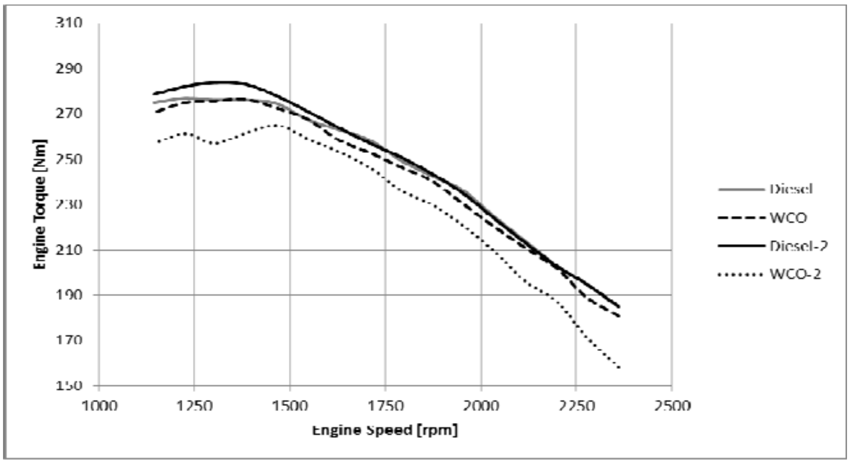

Fig. 2 Torque characteristics of the engine with diesel fuel and WCO at two stages (First test and after100 hours work test)

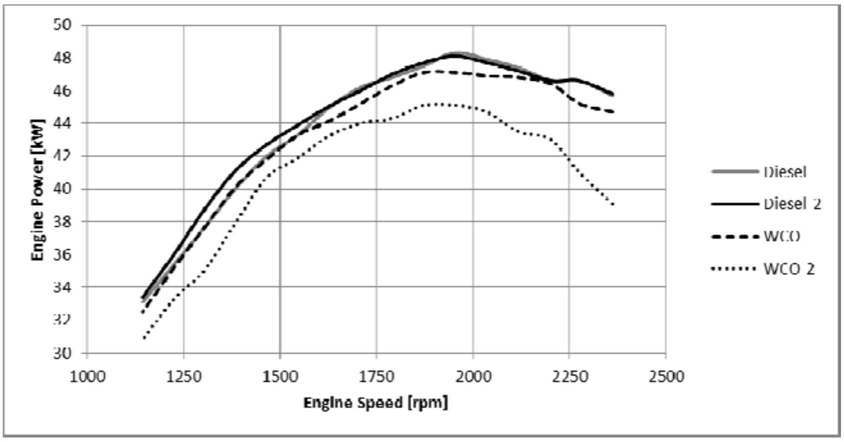

Fig. 3 Power characteristics of the engine with diesel fuel and WCO at two stage (First test and after100 hours work test)

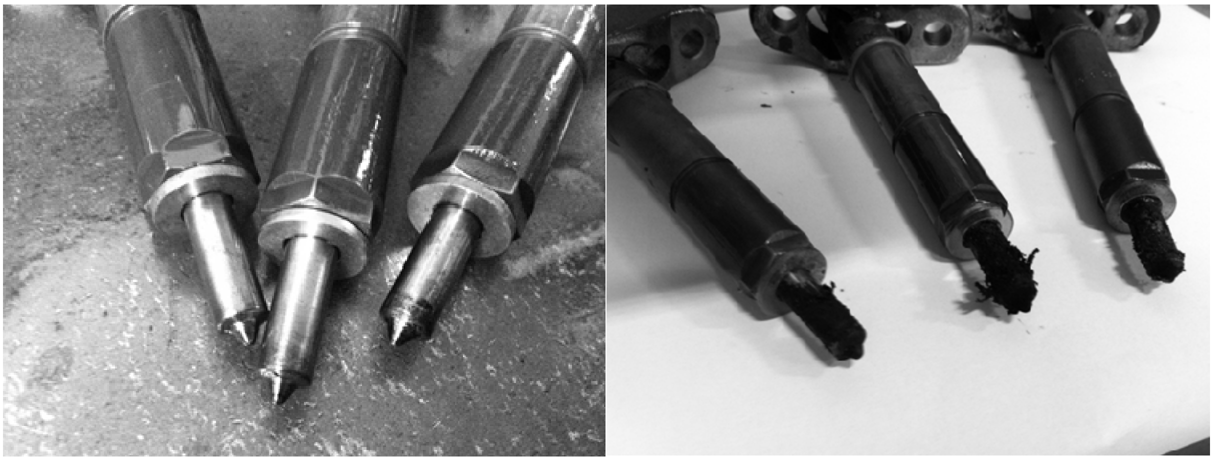

Fig. 3 Appearance of the injectors that are removed at the end of a 100-hour operation

Conclusion

In this study that is performed in two stages; the effects of WCO on their usage in diesel engines are investigated and in the first stage tests, it is seen that WCO and diesel fuel have similar performance values and as expected again, torque values of WCO are approximately 3 % lower than the torque values of diesel. However it is significant that this difference reaches 14 % at the end of a 100-hour operation and this result shows that WCO cannot be used in the engine without making any alterations or without mixing WCO with diesel fuel at specific ratios.

Considering the energy crisis of the countries; it can be stated that the usage of such alternative fuels will make significant economical contributions. For this reason; it is required to provide legal procedures and investment supports in order to collect and assess the waste oils via the organizations of the governments and civil society organizations. On the other hand; it should is required to deepen the investigations regarding to the assessment types of WCOs and their direct usages or usages at different mixture ratios. Investigation of the reasons of performance losses at the end of the long-term studies that arise in this study will be realized and the effects of WCO on engine and fuel system will be investigated.

Acknowledgement

The author would like to thank the Türk Tractor Factory for their support.

References

Altın R., Cetinkaya S., Yücesu H.S., 2001. The potential of using vegetable oil fuels as fuel for diesel engines. Energy conversion and management, 42(5): 529-538.

Arslan R., 2011. Emission characteristics of a diesel engine using waste cooking oil as biodiesel fuel. African Journal of Biotechnology, 10(19): 3790-3794.

Bari S., Yu C.W., Lim T.H., 2004. Effect of Fuel injection timing with waste cooking oil as a fuel in a direct injection diesel engine. Journal of Automobile Engineering, 218(1): 93-104.

Canakci M., Van Gerpen J.H., 2003. Comparison of engine performance and emissions for petroleum diesel fuel, yellow grease biodiesel, and soybean oil biodiesel.Trans ASAE,46(4): 937–44.

Çetinkaya M., Ulusoy Y., Tekin Y., Karaosmanoğlu F., 2005. Engine and Winter Road Test Performances of Used Cooking Oil Originated Biodiesel. Energy Conversion And Management, 46(7-8): 1279-1291.

Cetinkaya M., Karaosmanoglu F., 2005. A new application area for used cooking oil originated biodiesel: Generators. Energy & Fuels, 19(2): 645-652 .

Hamasaki K., Kinoshita E., Tajima H., Takasaki K., Morita D., 2001. Combustion characteristics of diesel engines with waste vegetable oil methyl ester. The fifth International Symposium on Diagnostics and Modeling of Combustion in Internal Combustion Engines (COMODIA).

Kaplan C., Arslan R., Sürmen A., 2006. Performance Charecteristics of Sunflower Methyl esters as Biodiesel. Energy Sources, 28: 751-755.

Naima K., Liazid A., 2013. Journal Waste oils as alternative fuel for diesel engine: A review. Journal of Petroleum Technology and Alternative Fuels, 4(3): 30-43.

Isa M.D., Shahrir A., Taib A., Mohamad I., 2009.Performance and emission characteristics of a diesel engine fuelled with waste cooking oil/diesel fuel blends. Proceedings of

International Conference on Applications and Design in Mechanical Engineering, iCADME 2009.

Lapuerta M., Agudelo J.R., Rodríguez-Fernández J., 2008. Diesel particulate emissions from used cooking oil biodiesel. Bioresour Technol, 99: 731–40.

McDonnell K.P., Ward S.M., McNulty P.B., Howard-Hildige R., 2000. Results of engine and vehicle testing of semirefined rapeseed oil. Transactions of the ASAE-American Society of Agricultural Engineers, 43(6): 1309-1316.

Mittelbach M., Tritthart P., 1988. Diesel fuel derived from vegetable oils, III. Emission tests using methyl esters of used frying oil. J American Oil Chemists' Soc., 65(7): 1185–1187.

Payri F., Macián V., Arregle J., Tormos B., Martínez J.L., 2005. Heavy-duty diesel engine performance and emission measurements for biodiesel (from cooking oil) blends used in the ECOBUS project. SAE paper, 01-2205.

UFOP, Union zur Förderung von Oel- und Proteinpflanzen e.V,2013.

Ulusoy Y., Tekin Y., Çetinkaya M., Karaosmanoğlu F., 2004. The Engine Tests of Biodiesel from Used Frying Oil. Energy Sources, 26: 927-932.

Ulusoy Y., Arslan R., Tekin Y., Sürmen A., Bolat A., Şahin R., 2010. Investigation of Performance of waste frying Oil as a Biofuel in a Diesel Engine. 11. International Combustion Symposium, 24 – 27 Haziran 2010, Sarajevo.

BIOGAS PRODUCTION FROM AGRICULTURAL WASTES IN TURKEY-A CASE STUDY

Yahya Ulusoy[1*], Ayse Hilal Ulukardesler[1], Ridvan Arslan[1], Reyhane Arslan[2]

[1]Uludag University, Vocational School of Technical Sciences, Bursa-Turkey,
Phone: +90 224 2942307, Fax: +90 224 2942303, E-mail: yahyau@uludag.edu.tr
[2]Uludag University, Yenisehir Ibrahim Orhan Vocational School, Bursa-Turkey

Abstract

Since the cost of production and use of energy from fossil energy sources increase every day, renewable energy sources that can compete with fossil energy sources come to the forefront of our country and world. Although Turkey has wide spectrum of energy resources, these resources are insufficient in terms of usage, and Turkey is currently an energy importing country. Approximately 75% of our country's energy consumption met by imports and the share of imports continues to increase each year. According to the literature, although approximately 50 to 65 Million Tonnes of Oil Equivalent (MTOE) agricultural waste and 11.05 MTOE animal wastes were produced and 60% of this value can be used for energy production, they are not assessed. It is known that, energy potential to be obtained from agricultural and animal waste can cover 22-27% of Turkey's annual energy consumption. In 2010, primary energy demand in Turkey was 109.266 MTOEwhile energy production value 32.228 MTOE. Energy demand in Turkey shows an increase of 8-10% annually, and it is estimated that in 2020 primary energy demand will reach 298,4MTOEwhile energy production will be 70.2 MTOE, and energy import will be 76 %.

In this study, the capacities of the collected and grouped agricultural organic waste were determined in Turkey and in Bursa, which is the fourth largest city in Turkey. According to these capacities, valuable organic matter amounts and amount of energy were calculated.

Keywords: Agricultural wastes, anaerobic digestion, Biogas

Introduction

In today's energy demanding life style, need for exploring and exploiting new sources of energy which are renewable as well as eco-friendly is a must (Yadvika et al., 2004). Renewable energy resources draw attention all over the world because they are sustainable, improve the environmental quality and provide new job opportunities in rural areas. Every year in the world several million tons of agricultural wastes are being disposed through different ways such as incineration, land applications and land filling. This global waste has a high potential as a bio renewable energy resource and can be turned into high-value by-products (Isci, Demirer, 2007)

The anaerobic digestion of various organic feedstocks, predominantly animal manures and municipal wastewater sludge's, produce a methane rich gaseous mixture called biogas (White et al., 2011). The produced biogas is a valuable biofuel for the replacement of fossil fuels in various technical applications (e.g. heating, electricity, transport fuel), which in turn determine its quality requirements. Owing to the high levels of methane, biogas can be used as a heating fuel, and can even be used in an engine to generate electricity (White et al., 2011).

According to some studies, biogas produced from anaerobic digestion is one of the most favorable bioenergy forms mainly because of the high net energy yields per acreage and the substrate flexibility (Persson et al., 2006).Biogas generally contains between 40% and 70% methane, with the balance of the gas consisting of carbon dioxide and anywhere from 100 to more than 3000 ppmv of hydrogen sulphide (H_2S).

Biogas is considered a carbon dioxide-neutral biofuel and if used as vehicle fuel, emits lower amounts of nitrogen oxide, hydrocarbon and carbon monoxide emissions than petrol or diesel engines (Wellinger, Linberg, 2000). Upgrading of biogas for use as vehicle fuel is feasible in large-scale sewage and biowaste digesters (e.g.), and pioneering work has recently also been done on farm-scale biogas concepts in this field (Rasi et al., 2007).

Known as the "20-20-20" targets, set three key objectives for 2020:a 20% reduction in EU greenhouse gas emissions from 1990 levels; raising the share of EU energy consumption produced from renewable resources to 20%; a 20%

improvement in the EU's energy efficiency. Currently, the amount of the primary energy consumption in Turkey is 1.36 toe per capita, world average is 1.80 TOE per capita and the OECD average is 4.64 TOE per capita. According to these data, Turkey is 30% compared to the OECD and when compared to the world Turkey also has the lower energy consumption. Although Turkey has lower greenhouse gas emissions per capita than in developed countries, the energy density must be reduced further. Accordingly, Turkey on energy efficiency target by 2023, to reduce energy intensity by 20% compared to 2008.

In this study, the capacity of organic waste potential and produceability of biogas capacity are evaluated for Turkey and Bursa.

An Overview of Biogas Potential and Productionfrom Wastesin Turkey

The organic wastes that can be used in biogas production can be sorted into three main categories. The next section examines the potential of these resources in our country and in the province of Bursa.

Urban Organic Wastes

Urban agricultural wastes are the city sewage sludge released from waste water treatment centers, food industry wastes, crop wastes and urban open market wastes. Instead of storing this waste-waste, biogas produced from organic content is an important source of raw materials for municipalities to use. Also industrial facilities can establish their own biogas plants in order to use their own waste.

According to the 2010 Turkish Statistical Institute (TSI) data, the cities that established composting plants in our country, and the province of Bursa are given in Table 1.Only 194.452 tons of 25.276.698 tons waste could be evaluated as compost in Turkey and the rest is stored in landfills is made of an important place, as well as environmental pollution. According to TSI, although a significant potential for organic waste present in the province of Bursa, no treatment has occurred. After 2010 many studies have been initiated in many cities for the gas production from garbage storage areas and separation of organic wastes.

Vegetable-Agricultural Organic Wastes

Products remaining after the seeds, unused stalks and straw parts, peas, beans, corn, tomatoes and other scraps left over from the production of products, nuts and cotton harvesting and processing of certain products of local stage consists of the remaining residues (Table 2).

Tab. 1 Cities founded compost facilities in Turkey and biogas data (TSI, 2012)

	Taken to landfills (ton/year)	**Biogas amount m^3/year**	**Energy equivalent (Tj/year)**	**Taken to compost (Ton/yıl)**	**Biogas amount m^3/year**	**Energy equivalent (Tj/year)**
TURKEY	13.746.876	1.752.726.690	36.807	194.452	24.792.630	521
Antalya	572.294	72.967.485	1.532	52.110	6.644.025	140
Aydın	181.219	23.105.423	485	1.806	230.265	5
Denizli	169.476	21.608.190	454	376	47.940	1
İstanbul	5.590.843	712.832.483	14.969	140.160	17.870.400	375
Bursa	605.836	77.244.090	1.622	15.146	1.931.102	41
Bursa	605.836	77.244.090	1.622	54.525	6.951.980	146

Tab. 2 Comparison of Vegetable-agricultural organic wastesin Bursa and Turkey (TSI,2012)

	Production		**Draff (Ton)**		**Biogas (m^3 /year)**		**Energy equivalent (Tj/year)**	
	Bursa	**Turkey**	**Bursa**	**Turkey**	**Bursa**	**Turkey**	**Bursa**	**Turkey**
Wheat	231.372	21.800.000	279.801	24.471.328	97.370.844	8.516.022.161	2.045	178.836
Corn	159.507	4.200.000	241.903	8.717.200	110.307.786	3.975.043.200	2.316	83.476
Silage corn	906.470	15.258.471	906.470	15.258.471	172.229.300	2.899.109.490	3.617	60.881
Rice	18.272	900.000	10.963	596.400	5.192.172	282.455.040	109	5.932
Barley	24.892	7.600.000	22.360	5.497.533	9.257.040	2.275.978.579	194	47.796
Sunflower	19.064	1.335.000	39.272	2.750.100	4.123.543	288.760.500	87	6.064
Sugar beet	85.544	16.126.489	59.881	11.288.542	26.317.612	4.961.314.341	553	104.188
Potatoes	38.459	4.648.081	17.307	2.091.636	1.739.308	210.209.463	37	4.414
Bean-pea	223.979	223.979	2.239.790	2.239.790	156.785.30	156.785.300	3.292	3.292

	Production		Draff (Ton)		Biogas (m^3 /year)		Energy equivalent (Tj/year)	
	Bursa	Turkey	Bursa	Turkey	Bursa	Turkey	Bursa	Turkey
Tomatoes	1.198.320	10.052.000	952350	4.523.400	53.331.600	253.310.400	1.120	5.320
Total	100%		4.770.097	77.434.401	636.654.50	23.818.988.47	13.370	500.199
Availability	50%		2.385.048	38.717.200	318.327.25	11.909.494.23	6.685	250.099
	10%		477.010	7.743.440	63.665.450	2.381.898.847	1.337	50.020

Animal Wastes

Cattle-sheep and poultry manure, slaughterhouse waste and waste generated during the processing of animal products-residues. 60% of the total numbers of animals are cattle and 33% are poultry. According to TSI, in 2010 there exist 11.518.827 cattle in Turkey (Table 3). Cattle population spread all over Turkey. But poultry sector usually developed in the western region. However, the chicken meat sector, particularly common in the western and northeastern Anatolia, while in egg sector spread over the entire country.

For determination of biogas potential, different approaches in terms of general academic studies and general analyzes exist. In this context, analysis of the theoretical, technical, economic, and consists of different methods can be performed. The first two of these approaches is relatively easy to reach the conclusion. Here, the theoretical potential means, the all theoretical potential assessed in the intent biomass, and the technical potential of biomass means the potential that could be used as a result of the structural potential of ecological constraints, and refers to the technical possibilities.

However, for the calculation of the technical potential of biogas should be dealt with separately in the west and east of Turkey. Because, the west of Turkey, has larger operations than the east and animals generally lives in barns. But in the east, long days of grazing make it impossible to collect animal waste for biogas production. For the potential calculations in Table 3, similar studies in theoretical biogas potential approaches were adopted (Ekinci et al., 2010; Kulcu, 2007; Ekinci, 2011).In this case available wastes for potential technical biogas were taken as 50% for cattle, 99% for poultry is to be used. This means that the waste can be used for cattle was 50% in the west, whereas this value is 15% for the cattle in the east.

It is practically possible to use different organic wastes as raw materials for biogas across the country. Among these sources, the most important sources are animal waste and agricultural organic wastes. Besides biogas production from animal waste, the maturation of these wastes as little as 1 to 1.5 months, and the availability of organic fertilizer is also possible. In the case that these waste are not evaluated, underground and above pollution of the environment in rural areas, especially in the troubled state of disposal to affect the health of humans and the environment. Biogas production from these wastes also prevent the loss of nutrients during standing by the fertilizer .Thus, energy (electricity and heat) production from organic wastes and also the improvement of agricultural soils poor in organic matter may be possible. Also, increasing efficiency in these areas is recognized.

Tab. 3 Animal wastes in Bursa and Turkey, and energy equivalent data (TSI,2012)

	Manure (ton/animal*year)		Biogas (m^3 /year)		Energy equivalent (Tj/year)	
	Bursa	Turkey	Bursa	Turkey	Bursa	Turkey
Cattle	622.278	40.931.280	20.535.174	1.350.732.240	431,239	28.365
Buffalo	3.128	305.014	103.237	10.065.449	2,168	211
Sheep	196.411	16.162.784	11.391.832	937.441.455	239,228	19.686
Goat	67.161	4.405.263	3.895.326	255.505.260	81,802	5.366
Chicken	174.750	5.168.196	13.630.497	403.119.288	286,240	8.466
Turkey-goose	177	89.210	13.833	6.958.380	0,290	146
Total	1.063.905	67.061.746	49.569.899	2.963.822.071	1.041	62.240
Availability 50%	531.953	33.530.873	24.784.950	1.481.911.036	520	31.120
10%	106.391	6.706.175	4.956.990	296.382.207	104	6.224

Result and Discussion

Bursa, located in Marmara Region of Turkey, has 429.323 ha fields in 40% of which are suitable for agriculture. This field is usable for almost all kinds of agricultural products. Currently 58% of this field is used for field plant and 11% for vegetables.

In recent years, the introduction of the private sector and entrepreneurs as well as in other regions, the agricultural production in the province of Bursa waste to biogas and converted to electrical energy and can be sold to state with 0,145 Turkish Lira incentive interconnected system. Water treatment systems of food and agro-based industries equipped with the mesophilic biogas system and produced biogas can be utilized in electricity-heat conversion facilities. There are many different samples for these facilities. Milk processing plant and animal husbandry plant has 350 kWh installed capacity. Also there exist a 4 MW installed capacity plant processing animal wastes.

Studies on the storage and processing of urban waste water treatment plants gained momentum. In that regard, the capacity of the stored waste that can be treated as municipal waste gas is 8.960.797 tons by the year 2012. On 19.05.2012, energy production was started and works with 30-40% efficiency.There exist 7 generators each having a capacity of 1.4 MWh and 5400 m3 waste gas is collected hourly and approximately 9.8 MWh electricity produced. The electricity generated is given Turkish Electricity Transmission Co. By production of energy from landfill gas, methane gas emissions 235.000 tons / year of CO2 equivalent reduced, annual lighting of 47.000 housing units produced which is approximately 76.204.800 kWh of electrical energy. In addition, to evaluate organic waste from urban-treatment study conducted by the Municipality of Bursa organic matter that can be collected and evaluated data are given in Table 4.

According to these data, especially about 100,000 tons / year of sludge and from different sources of organic solid waste may be collected. Resulting from treatment of urban waste resources in order that waste sludge 80.000 tons, the market place waste12.000 tons, park and garden waste 5.695 tons, bazaar waste 1.892 tons and food industry wastes 92 tons have been obtained respectively. Although theamount of methane may vary with respect to type and quantity of waste material, it is calculated as 1.000.000 Nm^3/year. According to the literature values, the amount of methane gas production is equal to 640000 natural gas is Nm3/year. By this production 7.315.000 kWh electricity and 7.022.400 kWh heat can be obtained. This amount of electricity and heat meet the needs of electric and heat capacity of the 14.000 houseapproximately. Thus, instead of a specific cost for the disposal of polluting the environment and the disposal of waste, significant contribution to the country's economy may be provided.

Tab. 4 Municipal wastes in Bursa, and energy equivalent data(TSI,2012)

	(Ton)	Dry Matter(Ton)	Organic dry matter(Ton)	Methane production (Nm^3)	Energy equivalent (Tj/year)
Sludge	80.000	4.800	3.154	402.306	8,45
Bazaar waste	12.000	1.980	1.643	376.470	7,91
Park waste	5.595	951	856	196.460	4,13
Vegetable waste	1.892	284	253	57.861	1,22
Food waste	92	16	15	5.323	0,11
Zoo waste	100	31	25	5.422	0,11
Total	19.679	3.262	2.794	641.536	13,47
General Total	99.670	8.062	5.947	1.043.842	21,92
Solid material	16.209	4.052			
Liquid material	81.332	1.872	1.203.836	127.5 ltr CH_4/kgOM	

References

Ekinci K., Kulcu R., Kaya D., Yaldız O., Ertekin C., 2010. The Prospective of Potential Biogas Plants That Can Utilize Animal Manure in Turkey. Energy Exploitation and Exploration, 28 (3): 187 - 206.

Ekinci K., 2011. Utilization of Apple Pruning Residues as a Source of Biomass Energy: A Case Study in Isparta Province. Energy Exploitation and Exploration, 29(1): 87 - 107.

Isci A., Demirer G. N., 2007. Biogas production potential from cotton wastes, Renewable Energy 32: 750 – 757.

Kulcu R., Yaldız O., 2007. Composting of goat manure and wheat straw using pine cones as a bulking agent.BioresouceTecnology, 98, 2700 - 2704.

Persson M., Jönsson O., Wellinger A., 2006. Biogas Upgrading to Vehicle Fuel Standards and Grid Injection. Report in IEA Bioenergy Task 37-Energy from Biogas and Landfill Gas.

Rasi S., Veijanen A., Rintala J., 2007. Trace compounds of biogas from different biogas production plants, Energy 32: 1375 - 1380.

Wellinger A., Linberg A., 2000. Biogas upgrading and utilization-IEA Bioenergy Task, vol. 24. Paris, France: International Energy Association.

White A. J., Kirk D. W., Graydon J. W., 2011. Analysis of small-scale biogas utilization systems on Ontario cattle farms, Renewable Energy 36: 1019 - 1025.

Yadvika, Santosh, Sreekrishnan T. R., Kohli S., Rana V., 2004. Enhancement of biogas production from solid substrates using different techniques- a review, Bioresource Technology 95: 1 – 10.

EFFECT OF THE LOAD ON TWO-BODY ABRASION PROCESS OF COMPOSITES BASED ON WASTE

Petr Valášek*, Petr Chocholouš

Czech University of Life Sciences Prague, 165 21 Prague 6 – Suchdol, Czech Republic, Phone: +420224383262, E-mail: valasekp@tf.czu.cz

Abstract

In case of the dispersion of solid inorganic particles based on waste in polymer matrix results in formation of the composite system together with kind of material recycling. Either primary or secondary hard inorganic particles increases material wear resistance. The article defines dependence of volume losses of particular composites with different types of waste filler on load of specimens. Composite particle systems showed significant increase of wear resistance compared to unfilled resin. The impact strength of specimens was assessed also, where significant decrease of particle composites has occurred compare to unfilled resin.

Keywords: Epoxy resin, polymers, recyclation, waste

Introduction

The wear can be defined as undesirable change on surface or dimension change of rigid bodies. The most represented wear in agricultural production area is abrasive wear. The abrasive wear means separating particulate material during scribing and cutting by hard particles. A typical example of this type of wear in agriculture can be worn functional surfaces of machine parts processing soil or functional surfaces coming into contact with the material being processed. Material behavior under abrasive wear can be experimentally defined by two-body abrasion using abrasive cloths with firmly bonded inorganic particles of corundum (Muller, Hrabe, 2013; Muller, Valasek, 2012).

Composite materials are composed of two or more phases that have different mechanical and tribological properties. The presence of solid inorganic particles in the polymer matrix increases resulting wear resistance. Chruscov, Babicev (1970) state that the wear rate of the composite filler is less than wear rate of the matrix, they assume that abrasive wear is governed by the filler. ZumGahr (1976) states that the tribological properties of the composite systems are not controlled by one phase only, but the contribution of each phase is linearly proportional to its volumetric share. According to this model abrasive wear of the composite linearly decreases with increasing volume of filler. This model has been confirmed by experiments carried out by Valasek, Muller (2010) and Valasek et al. (2012). He observed increasing of wear resistance of polymer composites based on thermosetting with increasing share of waste corundum particles.

Composite matrix can be formed also by thermoplastics – Panin et al. (2012) filled Super High Molecular Polyethylene by particles of Al_2O_3 (50 μm) which led to 18 times improvement of wear resistance. Similar tribological properties were also recorded by Basavarajappa et al. (2012) and Mohan et al. (2012) who used particles of SiC as filler.

Primary filler particles can be substituted by secondary material therefore waste. Valasek, Muller (2010), Valasek et al. (2012) and Valasek, Brozek (2013) describe a micro-particle systems filled with waste of corundum, glass beads and ferrous metal chips which distinctly increased the wear resistance. These experiments were carried out at constant loading. In practice, define the behavior of wearing materials under different loads is necessary. Tenenbaum (1976) determined relationship between abrasion (W) and load (F) of metallic and polymeric materials according to the formula 1.

$$W = k \cdot F^n \qquad (1)$$

The carried out experiment aims to define dependence of the volume losses of polymer micro-particle composite with a filler based waste on loading. Verify the hypothesis that even in composite systems based on waste the dependence between abrasion wear and loading will be exponential. Furthermore, to describe the temperature rise occurring during the tribological tests depending on load of specimens as one of the factors affecting abrasion wear of polymeric materials.

Material and Methods

Composite matrix were formed by thermosetting - epoxy resin Eco epoxy 1200/324. Microparticle filler was represented by waste of corundum particles (30 vol.%) with different fractions: F80 153 ± 48 μm (middle particle size), F240 46 ± 9 μm, F800 5 ± 1 μm. Individual fractions were combined together in a ratio of 1:5 and 5:1. Composite systems based on corundum waste were compared with systems of Epoxy/30 vol% SiC filler (129 ± 34 mm) and Epoxy/Chips 25 vol% filler (two kinds of ferrous metal chips – cast-iron weld deposits, which formed by machining solid material on a turning lathe without process fluids usage). The middle particle size of ferrous metals was due to their irregular shapes measured in a 2D plane through the surface: middle size of Chips 1 (0.41 ± 0.18 mm^2), Chips 2 (0.59 ± 0.20 mm^2). Chip measurements of ferrous metals demonstrate broad size distribution of particles. Due to saturation of the matrix by filler concentration of 25% for Epoxy/Chips and for other composites concentration of 30% was used. The chosen concentrations were selected according to hypothesis that the increasing proportion of particles in the matrix material increases resistance to abrasive wear. The composites were prepared by mechanical mixing in an ultrasonic bath. Subsequently, the prepared mixture was casted into rubber molds and cured according to the technological requirements of resin manufacturer.

Tribology

The two body abrasion was tested on a rotating cylindrical drum device with the abrasive cloth of the grain size P120 (Al_2O_3 grains) according to the standard CSN 62 1466. The testing machine with abrasive cloth consists of the rotating drum on which abrasive cloth is fastened by a bilateral adhesive tape. The test specimen is secured in the pulling head and during the test it is shifted by means of a mowing screw along the abrasive cloth from the left edge of the drum to the right one. The test specimen is in contact with the abrasive cloth and it covers the distance of 60 m. During one drum turn of 360° it is caused the test specimen left above the abrasive cloth surface. Consequent impact of the testing specimen on abrasive cloth simulates the concussion. Test specimen load was changed by replaceable weights. Load corresponds to 0.08 $N\cdot mm^{-2}$, 0.12 $N\cdot mm^{-2}$, and 0.16 $N\cdot mm^{-2}$. The mean diameter of the test specimens was 15.5 ± 0.1 mm and their height was 20.0 ± 0.1 mm. The volume losses were measured on analytic scales weighing on 0.1 mg. The volume losses were calculated on the basis of the found out volume and the density of the composite systems. The highest temperature value observed in the interface of the test sample and temperature of abrasive cloth was recorded by a contactless thermometer Testo 845. For the composite system comparison with the steel S235JR the relative wear resistance (ψ) was used according to (2):

$$\psi = \frac{W_{St.}}{W_{Ts.}} \tag{2}$$

where ψ – relative abrasive wear resistance,
W_{St} – average volume loss of standard (S235JR) (cm^3)
$W_{Ts.}$ – average volume loss of tested specimens (cm^3).

Impact strength

The impact strength was evaluated according to standard CSN 64 0611 (Determination of the impact resistance of rigid plastics by means of Dynstat apparatus). During these destructive tests the Dynstat device stated impact strength a_n, which expresses kinetic energy the hammer needed to crush the tested object without notches in relation to the surface of its diagonal cut, as expressed by the following formula (3)

$$a_n = \frac{A_n}{b \cdot h} \tag{3}$$

where a_n – impact strength ($kJ\cdot m^{-2}$)
A_n – energy required to shift the specimen (kJ),
b – width of the test specimen (m),
h – thickness of the test specimen (m).

Results

Due to the different density of composites the volume losses were used for comparison wear resistance. Comparison of the theoretical density (ρ_T) calculated based on the density of the epoxy (1.15 $g\cdot cm^{-3}$) and the density of each filler with actual density (ρ_R) is shown in Tab. 1. The difference of density is caused due to the presence of air bubbles which can not be completely eliminated by chosen procedure preparation. Actual density will affect the uneven distribution of the filler in matrix in dependence of composites preparation method.

Tab. 1 Density of composites

Material	ρ_T	ρ_R
Epoxy/Chips 1	2.78	2.56
Epoxy/Chips 2	2.78	2.62
Epoxy/SiC	1.77	1.61
Epoxy/Corundum 5:1 80:240	2.01	1.93
Epoxy/Corundum 1:5 80:240	2.01	1.89
Epoxy/Corundum 5:1 80:800	2.01	1.87
Epoxy/Corundum 1:5 80:800	2.01	1.86

Inclusion of micro-particle filler always significantly increased resistance to abrasive wear. From graphic representation of the load and volume losses (Fig. 1), it is clear that with increasing load there was an increase of volume losses. High resistance to two-body abrasion showed composite Epoxy/Chips. When load 0.08 $N{\cdot}mm^{-2}$ and 0.12 $N{\cdot}mm^{-2}$ the smallest volume losses showed Epoxy/Chips 1 - 0.0407 ± 0.0008 cm^3 (0.0487 ±0.0007 cm^3), when load 0.16 $N{\cdot}mm^{-2}$ Epoxy/Chips 2 - 0.0799 ± 0.0001 cm^3. Influence of corundum particle size on wear resistance was clearly showed in case of using Epoxy/corundum composite. Composites with a higher fraction (dimension 153 μm) had higher wear resistance (abrasive cloth P120 was used).

Middle values of volume losses were fitted by exponential functions whose functional equation and coefficient of determinance describes Tab. 2. The table also shows a comparison of volume losses of composites with ordinary carbon steel for each load (relative abrasive wear resistance $\psi_{0.08}$, $\psi_{0.12}$ a $\psi_{0.16}$). From the comparison it is clear that with increased load volume losses are significantly increasing in all cases of filled systems compare to steel.

During the tribological tests temperature was measured on interface of specimen and abrasive cloth. The highest recorded temperature for each load and materials are graphically presented in Fig. 2. The highest temperature was recorded by unfilled resin, the lowest by steel. Friction creates heat - part of the mechanical energy is converted into heat. Effects of heat and its size can affect many material characteristics. The heat transfer through the vibratory motion of atoms is characteristic for polymeric materials, for metal materials is characteristic heat transfer mainly by kinetic energy of the electrons. For this reason polymer materials have mostly lower thermal conductivity.

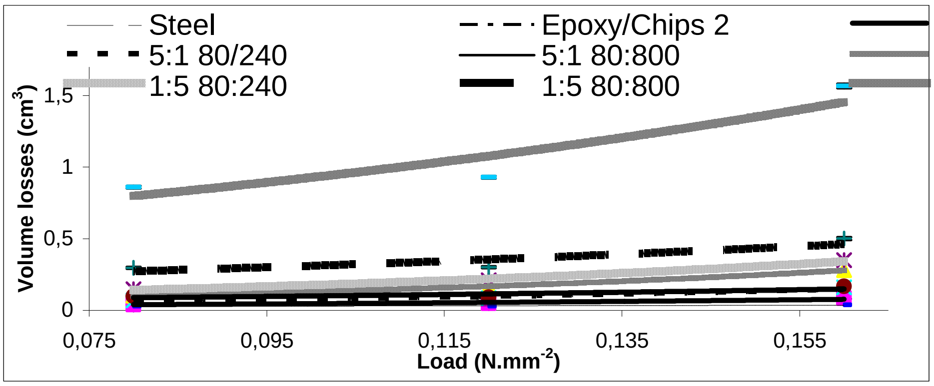

Fig. 1 Dependence of volume losses on load

Tab. 2 Functional equation

Material	$\psi_{0.08}$	$\psi_{0.12}$	$\psi_{0.16}$	Functional equation	R^2
Epoxy/Chips 1	0.70	0.56	0.48	$y = 0.0204e^{8.301x}$	0.96
Epoxy/Chips 2	0.71	0.59	0.45	$y = 0.0183e^{9.2338x}$	0.92
Epoxy/SiC	0.28	0.18	0.14	$y = 0.037e^{12.626x}$	0.99
Epoxy/Corundum 5:1 80:240	0.41	0.34	0.24	$y = 0.0283e^{10.358x}$	0.90
Epoxy/Corundum 1:5 80:240	0.20	0.14	0.11	$y = 0.0593e^{10.936x}$	0.99
Epoxy/Corundum 5:1 80:800	0.29	0.32	0.23	$y = 0.052e^{6.5674x}$	0.63
Epoxy/Corundum 1:5 80:800	0.10	0.10	0.08	$y = 0.1611e^{6.5761x}$	0.77
Epoxy	0.03	0.03	0.02	$y = 0.4381e^{7.5008x}$	0.85
Steel	*1*	*1*	*1*	$y = 0.0209e^{3.4544x}$	0.75

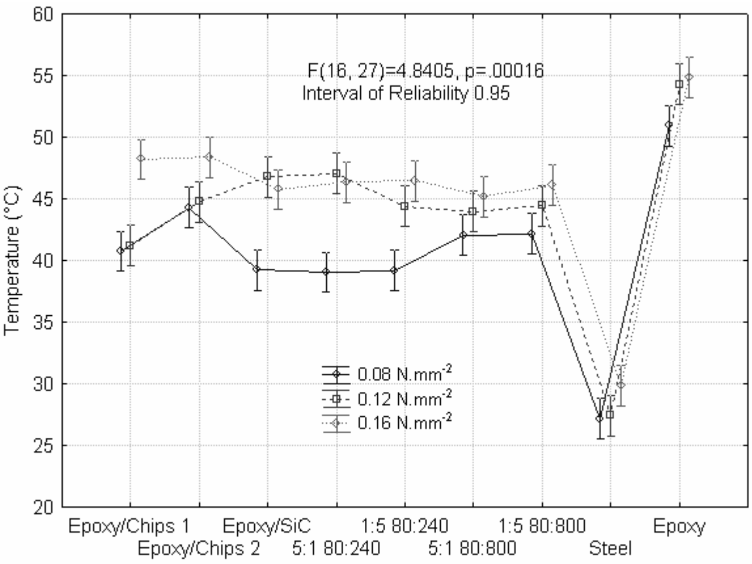

Fig. 2 Dependence of load on temperature

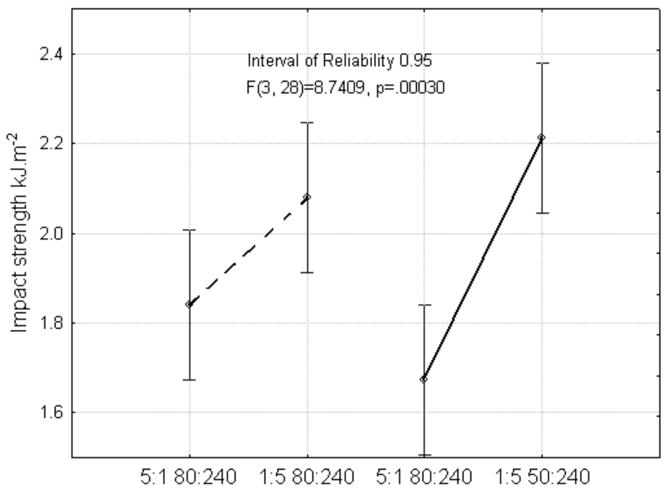

Material	Mean kj·m^{-2}	agreement		
5:1 80:800	1.67	*		
5:1 80:240	1.84	*	*	
1:5 80:240	2.08		*	*
1:5 80:800	2.21			*

Fig. 3 Impact strength and Tukey´s HSD Test of Epoxy/Corundum systems

The values of impact strength are graphical shown in Fig. 3 and by Tukey's HSD test are compared middle values. From the results it is clear that a higher proportion of small particles of corundum in epoxy resin resulted in lower reduce of impact strength compared to the resin without filler (8.24 ± kJ·m^{-2}).

Discussion

Inclusion of microparticulate fillers based on waste led to an increase resistance to two-body abrasion in accordance with the conclusions of authors (Valasek, Muller, 2010; Valasek et al., 2012; Panin et al., 2012; Valasek, Brozek, 2013). The most significantly decrease of volume losses - up to 95% caused inclusion of microparticles in form of ferrous metal chips. Epoxy/Corundum composites with a higher proportion of particles with an average diameter of 153 μm had up to 92% smaller volume losses than unfilled Epoxy. However, composites did not reach the same resistance to two-body abrasion as steel.

With increasing load there was an increase of volume losses compared to steel - under load 0.08 N·mm^{-2} composite Epoxy/Chips 2 reached $\psi_{0.08}$ = 0.70. With increasing load relative abrasive wear resistance decreased from this value by 20% and 31%.

The experiment confirmed Tenenbaum (1976) hypothesis about exponential dependency of load and abrasion of micro-particle composites.

Filled microparticle composite Epoxy/Corundum clearly showed decrease of impact strength at least about 73% compared to unfilled resin.

Due to the mechanical properties of polymer composites described above, those materials can be applied on functional surfaces of machines and for quick restoration of machine parts. In the agrocomplex these materials can assert at renovation of screw conveyors, fan vanes, at cementing and bonding scuttle, cracks in machine boxes, it can serve for planishing welding seams, for reparation of small cracks, for caulking cracks in tanks, for filling splits and microsplits and imperfections and not last for bonding materials.

Conclusion

- Hypothesis about the exponential increase of volume losses depending on the increasing load was confirmed.
- The assumption that composites with a higher proportion of particles with larger middle dimension will have better abrasive wear resistance (on selected abrasive cloth) was confirmed but larger particles significantly reduce the impact strength compared with a smaller size of particles.
- The dispersion of solid inorganic particles based on waste in thermosetting is kind of material recycling that should be prioritized.

Acknowledgement

Supported by Internal grant agency of Faculty of Engineering, Czech University of Life Sciences in Prague.

Reference

Basavarajappa S., Joshi A. G., Arun K., Kumar A. P., Kumar M. P., 2012. Three-Body Abrasive Wear Behaviour of Polymer Matrix Composites Filled with SiC Particles. Polymer-Plastics Technology and Engineering. 14: 8 - 12.

Chruscov M. M. M., Babicev M. A., 1970. Abrazivnoje iznasivanije. Izd. Nauka, Moskva.

Muller M., Valasek P., 2012. Abrasive wear effect on Polyethylene, Polyamide 6 and polymeric particle composites, Manufacturing Technology. 12: 55 - 59.

Mohan N., Natarajan S., KumareshBabu S. P., 2012. The role of synthetic and natural fillers on three-body abrasive wear behaviour of glass fabric-epoxy hybrid composites. Journal of applied polymer science. 124: 484 - 494.

Muller M., Hrabe P., 2013. Overlay materials used for increasing lifetime of machine parts working under conditions of intensive abrasion. Research in Agricultural Engineering. 59(1): 16 - 22.

Panin S. V., Kornienko L. A., Sondghaitamb N. et al., 2012 Abrasive Wear of Micro and Nanocomposites Based on Super High Molecular Polyethylene (SHMPE). Part 1. Composites Based on SHMPE Filled with Microparticles AlO(OH) and Al2O3. Journal of Friction and Wear. 33(5): 381 - 387.

Tenenbaum M. M., 1976. Soprotivlenije abrazivnomu iznašivaniju. Mašinostrojenije, Mosow, 271. (in Russian)

Valasek P., Muller M., 2010. Possibilities of use of mechanical surface treatment waste in form of polymeric particle composite fillers. In 9th International scientific conference engineering for rural development. Jelgava: LUA: 267 - 270.

Valasek P., Muller M., Proshlyakov A., 2012. Effect of sedimentation on the final hardness of polymeric particle composites. Research in Agricultural Engineering, 58(3): 92 - 98.

Valasek P., Brozek M., 2013. Two body abrasion of composites containing filler on the basis of hard cast iron deposits utilizable in agrocomplex. Agronomy Research. 11(1): 163 - 170.

ZumGahr K. H., 1976. Einfluβ der Bruchzähigkeit auf die Reibungskraft bei abrasivem Verschleiβ. Z. Metallk.67: 678 - 682.

ANALYSIS OF PARTICLE ABRASIVE WEAR OF ENGINE OIL WHEN USING LASERNET FINES ANALYZER

Kateřina Veselá*, Martin Pexa, Jakub Mařík

University of Life Science Prague, 16521 Prague 6 – Suchdol, Czech Republic, Phone: +420603110390, E-mail: kvesela@tf.czu.cz

Abstract

For technical practice, it is necessary to objectively analyze oil pollution. Quantification of the number and types of particles in the engine oil can be realized by various methods tribotechnickými. In this case the use analyzer of particles LNF for determining the abrasive particles in the oil. This device is not only used for classification of particles the oil, but also for the direct analysis of wear and contamination according to the standardized code purity. This paper describes the use of this particle analyzer for the analysis of engine oil from the machine Skoda Felicia Combi 1.3 MPI, which has undergone total general overhaul and went through a period of operation.

Key words: Oil, Wear, Laser Analyser, Clean of Purity

Introduction

Disorders and their induced disruption of machinery are caused by a wide range of factors and processes that affect and are pending directly in the machine. These factors have resulted in changes in the properties of mechanical parts. These technical changes are the primary cause of a fault. The set of these processes is called a mechanism faults. According to various combinations of factors that affect the deterioration of functional areas, there are the following categories: wear, corrosion, deformation, distortion, cracks and fractures, other injuries (Pošta, 2006).

When approaching surfaces violates the integrity of the adsorption layer and the oxide layers and surfaces that are transferred to metal contact (Buyanovskii, 2010). This has resulted in the creation of micro joints. As a result of the relative motion of the surface there is the separation metal particles and movement of material surfaces (Kotus et al., 2011). The intensity of this process depends on many factors, among which the most important are to be classified kind and properties of interacting surface, the presence and properties of the medium between the surface characteristics of the relative motion of surfaces and load. Various combinations of these factors are different kinds of damage to functional areas (Pošta, 2006).

Wear is persistent undesirable change in surface or dimensions of rigid bodies, caused by the interaction of functional surfaces or functional surfaces and media that causes wear. Wear is manifested as removing or moving particles of matter from a functional surface mechanical effects, sometimes accompanied by other factors, for example as chemical or electrochemical. Commonly distinguishes six basic types of wear: adhesive, abrasive, erosive, cavitation, vibration and fatigue (Pošta, 2006). The nature of wear characterizes the shape, size and surface texture of particles (Podsiadlo, Stachowiak, 2000; Stachoviak, 1998). Further describes the types of wear and tear that can evaluate a laser analyzer LaserNet Fines.

Adhesive wear – adhesive wear is caused by the strong adhesion forces that have formed between the materials in contact. Given that the contact surfaces are smooth, the contacts occur locally in contact with uneven surfaces. The micro-contact leads to elastic and plastic deformation (Stodola, 2010; Suchánek, 2010).

Abrasive wear – abrasive wear is damaging the surface material of hard particles or hard rough surface of another material, whereby the formation occurs grooves (Fig. 1 and Fig. 2). Solid particles in the process may penetrate into the material surface. Size of abrasive wear increases with increasing hardness of the abrasive particles and falls with increasing hardness worn with use material (Stodola, 2010; Vojtěch, 2006).

Fatigue wear – fatigue wear is characterized by gradual accumulation of faults in the surface layer during repeated contact stress. Achieve if the voltage values of the yield stress for the low cycle fatigue, where the yield strength, it is a hightccyclic fatigue (Pošta, 2006; Stodola, 2010).

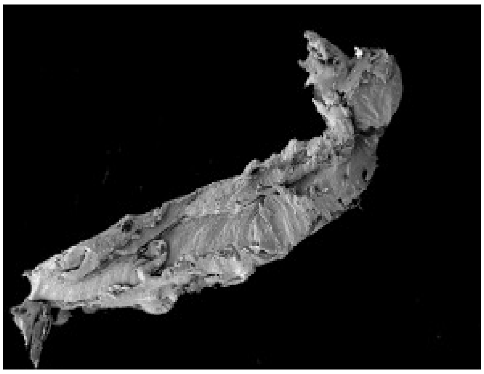

Fig. 1 Abrasive wear particles
(Stachowiak et al., 2008)

Fig. 2 Sample preparation before analysis surface
(Morin et al., 2011)

But here arises the question of how best to identify what type damage the machine when the machine is not possible to dismantle individual parts. Among other options as Vibrodiagnostics (suitable for rotary machines - Vibration spectrum), (Fernández-Francos et al., 2012; Fryščok, 2012) and Thermodiagnostics (Nondestructive testing) (Li et al., 2011) as one of the main solutions provides analysis of lubricating oils, called Tribodiagnostics. The oil is directly in contact with the functional surfaces of the exposed part and wear it directly deposited (Reintjes et al., 1994). In this paper, the analysis of abrasive particles through laser particle analyzer LNF-C in samples of semi-synthetic engine oil Mogul GX-FE 10W-40 engine of Skoda Felicia 1.3 MPI after overhaul. Furthermore, the waveforms wear complemented the consumption of fuel, depending on the distance traveled.

Material and methods

For determining the number of abrasive particles in the oil is used desktop laser particle counter and classifier LaserNet Fines ®-C. This analytical instrument is capable of analyzing hydraulic fluids and lubricating oils of various types of machinery and equipment and based on these analyzes to assess their current technical status and suggest possible measures that relate to their own maintenance. This monitoring is based on the evaluation of the morphology and number of wear particles generated during the operation of machines and equipment. LaserNet Fines ®-C is composed of two components. The first part is the analyzer, which analyzes the sample itself. The second part is a personal computer that is necessary to evaluate data from the analyzer.

Preparation of the oil sample for analysis is based on the perfect homogenization and removal of air bubbles in an ultrasonic bath. After removing the sample from the bath and enter the necessary information about the analyzed sample into the computer analysis is performed. The analysis takes about three minutes and after evaluation of the sample is operating the analyzer shows the result of analysis.

From the perspective of diagnostic machinery and determine its wear, the best combination of determination of wear metals and determine the size and character of particles, which particles analyzer is able to analyze. According to the contour are classified particles with the longest dimension greater than 20 micron in several categories. The paper analyzed particles of abrasive wear. Particle shape specifies the software under test circularity to remove bubbles and droplets larger than 20μm particles from the program calculates the result. The instrument is also capable of this function give approximate results of free water. An LNF process requires thousands of images to obtain a result with regard to statistics.

The amount of particles and their size is also evaluated, so that the results can be displayed in accordance with ISO 4406:1999, the so-called code cleanness (number of particles in a fluid - oil). Original writing by the standards of 1987 was based on the assessment in two dimensions ≥ 5 μm and ≥ 15 μm. Following the amendment of standards of 1991 and 1999 has been adjusted from the three border zone and ≥ 4 μm, ≥ 6 μm ≥ 14 μm. It is also used another division, according to NAS1638 (5-15 μm, 15-25 μm, 25-50 μm, 50-100 μm and more than 100 μm), (Filický et al., 2002; SPECTRON).

In this paper, was analyzed synthetic motor oil Mogul GX FE 10W-40, which ensures lubrication of the engine 1.3 MPI Skoda Felicia Combi. Currently the vehicle is driven about 150 thousand km, but the mileage of about 108 thousand. Km (see graph is referred to as the mileage traveled distance 0 km) was carried Engine overhaul, which included the replacement bearing crankshaft, piston inserts replace the pistons. Basic technical details of the vehicle are shown in Table 1.

Table 1 Information on the test vehicle (Author)

Model Name	Skoda Felicia Combi	**Type of engine**	four-stroke four-cylinder
Vehicle Category	personal	**Number of speeds**	5 manual
Stroke Volume	1289 cm^3	**Max. performance**	50 kW at 5 000 1/min
Top speed	163 km/h	**Total weight**	1460 kg
Number of kilometres	about 150000 km	**Year of construction**	1998

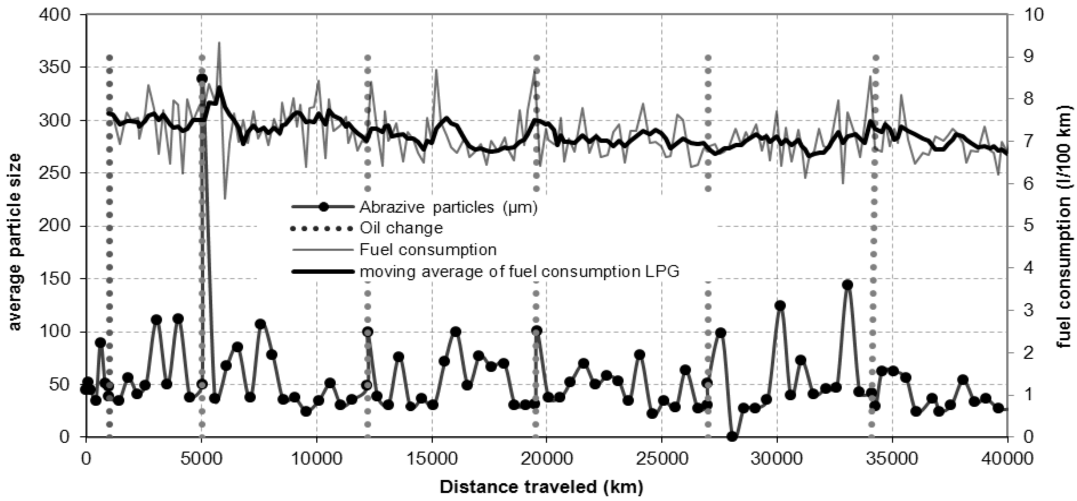

Fig. 3 Fuel consumption (LPG) and an average particle size depending on the distance traveled (Author)

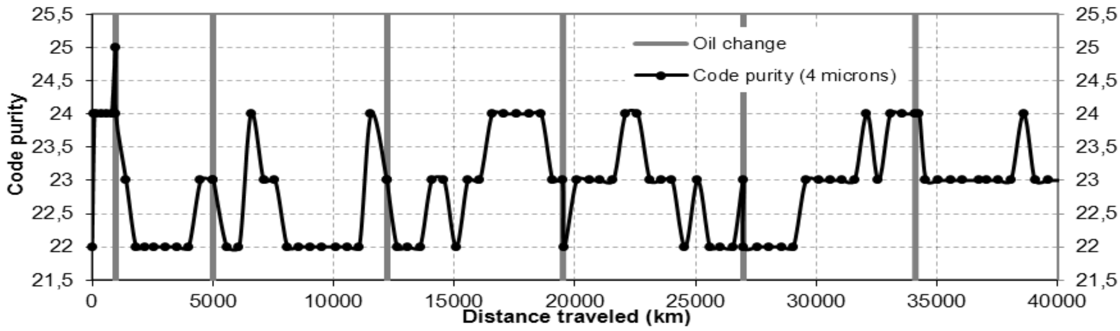

Fig. 4 Code of purity for 4 micron, depending on the distance traveled (Author)

Results

In Fig. 3 shows the course of an average particle size of the abrasive wear of the engine depending on the distance traveled in kilometers of marked change intervals oil filling and during the whole period was monitored fuel consumption (LPG). First oil was over 1,000 kilometers, which completed vehicle fuel Natural 95. Then it runs on liquefied petroleum gas (LPG). The second interval was over 4.000 km and still is being replaced at an interval of 7.500 km.

From the depending on the Fig. 3 shows that process the average particle size of abrasive wear in different oil samples is constant despite the fact that the distance traveled is noticeably changed the total number of particles. Front of the first exchange (distance 1.000 km), the total number of particles in a sample of engine oil to 6 times higher than in the next period. These are however predominantly particles smaller than 20 microns. Also in oil samples almost absent particles larger than 50 micron on which affects filtration used oil. As for the consumption of fuel (LPG), the figure shows that during operation time gradually decreased fuel consumption during start up. Compared with the first 10.000 km is a reduction in fuel consumption of 0.4 liters per 100 km. This downward trend is visible in the distance traveled from 25.000 to 30.000 km and from that distance, fuel consumption be even.

As an indicator of wear particles in engine oil, which is illustrated in Fig. 4, Fig. 5 and Fig. 6, the code cleanliness according to ISO 4406:1999, the particle size of 4 micron, 6 micron and 14 micron.

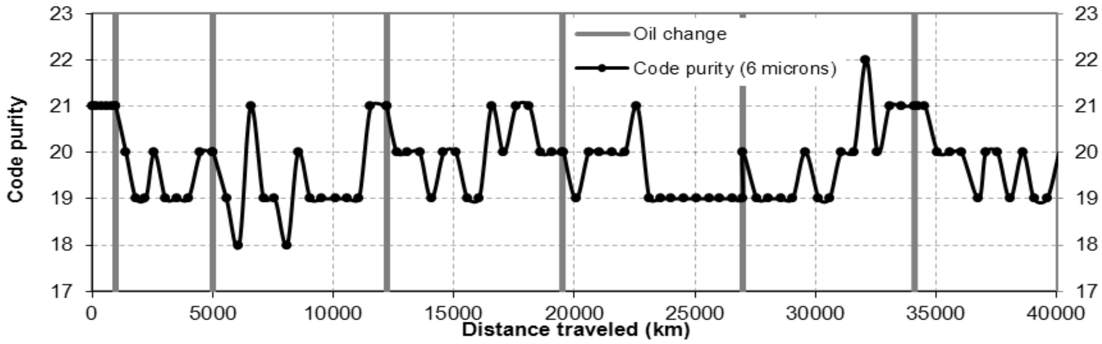

Fig. 5 Code of purity for 6 micron, depending on the distance traveled (Author)

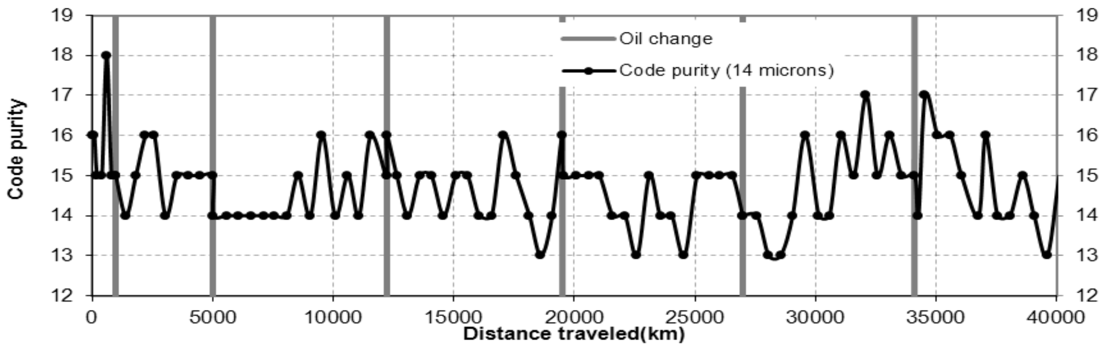

Fig. 6 Code of purity for 14 micron, depending on the distance traveled (Author)

From the aspect of the number of particles it is possible to say that it also remains constant. The gradual increase in the number of particles is evident only before the first engine oil change, where occurred significant run of the engine. In the next time, the number of particles does not change, in which they also clearly involved filtering engine oil.

Discussion and conclusion

The paper presents the use of laser analyzer LNF-C for the analysis of particles in the oil motor vehicles Skoda Felicia Combi 1.3 MPI petrol engine after overhaul, which included in particular the exchange of main bearings and cylinder liners with pistons. Repairs were carried out at 107.898 km, which is also marked as the starting point for the measurement and 0 mileages.

We were supposed to; the break-in period will be noticeable numbers of particles mainly large particles, resulting in a larger average particle size. From the results but it can be said that there has been a significant run only during the first 1,000 kilometers driven (i.e., the first oil change). In other cases are the size and number of particles expressed by a code of purity constant. Significant effect on those Constant was especially continuous oil filtration, which reduces oil mainly particle size and nature of the impact could have advanced production technology of the parts used for the overhaul. Just in Fig. 3, the measured value of abrasive particles at 5,000 kilometers climbed disproportionately compared to others. This deviation was probably caused by improperly take away the oil sample, and this distorted the measurements.

Simultaneously with the assessment of the number and size of abrasive wear was evaluated by the percentage of the analyzed sample oil. It is possible to say that these values are also too settled with no major changes. Order to give evidence that indeed been running engine, the fuel consumption was observed. Its dependence on kilometers driven is shown in Fig. 3, where it is clear that during the time period gradually dropped fuel consumption. Compared with the first 10.000 km is a reduction in fuel consumption of 0.4 liters per 100 km. This decreasing trend is evident in the distance traveled from 25.000 to 30.000 km and since then fuel consumption is uniform with.

When analyzing the filtered oil filling is very important to monitor the status of filtration, as a condition gives more information than the sample, which is taken directly from the oil tank. In fact it is possible to record up to increased wear, which manifests hike by increasing the number of particles and their size towards emergency breakdown. Despite these difficulties a laser particle analyzer in tribodiagnostic of machines for their location and filtered or unfiltered systems with a small number of circulating brings invaluable information for decision making or non-maintenance and contributes to savings, manifested delaying maintenance or bare impending lockout.

The paper is developed with grant support – 2013:1190 / 1312/3123 – Comparison of tribodiagnostics methods for the determination of particle

References

Buyanovskii I.A., 2010. Boundary lubrication by an adsorption layer. Journal of friction and wear, 31(1): 33-47. ISSN 1068-3666

Fernández-Francos D., Martínez-Rego D., Fontenla-Romero O., Alonso-Betanzos A., 2012. Automatic bearing fault diagnosis based on one-class ν-SVM. Computers and Industrial Engineering, 64(1): 357-365. ISSN: 0360-8352

Filicky D., Sebok T., Matle L., Anderson D., 2002. LaserNet Fines – A New Toolforthe OilAnalysisToolbox. MachineryLubrication, Noria. [online]. Avaible at: www.machinerylubrication. com/Read/383/lasernet-fines-oil-analys (accessed June 10, 2013).

Fryščok T., 2012. Rotor dynamics of modern turbochargers. Perner´s Contacts, 7(2): 40-50. ISSN 1801-674X

Kotus M., Andrássyová Z., Čičo P., Fries J., Hrabě P., 2011. Analysis of wear resistent weld materials in laboratory conditions. Research in Agricultural Engineering (RAE), 57, Special issue: 74-78. ISSN 1212-9151

Li T., Almond D.P., Rees D.A.S., 2011. Crack imaging by scanning laser-line thermography and laser-spot thermography. Measurement Science and Technology, 22(3). ISSN: 0957-0233

Morina A., Lee P.M., Priest M., Neville A., 2011. Challenges of simulating 'fired engine' ringliner oil additive/surface interactions in ringliner bench tribometer. Tribology - Materials, Surfaces and Interfaces, 5(1): 25-33. ISSN: 1751-5831

Podsiadlo P., Stachowiak G.W., 2000. Scale-invariant analysis of wear particle morphology — a preliminary study, Tribology International, 33(3–4): 289-295. ISSN 0301-679X

Pošta J., 2006. Provozuschopnost strojů. Česká zemědělská univerzita v Praze, 2. vydání, Praha. ISBN 80-213-0966-0

Reintjes J., Mahon R., Duncan M.D., Tankersley L.L., Schultz A., Chen V.C., Kover D.J., Howard P.L., Chamberlain M., SriniRaghavan, NareshGupta, 1994. "Optical Debris Monitoring", JOAP Annual Meeting, Pensacola FLA, November.

Specron, INC. LaserNet Fines – ParticleCounting and ShapeRecognitionfor In-ServiceOils. Industrytribology Systems, USA, 1 – 13.

Specron, INC., 2013. Automatic Sample Processorfor LaserNet Fines. USA [online]. Avaible at: www.omnitek.nl/en/products/particle/asp/asp.pdf (accessed June 11, 2013).

Stachowiak G.W., 1998. Numerical characterization of wear particles morphology and angularity of particles and surfaces, Tribology International, 31(1–3): 139-157. ISSN 0301-679X

Stachowiak G.P., Stachowiak G.W., Podsiadlo P., 2008. Automated classification of wear particles based on their surface texture and shape features. Tribology International, 41(1): 34-43. ISSN 0301-679X

Stodola J., 2010. Mechanical systeme wear and degradation processes modelling. Perner´s Contacts, 5(4): 248-264. ISSN 1801-674X

Suchánek J., 2010. Adhezivní opotřebení. TriboTechnika, 2: 66 – 71.

Vojtěch D., 2006. Kovové materiály. 1. vyd. Praha: Vysoká škola chemicko-technologická v Praze, 185. ISBN 80-7080-600-1

SPEED OF SEED PASSAGE THROUGH DELIVERY TUBES

Patrik Vitek, Josef Hula*, Adolf Rybka

Czech University of Life Sciences Prague, 165 21 Prague 6 – Suchdol, Czech Republic,
Phone: +420-224383123, E-mail: hula@tf.czu.cz

Abstract

The trend of development and innovation of precision seed drills is the use of central seed hopper and central seeding unit on these seed drills. These construction changes of seed drills need a new solution to the transport of seeds from the central sowing unit to drill coulters. As the most preferred solution is the use of delivery tubes. The airstream speed measurement by Pitot tubes has been used to determine the airstream parameters. The passage speed of wheat seeds was higher than that of maize seeds but the differences were not statistically significant. With the increasing length of delivery tubes the passage speed of seeds was decreasing. The passage speed of seeds in delivery tubes was further influenced by the placement of delivery tubes (straight, curved).

Keywords: seed drills; precision drilling; delivery tubes

Introduction

In precision seed drills separate seed hoppers are used for each seeding unit when seeds fall from a low height from the seeding mechanism directly into a furrow in the soil created by drill coulters. In recent years the manufacturers of precision seed drills have focused their efforts on the development of machines with central seed hopper and central seeding mechanism due to operating advantages of such a solution. Pneumatic transport of seeds in delivery tubes is one of the important factors of the appropriate function of seeding machines. When central seed hopper and central seeding mechanism are used in precision seed drills, an emphasis is laid on the regular distribution of seeds in the soil. It is to ensure that seeds will be conveyed by the airstream in delivery tubes at regular distances in order to avoid clustering or retaining of seeds during their transport and to observe the required seed distance in rows during sowing.

The study of seed passage through delivery tubes is based on data cited in literature dealing especially with aerodynamic conditions in tubes, airstream pressure and speed and with the overpressure transport of grains.

The objective of measuring the seed passage through delivery tubes was to specify the influence of basic parameters (airstream speed, curvature of tubes) on the precision of transport of selected seeds into drill coulters in conditions of precision drilling.

Material and method

Delivery tubes were connected to the outlet of a fan used in FARMET Excelent seed drills. The fan was driven by a CULS hydraulic unit allowing a fluent change in the rotation frequency of the fan rotor.

To measure the airstream speed in delivery tubes two devices were used: a TESTO pressure probe, 0638.1445 model (±10 hPa) connected to a TESTO 445 device with internal memory (3 000 values). Pressure probes were connected to Pitot tubes to measure differential pressure and airstream speed (Russo, 2011). The parameters of streaming air were measured with Pitot tubes in the axis of delivery tubes. Pitot tubes were installed in delivery tubes at a distance of 0.55 m from the air ingress into delivery tubes and 0.40 m in front of the end of delivery tubes.

After measuring the airstream speed in delivery tubes of 0,016 m in inside diameter and of the lengths 2, 3, 4 and 5 m, at a different frequency of the fan rotor revolutions and with straight and curved delivery tubes the passage speed of winter wheat and maize seeds was measured in these delivery tubes. To measure seed passage BALLUFF optical sensors, BLG 30C-005-S4 model, connected to a logger, were used. Seed passage was measured in straight parts of delivery tubes and subsequently in curved parts according to the requirements on the sowing machine construction - examples on scheme in Fig. 1. The curvature of tubes was chosen in line with the assumed placement of delivery tubes in a seed drill. The frequency of the fan rotor revolutions was changed in steps of $8{,}3.s^{-1}$, in the range from 16,7 to $58{,}3.s^{-1}$. The speed of seed passage was calculated from the measured time segments. Measurements were done in ten replications.

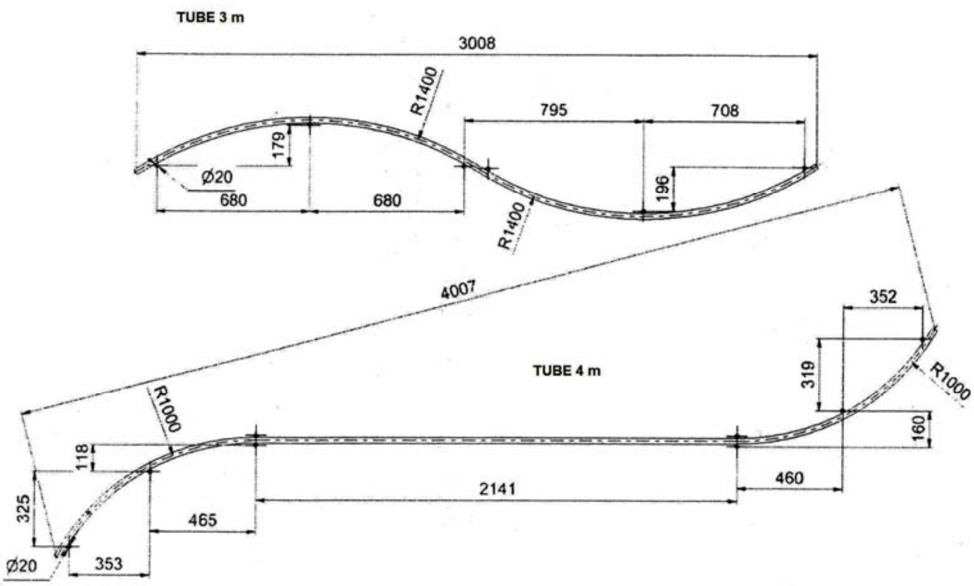

Fig. 1 Curved placement of delivery tubes

Results and discussion

It was found out in the course of measuring the speed of wheat and maize seed passage through delivery tubes that at the lower frequency of the fan rotor revolutions (the range of 16,7 to 41,7.s^{-1}) the airstream speed in delivery tubes necessary for the fluent movement of seeds in delivery tubes was not reached. This is the reason why for statistical data processing the values of seed passage at a frequency of the fan rotor revolutions 58,3.s^{-1} were chosen.

Fig. 2 illustrates that a higher speed of seed passage was measured for the straight placement of delivery tubes compared to the curved placement (delivery tube length of 2 m). In variant 3 the values of this characteristic were statistically significantly lower than in the variants with straight placement of delivery tubes. A similar trend of differences among measurement variants was observed for the delivery tube of 3 m in length (statistically significantly difference between the variants 3 and 2) – the graph in Fig. 3.

In delivery tubes of 4 m in length the lowest speed of wheat seed passage was recorded for the straight placement of delivery tubes, which is different from the results of measurement at delivery tube lengths of 2 and 3 m (Fig. 4). For the largest length of delivery tubes (5 m) the speed of seed passage was not statistically significantly different among measurement variants (Fig. 5).

Graphs in Fig. 6 and Fig. 7 allow a different view on results of measurements. In the curved placement of delivery tubes the passage speed of winter wheat seeds and also of maize seeds decreased with the increasing length of delivery tubes. The values measured at a delivery tube length of 4 m were an exception. At this length of delivery tube and its curved placement the statistically significantly lower speed of seed passage was measured compared to the delivery tube length of 2 and 3 m. Parameters of the delivery tube curvature at its length of 4 m are an assumed cause.

The results of measuring the airstream speed in delivery tubes may help elucidate differences in the speed of seed passage through delivery tubes. Tab. 1 documents the results of measuring the airstream speed when delivery tubes of 0,016 m in inside diameter, with the straight placement of tubes and tube length of 2 m and 5 m were used. For regression analysis a linear model of the function was chosen to express the relation between the airstream speed (vv) and the frequency of the fan rotor revolutions (nv). Correlation coefficient r indicated a high degree of correlation closeness in all cases. The airstream speed increased with the decreasing length of tubes at the same frequency of the fan rotor revolutions.

For the curved placement of delivery tubes a linear model of the function was chosen again to express the relation between the airstream speed and the frequency of the fan rotor revolutions because it is the most suitable for the relation between the studied variables. Using the curved placement of tubes, the airstream speed in tubes was lower than in tubes with the straight placement.

The results of measurements are consistent with literature sources that deal with the principles of airflow in piping and with pneumatic transport of grains (Flandro et al., 2012; Jech et al., 2011).

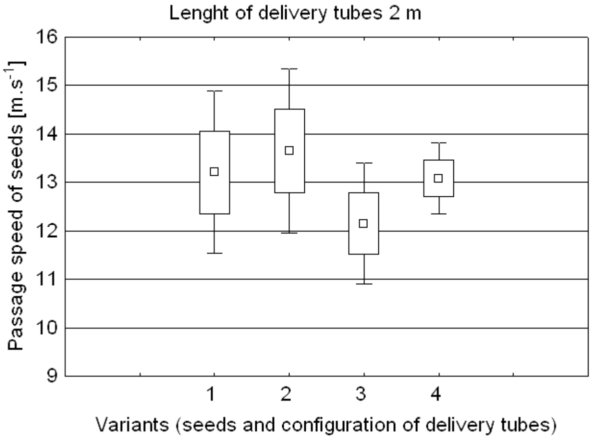

Fig. 2 Speed of seed passage (delivery tube length of 2 m)

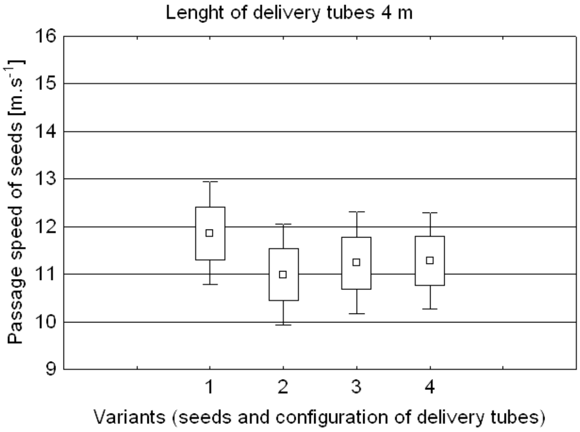

Fig. 4 Speed of seed passage (delivery tube length of 4 m)

Variants:
1 – Maize, straight placement
2 - Winter wheat, straight placement
3 – Maize, curved placement
4 - Winter wheat, curved placement
Average ± St. error
Average ± 1,96 St. error

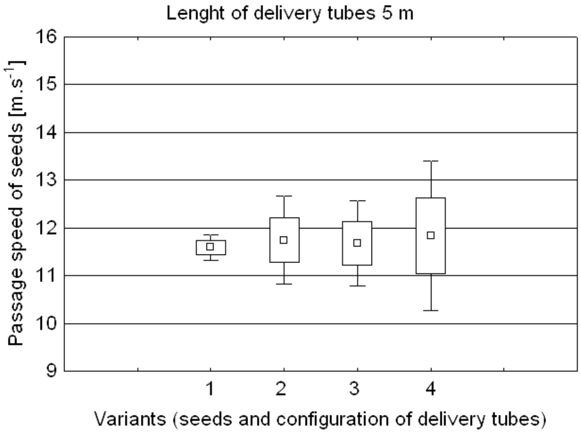

Fig. 5 Speed of seed passage (delivery tube length of 5 m)

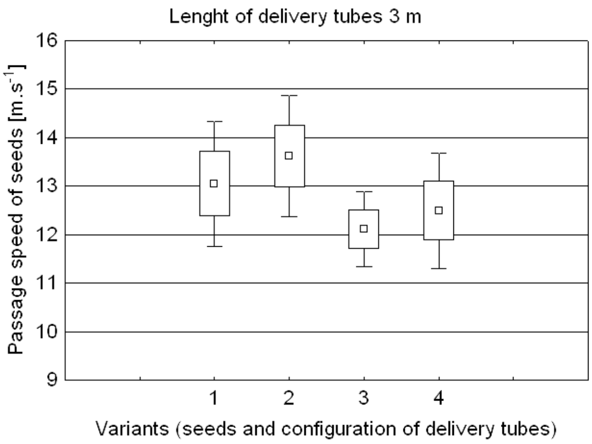

Fig. 3 Speed of seed passage (delivery tube length of 3 m)

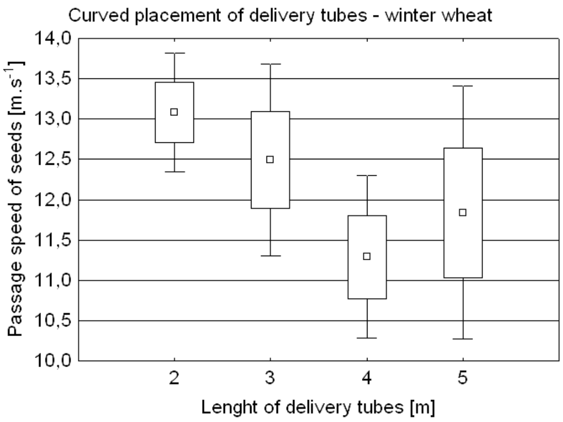

Fig. 6 Speed of seed passage (curved placement of delivery tubes, winter wheat)

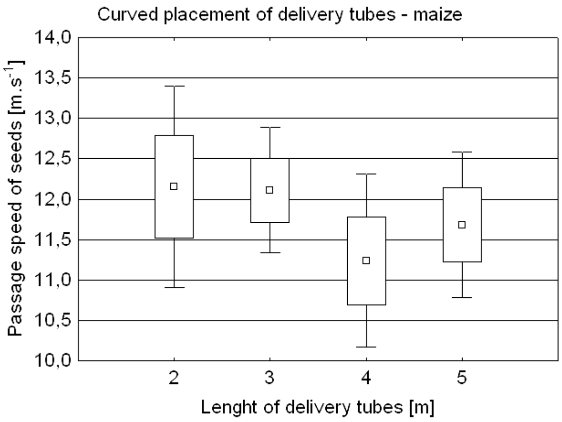

Fig. 7 Speed of seed passage (curved placement of delivery tubes, maize)

Tab. 1 Dependence of airstream speed on frequency of the fan rotor revolutions - straight placement of tubes

Lenght of tubes (m)	Equations of regression	Correlation coefficient
2	$v_v = 0{,}684\ n_v - 1{,}323$	$r = 0{,}98$
5	$v_v = 0{,}609\ n_v – 2{,}018$	$r = 0{,}99$

where:
v_v - airstream speed (m.s^{-1})
n_v - frequency of the fan rotor revolutions (1.s^{-1})

Conclusion

The results of measurement of the seed passage speed in delivery tubes revealed a problem connected with the use of delivery tubes of uneven lengths in a new generation of precision seed drills. The uneven length of delivery tubes may cause differences in the speed of seed passage through delivery tubes while the parameters of precision drilling are worsened in this way. Another source of drilling imprecision may be the placement of delivery tubes. Differences in the speed of seed passage were recorded between wheat and maize seeds. The results provide information applicable to the development of precision seed drills complying with requirements for drilling quality at a relatively high travel speed of machines.

Acknowledgement

Supported by the research project of Ministry of Industry and Trade of the Czech Republic No. FR-TI3/069.

Reference

Flandro G.A., McMahon H.M., Roach R.L., 2012. Basic aerodynamics. Cambridge; University Press., 419.
Jech J., 2011. Machinery for plant production 3. Machinery and equipment for postharvest processing and storage of materials. Prague, Profi Press, 368. (in Slovak and Czech
Russo G.P., 2011. Aerodynamic measurements. Cambridge, Woodhead Publishing, Ltd., 257.

LOGICAL AND EXPERIMENTAL VERIFICATION OF COMPUTER MODEL FOR HEAT DISTRIBUTION IN THE OBJECTS UNDER COVER

Jan Vogelgesang, Kazimierz Rutkowski, Krzysztof Kempkiewicz*

University of Agriculture in Krakow, Faculty of Production and Power Engineering,
Balicka 116 B, 30-149 Krakow, Poland,
Phone: +48 126624688, E-mail: Jan.Vogelgesang@ur.krakow.pl

Abstract

The technical system that gains heat from deep in the ground by heat pump is complicated and any attempt to implement innovative solutions requires a comprehensive analysis. The developed computer program had to predict the effects of design changes in the system: the lower source - heat pump - buffer tank - heaters - the greenhouse and its environment. The goal of this paper is to present the method to verify and determine the directions of model improvement (Vogelgesang et al., 2010). The verification process consists of two stages. First, a computer model with logical and some other tests was experienced to check the behavior of desired quality features. In this model, the fiction experiences were implemented changing about 20 input variables, and their results to logic and expert analysis were subjected. No unexpected program behaviors were occurred, also in limit situations. In this analysis the expected and known quality relations were confirmed as "increase", "decrease". Next, an experiment in the real object was carried, to calibrate the model and to determine the numerical values of some parameters, in particular related to environmental variables, including coefficient of heat transfer. After obtaining adjusted values, the model was experimentally verified conducting a series of experiments, similarly to the quality verification, but this time expecting confirmation of the simulated values with these obtained in the real object. Due to technical limitations, experiments included only variables related with the buffer tank operation. In this scope, the satisfactory quality of applied model was stated. Obtained consistency of results allows choose an optimal size of the buffer tank in the technical system with heat pump having a model as a base including expected time of its use, the object type and the projected weather scenario. There was found that further development requires modeling of thermal processes in the greenhouse, in particular the internal heat distribution in the context of diverse and changing in time: geometry, thermal capacity, spatial objects location (Rutkowski, 2009).

Keywords: computer model, heat distribution

Introduction

Most of the sub-processes of heating system in objects under cover with heat pump have been described in the literature (Hepbasli, 2011). The description uses the known laws of heat balance, conduction equation, heat and mass transfer.

In addition, a number of empirical models were obtained (Panwai et al., 2011). These works show that any attempt to modify a significant component or setting its work makes necessary analysis of all elements to re-tuning parameters and then the experimental verification is required. The computational arduousness of processes and a need to their improvement, led the authors to develop a computer application that is intended to simulate the described system operation. This application should facilitate to make decisions about initial selection of design and operation parameters of carried research activities.

The goal of this paper is method presentation of quality and experimental verification of a computer model simulating the selected heating process with heat pump based on the mathematical elements of experimental design. Discussed relationships were based on the results obtained in the experimental object located at the Faculty of Production and Power Engineering, University of Agriculture in Krakow.

Research subject

Designed computer software that maps the process physics of complicated technical system consists of partial interchanging relevant parameters. For a proper quality of complex program, several verification levels are required. It should include:

- IT validation,
- logical consistency,
- and at the end - results consistency.

It is possible to calibrate a computer model during the experimental verification i.e. more precise determination of some characteristic values.

A software module simulating buffer tank operation was selected for analysis. The buffer tank has a various features. According to Adamski (2008), it allows cyclic pump operation, and thereby enables bed regeneration, where lower heat source is placed. Tank allows also control the frequency and the start times of heat pump. It is used for heat supplies gathering when the object does not require heating.

The buffer tank is supplied through the heat pump pipe heat exchanger. The pump runs regularly, because regular operation breaks are forced by lower heat source regeneration.

Heat accumulated in the buffer tank is distributed through the induced circulation into the greenhouse heating system. Processes of heat filling and reception can run in various time configurations. They can run parallel or separated. By the separated process, the tank is first heated to a preset temperature and then the heat can be received. Tank operation is then cyclic. The intensity of the heat supply to the object depends on the weather.

The model of elementary exchange was the software core. There the mass element gives heat to the other and consequently their temperature equalizes. In the module describing the buffer tank operation the allocation method of heat carriers (medium)) into finite elements was used. Each element exchanges heat according to the elementary model.

Simultaneously these elements can move relative to each other or to the other objects and also remain stationary. The application had to recognize a few threads, according to the number of parallel processes.

Logical verification

Input variables of the examined software module:

$t_{we\_}a$ ($^{\circ}$C) - input temperature of a medium “a” flowing from the heat pump to the heat exchanger in buffer tank,

$t_{we\_}\ b_0$ (°C) - initial temperature of a medium “b” located in buffer tank,

T_{ab} (s) - time needed for medium “an”element to flow through the heat exchanger.

This variable depends on volume velocity of the flow in following formula:

$$T_{ab} = 10^3 . \frac{V}{v} \qquad (1)$$

where: V (m^3) - volume of the heat exchanger, v (dm^3. s^{-1}) – stream of the flow, S_{ab} (m^2) - transfer surface of the pipe heat exchanger, U_{ab}(W.m^{-2}.K^{-1}) - coefficient of the heat exchange, m_a (kg) - mass of medium “a” located in buffer tank, m_b (kg) - mass of medium “b” located in heat exchanger, c_a (J. kg^{-1}.K^{-1}) - specific heat capacity of medium “a” c_b (J. kg^{-1}.K^{-1}) - specific heat capacity of medium “b”, N - the number of discretization of the heat exchanger $O(n^2)$ calculations are complex, and its importance was needed to determine)

Output variables of the examined software module:

a. T (s) - time of warming up medium “b” to the defined temperature

In case of realization complete two-level plan the number of reference points would be:

$K = 2^{\ 10} = 1024$

Analyzing of such many points is not rational and would be time-consuming even with help of computer. For further analyze fractional, orthogonal and rotatability type 2^{n-p} plan was used. In this case $2^{\ 10-6}$ type plan with resolution R = 3 was chosen, which is connecting level- two interaction (two-factors) or higher with main effects. There is drawing, proper plan of research on Tab. 1, generated by Statistica program by Statsoft.

The result of the simulation, received from Statistica, is showed on the Pareto chart (Fig. 1). This chart is characterizing the meaning of each input factor and also is showing the change trends.

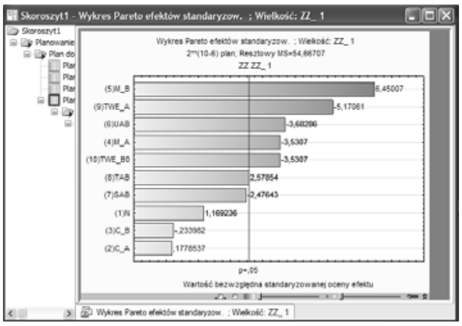

Fig. 1 Graph Pareto received from examinated program with help of two-level plan from *Statistica*

Tab. 1 Chart of fractional plan for logical and experimental verification of computer model

Configuration	n	c_a	c_b	m_a	m_b	U_{ab}	S_{ab}	T_{ab}	$t_{we}a$	$t_{we}b_0$
	-	-	-	-	-	-	-	-	-	-
1	-1	-1	-1	-1	-1	-1	-1	-1	1	1
2	-1	-1	-1	1	-1	1	1	1	-1	1
3	-1	-1	1	-1	1	1	1	-1	-1	1
4	-1	-1	1	1	1	-1	-1	1	1	1
5	-1	1	-1	-1	1	1	-1	1	-1	-1
6	-1	1	-1	1	1	-1	1	-1	1	-1
7	-1	1	1	-1	-1	-1	1	1	1	-1
8	-1	1	1	1	-1	1	-1	-1	-1	-1
9	1	-1	-1	-1	1	-1	1	1	-1	-1
10	1	-1	-1	1	1	1	-1	-1	1	-1
11	1	-1	1	-1	-1	1	-1	1	1	-1
12	1	-1	1	1	-1	-1	1	-1	-1	-1
13	1	1	-1	-1	-1	1	1	-1	1	1
14	1	1	-1	1	-1	-1	-1	1	-1	1
15	1	1	1	-1	1	-1	-1	-1	-1	1
16	1	1	1	1	1	1	1	1	1	1

For example, the volume of the heat container (M, B on Pareto chart) has the biggest influence on the time of its warming. Then, the quality comparison of the experimental results and expected data was made. It is presented on the Tab. 2. The tendency was marked with arrows adequately to the comparison results. Independently program was checked in border situations, and at the stage of constructing the parts of the code were put to the unit tests. All mentioned above details are confirming its credibility.

Tab. 2 Comparison the meaning of factors according to expert opinion and simulation results

Factors	symbol	expert opinion	simulation results
mass of medium “b”	m_b	↑↑	↑↑
input temperature of a medium “a .	$t_{we}a$	↓	↓↓
coefficient of the heat exchange	U_{ab}	↓↓	↓↓
mass of medium “a”	m_a	↓	↓↓
initial temperature of a medium “b”	$t_{we}b_0$	↓	↓↓
Time to flow through heat exchanger	T_{ab}	↑↑	↑
exchange surface	S_{ab}	↓↓	↓
the number discretization	N	?	↑
specific heat capacity of medium “b”	c_b	↓	↓
specific heat capacity of medium “a”	c_a	↑	↑

Tab. 3 Ranges of input variables

Value	c_a	c_b	m_a	m_b	U_{ab}	S_{ab}	T_{ab}	$t_{we}a$	$t_{we}b_0$
	(J. kg^{-1} .K^{-1})	(J. kg^{-1}.K^{-1})	(kg)	(kg)	(10^3 W. m^{-2} .K^{-1})	(m^2)	(s)	(°C)	(°C)
minimum	3500	3500	3	120	380	0,8	15	48	20
maximum	4200	4200	5	240	475	1	25	53	35

Tab. 4 Comparison the results of the simulation with experimental data

Configuration according to Tab. 1	Time of warming T (s)		
	Simulation T_{sym} (s)	Experiment T_{emp} (s)	Difference (s)
13	420	720	-300
14	780	840	-60
1	840	1080	-240
6	840	1200	-360
8	840	1140	-300
2	900	900	0
12	960	1440	-480
16	960	1560	-600
10	1020	1440	-420
4	1200	1500	-300
7	1380	1500	-120
11	1740	1380	360
15	1740	1380	360
3	2100	2400	-300
5	3720	3300	420
9	4500	4500	0

Empirical verification

The variable values from the empiric research, corresponding to the levels "1" or "-1" in Tab. 1, are shown in the Tab. 3. The N number of discretization, for obvious reasons, was omitted. Water or glycol were the medium. To get the variation of heat transfer coefficient, two types of copper pipes with varying wall thickness were applied. They were placed into the tanks in spiral shape. U_{ab} values correspond to the theoretical values of thermal conductivity for pure copper and for partitions of 0.001m and 0.0008 m thickness. They are included in the table only as starting values.

The measurements of temperature, medium flow and times were automatic.

To ensure the variation of medium mass in the exchanger (ma) and variable transfer surface (Sab) the proper tubes diameters and lengths were selected.

There were used several different copper pipes with diameters ranging from 0.015 to 0.03 m and with length from 8 to 26 meters. The pump to circulate medium flow through the exchanger and through the heat pump could change the flow from 0,1 to 0,4 $dm^3.s^{-1}$

Results are presented in the Tab. 4. There are summarized the heating times T_{sym} obtained in simulations, where $T_{ab} = T_{sym}$, and times obtained in the empirical researches (T_{emp}). The values are rounded to 10 seconds. Results are sorted by increasing times T_{sym}.

High correlation coefficient between obtained times r = 0,95 shows a good simulation quality. The average of experimental heating time (1630 seconds.) was little longer than the simulated value (1490 seconds.). To eliminate this difference, model was calibrated correcting U_{ab} values. Average reliability was found at U_{ab} = 1500 $W m^{-2}.K^{-1}$ for lower level and at U_{ab} = 2000 $W.m^{-2}.K^{-1}$ for the higher level.

However, such considerable reduction of their value in model means, they are losing importance as an exchanger characteristic. They rather reflect to averaged heat transfer both through the walls as well through the medium directly adjacent to these walls. The continuous exchange of medium particles (mixing) accelerating the heat transfer process was the model assumption.

Summary

To determine an optimal buffer tank capacity, with limited potential of lower source operation and by the expected weather scenarios, the tank heating time is particularly important. Method of logical and empirical verification of the model determining this time was presented. The verification is based on a mathematical method of experiment design with help of Statistica software. Reliability of the computer model was confirmed.

However, this model with a more detailed data of medium movement can be improved (convection and the Grashof number, stirring, heat losses, etc.). The model appears sufficient for the intended optimization test. For other software modules (still elaborating), especially those stimulating heat delivery into greenhouse, spatial modeling of thermal field is important. This element is significant because it determines the steady crops yielding and energy and materials consumption in the production process.

Acknowledgment

This work is financed by research project No. N 313 445137 National Science Centre Poland.

References

Adamski M., 2008. Longitudinal flow spiral recuperators in building ventilation systems. Energy and Buildings, 40(10): 1883 – 1888.

Hepbasli A., 2011. A comparative investigation of various greenhouse heating options using exergy analysis method. Applied Energy, 88(12): 4411 - 4423.

Panwai N.L., Kaushik S.C., Kothari S., 2011. Solar greenhouse an option for renewable and sustainable farming. Renewable and Sustainable Energy Reviews, 15(8): 3934 - 3945.

Rutkowski K., Wojciech J., 2009. Horizontal Temperature Profile In Selected Glasshouses.Media4u Magazine, 11: 27 – 35.

Vogelgesang J., Molenda K., Waciega M., 2010. Guidelines for micro- and mesoscale computer modeling of fluid flows in the soil-root system. Agricultural Engineering, 6(124): 113-119

IMPACT ASSESSMENT OF TRIM LEVELS OF MECHANIZATION IN COMPANY ON YIELD OF WINTER WHEAT

Václav Voltr[1*], Pavel Froněk[1], Martin Hruška[1], Petr Šařec[2]

[1]Institute of Agricultural Economics and Information, Mánesova 75, 252 64 Prague 2, Czech Republic, Phone: +420222000390, E-mail: voltr.vaclav@uzei.cz
[2]Czech University of Life Sciences Prague, 165 21 Prague 6– Suchdol, Czech Republic

Abstract

Yields of winter wheat were investigated in the years 2002–2010 along with production factors at more than 500 plots in the Czech Republic. Based on standardized yield values for individual soil quality categories using valuated soil ecological units (BPEJ), a model with relationship of quality of mechanization and actual yields of winter wheat was evaluated. Evaluation of standardized yield values has been used on more than 1,000 observations of winter wheat yield. Quality of mechanization was sorted using classification of machinery into groups according to progressiveness of technology within the soil preparation. Regression model to address the dependency of factors determining the quality of mechanization and depth of tillage is significant enough. Difference between categories of quality of used mechanization achieved an average of 0.1 t.ha^{-1}. The difference in winter wheat yield depending on the quality of equipment used in tillage reached the national average of 0.23 t.ha^{-1}. The resulting conclusion corresponds with the findings of Van den Putte et al. (2010). At an average depth of reduced tillage (RT) 0.12 m and at an average depth of 0.22 m for ploughing, the yield declines for RT by about 5 %. Increasing the depth of reduced tillage can reduce the yield difference. As Van den Putte et al. (2010) found, decline of yields in drier conditions was surprisingly large. Achieved way of evaluation of the model using the categorization of income to BPEJ can be used to extrapolate evaluation of machinery used in the Czech Republic.

Key words: production function, quality of mechanization, winter wheat, yield

Introduction

Soil as a basic means of production in agricultural practice provides different amounts of revenues depending on soil fertility, and is based on the need for different technological inputs. Orientation in relation to the profitability of land in technology assessment is an important prerequisite for the comparability of revenue and expenses. Assessment of technological processes with the use of crop production functions allows the inclusion of soil quality in the evaluation of the results and a better opportunity to assess the economic impact of mechanization. Many authors deals with the way of tillage and its evaluation. Šíp et al. (2009) points out the small differences between reduced tillage (RT) and conventional tillage (CT). Over the long term, the yield of winter wheat under RT should not be very different from that delivered by CT. Both conventional tillage in combination with standard N rates and reduced (shallow) tillage in combination with increased N rates could be considered in the central European area as promising tillage/nitrogen strategies (Gandorfer et al., 2011). High input reduced tillage system appears to be preferable to the more commonly utilized convention tillage systems.

Van den Putte et al. (2010) present a meta-regression analysis (47 European studies, 563 observations). Their analysis shows that, while the introduction of conservation tillage in Europe may indeed have some negative effect on yields, these effects can be expected to be limited: the overall average reduction they found was approximately 4.5 %. Surprisingly, no-tillage did perform worse under drier climatic conditions.

Material and methods

Currently, the evaluation of the effects of technology on crop yield used in the Czech Republic (CR) system of production areas describing the soil texture and optionally basic climatic characteristics has taken place. Results or estimates are not available that would compare to other conditions of the natural fertility of the soil. There is an established relationship of revenues and expenses based on soil and climatic conditions acceptable for technology assessment with sufficient accuracy under different conditions, including various weather phenomena and the supply of nutrients. Unbalanced evaluation cannot be eliminated at a specific selection of plots with different production capacity to monitor the impact of technology.

This article deals with the relationship of observed level of technological equipment for soil preparation and of yield based on the categorization of soil-climatic conditions using valuated soil ecological units (BPEJ). The main research aim is to verify whether an impact of the equipment level of mechanization can be demonstrated on the size of the yield based on production functions in several soil-climatic conditions. For description of farm land, a comprehensive evaluation method of achieved yields using multilevel regression equation (Voltr at al., 2011) was developed, covering all the major influences on crop yields. The most balanced results are obtained in the case of winter wheat with more than 1,000 measurements, and therefore it is suitable for verifying results of the proposed method. During the years 2002–2010 on individual homogenous plots, the following items were monitored: detailed information about soil texture, soil properties described by a comprehensive soil survey, a description of the main soil units, temperature, precipitation, soil moisture in each month, the manifestation of dry depending on humidity and temperature in pentads in the growing period, the amount of fertilizers of organic and inorganic origin, nutrient status of the soil by agrochemical soil testing, characteristic configuration of the land and some other specific investigations. The purpose of the experiment was to evaluate the influence of soil conditions on the comparison results. The problem with the current concept of experiments and evaluation of results is the poor transferability between soil and climatic conditions. For this reason, when calculating the effect of machinery on the crop yield, standardized yield under the given conditions for the application of the main factors affecting the yield formation is suggested for use.

Evaluation of a standardized yield

The production features influencing manufacturing conditions are formed by soil texture, soil description by the main soil units (MSU), weather, fertilization, technological process and the configuration of the terrain. Knowledge of the effects of natural conditions affecting the size of the input and generating revenues allows us to estimate the specific impact of the technology to other features under standardized conditions.

Voltr et al. (2011) compiled a standardized framework for assessing the impact of various factors on the size of the income and expenses. Impact of technological progress on yield is given by the individual above factors of yield formation and time T defining the size of technological progress.

$$Y_{tech} = f(TECH_t ; T) \quad (1)$$

Where TECH are technological factors: number of interventions to the protection of plants-application of herbicides, insecticides, fungicides, combined applications, other pests and methods of sowing.
The basic approach to the derivation of production functions for standardized yield is based on the following function:

$$Y_{st} = f\left(Y_{weather}; Y_{MSU}; Y_{tech}; Y_{fert}; Y_{local}; Y_{texture}\right) \quad (2)$$

Where Y_{st} is the stabilized crop yield, $Y_{weather}$ the estimated value of the dependent variables as measured by the weather, Y_{MSU} values influence the main soil units, Y_{tech} values describing number of applications of protection chemicals and methods of sowing, Y_{fert} depending on the model yield given by fertilization, Y_{local} values describing of exposure, depth, stoniness and slope of the farmland, $Y_{texture}$ values describing relationship models of grain size components in the soil to yield. Effect of nitrogen dosage is evaluated in the next step based on the derivation of dependence Y on the N.

$$Y_N = f\left(Y, Y_{st}, N, N_{st}\right) \quad (3)$$

Where N_{st} is standardized dosage of N on MSU, determined by a procedure analogous to the dependent variable N in the groups referred to in the equation (2).
Schematically, the approach to the evaluation of production functions is displayed in Fig. 1, which describes the weight of the major influences on the yield of winter wheat, evaluated on the basis of statistical analysis of the individual factors.

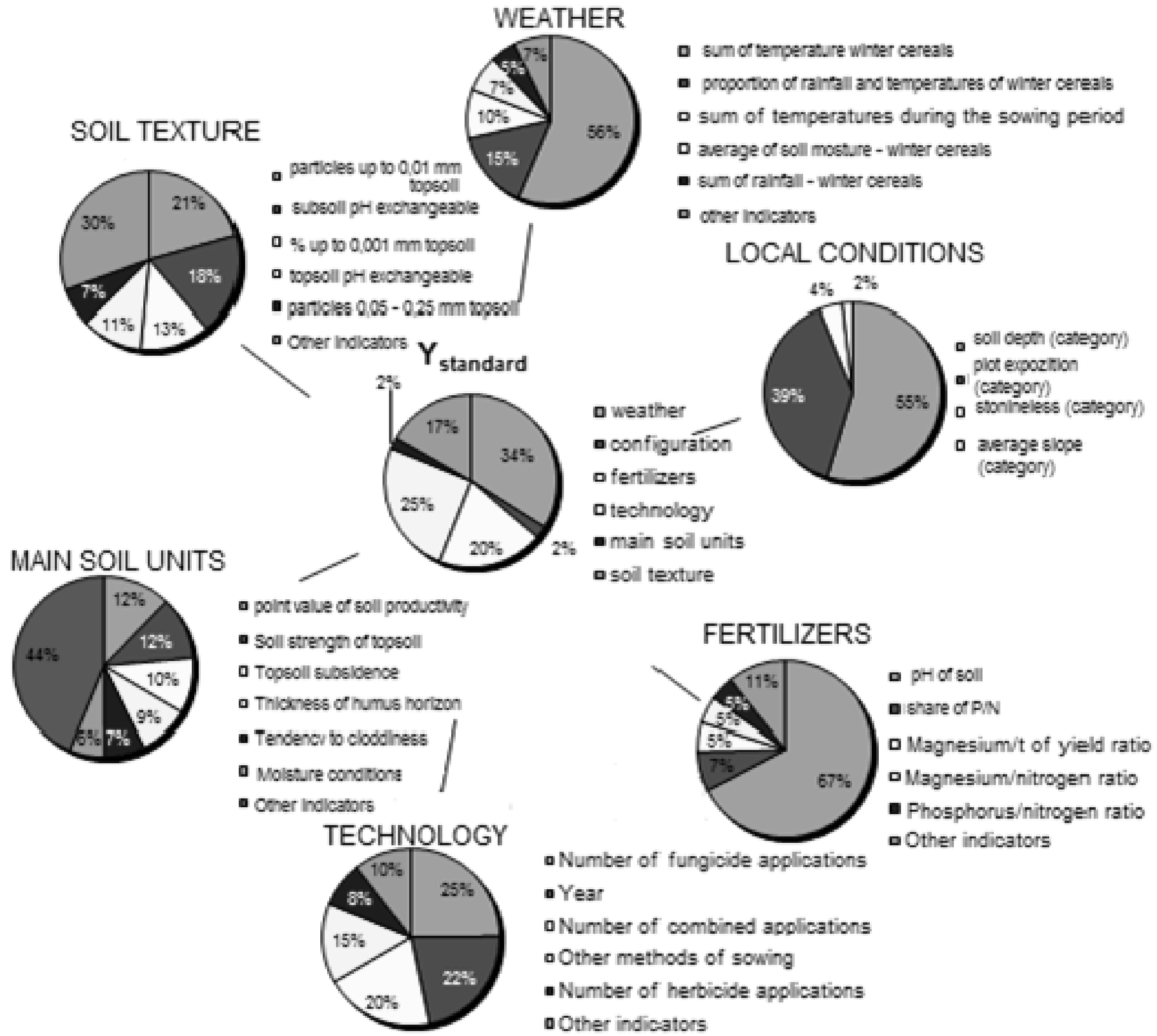

Fig. 1 The importance of production factors on the size of the yield of winter wheat (Voltr et al., 2011)

The approach to the assessment of production functions is formed by a system of linear equations with the main groups of factors influencing the yield of winter wheat. The resulting equation for the dependence of wheat yield on production conditions is formed by the equation:

$$Yst = -4.663 + 0.4667 \cdot Y_{tech} + 0.0427 \cdot Y_{local} + 0.6295 \cdot Y_{weather} + 0.3651 \cdot Y_{fert} - 0.0393 \cdot Y_{MSU} + 0.3096 \cdot Y_{texture} \quad (4)$$

Quality of mechanization

Quality of mechanization or method of tillage were not included in the statistical evaluation, they are subject to a separate evaluation.

Rating of technological factors is based on categorization quality of the equipment. Mechanization is subjected to the segmentation process with reduced tillage and ploughing and furthermore broken down to seedbed preparation methods: classical preparation (shear, gateway) use of PTO driven implements for soil preparation, soil preparation and sowing in one operation, other tillage methods. The above is used for the statistical evaluation of the results of the mechanical equipment for seedbed tillage divided into groups according to the expected quality of the work.

1. best – compactors, Köckerling, Allrounder, preparation and sowing in one operation
2. average – stubble or disc harrows
3. worst – spike-tooth harrow, skids

This information has been inserted into the database during years 2002–2010, along with other collected information of production characteristic.

Results

Comparison of the results of revenues by pre-sowing tillage using defined three categories depending on the way of reduced tillage and conventional tillage is shown in Tab. 1.

The Tab. 1 shows the yield of winter wheat at dry matter content of 85 %, the yield difference from each category average due to the actual yield and difference of reached a standardized yield.

Comparison shows that the differences from the average yields in each way of tillage differ. In that case, the different impact, especially that of reduced tillage in the third level quality of machinery is discernible. While the evaluation of the yield difference only by achieved yield between various conditions is -1.15 $t.ha^{-1}$, in the case of inclusion of all terms of yield formation decreased yield only by about 0.24 $t.ha^{-1}$. In the case of conventional tillage, the differences between is worst levels of quality machinery and average yields are also lower.

Effect of deep tillage is also dependent on a number of specific conditions, especially by soil moisture.

To compare the influence of climatic conditions, particularly rainfall, and the influence of soil type, which is also important for the method of tillage (Voltr et al., 2011), observed yields of winter wheat were divided into groups according to the values achieved annual precipitation from seeding winter wheat after harvest and according to the percentage of clay particulate matter in the topsoil. The results are shown graphically in Fig. 2, the statistical evaluation is shown in Tab. 2 and Tab. 3.

Tab. 1 Rating tillage achieved by a real and standardized yield

	Quality level of seedbed preparation	N	Yield of winter wheat ($t.ha^{-1}$)	Difference from the average yield Δ Y	Difference reached and standardized yield Y_N	Difference from the average standardized yield Δ Y_N
Reduced tillage	1	127	6.55	0.22	0.01	0.15
	2	151	6.33	0.00	-0.20	-0.06
	3	31	5.18	-1.15	-0.38	-0.24
	Total	309	6.33		-0.14	
Conventional tillage	1	153	6.80	0.55	0.42	0.25
	2	69	5.60	-0.65	-0.26	-0.43
	3	99	5.85	-0,40	0.12	-0.05
	Total	321	6.25		0.17	
Total	1	280	6.70	0.41	0.25	0.24
	2	220	6.14	-0.15	-0.22	-0.23
	3	130	5.73	-0.56	0.02	0.02
	Total	630	6.29		0.01	

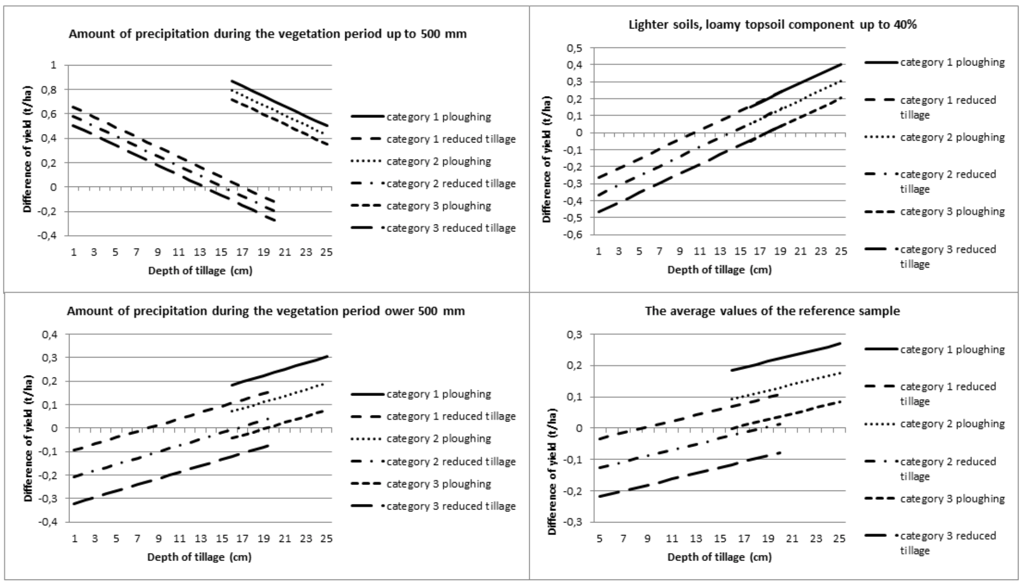

Fig. 2 Difference of yields of winter wheat depending on the depth of tillage, quality of seedbed tools and basic tillage

Tab. 2 Models summary

Model	R	R Square	Adjusted R Square	Std. Error of the Estimate	Sig.
Texture topsoil particle till 0.01mm < 40 %	0.156[a]	0.024	0.024	1.00079	0.000[a]
Precipitation over 500 mm	0.123[a]	0.015	0.015	1.04472	0.000[a]
Precipitation up to 500 mm	0.153[a]	0.024	0.022	0.93439	0.000[a]
Average values	0.115[a]	0.013	0.013	1.03350	0.000[a]

Tab. 3 Models coefficients

	Texture topsoil particle till 0.01mm < 40 %		Precipitation over 500 mm		Precipitation up to 500 mm		Average values	
	Coefficients		Coefficients		Coefficients		Coefficients	
Model	B	Std. Error	B	Std. Error	B	Std. Error	B	Std. Error
(Constant)	-0.189	0.037	-0.070	0.032	-0.056	0.079	-0.103	0.029
tillage category [1)]	-0.003	0.035	0.077	0.031	0.827	0.083	0.115	0.029
category of seedbed preparation	-0.100	0.011	-0.114	0.011	-0.075	0.007	-0.093	0.010
depth of tillage (cm)	0.028	0.003	0.013	0.003	-0.041	0.027	0.009	0.003

1) 1= reduced tillage, 2= ploughing

Discussion

Proposed models are presented for reduced tillage to 0.20 m, and for ploughing 0.16 to 0.25 m. In drier conditions to 500 mm of precipitation, yield of winter wheat with deep tillage decreases. In the other cases, yield increases with depth of processing. Differences proceed from the standardized values at the inclusion of other effects on the yield of winter wheat, and vary depending on the depth of tillage from -0.5 $t.ha^{-1}$to 0.8 $t.ha^{-1}$. The smallest importance is the basic method of soil preparation on lighter soils and soils with higher rainfall. The actual impact of the tillage tool quality on yield varies according to soil and climatic conditions, reaching 0.2 $t.ha^{-1}$. Average increase of yields with the implementation and conventional tillage was by about 0.1 $t.ha^{-1}$ at the same processing depth. The cost savings due to excluding ploughing are the main benefit of reduced tillage.

The obtained statistical evidence suggests that all proposed models are statistically significant, but the correlation coefficient R and coefficient of determination are very small. That means the total variation in YN can be explained by the linear relationship only from about 2 %. There exists a big variance in reached data. Function with results primarily indicates trends and interrelationships between these factors and results may vary according to the specific dispositions.

Conclusions

- The work was carried out analysing the possibilities of using production functions when evaluating the impact of different variants of tillage on yield of winter wheat. The resulting conclusion corresponds with the findings of Van den Putte et al. (2010). With an average depth of reduced tillage 0.12 m and an average depth of 0.22 m for ploughing, revenues for reduced tillage are about 5 %.
- Increasing the depth of reduced tillage can reduce the yield difference. As found Van den Putte et al. (2010), decline in yields in drier conditions was surprisingly large. The difference in quality of seedbed preparation stage leads to the difference of yields at approximately 0.1 $t.ha^{-1}$.
- Method for determining the production function allows evaluation of technological measures between different soil-climatic conditions, including evaluation of economic context of the other inputs involved in the production yield. Further research will be directed to determine the relation to the downstream environmental context.

Acknowledgment

We would like to express our gratitude towards the financing the NAZV – project of MoA QH72257 'Valuation of agricultural land taking into account environmental protection (www.uzei.cz).'

References

Šíp V., Růžek P., Chrpová J., Vavera R., Kusá H., 2009. The effect of tillage practice, input level and environment on the grain yield of winter wheat in the Czech Republic. Field Crops Research, 113(2): 131–137.

Gandorfer M., Pannell D., Meyer-Aurich A., 2011. Analyzing the effects of risk and uncertainty on optimal tillage and nitrogen fertilizer intensity for field crops in Germany. Agricultural Systems, 104(8): 615–622.

Van den Putte A., Govers G., Diels J., Gillijns K., Demuzere M., 2010. Assessing the effect of soil tillage on crop growth: A meta-regression analysis on European crop yields under conservation agriculture. European Journal of Agronomy, 33(3): 231–241.

Voltr V., Hruška M., Šařec P., 2011. Hodnocení půdy v podmínkách ochrany životního prostředí. (Evaluation of land in terms the context of environmental protection). Prague: ÚZEI, 480. (in Czech)

COMPUTER-AIDED IDENTIFICATION OF AGRO-FOOD AND FOREST PRODUCT PROPERTIES FOR HEAT AND WATER TRANSPORT SIMULATIONS

Jerzy Weres[1*], Wiesław Olek[2], Sebastian Kujawa[1], Michał Siatkowski[1]

[1]Poznan University of Life Sciences, Institute of Biosystems Engineering, Department of Applied Informatics, Wojska Polskiego 28, 60-637 Poznań, Poland,
Phone: +48 618487158, E-mail: weres@up.poznan.pl
[2]Poznan University of Life Sciences, Faculty of Wood Technology, Department of Mechanical Engineering and Thermal Techniques, Poznań, Poland

Abstract

It is difficult to represent properties of agro-food and forest products in mathematical models to simulate heat and water transport processes. Geometry of such products is complex, material structure is non-homogeneous and anisotropic, and properties vary with temperature and moisture content. Heat and water transport processes affect the end-use quality of agro-food and forest products, so it is important to support design and management of advanced systems of processing and storage of such products with mathematical modelling and computer predictions. In the paper an integrated computer-aided approach to estimate geometric and physical properties of agro-food and forest products was developed. The method was effective and it resulted in more accurate predictions of heat and water transport processes in investigated products.

Key words: image analysis, geometry measurement, geometry modeling, finite element algorithms, optimization algorithms, software development.

Introduction

Geometry of agro-food and forest products is difficult to describe, material structure is non-homogeneous and anisotropic, their behavior strongly depends on variable microclimate conditions, and physical properties vary with temperature and moisture content (Weres, Jayas, 1994; Pabis et al., 1998; Olek, Weres, 2007). Heat and water transport processes during drying and storage of such products definitely affect the end-use quality expected by consumers. It is essential to know thermal and diffusive properties of agro-food and forest products to undertake any analyses and management of advanced systems of processing and storage of biomaterials. Achievements in image analysis make it possible to measure geometry of complex 3D objects, and data acquired can be used for representing investigated product shapes in the 3D domain, and also for visualization of products subjected to thermo-mechanical processing (Frączek, Wróbel, 2009; Shih, 2010; Weres, 2010). Such approach can improve quality of mathematical models (Weres, 2010). Inverse finite element analysis algorithms (Weres et al., 2009, Olek et al., 2011) can be used to support identification of physical properties of examined biomaterials and thus to improve accuracy of computer simulations of heat and water transport processes.

The objective was to develop an integrated computer-aided approach to estimate geometric and physical properties of agro-food and forest products to improve analysis of heat and water transport processes.

Material and methods

Several methods depicted in Fig. 1 were implemented and integrated. They were based on:

1) Measurement of product geometry based on image acquisition, processing and analysis (digital photographs of consecutive product layers, edge detection for external and internal boundaries, construction of a model of geometry in a form of a mesh of 3D isoparametric finite elements, enhanced with NURBS and textures.
2) Identification of unknown values of mathematical model coefficients with the use of original inverse FE algorithms, and prediction of moisture content and temperature, with the use of original direct FE algorithms. Products investigated: dried cereal kernels, carrot roots, pine and beech wood, and wood-based panels (non-homogeneity, anisotropy and 3D shape irregularity).
3) Visualization of product property changes in space and time.

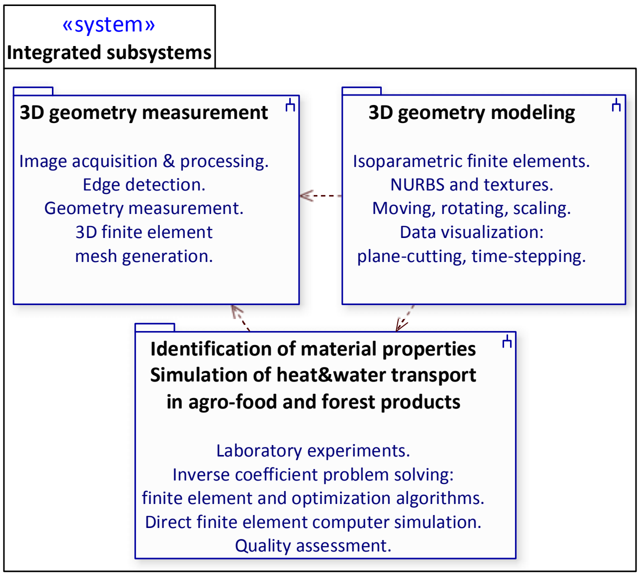

Fig. 1 Computer-aided identification of agro-food and forest product properties for heat and water transport simulations – a UML package diagram of nested subsystems

Original software packages were designed and integrated according to software engineering standards (Sommerville, 2010; Gomaa, 2011) with the use of UML 2.4.1. The software was implemented in two programming environments: Visual Studio 2012 (C#, C++/CLI) and Intel Parallel Studio XE 2013 with VS2012.

A subsystem depicted in Fig. 2 was developed for identifying unknown values of coefficients of the heat and water transport models (inverse finite element analysis supported with experimental data and original optimization algorithms), for predicting temperature and moisture content in investigated products (direct finite element analysis based on mathematical models of heat conduction and water diffusion with identified coefficient values and appropriate initial and boundary conditions of the third kind), and for assessing quality of algorithms.

Heat and water transport simulations were performed for cereal kernels, for pine and beech wood, and for wood-based panels. All investigated biomaterials manifested non-homogeneity, anisotropy, and 3D shape irregularity. Geometry and physical properties (specific heat, in-plane and transverse thermal conductivities, moisture transport coefficient, and convective heat/moisture transfer coefficients) were identified. Exemplary simulation results and their experimental validation are shown in Fig. 3. For all simulations global and local relative errors of prediction were computed, and values of the global relative error varied from 0.28 to 1.01 % for cooling processes in particle boards, and from 5.8 to 6.9 % for drying processes in individual corn kernels.

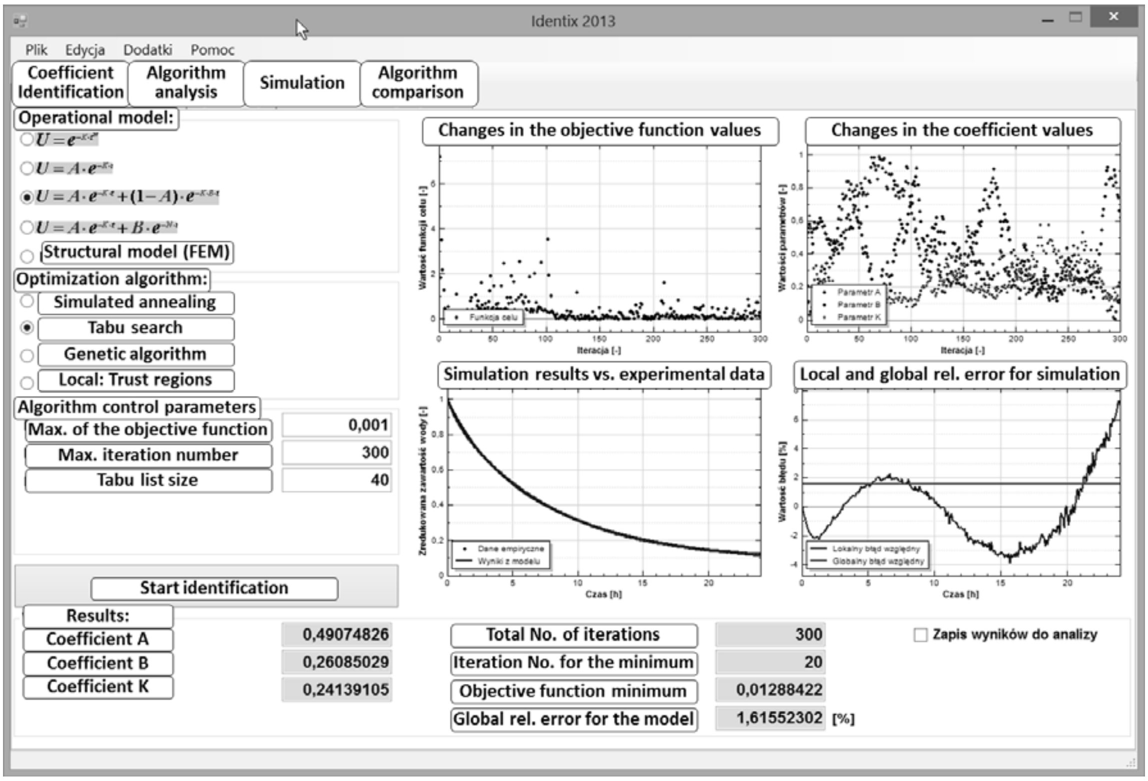

Fig. 2 Subsystem for running inverse and direct finite element analysis (identification of coefficients and simulation of the heat and water transport processes), and for assessing quality of algorithms

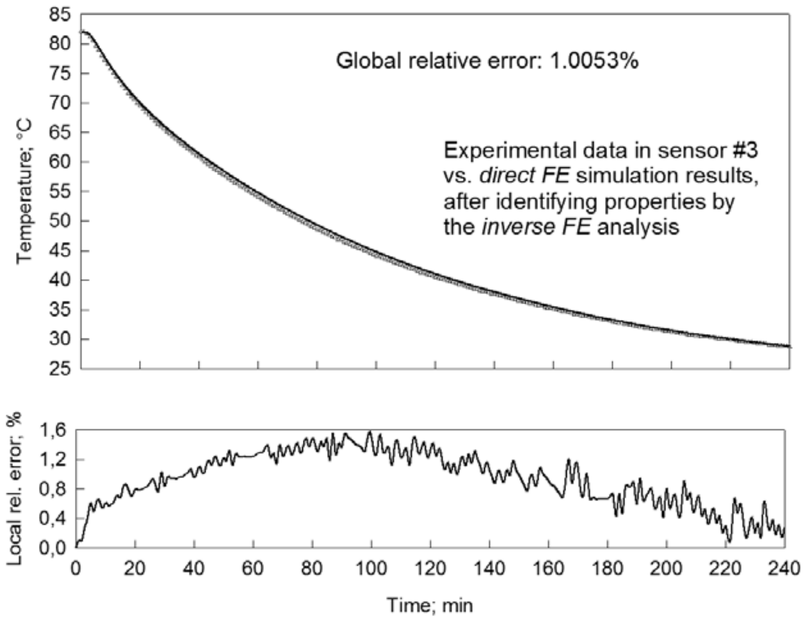

Fig. 3 Validation of temperature predictions for the particle board by the finite element structural model. Identified properties: specific heat, in-plane and transverse thermal conductivities. The developed algorithm is absolutely stable for non-linear problems for $\theta \geq 0.5$. Global relative error of the predictions: 1.0053 %

Conclusions

Identification of agro-food and forest product properties for heat and water transport simulations was enhanced with original algorithms. The integrated software developed in the paper was used to identify geometry and physical properties of investigated products, and the analysis of heat and water transport processes was more effective and accurate, measured by relative errors of predictions versus experimental data. The developed software showed satisfactory functionality, and also usability, effectiveness and efficiency, the software fulfilled the requirements.

Predictions of heating, cooling and drying processes in investigated biomaterials, performed with the software developed, resulted in significantly lower values of the relative errors for the developed model.

Acknowledgment

The work was financially supported by the National Science Centre as 2011/01/B/NZ9/03169 research grant.

Reference

Frączek J., Wróbel M., 2009. Using computer graphics for 3D reconstruction of seeds (in Polish). Inżynieria Rolnicza, 6(115): 87-94.

Gomaa H., 2011. Software Modeling and Design: UML, Use Cases, Patterns, and Software Architectures. Cambridge, UK, Cambridge University Press.

Olek W., Weres J., 2007. Effects of the method of identification of the diffusion coefficient on accuracy of modeling bound water transfer in wood. Transport in Porous Media, 66(1-2): 135-144.

Olek W., Perré P., Weres J., 2011. Implementation of a relaxation equilibrium term in the convective boundary condition for a better representation of the transient bound water diffusion in wood. Wood Science and Technology, 45: 677-691.

Pabis S., Jayas D.S., Cenkowski S., 1998. Grain Drying: Theory and Practice. Hoboken, NJ, USA, Wiley.

Shih F.Y., 2010. Image Processing and Pattern Recognition: Fundamentals and Techniques. Hoboken, NJ, USA, Wiley-IEEE Press.

Sommerville I., 2010. Software Engineering. 9th ed. Upper Saddle River, NJ, USA, Addison Wesley.

Weres J., 2010. Information system for acquiring data on geometry of agricultural products exemplified by a corn kernel (in Polish). Inżynieria Rolnicza, 7(125): 229-236.

Weres J., Jayas D.S., 1994. Effects of corn kernel properties on predictions of moisture transport in the thin-layer drying of corn. Transactions of the ASAE, 37(5): 1695-1705.

Weres J., Olek W., Kujawa S., 2009. Comparison of optimization algorithms for inverse FEA of heat and mass transport in biomaterials. Journal of Theoretical and Applied Mechanics, 47(3): 701-716.

EFFECTS OF INTERLIGHTING REGIMES ON GROWTH AND YIELD OF GREENHOUSE-GROWN TOMATOES

Chia-Chyi Wu*, Ming-Yih Chang, Fang-Jie Lian, Szu-Hua Chen

National Ilan University, 1. Shen-Lung Rd., Sec.1, I-Lan, Taiwan,
Phone: +886 39317641, E-mail: angwu@niu.edu.tw

Abstract

Limited amount of available natural sunlight and diminished light intensity in winter reduce the growth and yield of tomatoes in the greenhouse. Supplement of artificial lights in greenhouse is a better method to alleviate this drawback. The objective of this study was to investigate the effects of interlighting regimes to extend photoperiod and to increase light intensity on the growth and yield of greenhouse-grown tomatoes. Artificial interlighting was provided by light-emitting diode tubes, which were mounted vertically 1 m above the ground and 15 cm to the plant row horizontally. The lighting regimes were setup by lighting 3 hr, 6 hr before dawn, 3 hr, and 6 hr after dusk, with two levels of photosynthetic photon flux (PPF) 70 and 45 µmol m^{-2} s^{-1} *on the effective lighting area, 1.2 m wide by 0.6 m high, for lateral interlighting. The long extended photoperiod (6 hr) and high light intensity (70 µmol* m^{-2} s^{-1}*) significantly promoted the plant growth and yield. Compared with the control treatment with natural sunlight, the interlighting treatment of 6 hr and PPF 70 µmol* m^{-2} s^{-1} *shortened the days to anthesis and the days to ripen by 17 and 20 days, respectively. It also increased fruit number by 189 % and the yield by 179 %. It is recommended to use the interlighting regime of 6 hr before dawn to cultivate greenhouse-grown tomatoes in winter.*

Keywords: yield, growth, greenhouse, tomatoes

Introduction

In the past centuries, tomato had become one of the worldwide popular fruits due to its high nutritional value, low in calories, tolerance to storage and transportation, diverse cooking methods, etc. In tomato production, healthy plants are the most important factor in obtaining good yields. The good yield and quality tomatoes are usually produced from greenhouse or protected culture. Light is one of the main factors limiting the yield of tomato plants grown under greenhouse. The demand for fresh market tomatoes usually exceeds its production capacity, particularly during the winter months. However, limited amount of available natural sunlight and diminished light intensity in winter reduces the growth and yield of tomatoes in the greenhouse. Supplement of artificial lights in greenhouse is a better approach to alleviate this drawback. Lu et al. (2012) reported inter-lighting was considered an effective method to increase tomato yield and to improve the quality of tomato. Their results indicated that tomato yield and sugar content might increase with the increase of the amount of supplemented light. The objective of this study was to investigate the effects of interlighting regimes to extend photoperiod and to increase light intensity on the growth and yield of greenhouse-grown tomatoes.

Material and method

The tomato seedlings of Lycopersicon esculentum L. ‘Harvest II’ grown in 50-plug tray filled with commercial peat N2 (Neuhaus, Germany) as the growing substrate for 30 days, were transplanted to 38 cm-diameter pots. These tomato seedlings were moved into a glass greenhouse since 21 Dec. 2012 (day 1). Artificial interlighting was provided by cool-white light-emitting diode tubes, which were hung vertically 1 m above the ground and 15 cm to the plant row horizontally (Fig. 1). The lighting regimes were setup by lighting 3 hr before dawn (D3), 6 hr before dawn (D6), 3 hr after dusk (N3), and 6 hr after dusk (N6), with high (H) and low (L) levels of photosynthetic photon flux (PPF) 70 and 45 µmol m^{-2} s^{-1}, provided by two and one LED tube, respectively. The effective area for lateral interlighting was 1.2 m wide by 0.6 m high. The light intensity was measured at the distance of 15 cm to the light tube horizontally by the quantum sensor (LI-250A/LI-190, LI-COR, USA). The plants were watered above the pots every one or two days and fertilized with the fertilizer solution every week. Control tomato plants were grown in the greenhouse without any light supplement.

Fig. 1 Supplemental lighting method

Data collection and analysis

Six tomato plants were used in each treatment. The date of the first flowering and harvest were recorded. The yield, the truss and fruit number for each plant were measured. Fruit diameter, fruit length, peel thickness and quality indices, such as total soluble solid (TSS), titratable acidity (TA), Vitamin C content, and carotenoid content were analyzed. Lightness (L* value) and color-opponent dimensions (a* value) were measured with portable colorimeter (BYK-Gardner Color-Guide 45/0, Germany). The data were analyzed by the analysis of variance (ANOVA) with the means comparison by the Least Significant Differences (LSD at P≤ 0.05).

Result and discussion

Tab. 1 shows the data of the tomato flowering, harvest, and yield after supplemental lighting treatment. Tomato plants under supplemental lighting shortened the days to anthesis and the days to harvest. It also increased truss and fruit number and significantly higher yield than those control tomato plants without any light supplement. Compared with natural sunlight, the plants subjected to 3 or 6 hours lighting daily, only 6 hours supplemental lighting treatments could advance the days to anthesis by 7-17 days. The earliest anthesis was the plants under HN6, HD6, LD6 treatments, which only took 46 days to anthesis. All supplemental lighting treatments could also shortened the days to ripen by 1-20 days. The plants under HN6 treatment had the earliest harvest time among the treatments, which almost advanced 20 days to harvest comparing with the control treatment. It means that the annual greenhouse turnover rate in the supplemental lighting regimes was higher than the rate in a conventional greenhouse without any light supplement.

The LD6 treatment had the maximum truss number (10.66 truss/plant), which is significantly more than the control 7.67 truss/plant. The fruit number in all treatments ranged from 3.00 to 8.67, and the HD6 treatment had the maximum fruit number (Table 1). All supplemental lighting treatments signicantly increased the yield by 18.9 % to 179 %. The HD6 treatment had the highest yield (815.54 g/plant), which significantly increased 179 % than the control treatment. Under 6-hr interlighting daily, the plants subjected to higher PPF (70 μmol m^{-2} s^{-1}) increased 33.8 % fruit number and 32.23 % yield than those under lower PPF (45 μmol m^{-2} s^{-1}) plants. The 6-hr interlighting also advanced 5 days to anthesis and 7 days to harvest.

Tomato requires a relative high level of light for proper plant growth. Light intensity is a major factor governing the rate of photosynthesis and photoassimilates allocation. McAvoy et al. (1989) reported that the yield of tomato increased with the increase in the amount of light received from anthesis to harvest. Adams et al. (2008) reported that the low light intensity and long-day lighting promote the growth of tomato. These results agree with our experiment, the long extended photoperiod (6 hr) and higher light intensity (70 μmol m^{-2} s^{-1}) promoted the plant growth and yield significantly.

In the higher PPF and 6-hr supplemental lighting treatments (H6), the supplemental lighting before dawn treatments had higher yields than those in lighting after dusk. The spectrum of natural light may be different between dawn and dusk. It is possible to affect the stomatal movement and photosynthesis of plant. The stomatal movement is regulated by a variety of environmental and internal factors such as light, CO2 levels, water status of the plant, and temperature. The blue light effect has been demonstrated in a variety of ways. Stomatal opening is promoted by both red and blue light. It is generally more sensitive to blue light than to red. At low irradiance level, below 15 μmol m^{-2} s^{-1}, blue light will cause stomatal opening but red light is ineffective (Hopkins and Huner, 2008).

There was no significant difference on fruit diameter and length, and peel lightness among all treatments (Tab. 2). However, the peer thickness of fruit was thinner and maintained higher sugar-acid (TSS/TA) ratio in H6 treatments (Tab. 3). The a* value of peel color in supplemental lighting treatments was higher than those in control, and high a* value was showed redder. The highest sugar-acid ratio and vitamin C content were the fruits in HN6 treatment (Tab. 2 and Tab. 3). The higher supplemental light regime could increase fruits sugar-acid ratio and vitamin C content. However, the carotenoid content of fruits shows the opposite result. Tab. 3 shows that the fruits of LN3 had the highest carotenoid content among all treatments. The higher light PPF seems to decrease the carotenoid content of fruits. Irradiance can affect mineral accumulation and plant secondary compounds, such as carotene (Havaux et al., 1998). Increases in photosynthesis will increase plant biomass and can result in a dilution effect on elemental concentrations (Mills, Jones, 1996). Lefsrud et al. (2006) indicated that environmental modification of irradiance levels resulted in changes in crops fresh biomass production and the accumulation of carotenoid content. However, the effect of irradiance level depends on crop species and growing conditions.

Conclusion

Supplemental light regime was found critical not only to grow, but also to promote fruit yield and quality of tomato. Our result shows using interlighting regime for greenhouse tomato production was better than those of no supplymental lighting. Moreover, the electric cost was only NT$ 0.024 (EUR$ 0.0006) for every gram fruit yield production. Therefore, to use the interlighting regime of 6 hours before dawn and PPF 70 μmol m^{-2} s^{-1} to cultivate greenhouse-grown tomatoes in winter is recommended.

Tab. 1 Effects of different supplemental lighting regimes on the first flowering and harvest time, truss and fruit number, and yield of tomato ‘Harvest II’

Treatment	**DAT**^{z}		**Truss number**	**Fruit number**	**Yield**
	First Flowering	**First Harvest**	**(pl^{-1})**	**(pl^{-1})**	**(g pl^{-1})**
HN6	46 c^y	111 g	10.00 b	7.83 b	732.73 b
HD6	46 c	120 f	09.50 c	8.67 a	815.54 a
HN3	63 a	128 c	08.16 g	7.17 c	699.12 c
HD3	63 a	130 b	10.00 b	4.67 f	466.06 f
LN6	56 b	125 e	08.40 f	6.33 d	627.62 d
LD6	46 c	120 f	10.66 a	6.00 e	545.22 e
LN3	63 a	127 d	08.60 e	3.50 g	348.22 h
LD3	63 a	127 d	08.83 d	3.33 h	349.57 g
CK	63 a	131 a	07.67 h	3.00 i	292.75 i

^{z}DAT : the days after transplant.
^{y}Means followed by the different letters in each column are significantly different at 5 % level by LSD Test.

Tab. 2 Effects of different supplemental lighting regimes on the fruit diameter and length, peel thickness and color **(**L* and a* value) of tomato ‘Harvest II’

Treatment	**Fruit**		**Peel thickness (mm)**	**L* value**	**a* value**
	Diameter (mm)	**Length (mm)**			
HN6	59.39 ab^y	45.83 de	4.71 de	27.31 bc	15.95 ab
HD6	57.27 ab	45.11 ef	3.88 f	26.97 bc	15.10 abc
HN3	58.19 ab	46.34 cd	4.26 ef	26.54 c	14.90abc
HD3	59.78 ab	47.55 b	6.20 ab	28.10 abc	13.95 bc
LN6	61.38 ab	47.68 b	6.44 a	27.78 bc	16.13 a
LD6	56.34 ab	44.75 f	5.00 cd	26.75 bc	13.62 c
LN3	64.56 a	49.37 a	5.51 c	28.50 ab	15.84 ab
LD3	55.80 b	48.01 b	5.60 bc	29.20 a	13.75 c
CK	59.04 ab	47.02 bc	5.46 c	28.31 ab	13.57 c

^{y}Means followed by the different letters in each column are significantly different at 5 % level by LSD Test.

Tab. 3 Effects of different supplemental lighting regimes on the fruit quality parameters of ripen tomato 'Harvest II'

Treatment	Total soluble solid (°Brix)	Titratable acidity (%)	TSS/TA[z] ratio	Vitamin C content (mg ml^{-1})	Carotenoid content (mg g^{-1})
HN6	4.48 abc[y]	0.46 b	9.88 a	11.70 a	935.5 ab
HD6	4.54 ab	0.51 ab	8.95 ab	10.23 ab	744.7 b
HN3	4.88 a	0.54 ab	9.31 ab	8.28 bcd	804.4 b
HD3	4.10 bc	0.50 ab	8.32 abc	8.39 bcd	1091.7 a
LN6	4.20 abc	0.58 a	7.44 bc	10.16 ab	965.6 a
LD6	3.80 c	0.57 ab	6.67 c	7.24 d	1100.2 a
LN3	4.20 abc	0.51 ab	8.21 abc	10.34 ab	1129.1 a
LD3	4.52 abc	0.55 ab	8.67 ab	9.86 abc	918.9 ab
CK	4.52 abc	0.53 ab	8.74 ab	7.95 cd	977.8 ab

[z]TSS/TA: Total soluble solid / Titratable acidity
[y]Means followed by the different letters in each column are significantly different at 5% level by LSD Test.

Reference

Adams S. R., Valdes V., Langton F., 2008. Why does low intensity, long-day lighting promote growth in Petunia, Impatiens, and tomato? J. Horti. Sci. Biotech., 83: 609 - 615.

Havaux M., Tardy F., Lemonine Y., 1998. Photosynthetic light-harvesting function of carotenoids in higher-plant leaves exposed to high light irradiances. Planta, 205: 242 - 250.

Hopkins W. G., Huner N. P. A., 2008. Light and carbon dioxide regulate stomatal opening. Introduction to Plant Physiology, USA, 135 - 136.

Lefsrud M. G., Kopsell D. A., Kopsell D. E., Curran-Celentano J., 2006. Irradiance levels affect growth parameters and carotenoid pigments in kale and spinach grown in a controlled environment. Physiol. Planta., 127: 624 - 631.

Lu N., Maruo T., Johkan M., Hohjo M., Tsukagoshi S., Ito Y., Ichimura T., Shinohara Y., 2012. Effects of supplemental lighting within the canopy at different developing stages on tomato yield and quality of single-truss tomato plants grown at high density. Environ. Control Biol., 50: 1 - 11.

Lu N., Maruo T., Johkan M., Hohjo M., Tsukagoshi S., Ito Y., Ichimura T., Shinohara Y., 2012. Effects of supplemental lighting with light-emitting diodes (LEDs) on tomato yield and quality of single-truss tomato plants grown at high planting density. Environ. Control Biol., 50: 63 - 74.

McAvoy R. J., Janes H. W., 1989. Tomato plant photosynthetic activity as related to canopy age and tomato development. J.Am.Soc.Hort.Sci., 114: 478 - 482.

Mill H. A., Jones J. B. J., 1996. Plant analysis handbook II: A practical sampling, preparation, analysis, and interpretation guide. MicroMacro Publishing, GA.

DETECTION AND COUNTING OF INTACT TOMATO FRUITS ON TREE USING IMAGE ANALYSIS AND MACHINE LEARNING METHODS

Kyosuke Yamamoto[1*], Yosuke Yoshioka[2], Seishi Ninomiya[1]

[1]The University of Tokyo, 1-1-1 Midori-cho, Nishitokyo, Tokyo, Japan
Phone: +8142-463-1611, E-mail: 8244012644@mail.ecc.u-tokyo.ac.jp
[2]University of Tsukuba, Ibaraki, Japan

Abstract

Fully automated yield estimation of intact fruits before harvesting provides various benefits. For instance, it reduces the labor cost for site-specific management based on a yield mapping. Until now, many studies on crop yield estimation have been carried out. Previous studies (Kurtulmus et al., 2011; Zhou et al., 2012) estimated yield of intact fruits using image analysis and achieved high detection rate. The proposed method, however, required many parameters such as window size and thresholds for color and shape features. In this study, we introduced a new approach to detect and count intact immature and mature tomato fruits on tomato tress, using image analysis and a machine learning method. Our approach consists of two steps. The first is pixel-based segmentation. We extracted the color features of each pixel, and manually labeled them into four classes; i.e. fruit, leaf, stem, and background. Then we built a decision tree using the color features of the training images by using the Classification and Regression Tree (CART) classifier. The decision tree was applied to test images to classify pixels into the classes. The second step is blob-based segmentation. We extracted pixels classified as the fruit class by the pixel-based segmentation, and used connected regions as blobs. Since the misclassification at the first step generates the blobs which also include non-fruit regions, we conducted the classification of the blobs using the CART classifier. Blobs obtained from the training images were manually classified into fruit and non-fruit blobs, and used as a training data set. Then we built a decision tree using the average color values and texture feature of the blobs. The decision tree was applied to the blobs extracted from the test images to identify the fruit blobs. A total of 45 tomato images were acquired in February 2012 at the Tsukuba Plant Factory of Institute of Vegetable and Tea Science. All the images were acquired in the nighttime using a built-in flash of a camera. Five of the images were used for training, while the rest of the images were used for testing. The results showed that the test images taken under various growing condition of tomato trees, were correctly segmented into the four classes in the first step. Although some pixels especially those of stem parts were misclassified as fruits, they were removed by the blob-based segmentation. In addition, our approach was able to properly count more than 80 % of the fruits including not only mature fruits but also immature fruits that are usually difficult to discriminate from leaves or stem because of their similar color.

Keywords: tomato fruit, image analysis

Introduction

Fully automated yield estimation of intact fruits before harvesting provides various benefits. For instance, it reduces the labor cost for site-specific management based on a yield mapping. Until now, many studies on crop yield estimation have been carried out. Previous studies (Kurtulmus et al., 2011; Zhou et al., 2012) estimated yield of intact fruits using image analysis and achieved high detection rate. The proposed method, however, required many parameters such as window size and thresholds for color and shape features. Some researchers used hyperspectral and thermal imaging techniques for fruit detection (Safren et al., 2007; Stajnko et al., 2004). Though the detection rate was usually better than that of conventional color image analysis, the devices are rather costly. In this study, we aimed to develop a low price system to accurately detect intact fruits using a conventional RGB digital camera with a machine learning approach.

The method is based on two steps of image segmentation algorithm; pixel-based and blob-based segmentations. For both of the steps classification models were generated using the color and/or texture features of images. The model based proposed does not require thresholding for each image. We evaluated the fruit detection rate to identify the effectiveness of our approach for the yield estimation of intact tomato fruits.

Materials and Methods

Image Segmentation and Fruit Counting

Our approach for image segmentation consists of two steps. The first is pixel-based segmentation based on decision tree based segmentation model (Guo et al., 2013). We extracted the color features (B, G, R, H, S, V, L*, a*, b*, L*, u*, v*, Y, Cr and Cb) of each pixel, and manually labeled them into four classes; i.e. fruit, leaf, stem, and background (Fig. 1). Then we built a decision tree using the color features of the training images by using the Classification and Regression Tree (CART) classifier (Olshen and Stone, 1984). The decision tree was applied to test images to classify pixels into the classes.

The second step is blob-based segmentation. We extracted pixels classified as the fruit class at the pixel-based segmentation, and used connected regions as a blob. Since the misclassification at the first step made the blobs also include non-fruit regions, we conducted the classification of the blobs using the CART classifier again. Blobs obtained from the training images were manually classified into multi-fruits, single-fruit and non-fruit blobs (shown in Fig. 2), and used as a training data set. Then, we built a decision tree using the average values of the color features, texture features and size of the blobs. For the texture features, we generated histogram and gray level co-occurrence matrix (Haralick et al., 1973) of the blobs that are converted to gray scale image and calculated the contrast feature of them. The decision tree was applied to the blobs extracted from the test images to identify the blobs that contain fruit.

Each blob classified as a multi-fruits blob might include more than one fruit in the blob, therefore, we estimated the number of fruits in the blob based on the S and V values of HSV color space. Fig. 3 shows the distribution of S and V values in a multi-fruits blob. There were over-exposed regions on each fruit caused by reflection of the built-in flash of the camera. At the over-exposed regions, S value was lower, while the V value as higher than others. Therefore, we extracted the pixels whose S and V values are:

$$S_{xy} > \frac{\bar{S}}{2} \qquad (1)$$

$$V_{xy} > \bar{V} \times 1.8 \qquad (2)$$

where S_{xy} and V_{xy} are the S and V values at the point of (x, y), and $\bar{S}$ and $\bar{V}$ are the mean of S and V values within the blob. Fig. 3d shows the over-exposed regions extracted by using Eqs. (1) and (2). The number of over-exposed regions was used as the estimated number of fruits contained in the blob.

Image Acquisition

Tomato plant images were acquired at Tsukuba plant factory of Institute of Vegetable and Tea Science. For the image acquisition, a digital single-lens reflex camera (EOS Kiss X3, Canon Inc., Japan) was set up in the plant factory. A total of 154 images were captured every two hours during the nighttime from February 5th to March 7th, 2013. Then, 45 images were randomly selected from the 154 images, and five of the images were used for training, while the rest of the images were used for testing.

Results and Discussion

Fig. 4 shows the results of the image segmentation and fruit detection. The result of the pixel-based segmentation showed test images taken under various growing condition of tomato trees were correctly segmented into the four classes. However, some pixels especially those of stem parts were misclassified as fruits. For instance, in the result of the pixel-based segmentation of Fig. 4a, while 2,616 blobs were identified, there were only 28 fruits in the image (Fig. 4c). However, the number of candidates was reduced to 27 by conducting the blob-based segmentation. As a result, 29 fruits were detected as shown in Fig. 4d.

Tab. 1 describes the result of fruit counting in the test images. Our approach was able to properly count almost 80 % of the fruits in the test images. In addition, we were able to detect fruits including not only mature fruits but also immature ones that are usually difficult to discriminate from leaves or stems because of their similar color features. Furthermore, a fruit 80 % of whose surface was covered with leaves and stems was also detected in our approach.

Fig. 1 Example of training data collection.
Pixels drawn with red, green, yellow and blue colors were used as training data of fruit, leaf, stem and background, respectively

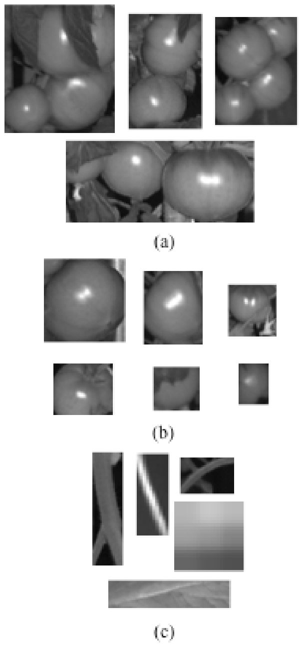

Fig. 2 Examples of training dataset for the blob-based segmentation: (a) multi-fruits blobs, (b) single-fruit blobs, (c) non-fruit blobs

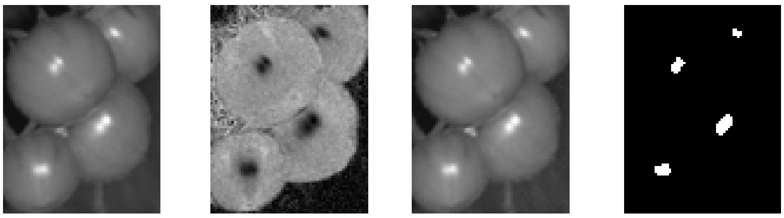

(a) (b) (c) (d)

Fig. 3 Extraction of over-exposed regions
(a) Original image, (b) Saturation image, (c) Value image, (d) Extracted over-exposed regions

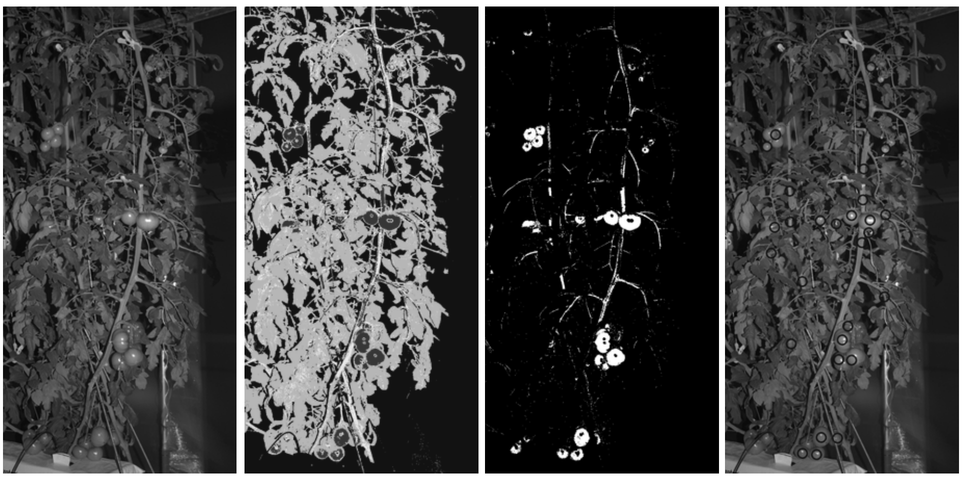

(a) (b) (c) (d)

Fig. 4 Example step of image segmentation and fruit detection
(a) Original image, (b) Result of pixel-based segmentation,

(c) Detected blobs, (d) Detected fruits by blob-based segmentation

Tab. 1 Average rates of fruit detection in the test images

	Detection rate[1]	**Accuracy rate[2]**	**Misdetection rate[3]**
Percentage [%]	79.7	83.1	16.9

[1]: number of detected fruit / number of fruits in an image
[2]: number of accurate detection / number of detected fruit
[3]: number of misdetection / number of detected fruit

Although we achieved high fruit detection rate, the misdetection rate was not sufficiently low. Since we used only color features for the pixel-based segmentation, some pixels were misclassified as a stem part, and this caused the misdetections of fruits. In a preliminary study, we have already confirmed that there are differences on texture features between fruit and stem parts and the misdetection rate can be improved by utilizing such information at the pixel-based segmentation. In addition, since we were able to extract not only fruit, but also leaf and stem parts from the images, another important information such as leaf area index and the distance between branches could be measured in the future study.

Conclusion

A new approach based on the image analysis and machine learning methods for the detection and counting of intact tomato fruit on trees was presented. Since the image segmentations were conducted by two-step process based on decision trees, our approach did not require any parameters such as window size and thresholds for color and texture features. The results of image segmentation showed that images taken under various growing condition of tomato tree were segmented correctly. Furthemore, the result of fruit detection showed that almost 80 % of the fruits were properly detected and counted in the test images.

References

Guo W., Rage U.K., Ninomiya S., 2013. Illumination invariant segmentation of vegetation for time series wheat images based on decision tree model. Computers and Electronics in Agriculture, 96: 58–66.

Haralick R.M., Shanmugam K., Dinstein I., 1973. Textural Features for Image Classification. IEEE Transactions on Systems, Man, and Cybernetics, 3: 610–621.

Kurtulmus F., Lee W.S., Vardar A., 2011. Green citrus detection using “eigenfruit”, color and circular Gabor texture features under natural outdoor conditions. Computers and Electronics in Agriculture, 78: 140–149.

Olshen L.B.J.H.F.R.A., Stone C.J., 1984. Classification and Regression Trees. Wadsworth International Group.

Safren O., Alchanatis V., Ostrovsky V., Levi O., 2007. Detection Of Green Apples in Hyperspectral Images of Apple-Tree Foliage using Machine Vision. Transactions of the ASABE, 50: 2303–2313.

Stajnko D., Lakota M., Hočevar M., 2004. Estimation of number and diameter of apple fruits in an orchard during the growing season by thermal imaging. Computers and Electronics in Agriculture, 42: 31–42.

Zhou R., Damerow L., Sun Y., Blanke M.M., 2012. Using colour features of cv. “Gala” apple fruits in an orchard in image processing to predict yield. Precision Agriculture, 13: 568–580.

SIMULATION OF SALT TRANSPORT AND CROP YIELD IN A RECLAIMED AREA WITH SALINE GROUNDWATER IN JAPAN

Kozue Yuge[1*], Jos C. van Dam[2], Joop G. Kroes[2], Mitsumasa Anan[3]

[1]Kyushu University, 6-10-1 Hakozaki Higashi-ku Fukuoka, Japan, Phone: +81-92-642-2912, Fax: +81-92-642-2912, E-mail: yuge@bpes.kyushu-u.ac.jp
[2]Wageningen University and Research Centre, Wageningen, the Netherlands
[3]Takasaki Sogo Consultant, Co. Ltd., Kurume, Japan

Abstract

Central polder in Isahaya Bay in south-west Japan was reclaimed in 1997. Farming started in 2008 after improvement of soil salinity and hydraulic conductivity conditions. Although the present soil conditions in the root zone are favourable and agricultural productivity has been increased, soil salinization will be of increasing concern because plans are considered to open the gates of the reclamation dike. Also irrigation scheduling is necessary to decrease drought stress, which may increase the salinity stress. The aim of this study is to evaluate salt transport in reclaimed fields of Central polder and to evaluate the effect of root zone salinization on crop yields. Annual change of the solute transport was simulated with SWAP model, assuming that groundwater is salinized after opening of the reclamation dike and salt groundwater flows upward as seepage. In the simulation scenario, potatoes were grown from 20 February to 30 June and from 10 August to 20 December. Simulation results indicated that solute concentrations around root zone were relatively low until July because of high and frequent precipitation in winter and early summer. After the rainy season, solute concentration increased gradually and salts from groundwater reached the root zone after successive dry days in summer. In addition, transpiration reduction due to wetness and drought also occurred in the rainy season and the successive dry season, respectively.

Keywords: simulation, salt, transport, saline groundwater, japan.

Introduction

More than 70 % of Japanese lands are classified as mountainous or hill slope land. Particularly the Nagasaki prefecture located in the south-west of Japan is well-known for its fields with steep slopes. In this region it is hard to develop flat and large scale crop fields and there is a serious problem to achieve sufficient agricultural productivity and farming efficiency.

A project to reclaim the Isahaya Bay in Nagasaki prefecture and develop prime and large-scale agricultural lands has been conducted. Cultivation in the newly reclaimed land known as Central polder started in 2008. As the crop fields in Central polder are flat and large-scale, agricultural productivity and farmingefficiency is relatively high.

However serious concerns exist on future cultivation in Central polder because plans are made to open the gates of the reclamation dike because of seaweed crop failure. Environmental assessment has been conducted and the effect of sea water seepage on the crop fields was evaluated using simulation model describing soil water and solute transport. However in this study, the crop effects on soil water and solute transport, including root extraction, crop stresses due to salinity and ground cover effects on evaporation, were not considered. As these effects may play a significant role in soil water and solute transport, these factors should be taken into account to predict accurately the saline effect on the crop fields.

The aim of this study is simulation of soil water and salinity transport in a reclaimed crop field in Central polder and to evaluate the effect of groundwater salinization on crops taking into account the crop effects on soil water and solute transport, including root extraction, crop stresses due to salinity and ground cover by crop canopy. Annual change of the solute transport was simulated with Soil-Water-Atmosphere-Plant (SWAP) model (Kroes et al., 2008; Van Dam et al., 2008), assuming that groundwater is salinized after opening of the reclamation dike and saline groundwater flows upward.

Study site

Central polder of Isahaya Bay shown in Fig. 1 is located in Nagasaki Prefecture, south-west of Japan (32.86°N, 130.13°E).Isahaya Bay was closed with a dike of about 7 km in 1997 and next the Central polder was reclaimed. Soil physical and chemical conditions have been improved for cultivation (Marui et al., 2002) and farming in Central polder started in 2008. Saline water in the detention pond was desalinized and the fresh water in this pond has been used for irrigation water. The area of agricultural fields in Central polder is about 700 ha and various crops including potatoes, onions and wheat are produced. Greenhouse cultivation and eco-friendly farming have gradually increased.

Methodology

Annual change of the soil water and solute transport was simulated with SWAP, assuming that groundwater is salinized after opening of the reclamation dike and saline groundwater flows upward as seepage. The vertical soil water movement in unsaturated/saturated soils can be described as follows;

$$\frac{\partial\theta}{\partial t}=\frac{\partial}{\partial z}\left[K(h)\left(\frac{\partial h}{\partial z}+1\right)\right]-S_a(h)-S_d(h)-S_m(h) \qquad (1)$$

where θ is volumetric water content (cm^3cm^{-3}), t is time (d), $K(h)$ is hydraulic conductivity ($cm\ d^{-1}$), h is soil water pressure head (cm), $S_a(h)$ is soil water extraction rate by plant roots ($cm^3\ cm^{-3}\ d^{-1}$), $S_d(h)$ is the extraction rate by drain discharge in the saturated zone (d^{-1}) and $S_m(h)$ is the exchange rate with macro pores (d^{-1}) .

The governing equation of solute transport in the soil can be described as follows;

$$\frac{\partial(\theta c+\rho_b Q)}{\partial t}=\frac{\partial(qc)}{\partial z}+\frac{\partial}{\partial z}\left[\theta(D_{dif}+D_{dis})\frac{\partial c}{\partial z}\right]-\mu(\theta c+\rho_b Q)-K_r S_a(h)c \qquad (2)$$

where c is the solute concentration in soil water ($mg\ cm^{-3}$), ρ_b is dry soil bulk density ($mg\ cm^{-3}$), Q is amount of adsorbed solute ($g.g^{-1}$), q is average soil water flux, D_{dif} is diffusion coefficient ($cm^2.d^{-1}$), Ddis is the dispersion coefficient ($cm^2.d^{-1}$) and K_r is root uptake preference factor (-). In this study, chloride concentration in the soil was simulated using eq. (2) as the solute c.

Simulation scenario

Fig. 2 shows a schematic view of the simulation model describing soil water and solute transport. To solve eq. (1), boundary conditions at soil surface were set taking into account the water balance at the soil surface, including precipitation, interception, soil evaporation and run-off (van Dam et al., 2008). There is no irrigation at the study site. Actual transpiration and soil evaporation were separately simulated from potential evapotranspiration taking into account the crop growing stage. The potential evapotranspiration was calculated using meteorological data of year 1994 which was a relatively dry year with probably salinity stress. The crop consists of potatoes which is one of main crops of the study site and the growing periods are 20 February - 30 June and 10August - 20 December. The maximum rooting depth amounts 50 cm. Reduction of the root extraction due to water and salinity stress was considered using critical values suggested by Feddes et al. (1978), Maas and Hoffman (1977), and Skaggs et al. (2006). An upward seepage flux from the groundwater was prescribed as the bottom boundary condition, as the polder resides below sea level. Using measured soil water retention curves and saturated hydraulic conductivities in 3 layers, the unsaturated hydraulic conductivities were specified by Mualem-van Genuchten functions (Van Genuchten, 1980). Fitting parameters of Mualem-van Genuchten functions are shown in Tab. 1.

Fig. 1 Location of Central polder and dike in Isahaya bay

The boundary condition at the soil surface to solve the eq. (2) are specified by solute concentrations in irrigation and rain water.These consentrations were assumed to be 0 mg cm^{-3} in this study. As the bottom boundary condition for the solute transport, a constant seepage flux of 1 mm d^{-1} was specified with a solute concentration of 5760 mg/L. The drainage flux by subsurface drainsat a depth of 0.8 m and with a spacing of 10 m, as shown in Fig .2**,**was estimated by SWAP using the drainage equation of Hooghoudt (1940). As initial soil moisture condition we adopted ? and as initial solute concentrations 0 mg cm^{-3}.

Result and discussion

Fig. 3 shows the simulated daily changes of chloride concentration at various depths. Upward movement of the solute was not remarkable until July because of relatively high precipitation as shown in Fig. 4. Simulated groundwater level shown in Fig. 5 fluctuated with the precipitation and floods were simulated between April and June. As the amount and frequencyof precipitation were low after July, the chloride concentration in every layer gradually increased as shown in Fig. 3. According to the Japanese standard for cultivation of vegetables, the chloride concentration which affects vegetables' growing amounts 250 mg/L and chloride concentrations should be kept under this level. As shown in Fig. 3, at the depth of 40cm this critical level is reached and this will affect crop growing and yields.

Fig. 6 shows the dairy changes of the transpiration reduction due to wet, dry and saline conditions. As shown in this figure, stress due to wetness occurred in the first half year because of high precipitation. Dry stress was remarkable after September. Although saline stress was relatively low comparing with the stresses due to wetness and drought, it slightly increased at the end of year. There is risk of accumulated residual salinity effect on crop growing and yield. In most of the crop fields in Central polder, irrigation is rarely conducted. However the simulated results indicated that proper irrigation and drainage management is needed to prevent stresses due to wetness, drought, and salinity.

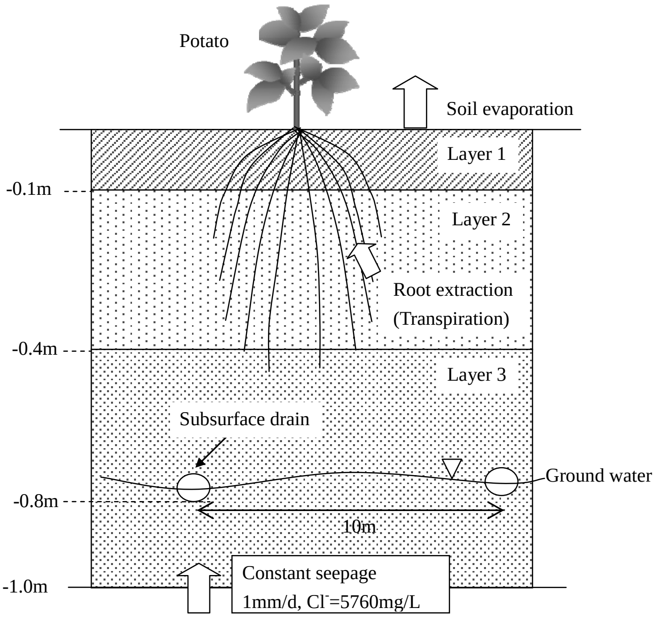

Fig. 2 Schematic view of simulation model describing soil water and solute transport

Tab. 1 Parameters of Mualem–van Genuchten soil hydraulic functions

Layer No.	Saturated hydraulic conductivity (cm s^{-1})	θs (%)	Θr (%)	Parameters of Mualem–van Genuchten		
				α (/cm)	*N* (-)	*L* (-)
1 (0 - 0.1 m)	1.15×10^{-3}	52.6	16.2	0.078	1.23	0.5
2 (0.1 - 0.4 m)	1.00×10^{-3}	52.9	3.2	0.070	1.13	0.5
3 (0.4 - 1 m)	7.54×10^{-4}	52.5	1.1	0.070	1.10	0.5

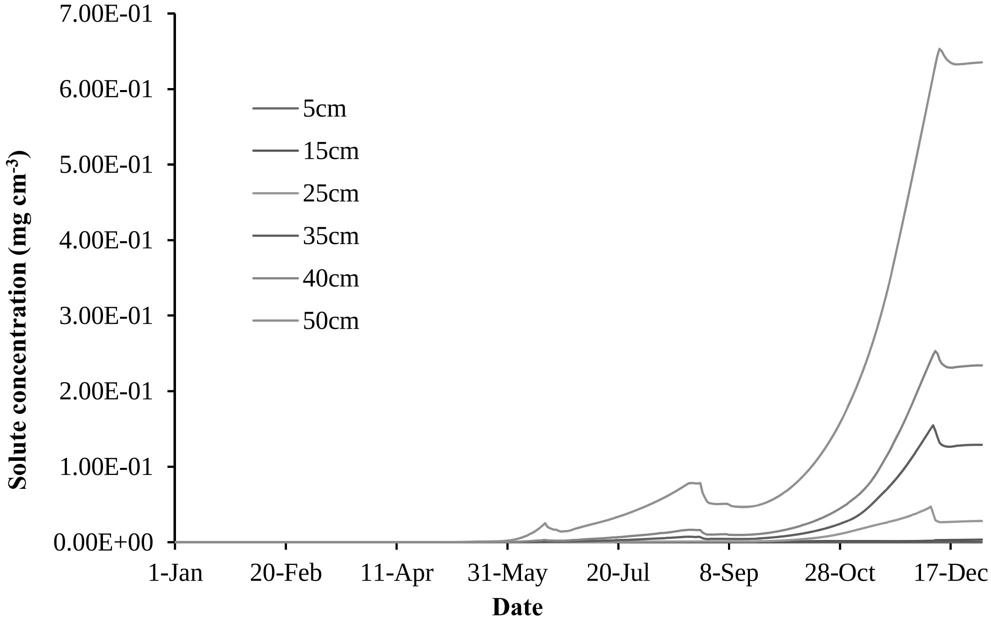

Fig. 3 Simulated daily changes of chloride concentration

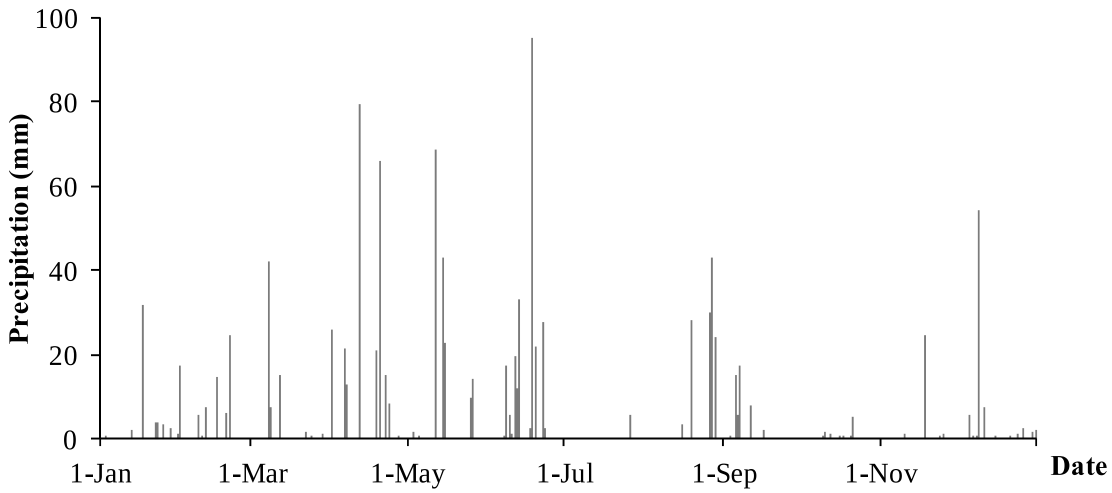

Fig. 4 Daily change of precipitation

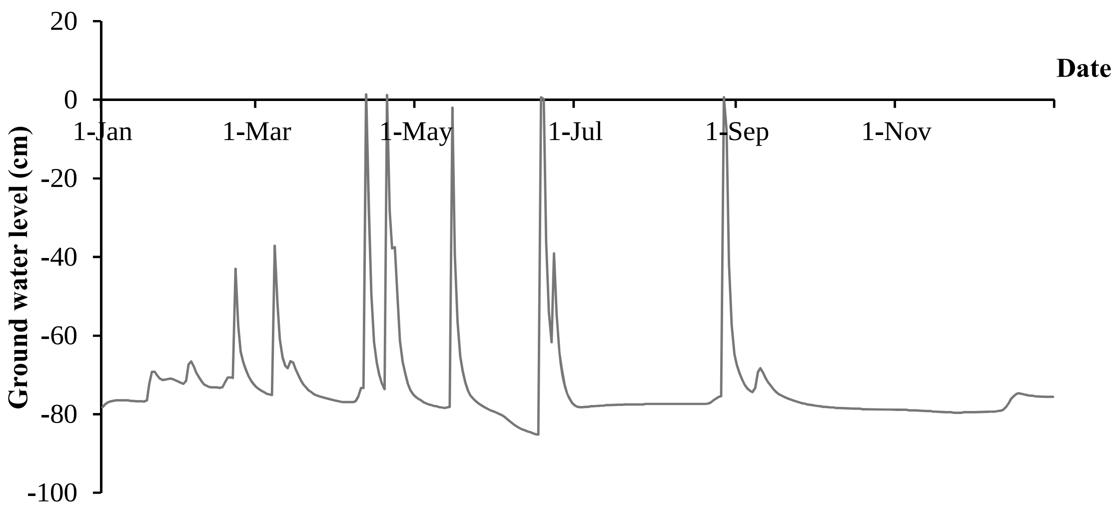

Fig. 5 Simulated daily change of groundwater level

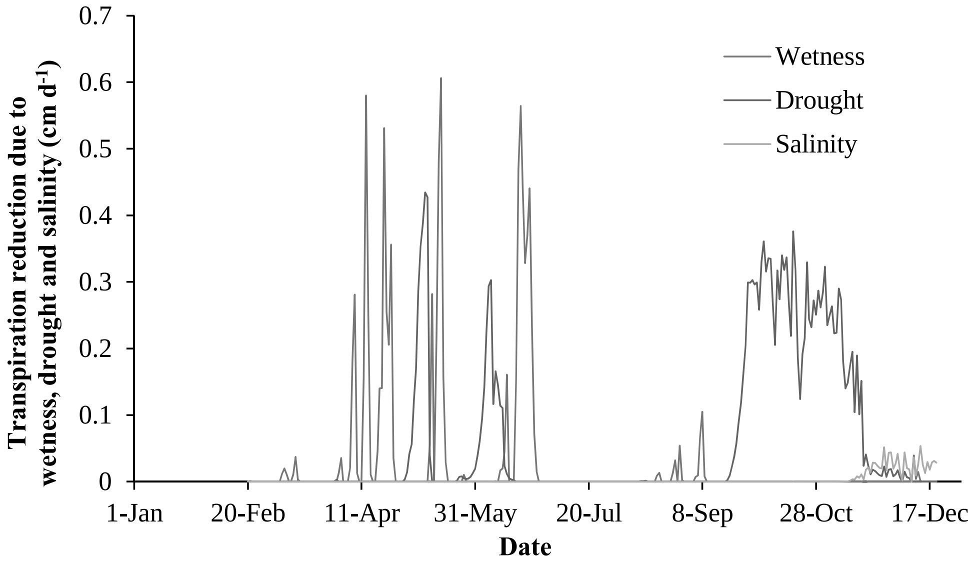

Fig. 6 Simulated transpiration reduction due to wet, dry and saline conditions

Conclusion

To simulate soil water, solute transport and crop yield in the Central polder of Isahaya Bay, the SWAP model was used in this study. The simulated solute concentration indicated that upward movement of salinity was inhibited in the rainy season and chloride concentration in every layer gradually increased during successive dry periods. The crop growing and yield could be affected by salinity in the soil when the groundwater is salinized because the simulated chloride concentration in the root zone exceeded the critical salinity level suggested in Japan. Transpiration reduction due to wetness and drought were also simulated in the rainy season and successive dry periods, respectively. To control the stresses due to wetness, drought and salinity, proper irrigation, drainage and leaching is important for sustainable agricultural production in Central polder in Isahaya Bay.

Using SWAP, the soil water and solute transport could be evaluated taking into account crop effects including root extraction, transpiration reduction caused by wet, dry and saline stress and partial ground cover by the crop canopy. In the future field observation will be conducted to verify the model accuracy in the Central polder of Isahaya Bay.

Reference

Feddes R.A., Kowalik P.J., Zaradny H., 1978. Simulation of field water use and crop yield. Simulation Monographs. Pudoc. Wageningen, 189.

Kroes J.G., Van Dam J.C., Groenendijk P., Hendriks R.F.A., Jacobs R.F.A., 2008. SWAP version 3.2. Theory description and user manual. Alterra report 1649, Wageningen University and Research centre, Wageningen, 262.

Maas E.V., Hoffman G.J., 1977. Crop salt tolerance-current assessment. J. Irrig. and Drainage Div., ASCE, 103: 115 - 134.

Marui A., Haraguchi T., Sakamoto T., Yuge K., Nakano Y., Funakoshi T., 2002. Irrigation Scheduling and Upland Utilizing of the Newly Reclaimed Land. Science bulletin of the Faculty of Agriculture, Kyushu University, 57(1): 125 – 133. (in Japanese)

Skaggs T.H., Van Genuchten M.T., Shouse P.J., Poss J.A., 2006. Macroscopic approaches to root water uptake as a function of water and salinity stress. Agric. Water Man., 86: 140 - 149.

Van Dam J.C., Groenendijk P., Hendriks R.F.A., Kroes J.G., 2008. Advances of modellingwater flow in variably saturated soils with SWAP. Vadose Zone J. 7: 640 – 653.

Van Genuchten M.T., 1980. A closed form equation for predicting the hydraulic conductivity of unsaturated soils. Soil Sci. Soc. Am. J., 44: 892 - 898.

NEW SOLUTIONS IN HARVESTING PLANTS FOR POWER PURPOSES

Marcin Zastempowski, Sylwester Borowski, Jerzy Kaszkowiak*,

University of Technology and Life Sciences in Bydgoszcz
Faculty of Mechanical Engineering, Institute of Machine Operation and Transport
ul. Prof. S. Kaliskiego 7, 85-789 Bydgoszcz, Poland
Phone: +48523408208, Fax: +48523408462
e-mail: kaszk@utp.edu.pl

Abstract

At the Farm Engineering Department of the University of Technology and Life Science in Bydgoszcz, there have been conducted continuous studies aiming at drawing up new solutions concerning harvesting of plants for power purposes. New constructions of working assemblies of farm machines with special consideration of cutting units are being designed, as well as technologies of preservation of plant material are being improved.

In the article there are presented new constructions of shear-finger cutting blocks and the drum cutting unit as well as selected issues connected with application of preserving formulations at the time of plants' harvesting with the use of chaff cutters.

Keywords: plant, harvesting, power purpose

Introduction

The technological process of cutting of plant material is one of the most important processes realised within the frames of acquiring plant material for power purposes. One of the basic working cutting units, that task of which is cutting of plant material, is the shear-finger cutting block.

The existing constructional solutions of shear-finger cutting blocks are characterised by high energy consumption of the realised cutting process, and their constructional solutions haven't changed considerably for a long period of time.

The drum cutting unit is the second basic cutting unit, the task of which is cutting of the layer of the plant material into chaff. It is widely used in field chaff cutters. Similarly like in case of the shear-finger cutting unit, its construction was not substantially affected by changes related to big demand for power in the phase of the cutting process.

The subject matter of the cutting process modeling was already described by Guarnieri, Maglioni and Molari (2007). In their studies, a mathematical lumped-mass model for a reciprocating single-blade cutting bar with a slider-crank mechanism was developed. The equation of motion was numerically integrated, and the influence of geometric, kinematic, dynamic, and biological parameters was investigated. The analysis demonstrated the uselessness of the crank disc inertia and pointed out that the system imbalance was due more to the periodic instability of the motion and torque than to the alternative inertia force of the blade. The analysis also demonstrated the existence of an optimum running speed that minimizes instability and, thus, imbalance and demonstrates that the cutting resistance decreases as the running speed increases (Guarnieri et al., 2007).

That is why, at the Faculty of Mechanical Engineering of the University of Technology and Life Science in Bydgoszcz, there have been conducted continued activities timing at drawing up of new constructions of operating units of farm machines with particular consideration of cutting units and the improvement of the technology of plant material's preservation

The main effect of the conducted studies on energy-consumption of the shear-finger and the drum cutting units, was drawing up of new energy-saving constructions of both the cutting units (Zastempowski, Bochat, 2012; Bochat, 2010).

New constructions of cutting units

The essence of a new shear-finger cutting unit's construction (Fig. 1) is characterized by the fact, that in place of standard slide buttons there have been used innovative buttons (new construction) having a hole in which a roller embedded on a bolt is placed. Additionally, there is used a knife strip of a decreased cross-section and the surface of fingers, the knife strip cooperates with, were subject to the process of electroplating. These treatments are to allow to lower the demand for power necessary to overcome the friction forces in the dead movement of the cutting unit.

The shear-finger cutting unit presented in Fig. 1 consists of two basic elements: an immovable finger beam (2) and a knife strip (4). Double fingers (6), the lateral edges of which constitute a counter-cutting edge, are attached to the finger beam. In the curse of operation of the cutting unit, the knife strip (4) makes a plane-return movement, and together with it the knives (5) attached to the knife strip (4) move . In the described shear-finger cutting unit, to assure correct adherence of knives to the counter-cutting edges, there are applied buttons (3) of innovative construction, that are placed at every second double finger. On the surface of knives there are mounted cover plates (1) constituting a raceway for rollers. Such a solution made it possible to eliminate slide friction between the button and the knife (occurring in known shear-finger cutting units), replacing them with rolling friction between the button's roller and the knife's cover plate. As a result, such a construction of the cutting unit causes the decrease of resistance to motion coming from friction forces.

Moreover, the surfaces of fingers, along which knives and the knife strip move, are covered with chromium by the use of the process of electroplating. Layers of that type on specific surfaces are characterized by increased hardness, abrasion resistance and there was obtained the effect of the decrease of the friction coefficient between the cooperating elements.

Additionally, in this new construction of the cutting unit, to make the knife strip there has been used steel 15H. This fact resulted in the increase of resistance and hardness of the knife strip as compared to the traditional solution. Thanks to that, it was possible to reduce the area of the knife strip's cross-section by half, the result of what is lowering of its mass.

Changes of that type have a considerable impact on the decrease of friction and inertial forces, what directly translates into the decrease of demand for the power from the shear-finger cutting unit.

In Fig. 2 there is presented a new, energy-saving construction of the drum cutting unit.

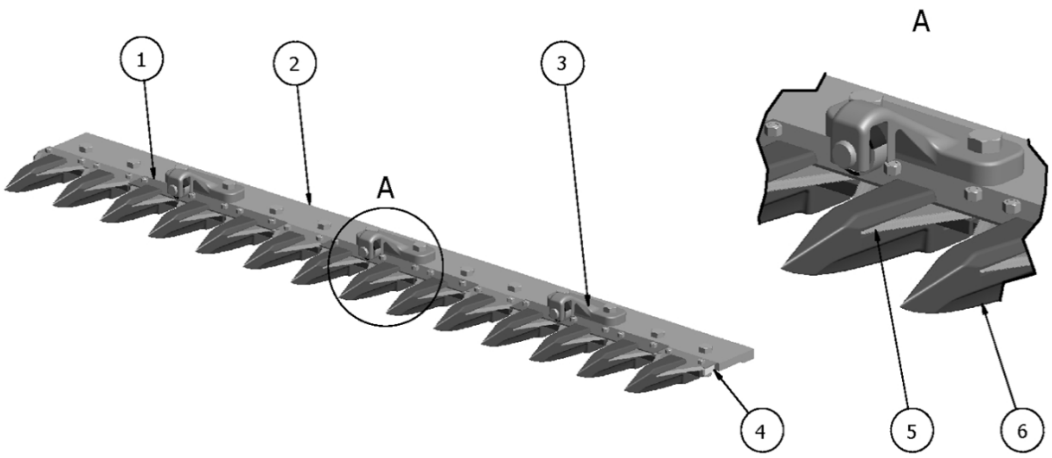

Fig. 1 New construction of the shear-finger cutting unit
1 - tool tip, 2 – finger beam, 3 – push button, 4 – knife strip, 5 – knife, 6 –finger

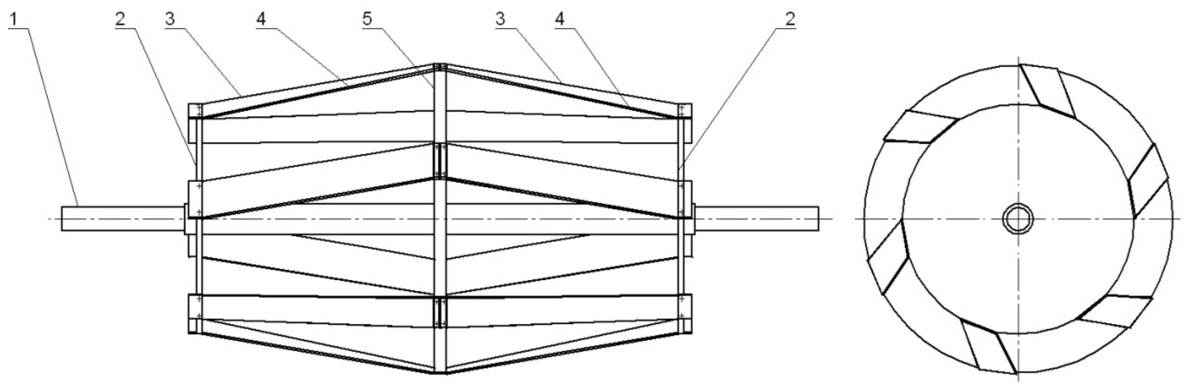

Fig. 2 New construction of the cutting drum
1 – shaft, 2 – external shields, 3 – knives, 4 – cutting edges of knives, 5 – center shield

New construction of the cutting drum is the subject matter of the patent application. The essence of the new construction, presented in the Fig. 2 consists in the fact, that the cutting drum constitutes the driving shaft on which three shields are mounted. The center shield has a bigger diameter as compared to side ones having equal diameters. Knives in the V configuration of straight or bended edges are screwed down to the shield directly with screws along the screw line. Novelty of the cutting drum's construction lies in the fact, that the material will be cut in a sloping and not in a lateral mode, what occurs in case of application of the existing constructions of cutting drums. The result of it is considerable lowering of energy-consumption of the process of plant material's cutting into chaff.

Additives used at silaging of biogas works' substrates

Lactic fermentation conducted by lactic acid's bacteria is a common method of preservation of plant raw material to be used for production of fodder and acquiring substrate for biogas works (Kalač, 2011; Dorszewski, 2005). The technology of preparing silages to be used as charge – coenzyme for biogas production in farm biogas works is almost the same as in case of silaging of fodder for animals. Moldy fodders do not fit to be used for biogas production, as on their quality there depends the volume of obtained gas and bioethane included in it. Strong pollution with soil results in the fact, that biomass includes lots of bacteria Clostridium, what results in secondary fermentation (butyric fermentation) in the stable phase of silaging. Saccharolitic species decompose sugar essential for lactic bacteria, while proteolytic species - protein (McEniry et al., 2006). Decomposition of that nutrient leads to formation of amines and ammonia, which inhibit expansion of methanogenic bacteria. On the other hand moulds produce mycotoxines (secondary metabolites), which also inhibit expansion of these bacteria due to what lowering of efficiency of biogas production occurs.

In case of shredding of raw material to be silaged, green fodder that is silaged to be the fodder for animals, should be shredded into chaff of the length from 15 to 30 mm, what results from physiological needs of ruminants. In case of raw material for agro-biogas Works shredding should be smaller – 4 to 8 mm, what increases the area available to bacterial enzymes, and at the same time the volume of biogas production.

In case of production of silages for ruminants, important is to obtain fodder of high content of lactic acid and lower of acetic acid. Application of such silage as batch – coenzyme in biogas works is limited, as methane bacteria poorly decompose lactic acid, while quite well as acetic acid, propanoic acid and alcohols (Kalač, 2011). Due to that, to silage plants for that purpose, recommended is the use of silage additives including lactic heterofermentative bacteria, in particular Lactobacillus buchneri, which shall not result in excessive acidification of future batch –coenzyme with lactic acid but with acetic acid (Kalač, 2011). However, the process of heterofermentation leads to fermentation losses (Banemann et al., 2008, 2009; Nussbaum, 2012).

It is the best to apply additives controlling the process of fermentation during harvest of biogas works' substrates, at their harvest time. Then, the best mixing of an additive with the harvested plant material is obtained. However, due to the costs of preserving formulas, farmers often tend to decrease the volumes of formulas added to silage green mass. It may result in formation of places without the access of formula, in which detrimental processes occur. In order to prevent that, in the Farm Technology Department there are conducted studies on the use of automatic regulation of the formula's dose depending on temporary efficiency of picking-up machine (Borowski, 2012).

One of the used innovative methods is marking of biologically active additives with the use of n-hexane. With reference to the so-far used methods, it allows to maintain full safety, and silages obtained in such a manner may be used for production of biogas or feeding animals (Borowski, 2012).

Conclusion

Due to the continuous increase of demand for plant material for power purposes, attention started to be paid to not only the manner and the costs of its generation but also at the costs related to the losses generated by its incorrect storage or processing.

In order to limit the costs efficiently, attention should be paid to Power-consumption of the cutting process and effectiveness of conducting of the process of plant material's silaging. Agricultural Technique Faculty of the University of Technology and Life Sciences in Bydgoszcz has been dealing with these issues. New constructions of cutting units that are to guarantee lowering of the power demand in the process of plant material's cutting have been drawn up. There have also been conducted works on optimization of application of additives steering the process of fermentation at the time of collection of substrates for biogas works.

Due to the fact, that the time of material's harvesting is the best moment for formulations' application, that is why in particular works have been conducted on automation of formulation dosage's regulation depending on temporary machine's efficiency.

References

Banemann D., Mayrhuber E., Schein H., Nelles M., 2008. Effect of homo- and heterofermentative silagen additive on the methan yield of mais silage. Proc. of 13th Int. Conf. Fooder conservation, Nitra, Slovak Republic, 156-157.
Banemann D., Nelles M., Thaysen J., 2009. Silages as feedstock for biogas: Novel perspectives for silage additives. Proc. of XVth Int. Silage Conf., Madison, Wisconsin, USA, 355-356.
Bochat A., 2010. Theory and design of cutting units of agricultural machines. (Teoria i konstrukcja zespołów tnących maszyn rolniczych. Published by University of Technology and Life Sciences in Bydgoszcz , Bydgoszcz.
Borowski S., 2012. Controlling Rate Of Delivery Of Applicators At The Harvest Of Substrates Biogasworks - Preliminary Issues, Journal of POLISH CIMAC, 7(3): 17-22.
Dorszewski P., 2005. Effect of different additives to pickling on the number of yeats, moulds and arobic instability of maize silages (Wpływ różnych dodatków kiszonkarskich na liczebnośc drożdży, pleśni i niestabilność tlenową kiszonek z kukurydzy). Med. Weter. 61(8): 919-922.
Guarnieri A., Maglioni C., Molari G., 2007. Dynamic analysis of reciprocating single-blade cutter bars. Transaction of ASABE, 50(3): 755-764.
Kalač P., 2011. The required characteristics of ensiled crops used as a feedstock for biogas production: a review. J. Agrobiol, 28: 85-96.
McEniry J., O'Kiely P., Clipson N.J.W., Forristal P.D., Doyle E.M., 2006. The microbiological and chemical composition of baled and precision-chop silages on a sample of farms in County Meath. Irish J. Agric. Food Res., 45: 73-83.
Nussbaum H., 2012. Effects of silage additives based on homo- and heterofermentative lactic acid bacteria on methane yields in the biogas processing. Proc. of XVIth Int. Silage Conf., Hämmenlinna, Finland, 452-453.
Weissbach F., 2009. Prediction of biogas production potential of silages. Proc. of XVth Int. Silage Conf., Madison, Wisconsin, USA, 189-190.
Yiljep Y.D., Mohammed U.S., 2005. Effect of knife velocity on cutting energy and efficiency during impact cutting of sorghum stalk. Agricultural Engineering International. Manuscript PM 05 004, VII.
Zastempowski M., Bochat A., 2012. Selected aspects of the designing an energy efficient constructions of scissor-finger cutting unit (Wybrane aspekty projektowania energooszczędnej konstrukcji nożycowo-palcowego zespołu tnącego). Journal Research and Applications in Agricultural Engineering, 57(4): 212-216.

CORRELATION OF SOIL MOISTURE AND DAILY DISCHARGE OSCILLATIONS OF STAROSUCHDOLSKÝ BROOK

Josef Zeman[1*], Šárka Dvořáková[1]

[1]Czech University of Life Sciences Prague, Faculty of Engineering, Kamýcká 129, 165 21 Prague 6 – Suchdol, Czech Republic, e-mail: zeman@dzeta.cz

Abstract

In some cases, the evaluation of the watershed structure with the classic methodology, which is based on the idea of grouping of flood waves of all soil zones, is not suitable. In the case of some watersheds there is a large time shift in start of separate waves coming from different layers of soil and unabsorbed water. An example of such watershed is the watershed of Starosuchdolský brook in which we measure the discharge continuously for two years. The content of this paper is to describe the process of separation of individual waves and to find out all hydrological characteristics for each absorbing zone separately already in compliance with the original methodology. Also, it is possible to determine the permeability coefficient already beyond the original methodology.

Keywords: soil moisture, Starosuchdolský brook

Introduction

The part of water, which comes into the watershed with a rain, flows through the water channel with time. Through this water channel then subsequently runs away from the watershed. The flows, by which precipitation water reaches the water channel, we can usually divide into three main groups (Fig. 1).

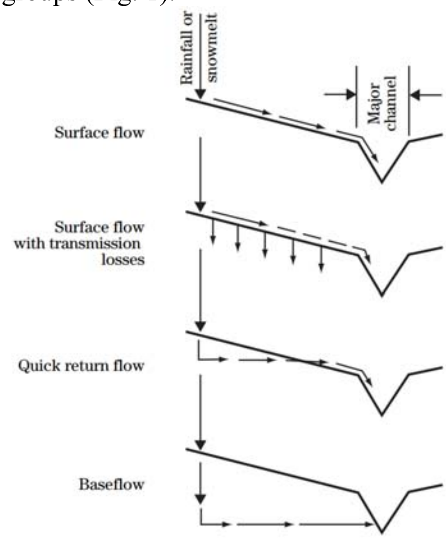

Fig. 1 Types of flow

The first part is formed by the water, which does not infiltrate at all after falling on the ground. This part therefore only runs along the surface and it is therefore in the channel as first. Time, in which this water reaches the water channel, is influenced by the segmentation of the surface and by the watershed slope. The porosity of the soil does not play any role however. The size of this component, i.e. the percentage of non-infiltrated water, however, may depend on the water saturation of the upper soil zone. The second part of the precipitation water leaving through the water channel forms the contribution which is infiltrated after falling on the ground, but already slightly lower rises to the surface again and continues to the water channel already along the surface. The third group consists of paths of water that are all implemented under the surface and can pass also through deep soil zones. Infiltration through these layers may take a very long time. The time needed for the transport of precipitation water to the water channel is proportional both to the distance from the water channel and to the slope of this path of water. Generally the effects of the separate tributaries are summed in the water channel and they form together the shape of the runoff hydrograph (Fig. 2).

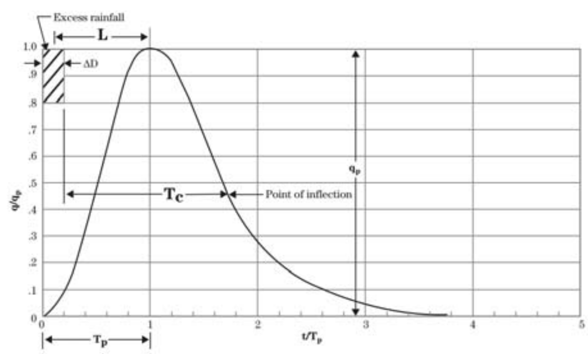

Fig. 2 A shape of the runoff hydrograph with marked characteristic values

where:

L	…	lag [day]
ΔD	…	duration of excess rainfall [day]
q	…	discharge at time t [litre.s^{-1}]
q_p	…	peak discharge at time T_p [litre.s^{-1}]
T_p	...	time to peak [day]
T_c	…	time of concentration [litre.s^{-1}]

As we usually don´t know the analytical shape of the final hydrograph, we characterize the drainage curve with the help of the following time indicators. The first point of inflection of the curve is called the starting part T_s, the runoff curve maximum is denoted as T_p and the second inflection point T_k. The distance between inflection points T_k and T_s is the time of concentration T_c. By flowing through the water channel the runoff wave is gradually modified and it changes to the flood wave with increasing slope of the forehead, in accordance with the Navier-Stokes equations. But this effect may be neglected in small rugged basins because we are not able to verify it experimentally. In some watersheds, the times T_c for the separate three groups of paths of water are so different that even inflection points of runoff curves of each type create time disjoint intervals. The watershed of the Starosuchdolský brook is one such example. The aim of this paper is to demonstrate a possible procedure for finding a set of characteristic times for each different type of paths of water of this watershed. The work is a part of a broader systematic survey of this experimental watershed, whose aim is to verify some of the physical models and their applicability to similar small watersheds.

Material and method

From the midyear 2011 we have continuously measured the discharge of the Starosuchdolský brook in two second intervals just before its outlet into the Únětický brook. The average discharge at this location for the last two years was approximately 1.1 (litre.s^{-1}). The discharge over 100 (litre.s^{-1}) occurred in nine episodes and over 10 (litre.s^{-1}) was 116 times. During the survey of behaviour of this brook within the grant study the status of this twelve-hectare watershed was analysed especially in rainless periods. In the first analyses of precipitation episodes according to the methodology described in National Engineering Handbook of United States Department of Agriculture, this method, which is widely used in many other works, proves to be difficultly applicable in this concrete watershed. The main difficulty lies in the fact that in the watershed investigated by us the runoff curve with one peak does not arise, but it has three peaks. These peaks are formed by gradual drainage of separate soil zones. There is a way how to separate these three virtually independent flood wave from each other.

This fact makes somewhat difficult to use the conventional methodology described in National Engineering Handbook of United States Department of Agriculture (Woodward, 2010), but allows to analyse in more details the flow contribution of each zone to the total measured discharge of the Starosuchdolský brook. The actual separation of the individual contributions is always carried out in several steps. We can show this method on the precipitation episode of 29.4.-3.5.2013 when, according to the CULS meteorological station measurement, 0.7 mm of precipitation fell down in 6 minutes. This episode was chosen because it was a quick rainfall, which however does not significantly affect the weather of this day and evapotranspiration conditions remained for all this day practically the same as in the preceding rainless days. It allows to make the first step in the following separation process. The hydrograph of the measured discharge of Starosuchdolský brook affected by this episode we can see on Fig. 3.

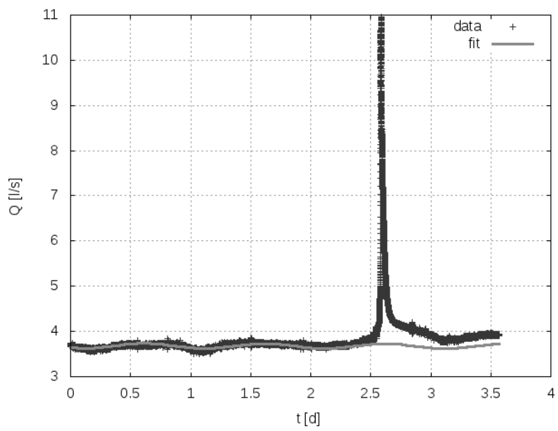

Fig. 3 Measured data at 29.4.-3.5.2013 approximated by function (1), which allows to find rainless days trends

At the first glance, it is evident that the discharge through the water channel differs significantly from the curve under consideration of methodology described in National Engineering Handbook of United States Department of Agriculture. Before the separation it is necessary to eliminate the influence of evapotranspiration and the retention trend of the previous days. From the linear model (Dvořáková et al., 2012) follows the shape of the curve given by equation (1) in which for the inclusion of evapotranspiration two main members of the Fourier series are taken (Mošna et al., 1999).

$$Q(t) = A \cdot e^{\frac{-t}{\tau_0}} + B \cdot e^{\frac{-t}{\tau_1}} + C \cdot \sin(2\pi(t+t_0)) + D \cdot \sin(4\pi(t+t_1)) \qquad (1)$$

where:

Q(t) [litre.s-1]	Starosuchdolský brook discharge
A, B	initial relative water storages in the upper (A) and middle (B) soil zone of the brook's riparian section [litre.s^{-1}]
τ_0, τ_1	half term duration during which the water reserve in zones A, B on 1/e, with the Euler constant [day]
C, D	depth of evapotranspiration [litre.s^{-1}]
t	duration of the time lapse [day]
t_0, t_1	time shift between the maximum evapotranspiration and midnight UTC [day]

Approximation of the function (1) from measured data we can see also on Fig. 3. By subtraction of this relation we obtain the function, which we can see on Fig. 4.

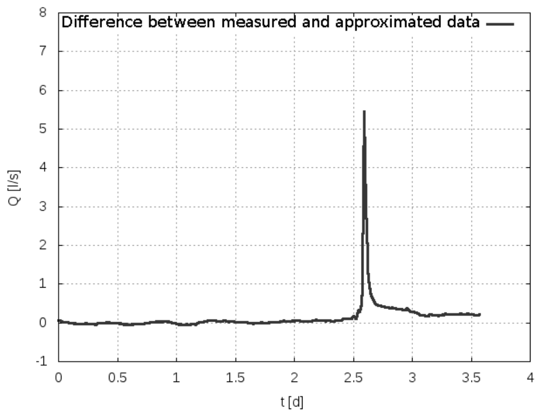

Fig. 4 Hydrograph of the rainfall event after subtraction of long-time trends and evapotranspirational fluctuations

We can see that in the rainless period there are only small fluctuations up to 0.018 l / s. Fig. 4 shows a detail of the same period, only with showing the rainfall episode and its effects to the flow through the Starosuchdolský brook water channel. In this way we get over, under the assumption of the separability of this problem, the influence of the long-term trends of runoff.

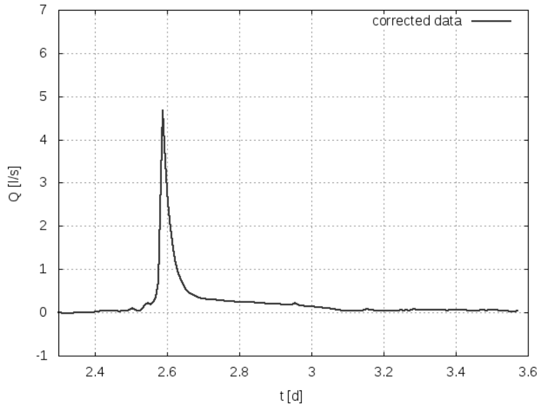

Fig. 5 Detailed hydrograph of flood wave

The starting limb of the hydrograph we cannot describe without solving the Navier-Stokes equations, but behind an inflection point in the decreasing part of the hydrograph we are able to develop their solution into a series of decreasing exponential curves effectively. We are satisfied with the first two terms of these series, as the residue is much smaller than the accuracy of our measurements. Thus in this section we use the approximate prescription (2).

$$Q(t) = E \cdot e^{\frac{-t}{\tau_2}} + F \cdot e^{\frac{-t}{\tau_3}} \qquad (2)$$

where:

E, F	main coefficients of the declining limb of runoff hydrograph
τ_2, τ_3	half term duration during which the water reserve in zones A, B on 1/e, with the Euler constant [day]
t	duration of the time lapse [day]

This separation, of course, cannot be done in general, but in the case of Starosuchdolský brook we are lucky. When we display the discharge through the water channel after subtracting the surface flood wave approximated by equation (2), we obtain the graph on Fig. 6. We can see that the accession of the flood wave coming from the infiltration of the surface zone comes after the absorption of the flood wave caused by the water flowing on the surface.

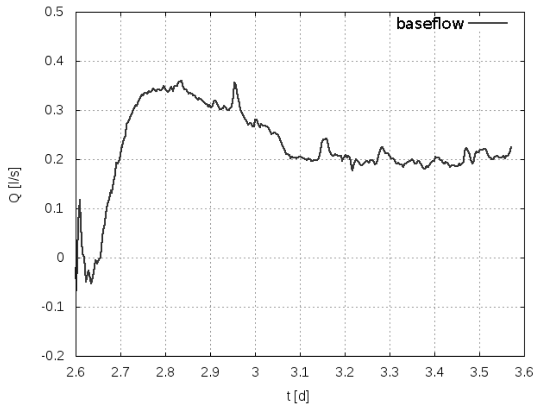

Fig. 6 Separated part of flood wave (It represents the sum of contributions of the middle and the lower zone.)

It is possible to separate the parts of the flow which flow through middle and lower soil zones in a similar way. For this analysis we need a longer rainless period than followed after this sample precipitation episode of 29.4.-3.5.2013. But the effect of a contribution of the lower zone is evident also in this episode, namely at the end of this period, where instead of exponential decrease of flow due to depletion of the upper zone there is again a small, but clear increase of the flow in the water channel.

The travel time to peak (3) is given partly by average slope of the trajectory, partly by the porosity of soil *P* and partly by average length of the trajectory *l*.

$$T_p = \frac{l}{v} \tag{3}$$

where:
T_p time to peak [day]
l average length of the trajectory of water [m]
v average velocity of discharge [m/s]

In the case of Starosuchdolský brook we can consider the average slope of all layers the same, namely 1/10. Also the average length of falling of the water to the water channel is 300 m for all layers.

Results and discussion

It is necessary to appreciate above all that thanks to the separation of individual contributions we are able to find times T_p and T_c for every type of flow separately and from them also separately determine mechanical parameters for separate zones. The time values found for Starosuchdolský brook are given in Tab. 1.

Tab. 1 Outflow characteristics of separate soil zones

Type of flow	T_p [day]	T_c [day]	q_p [litre.s^{-1}]	V [m^3]	v [m/s]
Surface flow	0.081	0.05	5.5	1.044	0.042
Quick return flow	0.293	0.56	0.34	0.684	0.012
Base-flow	1.8	4.51	0.23	3.6	0.002

where V … total runoff volume [m^3].

Conclusion

It appeared that with a certain modification of the conservative approach described in National Engineering Handbook of United States Department of Agriculture a successful separation of the effects of the contributions of soil zones to the resulting discharge can be implement, at least at some small streams, but certainly in the case of Starosuchdolský brook. We are able gradually to separate the part of flow caused by outflow of rainwater on the surface from the total flow and thus to see the total separated contribution of infiltrated waters, which then we can differentiate to the quick return flow and base-flow. In this way we are able to find also some watershed parameters that cannot be determined from the unmodified conservative analysis.

Acknowledgement

This paper was supported by the Czech Technological Agency, Project TA02020402 (Water regime optimisation to mitigate impacts on hydrological extremes).

Reference

Dvořáková Š., Kovář P., Zeman J., 2012. Implementation of conceptual linear storage model of runoff with diurnal fluctuation in rainless periods, Journal of Hydrology and Hydromechanics, 60(4): 217-226.
Mošna F., Nečas J., 1999. Nonlinear hyperbolic equations with dissipative temporal and spatial non-local memory, Zeitschrift fur Analysis und ihre Anwendungen 1999, Leipzig, 18(4): 939 – 951.

INVENTER´S EFFICIENCY IN SOLAR SYSTEM MĚNÍN

Beránek, V.*, Jan Sedláček

Czech University of Life Sciences Prague, Czech Republic

Abstract

The photovoltaic power plant was constructed according to our project and the monitoring was developed by us. Few types of inverters were compared during the data monitoring. The results are presented.

Keywords: energy, solar system, photovoltaic

Introduction

The objective of this testing is to determine the efficiency of the photovoltaic power plant (hereinafter referred to as PVP) mainly their sub-components such as inverters and transformers. At the Měnín 3.3 MW_p PVP are tested four types of inverters and also their long-term analysis are performed there. These are the decentralized inverters SMA 7000TL, Refusol 15, Fronius IG150+ and Vacon NXI 45 The benefit of this experiment is more accurate measurement of PVP from tens to units of percent and defining the appropriateness of the inverter technologies for construction of more power plants.

Experimental arrangement

The power plant Měnín (3.3 MW_p) was constructed by the author and the monitoring was developed by the corresponding author during his Ph.D. study (Beránek, Libra, 2010; Beránek, Libra, 2010). The power plant was created as research centre, it consists of 4 parts with different types of inverters. We tested 3 types of wiring of PV panels.

- 1. type of string – top line of PV panels is connected in series, each top line strings are parallel connected into one inverter,
- 2. type of string – lower line of PV panels is connected in series, each top line strings are parallel connected into one inverter,
- 3. type - combination of both types.

Fig. 1 shows the PV power plant Měnín 3.3 MW_p and the detail of the inverters SMA.

Results and discussion

Calculation of the overall effectiveness of PVP

The most important and the most wanted result of constructing, monitoring and diagnosing of the photovoltaic power plants is the overall efficiency of the plant. The literature often names it as the performance ratio (hereinafter referred PR). Tab. 1 shows energy losses measured during the August 2012 at the Měnín PVP. In order to run the measurements ideal conditions had to occur, therefore, the amount of incoming radiation to be larger than 500 W/m^2 at least 30 minutes. The difference in radiation during this period could not be greater than 10 %. After eliminating these values, these results can be considered very accurate. During measurement distortion due to varying incident radiation was avoided and measuring devices were in the range of the best accuracy class specified by the manufacturer. Overall, we were able to record 13 samples complying with the conditions. Measurements were carried out only at maximum output power. From Tab. 1 it is clear that we measured E_{dc}, which is the theoretical energy generated by panels in a given time period. In addition, we measured E_{ac} (energy measured at the output of the inverters), E_{tr} (energy run trough the electro-meter). E_{dc} is a theoretical value based on the panels. With this we can say that the loss of DC move at maximum load from 3 % to 7 % and average is 4.9 %. Losses in AC – it is losses on the plus substation, ranging from 0.8 % to 2.9 % and average is 1.9 %. Overall power plant efficiency is between 90 % and 94 %. Measurement was carried out on 18 samples of those, so that we can consider it very accurate. Measurement of this kind is done only at maximum load, because here it shows weakness of any part of PVP. The average annual efficiency of photovoltaic power Měnín is 13.5 %. This efficiency includes rainy days and start of the plant.

Calculation of inverters efficiency

Four kinds of inventors were installed on PVP Měnín for better choice of technology for future power plant construction. From January 2011 are measured inverters 2x VACON45k - NXI75, 2 FRONIUS12 5k - 150IG +, 2x and 2x REFUSOL15k SMA17000 TL. The same types of panels were installed and plugged in on these samples so the inverters efficiency was the biggest possible. Tab. 2 presents the statistics of energy produced - converted to unit power of the panel so called kilo watt peak (kW_p hereinafter) from January 2011 to April 2012. There are reported means of daily energy in months. The statistics show that the best inverters are REFUSOL and the inverters with the least efficiency are FRONIUS. However, during testing was found that some types of inverters - e.g. mentioned Fronius type of inverter work better in a bad weather, but when loaded on maximum these drives show a below-average efficiency. Furthermore, on SMA inverters there has been tested different connection to solar panels. If we connect the top and bottom panels separately, this means that annually we produce about 0.09 % more energy, which means that due to the results it is recommended to divide the wiring panels on the upper and lower range even at higher cost for wiring. The results show that the best solution is the REFUSOL technology. Tab. 4 shows the efficiency of individual technologies. This confirms the results in Tab. 2 only measured by other devices. Increased production is mainly due to better efficiency. It even has a greater impact than better connection of panels. Measurement was carried out again under the same conditions; measuring instruments are part of the inverters only in the tested samples (Tab. 2 and 3). Calibrated gauges were used and they were connected directly to the monitoring system SOLARMON.

The calculation comparing two types of solar panels wiring

Tab. 2 describes two options for connecting solar panels. Two SMA inverters 700TL were involved as test the drive. In the first test drive, the panels are connected top and bottom panel together and in the second test drive the panels are connected at the top and bottom line I separately. It is obvious that the largest energy differences are in the winter months, which also implies the way of connection. However we can say that it is a very small amount of energy, as in the winter months there is less sunshine hours. The connection system is therefore very suitable for plants where at the first place was counted with less land, respectively where the constructor must take into account the plot size and power output. Lines have to be closer together due to lack of space on the property. In other cases where the main requirement is not given to the size of the land, the use of upper and lower row does not increase power plant efficiency (number of panels may be at a greater distance from each other).

Tab. 1 Total energy losses of the power plant Měnín 3,3 MW_p

Date 2012	Day average solar radiation M_e (W/m^2)	Average of module temperature t_p (°C)	Theoretical DC energy E_{dc} (kWh)	DC losses (%)	AC energy of inverters E_{ac} (kWh)	AC losses (%)	Substation energy E_{tr} (kWh)	PV systems losses (%)	Performance ratio PR (%)
30.8.	890,5	51,1	1474	4,74	1404	1,9	1377	6,6	93,4
29.8.	941	53,8	1507	5	1431	2,0	1403	6,9	93,1
28.8.	938	45,4	1618	7,31	1500	1,9	1472	9,4	91,0
23.8.	791	49,6	1333	4,33	1275	1,6	1254	5,9	94,1
22.8.	892	57,8	1381	3,09	1339	2,3	1311	5,6	94,9
20.8.	885,5	56,1	1432	4,3	1370	2,0	1343	6,2	93,8
19.8.	907	55,7	1468	5	1394	2,0	1367	6,9	93,1
18.8.	910	55,5	1490	4,16	1428	2,0	1400	6,2	94,0
15.8.	911	49,4	1549	4,07	1486	1,8	1459	5,8	94,2
14.8.	985,5	43,3	1664	5,88	1566	1,8	1538	7,6	92,4
13.8.	580	34,0	1068	5,94	1004	0,8	997	6,7	93,4
10.8.	598	30,7	1116	6,66	1042	0,8	1034	7,4	92,6
9.8.	883,5	50,4	1485	2,97	1441	2,2	1410	5,8	94,9
6.8.	891,5	58,8	1415	4,69	1349	2,9	1321	6,7	93,3
5.8.	952	51,4	1602	7,94	1475	1,9	1446	9,7	90,3
4.8.	871,5	55,8	1427	3,34	1379	2,9	1350	5,4	94,6
2.8.	916	51,0	1533	6,58	1432	1,8	1406	8,3	91,7
1.8.	931,5	55,4	1545	4,54	1475	2	1445	6,5	93,6
Average	870,9	50,3	1450	4,9	1377	1,9	1352	6,8	93,2

Tab. 2 Average monthly energy amount per W_p of tested inverters (kWh/kW_p)

Date	SMA1 new part (modules are together) (kWh/kW_p)	SMA2 old part (modules are separate) (kWh/kW_p)	Difference of energy per kW_p
1/2011	0,82	0,84	-0,02
2/2011	1,80	1,90	-0,10
3/2011	3,73	4,00	-0,27
4/2011	4,07	4,21	-0,14
5/2011	5,22	5,28	-0,06
6/2011	3,96	3,92	0,03
7/2011	4,41	4,45	-0,04
8/2011	4,12	4,26	-0,14
9/2011	2,11	2,19	-0,08
10/2011	1,28	1,34	-0,06
12/2011	0,61	0,59	0,02
1/2012	1,26	1,33	-0,08
2/2012	2,37	2,55	-0,17
3/2012	3,64	3,79	-0,15
4/2012	4,10	4,18	-0,07
Yearly average on W_p	**2,90**	**2,99**	-0,09
Difference of power %	**2,95**		**-1,32**

Tab. 3 Average monthly energy amount per W_p of tested inverters (kWh/kW_p)

Date	VACON 1	VACON 2	FRONIUS 1	FRONIUS 2	REFU-SOL 1	REFU-SOL 2	SMA 1 new part	SMA 2 old part
1/2011	0,88	0,85	0,82	0,74	0,89	0,91	0,82	0,84
2/2011	1,88	1,87	1,88	1,77	1,88	1,76	1,80	1,90
3/2011	3,93	3,94	3,91	3,77	3,92	4,02	3,73	4,00
4/2011	4,20	4,22	4,16	4,11	4,20	4,30	4,07	4,21
5/2011	5,31	5,23	5,10	5,09	5,30	5,42	5,22	5,28
6/2011	3,99	4,00	3,81	3,81	3,99	4,09	3,96	3,92
8/2011	4,46	4,48	4,64	4,28	4,43	4,54	4,41	4,45
9/2011	4,20	4,20	4,14	4,04	4,17	4,27	4,12	4,26
10/2011	2,15	2,13	2,15	2,06	2,16	2,21	2,11	2,19
11/2011	1,37	1,33	1,30	1,21	1,37	1,05	1,28	1,34
12/2011	0,80	0,73	0,50	0,39	0,80	0,73	0,61	0,59
1/2012	1,41	1,36	1,28	1,16	1,41	1,45	1,26	1,33
2/2012	2,51	2,51	2,53	2,37	2,46	2,53	2,37	2,55
3/2012	3,74	3,74	3,71	3,58	3,72	3,82	3,64	3,79
4/2012	4,19	4,19	4,06	4,00	4,17	4,28	4,10	4,18
Annual average of mean values of daily energy calculated per kW_p	**3,00**	**2,99**	**2,93**	**2,83 the worst**	**2,99**	**3,03 the best**	**2,90**	**2,99**


Fig. 1 PV power plant Měnín 3.3 MW$_p$ and the detail of the inverters SMA

Tab. 4 Average monthly energy amount per kW$_p$ of tested inverters (different type of measurement) (kWh/kW$_p$)

Name of inverters	DC power P_{dc} (W)	Losses of inverter (%)	AC power P_{ac} (W)
SMA 7000TL	1880	2,81	1827
SMA 7000TL	1827	2,65	1779
Vacon NXI	8360	5,85	7871
Vacon NXI	8850	5,85	8332
Fronius 12,5k	3468	6,29	3250
Fronius 12,5k	3915	6,23	3671
Refusol 15k	1832	1,48	1806
Refusol 15k	1759	1,74	1758

Conclusion

Monitoring of the experimental power plant showed next results:

- Efficiencies of different types of inverters various, Refusol are the best, some types of inverters are more repairing,
- 1. type of string is the best type of wiring – top line of PV panels is connected in series, each top line strings are parallel connected into one inverter,
- The project engineers can use the results in the future for PV power plants planning.

The references (Poulek et al., 2012; Poulek, Libra, 2000) show the possibilities how to subsequently increase the lifetime and the efficiency of the PV power plant.

References

Beránek V., Libra M., 2010. Monitorovací systém pro fotovoltaické. Jemná mechanika a optika. 55, 9, 250-252, ISSN 0447-6441 (in Czech).

Beránek V., Libra M., 2010. Monitoring system for photovoltaic power plant. In Proc. 4th International Conference on Trends in Agricultural Engineering, Prague, 7-10 September 2010, 668-675, ISBN 978-80-213-2088-8.

Poulek V., Libra M., 2000. A New Low Cost Tracking Ridge Concentrator, Solar Energy Materials and Solar Cells, 61, 2, 199-202.

Poulek V., Strebkov D. S., Persic I.S., Libra M., 2012. Towards 50 years lifetime of PV panels laminated with silicone gel technology. Solar Energy, 86, 10, 3103–3108.

EFFECT OF ENVIRONMENTAL DEGRADATION ON THE ADHESIVE BONDS STRENGTH AND DURABILITY

Jan Cidlina*, Petr Henc

Czech University of Life Sciences in Prague, 165 21 Prague 6 – Suchdol, Czech Republic
Phone: +420224383263, E-mail: cidlina@tf.czu.cz

Abstract

Adhesive technology is currently perspective and dynamically evolving method of the material bonding. With the growing rate of the application of adhesives in the industry, there is need of further tests and studies of the effects which negatively influence on adhesive bond strength and durability. Environment is one of the aspects that influence bond strength and durability. The aim of the experiments was to determine interaction between bond strength and selected environmental degradation. The bond strength of all tested specimens in the environmental degradation decreased. The results also show that methyl methacrylate adhesives (MMA) are more durable than tested epoxy adhesives.

Keywords: degradation process, adhesives, methyl metacrylates, epoxy, ultimate strength

Introduction

In common-practice is adhesive bonding technology used as a complementary method to conventional methods of material joining. Currently it is difficult to imagine a variety of industries without adhesive technology, for example in the automotive or aerospace industry. Application of the adhesive bonding technology has a growing trend in these industries due to the positive properties of adhesive technologies, such as low weight of the bonds or a rate to make adhesive bond connection. Adhesive bonding technology has many advantages as well as many disadvantages, for example adhesive bonding durability, which is lower in a compare with conventional joining methods such as welding, riveting and so on. Instead of some type stress is durability affected mainly by conditions, which can greatly accelerate the degradation of adhesive bonds.

Process of the adhesive bond degradation respectively of the adhesive can be divided into the followed three phases: degradation during the storing of the adhesive, degradation during the curing process of the adhesive, degradation of the adhesive after the curing process.

In the cause of the first phases of degradation is pointed in experiments by Müller et al. (2005) importance of the expiration time respect and correct storing. The second phase of the degradation process is dealt in the papers by Henc et al. (2011). There was found that higher temperatures accelerate the curing process and have a positive effect on the ultimate strength. During the curing process the lower temperatures, than temperatures recommended by the manufacturer, lead to the extending of the curing process and ultimate strength is rapidly lower. Degradation of adhesive after the curing process is a long-term process in the adhesive bond life cycle. The main aspects that affect the strength and durability of bonds are time and conditions. Conditions to which are exposed the adhesive bonds have a various character according to broad range of adhesive application. Each condition to which is adhesive bond exposed affect final strength of the adhesive bond depending on time. One of the many factors is water, or atmospheric moisture.

The effect of moisture on the mechanical properties of epoxy adhesives is discussed in the article by Lapique and Redford (2002). The test specimens were in experiments exposed at 40 °C and humidity of 90 - 100 %. After 36 days of exposure the value of ultimate strength and elastic modulus decreased about 40 %. Experiments confirm the significant effect of moisture on the strength and durability of adhesive bonds.

The importance about relevance of different climatic environment or moisture is evident from experiments conducted by Herak et al. (2009). There was assessed the environmental condition effects on the strength of adhesive bonds which were exposed for eight months (measured with two month step) in the conditions of the tropical climate of Indonesia, specifically in the three regions with different altitudes, daily temperature and relative humidity. In all cases it was found that the strength of adhesive bonds rapidly decreased during the time. The highest and most stable strength values was achieved in Balige, moderate altitude with the "lower" temperature and relative humidity, while the lowest strength was measured in the region of Medan, at sea level with a "high" temperature and relative humidity. In the region of Medan the strength decreased by 76 %. By the prediction of the future process of the bond strength in these areas was found that in the case of areas Medan and Pagarbatu the strength dropped to zero value till end of one year. In the case of the Balige the strength would reach zero value in about 29 months. Adhesive bonds were not in any stress during the influence of the external conditions. In the case of load or stress exposure there would be expected significantly worse results.

Assertion by Herák et al. (2009) that adhesive bond strength is reduced by climatic conditions was confirmed also in the experiments by Valasek et al. (2012) focused on the effect of climatic conditions that affect the mechanical properties of adhesive bonds in the Czech Republic. Experiments were focused on short-term degradation effect and show downward trend of the ultimate strength of adhesive bonds.

According to Müller and Valasek (2011) it can be asserted that the degradation process has negative effect on all polymeric materials not only with the plastic based, such as adhesives.

Crocombe (1997) found that the degradation of the adhesive bonds depends on the type of adherend and the adhesive, the type of surface preparation of the adherend, configuration, stress configuration and ageing environments.

The beginning values of strength limits of the adhesive bonds can be reduced by degradation processes with time. On the experiments basis which were focused on the degradation processes affecting the adhesive bonds can be asserted that the final strength of adhesive bonds in a time and the simultaneous affecting of conditions decrease. Rate of decrease of the ultimate strength depends on the specific conditions, as pointed Müller and Valasek (2010).

Experimental arrangement

Adhesive bonds are used in a variety of environments due to the experiments were aimed at determining the effect of degradation and extreme environments, such as gasoline. Other environments were brine (salt water) and water bath. In this mediums were verified statements by manufactures about the adhesive strength. In the experiments were also investigated the influence of the exterior conditions.

Degradation of samples was in the regular cycles according to CSN EN ISO 9142 (2004). Selected cycle of degradation was uniform for all environments and occurred with cycle D4 according to CSN EN ISO 9142 (2004). The degradation time was also uniform for all environments, after the 168 hours were the specimens removed from degradation medium and placed in a laboratory conditions again for 168 hours.

In the experiment were used 6 structural adhesives (3 epoxy adhesives and 3 methyl methacrylate adhesives). Specifically were used epoxy adhesives: Uhu plus (hereinafter referred to as "Uhu Akr"), Novafix, Pegamento (hereinafter referred to as "Peg"); and methyl methacrylate adhesives: Novati, Uhu plus (hereinafter referred to as "Uhu Epo") and Perma Oxy (hereinafter referred to as "Oxy"). These adhesives were chosen for its ability to withstand in the range degradation media. Adhesives were applied on steel plates S235J0 with proportion 100 × 25 mm and thickness of 1.5 mm. Procedure for the bonding process was the same in all tested adhesives and occurred with CSN EN 1465 (2009). Steel plates were firstly mechanically surface treated with blasted by synthetic corundum (Al_2O_3) with size of fraction F80. Then was the surface of the sheets decreased in the Perchlorethylen bath. After the surface preparation was applied adhesive on the steel plate in the width 12.5 mm. To define the thickness of the adhesive between the bonded adherends were used distance wires with a diameter of 0.11 mm. To determine the constant pressure was used 0.5 kg weight. After the degradation process was observed ultimate strength on a Universal testing machine.

Results and discussion

The aim of the experiments was to determine the effect of environmental degradation to change the characteristics of adhesive strength. According to hypothesis prepared on the basis of the manufacturer statement is assumed that the structural adhesives are resistant to water. As mentioned above due to degradation the strength limits of adhesive bonds are changed in a time.

Figure 1 show the case of the influence of water, the degradation time on the ultimate strength. From Figure 1 clearly shows the decreasing trend of ultimate strength for all adhesives. Representatives of the methyl methacrylate adhesives are characterized by greater resistance to degradation in the aqueous media compared to epoxy adhesives. The ultimate strength of the methyl methacrylate adhesives “Novatit” decreased after 1.5 year in only about 35 %. Adhesive “Oxy” has low values of ultimate strength due to wrong reaction of two components and then improper curing of the adhesives.

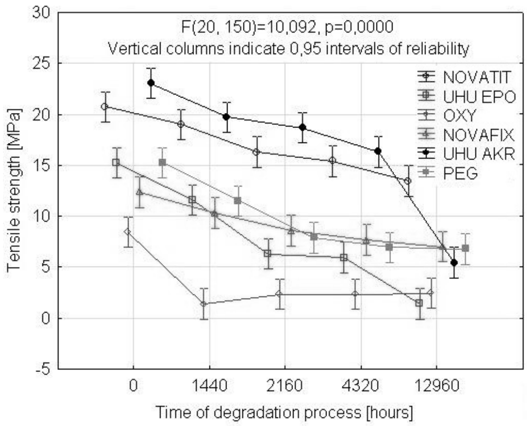

Fig. 1 Effect of the water bath on the adhesive bond strength

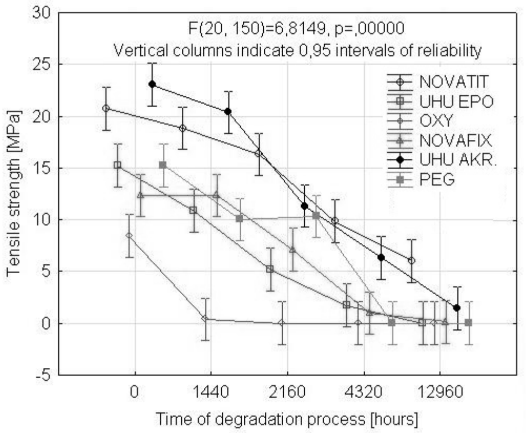

Fig. 2 Effect of the gasoline bath on the adhesive bond strengthIn the Figure 2 is shown effect of the aggressive degradation medium.

A disintegration of the adhesive and cohesive forces occurred after 6 months in the gasoline. Methyl metacrylate adhesives were more resistant in a compare to epoxy adhesives. After 18 months of degradation the ultimate strength of the methyl metacrylate adhesive "Novati" decreased by 70 %. It can be asserted that environment of gasoline is not suitable for above mentioned adhesives.

Some experiments were aimed to determine an effect of the brine as adegradation environment. The results clearly showed a downward trend of the ultimate strength in time for all tested adhesives. A disintegration of adhesive and cohesive forces of the epoxy adhesives occurred after 18 months, as well as the environment of gasoline. Methyl methacrylate adhesives were more resistant than epoxy adhesives as it can be seen in Figure 3, however there is also a decrease of ultimate strength by 65 % and 71 %.

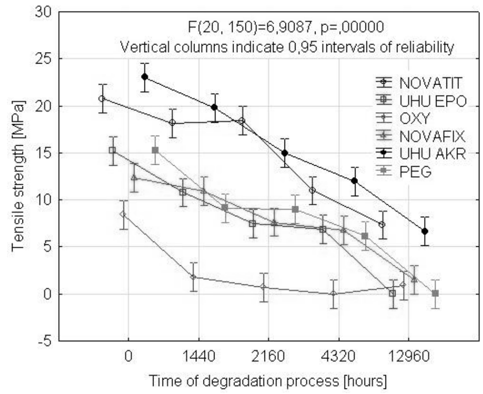

Fig. 3 Effect of the brine bath on the adhesive bond strength

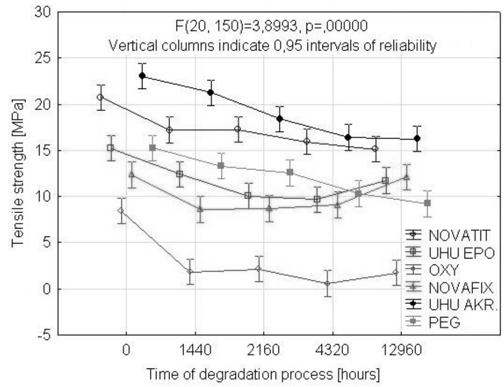

Fig. 4 Effect of the exterior environment on the adhesive bond strength

In a practice, there are a number of adhesive bonds exposed to common environment conditions, i.e. exterior environment. For that reason was the last part of the experiments focused on the degradation of adhesive bonds in exterior. In the case of methyl methacrylate adhesives has been shown a slight continuous decline of the ultimate strength in a time of degradation. In the case of "Novati" and "UHU acryl", the strength of adhesives decreased by 27 % (respectively by 30 %) after 18 months of degradation. The ultimate strength of epoxy adhesives decreases during the first 3 months of degradation. After this period of degradation there has been noticed increasing trend of ultimate strength. The increase trend of the ultimate strength is due to the different climatic conditions where the experiment was evaluated.

In the case of evaluating of the degradation interval of three months the climatic conditions were - 15 ° C ± 3 ° C, in the interval of 6 and 18 months the temperatures were well above the freezing point. In the research of Kejval et al. (2011) has been found that freezing temperatures have a negative effect on the ultimate strength of adhesive bonds. Therefore it can be assumed that the above mentioned fact about negative effects of low temperatures is reason of the decrease of ultimate strength about 50 %.

Tab. 1 Tukey's test for degradation media of brine and gasoline

		Brine				Gasoline			
Adhesive Designation	**Degradation Time [h]**	**Ultimate Strength [MPa]**	**Homogeneity of Variances**			**Ultimate Strength [MPa]**	**Homogeneity of Variances**		
Peg	12960	0.00	***			0.00	***		
Uhu Epo.	12960	0.00	***			0.00	***		
Novafix	12960	0.13	***			1.51	***		
Peg	1440	10.03		***	***	9.15		***	***
Uhu Epo.	1440	10.87			***	10.78			***
Novafix	1440	12.37			***	10.96			***
Uhu Epo.	2160	5.19	***	***		7.48		***	***
Novafix	2160	7.12		***	***	7.63		***	***
Peg	2160	10.33		***	***	9.00		***	***
Peg	4320	0.00	***			6.15		***	
Novafix	4320	0.99	***			6.78		***	
Uhu Epo.	4320	1.72	***			6.84		***	

Failure of epoxy adhesive bonds was in all measured intervals characterized by loss of adhesion power, i.e. it was an adhesive failure. In the case of methyl methacrylate adhesive bonds the cohesion failure has been changed to adhesive failure. Change occurred in the majority of cases of degradation after 6 months.

To verify the hypothesis of constant degradation of epoxy adhesives was performed by Tukey's test. The homogeneity of variances of epoxy adhesives was confirmed by Tukey's test in the gasoline and brine bath as the degradation medium, which is shown in Table 1. The Homogeneity is singed by symbols (***) in the column of the table. The hypothesis was not confirmed in the water bath and exterior environment.

Conclusion

Adhesive development spread the application possibilities of adhesives in a practice. Spreading of the adhesive application requires constant testing of adhesives in specific conditions and environments. The importance of these experiments is mainly in the fact of difficult build of the predictive equations to determine the ultimate strength during the durability of adhesive bonds, as pointed da Silva et al. (2009).

Experimental results demonstrated the following:

- Aggressive environments (such as gasoline or brine) are not suitable in a long-term for adhesive bonds;
- Methyl methacrylate adhesives seems to be very resistant, it reach high values of tensile strength and the degradation process;
- In the tests was confirmed resistant of the adhesives to the water environment.

Acknowledgement

This paper has been done when solving the grant of the title "Study of factors affecting the strength and durability of perspective bonds" Nr. 2013:31140/1312/3107.

Reference

CSN EN 1465 Adhesives – Determination of tensile lap-shear strength of bonded assembleies. Czech office for Standards, Metrology and Testing, Prague, Czech Republic. (in Czech)

CSN EN ISO 9142 Adhesives – Guide to the selection of standard laboratory ageing conditions for testing bonded joints). Czech office for Standards, Metrology and Testing, Prague, Czech Republic. (in Czech)

Crocombe, A. D., 1997. Durability modelling concepts and tools for the cohesive environmental degradation of bonded structures, International Journal of Adhesion & Adhesives, 17: 229 - 238.

da Silva, L.F.M., Carbas, R.J.C., Critchlow, G.W. , Figueiredo, M.A.V., Brown, K., 2009. Effect of material, geometry, surface treatment and environment on the shear strength of single lap joints. International Journal of Adhesion and Adhesives, 29: 621- 632.

Henc, P., Chocholouš, P., Müller, M., Kejval, J., 2011. Methyl methacrylate (adhesive) – the influence of climatic conditions on the properties of adhesive bond. Engineering for Rural Development. Jelgava.

Herák, D., Müller, M., Karanský, J., Dajbych, O., Simanjuntak, S., 2009. Bearing capacity and corrosion weight losses of the bonded metal joints in the conditions of Indonesia, North Sumatra province. Research in Agricultural Engineering, 55: 94 - 100.

Kejval, J., Henc, P., Müller, M., 2011. Effect of the temperature and curing time on the adhesive bond strength – bonding alloys of the AlCu4Mg with methyl methacrylate adhesives, Manufacturing technology, 16: 15-20. (in Czech)

Lapique, F., Redford, K.,2002. International Journal of Adhesion and Adhesives, 22, 337 - 346. Available at: www.sciencedirect.com/ science/article/pii/S0143749602000131. (accessed June 06, 2012).

Müller, M., Brožek, M., 2005. Adhesive bond technology – Effect of the expiration time of the adhesive to the adhesive bond strength, Manufacturing technology, 3: 10 – 16. (in Czech)

Müller, M., Valášek, P., 2011. Influence of specific degradation agents of agricultural production on recycled plastics mechanical properties. In The Fifth International Scientific Conference Rural Development in Global Changes 2011, 5. Aleksandras Stulginskis University, Lithuania: 384 - 388.

Müller, M., Valášek, P., 2010. In 9th International scientific conference engineering for rural development. Jelgava: LUA: 49 - 52.

Valášek, P., Müller, M., 2012. Vliv klimatických podmínek České republiky na pevnostní charakteristiky lepených spojů (Effect of climatic conditions that affect the mechanical properties of adhesive bonds in the Czech Republic). Strojírenská technologie (Manufacturing technology), 5-6: 343-348. (in Czech)

ANALYSIS OF SELECTED BIODEGRADABLE WASTE

David Houška*, Petr Hájek, Vlastimil Altmann

Czech University of Life Science, Prague, 16521 Prague 6 – Suchdol, Czech Republic,
Phone: +420 22438 3150, E-mail: houskad@tf.czu.cz

Abstract

For effective planning of logistics collection of biodegradable waste (BDW) and its subsequent use for composting is desirable to know its physical properties, especially density, which is striking for the selection of suitable containers for collection and further handling from the place of origin to place of further processing.

Keywords: biodegradable waste, analysis

Introduction

Measurement, on which is this post based on, was implemented at two golf courses, where there is a high diversity of resulting BDW and its physical properties. The source of BDW is green maintenance, which is carried out at different time intervals. The level of intensity of maintenance is determined by the desired final quality of playing surfaces and the expected value of the aesthetic field. Intervals are in range from daily maintenance to maintenance performed once a year.

Material and methods

For the detection of density of BDW can be used a method which is based on weighted known volume of material and the weight value is automatically calculated using the relationship bulk density. For the calculation it is necessary for m installed weight of material which is weighed in the container, where it occupies a known volume V.

$$m_V = k.\frac{m}{V} \quad [\text{kg.m}^{-3}] \qquad /1/$$

m_V - the resulting bulk density [kg.m-3]
m - sample weight [kg]
k - conversion factor from liters to m^3
V - volume of the vessel [l]

The most common collection system of BDW (Bilitewski et al., 1997) is a bin or container collection system, which is based on the re-use of receptacles. Frequently used bins for collection of BDW are bins (Fig. 1) of 120 and 240 liters. Containers (Amos, 1994) intended for collecting BDW are different from other containers about the same volume by aeration holes on the sides and above the bottom placed grate which provides separation of water from the waste introduced into the container. When measuring the mass of waste placed in containers, it is advisable to use a platform scale with adequate capacity, units and smallest piece of mass unit of weight. The smallest piece is the accuracy with which can be determine the weight measured by the scale.

The measurement was carried out by using a platform scales with capacity about 500 kg and the smallest unit 0.1 kg, on which was placed the bin with volume of 120 l filled with BDW of the same character or a common place of origin. Filling the container is done by free pouring of waste into the container without compressing. The recorded values of weight and known volume of 120 l filled containers are processed by using the formula for calculating of density.

Fig. 1 BDW Bin (120 l)

Results

In the Table 1 are shown selected values for comparison of density from used literature (Pliva et al., 2009). When comparing densities is important to realize that the density of the material in bin reaches different values according to the size and shape of the bin and even assuming that the volume of container remains the same. Therefore, to obtain values for all measurements is used container often used for collection of BDW. On the obtained data can be used for further calculation of BDW collection system with using one hundred twenty liter collecting bins.

Tab. 1 Density of selected BDW

Types of biodegradable waste - selection	
Type of BDW	**Density [kg . m^{-3}]**
Hay	66
Starin from bow	95
Dry leaves	119
Wet leaves	267
Waste of lawn maintenance	326
Farm compost	410

Some results of density measurements of golf course maintenance are shown in the Tab. 2. It is a waste of maintenance activity, which is characterized by a longer time interval between each operation, and some is done only once a year. In most cases it is a shortening of the crop. Tab. 2 also shows other type of BDW then from golf course maintenance to compare the values of density, which have been documented. Collection BDW value is reached by waste imported from municipal waste collection by waste truck from the actual collection processed by Prague Services company (after emptying the vehicle sample was taken). The last value is the density of compost, which is the end product of the composting process of BDW.

Tab. 2 The measured density of selected BDW

The measured density of	
Druh BRO Type BRO	**Density [kg . m^{-3}]**
Virginia creeper	30
Walnut leaves (dry)	50
Cotoneaster	59
Waste of flowerbeds	89
Thuja cuttings	97
Preshredded BDW before piling	267
Collection BDW Prague Services	271
Compost	519

During maintenance of lawns by mowing we get different lengths of cuttings which are associated with a main function of specific grassland. Property chop is also influenced by the type of lawn mower. On the golf courses are frequently used rotary and spindle mowers (Witteveen et al., 2012) with motor drive and one or more cutting unit. Table 3 shows the values of density of grass mass from maintenance of ornamental grass with cutting length 60 cm which is reaching very low values of density. Ornamental lawn meadow of nature is used to improvement of peripheral areas or to make more difficult playing conditions for golfers. High values are reached on intensive lawns mowed to a low height of cut. Tees are mown to a height of 9 mm and a length of cut is in the range of 0.3 to 2 cm. The greens are mowed at the height of 3-5 mm cutting length and the grass on green reaches length of 0.1 to 8 mm. Mown grass on the greens can achieve different values of density and not only because of changes in humidity but mainly because of the prior mechanical treatment or other interventions. These treatments may include mechanical scarifying and aeration which cause the lower value of density in measured in bin. On the contrary, higher values are obtained after sanding the greens, the green mowers during mowing collect the clippings also with sand.

Tab. 3 Measured values of different kinds of grass cuttings

measured values of different kinds of grass cuttings	
Type of BRO	**Density [kg . m^{-3}]**
Grass (5 - 7 cm)	138
Ornamental lawn – cuttings 60 cm	33
Grass after verticutation	41
Green of 1st golf course	320
Tee ground of 1st golf course	193
Green of 2nd golf course	284

Fig. 2 and Fig. 3 are the sample photographs of mowed grass of green lawn and ornamental lawn.

Conclusion

Density measurement of samples incurred in the maintenance of field is in the range of 30-320 [kg.m^{-3}]. On the basis of this knowledge it is possible to design a collection system of BDW and ensure by using appropriately selected bins and intervals optimized system of collection to ensure timely disposal of biodegradable waste from its point of origin and prevent the undesirable accumulation. The measurement results show that in the case of the maintenance of lawns, it was found that when the cuttings length is increased the value of the density is lower, and vice versa.


Fig. 2 Mowed grass mass of greens


Fig. 3 Mowed grass mass of ornamental grass (cutting length 5-7 cm)

Acknowledgement

This entry was written with the financial support of Objective No. 2013:31180/1312/3120

Reference

Amos J., 1994. Waste and Recycling. Steck. Vaughn Company, 81.

Bilitewski B., Härdtle G., Marek K., 1997. Waste Management, Springer, 699.

Plíva P., Banout J., Habart J., Jelínek A., Kollárová M., Roy A., Tomanová D., 2009. Composting in the open area in the belt piles. Profi Press, s.r.o., 136. (in Czech)

Witteveen G., Bavier M., Practical Golf Course Maintenance, 2012. The Magic of Greenkeeping John Wiley & Sons, 272.

CREATING OF THE SKELETON OF A DIGITAL DOMESTIC CATTLE MODEL

Michal Hruška; Jan Nevoral

Czech University of Life Sciences Prague, 16521 Prague 6 – Suchdol, Czech Republic, Phone: +420 22438 3215 E-mail: hruska@tf.czu.cz

Abstract

This paper presents the development of the method of creating the skeleton of a digital domestic cattle model. There are currently no source materials or data of this type and for this reason it is necessary to define all procedures entirely from the beginning and thus set out basic data models for further application. The method of differential photography with a reference object was used in order to set out a basic mechanical cattle model. Equations were determined that allowed for the extrapolation of the position of the camera in relation to the photographed object from the photographs taken. A 3D skeleton of the animal was created based on this data, on the basis of which all moving joints and basic dimensions were subsequently defined. Based on this experimentally obtained procedure, it was possible to define a precise method of obtaining a virtual, biomechanical domestic cattle skeleton model. The resulting method also provides the option of connecting the basic model to a statistical database of basic dimensions of domestic cattle and, with the help of defining mutual relations, allows for the morphing of the model according to statistical data. It therefore provides the option of displaying the skeleton model of any single animal. The resulting method will also be used as a fundamental biomechanical model for the onward development of a more complex dairy cow model intended for the testing of automatic milking machines.

Key words: automatic milking system; dairy cows; digital modelling; ergonomics; Tecnomatix Jack

Introduction

Animal production is currently undergoing a period of dynamic advancement. This mainly involves new technological possibilities, mechanisation and automation, with an ever-decreasing need for human work (Thornton, 2010). An expansion of automatic milking machines and automatic milking systems is currently underway (Cattaneo et al., 1996; Ipema, 1997). Given that increasing production is directly dependent on the comfort of the animals, it is essential to avoid stressful situations and stimuli in cattle breeding and in the milking process (Gygaxet et al., 2006). Recent studies, in fact, discovered that dairy cows in automatic milking systems show a higher concentration of stress hormones in the blood (Hagenet et al., 2004; Abeniet et al., 2005). This might be a result of discomfort caused by the inappropriate construction of automatic milking systems. There are currently no studies to identify the disruptive elements of technological equipment in animal production.

The absence of disruptive elements and the immediate comfort of the animal during milking in automatic milking systems can be ensured by the actual construction and technological realisation of automatic milking machines. The design and technological development of automatic milking machines proceeds on the basis of practical knowledge and decrees. There is not yet any suitable and sufficiently objective way of identifying any shortcomings that could cause discomfort among the animals.

For the work of humans, so-called work ergonomics are used to eliminate employee discomfort. Work ergonomics is currently based on the creation of a precise biomechanical human model and a model of his positioning in a defined virtual environment. Ergonomics software is able to enter a model of actions, monitor his performance and comfort and, using this modelling, is able to reveal any possible discomfort of the model or even situations in which collisions and injuries could occur. The generation of a functional, three-dimensional human model is termed Digital Human Modelling (Miller, Jenkins, 2002; Conradi, Alexander, 2002). It can be expected that, as in the case of humans, we can consider the generation of a three-dimensional model of an animal in similar contexts. Such technology can be termed Digital Animal Modelling and can be considered the foundation for ergonomics used in the breeding of farm animals.

Material and method

The animals

Images of Holstein breed heifers (n = 5) were used to produce a biomechanical dairy cow model. Measurement was done at the School Agricultural Enterprise in Lány, Ruda Farm.

In addition to live animals, three teaching skeletons of the Holstein breed were used to set out dimensions.

Hardware

Animals were photographed for the purpose of digitalising points defined on the body of the dairy cow. Digitalisation was therefore used to determine selected joints and their position and connection to each other. The process involved photographs taken using 4 x Nikon 1 J1 cameras. This type of camera is fitted with a fixed lens and focal length of 10 mm. After conversion using the so-called crop factor of 2.7, it provides a final focal length of 27 mm. The view angle of the camera is 65.5°.

To best take source photographs, as is described in the methodology, it was necessary to create a specific installation, whereby two cameras were invariably placed on a fixed bracket at a distance of N_{LR} (see Fig. 2) and their position secured. This installation was then placed on a tripod with a high load bearing capacity in order to maintain stability, as can be seen in Fig. 1.

Fig. 1 Installation of duo of Nikon 1 J1 cameras on a fixed bracket

The installation was supplemented by electronic equipment, of our own construction and production, for communicating with cameras and their remote connection and control by computer. This equipment allows for the functions of all 4 cameras to be synchronised and for data to be gathered from a camera in real time.

Results

A hypothesis was set, based on the information in print and the procedures used in human ergonomics, that the generation of a three-dimensional farm animal model can be used to detect elements of technological equipment used in animal production that cause the animal discomfort. The aim is to generate a three-dimensional dairy cow model that can be used in modified modules of Tecnomatix Jack software and to thus create a basis of knowledge and software for Digital Animal Modelling and animal ergonomics.

The generation of a complex dairy cow model is a process that must be dealt with in two stages. Stage one, the subject-matter of this paper, involves the generation of a digitalised skeleton with fully functional kinematics. Stage two, which follows on from this, involves the generation of the outside of the dairy cow and its subsequent connection to the skeleton.

The generation of the skeleton of a dairy cow consists of three consecutive stages. In the first stage, it is necessary to define the basic spacing of individual points, representing joints and vertebrae, which are subsequently joined and a basic model created. This first stage uses a model of the real skeleton of an animal as a source of data. However, given that it is impossible to reliably determine the precision of position of individual parts of the real model of a skeleton, this information must be made more specific using data obtained from live animals. This is the second stage, when live animals are photographed and basic dimensions taken from their photographs using the method described below, based on which the original, initial model is further modified. The process described in stage two can also be used as a source of data for a statistical database.

The digitalisation of an image and the creation of a basic model

The digitalisation of a model involves determining key points in space, invariably from two photographs taken at the same moment by two cameras positioned on a fixed bracket on a tripod (see Fig. 1). Cameras are positioned at a constant distance of N at a known angle (see Fig. 2). Using the principle of parallax, the defined points were measured on the photographed model of the skeleton or live animal. The resulting position of the monitored points is determined in space by the Cartesian system, whereby the zero point is the central point between the apparatus or the top of the tripod.

The first step in the actual digitalisation of the model was to determine one monitored point on both photographs and their relative positioning on the image towards its centre. Zero position corresponds to the axis that is found in the centre of the tripod head and which is parallel to the axes of the view of both cameras. When knowing the view angle, the next stage was to determine the angle by which the straight line between the sought point and the focus of the lens deviated from the view axis. This applies to seeking the angle at level X (vertical angle of image) and Y (horizontal angle of image). Vectors were determined following the measurement of these angles and subsequently an equation of the two straight lines that emanate from the cameras and meet at the monitored point. The calculation of the position of a point was completed with the establishment of the position of the cameras in which the result was the positioning towards the tripod head. The positioning and distance of points were expressed in mm.

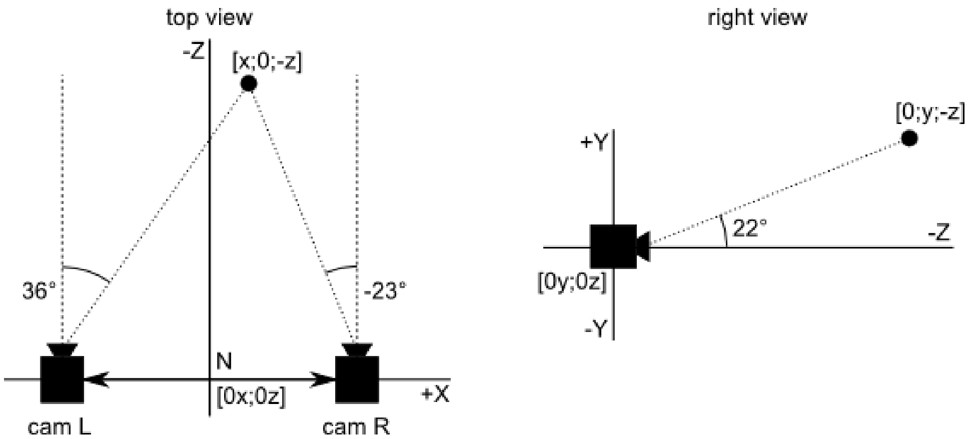

Fig. 2 Top and side view on the principle of ascertaining the distance of points from two photographs

The diagram (See Fig. 2) is an example of the positioning of two cameras from the top and side views. The zero point between the cameras is indicated [N], the right and left camera [cam R, cam L] and the individual axes [X, Y, Z].

$$horizontal\ angle = \arctan\left(\frac{2*pW-W}{W}*\tan\left(\frac{aW}{2}\right)\right)$$

$$vertical\ angle = \arctan\left(\frac{2*pH-H}{H}*\tan\left(\frac{aH}{2}\right)\right)$$

//in which
pH – the position of a point on a photograph in pixels from above
pW – the position of a point on a photograph in pixels from the right
H – the height of the photograph in pixels
W – the width of the photograph in pixels
aH – the vertical angle of the shot
aW – the horizontal angle of the shot

$$\begin{bmatrix} x & y*\tan(uW_{CamL}) & x_{CamL} \\ x & y*\tan(uW_{CamR}) & x_{CamR} \end{bmatrix} = 0$$

//in which
x, y – unknown
uWCamL – horizontal view angle from the left-hand camera
uWCamR – horizontal view angle from the right-hand camera
xCamL – position of the left-hand camera on axis X
xCamR – position of the right-hand camera on axis X

$$point = \left[X; Z = \frac{-x_{CamR} - X}{\tan(uW_{camL})}; Y = \tan(uH)*Z\right]$$

//in which
X, Y, Z – positions on axes
xCamR – position of the right-hand camera on axis X
uWCamL– horizontal view angle from the left-hand camera
uH – vertical view angle (both cameras should have the same)

The calculations and methods described above allowed for the generation of a basic animal skeleton in the Tecnomatix Jack program.

Data obtained on live animals and refining of the model

As stated above, the basic model needs to be further refined. This can be done using data obtained on live animals. This data represents individual defined points that can be determined on the skeleton model and on a live animal. The definition of points consists of the manual marking of joints on live animal using targets. These targets are photographed using two cameras positioned on a bar and on a tripod. This ensures stability of photographing and, given that we know the distance between the cameras, we can ascertain points in space using the method described in the previous section. The target is used to focus on a specific point on the animal on all photographs.

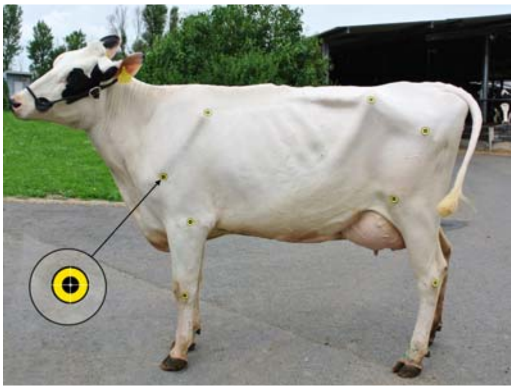

Fig. 3 Dairy cow with individual joints indicated by targets

It is important during this geometric measurement for the photograph to be taken from the side view (profile) and for fixed levels that are known and that may not be exceeded in the case of the possible movement of points to be determined on this photograph.

N.B. The further optimisation of the method counts on automating the distinguishing of targets from the surroundings and their automatic targeting.

The ratio of the difference between the basic (reference) model and the data measured in stage two on a live animal can be applied as a coefficient to a scale deformation of individual parts of the skeleton. This coefficient can also be used to ascertain the dimensions of those parts that could not be measured directly (points which are known only from the skeleton, but that cannot be targeted on the live animal). The reference model therefore helps put together a model accurately and more simply from the data obtained by measuring live animals.

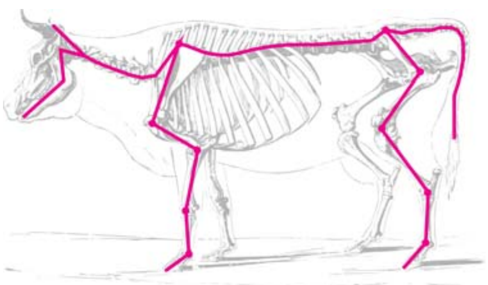

Fig. 4 Points defining the individual joints of an animal and their connection to each other

Scale deformation is one of the deformations in space given by a transformation matrix. In this case it is a matter of simple multiplication. In order to guarantee that the model obtained is accurate, the validity of the scope of movement of joints will be verified and the model must also apply the laws of kinematics.

The positions in space of individual points are already known from the previous method and now calculations of the distances of individual points, representing the length of specific bones, are completed with the use of analytical geometry. For each known bone, therefore, there is a reference length (ascertained from the skeleton model) and the length for a specific animal. Coefficients must be calculated separately for each bone and consideration must be made of the fact that points actually describe only peaks on the surface of the body. To achieve maximum precision and objectivity, the points compared are found translocated to the middle of the joint, which is another coefficient relevant for each joint and which represents its outer radius. This corrective translocation factor is experimentally determined, for example, on the skeleton of an animal. Moreover, the factor can areally proportionately change in relation to the overall size of the animal and has the form of the transformation matrix already mentioned, describing movements on individual axes by adding the measured value and the corrective factor. Since the coefficient is ascertained from the length of the bone, the result of measurement does not depend on the position of the animal or even on the angle of photographing. It is only necessary to guarantee that all targets are within the shot angle, i.e. ideally viewed from the profile.

The positions of points obtained in this way will be applied to a real 3D cattle model (see Fig. 4) and will be compared to the real sizes of the animal, in particular the determination of scopes.

The information obtained from photographing each animal is archived. Statistically-speaking, we can obtain the values of the average lengths of bones, total size and the ascertained scopes of the movement of joints, all categorised according to breed, sex and age.

Definition of the scope of movement of joints

The scopes of movement of joints are very difficult to ascertain from photographs, but we can compare the angles that hold selected bones in joints and use these to determine a minimum and maximum. The physiological limit will appear beyond the identified boundary, but will correspond to the scope in routine cattle activities (resting, standing, grazing, etc.).

As initial data, we can, in the case of the scope of movement of joints, use the available scientific literature that deals with the empirical identification of this data. This data can thereafter be transferred to the Tecnomatix Jack program and we can thus define the basic physiological scope of movement of the dairy cow model.

Tab. 1 Physiological range of the scope of movement of individual joints of a dairy cow (Komárek, 1993)

		name	min	max
Thoracic limb	A	articulatio humeri	90	120
	B	art. cubiti	50	135
	C	art. carpi	40	170
	D	art. metacarpophalangea	120	200
	E	art. interphalangea proximalis	160	180
	F	art. interphalangea distalis	170	190
Pelvic limb	1	art. coxae	75	120
	2	art. genus	60	150
	3	art. tarsi	60	160
	4	art. metatarsophalangea	120	200
	5	art. interphalangea proximalis	160	180
	6	art. interphalangea distalis	170	190

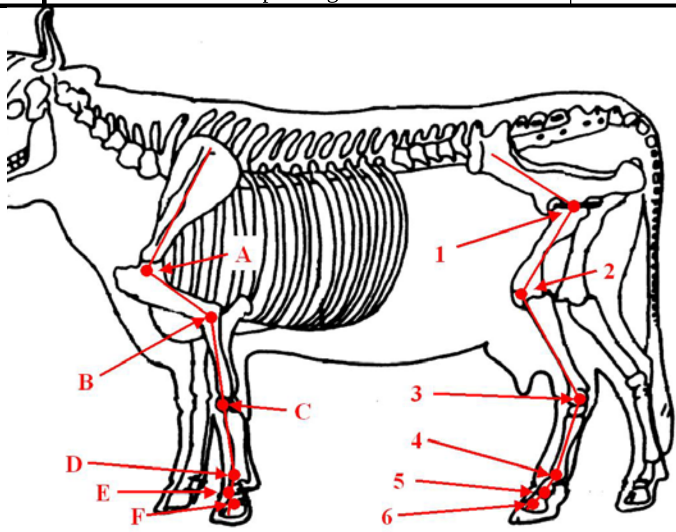

Fig. 5 Illustration and descriptions of individual joints, as they are described in Tab. 1

Discussion

The methodology presented above describes the first stage of the generation of a virtual dairy cow model. We were able to generate a fully functioning motion skeleton of a dairy cow whose scope of movement of individual joints corresponds to the empirically obtained data for actual animals. A new method of photographing was created based on successive photographing of a real skeleton model and of a live animal and the subsequent evaluation of the data obtained. Mathematical relations were defined that allow for statistical, dimensional variation based on an original reference model. This enables statistical data to be obtained with ease based on the actual dimensions of the set of specific animals examined.

Conclusion

The results obtained must be followed up with the creation of a database of bodily dimensions and their use in the creation of a specific type of farm animal, breed or individual animal. The procedures of Animal Digital Modelling and animal ergonomics can be used through a definition of the virtual environment of automatic milking systems and by applying a biomechanical dairy cow model to this environment as a means of marking out critical points of construction and improving the welfare of dairy cows (Jacobs, Siegford, 2012). Broadened applications can be used in advanced methods of constructing technological equipment (Thornton, 2012) and thus optimise production processes in the breeding of farm animals.

A software database with numerous population data and the relevant conversion algorithm allows us to generate further dimensions of frames based only on height, weight or representation in the population and so create a specific, three-dimensional model as in the Digital Human Modeling (Ge et al., 2007; Wang et al., 2007). The Jack system allows us to specify how the virtual model will behave in contact with other elements of the environment (Sekulová, 2010). In this way we can monitor any collision of the model in the environment or the optimum position of an object during work or during its examination.

Acknowledgement

This study was financed by a project of the Czech Agricultural University in Prague (CIGA 20133003): Animal ergonomy as a means for optimalization of the automatic milking systém).

Reference

Abeni F., Calamari C., Calza F., Speroni M., Bretoni G., Pirlo G., 2005. Welfare assessment based on metabolic and endocrine aspects in primiparous cows milked in a parlor or with an automatic milking system. Journal of Dairy Science, 88: 3542-3552.

Badler N.I., Phillips C.B, Webber B.L., 1993. Simulating Humans: Computer Graphics, Animation, and Control. Oxford Univ. Press. ISBN 978-0195073591.

Cattaneo M., Cavalchini A.G., Rognoni G.L., Zazueta F.S., Martinez-Austria P., Xin J.N., Garcia-Villanueva N.H., 1996. Design and construction of robotic milking system. Sixth International Conference on Computers in Agriculture, 155-160.

Chang M.-C., Leymarie F.F., Kimia B.B., 2004. 3D Shape Registration using Regularized Medial Scaffolds, 3dpvt, Second International Symposium on 3D Data Processing, Visualization and Transmission (3DPVT'04), 987-994.

Conradi I., Alexander T., 2002. Interrelation between empirical and motion simulation data of a digital human model. Digital Human modelling Conference, 1675: 343-353.

Exposé 4, 2006. Finest digital art in the known universe. Edited by Daniel Wade - Paul Hellard - Mark Snoswell - Leonard Teo. 1st ed. Mylor: Ballistic publishing, 223. ISBN 1-921002-30-1.

Ge B.Z., Tian Q.G., Young K.D., Sun Y.C., 2007. Color 3D digital human modeling and its applications to animation and anthropometry. Lecture Notes in Computer Science – Digital Human Modeling, 4561: 82-91.

Grandin T., 2003. Transferring results of behavioural research to industry to improve animal welfare on the farm, ranch and the slaughter plant. Applied Animal Behaviour Science, 81: 215-228.

Gygax L., Neuffer I., Kaufmann C., Hauser R., Wechsler B., 2006. Milk cortisol concentration in automatic milking systems compared with auto-tandem milking parlors. Journal of Dairy Science, 89: 3447-3457.

Hagen K., Lexer D., Palme R., Troxler J., Waiblinger S., 2004. Milking Brown Swiss and Austrian Simmental cows in herring bone parlour or an automatic milking unit. Applied Animal Behaviour Science, 88: 209-225.

Hulsen J., 2006. CowSignals: A Practical Guide for Dairy Farm Management. Roodbont Publishers. ISBN 978-90-75280-65-4.

Hulsen J., Rodenburg J., 2008. Robotic Milking. Roodbont Publishers. ISBN 978-90-8740-043-9.

Jacobs J.A., Siegford J.M., 2012. Invited review: the impact of automatic milking systems on dairy cow management, behavior, health and welfare. Journal of Dairy Science, 95: 2227-2247.

Miller J.J.; Jenkins G., 2002. The development of a functional visualization system for the creation of digital human model. 6th International Conference on Information Visualisation, Proceedings, 197-201.

Panagiotakis C., 2004. Construction of Animal models and motion synthesis in 3D virtual environments using image sequences, ISBN 0-7695-2223-8.

Pu J., Liu Y., Xin G., Zha H., Liu W., Yusuke U., 2004. 3D Model Retrieval Based on 2D Slice Similarity Measurements, 3dpvt, 95-101, Second International Symposium on 3D Data Processing, Visualization and Transmission (3DPVT'04).

Thornton P.K., 2010. Livestock production: recent trends, future prospects. Philosophical Transactions the Royal Society B., 365: 2853-2867.

Wang M.J.J., Wu W.Y., Lin K.C., Yang S.N., Lu J.M., 2007. Automated anthropometric data collection from three-dimensional digital human models. International Journal of Advanced Manufacturing Technology, 32: 109-115.

THE TREND OF OIL PALM PRODUCTION IN GHANA

Abraham Kabutey, David Herak, Riswanti Sigalingging

Czech University of Life Sciences Prague, Faculty of Engineering, Department of Mechanical Engineering, Kamycka 129, Praha 6, Prague 165 21, Czech Republic
kabutey@tf.czu.cz; herak@tf.czu.cz; sigalingging@tf.czu.cz

Abstract

This article is primarily focused on the current status of oil palm production in Ghana. The oil palm industry in Ghana has developed over the last two decades into huge and important industry which comes next only to cocoa in the agricultural sector of the economy. However, consumption of palm oil in Ghana for food and industrial purposes exceeds domestic supplies as a result palm oil is being imported. This paper highlights the contributions of major companies, research institutions, small to medium-scale farms and private holdings promoting oil palm cultivation to boost production. Most importantly, the Government interventions and plans to revive the oil palm industry in Ghana to meet both domestic and industrial demands as well as to compete on the global market have been addressed.

Key words: oil palm production, crude palm oil, major companies, small to medium-scale farms, government interventions

Introduction

The oil palm ranks among the most important edible oil producing crops in Sub-saharan Africa. It produces one of the major oils and fats traded on the continent (Tagoe et al., 2012). As far back in the early 1900s in Ghana (formally the Gold Coast) under the British rule, the oil palm plantation and mill was established by Alexander Cecil Goff at a location near the coast. In 1957, Ghana gained independence from the British, and Malaysia also a British colony achieved independence the same period. Malaysia, through the efforts of the Europeans travelled to the oil palm estate in Ghana to learn about oil palm cultivation and techniques. Consequently, the oil palm estates owned by the Europeans were established in Malaysia from 1917 onwards. By 1960, Malaysia had a well-established palm oil export industry while attempts were and still being under way to revive Ghana's oil palm industry to meet domestic and industrial demands and also to compete on the global market (Fold, Whitfield, 2012).

Globally, the production of palm oil has increased tremendously during the last 30 years as a result of rapid expansion of oil palm plantation in South East Asian countries controlled by Malaysia and Indonesia. These two countries have been the major suppliers of palm oil since the 1970s and still take dominance (Basiron, 2007; Oworlarafe et al., 2007). Presently, these countries account for about 87 percent of global production and about 91 percent of global trade. China, India and the European Union are also three major importers of palm oil. It is important to note that there is growing interest in palm oil for biodiesel production and this firmness of purpose is against the use of the edible oil primarily as food and industrial purposes.

In Ghana, the oil palm industry has developed over the last two decades into great and important industry which comes next only to cocoa in the agricultural sector of the economy. Consumption of palm oil in Ghana for food (cooking oil, margarine, etc.) and for industrial purposes (as an ingredient in the production of detergents, soap and cosmetics) exceeds domestic supplies as a result palm oil and other vegetable oils are being imported (Fold, Whitfield, 2012; Keshvadi et al., 2011). This limitation depends on a number of factors including poor agricultural practices, transportation cost of Fresh Fruit Bunches (FFB) to processing mills or market and limited access to land due to the traditional land ownership structure inherent in Ghanaian culture.

The objective of the study was to discuss the current situation of oil palm industry in Ghana and the measures so far designed especially by the government to promote oil palm production to meet both domestic and industrial demands, and most importantly, to compete on the international market.

Tab. 1 Projected crop area of oil palm of some major companies and medium farms in Ghana

Company	Area (Ha; '000)							
	Year							
	2003	**2004**	**2005**	**2006**	**2007**	**2008**	**2009**	**2010**
GOPDC	7.6	10.2	10.5	10.9	7.1	22.35	25	25
BOPP	6.5	5.7	6.3	6.3	6.1	6.34	6	5.2
TOPP	9.5	10.3	10.1	10	7.4	12.24	15	6.3
NOPL	6.7	7.3	8.1	8.9	9.7	4	6	6
MEDIUM FARMS	0.57	0.61	0.66	0.71	0.8	0.74	0.8	0.8

Source: (Agriculture in Ghana, Facts and Figures, 2010)

Tab. 2 Actual crude palm oil production and projections of major companies and medium scale mills in Ghana

Company	Crude palm oil production (MT '000)								
	Year								
	2002	**2003**	**2004**	**2005**	**2006**	**2007**	**2008**	**2009**	**2010**
GOPDC	19.425	19.9568	26.5302	27.0652	28.7431	17.8427	18.05568	20.143	20.143
BOPP	17.583	17.26	14.323	16.012	16.485	15.305	14.96018	14.124	11.838
TOPP	18.6889	19.8921	20.5882	20.2236	20.348	14.7971	14.24966	17.373	14.688
NOPL	4.794	5.274	5.801	6.381	7.019	7.721	8.49283	12.775	12.775
MEDIUM SCALE MILLS	5.729	6.301	6.932	7.625	8.387	9.2257	10.14807	10.836	10.836

Source: (Agriculture in Ghana, Facts and Figu

Overview of oil palm cultivation in Ghana

Areas suitable for cultivation

Ghana is made up of ten regions and soil fertility status differs accordingly for oil palm and other crops production. In the northern part of Ghana, for instance, yam and millet are among the most suitable crops for production as compared to the eastern or southern parts where food crops such as cassava, plantain and cocoyam thrives better. In case of oil palm production, the most ecological areas or regions include Western, Eastern, Central, Ashanti, Volta and Brong Ahafo. To ensure high production of oil palm, climatic and soil suitability are relevant factors. These potential areas in Ghana have the recommended climatic and soil suitability requirements. Minimum annual rainfall of 1500 mm which is able to yield about 15–30 MT per ha per annum at peak production can be observed. The sunshine requirement is 1,500 hours of sunshine per annum. This is equivalent to 5 hours per day of sunshine in all months. A minimum and maximum temperature requirement is between 18 °C and 32 °C respectively. Well drained loamy soil is suitable for oil palm production and soil suitability in these potential areas in Ghana is productive.

Major oil palm companies/mills in Ghana

There are four large-scale oil palm plantations that have their own processing mills namely Ghana Oil Palm Production Company (GOPDC) in the Eastern Region, Twifo Oil Palm Plantations (TOPP) in the Central Region, and NORPALM and Benso Oil Palm Plantations (BOPP) in the Western Region respectively. Also there are eight medium-scale mills and about 400 small-scale processing units or more across the country. In addition, Golden Star, a mining company in the Western Region of Ghana is engaged in oil palm plantations. The company has a nursery with the capacity to produce over 100,000 palm seedlings per year which is sufficient to plant about 700 ha.

Research Institutions

There is a considerable number of research institutions in Ghana but Oil Palm Research Institute (OPRI) at Kusi (Kade) in the Eastern Region of Ghana, is the only institution fully dedicated to research into oil palm. It is also the only institution that produces seed nuts in the country.

Government and international interventions

The government of Ghana is making considerable efforts to promote oil palm cultivation to increase production of crude palm oil to meet domestic and industrial demands. Recently, an amount of 6.62 million euros was secured from the Agence Francaise de Developpement (AFD), a French international development agency to support a 3000 ha outgrower project on oil palm cultivation which is currently ongoing in the Upper & Lower Denkyira Districts of the Central Region of Ghana. Under the World Bank sponsored Agriculture Services Sub-Sector Investment Programme (AgSSIP), the Government of Ghana has expanded the seed nuts production capacity of Oil Palm Research Institute (OPRI) from 2 million to 5 million seed nuts per year. Also cultivation of over 20,000 ha small-scale farms under the President's Special Initiative (PSI) on oil palm cultivation has been implemented.

Results and discussion

Ghana's agriculture accounts for roughly one-quarter of GDP and employs more than half of the workforce, mainly smallholders. The profitability of palm oil industry in Ghana, that is, major companies through small to medium-scale production) provides crude palm oil (CPO) for home consumption and industrial use. For instance, one out of every two households (54 percent) in Ghana uses crude palm oil as a vegetable oil in food preparation. In the rural areas, however, the proportion of households that uses palm oil as cooking oil is even higher (62 percent). As a result of this great use of crude palm oil (CPO), the demand of palm oil outstrips supply and the country faces a yearly deficit of 300,000 tonnes of crude palm oil. The production is limited by a number of factors including cost of transportation of Fresh Fruit Bunches (FFB) to the processing mills, poor agricultural practices and limited access to land due to the traditional land ownership system inherent in Ghanaian culture. Despite this hindrance, Ghana is the third biggest exporter of curde palm oil (CPO, >100, 000 mt; 2009) in Africa. It is important also to note that independent smallholders with typical holdings of less than two hectares of oil palm plantation account for the major supply of (FFB) for crude palm oil production in Ghana (Masterplan study, 2011).

Considering the large scale estates, medium scale mills and small-scale processing units as shown in Tab. 1, the total area cultivated in 2010 was 340,000 hectares, which was a major expansion of the amounts cultivated in 2002 through 2009. Although the large estates have the highest farm productivity, it is low compared to Malaysia. For instance, Malaysia oil palm yields 17.6 tons per hectare, whereas large estates in Ghana do not get more than 10 tons per hectare on their nucleus plantations, and smallholder yields can be as low as 2 tons per hectare. Currently, none of the mills in the country operate at 100 percent capacity mainly because of short supply of Fresh Fruit Bunches (FFB).

In terms of total production of crude palm oil provided by the estates, medium-scale farms and small and other private holdings in 2010 was much higher than in 2008 but lower compared to 2009 production estimates as given in Tab. 2. However, total crude palm oil production has shown an increasing trend over the years from 2002 to 2009 but in 2010, the production declined.

In addition, among the estates or large-scale oil palm plantations, Ghana Oil Palm Development Company (GOPDC) produces more of the Fresh Fruit Bunches as well as the crude palm oil compared to the other estates. Nevertheless, the other companies are also expanding their production. Last year NORPALM Ghana Ltd processed a record volume of 70,000 tonnes of fresh fruits bunches from out-growers and also from own estate and this year the company is targeting to process 80,000 tonnes. On the other hand, Benso Oil Palm Plantation Limited (BOPP) also produced 14,270 tonnes of palm oil between January and November last year, recording a 30 percent increase over the previous year's 10,966 tonnes.

The future of oil palm industry in Ghana

The future of oil palm production seems to be very promising as a result of Government's intervention. At the moment, the Government has launched an Oil Palm Development Master Plan which outlines how the nation can boost its competitiveness in the global vegetable oil markets over a 15-year period. The summary of the plan includes but not limited to the following: finding the right strategies to transform small-scale village oil palm farming and palm oil production into more commercial and sustainable cultivation and production; accelerating production of Fresh Fruit Bunches (FFB) to attract industrial investment; expansion of milling capacities following implementation of programmes which increases FFB supply; improvement in productivity of oil palm plantations and mills of all sizes; improvement in FFB and palm oil quality for edible and industrial consumption; improving competitiveness of Ghanaian palm oil in the domestic and international markets; generating regular employment and income through the rapid expansion of the industry; diversification of the structure of the economy which relies on cocoa, gold and timber exported as primary products and raw materials to greater contribution from exports of industrial goods and services. This includes import substitution and self sufficiency in vegetable oil production and growth and development of the capital goods manufacturing sector.

Conclusion

The Government of Ghana, international financial agencies, major oil palm companies, medium-scale farms, small-scale farms and private holdings are making concerted efforts to increase oil palm cultivation so that in the future Ghana becomes self sufficiency in palm oil production and can compete on the global market like Indonesia and Malaysia. However, the oil palm industry in Ghana, and Africa generally, has a great potential to achieve increased production and possible export of crude palm oil if best management and agronomic practices are adopted.

Reference

Agriculture in Ghana, facts and figures, 2010. Ministry of Food and Agriculture; Statistics, Research and Information Directorate (SRID). Avaible at: www.mofa.gov.gh (accessed May 1, 2011)

Basiron Y., 2007. Palm oil production through sustainable plantations. European Journal of Lipid Science and Technology, 109: 289–295.

Fold N., Whitfield L., 2012. Developing a Palm Oil Sector: The Experiences of Malaysia and Ghana Compared, Danish Institute for International Studies, 08: 1–23.

Keshvaldi A., Endan J.B., Harun H., Ahmed D., Saleena F., 2011. The relationship between palm oil index development and mechanical properties in the ripening process of Tenera variety fresh fruit bunches. Research Journal of Applied Sciences, Engineering and Technology, 3: 218 –226.

MASTERPLAN STUDY ON THE OIL PALM INDUSTRY IN GHANA, 2011. Final report revised November, 2011.

Oworlarefe O.K., Olabige M.T., Faborade M.O., 2007. Physical and mechanical properties of two varieties of fresh oil palm fruit. Journal of Food Engineering, 78: 1228–1232.

Tagoe S.M.A., Dickinson M.J., Apetorbor M.M., 2012. Factors influencing quality of palm oil produced at the cottage industry level in Ghana. International Food Research Journal, 19 (1): 271–278.

MECHANICAL PROPERTIES OF EPOXY COMPOSITES FILLED WITH Al_2O_3/GLASS BEADS

Jiri Kejval*

Czech University of Life Sciences Prague, 165 21 Prague 6 – Suchdol, Czech Republic,
E-mail: kejval@tf.czu.cz

Abstract

Composite materials are nowadays expanding into many fields. The use of composite materials is limited by their characteristics that affect its individual components. Properties required for a particular application can be achieved by combining the various components with specific characteristics. Adding micro particles of Al_2O_3 and glass beads is intended to influence and improve the mechanical properties of the particle composite. The aim of this paper is to find an optimal representation of the components of Al_2O_3/glass beads and their ratio depending on the resulting mechanical properties of the composite. Along with different ratios of the individual components were also used different particle sizes of the ingredients used. As the matrix of the composite was used epoxy resin.

Keywords: Al_2O_3/glass beads, mechanical properties, polymeric particle composite

Introduction

In the field of materials engineering is currently continuous development. Creating new material with properties that lead this industry forward. One of the dynamically growing areas is the composite materials and these are becoming an important part of the many modern industries. These heterogeneous materials consist of two or more phases, each with different mechanical, physical and chemical properties (Jančář, 2003). Combination of polymer matrix and particulate filler is referred to as a polymeric particle composite. They combine the mechanical properties of the filler with the suitable properties of the matrix (Suresha et al., 2011).

Sanchez-Soto et al. (2007) engaged in the mechanical properties of epoxy resin filled with glass beads of size 2-120 µm volume amounts ranging from 0 – 40 %. Mechanical properties such as tensile strength was the same in some cases higher than the actual matrix, such as tensile strength of the composite with 40 % reached 44.9 MPa compared with matrix 38.1 MPa. On the contrary values impact strength decreased to 50 % of the matrix itself. Liang and Wu (2012) has been added to the polypropylene matrix glass beads of size 34 µm, the achieved improvements in both tensile properties and impact strength. Volume of the glass beads ranged from 0-18%. Young's modulus increased nonlinearly, while the tensile strength decreased with increasing volume fraction. Charpy impact strength increased with increasing volume fraction of up to 11 %, which on the contrary decreased to 18 %. Glass beads also adding Tjong and Xu (2001) into a mixture of polyamide PA 6.6, which was prepared by extrusion and subsequent injection. The measurement showed very little effect adding glass beads to tensile and impact test showed a decreasing trend with increasing content of glass beads and the best ratio between mechanical properties was a mixture containing 20 %. The aim of this paper is to find an optimal representation of the components of Al_2O_3/glass beads and their ratio depending on the resulting mechanical properties of the composite. Along with different ratios of the individual components were also used different particle sizes of the ingredients used. As the matrix of the composite was used epoxy resin.

Materials and method

To measure the influence of particle size and concentration on the mechanical properties of polymeric particle composites were used as a matrix two-component epoxy resin EPOXY ECO-1200/324 based on bisphenol A hardening with curing agent P11. Al2O3 and glass beads with the total volume amount of the filler 30 % were added into the composite as the reinforcing phase. Glass beads are microscopic spherical glass particles. They are used primarily for fine blasting, polishing and cleaning of stainless steel parts. Manufacturers indicate glass beads also the name BALLOTINI (Pottersbeads 2013; Alumetal Technik 2013). Ratios among single fractions of the artificial corundum F80 and glass beads B10, B112, B134 and B112 were chosen in a following way: 1:5 and 5:1 (Al_2O_3:glass beads). Express the amount of filler in the matrix volume percent, respectively volumetric ratio, prevent the influence of different density matrix (density in the hardening state given by the manufacturer is 1.15 g·cm-3) and filler. The particles size of Al_2O_3 of the fraction F80 was 185 µm and the size of glass beads ranged according to the producer according to the fraction from 300 µm for the fraction B10 till 70 µm for B159.

The process of preparing composite system consisted of mixing the epoxy resin and the particulate filler, which has been always performed by the same procedure in order to guarantee reproducible results. Mechanical mixing was carried out in a plastic container, which was placed in an ultrasonic bath, where mechanical waves facilitate homogeneous dispersion of the filler particles in resin and minimize the formation of air bubbles, which may negatively effect on the mechanical properties of the test. Prepared mixture was cast into prepared molds that shape and dimensions specified in the standards. For the manufacture of molds for casting specimens were first made of steel specimens which represented negative for the molds made of Lukopren N. In these forms were then cast respective specimens.

To measure the shapes, sizes and angles edges filler particles used image analysis performed stereomicroscope using built-in camera and software Quick Photo Industry measured different dimensions and surface particles in a 2D plane.

The abrasive wear resistance was tested on rotating cylindrical drum device with the abrasive cloth of the grain size P120 and P220 according to the standard ČSN 62 1466. The diameter of the test specimens was 15.5 ± 0.1 mm and their height was 20 ± 0.1 mm (ČSN 62 1466, 1993). The shape and sizes of diameter test specimens were prepared by means of turning. The test specimen is in the contact with the abrasive cloth and it covers the distance 60 m. The pressures force is 10 N.

The hardness was evaluated in accordance with the standard ČSN EN ISO 2039-1. Experimentally measured hardness by a method according to Brinell (ČSN EN ISO 2039-1, 2003), in accordance with the above mentioned standard, was carried out on samples of sizes 35 x 20 x 10 mm which were loaded by a force 2.452 kN for the time 30 sec. A ball from a hard metal of a diameter of 10 mm was used as a penetrating indentor.

The impact tests were carried out according to the standard ČSN 64 0611 - determination of the impact resistance of rigid plastics by means of Dynstat apparatus (ČSN 64 0611, 1968). The test specimens for the tensile properties determination according to the standard ČSN EN ISO 527-1 (1997) were prepared according to the standard ČSN EN ISO 3167 (1997).

Results and discussion

Particle size was measured by image analysis on an optical microscope with built-in camera and software Quick Photo Industry. The measured particles size of Al_2O_3 of the fraction F80 was 145 ± 23 µm, for glass beads of the fraction B10 it was 217 ± 23 µm, of B112 169 ± 20 µm, of B134 148 ± 16 µm, of B159 94 ± 11 µm. Fig. 1 shows the dependence of the Brinell hardness of the impact strength of composite systems. The highest measured hardness was at the composite systems with the content of Al_2O_3 of F80 and glass beads of B159 in a ratio 1:5 which amounted 17.5 ± 0.45 HB. The hardness of the unfilled epoxy resin was 10.7 ± 0.19 HB but was measured at the highest impact strength 6.1 ± 0.77 kJ.m-2. Schroder et al. (2003) describe a significant improvement in impact strength and hardness but lower tensile strength in hybrid composites containing 5 – 10 % of the liquid rubber and 10 - 60 % of glass balls. A similar issue was discussed by the authors (Valášek 2012; Müller 2013) who examined the hardness of the polymer particle composites filled with recycled material from the blasting process.

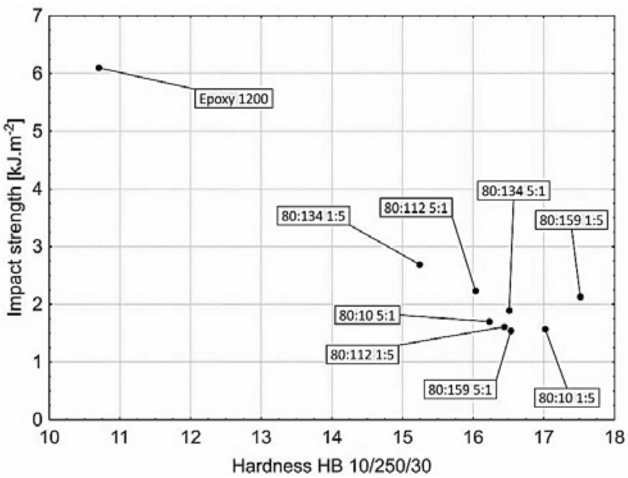

Fig. 1 Hardness and impact strength of tested polymeric system

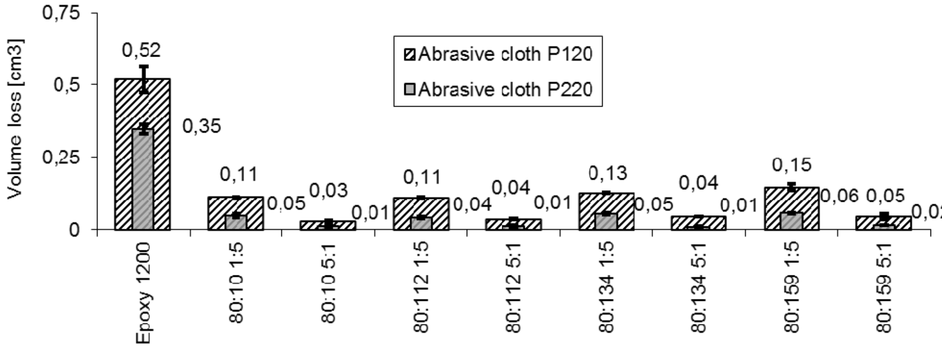

Fig. 2 Abrasive wear resistance - volume losses

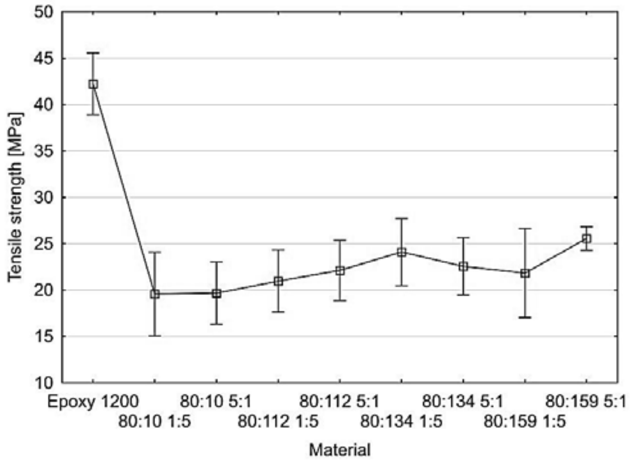

Fig. 3 Tensile strength

Fig. 2 shows the results of measuring the three-body abrasion. The volume losses for the epoxy resin without the filler were 0.3473 ± 0.0017 cm^{-3} for the cloth P220, 0.5198 ± 0.0021 cm^{-3} for the cloth P120. The smallest volume loss for the cloth P220 was at the composite systems with higher content of Al_2O_3, in the ratio 5:1 (Al_2O_3 : glass beads) at the composite 80:10 (the volume loss 0.012 ± 0.0025 cm^{-3}), at the composite 80:112, 80:134 and 80:159. The smallest volume loss for the cloth P120 was measured 0.028 ± 0.0028 cm^{-3} at the composite 80:10 with ratio 5:1. The measurement results confirmed the presumption of the authors (Müller 2012; Valášek 2013) who state considerable decrease of the volume losses at the composite systems filled with particles of Al_2O_3.

Tensile strength of composites was measured at various amounts of the individual components Al2O3 and glass beads with a maximum saturation of the mixture 30 %. The differences between the ratios of components had no significant effect compared to the particle size. From fig. 3 it is visible decreasing tensile strength depending on the increasing sizes of glass beads in the composite. The highest value of tensile strength 42.58 ± 1.28 MPa was measured in epoxy resin without added particles. The highest measured tensile strength 26.56 ± 0.54 MPa corresponded to the composite systems with the content of Al2O3 of F80 and glass beads of B159 in ratio 5:1. From the experiment has been confirmed the supposition of authors (Valášek, 2011; Müller 2010) that the addition of particles to reduce the tensile strength of the composite in comparison with the epoxy resin without fillers. Mechanical properties of polymers filled with 0 – 30 % glass beads have also examined the Balkan, Demirer (2010) who achieved the best properties at 2.5 % and 5 %, which increased impact strength, but there was also a reduction in the modulus of elasticity and tensile strength.

Conclusion

The experiments have shown that the addition of fillers in epoxy resins significantly influences the final mechanical properties. Been found a relationship between particle size, ratios of the individual components and the mechanical properties. Due to the hardness of the added particles of Al2O3 and glass beads also increased hardness of the composite, which is related to the resistance to abrasive wear. Applied filler significantly reduced tensile strength and impact strength. These mechanical properties depend on the interaction between the filler and the matrix. The interaction depends on the type, size, shape and amount of filler in the matrix. Carried out experiments whose aim was to map the influence of adding particles of Al2O3 and glass beads of various sizes and various mutual ratio combinations into the epoxy resin can be summarized into following points:

- Increasing the hardness of the composite compared to the epoxy resin.
- For all the tested composites decreased impact strength of more than 50 % of epoxy resin.
- At the three-body abrasion wear the systems created with higher content of Al_2O_3 together with glass beads were the most resistant.
- The decrease of the tensile strength at all composite systems of 39 % compared with the

unfilled epoxy resin, the difference among single concentration ratios is 27 %.

Acknowledgement

This paper has been done when solving the grant of the title “Study of factors affecting the strength and durability of perspective bonds” Nr. 2013:31140/1312/3107.

Reference

Alumetal-Technik. Available at: www.alumetal-technik.com (accessed June 26, 2013)

Balkan O., Demirer H., 2010. Mechanical properties of glass bead-and wollastonite-filled isotactic-polypropylene composites modified with thermoplastic elastomers. Polymer Composites 31 (7): 1285 – 1308.

CSN 62 1466 (1993): Determination of abrasion resistance using a rotating cylindrical drum device. Prague, Czech Standard Institute. (in Czech)

CSN EN ISO 2039-1 (2003): Plastics - Determination of hardness. Prague, Czech Standard Institute. (in Czech)

CSN 64 0611 (1968): Plastics testing. Determination of the impact resistance of rigid plastics by means of Dynstat apparatus. Prague, Czech Standard Institute. (in Czech)

CSN EN ISO 527-1 (1997): Plastics - Determination of tensile properties. Prague, Czech Standard Institute. (in Czech)

CSN EN ISO 3167 (1997): Plastics - Multipurpose test specimens. Praha: Prague, Czech Standard Institute. (in Czech)

Jančár J., 2003. Introduction to Materials Engineering polymer composites Brno: Brno University of Technology: 194. (in Czech)

Liang J. Z., Wu C. B., 2012. Effects of the glass bead content and the surface treatment on the mechanical properties of polypropylene composites. Journal of Applied Polymer Science 123 (5): 3054 – 3063.

Müller M., Hrabě P., 2013. Overlay materials used for increasing lifetime of machine parts working under conditions of intensive abrasion. Research in Agricultural Engineering, Vol. 59: 16 - 22.

Müller M., Valášek P., 2012. Abrasive wear effect on Polyethylene, Polyamide 6 and polymeric particle composites. Manufacturing Technology, Vol. 12,12: 55 - 59.

Müller M., Valášek P., Tomek L., 2010. Mechanical properties of polymeric particle composites. In Trends in Agricultural Engineering, Prague: Czech University of Life Sciences Prague, Faculty of Engineering: 454 - 458.

Potters Industries LLC. Available at: www.pottersbeads.com (accessed June 26, 2013)

Sánchez-Soto M., Pagés P., Lacorte T., Briceño K., Carrasco F., 2007. Curing FTIR study and mechanical characterization of glass bead filled trifunctional epoxy composites. Composites Science and Technology 67 (9): 1974 – 1985.

Schröder N., Könczöl L., Döll W., Mülhaupt R., 2003. Mechanical properties of epoxy-based hybrid composites containing glass beads and α,ω-oligo(butylmethacrylate)diol. Journal of Applied Polymer Science 88 (4): 1040 – 1048.

Suresha B., Ravi Kumar B. N., 2011. Two-body Abrasive Wear Behavior of Particulate Filled Polyamide66/Polypropylene Nanocomposites. Journal of Applied Polymer Science 119: 2292 - 2301.

Tjong S. C., Xu S. A., 2001. Ternary polymer composites: PA6,6/maleated SEBS/glass beads. Journal of Applied Polymer Science 81 (13): 3231 – 3237.

Valášek P., 2011. Strength characteristics of polymer particle composites with filler on basis of waste from mechanical surface treatment. 10th International Scientific Conference on Engineering for Rural Development Jelgava: 434 – 439.

Valášek P., Brožek M., 2011. Two body abrasion of composites containing filler on the basis of hard cast iron deposits utilizable in agrocomplex. Agronomy Research 11: 163 - 170.

Valášek P., Müller M., Proshlyakov A., 2012. Effect of sedimentation on the final hardness of polymeric particle composites, Research of. Agriculture Engineering. 58: 92 - 98.

TENSILE PROPERTIES OF POLYETHYLENE FILMS AND PAPER

Ľubomír Kubík*, Stanislav Zeman

Slovak University of Agriculture in Nitra, 94976 Nitra, Slovak Republic,
Phone: +421037- 6414879, Fax: +421037-7417003, E-mail: Lubomir.Kubik@uniag.sk

Abstract

The paper deals with the evaluation of the mechanical properties of the polyethylene films such as the stress, strain, modulus of elasticity and stress and strain in the moment of breaking. The thin films of thickness 50 μm which contained 91 % of polyethylene Bralen RA 2–63 and 9 % colored concentrate Maxithen were studied. "Chicken" paper is usually used for chicken breeding. "Chicken" paper is disintegrating and it decomposes due to a moisture and it don't glue on the chicken legs. We measured the tensile properties as modulus of elasticity, maximal elongations, maximal tensile forces, tensile strengths, tensile indexes and strain at breaks of the longitudinal and transversal samples by testing paper strips.

Keywords: polyethylene films, chicken paper, tensile properties

Introduction

Thin plastic films are used in a wide variety of applications such as packaging materials, heat shrink wrap, consumer plastic bags, and adhesive tape. The films evoke more favorable conditions of the growing and progression of the plants which consequence is enhancing of the harvest, quality and the realized production (Romic et al., 2003; Ibarra–Jimenez et al., 2006). The best responses on the application of polyethylene films have fruiting vegetables. Mechanical properties of the polyethylene films are important for determination of suitable mulch films to the various plants from the point of view to penetration of the plants through mulch films. Spadaro (1993) studied effect of ageing due to gamma radiation, at various dose rates and temperatures, on the mechanical tensile behaviour of low density polyethylene. Nazhad et al. (2010) studied two softwoods mechanical pulps from species of differing fibre length and coarseness which were fractionated by fibre length and formed into handsheets at standard handsheet consistency and at a headbox consistency. Kunnari et al. (2007) studied the effect of fibre shape factor on water removal, wet web tensile and especially relaxation properties, i.e. the tension holding capacity of wet web was studied. Chicken" paper is usually used for chicken breeding. Chicken paper is disintegrating and it decomposes due to a moisture and it don't glue on the chicken legs. The objective of this study was to examine the tensile behaviour of thin polyethylene films and the papers by testing paper strips in the linear region of straining. We measured the tensile properties as modulus of elasticity, maximal elongations, maximal tensile forces, tensile strengths, tensile indexes and strain at breaks of the longitudinal and transversal samples by testing polyethylene and paper strips.

Material and methods

Samples contained 91 % of polyethylene Bralen RA 2–63 and 9 % colored concentrate Maxithen. They were made by Plastika a.s. Nitra for mulch applications. Four sorts of films were examined: samples with Maxithen HP 1510 – white, Maxithen HP 231111 – yellow, Maxithen HP 533031 – blue and Maxithen HP 533 041 – violet. Thickness of the samples was 50 μm. Samples were cut in the longitudinal and transversal direction on the dimensions (150x15) mm. Ten samples of the films were used of each sort. The tensile behavior was monitored on the motorized test stand ANDILOG STENTOR 1000. The force F (N) and elongation δ (mm) were measured when the speed of flat grip fixtures was 200 mm.min^{-1} and data were stored in xls format in the computer.

„Chicken" paper is a special paper which is suitable for chicken breeding. The paper absorbs the drops of the water and makes the environment more hygienic for the chicken. The paper disintegrates with 100 % efficiency due to a moisture. The are three sort of the paper in dependence on disintegration, with the reducibility 2 - 3 days, 5 - 6 days or 8 - 9 days. The basic weight of paper is 40 g/m^2 , the thickness 100 μm and paper is packed in the rolls of the length 220 m with the width 68 cm. „Chicken" paper was measured in the same method as the polyethylene films. The dimensions of the samples were (180x15) mm and the speed of flat grip fixtures was 20 mm/min. The initial length of the sample was 150 mm for polyethylene films and 180 mm for paper. Tensile modulus of elasticity E (MPa) of the polyethylene film is defined as the stress change divided by change in strain within the linear region of the stress/strain curves:

$$E = \frac{\sigma_2 - \sigma_1}{\varepsilon_2 - \varepsilon_1}, \quad (1)$$

where σ_1 is the stress equivalent the strain ε_1 = 0.0005 mm/mm and σ_2 is the stress equivalent the strain ε_2 = 0.0025 mm/mm. Modulus values were calculated by taking the slope of stress versus strain curves but in the range of strains from 0.0005 mm/mm to 0.0025 mm/mm, (0.05% – 0.25%) where the stress/strain dependency is linear. There was problem to adhere the terms because the test stand fails to measure all data at the beginning of the measurement. The breaking strength determined by maximal stress at break σ_T (MPa) and maximal strain at break ε_T (mm/mm) of the polyethylene films were also measured in the time of the rupture of the films.Tensile modulus of elasticity of the paper E (MPa) was defined from the equation:

$$E = \frac{S_{max}\, l}{bt}, \quad (2)$$

where:

S_{max} – maximal slope of the curve of force versus elongation, N/mm
l – initial length of the specimen, mm
b – initial width of the specimen, mm
t – thickness of the paper, mm

Tensile strength of the paper σ_T^b (kN/m) is maximal tensile force referring on the unit of the width, which paper suffers before the breaking. The maximal tensile force of the each specimen was determined. The average maximal tensile force was calculated and than the tensile strength was evaluated from the equation:

$$\sigma_T^b = \frac{\overline{F_t}}{b} \quad (3)$$

where:

σ_T^b – tensile strength, kN/m
$\overline{F_t}$ – average maximal tensile force, N
b – initial width of the specimen, mm

Tensile index σ_T^w (kNm/kg) was defined from the equation:

$$\sigma_T^w = \frac{1000\, \sigma_T^b}{w} \quad (4)$$

where:

σ_T^w – tensile index, kNm/kg
w – basic weight, g/m^2.

Maximal strain at break ε_T (%) was defined as the percent of the initial length of the specimen from the equation:

$$\varepsilon_T = \frac{\delta_b}{l} 100 \quad (5)$$

where:

δ_b – maximal elongation , mm
l – initial length, mm.

The maximal elongation and maximal tensile force was measured in the moment of the breaking of the paper sample.

Results and discussion

At low stresses most polyethylene samples indicated a linear viscoelastic response. The example of tensile stress/strain diagram of the longitudinal polyethylene film sample with colored concentrate Maxithen HP 533041 – violet is presented at the Fig. 1. The dependency presents the region of linear viscoelasticity, to the value of the strain 0.0025 mm/mm than the region of the viscoelasticity to the value of the strain about 0.060 mm/mm and the region of the plasticity over the strain 0.060 mm/mm. The breaking strength was determined as the maximal stress 10.16 MPa at the maximal strain 1.59 mm/mm. The resulting modulus of elasticity was 288 MPa. Modulus of elasticity was obtained from the slope of the regression line in the range from 0.0016 mm/mm to 0.014 mm/mm and no from the Eq. (1), because the initial interval of the measured strains was measured only from 0.0016 mm/mm. This problem was caused by the fixation of the samples in the flat grip fixtures and the initial data acquisition. The results of the examined films are presented in the Tab. 1 and the Tab.2 for the longitudinal and transversal samples respectively.

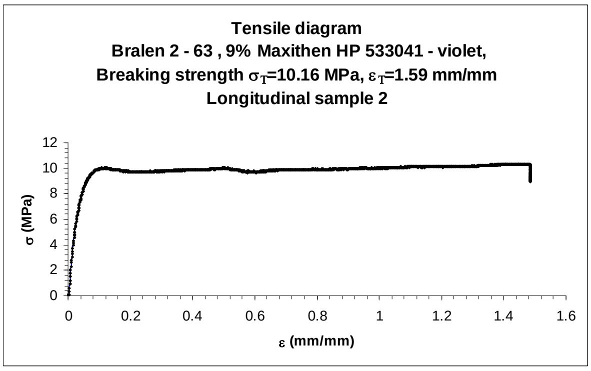

Fig. 1 Tensile stress – σ versus strain – ε diagram of polyethylene sample Bralen RA 2 – 63 with color concentrate Maxithen HP 533041 – violet for longitudinal sample 2 and values of maximal stress at break σ_T=10.16 MPa and maximal strain at break ε_T=1.59 mm/mm

The example of tensile stress versus strain diagram of the "chicken" paper of the longitudinal sample 1 is presented at the Fig. 2. We obtained values of maximal tensile force F_t = 3.7 N and maximal elongation δ_b = 5.4 mm. We determined the maximal slope of the curve of force versus elongation, S_{max} (N/mm) from the Fig. 2 in the range of the elongation from 0 mm to 2 mm (linear region). The value of S_{max} was 1.2 N/mm. The modulus of elasticity was determined from the Eq. (2). Its value was 136 MPa. We also determined tensile strength from the Eq. (3), it was 0.3 kN/m, tensile index from the Eq. (4), it was 6.1 kNm/kg and maximal strain at break from the Eq. (5), it was 3%.

The value of S_{max} was 1.4 N/mm. The modulus of elasticity was determined from the Eq. (2). Its value was 160 MPa. We also determined tensile strength from the Eq. (3), it was 0.5 kN/m, tensile index from the Eq. (4), it was 12.3 kNm/kg and maximal strain at break from the Eq. (5) and it was 7.9%. The results of the examined paper are presented in the Tab. 3 and the Tab. 4 for the longitudinal and transversal samples respectively. Tensile properties of the polyethylene films and paper are important for advisement of mechanical condition of the materials. Tensile properties of the films and paper were studied only in the linear viscoelastic region of film and paper deformations. In consequence viscoelastic behavior of the polymers a lot of properties depend not only on the temperature, but also on the time. The stress–strain dependency of the tensile test is nonlinear even in the range of linear viscoelasticity.

Tab. 1 Results of the modulus of elasticity E (MPa), the maximal stress and strain at break σ_T (MPa) and ε_T (mm/mm) respectively of the longitudinal samples and their standard deviations of the yellow, white, blue and violet films Bralen RA 2 – 63

Sample	**Longitudinal**					
	Mean	**Std**	**Mean**	**Std**	**Mean**	**Std**
	E (MPa)	s_E (%)	σ_T (MPa)	s_b(%)	ε_T (mm/mm)	s_ε (%)
Yellow	251	5.4	12	1.0	1.5	1.6
White	223	8.0	13	0.9	1.5	0.5
Blue	229	10.8	10	1.0	1.5	0.8
Violet	298	2.3	10	0.6	1.5	1.4

Std – standard deviation

Tab. 2 Results of the modulus of elasticity E (MPa), the maximal stress and strain at break σ_T (MPa) and ε_T (mm/mm) respectively of the transversal samples and their standard deviations of the yellow, white, blue and violet films Bralen RA 2 – 63

Sample	**Transversal**					
	Mean	**Std**	**Mean**	**Std**	**Mean**	**Std**
	E (MPa)	s_E (%)	σ_T (MPa)	s_σ(%)	ε_T (mm/mm)	s_ε (%)
Yellow	270	7.5	12	0.9	1.6	0.6
White	180	13.3	16	0.7	1.5	0.2
Blue	208	9.7	13	0.6	1.5	0.7
Violet	220	10.1	12	2.3	1.5	0.8

Std – standard deviation

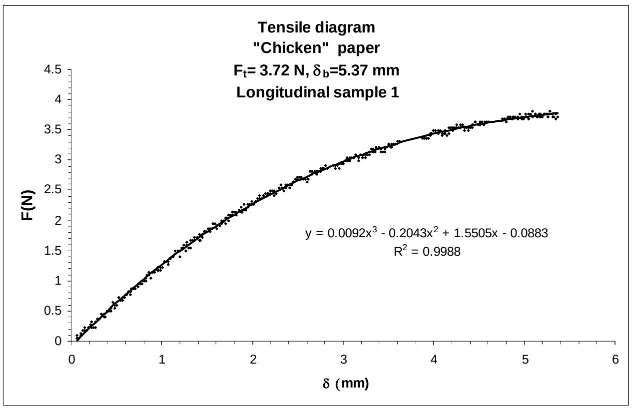

Fig. 2 Tensile force – F versus elongation – δ diagram of "chicken" paper sample for longitudinal sample 1 and values of maximal tensile force F_t = 3.72 N and maximal elongation δ_b = 5.37 mm

Tab. 3 Results of maximal elongation δ_b (mm), maximal tensile force F_t (N), tensile strength $\sigma^b{}_T$ (KN/m), tensile index $\sigma^w{}_T$ (kNm/kg), maximal strain at break ε_T (%), maximal slope of the curve of force versus elongation S_{max} (N/mm) and modulus of elasticity E_L (MPa) respectively of the longitudinal samples and their standard deviations of the "chicken" paper

"Chicken" paper	Longitudinal						
Sample	**δ_b (mm)**	**F_t (N)**	**$\sigma^b{}_T$ (kN/m)**	**$\sigma^w{}_T$ (kNm/kg)**	**ε_T (%)**	**S_{max} (N/mm)**	**E_L (MPa)**
Mean	4.4	3.5	0.2	5.9	2.5	1.3	155
s	0.3	0.1	0.01	0.2	0.2	0.1	5.2
s (%)	7.7	4.1	4.0	4.1	7.7	3.4	3.4

Tab. 4 Results of maximal elongation δ_b (mm), maximal tensile force F_t (N), tensile strength $\sigma^b{}_T$ (KN/m), tensile index $\sigma^w{}_T$ (kNm/kg), maximal strain at break ε_T (%), maximal slope of the curve of force versus elongation S_{max} (N/mm) and modulus of elasticity E_T (MPa) respectively of the transversal samples and their standard deviations of the "chicken" paper

"Chicken" paper	Transversal						
Sample	**δ_b (mm)**	**F_t (N)**	**$\sigma^b{}_T$ (kN/m)**	**$\sigma^w{}_T$ (kNm/kg)**	**ε_T (%)**	**S_{max} (N/mm)**	**E_T (MPa)**
Mean	12.7	6.8	0.5	11.3	7	1.4	158
s	0.4	0.2	0.01	0.3	0.2	0.03	3.3
s (%)	2.9	2.6	2.6	2.6	3	21	2.1

This effect is typical of the tenacious polymers. For that reason the values of the tangential modulus tenacious materials, determined from the initial part of the curve stress – strain, often depends on the applied scale factor. From that reason the method of the measurement of the modulus of elasticity of the polyethylene films was based on two specific values of the strain, i. e. 0.05 % and 0.25 %. Our measurements of the polyethylene films were realized in the near region of these values.

Conclusions

Mean values were determined from ten samples of the polyethylene films. Mean values of the moduli of elasticity E (MPa) of the longitudinal and transversal polyethylene samples exhibited similar size respectively. Brandrup et al. (1999) introduce the moduli of the polyethylene material into the range of 55 to 172 MPa. Our results were in average 250 MPa for longitudinal samples and 220 MPa for transversal samples. There were not significant differences among the elastic values of the longitudinal and transversal properties of the films.

The maximal stresses and maximal strains at the break σ_T (MPa) and ε_T (mm/mm) were also similar for longitudinal and transversal samples.

Mean values of the moduli of elasticity of the "chicken" paper of the longitudinal and transversal samples were almost identical. Mean values of the moduli of elasticity were in the linear region 155 MPa for longitudinal samples and 158 MPa for transversal samples. The values of the maximal elongation of the transversal samples were three times bigger than the longitudinal samples. The values of the maximal tensile force, tensile strength, tensile index and maximal strain at break were two times bigger for transversal samples than the longitudinal samples. Holik (2013) presents the tensile indexes of the pulp from 30 kNm/kg to 40 kNm/kg, which are in the same order with our measurements in Tab. 3 and Tab 4. Kataja – Aho et al. (2011) present the values of the tensile strength of the wet paper from 0.1 kN/m to 0.4 kN/m and the strain at break of the wet paper from 2% to 4% in dependence of the dry solids content which are in good agreement with our measurements. The results of our measurements for the tensile strength of samples of "chicken" paper were 0.2 kN/m for longitudinal samples and 0.5 kN/m for transversal samples. Our results of the strain at break of samples of "chicken" paper were from 2.5 % for longitudinal samples to 7.0 % for transversal samples. The measurements of the tensile properties of the "chicken "papers were realized also in the linear region, between 0.0 % and 1.1% of the strain values.

References:

Brandrup J., Immergut E.H., Grulke E.A., 1999. Polymer Handbook. 4nd Ed., Wiley, New York, 2000.

Holik H., 2013. Handbook of Paper and Board. Second, Revised and Enlarged Edition, Volume 1, 2, Wiley-VCH Verlag GmbH & Co., KGaA Boschstr. 12, Weinheim, Germany, 800.

Ibarra-Jimenez L., Quezada-Martin R., Cedeno-Rubalcava B., Rio A.J.L., de la Rosa-Ibarra M., 2006. Watermelon Response to Plastic Mulch and Row Covers. In: European Journal of horticultural science, 71 (6): 262–266.

Kataja, Aho J., Haavisto S., Asikainen J., Hyvärinen S., Vuoti S., 2011. Web Strength and Xylan, BioResources, 7(2): 1713 – 1728.

Kunnari V., Salminen K., Oksanen A., 2007. Effects of Fibre Deformations on Strength and Runnability of Wet Paper, Paperi Ja Puu-Paper and Timber, 89 (1): 46 – 49.

Nazhad M.M., Harris E.J., Dodson Ch.T.J., Kerekes R.J., 2010. The Influence of Formation on Tensile Strength of Paper Made from Mechanical Pulps, Tappi Journal, 83 (12): 1 – 9.

Romic D., 2003. Polyethylene Mulches and Drip Irrigation Increase Growth and Yield in Watermelon (Citrullus lanatus L.). In: European Journal of Horticultural Science, 68 (4): 192–198.

Spadaro G., 1993. Effect of Irradiation Temperature and Dose Rate on the Mechanical Tensile Behaviour of Low Density Polyethylene, European Polymer Journal, 29 (9): 1247–1249.

INFLUENCE OF AN AUTOMATIC BIOMASS GASIFIER ON THE QUALITY OF DRYING RIPE COFFEE CHERRIES

Jadir N. Silva[1*], Svetlana F. S. Galvarro[2]

[1]Federal University of Viçosa - Viçosa/MG, Brazil, Phone: (+55) (31) 3899-1928,
E-mail: jadir@ufv.br
[2]Master's student of the Graduate Program in Agricultural Engineering, Viçosa /MG, Brazil

Abstract

In order to maintain coffee quality within the commercialization standards, the post-harvest stages must be very well conducted, especially those related to cleaning, drying and storing, so that quality is not lost during storage. Among these stages, drying is the most important and if poorly conducted could put the quality of the product at risk. Drying requires clean warm air in order not to contaminate the product. Few studies have been performed on gasification, especially application of this process to drying grains. Therefore, the objective of the present study was to apply heated air generated by an automated biomass gasifier (eucalyptus charcoal) in coffee drying. Drying of the ripe coffee cherry in this study was performed in two drying silos attached to an automated biomass gasifier which generates the heated air used in the process. Two treatments were determined to conduct the study: treatment 1 consisted of 8 hours of drying per day, with revolving the grain mass every 2 hours; and treatment 2 consisted of drying the coffee on a suspended terrace and on concrete. In order to evaluate the influence of coffee drying in the system proposed, the following parameters were analyzed: beverage classification, electrical conductivity, potassium lixiviation and one thousand grain weight. Coffee dried in the proposed system was classified as a soft beverage, obtaining an average grade of 79 points. Based on the results, the following average values were obtained: 146.86 $\mu Scm^{-1}g^{-1}$ for the electrical conductivity; 34.04 $ppm.g^{-1}$ for potassium lixiviation; 160.90 g as the one thousand grain weight. Drying performed using the proposed method showed to be viable since the dry coffee obtained presented good qualitative results regarding the specific mass, electrical conductivity, potassium lixiviation, color and other parameters which indicated that there was no risk of final quality loss in the beverage.

Keywords: biomass, coffee, drying, gasifier, weight

Introduction

Knowledge on gasification has grown in recent years due to the necessity for technologies that provide efficient and viable methods of energy conversion. Biomass gasification technology can provide benefits such as economic and social development if incorporated in the process of agricultural production. Because it is an easily applied technology that uses biomass, it can be easily integrated in the rural regions. It also favors energy independence, since from gasification both electrical and mechanic energy can be generated, offering a non-dependence on generation units (Lora et al., 2009). However, there are still few studies on the gasification technology, especially its application for the grain drying. Therefore, the objective of this study was to apply an automated gasifier (eucalyptus coal) for air heating in a coffee drying process.

Objective

To evaluate the quality of ripe coffee cherries dried in a fixed layer, using charcoal as an energy source (eucalyptus) for air heating, using an automated gasifier.

Materials and methods

The study was conducted in the Area of PreProcess and Storing of Plant Products at the Agricultural Engineering Department, Federal University of Viçosa.

A concurrent gasifier was projected by Rezende (2012), in which the biomass feeding was performed at the top. An external ring (Figure 01) was built in the body of the reactor, with five openings for the entrance of primary air to the inside of the reactor oxidation area via a system of positive forced ventilation, in order to facilitate the process of combustion and later, the gasification of the fuel.

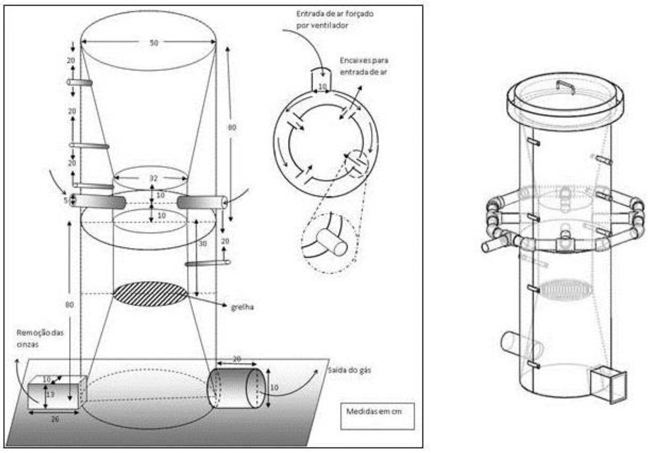

Fig. 1 Schematic Diagram of the gasifier

A masonry gas burner was constructed just where the gases exit the reactor, where the produced gases were immediately combusted to produce heated air destined for the drying process; after exiting the gas burner, it was directed to a mixture chamber where this heated air was mixed with ambient air. Figure 02 below represents the reactor together with the adjacent gas burner composing the concurrent gasifier used in this study.

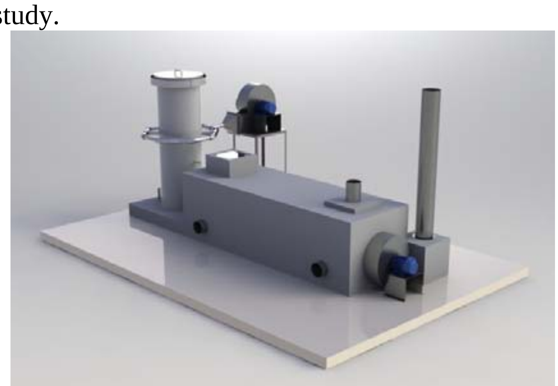

Fig. 2 Gasifier reactor together with the gas burner and mixing chamber, forming the gasifier

This system was connected to two silos by means of metal ducts. The drying silos, after being constructed and attached to the hot air generation system, had the following dimensions: radius of 0.5 m and diameter of 1 m; total height of 1.20 m; effective height of 0.80 m; plenum height of 0.40 m.

The silos were filled with a 0.4 m thick layerand at every 0.10 m a thermocouple was installed connected to a system of data acquisition in order to monitor the temperature of the grains to keep them at approximately 50 ºC +/- 5 ºC.

The drying system proposed in this study, which was composed of an automatic biomass gasifier attached to the silos, can be observed in Figure 03.

Fig. 3 Silo-gasifier system built to dry coffee

The experimental tests were performed using two treatments:

Treatment 01 – 8 hours of drying with manual revolving of the mass at 2h intervals.

Treatment 02 – Drying on a suspended terrace and on concrete. The suspended terraces were .94 m high, 2.04 m long and 1m wide. In total there were 8 terraces, 4 repetitions for each terrace type (Figure 04).

For treatment 1, four drying tests were performed, where the fuel used was charcoal.

(a) (b)

Fig. 4 (a) Drying on concrete terraces; (b) Drying on suspended terraces

The physical characteristics of the coffee were evaluated during the drying tests, including: impurity, water content and apparent specific mass of the grains. The methodology described in the Brazilian Rules for Seeds Analysis was used to determine the moisture content by the method of drying in an oven at 105±3 ºC during 24 hours.

The apparent specific mass was measuredusing a hector scale with the capacity of 1 liter, according the standard method. The chemical characteristics analyzed were potassium lixiviation and electrical conductivity. The values obtained for these characteristics were the average of the samples removed.

The official classification of coffee quality in Brazil is based on Regulatory Instruction no.16, on May 24th 2010, which establishes the Technical Regulation for Toasted Coffee Grains and Toasted and Ground Coffee Grains. The beverage classification was defined according to the grade attributed to it, and also according to the limits defined below:

- Grade equivalent to or higher than 86 refers to a strictly soft beverage;
- Grade between 80-85 refers to a soft beverage;
- Grade between 75-79 refers to an strictlysoft beverage;
- Grade equivalent to or lower than 74 refers to a hard beverage.

Results and discussions

The average values obtained for the apparent specific mass of coffee grains for treatment 01 were 400.60 kg.m^{3}for moisture content of 37.8 % (d.b.) and 382.76 kg.m^{3}for moisture content of 12.6 % (d.b.). The results obtained are in accordance with Afonso (1994), who concluded that the apparent specific mass of coffee in the husk is higher for a higher moisture content, and in this case the resistance of the product to the air flow is lower. The average values of electrical conductivity for treatment 01 are found in TABLE 01.

Table 1 Average results of the electrical conductivity analysis for treatment 01

Treatment	Test	EC (µS cm^{-1} g^{-1})
01	1	155.39
	2	134.73
	3	143.13
	4	154.18
Average		146.86
StandardDeviation		9.79

EC = electrical conductivity

The average values of the potassium lixiviation analysis for treatment 01 are presented below.

Table 2 Average values of the potassium lixiviation analysis for treatment 01.

Treatment	Test	KL (ppm g^{-1})
01	1	27.9
	2	33.06
	3	31.22
	4	43.98
Average		34.04
StandardDeviation		6.96

The values of the grade obtained in the sensory analysis of the coffee submitted to drying in the proposed system are found in TABLE 03. The sensory analysis of the cup test was performed in the 3 Irmãos Coffee Center, located in Viçosa-MG.

Table 3 Beverage grades for the coffee submitted to treatment 01.

Treatment	Test	Grade	Bevarage
01	1	79	Strictly soft
	2	79	Strictly soft
	3	79	Strictly soft
	4	79	Strictly soft
Average		79	
Standard Deviation		0.0	

From these results, it is observed that the beverage quality resulting from treatment 01 was not compromised, which makes the use of the automated biomass gasifier to dry coffee a viable alternative.

Conclusions

According to the results obtained, for the experimental conditions in which this study was conducted, it can be concluded that:

1–The proposed drying system showed to be feasible with regards to quality of the coffee beverage, since the dry coffee has had good qualitative results referring to the specific mass, electrical conductivity, potassium lixiviation, color and other parameters that did not compromise the final beverage quality, and therefore did not lose commercial value.

2–Higher values of electrical conductivity and potassium lixiviation were observed for the dry coffee for the proposed system and the concrete terraces in comparison to the dry coffee on the suspended terraces. However, these values did not affect the quality of the coffee regarding classification of the beverage.

3–It was observed that the classification of the coffee beverage dried using the proposed system and on the suspended terraces was superior to the that obtained for coffee dried on the concrete terrace, indicating a quality loss of coffee dried on this terrace due to contact with the wet floor, resulting from the rain during the drying period.

Acknowledgements
To CNPq, CAPES, FAPEMIG

Reference

Lora E. E. S., Cortez L. A. B., Gómez E. O., 2009. Gasification. In: Biomass for Energy. 2. ed. Campinas- SP: Unicamp, Cap. 9: 241-332.

Rezende O. L. T., 2012. Using fuzzy logic to control ventilation and exhaust systems of the set gasifier/combustor in order to keep combustion zone and exhaust air temperatures at preset values. (Thesis-DS). Viçosa, MG, UFV: 145p.

FINANCIAL ANALYSIS OF OIL PALM PLANTATION CULTIVATION IN INDONESIA

Tereza Svatonova*

Czech University of Life Sciences Prague, 16521 Prague 6 – Suchdol, Czech Republic,
E-mail: svatonovat@tf.czu.cz

Abstract

Oil palm cultivation in Indonesia is increasing. This study investigates the financial and economic aspects of establishing an oil palm plantation using data collected in 2012. The financial case study is undertaken from the perspective of company in North Sumatra, Indonesia. A spreadsheet model was used to develop and calculate the net present value (NPV), benefit: cost ratio (BCR) and internal rate of return (IRR). Sensitivity analysis of the NPV to the default discount rate (4 %) was included. A 5000 ha plantation over 25 years was estimated to result in a positive NPV of 264 million IDR (29,300 US$) with a BCR of 2.32 and an IRR at 26.9 %. The payback period was about six years. Establishing an oil palm plantation seems to be very profitable investment on the basis of the assumptions made.

Keywords: Capital cost, fresh fruit bunch (FFB), labour need, plantation, recurrent cost and sensitivity analysis.

Introduction

Palm oil is one of the raw stocks of vegetable oil used for producing biodiesel with annual yields of 3.94 t/ha (average value from: Yusoff, Hansen, 2007; Ong et al., 2012; Mekhilef et al., 2010; Lim, Teong, 2012). Biodiesel is a biological non-petroleum diesel derived using transesterification process (Fisher et al., 2009; Yee et al., 2009) and it has similar characteristics as petroleum-derived diesel and when both mixed together it can be used in any Compression Ingition engines without regulation (Lim, Teong, 2012). Indonesia is the largest global producer of palm oil. In Indonesia, 50 % of palm oil plantations are owned by huge companies with mills. Small farmers in Indonesia own 40 % of Indonesian plantations (produced 9.4 Mt in 2008). The remaining 10 % of plantations are owned by Indonesian Government (Rist et al., 2010; Rianto, 2010).

Indonesia and Malaysia supply 85 % of total demand. Thailand which produced 2.8 % of total world production in 2010 is the third largest producer in the world.

The aim of this study is to collect the financial data of oil palm production (from the perspective of a plantation) in Indonesia.

Material and methods

Area description

The research was carried out in North Sumatra. The oil palm plantation is located in Eastern region in Serdang Bedagai Regency around city of Tebing Tinggi, at an altitude of about 100 m above sea level. The climate is tropical with a mean daily temperature of 27 °C and a mean annual rainfall of around 2 000 mm, which is primarily distributed from November to March. The relative humidity is around 85 %. The topography is relatively flat including some hills with slopes of less than 8 %. The underlying geology is sedimentary rock, and the mineral soils have a pH of about 4.5. The oil palm company plantations were selected, because they are one of the largest plantations owners in North Sumatra.

Data collection

Data were collected during face to face interviews with oil palm plantation managers involved in the production process. Data related to quantities and costs of all inputs and outputs of the establishment, maintenance, production, harvesting and sales. Future amounts of inputs and outputs were estimated from past experience. A spreadsheet model, developed in Microsoft Excel 2010, was found as appropriate method of summarising the data. The area of the case study plantation is 5 000 ha. See system assumptions in Tab. 1. The typical life cycle production chain is 26 years, while in first year the pre-nursery and nursery plantation is planted. Concurrently the establishment of palm oil field is conducted, but the costs of overall establishment and nursery costs are summarised only in year zero. The main costs in each operation relate to labour, machinery, and input materials. Labour costs are expressed in "person-days" which is equal to 8 hours. The net salary for labour for one day is 45 000 IDR and men and women are equivalent. The sensitivity analysis compares the economics on the effects in prices of inputs and outputs.

Tab. 1 System assumptions

System	Unit	Value
Area of plantation	ha	5000
Area of pre-nursery per ha of plantation	ha of pre-nursery (ha of plantation)$^{-1}$	0.0089375
Area of nursery per ha of plantation	ha of nursery (ha of plantation)$^{-1}$	0.0103623
Length of access road per ha	(km ha^{-1})	0.0005
Length of main road per ha	(km ha^{-1})	0.01
Length of collection road per ha	(km ha^{-1})	0.034
Length of drainage per ha	(km ha^{-1})	0.3

Results and discussion

This study has sought to estimate the financial outcome of a new oil palm plantation. Externalities are not included in this study and are recommended for future studies.

The financial indicators used to evaluate oil palm production are: Net present value (NPV), Benefit: Cost ratio (BCR) and Internal rate of return (IRR). The costs of production taken into account are capital and recurrent costs, both including labour and material costs. Total discounted revenue and cost were calculated yearly over a 25 years period using 4 % discount rate.

Capital and recurrent costs

Capital costs are shown in Tab. 2 and the greatest capital cost per hectare of plantation was associated with land clearing.

Tab. 2 Total capital costs of palm oil plantation

Operation	Total cost (IDR/ha)
Survey	299
Pre-nursery	1 105 734
Nursery	1 269 762
Land clearing	5 730 375
Buildings and facilities	1 119 600
Roads infrastructure	1 640 978
Drainage infrastructure	1 572 000
Planting in the field	4 253 853
Operating costs	500 000
Total capital costs	**17 192 601**

These are the costs associated with cultivation and occur every year: weeding, pest and disease control, pruning, fertilising, harvesting and transport (Fig. 1).

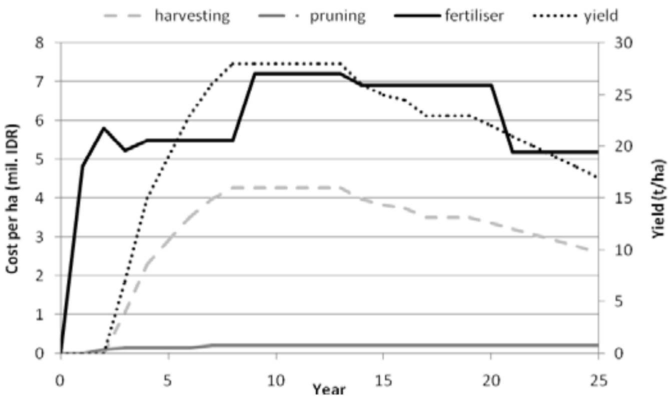

Fig. 1 Annual cost for fertilising, pruning and harvesting in relationship to yield

Financial assessments

The key factors influencing financial side of the project are: the cost of inputs (material, labour and machinery), the market price of selling fruits, which affect the revenue and profit for company and discount rate. Fig. 2 shows annual cash flow for plantation. Costs are the biggest in the beginning of the project because of the significant capital costs, mainly for clearing. In the next two years, the annual costs are reduced, but overall costs are still rising and then start to go down. Within the first three years there is no income because oil palms still not yield. Revenue begins to growth sharply during the fourth year, when oil palms begin to produce FFB. Subsequently, income starts to vary but stays stable up to Year 15 and begins to decline. The NPV suggest the total financial achievement of investment. For this cost-benefit analysis the annual income and costs are calculated for 25 years, and then discounted. Discounted cumulative net margin is the NPV of this investment. Using the discount rate at 4 %, the NPV of the project, the discounted total revenue is 463 million IDR and the present value of total costs is 199 million IDR. The NPV was calculated as 263 million and the BCR is 2.32:1. These values suggest that oil palm cultivation is profitable. The derived IRR was 27 %, which is 7 times higher than 4 % discount rate.

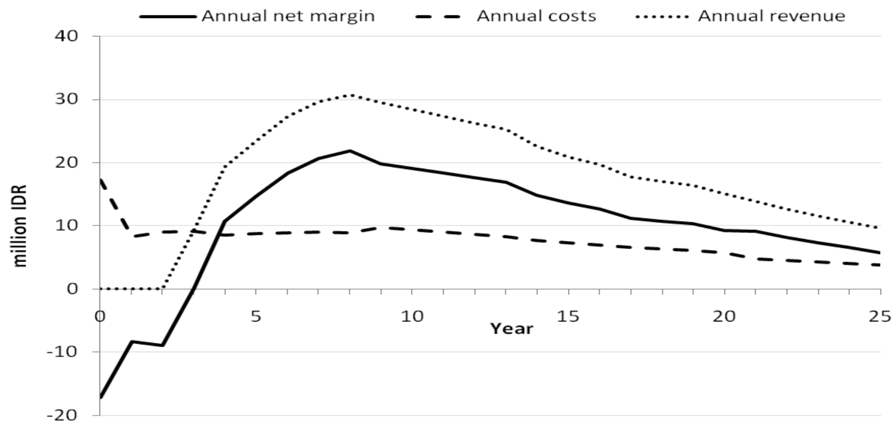

Fig. 2 Estimated discounted annual cost, revenue and profit per hectare of oil palm plantation in IDR

The cash flow for each year and the cumulative cash flow over 25 years have been calculated. The biggest difference is visible when the cash flow benefits became evident. The oil palm plantation system is highly profitable assuming a discount rate of 0-8 % (Tab. 3). Beyond this, it is necessary to take into consideration a high risk of establishing a plantation, because of high establishment costs and the fact that the plantation will first yield after 3 years from planting. It is necessary to consider the risk of possibility that the forest burns before it starts getting profit. System is loaded by negative cash flow for six years and records a rapid growth after that. There are three ways of shifting NPV: 1) changing the discount rate changes the NPV. Higher discount rate makes minor NPV; 2) higher income amounts heighten the NPV and conversely; 3) formerly profits elevate the NPV and later profits reduce the NPV.

Tab. 3 Comparison of net revenue from oil palm plantation system IDR ha^{-1} in different discount rates

Discount rate (%)	**NPV (million IDR ha^{-1})**	**BCR**	**IRR (%)**
0%	467	2.50	32.0
4%	**264**	**2.32**	**26.9**
8%	156	2.11	22.2

Conclusion

In this study the economic analysis of oil palm plantation was developed. The practical part calculates the NPV for the system during 25 years long period in Indonesian agriculture production. The timber revenue from the trees when replanting was not included in this case study. With incorporation of 4 % discount rate the discounted total revenue is 463 million IDR and the present value of total costs is 199 million IDR. The NPV of the system is positive at 263 million IDR and indicates that this investment is good and profitable. The BCR of 2.32 is greater than zero and ensures a considerable return per hectare. This is obtainable due to inexpensive labour need in oil palm plantation. The IRR of 27 % is nearly 7 times higher than interest rate and forecasts high returns.

Refferences

Fisher B., Turner R.K., Morling P., 2009. Defining and classifying ecosystem services for decision making. Ecological Econonomics, 68: 643-653.

Lim S., Teong L.K., 2010. Recent trends, opportunities and challenges of biodiesel in Malaysia: An overview. Renewable and Sustainable Energy Reviews, 14: 938-954.

Mekhilef S., Siga S., Saidur R., 2011. A review on palm oil biodiesel as a source of renewable fuel. Renewable and Sustainable Reviews, 15: 1937-1949.

Ong H.C., Mahlia T.M.I., Masjuki H.H., Honnery D., 2013. Life cycle cost and sensitivity analysis of palm biodiesel production. Fuel (in press).

Rianto B., 2010. Overview of palm oil industry landscape in Indonesia. Price water house Coopers Indonesia, Jakarta.

Rist L., Feintrenie L., Vevang P., 2010. The livehood impacts of oil palm: smallholders in Indonesia. Biodivers Conserv, 19: 1009-1024.

Yee K.F., Tan K.T., Abdullah A.Z., Lee K.T., 2009. Life cycle assessment of palm biodiesel: Revealing facts and benefits for sustainability. Applied Energy, 86(1): 189-196.

Yusoff S., Hansen S.B., 2007. Feasibility Study of Performing an Life Cycle Assessment on Crude Palm Oil Production in Malaysia. The International Journal of Life Cycle Assesment, 12(1): 50-58.

SECURITY SYSTEMS AS PART OF THE CONTROL SYSTEM IN BUILDING TECHNOLOGY

Zdeněk Votruba*

Czech University of Life Sciences Prague, 16521 Prague 6 – Suchdol, Czech Republic, Phone: +420 224383158, Fax: +420 224383168, E-mail: votruba@tf.czu.cz

Abstract

The aim of this paper is consider the technical, technological, security and commercial possibility of integration security systems (I&HAS, CCTV systems, fire alarm systems, access control) to the global information system usually called intelligent system buildings. It is not detailed and complete description of all these systems, equipment, technologies and techniques in the fields. Essential is define the basic systems and assess them in terms of integration possible, taking into account mainly to security and legislative risks. Chapters of contribution to provide a general overview of the present situation in the integration issues. Based on theoretical calculations and experimental measurements which were carried out both under laboratory conditions and in normal operating conditions too, it was necessary to formulate the basic premise of the properties of subsystems and their integration, then is to compare with the legislative and normative base in CR and in EU. The final output is drafting proposal technology to safe and modular integration of safety systems, including put into partial operation physical solution.

Keywords: security, system, building

Introduction

The current market environment, along with the ever increasing pressure on automation, reliability and above all the safety of persons, objects and technologies, building our usual view of designing buildings still more pressure on the essential and fundamental change. Nowadays, it is already quite common that the object is installed parallel **information systems** (computer networks, telephony, audio and video distribution), **security systems** (alarm systems, CCTV systems, access control systems, fire protection systems, explosion, systems against flooding, etc.) and **large technological systems** (air conditioning, ventilation, heating, lifts, technological lines). Consequently, the user an ever greater pressure to centralize the installed systems and their interconnection, and then ultimately, their interaction and automatically optimize operation and diagnostics.

This trend is evident for decades, but the results are not significant. Integration of a number of internal systems, in many cases, although technically possible, due to the reliability, safety from the perspective of current standards but **very problematic**. Given this, it is first necessary to define the parameters of the systems (per formative indicators) used in different types of buildings and subsequently determine their suitability for possible integration. Only then it is possible to identify ways of integrating with a view to maintaining the necessary operational, technological and especially security conditions.

Material and method

From the point of history the first "**intelligent house**" was in the 60th of 20th century presented in Japan (Dušek, 2010; Li, 2013). As it was at this time common practice, all technologies and functionalities were controlled via central unit. Nowadays we would assign it as a PCL computer. These introductory practical experiments, however, have not met with great interest amongst builders and engineers and therefore they were not significantly applied in practice.

Approximately 10 years later, in the early 70th of the last century the energy crisis and soaring oil prices caused resurgence of interest in this project. Primarily because this would lead to a significant and global reduction of electricity consumption for heating, lighting, air conditioning and the overall increase of user comfort. Quite quickly were achieved first successes - many, especially German manufacturers began offering not only quality heating and other systems, but also they began to offer a newly designed, mutually cooperating electrical installation. The beginning of the birth of the concept of a single intelligent electrical installation technology can be considered for 1987. At this time the companies Berker, Gira, Merten and Siemens commonly founded the **Instabus Gemeinschaft**. The goal act was to design and develop a system for monitoring, measurement, and control of operating conditions in buildings (Dušek, 2010; Li, 2013).

In the Czech Republic (and it is similar in most EU countries) the issue of integration of information and security systems in intelligent buildings deals with a single standard - ČSN CLC / TS 50 398:2009. And its formulation is rather unfortunate from the perspective of the requirements of security systems and significantly out of date, which I will try to demonstrate in the next section.

Subsequently a number of tools and protocols ensuring the connectivity of systems began to develop (see details below). On the other hand it is true till now, that there is still no clear definition of what an intelligent house actually is and how it can be specified. We attempt within this paper to define the concept of intelligent buildings at least with regard to the interdependence of internal security systems.

Nowadays, it is already quite accurately defined and legislated activity and the function of alarm systems (formerly known as SAS, now I&HAS) (Votruba, 2012) as well as fire protection and extinguishing systems (FPS and SHZ). The field of CCTV (at first IP cameras, but also CCTV) is currently undergoing a dramatic progress as well as gradual standardization. Individual manufacturers and specialized companies attempt certain degree of interconnection systems, they face however to significant technical, technological and especially legislative (and unfortunately also strong commercial) problems.

These issues will be described in the following paragraphs, as they are crucial for a correct and meaningful integration of security systems to control building systems.

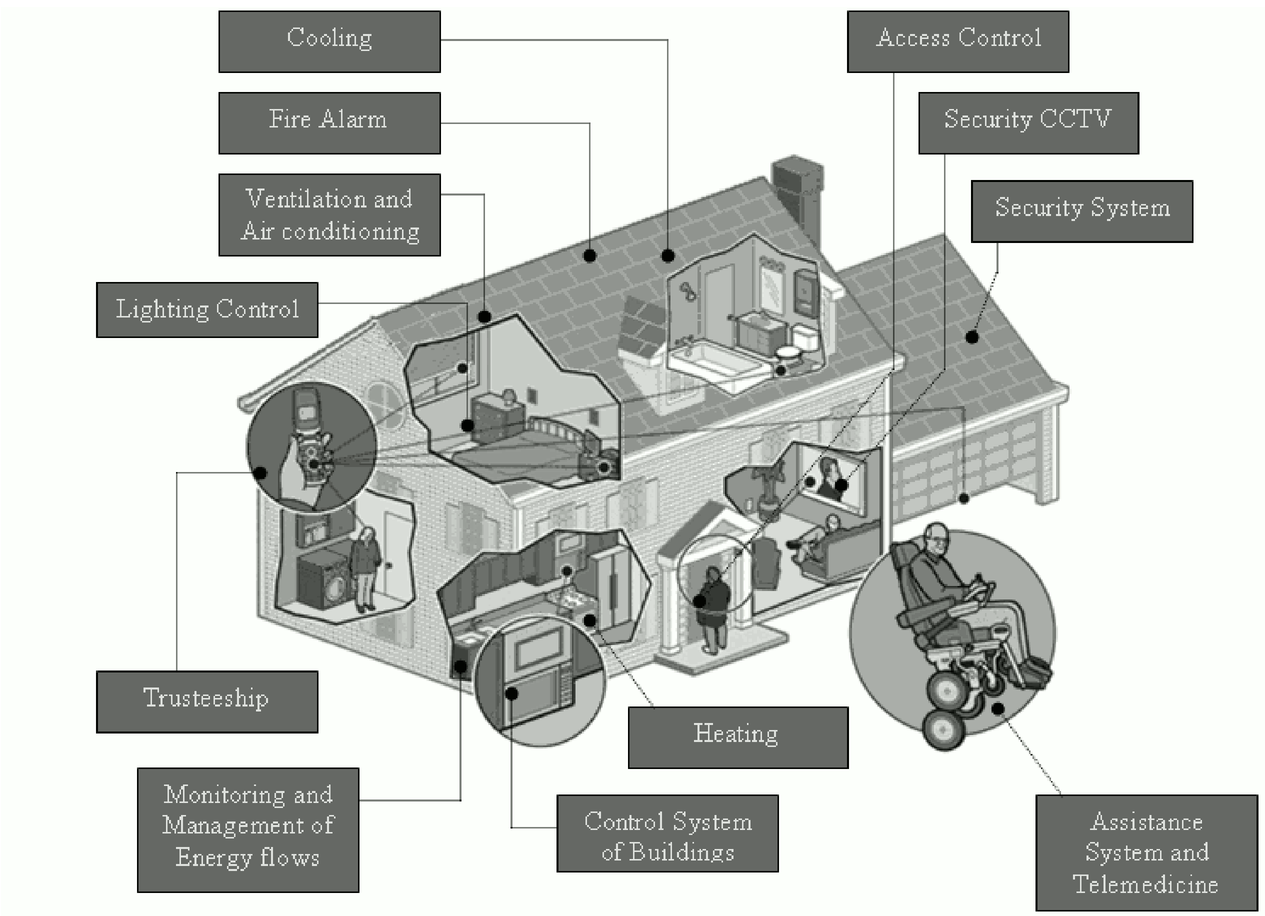

Fig. 1 Example of integration of smart building - living type

Results and discussion

Precise and general definition of intelligent building does not exist. However, it is feasible to define different points of view, according to which the concept can be partially defined. For our basic needs, it is sufficient if you simplify the issue of intelligent buildings in terms of architecture, automation and communication.

From an **architectural point of view** it is a building that's design ensures maximum energy efficiency. It is of course a number of ways to achieve this, from the basic location of the building, through its orientation, materials, and construction methods chosen, to the careful and precise execution of work. This definition is not in itself for the problem of information systems essential, but important is its consequence***. Since the very beginning of the project must be obvious that this is the construction of an intelligent building***. Attempts to implement advanced integration of internal systems into existing conventional buildings, although quite often implemented, is very often associated with many problems and significant financial costs. For the design of intelligent building is therefore essential tight cooperation of architects with the designers of internal system. It is obvious that the requirements of these two groups may vary somewhat, but it is necessary to find an adequate solution enabling the realization (Zhou et al., 2013).

From the perspective of **internal systems**, the concept of "intelligent building" is to be reserved for such an object, where the set of all (most) of the installed systems (I&HAS, CCTV, ACC, FAS, air conditioning, heating, shading equipment, multimedia, computer and communication systems) is connected to one control (this of course does not define the very concept of intelligent buildings, but the user-specified impact of such a project). This can not only save the cost of a stand-alone installation of individual systems, but also significantly eliminate redundant controls (Althoff, 2001; Milenkovic et al., 2013; Zhou et al., 2013). This merger can achieve significant simplification of control and usually also the increase of functionality and quality of interior.

However, this is not the only reasons for the introduction of the integration of these systems. For the future owner of the building is particularly important (even the partial) the **energy saving**. For example, smart thermostats can regulate the temperature throughout the house as needed (exposure to sunlight, the presence of people, and the influence of other heat sources) just in rooms which are in use. For private facilities could be for example interesting if you can heat the hot water only when someone is inside the room. It is possible e.g. to disconnect heating radiators in the rooms where the window is open (there is a source of data from security systems which can be utilized for this purpose). System installations are increasingly deployed not only to the control of lighting, blinds, heating, air conditioning, ventilation (and similar features of buildings), but together with a range of optional features, such as solar panels or photovoltaic power plants. The systems I&HAS and FPS can also cooperate, and these functions may be provided without the need for independent security systems. Cooperation is increasingly common with modern audio and video systems. The future system installations are to manage all the functions that are intended for the complex activity of buildings as well as their surroundings. Current ideas go even to the imaginable situations where the installation will thus conceived independently decide ("think") – they will immediately respond to behavior and feelings of users of the building. Only then will it be really true now perhaps erroneously used term "intelligent installation". First attempts in this area already exist today - for example, the noteworthy system STAY-D Paradox Ltd. .In this system, depending on the behavior of the object user the behavior of the security system self-adjusts. This system is not required in the usual way to be switched on and off, it to some extent predicts the security requirements by sensing the motion (behavior) of people staying in the building.

Although projects of intelligent buildings (IB) are already quite popular nowadays, their massive expansions prevent certain obstacles. Most crucial of them is probably the state-of-the art of intelligent control system technology.

In principle there are two ways to control the IB. Historically; older and still the most widely used is the system with central unit. This attempt has its advantages primarily in the simplicity of implementation of the information system; as usual tools for an information system (IS) with central management can be used. However, major difficulties are encountered in the cases of extending the system, its modernization and integration of new modules. The fundamental problem is then looking at the reliability of the central system. It is hypothetical equivalent of an idea of being able to set up Internet as the central control node (server).

Modern and undoubtedly progressive control technology of IB system is based on a distributed control ie without a central unit, respectively with the central unit of the intelligent modules that mutually communicate via smart bus. Moving information among modules is then solved by a specialized protocol. This method has many advantages especially from the perspective of development - new modules (with standard bus) can be easily supplemented - designer, or subsequently the user is not bound to the specific solution of a particular manufacturer - it is relatively easy to define faults and "bottlenecks" in the system. The main drawback is the need for thorough preliminary analysis of the IS building, a well- designed and well- implemented installation and well trained personnel. Unfortunately, the price of this solution is much higher than in the case of use of a central model IS of building control (Dušek, 2010; Milenkovic et al., 2013).

	Advantage:	Disadvantage:
Centralized system		
thus includes a central control unit, which is connected with other elements by bus. Information from the sensors is sent to the central unit, where it is processed and the resulting aggregated information is sent to the actuators	o cheap sensors and actuators	o complex functionality of the central unit o need to connect the central unit with all the other elements of the system o lower overall system reliability, reliability adversely affected by the central unit and not backed up architecture
Decentralized system		
contains elements which are interconnected via communication bus, after which they send or receive information. There is no central element, which means that all elements are equivalent ones.	o easier and cheaper interconnections of elements o variability of the system o failure of the element does not result in dysfunction of the whole	o higher price due to build- in intelligence of individual elements

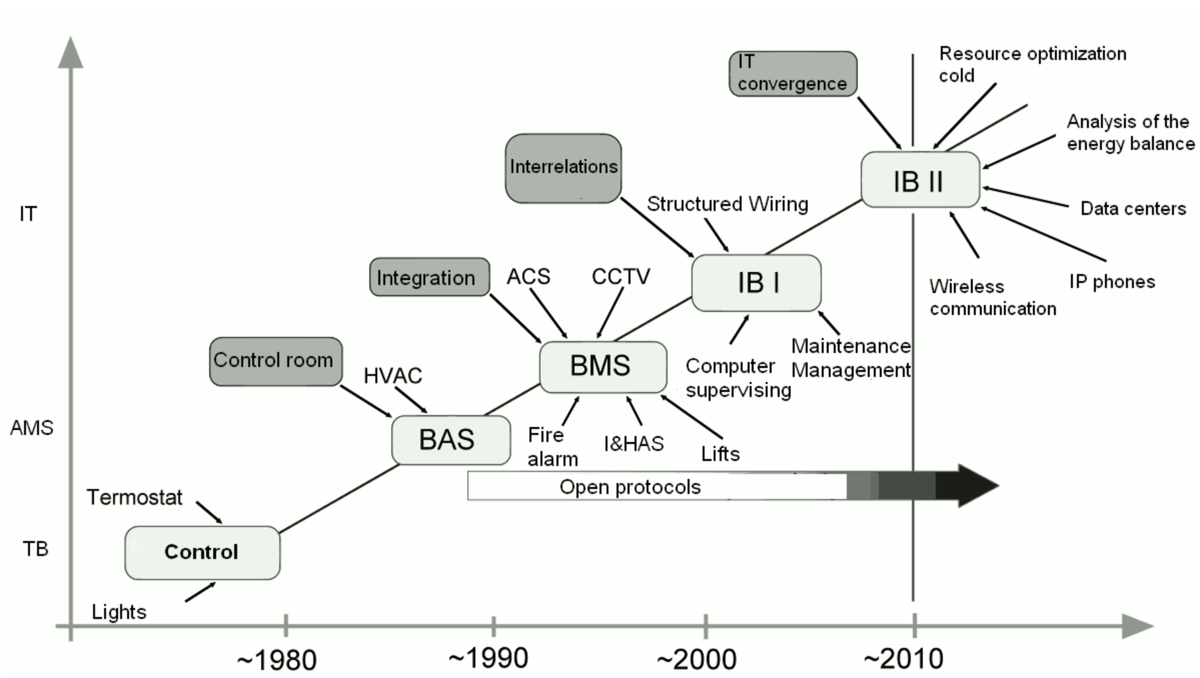

[(3)]

Fig. 2 Convergence of technologies in IB projects

When deciding on the choice of a particular methodology of systems integration is of course also need to consider the extent level and integrability of respective technology. These relations are quite well reflected in the following chart.

There is obvious in this graph that from intelligent building systems integration point of view we are just now in the phase in which the integration of individual modules is primarily carried out by the mean of computer communication technology. Such a procedure is of course optimal in terms of cost and ease of system integrability, however, it is highly disadvantageous in terms of the safety systems integration. If we take into consideration, as a starting point for other requisites in this time prevailing method of communication networks (TCP / IP over Ethernet), if we take into account also (variable and not too high) reliability of common network components and servers, including PLC, we can therefore deduce that expected reliability of integrated security systems is much lower than the current non-integrated modular system (Althoff , 2001; Votruba, 2012) -see. eg. **Anthony Mykiska,: Guarantee reliability of technical systems in the design phase** (Automa, 11/2001), **Mirko Novak, General terms of reliability and safety of technical systems** (LSS Research Report No. 100/01).

And that is the key problem of integrating safety systems into the current model of intelligent building projects! Even aside from the issue of standards (existing standards do not allow bidirectional communication for system integration as well as I&HAS and FPS to higher systems), the method of integration utilizing TCP / IP and PC servers (partly PLC) is completely wrong. In the long term perspective we would meet similar problems, as does Internet today – e.g. in the case of QoS and the like. Unfortunately, with the significant difference as in the case of security systems is resulting thread much more serious than in the case of loading a Web page or an e-mail!

It is just the issue of legislation and standards which currently stops all the correct attempts to integration of security systems in intelligent buildings. It is unfortunately true that now many companies and manufacturers offer security systems integration to internal systems of the building. But this can be accepted on the trivial level only, where security systems are completely separate, and they are in any case not influenced (controlled) through any other systems. In principle, only one-way communication is allowed to be used, where outputs from security systems are transposed "out" into an integrated building system. Under current standards (e.g. for security systems CSN 33 4590:1986 + Amendment 1:1999, EN 50130-4:1997, EN 50131-X, for fire protection systems Act 67/2001 Coll., Decree No. 246 / 2001 Coll. standards of EN 54, for camera systems currently valid EN 50132, the important issue is, the law 101/2000 Sb., and 127/205Sb.) no element which does not have adequate safety class corresponding to class security system (e.g. the communication bus) is allowed to be connected to the system . Perhaps, if this happens, the entire security system is consequently classified in safety class 0 (EN 50131-1).

Therefore, in reality a very serious stage arises in the process of integration, if the existing security system in safety class 2 is interconnected (usually via TCP / IP module) with any other building systems using KNX / EIB and BACnet. Because these systems and their individual modules do not have a security certificate for any class of security, respective security system automatically falls also to the class 0! If you choose for the purposes of integration an extra transmission over UTP using TCP / IP, the situation is the same or the even worse (Althoff, 2001; Dušek, 2010; Votruba, 2012).

It goes without saying that most of the integration companies do not inform its clients about this serious consequence. **In case of incident an insurance company carries out its own investigation and when it detects this type of system degradation, it logically refuses not only performance claims, but it can be expected that it will require reimbursement of all discounts on insurance arising from the installation of security systems. Furthermore, if the security systems are for respective object prescribed by law (in pre-defined class), this situation probably can classified as a criminal offense of public threats!**

From this perspective, it seems like a very tragic solution introducing the above-mentioned standards ČSN CLC / TS 50 398:2009. The standard is very general but nevertheless in point 4.2. clearly defines: "The integrated alarm systems must be provided for each application system used in the relevant standards."

This goes back to the originally defined problem. Although the standard defines three types of configuration of the integrated system, it is divided by interaction and autonomy of individual systems (Type 1, Type 2A, Type 2B). And just systems defined by the type 2A and 2B can interact, which is in accordance with other standards (eg ČSN CLC / TS 50 131:2007, EN 50132 and others) totally unacceptable!

Personally, I think that now we are currently in the situation where we have to find appropriate technological solutions for the interconnection and integration of security systems and only on the solid basis of its verification, valuation and testing this method introduce to the standards. This is not a task for the Czech Republic, or even the Europe, it is a global problem.

Legislative solve this problem is very important not only in terms of technical solutions, but also financial. According to our research (projects: 31170/1312/3136, 31170/1312/3126) a mathematical model of a financial return on investment in intelligent building systems in residential buildings, although still quite excellent long term, in the case of commercial buildings, however, is about the importance of returns.

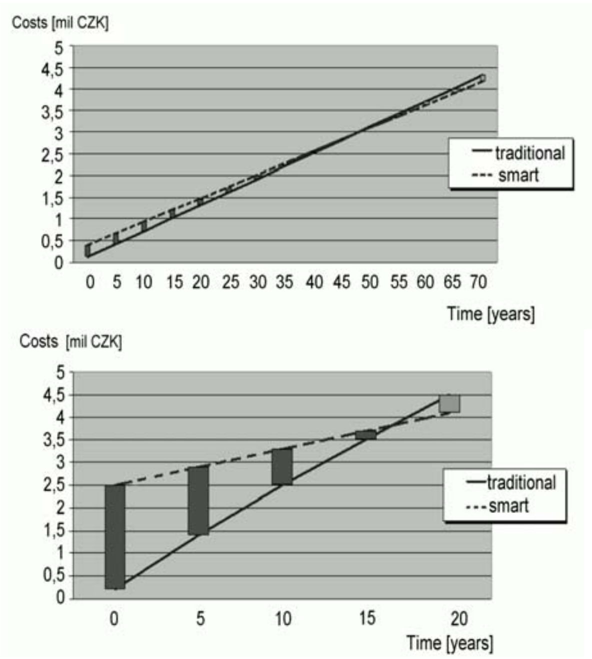

Fig. 3 Investment difference return for residential buildings and for commercial buildings

Conclusions

Within the frame of this paper is really not possible to describe in detail all the options, parameters, and utilizations (especially the pitfalls) of the security systems integration to the "intelligent" buildings. Perhaps, however the outline of the basic solutions and especially the presentation of dangers that this integration can bring was briefly done. To summarize the attempts the situation could be characterized as follows:

- an integration of safety systems into information systems of buildings Is in the so-called "intelligent building" a need,
- there are a number of technological solutions (computer networks, fieldbus application protocols, application extensions) that can solve this problem,
- nowadays, there is no technical solution, which according to current standards allows the full (two-way) integration; keep in mind that for this integration is necessary to solely use components and software tools that have the appropriate safety certification (as an example can be mentioned rail safety systems),
- due to the required reliability and safety an universal distributions (Ethernet) cannot be used and certainly universal protocols (TCP / IP), cannot be applied,
- due to the required reliability and safety, it is unrealistic to use centralized systems, but it is necessary to use systems with distributed intelligence (substitutability of modules) - from this point of view LONWORKS is better, but it has other disadvantages described above.

It is obvious that the integration of safety systems to information systems IB today is a problematic task, especially for reasons of legislation, standards and regulation of implementations. Significant changes are expected in this field, **it is up to professionals to focus on conceptual strategic evolution**. Today, the typical centrally controlled systems have no perspective, it is necessary to introduce technical and especially standardization documents for the implementation of decentralized information systems of buildings so that they can be used in order to integrate all security systems. Therefore, at this point I think the efforts of some companies and trade associations to quickly change the standards without in depth discussion and thorough testing of possible solutions seems to be rather harmful and dangerous.

The estimate of future developments is quite difficult. When analyzing the current technical possibilities, trends and consumer requirements can be assumed that in the perspective of a few years it will be possible to implement truly intelligent buildings IS with full integration (i.e. also with integration with security systems), probably on LonWorks bus, or (hopefully not) with the support of BACnet communication protocol. In the longer term, however, I believe that the development will be oriented in a different direction - toward neural network control which is created just on the LonWorks bus. Currently in our laboratory the tests of this technology are carried out and the results are very promising (Althoff, 2001; Votruba, 2012; Zhou et al., 2013).

The key to dealing with the legislative and normative inaccuracies, in the author's view, is correct and professional work of the national standardization committees, which can correct inaccuracies and questionable interpretation of the submitted standards. It is unfortunately true (as the author knows from his own experience working in technical standardization committee), that a relatively often promotes to the working of this committee the interest of companies and professional organizations.

References

Althoff J., 2001. Preface. In Safety of Modern Systems. Congress Documentaion Saarbruecken 2001. Cologne : TŰV- Verlag GmbH, 5-6. ISBN 3-8249-0659-7.

Anttiroiko A.V., Valkama P., Bailey S.J., 2013. Smart cities in the new service economy: building platforms for smart services. AI and Society, 1-12. ISSN 0951-5666.

Dušek B., 2010. Intelligent buildings and their implementation, presentation at the conference "Intelligent Buildings 2010", Prague 14.4.

Junqi D., Sidong Z., Tao Z., 2011. Improved implementation and evaluation of wireless sensor networks in intelligent building. China Communications, 8(8): 64-71.

Li M., 2013. The construction and development of the green intelligent building, International Journal of Advancements in Computing Technology, 6(5): 28-35.

Milenkovic M., Dang T., Hanebutte U., Huang Y., 2013. Platform-integrated sensors and personalized sensing in smart buildings. SENSORNETS 2013 - Proceedings of the 2nd International Conference on Sensor Networks, 47-52.

Votruba Z., 2012. Safety systems in intelligent building project. Security magazine, 4. ISSN 1210-8723. (in Czech)

Zhou Q., Zhang Z., Cui F., 2013. Research on the integrated control teaching system of building based on fieldbus. Applied Mechanics and Materials, 278-280: 1952-1955.

Faculty of Engineering

Title: **Trends in Agricultural Engineering 2013**

Editor: © 2013 Czech University of Life Sciences Prague; Faculty of Engineering (www.tf.czu.cz)

The conference is organised in cooperation with CIGR (www.cigr.org)

Type publication: Conference Proceedings

Approved: Deanship of Faculty of Engineering; Czech University of Life Sciences Prague

Edition: First

Circulation: 180

Imprint date: 2013

The articles in the publication are reviewed

The Conference Proceedings designed by Jan Malaťák and Martin Libra

ISBN: 978-80-213-2388-9

Note: Objective correctness and language guaranteed by authors